

62

12 11/92

cup-Hor-4-37-3244

AJR

37

ucm

[Handwritten signature]

American
Journal of
Roentgenology



November 1991

Served only in the best hospitals!

NuLYTELY®

PEG 3350, Sodium Chloride, Sodium Bicarbonate
and Potassium Chloride for Oral Solution

A double-blinded multicenter study¹ comparing
NuLYTELY® and GOLYTELY® demonstrates:

**Preference. Patients prefer
the taste of NuLYTELY 3 to 1.¹**

Manufactured for Braintree Laboratories, Inc., Braintree, MA 02184
by Lyne Laboratories, Inc., Stoughton, MA 02072.

Reference: 1. Gastrointest Endosc 1990; 36: 285-289

LABORATORIES, INC.
Braintree

© 1991 BRAINTREE LABORATORIES, INC. THE-1081

Official Journal of the American Roentgen Ray Society



P 24,466

American Journal of Roentgenology
Diagnostic Imaging and Related Sciences

Editor-In-Chief Robert N. Berk, *La Jolla, California*
University of California, San Diego
School of Medicine and Medical Center

Editor Emeritus Melvin M. Figley, *Seattle, Washington*

Associate Editor Karim Valji, *San Diego, California*

Consulting Editor A. James Barkovich, *San Francisco, California*

Statistician Charles C. Berry, *San Diego, California*

P 24,466

Editorial Board

John R. Amberg
Ithamar Aviad
Mark E. Baker
Lawrence W. Bassett
Michael A. Bettmann
Felix S. Chew
N. Reed Dunnick
David K. Edwards
Ronald G. Evens
David S. Feigin
Sandra K. Fernbach
Richard H. Gold
William R. Hendee

John R. Hesselink
Charles B. Higgins
Melvyn T. Korobkin
Faye C. Laing
Thomas L. Lawson
Robert G. Levitt
Bruce L. McClennan
Richard P. Moser
Albert A. Moss
Jeffrey H. Newhouse
Donald L. Resnick
Stewart R. Reuter
Charles A. Rohrmann, Jr.

Peter M. Ronai
Sjef H. J. Ruijs
Stuart S. Sagel
David J. Sartoris
Stefan C. Schatzki
William P. Shuman
Edward A. Sickles
Barry A. Siegel
David D. Stark
Edward T. Stewart
Murali Sundaram
Eric vanSonnenberg
Robert K. Zeman

Editorial Staff: Margaret Levene, *managing editor*; Katie L. Spiller, Barbara Rose, Barbara L. Halliburton, and Janine Anderson, *manuscript editors*; Nancy Rydbeck, *office manager*; Sheri Smith, *administrative assistant*; Linda J. Waggoner, *administrative secretary*

AJR, AMERICAN JOURNAL OF ROENTGENOLOGY (ISSN 0361 803X) is the official journal of the American Roentgen Ray Society and is published monthly by Williams & Wilkins, 428 E. Preston St., Baltimore, MD 21202. Annual dues include \$50 for journal subscription. Second-class postage paid at Baltimore, MD, and at additional mailing offices. Postmaster, send address changes (Form 3579) to AJR, 428 E. Preston St., Baltimore, MD 21202. Subscription rates \$125 (\$180 foreign); institutions \$135 (\$190 foreign); in training \$25 (\$80 foreign); single copy \$18 (\$22 foreign). The GST number for Canadian subscribers is 123394371. Airmail rates furnished on request. Indexed by *Current Contents* and *Index Medicus*. Copyright © 1991 by American Roentgen Ray Society. 0361-803X/90\$3.00



F R O M M A L L



Perspective

AIDS Risk and Risk Reduction in the Radiology Department

Susan D. Wall,¹ Eric W. Olcott,² and Julie L. Gerberding³

As the AIDS epidemic progresses, concern about the risk of occupational transmission of the causative organism, human immunodeficiency virus (HIV), is increasing. In this article, we summarize the risk of occupational acquisition of HIV in the health care setting and specify protocol and equipment that can reduce this risk in the radiology department. Accidental needle-stick injury is the most common form of exposure to infected blood, which is the only body fluid implicated to date in the occupational transmission of HIV. Prospective cohort studies demonstrate a 0.3–0.4% risk of infection for each needle-stick event. The most important instruction to health care workers that can reduce this risk is the following: Do not recap needles. Other risk-reduction measures include the adoption of universal precautions against transmission of infectious disease; sharp-instrument precautions; the use of protective garb to prevent skin and mucous membrane contamination when blood or bloody body fluid may splash; the availability of stable, puncture-resistant disposal containers for sharp instruments; the exclusion of breakable glass syringes; and the accessibility of resuscitation equipment in all rooms in order to avoid direct mouth-to-mouth contact. These and other measures discussed here are designed to prevent exposure of skin or mucous membrane to blood. If exposure does occur, the contaminated area should be washed immediately. A multicenter research protocol to evaluate the effectiveness of zidovudine (AZT) therapy in preventing seroconversion after exposure to HIV-contaminated blood recommends AZT therapy after massive exposure (e.g., injection of measurable quantities of blood) and endorses it for serious parenteral exposure (e.g., deep needle sticks).

The AIDS epidemic continues to progress. Indeed, AIDS will be diagnosed in approximately 35,000 patients in the United States this year. It is estimated that 1 million people in the United States currently are infected with the human immunodeficiency virus (HIV) and that the infection eventually will progress to AIDS [1]. A cumulative total of 365,000 cases of AIDS by 1992 is predicted [2]. Improved treatment protocols have extended the latency period from the initial infection with HIV to the development of clinical AIDS to a current mean of 11 years, and the progression to death has been slowed to a mean of 21 months from the time of diagnosis [3]. Nonetheless, the 100% fatality rate persists.

Opportunities for encounters between health care workers and HIV-infected patients will increase as the epidemic progresses. During the next decade, increasing numbers of currently asymptomatic but infected persons will require health care as their infections progress to AIDS. In addition, because drug therapies have increased the life expectancy of infected patients, more will need health care for both AIDS-related and non-AIDS-related illnesses and for longer periods. Furthermore, some patients receiving health care are unknowingly HIV positive and may also pose a risk of transmitting the disease to health care workers.

Although the available data indicate that the risk of acquiring HIV infection from occupational exposure is low, the risk for progression to AIDS is high once infection occurs [4]. Con-

Received April 1, 1991; accepted after revision June 13, 1991.

¹ Department of Radiology, University of California, San Francisco, Veterans Administration Medical Center, 4150 Clement St., San Francisco, CA 94121. Address reprint requests to S. D. Wall.

² Department of Radiology, University of California, San Francisco, San Francisco General Hospital, 1001 Potrero Ave., San Francisco, CA 94110.

³ Department of Medicine, University of California, San Francisco, San Francisco General Hospital, 1001 Potrero Ave., San Francisco, CA 94110.

AJR 157:911–917, November 1991 0361–803X/91/1575–0911 © American Roentgen Ray Society

sequently, protection against the transmission of HIV in the health care setting is important. Health care personnel are understandably concerned about their cumulative professional risk of infection. The purpose of this discussion is to summarize the currently available data on the risk of occupational transmission of HIV and to delineate measures used at our institution to reduce this risk in the radiology department.

Assessing Occupational Risk

The risk to health care workers of occupational transmission of HIV has been addressed by several types of epidemiologic investigations, including the case report method and the prospective cohort study method. Both are important; they are quite different methods. Case reports are anecdotal, and therefore do not provide data sufficient to compute an estimate of the magnitude of risk. However, they do document the existence of risk, determine potential routes of transmission, and suggest hazards that may be amenable to intervention. By June 1991, 27 definite and nine possible cases of occupational acquisition of HIV infection had been reported [5–8]. In addition, the Centers for Disease Control (CDC) is investigating 36 more cases that may represent occupational infections. Twenty-five of the 27 documented cases involved health care workers exposed to infected blood or blood-contaminated body fluids. The remaining two cases involved exposure to highly concentrated virus preparations in research laboratories [9]. In 22 of the 27 definite cases, seroconversion was temporally related to needle-stick or similar percutaneous injury. In the other five cases, infection was attributed to exposure via inoculation of the mucous membranes or contamination of open skin wounds [10, 11]. In the nine cases of possible occupational infection, seroconversion after exposure could not be proved rigorously because no baseline testing for HIV antibodies had been performed. However, the virus was identified in the exposure source.

Review of the anecdotal case reports suggests that seroconversion is apt to be symptomatic in health care workers [12]. An acute febrile illness at the time of seroconversion, with fever, rash, malaise, weight loss, and lymphadenopathy, has been observed in more than 75% of occupationally infected health care workers. Seroconversion usually occurs within the first 4–12 weeks after exposure, and conversion more than 6 months after exposure has never been reported in health care workers.

Prospective cohort studies, on the other hand, provide a numerator (number of infections) and a denominator (number of exposed persons or number of discrete exposures) and thereby allow an estimation of the magnitude of risk of HIV infection once exposure has occurred [10]. On the basis of cumulative data from 14 studies since 1983, the risk of infection after an accidental needle-stick injury is estimated to be 0.3–0.4% (six infections per 2008 needle sticks) [5, 12]. In these studies, no infections occurred after exposure via the mucous membranes or skin. All were due to needle-stick or similar percutaneous injuries, and blood was the only body

fluid implicated in HIV transmission [12, 13]. Although the risk from mucocutaneous exposure is not zero—as evidenced by the anecdotal case reports described earlier—to date, the hazard in these prospective cohort studies is too small to be quantified.

The average risk estimate (0.3–0.4%) must be interpreted with caution, because it is likely that not all of the factors that influence the infectivity of a given needle-stick injury are known. Most authorities agree that the volume of blood transferred during the exposure and the concentration of the virus in the source fluid are apt to be the most important predictors of risk in individual cases. Injection of blood, injuries caused by large-bore hollow needles, and deep penetration are features of exposure reported with frequency among cases of occupational infection. Therefore, it is probable that the true risk of transmission is substantially greater than 0.4% when such “severe” exposures occur. In contrast, exposures involving superficial injuries with small, nonhollow needles may be less hazardous than the average risk estimate suggests.

Most of the exposures evaluated in the prospective studies have involved source patients hospitalized with a known diagnosis of AIDS. This is important because these patients have plasma concentrations of HIV 100–1000 times higher than HIV-seropositive patients who do not yet have symptoms of AIDS. Consequently, the true risk of infection after exposure to blood from patients with undiagnosed or asymptomatic HIV infection could be substantially lower than the reported 0.3%. In summary, needle-stick injury poses the greatest risk of occupational transmission of HIV. And, although the average risk of transmission per event appears low relative to the hazards associated with a similar exposure to hepatitis B virus (10–35%) [14], it is likely that the degree of risk inherent in specific HIV exposure events can vary from this average, depending on several factors.

The cumulative risk of HIV infection encountered by various categories of health care workers is influenced by the frequency of the workers' exposure to blood or other infectious materials, the severity of such exposures, and the prevalence of HIV in the population of patients served. Surgeons, dentists, emergency personnel, labor and delivery personnel, and laboratory staff have the highest prevalence of hepatitis B infection, primarily because exposure to blood is ubiquitous among these professionals. In contrast, most health care workers with occupational infection with HIV appear to be nurses, phlebotomists, and laboratory workers [15]. Although underreporting may contribute somewhat to this dissimilarity, it may reflect the fact that most hospitalized AIDS patients are cared for on medical wards rather than on surgical wards, and these are the workers who most frequently perform bedside procedures. Therefore, they may be the health care workers at highest risk for occupational infection. However, as the AIDS epidemic expands, the prevalence of infection among health care workers in surgical, obstetric, and pediatric wards will no doubt increase.

Radiology personnel frequently perform invasive diagnostic and therapeutic procedures involving needles, scalpels, and vascular access. Because patients from the emergency and outpatient departments and from all inpatient units may be

candidates for these procedures, the prevalence of HIV infection in the radiology department may vary widely. For this reason, we urge strict attention to infection control for all patients at our institution.

Infection-Control Precautions in the Radiology Department

Developing, implementing, and maintaining a comprehensive infection control program is essential. This is so not only because of known HIV-positive patients, but also because HIV infection may not have been diagnosed in an infected patient, and because negative HIV tests are not 100% reliable. The prevalence of HIV infection is high at our institution. Consequently, the use of a cautious universal standard of infection control for all patients regardless of diagnosis is the most prudent approach for protection against occupational transmission [16–18]. This approach will protect health care workers from exposure to other blood-borne pathogens as well. Some of the specific infection control precautions described here require additional expense (Table 1), but most do not.

The single most important change in behavior that our health care workers have been asked to adopt is the following: Do not recap needles. Most needle-stick injuries have been

associated with the recapping of needles (Fig. 1) or the improper disposal of needles [19, 20]. If a needle must be recapped, we recommend a single-handed method. If a needle must be removed from the syringe, we recommend use of a hemostat or forceps to grasp the needle. In addition, all needles (with syringe attached) and other sharp instruments should be disposed of immediately in a puncture-resistant container, which should be easily accessible in all rooms. The containers should be stabilized (to prevent spillage; Fig. 2), waterproof, brightly colored, clearly labeled, and should be emptied when they are two thirds full. Twenty-two percent of the reported needle sticks in a recent survey [21] of house officers could have been avoided if the guidelines discussed here had been used. As new products such as resheathing devices and retracting needles are developed, the safety of many procedures may be improved, but such devices will require thorough evaluation during actual clinical use.

Several other measures can reduce the risk of sharp-instrument injury during percutaneous biopsy or interventional procedures. For instance, a stable container can be used to hold nondisposable sharp instruments, rather than allowing them to lie atop a draped patient or on an instrument tray. A flat metal container (Fig. 3) can be used or the plastic canister for 105-mm spot X-ray film can be adapted by drilling holes in the lid [22]. A commercially available universal precaution aspiration tray (Picker International, Highland Heights, OH) [23] includes a foam pad for placement (point first) of sharp objects. It has been a common angiographic practice to remove the puncture needle from the guidewire after vascular access by grasping the needle tip with a piece of gauze held between the fingers while simultaneously wiping remaining droplets of blood from the wire (Fig. 4). This is a high-risk maneuver, however, and should be replaced by a two-step technique that involves careful removal of the needle by the hub before the wire is wiped. Glass syringes and glass vials are not advised unless absolutely necessary. They could break, and their accidental shattering during routine use has been known to cause hand lacerations. Technologists removing used instruments from procedure trays should use long-handled forceps and maintain eye and skin protection.

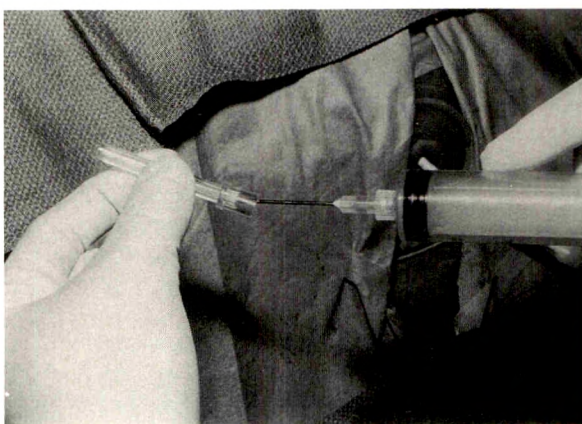
In addition, frequent verbal communication among personnel is helpful when several people are involved in a procedure

TABLE 1: Safety Devices

Equipment	Manufacturer	Location	Price (\$)
Transparent plastic shield	Anago, Inc.	Hayward, CA	1.89
Closed angiographic flush system ("Custom angiographic kit")	NAMIC, Inc.	Glens Falls, NY	9.75
Safe Stick arterial puncture adapter	Cook, Inc.	Bloomington, IN	7.00
Angio-Sac bag with tubing	NAMIC, Inc.	Glens Falls, NY	5.00
Ureteral tubing connector	Cook, Inc.	Bloomington, IN	6.95
Universal precaution biopsy tray	Picker Intl.	Highland Heights, OH	19.65

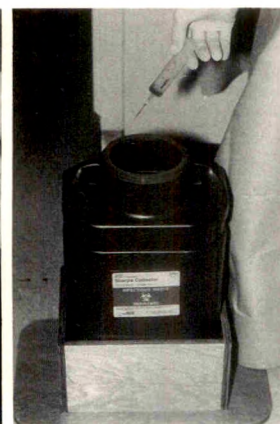
Note.—This list is intended to give examples and is not intended to be exhaustive; other products are or will be available from other manufacturers. The prices listed are those at our institution.

Fig. 1.—Recapping needle. Needle-stick injuries occur when needle misses sheath or when needle passes through sidewall of sheath and into operator's hand.

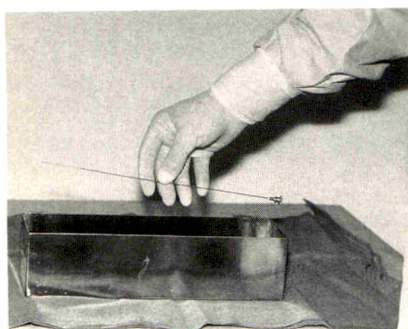


1

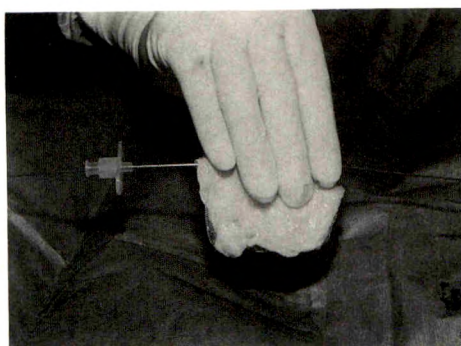
Fig. 2.—Plastic container with nontip base for disposal of sharp instruments. Sharp instruments are deposited in container immediately after use. Wooden base prevents tipping and spillage.



2



3



4

Fig. 3.—Stainless steel container for nondisposable sharp instruments used during angiographic or interventional procedures.

Fig. 4.—Wrong wiping method. Conventional, but hazardous, method of simultaneous wiping of guidewire and removal of angiographic needle by grasping needle at its point. Rather, needle should be removed first, in a dedicated motion, and by its blunt end. Then, with a second motion, wipe wire clean with a sponge.

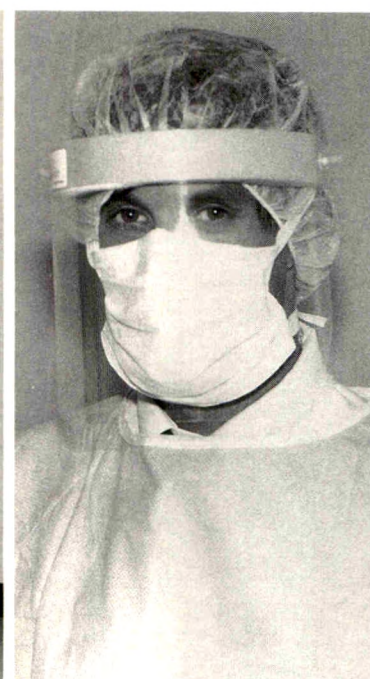
that requires use of sharp instruments. Many of our physicians and technologists voice the word "sharp" whenever a sharp instrument is handled or transferred to a new location. Sharp instruments are not handed from one person to another; instead, one person lays the instrument on a stable surface and withdraws his or her hand before another person reaches for the instrument. Physicians speak freely to each other in order to anticipate movements and to avoid splashes; the patient is told to expect to hear discussion throughout the procedure. Also, adequate light is important for any procedure involving sharp instruments. Control of the overhead lighting in fluoroscopic rooms can be made available to the radiologist via foot pedal or tabletop button to permit bright illumination whenever sharp instruments are being used as well as the dim lighting necessary for dark adaptation.

Other risk-reduction measures are designed to prevent exposure of skin or mucous membrane to blood. For instance, protective garb is recommended when blood or other bloody body fluid might splash (Fig. 5). Blood-filled transfusion bags and tubing can leak or even burst. Therefore, eye protection and gloves are advised whenever transfusion equipment is handled. Gloves are recommended when needles or other sharp instruments are used. Although gloves do not prevent needle sticks, they are likely to decrease the volume of blood transferred to the skin during such injuries by 50% [22]. Gloves also are recommended whenever blood or other body fluids may contaminate the field. Wearing two pairs of gloves and changing gloves in midprocedure are advised for prolonged procedures in bloody fields [13]. Goggles or face shields are used by persons inserting needles for IV access or for drainage procedures and by technologists who must remain close during such procedures. Protection is especially important during interventional procedures when vascular access is expected, and we recommend that it be routine. Disposable gown, gloves, hat, mask, boots, and transparent plastic face shield should be considered. These precautions not only enhance the sterility of the procedure but afford broad skin surface protection against splash. Furthermore, they minimize the risk of transmitting the various non-HIV pathogens among patients susceptible to them.

Some devices designed to reduce the risk of exposure are commercially available, and some previously existing equip-



A



B

Fig. 5.—A, Standard garb for interventional procedures: disposable (but reusable) face shield (Anago, Inc.), hat, mask, gown, gloves, and boots. B, Close-up view of face protection. Note transparent plastic face shield (which does not impair vision), hat, and mask.

ment can be used for the same purpose. For instance, the Cook (Bloomington, IN) Safe Stick puncture device [24] protects against splashing during arterial puncture by containing blood within a clear plastic sleeve. However, the diminished tactile sensation during guidewire manipulation precludes its use routinely at our institution, and it is hoped that a modified version can be developed. Also, a closed angiographic flush system (Fig. 6) reduces the chance of splashing and aerosolizing blood as compared with conventional open systems. Fluid collections can be drained with a similar closed system [25]. Such a unit (Fig. 7) can be created with a three-way

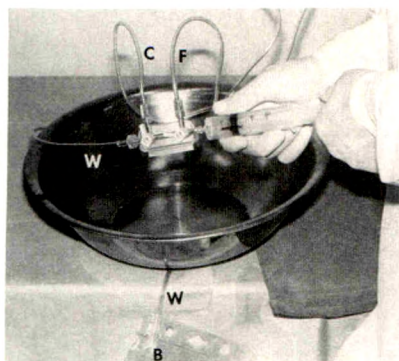


Fig. 6.—Closed flush system for angiography (NAMIC, Inc.) minimizes aerosolization and splatter. Inlet lines are flush solution (F) and contrast media (C). Waste outlet line (W) leads to collection bag (B).

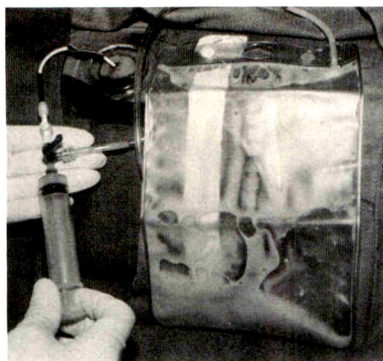


Fig. 7.—Closed aspiration system for fluid drainage procedures. A three-way stopcock first permits withdrawal of fluid from patient into syringe, and then directs fluid expelled from syringe into a collection bag (NAMIC, Inc.). Splashing is avoided.

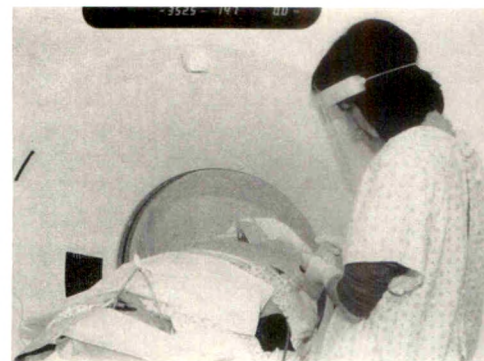


Fig. 8.—Fine-needle aspiration biopsy with CT guidance. Risk-reduction measures include use of transparent face shield, gloves, gown, and sharp-instrument precautions.

stopcock, a syringe, and an Angio-Sac (NAMIC, Inc., Glens Falls, NY), which includes a collection bag and connector tubing in one unit. Or a standard urinary leg bag can be combined with a Cook ureteral tubing connector. We hope that innovative products such as these will gain in acceptance and that more will be developed.

Every radiology room used by patients should have a manual resuscitation bag readily available to facilitate resuscitation without direct mouth-to-mouth contact. Gowns, gloves, face shields, and containers for needle disposal are located on crash carts or are immediately accessible. Suction devices should be available for the removal of body fluids. Syringes with Luer-lock tips are recommended whenever blood or bloody fluid is expelled in order to prevent accidental separation and splattering from the syringe tip. Contaminated linen and plastic items are placed in brightly colored, clearly labeled plastic bags for disposal as hazardous material.

Because blood is the only body fluid that has been implicated in occupational HIV transmission, radiographic procedures that do not involve vascular or percutaneous access generally pose no additional risk of occupational acquisition of AIDS. Thus, most of these procedures require no HIV protection. They include plain film radiography, routine barium fluoroscopy, mammography, sonography, and both CT and MR imaging when IV contrast media is not used. However, in some cases, these procedures involve maneuvers that do introduce additional risk. For instance, protective garb to prevent skin and mucous membrane exposure to splash might be indicated during fluoroscopy if the patient's history includes hematemesis or hematochezia. Also, if glucagon or contrast media is administered IV, gloves are recommended and needle-stick precautions are advised. Percutaneous fine-needle aspiration biopsy with guidance by CT, sonography, fluoroscopy, or mammography should be performed with sharp-instrument precautions (Fig. 8), and if splashing is possible, face shields are indicated. Decisions regarding the use of protective measures require experience and judgment. The likelihood of accidental injury with a sharp instrument or

of splashing with blood or bloody body fluid provides a reasonable estimate of the potential hazard, and the precautions taken in each case are individualized.

If Exposure Occurs

If exposure does occur, take steps immediately to reduce the inoculum. Wash punctured or exposed skin with soap and water. Flush eyes with water or saline. Rinse the mouth and nose with clear water when contamination of mucous membranes occurs. Contaminated equipment and counter surfaces can be cleaned and then disinfected with a 1:10 to 1:100 dilution of 5% sodium hypochlorite (household bleach) or other virucidal hospital disinfectant.

Treatment or procedures for use after exposure remain incompletely studied and controversial. Zidovudine (AZT, azidothymidine, or Retrovir) delays but does not prevent disease progression in patients with AIDS. It inhibits reverse transcriptase, an enzyme essential for virus replication. Its use as prophylactic treatment to prevent seroconversion after exposure to HIV was stimulated by the results of several recent animal studies, which showed that retroviral infection in some animals could be prevented by the administration of AZT within 1 to 4 hr after exposure [26]. However, no proof is available that zidovudine therapy is efficacious in preventing seroconversion in humans or that the potential benefit outweighs the treatment risks [26]. Furthermore, a national double-blind, placebo-controlled study [27] to assess the efficacy of AZT as chemoprophylaxis after occupational exposure to HIV is under way, but may not be concluded for several years because of the relatively low risk of infection by occupational exposure.

If AZT treatment after exposure is used, most authorities agree that therapy should begin as soon as possible, preferably within 1 hr [28]. The treatment regimen currently used in the multicenter study of AZT by the University of California, San Francisco (UCSF), National Institutes of Health, and CDC

specifies an initial dosage of 200 mg by mouth every 4 hr for 3 days. Then 100–200 mg is taken by mouth five times per day for an additional 25 days. The adequacy of this regimen and the prevalence of AZT complications have not been determined. It is preferable to obtain a pretreatment blood sample for testing.

The toxicity of AZT (therapy) in health care workers is unknown. Studies evaluating AZT treatment of patients with AIDS have shown that the primary toxic effects are hematologic and dose related [29]. Anemia, neutropenia, and thrombocytopenia may occur within 4 weeks of the start of therapy. Other side effects include nausea, headache, fatigue, insomnia, myalgias, myositis, paresthesias, and hepatitis. Long-term effects are unknown, but concern exists about possible mutagenesis and teratogenesis. For these reasons, close monitoring of clinical and laboratory data at minimum intervals of 2 weeks during AZT treatment is advised. We defer treatment during pregnancy or lactation.

If AZT therapy is elected, it is provided immediately. AZT is recommended for persons who have had massive exposures (e.g., injections of measurable quantities of blood). It is endorsed for serious parenteral exposures (e.g., deep needle sticks). It is not encouraged, but is available, for less severe exposures. If the source patient's serostatus is unknown, he or she is urged to agree to testing, and if the result is negative, AZT for the injured health care worker is discontinued. However, serial retesting of the source patient for 6 months is encouraged because of the latency period between inoculation and seroconversion. Exposed health care workers are advised to have baseline and follow-up testing for seropositivity 6 weeks, 3 months, and 6 months later [12]. They are further advised not to donate blood for the next 6 months and to delay pregnancy for the same period.

Counseling is an important aspect of management after exposure. Exposure to HIV is a frightening event. The knowledge that the statistical risk of infection is low may not be reassuring when it is coupled with simultaneous advice to practice unfailingly safe sex, avoid pregnancy, and take a drug for 4 weeks. At UCSF, physician counseling is available 24 hr a day for health care workers who have been exposed to HIV. Expert advice on risk assessment, decontamination, care after exposure, and psychological support are provided immediately.

Summary

The complex nature of the protective measures should not be underestimated. Some will increase cost, prolong procedure time, or introduce new technical difficulties. For instance, a midprocedure change of gloves requires an interruption and it increases cost. In addition, experience and judgment are important regarding the use of some technical devices such as the Safe Stick puncture device, because it may reduce the angiographer's sensitivity to guidewire movement. Its use in difficult situations such as in children or for access via the brachial artery may be less advisable because of the added

risk of multiple punctures. Also, protective garb, if unexpected, may be alarming to the patient and its use enhances the importance of the preprocedure consultation. Habits are difficult to change, and change is not always welcomed. Indeed, even at our institution, where the prevalence of HIV infection is high, compliance with recommended risk-reduction measures is not universal [21]. However, knowledge of the risk of occupational acquisition of HIV provides a basis for case individualization and adoption of appropriate risk-reduction measures to minimize needle stick and splash.

The data indicate that the risk of occupational exposure to HIV is small for health care workers in general. It is prudent to assume, however, that radiologists are at increased risk because they use needles and sharp instruments in darkened rooms on a daily basis. Although the risk is low, the stakes are high. A large percentage of, if not all, seropositive patients will get AIDS. Because the serostatus of most patients is unknown, universal precautions against the transmission of infectious disease are recommended at our institution.

Each worker must be concerned for the safety of co-workers. Conversely, each person must work defensively. Continual real-time communication among physicians and technologists and scrupulous attention to safe technique are essential. In our experience, injury to even the most attentive worker can occur because of another's lack of vigilance with equipment, communication, or protocol. Maintaining a safe work environment is a realistic goal, but it requires resources, creativity, and planning.

REFERENCES

- Centers for Disease Control. Estimates of HIV prevalence and projected AIDS cases: summary of a workshop, October 31–November 1, 1989. *MMWR* 1990;39:110–119
- Heyward WL, Curran JW. The epidemiology of AIDS in the U.S. *Sci Am* 1988;259:72–81
- Lemp GF, Payne SR, Neal D, Temelso T, Rutherford GW. Survival trends for patients with AIDS. *JAMA* 1990;263:402–406
- Hessol NA, Rutherford GW, Lifson AR, et al. The natural history of HIV infection in a cohort of homosexual and bisexual men: decade of follow-up [abstract 4096]. In: *Program and Abstracts of the IV International Conference on AIDS*. Washington DC: Bio-Data, 1988
- Beekmann SE, Fahey BJ, Gerberding JL, Henderson DK. Risky business: using necessarily imprecise casualty counts to estimate occupational risks for HIV-1 infection. *Infect Control Hosp Epidemiol* 1990;11:371–379
- Centers for Disease Control. Update: acquired immunodeficiency syndrome and human immunodeficiency virus infection among health care workers. *MMWR* 1988;37:229–239
- Update on occupational HIV infection among health care workers. *Epidemiol Bull* 1990;6(10):41–44
- Centers for Disease Control. Guidelines for prevention of transmission of human immunodeficiency virus and hepatitis B virus to health-care and public-safety workers. *MMWR* June 23, 1989;[Suppl 38 (6S)]:1–37
- Weiss SH, Goedert JJ, Gartner S, et al. Risk of human immunodeficiency virus (HIV-1) infection among laboratory workers. *Science* 1988;239:68–71
- Gerberding JL. Occupational health issues for providers of care to patients with HIV infection. *Infect Dis Clin North Am* 1988;2(2):321–328
- Update: human immunodeficiency virus infections in health-care workers exposed to blood or infected patients. *MMWR* 1987;36:285–289
- Marcus R. Surveillance of health care workers exposed to blood from patients infected with human immunodeficiency virus. *N Engl J Med* 1988;319:1118–1123

13. Gerberding JL. Occupational HIV transmission: risk reduction. *Occup Med* **1989**;4:21-24
14. Palmer DL, Barash M, King R, Neil F. Hepatitis among hospital employees. *West J Med* **1983**;138:519-523
15. Gerberding JL. Risks to health care workers for occupational exposure to hepatitis B virus, human immunodeficiency virus, and cytomegalovirus. *Infect Dis Clin North Am* **1989**;3:735-745
16. Update: universal precautions for prevention of transmission of human immunodeficiency virus, hepatitis B virus, and other blood-borne pathogens in health-care settings. *MMWR* **1988**;37:377-382, 387-388
17. Recommendations for prevention of HIV transmission in health care settings. *MMWR* **1987**;[Suppl 2S]:3S-18S
18. Centers for Disease Control. AIDS and human immunodeficiency virus infection in the U.S.: 1988 update. *MMWR* **1989**;38:1-38
19. McCormick RD, Maki DG. Epidemiology of needle stick injuries in hospital personnel. *Am J Med* **1981**;70:928-932
20. Jagger J, Hunt EH, Brand-Elnaggar J, Pearson RD. Rates of needle stick injury caused by various devices in a university hospital. *N Engl J Med* **1988**;319:284-288
21. Magione CM, Gerberding JL, Cummings SR. Occupational exposure to HIV: frequency and rates of underreporting of percutaneous and mucocutaneous exposures by medical housestaff. *AJR* **1991**;90:85-90
22. vanSonnenberg E, Casola G, Maysey M. Simple apparatus to avoid inadvertent needle puncture. *Radiology* **1988**;166:550
23. Mueller RP, Silverman SG, Tung G, et al. New universal precaution aspiration tray. *Radiology* **1989**;173:278-279
24. Olsen WL, Jeffrey RB, Tolentino CS. Closed system for arterial puncture in patients at risk for AIDS. *Radiology* **1988**;166:551-552
25. Palestrant AM, Esplin CA, Shaw GT. A closed irrigation and drainage system for use with percutaneous abscess drainage: technical note. *Cardiovasc Intervent Radiol* **1990**;13:119-121
26. Mast S, Gerberding JL. Factors predicting infectivity during needle stick: an in vitro model (abstr). *Clin Res* **1991**;39(1):58A
27. Henderson DK, Beekmann SE, Gerberding J. Post-exposure antiviral chemoprophylaxis following occupational exposure to the human immunodeficiency virus. *AIDS Update* **1990**;3(1):1-8
28. Public Health Service statement on management of occupational exposure to human immunodeficiency virus, including considerations regarding zidovudine postexposure use. *MMWR* **1990**;39:1-30
29. Richman DD, Fisch MA, Grieco MH, et al. The toxicity of patients with AIDS and AIDS-related complex: a double-blind, placebo-controlled trial. *N Engl J Med* **1987**;317:192-197

The reader's attention is directed to the commentary on this article, which appears on the following pages.

Call for Papers on Neuroradiology

On January 1, 1992, The American Roentgen Ray Society and the American Society of Neuroradiology will terminate their agreement whereby manuscripts on neuroradiology submitted to the *AJR* are forwarded to the *AJNR* and selected *AJNR* papers are republished in the *AJR*.

To avoid any lag in the publication of neuroradiologic articles in the *AJR*, the Journal requests authors to submit neuroradiologic manuscripts effective immediately. We plan to expedite publication of these papers. Authors will receive an initial editorial decision in 3–4 weeks, and accepted papers will be published 3 months after revised manuscripts are accepted. This is more than twice as fast as most other journals.

The advantages of this rapid publication time and the *AJR*'s large circulation (24,000) are now available to all authors of neuroradiologic papers. An expanded section on neuroradiology, including review articles, pictorial essays, and commentaries, will accommodate more than the limited number of papers published under the previous agreement.

We invite authors of neuroradiologic articles to submit their papers for original publication in the *AJR* so that the Journal may continue to fulfill its commitment to supply timely and important original information about neuroradiology to general radiologists as well as to those who subspecialize in the field.

Robert N. Berk
Editor-in-Chief

Commentary

AIDS Risk and Risk Reduction in the Radiology Department

David M. Williams,¹ M. Victoria Marx, and Melvyn Korobkin

Because radiation dermatitis, squamous cell carcinoma, and leukemia developed in some radiology pioneers, radiologists became aware of the notion of occupational diseases. The nearly universal adoption of simple, low-tech precautions—liberal use of lead shielding around the X-ray source, beam path, and operator's body; exposure times as short as feasible; and distance from operator to primary and scatter radiation sources as long as feasible—has nearly eliminated ionizing-radiation-dependent diseases among radiologists. As with other occupational risks in medicine, however, the radiologist's health risk incurred by exposure to ionizing radiation is just one consideration to be integrated into the workup and treatment plan for patients.

The need for a balance between operator's exposure to radiation and diagnostic or therapeutic benefit to the patient is particularly evident during fluoroscopically guided interventional procedures. Indeed, one might argue that beyond a certain point, additional radiation protection to the operator shifts procedure-related risk from the operator to the patient. For example, a thyroid shield clearly protects the fluoroscopist at no risk to the patient. Lead gloves, however, while protecting the physician's hands, diminish tactile feedback and may increase the risk to the patient of subintimal dissection by the catheter or guidewire during angiographic procedures. How does one define the point beyond which additional protection of the physician from ionizing radiation increases the patient's morbidity? A conclusive definition would require a controlled prospective trial of the proposed innovation, with due allowance for the learning curve associated with a change in interventional techniques. No trial, however, will eliminate the need for experienced clinical judgment in the individual

case, where the demands of clinical care occasionally lead the interventionalist uncomfortably close to the X-ray beam and invite scrutiny by the local radiation safety officer.

The preceding article by Wall et al. [1] discusses the AIDS epidemic, another occupational risk that radiology workers must face. Their article is a timely summary of the risks, precautions, and current treatment recommendations regarding exposure to the human immunodeficiency virus (HIV). An analogy can be made between the well-known need to balance the interests of the operator and those of the patient with respect to the operator's radiation protection and the need to balance those interests with respect to potential exposure of the operator to HIV. Obviously, the analogy is not perfect. Chronic exposure to low-energy radiation may or may not be associated with health ill-effects. Seroconversion to HIV-positive status, on the other hand, has a high likelihood of resulting in the development of a uniformly fatal disease. Because of these high stakes, development of habits and techniques designed to minimize operators' risk is mandatory.

As Wall et al. imply, the workers at risk in radiology are primarily interventional radiologists (interventionalists) and those who establish IV access for injection of contrast medium or medications (phlebotomists). The risk of HIV infection to these workers depends on the local prevalence of HIV-positive persons and AIDS patients, the number of accidents per unit time, and the probability of HIV infection per accident [2]. The prevalence of HIV infection varies widely among hospitals. Few reports have been published on phlebotomy and interventional radiology accidents. The quoted risk of infection per needle-stick injury is 0.5% (upper 95% confidence limit, 1.1%) [3]. The risks of infection by mucocuta-

This article is a commentary on the preceding article by Wall et al.

¹ All authors: Department of Radiology (B1-D530), University Hospitals, University of Michigan, 1500 E. Medical Center Dr., Ann Arbor, MI 48109-0030. Address reprint requests to D. M. Williams.

neous contact (with blood-contaminated fluid catapulted by guidewire fling) or by percutaneous contact with blood-contaminated bile, abscess contents, or urine are unknown.

Wall et al. outline techniques used in their radiology departments to minimize operators' exposure to HIV, including the adoption of universal precautions against transmission of infectious diseases, recommendations regarding the handling of sharp instruments, suggestions for modifying the angiography tray and instruments, and recommendations regarding the use of protective clothing. They further imply that other radiology departments should follow their recommendations. We are in agreement with many of the authors' infection-control measures. However, their discussion excludes several important points, most significant of which is that there is more than one approach to the issue. We are pleased to have the opportunity to present another viewpoint and anticipate that much healthy discussion among peers will ensue.

First, the concept of universal precautions merits discussion. Universal precautions are based on the premise that, because the patient's true current HIV status is at best unknown, all blood should be considered toxic and maximal precautions should be used during all contact with patients. The authors imply that adoption of universal precautions against the transmission of infectious diseases is warranted throughout radiology departments. This approach may be warranted in institutions similar to their own, which has a high prevalence of HIV infection. Radiologists should be aware, however, that at hospitals in which the prevalence of HIV infection is low, universal precautions have been criticized as being neither cost-effective nor efficacious [4, 5]. Therefore, precautions appropriate for these authors' institutions may not be necessary or appropriate for all practice settings.

Universal precautions appear appropriate for the phlebotomist, whose duties are simple and routine, whose risks are limited and well known, and whose contact with the patient is relatively brief. Toxic fluid precautions should, like lead aprons, be incorporated into routine radiologic procedures. Incorporation of standard protection measures into procedural routine in this setting, such as the use of latex gloves during venipuncture, is likely to be easy to adapt to, not time-consuming, and relatively inexpensive.

Universal precautions may be unrealistic, however, for the interventionalist, if "universal" is interpreted as meaning that any procedural precaution undertaken for a known AIDS patient should be undertaken for every patient just because the patient's true current HIV status is unknown. For lengthy and/or technically difficult procedures involving risk to the patient, multiple needle passes, multiple guidewire and catheter exchanges, the duty to train residents and fellows, and the possible fatiguing of the operator, it is prudent to tailor the precautions to the level of risk.

For instance, a 65-year-old heterosexual man who denies IV drug use or previous transfusion has lower-extremity angiography because of claudication in the right buttock and calf. The right femoral pulse is absent and that on the left is palpable but weak. The universal precautions adopted by the hypothetical radiology department include the use of a Safe Stick set (Cook, Bloomington, IN) for all arterial punctures. Does the avoidance of a possible splash of blood to the

operator's face outweigh the potential increase in risk of inadvertent needle puncture to the operator's hand caused by the fact that the decreased sensation through the Safe Stick device may increase the number of passes required to access the left femoral artery? In addition, does the possibility of slightly increased operator safety (which is by no means assured) justify use of the device in a patient who is unlikely to be HIV-positive and who is at high risk for guidewire-induced arterial injury?

In a second scenario, an AIDS patient who is not a candidate for anticoagulation comes to a teaching hospital to have a filter placed in the inferior vena cava because of venous thrombosis in the left lower extremity. Would the operator's safety best be served by having a trainee who is well versed in the use of newly adopted departmental universal precautions do the procedure or by having an experienced interventionalist accomplish the task using the techniques with which he/she is most facile and familiar?

The issues regarding operator's safety and patient's care raised by these two hypothetical cases are complex. No simple answer is available, nor is a "universal" answer appropriate for all patients. It is imperative that procedural changes designed to protect the operator from contact with HIV not compromise patients' care.

We agree with the authors' emphasis on the hazards associated with and the need for safe disposal of sharp instruments. We add a point not addressed by Wall et al. Reassembly of a Seldinger-type needle during repeated attempts to cannulate an artery, bile duct, or other cavity is analogous to recapping the needle, a practice that is the single greatest source of occupationally acquired AIDS. This analogy is particularly true in instances where a needle with a hollow stylet is used because inadvertent puncture with a hollow needle is likely to result in a larger inoculum than that resulting from puncture with a solid stylet. Safe needle reassembly requires meticulous attention.

Some of the authors' specific recommendations appear to be influenced by the techniques and equipment particular to their institutions. For example, the authors state that retracting a vascular puncture needle in a single step while wiping the guidewire with gauze is a high-risk maneuver inviting a needle-stick injury. This may be true with certain one-wall puncture needles equipped with a sharp cannula. The cannula of one common Seldinger needle is blunt (INRAD, Grand Rapids, MI), and one-step removal is acceptable. We have mixed opinions on the use of the Safe Stick adapter and closed flush system. As Wall et al. note, the Safe Stick device adds resistance to guidewire movement, which may be difficult to distinguish from subintimal entrapment of the wire tip. In our own angiographic setup (intermittent hand flush of the catheter), the closed flush system requires full attention and two hands to mate the syringe to the flush port. One of us finds this acceptable, but a second considers it an annoying distraction in a complicated interventional case. It should be noted that many procedures may still require an open waste basin to allow flushing a catheter before and after use, wetting gauze wipes for cleaning wires, and so forth. Future design changes may make the Safe Stick and the closed flush systems easier to use.

We think that the face shield is somewhat clumsy and that it is premature to recommend it for routine use. Protection provided to the mucous membranes of the face by a mask and leaded glasses is likely to be adequate. Because no controlled study has favored a particular design of facial protection, the best option is simply unknown. The choice of facial protection should be dictated by the operator's comfort as well as infection-control principles, so that the smooth progress of the case is not hindered by physical discomfort of the operator.

Additional precautions against AIDS exposure, not mentioned in Wall's article, merit discussion. Adoption of new infection-control precautions should involve as little change as possible from what has been one's procedural routine. Administration of local anesthesia near the inguinal crease sometimes requires tensing the skin to achieve an adequate wheal. Sudden flinching by the patient has been known to cause unwary residents to stick themselves. It may be prudent to administer local anesthesia one-handed in order to avoid the danger altogether. An additional precaution in complex cases involving HIV-seropositive patients is for the interventionalist to work with an experienced assistant, to prevent inadvertent breaks in angiographic routine or other surprises that might be encountered when working with a novice. We obviously cannot exercise this precaution universally or else residents and fellows will not be properly trained.

The tone of future discussions of physicians' protection may be affected by two current political developments. The first is the recent congressional bill, passed by the United States Senate with an overwhelming majority, which asks for (among other things) mandatory HIV testing of all health care workers performing invasive procedures. Although the ultimate fate of this bill is, as of yet, unknown, it is certainly possible that it will become law in the near future. The second is a set of rules proposed by the Occupational Safety and Health Administration (OSHA) that enmeshes HIV-prevention measures, including universal precautions, engineering and work-practice controls, and personal protective equipment requirements, in a maze of rigid administrative rules [6, 7]. It is possible that these externally imposed controls will irritate members of the medical community, causing them to become distracted from the central issue: the need to provide optimal medical care as safely as possible.

As the controversy surrounding health care workers and AIDS prevention grows, it will become more important than ever not to let the doctor-patient relationship become hidden or lost behind an elaborate protective garb or siege mentality.

Although patients will have met some member of the interventional team when they consented to the procedure, it is imperative that the entire team, especially the physician primarily responsible for the procedure, become acquainted with the patient before donning boots, gown, mask, and goggles.

In summary, we suggest that a "lead-apron" level of precaution, which recognizes the unknown HIV status in the average patient and treats blood as a toxic fluid, should be incorporated into routine radiologic phlebotomy and interventional practice. Routine precautions should include vigilant attention to sharp instruments during prolonged attempts to establish vascular or other percutaneous access, scrupulous sequestration of sharp instruments after use, and the use of gloves and possibly barrier gown, face mask, and eye protection. A "lead-glove" level of protection should be undertaken in patients who have seropositive HIV status or are known to practice risk behaviors, recognizing that these measures may prolong or increase the complexity and morbidity of the procedure. These extraordinary measures include one-handed administration of local anesthesia, wearing two pairs of gloves or frequent glove changes, and the use of safety devices such as those listed in Table 1 of Wall et al. [1]. The decision whether to adopt routine universal or extraordinary precautions for a particular patient will depend on the clinical history, cost of the precautionary measures, nature of the interventional procedure, and local prevalence of AIDS. It is premature to define a standard of care at this time.

REFERENCES

1. Wall SD, Olcott EW, Gerberding JL. AIDS risk and risk reduction in the radiology department (perspective). *AJR* 1991;157:000-000
2. Leentvaar-Kuijpers A, Dekker MM, Coutinho RA, Dekker EE, Keeman JN, Ansink-Schipper MC. Needlestick injuries, surgeons, and HIV risks (letter). *Lancet* 1990;335:546-547
3. Marcus R, Group C. Health care workers exposed to patients infected with human immunodeficiency virus (HIV). In: *Abstracts of V International Conference on AIDS*. Montreal: V International Conference on AIDS, 1989
4. Becker CE, Cone JE, Gerberding J. Occupational infection with human immunodeficiency virus (HIV): risks and risk reduction. *Ann Intern Med* 1989;110:653-656
5. Stock SR, Gafni A, Bloch RF. Universal precautions to prevent HIV transmission to health care workers: an economic analysis. *Can Med Assoc J* 1990;142:937-946
6. OSHA. Occupational exposure to bloodborne pathogens: proposed rule and notice of hearings (29 CFR 1910). *Federal Register* 1989;54:23042-23139
7. Bachner P. The epidemiology of fear: scientific, social, and political responses to the occupational risk of blood-borne infection. *Arch Pathol Lab Med* 1990;114:319-323

Clarence Dally: An American Pioneer

Raymond A. Gagliardi¹

On December 28, 1895, Wilhelm Conrad Roentgen delivered to the secretary of the Würzburg Physical Medical Society his preliminary report entitled "On A New Kind of Rays" [1]. By early January 1896, the news had spread throughout the world. The first American newspaper articles suggested that it was a new form of light that would be a great boon for photographers [2].

As early as March 14, 1896, the Italian physicist Angelo Battelli called attention to the possible ill effects of roentgen rays on living tissue [3]. He followed this communication later in the same year with a detailed study of deleterious effects of the rays on the human eye [4]. Thomas Edison later observed some annoying symptoms of his own—which he attributed to eye strain—while working on glass-tube forms for X-rays [5], and a Boston dentist, William Rollins, recommended covering fluoroscopic screens with some filtration "to protect the eyes from x-light" [6]. Other concerns were raised largely by engineers and were published in the engineering literature, but these concerns were swept aside by the fervor ("Roentgen mania") of scientists, physicians, photographers, electrotherapists, and charlatans who, in trying to determine only what the new rays could do, ignored almost completely their potential for harm [7]. This brief report recounts the story of the first American to lose his life in the new field. He was Clarence Madison Dally, a researcher associated with Thomas Edison in the attempt to develop practical uses of the X-ray. Edison's laboratories were in some ways the forerunners of modern research and development laboratories. Research has been essential to economic progress, and the emphasis even in Edison's time was not just on good results but on speedy, usable results.

Clarence Dally was born in Woodbridge, NJ, in 1865, and grew up in an America struggling to heal the wounds of the Civil War. After serving in the United States Navy, he obtained employment at the Edison Lamp Works in Harrison, NJ, where he was trained by his father, a master glassblower. Clarence quickly matched his father's skills and became a key participant in the production of glass bulbs for the burgeoning incandescent lamp industry [6].

Edison recognized almost at once in Roentgen's discovery a possible tool for further improvement of the incandescent lamp and called young Dally to assist him in this new research in the main Edison laboratory in East Orange, NJ [5].

Dally personally produced thousands of Crookes tubes during the experiments designed to test a "fluorescent lamp" that might replace the electric light bulb. The principle was simple. The inner walls of the glass envelope were coated with a fluorescing material, and as the Crookes tube was activated, the X-rays produced would collide with the coated wall to produce a fluorescent light that might be brighter and less expensive than the current electric light bulb. Dally personally tested each tube he made by placing his hand directly in the beam. In retrospect, this seems like an extraordinarily stupid practice, but medical pioneers were also setting the appropriate milliamperage for their examinations of patients by placing their ungloved hand in the beam until they could clearly see the bones in their fingers. This was generally done without any adaptation to the dark, so the technique was many times more damaging.

Edison observed that Dally's skin had started to appear burned,

with persistent erythema and ulceration and striking local hair loss, leading the great inventor to abandon this line of investigation. The idea of an X-ray lamp was discarded.

Edison's research into the development of a practical complete X-ray unit was not halted, however. Some early workers did not believe the changes in their skin were caused by the X-ray but rather by an unexplained "electrostatic effect" in the tissue caused by the electric charge activating the Crookes tube. This and other denials of the real cause delayed the eventual recognition and acceptance of the dangerous side of the roentgen ray.

The first major breakthrough in Edison's laboratory was the discovery of calcium tungstate as a fluorescing agent to detect the presence of X-rays. It was superior to the original material, barium platinocyanide, used by Roentgen. Dally continued as a major player in this research, but with loss of his facial hair, eyebrows, and eyelashes and with severe pain and ulceration of the dorsum of his hand. Because Dally was right-handed, his left hand was usually placed in the beam. When his left hand became too extensively damaged, he switched and placed his right hand in the beam. Dally was seen by every prominent dermatologist and surgeon in the East, but this was a new phenomenon, and therapeutic approaches were trial and error.

All conventional burn therapies failed to stop the relentless destruction and malignant metamorphosis of Dally's skin. It soon became apparent that X-ray changes were cumulative, for when Dally was away from the laboratory, no demonstrable regression would occur, but with each new exposure, progression was obvious.

Finally, after ointments had failed and skin grafts would not take, the unfortunate Dally suffered amputation of the left arm at the shoulder and the other arm above the elbow. Death came mercifully to the 39-year-old martyr in 1904.

The roentgen ray had produced giant medical strides by this time, with its first specialty society, the American Roentgen Ray Society, firmly established, producing a respected scientific journal, and setting standards of training that served to establish the specialty as an equal to the older clinical disciplines. But the X-ray had also called its first victim. The death of Clarence Dally was a tragic but important milestone, and radiation protection became an integral part of the radiologist's work.

REFERENCES

1. Glasser O. *William Conrad Roentgen and the early history of the roentgen rays*. Springfield, IL: Thomas, 1934
2. *New York Sun*. 1896 January 6
3. Battelli A. The reaction of roentgen rays upon various human tissues. *Atti Acad Med Fis Fiorent* 1896 March 14
4. Battelli A. The transmission and effect of roentgen-rays upon the eye. *Arch Ital Biol* 1896;25:202
5. Josephson M. *Edison, a biography*. New York: McGraw-Hill, 1959
6. Brown P. *American martyrs to science through the roentgen rays*. Springfield, IL: Thomas, 1936
7. Gagliardi RA. 1987 ARRS meeting—presidential address. *AJR* 1987;149:415–417

¹ Department of Radiology, St. Joseph Mercy Hospital, 900 Woodward Ave., Pontiac, MI 48341.

Review Article

Radiologic Assessment of Impotence: Angiography, Sonography, Cavernosography, and Scintigraphy

Max P. Rosen,¹ Alan N. Schwartz,² Frederic J. Levine,³ and Alan J. Greenfield¹

Recent advances in the understanding of erectile dysfunction have led to new treatments for vasculogenic impotence and a need for improved imaging techniques. Although much controversy still exists in this evolving field, we provide a review of the concepts and techniques currently used in cavernosography, sonography, scintigraphy, and angiography to evaluate the impotent patient.

During the past decade, significant advances have been made in the understanding, evaluation, and treatment of impotence. Impotence may be the result of psychogenic, neurogenic, hormonal, or vasculogenic causes. Recent work by Krysiwicz and Mellinger [1] details an algorithm for the workup of the impotent patient. Once psychogenic, neurogenic, and hormonal factors have been eliminated, the focus of the workup shifts to an investigation of possible vasculogenic factors that may be amenable to arterial or venous reconstructive surgery, angioplasty, or venous embolization.

The evaluation of these vasculogenic factors depends on dynamic infusion cavernosometry and cavernosography (DICC), duplex sonography with pulsed Doppler analysis, and internal pudendal angiography. Scintigraphic studies may provide additional or complementary information.

In this review, we outline the technique of dynamic infusion cavernosometry and cavernosography and review recent advances in sonography, scintigraphy, and angiography for ex-

amining patients suspected of having vasculogenic impotence.

As is often the case in a new field, methods and interpretation of results are controversial. These issues are especially confounding in the field of impotence research because of the subjective nature of an "adequate" erection and the paucity of data from studies of "normal" control subjects. At all times, we have attempted to present a balanced review of the current literature. We hope that future studies will reduce much of the controversy in this evolving field.

Dynamic Infusion Cavernosometry and Cavernosography

Several methods are currently used to diagnose corporal venocclusive dysfunction [2]. Although most authors agree that informative studies require pharmaceuticals injected directly into the corpora cavernosa, significant differences in protocols exist. The approach of Goldstein et al. [3] is described in detail here. This should serve as an outline to understand the normal function of the corporal venocclusive mechanism and as a framework for understanding the various points at which the normal mechanism can malfunction. Alternative methods described by Freidenberg et al. [4] and Bookstein et al. [5, 6] also are reviewed.

DICC evaluates the hemodynamic and hydraulic function of

Received March 5, 1991; accepted after revision April 16, 1991.

¹ Department of Radiology, University Hospital, Boston University Medical Center, 88 E. Newton St., Boston, MA 02118. Address reprint requests to A. Greenfield.

² Pacific Northwest Center for Sexual Health, Department of Radiology, Stevens' Memorial Hospital, Edmonds, WA 98026 and Department of Radiology, University of Washington, Seattle, WA 98108.

³ Division of Urology, Case Western Reserve University and Mt. Sinai Impotence Center, Mt. Sinai Hospital, Cleveland, OH 44122.

AJR 157:923-931, November 1991 0361-803X/91/1575-0923 © American Roentgen Ray Society

the penis. By evaluating arterial inflow, venocclusive function, and the interaction of these two mechanisms, DICC can be used to determine the contribution of each of these components to the erectile process. The patient's susceptibility to pharmacologic manipulation of the erectile process also can be evaluated [3].

Normal erectile function depends on the hemodynamic interaction of cavernosal arterial inflow and perfusion pressure and the development of an adequate degree of venous outflow resistance [7, 8]. Sufficient pressure in the corpora cavernosa must be achieved and maintained for a functional erection to occur. The pressure in the corpora cavernosa during erection is equal to the perfusion pressure in the cavernosal artery minus the pressure loss from corporal venous drainage. Abnormalities of either arterial perfusion, corporal venocclusion, or both may result in erectile dysfunction [9].

Performed after the intracavernosal injection of vasoactive agents, DICC gives a functional diagnostic assessment of corporal venocclusion and of perfusion pressures in the left and right cavernosal arteries during erection. DICC is performed with local anesthesia, and approximately 45–60 min is required to complete the examination. The study is divided into four phases.

Phase 1

Baseline intracorporal pressure and penile circumference are recorded first. Vasoactive medication then is injected into the corpora cavernosa to stimulate corporal smooth-muscle relaxation and to achieve a pharmacologically induced erection. It is important to produce maximal smooth-muscle relaxation. A combination of 45 mg of papaverine hydrochloride and 2.5 mg of phentolamine mesylate currently is used by Goldstein et al. [3] for this purpose.

The corpora cavernosa consist primarily of a trabecular network of lacunar spaces whose walls are composed of smooth muscle and a fibroelastic frame. Smooth muscle also principally composes the walls of the cavernosal artery and its branching helicine arterioles, the resistance vessels that empty into the lacunar spaces [9, 10]. During a sexually induced erection, smooth-muscle relaxation occurs, resulting in (1) a decreased arteriolar resistance, allowing increased arterial flow and transmission of the systemic blood pressure directly to the lacunar spaces, and (2) an expansion of corporal volume, increasing venous outflow resistance. The result is an increase in pressure in the corpora cavernosa and the development of an erection [8, 9]. Phase 1 of DICC attempts to reproduce such an erection pharmacologically.

During phase 1, the rise in pressure in the corpora cavernosa and the change in penile circumference in response to the injected vasoactive medications is monitored for at least 10 min, or until an equilibrium level is reached.

In a normal phase 1 response, the equilibrium pressure in the corpora cavernosa should approach the systemic mean arterial blood pressure within 5–10 min (Fig. 1). Failure to achieve this in the corpora cavernosa is an indication of either

a decrease in the cavernosal artery perfusion pressure or an inability to adequately increase venous outflow resistance.

Patients with arteriogenic impotence and normal venocclusion typically show a slow but steady rise in pressure in the corpora cavernosa, never reaching the mean systemic arterial pressure. Conversely, patients with abnormal corporal venocclusion and normal cavernosal arterial pressures typically show an initial rapid increase in pressure in the corpora cavernosa that reaches an equilibrium early in the study, well below the mean systemic arterial pressure. More commonly, organically impotent patients will have a combination of these two processes.

Phase 2

Provocative tests of corporal venocclusive function are performed in phase 2 to determine the ability of the corpora cavernosa to optimally increase their venous outflow resistance. Corporal venous drainage normally emanates from the network of subtunical venules that lie in the potential space between the periphery of the erectile tissue and the tunica albuginea. As the lacunar spaces become engorged with blood during erection, the subtunical venules are compressed between them and the relatively noncompliant tunica albuginea [9–11]. Venous outflow resistance increases, decreasing corporal venous drainage.

Once the phase 1 equilibrium pressure has been achieved, pressure in the corpora cavernosa is increased, in 30 mm Hg intervals, by infusing heparinized saline (2 U heparin/ml) into the corpora cavernosa. As each preset pressure is reached, the flow of heparinized saline necessary to maintain that pressure is determined. This is continued until a pressure of 150 mm Hg is attained. At this level, the flow of heparinized saline is terminated and the drop in pressure in the corpora cavernosa during a 30-sec period is ascertained. Goldstein et al. [3] advocate repeating phase 2 tests while manual pressure is applied to the perineum, to determine if such perineal compression reduces the maintenance flow rates or the drop in pressure in 30 sec.

In normal phase 2 studies, the flow of heparinized saline necessary to maintain various pressures in the corpora cavernosa will be 3 ml/min or less and the drop in pressure in the corpora cavernosa in 30 sec from a pressure of 150 mm Hg will be less than 45 mm Hg (Fig. 2). Values greater than this indicate the presence of corporal venocclusive dysfunction. Those patients whose phase 2 studies normalize during perineal compression most likely will show only focal, proximal cavernosal/crural venous drainage on later cavernosography.

Phase 3

Systolic occlusion pressures in the left and right cavernosal arteries are measured in phase 3. Heparinized saline is infused into the corpora cavernosa, gradually increasing intracorporal pressure until pulsatile flow (as measured by a Doppler transducer) disappears. Infusion is stopped at this point, and the pressure in the corpora cavernosa is allowed to decrease until pulsatile flow returns. The pressure at which flow returns

Fig. 1.—A normal phase 1 dynamic infusion cavernosometry and cavernosography response to injection of 45 mg of papaverine hydrochloride and 2.5 mg of phentolamine mesylate. In 5.5 min, pressure in corpora cavernosa increases from a baseline level of approximately 10 mm Hg to an equilibrium pressure of 90 mm Hg. This approximates patient's systemic mean arterial pressure of 94 mm Hg.

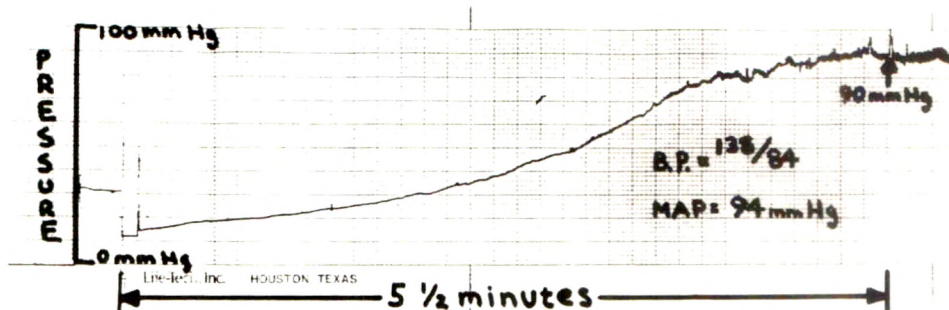
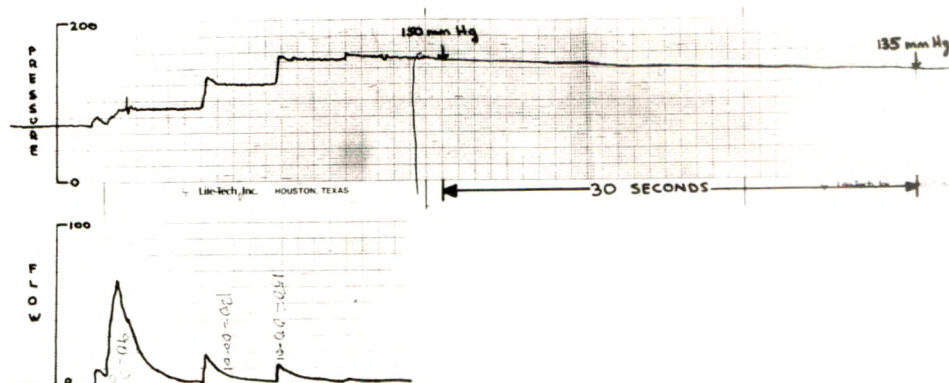


Fig. 2.—A normal phase 2 dynamic infusion cavernosometry and cavernosography examination. Flow of heparinized saline necessary to maintain pressures in corpora cavernosa of 90, 120, and 150 mm Hg are all less than 3 ml/min. Fall in pressure in 30 sec after pressure of 150 mm Hg is achieved is only 15 mm Hg, well within normal range.



is defined as the cavernosal artery systolic occlusion pressure and is the maximal pressure that can be transmitted to the erectile tissue.

Cavernosal artery systolic occlusion pressures are compared with the simultaneous recording of the systolic pressure in the brachial artery. The cavernosal artery systolic occlusion pressure should be approximately the same as the systolic pressure in the brachial artery. A large gradient between the two suggests significant arterial occlusion in the ipsilateral hypogastric-cavernous arterial bed.

Phase 4

Cavernosography is performed as the final stage of DICC to examine the corporal venous drainage system radiographically during erection. This is done by using a dilute ionic contrast agent (Conray 43, iothalamate meglumine, Mallinckrodt, St. Louis, MO), or a nonionic contrast agent (Omnipaque 240, iohexol, Winthrop Pharmaceuticals, New York, NY). Approximately 100–150 ml of contrast material is infused while the pressure in the corpora cavernosa is maintained at 90 mm Hg. Anteroposterior and right and left lateral radiographs of the entire corpora cavernosa are obtained.

The exact anatomy of the venous drainage of the penis is complex, and its description is often controversial. Normally, in the pendulous portion of the penis, the subtunical venules coalesce to form emissary veins that pierce the tunica albuginea to drain ultimately into the deep dorsal vein. Proximally, in each crus, an independent drainage system exists. The cavernosal veins appear to originate at the penile hilum and

empty into the internal pudendal vein [12] and/or the preprostatic plexus [13]. Near the crural tip, crural veins occasionally are seen to enter directly into the internal pudendal vein. Normally, no communication exists between the venous drainage systems of the corpora cavernosa and the venous drainage system of the glans and corpus spongiosum [10, 11, 13]. However, a few communications occasionally may be shown [12].

In a normal phase 4 study (using Goldstein's [3] technique) no venous drainage should be visualized (Fig. 3). The various patterns of abnormal drainage seen during cavernosography can be described as visualization of the dorsal, cavernosal, or crural veins; the glans; or the corpus spongiosum. Further drainage into the preprostatic plexus or the internal pudendal veins also may be seen (Fig. 4).

Conclusion of Study

At the end of DICC, the corpora cavernosa are aspirated to achieve detumescence. In those patients with normal or nearly normal venocclusive function, detumescence may not occur after aspiration alone. Such patients require the intracavernosal administration of phenylephrine, an alpha-adrenergic agent, in divided doses of 200–500 μ g. If detumescence is not achieved after the total administration of 2–3 mg of phenylephrine, the corpora cavernosa should be alternately aspirated and irrigated with a 10 μ g/ml solution of phenylephrine in normal saline until detumescence occurs.

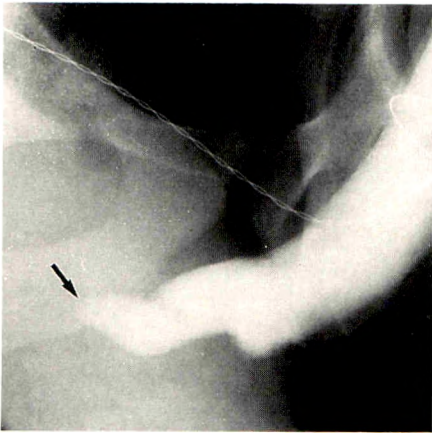


Fig. 3.—A normal cavernosogram with patient in right lateral position. Entire corpora cavernosa are filled with contrast material. A penile strain gauge is seen around the shaft. No contrast material is visualized exiting from the penis (arrow), indicating normal venocclusion. (Although no leakage is shown here, some leakage may be seen normally when a slow injection rate or different cavernosography techniques are used [14]).

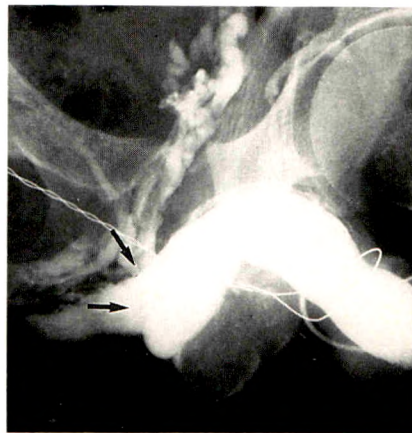


Fig. 4.—An abnormal cavernosogram seen with patient in right lateral position. Corpora cavernosa are filled with contrast material, but abnormal drainage occurs from proximal portion of penis (arrows). Cavernosal and crural veins are opacified and drain into preprostatic plexus.

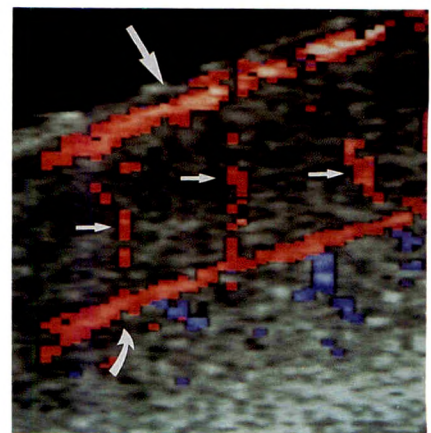


Fig. 5.—Color flow sonogram of corpora cavernosa shows dorsal artery (long straight arrow), cavernosal artery (curved arrow), and helicine branches (small arrows).

Alternative Methods

Several other methods of diagnosing corporal venocclusive dysfunction have been described and recently reviewed by Lewis [2]. Freidenberg et al. [4] calculated a venous outflow resistance measurement based on flow necessary to maintain pressure within the corpora cavernosa 20 mm Hg above mean arterial pressure 20 min after injection of 60 mg of papaverine into the corpora cavernosa. Bookstein et al. [5, 6] have described the pharmacologic maintenance erectile flow method (PMEF), in which volume of leak is expressed in milliliters per minute at systemic systolic pressure.

Penile Sonography

Once the presence or absence of a venous leak has been determined by cavernosometry and cavernosography, assessment of the penile arterial supply is necessary to show diminished penile arterial flow. A method for evaluating the cavernosal arteries that is less invasive than angiography is desirable, and many researchers have investigated the possibility of using duplex Doppler sonography to evaluate the patency of the cavernosal arteries and competency of the penile veins [15] and using gray-scale real-time sonography to assess the corporal architecture [16–18].

Several parameters have been used for quantifying penile blood flow: acceleration, peak flow velocity, arterial dilatation, visible pulsatility of the cavernous artery, increase of penile volume, and resistance index [19]. Although there is still no widely accepted consensus on which of these parameters is most valid, a range of normal and abnormal values is developing in the literature. A summary of this evolving field is provided here.

Peak Systolic Arterial Flow

Gray-scale duplex Doppler penile sonography, as introduced by Lue et al. [20], offered several important advances. As the arteries were imaged, the origin of the Doppler signal could be located and flow velocity measured. The diameter of the cavernosal arteries could be measured as well. Lue et al. also introduced the concept of measuring Doppler signals from the cavernosal artery before and after the intracorporal injection of vasoactive medications, in order to study the cavernosal artery during tumescence. In 1985, Lue et al. [20] reported that patients with normal cavernosal arteries had peak systolic velocities of 30 cm/sec and a poststimulation cavernosal artery diameter of more than 1 mm. In a follow-up study in 1989, this group found that the arterial reaction to vasoactive medications could be reported as normal if good concentric pulsations were present and a mean peak systolic velocity of 34.8 cm/sec and a mean diameter of 0.89 mm were found. Recently, Mueller et al. [21] found a 91% correlation between the results of selective internal iliac angiography and those of gray-scale duplex Doppler sonography. In contrast, however, Rajfer et al. [22] reported that duplex Doppler sonography did not correlate well with angiography.

As sonographic technology evolved, it was recognized that color flow Doppler imaging offered an improved method for visualizing the cavernosal arteries and measuring arterial velocity (Fig. 5). In 1989, Quam et al. [23] and Schwartz et al. [24] found that peak systolic velocities between 25 and 30 cm/sec represented borderline normal arterial function. Quam et al. found that the mean peak systolic velocity in control subjects was 35.6 cm/sec, and Schwartz et al. found that the mean peak systolic velocity in normal subjects during phases 1 or 2 was 32 cm/sec. More recently, in a study of 10 control subjects and 44 dysfunctional patients, it was shown that

when the systolic occlusion pressure was greater than 80 mm Hg, the mean peak systolic velocity was 38 ± 8.4 cm/sec for phase 1 and 2 (Schwartz AN, presented at the annual meeting of the Radiological Society of North America, November 1990). Benson and Vickers [25] described control subjects as having higher mean peak velocity of 47 ± 9 cm/sec; patients with mild to moderate arterial insufficiency had a mean peak systolic velocity of 35 ± 16 cm/sec. Two explanations could account for this variability. First, different sonographic units, transducers, and software packages may yield different systolic velocities. Second, the phase during which peak systolic velocities are measured greatly influences the measurement. Peak systolic velocities measured during the early phases of tumescence (at low intracorporal pressures) most likely are a more accurate reflection of arterial inflow than are velocities measured when the penis is more rigid [19].

Diastolic Arterial Flow

In contrast to peak systolic flow, both Quam et al. [23] and Schwartz et al. [24] found that diastolic cavernosal artery velocities were most useful in evaluating the mechanism of venous sinusoidal occlusion when measurements were obtained during maximal tumescence. Quam et al. reported that a diastolic velocity of 5 cm/sec or greater defined significant venous sinusoidal leakage. Schwartz et al. described a characteristic progression of spectral waveform patterns that corresponds to increasing intracorporal pressure [24]. Men who could generate an intracorporal pressure of 60 mm Hg or more had a diastolic velocity of 0 cm/sec. Men with an intracorporal pressure of 63–83 mm Hg (mean, 75 mm Hg) generated diastolic velocities that were negative. This corresponds well with clinical observations in which men with intracorporal pressures of approximately 60 mm Hg have borderline functional erections [4], whereas men with intracorporal pressures of 75 mm Hg have normal erections adequate for intercourse [26].

Systolic Occlusion Pressure

The integrity of the cavernosal artery can be analyzed by measuring systolic occlusion pressure. Systolic occlusion pressure is the intracorporal pressure required to reduce systolic flow in the cavernosal artery to approximately zero. Systolic occlusion pressures are measured after intracorporal injection of vasoactive medications and during intracorporal infusion of saline.

In 1990, Schwartz et al. [27] studied patients with abnormal cavernosal arteries and found a correlation between systolic occlusion pressures and peak systolic velocity. Patients with normal cavernosal arteries (systolic occlusion pressures of 80 mm Hg or greater) had a mean peak systolic velocity of 38 ± 8.4 cm/sec, whereas patients with abnormal cavernosal arteries (systolic occlusion pressures <50 mm Hg) had a mean peak systolic velocity of 10 ± 6.1 cm/sec. (Note: Systolic occlusion pressures cannot be obtained in some subjects who have severe venous sinusoidal leakage).

Penile Veins

King et al. (presented at the annual meeting of the Radiological Society of North America, November 1989) and Vickers et al. [28] examined the penile veins directly by using duplex Doppler color flow sonography and found variable and non-specific flow rates within the deep dorsal vein. Patients with normal erections occasionally had high flow rates within the deep dorsal vein. Patients with significant venous leakage occasionally had no significant flow within the deep dorsal vein. In patients with normal erections, this may reflect the presence of incomplete closure and an equilibrium state between inflow and outflow during full tumescence. In patients with significant venous leakage, as shown by cavernosometry and cavernosography, the absence of flow in the deep dorsal vein may represent the leakage of blood into sites other than the deep dorsal vein. Further investigation is necessary to document the correlation between these two techniques.

Summary

Doppler sonography, particularly duplex Doppler color flow sonography performed before and after the injection of intracorporal vasoactive medications, is useful in quantifying and understanding physiologic events during both abnormal and normal erections. The use of peak systolic and diastolic velocities and waveform analysis, especially in combination with systolic occlusion pressure, appears to be a valid approximation of data obtained by invasive measures.

Scintigraphy

Penile Arterial Inflow and Corporal Volume

The first attempts to image and quantify the vascular events occurring during erection by using radionuclides were performed by Shirai and Nakamura in 1970 [29]. In 1976, Shirai, Nakamura, and their colleagues [30] developed the method further to quantify the change in penile blood volume during erection by using ^{99m}Tc -labeled autologous RBCs.

As overlap between the response of patients with full erections and patients with incomplete erections was significant, Fanous et al. [31] developed a more precise and reproducible method for quantifying tumescence.

By synthesizing the results of many of the prior studies, Schwartz et al. [32] developed radionuclide penile plethysmography, a noninvasive technique to quantify blood flow in the corpora cavernosa during early penile tumescence by using ^{99m}Tc -labeled RBCs (Fig. 6). Peak corporal flow rates correlated well with angiography ($r = .91$). Patients with normal arteries had a mean peak corporal flow rate of 14.7 ± 4.4 ml/min, whereas patients with severe arterial disease had a mean peak corporal flow of 4.8 ± 1.5 ml/min during early tumescence.

Xenon Washout: Venous Assessment

In addition to measuring accumulation of radionuclide within the penis, attempts have been made to measure the washout

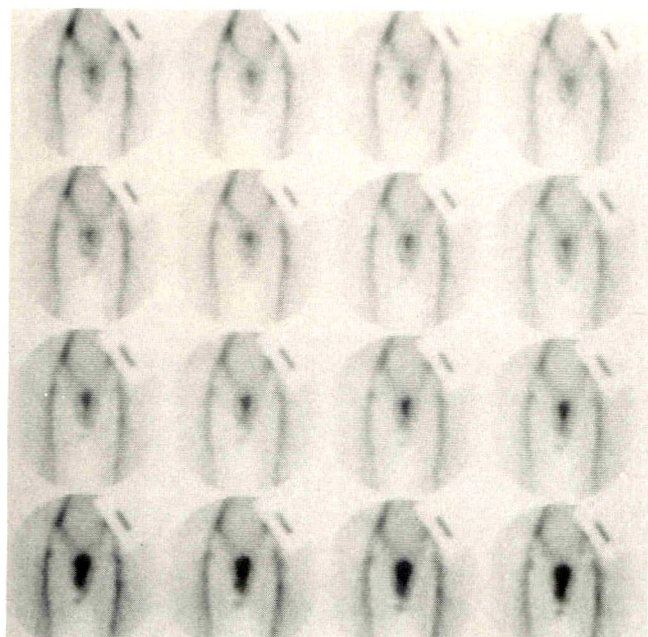


Fig. 6.— ^{99m}Tc -labeled RBC scintigrams in a patient with excellent arterial inflow and moderate venous leakage. Top row shows equilibrium and infusion of papaverine. Bottom three rows show penile blood flow 1, 2, and 3 min after intracorporeal papaverine infusion. Each row represents 1 min. (Reproduced with permission from Schwartz et al. [32].)

of radionuclides from the corpora cavernosa by using xenon-133.

In 1983 Metz et al. [33] measured xenon washout during penile erection and found that it was reduced or unchanged in patients who had normal erections, but was considerably increased in subjects with an insufficient venous sinusoidal occlusion mechanism.

Haden et al. [34] in 1989 used ^{133}Xe in saline injected directly into the corpora cavernosa to evaluate blood flow in the flaccid penis. No difference in xenon washout was detected between impotent patients and normal subjects, suggesting that measurements made when the penis is flaccid are not helpful in the evaluation of erectile failure.

In 1989 and 1990, both Miraldi et al. (presented at the 36th annual meeting of the Society of Nuclear Medicine, June 1990) and Schwartz and colleagues [35] presented techniques by which penile inflow and outflow could be measured simultaneously. Inflow was measured by using ^{99m}Tc -labeled RBCs, outflow was assessed with either ^{133}Xe or ^{127}Xe in saline injected intracorporally.

The rate of blood flow out of the penis during early tumescence depends on many variables. In order to evaluate the outflow mechanism, adequate arterial inflow and/or corporal relaxation and closure must be achieved. If these conditions are met, then xenon outflow rates may be useful in assessing the competence of the corporal venous sinusoidal occlusion mechanism.

Summary

Currently, scintigraphic studies can be used to measure both penile arterial inflow and outflow rates and provide a

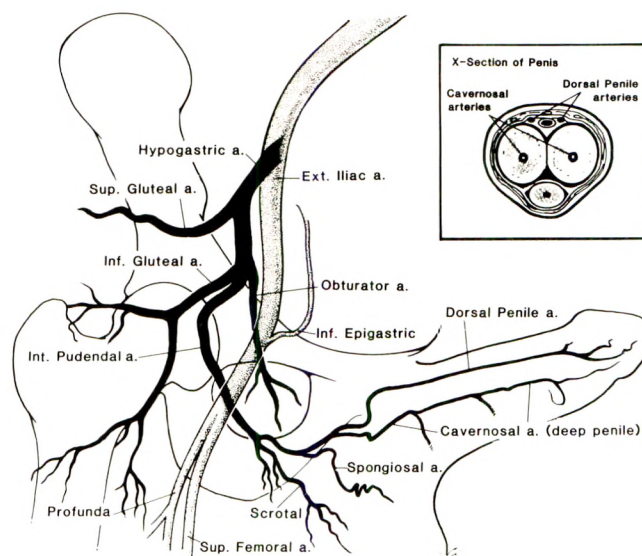


Fig. 7.—Schematic diagram shows normal penile arterial supply. (Reproduced with permission from Rosen et al. [36].)

convenient physiologic approach to quantify the events occurring during erections. The arterial inflow rates correlate well with estimates of normal and abnormal penile blood flow during erection.

Venous outflow also can be measured by using xenon washout studies. As venous outflow depends on many variables, the full usefulness of this technique remains to be determined. Prospective clinical trials are needed to fully assess the potential of scintigraphy in the evaluation of erectile dysfunction.

Internal Pudendal Angiography

The purpose of internal pudendal angiography is to provide precise localization of penile arterial lesions in patients who are selected as candidates for penile artery reconstruction on the basis of cavernosometric evaluation of penile hemodynamics. Internal pudendal angiography also may be useful in assessing arterial inflow in patients who have only marginally abnormal hemodynamics or who have large venous leaks.

The efficacy of such studies requires excellent visualization of the small arteries that constitute the penile blood supply. In order to achieve this objective, penile arterial inflow must be maximized. This requires pharmacologic induction of an erection. Care must be taken to avoid increasing intracorporal pressure to a point that arterial flow is terminated. Corporal venous outflow, autonomic sympathetic tone, and the patient's discomfort must be minimized as well.

Anatomy

Figure 7 shows the classic anatomy of the penile vascular supply. The anterior division of the internal iliac (hypogastric) artery supplies the internal pudendal artery. After giving off muscular, inferior rectal, and scrotal branches, the internal

pudendal artery continues as the common penile artery. The common penile artery gives off urethral and bulbar branches and terminates as the dorsal artery of the penis and the cavernosal (deep penile) artery [36].

The origin of the internal pudendal artery varies. The artery may arise independently from the main hypogastric trunk, as a branch of the anterior division of the hypogastric trunk (classic anatomy), or from the inferior gluteal artery [37]. An accessory internal pudendal artery has been reported in 7% [37] to 21% [38] of cases.

In a detailed review of penile anatomy, Bookstein and Lang [39] documented the great variability of the intrapenile arteries. Normal variations that easily could be confused with arterial obstruction were (1) unilateral origin of all cavernosal branches, (2) unilateral hypoplasia of a dorsal penile artery, and (3) aberrant origin of bulbar or cavernosal arteries.

Multiple collateral routes of flow within the penis have been documented; these may assume functional importance in patients with intrapenile obstructing arterial lesions. These routes include (1) cavernosal artery to cavernosal artery via transverse communicating branches at the penile root, (2) dorsal artery to cavernosal artery or cavernosal artery to dorsal artery via perforating branches, (3) cavernosal artery to ipsilateral cavernosal artery via bridging cavernosal branches, and (4) external pudendal artery to dorsal penile artery. A complete understanding of these anatomic variations and collateral pathways is essential for differentiating between true obstructing lesions and "nonvisualization" of an artery due to collateral flow or anatomic variation [39].

Pharmacangiography

In order to achieve optimal visualization of the intrapenile arteries, venous outflow should be minimized and arterial inflow maximized [40]. Intracorporal papaverine (30–60 mg), a smooth-muscle relaxant, now is administered routinely to induce an erection [41] either at the start of the angiographic procedure [36] or just before the injection of contrast material [42]. (Although some authors have advocated placing a tourniquet at the base of the penis to prevent escape of papaverine into the systemic circulation [43], this step was not used in most other studies.) As the sinusoidal muscles of the

corpora cavernosa relax, and the penis becomes rigid, arterial inflow will be reduced and may result in apparent "underfilling" of the cavernosal arteries during angiography.

In order to ensure maximal filling of the cavernosal arteries during the filming sequence, intraarterial vasodilators now are used routinely just before the injection of contrast material. Bookstein and Lang [39] had recommended 150–200 μ g of nitroglycerine mixed with 30 mg of papaverine but now prefer 60 mg of intracavernosal papaverine mixed with 1 mg phen-tolamine (personal communication). Rosen et al. [36] have used tolazoline (25 mg) diluted in 5 ml of isotonic saline.

Selective Catheterization

Earlier studies of penile arteries were performed via non-selective injection. Gray et al. [38] recommended injection of the internal iliac artery and warned that "the internal pudendal artery should not be selectively catheterized as an accessory pudendal artery supplying the penile vessels may originate separately from the iliac trunk." Schwartz et al. [42] also have advocated a nonselective technique in the past.

Although nonselective injections may be technically easier, especially in older patients, many authors think that selective injection of the internal pudendal artery maximizes detailed visualization of the intrapenile arteries and permits selective injection of intraarterial vasodilators [36, 41]. The use of the Waltman loop technique [44] with a Cobra catheter allows easy catheterization of both internal pudendal arteries from a single femoral artery puncture [36]. An ultralong reverse-curved catheter also has been advocated [45]; its use achieves the same effect.

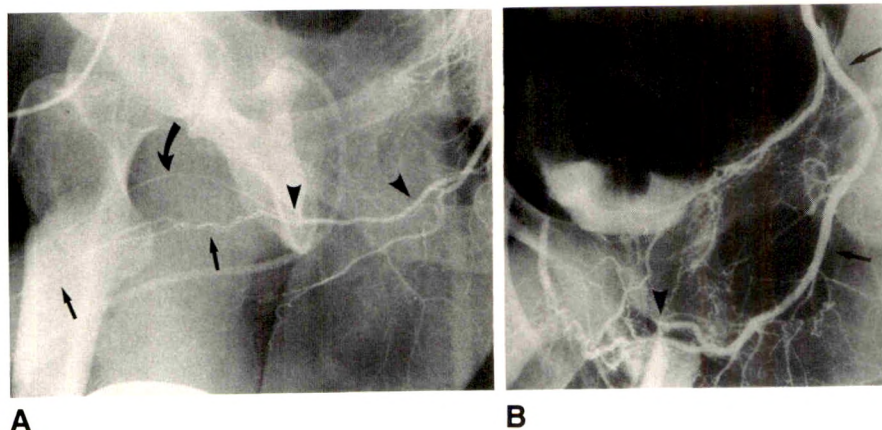
If the internal pudendal artery cannot be catheterized selectively by using these techniques, or if an accessory pudendal artery is suspected, a less selective injection can be performed.

Sedation

Early investigators in the field of pudendal angiography relied on general or epidural anesthesia [38] to reduce sympathetic tone and increase the patient's comfort. However, with the advent of low-osmolality contrast agents and selective internal pudendal pharmacangiographic technique, most

Fig. 8.—A, Magnified selective angiogram of left internal pudendal artery in a patient with normal penile arteries. Common penile artery (arrowheads) bifurcates into dorsal artery (curved arrow), and the cavernosal artery (straight arrows). Both cavernosal arteries are filled from this unilateral injection. Also note small helicine branches of cavernosal arteries best visualized between two straight arrows.

B, Selective angiogram of left internal pudendal artery in a patient who suffered pelvic trauma. Internal pudendal artery (arrows) is normal. Common penile artery is abruptly occluded at level of pubic ramus (arrowhead). This is a common site for arterial occlusion after pelvic trauma. (Reproduced with permission from Rosen et al. [37].)



authors today [36, 41, 46] find such measures unnecessary. Typically, internal pudendal angiography is performed by using only local anesthesia at the site of catheter insertion and mild sedation (commonly morphine and diazepam).

Distribution of Disease

The distribution of arterial lesions in the hypogastric-cavernous arterial bed depends strongly on the criteria used to select patients considered for pudendal angiography. The patient's age, history of perineal or pelvic trauma, and arterial risk factors (diabetes, hypertension, hypercholesterolemia, and cigarette smoking) are all important considerations [37, 47-49]. For example, Gray et al. [38] documented arterial lesions in the iliac or internal pudendal arteries of 44% of patients studied whose average age was 50.5 years. Schwartz et al. [42] showed disease at the base of the penis in 58% of patients and in the internal pudendal artery in 31% of patients whose average age was 55 years. In contrast to these two studies, Rosen et al. [37] found a different distribution of disease in a younger group of patients whose average age was 35.4 years. In this study, no patients had disease in the hypogastric arteries. The internal pudendal and common penile arteries had hemodynamically significant lesions in 9% and 29%, respectively. Disease was concentrated in the cavernosal arteries, which showed hemodynamically significant lesions in 62% of patients. Clearly, selection of patients will determine the angiographic findings (Fig. 8).

Conclusions

Vasculogenic impotence can be caused by a variety of factors. Evaluation of patients with suspected vasculogenic impotence should begin with assessment of the corporal venoocclusive mechanism and measurement of the perfusion pressures of the cavernosal arteries during erection. Angiography is necessary to assess the anatomy, patency, and distribution of arterial lesions in patients who are candidates for penile vascular reconstruction. Recent advances in sonography allow accurate assessment of the patency of the cavernosal arteries as well. Although several techniques have been developed to evaluate erectile function with scintigraphy, these methods do not play a major role in evaluating the impotent patient.

REFERENCES

- Krysiewicz S, Mellinger BC. The role of imaging in the diagnostic evaluation of impotence. *AJR* 1989;153:1133-1139
- Lewis RW. Diagnosis and management of corporal venoocclusive dysfunction. *Semin Urol* 1990;8:113-123
- Goldstein I, Krane RJ, Greenfield AJ, Padma-Nathan H. Vascular diseases of the penis: impotence and priapism. In: Pollack HM, ed. *Clinical urography*. Philadelphia: Saunders, 1989:2231-2252
- Freidenberg DH, Berger RE, Chew DE, Ireton R, Ansell JS, Schwartz AN. Quantitation of corporal venous outflow resistance in man by corporal pressure flow evaluation. *J Urol* 1987;138:533-538
- Bookstein JJ. Cavernosal venoocclusive insufficiency in male impotence: evaluation of degree and location. *Radiology* 1987;164:175-178
- Bookstein JJ, Fellmeth B, Moreland S, et al. Pharmacangiographic assessment of the corpora cavernosa. *Cardiovasc Intervent Radiol* 1988;11:218-224
- Saenz de Tejada I, Goldstein I, Blanco R, et al. Smooth muscle of the corpora cavernosa: role in penile erection. *Surg Forum* 1985;36:623-624
- Lue TF, Tanagho EA. Physiology of erection and pharmacological management of impotence. *J Urol* 1987;137:829-836
- Krane RJ, Goldstein I, Saenz de Tejada I. Impotence. *N Engl J Med* 1989;321:1648-1659
- Lue TF, Tanagho EA. Functional anatomy and mechanism of penile erection. In: Tanagho EA, Lue TF, McClure RD, eds. *Contemporary management of impotence and infertility*. Baltimore: Williams & Wilkins, 1988:39-50
- Levine FJ, Goldstein I. Vascular reconstructive surgery in the management of erectile dysfunction. *Int J Impotence Res* 1990;2:59-78
- Bookstein JJ, Lurie AL. Selective penile venography: anatomical and hemodynamic observations. *J Urol* 1988;140:55-60
- Puech-Leao P, Chao S. Venous drainage of the crura: an anatomic study. *Int J Impotence Res* 1990;2:105-110
- Bookstein JJ, Fellmeth B, Moreland S, et al. Pharmacangiographic assessment of the corpora cavernosa. *Cardiovasc Intervent Radiol* 1988;11:218-224
- Lue T, Hricak H, Marich K, Tanagho E. Vasculogenic impotence evaluated by high resolution ultrasonography and pulsed Doppler spectrum analysis. *Radiology* 1985;155:777-781
- Altofer L, Jordan G. Sonographic demonstration of Peyronie plaques. *Urology* 1981;3:292-295
- Balconi G, Angeli E, Nessi R, deFraviis L. Ultrasonographic evaluation of Peyronie's disease. *Urol Radiol* 1988;10:85-88
- Yamashita T, Ogawa A. Ultrasound in penile cancer. *Urol Radiol* 1989;11:174-177
- Meuleman EJH, Bemelmans BLH, van Asten WNJC, Doesburg WH, Skotnicki SH, Debruyne FMJ. The value of combined papaverine testing and duplex scanning in men with erectile dysfunction. *Int J Impotence Res* 1990;2:87-98
- Lue T, Hricak H, Marich K, Tanagho E. Evaluation of arteriogenic impotence with intracorporal injection of papaverine and the duplex ultrasound scanner. *Semin Urol* 1985;3:21-26
- Mueller SC, Wallenberg-Pachaly H, Voges GV, Schild HH. Comparison of selective internal iliac pharmacangiography, penile brachial index, and duplex sonography with pulsed Doppler analysis for the evaluation of vasculogenic (arteriogenic) impotence. *J Urol* 1990;143:928-932
- Rajfer J, Canan V, Dorey FJ, Mehlinger M. Correlation between penile angiography and duplex scanning of the cavernous arteries in impotent men. *J Urol* 1990;143:1128-1130
- Quam J, King B, James E, et al. Duplex and color Doppler sonographic evaluation of vasculogenic impotence. *AJR* 1989;153:1141-1147
- Schwartz A, Wang K, Mack L, et al. Evaluation of normal erectile function with color flow Doppler sonography. *AJR* 1989;153:1155-1160
- Benson C, Vickers M. Sexual impotence caused by vascular disease: diagnosis with duplex sonography. *AJR* 1989;153:1149-1153
- Lue T, Mueller S, Jow Y, Hwang T. Functional evaluation of penile arteries with duplex ultrasound in vasodilator induced erection. *Adv Urol Ultrasound* 1989;16:799-807
- Schwartz A, Lowe M, Ireton R, Berger R, Richardson M, Graney D. A comparison of penile brachial index and angiography: evaluation of corpora cavernosa arterial inflow. *J Urol* 1990;143:510-513
- Vickers MA, Benson CB, Richie JP. High resolution ultrasonography and pulsed wave Doppler for the detection of corporovenous incompetence in erectile dysfunction. *J Urol* 1990;143:1125-1127
- Shirai M, Nakamura M. Differential diagnosis of organic and functional impotence by the use of I-131 human serum albumin. *Tohoku J Exp Med* 1970;101:317-324
- Shirai M, Nakamura M, Ishii N, Mitsukawa S, Sawai Y. Determination of intrapenile blood volume using Tc 99m labeled autologous red blood cells. *Tohoku J Exp Med* 1976;120:377-383
- Fanous H, Jevtich M, Chen D, Edson M. Radioisotope penogram in diagnosis of vasculogenic impotence. *Urology* 1982;20:499-502
- Schwartz AN, Graham M, Ferency GF, Miura RS. Radioisotope penile plethysmography: a technique for evaluating corpora cavernosa blood flow during early tumescence. *J Nucl Med* 1989;30:466-473
- Metz P, Ebbehøj J, Uhrenholdt A, Wagner G. Peyronie's disease and

- erectile failure. *J Urol* **1983**;130:1103-1104
34. Haden H, Katz P, Mulligan T, Zasler N. Penile blood flow by xenon-133 washout. *J Nucl Med* **1989**;30:1032-1035
35. Schwartz AN, Graham MM. Combined technitium radioisotope penile plethysmography and xenon washout: a technique for evaluating corpora cavernosal inflow and outflow during early tumescence. *J Nucl Med* **1991**;32:404-410
36. Rosen MP, Walker TG, Greenfield AJ. Arteriography and radiology of impotence. *Urol Radiol* **1988**;10:136-143
37. Rosen MP, Greenfield AJ, Walker TG, et al. Arteriogenic impotence: findings in 195 impotent men examined with selective internal pudendal angiography. *Radiology* **1990**;174:1043-1048
38. Gray RR, Keresteci AG, St Louis EL, et al. Investigation of impotence by internal pudendal angiography: experience with 73 cases. *Radiology* **1982**;144:773-780
39. Bookstein JJ, Lang EV. Penile magnification pharminoarteriography: details of intrapenile arterial anatomy. *AJR* **1987**;148:883-888
40. Bookstein JJ. Penile angiography: the last angiographic frontier. *AJR* **1988**;150:47-54
41. Bookstein JJ, Valji K, Parsons L, Kessler W. Pharminoarteriography in the evaluation of impotence. *J Urol* **1987**;137:333-337
42. Schwartz AN, Freidenberg D, Harley JD. Nonselective angiography after intracorporal papaverine injection: an alternative technique for evaluating penile arterial integrity. *Radiology* **1988**;167:249-253
43. Delcour C, Vandenbosch G, Wespes E, Delatte P, Struyven J. Pudendal angiography. *Acta Urol Belg* **1988**;56:308-314
44. Waltman AC, Courey WR, Athanasoulis C, Baum S. Technique for left gastric artery catheterization. *Radiology* **1973**;109:732-734
45. Fellmeth B, Bookstein JJ, Lurie A. Ultralong, reverse-curve angiographic catheter. *Radiology* **1989**;172:872-873
46. St Louis EL, Gray RR, Grossman H. Simplified technique of internal pudendal angiography in the investigation of impotence. *Cardiovasc Intervent Radiol* **1986**;9:22-24
47. Levine FJ, Greenfield AJ, Goldstein I. Arteriographically determined occlusive disease within the hypogastric-cavernous bed in impotent patients following blunt perineal and pelvic trauma. *J Urol* **1990**;144:1147-1153
48. Forsberg L, Henderstrom E, Olsson AM. Severe arterial insufficiency confirmed with an improved angiographic technique: the impact of smoking and some other etiologic factors. *Eur Urol* **1989**;16:357-360
49. Rosen MP, Greenfield AJ, Walker TG, et al. Cigarette smoking: an independent risk factor for atherosclerosis in the hypogastric-cavernous arterial bed of men with arteriogenic impotence. *J Urol* **1991**;145:759-763

The reader's attention is directed to the commentary on this article, which appears on the following pages.

P 24, 466

The Arteriolar Component in Impotence: A Possible Paradigm Shift

Joseph J. Bookstein¹ and Karim Valji

Paradigm: the constellation of perspectives, constructs, and biases through which information is perceived and communicated between individuals in a field.

Derived from Thomas Kuhn [1].

The preceding article by Rosen et al. [2] presents an admirable and comprehensive review of the current opinions of major investigators in the field of erectile dysfunction. It considers much of the rationale for radiologic investigation of impotence and provides a foundation on which to base understanding of controversy and assimilation of further advances. We too have at one time or another subscribed to most of the concepts expressed. And yet, we must voice caution in fully accepting the validity of and justification for portions of the diagnostic workup. As Rosen et al. have pointed out, the subject is controversial. We feel obligated to take this opportunity to participate in the controversy, to articulate several alternative opinions, lest the reader express unwarranted optimism to patients regarding the therapeutic significance of proposed diagnostic investigations.

The article by Rosen et al. [2] reviews a paradigm that was developed during the past decade, based on discovery of the erectogenic effects of several smooth-muscle relaxants, as well as developments in arteriography and cavernosometry. Reduced to its most basic elements, the paradigm is as follows. Impotence is frequently caused by excessive cavernosal venous leak or arterial obstruction central to the mid-cavernosal arteries, usually near the root of the penis. Identifi-

cation of cavernosal venous leakage or arterial insufficiency by morphologic and/or physiologic methods will enable specific diagnosis of venogenic or arteriogenic impotence. Specific diagnosis will in turn often lead to rational and specific corrective vascular surgery or transluminal therapy.

But the paradigm itself is proving to be impotent: specific diagnosis does not usually lead to specific and effective therapy. Considering the huge reservoir of potential patients and the concerted efforts of urologists and interventional radiologists, where is the profusion of favorable reports after revascularization or venoablation? Where is the arteriographic documentation of long-term patency after arterial bypass? Such articles are conspicuous by their absence, and only in the treatment of young men with posttraumatic impotence does specific vascular therapy seem reasonably promising. Although almost 60% of our patients report cure or improvement after transcatheter venoablation, we have been unable to define reliable predictive indexes of success and have difficulty demonstrating objective evidence of improvement.

Currently favored treatments for impotence, such as vacuum devices, intracavernosal injection of smooth-muscle relaxants, and penile prostheses, are nonspecific and generally are applied regardless of the cause diagnosed. Although the diagnostic methods described by Rosen et al. [2] appear to be reasonable, the gold standard against which they should be objectively assessed, namely, results of specific therapy, simply does not exist. Thus the validity of the diagnostic methods in determining the cause of impotence cannot be evaluated at present. We are left to evaluate the correlation

This article is a commentary on the preceding article by Rosen et al.

¹ Both authors: Department of Radiology, University of California, San Diego, Medical Center, 225 Dickinson St., San Diego, CA 92103. Address reprint requests to J. J. Bookstein.

between diagnostic tests, that is, internal correlations, as for example between duplex sonography and arteriography. Even relative to this reduced standard of accuracy, major concerns remain.

Perhaps the unimpressive results of therapy can be attributed to inadequacies of the therapeutic techniques themselves. Long-term patency of a penile arterial bypass is rare in our experience; venous collaterals can develop promptly after venoablation. If these deficiencies could be overcome, perhaps therapeutic results would greatly improve and current diagnostic methods might assume greater clinical relevance.

But perhaps not. The possibility of an error of basic concepts—that is, an error in the paradigm—must be considered. Perhaps the arterial obstructions observed angiographically or the excessive venous leak defined manometrically are often incidental or secondary, rather than causative. Histologic and now clinical angiographic and physiologic evidence suggests that the critical disease may be at the arteriolar level. Dysfunction of the cavernosal endothelium also is suspected, with associated decreased production of endothelium-derived relaxation factor [3]. Arteriolar, endothelial, and other possible dysfunctional elements were not a part of the 1980s paradigm and are not ordinarily considered part of the radiologic assessment of impotence. The information is available, however, perhaps in occult form, and could be revealed by methodologic improvements, particularly in penile vascular catheterization [4, 5].

Let us further consider the possibility of an arteriolar component of erectile dysfunction. Such a component has long been suspected on the basis of histologic studies [6–8], but has lost favor recently in view of irrefutable arteriographic evidence of more central arterial obstructions. For several years, we have quantified the amplitude of pressure pulsations that are regularly observed during cavernosometry [5]. If one presumes that proper precautions are observed to avoid pitfalls (e.g., proper needle position, elimination of air bubbles, prevention of penile swing), our clinical and laboratory experience suggests that these pulsations reflect the degree of arterial patency from the aorta to the cavernosal lacunae. By this postulate, pulse amplitude also can serve as an index of arteriolar patency, particularly when the central arteries are widely patent. Our belief in an arteriolar component was reinforced when we noted a rather consistent diminution in the amplitude of cavernosal pressure pulsations in impotent patients, regardless of central arterial patency.

Diagnostic penile vascular catheterization at our institution regularly includes arteriography and cavernosometry, which allow correlation between arteriography and maximal amplitude of cavernosal pressure pulsations (MACPP). With our cavernosometric system (intracavernosal injection of 60 mg papaverine mixed with 1 mg phentolamine, 21-gauge needles, polyvinyl connecting tubes, non-degassed saline, and Hewlett-Packard transducer), the normal MACPP was 4.6 ± 0.8 mm Hg ($n = 9$), and the maximum almost always occurred at about 85 mm Hg intracavernosal pressure (Bookstein JJ et al., presented at the annual meeting of the Society of Cardiovascular and Interventional Radiology, February 1991). As expected, MACPP was reduced in patients with central arterial obstruction, to 2.5 ± 1.5 mm Hg ($n = 27$, $p < .03$).

Significantly, patients with venoocclusive dysfunction and patent central arteries had equally depressed MACPP. Furthermore, 11 patients had reduced MACPP (1.3 ± 1.6 mm Hg) despite normal findings on pudendal and cavernosal arteriography and normal venoocclusive function. These patients were noted to have inconspicuous helicine branches on magnification arteriography. Theoretically, this combination of observations (i.e., decreased MACPP, normal arteries through the level of the cavernosal arteries, and inconspicuous helicine branches) would be anticipated in the presence of arteriolar constriction or obstruction. The MACPP data suggest that excessive arteriolar resistance is a common underlying condition in erectile dysfunction. The presence of undiagnosed organic or functional arteriolar obstruction in impotence would be a plausible explanation for the frequent failure of specific arterial or venous therapy.

Few serious histologic studies of the cavernosal vascular bed in erectile dysfunction have been reported. Ebner [6] and Conti et al. [7] showed longitudinal pads (or polsters) within the intima of the helicine arterioles that were presumed to play a role in determining arterial flow. The nature and function of polsters, however, remain highly controversial. Benson [9], for example, reported that polsters were found infrequently in corpora from young subjects and concluded that polsters indicated arterial branch points or various stages of arteriosclerosis. On the other hand, Fugleholm et al. [10] observed cushions in the helicine arterioles of both monkeys and rats, with no signs to suggest that they were caused by atherosclerosis. Regardless of the nature of these structures, they may significantly obstruct the lumens of helicine arterioles (e.g., Fig. 5 in Conti et al. [7]) and could explain our evidence of frequent partial arteriolar obstruction. In a histologic study of 30 men, Ruzbarsky and Michal [8] found a direct correlation between age or diabetes and the degree of arteriolar compromise by Ebner pads; the data required to correlate histologic changes and erectile function were lacking. Histologic changes were primarily fibrous substitution and proliferation of the pad musculature. Late changes included microthromboses and occlusion of arteriolar lumens.

Assuming MACCP may partially reflect arteriolar patency, we have abundant clinical and laboratory evidence of functional variability of arteriolar caliber. For example, cavernosal pulsations are almost never observed unless an intracavernosal relaxant has been injected, and the pulsations vary with the dose and agent used and the time elapsed since injection. The MACCP also diminishes with exposure to cigarette smoke. Thus, high arteriolar resistance may be functional as well as organic in origin.

In summary, although our data cast limited light on the existence and function of pads and polsters, they do provide independent physiologic and angiographic confirmation of the frequency of functional or organic obstruction in the arteriolar vascular bed of impotent patients.

Beyond the major reservations discussed here regarding the accuracy of the impotence paradigm, questions also exist regarding the internal accuracy of the diagnostic methods. At least three publications express reservations regarding the degree of correlation between arteriography and existing sonographic indices of arterial disease [11–13]. We too have

found unimpressive arteriographic-sonographic correlation in diagnosing central arterial disease in an experience encompassing approximately 20 cases to date (Valji K, Bookstein JJ, to be presented at the annual meeting of the Radiological Society of North America, Chicago, December 1991). Although the reason(s) for poor sonographic-angiographic correlation in diagnosis of central arterial disease is not yet clear, arteriolar variables could be one explanation. On the other hand, we believe that combined consideration of sonography, cavernosometry, and arteriography provides means for evaluating both the arteries and the arterioles.

One other point should be made regarding internal correlations, in this instance with respect to the cavernosal occlusion-pressure method presented by Rosen et al. [2]. Although we have not found it useful, the method seems to be at least theoretically valid in detecting arterial obstruction central to the cavernosal arteries. However, isolated cavernosal arterial obstruction is quite common, and in this circumstance the occlusion-pressure method is theoretically flawed. The occlusion pressure is determined under conditions of near-zero flow in the cavernosal artery. But pressure gradients disappear under no-flow conditions. Thus, a stenosis of the cavernosal artery that produced a pressure gradient during a high-flow state might fail to cause a gradient at near-zero flow and could remain undetected by the occlusion-pressure method.

Summary

Despite a decade of rapid development in the field of erectile physiology, results of specific vascular therapy for impotence have not improved dramatically. This failure of specific therapy is of key import in assessing progress in impotence vis à vis mere change. Although failure of major advances in specific therapy may only reflect limitations of the therapeutic methods themselves, such failure also eliminates the major objective standard against which the appropriateness and accuracy of radiologic diagnosis can be assessed. Furthermore, such failure forces us to at least consider the possibility of deficiencies of current concepts regarding the cause of impotence. In other words, the therapeutic deficiencies jeopardize to some degree the currently favored impotence paradigm.

Perhaps venous leakage and arterial insufficiency are sometimes incidental or secondary, rather than causative, in impotence. We and others before us suspect that arteriolar abnormality, sometimes functional, may be a common underlying determinant. We believe that the scope of diagnosis should be expanded to evaluate the helicine arterioles and to consider other possible causes, such as cavernosal endothelial dysfunction, more strongly. We are anticipating a paradigm shift.

REFERENCES

1. Kuhn T. *The structure of scientific revolutions*. Chicago: University of Chicago Press, 1962
2. Rosen MP, Schwartz AN, Levine FJ, Greenfield AJ. Radiologic assessment of impotence: angiography, sonography, cavernosography, and scintigraphy. *AJR* 1991;157:923-931
3. Saenz de Tejada I, Goldstein I, Azadzi K, Krane RJ, Cohen RA. Impaired neurogenic and endothelium-mediated relaxation of penile smooth muscle from diabetic men with impotence. *N Engl J Med* 1989;320:1025-1030
4. Bookstein JJ, Vandeberg J, Machado T. The cavernosal acetylcholine/papaverine response—a practical in vivo method for quantification of endothelium-dependent relaxation: rationale and experimental validation. *Invest Radiol* 1990;25:1168-1174
5. Bookstein JJ, Fellmeth B, Moreland S, Lurie AL. Pharmacangiographic assessment of the corpora cavernosa. *Cardiovasc Intervent Radiol* 1988;11:218-224
6. von Ebner V. Über Klappenartige Vorrichtungen in den Arterien der Schwellkörper. *Anat Anz* 1990;18:79-81
7. Conti G, Virag R, von Niederhausen W. The morphological basis for the polster theory of penile vascular regulation. *Acta Anat* 1988;133:209-212
8. Ruzbarsky V, Michal V. Morphologic changes in the arterial bed of the penis with aging. *Invest Urol* 1977;15:194
9. Benson GS. Polsters: functional structure or atherosclerotic changes? *J Urol* 1981;125:800-803
10. Fugleholm K, Schmalbruch H, Wagner G. The vascular anatomy of the cavernous body of green monkeys. *J Urol* 1989;142:181-188
11. Meuleman EJH, Bemelmans BLH, van Asten WNJC, Doesburg WH, Skotnicki SH, Debruyne FMJ. The value of combined papaverine testing and duplex scanning in men with erectile dysfunction. *Int J Impotence Res* 1990;2:87-96
12. Junemann K-P. Editorial comment on the value of combined papaverine testing and duplex scanning in men with erectile dysfunction. *Int J Impotence Res* 1990; 2:97
13. Rajfer J, Canan V, Dorey FJ, Mehringer M. Correlation between penile angiography and duplex scanning of the cavernous arteries in impotent men. *J Urol* 1990;143:1128-1130

Review Article

Percutaneous Biopsy of Skeletal Lesions

Susan V. Kattapuram¹ and Daniel I. Rosenthal

Percutaneous needle biopsy of lesions affecting the musculoskeletal system should be considered a routine radiologic procedure. Although relatively safe, the procedure requires expertise. An experienced radiologist and the cooperation of a skilled pathologist are essential. Consultation with the orthopedic surgeon is also important, especially when resection of the lesion is contemplated. Recent advances in imaging techniques and the availability of various cutting and trephine needles have made it easier to perform biopsies safely and accurately, even in difficult locations. The procedure obviates surgery in many instances and facilitates appropriate surgical planning in others. This review offers a pragmatic approach to percutaneous needle biopsy of skeletal lesions. It is hoped that more radiologists will be encouraged to undertake these valuable procedures.

Radiologists have become increasingly involved in interventional procedures of all types. Although biopsy of the skeletal system is not a new procedure, advances in imaging technology, particularly the introduction of CT-directed biopsy, have greatly extended the potential of this procedure. Almost no part of the skeleton is inaccessible by a percutaneous route, and, with the assistance of a skilled pathologist and cytologist, accurate diagnoses can be obtained from very small specimens.

Biopsy of the musculoskeletal system is not a single procedure; rather, it consists of several procedures that differ greatly in technique depending on the type of lesion and its location. The choice of needle, potential complications, and probability of a successful outcome all depend on whether the lesion is blastic or lytic; whether it is located within bone,

bone marrow, or soft tissue; the amount of tissue that is likely to be needed by the pathologist; and the proximity of vital organs.

Because of these complexities, close cooperation with the pathologist and orthopedic surgeon is needed. The orthopedic surgeon is important in selecting appropriate cases for needle biopsy, and in the choice of the needle path. The pathologist should be consulted concerning handling of the tissue and the quantity required. In general, larger specimens are needed for primary tumors than for metastatic lesions. In cases in which an adequate specimen is in doubt because of technical difficulties, rapid cytologic evaluation or frozen section diagnosis can be accomplished while the patient is still on the biopsy table. These techniques can help ensure that the procedure is not terminated before an adequate specimen is obtained. Potentially infected materials must be handled with sterile technique and cultured. The pathologist should always be informed of the radiologic differential diagnosis.

In this article, we address some of the questions and difficulties encountered most often in percutaneous biopsies. It is our hope that this discussion will encourage more radiologists to undertake these procedures.

Needles

A large number of needles have been devised for various special applications [1-10]. In general, these can be divided into large- and small-gauge cutting needles, aspiration needles, and trephine needles (Table 1). Aspiration needles

Received December 21, 1990; accepted after revision April 29, 1991.

Presented at the annual meeting of the American Roentgen Ray Society, Washington, DC, May 1990, as an instructional course.

¹ Both authors: Department of Radiology, Massachusetts General Hospital and Harvard Medical School, 15 Parkman St., ACC-515, Boston, MA 02114. Address reprint requests to D. I. Rosenthal.

AJR 157:935-942, November 1991 0361-803X/91/1575-0935 © American Roentgen Ray Society

TABLE 1: Types of Needles Used for Percutaneous Biopsy of Skeletal Lesions

	Needle Type
Aspiration	
Spinal	
Westcott (Becton-Dickinson, Rutherford, NJ)	
Chiba (Cook Co., Bloomington, IN)	
Cutting	
Tru-Cut (Baxter Health Care Corp., Deerfield, IL)	
Jamshidi (Kormed Co., Minneapolis, MN)	
Trephine	
Craig (Becton-Dickinson)	
Turler (Turler Instruments, Inc., Southfield, MI)	
Ackermann (Slanco, Becton-Dickinson)	
Fraseen (Cook Co.)	
Vim-Silverman	

and fine-gauge cutting needles are used for radiologically guided biopsies of other organ systems, and will be familiar to most radiologists. Of the large-gauge cutting needles, the one in widest use and with which we have the greatest experience is the Tru-Cut needle (Baxter Health Care Corp., Deerfield, IL). This needle is available in two lengths, 11.5 and 7.5 cm, but only one gauge. It is a disposable, side-cutting needle (Fig. 1). It is particularly useful for biopsy of primary soft-tissue neoplasms because it produces a large specimen, free from maceration. In our experience, it is also extremely valuable for lytic lesions of bone and bone marrow lesions. In the latter cases, a cortical window must be made first, since the Tru-Cut needle can bend easily if hard bone is encountered.

The type of needle most closely associated with bone biopsy procedures is the trephine needle. These tend to be large-gauge [10–13] needles with a serrated or sawtooth cutting edge (trephine). In order to protect the soft tissues, the trephine is introduced with a coaxial technique through an outer protective sheath. The sheath in turn is introduced over a blunt obturator, which is intended to displace nerves and vessels, rather than cutting through them. In the case of the Craig needle, the obturator is introduced first, and the sheath is advanced over it by using a coaxial technique. The Turler and Ackermann needles introduce the obturator and sheath simultaneously. An additional blunt obturator is usually provided for expressing the specimen from the trephine.

Imaging

The choice of imaging technology depends on anatomic location [11–18]. Fluoroscopy is faster, easier to use [11, 12], and less costly than CT. However, CT introduces an additional element of safety because it can visualize the contiguous soft tissues, and can more readily place the needle within three dimensions [14–18]. Fluoroscopy in a single plane can be used when there is a dense bony cortex to limit the advance of the needle. For example, biopsy of destructive lesions of one cortex of an appendicular long bone can be performed safely with single-plane fluoroscopy because, after the needle traverses the destroyed area of bone, its further advance will

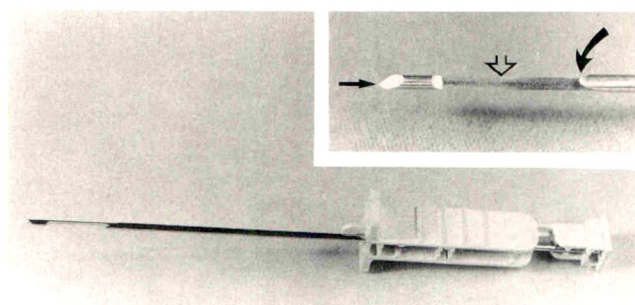


Fig. 1.—Photograph of Tru-Cut needle. Magnified view of tip (inset) shows blunt tip (straight solid arrow), inner specimen groove (open arrow), and outer cutting sheath (curved arrow).

be halted by contact with the solid cortex on the other side. However, if the examiner cannot determine when the lesion has been contacted, as, for example, with an extremely lytic process; or if it is necessary to judge the depth of the needle by visual cues; or if the approach to the lesion must be oblique to the plane of visualization, as in a spinal biopsy, then it is necessary to use biplane or C-arm fluoroscopy. In general, we have found fluoroscopy to be preferable for biopsies of the extremities and the lumbar spine. We prefer CT for biopsies of the pelvis because of the difficulty of obtaining biplane images of the pelvis, and we consider CT essential for biopsies of the thoracic and cervical spine because of complex anatomy and adjacent vital structures.

Before the biopsy procedure, a thorough radiologic evaluation should be performed. This is done to characterize and carefully locate the lesion with respect to surrounding anatomy. In addition, it is important to determine that the lesion is the best choice for biopsy. It is embarrassing (and potentially hazardous) to perform a biopsy of the cervical spine if a similar lesion is present in the pelvis!

Preparation and Technique

Before biopsy, patients should be evaluated for coagulopathy. In many cases a simple medical history will suffice. For lesions in the extremities in which it is possible to obtain hemostasis by pressure alone, clotting studies are usually unnecessary. For deeply situated lesions, particularly when use of a large-caliber needle is projected, we agree with Silverman et al. [19] regarding the appropriate protocol for selecting clotting studies. These will generally include a platelet count, prothrombin time (PT), and partial thromboplastin time (PTT). If there is any history of ingestion of nonsteroidal antiinflammatory drugs or a tendency to bruise easily, a study of bleeding time is added.

Most biopsies are done on outpatients with the use of local anesthesia, and therefore premedication is not essential. It is sometimes preferable to use sedation in apprehensive patients.

Figure 2 illustrates the approach to a destructive lesion of the left lateral aspect of the vertebral body and pedicle of T10 under fluoroscopic guidance. Access to the vertebral body is achieved through the paraspinous soft tissues (Fig. 3). In the

Fig. 2.—A and B, Posteroanterior (A) and lateral (B) fluoroscopic spot films show placement of a 20-gauge spinal needle used for local anesthesia. Note that in posteroanterior projection, tip of needle is lateral to medial edge of incompletely destroyed pedicle, indicating that needle is not within spinal canal. Lateral image shows that needle is in contact with posterolateral surface of vertebral body.

C and D, Posteroanterior (C) and lateral (D) spot films show placement of a Turkel needle in tandem with spinal needle. Inner trephine has been advanced to its full length. Lateral film shows that trephine has not violated anterior cortex. Posteroanterior film shows that trephine tip is approximately midline.

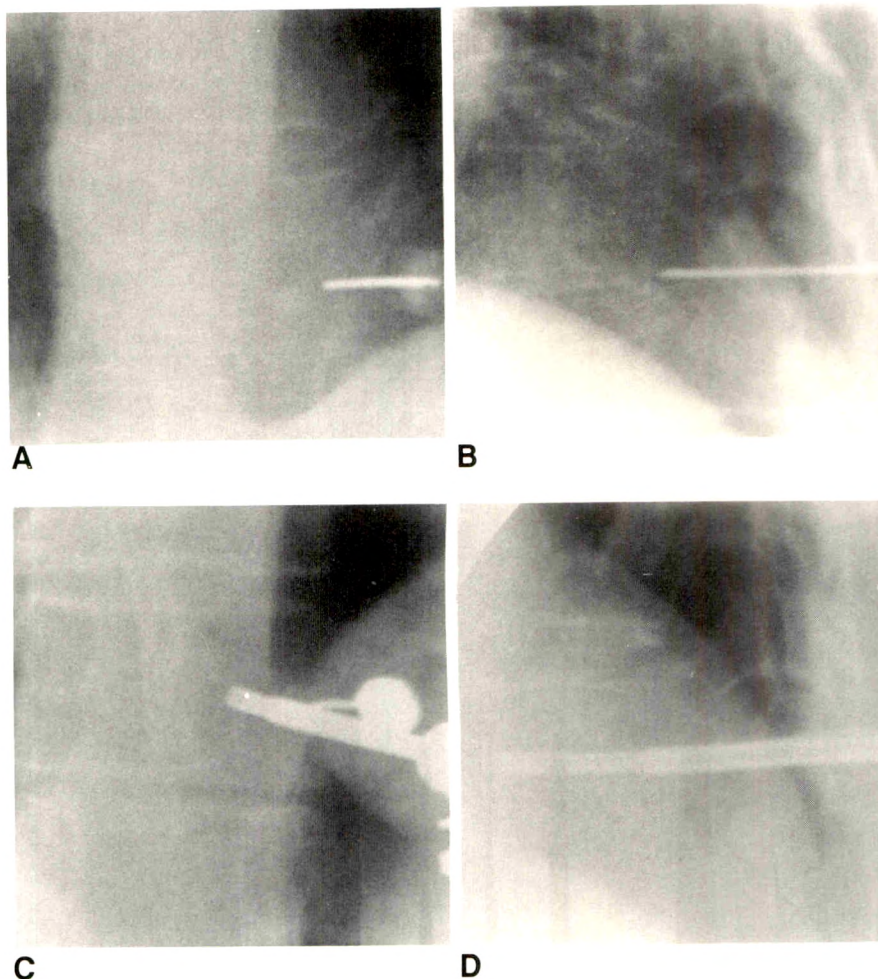
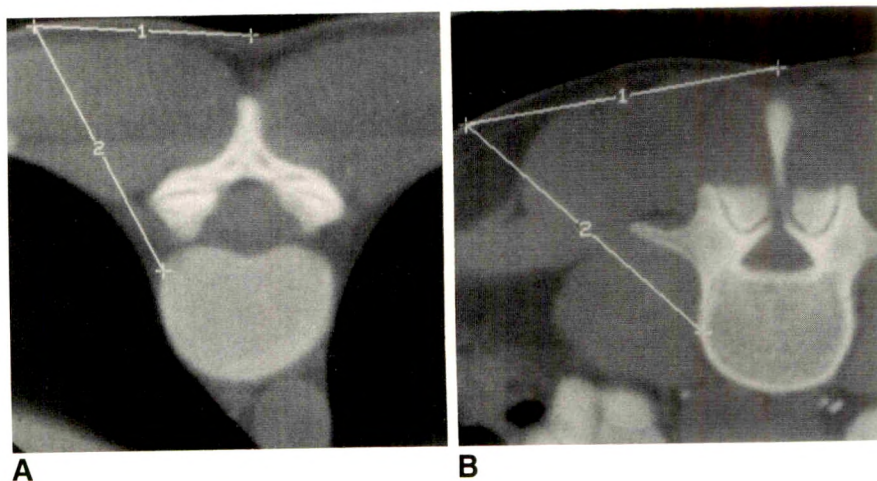


Fig. 3.—A, CT scan of extrapleural approach to a high thoracic vertebra. Distance from midline is measured and marked on patient's skin. Needle should be angled steeply (in this case approximately 30° from vertical).

B, CT scan of paraspinous approach to a lumbar vertebra. A more horizontal approach is used (in this case approximately 45° from vertical).



lumbar spine the skin puncture site is typically 10–12 cm lateral to the midline and the angle of approach is approximately 45° from the sagittal plane. It is desirable for the needle to be perpendicular to the posterolateral surface of the vertebral body at the point of contact. Higher levels require more medial skin punctures and a steeper angle of approach

(Fig. 3A). In the midthoracic spine, in order to avoid the pleura, the angle typically may be only $20\text{--}30^\circ$ from the sagittal plane and the puncture site 6–8 cm from the midline. CT may be helpful in these cases to determine the optimum approach. The approach to a lesion of a cervical vertebral body is often anterior (this is discussed separately).

For a lumbar or thoracic biopsy, the patient may be positioned either prone or lateral decubitus. The skin entry point is selected so that it is not necessary to angle the needle in a cranial or caudal direction. The skin is anesthetized with Xylocaine, and a spinal needle is advanced along the projected course. The position is checked frequently with biplane fluoroscopic images. The target is the posterolateral corner of the vertebral body. On the anteroposterior projection, the tip of the needle should always project lateral to the medial cortex of the adjacent pedicle to guarantee that the needle is outside the spinal canal (Fig. 2A). On the lateral view, the needle should encounter bone at approximately the posterior border of the vertebral body (Fig. 2B). Thus, with fluoroscopic guidance it is necessary to estimate the relative distances that the needle can be safely advanced anteriorly and toward the midline and adjust the angle of approach to reach this final destination.

With each centimeter's advance of the needle, 0.5–1.0 ml of Xylocaine is injected. Once the needle encounters the target, an incision is made in the skin adjacent to the needle and the trephine assembly is introduced. It is advanced in tandem with the needle used for anesthesia, and we make sure that it follows an identical route.

When the obturator encounters the posterolateral vertebral corner, as determined by feel, the sheath is advanced over the obturator until it strikes bone, and the cannula is removed. Using one hand to maintain the position of the sheath, we introduce the trephine through the sheath and advance it into the bone with a rotating movement. It is best to rotate the needle in only one direction to take advantage of its beveled teeth and to avoid maceration of the specimen. The amount of pressure necessary to advance the needle may vary. In the lumbar spine, firm manual pressure is almost always sufficient. Biopsy of dense cortical bone in the extremities may require considerable force and the assistance of a large hand drill [20]. If the force necessary to advance the needle becomes excessive or if the advance of the needle suddenly stops, the trephine should be withdrawn and examined. Occasionally, dense bone may bend the teeth of the trephine, closing its orifice. More often, the needle becomes impacted with dense bone. Expressing the specimen to clear the needle at this point will allow the biopsy to be resumed.

The trephine is advanced until its maximal length extends beyond the sheath or until the radiologist no longer considers it safe to proceed. The vertebral biopsy needles have been designed so that the maximal extent of the trephine will not transgress the anterior cortex of a typical lumbar vertebrae. The radiologist should not assume this to be the case, however. There is no substitute for exact knowledge of the location of the needle tip. Thoracic and cervical vertebrae are smaller and must be treated individually. The position of the trephine should be documented before the specimen is removed.

The needle can usually be removed without loss of the specimen. It is seldom necessary to use suction, as the firm bony tissue will usually be wedged into the trephine. In fact, it is often difficult to express the specimen from the trephine, even with the assistance of the obturator. It is suggested that

the trephine be placed within a sterile tube or covered loosely with a gauze pad before any force is applied to the obturator, as the specimen may suddenly be extruded. We have had the unfortunate experience of seeing a bony specimen rapidly ejected from a trephine needle and bounce off a flat surface or shallow dish. For this reason, it is recommended that the trephine be placed within a tube before this maneuver is attempted.

Special Circumstances

Most patients can tolerate this procedure easily. Local anesthesia with Xylocaine is virtually always effective as long as the entire needle path is anesthetized down to the surface of the bone. Patients with severely destroyed bones often appear to lose sensation and tolerate the procedure better than those with small lesions. If radicular pain is encountered in the course of advancing the needle, the needle is pulled back slightly and redirected. However, displacement of the lesion by the needle tip may in turn displace a nerve root that is not immediately contiguous with the needle, thus producing radicular symptoms. If we are convinced that the needle is not adjacent to a spinal nerve root, we sometimes proceed despite radicular symptoms. Occasionally, owing to hypervascular lesions or even the normal vascularity of the marrow, copious bleeding may occur through the sheath after the trephine is removed. Replacing the obturator in the sheath will tamponade the bleeding. We usually wait 3–5 min before obtaining a second sample or removing the needle. Usually, two or three samples of bone are obtained, depending on the size of the initial sample.

The procedure as thus described can be made more difficult by several factors. There may not be a convenient needle path to reach the lesion, although sometimes relatively inaccessible lesions can be approached by creative positioning of the patient (Fig. 4).

A more common concern is the presence of adjacent vital structures, which must be avoided. Biopsy of lesions in the chest wall potentially can cause a pneumothorax. CT is helpful in planning a needle path and in determining a safe depth (Fig. 5).

Proximity to the spinal canal also warrants the use of CT guidance, which we routinely employ for biopsy of the posterior elements. Biopsy of a cervical vertebral body requires a somewhat different technique. The bulky posterior elements and articular masses prevent a posterior approach. In the lower cervical spine, a lateral approach may be used; however, in the upper cervical spine the position of the carotid sheath dictates an anterior approach. The needle is advanced between the pharynx and the carotid sheath. It is sometimes helpful to retract the great vessels laterally. This is usually easily accomplished with one hand while the needle is advanced with the other. It is done more readily if the neck is not extended excessively. In most cases we prefer to do a fine-needle aspiration biopsy of cervical vertebrae; however, it is possible to use the same large-caliber cutting and trephine needles in the cervical spine as are used elsewhere (Fig. 6).

A difficulty that is unique to the skeletal system is the need to penetrate hard, round, bony surfaces. In bones such as



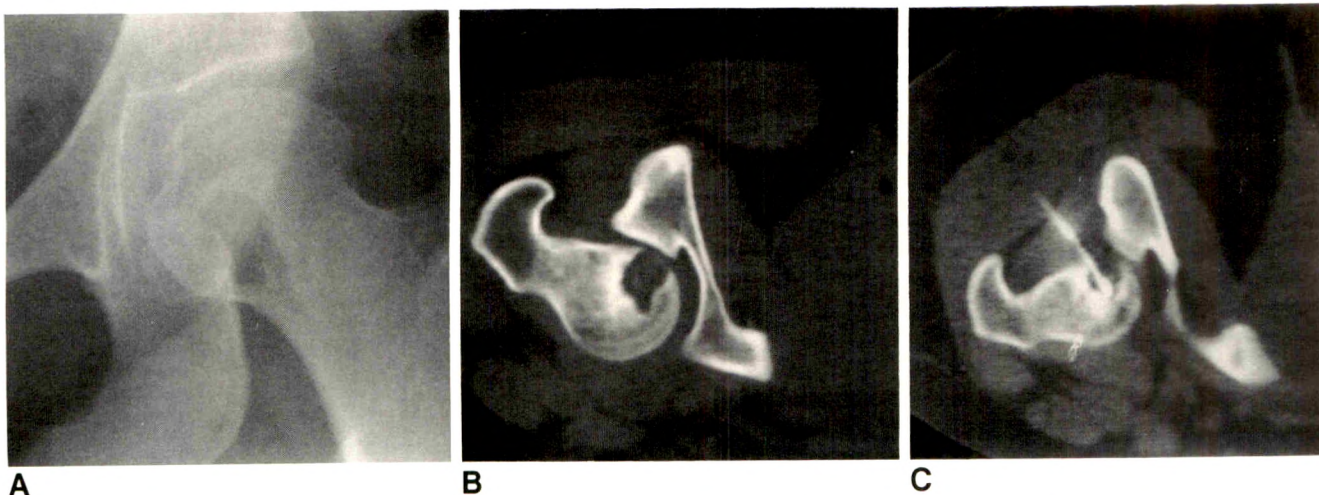


Fig. 4.—A, Anteroposterior plain film of hip shows a lytic lesion in medial femoral head. Appearance might suggest that this lesion is easily accessible, if femoral vessels can be avoided.

B, CT scan obtained with patient prone reveals that lesion is almost entirely covered by acetabulum, severely limiting ability to reach it by needle.

C, CT scan obtained with leg in marked internal rotation was used to guide placement of a Tru-Cut needle. Biopsy results indicated eosinophilic granuloma.

Fig. 5.—CT scan is used to guide depth of rib biopsy. With fluoroscopic guidance, it would have been difficult to be certain that needle did not transgress pleura.

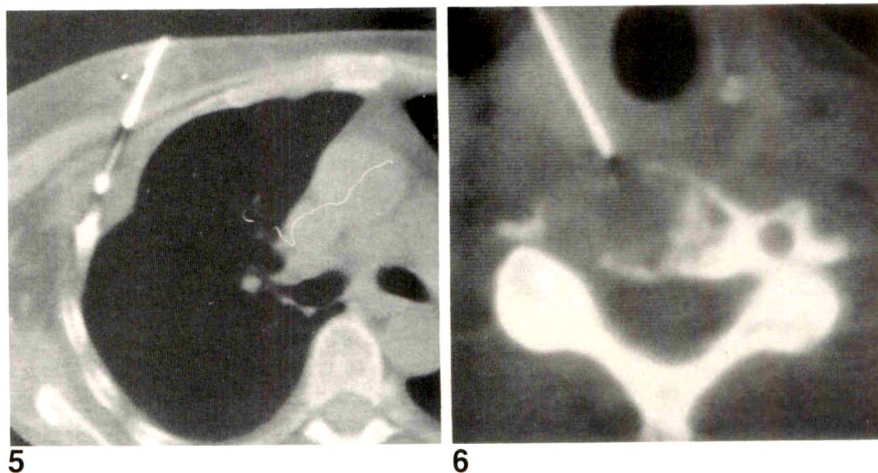


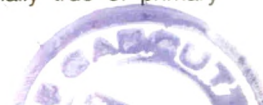
Fig. 6.—Cervical spine biopsy with CT guidance was done by using a large-caliber (Tru-Cut) needle introduced anteriorly. In this case there was easy access to lesion through thyroid gland, so that retraction of vessels was not necessary. Lesion was shown to be metastatic carcinoma. Primary lesion had not been determined at this time.

the clavicle and ischium, despite careful immobilization, it may be very difficult to obtain adequate "purchase" of the needle tip, which may skid along the surface to an undesirable position. This is a problem particularly when the cortical surface is intact and the intended target is endosteal or intramedullary. In such instances, the use of a hand drill is helpful [20]. The drill bit is introduced within a sheath, which is necessary to protect the surrounding soft tissues, and an assistant steadies the sheath while the examiner operates the drill. If it is necessary to include cortical bone in the sample, the drill may be adapted to the Luer-Lok fitting of the trephine [21]. Despite the somewhat frightening appearance of the hand drill assembly, patients seem to have less discomfort when this technique is used, perhaps because of the marked decrease in the time necessary to obtain the sample. We have found that a 2.8-mm drill bit creates a hole that is adequate to admit a Tru-Cut needle into the marrow for

purposes of biopsy. With the sheath in place, relocating the hole repeatedly for additional marrow samples is straightforward (Fig. 7).

Certain lesions may present particular difficulties. Lesions with dense ossification present several problems. It may be extremely difficult to penetrate densely ossified tissue with a trephine needle. Although the drill can be helpful, instances are still encountered in which it is almost impossible to advance the trephine because of plugging and bending of the needle. The presence of a large amount of ossified tissue may result in a macerated specimen that is difficult for the pathologist to interpret. In general, densely mineralized areas of lesions tend to represent the most differentiated portions, and therefore, when it is possible, a less mineralized area should always be selected as the target for biopsy (Fig. 8).

Certain types of diseases are relatively more difficult for the pathologist to interpret. This is especially true of primary



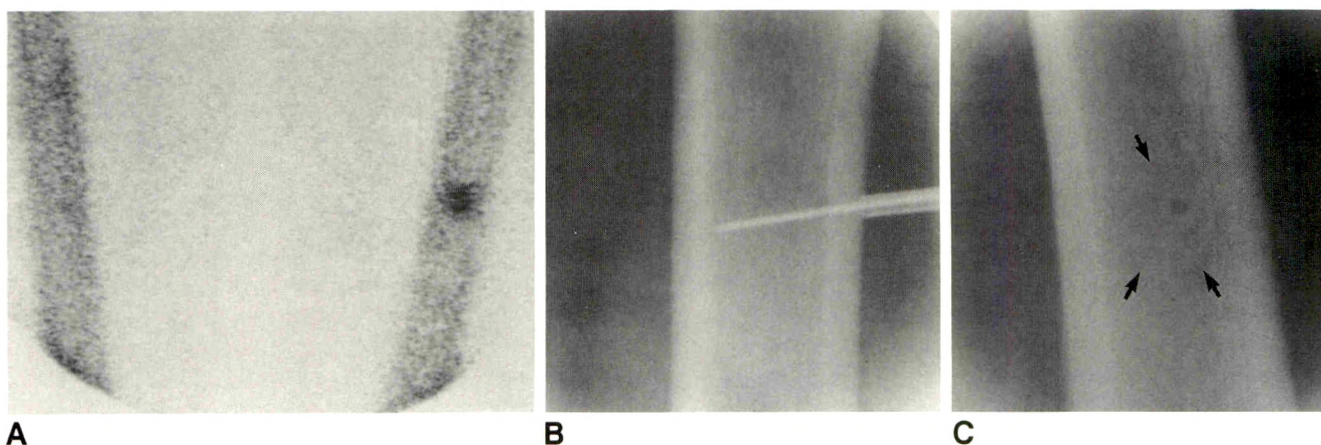


Fig. 7.—A, Solitary focal area of increased uptake is seen on radionuclide scan in patient with breast cancer.
 B, Hand drill within a protective sheath was used to penetrate intact cortex. Radiograph shows sheath still in place after drill was removed and spinal needle was introduced for biopsy of marrow, which indicated metastatic breast cancer.
 C, At conclusion of procedure, drill hole is readily visible on a spot film. The only radiographic manifestation of lesion is a faint zone of sclerosis (arrows).

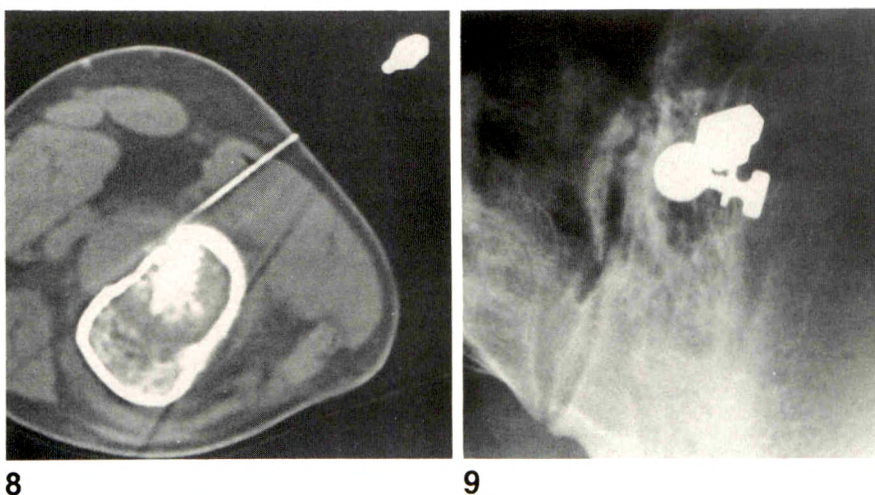


Fig. 8.—CT guidance is used for biopsy of nonmineralized soft-tissue component of this osteosarcoma. In this case, soft-tissue component was thought to represent highest-grade tissue. If it is possible to avoid cortical biopsy, risk of pathologic fracture is reduced.

Fig. 9.—Anteroposterior fluoroscopic spot film shows biopsy of angioma of posterior ilium with large-caliber (Turkel) needle.

tumors, in which the histology may vary from one portion to the other. Cartilage tumors are notoriously difficult. In such instances, as large a sample as possible should be obtained, and the radiologist must be alert to any discrepancies between the interpretation of the biopsy specimen and the probable diagnosis based on the imaging studies. Lymphomas also present difficulties because the pathologist may need to study the nodal architecture, which is something that cannot be easily accomplished with a needle biopsy. In our institution, lymphoma classification requires the study of cell surface markers, and for this reason, specimens of suspected lymphoma are always delivered fresh in saline rather than fixed in preservative.

Finally, hypervascular lesions present a relative, but not absolute, contraindication to biopsy with a large-caliber needle. Despite this, we have successfully performed biopsies on many hypervascular osteosarcomas, renal cell cancer metastases, and angiomas of the skeleton without problems (Fig. 9).

Results of the Procedure

Table 2 lists some of the accuracies reported over the years of bone biopsy procedures [2, 6, 8–10, 17, 18, 22–45]. Some of the early work was done without any radiographic guidance, and the results were fairly poor. The trend has been generally improving, with peak accuracy approaching 90%. Accuracy depends partly on the types of cases involved. The highest accuracy is generally achieved in the diagnosis of metastatic tumor, and the worst is in primary tumors. This is fortunate because metastatic lesions are usually the most common indication for bone biopsy. In our institution, the initial occurrence of metastasis is often documented by biopsy, even if more than one site is demonstrated. Other reasons for a biopsy of metastatic disease include uncertainty about diagnosis (e.g., pathologic fracture) and unknown primary tumor.

Nondiagnostic specimens may be obtained for a variety of reasons other than faulty technique. Densely osteoblastic

TABLE 2: Accuracies of Musculoskeletal Biopsy (Including Spine) Reported Since 1931

Source, Year	Accuracy (%)
Coley et al. [2], 1931	94
Snyder and Coley [26], 1945	68
Valls et al. [22], 1948	80
Mazet and Cozen [23], 1952	72
Frankel [29], 1954	59
Ottolenghi [24], 1955	95
Ackermann [6], 1956	11
Kendall [30], 1960	67
Ackermann [25], 1963	16
Cramer [32], 1964	71
Ottolenghi [31], 1964	79
Ottolenghi [27], 1969	73–92
Hajdu and Melamed [33], 1971; [34], 1973	81
Gladstein and Grantham [35], 1974	97
Armstrong et al. [37], 1978	68
De Santos et al. [39], 1979	93
Adler and Rosenberger [38], 1979	88
Murphy et al. [40], 1981	94
Ayala and Zornosa [42], 1983	79
Tehranezhadeh et al. [43], 1983	72
Haaga et al. [10], 1983	78
Hewes et al. [41], 1983	85–94
Bernardino [44], 1984	94
Laredo and Bard [28], 1986	78
Bender and Berquist [17], 1986	90
Kattapuram et al. [45], 1991	91

Note.—The numbers given for accuracy are those quoted by the authors. It was not possible to verify that the strict definition of accuracy ([true positive plus true negative]/total) was used in all cases.

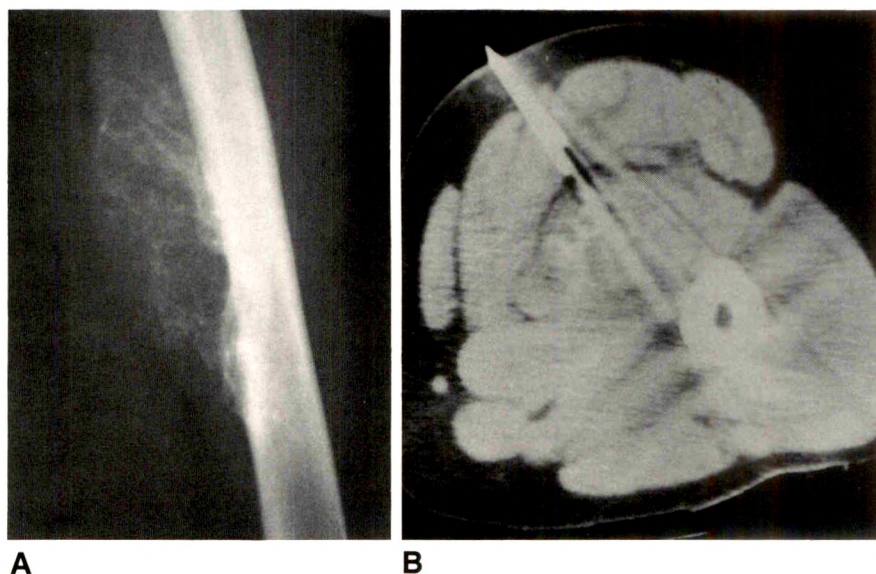
lesions are not only physically difficult to sample, but also frequently yield macerated specimens. It may be difficult to obtain diagnostic cellular material from lesions that are mostly cystic or necrotic. For highly vascular lesions, and lesions that are in particularly dangerous locations, the examiner may limit the number of needle passes that would otherwise be done.

Complications

Potential complications vary greatly depending on the anatomic location and the type of needle used. The reported prevalence has varied between zero and 10% [8, 13, 17, 18, 24, 35, 37, 40, 43, 46–55]. Some complications (pain, bleeding, infection, spread of disease) are generic. Others, such as pneumothorax, neurologic damage, and pathologic fracture, are site specific. In our opinion, the risk of significant complication (excluding mild to moderate discomfort and nondiagnostic tissue) should be much less than 1%. We have encountered several problems that deserve emphasis. Non-steroidal antiinflammatory drugs can markedly prolong the bleeding time [56]. In the case of aspirin, this effect can persist for a week or even longer after use is discontinued and may be seen in patients with normal platelet counts, PT, and PTT. We have seen significant bleeding when this hazard was overlooked. Tumor implantation in the needle track is really quite rare, but it can occur [8, 47]. For this reason it is important that when biopsy of a primary tumor is done, the biopsy be done in such a way that the needle track can be resected along with the specimen. The shortest needle path to the lesion is not always the most desirable. If the lesion is a suspected recurrence, it is usually desirable to place the needle near the original incision, since this area will be resected along with the recurrent lesion. Sometimes the surgical technique may not be intuitively obvious from the appearance of the lesion (Fig. 10), and in order to avoid contamination of additional compartments by the needle track, consultation with the surgeon regarding the proposed surgery is advisable. Finally, we have observed a minor complication in a number of instances that proved to be quite alarming. It is possible to anesthetize major motor nerves, leading to paresis or paralysis. The depth and extent of anesthesia can be slowly progressive as the anesthetic diffuses beyond the original injection site, and thus may simulate damage from the biopsy procedure. It is important to remain calm in such circum-

Fig. 10.—A, Lateral plain film of femur shows a destructive lesion extending posteriorly into thigh.

B, Under CT guidance, a Tru-Cut needle was introduced into lesion from a posterior approach. Histology revealed osteosarcoma. Although the posterior approach was most direct, and easiest for the radiologist, later consultation with the surgeon indicated that the preferred approach to this lesion was anterior. Thus, the needle track could not be excised, potentially compromising the outcome.



stances, as uneventful recovery should occur within 3 or 4 hr.

REFERENCES

- Martin HE, Ellis EB. Biopsy by needle puncture and aspiration. *Ann Surg* 1930;92:169-181
- Coley BL, Sharp GS, Ellis EB. Diagnosis of bone tumors by aspiration. *Am J Surg* 1931;13:215-224
- Hoffman WJ. Punch biopsy in tumor diagnosis. *Surg Gynecol Obstet* 1933;56:829
- Martin HE, Ellis EB. Aspiration biopsy. *Surg Gynecol Obstet* 1934;59:578-589
- Turkel H, Bethell FH. Biopsy of bone marrow performed by a new and simple instrument. *J Lab Clin Med* 1943;28:1246-1251
- Ackermann W. Vertebral trephine biopsy. *Ann Surg* 1956;143:373-385
- Craig FS. Vertebral body biopsy. *J Bone Joint Surg [Am]* 1956;38-A:93-102
- De Santos LA, Lukeman JM, Wallace S, Murray JA, Ayala AG. Percutaneous needle biopsy of bone in cancer patient. *AJR* 1978;130:641-649
- Zornosa J, ed. *Percutaneous needle biopsy*. Baltimore: Williams & Wilkins, 1981
- Haaga JR, Lipuma JP, Bryan PJ, Balsara VJ, Cohen AM. Clinical comparison of small and large caliber cutting needles for biopsy. *Radiology* 1983;146:665-667
- Lalli AF. Roentgen-guided aspiration biopsies of skeletal lesions. *Can Assoc Radiol J* 1970;21:71-73
- Lalli AF. The direct fluoroscopically guided approach to renal, thoracic and skeletal lesions. *Curr Prob Radiol* 1972;2:30-41
- Collins JD, Bassett L, Main GD, Kagan C. Percutaneous biopsy following bone scans. *Radiology* 1979;132:439-442
- Haaga JR. New techniques for CT-guided biopsies. *AJR* 1979;133:633-641
- Hardy DC, Murphy WA, Gilula LA. Computed tomography in planning percutaneous bone biopsy. *Radiology* 1980;134:447-450
- Zornosa J, Bernardino ME, Ordonez NG, Thomas JL, Cohen MA. Percutaneous needle biopsy of soft tissue tumors guided by ultrasound and computed tomography. *Skeletal Radiol* 1982;9:33-36
- Bender CE, Berquist TH. Imaging assisted percutaneous biopsy of the thoracic spine. *Mayo Clin Proc* 1986;61:942-950
- Kattapuram SV, Rosenthal DI. Percutaneous biopsy of the cervical spine using CT guidance. *AJR* 1987;149:539-541
- Silverman SG, Mueller PR, Pfister RC. Hemostatic evaluation before abdominal interventions: an overview and proposal. *AJR* 1990;154:233-238
- Cohen MA, Zornosa J, Finkelstein JB. Percutaneous needle biopsy of long bone lesions facilitated by the use of a hand drill. *Radiology* 1981;139:750-751
- Kattapuram SV, Rosenthal DI, Phillips WJ. Trephine biopsy of the skeleton with the aid of a hand drill. *Radiology* 1984;152:231
- Valls J, Ottolenghi CE, Schajowicz F. Aspiration biopsy in diagnosis of lesions of vertebral bodies. *JAMA* 1948;136:376-382
- Mazet R, Cozen L. The diagnostic value of vertebral body needle biopsy. *Ann Surg* 1952;135:245-252
- Ottolenghi CE. Diagnosis of orthopaedic lesions by aspiration biopsy: results of 1061 punctures. *J Bone Joint Surg [Am]* 1955;37-A:443-464
- Ackerman W. Application of the trephine for bone biopsy: results of 635 cases. *JAMA* 1963;184:11-17
- Snyder RE, Coley BL. Further studies on the diagnosis of bone tumors by aspiration biopsy. *Surg Gynecol Obstet* 1945;80:517-522
- Ottolenghi CE. Aspiration biopsy of the spine: technique for the thoracic spine and results of twenty-eight biopsies in the region and overall results of 1050 biopsies of other spinal segments. *J Bone Joint Surg [Am]* 1969;51-A:1531-1544
- Laredo JD, Bard M. Thoracic spine: percutaneous trephine biopsy. *Radiology* 1986;160:485-489
- Frankel CJ. Aspiration biopsy of the spine. *J Bone Joint Surg [Am]* 1954;36-A:69-74
- Kendall PH. Needle biopsy of the vertebral bodies. *Ann Phys Med* 1960;5:236-242
- Ottolenghi CE, Schajowicz F, DeSchant FA. Aspiration biopsy of the cervical spine: technique and results in thirty-four cases. *J Bone Joint Surg [Am]* 1964;46-A:715-733
- Cramer LE, Khun C III, Stein AH Jr. Needle biopsy of bone. *Surg Gynecol Obstet* 1964;118:1253-1256
- Hajdu SI, Melamed MR. Needle biopsy of primary malignant bone tumors. *Surg Gynecol Obstet* 1971;133:829-832
- Hajdu SI, Melamed MR. The diagnostic value of aspiration smears. *Am J Clin Pathol* 1973;59:350-356
- Gladstein MO, Grantham SA. Closed skeletal biopsy. *Clin Orthop* 1974;103:75-79
- Hajdu SI. Aspiration biopsy of primary malignant bone tumors. *Radiat Ther Oncol* 1975;10:73-81
- Armstrong P, Chalmers AH, Green G, Irving FD. Needle aspiration/biopsy of the spine in suspected disc space infection. *Br J Radiol* 1978;51:333-337
- Adler O, Rosenberger A. Fine needle aspiration biopsy of osteolytic metastatic lesions. *AJR* 1979;133:15-18
- De Santos LA, Murray JA, Ayala AG. The value of percutaneous needle biopsy in the management of primary bone tumors. *Cancer* 1979;43:735-744
- Murphy WA, Destouet JM, Gilula LA. Percutaneous skeletal biopsy 1981: a procedure for radiologists—results, review and recommendations. *Radiology* 1981;139:545-549
- Hewes RC, Vigorita VJ, Freiburger RH. Percutaneous bone biopsy. The importance of aspirated osseous blood. *Radiology* 1983;148:69-72
- Ayala AG, Zornosa J. Primary bone tumors: pathologic study of 222 biopsies. *Radiology* 1983;149:675-679
- Tehranchadeh J, Freiburger RH, Ghelman A. Closed skeletal needle biopsy. *AJR* 1983;140:113-115
- Bernardino ME. Percutaneous biopsy. *AJR* 1984;142:41-45
- Kattapuram SV, Khurana JS, Rosenthal DI. Percutaneous needle biopsy of the spine. *Spine* 1992 (in press)
- Hanafee WN, Tobin PL. Closed bone biopsy by a radiologist. *Radiology* 1969;92:605-606
- Engzeu V, Esposti PL, Rubio C, Sigurdson A, Zajicek J. Investigation of tumor spread in connection with aspiration biopsy. *Acta Radiol [Oncol]* 1971;10:385-398
- Debnam JW, Staple TW. Trephine bone biopsy by radiologists. *Radiology* 1975;116:607-609
- Debnam JW, Staple TW. Needle biopsy of bone. *Radiol Clin North Am* 1975;13:157-164
- McLaughlin RE, Miller WR, Miller CW. Quadripareisis after needle aspiration of the cervical spine: report of a case. *J Bone Joint Surg [Am]* 1976;58-A:1167-1168
- Stahl DC, Jacobs B. Diagnosis of obscure lesions of the skeleton: evaluation of biopsy methods. *JAMA* 1967;201:229-231
- Ramgopal V, Geller M. Iatrogenic *Klebsiella* meningitis following closed needle biopsy of the lumbar spine: report of a case and review of literature. *Wis Med J* 1977;76:41-42
- Moore TM, Meyers MH, Patzakakis MJ, et al. Closed biopsy of musculoskeletal lesions. *J Bone Joint Surg [Am]* 1979;61-A:375-380
- Southwick WO, Robinson RD. Surgical approaches to the vertebral bodies in the cervical and lumbar regions. *J Bone Joint Surg [Am]* 1957;39-A:631-644
- Nagel DA, Albright JA, Keggi KJ, Southwick WO. Closer look at spinal lesions: open biopsy of vertebral lesions. *JAMA* 1965;191:103-106
- Lind S. Prolonged bleeding time. *Am J Med* 1984;77:305-312

Pictorial Essay

Defects of the Interventricular Septum of the Heart: En Face MR Imaging in the Oblique Coronal Plane

Shi-Joon Yoo,¹ Tae-Hwan Lim,¹ In-Sook Park,² Chang Yee Hong,² Meong Gun Song,³ and Sam Hyun Kim³

MR imaging in the oblique coronal plane can provide an en face image of ventricular septal defects by visualizing the entire circumference of the defect. This pictorial essay illustrates various types of ventricular septal defects as seen on these images.

Identification of the precise location and size of a ventricular septal defect is important in determining the patient's prognosis and, when surgery is contemplated, the surgical approach and the technique of closure (Fig. 1) [1–3]. In echocardiographic and angiographic studies, ventricular septal defects are identified as areas of discontinuity on a cross-section or profile of the ventricular septum.

MR imaging, which can image the heart in any desired plane, can be used to visualize the entire circumference of the defect in the cross section of the ventricular septum [4]. Images in this particular plane, which are difficult to obtain with other diagnostic techniques, provide en face views of ventricular septal defects and make localization of defects simple and precise.

Imaging Technique

MR images were acquired with a 1.5-T MR unit (General Electric Medical System, Milwaukee, WI) by using standard ECG-gated spin-echo technique with the repetition time (TR) determined by the patient's heart rate and a short echo time

(TE). Each patient was examined while supine with the thorax elevated 5–15°. This maneuver generally makes the cranio-caudal axis of the ventricular septum parallel to the imaging table. Initial images of the heart were obtained in the transverse plane. Subsequently, after placing the slice-selecting line cursor on the ventricular septum, an oblique coronal imaging plane was chosen from the transverse image that shows the maximal dimension of the defect. The cursor was adjusted to the plane that passes through the center of each of the two margins of the cross-sectioned defect (Fig. 2). Imaging in this plane with slices 3- to 5-mm thick produced an en face view of the ventricular septal defect, comparable to seeing the defect directly. The defect shown in an oblique coronal image represents the true dimensions of the defect.

Perimembranous Ventricular Septal Defects

Perimembranous ventricular septal defects are defects that occur in and/or around the membranous septum. They typically abut the tricuspid-mitral-aortic fibrous continuity, which is called the "central fibrous body" [1, 2]. They may extend mainly into the inlet (Fig. 2), trabecular (Fig. 3), or outlet (Fig. 4) component of the right ventricular aspect of the muscular septum (Fig. 1B). Large perimembranous defects may involve all three components of the muscular septum; these are called confluent perimembranous defects.

Received March 12, 1991; accepted after revision May 2, 1991.

¹ Department of Diagnostic Radiology, Asan Medical Center, University of Ulsan, Kang-Dong P.O. Box 145, Seoul 134-600 Korea. Address reprint requests to S.-J. Yoo.

² Department of Pediatrics, Asan Medical Center, University of Ulsan, Kang-Dong P.O. Box 145, Seoul 134-600, Korea.

³ Department of Thoracic Surgery, Asan Medical Center, University of Ulsan, Kang-Dong P.O. Box 145, Seoul 134-600, Korea.

AJR 157:943–946, November 1991 0361–803X/91/1575–0943 © American Roentgen Ray Society

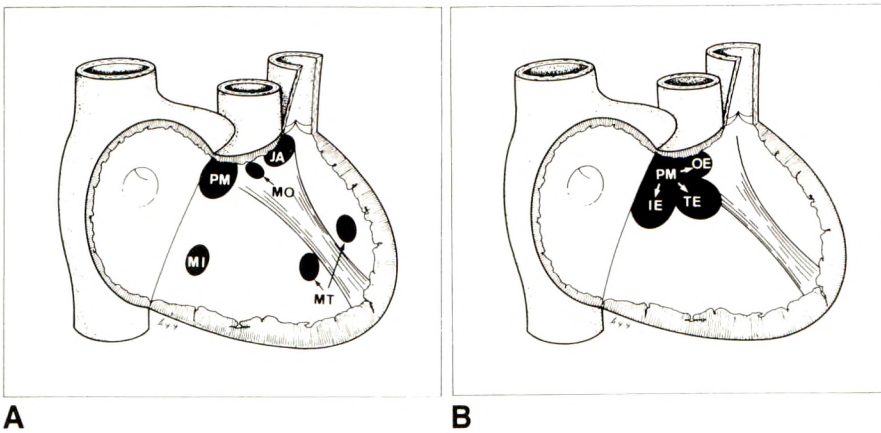


Fig. 1.—A and B, Diagrams show basic types of ventricular septal defects (A) and subdivision of perimembranous defects (B) as viewed from right ventricle. Muscular defects occur in inlet septum (MI), in trabecular septum (MT), and in outlet septum (MO). Perimembranous defects (PM) occur with inlet extension (IE), with trabecular extension (TE), and with outlet extension (OE). JA = doubly committed juxtaarterial defects. (Reprinted with permission from Yoo and Choi [2].)

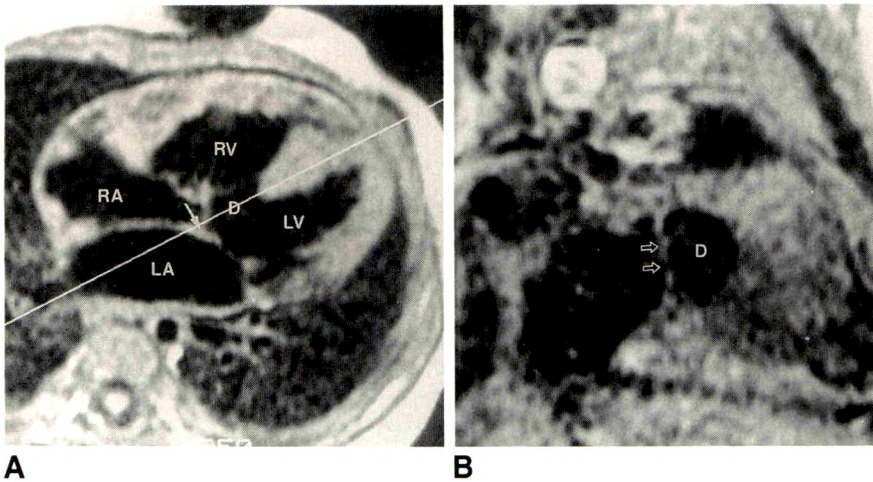


Fig. 2.—Perimembranous defect with inlet extension.

A, Transverse MR image shows that defect (D) abuts on tricuspid-mitral fibrous continuity (arrow). Oblique line represents plane at which oblique coronal MR image in B was obtained. RV = right ventricle, RA = right atrium, LV = left ventricle, LA = left atrium.

B, Oblique coronal MR image shows cross section (en face image) of ventricular septum that contains defect. Defect extends toward ventricular inlet along atrioventricular annulus (arrows).

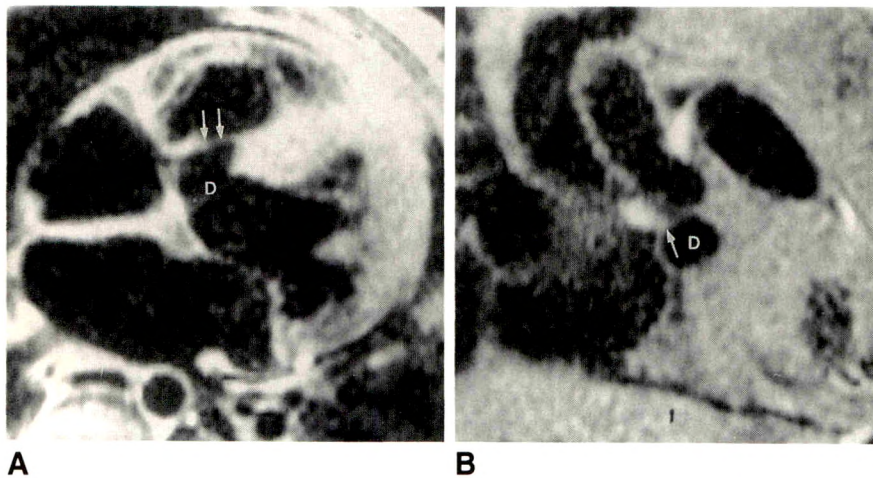


Fig. 3.—Perimembranous defect with trabecular extension.

A, Transverse MR image shows a defect (D) that is covered by adherent tricuspid valve leaflet (arrows).

B, Oblique coronal MR image shows a defect (D) that extends mainly toward apex of right ventricle. Defect abuts on central fibrous body (arrow).

Muscular Ventricular Septal Defects

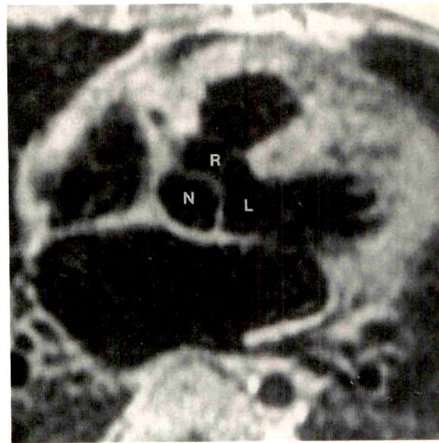
Muscular ventricular septal defects are defects that are surrounded entirely by the muscular rims and are separated from the pulmonary and atrioventricular valves [1, 2]. They

are subdivided into the muscular inlet, muscular trabecular (Fig. 5), and muscular outlet (Fig. 6) defects according to their position within the septum. Muscular trabecular defects are frequently multiple (Fig. 5).

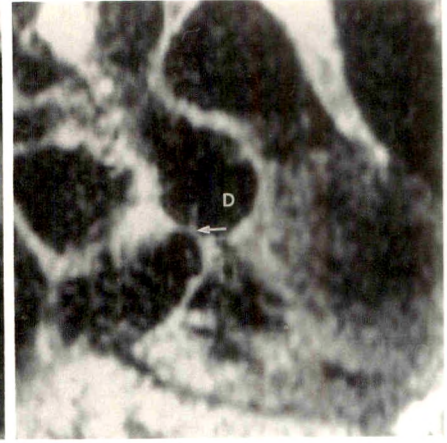
Fig. 4.—Perimembranous defect with outlet extension.

A, Transverse MR image shows that aortic valve, indicated by its right (R), left (L), and noncoronary (N) sinuses, overrides defect.

B, Oblique coronal MR image shows that defect (D) abuts on central fibrous body (arrow) and extends toward outlet of right ventricle.



A

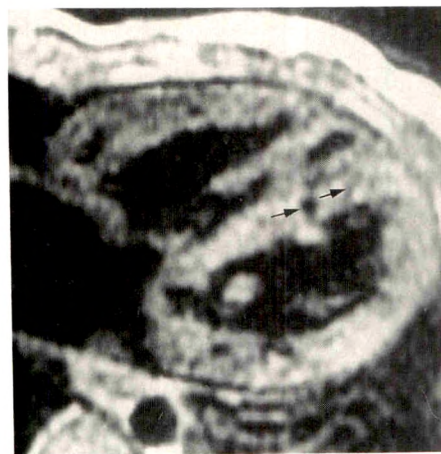


B

Fig. 5.—Multiple muscular trabecular defects.

A, Transverse MR image shows two small channels of defect (arrows) in apical muscular septum.

B, Oblique coronal MR image shows a large perimembranous defect (D) and three small holes of defect (arrows) in trabecular septum.



A

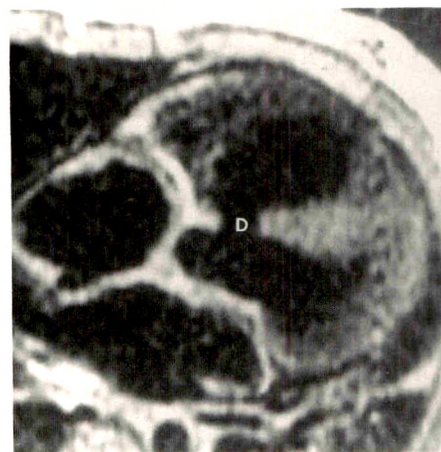


B

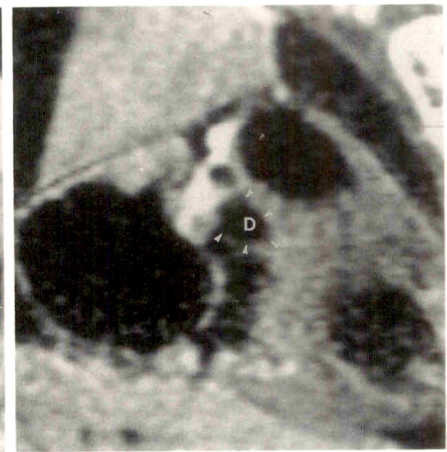
Fig. 6.—Muscular outlet defect.

A, Transverse MR image shows a small defect (D), both sides of which are bordered by muscular rims.

B, Oblique coronal MR image shows a small defect (D, arrowheads) located at center of so-called crista supraventricularis. Defect has entirely muscular rim.



A



B

Doubly Committed Juxtaarterial Ventricular Septal Defects

Doubly committed juxtaarterial ventricular septal defects involve the highest part of the outlet septum and are roofed

by the aortic and pulmonary valves, which are in fibrous continuity [1, 2] (Fig. 7). The rest of the rim usually is formed by the muscular septum. When the defect extends posteriorly to involve the membranous septum, it is both juxtaarterial and perimembranous.

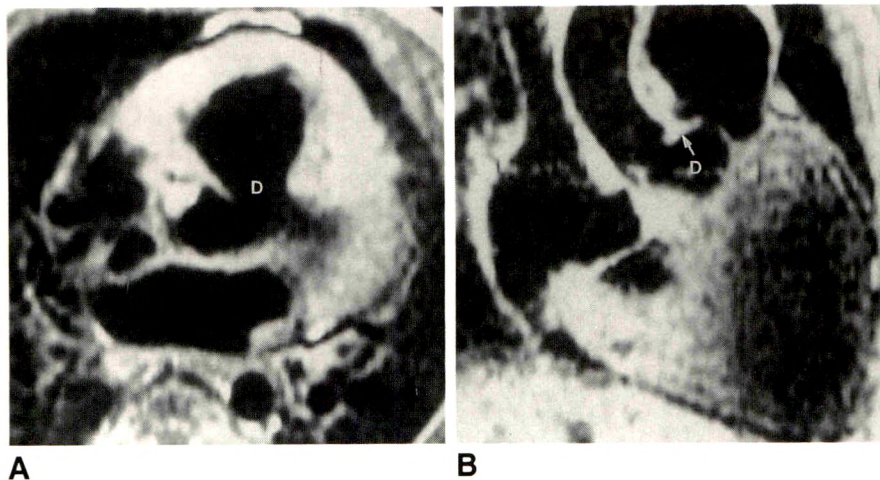


Fig. 7.—Doubly committed juxtaarterial defect.

A, Transverse MR image shows defect (D) in outlet septum.

B, Oblique coronal MR image shows that defect is roofed by aortic and pulmonary valves, which are in fibrous continuity (arrow).

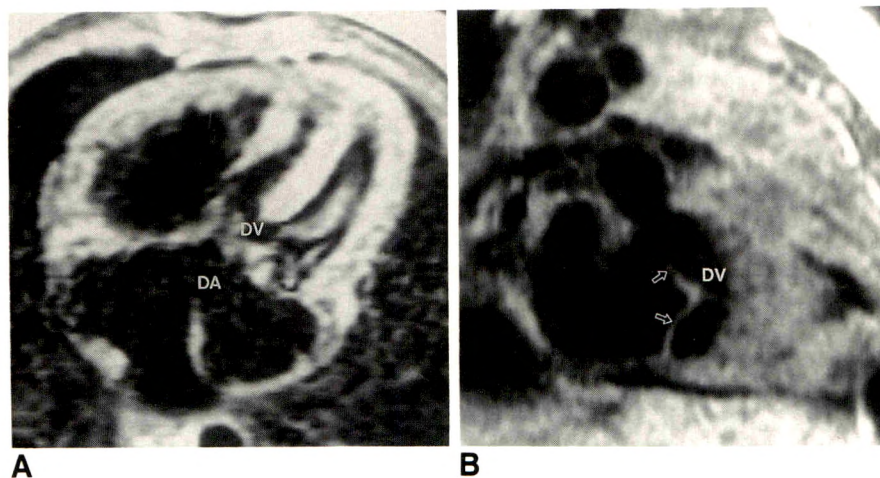


Fig. 8.—Atrioventricular septal defect.

A, Transverse MR image shows a large defect in atrioventricular junction. Defect is divided into interventricular (DV) and interatrial (DA) components by free-floating bridging leaflets of common atrioventricular valve.

B, Oblique coronal MR image shows characteristic "scooped-out" ventricular septum and free-floating bridging leaflets (arrows).

Atrioventricular Septal Defects

Atrioventricular septal defects involve the atrioventricular septum and the adjacent atrial and ventricular septa and are characterized by a "scooped-out" appearance of the ventricular septal crest [5] (Fig. 8). The atrioventricular bridging leaflets may attach to the ventricular septal crest (ostium primum defect) or to the lower margin of the defective atrial septum. Also, the bridging leaflets may have chordal insertion to the ventricular septal crest or may remain free floating (complete atrioventricular canal, Fig. 8).

REFERENCES

1. Soto B, Becker AE, Moulart AJ, Lie JT, Anderson RH. Classification of ventricular septal defects. *Br Heart J* 1980;43:332-343
2. Yoo SJ, Choi YH. Ventricular septal defect. In: *Angiocardiograms in congenital heart disease*. New York: Oxford Univ. Press, 1991:29-54
3. De Leval MR. Ventricular septal defect. In: Stark J, de Leval MR, eds. *Surgery for congenital heart defects*. London: Grune & Stratton, 1983:271-284
4. Baker EJ, Ayton V, Smith MA, et al. Magnetic resonance imaging at a high field strength of ventricular septal defects in infants. *Br Heart J* 1989;62:305-310
5. Becker AE, Anderson RH. Atrioventricular septal defects: what's in a name? *J Thorac Cardiovasc Surg* 1982;83:461-469

Case Report

Bronchopulmonary Sequestration: Dynamic, Ultrafast, High-Resolution CT Evidence of Air Trapping

Eric J. Stern,¹ W. Richard Webb,¹ Martha L. Warnock,² and Christopher J. Salmon¹

Intralobar bronchopulmonary sequestration is a congenital anomaly that consists of nonfunctioning, abnormal lung tissue that is contained within an otherwise normal lung and has an anomalous systemic blood supply [1-4]. Although intralobar sequestrations lack normal communications with the tracheobronchial tree, they can be ventilated by collateral air drift or through fistulous bronchial communications that may develop after an episode of infection. An air-containing intralobar sequestration can appear on chest radiographs as an area of hyperlucency, with or without associated visible cysts, or can appear as normal lung [5].

The CT appearances of bronchopulmonary sequestration have recently been reviewed [6], and the presence of lucent or low-attenuation areas of "emphysema" have been emphasized. It has been suggested that the emphysema seen in patients with sequestration results from collateral ventilation and air trapping [7]. We recently had an opportunity to test this hypothesis by using dynamic expiratory, ultrafast, high-resolution CT (HRCT) in a patient who subsequently had an intralobar pulmonary sequestration confirmed surgically and pathologically.

Case Report

A 19-year-old woman had a 3-cm, rounded soft-tissue mass on a routine chest radiograph. The surrounding right lower lobe appeared hyperlucent, but no air-containing cysts were visible. Five years before, a chest radiograph had shown consolidation in the right lower

lobe with an air-fluid level, and the patient was treated for presumed necrotizing pneumonia.

On conventional CT, obtained with contiguous 1-cm collimation, a nonsegmental area of abnormally lucent lung was visible in the posterior, medial, right lung base, adjacent and inferior to a homogeneous well-circumscribed soft-tissue density, corresponding to the mass visible on the chest radiograph. The lucent lung suggested the presence of one or more thin-walled, air-containing cysts (Fig. 1A).

Aortography showed an anomalous artery arising from the upper abdominal aorta and supplying the region of abnormal right lung. The venous drainage was not clearly shown.

Ultrafast CT (Imatron C-100, Imatron Inc., So. San Francisco, CA) was first performed immediately after the patient's aortogram was obtained, with the angiographic catheter still in place within the anomalous artery that was feeding the sequestration, in order to show the venous drainage of the sequestered lung. After the injection of 8 ml of contrast material, 10 CT scans, with 6-mm collimation, each 100-msec long, were obtained in 6 sec, at a single level through the atrial chambers. The "venous phase" of this CT angiogram showed opacification of the left atrium, indicating pulmonary venous drainage of the sequestration.

A series of ultrafast high-resolution CT (HRCT) scans (3-mm collimation, high-spatial-frequency reconstruction algorithm) were obtained through the abnormal right lower lobe at 1-cm intervals with the patient supine. These showed numerous, moderately thin-walled, air-containing cysts, 0.5 to 1.0 cm in diameter, that were not visible on conventional CT. Several larger air-containing cysts, up to 3 cm in diameter, were noted adjacent to the smaller cystic spaces.

Last, two series of dynamic, expiratory, ultrafast HRCT scans were obtained through the middle and lower portions of the sequestration in an attempt to show air trapping within the abnormally lucent

Received May 10, 1991; accepted after revision June 18, 1991.

¹ Department of Radiology, University of California, San Francisco, San Francisco, CA 94143-0628. Address reprint requests to E. J. Stern.

² Department of Pathology, University of California, San Francisco, San Francisco, CA 94143-0628.

AJR 157:947-949, November 1991 0361-803X/91/1575-0947 © American Roentgen Ray Society

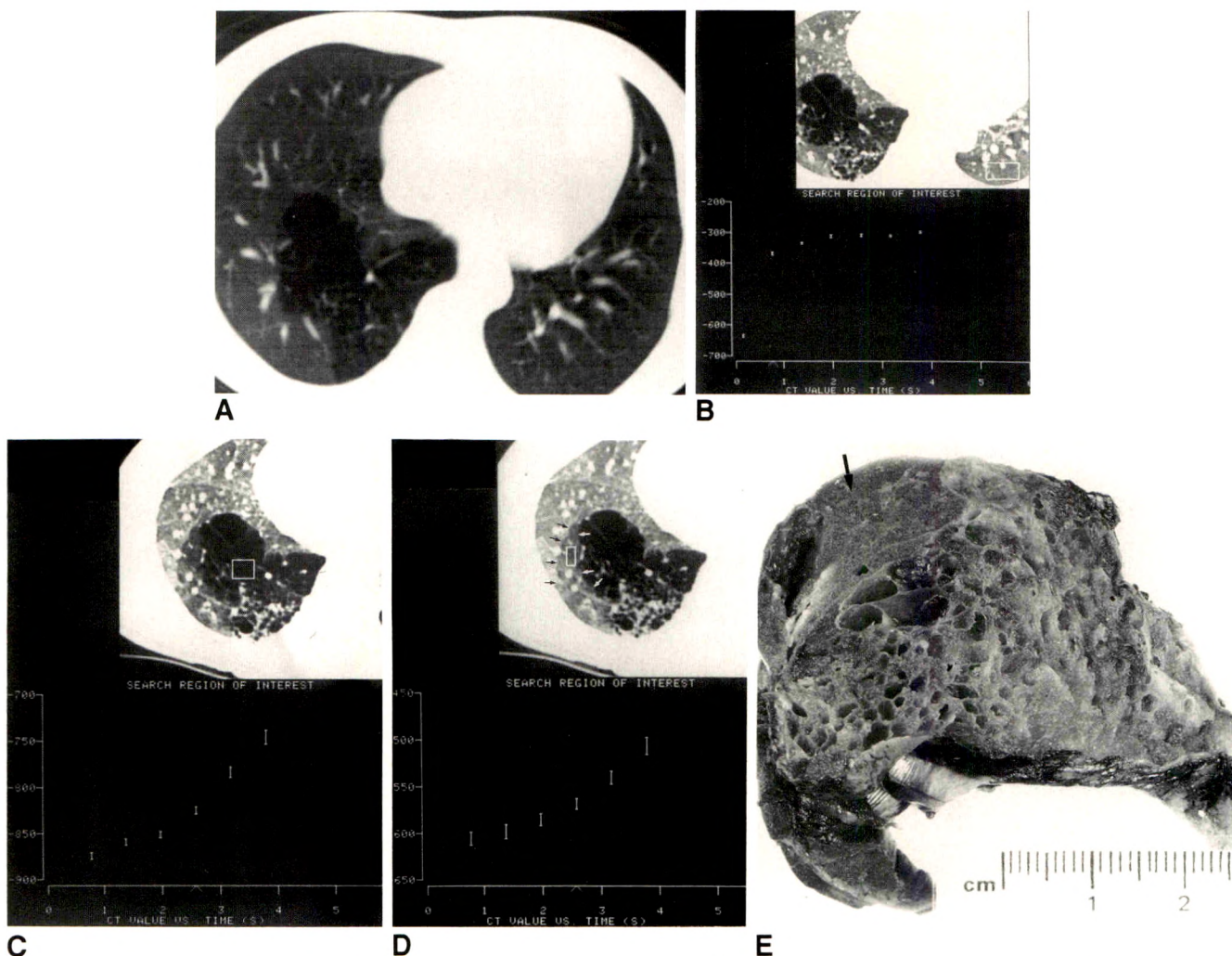


Fig. 1.—A, Conventional CT scan at level of right lung base. A nonsegmental area of hyperlucency is visible. Cystic components of sequestration are poorly seen.

B, Dynamic ultrafast high-resolution CT time-density analysis of normal left lung during a forced exhalation. Measurements were acquired from region of interest (ROI) shown. Hounsfield units are on y-axis, time in seconds on x-axis. Note rapid increase in lung density as patient exhales. During exhalation, lung increases in density by approximately 310 H, well within range of normal in patients we have studied. Note that rate of change in density yields a curve that is convex upward.

C, Time-density analysis of multicystic portion of sequestration in right lung, performed during same exhalation and at same level as in B, shows an increase in density as patient exhales, but at a slower rate than ROI in B. Rate of change in density yields a curve that is concave upward, as opposed to convex-upward curve seen in normal lung. Also, increase in lung density (+140 H) is considerably less than in normal left lung. These findings suggest that this area ventilates, but at an abnormally slow rate.

D, Time-density analysis from an area of apparently normal lung parenchyma (arrows) adjacent to sequestration also shows a slow and delayed increase in density during exhalation, yielding a curve that is concave upward. Note that this area of lung is qualitatively more lucent than normal anterior right lung.

E, Gross pathologic specimen obtained during partial right lower lobectomy shows multicystic honeycomblike lung that represents sequestration. Note normal lung parenchyma (arrow) adjacent to sequestration.

lung. Ten scans, each with a duration of 100 msec, were obtained in 6 sec, as the patient performed a forced vital capacity maneuver. Time-density analysis graphs and tabulated mean Hounsfield attenuation values were determined for normal and abnormal lung regions for each series of images. Selected lung regions also were visualized and displayed in the ciné-loop mode to show the dynamic processes that occurred during exhalation.

Several areas within the sequestration that contained small cysts showed an increase in attenuation density during exhalation, but this increase was at a delayed rate, and to a lesser degree, than the density increase that was seen in the normal contralateral lung. Several other areas of the sequestration that consisted of small air

cysts showed no increase in density during exhalation. Unexpectedly, a region of lung adjacent to the cystic sequestration, which appeared normal on the HRCT scans obtained during inspiration, showed dynamic CT findings of delayed and diminished increase in density. This region appeared to be transitional between the obvious cystic portion of the sequestration and normal subpleural lung, which showed a normal increase in density during exhalation (Figs. 1B–1D). This transitional lung had normal bronchovascular architecture on HRCT, which suggests that it was not part of the sequestration.

Ultrafast HRCT time-density analysis of the sequestration was done by using the normal contralateral left lung as a control. Although the lung moves cephalad through the scanning plane during exhalation,

tion, this motion was minimal, and the individual images were viewed to ensure that the lung region selected on each slice was substantially the same.

Partial right lower lobectomy was performed, and an intralobar pulmonary sequestration was diagnosed after pathologic examination of the specimen. On gross inspection, the resected specimen (14.0 × 8.0 × 2.3 cm) consisted primarily of thin-walled air-containing cysts, most of which were less than 1 cm in diameter; some cysts were filled with mucin and the largest contained clotted blood. This blood-filled cyst represented the rounded soft-tissue mass seen on the chest radiograph. Histologically, the cysts were lined by airway epithelium and contained rare cartilage elements. No bronchus was identifiable in this part of the specimen. However, some normal lung parenchyma was present in the subpleural region of the resected specimen; this normal lung blended gradually with the cystic abnormal lung, which represented the sequestration (Fig. 1E).

Discussion

It has been suggested that hyperlucent lung parenchyma seen in association with sequestration is the result of air trapping within the sequestration, within large air-containing cysts, or within the adjacent lung [5–7]. In each of these instances, the air trapping presumably occurs because the abnormal lung parenchyma lacks normal bronchial connections and is aerated collaterally [5, 6]. In a recent review, Ikezoe et al. [6] found the presence of lucent or low-attenuation areas of "emphysema" in six of 16 patients with an intralobar sequestration.

Because of the greater contrast and density resolution of CT, the hyperlucent lung associated with sequestrations is better seen on CT scans than on chest radiographs. However, heretofore CT has not clearly shown the relationship of the lucent areas to either cystic regions of the sequestration or to adjacent lung. Ikezoe et al. [6] were unable to show that areas of lucency were associated with small air-containing cysts, but HRCT was not performed in any of their cases, and cyst walls may not have been visible. In our case, the areas of lucency on CT corresponded to areas of the sequestration that contained both small and large air cysts, and these lucent areas also were seen in apparently normal lung at end exhalation.

The cystic portion of the sequestration that we studied showed a delayed and diminished increase in density during exhalation, best shown by using time-density analysis. These findings suggest that communication with the airway occurred in this case, but that an abnormal egress of air, or air trapping, occurred during rapid exhalation; if no communication were present, no change in density or cyst size would be expected during exhalation. Indeed, in several areas of the sequestration, little or no increase in density was measured during exhalation. Because no normal bronchial connection to the sequestration was seen on pathologic examination, we assume that the ability of some parts of the sequestration to ventilate, albeit at a reduced rate, must be because of the presence of anomalous bronchial connections or fistulas.

These features strongly support the hypothesis of air trapping via collateral pathways as the mechanism for the emphysematous parenchyma associated with intralobar pulmonary sequestrations. It is not clear if a previous or ongoing inflammatory process is a prerequisite for the development of these collateral pathways or emphysematous spaces. For example, in smoking-related pulmonary emphysema, a contributing factor to the formation of emphysematous cysts appears to be inflammatory degradation and disruption of elastic fibers in the alveolar walls [8].

Additionally, a region of apparently normal lung adjacent to the sequestration also showed a delayed and diminished increase in density during exhalation. Although we have no pathologic proof, we speculate that this segment of lung, which exhibited abnormal lucency only during exhalation, also must have been trapping air, either because of the mass effect of the sequestration and compression of the segment's subtending airway or as a manifestation of inherently abnormal lung parenchyma that was transitional between the sequestration and normal lung, detectable only with this technique.

The use of ultrafast CT to define the venous drainage of a sequestration has not been previously reported. Although we do not advocate the use of CT angiography in all such cases, the detection of the venous drainage of the sequestration into the left atrium, shown in this case, makes the diagnosis of intralobar sequestration likely. Extralobar sequestrations usually drain via systemic veins into the right atrium and only rarely empty via pulmonary veins.

We conclude that dynamic ultrafast HRCT clearly shows the air trapping that is proposed as a mechanism for the emphysematous changes that occur in association with intralobar sequestrations and that this air trapping occurs both in the sequestration and in adjacent normal-appearing parenchyma. Also, HRCT shows the characteristic multicystic component of pulmonary sequestrations better than conventional CT does, thus aiding in the diagnosis.

REFERENCES

1. Choplin R, Siegel M. Pulmonary sequestration: six unusual presentations. *AJR* 1980;134:695–700
2. Felker R, Tonkin I. Imaging of pulmonary sequestrations. *AJR* 1990;154:241–249
3. Paul D, Mueller C. Case report: pulmonary sequestration. *J Comput Assist Tomogr* 1982;6:163–165
4. Wimbish K, Agha F, Brady T. Bilateral pulmonary sequestration: CT appearance. *AJR* 1983;140:689–690
5. Felson B. Pulmonary sequestration revisited. *Med Radiogr Photogr* 1988;64:1–28
6. Ikezoe J, Murayama S, Godwin JD, Done SL, Verschakelen JA. Bronchopulmonary sequestration: CT assessment. *Radiology* 1990;176:375–379
7. Culiner M, Wall C. Collateral ventilation in intralobar pulmonary sequestration. *Dis Chest* 1965;47:118–122
8. Fukuda Y, Basset F, Soler P, Ferrans VJ, Masugi Y, Crystal RG. Intraluminal fibrosis and elastic fiber degradation lead to lung remodeling in pulmonary Langerhans cell granulomatosis (histiocytosis X). *Am J Pathol* 1990;137:415–424

Bilateral Bronchogenic Cysts

William E. Palmer,¹ S. Mitchell Rivitz, and Felix S. Chew

The esophagogram of a 27-year-old man admitted for evaluation of epigastric pain showed bilateral paraspinous soft-tissue masses (Fig. 1). The masses were sharply margined and homogeneous on CT scans. The structures next to the masses, including the lungs, appeared normal. Both lesions were homogeneous and bright on both T1- and T2-weighted MR images. Percutaneous needle aspiration of the right-sided mass produced mucoid material. At surgery, the masses were found to be completely separate from each other. A tense, mucus-filled, thin-walled cyst was resected from the left side; no hematoma was found. The wall of the cyst was lined by respiratory epithelium and contained cartilage, smooth muscle, and glands. The final pathologic diagnosis was mediastinal bronchogenic cysts.

Because the walls of uncomplicated bronchogenic cysts are relatively thin and are interposed between the cyst contents and the adjacent structures, the imaging characteristics of these lesions are essentially those of the contents of the cyst. Radiographs show a soft-tissue mass, frequently subcarinal, less frequently in other mediastinal locations or within the lung. CT scans show sharp margination and no contrast enhancement. The high protein content of the cystic fluid apparently shortens the T1 sufficiently to result in bright signal

on T1-weighted images [1]. The fluid is also bright on T2-weighted images. When complicated by infection or hemorrhage, various attenuation values on CT [2] and a spectrum of possible signal intensities on MR may be found [1, 3], sometimes with fluid-fluid levels or air-fluid levels. Bright signal on T1-weighted images is uncommon in mass lesions and suggests the specific tissue compositions of fat, subacute hematoma, proteinaceous material, and cells with a high nucleocytoplasmic ratio [1]. A homogeneous appearance and concurrent bright signal on T2-weighted images eliminate fat and subacute hematoma as diagnostic possibilities.

Bronchogenic cysts probably result from aberrant budding of the developing tracheobronchial tree. Adults usually present with asymptomatic masses.

REFERENCES

1. Barakos JA, Brown JJ, Brescia RJ, Higgins CB. High signal lesions of the chest in MR imaging. *J Comput Assist Tomogr* 1989;13:797-802
2. Nakata H, Nakayama C, Kimoto T, et al. Computed tomography of mediastinal bronchogenic cysts. *J Comput Assist Tomogr* 1982;6:733-738
3. Naidich DP, Rumancik WM, Ettenger NA, et al. Congenital anomalies of the lungs in adults: MR diagnosis. *AJR* 1988;151:13-19

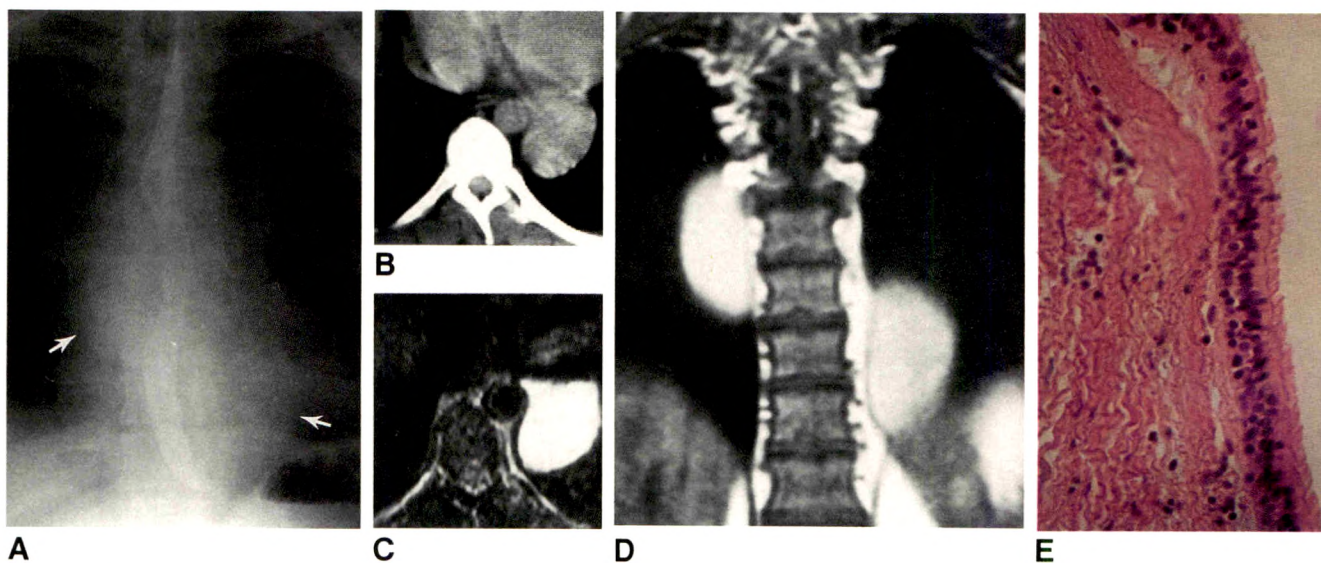


Fig. 1.—Bilateral bronchogenic cysts.

A, Anteroposterior esophagogram shows bilateral paraspinous masses (arrows).

B, CT scan at level of lesion on left side shows sharp margination.

C, T2-weighted axial MR image shows lesion as bright, homogeneous signal.

D, T1-weighted coronal MR image shows bright signal in both lesions.

E, Histologic specimen shows thin wall of cyst lined by ciliated, pseudostratified, columnar, respiratory epithelium (H and E, original magnification $\times 390$).

From the weekly radiologic-pathologic correlation conferences conducted by Jack Wittenberg. Pathology editor: Andrew E. Rosenberg. Radiology editors: Felix S. Chew, Daniel P. Barboriak, William E. Palmer, Daniel I. Rosenthal.

¹ All authors: Department of Radiology, Massachusetts General Hospital and Harvard Medical School, 32 Fruit St., Boston, MA 02114. Address reprint requests to F. S. Chew.

The Radiologic Diagnosis of Barrett Esophagus: Importance of Mucosal Surface Abnormalities on Air-Contrast Barium Studies

Seth N. Glick¹
Steven K. Teplick²
Peter S. Amenta³

Patients with Barrett esophagus are predisposed to the development of esophageal adenocarcinoma. Identification of these patients before this complication develops is essential. We prospectively made the diagnosis of Barrett esophagus on routine biphasic upper gastrointestinal series in nine patients in whom a mucosal surface pattern alteration was the only radiologic abnormality on the esophagogram. The diagnosis was confirmed by biopsy in eight patients and during surgery in one patient. Only a third of the patients had symptoms related to the esophagus. Two types of surface changes were noted. A reticular pattern was present in six cases and a villous pattern in five cases. Both patterns were noted in two patients. This series was obtained in a 5-year interval during which there were 15 additional patients with Barrett esophagus and corresponding esophagograms. None of these patients had normal results on esophagograms.

Recognition of these subtle surface patterns, particularly in the absence of other reflux-induced abnormalities, may improve detection of Barrett esophagus and aid in the selection of patients for subsequent surveillance.

AJR 157:951-954, November 1991

Columnar metaplasia of the esophageal mucosa (Barrett esophagus) associated with gastroesophageal reflux is recognized as a premalignant condition. Definitive diagnosis of Barrett esophagus usually occurs during endoscopic examination of patients with severe symptoms of gastroesophageal reflux or dysphagia from associated stricture. However, many patients do not undergo endoscopic examination unless the characteristic radiologic findings of a midesophageal stricture or a deep ulcer are discovered. A reticular mucosal pattern also has been described [1] as highly predictive of Barrett esophagus, but almost all previously reported cases were associated with the typical abnormalities.

During a 5-year period, we examined nine patients in whom an abnormal mucosal surface pattern was the only structural finding on the esophagogram. In each case, the diagnosis of Barrett esophagus was made prospectively on the basis of the radiographs. Thus, the radiologic sensitivity for Barrett esophagus can be improved by recognition of these features, particularly in the absence of other suggestive findings.

Subjects and Methods

During a 5-year period, a radiologic diagnosis of Barrett esophagus was made in nine patients solely on the basis of detection of an abnormal mucosal surface pattern on air-contrast esophagogram. The patients were six men and three women from 34 to 68 years old (mean, 55 years). Four were younger than 50 years old. Only three (33%) had esophageal symptoms, and in only two of these could the symptoms be directly attributed to reflux (i.e., heartburn or regurgitation). The third patient had hiccups and vague chest discomfort. The remaining six (66%) patients were being studied for nonesophageal signs or symptoms,

Received April 15, 1991; accepted after revision June 6, 1991.

¹ Department of Diagnostic Radiology, Hahnemann University Hospital, Broad and Vine Sts., Philadelphia, PA 19102. Address reprint requests to S. N. Glick.

² Department of Diagnostic Radiology, University of Arkansas for Medical Science, 4301 W. Markham, Little Rock, AR 72205.

³ Department of Pathology, Robert Wood Johnson University—University of Medicine and Dentistry of New Jersey, 1 Robert Wood Johnson Place, New Brunswick, NJ 08903-0019.

0361-803X/91/1575-0951

© American Roentgen Ray Society

including upper abdominal pain or discomfort (five cases) and anemia with indigestion (one case).

The esophagus was evaluated as part of the routine biphasic upper gastrointestinal series. The studies were interpreted by one radiologist with a special interest in gastrointestinal radiology. Two distinct types of surface patterns were noted. The first was a reticular pattern similar to that reported by Levine et al. [1]. This pattern was present in six patients and it appeared as a coarse network of intersecting lines of barium producing an angular or round mosaic configuration (Fig. 1A). The other pattern, which has not been described before, was termed the villous pattern. This was noted in five patients and it appeared as tiny, uniform, confluent, round lucencies, similar to the villi of the duodenum (Fig. 1B). Both patterns were shown in two patients.

Eight of the nine patients had endoscopy and biopsy performed within 1 month of the barium study. In the remaining patient, esophageal adenocarcinoma developed 9 months later, and Barrett mucosa was found adjacent to the neoplasm (Figs. 2A and 2B). No false-positive radiologic diagnoses of Barrett esophagus were made on the basis of these criteria.

The pathology records were reviewed in order to determine all of the cases of Barrett esophagus diagnosed by biopsy during this 5-year interval. Twenty-two cases were noted, and 15 had esophagograms obtained before this disease was documented. The films and initial reports of these studies were reviewed to determine the prevalence of isolated mucosal abnormalities and to ascertain whether inclusion of this group of patients affected our overall sensitivity for the diagnosis of Barrett esophagus.

The radiographs were obtained by using air-contrast technique after the patient had ingested E-Z HD barium (250% w/v, E-Z-EM, Inc., Westbury, NY) and E-Z Gas (E-Z-EM, Inc.). Studies were performed with high-speed, double-contrast, blue-sensitive film and mr 400 rare-earth screens (Agfa Corp., Ridgefield Park, NJ). The focal spot of the fluoroscopic equipment varied from 0.3 mm to 1.2 mm, but in most of the cases was 0.6 mm.

Results

In all six patients in whom the villous pattern was seen, the distal 5 cm of the esophagus was involved in a diffuse (four cases) or circumscribed (two cases, Fig. 3) manner. In three of the four in whom the changes were diffuse, they extended proximally to the level of the carina. The reticular pattern was confined to the mid esophagus and was focal in two of the

five patients in whom it occurred (Fig. 4). In two other patients, this pattern was present in the mid esophagus but extended throughout the esophagus, including the distal portion in both. In one patient, the reticular pattern was isolated to the distal 5 cm of the esophagus. In the two patients in whom both patterns were present, the villous pattern was located distal to the reticular pattern. In two patients with the diffuse villous pattern, fine linear striations parallel to the long axis of the esophagus were noted when the esophagus was slightly less distended (Fig. 5). All of the patients had marked gastroesophageal reflux. The region of the lower esophageal sphincter was patulous in all cases. A hiatal hernia was noted in only two patients, but maneuvers to show this were not done.

The endoscopic results suggested Barrett esophagus in all eight cases. In four patients, this was the only abnormality observed. Two patients had mild friability or erythema, and the remaining two patients each had one superficial erosion. Biopsy in each case showed columnar metaplasia. A review of the histologic subtypes revealed five patients with both the intestinal and cardia types, one of whom had high-grade dysplasia. Two patients had only the cardia type, and one patient had the intestinal type. In the patient with adenocarcinoma, only the fundal type was present; however, the possibility that the other types had been obliterated by the malignant process could not be excluded.

Fifteen additional patients with histologically proved Barrett esophagus had recent prior esophagograms. Five (33%) of these patients had midesophageal strictures, and the accurate prospective diagnosis of Barrett esophagus was made. The remaining 10 patients had esophagitis and/or distal stricture on the barium study. Thus, patients with isolated abnormalities of surface pattern constituted 38% of all patients with Barrett esophagus. The overall radiologic sensitivity for this diagnosis was 58%, and no patient with Barrett esophagus had a normal esophagus. All had either abnormal surface patterns or reflux-induced pathologic changes.

Discussion

The concept that Barrett esophagus is a sequela of gastroesophageal reflux and that patients with this condition are predisposed to the development of adenocarcinoma of the

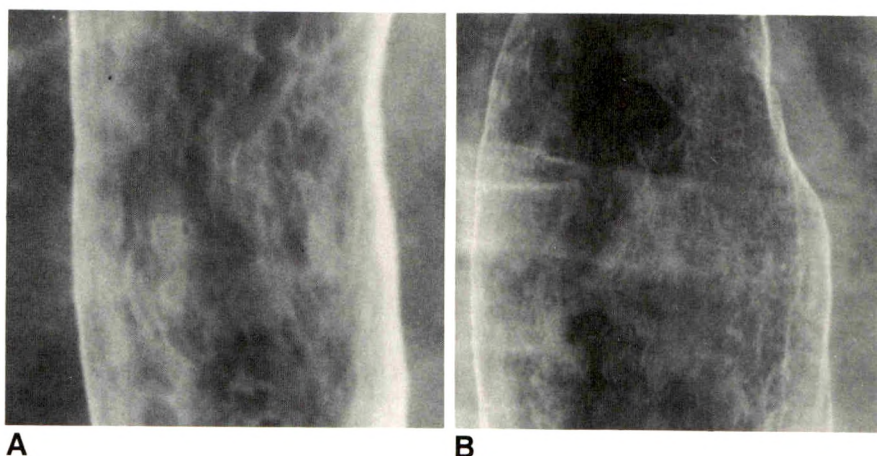


Fig. 1.—A, Reticular pattern. Air-contrast esophagogram of 48-year-old man with discomfort in right upper quadrant shows a network of intersecting lines of barium in mid esophagus, producing angular and round mosaic pattern. These changes extended to gastroesophageal junction. Biopsy showed columnar epithelium of cardia type.

B, Villous pattern. 68-year-old woman with anemia. Air-contrast esophagogram at level of left main bronchus shows diffusely distributed, tiny, confluent, round lucencies resembling villi of small intestine. Both specialized and cardia types of Barrett mucosa were noted on biopsy.

Fig. 2.—A, 65-year-old man with hiccups and vague discomfort in chest. A fine villous pattern was noted in distal esophagus on air-contrast study. Barrett esophagus was suggested, and endoscopy was recommended but not performed.

B, 9 months later, patient returned with dysphagia, and an esophagogram showed an ulcerating mass just proximal to gastroesophageal junction. Resected specimen showed infiltrating adenocarcinoma with adjacent fundal-type columnar mucosa. Superficial carcinoma was most likely present when first study was done.

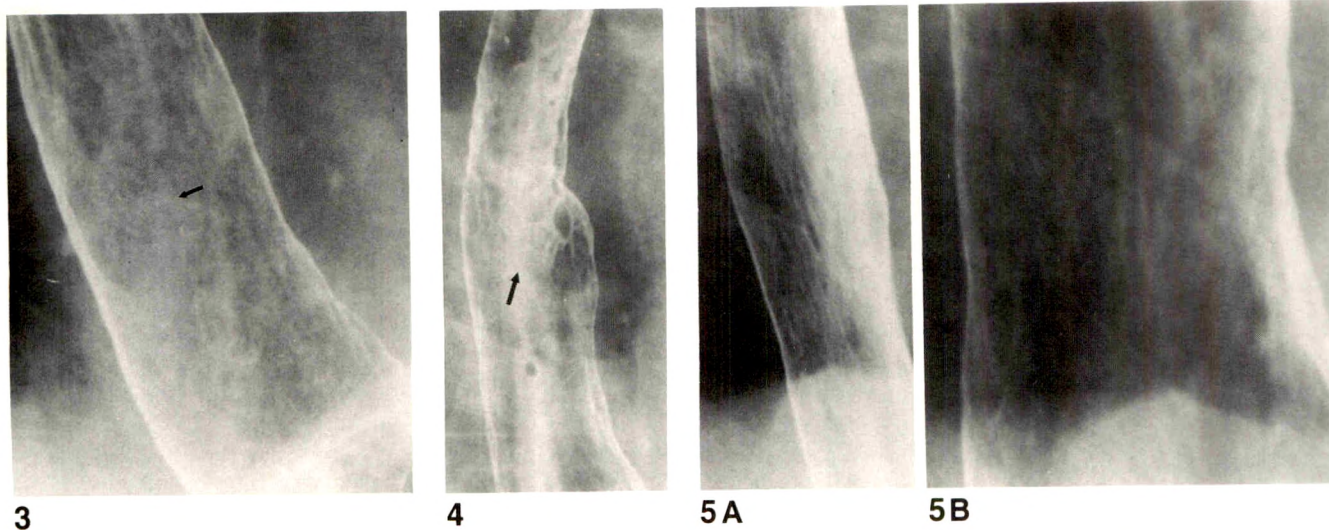
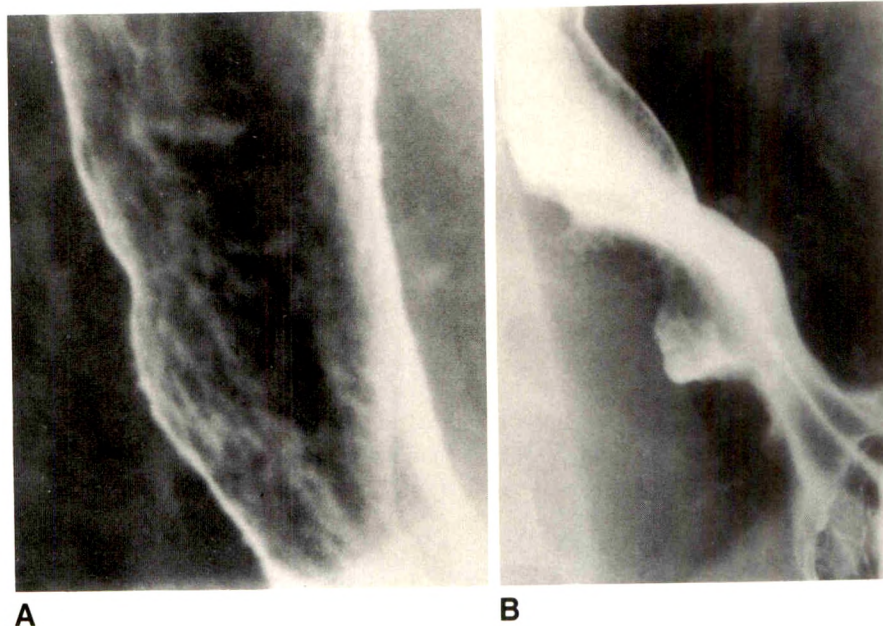


Fig. 3.—50-year-old woman with periumbilical discomfort. Villous pattern is identified on air-contrast study as a focal patch (arrow) just proximal to gastroesophageal junction. Remainder of esophagus appeared normal. Biopsy showed specialized-type columnar mucosa.

Fig. 4.—62-year-old man with a 6-month history of heartburn. Air-contrast esophagogram shows reticular pattern (arrow) confined to mid esophagus. Patient also had a focal villous patch (not seen here) just proximal to gastroesophageal junction. No other abnormalities were seen. Specialized and cardia types of Barrett epithelium were seen on biopsy.

Fig. 5.—Air-contrast esophagograms of a 34-year-old man with pain across upper abdomen.
A, With slight underdistension, villous pattern may manifest as fine linear striations parallel to longitudinal axis of esophagus. This should not be confused with longitudinal folds.
B, With further distension, villous pattern can be readily seen, producing a velvety texture to normally smooth esophageal surface. Biopsy showed specialized columnar epithelium.

esophagus is well established. The cost-effectiveness of routine endoscopic surveillance of these patients is controversial, and the value of this approach depends on the magnitude of the risk of malignant degeneration. Although initial retrospective studies reported a low incidence of malignant transformation, prospective studies have found an annual incidence of 1–2% [2, 3]. Although the issue of cost-effectiveness

remains to be clarified, detection of Barrett esophagus and surveillance before the development of carcinoma can result in a greater number of curable malignant lesions.

Unfortunately many cases of Barrett esophagus go undetected. The prevalence of this condition in the general population may be much greater than predicted from clinical records. Cameron et al. [4] compared the number of cases found

at autopsy with the number of clinically diagnosed cases in a defined population and determined that the prevalence of unrecognized cases was 20 times greater than the number of patients who had diagnostic investigation. This may be related to the fact that reflux symptoms are frequently treated empirically. However, in many patients, signs and symptoms of reflux are minimal or nonexistent. Approximately 20–40% of patients with Barrett esophagus do not have reflux symptoms or even symptoms that suggest esophageal disease [5, 6]. It is not surprising that in patients with adenocarcinoma in Barrett esophagus a history of reflux symptoms is absent in 23–58% (mean, 36%) [7, 8]. Our finding of classic reflux symptoms in only two of our nine cases is consistent with these data. In addition, two of our nine patients had malignant or premalignant changes in the absence of signs or symptoms or significant inflammatory pathologic changes.

Although endoscopy with biopsy has a major role in the management of patients with Barrett esophagus, initial detection requires appropriate selection for this procedure. The value of barium studies is unclear. A prospective radiologic diagnosis of Barrett esophagus by using suggestive criteria is possible in only 25–45% of cases [9, 10]. However, it has been shown that the barium study is highly sensitive in detecting reflux-induced pathologic changes that are severe enough to be associated with Barrett esophagus [9, 11]. When nonspecific reflux esophagitis and/or scarring is included with the characteristic appearances, more than 95% of cases of Barrett esophagus can be detected. It is extremely rare for Barrett esophagus to be overlooked when esophagographic findings are normal, making this study an effective tool for predicting which patients can benefit from endoscopy. In one study, 58% of patients with reflux symptoms would have been spared the more invasive procedure [11].

We describe two types of mucosal surface patterns that not only are highly predictive for Barrett esophagus but also may be the only structural abnormalities visible on the barium study. The villous pattern has not been described before. The reticular pattern was initially reported by Levine et al. [1] and has been seen in 5–30% [1, 9, 12–14] of patients with Barrett esophagus. The specificity of this finding has been questioned [12], but this discrepancy may represent differences in interpretation. In previous reports, the reticular pattern has almost always been associated with other radiologic abnormalities suggestive of Barrett esophagus. Thus, while further supporting the diagnosis, detection of a reticular pattern under these circumstances would not significantly improve the yield even if the more liberal screening criteria were used. However, the study of Gilchrist et al. [11] included only patients with reflux symptoms, and patients with reflux symptoms and/or dysphagia may be more likely to have other findings. This is supported by the presence of classic reflux symptoms in only 22% of our patients.

The histologic basis for these mucosal surface patterns remains obscure. Levine et al. [1] suggested that the reticular pattern may represent specialized columnar epithelium. Specialized epithelium was present in 75% of our patients (excluding the patient with carcinoma). However, specialized epithelium is the most common histologic subtype and is found in a similar percentage of patients with Barrett esoph-

agus. Furthermore, it is impossible to correlate the biopsy sites precisely with the location of the radiologic surface pattern in all cases, although in those patients with a diffuse distribution, such an association could be assumed. Specialized epithelium may be the only type present or may occur in conjunction with the other types. In the latter setting, it is invariably found most proximally in the esophagus. We noted a tendency for the reticular pattern to be located more proximally than the villous pattern, but whether this is related to histologic differences between the two patterns is unknown.

Radiologic studies can make a significant contribution through the appropriate selection of patients for endoscopy. Although implementation of the criteria of Gilchrist makes the value of a specific radiologic diagnosis of Barrett esophagus less crucial, not all patients with nonspecific reflux-related abnormalities, especially when signs and symptoms are minimal, will be referred for endoscopy. A more definitive radiologic diagnosis may provide the impetus for aggressive management. Furthermore, recognition of an abnormal surface pattern on a barium study as the sole structural abnormality, particularly as an incidental observation not obviously related to the indication for the examination, should improve the detection of a condition whose prevalence is greater than generally is recognized.

REFERENCES

1. Levine MS, Kressel HY, Caroline DF, Laufer I, Herlinger H, Thompson JJ. Barrett esophagus: reticular pattern of the mucosa. *Radiology* 1983;147:663–667
2. Hameeteman W, Tytgat GN, Houthoff HJ, van den Tweel JG. Barrett's esophagus: development of dysplasia and adenocarcinoma. *Gastroenterology* 1989;96:1249–1256
3. Robertson CS, Mayberry JF, Nicholson DA, James PD, Atkinson M. Value of endoscopic surveillance in the detection of neoplastic change in Barrett's oesophagus. *Br J Surg* 1988;75:760–763
4. Cameron AJ, Zinsmeister AR, Ballard DJ, Carney JA. Prevalence of columnar-lined Barrett's esophagus: comparison of population-based clinical and autopsy findings. *Gastroenterology* 1990;99:918–922
5. Cooper BT, Barbezat GO. Barrett's oesophagus: a clinical study of 52 patients. *Q J Med* 1987;62:97–108
6. Kerlin P, D'Mellow G, Van Deth A. Barrett's esophagus: clinical, endoscopic, and histologic spectrum in fifty patients. *Aust N Z J Med* 1986;16:198–205
7. Saubier EC, Goullat C, Samaniego C, Guillaud M, Moulinier B. Adenocarcinoma in columnar-lined Barrett's esophagus: analysis of 13 esophagectomies. *Am J Surg* 1985;150:365–369
8. Witt TR, Bains MS, Zaman MB, Martini N. Adenocarcinoma in Barrett's esophagus. *J Thorac Cardiovasc Surg* 1983;85:337–345
9. Chen YM, Gelfand DW, Ott DJ, Wu WC. Barrett esophagus as an extension of severe esophagitis: analysis of radiologic signs in 29 cases. *AJR* 1985;145:275–281
10. Winters C, Spurling TJ, Chobanian SJ, et al. Barrett's esophagus: a prevalent, occult complication of gastroesophageal reflux disease. *Gastroenterology* 1987;92:118–124
11. Gilchrist AM, Levine MS, Carr RF, et al. Barrett's esophagus: diagnosis by double-contrast esophagography. *AJR* 1988;150:97–102
12. Vincent ME, Robbins AH, Spechler SJ, Schwartz R, Doos WG, Schimmel EM. The reticular pattern as a radiographic sign of the Barrett esophagus: an assessment. *Radiology* 1984;153:333–335
13. Shapir J, DuBrow R, Frank P. Barrett oesophagus: analysis of 19 cases. *Br J Radiol* 1985;58:491–493
14. Agha FP. Radiologic diagnosis of Barrett's esophagus: critical analysis of 65 cases. *Gastrointest Radiol* 1986;11:123–130

Disseminated Histoplasmosis: Abdominal CT Findings in 16 Patients

D. Randall Radin¹

Since the onset of the AIDS epidemic, disseminated *Histoplasma capsulatum* infection has been reported with much greater frequency in both endemic and nonendemic areas. Abdominal CT scans of 16 patients with disseminated histoplasmosis were reviewed retrospectively to identify radiologic features of this disease. The diagnosis was confirmed by autopsy (three patients), bone marrow biopsy (10 patients), lymph node biopsy (three patients), bronchoscopic biopsy (three patients), liver biopsy (two patients), and/or colonoscopic biopsy (one patient). Fourteen patients had serologic evidence of human immunodeficiency virus infection. Disseminated histoplasmosis was either the only initial manifestation of AIDS (seven patients) or was accompanied simultaneously by cytomegalovirus infection (four patients), or Kaposi sarcoma, *Toxoplasma* encephalitis, or cryptosporidiosis (one patient each). Abdominal CT findings included hepatomegaly (63%); splenomegaly (38%); diffuse splenic hypoattenuation (19%); bilateral adrenal enlargement or hypoattenuating masses (13%); and enlarged lymph nodes with homogeneous soft-tissue density (44%), diffuse or central low density (13%), or both (19%).

Histoplasmosis should be included in the differential diagnosis when abdominal CT scans show such nonspecific findings as hepatomegaly, splenomegaly, enlarged soft-tissue-density or hypoattenuating lymph nodes, or adrenal enlargement or masses in an immunodeficient patient. An uncommon but possibly specific CT finding in histoplasmosis is diffuse splenic hypoattenuation.

AJR 157:955-958, November 1991

Histoplasmosis is the most common systemic fungal disease in the United States [1]. Primary pulmonary infection results from inhalation of airborne spores of *Histoplasma capsulatum* [2]. Progression to disseminated infection is uncommon, occurring in one of 2000-5000 cases and usually involving infants, the elderly, or patients with impaired cellular immunity [1]. Since 1984, disseminated histoplasmosis has been reported with increasing frequency in patients with AIDS, first in the central United States, where histoplasmosis is endemic, and then in New York and California, where the AIDS epidemic is concentrated [3]. In 1987, disseminated histoplasmosis was added to the list of diseases that indicate a diagnosis of AIDS in patients with laboratory evidence for infection with human immunodeficiency virus (HIV) [4]. Abdominal CT findings in 16 patients with disseminated histoplasmosis, 14 of whom also had AIDS, are the subject of this report.

Materials and Methods

According to mycology laboratory records at our hospital, cultures of specimens from lymph node biopsies, bone marrow biopsies, or blood yielded *H. capsulatum* in 45 patients between April 1984 and April 1991. In 16 of the 45 patients, an abdominal CT examination done within 2 weeks of the date on which the biopsy with positive results was performed was available. Medical records and chest radiographs of these 16 patients were reviewed.

All 16 patients were men 24-64 years old (average, 40 years). None of the patients were born in Los Angeles. They had moved from Mexico (seven patients), Central America (six

Received June 5, 1991; accepted after revision July 10, 1991.

¹ Department of Radiology, University of Southern California School of Medicine, Los Angeles County-USC Medical Center, 1200 N. State St., Los Angeles, CA 90033-1084. Address reprint requests to D. R. Radin.

0361-803X/91/1575-0955
© American Roentgen Ray Society

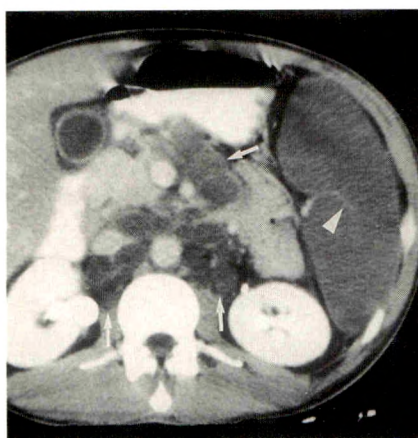


Fig. 1.—CT scan shows enlarged spleen of homogeneous low density. Enhancing vessels (arrowhead) course through splenic parenchyma. Multiple enlarged lymph nodes of diffuse homogeneous low density (arrows) are seen in retroperitoneum and mesentery. Blood culture, bone marrow biopsy, and submandibular lymph node biopsy yielded *Histoplasma capsulatum*.



Fig. 2.—CT scan shows massively enlarged spleen of decreased density filling most of left side of abdomen. Smaller area of relatively lower density in lateral aspect of spleen represents infarct. Bilateral low-density adrenal masses (arrows) are seen. Inferior vena cava is compressed by right adrenal mass. Blood culture, bone marrow biopsy, and cervical lymph node biopsy specimens grew *Histoplasma capsulatum*.

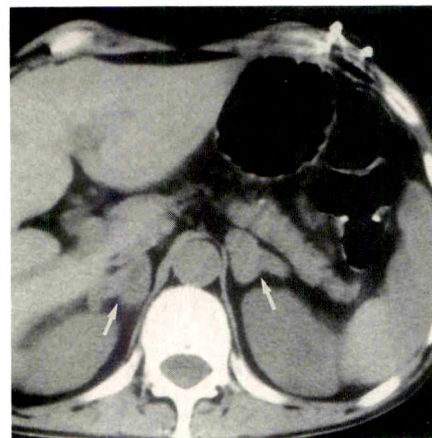


Fig. 3.—CT scan shows marked enlargement of right and left adrenal glands (arrows).

patients), or Ecuador, Ohio, or Vietnam (one patient each). Fourteen of the 15 patients tested had serologic evidence of HIV infection. A 64-year-old Vietnamese man with no known risk factor was not tested for antibodies to HIV. HIV risk factors in the 14 seropositive patients were homosexuality (10 patients), IV drug use (one patient), or unknown (three patients). Although none of the patients had a previous AIDS-defining illness, a concurrent diagnosis of cytomegalovirus infection (four patients) or Kaposi sarcoma, *Toxoplasma* encephalitis, or cryptosporidiosis (one patient each) was made in half of the HIV-seropositive patients with histoplasmosis. The most common complaints were fever (11 patients); weight loss (nine patients); abdominal pain (five patients); and diarrhea, cervical lymphadenopathy, cough, and dyspnea (four patients each).

CT examinations of the 16 patients were performed on a Picker 1200 SX scanner. Slices 10-mm thick were obtained at 10- or 15-mm intervals. IV contrast medium was administered in all but three cases. The studies were reviewed retrospectively and evaluated for liver and spleen size; the presence of visceral lesions and ascites; and the location, size, and density of abdominal lymph nodes.

Three patients died within 2 weeks of the CT examination. Autopsy results showed that histoplasmosis involved lung, liver, spleen, and lymph nodes in all three patients; and bone marrow, small bowel, colon, adrenal gland, kidney, pancreas, and gallbladder in one patient each. In the other 13 patients, biopsy-proved sites of *Histoplasma* infection were bone marrow (10 patients), lung (three patients), lymph node (three patients), liver (two patients), and colon (one patient). Two patients with bilateral adrenal masses had evidence of adrenal insufficiency but no pathologic confirmation.

Results

CT showed hepatomegaly in 10 (63%) and splenomegaly in six (38%) of the 16 patients. Enlargement of the liver was mild (cephalocaudal span of 19–21 cm) in eight patients (50%) and marked (cephalocaudal span of 24–25 cm) in two patients

(13%). Splenic enlargement was moderate (cephalocaudal span of 16–17 cm) in three patients (19%) and massive (cephalocaudal span of 22–26 cm) in three patients (19%). In all six patients with splenomegaly, the liver also was enlarged. In six patients (38%), neither the liver nor the spleen was enlarged.

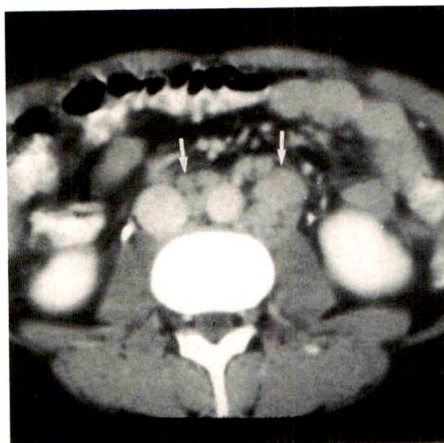
No focal or diffuse abnormality in hepatic attenuation was seen in any of the 16 patients, including five patients with biopsy or autopsy proof of hepatic histoplasmosis. In three of the six patients with splenomegaly, the spleen was diffusely decreased in attenuation, measuring at least 30 H less than the liver (Figs. 1 and 2). Enhancing vessels were seen within the hypoattenuating splenic parenchyma in all three cases. In two of these three patients and in the other three patients with splenomegaly, one or more splenic infarcts were present. No splenic abnormality was seen in the 10 patients with normal-sized spleens (cephalocaudal span of 9–13 cm).

Two patients with adrenal insufficiency had bilateral adrenal abnormalities—hypoattenuating masses in one (Fig. 2) and marked diffuse enlargement in the other (Fig. 3). No renal, pancreatic, biliary, or gastrointestinal abnormality was seen in any of the 16 patients. A small volume of ascites was present in three patients (19%).

Enlarged abdominal lymph nodes 1–2 cm in diameter were seen in 12 (75%) of the 16 patients. Sites of lymphadenopathy included retroperitoneum, mesentery, retrocrural space, gastrohepatic ligament, and porta hepatis. In seven patients, all of the enlarged nodes were of homogeneous soft-tissue density (Fig. 4). Five patients had enlarged nodes with diffuse or central low density (Figs. 1 and 5). Enlarged soft-tissue-density nodes also were present in three of these patients.

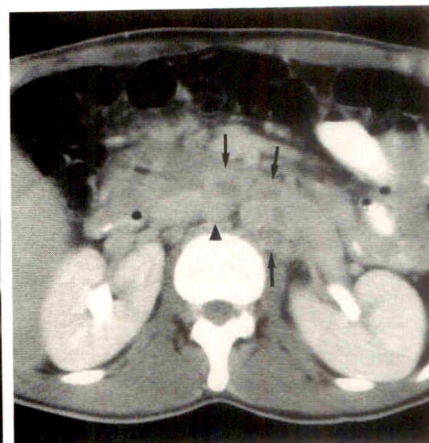
No abdominal visceral or nodal calcification was seen in any of the 16 patients. In two patients (13%), abdominal CT

Fig. 4.—CT scan shows enlarged paraaortic lymph nodes of homogeneous soft-tissue density (arrows). Blood culture and bone marrow biopsy yielded *Histoplasma capsulatum*. No evidence of other infection or neoplasm was seen.



4

Fig. 5.—CT scan shows enlarged paraaortic lymph nodes with central low density (arrows). Homogeneous lymph node of soft-tissue density (arrowhead) is also seen between aorta and inferior vena cava. *Histoplasma capsulatum* was obtained by bronchoscopic biopsy and biopsy of cervical lymph nodes. Follow-up chest radiograph after treatment with amphotericin B showed resolution of enlarged mediastinal lymph nodes.



5

showed no abnormality. Findings on the chest radiograph were normal in seven of the 16 patients, including two patients with autopsy proof of pulmonary histoplasmosis. In only one patient was there evidence of previous granulomatous disease, consisting of several small calcified apical nodules. In one patient with pulmonary infiltrates, bronchoscopic biopsy showed *Aspergillus fumigatus*. Radiographs of the remaining seven patients showed diffuse nodular or reticulonodular pulmonary infiltrates, accompanied by mediastinal lymphadenopathy in three cases. In four of these seven patients, biopsy or autopsy proof of pulmonary histoplasmosis was available.

Discussion

Evidence suggests that the occurrence of disseminated histoplasmosis in nonendemic regions such as California and New York is due to endogenous reactivation in immunodeficient patients with remote exposure in highly endemic areas, such as the central United States or Central America [2, 3, 5]. However, radiologic evidence of previous infection (i.e., pulmonary, nodal, hepatic, or splenic calcification) was absent in 15 of the 16 patients in this series.

Of the 14 HIV-seropositive patients in this series, disseminated histoplasmosis was initially the only AIDS-defining disease in seven patients and was accompanied simultaneously by a second AIDS-defining disease in seven patients. This finding echoes reports from endemic areas, in which disseminated histoplasmosis was the AIDS-defining illness or occurred shortly after the diagnosis of AIDS [3, 6].

Findings on chest radiographs in this series were similar to those previously reported [3, 5, 6]. The lungs may be clear or may show diffuse small nodules, suggesting miliary tuberculosis, or diffuse reticulonodular infiltrates, suggesting *Pneumocystis carinii* pneumonia. Hilar and mediastinal lymph node enlargement is seen occasionally.

Reports of abdominal CT findings in disseminated histoplasmosis are few. Nonspecific enlargement of retroperitoneal and mesenteric lymph nodes was seen in one patient with AIDS and CT-guided needle-biopsy proof of histoplasmosis

[7]. In a second patient with AIDS and open-biopsy proof of histoplasmosis, CT showed fine nodularity and strands in the omentum and mesentery [8].

In most patients in this series, abdominal CT findings were abnormal but nonspecific. Hepatomegaly was mild (cephalocaudal span of 19–21 cm) in 50% of cases and marked (cephalocaudal span of 24–25 cm) in 13% of cases. Splenomegaly was moderate to massive (cephalocaudal span of 16–26 cm) in 38% of cases. Mild hepatomegaly and splenomegaly are common in patients with AIDS and are not useful features for differentiating among the various infectious and neoplastic complications of AIDS. However, moderate to massive enlargement of the liver and spleen is less common. Slight hepatomegaly was seen in 19% of 31 patients with AIDS-related Kaposi sarcoma [9]; splenomegaly was present in 65% of these 31 patients, but the degree of splenic enlargement was not described. Hepatomegaly is common in patients with AIDS-related lymphoma but is usually associated with focal hepatic lesions [10]. Splenomegaly was reported in 84% of 19 patients with AIDS-related lymphoma, but the degree of splenic enlargement was not noted [11]. Marked hepatomegaly and marked splenomegaly were seen in 20% and 14%, respectively, of 44 patients with AIDS and disseminated *Mycobacterium avium-intracellulare* infection but in none of 27 patients with AIDS and disseminated *M. tuberculosis* infection [12]. Thus, the differential diagnosis of marked homogeneous enlargement of the liver and spleen in a patient with AIDS includes lymphoma, *M. avium-intracellulare* infection, and histoplasmosis. However, a unique finding in 19% of the 16 patients in this series was diffuse hypoattenuation of the spleen. Pathologic correlation in one case and CT demonstration of enhancing intrasplenic vessels in all three cases indicated that the hypoattenuation was not due to splenic infarction.

Enlargement of abdominal lymph nodes was common in this series, occurring in 75% of the 16 patients. Adenopathy of homogeneous soft-tissue density was slightly more common than nodes with diffuse or central low density. The differential diagnosis of soft-tissue-density lymphadenopathy in a patient with HIV infection includes lymphoma, Kaposi

sarcoma, lymphadenopathy syndrome, and *M. avium-intracellulare* infection in addition to histoplasmosis [12]. The other major cause of low-density adenopathy in patients with AIDS is mycobacterial infection, occurring in 93% of patients with *M. tuberculosis* infection and 14% of patients with *M. avium-intracellulare* infection in one large series [12].

Bilateral adrenal enlargement or masses were seen in only two patients, one of whom was HIV-seronegative. CT demonstration of adrenal masses has not been reported in large series of patients with AIDS-related lymphoma [11], Kaposi sarcoma [9], or disseminated mycobacterial infection [12]. However, bilateral adrenal masses were shown by sonography in one patient with AIDS-related lymphoma [13]. The CT appearance of bilateral adrenal enlargement or hypoattenuating masses in our two patients is similar to that reported in several patients with disseminated histoplasmosis in an endemic area who had risk factors other than AIDS [14].

It seems likely that the abnormal CT findings in the patients in this series were due to histoplasmosis. Only one of the 16 patients had an additional AIDS-related disease (Kaposi sarcoma) that is occasionally associated with some of these findings.

In conclusion, histoplasmosis should be included in the differential diagnosis when chest radiographs show a diffuse nodular or reticulonodular pattern and when abdominal CT scans show marked hepatomegaly, marked splenomegaly, enlarged soft-tissue-density or hypoattenuating lymph nodes, or adrenal enlargement or masses in an immunodeficient patient. An uncommon but possibly specific CT finding in histoplasmosis is diffuse splenic hypoattenuation. Awareness of the radiologic findings of histoplasmosis is important because, as the AIDS epidemic continues, an increasing number

of cases will be encountered in both endemic and nonendemic areas.

REFERENCES

1. Wheat JL. Histoplasmosis. *Infect Dis Clin North Am* **1988**;2:841-859
2. Davies SF. Histoplasmosis: update 1989. *Semin Respir Infect* **1990**;5:93-104
3. Sarosi GA, Johnson PC. Progressive disseminated histoplasmosis in the acquired immunodeficiency syndrome: a model for disseminated disease. *Semin Respir Infect* **1990**;5:146-150
4. Centers for Disease Control. Revision of the CDC surveillance case definition for acquired immunodeficiency syndrome. *MMWR* **1987**;36[suppl 1S]:3S-15S
5. Salzman SH, Smith RL, Aranda CP. Histoplasmosis in patients at risk for the acquired immunodeficiency syndrome in a nonendemic setting. *Chest* **1988**;93:916-921
6. Nightingale SD, Parks JM, Pounders SM, Burns DK, Reynolds J, Hernandez JA. Disseminated histoplasmosis in patients with AIDS. *South Med J* **1990**;83:624-630
7. Megibow AJ, Balthazar EJ, Hulnick DH. Radiology of nonneoplastic gastrointestinal disorders in acquired immune deficiency syndrome. *Semin Roentgenol* **1987**;22:31-41
8. Alterman DD, Cho KC. Histoplasmosis involving the omentum in an AIDS patient: CT demonstration. *J Comput Assist Tomogr* **1988**;12:664-665
9. Moon KL Jr, Federle MP, Abrams DI, Volberding P, Lewis BJ. Kaposi sarcoma and lymphadenopathy syndrome: limitations of abdominal CT in acquired immunodeficiency syndrome. *Radiology* **1984**;150:479-483
10. Townsend RR. CT of AIDS-related lymphoma. *AJR* **1991**;156:969-974
11. Nyberg DA, Jeffrey RB Jr, Federle MP, Bottles K, Abrams DI. AIDS-related lymphomas: evaluation by abdominal CT. *Radiology* **1986**;159:59-63
12. Radin DR. Intraabdominal *Mycobacterium tuberculosis* vs *Mycobacterium avium-intracellulare* infections in patients with AIDS: distinction based on CT findings. *AJR* **1991**;156:487-491
13. Townsend RR, Laing FC, Jeffrey RB Jr, Bottles K. Abdominal lymphoma in AIDS: evaluation with US. *Radiology* **1989**;171:719-724
14. Wilson DA, Muchmore HG, Tisdal RG, Fahmy A, Pitha JV. Histoplasmosis of the adrenal glands studied by CT. *Radiology* **1984**;150:779-783

Primary Sclerosing Cholangitis: Value of Cholangiography in Determining the Prognosis

Daniel A. Craig¹
Robert L. MacCarty¹
Russell H. Wiesner²
Patricia M. Grambsch³
Nicholas F. LaRusso²

We studied cholangiograms in 129 patients with primary sclerosing cholangitis (PSC) to determine if there was a correlation between any of the findings and the prognosis of the disease. The grade, length, and extent of strictures, the degree of bile duct dilatation, and the distribution of lesions were evaluated. Survival curves were generated to test the association of these radiologic signs with subsequent survival. High-grade intrahepatic duct strictures (>75% narrowing) were associated with a 19% decrease in 3-year survival ($p = .05$) compared with lower-grade strictures. Diffuse intrahepatic strictures (involving >25% of the ducts) were associated with a 16% decrease in 3-year survival ($p = .012$) compared with localized strictures. Statistically insignificant ($p > .05$) but measurable decreases in survival were observed with high-grade extrahepatic duct strictures, diffuse involvement of the extrahepatic ducts, long confluent strictures anywhere in the biliary tree, and marked dilatation of the intrahepatic ducts. In general, intrahepatic duct disease was found to have greater prognostic significance than extrahepatic duct disease.

High-grade strictures and diffuse strictures of the intrahepatic ducts were found to be indicators of a poor prognosis in PSC and were more predictive of a poor prognosis than was extrahepatic duct disease.

AJR 157:959-964, November 1991

Primary sclerosing cholangitis (PSC) is a chronic cholestatic disease of unknown cause. It is characterized by chronic fibrosing inflammation of the bile ducts and generally leads to bile duct obliteration and biliary cirrhosis [1-6]. This progression is insidious and unpredictable. There is no known effective medical therapy [5, 7, 8]. Seventy percent of patients with PSC have inflammatory bowel disease, usually ulcerative colitis. However, the relationship is probably a shared cause rather than one disease causing the other [6]. Treatment for inflammatory bowel disease has not been shown to influence the activity of PSC [6]. Biliary drainage procedures provide palliative treatment at best [5, 9]. Orthotopic liver transplantation currently provides the greatest hope for a possible cure for this enigmatic disease [8].

Cholangiography is the gold standard for diagnosing PSC in the proper clinical setting [7]. In this study, we reviewed the initial cholangiograms in a large group of patients with well-established PSC. Our goal was to determine retrospectively whether any cholangiographic features are useful in predicting clinical outcome. This information should be useful in treating patients (e.g., in planning the timing for liver transplantation or in determining the usefulness of surgery or balloon dilatation for a dominant extrahepatic duct stricture) and in counseling patients and stratifying patients for therapeutic trials.

Materials and Methods

Using our prospective clinical trials of medical therapy and the computerized record system in our institution, we identified 174 patients between 1970 and 1984 who met the clinical,

Received March 21, 1991; accepted after revision June 17, 1991.

¹ Department of Diagnostic Radiology, Mayo Clinic and Mayo Foundation, 200 First St., S. W., Rochester, MN 55905. Address reprint requests to R. L. MacCarty.

² Division of Gastroenterology and Internal Medicine, Mayo Clinic and Mayo Foundation, 200 First St. S. W., Rochester, MN 55905.

³ Section of Biostatistics, Mayo Clinic and Mayo Foundation, 200 First St. S. W., Rochester, MN 55905.

0361-803X/91/1575-0959
© American Roentgen Ray Society

biochemical, radiologic, and histologic criteria for the diagnosis of PSC. Patients with evidence of cholangiocarcinoma were excluded. Of these patients, 129 had cholangiograms on file that had been obtained within 1 year of their presentation at our institution. Cholangiograms from the remaining 45 patients were not available for review, and this group of patients was not included in the study. The final study group consisted of 83 men and 46 women. The mean age was 42 years, with a range from 18 to 71 years.

The starting point for follow-up was the date of the cholangiogram used for the initial diagnosis at our institution. Many patients had a previous diagnosis of PSC or a misdiagnosis of another hepatobiliary disease before coming to our institution. Most patients were seen for follow-up care at our institution. For the remainder, follow-up data were obtained from questionnaires completed by the patients or their physicians. Of the 129 patients, 36 had died by February 1, 1986, 14 had received a liver transplant, and 79 were still alive without liver transplants. The end points for our follow-up were the date of death, the date of liver transplantation, and February 1, 1986. The mean follow-up was 3.8 years (range, 0.1–9.7 years).

The 129 cholangiograms were reviewed retrospectively by one radiologist without knowledge of clinical findings and outcomes. There were 101 ERCPs, 14 transhepatic cholangiograms, 12 T-tube cholangiograms, and two intraoperative cholangiograms. Each cholangiogram was scored for a number of specifically defined characteristics. Each characteristic was scored as being present, absent, or unknown because of technical factors. Technical problems included nonfilling or partial filling of the biliary tree and insufficient plain film documentation. For all cholangiographic films, we assumed 15% magnification except for 100-mm spot films, for which we assumed 20% minification.

The intrahepatic and extrahepatic portions of the biliary tree were evaluated separately. The extrahepatic portion was defined as the common bile duct, common hepatic duct, and distal 1 cm of the left and right hepatic ducts [10]. The remainder of the proximal biliary tree was considered intrahepatic.

Three characteristics of bile duct strictures were evaluated: grade, length, and extent (Table 1). For both the intrahepatic and extrahepatic biliary trees, the highest grade stricture identified was recorded. The greatest length of stricture present also was identified for both intrahepatic ducts (IHDs) and extrahepatic ducts (EHDs) (Figs. 1A and 1B). The extent of involvement was categorized separately for the IHDs and EHDs as either localized or diffuse (Fig. 1C). Finally, the presence and degree of bile duct dilatation [4] (Table 2, Fig. 1D) were evaluated and recorded separately for IHDs and EHDs.

Survival curves were generated on the basis of clinical outcome during the follow-up period by using the Kaplan-Meier method. A good outcome was defined as survival through February 1, 1986, without the need for a liver transplant. Liver transplantation at our institution during this study was restricted to patients with histologic

TABLE 1: Classification of Three Independent Characteristics of Bile Duct Strictures

Characteristic		Classification
Grade	Grade 1	0–25% narrowing of duct
	Grade 2	>25–50% narrowing of duct
	Grade 3	>50–75% narrowing of duct
	Grade 4	>75–100% narrowing of duct
Length	Band	1–2 mm of involvement
	Segmental	3–10 mm of involvement
	Confluent	>10 mm of involvement
Extent	Localized	≤25% of ducts involved
	Diffuse	>25% of ducts involved

TABLE 2: Bile Duct Dilatation According to Location Within the Biliary Tree

Degree of Dilatation	Luminal Diameter (mm)			
	Common Duct ^a	Left Main Hepatic Duct	Right Main Hepatic Duct	Secondary Intrahepatic Ducts
None	<15	<7	<6	<4
Mild	15–19	7–9	6–7	4
Marked	≥20	≥10	≥8	≥5

^a Common hepatic or common bile duct.

evidence of cirrhosis and life-threatening complications of portal venous hypertension. Patients who died and patients who required a liver transplant because of end-stage liver disease were considered to have equally poor outcomes. We compared the survival curves of patients with various combinations of cholangiographic findings. A log-rank test, which takes into account the number of patients in each group and the amount of follow-up time available for each patient, was used to determine the level of statistical significance of any observed difference between survival curves. A *p* value of .05 or less was considered to represent statistical significance. A prognostic factor associated with an apparent difference in survival, but with a *p* value greater than .05, was considered to have shown a trend toward prognostic usefulness.

We attempted to validate our results by comparing several of our cholangiographic prognostic factors with two of the previously known clinical prognostic factors [10]. Specifically, we compared the mean serum total bilirubin level and the histologic stage after liver biopsy [7] in patients with high-grade and low-grade intrahepatic and extrahepatic strictures and in patients with and without marked dilatation of the intrahepatic bile ducts.

Results

Results showed a 5-year survival rate of 57%; the rest of the patients (43%) died or received a liver transplant (Fig. 2). When evaluating the highest grade stricture present, we found that relatively few patients had only grade 1 or grade 2 strictures. Therefore, we combined these patients with patients who had grade 3 strictures and compared them as a group (i.e., patients with grade 1, 2, or 3 strictures) with patients who had grade 4 strictures. Fifty-three percent of our patients had grade 4 IHD strictures. Figure 3 (top) shows the influence of the highest grade IHD strictures on survival without regard for the presence of EHD strictures. A significant decrease in survival occurred among patients who had grade 4 IHD strictures compared with those with grade 1, 2, or 3 IHD strictures. Similarly, Figure 3 (bottom) shows the influence of the highest grade EHD stricture on survival without regard for IHD strictures. A trend toward decreased survival occurred with high-grade (i.e., grade 4) EHD strictures also, but this was not statistically significant.

The influence of the IHD stricture length (without regard for length of EHD strictures) on survival is shown in Figure 4 (top). No patients in our study had only band strictures involving the IHDs, and therefore the effect of IHD band strictures on survival could not be evaluated. We did not find a significant difference in survival between patients with seg-

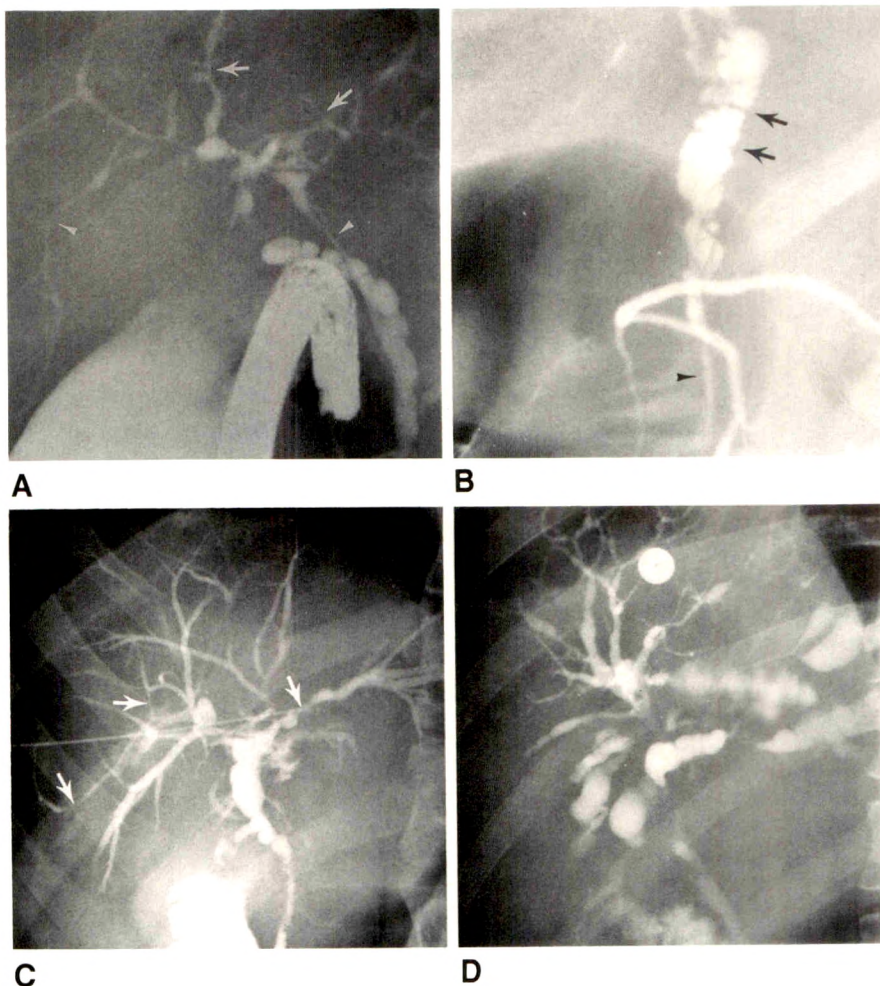
Fig. 1.—Cholangiograms show characteristics of bile duct strictures in patients with primary sclerosing cholangitis.

A, Multiple segmental (arrows) and confluent (arrowheads) strictures. (Reprinted from MacCarty et al. [4]. By permission of the Radiological Society of North America, Inc.)

B, Multiple band strictures (arrows) and a confluent stricture (arrowhead) of extrahepatic ducts. (Reprinted from MacCarty et al. [4]. By permission of the Radiological Society of North America, Inc.)

C, Localized involvement of intrahepatic ducts (arrows) and diffuse involvement of extrahepatic ducts.

D, Marked dilatation of segments of intrahepatic ducts.



mental strictures and those with confluent strictures of the IHDs. The influence of the length of the longest EHD stricture (without regard for length of IHD strictures) on survival is shown in Figure 4 (bottom). Although a trend for decreased survival occurred with longer strictures of the EHDs, this was not statistically significant.

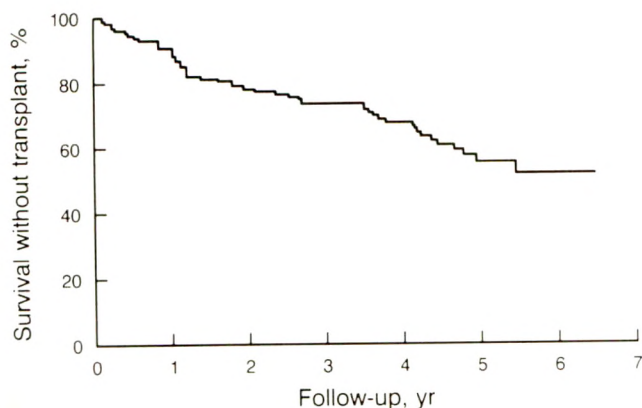


Fig. 2.—Survival curve for all patients with primary sclerosing cholangitis ($n = 129$). End point was either death or liver transplantation.

Patients who had IHD strictures limited to less than 25% of the IHDs (i.e., localized strictures)—a finding in 21% of our patients—had a significantly better survival rate than did those who had diffuse IHD strictures (Fig. 5, top). Prognosis tended to be poorer in patients with EHD strictures involving more than 25% of the EHDs than in patients with localized EHD strictures (Fig. 5, bottom), but the difference was not statistically significant.

We found no perceptible difference between patients with mild IHD dilatation and those with no dilatation, so these groups were combined and compared with patients who had marked IHD dilatation. As shown in Figure 6, patients with marked IHD dilatation tended to die or require a transplant much sooner than did those who had mild or no dilatation of the IHDs. This was particularly true in the first 2 years of follow-up. Although a trend toward decreased survival was seen with marked IHD dilatation, this was not statistically significant. There were not enough patients with marked EHD dilatation to compare these with patients with mild or no dilatation.

A higher proportion of patients with high-grade IHD strictures than with lower-grade IHD strictures had histologic evidence of cirrhosis (stage 4 hepatic histology) as indicated in Figure 7. Similarly, mean serum total bilirubin level was

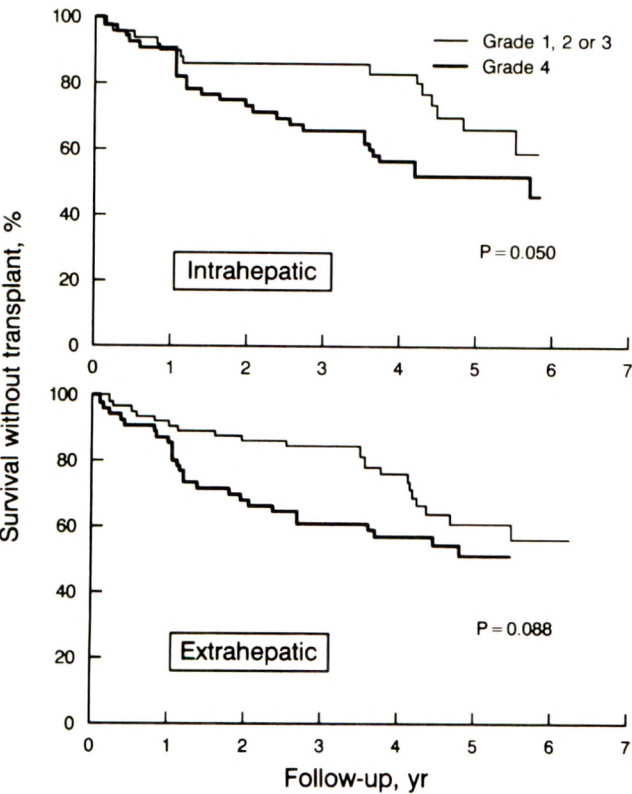


Fig. 3.—Effects of intrahepatic (top) and extrahepatic (bottom) stricture grade on survival curves for patients with primary sclerosing cholangitis. End point was either death or liver transplantation.

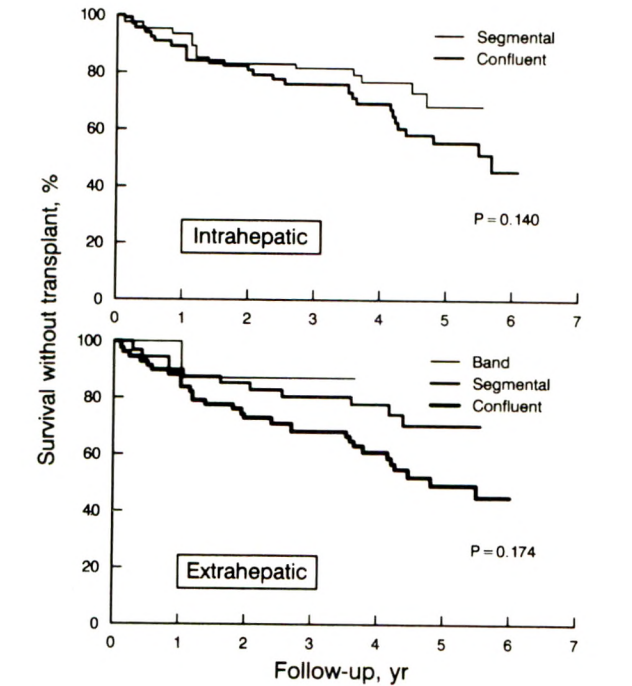


Fig. 4.—Effects of intrahepatic (top) and extrahepatic (bottom) stricture length on survival curves for patients with primary sclerosing cholangitis. End point was either death or liver transplantation.

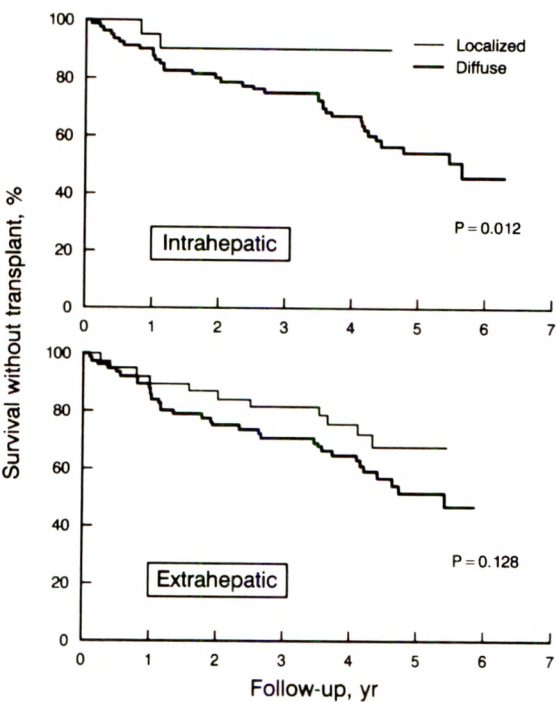


Fig. 5.—Effects of extent of intrahepatic (top) and extrahepatic (bottom) strictures on survival curves for patients with primary sclerosing cholangitis. End point was either death or liver transplantation.

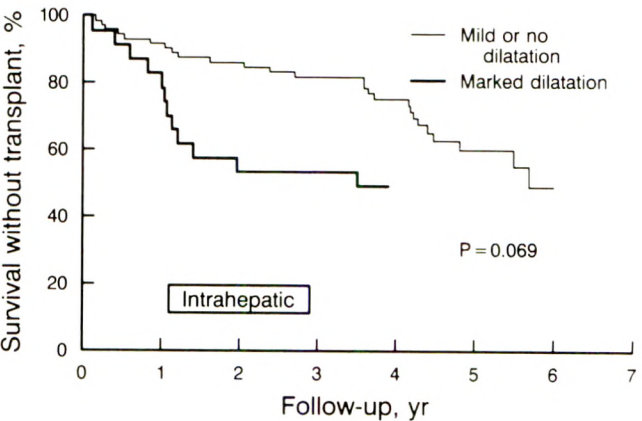


Fig. 6.—Effect of marked dilatation of intrahepatic bile ducts on survival in patients with primary sclerosing cholangitis. End point was either death or liver transplantation.

higher among patients with high-grade IHD strictures, as shown in Figure 8. Similar associations were observed when we compared high-grade EHD strictures with lower-grade strictures and when we compared marked IHD dilatation with mild or no dilatation.

Discussion

The 5-year overall survival rate of 57% in our study group was somewhat lower than other previously published figures

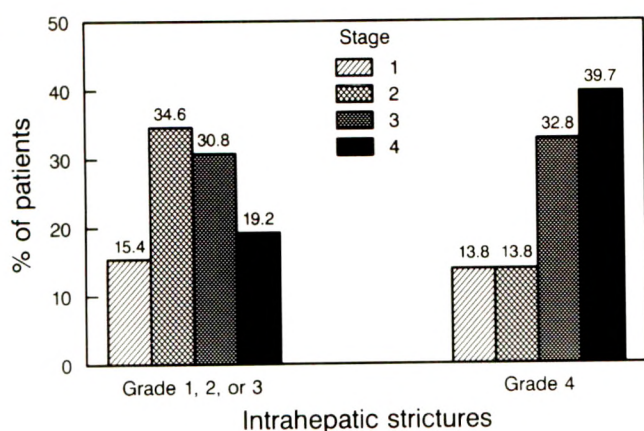


Fig. 7.—Distribution of hepatic histologic stage for patients with and without high-grade intrahepatic duct strictures.

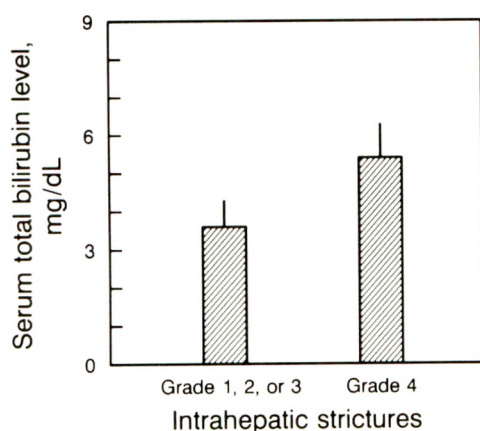


Fig. 8.—Mean serum total bilirubin level for patients with and without high-grade intrahepatic duct strictures.

[11]. This finding is partially explained by our definition of survival as being alive without having a liver transplant; that is, transplantation patients were added to our mortality figures owing to the advanced state of liver failure that existed at the time of transplantation. Also, the survival rate in our study reflects the fact that our institution is a tertiary care referral center. The calculation of survival figures used the date of the cholangiogram available on presentation at our institution; calculations did not necessarily use the date of either disease onset or original diagnosis. The relatively advanced state of disease in our patients was illustrated by the fact that only 3% of our patients had intrahepatic disease alone, a condition that may represent an early stage of disease with a better prognosis [11].

In this study, univariate analysis was used to identify cholangiographic prognostic signs in PSC. We found that patients who had IHD strictures that narrowed the luminal diameter by 75% or more had a poorer prognosis than did patients

with lesser grade IHD strictures. That patients with high-grade IHD strictures tended to be the same patients who had an advanced hepatic histologic stage and an increased serum total bilirubin level supports our conclusion that high-grade IHD strictures are a poor prognostic factor. In fact, the presence of biliary strictures may contribute to the development of hyperbilirubinemia and to more extensive pathologic changes in the liver. It is interesting that high-grade EHD strictures were not a significant predictor of a poor outcome. One explanation might be that some of these patients had procedures performed on their EHDs (surgery or balloon dilatation) that favorably influenced their survival. However, only seven patients had such procedures performed during the follow-up period (including one patient with multiple procedures and excluding 12 patients with short-term T-tube placement after cholecystectomy or exploratory laparotomy). Of these, four were alive at the end of follow-up and three had died; these mortality figures are not significantly different from the overall mortality rate for the rest of our study group. Therefore, we conclude that the small number of biliary drainage procedures performed during the follow-up period did not significantly influence the results of our survival analysis. A large prospective series would be necessary to determine definitely the effect of biliary drainage procedures on survival.

In this series, stricture length was not found to be a significant predictor of survival. However, a trend toward decreased survival was seen with longer strictures. The reason may be that longer confluent strictures represent a more advanced stage of disease than do shorter segmental strictures and band strictures. We have observed that band strictures progress to confluent strictures on serial cholangiograms in some cases, but this change has not been shown in a large series. Furthermore, confluent strictures—with their greater extent of fibrosis—are more likely to be high-grade strictures with concomitant obstruction. Therefore the grade of the stricture may be a more important prognostic factor in PSC than stricture length is.

Although not a statistically significant prognostic factor, marked IHD dilatation showed a stronger trend toward decreased survival than did mild or no dilatation of the IHDs. Marked dilatation is usually indicative of high-grade obstruction and should logically portend a poor prognosis. However, patients with PSC have a great deal of fibrosis about the biliary tree and may have significant obstruction and cholestasis without showing evidence of marked bile duct dilatation. Bile ducts that can markedly dilate may represent regions of the liver that are relatively less involved by this chronic fibrosing disease. The IHD dilatation occurring with PSC typically involves alternating dilatation and strictures of short segments, giving the characteristic beaded appearance of PSC [4]. When cholangiocarcinoma develops in patients with PSC, large, nonsegmental areas of marked dilatation typically occur; this often provides the first clue to the development of this ominous complication [12, 13]. The radiologic appearances of PSC alone and of PSC complicated by cholangiocarcinoma overlap considerably. Although effort was made to exclude patients with PSC complicated by cholangiocarcinoma from our study, it is possible that some of the early

TABLE 3: Prognostic Predictors of a Poor Outcome in Patients with Primary Sclerosing Cholangitis

Duct Location	Predictors	
	Statistically Significant (<i>p</i>)	Trend Indicated ^a (<i>p</i>)
Intrahepatic	Grade 4 strictures (.050)	Confluent strictures (.140)
	Diffuse strictures (.012)	Marked dilatation (.069)
Extrahepatic	None	Grade 4 strictures (.088) Confluent strictures (.170) Diffuse strictures (.128)

^a Decreased survival observed, but *p* > .05.

deaths that occurred in the first 2 years (Fig. 6) were the result of unrecognized cholangiocarcinoma.

Table 3 summarizes the prognostic factors that were shown to be statistically significant and those that, although not significant, suggested a trend toward prognostic usefulness. The finding that IHD disease has a greater effect on survival than EHD disease has important therapeutic implications. Procedures aimed at relieving EHD obstruction, such as balloon dilatation or choledochojejunostomy, may not have a significant effect on survival if the patient also has high-grade IHD strictures. However, biliary drainage procedures can be highly effective in relieving symptoms [6, 9] and should be performed in selected patients. Transhepatic or endoscopic balloon dilatation is preferable to surgery because previous surgery makes transplantation technically more difficult [3, 6, 8].

REFERENCES

1. Wiesner RH, LaRusso NF. Clinicopathologic features of the syndrome of primary sclerosing cholangitis. *Gastroenterology* **1980**;79:200-206
2. Chapman RWG, Arborgh BÄM, Rhodes JM, Summerfield JA, Scheuer RD, Sherlock S. Primary sclerosing cholangitis: a review of its clinical features, cholangiography, and hepatic histology. *Gut* **1980**;21:870-877
3. LaRusso NF, Wiesner RH, Ludwig J, MacCarty RL. Primary sclerosing cholangitis. *N Engl J Med* **1984**;310:899-903
4. MacCarty RL, LaRusso NF, Wiesner RH, Ludwig J. Primary sclerosing cholangitis: findings on cholangiography and pancreatography. *Radiology* **1983**;149:39-44
5. Lindor KD, Wiesner RH, LaRusso NF. Recent advances in the management of primary sclerosing cholangitis. *Semin Liver Dis* **1987**;7:322-327
6. Wiesner RH, Ludwig J, LaRusso NF, MacCarty RL. Diagnosis and treatment of primary sclerosing cholangitis. *Semin Liver Dis* **1985**;5:241-253
7. Ludwig J, LaRusso NF, Wiesner RH. The syndrome of primary sclerosing cholangitis. *Prog Liver Dis* **1990**;9:555-566
8. Marsh JW Jr, Iwatsuki S, Makowka L, et al. Orthotopic liver transplantation for primary sclerosing cholangitis. *Ann Surg* **1988**;207:21-25
9. May GR, Bender CE, LaRusso NF, Wiesner RH. Nonoperative dilatation of dominant strictures in primary sclerosing cholangitis. *AJR* **1985**;145:1061-1064
10. Wiesner RH, Grambsch PM, Dickson ER, et al. Primary sclerosing cholangitis: natural history, prognostic factors and survival analysis. *Hepatology* **1989**;10:430-436
11. Hermann R, Dooley JS, Sherlock S, McIntyre N. Natural history and mortality in primary sclerosing cholangitis (abstract). *Gut* **1988**;29:A1430
12. MacCarty RL, LaRusso NF, May GR, et al. Cholangiocarcinoma complicating primary sclerosing cholangitis: cholangiographic appearances. *Radiology* **1985**;156:43-46
13. Coffey RJ, Wiesner RH, Beaver SJ, et al. Bile duct carcinoma: a late complication of end-stage primary sclerosing cholangitis (abstract). *Hepatology* **1984**;4:1056

Case Report

Color Doppler Sonography in a Case of Splenic Hemangioma: Value of Compressing the Tumor

Makoto Niizawa,¹ Hideaki Ishida, Pablo Morikawa, Hiroko Naganuma, and Osamu Masamune

Color Doppler sonography is frequently used for the diagnosis of abdominal abnormalities, especially in cases of liver and vascular disease. However, color Doppler findings of splenic diseases have been reported only rarely.

We describe a case of a splenic hemangioma in which color Doppler sonography showed blood flow within the tumor. Many color echoes appeared in the tumor immediately after it was compressed by the probe, suggesting that flow in the vessels in the hemangioma was obliterated by the probe.

Case Report

An abdominal sonogram was obtained as part of a routine medical examination in a 70-year-old man with diabetes mellitus. An echogenic mass measuring 29 × 24 mm was detected at the lower pole of the spleen. The mass was round, homogeneous, and solid, without a halo, lateral shadowing, or posterior enhancement. Plain and drip-infusion enhanced CT showed no abnormality, but splenic angiography revealed an avascular area at the inferior aspect of the spleen. Color Doppler sonography showed an artery at the periphery of the tumor and a few color echoes in the mass, indicative of blood flow within the lesion (Fig. 1A). Arterial flow was detected in the lesion. A Doppler examination performed with and without compressing the lesion with the probe showed that the color echoes within the lesion disappeared during compression and reappeared immediately afterward (Figs. 1B and 1C). This phenomenon was observed repeatedly, suggesting that the tumor was vascular and soft. Splenectomy was performed. The tumor was solitary, round, soft, and nonencapsulated. Histologically, the tumor was composed of a proliferation of vascular channels lined by a single epithelial layer. The diagnosis was splenic capillary hemangioma.

Discussion

Hemangioma is the most common tumor of the spleen. Such tumors may be solitary or may occur in connection with multiple disseminated hemangiomatosis. The prevalence of splenic hemangioma varies from 0.03% to 14% in reported autopsy studies [1]. Histologically, splenic hemangioma can be divided into capillary and cavernous forms. When the tumor is small, it is asymptomatic and is discovered only occasionally during routine examinations.

The sonographic appearance of a splenic capillary hemangioma is a round, echogenic mass with or without cystic areas [1]. When an echogenic solid tumor is seen in the spleen, as in our case, the possibilities of healed infarction, hemangioma, hemangiosarcoma, and metastatic tumor are considered [2]. Among these diseases, healed infarction appears wedge-shaped [2, 3] or as a round mass [3].

Doppler features of hepatic hemangiomas have seldom been described in the literature [4, 5]. Ishida et al. [4] reported a constant wave flow in the hypoechoic areas within the hemangioma. Tanaka et al. [5] reported a color Doppler image showing focal echoes in the central region of the tumor. However, in our case, small color echoes were seen within the mass, and arterial flow was detected in the lesion. A Doppler examination performed with and without compressing the lesion with the probe showed that the color echoes within the lesion disappeared during compression and reappeared immediately afterward. This phenomenon was observed repeatedly, suggesting that the tumor was vascular and soft. From these results, it may be possible to differentiate

Received March 14, 1991; accepted after revision May 17, 1991.

¹ All authors: First Department of Internal Medicine, Akita University School of Medicine, 1-1-1, Hondo, Akita (010), Japan.

AJR 157:965-966, November 1991 0361-803X/91/1575-0965 © American Roentgen Ray Society

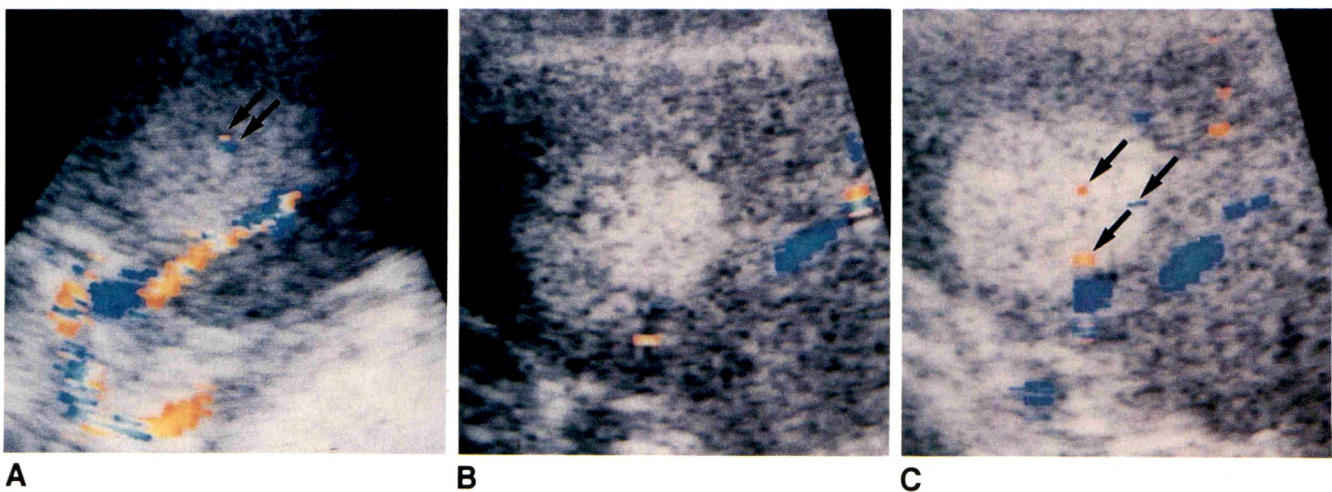


Fig. 1.—A, Color Doppler sonogram of spleen obtained without compression. Artery at periphery of tumor and a few color echoes in mass, indicative of blood flow within lesion (arrows), are shown.

B, Sonogram obtained with compression shows reduced blood flow.

C, Sonogram obtained immediately after release of compression shows reappearance of blood flow (arrows).

splenic vascular tumors from infarction, which is usually avascular, by color Doppler sonography. Furthermore, it may be possible to distinguish splenic hemangiomas from other splenic masses by color Doppler sonography after the study of a large number of cases.

Sonograms obtained with and without compression of hepatic hemangiomas as part of intraoperative studies have been described [6]. The echogenicity of the tumors was markedly decreased during compression. The mechanism of this phenomenon was presumed to be the collapse of many sinuses in the hemangioma caused by the compression, resulting in a reduced flow. In our case of splenic hemangioma, color echoes in the tumor diminished during compression with the probe and reappeared immediately afterward. Microscopically, all splenic hemangiomas, as in hepatic hemangiomas, are composed of a proliferation of vascular channels lined by a single layer of endothelium [1]. On the other hand, it is also well known that color noise appears from moving tissue or moving transducers at low gain [7], and that such noise appears over the monitoring field. In our case, the color echoes appeared repeatedly only within the tumor, and, therefore, they did not correspond to noise from unsatisfied gain. It is also possible, however, that the color spots, which reappeared after arrest of compression, indicated the expansion of the hemangioma tissue itself, because the heman-

gioma tissue was relatively soft and the movement of the hemangioma, after arrest of compression, was larger than the surrounding parenchyma. From these results, we concluded that the detected tumor was relatively soft.

We conclude that the compression test, under color Doppler monitoring, is potentially a new method for the differential diagnosis of hemangioma and other echogenic tumors of the abdomen.

REFERENCES

1. Ros PR, Moser RP, Dachman AH Jr, Murari PJ, Olmsted WW. Hemangioma of the spleen: radiologic-pathologic correlation in ten cases. *Radiology* 1987;162:73-77
2. Solbiati L, Bossi MC, Bellotti E, Ravetto C, Montali G. Focal lesions in the spleen: sonographic patterns and guided biopsy. *AJR* 1983;140:59-65
3. Goerg C, Schwerk WB. Splenic infarction: sonographic patterns, diagnosis, follow-up, and complications. *Radiology* 1990;174:803-807
4. Ishida H, Morikawa P, Niizawa M, Naganuma S, Arakawa H, Masamune O. L'apport du Doppler à émission pulsée dans l'exploration des tumeurs du foie. *JEMU* 1988;9:178-185
5. Tanaka S, Kitamura T, Fujita M, Nakanishi K, Okuda S. Color Doppler flow imaging of liver tumors. *AJR* 1990;154:509-514
6. Choji K, Shinohara M, Nojima T, et al. Significant reduction of the echogenicity of the compressed cavernous hemangioma. *Acta Radiol* 1988;29:317-320
7. Mitchell DG. Color Doppler imaging: principles, limitations, and artifacts. *Radiology* 1990;177:1-10

Transfemoral Venous Catheterization Through Inferior Vena Caval Filters: Results in Seven Cases

Margaret E. Hansen^{1,2}
 Stuart C. Geller
 E. Kent Yucel
 Thomas K. Eggin
 Arthur C. Waltman

Use of the transfemoral route for venous catheterization has been considered contraindicated in patients with inferior vena caval (IVC) filters. The transjugular route has been used instead in such patients when subsequent diagnostic or therapeutic procedures are required. Many radiologists, however, are more accustomed to the transfemoral approach, and may not find the transjugular route a desirable alternative. We describe seven patients with previously placed IVC filters in whom the transfemoral route was used to perform pulmonary arteriography (five patients) or to place additional IVC filters (two patients). After venographic confirmation of caval patency, filters were catheterized under fluoroscopic control and the procedures were performed. All procedures were technically successful; no complications occurred.

We believe the transfemoral route to be a safe and feasible approach for performing venous procedures in selected patients with IVC filters, obviating the less familiar and potentially more hazardous transjugular approach.

AJR 157:967-970, November 1991

Patients with IVC filters may later need diagnostic or therapeutic procedures most easily accomplished from a femoral vein approach. Transfemoral venous catheterization may be avoided in such patients because of concerns about the safety or technical feasibility of this method in the presence of an IVC filter [1]. Such concerns include possible filter displacement and the risk of dislodging trapped thrombi within the filter, which would then cause an embolism in the pulmonary circulation.

Technical difficulties in filter deployment occasionally result in unsatisfactory filter positioning for prophylaxis of pulmonary embolism. This may occur if the filter is too low, if the filter struts do not open fully, or if the filter is excessively tilted. In such cases, a second filter is often placed cephalad to the first via the transjugular route [2, 3].

We have performed both diagnostic and therapeutic procedures from a femoral vein approach without difficulty or complications in patients with IVC filters and consider the transfilter approach safe and feasible.

Methods and Results

Procedures were done via the transfemoral venous approach in seven patients with IVC filters. There were three women and four men, ranging in age from 28 to 70 years (mean age, 59 years). Filters present in these patients included stainless steel Greenfield (Medi-tech, Watertown, MA; two patients), Vena-Tech (LG Medical SA, Chassenuel, France; distributed by Vena-Tech Corp., Evanston, IL; three patients), and bird's nest (Cook Inc., Bloomington, IN; two patients) models. Filters had been in place from less than 1 day to 21 months.

Five patients were referred for pulmonary arteriography. In three patients with

Received April 2, 1991; accepted after revision May 10, 1991.

¹ All authors: Vascular Radiology Section, Department of Radiology, Massachusetts General Hospital, Boston, MA 02114. Address reprint requests to S. C. Geller.

² Present address: Special Procedures Section, Department of Radiology, University of Texas Southwestern Medical Center, Dallas, TX 75235.

0361-803X/91/1575-0967
 © American Roentgen Ray Society

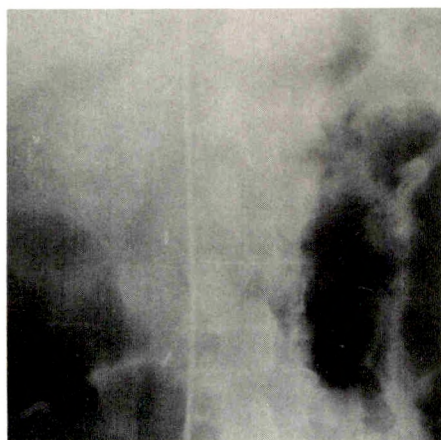
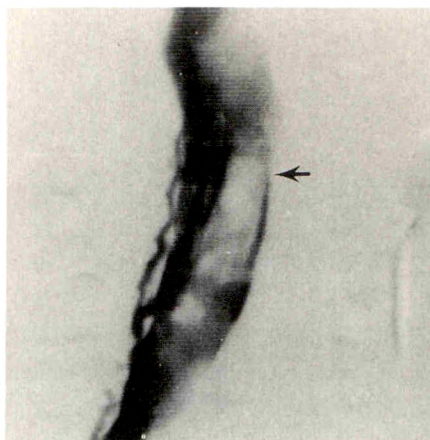


Fig. 1.—61-year-old woman with bird's nest filter placed previously for pulmonary emboli. New symptoms suggested recurrent emboli. Radiograph shows pigtail catheter and guidewire passing through filter.



A



B

Fig. 2.—69-year-old woman with deep venous thrombosis in lower extremity and contraindication to heparin therapy.

A, Venacavogram shows initial Vena-Tech filter is prevented from opening fully by eccentric caval thrombus (arrow); clot extends to renal veins.

B, Digital subtraction venacavogram shows second Vena-Tech filter, placed through first, is positioned above top of thrombus.

previous pulmonary emboli or deep venous thrombosis, IVC filters had been placed because heparin therapy was contraindicated. New pulmonary emboli were suspected clinically. In two cases, massive pulmonary emboli had been documented by previous pulmonary arteriography, and thrombolytic therapy had been instituted; IVC filters had been placed at the time of the initial studies because of limited cardiac reserve. Follow-up studies were requested to assess results of thrombolytic therapy. Both of these patients had thrombi trapped within their IVC filters when the follow-up arteriogram was obtained.

Two patients with deep venous thrombosis of the lower extremity required placement of IVC filters because of contraindications to heparin therapy. In both patients, technical problems with deployment of the filters necessitated placement of additional filters.

The method of pulmonary arteriography used in these cases involved catheterization of either the right or left common femoral vein by using the Seldinger technique and insertion of a 7.1-French, 100-cm-long pigtail catheter (Cook Inc.) to the level of the iliac vein confluence. Injection of 43–60% iodinated contrast material was performed with fluoroscopic observation or digital subtraction filming of the IVC to confirm patency. A 0.038-in. (0.97-mm) Newton LLT guidewire with a 15-mm J tip (Cook Inc.) was inserted into the catheter and threaded through the struts of the filter, after which the catheter was advanced (Fig. 1) and selective pulmonary arteriography was done in the usual fashion [4]. All catheters were straightened by using a guidewire and fluoroscopic monitoring before removal.

In two patients, a filter was inserted through another filter already in place. In the first case, the initial Vena-Tech filter was placed into the infrarenal IVC, but the struts did not open fully. A venacavogram after filter placement showed eccentric caval thrombus compressing the filter and extending to the

level of the renal veins. This thrombus was not seen on a venacavogram obtained before filter placement, because it caused only minimal impression on the lumen of the IVC. A guidewire was passed through the introducer sheath and filter into the suprarenal IVC, and the dilator from a second Vena-Tech kit was introduced into the sheath over the wire; both sheath and dilator were advanced through the filter to a position above the clot. A second Vena-Tech filter was then inserted, and a digital subtraction venacavogram showed it was above the top of the thrombus (Fig. 2). In the second case, one of the hooks of the first Vena-Tech filter caught on the introducer sheath, and the entire assembly was withdrawn into the right common iliac vein before the filter could be disengaged. Because the patient had thrombus in the left common iliac vein, a second Vena-Tech filter was introduced through the first one and placed in the infrarenal IVC.

Procedures were technically successful in all cases. No major or minor complications occurred. No new respiratory symptoms developed in any of the patients, including the two patients whose filters contained trapped thrombi. In no case was the IVC filter displaced or significantly altered in orientation.

Discussion

Since the development of percutaneous methods of placement [5], IVC filters have come into widespread clinical use. The most common location for these devices is in the infrarenal IVC. Most currently used models are intended to be permanent indwelling devices. This is not a problem for most patients. However, patients may later need diagnostic or therapeutic procedures requiring central venous access.

The presence of an IVC filter has been considered by some to contraindicate the use of the femoral vein approach for subsequent procedures [1]. In most cases, however, the IVC

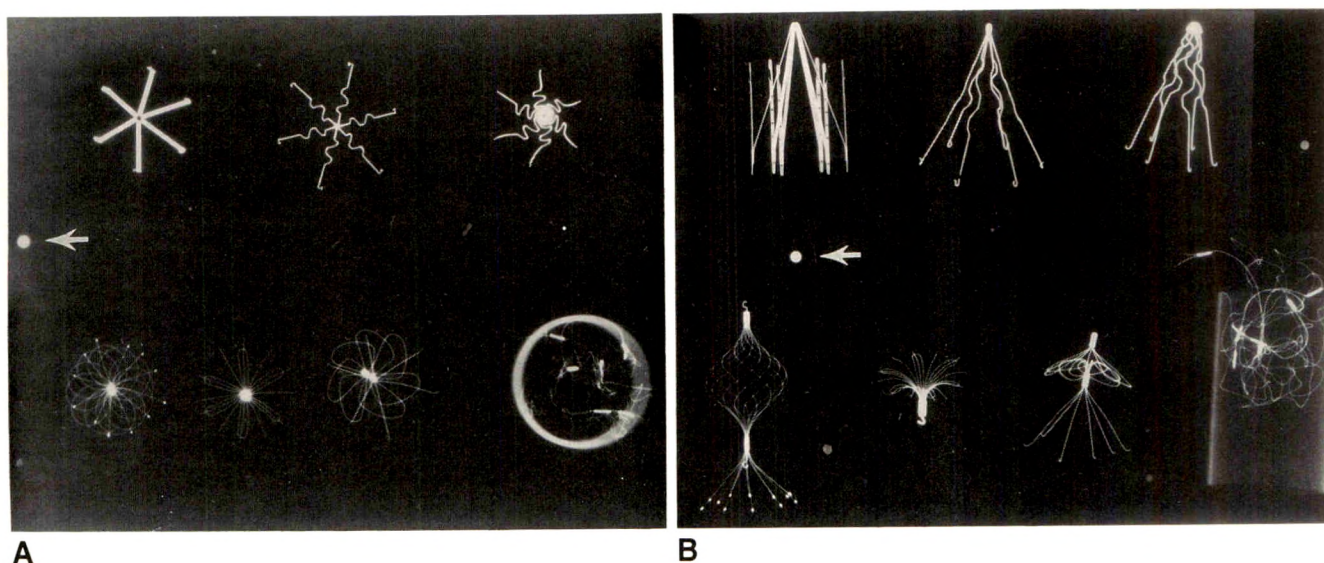


Fig. 3.—A and B, Axial (A) and lateral (B) radiographs of seven filter models show spacing of filter elements. Top row (left to right): Vena-Tech, titanium Greenfield, and stainless steel Greenfield; bottom row (left to right): Gunther, Amplatz, Simon nitinol, and bird's nest. A 3-mm BB (arrow) is shown to allow estimation of sizes of gaps between filter elements; outer diameter of a 7.1-French catheter is less than 3 mm.

remains patent and could serve as a route of access for pulmonary arteriography, venous sampling, hepatic vein manometry, catheterization of the right side of the heart, and other studies. Caval patency rates as high as 98% have been reported with the stainless steel Greenfield filter [6]. Studies on newer models also indicate high caval patency rates [7, 8], which makes the transfilter approach feasible.

Stability of the filter's position (and the likelihood of displacement) is also a theoretical concern. Experimental studies with the Gunther retrievable filter have shown adherence of filter struts to the IVC wall as early as 5 days after placement, although filters were easily removed up to 14 days after insertion. After follow-up of 3–4 months, parts of the filter were firmly incorporated into the vessel wall and partially covered by neointima [9]. The low prevalence of filter migration reported in numerous clinical series with various filter types also suggests that most such devices are in fact quite stable [6, 7, 10]. The lack of significant change in the position of the filters in our series, including two filters that had been in place less than 1 day, confirms this impression. However, care should be taken during catheter manipulation via this approach, particularly when passage through the right side of the heart is attempted during pulmonary arteriography. In some cases, it may be prudent to insert a long sheath, which would reduce the chance of complications at the filter site during transfilter procedures, especially if catheter exchanges are required. In addition, this would reduce the chance of entangling the catheter in the filter while removing the catheter at the end of the procedure.

The presence of thrombi trapped within or extending cephalad from the filter poses a theoretical risk of inducing pulmonary emboli by passing wires and catheters through the filter. Such thrombi can also form emboli spontaneously [11, 12]. In two of our cases, trapped thrombi were present in the

filters, yet passage of guidewires and catheters was readily accomplished, and no new respiratory symptoms occurred. Both of these patients had previously documented emboli and were being studied to assess results of thrombolytic therapy. No new emboli were detected on the follow-up arteriogram in either case. Accordingly, we do not consider the presence of nonocclusive thrombi within the filter a contraindication to use of the transfilter approach if the IVC itself is patent. In all such cases, however, caution should be exercised when attempting to negotiate the filter and thrombus. Catheterization through massive or occlusive thrombus should not be attempted. Although none of our patients had thrombus extending cephalad from the filter, this is not an uncommon finding [11, 12], and caution should be used in this situation as well.

We have successfully performed transfilter procedures with guidewires with 3-mm J or straight tips and with our standard 15-mm J wire. Catheters should be straightened under fluoroscopic observation before they are withdrawn through the IVC (and the filter) to avoid catching them on the filter elements, which could result in displacement of the filter. Although the tip-deflecting wire technique is our standard method of pulmonary arteriography, we see no technical reason why the transfilter technique could not be used with a Grollman catheter as well.

We have performed transfilter procedures without difficulty or complication in patients with stainless steel Greenfield, Vena-Tech, and bird's nest filters. We have not as yet performed such procedures in patients with Simon nitinol, titanium Greenfield, Amplatz, or other filter types. Most currently available models contain large enough spaces between their elements to allow passage of a 7-French catheter, and some, such as the Vena-Tech, have even larger spaces (Fig. 3). The Gunther model has tightly spaced wires, and transfilter pro-

cedures probably would not be possible with this type of filter. Others, such as the Amplatz and the Simon nitinol, have relatively tightly spaced wires but could probably be negotiated successfully if caution were used. More complicated procedures, such as percutaneous removal of foreign bodies, may not be possible with the transfilter approach. Displacement of the filter or injury to the IVC could result from such attempts, particularly if the foreign body is large.

Clinical judgment on the use of this method should be exercised in each case. Further experience with a broader range of filter models would be helpful to expand on our results, but we think this method is safe, easily performed, and of wide potential use.

REFERENCES

1. Miller DL, Doppman JL. Petrosal sinus sampling: technique and rationale. *Radiology* **1991**;178:37-47
2. Cho KJ, Proctor MC, Greenfield LJ. Interim results of a multicenter trial of the modified hook titanium Greenfield. *J Vasc Intervent Radiol* **1991**;2:6
3. Awh MH, Taylor FC, Lu CT. Continued experience and follow-up with the Vena-Tech filter. *J Vasc Intervent Radiol* **1991**;2:9
4. Courey WR, Merino DeVillasante J, Waltman AC. A quick simple method for percutaneous transfemoral pulmonary arteriography. *Radiology* **1974**;113:475-477
5. Tadavarthy SM, Castañeda-Zúñiga W, Salomonowitz E, et al. Kimray-Greenfield vena cava filter: percutaneous introduction. *Radiology* **1984**;151:525-526
6. Greenfield LJ. Current indications for and results of Greenfield filter placement. *J Vasc Surg* **1984**;1:502-504
7. Roehm JOF, Johnsrude IS, Barth MH, Gianturco C. The bird's nest inferior vena cava filter: progress report. *Radiology* **1988**;168:745-749
8. Murphy TP, Dorfman GS, Yedlicka JW, et al. LGM vena cava filter: objective evaluation of early results. *J Vasc Intervent Radiol* **1991**;2:107-115
9. Gunther RW, Schild H, Fries A, Storkel S. Vena caval filter to prevent pulmonary embolism: experimental study. *Radiology* **1985**;156:315-320
10. Epstein DH, Darcy MD, Hunter DW, et al. Experience with the Amplatz retrievable vena cava filter. *Radiology* **1989**;172:105-110
11. McAuley CE, Webster MW, Jarrett F, Hirsch SA, Steed DL. The Greenfield intracaval filter as a source of recurrent pulmonary thromboembolism. *Surgery* **1984**;96:574-576
12. Geisinger MA, Zelch MG, Risius B. Recurrent pulmonary embolism after Greenfield filter placement. *Radiology* **1987**;165:383-384

LIST OF BOOK AND VIDEOTAPE REVIEWS

- | | |
|------|--|
| 1022 | Creative Medical Teaching. <i>Whitman N</i> |
| 1028 | The Radiologic Clinics of North America: Metabolic Bone Disease. <i>Rosenthal DI, ed</i> |
| 1034 | Cartilaginous Tumors of the Skeleton. <i>Moser RP Jr</i> |
| 1038 | Radiology Review Manual. <i>Dähnert W</i> |
| 1050 | Effective Choices for Diagnostic Imaging in Clinical Practice. <i>World Health Organization</i> |
| 1064 | RSNA Today, Vol. 4, No. 6. <i>The Radiological Society of North America</i> |
| 1072 | Three-Dimensional Neuroimaging. <i>Toga AW, ed</i> |

Case Report

Multiple Intrahepatic Portohepatic Venous Shunts: Treatment with Steel-Coil Embolization

Yoshitaka Okada,¹ Takashi Endo,¹ Shoichi Kusano,¹ and Muneki Yoshida²

Large intrahepatic shunts between the portal vein and the hepatic vein are rare vascular abnormalities that frequently cause hepatic encephalopathy [1–6]. Surgery for this condition is often associated with high morbidity and mortality rates [1]. Angiographic intervention for treatment of intrahepatic portohepatic venous shunts has been limited. To our knowledge, only one case report has been published in the English-language literature [5]. We recently used steel-coil embolization through an angiographic catheter introduced from the ileocolic vein under minilaparotomy to treat a patient who had numerous large intrahepatic portohepatic venous shunts.

Case Report

A 42-year-old man had had frequent disturbances in consciousness for 8 years. He had had a liver biopsy, and alcoholic liver cirrhosis had been diagnosed. Hepatic encephalopathy was diagnosed on the basis of clinical signs and symptoms, results of laboratory tests, and the finding of triphasic waves on EEG. The patient subsequently had sonography and CT, both of which revealed multiple aneurysmal dilatations of the intrahepatic portal branches connecting with the hepatic veins (Fig. 1A). These findings were confirmed by arterial portography with selective injection of contrast material into the superior mesenteric artery. Because of the number of portohepatic venous shunts, the patient was not considered a candidate for surgical repair. Therefore, transcatheter embolization was attempted.

The procedure was performed in the angiography suite by a team of interventional radiologists, surgeons, and anesthesiologists. After administration of epidural anesthesia, minilaparotomy was performed, and a 7-French sheath introducer (Cordis, Miami, FL) was inserted

into a tributary of the ileocolic vein and then advanced into the superior mesenteric vein. A cobra-shaped, 6.5-French long-tapered curved catheter (Cook, Bloomington, IN; size of the tapered tip, 5-French) was introduced through the sheath into the portal system by means of a standard angiographic technique. The portogram was obtained with a direct injection of contrast material into the portal vein (Fig. 1B). In order to evaluate the number, location, and size of the portohepatic venous shunts, the catheter tip was subsequently advanced into the shunt channels as selectively as possible by using a 0.035-in. (0.89-mm) Radifocus Glidewire (Terumo, Tokyo) for guidance, and the shunts were occluded one by one with Gianturco coils (Cook) 5 to 8 mm in diameter (Fig. 1C).

Because the abrupt closure of all the shunt channels might exacerbate the patient's portal hypertension, the embolization was performed in three separate sessions. Two months elapsed between the first and the second embolizations, and 6 months between the second and the third. A total of 59 coils was used to occlude all the shunt channels. At the end of the third embolization session, virtually no shunts were seen on the portogram, and uninvolved intrahepatic portal branches, which were unclear on the initial portograms because of the preferential flow of contrast medium to the large shunts, were visualized clearly (Fig. 1D). No encephalopathy occurred during the 15-months of follow-up after the third embolization, and no sign of exacerbation of portal hypertension was observed clinically.

Discussion

Although intrahepatic portohepatic venous shunt had been thought to be a rare disorder, recent advances in sonography and CT have shown asymptomatic intrahepatic shunts in an increasing number of patients. Nevertheless, large intrahe-

Received April 23, 1991; accepted after revision May 31, 1991.

¹Department of Radiology, Kitasato University East Hospital, 2-1-1 Asamizodai, Sagami-hara, Kanagawa 228, Japan. Address reprint requests to Y. Okada.

²Department of Surgery, Kitasato University East Hospital, 2-1-1 Asamizodai, Sagami-hara, Kanagawa 228, Japan.

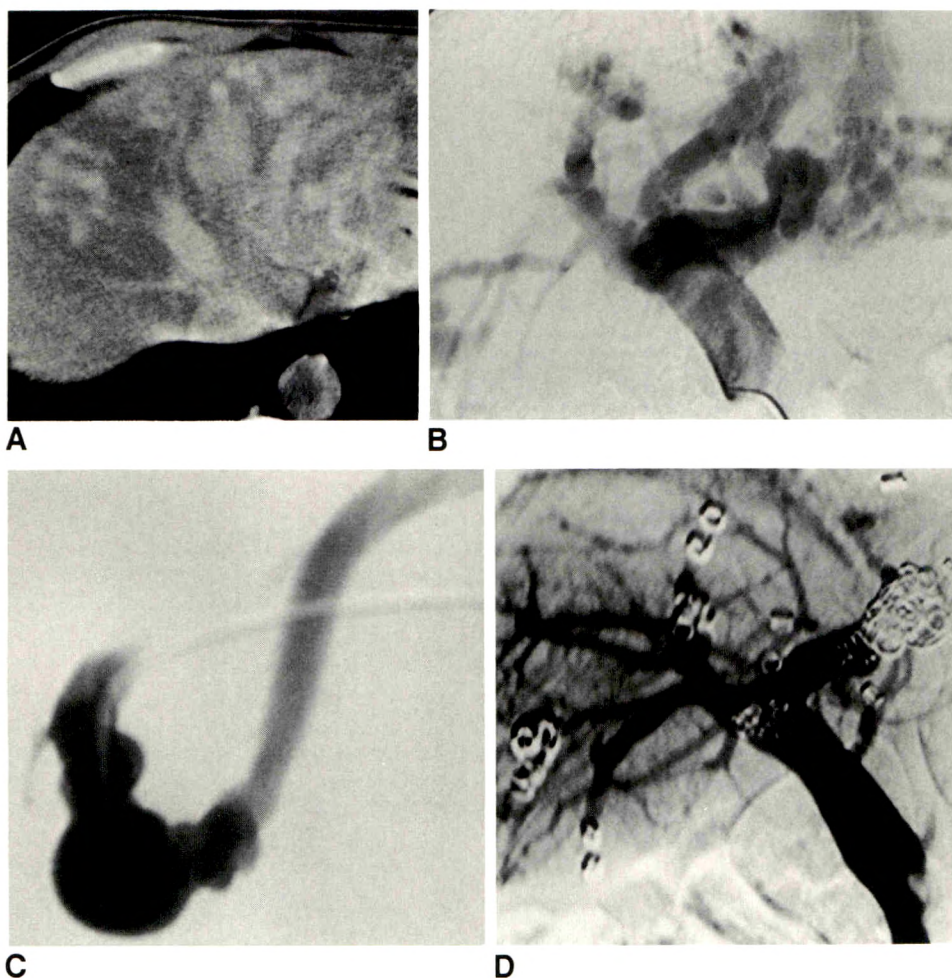


Fig. 1.—Steel-coil embolization of multiple intrahepatic portohepatic venous shunts.

A, Contrast-enhanced CT scan shows multiple abnormal serpentine intrahepatic vessels.

B, Portogram obtained before treatment shows multiple enlarged intrahepatic portal branches communicating with hepatic veins. Uninvolved portal branches are scarcely seen because of preferential flow into large shunt channels.

C, Portogram obtained after selective catheterization into shunt vessel in right lobe shows communication between portal branch and right hepatic vein more clearly. This vessel was subsequently occluded with coils. Other shunt vessels were treated likewise.

D, Portogram obtained after third embolization procedure shows absence of shunts. Uninvolved portal branches in right lobe are clearly depicted.

patic shunts that cause hepatic encephalopathy are still uncommon; fewer than 20 cases have been reported [1–7]. The cause is thought to be a congenital vascular anomaly in some patients [1, 2, 4], and an acquired event is suspected in others [3]. The cause of the shunts in our patient was unknown. We speculate, however, that the acquired changes due to liver cirrhosis may have contributed somewhat to the development of the patient's large shunts. It is uncertain whether there were any underlying congenital abnormalities.

Unlike small asymptomatic shunts, large shunts causing hepatic encephalopathy require appropriate therapeutic intervention. Because of the rarity of this disorder, however, the choice of treatment is controversial. To our knowledge, three patients, each of whom had a single shunt channel, have been treated successfully by surgical intervention, including shunt ligation and hepatic resection [2–4]. As far as multiple large intrahepatic shunts are concerned, however, only one case, a patient who had surgery, has been reported [1], and the patient died 2 days after surgery. Creation of the alternative portosystemic shunt by surgery, such as the distal splenorenal shunt (Warren's operation), also may be considered. The splenorenal shunt would reduce the portal inflow and therefore diminish the size of intrahepatic shunt channels.

Because of the large size and number of the intrahepatic shunts, however, complete disappearance of all the shunts seemed unlikely in this patient. Had some shunt channels remained patent, the patient might still have suffered from encephalopathy.

The first patient with intrahepatic portohepatic venous shunts treated with angiographic intervention was reported by Ohtomo et al. in 1986 [5]. That patient had multiple large intrahepatic shunts throughout the liver and was treated with steel-coil embolization through a catheter introduced from the ileocolic vein, a technique we used with our patient. The transileocolic vein approach was first described by Ueda et al. [7] as an access to the portal system for the embolotherapy of gastroesophageal varices. This method, although admittedly more invasive than the percutaneous transhepatic approach, makes it possible to manipulate a catheter more easily and to avoid inadvertent hemorrhage associated with the transhepatic route [7, 8]. These factors were critical in our patient because the catheterization into the complicated intrahepatic shunt vessels was technically demanding and required better catheter maneuverability. Furthermore, the unusual intrahepatic vasculature could increase the risk for hemorrhagic complication of the transhepatic approach.

Potential complications of steel-coil embolization may include exacerbation of portal hypertension caused by abrupt changes in the portal hemodynamics and dislodgement of coils into the systemic circulation. Although neither was observed in our patient, the long-term outcome of this treatment still needs to be evaluated. When the difficulty of surgical repair is considered, transcatheter steel-coil embolization is a promising treatment for the management of multiple large intrahepatic portohepatic venous shunts that cause hepatic encephalopathy.

REFERENCES

1. Raskin NH, Price JB, Fishman RA. Portal-systemic encephalopathy due to congenital intrahepatic shunts. *N Engl J Med* **1964**;270:225-229
2. Chagnon SF, Vallee CA, Barge J, Chevalier LJ, Gal JL, Blery MV. Aneurysmal portohepatic venous fistula: report of two cases. *Radiology* **1986**;159:693-695
3. Kitami Y, Usui Y, Rai F, Tominaga S, Hashino H. A surgical case of portal systemic encephalopathy due to an enormous portahepatic venous shunt. *Nippon Rinsho Geka Igakukai Zasshi (J Jpn Soc Clin Surg)* **1985**;46:1000-1005 [in Japanese]
4. Nakatsuji Y, Kiyosawa K, Furuta K, et al. A case of hepatic encephalopathy and pulmonary hypertension due to intrahepatic portacaval shunt. *Kanzo (Acta Hepatol Jpn)* **1991**;32:197-204 [in Japanese]
5. Ohtomo K, Furui S, Saito M, Kokubo T, Itai Y, Iio M. Case report: enormous intrahepatic communication between the portal vein and the hepatic vein. *Clin Radiol* **1986**;37:513-514
6. Mori H, Hayashi K, Fukuda T, et al. Intrahepatic portosystemic venous shunt: occurrence in patients with and without liver cirrhosis. *AJR* **1987**;149:711-714
7. Ueda T, Isobe Y, Tsutsui T, Aoki Y, Ando M, Ishibashi T. Trans-ileocolic vein obliteration of the gastroesophageal varices. *Rinsho Geka* **1979**;34:685-694 [in Japanese]
8. Goldman ML, Philip PK, Shah DM, Sarrafizadeh MS. Minilaparotomy for occlusion of coronary veins and control of varices. *Radiology* **1982**;144:924-926

American Roentgen Ray Society Residents' Award Papers, 1992

The ARRS announces competition for the 1992 President's Award and two Executive Council Awards for the best papers concerning the clinical application of the radiologic sciences.

Awards

The winner of the President's Award will receive a certificate and a \$2000 prize. The winners of the two Executive Council Awards will each be given a certificate and a prize of \$1000. The winners will be announced on March 16, 1992. Winning papers will be presented at the ARRS annual meeting at Marriott's Orlando World Center, Orlando, FL, May 10-15, 1992. Winning papers will be submitted for early publication in the *American Journal of Roentgenology*. All other papers will be returned to the authors.

Regulations

Eligibility is limited to residents or fellows in radiology who have not yet completed 4 years of approved training in a radiologic discipline. A letter from the resident's department chairman attesting to this status must accompany the manuscript. The resident must be the sole or senior author and be responsible for all or most of the project.

Submitted manuscripts must not exceed 5000 words and have no more than 10 illustrations. Four copies of the manuscript and illustrations are required. Submitted manuscripts should not contain previously presented or published material and should not be under consideration for publication elsewhere.

Deadline for submissions is February 14, 1992. Send papers to

Nancy O. Whitley, M.D.
Chairman, Committee on Education & Research
American Roentgen Ray Society
Department of Radiology
University of Maryland Medical Systems Hospital
22 S. Greene St.
Baltimore, MD 21201

Edith Cavell

Stefan C. Schatzki¹

George Wesley Bellows was a successful and important realistic chronicler of early 20th century America. Even though he was considered part of the Ashcan School, his paintings depicted a much broader part of society than those of other painters in this group. He was able to capture uniquely the drama of the movement and excitement of his surroundings, and he achieved success at a very early age.

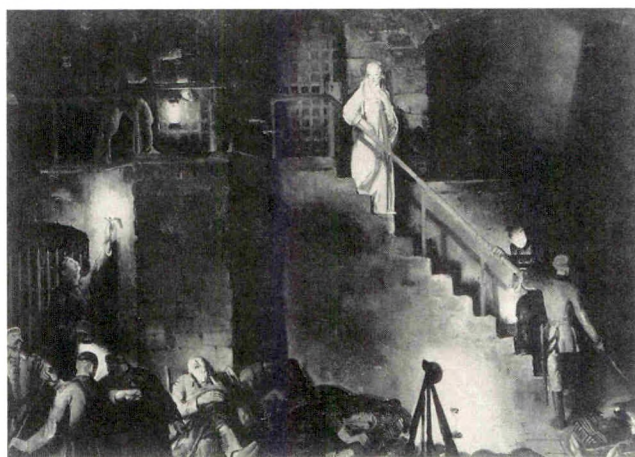
Bellows was born in 1882 in Columbus, OH. His mother was a devout Methodist, and hoped, as his middle name indicates, that he would become a bishop. However, he attended Ohio State University, where, in addition to being a very prolific cartoonist, he was an excellent basketball and baseball player, even being offered a tryout by the Cincinnati Reds. In 1904 he left Ohio State at the start of his senior year and entered the New York School of Art, which was operated by the famous American artist, William Merritt Chase. Soon after, he became a student of Robert Henri, the major mentor of the Ashcan artists. During the next several years, Bellows had phenomenal success. Within 5 years he had sold his first painting to a major museum and became, at the age of 26, the youngest associate member of the National Academy of Design. Four years later, before he turned 30, he became a full member.

Bellows was considered by most critics to be a member of the Ashcan School because of his honest pictures of New York and its people. However, he did not participate in the seminal exhibit in 1908, which directly challenged academic authority, by a group of painters known as The Eight, several of whom were prominent members of the Ashcan School. His popularity with critics and patrons of the arts was thus not damaged by controversy. In addition, the athletic Bellows was so personally pleasant that his popularity was equally great among his fellow artists, most of whom could claim only a small part of his success.

Bellows today is best known for his pictures of boxing. He did not paint from sketches but used his unusual memory to recreate scenes later in the studio. He was thus sitting at ringside during the famous Dempsey-Firpo fight in 1923 when Luis Angel Firpo knocked Jack Dempsey out of the ring into—according to Bellows's story—Bellows's lap. This moment was captured later by Bellows in one of America's most memorable paintings (Whitney Museum, New York). The titles of just a few of his other works, *River Rats*, *Dance in a Mad House*, *Forty-Two Kids*, *Up the Hudson*, *Excavation at Night*, *Steaming Streets*, *The Lone Tenement*, *Polo at Lakewood*, *Men of the Docks*, *Big Dory*, *Nude with Parrot*, *Tennis at Newport*, and *My Mother*, demonstrate the wide range of his genre subjects. In addition to the large body of paintings that he rapidly produced, Bellows became a skillful and successful printmaker, often making etchings related to his paintings.

In 1918, Bellows made a rare excursion into historical art for the painting *Edith Cavell*. Edith Cavell was a British nurse who served at the Red Cross Hospital in Brussels during World War I. She almost single-handedly helped 200 Allied soldiers to escape to Holland from Belgium in 1914 and 1915. She was subsequently caught by the Germans, court-martialed, and executed on October 12, 1915. Her execution had a dramatic impact both in England and the United States. The painting is one of the works of art that Bellows painted between 1916 and 1918 in reaction to reports of German atrocities. In the painting, and in the lithograph that Bellows also produced, Edith Cavell is dramatically silhouetted in white at the top of a staircase, defiant as her captors begin to ascend the stairs to capture her. Another American painter complained that Bellows should not have depicted the scene, as he could not have been present at Nurse Cavell's capture. Bellows responded that he did not think that Leonardo da Vinci "had a ticket to the Last Supper."

History will never know how great George Wesley Bellows would have been. Early in 1925 he developed appendicitis and died shortly thereafter on January 8 at the age of 42. In the 21 years since his arrival in New York as a 22-year-old student, he had produced more than 600 paintings. Today his paintings are in the collections of all major American museums. He uniquely captured the varied vitality, mood, and excitement of the times in which he lived.



George Wesley Bellows (1882–1925), *Edith Cavell*, 1918. Oil on canvas, 45 × 63 in. Museum of Fine Arts, (The James Philip Gray Collection), Springfield, MA.

¹ Department of Radiology, Mount Auburn Hospital, 330 Mount Auburn St., Cambridge, MA 02238.

Detection of Renal Stones with Real-Time Sonography: Effect of Transducers and Scanning Parameters

Carolyn Kimme-Smith¹
 Rita R. Perrella
 Laszlo P. Kaveggia
 Sachiko Cochran
 Edward G. Grant

Three experiments with a variety of transducers and scanning parameters were designed to investigate if renal stones could be detected with greater certainty by using particular transducers or scanning parameters. First, the lateral resolution, derived from the -6 -dB size of the beam profile, was measured at various depths for five transducers commonly used for renal sonography. Second, an in vitro test object was constructed from bovine liver, porcine kidneys, and two renal calculi to assess gray-scale map effects on shadow visibility before and after storage in the digital scan converter. The third experiment combined 15 lithotripsy patients with known renal stones with 16 patients in whom the results of renal sonography and other radiographic procedures suggested renal calculi. The group of 15 patients was scanned several times with the transducers and gray-scale maps studied earlier, and the group of 16 patients was scanned only with one transducer and one gray-scale map. On radiographs, 12 of the 16 patients did not have renal calculi.

Sonograms of the test object showed that low-contrast images were best for detection of posterior shadows. Three radiologists interpreted the 31 sonograms with a sensitivity of 81% and a specificity of 86% for detecting renal stones. For the 15 cases of renal stones scanned with a variety of transducers, the three radiologists found that annular-array transducers depicted stone shadowing with less ambiguity than mechanical sector transducers did 81% of the time.

AJR 157:975-980, November 1991

Use of sonography for detecting renal calculi has been disappointing. Of the factors that may contribute to sonography's lack of specificity, the need to show posterior acoustic shadowing may be the most problematic. The factors contributing to shadowing by renal stones were first described for B-mode sonography in an in vitro experiment by King et al. [1]. Since that paper was published, two other investigations in which the accuracy of real-time sonography for in vivo detection of renal stones was assessed have been reported [2, 3]. In both investigations, the stone size was estimated from radiographs, although the effect of variable magnification was not described. Baumgartner et al. [2] could not detect stones less than 5 mm in diameter and missed 19 (42%) of the 45 stones whose largest dimension was between 6 and 10 mm. The sonographic equipment in this study consisted of mechanical 3- or 5-MHz transducers. Middleton et al. [3] did not describe the type of equipment they used or the criterion they used for stone detection. The authors were, however, able to detect 24 of the 25 stones 5 mm or less in diameter. More recently, an in vitro experiment with renal calculi embedded in tissue-equivalent gel established that higher frequency transducers could be used to detect calculi as small as 0.8 mm in diameter [4].

Our clinical experience did not support the results of the last two studies. Stones smaller than 5 mm in diameter were extremely difficult to detect with or without posterior shadowing. We therefore undertook our own study in an effort to improve stone detection.

Received April 22, 1991; accepted after revision July 3, 1991.

¹ All authors: Department of Radiology, University of California, Los Angeles, School of Medicine, Los Angeles, CA 90024. Address reprint requests to C. Kimme-Smith.

0361-803X/91/1575-0975
 ©American Roentgen Ray Society

Methods

We tested a variety of transducers and scanning parameters in order to duplicate the results of Middleton et al. [3]. As part of this effort, the effects of beam profile on stone shadowing were investigated. First, we tested a variety of transducers to characterize the depth at which they were most likely to detect small stones; then we used those transducers in a series of in vitro experiments to scan renal calculi embedded in porcine kidneys to test the effects of scanning parameters on stone shadowing; finally, we scanned a series of patients after extracorporeal shock-wave lithotripsy (ESWL) with the tested (and some untested) transducers and asked a panel of three radiologists specializing in sonography to evaluate the multiformat scans generated.

Transducers' Lateral and Elevation Resolution Characteristics

The position of the focal zone with respect to the position of the renal stone has been shown to be critical for stone shadowing [1]. In particular, when phased-array transducers were included among the imaging equipment, out-of-the-imaging-plane focusing (slice thickness) at the depth of the stone was a critical factor for the reproduction of posterior shadowing [5]. If each A-line intersecting the renal stone is completely attenuated by the stone, posterior shadowing will result. If the dimensions of the stone are smaller than a cross section of the ultrasound beam, the transducer will receive a signal from tissue posterior to the stone, which will decrease shadowing there (Fig. 1). For example, if the resolution of a transducer in the lateral direction is 4 mm at a depth of 6 cm, a 2-mm renal stone located 6 cm from the transducer will block only about one fourth of the beam; echoes posterior to the stone will be only slightly decreased. Furthermore, scatter from the surrounding tissue will help fill in the area posterior to the stone. For phased-array transducers, the slice-thickness resolution does not necessarily match lateral resolution. Therefore, a phased-array transducer can be correctly focused for a depth of 6 cm, and have lateral resolution of 2 mm, but the slice-

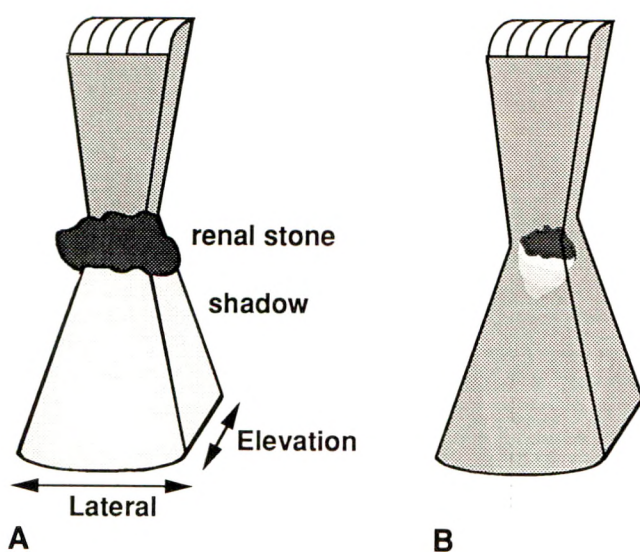


Fig. 1.—A linear- or phased-array transducer can have variable focus at different depths only in lateral direction. Elevation or slice-thickness focus is fixed.

A, If renal stone is larger than beam volume, a posterior shadow will result.

B, If stone is smaller than beam volume, posterior shadow will be filled in.

thickness resolution may still be 4 mm at that depth. Then a 2-mm stone will block only about half the sonography beam posterior to the stone. Unfortunately, manufacturers do not include information concerning slice-thickness resolution at various depths in their transducer documentation. For this reason, beam profile and slice-thickness resolution were measured on a commercial phantom [6] for the types of transducers commonly used for renal imaging at our facility.

Lateral resolution was measured for five transducers: two mechanical, one phased-array, and two annular-array. These 3- or 5-MHz transducers were used to image lightweight monofilament (fishing line) targets in a water tank. This technique is similar to quality-control testing with either the American Institute of Ultrasonographers in Medicine (AIUM) 100-mm test object or a gray-scale test object. By scanning across the monofilament (as opposed to scanning in the same direction as the monofilament), a point target is established. The dimensions of the image of the monofilament depend on the dimensions of the ultrasound beam at that depth and on the intensity of the reflected ultrasound. If the edge of the beam is measured where the intensity is half of the intensity at the center of the image of the monofilament (full-width-half-maximum), then this point is called the -6 -dB contour. A feature of the Advanced Technology Laboratories (ATL, Bothell, WA) Ultramark (UM) 8, used in manufacturing quality control, allowed -6 -dB contours to be marked around magnified images of the monofilament targets (Entrekin R, ATL, personal communication) (Fig. 2). As a result, the -6 -dB beam profile could be calibrated at depths from 2 to 8 cm. We next used an Advanced Technology Systems (ATS, Bridgeport, VT) test object (#538N) to measure slice-thickness resolution at the same range of depths for the three ATL array transducers, already tested for lateral resolution, and an Acuson (Mountain View, CA) phased-array transducer commonly used for renal imaging. The Acuson transducer could not be tested for its -6 -dB contour because this feature was unique to ATL transducers.

Slice-thickness focusing characteristics are the same as those for lateral focusing for mechanical transducers, so they did not need to be tested. The slice-thickness phantom consists of an inclined plane in a rubber-based material that attenuates the ultrasound at -0.5 dB/cm/MHz. By imaging across the inclined plane, the thickness of the slice can be qualitatively related to the slice-thickness resolution at that depth. Because gain affects measurements of slice-thickness resolution and is not calibrated, quantitative comparison measurements for slice-thickness resolution such as those done for lateral resolution were not possible; only ranges of relative focus could be established.

Selection of In Vitro Scanning Parameters

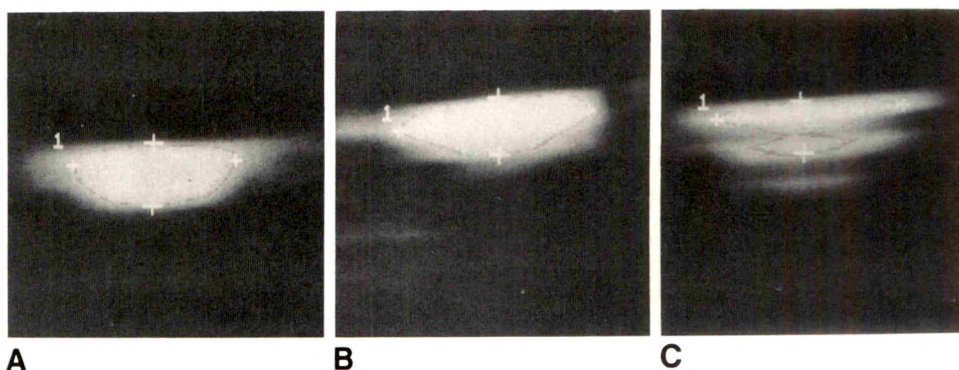
Once the transducers had been calibrated, a series of in vitro experiments were performed to assess the transducers' ability to image various renal stones embedded in porcine kidneys. As in an earlier study [1], bovine liver was used as intervening tissue. The purpose of these preliminary imaging exercises was to establish preprocessing gray-scale map effects on the visibility of shadows. Earlier tests with B-mode equipment did not have the range of processing options that are available on real-time equipment. The ATL UM 4, ATL UM 8, and an Acuson 128 transducer were tested with two renal stone sizes: $3.5 \times 5.0 \times 7.0$ mm and $11.0 \times 8.0 \times 4.5$ mm. Three test objects were constructed on 3 separate days, to ensure fresh tissue for all the combinations of parameters tested. The renal stone was inserted into the pelvis of the porcine kidney, which was then placed at the bottom of a container. The kidney was then covered with 3 cm of bovine liver and the container was flooded with saline. The tissues were pressed periodically during the next hour to aid the emergence of gas bubbles. Then the tissue was left

Fig. 2.—Transverse images of a monofilament submerged in a water tank, magnified eight times and contoured at -6 -dB level to show beam-profile characteristics of three transducers (all Advanced Technology Laboratories Ultramark 8 transducers).

A, 3.5-MHz annular-array transducer in far field.

B, 5-MHz phased-array transducer at last clearly imaged monofilament.

C, 5-MHz mechanical sector transducer near same depth as B.



alone for an hour, after which scanning was started. Dynamic range variations and the selection of gray-scale maps were evaluated with these renal stone test objects. An experienced technologist scanned the phantom until the stone was located. Then transverse and longitudinal views were made for each dynamic range available and for four gray-scale maps for each of the five ATL transducers as well as two Acuson transducers. Multiformat images were made of each view, each transducer, and each parameter variation. For two of the three test objects constructed, the large stone was used. The small stone ($3.5 \times 5.0 \times 7.0$ mm) was inserted into only one porcine kidney because of poor stone shadowing. Fresh tissue was used for each experiment, but because it was transported from commercial markets, it was at least 48 hr old at the time of imaging.

After all three experiments were completed, the multiformat images were reviewed by the physicist, technologist, and one of the three radiologists specializing in sonography. Each transducer was graded independently of the others, so that the multiformat image with the sharpest posterior shadowing was selected for each transducer and each sonography unit.

Clinical Evaluation

Finally, a series of 15 post-ESWL patients with known renal stones 1 cm or less in diameter, according to sonographic data, were scanned with two or more transducers. Stone size was determined by sonography because of the variable magnification associated with kidney, ureter, bladder (KUB) radiographs. The Acuson 128 and ATL UM 4 and ATL UM 8 sonography units were adjusted with gray-scale and focusing protocols established by the *in vitro* experiments. In addition to this group of 15 patients with renal stones, 16 of 49 patients who had renal studies were selected on the basis of the difficulty of sonographic diagnosis. All 16 sonograms had been interpreted as showing a suspected renal stone, but in fact the radiographic findings included a combination of normal kidneys, cases of echogenic foci in and near the kidneys, and a few complex cases with renal cysts and masses. Only five of these 16 patients had calculi. Selection and diagnosis were done by a radiologist specializing in genitourinary diagnosis who was not included among the three radiologists who later evaluated the sonograms. For all 31 cases, the urologist interpreted the abdominal plain films, tomograms, and excretory urograms that established whether a stone was present and its location. Location of the stone determined sonographically was confirmed radiographically; not all patients had all three radiographic studies. One lithotripsy patient had a stone beside a kidney and so was counted among the 12 control subjects (i.e., those without renal stones) in this study. The previous studies [1–4] did not include patients who did not have renal stones. Patients without renal stones were included in our study to assess the usefulness of sonography

for differentiating between true calculi and other highly echogenic intrarenal structures that produce some degree of acoustic shadowing. No attempt was made to make this a population without disease, so that sensitivity should be higher and specificity lower than in most populations of patients with renal disease.

The 31 cases were reviewed independently by three radiologists 6 to 10 months after the patients were originally scanned in order to decrease the likelihood that the radiologists would remember the original diagnosis for any of the patients. The two groups of patients were combined and then were split into two groups of 20 and 21 cases, with 10 cases present in both groups to establish consistency. As each case had from 12 to 36 images associated with it (two to six multiformat films), 20 cases took more than an hour to interpret, so the films were split into two groups to reduce interpreters' fatigue. The 10 duplicated cases consisted of three control subjects and seven patients who had renal calculi that had been misdiagnosed by at least one radiologist on the first review. The reinterpretation of these cases enabled the ambiguity of the decisions to be tested.

Each of the three radiologists was asked to decide if a stone was present in the kidney; the possible responses were "definitely," "maybe," and "no." When the radiologist answered that a stone was definitely present, he or she was then asked to select one or two images that best illustrated the presence of the stone.

Results

Transducers' Lateral and Elevation Resolution Characteristics

The lateral resolution of the five transducers tested with monofilament targets is given in Table 1. Images of three of these beam patterns are illustrated in Figure 2. Although the phased- and annular-array transducers' beam profiles have a similar shape, the externally focused mechanical-sector transducer (Fig. 2C) has a smaller, but more distorted, beam pattern. At less than a depth of 6 cm, the 3.5-MHz annular-array transducer is likely to represent stone shape and posterior shadowing of renal stones with greater resolution than the 3.0-MHz mechanical transducer would. At a depth of 7 cm, we would expect the same performance from the two transducers. Because these measurements were made in water, the defocusing effects of tissue are not represented by our results. Clinical scanning will reduce the depth at which both transducers are in focus. The difference between the 5-MHz annular- or phased-array transducers and the 5-MHz mechanical transducers is definitive at depths of 2 and 3 cm

also, but this is not helpful for most imaging of renal stones. Slice-thickness resolution was compared for two phased-array and two annular-array transducers. However, differences in gain, required for adequate penetration, made quantitative measurements impossible. Different types of sonographic equipment have different procedures for amplifying the received signal. Many of these procedures are nonlinear, noncalibrated, and proprietary. Their application changes the measurements of slice-thickness resolution.

The main purpose of calibrating the slice-thickness resolution of the phased- and linear-array transducers was to establish the range of depths at which the thickness of the image slice was focused. The four transducers tested were slice-focused at 7.5–9.5 cm for the 3-MHz probes and at 2.5–5 cm for the 5-MHz probes. Three transducers were phased arrays; one 5-MHz transducer was a linear array (L558).

Selection of In Vitro Scanning Parameters

Experiments with the smaller stone in the in vitro test object showed no shadowing posterior to the stone with either an annular- or a phased-array transducer. These experiments could show posterior shadowing with the larger stone only, possibly because of diffraction from intervening tissue and air trapped in the tissue before the tissue was submerged in the water bath. The sizes of stone tested were larger than those of stones routinely diagnosed in our clinic. Experiments with the larger stone clarified the effects of dynamic range and other gray-scale maps on visualization of renal stones (Fig. 3). Changing the gray-scale map did not improve detection of posterior shadows enough to change diagnosis for the two sizes of stones tested. For each transducer tested, the highest dynamic range and a linear gray-scale map improved visualization of stone shape and reduced posterior shadow fill-in, thus decreasing the ambiguity of stone recognition.

Dynamic range had more effect than the gray-scale map (postprocessing) on shadow fill-in for the Acuson than for the two ATL units tested. The ability to verify the shape of the gray-scale map on the Acuson unit was helpful, because the ATL map shape could only be assumed by its effect on contrast. The evaluation of the multifformat images for each transducer produced concurrence for the choice of linear gray-scale maps for all transducers and near concurrence (two out of three readers) for the highest dynamic range for all but one transducer. The ATL 5-MHz phased-array transducer with a short focus was preferred with a medium dynamic range to improve penetration. The radiologist inter-

preter generally preferred the next to highest dynamic range rather than the highest dynamic range because the highest dynamic range made the images look "flat."

Clinical Evaluation

The review of the 31 cases is reported in Table 2 as two truth tables. The first truth table reports the results of reviewing the 31 cases, including the first interpretation of the 10 cases that were reinterpreted later. The second truth table contains the results when the second interpretation of the 10 repeated cases is included instead of the results of their first interpretation. Sensitivity remained the same for both truth tables, but specificity decreased because some of the no answers moved into the uncertain category on the second interpretation. Differences between the three radiologists for each interpretation were less than 4%, and this difference mainly consisted of one radiologist's uncertain diagnosis replacing a no-stone diagnosis. However, as an uncertain diagnosis will result in further treatment of the patient (such as further imaging), uncertain diagnoses should probably be counted as stone-present diagnoses. In this case, true-positive values would have increased to 93%.

The three radiologists selected the multifformat images of the 19 cases of renal stones in which the stones were shown with the least ambiguity. They selected annular transducers 34 times, both annular and mechanical transducers 11 times, and mechanical transducers 12 times. Phased-array transducers represented a relatively small proportion of the transducers tested (three cases) because of radiologists' preferences when scanning, so that the usefulness of these transducers for detection of renal stones cannot be assessed in this study. For stones located no more than 6 cm from the transducer, the annular-array transducer clearly produced a sharper posterior shadow than did the mechanical sector transducers (Fig. 4). At a depth of 5 cm, lateral resolution of the stone illustrated was twice as good for the annular array as it was for the mechanical array. However, when a small patient with a 5.6-mm stone was imaged with a 5-MHz phased-array transducer focused at 2.5 cm, better shadowing resulted than when the annular-array transducer was used to image the same stone at a depth of 4 cm (Fig. 5).

Discussion

Recently purchased sonographic units have a variety of processing options and transducers that were not available 4

TABLE 1: Lateral Resolution (cm) When Scanning Monofilament Target

Transducer	Depth (cm)						
	2.1	3.1	4.2	5.2	6.1	7.1	8.1
3-MHz mechanical	1.10 ^a	0.87	0.79	0.61	0.51	0.42	0.51
5-MHz mechanical	0.61	0.50	0.32	0.34	0.41	0.42	0.52
3.5-MHz annular ^b	0.75	0.25	0.30	0.31	0.35	0.41	0.46
5-MHz annular ^b	0.18	0.20	0.25	0.28	0.39	0.42	0.44
5-MHz phased ^b	0.17	0.26	0.29	0.46	No penetration		

^a Lateral dimensions in centimeters at the -6-dB contour.

^b Focused at the depth measured.

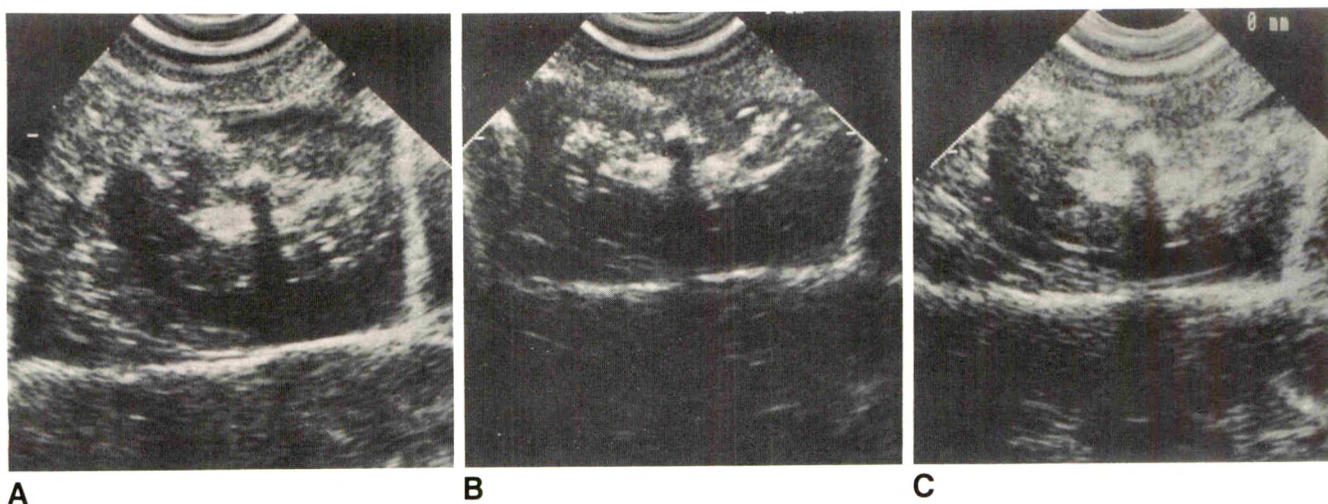


Fig. 3.—When an 11.0 × 8.0 × 4.5 mm stone is inserted into porcine kidney, a posterior shadow is present for all transducers tested.

A, Decreased dynamic range increases gray-scale contrast, which obscures shape of stone.

B, Higher dynamic range is less likely to fill in posterior shadow.

C, A logarithmic rather than a linear gray scale does not improve visualization of renal stone and fills in posterior shadow.

TABLE 2: Accuracy of Sonographic Detection of Renal Stones in 31 Cases

Sonographic Diagnosis	Radiographic Diagnosis	
	Stone Present	No Stone
First interpretation ^a		
Stone present	(TP) 46 (81%)	(FN) 0
Uncertain	7	5
No stone	(FP) 4	(TN) 31 (86%)
Total	57	36
Second interpretation ^a		
Stone present	(TP) 46 (81%)	(FN) 0
Uncertain	8	8
No stone	(FP) 3	(TN) 28 (78%)
Total	57	36

Note.—TP = true-positive, FN = false-negative, FP = false-positive, TN = true-negative.

^a Sum of three radiologists' interpretations.

years ago. Radiologists and technologists do not always select appropriate scanning equipment and parameters for detection of renal calculi because optimal scanning parameters are unknown. In this study, we hypothesized, on the basis of an early in vitro study [1], that characterizing the beam profile of transducers used for renal studies would facilitate the detection of renal stones. Furthermore, the use of gray-scale maps that tend to fill in anechoic shadows posterior to renal calculi will decrease detection of renal stones. The first two experiments provided information about optimal depths at which suspected renal calculi should be scanned with specific transducers and illustrated the deleterious effects of high-contrast gray-scale maps on posterior shadows. To test these two recommendations, we scanned 15 patients with known renal stones (after ESWL) by using the technique determined in our initial tests with several transducers. Because all 15 patients had renal calculi, we

added 16 patients in whom the diagnosis of renal calculi was equivocal.

Annular-array transducers can produce sharper images of renal stones and less noise in the posterior shadow of the scans than mechanical real-time transducers can. Phased- and linear-array transducers can produce diagnostic images similar to those produced by annular-array transducers when the stone is in the slice-thickness focus of the array. The thickness of a phased-array beam at a depth of 4 cm is dependent on a fixed-focus lens, whereas an annular-array transducer can focus in both the lateral and elevation directions dynamically. If the renal stone is located out of the elevation focal zone of a phased- or linear-array transducer, and if the stone is smaller than the beam profile at that depth, then little or no shadowing will result. However, stones smaller than 5 mm rarely have posterior shadows, even when imaged in the focal zone of the transducer. When a 5-MHz transducer was used, we found posterior shadowing of only one stone 5.6 mm in diameter (Fig. 5).

The two previous clinical investigations that used modern real-time sonographic equipment [2, 3] did not include control patients with renal disease that might mimic renal stones on sonography. When these results are compared with those of an in vitro study [4], it is clear that the heterogeneous tissue surrounding renal calculi defocuses the ultrasound beam significantly. The detection of small stones in a homogeneous gel was far superior to detection in our in vitro experiments with porcine kidney and to our clinical results. This corroborates the well-known ease of finding gallbladder stones when they are surrounded by anechoic bile. Our study has shown that echogenic foci in the kidneys that have posterior shadowing can be diagnosed correctly as renal stones 81% of the time; detection of the absence of a stone was more likely to vary with reinterpretation: 86% compared with 78%. All of the errors due to reinterpretation were the result of three of the 16 difficult cases, which had been chosen specifically for

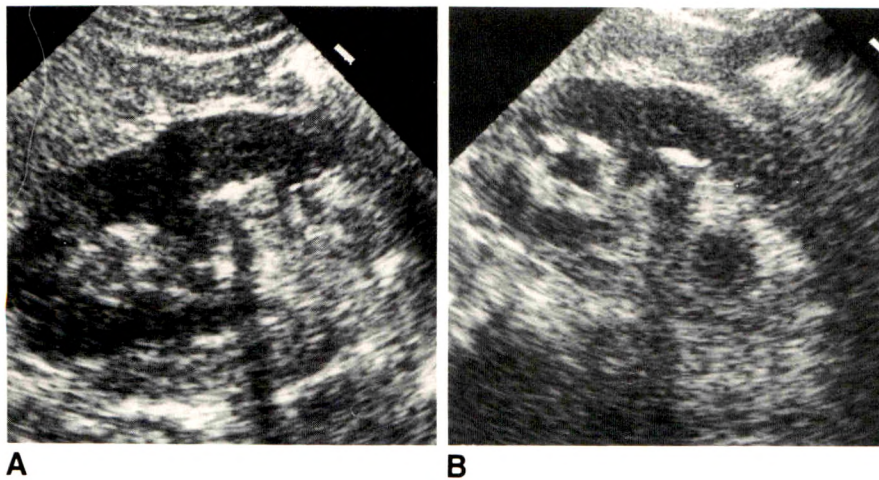


Fig. 4.—A and B, Largest stone imaged was similar in dimensions to that in Fig. 3. With high dynamic range and linear gray-scale map, posterior shadow is much more pronounced for an annular-array transducer operating at 3.5 MHz (A) than for a mechanical sector transducer operating at 3 MHz (B). All three radiologists preferred A. (Note that magnification differs for A and B.)

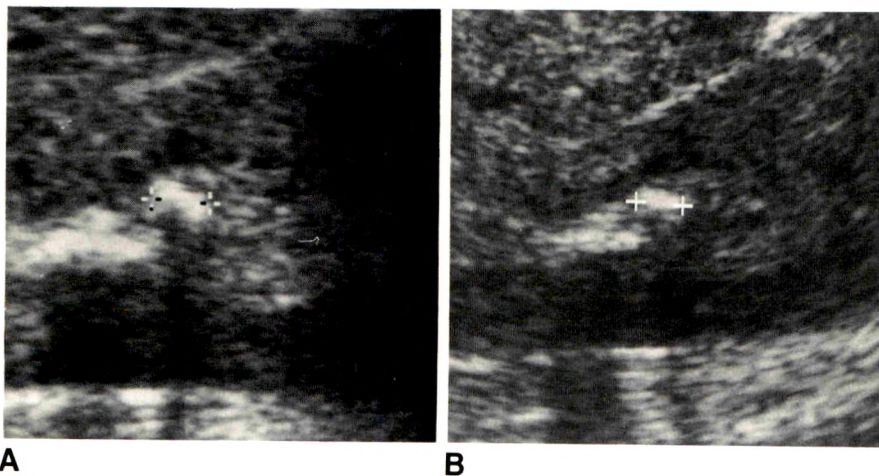


Fig. 5.—A and B, Smallest stone imaged was a 5.6-mm stone imaged with six transducers operating on three units. Larger stones are to left and below small stone. Acuson 128 operating with an L558 linear 5-MHz transducer (A) shows better shadowing than the ATL UM8 5-MHz annular-array transducer (B).

their ambiguity. In one case, a renal carcinoma with calcifications had a significant echogenic focus but no shadowing. In another, renal cysts with strong backwall echoes provided both echogenic foci and posterior shadowing from the cyst capsule. The second interpretation of these difficult cases emphasizes the problems associated with the use of sonography to rule out the presence of renal stones. Most radiologists specializing in sonography are more concerned when they cannot rule out a stone or when they are uncertain of the diagnosis (13%) than when they confirm what has been detected with a plain radiograph or tomogram. Sonography is often the first diagnostic procedure for many patients, so equivocal results do not encourage wider use of the technique. Radiologists should, therefore, choose transducers, scanning windows, and scanning parameters that will detect abnormalities unambiguously.

With all transducers, it remains difficult to rule out renal stones in highly echogenic kidneys. This effect can be reduced by reducing contrast, either by increasing dynamic range or by selecting a linear gray-scale map. Focal zones that can be varied should always be placed at the depth of the suspected stone, or slightly deeper than the stone. Placement of the focal zone for phased-, linear-, and annular-array transducers

was critical to stone shadowing. Placement of the focal zone at or slightly below the echogenic focus representing the renal stone made posterior shadowing sharper with less noise in the shadow. Because plain radiographs and tomograms are often used as a gold standard, and because the accuracy of these examinations also depends on the equipment and the patient, some ambiguity will remain about the size and position of the stone in any controlled clinical study.

REFERENCES

1. King W, Kimme-Smith C, Winter J. Renal stone shadowing: an investigation of contributing factors. *Radiology* 1985;154:191-196
2. Baumgartner BR, Steinberg HV, Ambrose SS, Walton KN, Bernardino ME. Sonographic evaluation of renal stones treated by extracorporeal shock-wave lithotripsy. *AJR* 1987;149:131-135
3. Middleton WD, Dodds WJ, Lawson TL, Foley WD. Renal calculi: sensitivity for detection with US. *Radiology* 1988;167:239-244
4. Choyke PL, Pahira JH, Dauros WJ, Nilges E, Dwyer AJ, Mun SK. Renal calculi after shock wave lithotripsy: US evaluation with an in vitro phantom. *Radiology* 1989;170:39-44
5. Goldstein A, Madrazo BL. Slice-thickness artifacts in gray-scale sonography. *JCU* 1981;9:365-375
6. Goldstein A. Slice-thickness measurements. *J Ultrasound Med* 1988;7:487-498

1991 ARRS Executive Council Award

Imaging of the Renal Arteries: Value of MR Angiography

Jörg F. Debatin¹
Charles E. Spritzer¹
Thomas M. Grist¹
Craig Beam¹
Laura P. Svetkey²
Glenn E. Newman¹
H. Dirk Sostman¹

We compared the efficacy of MR angiography with that of conventional angiography for visualizing the renal arteries and detecting renovascular disease. Thirty-three MR angiographic studies, consisting of axial two-dimensional (2-D) phase-contrast, coronal 2-D phase-contrast, and coronal 2-D time-of-flight acquisitions, were performed within 48 hr of conventional arteriography. The studies were done to evaluate possible renovascular hypertension ($n = 25$) or potential donor nephrectomy ($n = 8$). The three MR image sets were interpreted independently, in random order by three observers, with regard to the number of renal arteries, degree of vessel visualization, arteriovenous overlap, and presence of renovascular disease. A fourth interpretation was based on the combined axial and coronal phase-contrast image sets. Evaluation was limited to the proximal 35 mm of each renal artery. Renal artery visualization and detection of renovascular disease were more complete with coronal phase-contrast (80% sensitivity, 91% specificity) than with time-of-flight (53% sensitivity, 97% specificity) images. Combined axial and coronal phase-contrast images permitted visualization of the proximal 35 mm of all dominant renal arteries and detection of 13 of 15 stenoses (87% sensitivity, 97% specificity).

Our data suggest that biplanar MR angiography has considerable potential as a noninvasive screening technique for the evaluation of renovascular disease.

AJR 157:981-990, November 1991

Interest in the identification of renovascular disease in patients with hypertension has increased because of the availability and effectiveness of treatment with percutaneous transluminal angioplasty [1, 2].

To date, conventional arteriography and intraarterial digital subtraction angiography are the most accurate means of assessing the presence and severity of renal artery stenosis [3, 4]. Because these techniques are invasive, require contrast material, and are expensive, they are not well suited for screening a population of patients with a low prevalence of renal artery stenosis. Many other diagnostic screening techniques have thus been evaluated [1-8].

Although MR angiography has been reasonably successful in the evaluation of circulation in the head and neck [9, 10], renal artery imaging poses a number of particular challenges. These include artifacts from cardiac, respiratory, and bowel motion; problems with stationary tissue suppression; the inherent complex flow patterns and directions of the renal arteries; and vessel overlap from renal veins, the inferior vena cava, and the adrenal and gonadal vasculature [11, 12]. These difficulties have translated into variable success in the assessment of renovascular disease with MR angiography, ranging from not accurate (50% sensitivity) [13] to very accurate (100% sensitivity) [14].

We performed a prospective study to evaluate four MR angiographic image sets (axial two-dimensional [2-D] phase-contrast, coronal 2-D phase-contrast, coronal 2-D time-of-flight, and combined axial and coronal 2-D phase-contrast) with respect to image quality and the degree of visualization of dominant renal arteries, acces-

Received March 20, 1991; accepted after revision July 5, 1991.

Presented at the annual meeting of the American Roentgen Ray Society, Boston, May 1991.

¹ Department of Radiology, Box 3808, Duke University Medical Center, Durham, NC 27710. Address reprint requests to C. E. Spritzer.

² Department of Medicine, Duke University Medical Center, Durham, NC 27710.

0361-803X/91/1575-0981
© American Roentgen Ray Society

sory renal arteries, and renovascular disease. Conventional arteriography was used as the reference standard.

Subjects and Methods

Population of Patients

During a 6-month period, MR angiography of the renal arteries was performed in 32 patients, 18 men and 14 women 30–77 years old (average age, 52 years), who had undergone routine conventional arteriography for evaluation of possible renovascular hypertension ($n = 24$) or for possible donor nephrectomy ($n = 8$). One patient was examined twice, once before and once after percutaneous transluminal renal artery angioplasty. Criteria for participation in the study included willingness to give informed consent as set forth by our institutional review board, lack of standard contraindications to MR imaging (e.g., pacemaker, ocular metallic foreign bodies, claustrophobia, or recent surgery), and our ability to perform the MR examination within 48 hr of conventional arteriography.

MR Angiography

MR angiography of the renal arteries was performed with a 1.5-T MR imager (Signa System, General Electric, Milwaukee, WI) with the patient in shallow respiration. The body coil was used for signal transmission and reception. To localize the aorta and renal arteries, spin-echo scout images, 500/14 (TR/TE), were obtained in the coronal projection through the kidneys by using a 256×128 matrix, a 40-cm^2 field of view, and 10-mm-thick sections.

The MR angiography techniques, 2-D phase-contrast and 2-D time-of-flight, are part of the Signa System Vascular Magnetic Resonance Package. 2-D phase-contrast images were obtained in both axial and coronal planes with the following parameters: 40/8.4 (TR/TE), 60° flip angle, 256×128 matrix, 28-cm^2 field of view, two excitations, and first-order gradient-motion nulling. The velocity-encoding value (velocity-yielding π radians of phase shift) was 40 cm/sec. Seven-millimeter axial sections with 2-mm overlap between consecutively acquired images were obtained from the more cephalad superior pole to the more caudad inferior pole of either kidney. The same slice parameters were used to obtain coronal images from 10 mm anterior to 25 mm posterior to the aorta.

For each phase-contrast image, the system acquires a magnitude gradient-recalled echo image and three raw data sets for the three flow-encoding directions: right to left, superoinferior, and anteroposterior. The magnitudes of these data sets are then combined into a total flow diagram for that particular section [15]. Depending on kidney size and location, between 11 and 23 image sections (average, 16) were obtained in the axial projection, with acquisition times of 8–16 min. On average, only 11 images were obtained in the coronal projection (range, 9–14), with acquisition times between 7 and 12 min.

2-D time-of-flight MR imaging was performed in the coronal plane with the following scan parameters: 40/8.4 (TR/TE), 60° flip angle, 256×128 matrix, 32-cm^2 field of view, an average of two excitations, and first-order gradient-motion nulling. Between 20 and 28 consecutively acquired 4-mm-thick sections with 2-mm intersection overlap were obtained from 10 mm anterior to the aorta to 25 mm posterior to the aorta. Acquisition times ranged from 4 to 6 min.

In order to reduce venous signal from the inferior vena cava and the renal veins, 40-mm-wide saturation pulses were placed inferior to the lower pole of the kidneys and over the renal cortex on either side, extending with its medial margin into the renal medulla. These saturation pulses remained unchanged for phase-contrast and time-of-flight acquisitions.

Two maximum-pixel-intensity projection (MIP) images along the slice direction [16, 17] were created for each of the three MR angiography acquisitions. The first was based on all obtained sections. The second, based on fewer selected images and containing only major portions of the renal arteries, was obtained in an attempt to minimize overlap from extraneous vessels.

Conventional Angiography

Conventional angiography was performed by using a 5-French pigtail catheter. Contrast material was injected at 25 ml/sec for 2 sec, and films were obtained in the anteroposterior projection at three frames per second. If the renal arteries were not clearly visualized, the arteriogram was repeated in oblique projections. If selective renal artery injections were required to adequately define the renovascular anatomy, a preformed end-hole catheter was used, and the injection rate varied with the vessel size.

Image Analysis

Each of the 33 MR angiograms was independently evaluated by three experienced MR radiologists, all of whom had no knowledge of the clinical histories of the patients or the results of the conventional arteriograms. For each study, four separate interpretations, based on four different image sets (axial 2-D phase-contrast, coronal 2-D phase-contrast, coronal 2-D time-of-flight, and a combination of axial and coronal 2-D phase-contrast), were rendered in random order. Although each evaluation was initially based on the MIP images only, the final interpretation included both MIP images and images of individual sections.

Each image set was assessed with regard to the number of renal arteries present, the degree of vessel visualization, the degree of venous overlap, and the presence of renovascular disease. Each renal artery was divided into three segments: the ostium, the proximal 15 mm (1–15 mm), and the distal 20 mm (15–35 mm). Each segment was characterized as either seen, not seen owing to stenosis, or not seen owing to artifact. It was noted separately if venous overlap impaired proper assessment of the renal artery.

On the basis of previous *in vivo* MR angiographic evaluations of stenosis (Porges R et al., presented at the annual meeting of the Radiological Society of North America, November 1990; Grist TM et al., unpublished data), renovascular disease was defined as a segment of luminal narrowing and/or signal loss and graded on a four-point scale ranging from mild stenosis to occlusion. Mild disease ($<50\%$ stenosis) was defined as mere luminal narrowing; moderate disease (50–74% stenosis), as reduction of the arterial diameter with a focal flow void (<5 mm); and severe disease (75–99% stenosis), as a longer region of signal void (>5 mm) with distal reconstitution of flow. Vessel occlusion was suggested by total lack of signal distal to the lesion.

Conventional arteriograms, considered adequate for diagnosis in all cases, were interpreted independently with regard to the number of renal arteries and the presence of renal artery stenosis by a vascular radiologist who had no knowledge of the identity or clinical history of the patient. It was noted if lesions were caused by fibromuscular dysplasia. Stenoses were classified as ostial, proximal (first 15 mm), distal (15–35 mm), or very distal if they occurred beyond the proximal 35 mm. Analogously to the MR angiographic interpretations, disease was characterized as mild ($<50\%$), moderate (50–74%), severe (75–99%), or as occlusion. The grade was based on the most severe reduction of the arterial diameter.

As the evaluation of the MR angiographic images did not include analysis of the renal arteries distal to the first 35 mm, lesions detected

with conventional angiography beyond 35 mm were not included in the analysis.

Statistical Analysis

In order to evaluate the diagnostic accuracy of each image set for the three observers, the median rating of the observers was used. The McNemar test was used to compare the degree of vessel visualization for the four evaluated image sets [18].

Results

Renal Artery Visualization

Regardless of technique or projection, adding images of individual sections to the processed MIP images reduced the number of nonvisualized renal artery segments by 50% or more (Table 1).

Renal arteries were visualized more completely with the coronal phase-contrast technique than with the time-of-flight technique regardless of whether interpretation was based on processed MIP or images of individual sections (Table 1). The difference in the number of visualized renal artery segments between coronal phase-contrast and coronal time-of-flight acquisitions was statistically significant ($p < .05$).

Axial and coronal projections complemented one another in the full evaluation of the renal arteries (Fig. 1). While evaluation of the renal ostium was superior in the coronal projection, distal renal artery segments were better visualized in the axial plane. Combined interpretation of axial and coronal phase-contrast projection and individual images allowed complete assessment of the renal ostia and proximal 35 mm of all 66 dominant renal arteries (Table 1).

Venous Overlap

Overlap by extraneous vessels, particularly the renal veins, was one of the major causes of nonvisualization of renal artery segments. The lack of arteriovenous differentiation affected interpretations based on processed MIP images in a similarly adverse fashion regardless of technique or imaging plane (Fig. 2): venous overlap impaired assessment of 47

dominant renal arteries (19 right-sided and 28 left-sided) on coronal time-of-flight MIP images and of 28 renal arteries (11 right-sided and 17 left-sided) on coronal and 24 renal arteries (10 right-sided and 14 left-sided) on axial phase-contrast MIP images. Addition of the images of individual sections sensitive to flow direction eliminated all confusion due to venous overlap on both axial and coronal phase-contrast images (Figs. 2 and 3). However, venous overlap remained a factor in the evaluation of the coronal time-of-flight image set, impairing complete assessment of 10 right-sided and 20 left-sided dominant renal arteries.

Number of Renal Arteries

Conventional arteriography revealed unilateral accessory renal arteries in five patients and bilateral vessels in two patients. With MR angiography, these were seen better in the coronal than in the axial plane. Five accessory renal arteries were identified on the coronal phase-contrast MR images, whereas only two were detected in the axial plane. A sixth accessory vessel was identified when interpretation was based on both the axial and the coronal phase-contrast images. Only three of the seven accessory renal arteries were identified correctly on the coronal time-of-flight images.

Renovascular Disease

Including the seven accessory renal arteries, a total of 73 renal arteries were shown on conventional arteriography in 33 patients. Of these, 54 renal arteries were angiographically classified as normal. Abnormalities in the proximal 35 mm were identified in 12 dominant and three accessory renal arteries. In five of these 15 cases, disease was classified as mild ($<50\%$); in four, as moderate ($50\text{--}74\%$); in five, as severe ($75\text{--}99\%$); and in one, as occlusion. Four additional lesions were detected beyond 35 mm from the renal ostia. Bilateral lesions were detected in two patients, both of whom had angiographic evidence of bilateral fibromuscular dysplasia. They were graded as moderate ($50\text{--}75\%$) in one and as mild ($<50\%$) in the other patient. Since only the proximal 35 mm of each renal artery was evaluated on the MR angiographic

TABLE 1: Summary of Renal Artery Segments Not Visualized with MR Angiography

Acquisition/Images Evaluated	No. Not Visualized, by Segment ($n = 198$)			
	Ostium	1–15 mm	15–35 mm	Total
Coronal time-of-flight				
MIP	8	15	29	52
MIP + images of individual sections	0	3	15	18
Coronal phase-contrast				
MIP	0	4	14	18
MIP + images of individual sections	0	1	8	9
Axial phase-contrast				
MIP	3	2	7	12
MIP + images of individual sections	3	1	2	6
Axial + coronal phase-contrast				
MIP	0	2	3	5
MIP + images of individual sections	0	0	0	0

Note.—MIP = maximum-intensity projection.

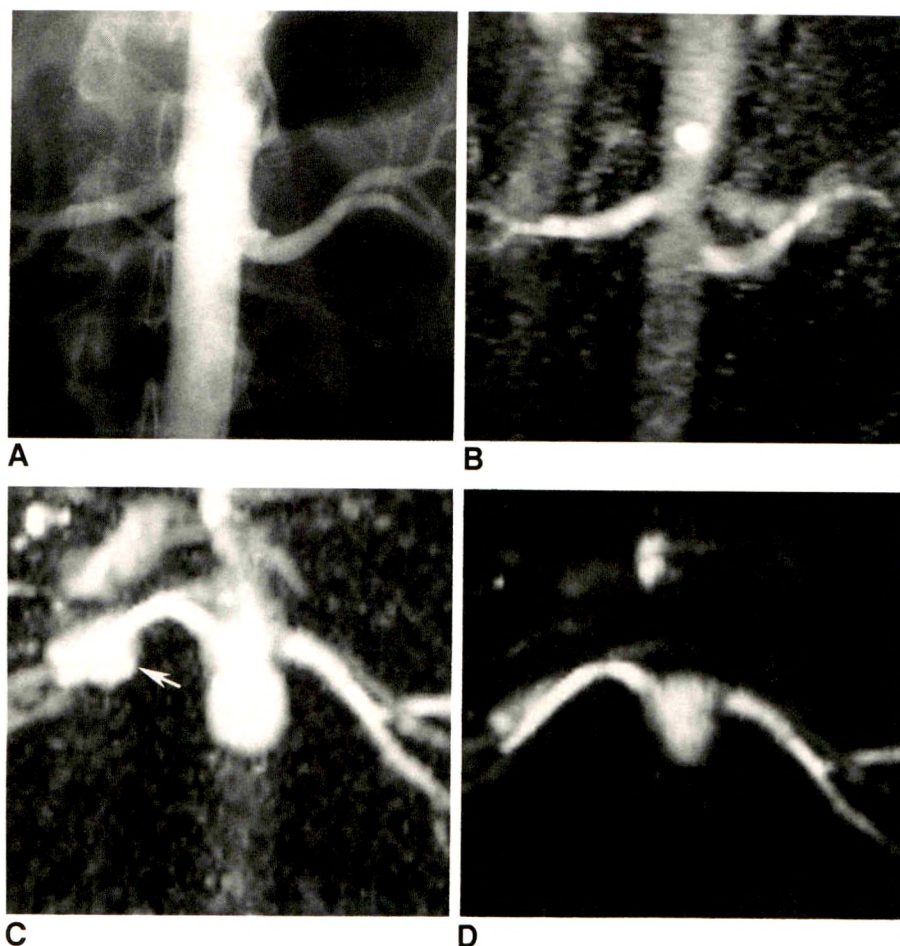


Fig. 1.—A and B, Normal bilateral renal arteries are seen on conventional angiogram (A) and coronal maximum-pixel-intensity projection (MIP) phase-contrast image (B).

C, Axial MIP phase-contrast image based on all acquired image sections complements coronal MR angiogram by depicting more distal renal artery segments as they extend into renal hila. Overlapping inferior vena cava (arrow) obscures parts of right renal artery, mimicking focal dilatation.

D, MIP image based on selected sections only, with extraneous vessels eliminated from image. Full extent of both renal arteries can now be adequately assessed.

images, these peripheral lesions were not included in further analysis.

Although both coronal image sets were equally specific in the detection of renal artery disease (91% for phase-contrast, 97% for time-of-flight), more lesions were detected on coronal phase-contrast than on time-of-flight images. The overall sensitivity for the coronal time-of-flight image set of 53% was considerably lower than the 80% sensitivity for the coronal phase-contrast acquisition (Table 2).

Phase-contrast images in the axial plane (97% specificity, 67% sensitivity) were slightly more specific but less sensitive than were coronal phase-contrast images (91% specificity, 80% sensitivity). In the axial projection, two normal renal arteries were interpreted as having mild stenosis, and interpretation of the coronal phase-contrast images suggested moderate stenosis in one and mild stenosis in four non-diseased renal arteries. Five stenoses were missed on the axial images; three stenoses were not detected on the coronal images.

The presence of renovascular disease was assessed most accurately when interpretation was based on both axial and coronal phase-contrast images (Table 2, Fig. 4). Only two of 58 normal renal arteries were thought to harbor mild stenosis, for an overall specificity of 97%. Mild stenoses (<50%) were undergraded as normal and overgraded as moderate in one

case each and were identified correctly in three cases. Moderate stenoses were correctly identified in two renal arteries, overgraded as severe in one case, and not identified in a branch vessel arising proximally off the main renal artery (Fig. 5). All five severe stenoses and one occluded vessel were identified correctly as such on the combined axial and coronal phase-contrast images. The overall sensitivity of the combined axial and coronal phase-contrast image sets was 87% for all stenoses and 91% for significant stenoses (>50%).

Interobserver Variability

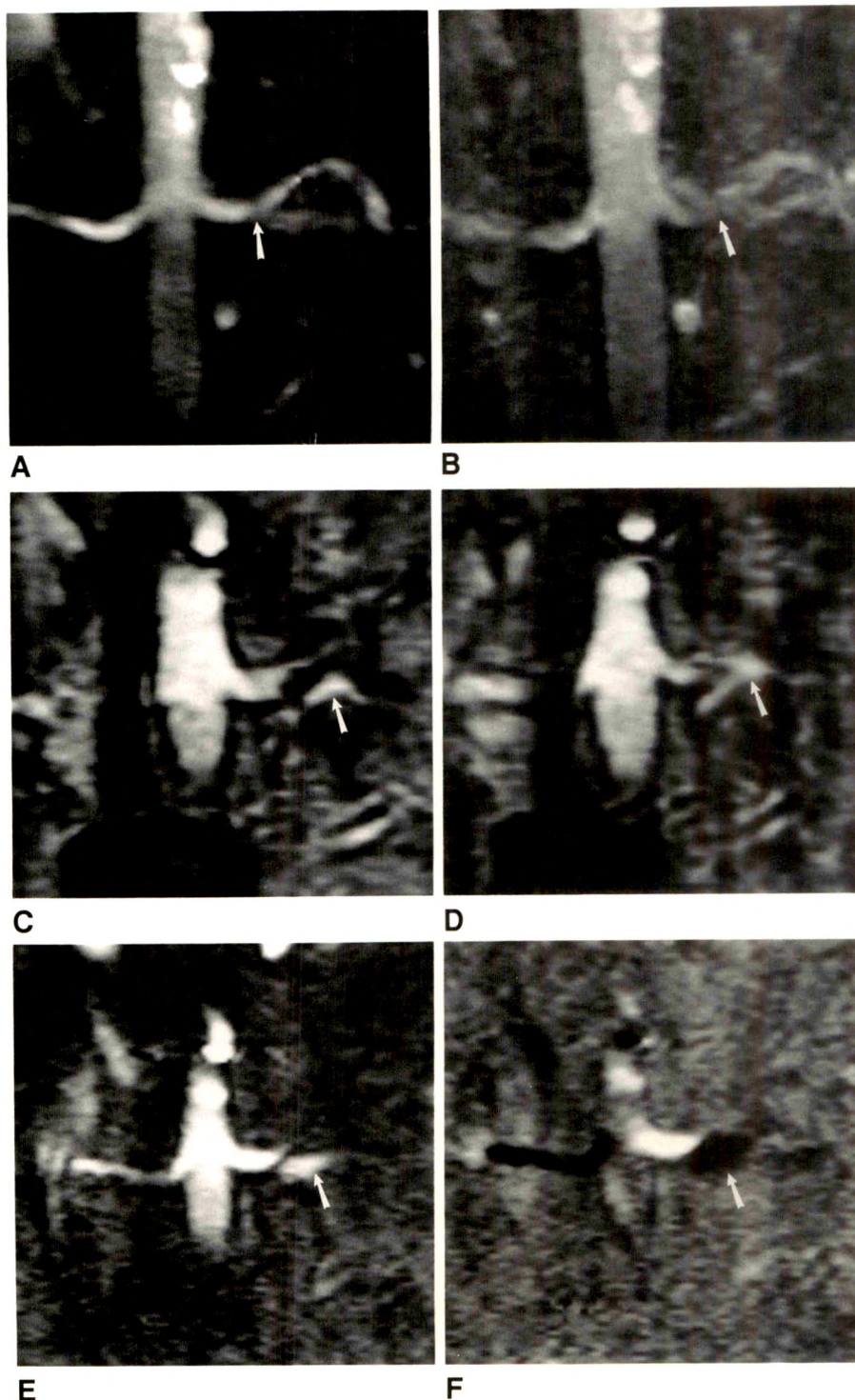
On the basis of combined axial and coronal phase-contrast image sets, the independent interpretations made by the three observers showed overall concurrence. Observer 1 correctly assessed the proximal 35 mm in 65 of the 73 renal arteries. Three renal artery stenoses were overgraded and five renal artery stenoses were undergraded by that observer. Observer 2 correctly graded 65 of 73 renal artery stenoses and overgraded and undergraded four stenoses each. Observer 3 correctly assessed 64 artery stenoses, overgraded six, and undergraded three. All stenoses greater than 50% were correctly identified and classified by all three observers. Of 54 angiographically disease-free vessels, 49 were characterized as normal by all three observers.

Fig. 2.—A and B, Coronal phase-contrast (A) and time-of-flight maximum-pixel-intensity projection (B) images of normal bilateral renal arteries. Vessel contrast is better and signal is greater in distal renal artery segments on phase-contrast image. Because of vessel overlap, a small segment in midportion of left renal artery is poorly shown on both images (arrows).

C and D, Individual time-of-flight images aid in evaluation of left ostium and proximal left renal artery. It cannot be determined whether signal distal to proximal left renal artery segment (arrows) is arterial or venous.

E, Individual-section phase-contrast modulus image shows same region of signal (arrow) distal to proximal segment of left renal artery.

F, Right/left flow-encoded image eliminates arteriovenous confusion. Dark signal distal to left proximal renal artery (arrow) indicates a left-to-right flow direction corresponding to left renal vein.



Discussion

Potentially correctable renovascular disease is the cause for hypertension in up to 5% of the 60 million Americans who have increased blood pressure [3] and is implicated in an undetermined number of patients with renal failure [2, 6]. These numbers emphasize the need for a highly sensitive and

specific screening method that is noninvasive, easily available, and relatively inexpensive.

The capability for studying blood flow noninvasively with MR has long been recognized [19, 20] and is dependent on two principles: time-of-flight effects and the phase difference between flowing and stationary spins [21, 22]. The signal of flowing blood is furthermore influenced by the character (ve-

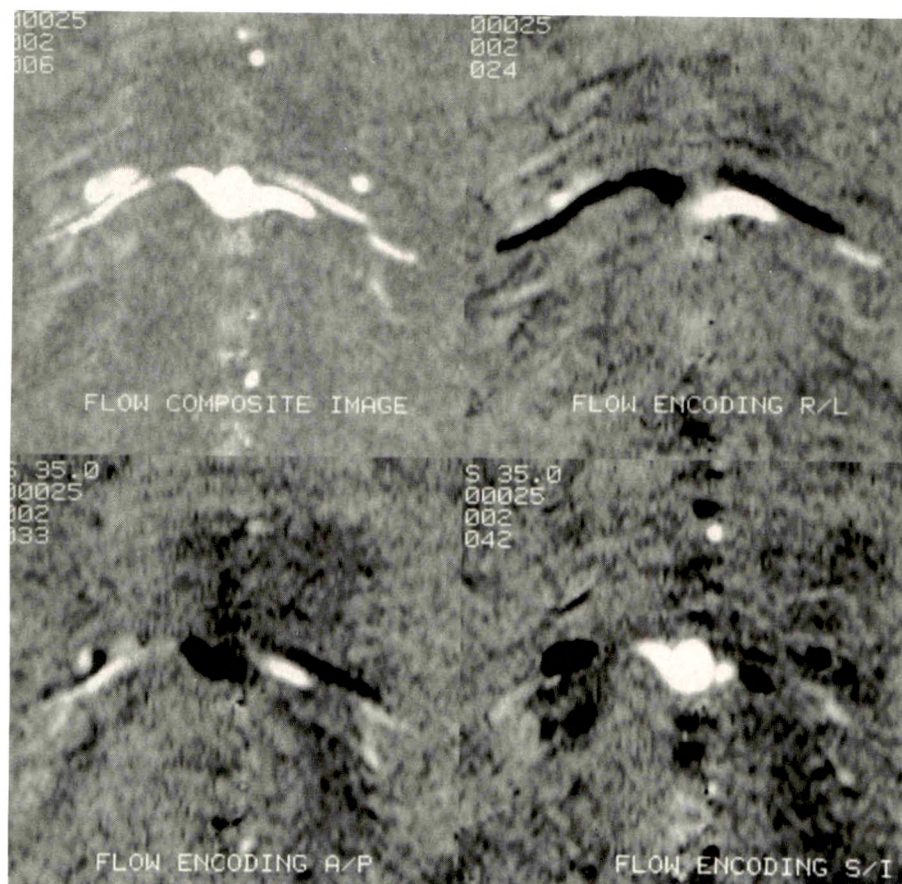


Fig. 3.—By showing flow direction, individual phase-sensitive images are very useful in differentiating arterial from venous vessels. Composite flow image (upper left) shows bright signal for all flowing spins and is generated from remaining three images, which are sensitive to flow moving side to side (upper right), anteroposteriorly (lower left), and superoinferiorly (lower right). Flowing spins moving right to left, anterior to posterior, and superior to inferior are displayed as bright pixels, whereas flow left to right, posterior to anterior, and inferior to superior is displayed in black.

TABLE 2: Detection of Renovascular Disease with MR Angiography

Acquisition	% Sensitivity	% Specificity
Coronal time-of-flight	53	97
Coronal phase-contrast	80	91
Axial phase-contrast	67	97
Axial + coronal phase-contrast	87	97

locity and acceleration) of flow as well as by sequence parameters and the orientation of the vessel to the imaging plane [21, 23]. MR imaging has shown considerable promise as a noninvasive tool in the evaluation of vascular morphology throughout the body [9, 10, 16, 21, 22, 24]. If sufficiently accurate, MR angiography could prove cost-effective as a noninvasive screening tool for assessing renovascular disease.

Each of the two fundamental approaches to vascular MR, time-of-flight and phase-contrast imaging, offer theoretical advantages and disadvantages over MR imaging of the renal arteries.

Time-of-flight imaging is based on conventional gradient-echo scanning with gradient-moment nulling and relies on flow-related enhancement to distinguish moving from stationary spins. Advantages include its minimal saturation effects for normal flow velocities and its short acquisition time (4–6 min in this study). These must be weighed against reduced

sensitivity to in-plane blood flow and its difficulty in distinguishing venous from arterial blood flow. Phase-contrast imaging uses flow-induced phase shifts to distinguish flowing blood from surrounding tissue. Advantages include excellent background suppression; reduced intravoxel dephasing; the ability to encode for variable velocities; and the ability to generate magnitude and phase images in three different flow-encoding directions, facilitating differentiation of arterial from venous flow. These are offset by relatively long image acquisition times and increased sensitivity to signal loss from intravoxel spin-phase dispersion due to turbulent flow [24].

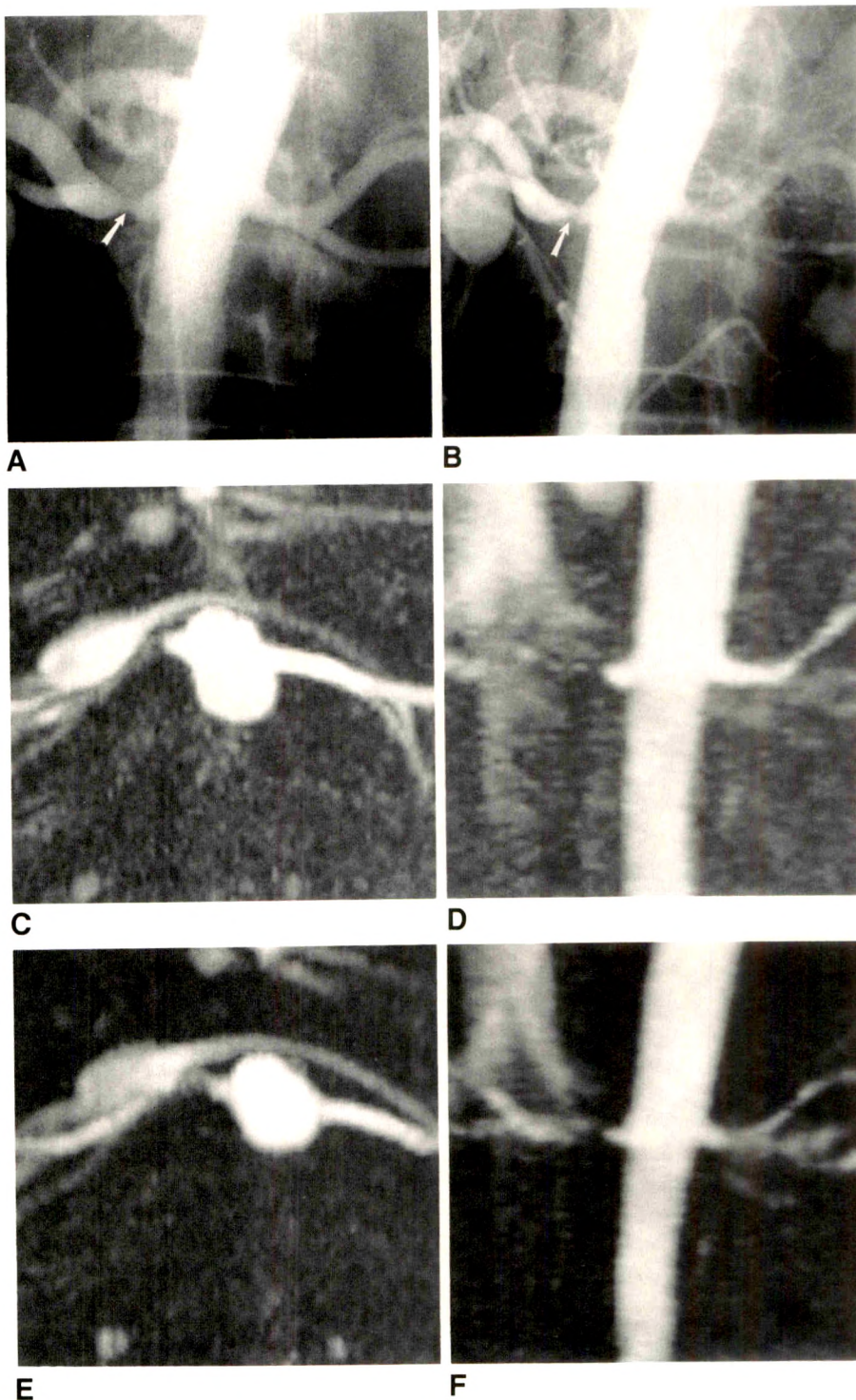
To determine which imaging sequence best meets the specific challenges of renal artery MR angiography, we evaluated both techniques. The choice of imaging parameters was based on prior MR angiographic work [9, 14, 22] (Porges R et al., RSNA, November 1990; Grist TM et al., unpublished data). In order to minimize motion artifacts and avoid overgrading of stenotic lesions, TRs and TEs as short as possible were chosen. Flow-related enhancement in distal vessels was maximized by use of a relatively large flip angle of 60°. Choice of the phase-encoding direction, anteroposterior in the axial and right to left in the coronal projections, limited the effects of associated ghosting artifacts. Acquisitions were performed with the patient breathing shallowly, mainly in an effort to keep the total study time under 40 min. Breath-holding would have lengthened acquisition times, but would be possible especially for the shorter time-of-flight acquisition. For phase-

Fig. 4.—A, Conventional arteriogram shows high-grade stenosis (75–99%) in proximal right renal artery (arrow) of a 35-year-old man.

B, Arteriogram shows reduction to a moderate lesion (arrow) after percutaneous transluminal angioplasty.

C and D, Axial (C) and coronal (D) preangioplasty maximum-pixel-intensity projection (MIP) phase-contrast images show extended area of signal void (>5 mm) in proximal right renal artery with reconstitution of signal distally.

E and F, Axial (E) and coronal (F) postangioplasty MIP phase-contrast images show reduced area of signal void (<5 mm) corresponding to a moderate lesion (50–75%). Stenosis was correctly detected and graded on phase-contrast MR angiography both before and after angioplasty.



contrast acquisitions, higher resolution was sacrificed by obtaining thicker sections in favor of shortening imaging times. As four data sets are acquired for each phase-contrast sequence, it still took about twice as long as the time-of-flight acquisition, thus introducing a signal-to-noise bias favoring the phase-contrast sequence.

Basic to the effective detection and proper characterization of renovascular disease with MR angiography is full visualization of the renal arteries. One of the major determinants of image compromise is vessel overlap, which is directly proportional to the concentration of vascular structures in the area of interest. The renal arteries are closely associated with renal

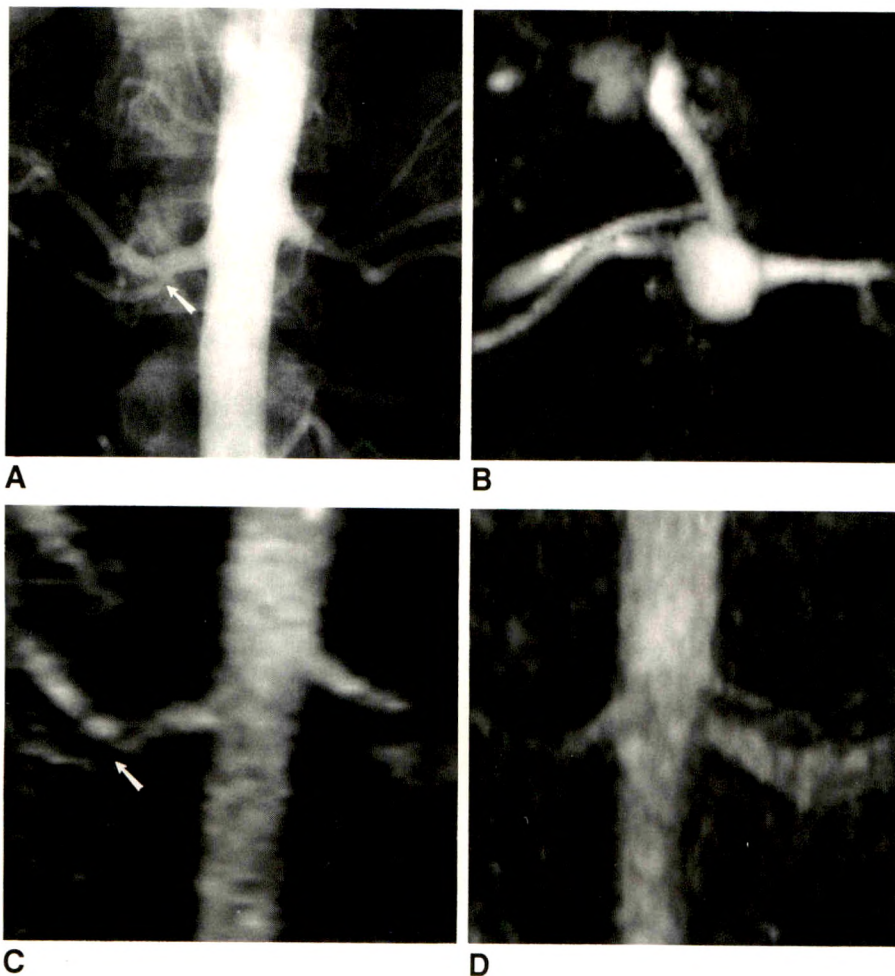


Fig. 5.—A, Conventional angiogram shows moderate stenosis (50–75%) in proximal right renal artery branch (arrow) that was missed prospectively with MR angiography.

B, Corresponding axial maximum-pixel-intensity projection (MIP) phase-contrast image shows normal bilateral renal arteries. Lesion is not visualized in axial plane because normal right renal artery is projected over diseased branch.

C, Coronal MIP phase-contrast image reveals area of signal void at point where proximal right renal artery branches off (arrow). This was not identified by any observers prospectively. In retrospect, however, lesion is apparent.

D, Lesion is not visualized on coronal time-of-flight MIP image owing to lack of signal in distal right renal artery.

veins, the inferior vena cava, and adrenal and mesenteric vessels. Despite saturating venous flow as suggested by Edelman et al. [9] by placing inferior and lateral presaturation bands, signal from the renal veins was never totally eliminated (Figs. 1–5). In order to avoid saturating the more distal renal arteries, lateral presaturation bands could be placed only over the renal cortices. Blood in the renal medulla thus escaped presaturation. The problem appeared worse on the left side, reflecting the longer course and larger size of the left renal vein because of inflow from only partially saturated adrenal and gonadal venous blood.

Despite excellent vessel contrast, MIP images were degraded by vessel overlap. Depending on the signal intensity of flowing spins, the renal arteries were concealed or narrowed by overlying vessels, thereby even simulating the presence of stenosis (Fig. 2). Although restricting the range of sections used for MIP processing to those containing renal arteries was often able to eliminate some extraneous vessels (Fig. 1), renal vein overlap remained a significant problem in the evaluation of MIP images for both phase-contrast and time-of-flight acquisitions. Images of individual sections were thus essential in the interpretation of renal artery MR angiograms. In our study, renal artery visualization for all four

evaluated image sets was greatly enhanced by adding images of individual sections (Table 1), largely through improved vessel differentiation. Despite careful examination of the images of individual sections, vessel overlap remained a problem in the assessment of 30 renal arteries on time-of-flight images (Fig. 2). In contradistinction, analysis of individual flow-encoded phase-contrast images, permitting directional determination of blood flow, virtually eliminated confusion due to venous overlap (Figs. 2 and 3). This contributed to the overall better performance of phase-contrast imaging compared with time-of-flight with regard to renal artery visualization ($p < .05$). More effective stationary tissue suppression, resulting in greater vessel contrast and more signal, especially in distal vessel segments, were other factors responsible for better renal artery visualization with phase-contrast images (Figs. 2 and 5).

The particular choice of imaging parameters also may have influenced these findings. Use of a lower flip angle, larger number of excitations, different section thickness, or imaging with breath-holding may improve time-of-flight images with regard to signal and vessel contrast. Confusion due to overlap of extraneous vessels, however, will remain a fundamental problem for time-of-flight imaging regardless of imaging pa-

rameters. This leads to confusion, especially in the presence of accessory renal arteries. Although five of seven accessory vessels were correctly identified on coronal phase-contrast images, only three were seen on the time-of-flight images.

Axial and coronal phase-contrast images complement one another (Figs. 1 and 4). Although ostia were better seen in the coronal plane, distal renal artery segments were better visualized in the axial projection. The coronal plane proved essential in the detection of accessory renal arteries. Only two of seven accessory vessels were prospectively identified on the axial images. Combined axial and coronal phase-contrast images allowed visualization of the proximal 35 mm of all 66 dominant renal arteries and allowed detection of six of seven accessory renal arteries.

The ability to detect and characterize renovascular disease based on the four different image sets was directly related to the degree of visualization. For all image sets, interpretations were more accurate once images of individual sections were added to the MIP reprojected images.

More lesions were correctly identified with phase-contrast than with time-of-flight images. Although both techniques were similarly specific (97% for time-of-flight, 91% for phase-contrast), the sensitivity for the detection of renovascular lesions was 80% for the coronal phase-contrast acquisition and only 53% for the coronal time-of-flight image sets. Failure to identify three diseased accessory arteries with time-of-flight images significantly contributed to this difference.

More lesions were detected in the coronal plane (80% sensitivity) than in the axial plane (67% sensitivity). This difference predominantly reflects nonvisualization of diseased accessory renal arteries in the axial images and thus reemphasizes the need for biplanar MR angiographic evaluation of renal arteries.

Interpretations based on combined axial and coronal phase-contrast images elicited the highest sensitivity and specificity. Thirteen of 15 lesions diagnosed in the proximal 35 mm of the renal arteries with conventional angiography were correctly identified, yielding a sensitivity of 87% with a specificity of 97%. Not detected was a moderate stenosis (50–75%) of a proximal branch vessel (Fig. 5). Missing this lesion may partially be attributed to the inexperience of the observers in evaluating MR angiographic examinations of the renal arteries. In retrospect, it is believed that diagnosis was possible. A second lesion, a mild stenosis (less than 50%), was missed in a small accessory renal artery. This vessel was not visualized on any of the MR acquisitions. This highlights the diagnostic dilemma caused by nonvisualization of accessory renal arteries. Owing to the small size of the accessory vessel involved in this case, the lesion was not thought to be functionally significant. However, lesions in larger accessory arteries may cause hypertension. Further evaluation of this potential pitfall is needed.

A higher overall sensitivity for MR angiography in the detection of renovascular disease was reported by Kim et al. [14]. Coronal and axial breath-hold gradient-echo images (time-of-flight technique) were found to be 100% sensitive and 92% specific for significant lesions (>50%). As the authors themselves point out, the spatial resolution of the technique used was adequate only for evaluating the proximal

renal arteries. Thus, their excellent results may be explained at least in part by the atherosclerotic origin of all detected lesions. Their very proximal location makes them particularly accessible to diagnosis by MR angiography. No branch vessel lesions, fibromuscular dysplasia-induced stenosis, or lesions in accessory renal arteries were among the detected lesions [14].

In our study, consensus interpretation overestimated one mild and one moderate lesion, each by one category. Some degree of overestimation is to be expected, since signal loss from turbulent flow distal to a stenosis will tend to exaggerate the stenosis. In anticipation of such overestimation, the degree of signal void was used to classify stenosis seen with MR angiography. One moderate lesion was underestimated by one category by most of the observers.

Underestimating and overestimating lesions in the mild and moderate categories and missing the moderate branch stenosis (Fig. 5) reflect our lack of experience with MR angiography of the renal arteries. As our experience grows, our accuracy should increase. In this regard, we are encouraged by the overall low interobserver variability and virtually 100% agreement among the three observers in the detection of severe lesions.

Four very distal (beyond 35 mm) stenoses induced by fibromuscular dysplasia that were diagnosed with conventional angiography were not included in our analysis. If they were to be included on the assumption that they would not have been visualized on the MR angiogram, the sensitivity would decrease to 68% for all stenoses and to 75% for stenoses greater than 50%, based on combined axial and coronal phase-contrast images. These numbers emphasize the need to include the very distal renal artery bed in any future evaluation of MR angiography.

These preliminary results suggest that MR angiography can visualize renal arterial disease and holds considerable promise as a noninvasive screening tool. Before MR angiography can be recommended for clinical screening however, other studies need to assess its usefulness in the evaluation of distal renal artery disease, particularly in patients with fibromuscular dysplasia. Further refinements, such as the implementation of surface coils, shortening of TEs, use of gradient reordering, and modification of the velocity-encoding value may aid in this pursuit.

ACKNOWLEDGMENTS

We thank J. Weinerth, T. Bashore, M. Harding, and R. McCann for referring patients; L. Upchurch and R. Negro-Vilar for help in data management and analysis; and R. Boyd and M. Cudic for manuscript preparation.

REFERENCES

1. Tegtmeier CJ, Hefler TJ, Ayers CA. Renal angioplasty: current status. *AJR* 1984;142:17–21
2. Martin LG, Casarella WJ, Gaylord GM. Azotemia caused by renal artery stenosis: treatment by percutaneous angioplasty. *AJR* 1988;150:839–844
3. Hillman BJ. Imaging advances in the diagnosis of renovascular hypertension. *AJR* 1989;153:5–14

4. Svetkey LP, Himmelstein SI, Dunnick NR, et al. Prospective analysis of strategies for diagnosing renovascular hypertension. *Hypertension* **1989**;14:247-257
5. Berland LL, Koslin DB, Routh WD, Keller FS. Renal artery stenosis: prospective evaluation of diagnosis with color Doppler US compared with angiography. *Radiology* **1990**;174:421-423
6. NHLBI Workshop on Renovascular Disease. Summary report and recommendations. *Hypertension* **1985**;7:452-456
7. Havey RJ, Krumlosky F, del Graco F, Martin HG. Screening for renovascular hypertension. Is renal digital-subtraction angiography the preferred noninvasive test? *JAMA* **1985**;254:388-393
8. Chen CC, Hoffer PB, Vahjen G, et al. Patients at high risk for renal artery stenosis: a simple method of renal scintigraphic analysis with Tc-99m DTPA and captopril. *Radiology* **1990**;176:365-370
9. Edelman RR, Mattle HP, Atkinson DJ, Hoogewoud HM. MR angiography. *AJR* **1990**;154:937-946
10. Bendel P, Buonocore E, Bockisch A, Besozzi M. Blood flow in the carotid arteries: quantification by using phase-sensitive MR imaging. *AJR* **1989**;152:1307-1310
11. Steinberg FL, Yucel EK, Dumoulin CL, Souza SP. Peripheral vascular and abdominal applications of MR flow imaging techniques. *Magn Reson Med* **1990**;14:315-320
12. Alfidi R, Masaryk TJ, Haacke EM, et al. MR angiography of peripheral, carotid, and coronary arteries. *AJR* **1987**;149:1097-1109
13. Linden A, Krestin GP, Theissen P, Friedmann G, Schicha H. Renal artery stenosis: potentials of MR tomography. *Nuklearmedizin* **1989**;28:226-233
14. Kim D, Edelman R, Kent K, Porter D, Skillman JJ. Abdominal aorta and renal artery stenosis: evaluation with MR angiography. *Radiology* **1990**;174:727-731
15. Dumoulin CL, Souza SP, Walker MF, Wagle W. Three-dimensional phase-contrast angiography. *Magn Reson Med* **1989**;9:139-149
16. Edelman RR, Wentz KU, Mattle H, et al. Projection arteriography and venography: initial clinical results with MR. *Radiology* **1989**;172:351-357
17. Lenz GW, Haacke E, Masaryk TJ, Laub G. In-plane vascular imaging: pulse sequence design and strategy. *Radiology* **1988**;166:875-882
18. Bishop YMM, Feinberg FE, Holland PW. *Discrete multivariate analysis: theory and practice*. Cambridge: MIT Press, **1984**:258-259
19. Hahn HL. Spin echoes. *Phys Rev* **1950**;80:580-594
20. Singer JR. NMR diffusion and flow measurement: an introduction to spin-phase graphing. *J Phys [E]* **1978**;11:281-291
21. Axel L. Blood flow effects in magnetic resonance imaging. *AJR* **1984**;143:1157-1166
22. Spritzer CE, Pelc NJ, Lee JN, Evans AJ, Sostman HD, Riederer SJ. Rapid MR imaging of blood flow with a phase-sensitive, limited-flip-angle, gradient recalled pulse sequence: preliminary experience. *Radiology* **1990**;176:255-262
23. Evans AJ, Hedlund LW, Herfkens RJ, Utz JA, Fram EK, Blinder RA. Evaluation of steady and pulsatile flow with dynamic MRI using limited flip angles and gradient refocused echoes. *Magn Reson Imaging* **1987**;5:475-482
24. Spritzer CE, Blinder RA. Vascular applications of magnetic resonance imaging. *Magn Reson Q* **1989**;5:205-227

Arteriovenous Malformations of the Kidneys: Diagnosis and Follow-up with Color Doppler Sonography in Six Patients

Shigeo Takebayashi¹
Noriko Aida
Kengo Matsui

We performed color Doppler sonography in six patients with arteriovenous malformations of the kidneys. The diagnosis was established by angiography in all patients. Color Doppler sonograms were obtained at a large Doppler frequency-shift range (55 cm/sec of maximal average flow velocity at zero Doppler angle) to depict high-velocity blood flow in the malformation. In all patients, the malformations were seen as focal areas of flow, portrayed as a mixing of lighter colors. These were reflected by a rapid flow rate and marked tortuosity of the vessels. The sonograms showed a small peripheral malformation that was indistinct on selective renal angiography. However, flow in normal vessels grouped in the hilum obscured lighter-color flow of a small central malformation. In three patients who had total or partial ablation of the malformations with alcohol, follow-up color Doppler sonograms showed that the focal areas of flow, represented as mixing of lighter colors, disappeared or became smaller.

This study shows that color Doppler sonography is a useful noninvasive procedure for diagnosing arteriovenous malformations of the kidney.

AJR 157:991-995, November 1991

The use of color has expanded the role of Doppler sonography significantly, and in many instances, color flow imaging is being used as a definitive diagnostic study without the need for correlative angiography [1]. Color Doppler imaging also has been used to detect high-flow velocity shunting of postbiopsy arteriovenous fistulas in transplanted kidneys [2], to locate intracerebral arteriovenous malformations (AVMs) through a craniotomy [3], and to detect peripheral AVMs [4]. We recently used color Doppler sonography in six patients with renal AVMs. In this article, we compare color Doppler sonograms with angiographic findings and discuss the usefulness of the procedure for detecting and monitoring AVMs.

Materials and Methods

From April 1989 to September 1990, we performed color Doppler sonography and angiography in 46 consecutive patients who had gross hematuria but had no lesion on CT scans obtained with and without IV injection of contrast material. Six of the patients had renal AVMs, for which the diagnosis was established by angiography. This group comprised five women and one man 29-55 years old (mean, 37 years). The malformations involved the right kidney in five patients and the left kidney in one. We applied the following angiographic scale to the AVMs: grade 1 = smaller than 2 cm, minimal degree of arteriovenous shunting (this was not observed on selective renal arteriography but by superselective arteriography); grade 2 = smaller than 2 cm, marked arteriovenous shunting (this was shown clearly on selective arteriography); grade 3 = 2-4 cm, marked arteriovenous shunting; and grade 4 = larger than 4 cm, marked arteriovenous shunting. We also documented the locations of the AVMs by the following classifications: 1 = central, located in the peripelvic area; 2 = peripheral, located in the pericaliceal area; and 3 = mixed, extending from the peripelvic to the pericaliceal areas.

All color Doppler sonographic examinations were performed by one of the authors. The sonograms were obtained by using a 3.75-MHz sector transducer (SSH-160A, Toshiba Co.,

Received December 6, 1990; accepted after revision May 31, 1991.

¹ All authors: Department of Radiology, Yokohama City University, School of Medicine, 3-9, Fukuura, Kanazawa-ku, Yokohama 236, Japan. Address reprint requests to S. Takebayashi.

0361-803X/91/1575-0991
© American Roentgen Ray Society

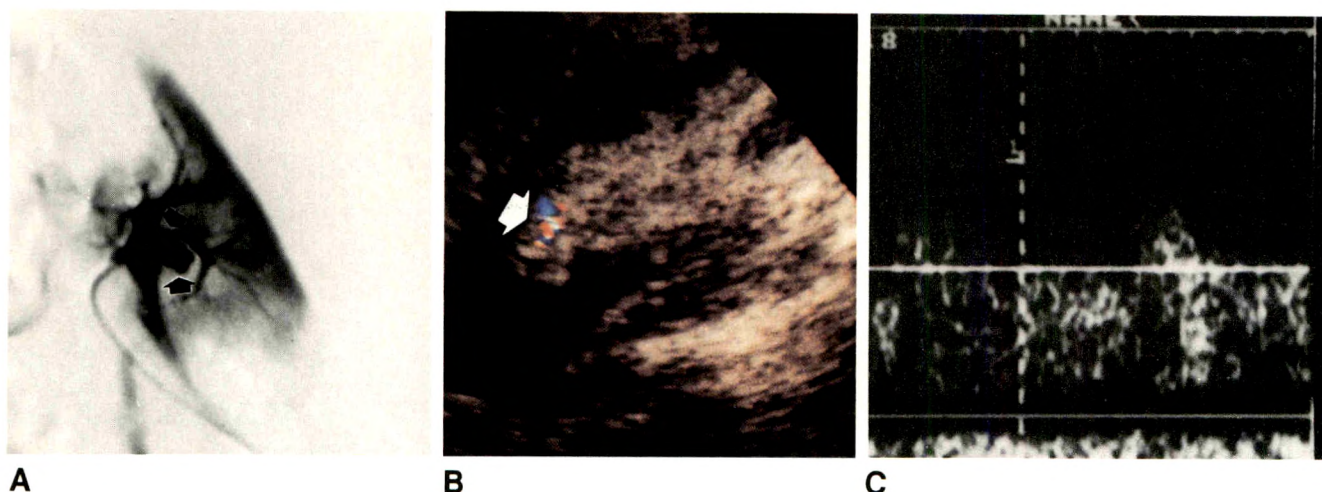


Fig. 1.—43-year-old woman with massive gross hematuria.

A, Superselective arteriogram, in which a catheter is placed in an interlobar artery of right renal upper pole, shows a small peripheral, grade 1 arteriovenous malformation (AVM, arrows) in pericaliceal area. Lesion was not seen on a selective renal arteriogram (not shown).

B, Longitudinal large frequency-shift range (55-cm/sec maximal average flow velocity at zero Doppler angle) color Doppler sonogram of right kidney. Small focal area of flow appears as mixing of lighter colors (arrow) corresponding to AVM in A. Flow of normal vessels is suppressed for demonstration purposes. Focal flow of lighter colors disappeared on follow-up sonography after total ablation of AVM with alcohol.

C, Doppler waveform from vessel with flow of lighter colors shows a pulsatile waveform with low resistivity (resistive index, 0.42). Horizontal line indicates large end-diastolic frequency shift.

Tokyo) or a 3.5-MHz convex transducer (U-sonic RT8000, Yokogawa Medical System Co., Tokyo). Sonography was done before angiography in all but one patient (in that case, the operator was blinded to the angiographic result). Color assignment for these units is such that flow toward the transducer is red and flow away from the transducer is blue. A light hue is used to show a greater frequency shift. Light yellow represents flow toward the transducer, and light blue represents flow away from the transducer. These lighter colors show only in a quarter of each color scale. Aliasing, which results in the reverse color assignment, occurs when the velocity of blood flow results in a frequency shift exceeding the recorded Doppler frequency range. The median flow velocity, estimated from a color and duplex Doppler study of transplanted kidney [2], is about 40–138 cm/sec in the arteries supplying an arteriovenous fistula and 12–32 cm/sec in the normal intrarenal artery. Therefore, in our study, the color scale was set for a large frequency-shift range that corresponded to a 55-cm/sec maximal average flow velocity at zero Doppler angle. At this setting and Doppler angle, slight high-velocity flow averaging about 40–70 cm/sec is light yellow or light blue, as is marked high-velocity flow averaging 150–180 cm/sec, whereas normal flow in the intrarenal artery is expected to be red, orange, or blue. The zero-degree Doppler angle also causes aliasing and lighter colors [1]. Therefore, the AVM, which is composed of a tangle of small tortuous vessels, is expected to be a focal area of flow, represented as a mixing of lighter colors. When the focal area of flow portrayed as a mixing of lighter colors was observed in the kidneys, a Doppler spectrum was obtained at the point of the light color codes with the wall filter set at 100 Hz. The resistive index (RI) of the vessel with flow of lighter colors was obtained by using the following equation: $(\text{peak systolic frequency shift} - \text{end-diastolic frequency shift}) / (\text{peak systolic frequency shift})$. Measurements of velocity corrected by the angle of insonation were impossible because the accurate direction of blood flow could not be determined in the tortuous vessels of the AVM. Regarding flow of the normal intrarenal arteries, we compared the sonograms at the large frequency-shift range and those at the moderate frequency-shift range, corresponding to a 31-cm/sec maximal average flow

velocity. The RI of the artery not exhibiting lighter-color flow was compared with the RIs of the vessels with lighter-color flow. The pulse rates in all patients ranged from 60 to 76 beats per minute during the Doppler spectrum examinations.

Of the six patients, three who had massive and persistent hematuria had transcatheter arterial ablation of their AVMs with absolute alcohol. The AVMs were ablated completely in two and partially in one. The patients had follow-up color Doppler sonography. The findings were compared with the findings of postablation angiography.

Results

The AVMs in the six patients were shown as distinct, tortuous, and coiled vascular channels on angiograms. They were grade 1 (Fig. 1A) in one, grade 2 in one, grade 3 (Fig. 2A) in two, and grade 4 (Fig. 3A) in two. Each of the grade 1 and grade 2 AVMs was located in the periphery. The two grade 3 lesions included one central type and one mixed type, as did the two grade 4 lesions. A gray-scale sonogram of the kidneys showed small peripelvic cystic masses corresponding to aneurysmal dilated vessels of one grade 4 AVM, and a tubular cystic echo corresponding to the draining vein of another grade 4 lesion. However, sonograms showed no abnormal echo in other patients with AVMs.

Flow in peripheral vessels at the moderate frequency-shift range disappeared or decreased at the large frequency-shift range. In the hilum, condensed flow of crowded, lighter colors at the moderate frequency-shift range was changed into flow of red, blue, or orange at the large frequency-shift range; however, these were still grouped in most cases. The RI of the normal vessels ranged from 0.62 to 0.84 (mean, 0.76). The focal areas of flow, represented as mixing of lighter

Fig. 2.—52-year-old woman with massive gross hematuria.

A, Right renal arteriogram shows grade 3 arteriovenous malformation (AVM, arrows) in both peripelvic and pericaliceal portions.

B, Longitudinal color Doppler sonogram of right kidney. Focal area of flow appears as mixing of lighter colors (arrow) corresponding to peripheral AVM in A. However, small central AVM was not distinct on color Doppler sonogram of right renal hilum (not shown) because flow of grouped normal vessels obscured light colors of AVM.

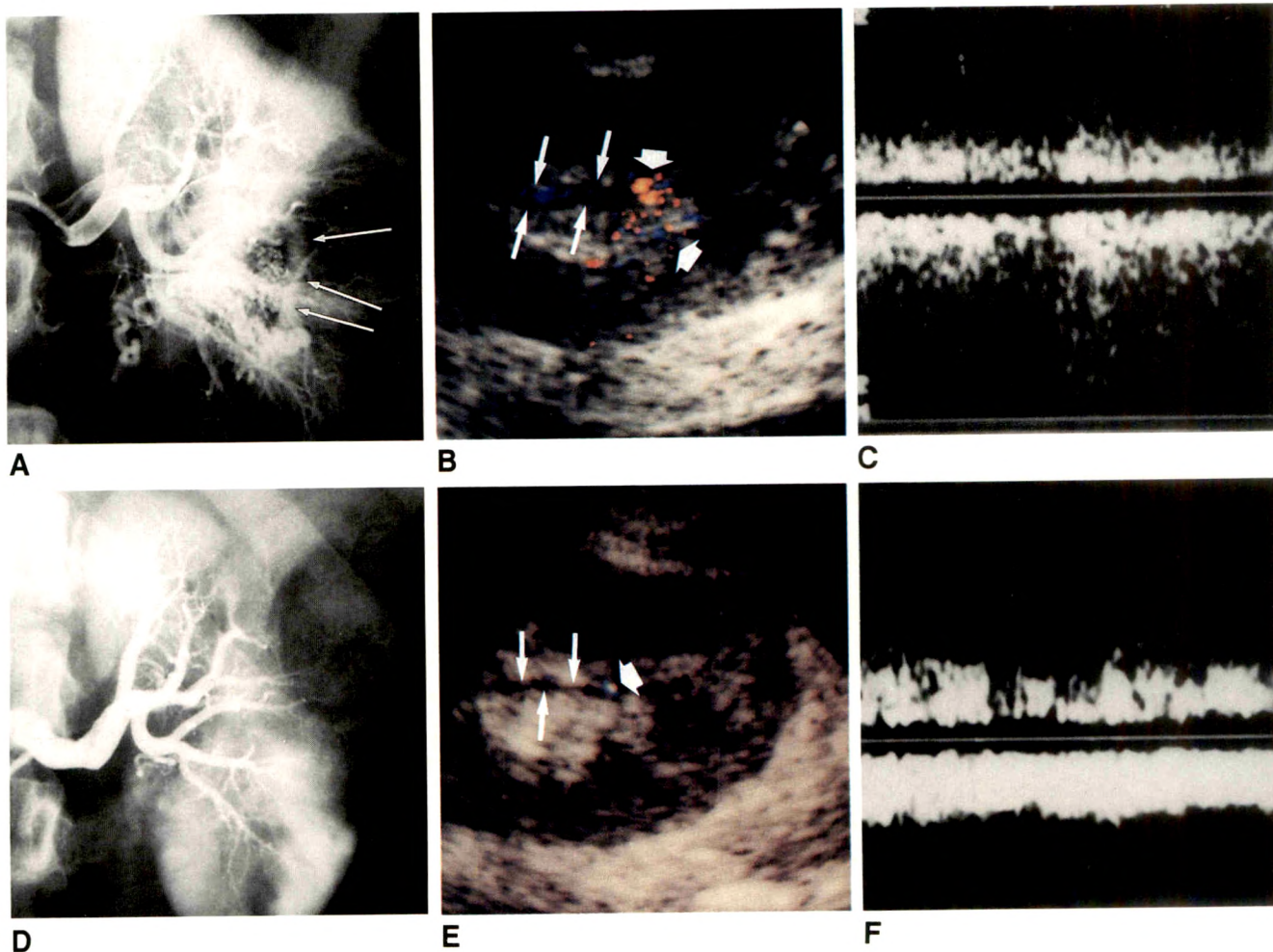
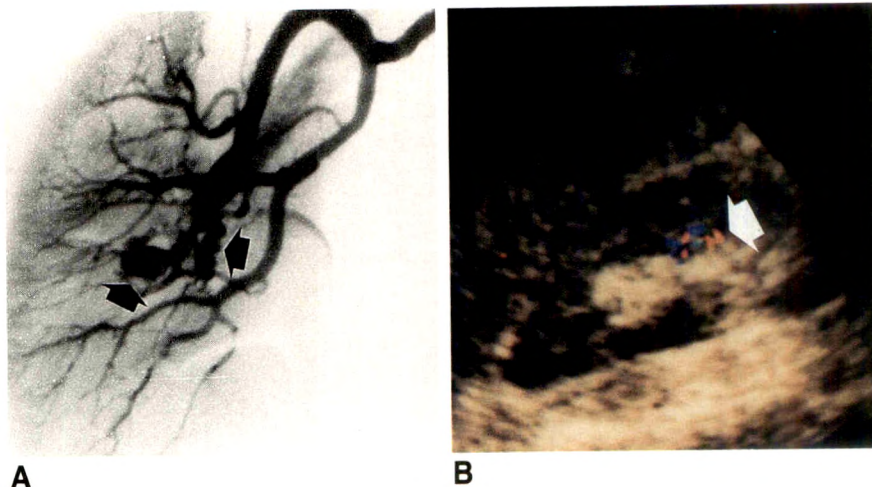


Fig. 3.—32-year-old woman with massive gross hematuria.

A, Left renal arteriogram shows grade 4 arteriovenous malformation (AVM). A draining vein (arrows) runs craniocaudally.

B, Longitudinal color Doppler sonogram of left kidney. Large area of flow is seen as mixing of lighter colors (short arrows). Draining vein (4 mm in diameter, long arrows) corresponds to vein in A.

C, Doppler waveform from draining vein shows arterial pulsations with large frequency shift.

D, Left renal arteriogram shows disappearance of AVMs after transcatheter arterial infusion of alcohol into supplying arteries.

E, Follow-up color Doppler sonogram 1 day after total ablation of AVMs shows disappearance of focal flow of lighter colors. However, a solitary spot of light color (short arrow), which corresponds to end of an ablated artery, remains. Diameter of draining vein (long arrows) is reduced to 1.5 mm.

F, Waveform from draining vein on follow-up examination shows disappearance of arterial pulsations and decrease in frequency shift.

colors, corresponded well to the AVMs, which were seen as tortuous and coiled vascular channels on angiography in five patients. In the remaining patient, the size of a mixed-type grade 3 AVM was underestimated because normal flow grouped in the hilum obscured flow of lighter colors in the central AVM (Fig. 2). The focal area of flow, portrayed as a mixing of lighter colors, was not observed in other patients in whom AVMs were not seen on angiography. However, a solitary spot flow of lighter color, which corresponded to a right-angle bifurcation of an interlobar artery on the angiogram, was noted in one patient. Color Doppler imaging yielded neither false-positive nor false-negative cases of AVM when the AVM was diagnosed on the basis of a focal area of flow manifested by a mixing of lighter colors. In the three patients who had total or partial ablation of the AVMs with alcohol, color Doppler sonograms obtained after ablation showed that the focal areas of flow manifested as mixing of lighter colors disappeared or diminished in size. However, a solitary spot of lighter color remained, which corresponded to an end of an ablated artery. Spectral waveforms, obtained from the vessels with flow of lighter colors, showed large peak-systolic and end-diastolic frequency shifts with smaller RIs than those of a normal intrarenal artery (Fig. 1C). The RI ranged from 0.32 to 0.52 (mean, 0.40) in AVMs with marked arteriovenous shunting (grades 2–4) and was 0.42 in the AVM with minimal arteriovenous shunting (grade 1). We found no correlation between the RI and the degree of arteriovenous shunting. In one patient who had partial ablation of the AVM, the RI of the vessels with flow of lighter colors had changed from 0.41 to 0.51 1 day after ablation; it was 0.53 1 month after ablation. Doppler waveforms from the draining vein were obtained in two patients. These showed both an increased shift frequency and arterial pulsations (Fig. 3C). One day after total ablation, they showed a normal venous pattern (Fig. 3F).

Discussion

In the past, renal arteriography or IV digital subtraction angiography has been the definitive study used to survey AVMs of the kidney in patients with gross hematuria [5], although a large aneurysmal AVM can be detected with a noninvasive imaging technique such as CT, gray-scale sonography, or MR [5, 6].

In color Doppler sonography, pulsed Doppler signals are used to produce flow images in color. At each color pixel, the average Doppler shift frequency is encoded [7]. Diminished flow patterns have been reported in patients with renal parenchymal disease on renal color Doppler sonography [8]. Unfortunately, it is not easy to distinguish the minimal flow from a pattern seen in normal kidneys, because the depiction of flow is reflected by the angle between the Doppler beam and the vessels, as well as by the depth of the kidneys. Fortunately, the increased flow pattern can be detected more easily than the diminished pattern when operators are careful to set the proper range of the recorded frequency shift. When the flow rate alone is considered, only slightly or markedly high-velocity flow of the AVM is shown by flow of lighter colors. However,

the hue depends on the angle of insonation between the ultrasound beam and the moving blood, as well as on the frequency shift, which is determined by the velocity of the moving reflectors [1]. The zero Doppler angle causes aliasing and flow of lighter colors [1]. Thus, the AVM, which is composed of a tangle of small tortuous vessels, is seen as a focal area of flow, mixing of lighter colors. The flow of normal peripheral vessels disappears or diminishes on the sonogram at the large frequency-shift range, because the frequency-shift cutoff was increased in the units used in this study. Therefore, a peripheral AVM, even a small one, is easily detected at the large frequency-shift range. In the renal hilum, however, flow of colors is still grouped at even the large frequency-shift range. The normal grouped flow of colors may obscure the flow of lighter colors of a small central AVM.

Doppler spectral analysis after color Doppler sonography appears to be the definitive study for diagnosing arteriovenous shunting in transplanted kidneys when the increased flow velocity of the supplying artery, the decreased resistivity of the artery, and the arterial pulsations in the draining vein are observed [2]. However, the application of this technique is limited to diagnosing the AVM in a native kidney. One of the reasons for this is that it is difficult for patients to hold their breath to avoid moving the kidneys until the Doppler cursor is adjusted to the objective color codes. This can be accomplished with the cooperation of the patient and considerable effort by the operator. A second hindrance is that the accurate flow velocity in the tortuous vessels is extremely difficult to measure because correction for the angle of insonation is unreliable in the vessels. Nevertheless, a small RI, indicative of low resistivity in the vessel, is a useful sign in diagnosing the AVM. The RI of the normal intrarenal artery in transplanted kidneys was 0.60–0.92 [2]. In this study, the RI of native kidneys was 0.62–0.84. Mostbeck et al. [9] reported that the RI was 0.70 ± 0.06 at a pulse rate of 70 beats per minute. It decreased to 0.57 ± 0.06 at a pulse rate of 120 beats per minute. An increased pulse rate and shortening of the diastolic component increase the end-diastolic frequency shift. Therefore, in interpretation of the RI, the actual pulse rate must always be considered. The Doppler waveform from the draining vein, if detected on the sonogram, is also useful in diagnosing AVMs.

Color Doppler sonography is also a useful, noninvasive procedure for follow-up in patients who have transcatheter arterial embolization or ablation as well as conservative therapy. Disappearance or diminution of flow, shown as mixing of lighter colors, as well as disappearance of arterial pulsations in the draining vein, implies success in therapeutic intervention. However, the RI is of little use in evaluating the grading of arteriovenous shunting, because the Doppler waveform is obtained from only one or a few of the multiple small vessels of the AVM [7]. Periodic follow-up color Doppler sonography is required to rule out growing or recanalization, which is usually seen in AVMs occluded by Gelfoam (an absorbable gelatin sponge) [10]. In conclusion, color Doppler sonography can be used for diagnosing and monitoring AVMs, and could eliminate a considerable number of angiograms.

REFERENCES

1. Foley WD, Erickson SJ. Color Doppler flow imaging. *AJR* **1991**;156:3-13
2. Middleton WD, Kellman GM, Melson GL, Madrazo BL. Postbiopsy renal transplant arteriovenous fistulas: color Doppler US characteristics. *Radiology* **1989**;171:253-257
3. Rubin JM, Hatfield MK, Chandler WF, Black KL, DiPietro MA. Intracerebral arteriovenous malformations: intraoperative color Doppler flow imaging. *Radiology* **1989**;170:219-222
4. Liu JB, Merton DA, Mitchell DG, Needleman L, Kurtz AB, Goldberg BB. Color Doppler imaging of the iliofemoral region. *RadioGraphics* **1990**;10:403-412
5. Hillman BJ. Disorders of the renal arterial circulation and renal vascular hypertension. In: Pollack HM, ed. *Clinical urography*. Philadelphia: Saunders, **1990**:2127-2172
6. Rao AKR, Kimball WR. Ultrasonic appearance of an arteriovenous fistula of the kidney. *JCU* **1978**;6:345-346
7. Powis RL. Color flow imaging: understanding its science and technology. *J Diagn Med Sonogr* **1988**;4:236-245
8. Merritt CRB. Doppler color flow imaging. *JCU* **1987**;15:591-597
9. Mostbeck GH, Gossinger HD, Mallek R, Siostrzonek P, Schneider B, Tscholakoff D. Effect of heart rate on Doppler measurements of resistive index in renal arteries. *Radiology* **1990**;175:511-513
10. Takebayashi S, Hosaka M, Ishizuka E, Hirokawa M, Matsui K. Arteriovenous malformations of the kidneys: ablation with alcohol. *AJR* **1988**;150:587-590



The Radiology Outreach Foundation (ROF) is a nonprofit corporation whose goal is to help disadvantaged countries improve their health care by providing radiology equipment, books, consultation, education, and training to their practitioners. This assistance is on an application basis that is independent of political, ethnic, or religious orientation of the grantee. It depends on the need of the people and the ability of the ROF to meet that need. The ROF is approved by the U.S. Internal Revenue Service as a tax-exempt organization. It is endorsed by the following radiologic societies: American Association of Women Radiologists, American College of Radiology, American Roentgen Ray Society, Association of University Radiologists, Radiological Society of North America, Society of Chairmen of Academic Radiology Departments, Society for Pediatric Radiology, European Society of Pediatric Radiology.

All donations to the ROF are tax deductible. Persons who would like to contribute financially to the ROF, would be interested in being a visiting professor, would like to send books or journals to any of the institutions supported by the ROF, or would like further information about the ROF should write to Charles A. Gooding, M.D., President, Radiology Outreach Foundation, 3415 Sacramento St., San Francisco, CA 94118 USA.



Come to the
American Roentgen Ray Society

92nd

ANNUAL MEETING

Orlando, FL

Marriott's Orlando World Center
May 10-15, 1992

Scientific Program (200 papers)
Instructional Courses (60 hours)
Categorical Course on Neuroradiology
The Caldwell Lecture
Award Papers
Scientific Exhibits
Social, Golf, and Tennis Programs
Guest Programs

Case Report

Nonobstructing Periureteric Venous Ring: Diagnosis with Conventional and Three-Dimensional Reconstruction CT

Evan H. Dillon¹ and Catherine Camputaro

Periureteric venous ring is a rare congenital abnormality resulting from anomalous development of the inferior vena cava (IVC). In the few previously reported cases [1–6], the anomaly was detected in the course of evaluation for urinary complaints. In our case, a nonobstructing periureteric venous ring was detected incidentally on a conventional CT scan obtained for the evaluation of gastric lymphoma. The diagnosis was confirmed by three-dimensional (3-D) reconstruction of these images. Recognition of this anomaly is clinically important in explaining the cause of a patient's hydronephrosis and in planning interventional procedures involving the IVC.

Case Report

A 50-year-old woman had dysphagia and weight loss. Unenhanced CT showed an abnormality of the IVC. Just below the renal veins, the IVC divided into two parallel vascular structures that continued down toward the bifurcation, where they fused into a single vessel before bifurcating. Contrast-enhanced CT confirmed the presence of two parallel infrarenal inferior venae cavae (Fig. 1A). No hydronephrosis was evident. The right ureter was medially displaced, passing behind the lateral vena cava and then coursing anteriorly between the two venae cavae before descending into the pelvis (Fig. 1B). 3-D reconstruction of the CT scans, performed on an independent 3-D system (ISG Technologies, Toronto, Ont.) by using a combination of computerized and manual segmentation, confirmed the diagnosis (Fig. 1C).

Discussion

Only a few cases of periureteric venous ring have been reported. The possibility of such an anomaly was first theoretically postulated by Huntington and McClure [7]. This anomaly of the infrarenal portion of the IVC is a variant of retrocaval ureter. In cases of retrocaval ureter, the infrarenal IVC is a single channel behind which the ureter passes before descending into the pelvis. In periureteric venous ring, the infrarenal IVC divides into two parallel venous channels just below the renal veins. These two channels fuse to form a single IVC just above the bifurcation. The ureter passes behind the lateral channel and then anteriorly between the two channels before descending into the pelvis. These two channels typically compress the ureter to some degree, which may result in urinary symptoms as has occurred in the previously reported cases [1–6]. If no compression occurs, the anomaly will be detected only incidentally, as in our case.

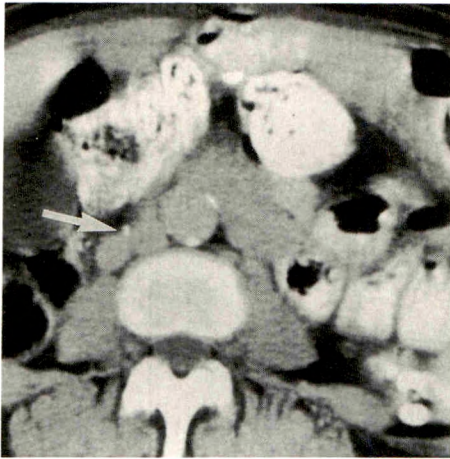
Recognition of this anomaly is clinically important, because it is a possible cause of hydronephrosis. Also, because there are two parallel infrarenal venae cavae, placement of a single vena caval filter in the infrarenal IVC would be ineffective in preventing pulmonary emboli.

Periureteric venous ring is easily diagnosed on contrast-enhanced CT scans. 3-D reconstruction of the CT scans is not necessary to make the diagnosis, but it provides an easily recognizable frontal projection of the anomaly.

Received February 27, 1991; accepted after revision May 21, 1991.

¹ Both authors: Department of Diagnostic Radiology, Yale University School of Medicine, 333 Cedar St. (2-NF), New Haven, CT 06510. Address reprint requests to E. H. Dillon.

AJR 157:997–998, November 1991 0361–803X/91/1575–0997 © American Roentgen Ray Society



A

Fig. 1.—Nonobstructive periureteric venous ring.

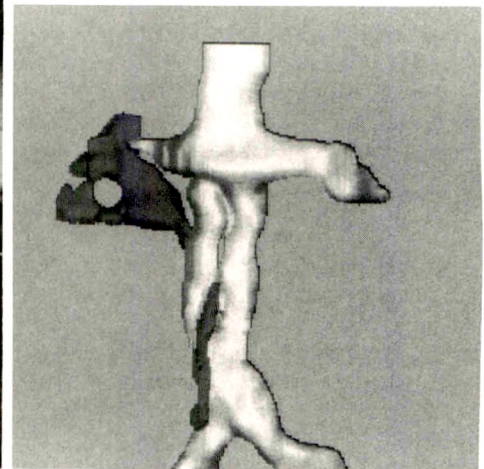
A, Contrast-enhanced CT scan shows two parallel venous channels in position of infrarenal portion of inferior vena cava. Ureter (arrow) can be seen in anterior notch between these two channels.

B, Contrast-enhanced multifformat CT scan shows normal inferior vena cava at level of renal veins, two parallel venous channels in infrarenal portion, and single inferior vena cava just above bifurcation. Contrast-opacified ureter (arrows) passes posterior to lateral venous channel and then anteriorly between two channels before descending into pelvis.

C, Anterior view of three-dimensional reconstruction of CT scans shows ureter (dark gray) passes between two channels of inferior vena cava (white).



B



C

REFERENCES

1. LePage JR, Baldwin GN. Obstructive periureteric venous ring. *Radiology* 1972;104:313-315
2. Djurhuus JC, Efsen F, Nerstrom B. Duplication of the inferior vena cava in retrocaval ureter. *Acta Chir Scand* 1976;472:87-90
3. Carrion H, Gatewood J, Politano V, Morillo G, Lynne C. Retrocaval ureter: report of 8 cases and the surgical management. *J Urol* 1979;121:514-517
4. Dharman K. Transcaval ureter. *J Urol* 1980;123:575-576
5. Radcliffe A, Goode AW. A case of ureteric obstruction due to a double right vena cava forming a periureteric venous ring. *Br J Urol* 1981;53:478
6. Sasai K, Sano A, Imanaka K, et al. Right periureteric venous ring detected by computed tomography. *J Comput Assist Tomogr* 1986;10:349-351
7. McClure CFW, Butler EG. The development of the vena cava inferior in man. *Am J Anat* 1925;35:331-383

Transitional Cell Carcinoma of the Bladder: Patterns of Recurrence After Cystectomy As Determined by CT

James H. Ellis^{1,2}
 Neil B. McCullough¹
 Isaac R. Francis¹
 H. Barton Grossman²
 Joel F. Platt¹

CT scans have been recommended for examination of patients at risk for recurrent transitional cell carcinoma after cystectomy. For CT to be useful in this regard, the location and type of recurrences must be known, so that appropriate scans can be made. Therefore, we retrospectively studied CT scans in 27 postcystectomy patients with recurrent transitional cell carcinoma of the bladder to identify the type and location of the recurrent disease. Recurrence was documented by biopsy in 18 patients and by progression of disease shown on serial CT scans in nine patients. All 27 patients had pelvic CT, and 23 had concomitant abdominal CT. Tumor recurred at the cystectomy site in 10 (37%) of 27 patients, pelvic adenopathy was present in 18 (67%) of 27 patients, and retroperitoneal adenopathy was present in 13 (57%) of 23 patients. Tumor recurrence at the cystectomy site was associated with pelvic adenopathy in seven of 10 patients, and the cystectomy site was the solitary site of disease in the remaining three patients. Conversely, in 11 of 18 patients with pelvic adenopathy no recurrence was seen at the cystectomy site. Combined retroperitoneal and pelvic adenopathy was identified in 11 of 23 patients, but two patients had retroperitoneal lymphadenopathy as their only site of recurrence. Hepatic metastases were seen in seven (30%) of 23 patients; six of these seven patients had metastases elsewhere. In four of five patients in whom underestimation of recurrent disease occurred, the deep pelvis and/or deep perineal space were involved.

Our results show that the pelvis is the most common site for recurrence. Cystectomy site or retroperitoneal nodal recurrences are usually accompanied by pelvic adenopathy, but the converse is not as common. Our findings of deep perineal and isolated abdominal recurrences indicate that proper protocol for CT follow-up of the postcystectomy patient should include abdominal scans and scans through the perineum.

AJR 157:999-1002, November 1991

Although CT has been used extensively in the preoperative staging of transitional cell carcinoma (TCC) of the bladder [1-5], only a few reports have described the use of pelvic CT for detecting recurrence of the disease after cystectomy [6, 7]. However, because little is known about whether this approach is adequate, we retrospectively studied CT scans in 27 patients with TCC recurring after cystectomy to identify the types and locations of recurrence.

Materials and Methods

Using a tumor registry and a computerized data base of pathologic reports, we identified 70 patients seen at our medical center between 1981 and 1988 who had undergone cystectomy (either here or elsewhere) for TCC of the bladder. Preoperatively, the patients had been free of known metastases. Of these, 27 patients who had both evidence of recurrence and postoperative CT examinations were selected for study. Their medical charts, pathology reports, and surgical reports were reviewed retrospectively. Recurrence was proved by biopsy in 18 patients. In the remaining nine patients, biopsy was not done, and recurrence was proved by progression of disease shown on serial CT scans.

Received March 18, 1991; accepted after revision June 18, 1991.

¹ Department of Radiology, University of Michigan Medical Center and VA Medical Center, 1500 E. Medical Center Dr., Ann Arbor, MI 48109-0030. Address reprint requests to J. H. Ellis.

² Department of Surgery, Section of Urology, University of Michigan Medical Center, Ann Arbor, MI 48109-0330.

0361-803X/91/1575-0999
 © American Roentgen Ray Society

There were 19 men and eight women, with a mean age of 66 years (range, 49–81 years). Staging of the primary tumor was available in 26 of the 27 patients. One patient had carcinoma in situ (T_{is}), three had invasion of the lamina propria (T_1), four had invasion of the superficial muscular layer (T_2), nine had deep muscle invasion (T_{3a}), seven had infiltration into the perivesical fat (T_{3b}), and two had extension to pelvic viscera (T_4). Twelve patients had no involved lymph nodes (N_0), three patients had involvement of a single homolateral node (N_1), and seven patients had involvement of contralateral or bilateral nodes (N_2). In four patients, nodal status was unknown (N_x).

All patients were scanned with either a General Electric CT/T 8800 or 9800 scanner (GE Medical Systems, Milwaukee, WI), using 10-mm-thick contiguous axial scans after the administration of oral and IV contrast material. IV contrast material was administered in a bolus. Scans obtained within 3 months of cystectomy were not included in the analysis, in order to exclude scans that had been obtained to evaluate for immediate postoperative complications such as hematomas or abscesses.

The CT scans were retrospectively reviewed jointly by two radiologists looking for local recurrence, adenopathy, and distant metastases. The scans were interpreted without knowledge of the clinical history or subsequent biopsy reports and were then reviewed again with this information. The final retrospective interpretation of the first CT examination showing recurrence after cystectomy was used for this study.

The staging of the original bladder tumor (perivesical fat invasion, lymph node involvement) was compared with the common sites of recurrence (cystectomy site, pelvic nodes, retroperitoneal nodes, liver, and skeletal metastases) to determine if the initial stage could predict the subsequent pattern of recurrence. Data were evaluated for statistical significance with Fisher's exact test. The Bonferroni correction (which attempts to correct for the possibility that, by chance alone, one or more of many tests may appear to reflect statistical significance) was used to correct for the number of comparisons being made simultaneously (e.g., p value for null hypothesis at 95% confidence level is .01 [.05/5]).

Results

All 27 patients had pelvic CT as the initial postoperative examination done at least 3 months after cystectomy; 23 of the 27 patients had abdominal CT as well. In 24 patients, the first postoperative scan showed recurrence; in the remaining three patients, the first scan did not show recurrence but a subsequent scan did show recurrence. The average time from cystectomy to the first scan showing recurrence was 14.5 months (range, 4–52 months; Fig. 1).

Tumor recurrence at the cystectomy site was seen in 10 (37%) of the 27 patients, and pelvic adenopathy was seen in 18 (67%) of the 27 patients. In seven of the 10 patients with recurrence at the cystectomy site, pelvic adenopathy was concomitant (Fig. 2). In the remaining three patients, the cystectomy site was the only site of recurrence. In 11 of the 18 patients with pelvic adenopathy, no evidence of recurrence at the cystectomy site was seen.

Retroperitoneal adenopathy was seen in 13 (57%) of the 23 patients who had abdominal CT. Eleven of these 13 patients also had associated pelvic adenopathy, whereas the remaining two patients had retroperitoneal adenopathy as the only sign of recurrence.

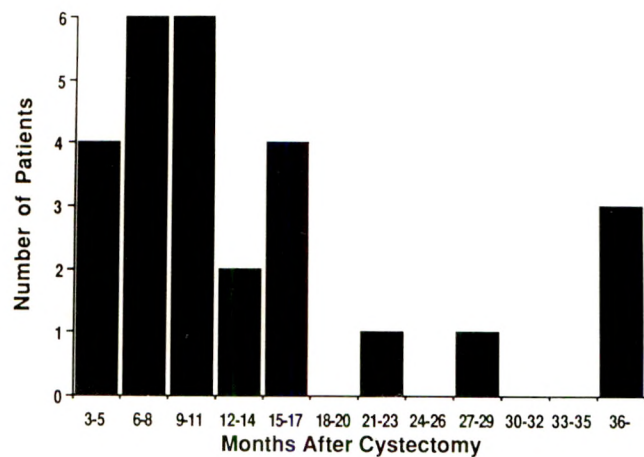


Fig. 1.—Histogram of months from date of cystectomy to date of first scan showing recurrence.

Hepatic metastases were seen in seven (30%) of 23 patients. One patient had hepatic metastases as the only sign of recurrent TCC. The other six of these patients had evidence of extensive recurrent disease at other sites (Fig. 3), most commonly involving the pelvic nodes (six of six), the retroperitoneal nodes (five of six), or the cystectomy site (three of six).

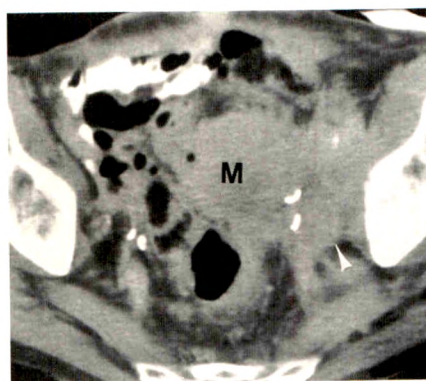
Three patients had evidence of distant bone involvement, including one patient with spinal metastases and two patients with acetabular metastases. Tumor recurrence at the cystectomy site extended into adjacent bony structures in four patients: two patients with involvement of the symphysis pubis (Fig. 4), one patient with involvement of the right pubic bone, and one patient with invasion into the sacrum and both posterior iliac wings.

Other sites of recurrence included splenic and renal metastases in one patient and anterior abdominal wall involvement in two patients.

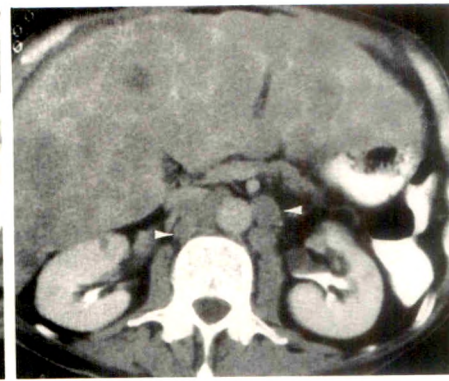
A statistically significant ($p < .026$, Fisher exact test) relationship was found between recurrence in pelvic lymph nodes and involvement of lymph nodes at the time of cystectomy. However, if the Bonferroni correction for the number of simultaneous comparisons is made, this relationship is not significant. The relationship between other sites of recurrence and the presence of either perivesical fat invasion or involved lymph nodes at cystectomy was not statistically significant.

The CT scans of three patients were interpreted as not showing recurrence on the initial prospective review. However, on the retrospective review with knowledge of the results of clinical investigations, recurrences were detected. Two of these cases involved small tumor recurrences at the cystectomy site (Fig. 5). The third case involved recurrent tumor in the deep perineal space at the base of the penis extending under the pubic bone to the pelvic floor and involving the abdominal rectus muscle. The scanning in this case was not continued far enough inferior to detect the tumor below the pelvic floor, although the involvement of the rectus muscle was identified retrospectively.

Fig. 2.—Recurrence at cystectomy site with concomitant pelvic nodal involvement in a 77-year-old man. CT scan shows large mass (M) of recurrent transitional cell carcinoma (TCC) growing up from pelvic floor with associated pelvic adenopathy (arrowhead). Needle biopsy was positive for TCC.



2



3

Fig. 3.—59-year-old man with multiple metastatic sites including liver, spleen, spine, cystectomy site, and retroperitoneal and pelvic nodes. CT scan shows innumerable hepatic metastases and retroperitoneal adenopathy (arrowheads). Surgical biopsy of recurrent pelvic tumor was performed concurrently with colostomy.

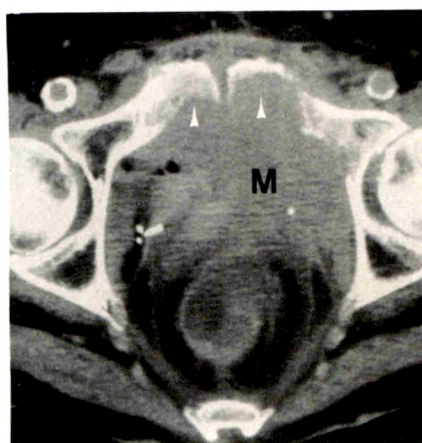


Fig. 4.—Local tumor recurrence with direct extension into bone after cystectomy in an 81-year-old man. CT scan shows low pelvic mass (M) with extension into symphysis pubis (arrowheads). Needle biopsy of pelvic mass showed transitional cell carcinoma.



Fig. 5.—Local vaginal recurrence seen only in retrospect in a 73-year-old woman. CT scan shows thickening of apex of vaginal cuff (M) with minimal indentation on rectum. Transvaginal biopsy showed transitional cell carcinoma.

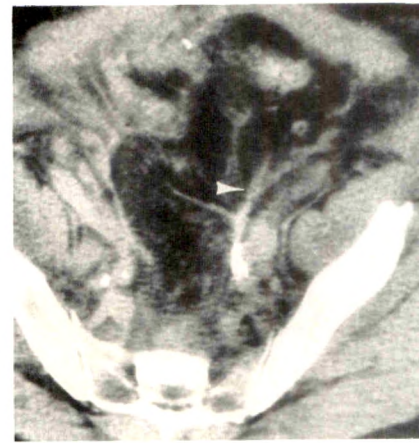


Fig. 6.—Underestimation of extent of disease by CT in a 59-year-old man with mesenteric recurrence. CT scan shows soft-tissue strands in mesentery (arrowhead). Surgery later revealed extensive tumor infiltration. Interpretation was made more difficult because bowel loops did not opacify with contrast material.

Disease was obviously underestimated in two other cases. In one case, extensive tumor infiltrating the mesentery was found 30 days after CT examination, when surgical exploration was required for revision of an ileal conduit. A mass was not discernible on CT even after the operative findings were known, although some increase in soft-tissue strands in the mesentery was noted on initial review (Fig. 6). However, this CT examination did show retroperitoneal and pelvic adenopathy. In the second case, the original postoperative scan did not reveal any abnormality even with the knowledge that a small anterior rectal mass was present on rectal examination. This mass ultimately grew to the point where it was evident on a follow-up scan.

Discussion

Previous studies have shown that CT can be used to detect both recurrence of bladder cancer and postoperative complications [6, 7]. Local recurrence may appear as asymmetric

soft tissue within the pelvis or as focal masses [7]. Lee et al. [6] were able to detect seven of eight local recurrences. Distant metastases are not distinguishable from metastases from many other primary tumors [6, 7].

Our study shows patterns of recurrence of transitional cell carcinoma of the bladder after cystectomy. Most patients had evidence of disease in more than one location. The pelvis was the most common site of recurrence; 37% of patients had evidence of tumor recurrence at the cystectomy site and 67% of patients had pelvic adenopathy. Patients with recurrence at the cystectomy site tended to have associated pelvic adenopathy (seven of 10), although in 11 of 18 patients with pelvic adenopathy no tumor recurrence was detected at the cystectomy site. Thus, pelvic recurrence tended to occur either in the lymph nodes alone or both in the nodes and at the cystectomy site. Recurrence at the cystectomy site alone was unusual, occurring in only three patients.

In earlier reports of postcystectomy CT, only the pelvis was studied [7], or the abdomen was examined only when the

pelvic scan showed abnormality or abdominal metastases were clinically suspected [6]. In our study, disease recurrence was detected on the abdominal portion of the CT examination in 17 (74%) of 23 cases. Retroperitoneal adenopathy was detected in 13 of 23 patients, and liver metastases were present in seven of 23 patients. Most of the patients with retroperitoneal adenopathy also had pelvic adenopathy (11 of 13 patients). This finding was not unexpected, as recurrent TCC does spread via lymphatics from pelvic nodes to retroperitoneal nodes. The pelvis was normal in three (13%) of 23 patients with recurrence shown on abdominal CT: two patients had retroperitoneal adenopathy and one patient had liver metastases as the sole site of recurrence. Thus, the need for both pelvic and abdominal scans in these patients is clearly evident, even when the pelvic portion of the examination does not show recurrence.

Hepatic metastases were usually associated with widespread involvement elsewhere. Extrahepatic sites of tumor in six patients with hepatic metastases included the pelvic nodes, retroperitoneal nodes, cystectomy site, spleen, kidney, spine, and anterior abdominal wall. However, in one patient, the liver was the sole site of recurrence.

We found that the extent of disease was underestimated on the initial CT interpretation in five of the 27 patients. Recurrent TCC that was underestimated occurred at the cystectomy site and perineal region in four patients and in the mesentery in one patient. In three of the five underestimated cases, small masses were located immediately superior to the perineal body and were originally thought to be part of that structure. Two were visible in retrospect as thickening or impression on the anterior rectal wall; one could not be seen in retrospect even knowing the location from a follow-up CT scan obtained when the mass had grown enough to be visible. In the other case of local recurrence, scanning had not been continued far enough inferior to evaluate the site of recurrence in the deep perineal space. Scans must be continued into the perineum to avoid missing recurrences in the urethra or other structures below the pelvic floor. In the case of mesenteric recurrence, mesenteric infiltration by tumor was missed because no sizable mass or no gross distortion of anatomic structures was present. Only an increase in soft-tissue strands could be appreciated in retrospect (which we interpreted as postoperative fibrosis). Even in retrospect, CT could not be used to predict the amount of disease found at surgery.

Limitations of our study include our inability to document disease status at each suspicious site on CT and to exclude disease definitively in all normal areas. In most patients, biopsy results proving recurrence are available from only one

location. In addition, not all examinations were continued through the perineum, which we recommend as the best technique. In general, regularly timed postoperative scans were not obtained, so that we did not have baseline postoperative scans for comparison in most cases. However, most recurrences in our series occurred within the first 18 months after surgery, suggesting the need for early follow-up examinations. This should be tempered by the knowledge that our population is skewed; because we are a tertiary-care referral center, some patients were referred to us for the treatment of metastatic disease. Finally, a selection bias exists in our population of patients because only patients with recurrent disease were studied. Thus the percentages of lesions at various sites in our patients are higher than should be expected when an unselected population of patients is scanned.

We and others [6, 7] have found CT to be useful in postcystectomy patients for detecting local and distant abdominal and pelvic recurrences; this raises the possibility that early, regularly scheduled, follow-up CT could promote earlier detection and perhaps prolong survival. Our study of 27 patients showed patterns of initial recurrence in which the most common sites are the pelvic and retroperitoneal nodes and the cystectomy site; however, hepatic and skeletal metastases are not infrequent. In our series, if scans through the perineum and abdomen were excluded from the follow-up scans, more than 10% of patients would not have had recurrent disease detected. A proper protocol for CT follow-up of the postcystectomy patient should include more than just routine pelvic scanning. Thorough technique requires excellent opacification of bowel (particularly small-intestine loops in the pelvis), IV contrast material (to opacify urinary diversions), and a scanning range that includes the abdomen and perineum.

REFERENCES

1. Hodson NJ, Husband JE, Macdonald JS. The role of computed tomography in the staging of bladder cancer. *Clin Radiol* 1979;30:389-395
2. Jeffrey RB, Palubinskas AJ, Federle MP. CT evaluation of invasive lesions of the bladder. *J Comput Assist Tomogr* 1981;5:22-26
3. Koss JC, Arger PH, Coleman BG, Mulhern CB Jr, Pollack HM, Wein AJ. CT staging of bladder carcinoma. *AJR* 1981;137:359-362
4. Morgan CL, Phil M, Calkins RF, Cavalcanti EJ. Computed tomography in the evaluation, staging and therapy of carcinoma of bladder and prostate. *Radiology* 1981;140:751-761
5. Salo JO, Kivisaari L, Lehtonen T. CT in determining the depth of infiltration of bladder tumors. *Urol Radiol* 1985;7:88-93
6. Lee JKT, McClennan BL, Stanley RJ, Levitt RG, Sagel SS. Use of CT in evaluation of postcystectomy patients. *AJR* 1981;136:483-487
7. Olivia L, Cariati M, Reggiani L, Romanzi F. CT evaluation of the pelvic cavity after cystectomy: observation in 40 cases. *J Comput Assist Tomogr* 1984;8:734-738

Case Report

Testicular Microlithiasis: Sonographic Features with Pathologic Correlation

W. Sean Smith,¹ Harry M. Brammer,^{1,2} Michael Henry,³ and Harold Frazier⁴

Testicular microlithiasis is a rare abnormality that histologically consists of concretions within the seminiferous tubules [1]. On sonograms, affected testes have small diffuse hyperechoic foci [2, 3]. We report a case that highlights this unique sonographic appearance. A radiograph of the scrotum confirmed the calcific nature of the hyperechoic foci.

Case Report

The patient is a 36-year-old man with a 4-month history of testicular pain unrelieved by antibiotics or antiinflammatory medications. Results of scrotal examination were normal. Sonography with an Acuson 128 unit and a 7.5-MHz transducer showed both testes to be of normal size and echogenicity. Diffusely scattered throughout both testes were small homogeneous, nonshadowing, hyperechoic foci (Fig. 1A). A radiograph of the scrotum made on a General Electric Sonographic 500T mammographic unit with a phototimed exposure of 25 kVp showed diffuse, homogeneous, 1- to 2-mm calcifications scattered throughout both testes (Fig. 1B). Because of persistent symptoms, exploratory surgery and biopsies of both testes were performed. On histologic examination, the parenchyma of the testes was normal except for laminated microcalcifications scattered randomly throughout. These calcifications were located in the tubular lumen or beneath the epithelium under a thin layer of connective tissue. The tubules containing the microliths had a variable loss of cellularity (Fig. 1C). One year after biopsy, the patient was asymptomatic and findings on a follow-up sonogram were unchanged.

Discussion

Although uncommon, testicular calcification usually is dystrophic and caused by previous infections, trauma, or tumor [4]. The presence of calcification in the lumen of seminiferous tubules, as in the case reported here, is unusual [2, 3]. Microlithiasis has been reported in males of all ages, in both cryptorchid and scrotal testes and in testes with normal and dystrophic spermatogenesis [1-3]. In our case, the testes were normal with normal spermatogenesis. A case of microlithiasis in a nonfunctioning testis is illustrated for comparison (Figs. 2A and 2B).

Intratubular microcalcifications result from formation of microliths from degenerating cells within the seminiferous tubule [1]. Formation of microliths appears to be a primary process and not a sequel of a more basic underlying process. Our cases underscore this point because the patients had no history of inflammation, infection, trauma, or infarction.

Sonographically, testicular microlithiasis has bilateral, diffusely scattered, intraparenchymal hyperechoic foci [2, 3]. In our cases, no significant beam attenuation occurred, and testicular architecture and echogenicity were normal. A radiograph of the scrotum showed the calcifications that had been seen on the sonogram and histologic section. The small, diffuse, uniform appearance of the calcifications is typical of testicular microlithiasis and not unlike the appearance of degenerative breast disease such as sclerosing adenosis.

Received May 7, 1991; accepted after revision June 26, 1991.

The opinions and assertions expressed herein are those of the authors and are not to be construed as reflecting the views of the Department of Defense.

¹ Department of Radiology, National Naval Medical Center, Bethesda, MD 20889-5000.

² Department of Radiology, Uniformed Services University of the Health Sciences, 4301 Jones Bridge Rd., Bethesda, MD 20889-5000.

³ Department of Pathology, National Naval Medical Center, Bethesda, MD 20889-5000.

⁴ Department of Urology, National Naval Medical Center, Bethesda, MD 20889-5000.

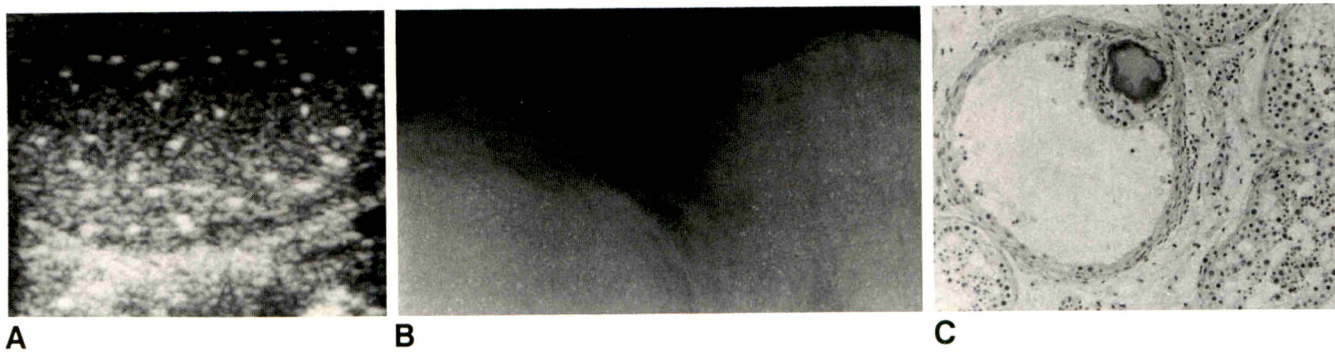


Fig. 1.—A, Longitudinal sonogram of right testicle shows multiple hyperechogenic foci caused by microlithiasis.

B, Radiograph of scrotum shows diffuse nature of testicular calcifications.

C, Histologic section shows microlith beneath an attenuated epithelium and surrounded by a layer of connective tissue. Testis is otherwise normal.

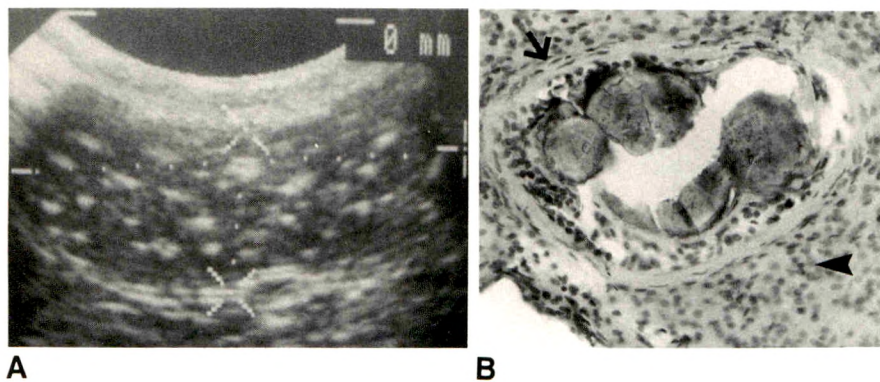


Fig. 2.—A, Sonogram of right testicle shows multiple hyperechoic foci in otherwise normal-appearing parenchyma.

B, Histologic section shows calcification in a sclerotic tubule without germ cells, surrounded by nonspecific fibrosis (arrow) and Leydig cell hyperplasia (arrowhead).

The distinctive microcalcifications of testicular microlithiasis separate them from the microcalcifications associated with tumor, inflammation, or scar, which tend to be solitary, focal, and frequently associated with a mass [5, 6]. If all the criteria for testicular microlithiasis are present, the diagnosis can be made without further clinical or surgical evaluation [3, 7]. If the characteristic sonographic findings are not present, further evaluation is warranted as clinically indicated [2].

ACKNOWLEDGMENTS

The authors thank Sudhir Arora, Paul Christenson, and Eric R. Sover for their contributions.

REFERENCES

1. Vegni-Talluri M, Bigliardi E, Vanni MG, Tota G. Testicular microliths: their origin and structure. *J Urol* **1980**;124:105-107
2. Jaramillo D, Perez-Atayde A, Teele RL. Sonography of testicular microlithiasis. *Urol Radiol* **1989**;11:55-57
3. Doherty FJ, Mullins TL, Sant GR, Drinkwater MA, Ucci AA. Testicular microlithiasis: a unique sonographic appearance. *J Ultrasound Med* **1987**;6:389-392
4. Krone KD, Carroll BA. Scrotal ultrasound. *Radiol Clin North Am* **1985**;23:121-139
5. Iking U, Wurster K, Terwey B, Möhring K. Microcalcifications in testicular malignancy: diagnostic tool in occult tumor? *Urology* **1982**;19:525-528
6. Martin B, Tubiana JM. Significance of scrotal calcifications detected by sonography. *JCU* **1988**;16:545-552
7. Bieger RC, Passarge E, McAdams AJ. Testicular intratubular bodies. *J Clin Endocrinol* **1965**;25:1340-1346

Perspective

Hemorrhage Associated with Pelvic Fractures: Causes, Diagnosis, and Emergent Management

Yoram Ben-Menachem,¹ Douglas M. Coldwell,¹ Jeremy W. R. Young,² and Andrew R. Burgess³

The high risk of exsanguinating hemorrhage in patients with pelvic ring disruption demands aggressive, yet balanced orthopedic and angiographic management as soon as patients are admitted to the emergency department. We present a perspective of our experience in two trauma centers and propose a logical approach to early prediction, diagnosis, and management of hemorrhage associated with pelvic fractures. Our method is based on knowledge of pelvic anatomy and an understanding of the mechanisms of injury and their wounding capacity, given that the mechanism of injury determines the type of pelvic ring disruption and that the probability of arterial hemorrhage is—to a great extent—a function of the type of pelvic fracture. The risks of diagnostic peritoneal lavage and of excessive radiologic studies of noncritical injuries are emphasized. The principles guiding arterial embolization and the application of external fixators are discussed.

Disruption of the pelvic ring and the hemorrhage that accompanies it call for an interdisciplinary exercise in diagnosis and management—one that quite often is complex and controversial. Given that hemorrhage is the common denominator of non-CNS death in pelvic fractures [1–4], delay in its diagnosis and hemostasis is directly responsible for death by exsanguination. Complications of undiagnosed hemorrhage further contribute to a high death rate and to severe, permanent disability in survivors. On the other hand, it has long been established that orthopedic-angiographic team management of hemodynamically unstable patients with pelvic ring disruption significantly lowers mortality rates [3, 5–8]. Frac-

ture of the pelvis is, therefore, an orthopedic/angiographic issue. This article emphasizes angiographic diagnosis and control of hemorrhage against the background—and within the context—of the orthopedic management of pelvic fractures. Intraabdominal and intrathoracic injuries that accompany pelvic fractures also are considered [9–14]; methods and timing for their diagnosis and treatment are discussed where relevant.

With the increasing use of external fixators and angiography, it has become important to understand the types and directions of forces responsible for pelvic fractures. With such an understanding, stabilizing devices can be applied rapidly and correctly and, at the same time, the probability of pelvic arterial hemorrhage can be assessed and hemorrhage controlled as early as possible.

Anatomy

The pelvis is basically a ring, comprising three bony components: the sacrum and two lateral components, each composed of ilium, ischium, and pubis. The ring formed by these units has no inherent stability, and its integrity relies totally on ligamentous support and stabilization of the sacroiliac joints; the symphysis pubis acts more as a supporting strut. The posterior portion of the pelvis is stabilized predominantly by the anterior and posterior sacroiliac ligaments, bridging the sacroiliac joints. Further stability is added by the inferior

Received April 11, 1991; accepted after revision July 12, 1991.

¹ Department of Radiology, University of Washington, Harborview Medical Center and the University of Washington Medical Center, Seattle, WA 98104. Address reprint requests to Y. Ben-Menachem, Department of Radiology, Harborview Medical Center, 325 Ninth Ave (ZA-65), Seattle, WA 98105.

² Department of Radiology, University of Maryland Medical Center, 22 S. Greene St., Baltimore, MD 21201.

³ Department of Orthopaedic Trauma, Maryland Institute of Emergency Medical Services Systems, 22 S. Greene St., Baltimore, MD 21201.

AJR 157:1005–1014, November 1991 0361–803X/91/1575–1005 © American Roentgen Ray Society

ligaments—the sacrotuberous and sacrospinous—that connect the sacrum and ischium (Fig. 1).

The major arterial structures are the common and external iliac arteries and the internal iliac artery with its branches. At least part of the course of each of the pelvic arteries is close to bone or across one of the supporting ligaments (Fig. 1). Understanding the paths of these vessels allows prediction of possible arterial injury when either the bones of the pelvic ring that lie in close relationship are fractured or there is an indication that supporting ligaments have been disrupted. For example, separation of the sacroiliac joints or posterior fractures of the iliac wings extending to the sciatic notch raise the possibility of trauma to the internal iliac and superior gluteal arteries. The superior gluteal artery may be severed by the sharp fascia of the piriformis muscle, even without a significantly displaced fracture [15, 16], and the internal pudendal artery may be disrupted proximally when the inferior supporting ligaments tear or may be injured anteriorly by fractures of the pubic rami.

Classification of Pelvic Fractures

The traditional classification of pelvic fractures was based primarily on the degree of instability of the pelvic ring. The assumption was that the least stable pelvic fractures were associated with increasingly severe hemorrhage [2, 17]. Although this is generally correct, it is clear that instability is not necessarily associated with hemorrhage, whereas a stable pelvic ring does not in itself guarantee immunity from significant arterial injury [6, 15]. Inasmuch as our experience has shown that the direction and intensity of the wounding force directly affects the degree of soft-tissue trauma, including arterial injury [18], we prefer to classify pelvic fractures according to the direction of the injurious force. Radiographs of the pelvis, obtained at admission and with proper technique

[19], provide not only information on the mechanism of injury but also an indication of pelvic stability.

Injury Force Patterns

The concept of classifying pelvic injuries according to the nature of the disruptive force was proposed by Tile [20] and Pennal et al. [21] and developed by Young and Burgess [19] and Young and Resnik [22]. Three main types of force can produce pelvic fractures: lateral compression, anteroposterior compression, and vertical shear. The three major groups of pelvic fracture in the Young/Burgess [18, 19, 23] classification are named accordingly.

Lateral compression is by far the most common pelvic fracture and is subdivided into three types (I, II, and III) depending on the severity of the injury and progressive involvement of the posterior pelvis [18, 22]. Fractures of the pubic rami are always present, and run horizontally or in the coronal plane, or present as "buckle" or "overlap" fractures. A "crush" impacted fracture of the sacrum is common.

In anteroposterior compression the force is generally from the front, tending to open the anterior pelvis, with diastasis of the symphysis pubis and/or fracture of the pubic rami. In this case, the fractures are sagittally oriented, appearing to run vertically. Again, three types of injury are seen (I, II, and III), depending on the severity of the ligamentous damage and disruption of the sacroiliac joints [18, 22].

In vertical shear the injury force is directed superiorly, as in falls from a height. Vertically oriented fractures occur through the anterior and posterior portions of the pelvis, with superior displacement of the major fragments [18, 22].

Finally, a combination of forces may act on the pelvis at the time of injury. In general where there is more than one force vector, one dominant vector is usually responsible for the major injury; however, on rare occasions, it may not be possible to define a single dominant vector. When there is no clear-cut dominant force vector, and the injury pattern suggests a combination of vectors, the fractures are classified as combined mechanical injury fractures. This group accounts for less than 7% of pelvic fractures [18, 22].

Equally uncommon is the isolated iliac wing fracture, without disruption of the integrity of the pelvic ring [18, 22].

Detailed discussion and illustration of the classes and types of pelvic fractures are outside the scope of this article and have been amply treated in recent publications [18, 22].

Prevalence of Arterial Hemorrhage in Association with Pelvic Fractures

In a significant number of persons killed in traffic accidents—for example, in up to 45% of pedestrians [24]—pelvic fractures are the cause of death [1, 17, 25]. Overwhelming evidence indicates that the high mortality rate in patients with pelvic fractures is related directly and primarily to hemorrhage [1, 2, 5–10, 24, 26–32]. Some of the victims die of exsanguination because of intractable shock and coagulopathy; others succumb to complications of hemorrhage, such as infected pelvic hematomas and renal or multiorgan failure.

Arterial injuries occur in direct relation to the mechanism and severity of the injury, and to a great extent to the degree

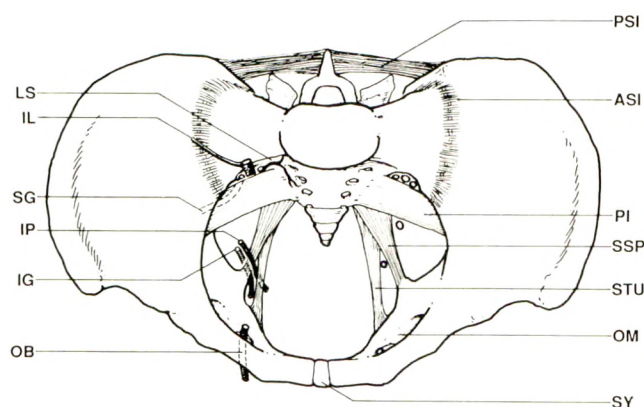
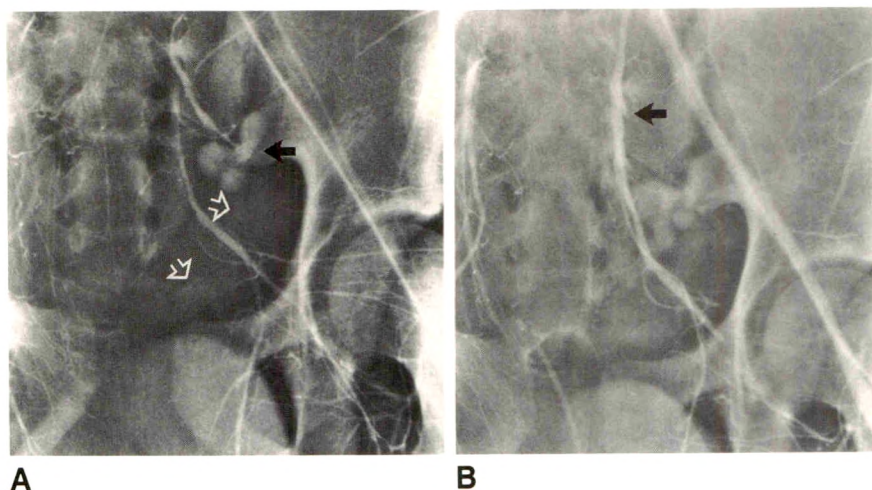


Fig. 1.—Drawing of pelvic ring and its supporting ligaments and a representation of branches of internal iliac artery. All arteries, at some phase of their course, are close to a bone, a joint, or a ligament, and disruption of one of these structures can lead to arterial tears. Piriformis muscle has a strong relationship to superior gluteal artery, as its fascia is sharp enough to tear superior gluteal artery even in the absence of a fracture. Arteries: IG = inferior gluteal, IL = iliolumbar, IP = internal pudendal, LS = lateral sacral, OB = obturator, SG = superior gluteal. Ligaments: ASI = anterior sacroiliac, PSI = posterior sacroiliac, SSP = sacrospinous, STU = sacrotuberous. Other: OM = obturator membrane, PI = piriformis muscle, SY = symphysis pubis.

Fig. 2.—Unremitting hemorrhage from superior gluteal artery in 16-year-old boy; anteroposterior compression type III mechanism from a motorcycle accident. Patient had complete diastasis of both sacroiliac joints, open symphysis pubis, sacrococcygeal dislocation, and avulsion of lateral portion of left part of sacrum. He had angiography because of progressive hypotension and drop of hematocrit. At angiography, his systolic blood pressure was 70–80 mm Hg and he had no measurable diastolic pressure.

A, Pelvic angiogram shows solitary, brisk hemorrhage from a transected left superior gluteal artery (solid arrow) and avulsion of sacrum (open arrows).

B, Angiogram obtained after selective embolization of left superior gluteal artery with a single 1 × 1 × 40 mm Gelfoam strip shows artery is occluded at its origin (arrow). Abdominal angiography did not reveal any abdominal injuries.



of instability of the pelvic ring. Therefore, arterial injuries are most prevalent in patients in whom the bony elements are fractured and the ligamentous elements are torn: anteroposterior compression types II and III, lateral compression type III, vertical shear, and combined mechanical injury [18]. As expected, the highest prevalence of arterial injury is in anteroposterior compression types II and III [18, 32, 33]. For this reason, the most frequently injured arteries are the superior gluteal (Fig. 2) [15, 16, 34] and internal pudendal [34] arteries, the former because of its relation to both the sacroiliac joint and the sharp fascia of the piriformis [15, 16], the latter because of its proximity to the inferior ligaments of the pelvis, the pubic rami, and the urogenital membrane. Other arteries are injured somewhat less frequently; the lateral sacral artery in disruptions of the posterior portion of the pelvic ring and the obturator and vesical arteries in anterior fractures. The inferior gluteal artery is injured when the inferior ligaments are injured [34].

Thus, the Young/Burgess classification allows us to predict, in general, the probability of pelvic arterial hemorrhage. The high frequency of arterial injuries in the anteroposterior compression, vertical shear, and combined mechanical injury groups should, by necessity, guide our early approach to the diagnosis and management of pelvic fractures.

Associated Injuries

Intraabdominal injuries are seen frequently in patients with pelvic fractures [11] and, although they are usually mild to moderate in severity, their diagnosis and management may sometimes interfere with or even complicate the management of the fractured pelvis [29, 35]. The reported frequency in which intraabdominal injuries accompany pelvic fractures is between 16% [12] and 26% [7] in all patients with pelvic fractures, and up to 55% in patients with unstable pelvic fractures [32].

Arterial hemorrhage in the posterior portion of the abdominal extraperitoneum, usually from transected lumbar (Fig. 3) or renal arteries, can be lethal [6, 7, 13, 35].

Intrathoracic injuries include, in addition to pulmonary and diaphragmatic trauma, an increased risk of rupture of the thoracic aorta. Panetta et al. [7], in their series of patients requiring embolization of pelvic arteries, found that 6.5% of these patients had ruptured thoracic aortas. In the series published by Ochsner et al. [14], 6% of all patients with pelvic fractures also had a ruptured thoracic aorta—six times the occurrence of ruptured aortas in the general population of trauma patients—and the same authors cite the Major Trauma Outcome Study, in which the percentage of patients with both pelvic fractures and ruptured aortas, although smaller (1.6%), was still 3.2 times greater than the percentage of ruptured aortas seen in the general trauma population.

Injuries to the CNS often dominate the clinical picture of patients with total body trauma and are also the primary cause of death in many of these patients. The occurrence of head injuries in patients with pelvic fracture is reported to be between 26% [7] to 50% [33] or 55% [2].

Urologic injuries closely parallel damage to the anterior components of the pelvic ring. Hence they are most likely to be found in patients with anteroposterior compression and vertical shear fractures, and in those with complex lateral compression fractures. The urethra is almost exclusively injured in males only. The frequency of urologic injuries is around 7%, with the male urethra dominating in the statistics [33].

Additional pelvic bleeding occurs from fractured bones and ruptured veins. Indeed, these two sources of hemorrhage always exist in patients with pelvic fractures and may be solely responsible for the entire volume of blood loss. Contrary to arterial hemorrhage, these two sources of bleeding respond well to application of external fixators.

Diagnostic Procedures on Admission

Initial Radiographic Examination

A single anteroposterior radiograph of the pelvis is made in every patient with wide-impact body trauma seen at any of

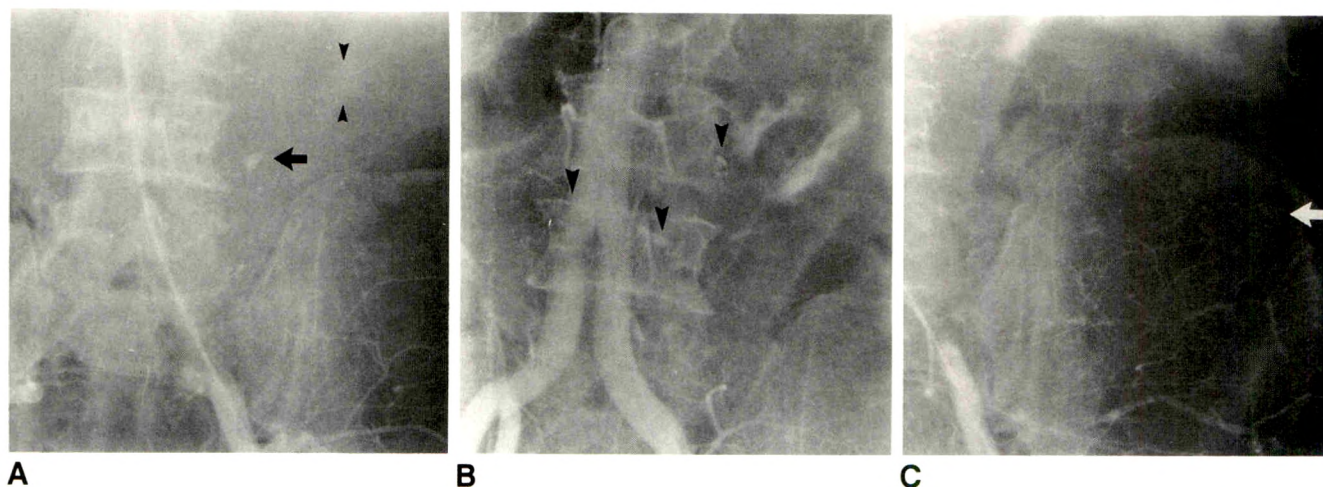


Fig. 3.—Lumbar artery injury in 63-year-old man injured in a work-related accident who had an isolated fracture of left iliac wing. Avulsion of left fourth lumbar transverse process was not found at time of admission. After several hours of unremitting hemorrhage, patient had no measurable blood pressure and was on total life support.

A, Diagnostic abdominopelvic angiogram shows hemorrhage from a transected left fourth lumbar artery (arrow) and avulsion of lumbar transverse process (between arrowheads). Embolization had to include left fourth lumbar artery as well as left third lumbar and right fourth lumbar arteries, because both of these arteries supplied collaterals to bleeding vessel.

B, Angiogram obtained after embolization shows that hemorrhage has been controlled. Arrowheads point to location of coils in lumbar arteries.

C, Selective arteriogram of left common iliac artery shows spotting along fracture line in left iliac wing (arrow). These hemorrhages are trivial and require no intervention. Patient had an uneventful recovery.

our institutions. This view allows a good general assessment and shows anatomic detail of the pelvis, but subtle fractures may be obscured. Therefore, in each patient in whom pelvic injury is either clinically suspected or previously diagnosed, two additional views of the pelvis are obtained: an "inlet" view, with the patient supine and the X-ray tube angled 45 degrees caudad and the beam centered on the umbilicus, and an "outlet" view, with the tube angled 45 degrees cephalad and the beam centered on the symphysis [19].

Examination of the plain radiographs will readily define the major force vector and type of fracture. The cardinal plain film findings are summarized in Table 1. On the basis of the plain film findings, we also assess the degree of instability of the fractures, the urgency and technique for application of an external fixator, and the probability of arterial hemorrhage requiring angiography and embolization.

Further Radiologic Assessment

In selecting the most appropriate method of diagnosis in acute trauma beyond the radiographs obtained at admission, one must bear in mind that angiography is the only means of obtaining direct evidence of vascular injury and hemorrhage. As much as unenhanced radiographs are beneficial to the diagnosis of skeletal injuries, they offer only indirect evidence of the likelihood of soft-tissue trauma. Repeatedly obtaining films at regular intervals will not elicit information that was not there in the first place, but will waste precious time and may eventually be detrimental to the patient [5, 35]. Physicians must concentrate on life-threatening injuries and should choose the minimum number of diagnostic procedures that provide direct, and hence the most reliable, evidence of critical injuries [4, 13, 36]. In the case of the fractured pelvis, the

TABLE 1: Features of the Primary Patterns of Pelvic Fractures

Type of Fracture	Lateral Compression	Anteroposterior Compression	Vertical Shear
Pubic rami fractures	Horizontal: buckle	Vertical	Vertical
Symphysis pubis diastasis	Rare, only with type III	Almost always present	Sometimes
Sacral fracture	Common, impacted	Rare, lateral sacral avulsion	Sometimes, vertical
Sacroiliac joint diastasis	Only in type III (contralateral)	Common	Sometimes
Iliac wing fracture	Type II or type III, oblique	Rare	Vertical
Acetabular fracture	Medial wall	Posterior column \pm anterior column	Roof
Displacement of major fragment	Medial (see type III)	Posterior or "open book"	Superior
Likelihood of arterial hemorrhage	Low, except in type III	High in types II & III	High

Note.—Based on material from Burgess et al. [18], Young and Burgess [19], Young and Resnik [22], and Young et al. [23].

diagnostic tool must allow rapid detection of both ongoing and imminent hemorrhage in the entire torso. The only technique capable of doing so is the arteriogram [6, 7, 35].

Therefore, initially, time should not be wasted on investigation of the urinary tract. Excretory urography offers only limited and uncritical information and should be avoided. Urethrography and cystography, no matter how attractive they may seem at the time, must not be considered before the patient is judged to be hemodynamically stable or before completion of angiographic diagnosis and management. Urologic diagnostic procedures, in addition to being irrelevant to preservation of the patient's life, also may greatly interfere with angiographic diagnosis if, when results are abnormal, the procedures result in extravasation of contrast medium into the area in which one must look for arterial hemorrhage [13, 36].

CT, on the other hand, has an important use in the diagnosis of pelvic fractures, but largely in the assessment of stable hematomas and in providing three-dimensional information regarding the status of the bony fragments [13, 37], especially in examining the acetabulum [38]. However, a serious logistical problem with CT is the need to transfer an acutely injured and hemodynamically unstable patient into the scanner and out of it, a transfer that can be difficult and may considerably aggravate hemorrhage. In the acute setting, CT should be reserved for those patients who are hemodynamically stable and probably do not need angiography. Even then one would be well advised to conduct CT investigation with IV contrast medium but without oral or rectal contrast medium because demonstration of large hematomas may result in immediate angiography, and the presence of contrast medium in the bowel would reduce the precision of the angiographic diagnosis.

Diagnostic Peritoneal Lavage and Exploratory Laparotomy

Ordinarily, in patients with isolated abdominal trauma, a diagnostic peritoneal lavage showing intraperitoneal blood is an indication for exploratory laparotomy. However, in the presence of pelvic fractures and large extraperitoneal hematomas, laparotomy not only fails to arrest the hemorrhage [39] but also may put the patient at great risk: by opening the abdominal cavity, the surgeon may contribute directly to aggravation of extraperitoneal hemorrhage and rapid expansion of hematomas due to decompression of tamponade. Breaching the pelvic peritoneum and the posterior portion of the abdominal peritoneum in an attempt to control this hemorrhage by packing the extraperitoneum and by ligating the internal iliac or other arteries is ineffective and may lead to death by exsanguination (Fig. 4) [2, 6, 10, 13, 29].

A false-positive diagnostic peritoneal lavage occurs in up to 29% of patients with pelvic fractures, largely because of slight bleeding from mild injuries and/or seepage of blood through small tears in the peritoneum. Therefore, diagnostic peritoneal lavage should not be relied on as an indicator for laparotomy [2, 29]. Indeed, unless there is clear clinical evidence that the patient has very large quantities of free blood

intraperitoneally, one would be wise to avoid diagnostic peritoneal lavage altogether [3], or else ignore an abnormal result and proceed with angiography and embolization [6, 8, 13]. Certainly, if a patient appears to need surgery, preoperative angiography and embolization may, if not obviate surgery, at least stabilize the patient and lower the risk of the surgery [6, 8, 35].

One should also bear in mind that normal findings on diagnostic peritoneal lavage merely indicate absence of free blood from the peritoneal cavity. The patient may still bleed to death into the extraperitoneum [6].

Angiographic Diagnosis of Acute and Imminent Hemorrhage

The diagnosis and subsequent treatment of arterial hemorrhage from pelvic fractures should be angiographically and not surgically directed because angiography is far more selective and direct and much less invasive and mutilating than any operation. The angiographer can survey all injuries, identify hemorrhage quickly and, without entering the extraperitoneal hematoma, reach the injury and treat it transarterially [5, 11, 31, 34, 40, 41].

As a matter of principle, therefore, one must be prepared to diagnose hemorrhage as soon as possible after the arrival of the patient in the emergency department. For this reason, a radiologist well trained in angiography must always be available, supported by technologists and nurses, and ready to start angiography on a moment's notice [35].

Patients with pelvic fractures do not necessarily bleed in the pelvis alone. Quite a few have multiple sources of bleeding, in the pelvis, abdomen, chest, and thigh; others bleed



Fig. 4.—Danger of exploratory laparotomy in presence of pelvic fractures. A 76-year-old woman, driver of a car hit broadside from left, was admitted in stable condition with lateral compression fractures of pelvis. Peritoneal lavage was unsuccessful. Because her blood pressure was starting to drop, she was taken directly to the operating room. Exploratory laparotomy showed no abnormalities. Immediately on opening of peritoneal cavity, patient began to bleed massively into pelvic extraperitoneum and died on the operating table. Arteriogram obtained during autopsy after injection of barium sulfate into left iliac artery shows multiple hemorrhages around entire left side of pelvic brim and in presacral region.

in the abdomen or chest only but not in the pelvis. Therefore, patients with pelvic fractures must undergo diagnostic angiography of both pelvis and abdomen [4, 6, 13, 35] and, should the slightest suspicion of thoracic injury exist, of the thoracic aorta as well [6].

Catheterization, transfemoral or (if both sides of the groin are indurated by large hematomas) left transaxillary, should be via an introducer sheath to allow easy and risk-free catheter changes. The sheath should have a reflux-preventing seal, be 13-cm long, and accommodate catheters up to 7-French. The procedure should always begin with midstream pelvic arteriography and abdominal aortography, which must include in it all soft tissues of the pelvis and abdomen—when treating patients who are bigger than average, one may have to study the right and left sides separately. Selective angiography should follow, as a preembolization procedure, if the midstream study fails to show to advantage third-generation and smaller branches of the internal iliac artery. As a general rule, an arterial hemorrhage requiring embolization is expected to show itself on the midstream study; however, this is not always true, and selective studies of the smaller arterial branches to the pelvis are recommended.

Any gently curved, 100- to 110-cm-long, selective cerebral catheter (e.g., H1, H1L, or H1H catheters, Cook Inc., Bloomington, IN) will do from a left axillary access. Selective pelvic angiography with a femoral access is easy with a specially designed catheter, such as the Torcon NB Advantage Curved HNB5, CD3932 (Cook Inc.); this 5-French modification of the Chuang-8-reverse-curve catheter (Cook Inc.) has a 24-cm descending arm and a distal H1L shape, most useful for entry into the ipsilateral internal iliac, external iliac, and deep femoral arteries, even when work is being done via a 13- or 15-cm sheath.

The purpose of abdominal angiography is to determine the most likely additional sources of hemorrhage. Because the most frequently injured organ is the spleen [7, 11, 12, 29, 32], it has to be shown well, at least on the midstream aortogram, and a selective splenic angiogram should be performed on the slightest suspicion of hemorrhage. One should also survey carefully all lumbar arteries, as these are often involved in patients with pelvic fractures [6, 7, 13].

When the chest radiograph obtained at admission shows a mediastinal hematoma of any size, a thoracic aortogram must be obtained, even with an otherwise low index of suspicion [7, 14].

Management

Priorities

In principle, most patients with combined high-risk pelvic fractures and intraabdominal injuries have only modest intraperitoneal hemorrhage, usually associated with minor intraabdominal injuries or diapedesis of RBCs from the extraperitoneal injuries. The pelvic fracture therefore is addressed first. For a patient with a low-risk disruption of the pelvic ring and findings of severe intraabdominal or other extrapelvic hemorrhage [18, 33], the pelvic injury is addressed only after

treatment of the more dangerous hemorrhagic injuries. The controversy, then, is the treatment priorities for a patient with both significant intraabdominal or thoracic hemorrhage *and* a high-risk pelvic fracture [18]. In this situation, it is the limits of the institution and available personnel, rather than the specifics of the injuries, that may determine the order of treatment. If highly specialized orthopedic surgeons are available, initial stabilization can be done with an external fixator, providing this can be accomplished in less than 20 min. This has been shown to stop venous, osseous, and minor arterial hemorrhage in a large proportion of cases at one of our institutions, thereby removing the need for angiography in most of the patients thus treated. If such orthopedic expertise is not available and if skilled interventional radiologists are available, the patient is transported to the angiography suite for diagnostic angiography and embolization. If such resources are unavailable, the bones should be stabilized in the emergency department while the operating theater is being readied. If experienced orthopedic and radiologic resources are not available, the patient may have to be treated with laparotomy to control the intraabdominal portion of the hemorrhage, and with symphysis plating before closure or pneumatic antishock garment after closure.

Physicians are often reluctant, for no valid reason, to transport hemodynamically unstable patients to the angiography suite. We urge them to abandon this attitude. Patients in hemorrhagic shock, with surgically correctable injuries, should be transported to the operating theater, regardless of shock. By the same token, patients in hemorrhagic shock, with unknown sources of hemorrhage—as well as those with hemorrhage best treated by embolization—should be transported to the angiographic suite, regardless of shock (Figs. 2, 3, and 5). Left where they are, be it the emergency department or intensive care unit, they may die of exsanguination [5].

External Fixation

Unless catastrophic hemorrhage is occurring with immediately life-threatening potential, we advocate initial pelvic stabilization with an external fixator. In a significant number of patients, such external fixation stabilizes the bony pelvic environment, providing immediate and longer-term benefits.

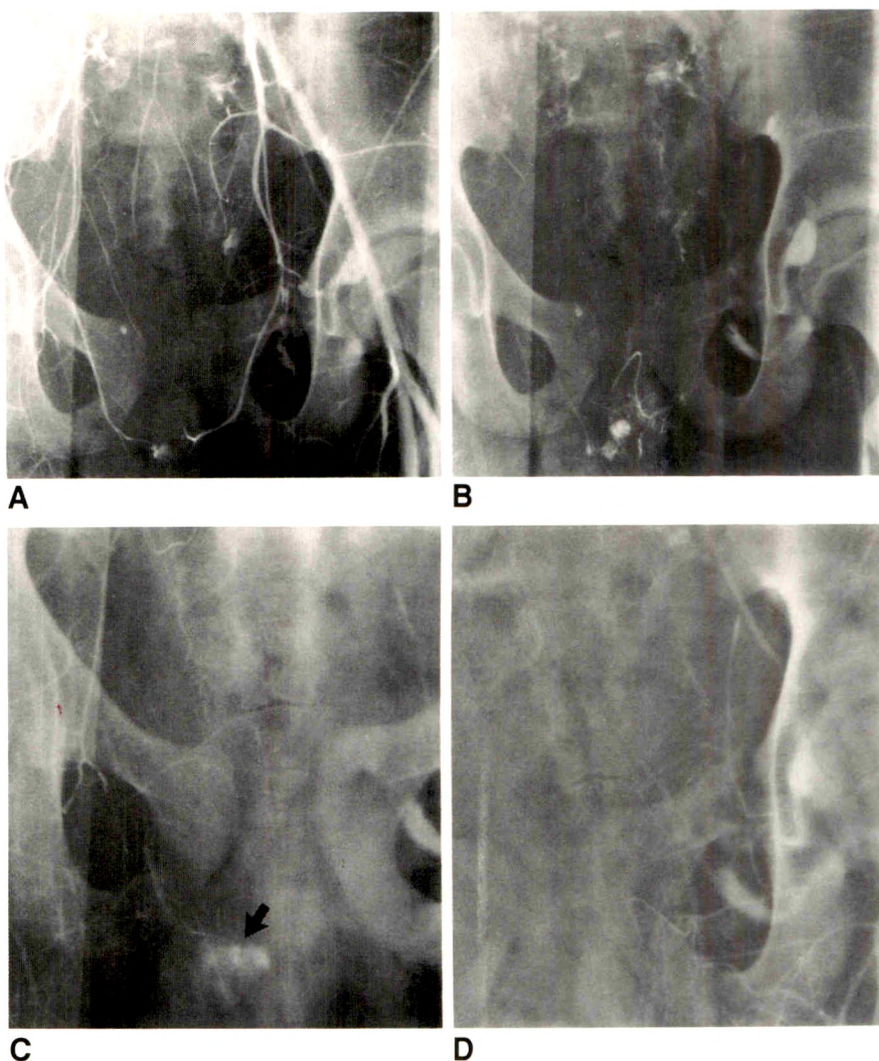
A pelvic fixator ensures that the body's first efforts at manufacturing clots are not disturbed as the patient is transferred for further diagnostic studies (e.g., angiography, CT) and concurrent emergent surgery. A pelvic fixator also helps control the volume of the true pelvic space into which much of the early hemorrhage occurs. By definition, high-risk pelvic injuries are those in which there is severe damage to the constraining ligaments of the pelvic ring, namely the anterior sacroiliac, sacrotuberous, and sacrospinous ligaments; in the most severe cases, the posterior sacroiliac ligaments also are damaged [19–21, 23]. The same force that has disrupted these ligaments also is responsible for the arterial and venous injuries causing the pelvic hemorrhage. The loss of these ligamentous "reins" hampers the body's natural effort to

Fig. 5.—Scatter embolization. A 16-year-old bicycle rider was hit by a car at high speed. He arrived at hospital without measurable blood pressure, with combined-mechanism pelvic fractures and severe head injury. Angiography was performed via left axillary approach because patient had to be kept in a pneumatic antishock garment.

A and B, Pelvic angiograms, arterial (A) and capillary (B) phases, show multiple brisk hemorrhages from lateral sacral and superior gluteal arteries bilaterally, left inferior gluteal and obturator arteries, and right internal pudendal and vesical arteries. Abdominal aortography (not shown) revealed massive extraperitoneal hematoma and a nonbleeding injury to left renal pedicle. Left internal iliac artery was occluded with three Gelfoam strips backed by coils; right internal iliac artery was occluded with small-particle Gelfoam suspension backed by coils.

C, Angiogram obtained after embolization shows right external pudendal artery supplies collateral blood flow to distal part of internal pudendal artery; slight, irrelevant bleeding is still seen (arrow).

D, Angiogram of left iliac artery after embolization shows complete control of hemorrhage. Patient became hemodynamically stable, but died of head injuries 2 days later.



achieve tamponade; the displacement of the bony elements of the true pelvis away from the midline enlarges the relative radius of the true pelvis. The true pelvis can be compared to a sphere, and as such its volume varies with the cube of its radius. Hence an injury that causes a 2-cm opening at the pubic symphysis can increase the pelvic volume in an adult from the normal 1.5 l to as much as 5.0 l. The fixator, therefore, by minimizing the change in pelvic dimensions, assists in tamponade.

In addition to these two immediate benefits, stabilization of the bony skeletal elements allows relatively painless immobilization of the elements of the fractured pelvis, permitting the patient maximal mobility with its attendant advantages.

The external fixator, by virtue of arresting venous, osseous, and in some cases, minor arterial hemorrhage, may render angiography predictably unproductive and therefore unnecessary. On the other hand, the presence of an external fixator should not interfere technically with angiography if the patient remains hemodynamically unstable after external fixation has

been accomplished. However, it is important to remember that the application of such a fixator may require between 1 and 2 hr, and that the patient might benefit from a swift angiographic procedure before its placement.

Embolization

If a patient is hemodynamically unstable, an immediate arteriogram and embolization is of great benefit [5, 6, 8, 36]. Even in cases in which an operation is necessary, the angiographer can accomplish almost instant hemodynamic stabilization by occluding the lower abdominal aorta with a balloon [35, 42].

In general, 7–11% of patients with pelvic fractures require embolization [18, 34, 43]. However, analysis of a large series of patients with pelvic fractures at the Maryland Institute for Emergency Medical Services Systems [18] revealed great differences in requirements of embolization within the group,

depending on the mechanism of injury: the larger group of patients—those with lateral compression mechanisms and isolated iliac wing fractures—required embolization in only 1.7% of cases. On the other hand, in the smaller group—those with anteroposterior compression, vertical shear, and combined mechanical injury mechanisms—20% of patients required embolization. This automatically creates two distinct categories of patients: one group in which the need for angiography and embolization could be considered marginal, and another in which early angiography should be mandatory, given the frequent need for embolization.

Three basic principles should guide the angiographer in performing embolization. (1) The purpose is to slow the bleeding to the extent that the body will control its own hemorrhage, rather than create large areas of ischemia or necrosis. (2) If ischemia or necrosis must be created, it should be limited to the smallest area possible. (3) The procedure must be done expeditiously. On the basis of the angiographic findings—numbers, locations, and intensity of hemorrhagic sources—and guided by these three principles, the occluding agents are selected [42]. Gelfoam (Upjohn, Kalamazoo, MI) is the ideal occluding agent, given the ease with which it can be prepared and injected in a sterile fashion, and because its longevity within the occluded artery is limited to several weeks, beyond which the artery is expected to recanalize.

If an isolated point of bleeding can be reached superselectively, embolization may be done with one or two Gelfoam strips (Fig. 2) [42]. The dimensions of each strip should conform with the inner diameter of the catheter and with the caliber of the target artery. Strips 1- to 2-mm thick (cut by scalpel from the commercially available block of Gelfoam), with lengths from 1 to 5 cm, are most suitable. Each Gelfoam strip is loaded separately into a 10-ml syringe with diluted contrast medium and injected via the catheter under constant fluoroscopic control.

Scatter Embolization

In the presence of multiple bleeding points, with or without difficult access because of anatomic variations, in a patient who is hemodynamically unstable, the radiologist is well-advised not to attempt individual arterial embolizations but to save much time and opt for scatter embolization, for which a small-particle (40 to 100 cubes, approximately 2 mm in each dimension) suspension of Gelfoam in diluted contrast medium (Fig. 5) [42] is the occluding agent of choice. Scatter embolization will usually occlude the larger branches of the internal iliac artery, usually the first two or three generations of branches, but will leave the smaller branches open to collateral blood flow. Thus immediate hemostasis is accomplished without significant ischemia.

When the bleeding artery is too large to accommodate Gelfoam, Gianturco coils [42] (Cook, Bloomington, IN) should be used instead. The vascular occlusion produced by the coil is sometimes incomplete, and the coil may then be used as matrix for deposition of Gelfoam in order to complete the hemostasis [6, 44, 45].

When the patient is extremely unstable and must go to the operating theater, or else when the injured artery is not expendable and must be repaired surgically, an occlusion balloon catheter (Medi-tech, Watertown, MA) can be introduced and the balloon inflated in the abdominal aorta or in the injured artery [6, 35].

Alcohol and phenol are destructive materials and must be avoided. Likewise, fine powders must not be used in trauma, as they disrupt circulation at the arteriolar or precapillary level and are therefore likely to cause infarction [45, 46].

Physicians are again reminded that, in treatment of hemodynamically unstable patients, time is of the essence, and therefore the simplest methods of embolization are preferable to sophisticated ones, because of the speed of their use. Unless the radiologist is certain that he or she has ample time for a more lengthy procedure, the use of coaxial systems and detachable balloons, for example, should be avoided unless the person performing the procedure is a very experienced specialist.

During the same session, the angiographer may occlude other points of hemorrhage as well. Intraabdominal and retroperitoneal bleeding, especially, should be so managed in order to avoid early laparotomy whenever possible [41, 47, 48].

Preemptive Embolization

When a branch of the internal iliac or another artery is found at angiography to be transected although not bleeding, the radiologist would be well advised to treat that artery as if it were bleeding at the time of examination and occlude it (Fig. 6). In this respect there is no difference between an angiographer occluding a transected artery during angiography and a surgeon ligating it during surgery. Avoiding preemptive embolization puts the patient at an unneeded risk of a delayed hemorrhage.

Embolization is not always the complete treatment for posttraumatic hemorrhage. Many patients with pelvic fractures may become hypothermic, and therefore coagulopathic, as well [49]. In these patients hemorrhage from the distal, unoccluded segments of the injured arteries may be resumed via retrograde collaterals and be severe enough to cause death [6]. Such rebleeding can be avoided if, during and after embolization, the patient is treated in an environment that allows rewarming and reversal of the coagulopathy.

Complications of Embolization

Unnecessary loss of functioning tissue may result from excessive embolization or from inadvertent occlusion of the wrong artery and can have rather unpleasant consequences. Overlapping embolizations, where a major artery is occluded and then the artery that supplies the only collaterals to the same area is occluded as well, are particularly dangerous; damage created by such excess can be fatal [42].

It is unknown whether a relationship exists between embolization and impotence. Given that many patients with pelvic fractures become impotent after rupture of the urethra, wide-

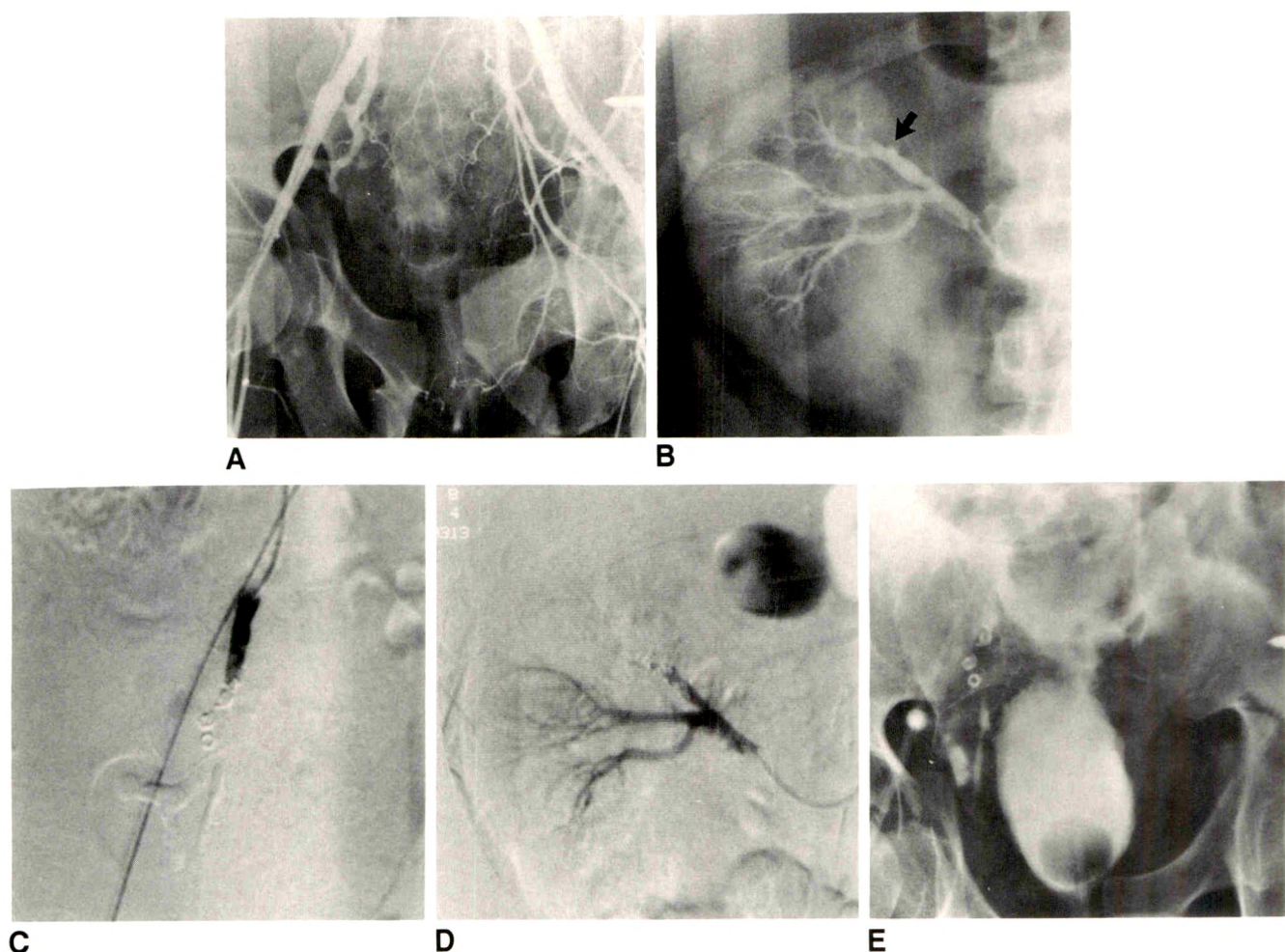


Fig. 6.—Preemptive embolization. A 33-year-old man who was crushed in a logging accident had severe injuries to pelvis and right flank, with a type III anteroposterior compression fracture consisting of fractures of all four pubic rami, extending into acetabula bilaterally and left sacrum, and dislocations of both sacroiliac joints and symphysis pubis. He had gross hematuria and was in hemorrhagic shock. Peritoneal lavage was avoided, and patient was taken directly to angiography.

A, Pelvic angiogram shows transection of all branches of right internal iliac artery except for descending arm of lateral sacral artery. There is no bleeding.

B, Selective right renal arteriogram shows transection, or dissection, and thrombosis of renal artery branches to upper pole (arrow). There is no bleeding. Findings on rest of abdominal arteriograms (not shown) were normal. Despite absence of arterial bleeding, urologist requested preemptive embolization of right renal artery branch and right internal iliac artery, to ensure that patient would not begin to bleed during surgery.

C and D, Angiograms of right internal iliac and renal arteries show successful embolization with coils. Patient became hemodynamically stable immediately after completion of embolizations. We could not explain this phenomenon, which could be due to purely favorable coincidence.

E, Retrograde cystogram obtained after completion of all angiographic work shows an intraperitoneal rupture of bladder. Patient had bladder repair and recovered uneventfully.

spread damage to the perineal veins, and lumbosacral plexus injury [50], it is impossible to ascribe impotence to embolization alone. In the series of Mucha and Farnell [3], five long-term survivors were impotent, but all five had lumbosacral plexus injuries. Irrespective of a possible causal relationship, most of us would rather have the patient alive but impotent, than dead.

REFERENCES

1. Rothenberger DA, Fischer RP, Strate RG, Velasco R, Perry JF Jr. The mortality associated with pelvic fractures. *Surgery* 1978;84:356-361
2. Gilliland MD, Ward RE, Barton RM, Miller PW, Duke JH. Factors affecting mortality in pelvic fractures. *J Trauma* 1982;22:691-693
3. Mucha P Jr, Farnell MB. Analysis of pelvic fracture management. *J Trauma* 1984;24:379-386
4. Ben-Menachem Y. Radiology. In: Moore EE, ed. *Early care of the injured patient*. Philadelphia: BC Decker, 1990:84-90
5. Ben-Menachem Y, Handel SF, Ray RD, Childs TL III. Embolization procedures in trauma: a matter of urgency. *Semin Intervent Radiol* 1985;2:107-117
6. Ben-Menachem Y, Handel SF, Ray RD, Childs TL III. Embolization procedures in trauma: the pelvis. *Semin Intervent Radiol* 1985;2:158-181
7. Panetta T, Sclafani SJA, Goldstein AS, Phillips TF, Shaftan GW. Percutaneous transcatheter embolization for massive bleeding from pelvic fractures. *J Trauma* 1985;25:1021-1029
8. Evers BM, Cryer HM, Miller FB. Pelvic fracture hemorrhage: priorities in

- management. *Arch Surg* **1989**;124:422-424
9. Sevitt S. Fatal road accidents: injuries, complications and causes of death in 250 subjects. *Br J Surg* **1968**;55:481-505
 10. Hawkins L, Pomerantz M, Wiscoan B. Laparotomy at the time of pelvic fracture. *J Trauma* **1970**;10:619-623
 11. Ben-Menachem Y. *Angiography in trauma: a work atlas*. Philadelphia: Saunders, **1981**;144-179
 12. Murr PC, Moore EE, Lipscomb R, Johnston RM. Abdominal trauma associated with pelvic fracture. *J Trauma* **1980**;20:919-923
 13. Ben-Menachem Y, Fisher RG. Radiology. In: Moore EE, Mattox KL, Feliciano DV, eds. *Trauma*, 2nd ed. Norwalk CT: Appleton & Lange, **1991**:195-218
 14. Ochsner MG Jr, Champion HR, Chambers RJ, Harviel JD. Pelvic fracture as an indicator of increased risk of thoracic aortic rupture. *J Trauma* **1989**;29:1376-1379
 15. Smith K, Ben-Menachem Y, Duke JH Jr, Hill GL. The superior gluteal artery at risk in blunt pelvic trauma. *J Trauma* **1976**;16:273-279
 16. Brumback RJ. Traumatic rupture of the superior gluteal artery, without fracture of the pelvis, causing compartment syndrome of the buttock. *J Bone Joint Surg [Am]* **1990**;72-A:134-137
 17. Dunn AW, Morris MD. Fractures and dislocations of the pelvis. *J Bone Joint Surg [Br]* **1972**;30-B:461-466
 18. Burgess AR, Eastridge BJ, Young JWR, et al. Pelvic ring disruptions: effective classification system and treatment protocols. *J Trauma* **1990**;30:848-856
 19. Young JWR, Burgess AR. Radiologic management of pelvic ring fractures. Baltimore: Urban & Schwarzenberg, **1987**
 20. Tile M. *Fractures of the pelvis and acetabulum*. Baltimore: Williams & Wilkins, **1986**
 21. Pennal GF, Tile M, Waddell JP, Garside M. Pelvic disruption: assessment and classification. *Clin Orthop* **1980**;151:12-23
 22. Young JWR, Resnik CS. Fracture of the pelvis: current concepts of classification. *AJR* **1990**;155:1169-1175
 23. Young JWR, Burgess AR, Brumback RJ, Poka A. Pelvic fractures: value of plain radiography in early assessment and management. *Radiology* **1986**;160:445-451
 24. Braunstein PW, Skudder PA, McCarroll JR, Mussolina A, Wade PA. Concealed hemorrhage due to pelvic fracture. *J Trauma* **1964**;4:832-846
 25. Huitinen VM, Slati P. Fractures of the pelvis: trauma mechanism, types of injury and principles of treatment. *Acta Chir Scand* **1972**;138:563-569
 26. Patterson FP, Morton KS. The cause of death in fractures of the pelvis. *J Trauma* **1973**;13:849-856
 27. Slati P. Injuries in fatal traffic accidents. *Acta Chir Scand (Suppl)* **1962**;297:1-15
 28. Peltier LF. Complications associated with fractures of the pelvis. *J Bone Joint Surg [Am]* **1965**;47-A:1060-1069
 29. Hubbard SG, Bivins BA, Sachatello CR, Griffen WO Jr. Diagnostic errors with peritoneal lavage in patients with pelvic fractures. *Arch Surg* **1979**;114:844-846
 30. Richardson JD, Harty J, Amin M, Flint LM. Open pelvic fractures. *J Trauma* **1982**;22:533-538
 31. Goldstein A, Phillips T, Sclafani SJA, et al. Early open reduction and internal fixation of the disrupted pelvic ring. *J Trauma* **1986**;26:325-333
 32. Cryer H, Miller FB, Evers BM, Rouben LR, Seligson DL. Pelvic fracture classification: correlation with hemorrhage. *J Trauma* **1988**;28:973-980
 33. Dalal SA, Siegel JH, Burgess AR, et al. Pelvic fractures in multiple trauma: classification by mechanism is key to pattern of organ injury, resuscitative requirements and outcome. *J Trauma* **1988**;29:981-1002
 34. Kam J, Jackson H, Ben-Menachem Y. Vascular injuries in blunt pelvic trauma. *Radiol Clin North Am* **1981**;19:171-186
 35. Ben-Menachem Y. Angiography in diagnosis of vascular trauma. In: Taveras JM, Ferrucci JT, eds. *Radiology: diagnosis, imaging, intervention*, Vol. 2, chapter 148. Philadelphia: Lippincott, **1988**:1-14
 36. Ben-Menachem Y. Logic and logistics of radiography, angiography, and angiographic intervention in massive blunt trauma. *Radiol Clin North Am* **1981**;19:9-15
 37. Gilula LA, Murphy WA, Tailor CC, Patel RB. Computed tomography of the osseous pelvis. *Radiology* **1979**;132:107-114
 38. Scott WW Jr, Fishman EK, Magid D. Acetabular fractures: optimal imaging. *Radiology* **1989**;165:537-539
 39. Yellin AE, Lundell CJ, Finck EJ. Diagnosis and control of posttraumatic pelvic hemorrhage. *Arch Surg* **1983**;118:1378-1383
 40. Stock JR, Harris WH, Athanasoulis CA. The role of diagnostic and therapeutic angiography in trauma to the pelvis. *Clin Orthop* **1980**;151:31-37
 41. Sclafani SJA. Angiographic control of intraperitoneal hemorrhage caused by injuries to the liver and spleen. *Semin Intervent Radiol* **1985**;2:139-147
 42. Ben-Menachem Y. Embolotherapy in pelvic trauma. In: Neal MP Jr, Tisnado J, Cho SR, eds. *Emergency interventional radiology*. Boston: Little, Brown, **1989**:91-106
 43. Goris RJA, Gimber JSF, van Niekerk, et al. Improved survival of multiple injured patients by early external fixation and prophylactic mechanical ventilation. *Injury* **1982**;12(1):39-47
 44. Sclafani SJA. Angiographic treatment of chronic post-traumatic arteriovenous fistulas of the extremities. *Semin Intervent Radiol* **1985**;2:125-129
 45. Ben-Menachem Y. Bleeding from trauma. In: Dondelinger RF, Rossi P, Kurdziel JC, Wallace S, eds. *Interventional radiology*. Stuttgart: Georg Thieme Verlag, **1990**:378-395
 46. Novak D. Embolization materials. In: Dondelinger RF, Rossi P, Kurdziel JC, Wallace S, eds. *Interventional radiology*. Stuttgart: Georg Thieme Verlag, **1990**:295-313
 47. Fisher RG, Ben-Menachem Y. Embolization procedures in trauma: The abdomen—extraperitoneal. *Semin Intervent Radiol* **1985**;2:148-157
 48. Hashimoto S, Hiramatsu K, Ido K, Yosii H, Motegi M, Yamamoto S. Expanding role of emergency embolization in the management of severe blunt trauma. *Cardiovas Intervent Radiol* **1990**;13:193-199
 49. Rutledge R, Sheldon GF. Bleeding and coagulation problems in trauma. In: Moore EE, Mattox KL, Feliciano DV, eds. *Trauma*, 2nd ed. Norwalk, CT: Appleton & Lange, **1991**:891-908
 50. Ellison M, Timberlake GA, Kerstein MD. Impotence following pelvic fracture. *J Trauma* **1988**;28:695-696

MR Imaging of the Labral-Capsular Complex: Normal Variations

Christian H. Neumann¹
Steve A. Petersen²
Arlon H. Jahnke²

Understanding the normal anatomy of the shoulder and its variations is important for the proper interpretation of MR images. This study was performed to describe variations in the normal labral-capsular complex as seen on MR images. MR images of 52 shoulders in 30 asymptomatic volunteers and 27 shoulders of symptomatic patients who had subsequent arthroscopy and/or reconstructive surgery were obtained with 1.5-T MR. The 52 scans of the asymptomatic group were reviewed by three radiologists in conference, and the assessment of labral shapes and capsular insertions was done by consensus. The 27 MR scans of the shoulders in the symptomatic group were reviewed by one radiologist before and after the asymptomatic cases were interpreted. Differences in these two interpretations were shown on receiver-operating-characteristic curves by using the results of subsequent arthroscopy and surgery as the gold standard. The anterior and posterior parts of the labra, respectively, varied in shape but showed several dominant features: triangular (45%, 73%), round (19%, 12%), cleaved (15%, 0%), notched (8%, 0%), flat (7%, 6%), and absent (6%, 8%). Most capsules inserted anteriorly on the labrum (47%) or glenoid rim (49%). All posterior insertions were on the labrum (100%). Intrinsic labral signal was noted on proton density-weighted images, but never on T2-weighted images. Receiver-operating-characteristic curves from interpretations of the symptomatic and clinical cases made before and after evaluation of the asymptomatic shoulders showed the interpretations improved considerably after scans of asymptomatic volunteers were studied.

Our study reveals a wide variability in the MR appearance of the labral-capsular complex in asymptomatic shoulders.

AJR 157:1015-1021, November 1991

The variability in the normal labral-capsular complex on CT arthrography has been documented [1] and is well recognized in the clinical and anatomic literature [2, 3]. Knowledge of these anatomic variations has improved the understanding and interpretation of arthroscopic and CT arthrographic examinations. Recently, several preliminary studies on the use of MR in the diagnosis of labral tears and capsular abnormalities have reported conflicting results [4-7]. In none of these studies has the normal variability of the labral-capsular complex been addressed. This may be because no systematic investigation of the appearance of normal shoulder structures on MR has been published.

The purpose of this study is to describe the variations in the MR appearance of the anterior and posterior parts of the labral-capsular complex in asymptomatic subjects in order to provide normal standards for the interpretation of MR images.

Subjects and Methods

All MR examinations were performed on a 1.5-T superconducting MR scanner (Signa, General Electric, Milwaukee, WI) operating on software versions 3.0 to 4.0. Two 5-in. (13-cm) surface coils were applied in sandwich configuration on the anterior and posterior surfaces of the shoulder and connected through a standard decoupler (Model A66GE, Wide Band

Received May 8, 1991; accepted after revision July 10, 1991.

This work was supported in part by clinical investigation grant ORTHO-8802Feb89 from Letterman Army Medical Center (principal investigator, S. A. Petersen).

¹ San Francisco Magnetic Resonance Center, 3333 California St., Suite 105, San Francisco, CA 94118. Address reprint requests to C. H. Neumann.

² Orthopaedic Surgery Service, Letterman Army Medical Center, Presidio of San Francisco, San Francisco, CA 94129.

0361-803X/91/1575-1015
©American Roentgen Ray Society

Engineering Co., Phoenix, AZ). After acquisition of a T1-weighted, large-field-of-view body-coil localizer in the coronal projection, four subsequent sequences were performed: an axial proton density-weighted multiplanar gradient-recalled acquisition in the steady state (GRASS) sequence, 300/10/4 (TR/TE/excitations), with a 90° flip angle, 256 × 192 matrix, 14-cm field of view (FOV), 4-mm slice thickness, and 0-mm skip; an axial proton density-weighted, 2000/10/2, and T2-weighted, 2000/70/2, double-echo sequence with a 256 × 192 matrix, 14-cm FOV, 4-mm slice thickness, and 1-mm skip; a modified coronal proton density-weighted, 1800/25/2, and T2-weighted, 1800/80/2, double-echo sequence with a 256 × 192 matrix, 15-cm FOV, 5-mm slice thickness, and 0.5-mm skip with rectangular pulse profile (contiguous space multi echo multi plane, CSMEMP); and a modified sagittally T1-weighted sequence, 700/10/1, with a 256 × 128 matrix, 18-cm FOV, 5-mm slice thickness, and 2-mm skip. The shoulder was kept in a neutral position with the arm along the patient's side and the thumb pointing upward or rotated slightly outward.

Images of 52 shoulders in 30 asymptomatic young, active, and healthy men and women enlisted in the Armed Forces and employees in medical services were included in the study. The 20 men and 10 women were 21–43 years old (mean, 26 years). Twenty-eight right and 24 left shoulders were scanned. In 22 volunteers, both shoulders were scanned. All volunteers were familiarized with the purpose of this study, and informed consent was obtained from all subjects.

Twenty-seven examinations had been performed in patients with clinical symptoms and surgical proof of shoulder instability. Twenty-two had arthroscopy and five had reconstructive surgery. The 22 men and five women were 17–44 years old (mean, 28 years). Thirteen left and 14 right shoulders were examined.

All scans of the shoulders in the normal volunteer group were evaluated in conference by two orthopedic surgeons and one radiologist with experience in interpretation of MR images of the shoulder. The signal intensity, shape, and size of the anterior and posterior portions of the labrum were evaluated. Descriptive terms such as triangular, round, cleaved, notched, flat, and absent were applied to the shape of the anterior and posterior sections of the labrum at their respective superior, mid, and inferior levels [1]. Size and labral signal were assessed subjectively. The anterior and posterior areas of the capsular insertion were classified into one of three categories accord-

ing to the system of Mosely and Oevergaard [2]: type 1 was a capsular insertion on the labral tip or its outer surface, type 2 was an insertion immediately medial to the labrum on the glenoid rim, and type 3 was an insertion 1 cm or more medial to the cartilaginous labral tip on the cortical surface of the glenoid neck. Anterior and posterior labral and capsular structures of the right and left shoulders were compared in the 22 volunteers in whom scans of both shoulders were obtained. Fluid in the joint and biceps tendon sheath and Hill-Sachs lesions were noted.

The 27 MR images of patients with clinically suspected glenohumeral instability and arthroscopic and/or surgical confirmation were interpreted by the radiologist who had been blinded to history and diagnosis before and after the evaluation of the 52 normal MR images. Anterior and posterior sections of the labrum were classified as normal, probably normal, equivocal, probably abnormal (torn), or abnormal (torn). Receiver-operating-characteristic (ROC) curves for the first and second interpretations of labral structures were calculated to determine the improvement in interpretation gained by the study of normal images.

Results

On the 52 MR images of the shoulder in the asymptomatic volunteers, considerable variability of the morphology of the anterior and posterior sections of the glenoid labrum was noted, with several common variants dominating. The most common labral shape was triangular, found anteriorly in 45% and posteriorly in 73% (Fig. 1). The second most common shape was rounded, found anteriorly in 19% and posteriorly in 12% (Fig. 2). The cleaved and notched patterns were found anteriorly only in 15% and 8%, respectively (Figs. 3 and 4). A flat labrum was noted anteriorly in 7% and posteriorly in 6%, and absence of labrum was seen in 6% anteriorly and 8% posteriorly (Figs. 5 and 6). The assessment of the labra at their superior, mid, and inferior thirds individually revealed similar variability (Table 1). No dominant trend in labral shape was found when the left and right shoulders were correlated

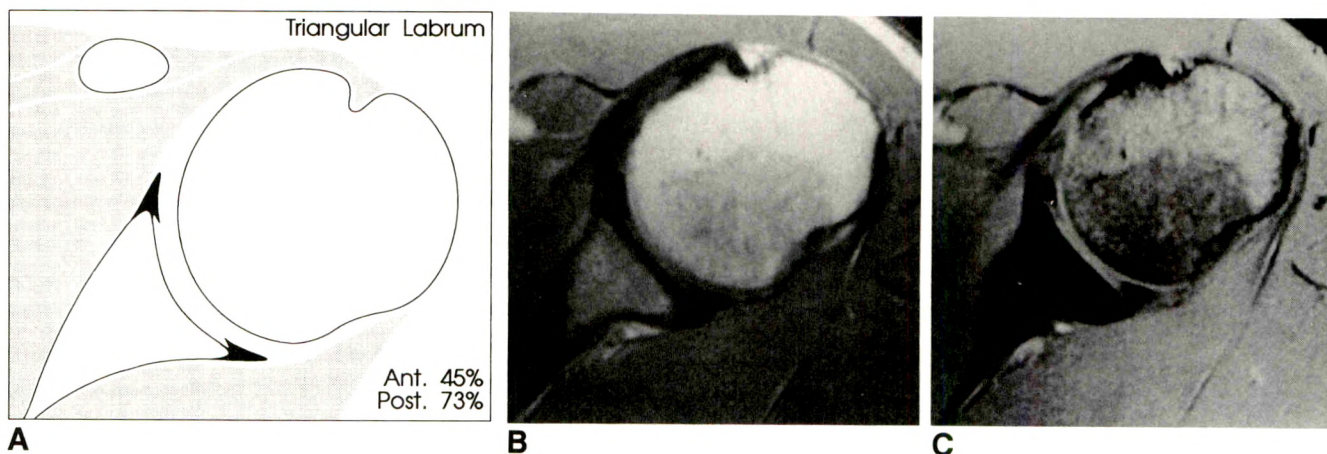
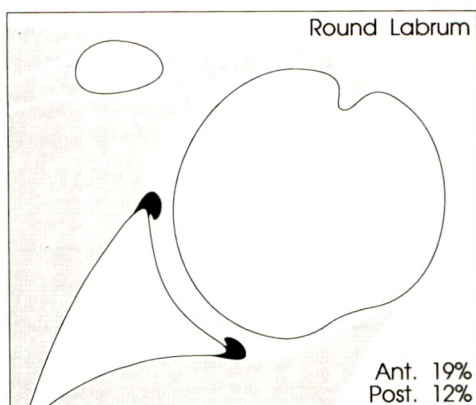


Fig. 1.—Triangular labrum. This labral shape was most common and was encountered anteriorly (Ant.) in 45% and posteriorly (Post.) in 73%.
 A, Artist's depiction of triangular labral shape, anteriorly and posteriorly.
 B, Axial T1-weighted MR image through mid glenoid level shows a triangular labrum anteriorly and posteriorly of homogeneous low signal intensity.
 C, Multiplanar GRASS image through mid glenoid level shows same triangular, sharply defined labrum with diffuse inhomogeneous low signal intensity. Thin band of higher signal on surface of humeral head and opposing surface of glenoid fossa represents hyaline cartilage, which in part extends underneath anterior and posterior portions of labrum.

Fig. 2.—Round labrum. This labral shape was encountered anteriorly (Ant.) in 19% and posteriorly (Post.) in 12%.

A, Artist's depiction of anteriorly and posteriorly round labrum.

B, Axial multiplanar GRASS MR image through mid glenoid fossa shows round labrum posteriorly and triangular labrum anteriorly.



A

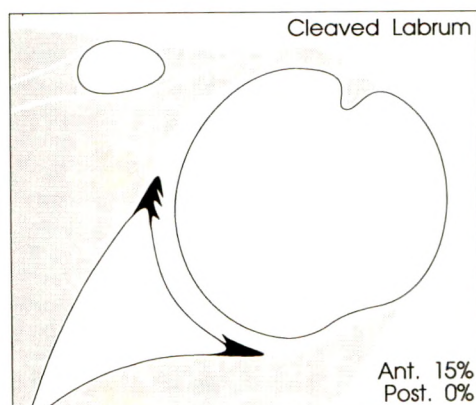


B

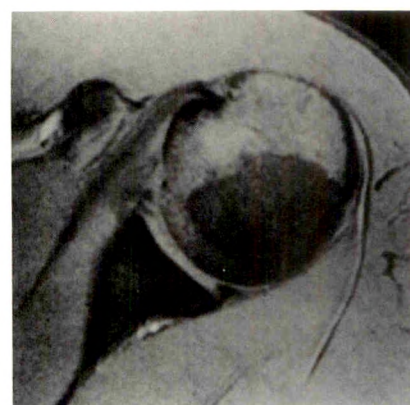
Fig. 3.—Clefted labrum. Cleft in anterior (Ant.) portion of labrum was seen in 15%. This labral type was never found posteriorly (Post.).

A, Artist's depiction of several clefts in surface of anterior portion of labrum. A single cleft is most common. A double cleft may be encountered as well. At no time was cleft found to extend through entire thickness of labrum.

B, Axial multiplanar GRASS MR image through mid glenoid fossa shows cleft extending from central surface of anterior portion of labrum deep into its substance. Higher signal on multiplanar GRASS image highlights cleft against lower signal of fibrous connective tissue of anterior labrum. It has an appearance similar to adjacent hyaline cartilage lining glenoid fossa and humeral head.



A

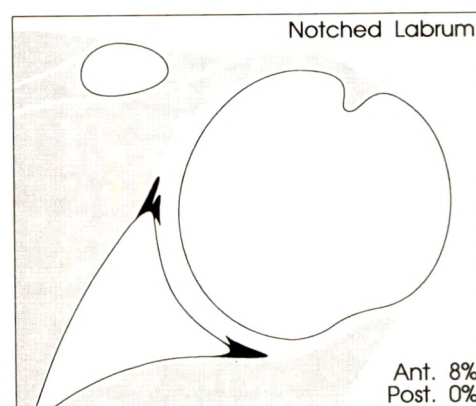


B

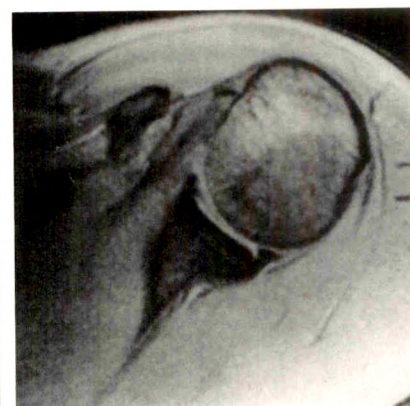
Fig. 4.—Notched labrum. This pattern was encountered only anteriorly (Ant.), in 8%. Post. = posteriorly.

A, Artist's depiction of notch in anterior part of labrum. Notch differs from cleft in its orientation, extending into labrum in a more vertical fashion than cleft, which is oriented horizontally.

B, Axial multiplanar GRASS MR image through mid glenoid fossa shows notch in anterior part of labrum.



A



B

in those 22 volunteers in whom both shoulders were scanned. Considering the superior, mid, and inferior glenoid levels individually, 45% (30 of 66 interpretations) had the same labral shape anteriorly. In the remaining 55% (36/66), different labral shapes were found in the right and left shoulders. Posteriorly, 65% (43/66) matched and 35% (23/66) differed.

If one considers the three sets of multiplanar GRASS, proton density-weighted, and more heavily T2-weighted im-

ages, some variation in the intrinsic labral signal was observed. Homogeneous signal void on multiplanar GRASS, proton density-weighted, and T2-weighted images was the dominant feature anteriorly in 39 of 52 and posteriorly in 52 of 52 shoulders (Fig. 1). Focally increased signal was seen on multiplanar GRASS and proton density-weighted images in only 13 cases anteriorly (Fig. 7). Increased labral signal was never seen on T2-weighted images. Thirty anterior and 18

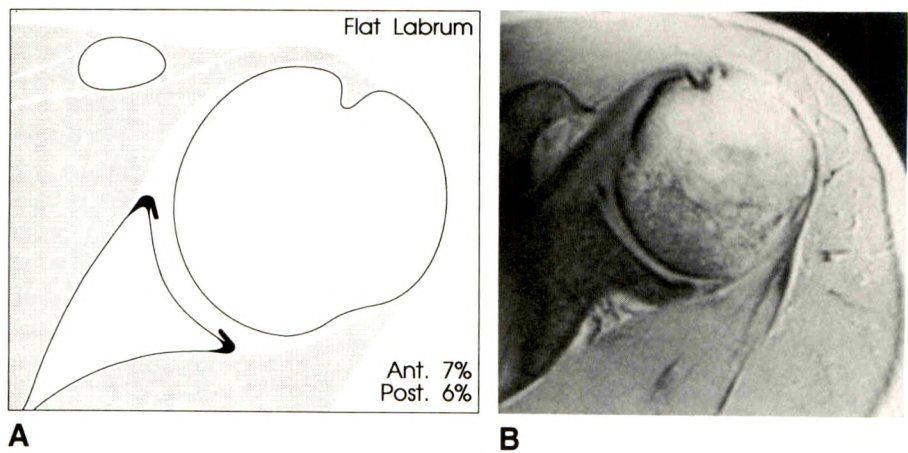


Fig. 5.—Flat labrum. A flat labrum was found anteriorly (Ant.) in 7% and posteriorly (Post.) in 6%.
A, Artist's depiction of flat labrum anteriorly and posteriorly.
B, Axial multiplanar GRASS MR image through mid glenoid fossa shows flat labrum anteriorly and posteriorly. Anteriorly, hyaline cartilage of glenoid fossa is seen extending underneath labrum, whereas posteriorly, labrum is difficult to differentiate from adjacent subcartilaginous cortex of posterior glenoid rim.

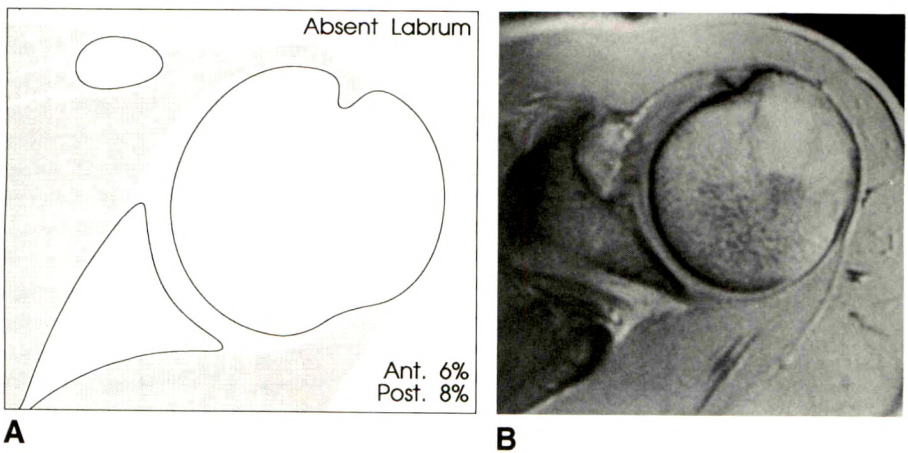


Fig. 6.—Absent labrum. Absence of labrum was encountered anteriorly (Ant.) in 6% and posteriorly (Post.) in 8%.
A, Artist's depiction of glenoid rim without visible labrum.
B, Axial multiplanar GRASS MR image through upper third of glenoid fossa. Posteriorly, capsule appears to attach in normal fashion on posterior glenoid rim without evidence of a discernible glenoid labrum. Anteriorly, an irregular structure is seen that represents attachment site of middle glenohumeral ligament on a small superior anterior labrum.

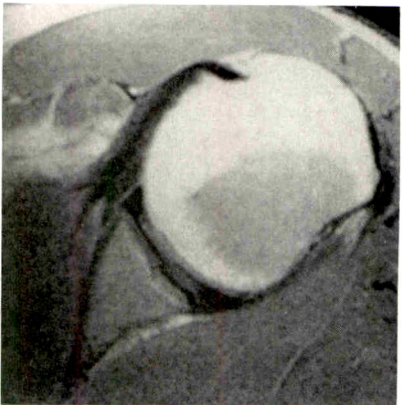


Fig. 7.—Increased intralabral signal. Axial proton density-weighted image through mid glenoid fossa shows faintly increased signal in substance of anterior part of labrum. This could not be confirmed on T2-weighted image, which showed homogeneously low signal. Finding is presumed similar to changes encountered in menisci of knee, most likely representing some degree of intrasubstance degeneration or increased water content.

TABLE 1: Variability in Anterior and Posterior Labral Shapes in 52 Asymptomatic Shoulders at Inferior, Mid, and Superior Glenoid Levels

Shape	Anterior Part of Labrum (%)			Posterior Part of Labrum (%)		
	Inferior	Mid	Superior	Inferior	Mid	Superior
Triangular	24 (46)	21 (40)	25 (49)	42 (81)	42 (81)	30 (58)
Rounded	8 (15)	4 (8)	17 (32)	7 (13)	7 (13)	5 (10)
Cleaved	9 (17)	13 (25)	2 (4)	0	0	0
Notched	7 (13)	6 (11)	0	0	0	0
Flat	2 (4)	6 (11)	3 (6)	3 (6)	3 (6)	4 (8)
Absent	2 (4)	2 (4)	5 (9)	0	0	13 (25)

posterior labral sections were considered unusually small. This was observed most often anterosuperiorly, in 13% (20/156). Extraordinarily large labra were found three times, two anteriorly and one posteriorly. All labra appeared otherwise

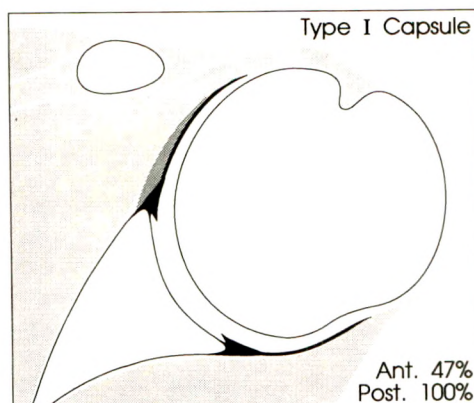
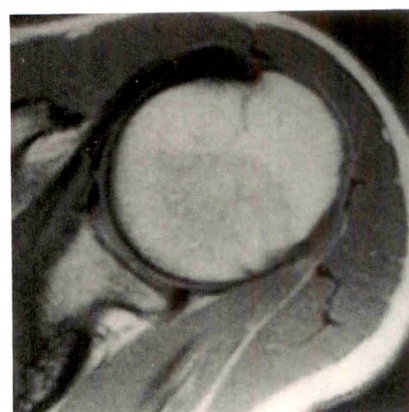
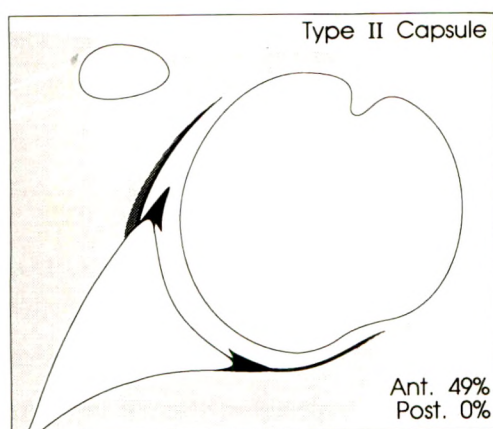
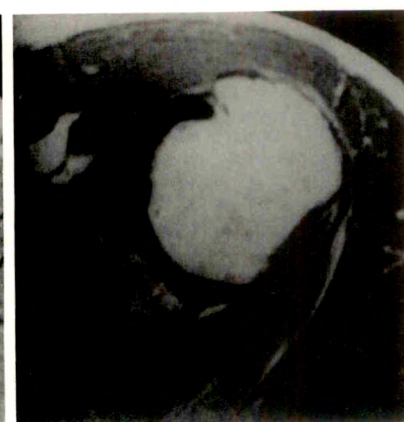
to have a smooth surface without fragmentation or displacement from the glenoid rim.

The capsular insertion classification of Mosely and Oevergaard [2] could be applied satisfactorily to all shoulders

Fig. 8.—Type 1 capsular insertion.

A, Artist's depiction of type 1 capsule anteriorly and posteriorly. Type 1 anterior capsular insertion is characterized by insertion of capsule on tip or outer surface of glenoid labrum. This was encountered anteriorly (Ant.) in 47% and posteriorly (Post.) in 100%. Shaded area on outer surface of anterior part of glenoid labrum shows variability of insertion encountered within type 1.

B, Axial proton density-weighted image through upper third of glenoid fossa shows a type 1 capsular insertion anteriorly and posteriorly on tip of labrum.

**A****B****A****B****C****Fig. 9.—Type 2 capsular insertion.** This type of capsular insertion was found anteriorly (Ant.) in 49%, but never posteriorly (Post.).

A, Artist's depiction of a type 2 anterior capsular insertion. A type 2 capsule should not insert more than 1 cm medially, as measured from tip of glenoid labrum. Shaded area adjacent to anterior part of capsule marks potential variability.

B, Axial multiplanar GRASS MR image through lower third of glenoid fossa shows slightly thickened type 2 capsule anteriorly inserting on anterior part of glenoid cortex just medial to anterior portion of labrum.

C, Axial proton density-weighted MR image at same level as **B**.

scanned. Considerable variability in capsular insertion was found anteriorly, with type 1 being present in 47%, type 2 in 49%, and type 3 in 4% of 156 interpretations at the three individual glenoid levels (Figs. 8–10). The variability at the mid, superior, and inferior glenoid levels individually is shown in Table 2. As in the appearance of the labra, no useful trend was found when correlating the anterior capsules of the 22 individuals with right and left shoulder scans, except at the superior level, which was predominantly of type 1 (Table 2). In the 66 interpretations at the three glenoid levels, the same attachment type was present in 73% (48/66) overall and 59% (13/22) at the inferior, 64% (14/22) at the mid, and 95% (21/22) at the superior levels. All posterior capsular insertions were of type 1 (Fig. 8).

The humeral head had a consistent configuration in all shoulders, being slightly flattened posteroinferiorly and otherwise in all aspects round, particularly posterosuperiorly. No Hill-Sachs lesions were observed. A small amount of joint fluid was noted occasionally (3/52). In 17% (9/52) of these

asymptomatic shoulders, however, isolated fluid was seen in the biceps tendon sheath.

The ROC curves of the two blinded interpretations of the 27 clinical cases before and after analysis of these normal volunteers are given in Figure 11. They show improved true-negative and true-positive fractions at all sensitivity levels at the time of the second interpretation.

Discussion

Awareness of the normal appearance and variations of the labral-capsular complex is an important prerequisite to meaningful interpretation of single- and double-contrast arthrography or CT arthrography in patients with clinically suspected instability. Our study provides an overview of patterns of capsular insertion, labral shape, and labral signal seen on MR in asymptomatic subjects. It confirms the variability previously documented by other techniques [1–3], but delineates the

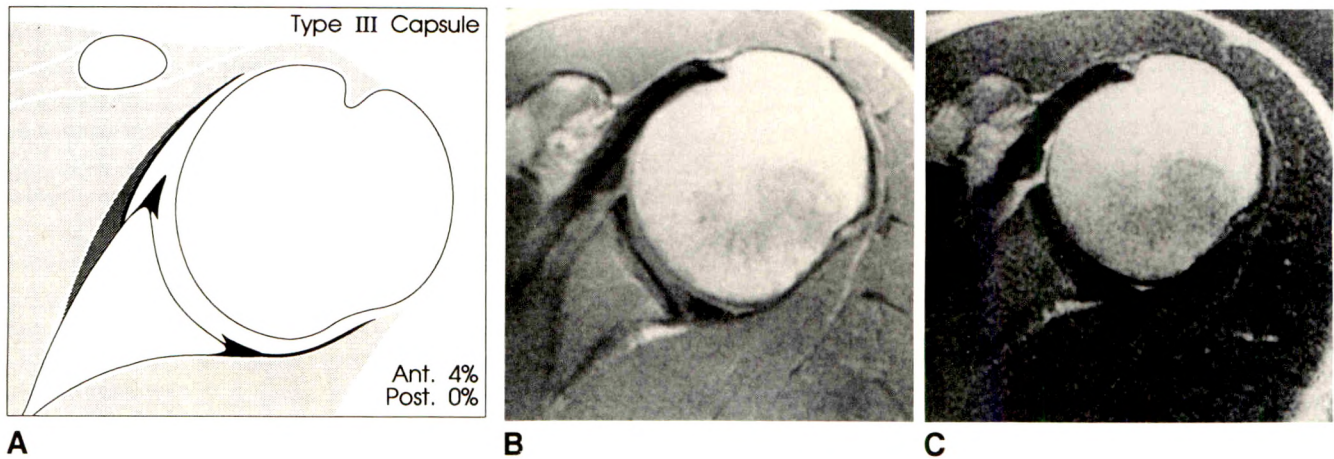


Fig. 10.—Type 3 capsular insertion found in 4% of labrum anteriorly (Ant.) and never posteriorly (Post.).
A, Artist's depiction of a type 3 anterior capsular insertion, characterized as an insertion of capsule more than 1 cm medial to tip of glenoid labrum. Type 3 capsular insertion can be quite variable, as shown by shaded area.
B, Axial proton density-weighted MR image through mid glenoid fossa shows intermediate signal intensity between middle glenohumeral ligament and anterior part of labrum extending along anterior surface of glenoid. Capsule is not clearly seen, unlike posterior portion of type 1 capsule.
C, Axial T2-weighted MR image at same level (second echo of same sequence) shows fluid separating anterior part of labrum from middle glenohumeral ligament and tracking along anterior surface of glenoid farther than 1 cm distal to tip of labrum. Although capsule is not clearly identified as low-signal-intensity band, as in other cases, high signal intensity of joint fluid allows appropriate diagnosis. This volunteer had possible shoulder trauma during adolescence. Possibility of a type 3 insertion representing, in this case, posttraumatic change without clinical symptoms or instability cannot be excluded.

TABLE 2: Variability in Capsular Attachment in 52 Shoulders at the Inferior, Mid, and Superior Levels of the Glenoid Cavity

Type of Insertion	Anterior Part of Glenoid (%)			Posterior Part of Glenoid (All Levels) (%)
	Inferior	Mid	Superior	
1	17 (33)	6 (12)	50 (96)	52 (100)
2	33 (63)	42 (80)	2 (4)	0
3	2 (4)	4 (8)	0	0

Note.—Type 1 = capsular insertion on labral tip or its outer surface; type 2 = insertion immediately medial to labrum on glenoid rim; type 3 = insertion 1 cm or more medial to cartilaginous labral tip on cortical surface of glenoid neck.

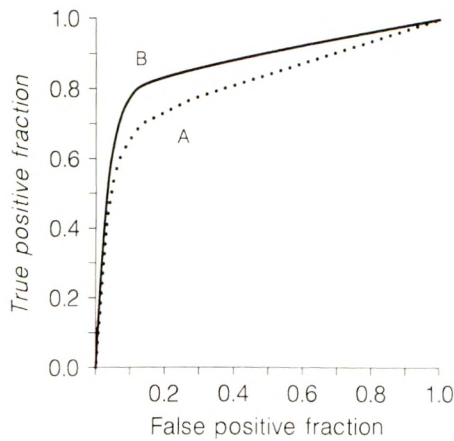


Fig. 11.—Receiver-operating-characteristic curves of two blinded interpretations in 27 patients with clinically suspected or diagnosed shoulder instability. After MR imaging, all patients had arthroscopy or arthrotomy, results of which served as a gold standard. Curve A represents first blinded reading of one radiologist. Curve B represents second blinded reading of same radiologist after studying MR images of volunteers. Second reading shows improved diagnostic results at all sensitivity levels, suggesting radiologist learned from images of normal shoulders.

specific appearance and signal patterns on MR and documents several dominant trends.

The attachment of the posterior part of the capsule was most consistent and was always type 1 on the tip or outer surface of the labrum, suggesting that deviation from this pattern may well indicate capsular stripping (Fig. 8). Anteriorly, a type 1 attachment was most commonly seen superiorly and a type 2 attachment, in the mid and lower thirds of the glenoid rim. A type 3 capsule was uncommon. It was seen only at mid and inferior levels and in 4% of all interpretations when individual levels were combined and in 8% (4/52) of all shoulders (Fig. 10). This may support observations previously published that a type 3 capsule in symptomatic and asymptomatic persons is the result of prior injury, implying stripping [2–8].

Anteriorly, labral variability was the rule. The most common labral shape was triangular (Fig. 1). Rounded labra were not rare, but were more common superiorly (Fig. 2). Cleaved and notched labra, when present, were more often seen in the mid and lower thirds (Figs. 3 and 4). The flat configuration of the labrum was more commonly seen at mid and superior levels (Fig. 5). Occasionally, no labrum was found at all. This was more common superiorly; however, in one volunteer, no labrum was found in the mid and lower thirds of both shoulders.

The morphology and shape of the labra were more consistent posteriorly. The triangular labral shape was dominant by far (Fig. 1). Relatively few labra were rounded or flat (Figs. 2 and 5). Total absence of the superior third of the posterior part of the labrum was not uncommon (25%), whereas absence was not seen in the mid and inferior thirds (Fig. 6). Importantly, the common normal cleaved and notched shapes of the anterior part of the labrum were not observed posteriorly.

Great care was taken in the selection of the volunteers to ascertain that only truly asymptomatic persons were included in this study. This was important, as proof for the findings described could not be provided through a gold standard such as arthroscopy or surgery. Nevertheless, some of our volunteers were questioned again about potential prior trauma to the shoulder because of an unusual pattern found that had been associated with abnormality by other authors, in particular, labral absence and type 3 capsular insertion [2] (McCauley R et al., presented at the annual meeting of the Radiologic Society of North America, November 1990). A type 3 insertion was found in both shoulders in one volunteer (Fig. 10). In this case, remote trauma from high school football could not be excluded. Nevertheless, no symptoms or dysfunction were remembered for at least the last 15 years. Another volunteer with bilaterally absent labra anteriorly at mid and inferior levels gave a similar history on second questioning. Therefore, it cannot be excluded that labral absence anteriorly and type 3 capsular insertion anteriorly in these volunteers were the result of an old dislocation or subluxation injury that did not lead to chronic instability or symptoms.

We were not able to confirm the belief that examining the contralateral shoulder is useful in patients in whom equivocal findings are encountered on the initial scan. Matching of capsular patterns was found only posteriorly and anterosuperiorly, owing to the fact that a type 1 capsule was the exclusive finding posteriorly and the nearly exclusive finding anterosuperiorly. Otherwise, no intersoulder matching of capsular insertion or labral shape was encountered. This may, however, not apply to pathologic patterns not considered in this study.

Hill-Sachs lesions were never found and should remain a strong indirect sign for instability with preceding dislocation. A small to moderate amount of fluid in the joint or biceps tendon sheath is a normal variant and does not predict biceps tendon abnormality.

The difference in ROC curves indicates that considerable learning occurred between the first and second interpretations of MR images in the 27 patients with clinical symptoms of instability, improving the diagnostic ability of one interpreter in the evaluation of shoulders with suspected labral abnormality (Fig. 11). The improvement was observed at all five sensitivity levels. These pathologic cases are the subject of a prospective comparison study between MR images and CT arthrography, and the initial encouraging results with MR have been reported elsewhere [9].

The young age of the volunteer group may have introduced a bias. Owing to the normal aging process, different patterns not necessarily associated with instability may prevail in an

older population. This subject deserves further attention. However, shoulder instability is a disease of the young and active. The results of this study, therefore, will apply to most patients who are imaged for instability.

In summary, considerable normal variability in the anterior and posterior portions of the labrum was confirmed. Its MR appearance was described and common patterns recognized, with a rounded and flat pattern being less common than a triangular pattern. The cleaved and notched patterns are common normal variants anteriorly, but should raise the suspicion of a tear when encountered posteriorly. Posterosuperior labral absence can be considered a common normal variant. At no time was detachment, displacement, or fragmentation seen. Anterior type 3 capsular attachment is uncommon and suggests prior injury and instability. At the posterior part of the capsule, type 2 and 3 patterns were never found, indicating a high likelihood of this being an abnormal finding when encountered in the interpretation of clinical cases.

ACKNOWLEDGMENTS

We thank the technical staff of the San Francisco Magnetic Resonance Center and the Orthopaedic Surgery Service at Letterman Army Medical Center for providing the technical and administrative support that made this study possible. We also thank Kara Reynolds for manuscript preparation and Gill Gardner for artwork.

REFERENCES

- McNiesh LM, Callaghan JJ. CT arthrography of the shoulder: variations of the glenoid labrum. *AJR* 1987;149:963-966
- Mosely HF, Oevergaard P. The anterior capsular mechanism: recurrent anterior dislocation of the shoulder. *J Bone Joint Surg [Br]* 1962;44-B: 913-927
- Detrisak DA, Johnson LL. *Arthroscopic shoulder anatomy: pathologic and surgical implications*, 1st ed. Thorofare, NJ: Slack, 1986:35-90
- Gross ML, Seeger LL, Smith JB, Mandelbaum BR, Finerman EAM. Magnetic resonance imaging of the glenoid labrum. *Am J Sports Med* 1990;18:229-234
- Kieft GJ, Gloem JL, Rozing PM, Obermann WR. MR imaging of recurrent anterior dislocation of the shoulder: comparison with CT arthrography. *AJR* 1988;150:1083-1087
- Legan JM, Burkhard ThK, Gott WB II, et al. Tears of the glenoid labrum: MR imaging of 88 arthroscopically confirmed cases. *Radiology* 1991;179:241-246
- Garneau RA, Renfrew DL, Moore TE, El-Khoury GY, Nepola JV, Lemke JH. Glenoid labrum: evaluation with MR imaging. *Radiology* 1991;179: 519-522
- Rafii M, Firooznia H, Golimbu C, Minkoff J, Bonamo J. CT arthrography of capsular structures of the shoulder. *AJR* 1986;146:361-367
- Neumann CH, Petersen SA, Jahnke AH, et al. MRI in the evaluation of patients with suspected instability of the shoulder joint including a comparison with CT-arthrography. *ROFO* 1991;154:593-600

Book Review

Creative Medical Teaching. By Neal Whitman. Salt Lake City: University of Utah School of Medicine, 235 pp., 1990. \$24

It is most refreshing to open a book, especially a medical book, and find the author's explicit instructions to not read the book from cover to cover. In fact, the main point of *Creative Medical Teaching* is acquired simply by understanding the methodology of the book itself. The intention of this terse volume is to exemplify and demonstrate that effective medical teaching involves innovation, surprise, and originality. The author is obviously an excited teacher and has engineered this method of communicating his joy in education.

The book is divided into short sections with highlighted words in each section that refer the reader to other sections. The sections are alphabetized to make them easy to find and find again. The terseness of each section reflects the importance of limited attention span in effective teaching. The reader is encouraged to jump from section to section only when and if interested in doing so. The various sections thus lead the reader through a wide variety of pearls, which are accompanied by a wide variety of rhinestones, a few pebbles, and even fewer rubies and diamonds. A reader might well pick up the book, read a few random sections until he or she finds something of true usefulness, and then toss the book aside for another hour, day, or week.

Some of the more cogent points for me include the section in which the author stresses that a distinct difference exists between

teaching children and teaching adults. It is obvious that a postgraduate course is taught on an adult level, with the total avoidance of pedantry. Such avoidance is less efficacious with medical students because some talking down might be necessary, and must be individualized even with residents. Another section that piqued my interest discusses the avoidance of stress in medical teaching and the need to create a professional intimacy (with feelings of empathy) with students. I am certain that many of the sections that I found repetitive, self-evident, or otherwise useless might be of particular interest to other readers. Certainly useful tidbits for every teacher can be found on these pages.

This book ought to be available in the reference section of departmental libraries, even though it is not truly a reference work. As the author clearly intends, it is a book to pick up and browse through, and possibly to reread, when sudden inspiration or recollection is useful. Those who teach a lot, get too little feedback, and tend toward frequent discouragement might find the purchase of *Creative Medical Teaching* quite worthwhile.

David S. Feigin
University of California, San Diego
La Jolla, CA 92093

Dialysis-Related Amyloid Arthropathy: MR Findings in Four Patients

Mark J. Cobby¹
 Ronald S. Adler¹
 Richard Swartz²
 William Martel¹

Dialysis-related amyloidosis is a recently recognized complication of long-term hemodialysis. It is caused by the deposition of a unique form of amyloid derived from circulating β_2 -microglobulin. This study describes the MR imaging characteristics in five articular sites of four symptomatic patients with biopsy-proved (three patients) or clinically and radiographically suspected (one patient) dialysis-related amyloidosis. Three wrists, one knee, and one cervical spine were examined. The extent of osseous and soft-tissue involvement at each joint site was well shown by MR imaging. Lesions that were apparently intraosseous on conventional radiographs were shown to be caused by well-defined erosions that extended to the articular surface. The MR signal characteristics of the amyloid deposition were intermediate between those of fibrocartilage and muscle on all sequences, distinguishing the deposition from cellular lesions or those containing large amounts of water, such as inflammatory masses, acute or chronic synovitis, and brown tumors of hyperparathyroidism. The intraarticular masses were associated with a moderate joint effusion in the large joint imaged, and small effusions were present in the wrist. Use of a fat-suppression sequence enhanced visualization of amyloid deposits within the wrist of one patient but provided no additional information in the knee of a second patient.

Our experience suggests that MR imaging is well suited to showing the extent and distribution of articular disease in dialysis-related amyloidosis.

AJR 157:1023-1027, November 1991

Dialysis-related arthropathy is a severe and often disabling complication of long-term maintenance hemodialysis unrelated to crystal deposition or renal osteodystrophy [1, 2]. The full extent of this disease is only just beginning to be realized. Clinically, it manifests as a symmetric progressive polyarthropathy, with pain and stiffness that usually involves the shoulders first and subsequently the wrists, knees, hips, and other large joints. Symptoms are often exacerbated during dialysis. The onset of the arthropathy is frequently preceded by carpal tunnel syndrome and tenosynovitis. Joint effusions, recurrent hemarthrosis, and a destructive spondyloarthropathy also may occur [1-3]. The prevalence of this condition is related to the duration of treatment and to the use of cuprophane dialysis membranes. It is seldom seen before the patient has had 5 years of hemodialysis, but after 10 years, up to 80% of patients may be affected [2]. Currently, it is uncertain whether dialysis-related arthropathy is a single entity or represents a number of disease processes. It is increasingly apparent, however, that many of the findings are associated with the intraosseous, articular, and periarticular accumulation of a unique form of amyloid derived from circulating β_2 -microglobulin [4-6].

This study describes the MR imaging characteristics of dialysis-related amyloidosis in five articular sites of four patients.

Subjects and Methods

Our study group comprised two men and two women 34-66 years old (mean age, 52 years) who have been monitored at the University of Michigan throughout their courses of

Received June 3, 1991; accepted after revision July 10, 1991.

¹ Department of Radiology, University of Michigan Medical Center, 1500 E. Medical Center Dr., Ann Arbor, MI 48109-0030. Address reprint requests to R. Adler.

² Department of Internal Medicine (Nephrology Division), University of Michigan Medical Center, Ann Arbor, MI 48109-0030.

0361-803X/91/1575-1023
 © American Roentgen Ray Society

hemodialysis. Three of the patients were studied prospectively. A fourth patient was included in whom amyloid spondyloarthropathy had been documented previously. The mean duration of hemodialysis was 15 years (range, 12–18). Cuprophane dialysis membranes were used throughout. Renal insufficiency was caused by congenital renal hypoplasia in two patients and associated with hypertension and abuse of analgesics in one patient each. All patients had clinical and radiologic findings compatible with amyloidosis. A symmetric polyarthropathy, involving at least the shoulders and wrists, was present in all patients. Three patients had bilateral carpal tunnel syndrome, and two had recurrent joint effusions of the knee. On the basis of hand radiographs and review of the medical charts, there was no current radiologic or biochemical evidence of active secondary hyperparathyroidism.

Conventional radiographs were reviewed by three radiologists; these showed numerous subarticular cystic radiolucencies at various joint sites in four patients and an erosive spondyloarthropathy of the cervical (C5–C6 level) and thoracic (T7–T8 level) spine in one of these. In one patient, a pathologic fracture of the hip occurred through scalloped cystic erosions of the femoral neck.

Histologic confirmation of amyloid deposition was available in three patients: after carpal tunnel release in two (one patient also had amyloid deposition confirmed in the hip after a total hip replacement for pathologic fracture) and from an open biopsy of a cervical vertebral body in one (reported previously [7]).

MR studies of three wrists, one knee, and one cervical spine were performed with conventional spin-echo (SE) techniques. Fat-suppression sequences (Dixon sequence [8, 9]) were obtained for one wrist and the knee. Examinations of the cervical spine and knee were performed on a 1.5-T Signa unit (General Electric) and examinations of the wrist on a 0.5-T Picker unit. All examinations were performed

in standard axial, sagittal, and coronal planes, emphasizing T1 and T2 contrast; technical factors such as field of view (FOV), matrix size, number of signal averages, and TR and TE values varied depending on specific anatomy and the MR imager used. Wrist imaging was typically performed by using a 12-cm FOV, 192 matrix, and two excitations. T1 and T2 contrast were provided by SE 500/20 (TR/TE) and SE 2000/40,80 pulse sequences, respectively. Imaging parameters for the cervical spine and knee cases included T1-weighted (600/20) and T2-weighted (2250–2500/25,80) SE sequences with a 128 (spine) or 256 (knee) matrix, two or four excitations, and a 24-cm (spine) or 16-cm (knee) FOV. Biochemical, biopsy, and clinical data pertaining to these patients were obtained from review of the medical charts and from the nephrologist.

Results

MR of the three wrists showed extensive deposition of abnormal soft tissue within the carpal canal, surrounding and displacing the flexor tendons, that remained low to intermediate in signal intensity on all pulse sequences. Less marked involvement of the extensor tendons and around the radial styloid process was present in two wrists. Synovial deposition of similar-appearing abnormal soft tissue within the wrist resulted in widening of the distal radioulnar joint and obliteration of the triangular fibrocartilage in two patients. Some degree of dissociation of the scaphoid and lunate bones was shown in all three wrists (Figs. 1 and 2). A slight excess of joint fluid, apparent as thin crescents of high signal intensity on T2-weighted imaging, was present within each wrist. Nu-

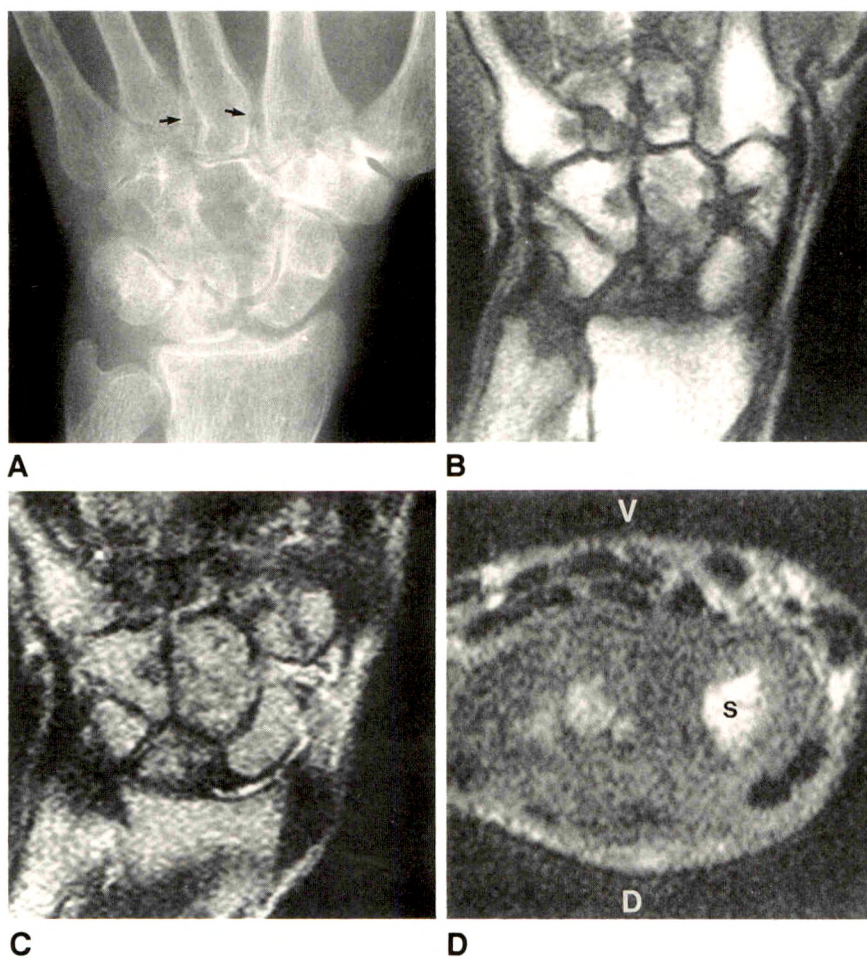


Fig. 1.—Right wrist. Biopsy-confirmed amyloid deposition.

A, Conventional radiograph shows numerous radiolucent lesions of various sizes involving carpal bones. Most have sclerotic margins and some have a lobulated outline. Erosions of intermetacarpal joints (arrows) and ulnar styloid are shown also. Scapholunate interosseous distance is widened. Other joint spaces are preserved or slightly widened.

B, Coronal T1-weighted MR image (SE 500/20) shows numerous erosions involving carpal bones, intermetacarpal joints, and distal ulna. Triangular fibrocartilage complex is destroyed, and lunate bone is almost completely replaced by abnormal material that has an intermediate signal intensity.

C, Corresponding T2-weighted MR image (SE 2000/80) shows that many of the erosions seen in **B** also have a low to intermediate signal intensity on T2-weighted image. Larger lesions, such as those in capitate bone, are isointense relative to surrounding marrow signal. A slight excess of joint fluid is evident.

D, Axial T1-weighted MR image (SE 500/20) through proximal carpal row shows mass with abnormal intermediate signal intensity surrounding carpal bones, displacing flexor and extensor tendons, and occupying expected location of lunate. V = volar surface, S = scaphoid bone, D = dorsal surface.

merous osseous erosions were shown involving all compartments of the wrist (two patients), the distal radioulnar joint (one patient), and the proximal intermetacarpal joints (one patient, Fig. 1). Erosions occurred most commonly on the volar or interosseous aspects of the carpus, but were also seen on the dorsal aspect in the most severely involved wrist. A number of lesions that appeared to be intraosseous on conventional radiographs were shown to be contiguous with articular surfaces (Fig. 2). The abnormal tissue showed a low to intermediate signal intensity on all pulse sequences, except for a larger lesion in the capitate of one wrist that had a signal intensity on the T2-weighted images equivalent to that of marrow. The fat-suppression sequence obtained in one patient was useful in distinguishing a lesion within the lunate bone, which was obscured on the T2-weighted images, by suppressing the marrow signal.

MR of the knee showed a moderate-sized joint effusion with large nodular masses of abnormal tissue arising from the synovium and associated with extensive osseous erosions of the tibial articular surface, the femur, and the dorsal aspect of the patella. On proton density-weighted images, the abnormal tissue had a slightly heterogeneous low signal intensity, similar to that of muscle, which in places was arranged in a whorl pattern. On T1-weighted images, the abnormal tissue had a signal intensity slightly lower than that of muscle and was more homogeneous. On T2-weighted images, the abnormal tissue had a low signal intensity, contrasting clearly with surrounding high-signal intensity joint fluid (Fig. 3). Most of the articular erosions were filled by low-signal-intensity material, although one tibial erosion contained fluid with a signal intensity matching that of the joint effusion. No additional information was provided by the fat-suppression sequence.

The MR images of the cervical spine showed a slight retrolisthesis of C5 on C6, decreased signal intensity on the T1-weighted images of the C5–C6 vertebral bodies, and destruction of the adjacent endplates. Abnormal soft tissue anterior and posterior to the thecal sac resulted in some compression of the spinal cord at the level of C5. On the T2-weighted images, the C5 and C6 intervertebral region had a

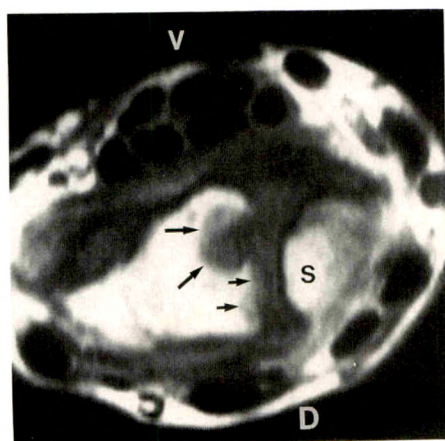


Fig. 2.—Right wrist. Axial T1-weighted MR image (SE 500/20) of wrist through proximal carpal row shows large erosion of lunate bone (*long arrows*). On conventional radiograph, this appeared to be an entirely intraosseous lesion. Abnormal material with intermediate signal intensity extends from erosion, fills widened scapholunate articulation, and displaces flexor tendons. Interosseous cortical surface of lunate bone is also eroded (*short arrows*). V = volar surface, S = scaphoid bone, D = dorsal surface.

signal intensity similar to that of adjacent vertebral bodies (Fig. 4).

Discussion

Conventional radiography in dialysis-related arthropathy shows a number of characteristic appearances that are similar to those of immunoglobulin-associated amyloidosis [5, 10–12]. Well-defined subarticular radiolucent lesions, usually with thin sclerotic margins, are shown in association with soft-tissue masses. These frequently involve the carpal bones (Fig. 1A), the acetabulum, the subcapital region of the femur, and the shoulder. Lesions of the femoral neck are associated with a high prevalence of pathologic fracture, as occurred in one patient in this series. The number and size of the lesions usually increase with the duration of dialysis. The joint space is preserved until late in the course of the disease. Bony expansion, internal mineralization, and periosteal reactions do not occur [10]. CT may provide additional information about the extent and location of involvement but does not always detect a soft-tissue component [10–12].

In the axial skeleton, a rapidly progressive destructive spondyloarthropathy, commonly involving the cervical spine, may simulate infectious diskitis [3, 13]. Characteristic findings on radiographs include progressive narrowing of the disk space; extensive, poorly defined end-plate erosions; and modest subchondral sclerosis that may progress rapidly over a period of months (Fig. 4A). The facet joints also can be involved. A useful differentiating feature from infection is the absence of an adjacent soft-tissue mass. MR imaging is also helpful in distinguishing the changes from an infectious spondylitis by showing abnormalities with low to intermediate signal intensity at the diskovertebral junction on all pulse sequences [14]. In this study, MR of the cervical spine showed a moderately low signal intensity on T1-weighted images and a signal isointense relative to adjacent bone marrow on T2-weighted images. These appearances contrast with the heterogeneous high signal intensity seen on T2-weighted images in infectious diskitis [15]. However, unlike previous studies, a localized soft-tissue mass was also evident (Figs. 4B and 4C).

The examples presented suggest that MR imaging is well suited for showing the extent and distribution of osseous, articular, and soft-tissue involvement in dialysis-related amyloidosis, providing considerable additional information to that obtained from conventional radiographic and CT studies. A number of lesions that were apparently intraosseous on conventional radiographs were shown to be contiguous with well-defined erosions of the articular surface on MR imaging (Fig. 2). In the wrist, these were observed most frequently on the volar and intraosseous borders of the carpal bones, but with extensive involvement, erosions of the dorsal aspects were also shown. Synovial involvement resulted in infiltration of the carpal tunnel, widening of the scapholunate and distal radioulnar articulations, disruption of the triangular fibrocartilage complex, and numerous erosions (Figs. 1B–1D). Articular erosions in the knee occurred in nonmarginal areas on the posterior aspect of the patella, on the tibial plateau, and around the origin and insertions of the cruciate ligaments (Figs. 3C and 3D). These, and the findings shown on conventional radiographs, suggest that some of the osseous lesions arise as a result of pressure defects from synovial-tissue

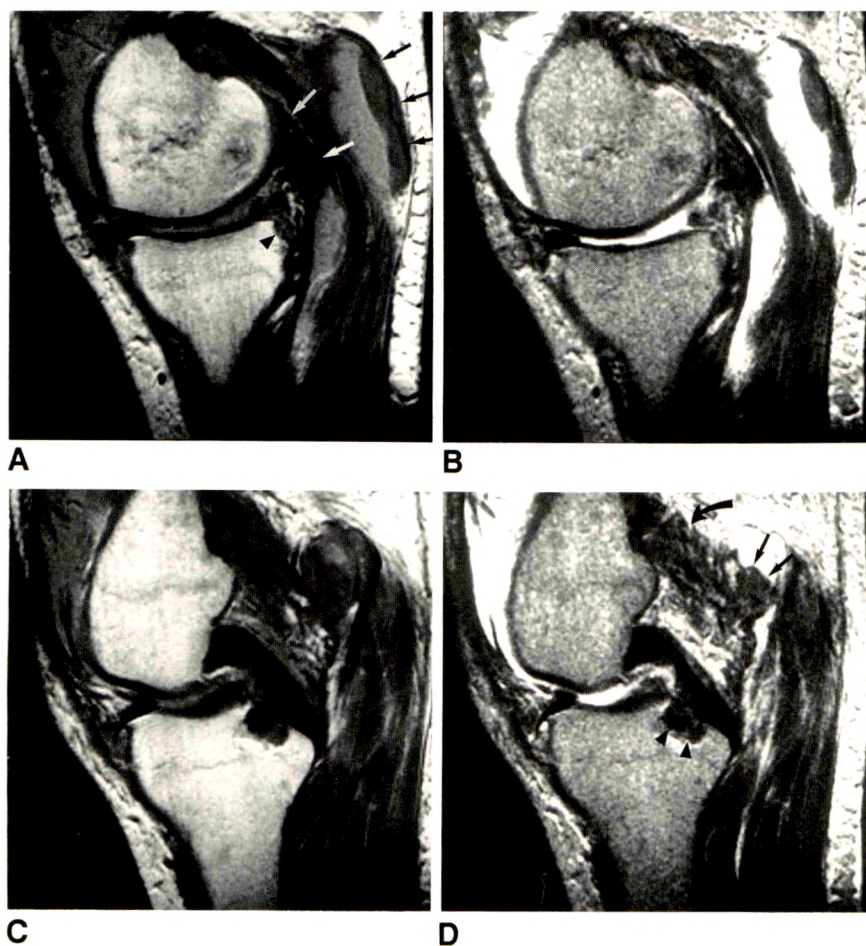


Fig. 3.—Left knee. Biopsy-confirmed amyloid deposition.

A–D, Sagittal intermediate (SE 2500/25, A) and T2-weighted (SE 2500/80, B) MR images through medial compartment and sagittal intermediate (C) and T2-weighted (D) MR images through intercondylar region show extensive deposition of abnormal soft tissue that has an intermediate signal intensity on both pulse sequences. Tissue distends joint capsule posteriorly (white arrows) and partially lines a large popliteal cyst (straight black arrows). Periarticular deposition is also evident (curved arrow). A large erosion around tibial insertion of posterior cruciate ligament and a smaller erosion of posterior surface of medial tibial plateau are also filled with same low-signal-intensity material (arrowheads). Posterior horn of medial meniscus is macerated. Large joint effusion is evident as high-signal material within joint and popliteal cyst.

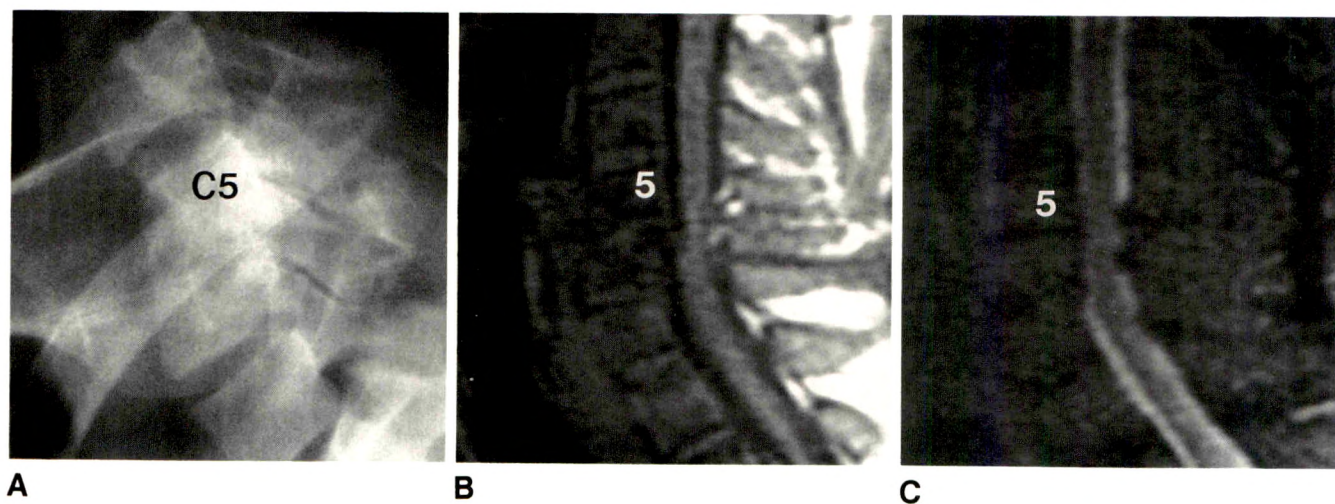


Fig. 4.—Cervical spine. Biopsy-confirmed amyloid deposition.

A, Lateral radiograph (swimmer's projection) shows an erosive spondyloarthropathy of C5–C6 intervertebral level with narrowing of intervertebral disk space and extensive erosion of adjacent endplates.

B, T1-weighted sagittal MR image (SE 600/20) shows patchy decreased signal intensity of C5 and C6 vertebral bodies. A retrolisthesis of C5 on C6 associated with a modest localized kyphosis is seen. Intervertebral disk and adjacent endplates are destroyed, and abnormal tissue anterior and posterior to thecal sac impinges on spinal cord.

C, T2-weighted sagittal MR image (SE 2250/80) shows that abnormal areas of decreased signal intensity seen in B also have a low to intermediate signal intensity on T2-weighted images.

masses rather than direct intraosseous deposition of amyloid tissue.

In addition, the MR signal characteristics of amyloid depositions were distinctive. The abnormal tissue had imaging characteristics compatible with relatively long T1 and short T2 relaxation times, resulting in a signal intensity intermediate between that of fibrocartilage and that of muscle on all pulse sequences. Some heterogeneity in the signal intensity was evident, however, on the T2-weighted images. Two of the larger lesions in the wrist and those involving the cervical vertebral bodies had signal intensities similar to that of adjacent bone marrow. These appearances distinguish amyloid infiltration from cellular lesions or lesions that contain large amounts of water, such as inflammatory masses, acute or chronic synovitis, and brown tumors of hyperparathyroidism, which have long T2 relaxation times and a high signal intensity on T2-weighted images [16–18].

Although amyloid deposition undoubtedly accounts for many of the articular and periarticular lesions seen in dialysis-associated arthropathy, the precise origin of the MR signal is unclear. Relatively few conditions result in a combination of long T1 and short T2 relaxation times. Tissues with few mobile protons, such as cortical bone, tendons, ligaments, and fibrous tissue, produce little or no signal on any pulse sequence. However, hemosiderin, by shortening T2 relaxation, does result in a low to intermediate signal intensity on both T1- and T2-weighted sequences, and so situations in which hemosiderin is deposited should be considered in the differential diagnosis of the MR findings of this study.

In hemophilia and other bleeding disorders, subacute or chronic hemarthrosis results in a hyperplastic, hemosiderin-laden synovium that may show MR characteristics similar to those of dialysis-related amyloidosis [19]. Loss of joint space is a more frequent finding in hemophilia, and other changes, such as bone overgrowth, do not occur in dialysis-related arthropathy. The distribution of joint involvement in the two also differs; the wrist is not commonly affected in cases of hemophilia.

Many of the conventional radiographic and MR findings of dialysis-related amyloidosis are mimicked by pigmented villonodular synovitis [20, 21]. This is an uncommon arthropathy characterized by synovial proliferation and hemosiderin deposition. In some instances, increased signal intensity within the thickened synovium may be seen on T2-weighted images. This finding is not observed in dialysis-related amyloidosis [20]. In addition, pigmented villonodular synovitis is almost invariably monoarticular, most frequently involves the knee (66%) and hip (16%), and only rarely affects the wrist (2% of cases) [22]. Long-standing ischemic necrosis may have an MR appearance similar to that of isolated intraosseous amyloid deposits [23], but the associated nodular soft-tissue masses and surface erosions are distinguishing characteristics. Indolent infections, particularly in the spine, may be difficult to distinguish, but usually the clinical setting and relatively increased water content of the inflammatory lesions are helpful differential features [15, 16, 24]. Interestingly, MR findings similar to those described in this study have been reported in the ankle, shoulder, and hip of a patient with immunoglobulin-associated amyloidosis [25].

The current investigation, albeit in relatively few articular sites, suggests the usefulness of MR in characterizing suspected soft-tissue and osseous changes caused by dialysis-

related amyloidosis. For instance, early "cystic" changes on plain radiographs of the wrists may be shown to be caused by extraosseous erosions from intraarticular amyloid soft-tissue deposits. This was, in fact, the case in one of our patients. Further, the relatively distinctive features of amyloid deposits may allow differentiation from other lytic processes (e.g., infection) seen at articular sites other than the wrist.

REFERENCES

1. Brown EA, Arnold IR, Gower PE. Dialysis arthropathy: complication of long-term treatment with hemodialysis. *Br Med J* 1986;292:163–166
2. Bardin T, Kuntz D. The arthropathy of chronic haemodialysis. *Clin Exp Rheumatol* 1987;5:379–386
3. Orzincolo C, Bedani PL, Scutellari PN, Cardoma P, Trotta F, Gilli P. Destructive spondyloarthropathy and radiographic follow-up in hemodialysis patients. *Skeletal Radiol* 1990;19:483–487
4. McClure J, Bartley CJ, Ackrill P. Carpal tunnel syndrome caused by amyloid containing β_2 microglobulin: a new amyloid and a complication of long-term haemodialysis. *Ann Rheum Dis* 1986;45:1007–1011
5. Bardin T, Zingraff J, Shirahama T, et al. Hemodialysis-associated amyloidosis and β_2 -microglobulin: clinical and immunohistochemical study. *Am J Med* 1987;83:419–424
6. Nakazawa R, Hamagudnik, Hosaka E. Synovial amyloidosis of β_2 -microglobulin type in patients undergoing long-term hemodialysis. *Nephron* 1987;44:379–380
7. Welk LA, Quint DJ. Amyloidosis of the spine in a patient on long-term hemodialysis. *Neuroradiology* 1990;32:334–336
8. Dixon WT. Simple proton spectroscopic imaging. *Radiology* 1984;153:189–194
9. Szumowski J, Eisen JK, Viritski S, Haake PW, Plewes DB. Hybrid methods of chemical shift imaging. *Magn Reson Imaging* 1989;9:379–388
10. Sargent MA, Fleming SJ, Chattopadhyay C, Ackrill P, Sambrook P. Bone cysts and haemodialysis-related amyloidosis. *Clin Radiol* 1989;40:277–281
11. Gielen JL, vanHolsbeeck MT, Hauglustaine D, et al. Growing bone cysts in long-term hemodialysis. *Skeletal Radiol* 1990;19:43–49
12. Ross LV, Ross GR, Mesgarzadeh M, Edmonds PR, Bonakdarpour A. Hemodialysis-related amyloidomas of bone. *Radiology* 1991;178:263–265
13. Naidich JB, Mossey RT, McHeffey-Atkinson B, et al. Spondyloarthropathy from long-term hemodialysis. *Radiology* 1988;167:761–764
14. Rafto SE, Dalinka MK, Schiebler ML, Burk DL, Kricun ME. Spondyloarthropathy of the cervical spine in long-term hemodialysis. *Radiology* 1988;166:201–204
15. Modic MT, Feiglin DH, Piraino DW, et al. Vertebral osteomyelitis: assessment using MR. *Radiology* 1985;157:157–166
16. Mason MD, Zlatkin MB, Esterhai JL, et al. Chronic complicated osteomyelitis of the lower extremity: evaluation with MR imaging. *Radiology* 1989;173:355–359
17. Yulish BS, Lieberman JM, Strandjord SE, Bryan PJ, Mulopulos GP, Modic MT. Hemophilic arthropathy: assessment with MR imaging. *Radiology* 1987;164:759–762
18. Yulish BS, Lieberman JM, Newman AJ, Bryan PJ, Mulopulos GP, Modic MT. Juvenile rheumatoid arthritis: assessment with MR imaging. *Radiology* 1987;165:149–152
19. Wilson DS, Prince JR. MR imaging of hemophilic pseudotumors. *AJR* 1987;150:349–350
20. Spritzer CE, Dalinka MK, Kressel HY. Magnetic resonance imaging of pigmented villonodular synovitis: a report of two cases. *Skeletal Radiol* 1987;16:316–319
21. Steinbach LS, Neumann CH, Stoller DW, et al. MRI of the knee in diffuse pigmented villonodular synovitis. *Clin Imaging* 1989;13:305–316
22. Myers BW, Masi AT. Pigmented villonodular synovitis and tenosynovitis: a clinical epidemiologic study of 166 cases and literature review. *Medicine (Baltimore)* 1980;59:233–238
23. Lang P, Jergesen HE, Moseley ME, et al. Avascular necrosis of the femoral head: high-field strength MR imaging with histologic correlation. *Radiology* 1988;169:517–524
24. Modic MT, Pflanze W, Feiglin DH, Belhobek G. Magnetic resonance imaging of musculoskeletal infections. *Radiol Clin North Am* 1986;24:247–267
25. Tagliabue JR, Stull MA, Lack EE, Lloyd RJ, Nelson MC. Amyloid arthropathy of the left ankle: case report 610. *Skeletal Radiol* 1990;19:448–452

Book Review

The Radiologic Clinics of North America. Metabolic Bone Disease. Guest editor: Daniel I. Rosenthal. Philadelphia: Saunders, January 1991;29(1):1-177. \$28; by subscription, 6 issues annually for \$98

Daniel Rosenthal, guest editor of this issue of *The Radiologic Clinics of North America*, states in a lucid preface that metabolic bone diseases provide a tremendous challenge and an opportunity for radiologists, for "in no other area does imaging offer such precise, detailed and quantifiable information about physiology as well as anatomy. . . . The subject, however, is difficult. . . . So much is unknown that it is often impossible to tie facts and ideas into coherent packages. . . . Another source of difficulty for the radiologist is that many of the thought processes required for understanding this field are more quantitative and mechanistic than those used elsewhere in radiology." With this in mind, Rosenthal and his team of author-experts have emphasized a mechanistic basis for radiologic observations.

An enlightening introductory chapter on prediction of fracture risk based on the results of quantitative CT stresses the correlation of quantitative CT data with bioengineering concepts of in vivo load vs strength estimates for the hip and spine. Another chapter reviews, at a basic level, the histology of bone disease and the pathology of metabolic bone disease. The radiologic appearances of osteopenia are described in another chapter, which emphasizes the different radiologic appearances and differential diagnosis of slow vs rapid bone loss.

The highlight of the book is a cogent and far-sighted review, "Osteoporosis: Current Techniques and Recent Development in Quantitative Bone Densitometry," by Philipp Lang and colleagues. These authors rationally discuss indications for bone densitometry and describe the advantages and limitations of each of the current densitometric techniques. Reinforcing the views of the editor, the authors decry the deficiency in medical and technical expertise that is the principal deterrent to the widespread implementation of their

recommended clinical applications. Additional chapters review radiographic bone morphometry (a technique that is admittedly too time-consuming to be practical), osteoporosis at a pathophysiologic level, the pathophysiology and radiology of hyperparathyroidism, rickets and osteomalacia, endocrine disorders and ectopic endocrine (paraneoplastic) syndromes involving bone, and inherited diseases of bone density in children.

A reviewer must dutifully search for glitches, but I could discover only a few: Howard Steinbach's name is misspelled three times in a row in the references for the chapter on rickets and osteomalacia, the legends for the radiographs in the chapter on inherited diseases of bone density in children do not always mention the diagnosis, and the features of pyknodysostosis presented in the same chapter do not include increased fragility of bone. Although some duplication is inevitable in any book that has more than one author, the generally high standard of excellence of previous Clinics is maintained. The illustrations are of the highest quality, the text is lucid and concise, and the references are up-to-date and plentiful (one chapter contains 94 references, another 135, yet another 138).

In summary, this book provides an excellent and relatively inexpensive review of the current knowledge of the radiology, pathophysiology, and biomechanics of metabolic bone disease and the state of the art (and science) of in vivo quantification of bone density and strength. I recommend it highly to all physicians, especially radiologists, who have an interest in skeletal disease in general and osteopenia in particular.

Richard H. Gold
University of California, Los Angeles
Los Angeles, CA 90024

Pictorial Essay

Hallux Rigidus Deformity: Radiologic Assessment

David Karasick¹ and Keith L. Wapner²

Hallux rigidus (osteoarthritis leading to reduced motion) is one of the most common afflictions of the first metatarsophalangeal joint. The diagnosis is based on the presence of pain, specific physical findings, and certain radiologic features. In this essay, we illustrate the grades of radiologic changes, which are an integral part of the surgeon's preoperative evaluation, and show examples of the postoperative radiologic appearance.

Hallux rigidus (osteoarthritis with restricted motion) is the second most common disabling deformity of the first metatarsophalangeal joint after hallux valgus (medial deviation of the first metatarsal with lateral deviation of the proximal phalanx). The "stiff great toe" is also known as hallux limitus, hallux flexus, metatarsus primus elevatus, and dorsal bunion. The disability with hallux rigidus is greater than that seen in hallux valgus because removal of shoes does not relieve the pain; dorsiflexion at the metatarsophalangeal joint is severely restricted and painful. The diagnosis of hallux rigidus is based on the presence of pain in the first metatarsophalangeal joint and physical findings of restricted dorsiflexion ($<30^\circ$), increased joint bulk (particularly dorsally), and often an associated synovitis [1]. Hallux rigidus is most commonly seen in middle-aged patients, but can develop during adolescence; unlike hallux valgus, males appear to be slightly more affected than females.

Pathogenesis

Hallux rigidus is the result of degenerative osteoarthritis of the first metatarsophalangeal joint leading to the great toe

being fixed in neutral position and limited in dorsiflexion. The restricted range of motion is related to bone proliferation adjacent to the articular cartilage at the first metatarsophalangeal joint, particularly dorsally. The plantar two thirds of the surface of the first metatarsal head is usually spared. Coexistent degenerative changes on the dorsal aspect of the base of the first proximal phalanx also are seen commonly. Similar to degenerative joint disease elsewhere, the joint cartilage begins to deteriorate, with resultant joint-space narrowing. The subchondral bone shows increased sclerosis and eburnation. Osteophytic spurs develop, usually over the dorsal aspect of the metatarsal head, and dorsal medial and dorsal lateral extensions are common. Subchondral cysts on either side of the joint may develop as well [2].

Although congenital causes of hallux rigidus can be found, the two most common causes are traumatic arthritis and arthritis associated with systemic disease. Predisposing factors include an abnormally long first metatarsal bone, dorsal hyperextension of the first metatarsal bone, and pronation of the forefoot [2]. The development of osteoarthritis at this joint may be due to injury of the first metatarsophalangeal joint, intraarticular microfracture, or osteochondritis dissecans. Most often it is the consequence of repetitive loading in a patient with a relatively flat metatarsal head, which limits medial and lateral motion [2]. Acquired hallux rigidus may be due to systemic conditions such as gouty arthritis, psoriatic arthritis, or rheumatoid arthritis.

The first metatarsal head varies in contour because of genotype variation. The shape of the head is important in the development of both hallux rigidus and hallux valgus. A

Received April 2, 1991; accepted after revision June 4, 1991.

¹Department of Radiology, Thomas Jefferson University Hospital and Jefferson Medical College, 111 S. 11th St., Philadelphia, PA 19107. Address reprint requests to D. Karasick.

²Department of Orthopedic Surgery, Thomas Jefferson University Hospital and Jefferson Medical College, 111 S. 11th St., Philadelphia, PA 19107.

AJR 157:1029-1033, November 1991 0361-803X/91/1575-1029 © American Roentgen Ray Society

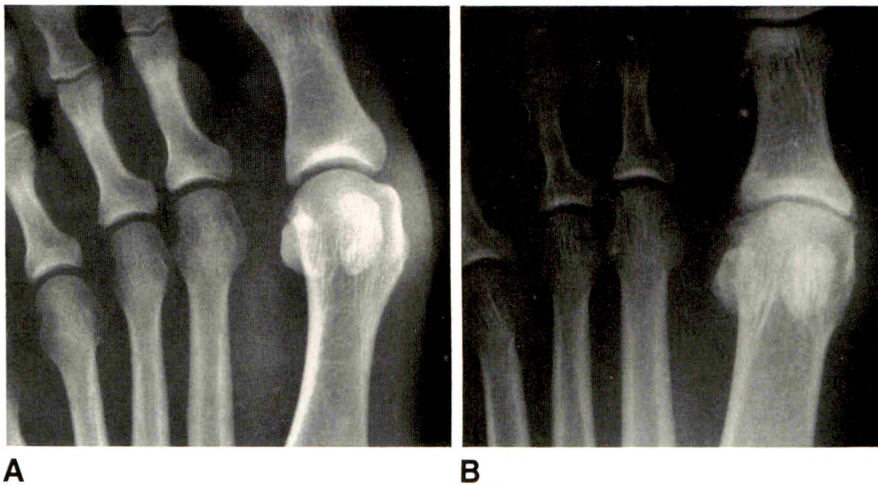


Fig. 1.—Hallux rigidus vs hallux valgus.
 A, Hallux valgus: Round first metatarsal head is more prone to development of hallux valgus deformity.
 B, Hallux rigidus: Flat first metatarsal head is more stable and resists dorsiflexion. Joint-space narrowing and marginal spurring reflect changes of hallux rigidus.

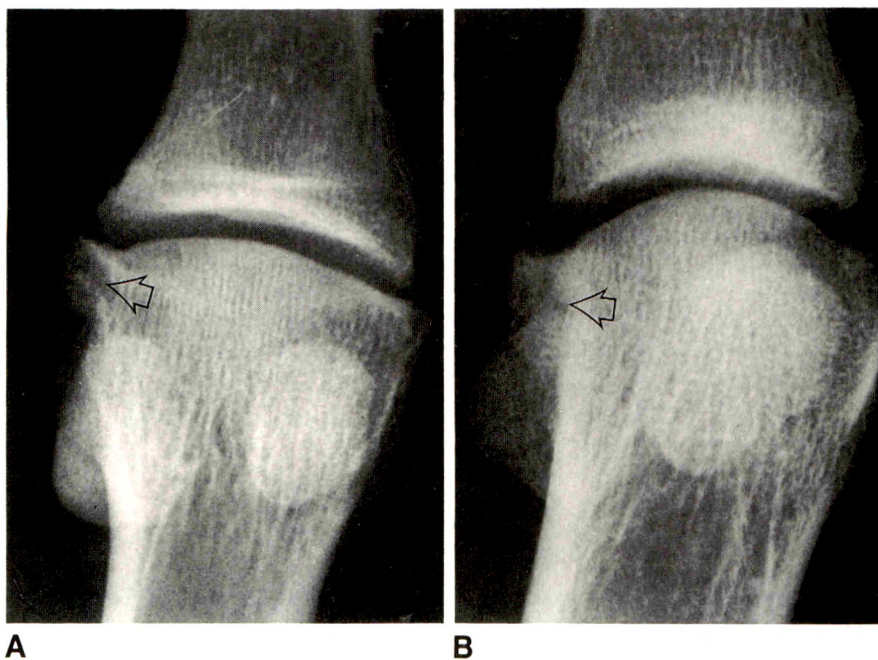


Fig. 2.—A and B, Mild hallux rigidus (grade 1). Anteroposterior radiographs of two examples show minimal metatarsophalangeal joint-space narrowing and lateral bone spurs (arrows).

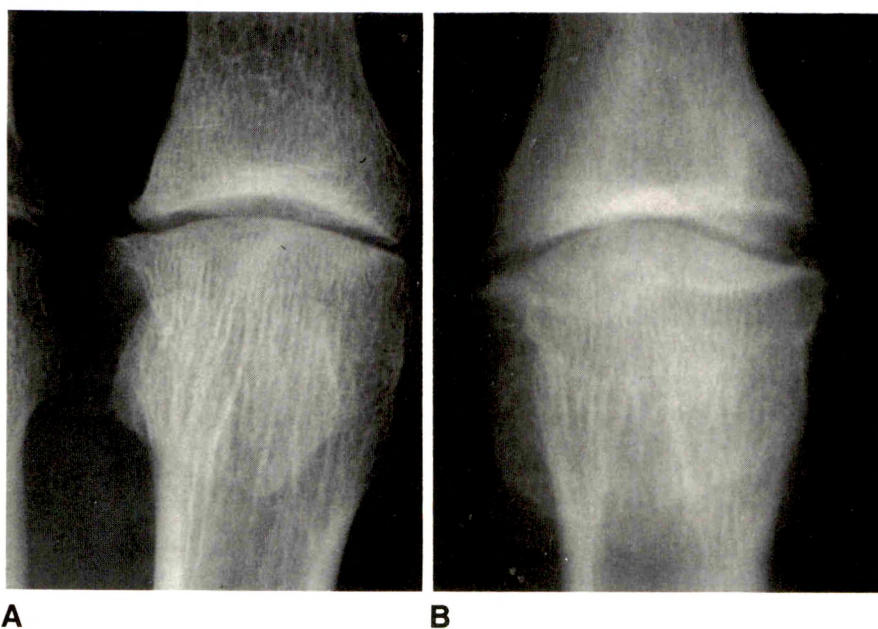


Fig. 3.—A and B, Moderate hallux rigidus (grade 2). Anteroposterior radiographs of two examples show progressive joint-space narrowing, marginal spurs, and subchondral sclerosis and/or cyst formation.

Fig. 4.—A and B, Severe hallux rigidus (grade 3). Anteroposterior radiographs of two examples show marked joint-space narrowing, advanced subchondral sclerosis, and spurring at hallux-sesamoid articulations.

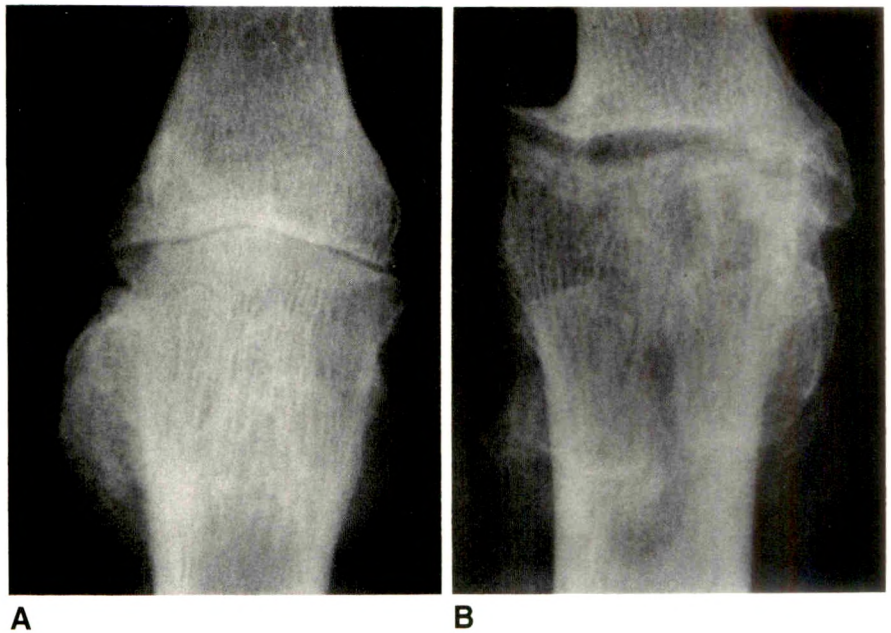


Fig. 5.—A and B, Dorsal ossicles with hallux rigidus. Lateral radiographs show dorsal ossicles (arrow) in conjunction with dorsal spurs of metatarsal head. Dorsal ossicles or intraarticular bone fragments result from repetitive micro-trauma or synovial chondrometaplasia.

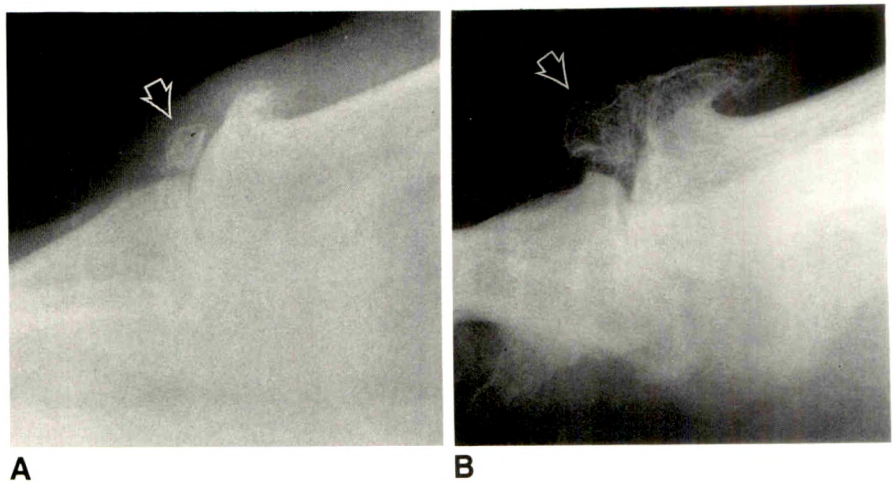
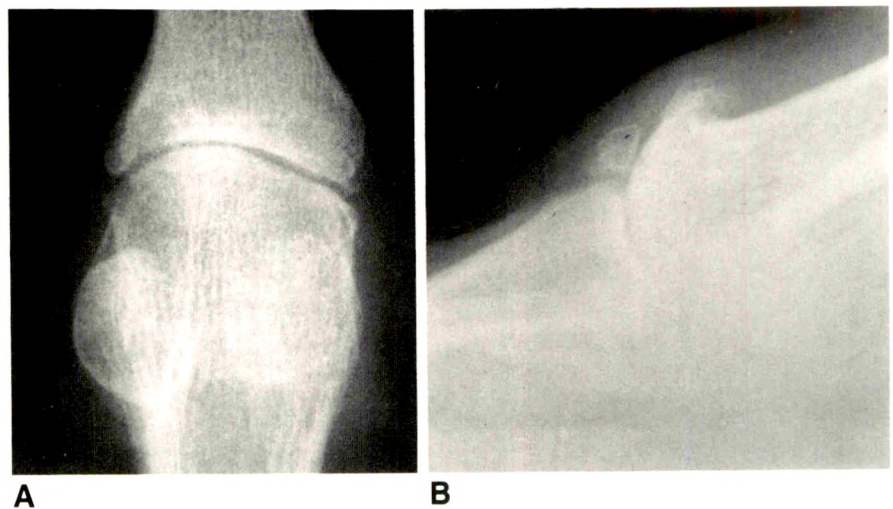


Fig. 6.—Value of erect lateral radiograph.
A, Erect anteroposterior radiograph does not show dorsal spur or ossicle with grade 2 hallux rigidus.
B, Erect lateral radiograph clearly defines degree of dorsal spurring at first metatarsophalangeal joint and presence of dorsal ossicle. Size and shape of dorsal spur affect degree of impingement of proximal phalanx against metatarsal head, thereby limiting dorsiflexion.



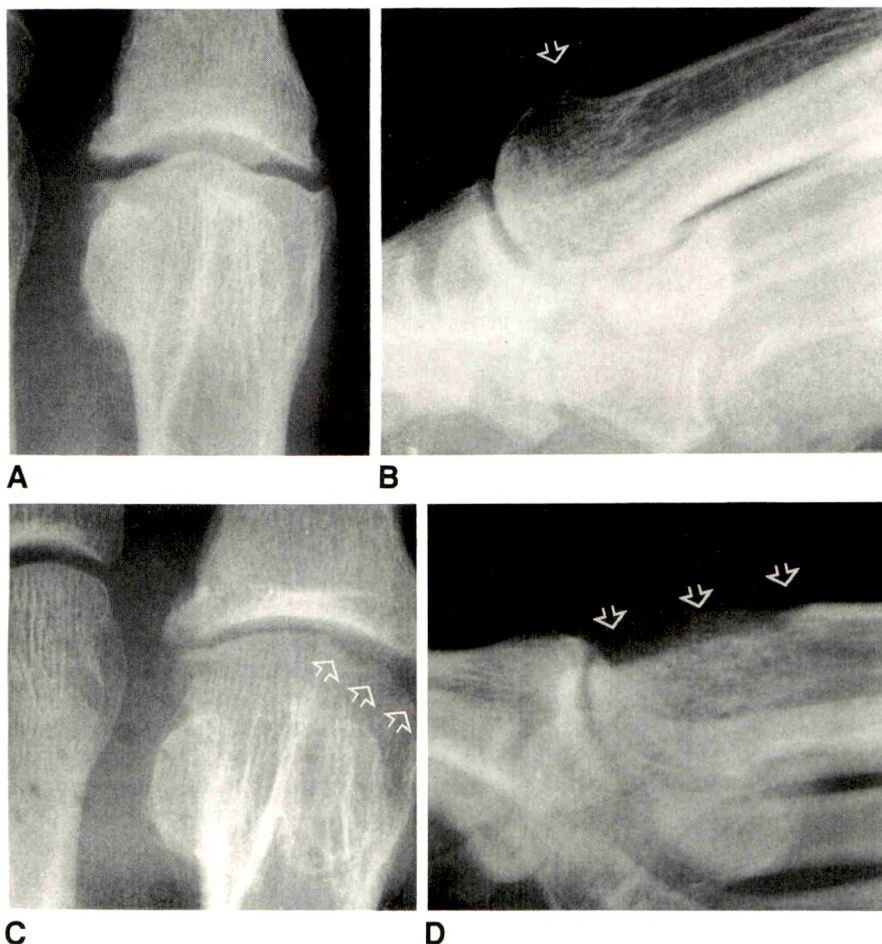


Fig. 7.—Radiographic findings after cheilectomy.

A and B, Preoperative anteroposterior (A) and lateral (B) radiographs of grade 1 hallux rigidus. Note prominent dorsal spur (arrow).

C and D, Postoperative anteroposterior (C) and lateral (D) radiographs show removal of medial spur and dorsal spur of metatarsal head below level of metatarsal shaft dorsally (arrows).

metatarsophalangeal joint with a rounded head is less stable in resisting dorsiflexion and adductory forces and is more prone to the development of a hallux valgus deformity. A flattened head is more stable and resists these forces; this leads to repetitive trauma to the articular surface of the first metatarsophalangeal joint, ultimately resulting in the development of hallux rigidus (Fig. 1).

Preoperative Radiography

The preoperative radiographic assessment of hallux rigidus deformity is similar to that of hallux valgus deformity [3]. Erect weight-bearing radiographs are obtained in the anteroposterior (dorsoplantar) and lateral projections. The anteroposterior radiograph is obtained with 15° cephalic tube angulation. The lateral radiograph is unangled and enables proper evaluation of pes planus as well as dorsal spurring at the first metatarsophalangeal joint. An accompanying oblique radiograph is obtained without tube angulation; this projection is helpful in the evaluation of joint-space narrowing and to visualize marginal spurring and subchondral cysts not optimally seen in the other two standard views.

Radiographically, hallux rigidus can be divided into mild

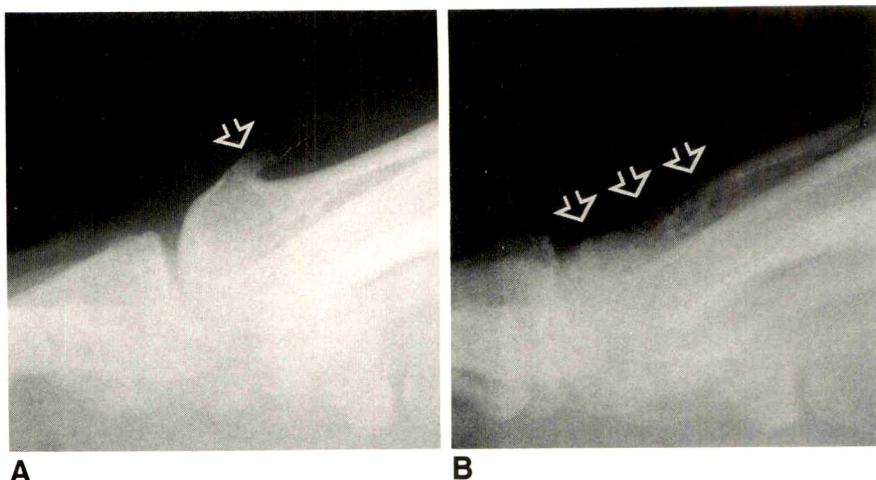
(grade 1), moderate (grade 2), and severe (grade 3) forms [4]. The mild form consists of minimal or no joint-space narrowing and minimal spurring dorsally or laterally (Fig. 2). The moderate form consists of progressive joint-space narrowing, larger spurs, and the development of subchondral sclerosis and/or cysts (Fig. 3). Severe hallux rigidus consists of marked joint-space narrowing, advanced subchondral sclerosis, and/or large circumferential spurs (especially dorsally) and degenerative changes at the hallux-sesamoid articulations (Fig. 4). Ossicles or dorsal intraarticular bone fragments can be seen resulting from either repetitive microtrauma or synovial chondrometaplasia (Fig. 5).

Proper positioning of the foot radiographically is crucial to the optimal selection of treatment for hallux rigidus. Without erect lateral views of the foot, dorsal spurs can be obscured (Fig. 6). The degree of dorsiflexion can be measured and assessed both before and after surgery. Dorsal spurring at the first tarsometatarsal articulation and talonavicular articulation also can be evaluated on this lateral view. The erect anteroposterior view of the foot is essential for evaluating for possible associated hallux valgus; abnormalities related to the other metatarsal bones such as fracture, cortical hypertrophy, and osteonecrosis also can be assessed.

Fig. 8.—Radiographic findings after cheilectomy.

A, Preoperative lateral radiograph shows grade 1 hallux rigidus with dorsal spur (arrow) of metatarsal head.

B, Postoperative lateral radiograph shows resection of dorsal spur of metatarsal head (arrows).



Surgical Options

On the basis of radiologic findings, the surgical options available include dorsal wedge osteotomy, arthrodesis, resection or implant arthroplasty, and cheilectomy (osseous rim excision) [2]. Wedge osteotomy of the proximal phalanx has been advocated in adolescents with little or no degenerative joint disease, but is rarely performed today. Arthrodesis of the first metatarsophalangeal joint has been considered as a primary choice in patients with advanced disease who require heavy use of their feet. Resection and implant arthroplasties have been advocated in low-demand patients, but have their shortcomings; the high rate of loosening, prosthetic fracture, and development of silicone synovitis have curtailed the use of these replacements at the first metatarsophalangeal joint.

The surgical procedure most often used is a cheilectomy because it offers the theoretical advantage of preserving hallux function that otherwise would be lost after resection arthroplasty or arthrodesis, while avoiding the potential complications of implant arthroplasty. Cheilectomy is the surgical procedure of chiseling off the irregular bony edges or lip of a joint cavity that interferes with motion. Cheilectomy has been recommended as the procedure of choice for grade 1 radiologic changes [4]. It can be attempted for grade 2 lesions, but grade 3 lesions usually require arthrodesis if push-off function is to be preserved. The success of cheilectomy is based on the removal of the dorsal third of the first metatarsal

head to allow 90° of dorsiflexion at the time of surgery [1]. The procedure avoids hallux shortening and eliminates impingement of the proximal phalanx against the large dorsal osteophyte of the metatarsal head, thereby permitting additional dorsiflexion. During surgery, bone spurs medially or laterally can be removed as well as any proliferative synovial tissue, debris, or loose bodies about the joint. The radiologic appearance of the great toe after cheilectomy is best evaluated in the erect lateral and oblique projections. The lateral view enables visualization of the dorsal aspect of the first metatarsal head after removal of spurs and a portion of the normal articular surface dorsally (Figs. 7 and 8).

In summary, hallux rigidus deformity is a common foot disorder that can be quite disabling to the patient. Recognition and grading of specific radiologic features are crucial to successful orthopedic management, including choice of surgical procedures.

REFERENCES

1. Mann RA, Clanton TO. Hallux rigidus: treatment by cheilectomy. *J Bone Joint Surg [Am]* **1988**;70-A:400-406
2. Mann RA, Coughlin MJ. Arthritides. In: Mann RA, ed. *Surgery of the foot*, 5th ed. St. Louis: Mosby, **1986**:158-179
3. Karasick D, Wapner KL. Hallux valgus deformity: preoperative radiologic assessment. *AJR* **1990**;155:119-123
4. Hattrup SJ, Johnson KA. Subjective results of hallux rigidus following treatment with cheilectomy. *Clin Orthop* **1988**;226:182-191

Book Review

Cartilaginous Tumors of the Skeleton. By Richard P. Moser, Jr. (Fascicle II in AFIP Atlas of Radiologic-Pathologic Correlations. Series editor: Alan J. Davidson.) Philadelphia: Hanley & Belfus (distributed by Mosby-Year Book, St. Louis), 208 pp., 1990. \$50, softcover

This softcover book is the second fascicle of the series AFIP Atlas of Radiologic-Pathologic Correlations from the Armed Forces Institute of Pathology (AFIP). Other fascicles are planned. Alan Davidson of the AFIP is the series editor. Six contributors assisted with this fascicle, all associated with the AFIP (present or past) and/or the Uniformed Services University of the Health Sciences. Part of the dedication is unique in these special times: "To all the dedicated men and women . . . who have served proudly in the Armed Forces of the United States of America, often at considerable personal sacrifice, so that all citizens of our great nation might enjoy a better life."

Is another book on a selected segment of bone tumors needed? How does this volume differ from already available texts? The preface states, "This book was developed to fill the need for a concise reference on cartilaginous lesions of the skeleton."

The book is simply organized. It has a brief opening chapter on the biology of cartilage, then four chapters on benign tumors (enchondroma, osteochondroma, chondroblastoma, and chondromyxoid fibroma), and a final chapter on chondrosarcoma. Periosteal (juxtacortical) chondroma is not mentioned. Each of the chapters on tumors discusses pathogenesis, pathology, clinical findings, and radiology. Differential diagnosis is included. The illustrations are mostly plain films, but each chapter does have CT scans, MR images, and scintigrams. Angiography and plain tomograms are included also. References at the end of each chapter include many important older citations and are also up-to-date, with 1988 and even 1989 listings.

This book is, as stated in the series name, an atlas. Pages of figures in each chapter outnumber pages of text by factors from 5:1 to 8:1. The text is clear and easy to read. The figures are large and clear, mostly full page or half page; radiographs predominate. Figures

showing pathologic changes are mostly macroscopic sections, in color, and many are juxtaposed with matching radiologic images for radiologic-pathologic correlation. The atlas also has specimen figures and specimen radiographs and only a few microscopic sections. The author does not state for whom this book was written. The figures and text suggest it is oriented primarily to those more interested in radiology than pathology. It has little in the way of detailed descriptions of micropathologic changes. The AFIP has previously published a multiple-fascicle tumor series for pathologists, *Atlas of Tumor Pathology*.

So, does this volume provide a needed concise reference on cartilaginous tumors? It has about one half the total pages and figures on cartilaginous tumors compared with Wilner's five-volume book on bone tumors. On the other hand, it has two to three times the text and figures on the same subject compared with Ediken's two-volume book on diseases of bone and Resnick's six-volume text on bone and joint disorders. The unique aspect of this book lies, as the series name states, in the many beautiful examples of radiologic-pathologic correlation from the large collection of material at the AFIP and in the text written with the experience and, hence, authority of the AFIP.

This fascicle should be of interest to radiologists and others who have a special interest in bone tumors. Most general radiologists will not personally need such a text on so small a topic, but it is hoped that it will be available to them at libraries and in radiology departments and group practices whose members see such tumors.

Stanley P. Bohrer
Bowman Gray School of Medicine, Wake Forest University
Winston-Salem, NC 27103

Case Report

Skeletal Lymphoma in a Patient with Castleman Disease

John G. Buckley¹ and Murali Sundaram

Castleman disease (angiofollicular hyperplasia) is a relatively rare disease of unknown cause that is characterized by the development of enlarged lymph nodes [1]. Keller et al. [2] subdivided the disease into two histologic types: the hyaline vascular and the rarer plasma cell type.

Both types of Castleman disease may be localized or widespread. The widespread form is frequently associated with malignancy; however, malignancy is uncommon in the localized form, and prognosis is uniformly good [1].

We describe a patient with Castleman disease of the plasma cell type localized to the mediastinum in whom skeletal lymphoma developed 5 years later.

Case Report

The patient, a 30-year-old man, had an infection of the upper respiratory tract. A chest radiograph showed right hilar lymphadenopathy (Fig. 1A). The patient was treated with antibiotics and had a good clinical response. However, a second chest radiograph showed persistence of the lymphadenopathy.

CT of the thorax and abdomen showed right hilar and subcarinal lymphadenopathy. No lymphadenopathy was seen in the abdomen. Washings obtained from the right bronchial tree at bronchoscopy were normal, and biopsy specimens showed normal mucosa.

Three months later, an anterior mediastinotomy was performed, and biopsies of several hilar lymph nodes were done. Cultures for fungi and for acid-fast bacilli were negative. Histologic findings of biopsy specimens were consistent with angiofollicular lymph node hyperplasia of the plasma cell type. The patient was asymptomatic, and the results of routine hematologic tests were within normal limits.

A year after the mediastinotomy, the patient was readmitted with a 2-month history of right-sided chest pain that was unresponsive to antiinflammatory medication. There was associated mild wheeze and cough. The right hilar adenopathy had grown since the initial presentation, and right paratracheal lymphadenopathy was noted (Fig. 1B). A right-sided thoracotomy was performed, and right hilar and mediastinal lymph nodes were obtained. Histologic examination showed partial effacement of the nodal architecture by plasma cells and a prominent vascular component. No Reed-Sternberg cells were identified. The features were again consistent with a diagnosis of angiofollicular lymph node hyperplasia of the plasma cell type. The patient had an uneventful postoperative course and was asymptomatic on discharge. No treatment was instituted.

Four years eight months after the initial presentation, the patient returned to the hospital because of a 3-month history of pain in the right arm. Plain radiographs of the chest (Fig. 1C) and right humerus (Fig. 1D) showed further increase in nodal size on the right side and a lytic lesion involving the proximal humerus, respectively. A bone biopsy was performed, and pathologic examination showed a malignant T-cell lymphoma. CT showed no lymphadenopathy in the left side of the mediastinum, abdomen, retroperitoneum, or pelvis. The patient was not seropositive for the human immunodeficiency virus.

The patient was treated with combination chemotherapy for lymphoma and has responded well, with diminution of mediastinal node size and relief of symptoms in the arm.

Discussion

Angiofollicular lymph node hyperplasia (Castleman disease) was originally described by Castleman et al. [1]. They identi-

Received April 22, 1991; accepted after revision May 21, 1991.

¹ Both authors: Department of Radiology, St. Louis University Medical Center, 3635 Vista at Grand, St. Louis, MO 63110-0250. Address reprint requests to M. Sundaram.

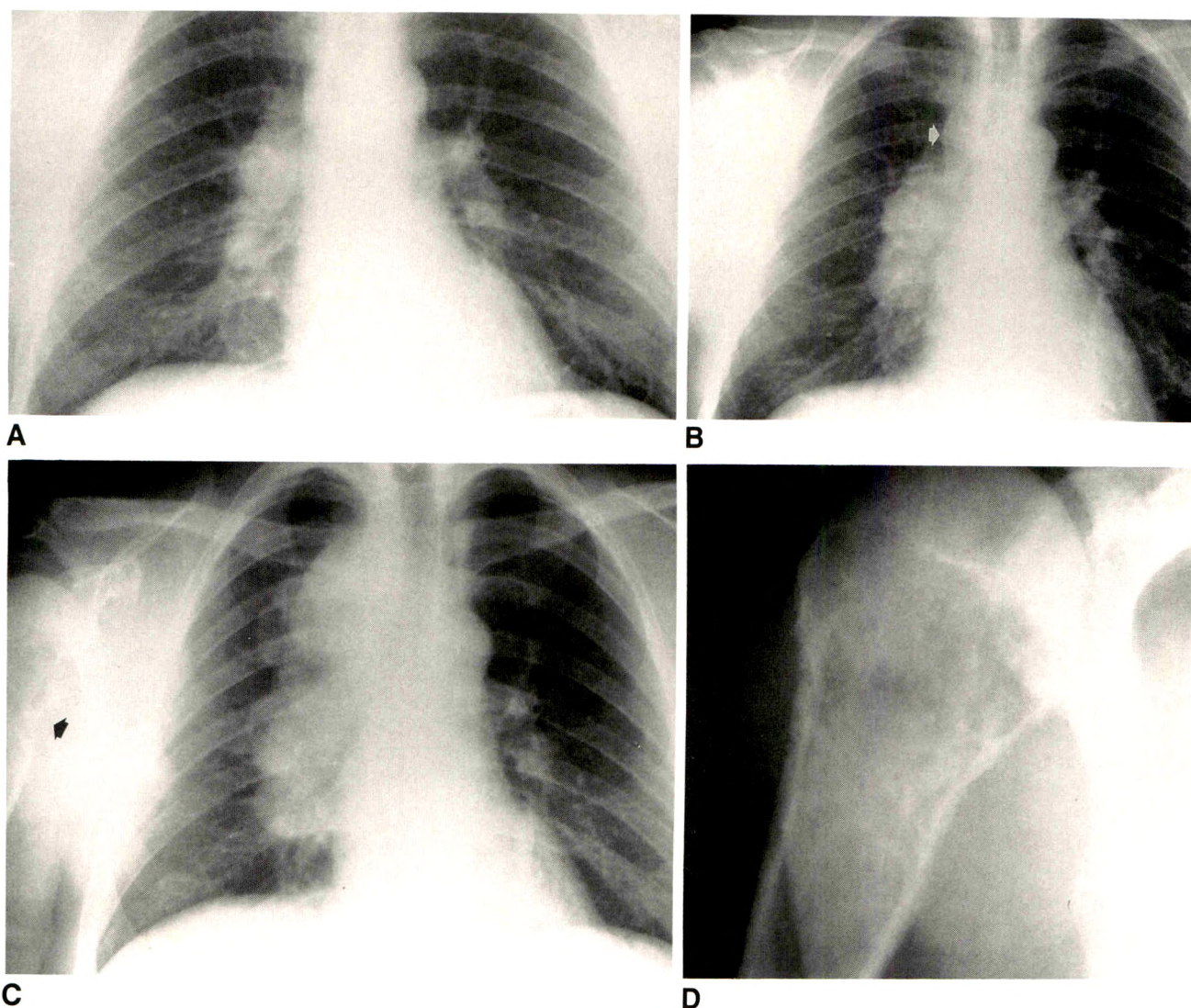


Fig. 1.—Development of skeletal lymphoma in localized Castleman disease.

A, Initial chest radiograph shows right hilar lymphadenopathy. Anterior mediastinotomy and biopsy of lymph nodes revealed angiofollicular hyperplasia. B, Radiograph obtained 15 months after A shows further enlargement of right hilar lymphadenopathy and development of right paratracheal lymphadenopathy (arrow). A right thoracotomy was performed at this time. C, Radiograph obtained 4 years 8 months after A shows further enlargement of lymphadenopathy shown in B. Note no lymphadenopathy on left side and destructive lesion in right humerus (arrow).

D, Radiograph of proximal right humerus obtained at same time as C shows a destructive lesion with a wide zone of transition and cortical destruction.

fied a group of patients with asymptomatic, large, benign, hyperplastic mediastinal lymph nodes that resembled thymomas. Various other names such as benign giant lymphoma, angiomatous lymphoid hamartoma, and giant lymph node hyperplasia have also been applied.

Keller et al. [2] divided Castleman disease into two distinct histologic subtypes: the hyaline vascular form, which constitutes 90% of the cases, and the plasma cell variant, which constitutes the remaining 10%. In the first subtype, numerous small folliclelike structures with prominent central vascular tufts are seen. A perifollicular concentric layering of small lymphocytes is characteristic. The distinguishing feature of

the plasma cell type is the presence of interfollicular layers of plasma cells.

Whereas patients with the hyaline vascular type of Castleman disease usually have no clinical signs and symptoms, those with the plasma cell variety frequently have fever, anemia, and polyclonal hypergammaglobulinemia. In our case, the patient did not have an abnormal blood count or hypergammaglobulinemia.

Castleman disease may be localized or widespread [2]. The latter type frequently has an aggressive course, with multifocal lymphadenopathy, hepatosplenomegaly, and alteration of the immune system often resulting in death from sepsis. The

development of neoplasia such as lymphoma, Kaposi sarcoma, plasmacytoma, and colonic carcinoma has been described in the systemic form of Castleman disease [3-5].

The association of localized Castleman disease and neoplasia has been reported rarely. Our review of the literature revealed two cases of localized Castleman disease associated with development of plasmacytoma [6, 7]. In addition, one letter to the editor described a patient with mediastinal Castleman disease in whom Hodgkin disease subsequently developed [8].

To our knowledge, however, this is the first report of a patient with localized Castleman disease who subsequently had skeletal lymphoma. It could be argued that the skeletal lymphoma is unrelated to the mediastinal lymphadenopathy. The development of the skeletal lesion with increase in nodal size and subsequent decrease in arm symptoms and nodal size after chemotherapy would suggest that they are related. Lymphomas that have developed in association with systemic Castleman disease have no features to distinguish them from lymphomas arising de novo.

This case further supports the concept that localized Castleman disease has a low but definite neoplastic potential. Surgical removal of lymph nodes has been advocated as therapy for symptomatic localized Castleman disease. Per-

haps this form of treatment has a place in asymptomatic patients with enlarging lymph nodes.

REFERENCES

1. Castleman B, Ivers M, Menendez V. Localized mediastinal lymph node hyperplasia resembling lymphoma. *Cancer* **1956**;9:822-830
2. Keller AR, Hochholzer L, Castleman B. Hyaline-vascular and plasma-cell types of giant lymph node hyperplasia of the mediastinum and other locations. *Cancer* **1972**;29:670-683
3. Weisenburger DD, Nathwani BN, Winberg CD, Rappaport H. Multicentric angiofollicular lymph node hyperplasia: a clinicopathological study of 16 cases. *Hum Pathol* **1985**;16:162-172
4. Dickson D, Ben-Ezra JM, Reed J, Flax H, Janis R. Multicentric giant lymph node hyperplasia, Kaposi's sarcoma and lymphoma. *Arch Pathol Lab Med* **1985**;109:1013-1018
5. Gould SJ, Diss T, Isaacson PG. Multicentric Castleman's disease in association with a solitary plasmacytoma: a case report. *Histopathology* **1990**;17:135-140
6. Cousineau S, Beauchamp G, Boileau J. Extramedullary plasmacytoma associated with angiofollicular lymph node hyperplasia. *Arch Pathol Lab Med* **1986**;110:157-158
7. Schlosnagle DC, Chan WC, Horgreaves HK, Nolting SF, Brynes RK. Plasmacytoma arising in giant lymph node hyperplasia. *Am J Clin Pathol* **1982**;78:541-544
8. McAloon EJ. Hodgkin's disease in a patient with Castleman's disease. *N Engl J Med* **1985**;313:758

Book Review

Radiology Review Manual. By Wolfgang Dähnert. Baltimore: Williams & Wilkins, 583 pp., 1991. \$55, softcover

"All Summer Long Emily Ogled Peter's Sporty Isuzu."

How does anyone remember the 1001 facts on the significant signs and differential diagnosis of the many syndromes and associated conditions inherent in the practice of radiology? Residents preparing for board examinations have long used some form of outline or notes as a memory aid or refresher. Those with imagination construct some catchy acronym or mnemonic to provide the necessary mental crutch to facilitate recall. Wouldn't it be nice to have at hand such an outline prepared and ready for use? Dr. Dähnert has provided just that help in the form of a softcover book: *Radiology Review Manual*.

The book has several sections organized in the usual organ orientation and one section on nuclear medicine. Each section follows a general pattern. The beginning of the section has lists of differential diagnoses. These are followed by a concise outline of the disease entities related to that organ system. The style of writing should be familiar to most residents (and radiologists); it tends to be brief and nonwordy and uses some of the medical shorthand common to housestaff officers. Commendably, the author has included a liberal dose of general medical facts to flesh out the skeleton of bare radiologic facts. Memory aids in the form of acronyms and mnemonics are used throughout the book. These include those generally well known and many others. A helpful and amusing feature is a separate list of the 106 acronyms and mnemonics used in the book. Do you remember the meaning of the line at the head of this review or of "POSTCARD" or "EPIC"? (For translation, see the note at the end of the review.) These and 103 other memory joggers are on the list. The book has no photographs, but it uses line drawings judiciously to clarify many conditions and anatomic relationships. The author credits many radiologic textbooks and articles in the introduction, but

no effort is made to cite the material in the body of the book. I would not expect to use this type of outline for a literature search and therefore do not find this a major criticism. In addition to the list of mnemonics, the book has a table of contents, a list of abbreviations, and a good index.

Who is the target audience of this book? The title suggests that it is those who are preparing themselves for a review or a board examination. I think that it will be used for more than this. It would be handy to have a copy of this book at the reading station as a quick reference to those things that are vaguely but inexactly remembered. This type of outline is also helpful to beginning residents, but only to complement standard references. Seeing the radiographic findings is still vital to the learning process. At 21.5 × 28.0 × 3.0 cm, about the size of a telephone book of a medium-sized city, the review is too big to carry around in your pocket. I wish that it could be minified for that purpose.

Note.—The sentence at the beginning of the book review is the mnemonic for the branches of the external carotid artery: *A*scending pharyngeal artery, *S*uperior thyroid artery, *L*ingual artery, *E*xternal maxillary (= facial artery), *O*ccipital artery, *S*uperficial temporal artery, and *I*nternal maxillary artery. POSTCARD is the acronym for the causes of papillary necrosis: *P*yelonephritis, *O*bstruction, *S*ickle cell disease, *T*uberculosis, *C*irrhosis (= alcoholism), *A*nalgesic nephropathy, *R*enal vein thrombosis, and *D*iabetes. EPIC is the acronym for the causes of discoid atelectasis: *E*mbolus, *P*neumonia, *I*nadequate inspiration, and *C*arcinoma, obstructing.

Marvin E. Goldberg
University of Minnesota
Minneapolis, MN 55455

Review Article

Drug-Related Complications in Infants and Children: Imaging Features

E. George Kassner¹

Iatrogenic disorders continue to be an important cause of morbidity and mortality in infants and children. Most adverse drug reactions have no distinctive radiologic features. Of those with radiologic manifestations, it is usually impossible to differentiate iatrogenic disorders from their spontaneously occurring counterparts. However, certain iatrogenic disorders have distinctive imaging characteristics that allow their recognition in specific patient populations. This review considers a variety of drug-related disorders and phenomena that have been the subject of original articles in the English language literature since 1984.

Drug-related complications remain an important cause of morbidity and mortality in infants and children. During a recent 11-year period (1974–1985), 131 (2.0%) of 6546 admissions of children (other than neonates and children with cancer) to seven American teaching and community hospitals were prompted by adverse drug reactions [1]. The most common offending drugs (five or more admissions each) were phenobarbital, aspirin, phenytoin, ampicillin or amoxicillin, theophylline or aminophylline, trimethoprim/sulfamethoxazole, and diphtheria-pertussis-tetanus vaccine. The reactions tended to be in one of two general categories: those that may have been related to excessive drug levels (e.g., phenobarbital-induced lethargy) and those related to acute hypersensitivity (e.g., sulfa-induced erythema multiforme, phenytoin-induced hepatitis).

Most adverse drug reactions have no distinctive radiologic features. Of those with radiologic manifestations (e.g., aspirin-induced peptic ulceration, furosemide-induced cholelithiasis),

it is usually impossible to differentiate iatrogenic disorders from their spontaneously occurring counterparts. However, certain iatrogenic disorders have distinctive imaging characteristics that allow their recognition in specific populations of patients (e.g., prostaglandin-induced periostitis in neonates with ductus-dependent congenital heart disease and medullary nephrocalcinosis in children with X-linked hypophosphatemic rickets being treated with vitamin D and oral phosphate supplements).

This review considers a number of drug-related disorders (omitting those related to cancer therapy and neonatal intensive care) that have been the subject of original articles in the English language literature since 1984. Other iatrogenic conditions have been reviewed elsewhere [2, 3].

Skeletal Disorders

Cortical Hyperostosis After Long-Term Therapy with Prostaglandins E₁ and E₂ for Ductus-Dependent Congenital Heart Disease

Since 1975, many articles have reported the effectiveness of IV infusions of prostaglandin E₁ (PGE₁) and prostaglandin E₂ (PGE₂) in maintaining the patency of the ductus arteriosus in neonates with ductus-dependent cardiac defects until palliative or corrective surgery can be performed. Long-term treatment with PGE₁ or PGE₂ may be necessary in infants in whom growth of the pulmonary arteries must occur before surgical treatment can be undertaken. Bone changes resem-

Received May 6, 1991; accepted after revision June 20, 1991.

¹Department of Radiology (Box 45), State University of New York–Health Science Center at Brooklyn, 450 Clarkson Ave., Brooklyn, NY 11203. Address reprint requests to E. G. Kassner.

AJR 157:1039–1049, November 1991 0361–803X/91/1575–1039 © American Roentgen Ray Society

bling infantile cortical hyperostosis (Caffey disease) have been reported in a number of these infants [4, 5] (Fig. 1). Pseudowidening of the cranial sutures [6] and soft-tissue swelling [7] also have been described. (*Pseudowidening* denotes a wide, unossified zone at the suture margins that can be mistaken for splitting of the suture.) Whereas the mandible is commonly involved in Caffey disease, it is only rarely affected in prostaglandin-induced periostitis. In general, the bone changes appear after several weeks of therapy and slowly regress after therapy is discontinued, leaving no residual bony abnormality [8]. Growth is not disturbed. The mechanism of prostaglandin-induced hyperostosis appears to be a direct, dose-related stimulation of osteoblastic cells. Because prostaglandins are cleared rapidly during the first passage through the lungs, no bone changes would be anticipated in a healthy infant who received a venous infusion of PGE₁ or PGE₂. However, in infants with congenital cardiac defects associated with diminished pulmonary blood flow and right-to-left shunting, clearance of prostaglandins from the systemic circulation is impaired. The calvarial changes have been attributed to a prostaglandin E-mediated imbalance between bone deposition and bone resorption [6].

Aluminum Bone Disease

Infants and children with chronic renal failure who ingest large doses of aluminum-containing phosphate binders are particularly susceptible to aluminum intoxication (manifested by microcytic anemia and encephalopathy) and aluminum-induced musculoskeletal disease (aluminum bone disease). The latter is characterized clinically by myopathy and a poor response to vitamin D therapy and radiologically by osteopenia, nonhealing pathologic fractures, and the absence of subperiosteal resorption or other changes suggestive of hyperparathyroidism. Biochemical features include normal to elevated levels of serum calcium and relatively low levels of immunoreactive parathyroid hormone and alkaline phosphatase activity. Although the radiologic changes are nonspecific (they may be seen in osteomalacia and renal osteodystrophy due to other causes), the absence of features of hyperparathyroidism should suggest aluminum bone disease in a child with chronic renal failure. Bone biopsy reveals marked osteomalacia in the absence of osteitis fibrosa, aluminum deposition at the bone-osteoid junction, and a severe mineralization defect manifested by markedly reduced uptake of tetracycline [9, 10].

A characteristic feature of aluminum bone disease is the unusual radiologic appearance of the healing phase. In two patients reported by Andreoli et al. [10], discontinuation of aluminum hydroxide therapy was followed by calcification of the metaphyses and disappearance of the osteopenia. The metaphyseal calcification was seen first in the most recently formed osteoid in the metaphyses, leaving a radiolucent zone between newly calcified and previously calcified bone. Calcification of the epiphyses began in the periphery and proceeded centrally, transiently creating a "bone-in-bone" appearance. These radiologic findings coincided with dramatic clinical improvement and a decrease in the aluminum content

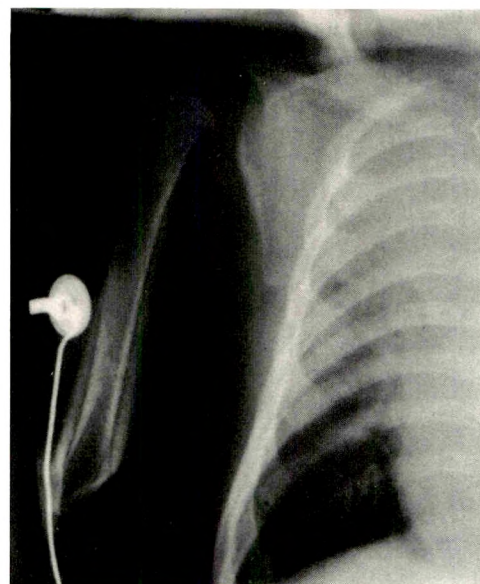


Fig. 1.—Hyperostosis associated with prostaglandin E₁ (PGE₁) therapy. Chest radiograph obtained after 2 months of IV PGE₁ therapy in neonate with ductus-dependent cyanotic congenital heart disease shows periosteal new bone cloaking ribs, humeral shafts, and scapulae. (Courtesy of J. Marquis, Newark, NJ.)

of the bone, indicating repair. Craniosynostosis requiring surgical decompression occurred in one patient, an infant who was 5 months old when radiologic signs of aluminum bone disease appeared.

Significant aluminum overload, with bone aluminum levels 10-fold greater than those of control subjects, is common in infants receiving chronic total parenteral nutrition. The sources of aluminum are primarily calcium and phosphate salts, but also heparin and albumin, in the infusate. Aluminum overload appears to be a significant factor in the osteopenia and rachitic changes that are commonly observed in these infants [11].

Deferoxamine-Induced Bone Dysplasia in Patients with Thalassemia Major

Current treatment of severe beta thalassemia (thalassemia major) consists of blood transfusions to maintain hemoglobin at acceptable levels ("hypertransfusion") and chelation to remove excessive iron stores resulting from multiple transfusions. De Virgiliis et al. [12] have reported metaphyseal abnormalities in children with thalassemia major who were undergoing combined hypertransfusion-chelation therapy. They related the bony abnormalities to the early start of chelation therapy (with deferoxamine) and theorized that a direct toxic effect of the chelating agent on growing bone or the loss of minerals other than iron, or both, might be responsible. Brill et al. [13] have recently reported a retrospective radiologic study of 27 patients with thalassemia major who were treated with hypertransfusion and who began chelation therapy with deferoxamine before the age of 7 years. Meta-

physeal irregularities and abnormal vertebral bodies were seen in two of five children in whom treatment was begun before the age of 3 years. These changes were not seen in any of the 22 children in whom treatment was begun after the age of 3 years.

Clinically, the affected patients have a short trunk with moderate sternal protrusion, genu valgum, and widening of the distal ends of the radius and ulna. A few patients have had moderate generalized joint stiffness [12]. In general, the skeletal changes resemble those of a spondylometaphyseal dysplasia; however, the findings are not identical to any of the recognized genetic dysplasias. The radiologic findings include flattening of the thoracic and lumbar vertebral bodies (Fig. 2), circumferential metaphyseal osseous defects, short zones of provisional calcification, and widened growth plates. The evolution of the metaphyseal changes has been described in detail by de Virgiliis et al. [12]. The metaphyseal abnormalities typically begin at 2–4 years of age and are progressive. Initially, the affected metaphyses appear concave and widened, but the metaphyseal line is intact; later the metaphyses become cupped (Fig. 3A). Eventually the metaphyseal line becomes irregular and thickened, and the metaphyseal margin becomes frayed (Fig. 3B). Later, small cavities surrounded by a border of osteosclerotic tissue appear. With time, the sclerosis becomes more pronounced, and longitudinal striations appear; in some patients, the metaphyseal zone is irregular, containing cystic foci with sclerotic margins and linear streaks of osteosclerosis (Fig. 3C). A valgus deformity develops in some patients with involvement of the proximal tibial metaphysis (Fig. 3D). Radiologic evidence of healing may be seen after the dose of deferoxamine is decreased [13].

A relationship between the dose of deferoxamine, the age of the patient, and the severity of the radiologic abnormality has not been established. More data are needed to determine if the skeletal abnormalities are related to chelation-induced deficiencies of trace metals such as zinc or copper. To decrease the risk of dysplastic bone growth, de Virgiliis et al. [12] recommend that chelation therapy be delayed until the patient is older than 3 years and has received 20 to 30 blood transfusions, as evidenced by a serum ferritin level of 800–1000 ng/ml.

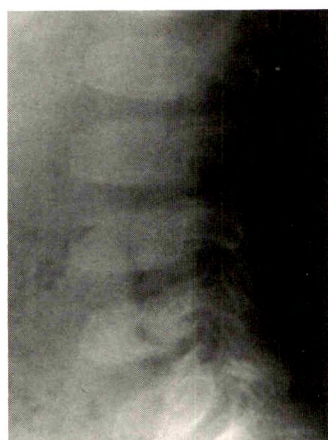


Fig. 2. — Deferoxamine-induced bone dysplasia in a 7-year-old boy with thalassemia major who had been on combined transfusion-chelation therapy for 5 years and had received a total of 48 units of RBCs. Serum ferritin level was 4068 ng/ml. Lateral radiograph of lumbar spine shows flattening of vertebral bodies. Metaphyseal irregularities were present in long bones (not shown). (Reprinted from Brill et al. [13].)

Gastrointestinal Disorders

Hemorrhagic Pancreatitis Caused by Valproic Acid

Hemorrhagic pancreatitis, a frequently lethal disorder, has been reported in a small number of children receiving valproic acid therapy for seizure disorders. Valproic acid-related hemorrhagic pancreatitis is usually associated with long-term administration of the drug but can occur as early as 1 week after the onset of therapy. This complication, which is not dose related, should be considered when severe abdominal pain, nausea, and vomiting develop in a patient receiving the drug. Sonography, which can be performed at the bedside in these critically ill patients, can help establish the diagnosis. As in other forms of hemorrhagic pancreatitis, sonograms show pancreatic enlargement, diffusely increased pancreatic echogenicity with superimposed brighter focal areas, and ascites [14] (Fig. 4). Complications such as pseudocysts, abscesses, and other fluid collections are readily detected by serial sonograms [14].

Reversible Ceftriaxone-Associated Biliary Sludge ("Biliary Pseudolithiasis")

Shaad et al. [15] have reported transient biliary concretions in 16 (43%) of 37 severely ill children being treated with high doses of ceftriaxone, an antibiotic with high antimicrobial activity and a long half-life (which allows once-daily treatment even in severe infections). Gallbladder sonography showed multiple mobile, strikingly hyperechoic concretions with acoustic shadowing—a finding the authors termed biliary pseudolithiasis. In one patient, multiple obstructing urinary calculi developed also. Three (19%) of 16 patients with gallbladder concretions had unequivocal biliary symptoms (colicky upper abdominal pain, nausea, vomiting) that subsided a few days after ceftriaxone treatment was discontinued. Biliary pseudocalculi were demonstrated sonographically after 4–22 days (mean, 9 days) of treatment and had completely resolved 2–63 days (mean, 15 days) after ceftriaxone was stopped.

Ceftriaxone-related biliary pseudolithiasis can be regarded as a form of biliary sludge with atypical sonographic features. Unlike typical gallbladder "sludge"—which is characterized sonographically by low-amplitude echoes within the lumen, layering in the most dependent part of the organ, and absence of acoustic shadowing—ceftriaxone-associated sludge gives rise to high-amplitude echoes and prominent acoustic shadows, an appearance similar to that of gallstones [16]. Lee et al. [16] examined cholecystectomy specimens from four ceftriaxone-treated patients who were believed to have gallstones on the basis of sonographic examination. Each specimen contained sediments with fine granules measuring 20–250 μm ; no structures resembling a macroscopic concretion or stone were found. Chemical analysis of the gallbladder sediments in adult patients with typical sonographic findings has revealed small amounts of cholesterol and bilirubinate, a trace of ceftriaxone, and a high content of various calcium salts [15].

Fully reversible biliary pseudolithiasis with no laboratory evidence of hepatic or pancreatic damage is probably of no consequence in children who have a normal gallbladder, biliary

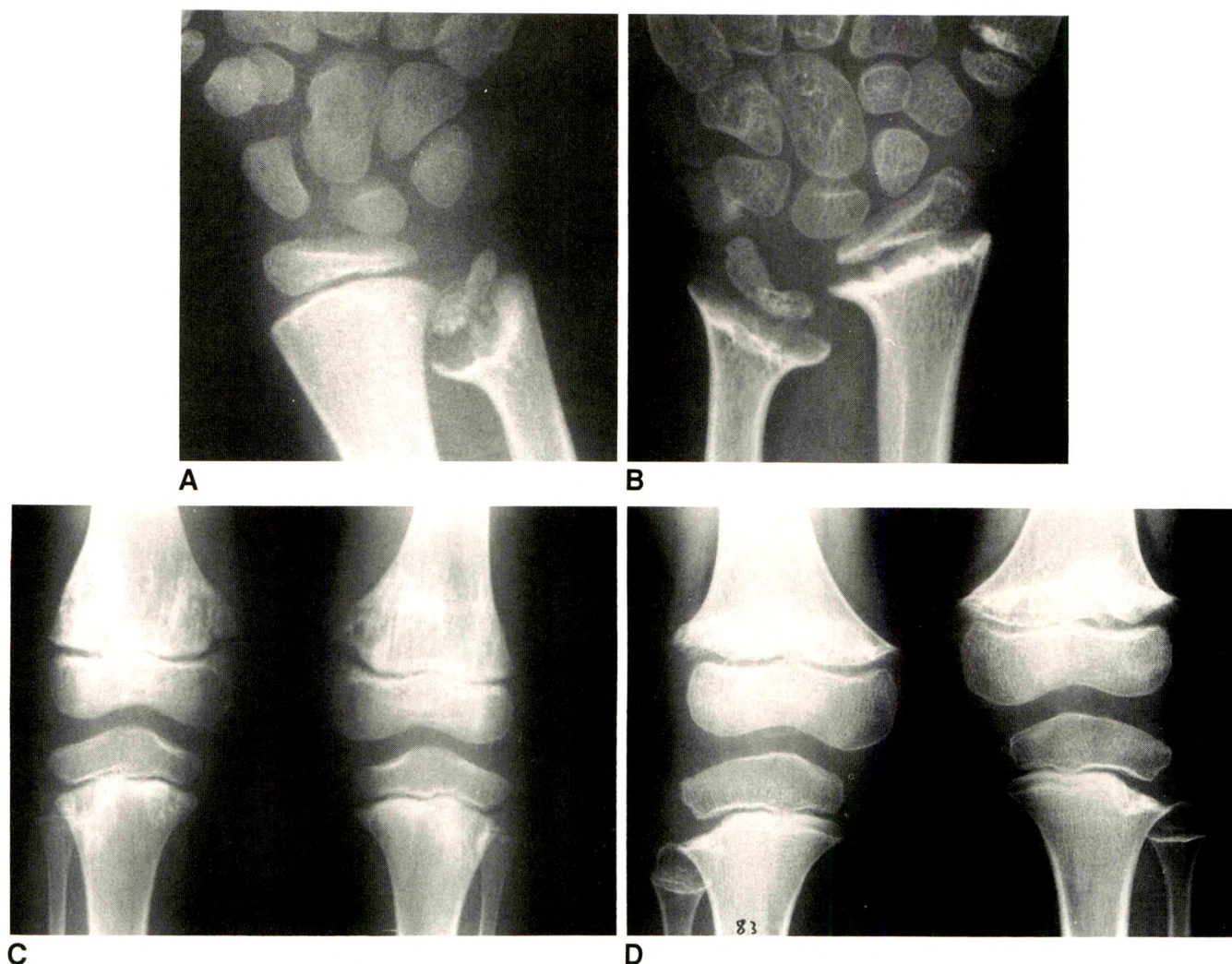


Fig. 3.—Deferoxamine-induced bone dysplasia associated with combined transfusion-chelation therapy for thalassemia major.
 A, Radiograph of wrist in 5-year-old child shows early ricketslike lesions in distal ulna; distal metaphysis is widened, cupped, irregularly mineralized, and frayed. Distal metaphysis of radius is normal.
 B, Radiograph of wrist in 6-year-old child shows advanced lesions in distal radius and ulna. Metaphyseal line is widened and thickened.
 C, Radiograph of knees in 7-year-old child shows symmetric longitudinal striations and cystic areas margined by sclerotic bone in distal femurs and proximal tibias.
 D, Radiograph of knees in 5-year-old child shows symmetric deformity of lateral portions of proximal tibial metaphyses. Proximal ends of fibulas are widened and cupped. Metaphyseal line of femur is irregular and thickened. There is a mild genu valgum deformity.
 (Reprinted with permission from de Virgiliis et al. [12].)

tract, liver, and pancreas. However, it may be clinically important in patients with preexisting disease. Schaad et al. [15] recommend that such patients have serial abdominal sonograms when they are receiving ceftriaxone; that any patient on ceftriaxone therapy in whom colicky abdominal pain develops have abdominal sonography and appropriate laboratory tests; and that a change in antibiotic therapy be considered if biliary pseudocalculi are demonstrated.

Medication Bezoars in Patients Undergoing Dialysis for Chronic Renal Failure

Formation of bezoars is an unusual but well-documented complication in patients who receive antacids to control the

hyperphosphatemia associated with renal failure. Aluminum hydroxide gels have been responsible for nearly all reported cases of antacid-induced medication bezoars in children [17]. In addition, aluminum, which is absorbed in significant amounts from the gut, accumulates in patients with renal failure and can cause anemia and severe bone and CNS disease, particularly in children. In order to avoid this complication, high-dose calcium carbonate, which has been shown to be an effective phosphate binder, is now considered the agent of choice in children with chronic renal insufficiency who are unable to tolerate a low-phosphate diet. Fildes et al. [18] described a 5-year-old child on long-term calcium carbonate therapy who had bowel obstruction caused by a bezoar in the transverse colon that was the leading point of

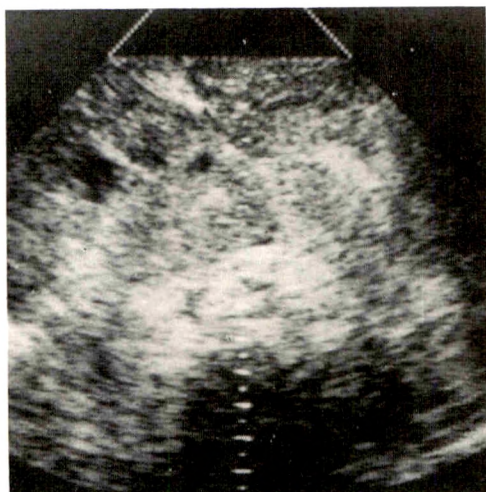


Fig. 4.—Hemorrhagic pancreatitis caused by valproic acid in a 4.5-year-old boy. Abdominal sonogram shows diffuse pancreatic enlargement with overall increased echogenicity and focal areas of brighter echogenicity. Other images showed generalized bowel distension and ascitic fluid. Repeat sonogram on hospital day 19 (not shown) showed a large pseudocyst. (Reprinted with permission from Rosenberg and Ortega [14].)

a cecocolic intussusception. Crystallographic analysis showed that the bezoar consisted of layers of proteinaceous material and pure calcium phosphate. It is hoped that the problem of antacid-induced bezoars can be eliminated by using alternative phosphate-binding regimens that are currently under investigation (e.g., aluminum-free phosphate-binding compounds and magnesium carbonate combined with magnesium-free dialysate to prevent accumulation of toxic amounts).

Medication-Induced Esophagitis

During the past decade, an increasing number of cases of medication-induced focal esophagitis in children have been reported. A great many drugs, including antibiotics, nonsteroidal antiinflammatory agents, multivitamins, digoxin, potassium chloride, theophylline, cromolyn inhalant, ferrous sulfate, ascorbic acid, and carbachol, are known to cause focal esophagitis in adults. Several agents (doxycycline, sulfonamides [trimethoprim, sulfamethoxazole], aspirin, quinidine, emetopium bromide) have been implicated in both children and adults. Over-the-counter Eucalyptus oil/menthol cough tablets have recently been added to the list of agents known to cause focal esophagitis in children [19]. The pathogenetic mechanism varies with the causative agent. Doxycycline produces a highly acidic solution when dissolved, which may cause local ulceration. Ferrous sulfate produces a hyperosmolar solution that can damage squamous mucosa by tissue desiccation. The mechanisms by which theophylline, nonsteroidal antiinflammatory drugs, and certain antibiotics injure the esophageal mucosa are unknown. Predisposing factors include the patient's ingesting the pills or tablets while supine or with an inadequate amount of liquid.

Patients with medication-induced esophageal ulceration

typically have odynophagia (often severe and of sudden onset), retrosternal chest pain, and dysphagia. Double-contrast esophagography is more reliable than single-contrast esophagography in detecting the lesions, which usually occur at areas of physiologic delay in the mid esophagus (i.e., the aortic arch and left atrium). Double-contrast studies typically show a cluster of discrete, superficial ulcers, sometimes surrounded by a zone of edema, in an otherwise normal esophagus; linear ulceration also may be present [20]. The radiologic differential diagnosis includes infections with opportunistic organisms such as *Candida* and herpesvirus and erosive or ulcerative esophagitis associated with gastroesophageal reflux [21]. Optimal double-contrast technique generally obviates esophagography in adults; however, this may not be feasible in young children, in which event esophagoscopy may be necessary for definitive diagnosis. Esophageal perforation and stricture formation are infrequent sequelae of medication-induced esophageal ulceration.

Xanthine-Related Gastroesophageal Reflux

Because of their potency as CNS stimulants, xanthine derivatives frequently are given to infants with evidence of "infant apnea" or a history of a "near miss" sudden infant death syndrome (SIDS) episode. Theophylline and caffeine decrease lower esophageal sphincter pressure, which in turn may increase gastroesophageal reflux and the consequent risk of aspiration and respiratory problems. In one study of infants at risk for SIDS who were receiving theophylline or caffeine, 24-hr pH monitoring showed a significantly increased number of episodes of gastroesophageal reflux and a marked increase in the total reflux time [22]. Because gastroesophageal reflux is a recognized risk factor for SIDS, the authors recommend that xanthines be administered with caution to infants at risk for SIDS who have not been screened for gastroesophageal reflux.

Renal Disorders

Renal Papillary Necrosis Caused by Nonsteroidal Antiinflammatory Drugs

Renal papillary necrosis, with typical urographic findings, has been reported in a small number of children with various types of chronic arthritis who were being treated with nonsteroidal antiinflammatory drugs (NSAIDs), a class of drugs that includes aspirin, ibuprofen, tolmetin, indomethacin, and acetaminophen. Several children also had ingested over-the-counter acetaminophen preparations intermittently. The wide range of drugs that have been implicated suggests that their common pharmacologic effect (inhibition of prostaglandin synthesis) might be the underlying pathogenic process. NSAID-related papillary necrosis was initially described by Wortmann et al. [23] in three severely disabled children with juvenile rheumatoid arthritis, leading the authors to speculate that dehydration might have been an important contributory factor. However, NSAID-related renal papillary necrosis has since been documented in six ambulatory children whose functional

disability ranged from mild to none [24, 25]. Allen et al. [24] advise that children receiving long-term NSAID therapy should have regular urinalysis and be counseled about the use of nonprescribed preparations. They recommend that excretory urography be performed in children with persistent hematuria, and that the study be repeated in a few months if the urogram is normal and the hematuria persists.

Other renal complications of NSAID therapy (e.g., renal insufficiency or acute renal failure, interstitial nephritis, nephrotic syndrome, water retention, sodium retention, and hyperkalemia) are less common in children than in adults [25].

Nephrocalcinosis Associated with Treatment of X-linked Hypophosphatemic Rickets

The clinical manifestations of X-linked hypophosphatemic rickets—metabolic bone disease and short stature—can be attributed to defective renal resorption of phosphate and impaired renal synthesis of 1,25(OH)₂D (dihydroxyvitamin D). The goal of therapy is to optimize the local conditions for mineralization by providing oral phosphate supplements together with a metabolically active form of vitamin D (chronic combination therapy) until the patient has achieved adult height. However, therapy does not repair the underlying renal pathophysiologic changes and occasionally may lead to significant complications. For example, excessive oral phosphate supplementation stimulates secretion of parathyroid hormone and, if prolonged, may lead to tertiary hyperparathyroidism necessitating parathyroidectomy. On the other hand, excessive administration of phosphate can lead to hyperabsorption of dietary calcium with consequent hypercalciuria and hypercalcemia; the latter can cause medullary nephrocalcinosis. Goodyer et al. [26] found sonographic evidence of medullary nephrocalcinosis (markedly increased echogenicity of the renal pyramids without acoustic shadowing) in 11 (48%) of 23 patients with X-linked hypophosphatemic rickets receiving chronic combination therapy. They concluded that medullary nephrocalcinosis was not an inherent feature of untreated disease.

Jequier et al. [27] observed three abnormal sonographic patterns in patients with chronic combination therapy-related nephrocalcinosis: pattern 1 comprised homogeneously echodense renal pyramids with normal renal cortex (Fig. 5); pattern 2 comprised inhomogeneously dense renal pyramids with normal renal cortex (in some instances, a "doughnut" pattern was produced by an echodense rim surrounding the anechoic tip of each renal pyramid); and pattern 3 comprised echodense renal pyramids with echodense cortex. They concluded that patterns 1 and 2 reflected "pure" medullary nephrocalcinosis (pattern 2 could be an early or mild form of pattern 1). Pattern 3, which was observed in patients with documented secondary hyperparathyroidism and a history of repeated episodes of vitamin D intoxication, was thought to represent more complex disease. Patients with abnormal renal sonograms were usually those receiving higher doses of vitamin D and phosphate; none had pain or microscopic hematuria [26]. Sonography is clearly the method of choice for detecting iatrogenic medullary nephrocalcinosis: plain films were normal

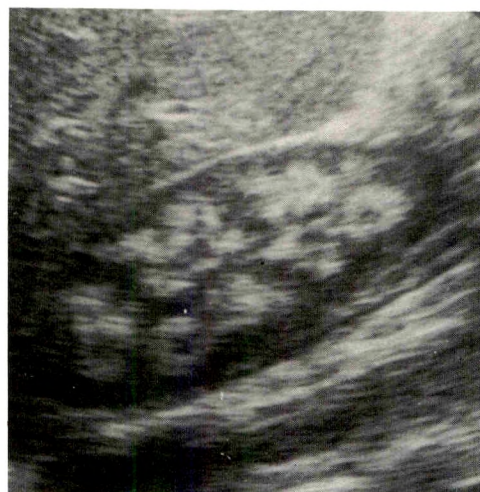


Fig. 5.—Nephrocalcinosis associated with treatment of X-linked phosphatemic rickets in a 3-year-old child. Sonogram of right kidney obtained after several months of combined therapy shows markedly echogenic renal pyramids. Similar changes were present in left kidney. Laboratory studies revealed mild hypercalcemia and hyperphosphatemia. Renal function test results were normal.

in all of the patients with sonographic evidence of medullary nephrocalcinosis. Faint medullary calcifications were detected by CT in only one patient.

The clinical significance of patterns 1 and 2 is unclear. In experimental models of renal failure, medullary nephrocalcinosis appears to be an important contributor to progressive renal damage and loss of glomerular filtration rate. However, none of the patients reported by Goodyer et al. [26] had laboratory evidence of impaired renal function (e.g., elevated levels of serum creatinine or significant impairment of urinary concentrating ability); renal biopsies were not performed. Alon et al. [28] reported two patients with chronic combination therapy-related medullary nephrocalcinosis in whom renal biopsies showed evidence of significant renal damage (interstitial nephritis, glomerulosclerosis). Until the natural history of this disorder is fully known, it seems prudent to perform renal sonography at regular intervals in all patients with X-linked hypophosphatemic rickets who are having chronic combination therapy, and to closely monitor renal function in those whose sonograms show evidence of medullary nephrocalcinosis.

Cardiopulmonary Disorders

Congestive Heart Failure After Chicken Soup Rehydration for Gastroenteritis

Gastroenteritis is a common disease in infants and children and is usually adequately treated on an outpatient basis. Many "at-home" therapeutic regimens used for infants with mild dehydration from gastroenteritis employ a variety of clear liquids, including chicken soup and chicken soup broth. However, because of its high concentration of sodium, chicken soup is potentially dangerous when used as a rehydrating

solution. Indeed, the sodium concentration of several national brands of clear chicken soup or broth ranges from 152 to 183 mEq/l, which exceeds the sodium concentration (90 mEq/l) of the rehydrating solution recommended by the World Health Organization (WHO) for oral rehydration of infants with gastroenteritis in developing countries. Oral rehydration therapy with the WHO solution, which has been associated with such complications as hypernatremia and periorbital and peripheral edema when used improperly, requires close supervision by a physician or other trained personnel, and is preferably carried out in a health care facility.

Garland et al. [29] have reported an unusual complication of poorly supervised replacement therapy with chicken soup. Their patient, a 2-month-old infant with gastroenteritis, had clinical and radiologic evidence of congestive heart failure (hepatomegaly, tachypnea, gallop rhythm, pitting edema, pulmonary edema) after receiving nearly a liter of a national brand of chicken soup and "large volumes" of water over a 16-hr period. The parents had been instructed to administer clear fluids, including chicken soup, in unspecified amounts. The authors estimate that the infant received 180 mEq of sodium—more than five times the amount required to rehydrate an infant of similar size with 5% isonatremic dehydration—over a 24-hr span. (Even if the infant had been severely [10%] dehydrated at the time rehydration therapy was begun, he should have received only 70 mEq of sodium over a 24-hr span.) The authors conclude that the chicken soup overdose, augmented by the large volume of water administered ad libitum, led to a combined salt/fluid overload resulting in transient congestive heart failure.

Lipoid Pneumonia

Lipoid pneumonia in children, first described in the 1920s as a complication of aspiration of mineral or cod liver oil, is still occasionally encountered in special circumstances. Wolfson et al. [30] recently reported a case of an infant with gastroesophageal reflux in whom biopsy-proved lipoid pneumonia developed while he was receiving medium-chain triglyceride oil mixed in formula via a nasogastric tube. Serial chest films showed progressive consolidation of the lungs with a diffuse alveolar pattern. Because of the nonspecificity and variability of the radiologic findings, the differential diagnosis is extensive. The findings on bronchial lavage are nonspecific; lipid-laden macrophages, once thought to be specific for lipoid pneumonia, also can be found in bronchial washings without clinical or radiologic evidence of pneumonia. Lung biopsy may be needed to exclude an opportunistic infection or other unsuspected process in a debilitated patient.

Whereas lipoid pneumonia in adults (usually associated with the long-term use of mineral oil-based medications) generally produces mild symptoms and only rarely progresses to respiratory failure, lipoid pneumonia in young children can be fatal. De Oliveira et al. [31] reported four Brazilian children less than 2 years old in whom severe lipoid pneumonia developed while they were receiving mineral oil via a nasogastric tube for treatment of partial small bowel obstruction by *Ascaris lumbricoides*. (In this technique, the stomach is

emptied by nasogastric tube and 20 ml of mineral oil is given every 2 hr. The tube is clamped for 30 min after each administration, and then opened to allow gravity drainage until the next dose is given. This sequence is repeated until oil is evacuated and the palpable abdominal masses disappear.) Progressive respiratory failure developed in three children, and two died. Whereas chest films of adults with chronic lipoid pneumonia typically show localized disease, which can simulate bronchogenic carcinoma, the chest films of these patients showed diffuse alveolar disease of rapid onset, with blurred margins, air bronchograms, coalescence, and "bat's-wing" distribution of infiltrates. Microscopic examination revealed evidence of both alveolar and interstitial involvement; free and phagocytosed fat droplets were seen in both the alveolar lumen and the interstitium. The dramatic clinical and radiologic findings probably reflect massive aspiration, possibly accompanied by simultaneous aspiration of gastric contents. In one child with chronic lung lesions, CT revealed an area of consolidated lung with negative Hounsfield numbers, a finding that is believed to be pathognomonic of this disorder.

CNS Disorders

Fatal Cerebral Edema During Treatment of Diabetic Ketoacidemia: An Iatrogenic Disorder?

Children with severe diabetic ketoacidemia (DKA) are known to be at risk for brain herniation associated with cerebral edema during the first 24 hr of treatment. Although the true prevalence of clinically apparent cerebral edema is unknown, it is believed to occur in as many as 2% of children with severe DKA (Fiordalisi I, personal communication). The clinical onset is typically abrupt, unheralded by warning signs or predictive indicators. Neurologic symptoms (abrupt changes of mental status, abnormal neurologic signs, rapid progression to coma) appear 6–10 hr after therapy has begun, at a time when severe acidosis has been partially corrected, the blood glucose level is falling, adequate circulation has been restored, and all indications suggest that the patient is recovering satisfactorily. Respiratory arrest may occur in association with brainstem herniation [32]. CT shows generalized brain swelling (small ventricles and obliteration of the subarachnoid space around the quadrigeminal plate and the quadrigeminal cistern) [33] and the classic signs of brain herniation. Hemorrhagic infarction of the basal ganglia, internal capsules, thalami, and lentiform nuclei has been shown by CT in survivors, who manifest persistent deficits in corticospinal and higher cognitive functions [34].

Although it has been difficult to implicate any single therapeutic maneuver as the causative factor in DKA-associated cerebral edema [35, 36], evidence is increasing that iatrogenic factors play an important role [37, 38]. DKA is a hypertonic state. Traditional therapeutic regimens aim to repair the deficit as quickly as possible with insulin and large volumes of hypotonic fluid (usually administered IV). Such treatment appears to favor a rapid shift of water across the blood-brain barrier. (Increased cerebral blood flow may also occur.) Although evidence of brain swelling, manifested by decreased

ventricular size on CT, is commonly seen before treatment is begun in asymptomatic children (subclinical cerebral edema) [33], fatal brain herniation is exceedingly rare in untreated patients. Harris et al. [38] concluded that traditional therapy—excessive rates of fluid administration, in particular—can cause *de novo* brain swelling and/or exacerbate preexisting brain swelling in susceptible patients (Fig. 6). Inappropriate regulation of plasma vasopressin levels, common in patients with DKA, may play an important role. Excessive plasma vasopressin concentrations enhance retention of free water and aggravate hyponatremia, leading to the movement of free water from the relatively hypotonic intravascular space into the relatively hypertonic brain tissues; Duck and Wyatt [37] theorized that such fluid shifts can exacerbate the cerebral edema that is already present as a result of other biochemical forces in patients with DKA, triggering fatal brainstem herniation. Another factor that may contribute to increased intracranial pressure in this setting is excessive elevation of the central venous pressure caused by a rapid increase in blood volume. It remains to be seen whether gradual correction of the metabolic aberrations, as recommended by Duck and Wyatt [37] and Harris et al. [38], can avoid life-threatening cerebral edema in patients with DKA.

Coma at any stage of treatment for DKA should be regarded as evidence of life-threatening cerebral edema until proved otherwise [35]; immediate mannitol therapy can be life-saving in such cases [37].

Cerebral Vasculitis Caused by Phenylpropanolamine

Nonprescription drugs are not without risk. Cerebral vasculitis and brain hemorrhage have been reported in adult patients taking phenylpropanolamine, a synthetic sympathomimetic drug available in small dosages in cough and cold medicines and in larger dosages in diet pills. Phenylpropanolamine-related cerebral vasculitis typically occurs in young women, usually at dosages that are within the manufacturer's

recommended therapeutic range (50–75 mg). It is not clear whether the vascular lesions represent a necrotizing vasculitis, a vasospastic phenomenon, or a combination of the two. Forman et al. [39] reported the first pediatric case of this entity (Fig. 7), and speculate that unrecognized use of diet aids may account for some of the unexplained strokes and subarachnoid hemorrhages that many children suffer each year.

Multisystemic Disorders

Complications of Amiodarone Therapy

Amiodarone, a benzofuran derivative initially used in the treatment of angina pectoris, has been shown to be effective in the management of supraventricular tachyarrhythmias, including those associated with the Wolff-Parkinson-White syndrome, and is being used with increasing frequency in infants and children. Although the drug appears to be less cardiotoxic than most other antiarrhythmic agents, it has been associated with a number of noncardiac adverse effects, including pulmonary fibrosis, hypothyroidism, hyperthyroidism, neurologic disturbances, and hepatic toxic effects. In adults, gallium scintigraphy can detect amiodarone-related toxic pulmonary effects and is useful in differentiating toxic lung injury from pulmonary edema [40]. Severe, potentially life-threatening adverse effects of this drug (e.g., pulmonary fibrosis) have been less common in children than in adults, a phenomenon that has been attributed to the relatively rapid metabolism of the drug in the former, presumably resulting in less tissue accumulation of the drug. However, a fatal Reye-like syndrome (vomiting, encephalopathy, severe hepatic failure without jaundice) developed in a child receiving amiodarone for Wolff-Parkinson-White syndrome [41]. Fatty changes characteristic of Reye syndrome were not evident on liver biopsy, leading the authors to conclude that the hepatic failure and encephalopathy in this patient were induced by amiodarone.

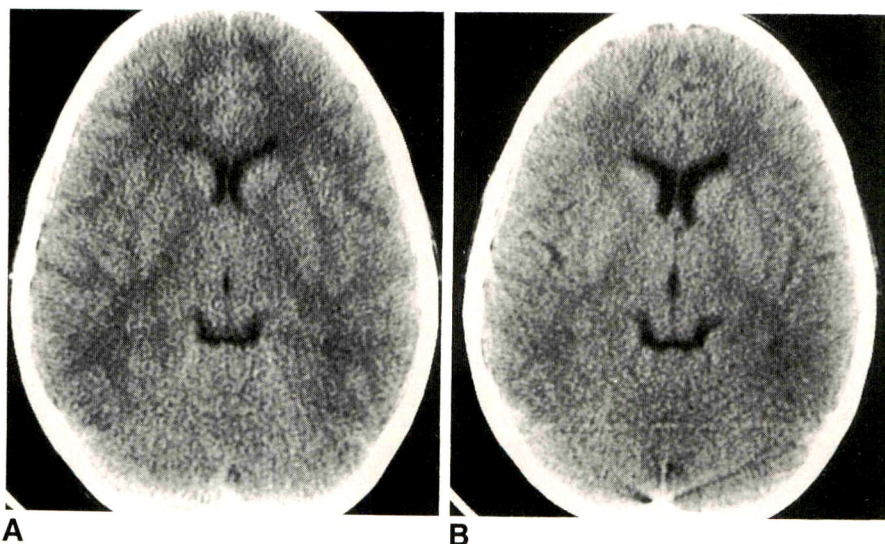


Fig. 6.—Cerebral edema during treatment of diabetic ketoacidosis. A 9-year-old boy had severe diabetic ketoacidosis (pH of 6.9, carbon dioxide tension of 3 mm Hg, and serum glucose of 855 mg/dl), severe dehydration, and extreme lethargy (irritable when stimulated).

A, Initial CT scan (9 hr after hospitalization) shows lateral ventricles are slightly smaller than normal.

B, CT scan obtained on hospital day 3, after slow correction of metabolic deficits with solutions of greater tonicity than are used traditionally, shows increased size of lateral ventricles. Patient made an uneventful recovery. (Courtesy of G. D. Harris and A. Brody, Buffalo, NY.)

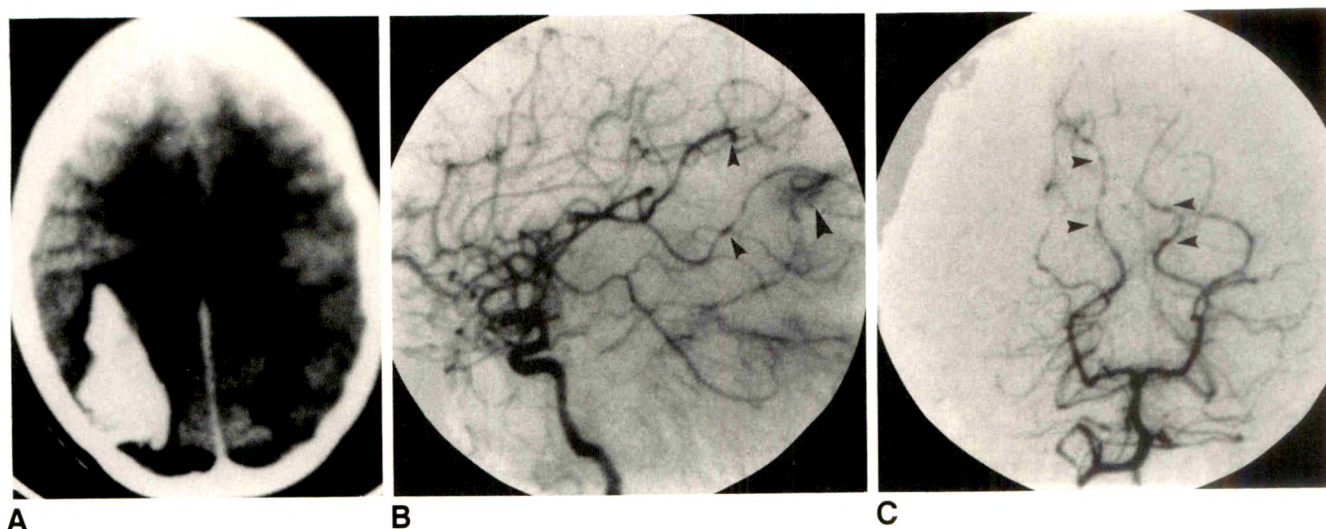


Fig. 7.—Cerebral vasculitis caused by phenylpropanolamine. This slightly obese 17-year-old girl had severe frontal headaches of abrupt onset associated with nausea, lethargy, and vomiting about 3–5 hr after ingesting five nonprescription diet pills containing 75 mg of propanolamine per tablet in a suicide gesture. Neurologic examination revealed blurry disk margins and minimal nuchal rigidity.

A, Unenhanced CT scan shows a large right-sided parietooccipital hematoma with a right-to-left midline shift. Patient's condition worsened until she was responding only to deep pain.

B, Right internal carotid intraarterial digital subtraction angiogram shows a stain (large arrowhead) corresponding to region of right cerebral hematoma and stenotic segments and beading in branches of right angular artery (small arrowheads).

C, Right vertebral intraarterial digital subtraction angiogram shows beading of branches of both posterior cerebral arteries (arrowheads).

(Reprinted with permission from Forman et al. [39].)

Amiodarone has a chemical structure similar to L-thyroxine (T_4) and contains 37% organic iodine by weight. Because of its high iodine content—400 mg of amiodarone contains 150 mg of iodine, equivalent to 24 drops of Lugol's solution—it can cause either hypo- or hyperthyroidism in certain susceptible persons. Amiodarone also acts as a competitive inhibitor of the enzyme that catalyzes the conversion of T_4 to triiodothyronine (T_3) and the conversion of the inactive reverse T_3 to 3,3'-diiodothyronine (T_2). Costigan et al. [42] found clinical and biochemical evidence of hypothyroidism in five (20%) of 20 children and teenagers being treated with amiodarone for various arrhythmias. A sixth patient had persistent hyperthyroxinemia without clinical evidence of hyperthyroidism. Interference with normal thyroid hormone homeostasis can profoundly affect young children during critical stages of brain and somatic development. Costigan et al. [42] urge careful follow-up of children on long-term amiodarone therapy to detect laboratory evidence of thyroid decompensation before clinical symptoms appear. Early diagnosis is particularly important in children younger than 1 year who are undergoing rapid brain growth and therefore are at greatest risk for the development of cerebral cortical deficiency of T_3 while receiving amiodarone.

Miscellaneous Drug-Related Phenomena

Subcutaneous Gas from Hydrogen Peroxide Administered Under Pressure

Hydrogen peroxide (usually as a 3.0% or 1.5% solution) is commonly used to irrigate dirty wounds. When hydrogen peroxide is administered under pressure (e.g., by using a

hydrogen peroxide-filled syringe to irrigate the wound), oxygen liberated in the wound and subsequently dissecting through the soft tissues can be mistaken clinically and on radiographs for an infection caused by a gas-forming organism. Schneider and Hebert [43] have reported this phenomenon in two children. In one patient, a 3-year-old child with a laceration of the forearm, plain films of the arm showed extensive subcutaneous emphysema, and a chest radiograph showed gas in the soft tissues of the lateral chest wall.

CT Demonstration of Hyperdense Cerebral Vasculature Caused by Bromide Therapy

Although the vein of Galen and the venous sinuses are often seen on unenhanced CT, the major cerebral arteries are visualized only occasionally. The visualization of major cerebral arteries is associated with various pathologic states, including encephalomalacia and cerebral edema (in which the attenuation of the adjacent brain is reduced), calcification of senescent or atherosclerotic plaque, arterial emboli, arterial thrombosis, calcification or thrombosis of a vascular malformation or aneurysm, and polycythemia; normal cerebral arteries can be visualized in subjects with unusually wide subarachnoid cisterns. Although bromides are used infrequently in the treatment of childhood epilepsy, their use is associated with enhanced visualization of the cerebral arteries, which can be a source of confusion. A 16-month-old girl who was taking tribromide elixir for a seizure disorder had markedly increased attenuation (70–75 H) of the middle cerebral arteries and their major branches on an unenhanced CT scan. Her blood bromide level was 258 mg/dl, well above the recom-

mended therapeutic range (80–120 mg/dl). A sample of whole blood containing 240 mg of bromide/dl had a similar CT attenuation number [44].

Drugs Causing Increased Attenuation of the Liver on CT

Increased attenuation of the liver is commonly observed in children receiving amiodarone, an antiarrhythmic drug that contains 37% iodine by weight [45] and *cis*-diaminedichloro platinum II, an antineoplastic drug used for a broad spectrum of malignant neoplastic disorders [46]. This phenomenon is of no clinical significance.

Tracheal and Bronchial Calcification Associated with Warfarin

Long-term anticoagulant therapy is necessary in the post-operative care of children with prosthetic cardiac valves. Taybi and Capitanio [47] noted asymptomatic tracheal and tracheobronchial calcification in three of 18 children and teenagers who had been taking warfarin sodium (Coumadin, DuPont Pharmaceuticals, Wilmington, DE) for several years after cardiac valve replacement (Fig. 8). One patient, a 9-year-old girl, also had costochondral calcification, a very unusual phenomenon at this age. A review of the literature uncovered three additional cases of warfarin-related tracheal or tracheobronchial calcification. The cause of the calcification is unknown. Noting that laryngeal and tracheobronchial calcification occur in warfarin embryopathy, the authors theorize that warfarin sodium may have an effect on the cartilaginous tissues of children.

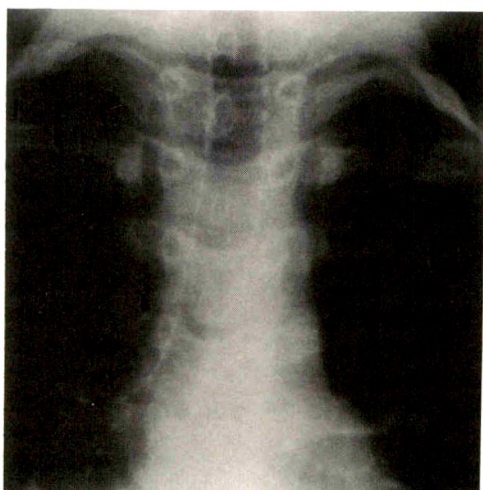


Fig. 8.—Tracheal and bronchial calcification associated with warfarin therapy in an 11-year-old girl who had mitral valve replacement when she was 5 years old. Chest radiograph shows calcification in wall of trachea and main bronchi. Calcifications were first noted when the patient was 8 years old, 3 years after start of warfarin therapy, and had progressively increased. There were no respiratory symptoms. (Reprinted with permission from Taybi and Capitanio [47].)

ACKNOWLEDGMENTS

I thank Irma Fiordalisi and Glenn Harris for sharing their unpublished material on cerebral edema in children being treated for diabetic ketoacidemia and for their helpful comments.

REFERENCES

1. Mitchell AA, Lacoutre PG, Sheehan JE, Kauffman RE, Shapiro S. Adverse drug reactions in children leading to hospital admission. *Pediatrics* 1988;82:24–29
2. Ansell G. *Radiology of adverse drug reactions and toxic hazards*. Rockville, MD: Aspen, 1985
3. Pathak A, Bernstein RM, Kassner EG. Complications of drugs, nutritional therapy, and immunizations. In: Kassner EG, ed. *Iatrogenic disorders of the fetus, infant, and child*. New York: Springer-Verlag, 1985:275–338
4. Ueda K, Saito A, Nakano H, et al. Cortical hyperostosis following long-term administration of prostaglandin E₁ in infants with cyanotic congenital heart disease. *J Pediatr* 1980;97:834–836
5. Ringel RE, Brenner JI, Haney PJ, Burns JE, Moulton AL, Berman MA. Prostaglandin-induced periostitis: a complication of long-term PGE₁ infusion in an infant with congenital heart disease. *Radiology* 1982;142:657–658
6. Hoevels-Guerich H, Haferkorn L, Persigehl M. Widening of cranial sutures after long-term prostaglandin E₂ infusion in two newborn infants. *J Pediatr* 1984;105:72–74
7. Jureidini SB, Chase NA, Albert BS, Vanderzalm T, Sheneflet RE. Soft-tissue swelling in two neonates during prostaglandin E₁ therapy. *Pediatr Cardiol* 1986;7:157–160
8. Host A, Halken S, Andersen PE Jr. Reversibility of cortical hyperostosis following long-term prostaglandin E₁ therapy in infants with ductus-dependent congenital heart disease. *Pediatr Radiol* 1988;18:149–153
9. Andreoli SP, Smith JA, Bergstein JM. Aluminum bone disease in children: radiographic features from diagnosis to resolution. *Radiology* 1985;156:663–667
10. Andreoli SP, Smith JA, Bergstein JM. Reply to letter from Daves MD: Aluminum bone disease in children: radiographic features from diagnosis to resolution. *Radiology* 1986;156:283–284
11. Klein GL, Snodgrass WR, Griffin MP, Miller NL, Alfrey AC. Hypocalcemia complicating deferoxamine therapy in an infant with parenteral nutrition-associated aluminum overload: evidence for a role of aluminum in the bone disease of infants. *J Pediatr Gastroenterol Nutr* 1989;9:400–403
12. De Virgiliis S, Congia M, Frau F, et al. Deferoxamine-induced growth retardation in patients with thalassemia major. *J Pediatr* 1988;113:661–669
13. Brill PW, Winchester P, Giardina PJ, Cunningham-Rundles S. Deferoxamine-induced bone dysplasia in patients with thalassemia major. *AJR* 1991;156:561–565
14. Rosenberg HK, Ortega W. Hemorrhagic pancreatitis in a young child following valproic acid therapy. *Clin Pediatr (Phila)* 1987;26:98–101
15. Schaad UB, Wedgwood-Krucko J, Tschaeppeler H. Reversible ceftriaxone-associated biliary pseudo-lithiasis in children. *Lancet* 1988;2:1411–1413
16. Lee SP, Lipsky BA, Teefey SA. Gallbladder sludge and antibiotics. *Pediatr Infect Dis J* 1990;9:422–423
17. Hurley JK. Bowel obstruction occurring in a child during treatment with aluminum hydroxide gel. *J Pediatr* 1978;92:592–593
18. Fildes RD, Springate JE, Jewett T, O'Shea MM, Feld LG. Colonic intussusception secondary to a calcium phosphate bezoar in a child receiving calcium carbonate for hyperphosphatemia. *J Pediatr Surg* 1989;24:1195–1197
19. Fiedorek SC, Casteel HB. Pediatric medication-induced focal esophagitis. *Clin Pediatr* 1988;27:455–456
20. Bova JG, Dutton NE, Goldstein HM, Hoberman LJ. Medication-induced esophagitis: diagnosis by double-contrast esophagography. *AJR* 1987;148:731–732
21. Creteur V, Laufer I, Kressel HY, et al. Drug-induced esophagitis detected by double-contrast radiography. *Radiology* 1983;147:365–368
22. Vandenplas Y, De Wolf D, Sacre L. Influence of xanthines on gastroesophageal reflux in infants at risk for sudden infant death syndrome. *Pediatrics* 1986;77:807–810

23. Wortmann DW, Kelsch RC, Kuhns L, Sullivan DB, Cassidy JT. Renal papillary necrosis in juvenile rheumatoid arthritis. *J Pediatr* **1980**;97:37-40
24. Allen RC, Petty RE, Lirenman DS, Malleson PN, Laxer RM. Renal papillary necrosis in children with chronic arthritis. *Am J Dis Child* **1986**;140:20-22
25. Lindsley CB, Warady BA. Nonsteroidal antiinflammatory drugs: renal toxicity. Review of pediatric issues. *Clin Pediatr* **1989**;29:10-13
26. Goodyer PR, Kronick JB, Jequier S, Reade TM, Scriver CR. Nephrocalcinosis and its relationship to treatment of hereditary rickets. *J Pediatr* **1987**;111:700-704
27. Jequier S, Cramer B, Goodyer P, Kronick J, Reade T. Renal ultrasound in metabolic bone disease. *Pediatr Radiol* **1986**;16:135-139
28. Alon U, Brewer WH, Chan JCM. Nephrocalcinosis: detection by ultrasonography. *Pediatrics* **1983**;71:970-973
29. Garland JS, Starshak RJ, Thomas JP. Fluid overload following chicken soup rehydration for gastroenteritis: the demything of a therapeutic legacy. *Clin Pediatr* **1986**;25:527-528
30. Wolfson BJ, Allen JL, Panitch HB, Karmizin N. Lipid aspiration pneumonia due to gastroesophageal reflux. *Pediatr Radiol* **1989**;19:545-547
31. De Oliveira GA, Del Caro SR, Bender Lamego CM, Merçon de Vargas PR, Vervloet VEC. Radiographic plain film and CT findings in lipoid pneumonia in infants following aspiration of mineral oil used in the treatment of partial small bowel obstruction by *Ascaris lumbricoides*. *Pediatr Radiol* **1985**;15:157-160
32. Krane EJ, Rockoff MA, Wallman JK. Subclinical brain swelling in children during treatment of diabetic ketoacidosis. *N Engl J Med* **1985**;312:1147-1151
33. Hoffman WH, Steinhart CM, El Gammal T, Steele S, Cuadrado AR, Morse PK. Cranial CT in children and adolescents with diabetic ketoacidosis. *AJNR* **1988**;9:733-739
34. Rogers B, Sills I, Cohen M, Seidel FG. Diabetic ketoacidosis: neurologic collapse during treatment followed by severe developmental morbidity. *Clin Pediatr* **1990**;29:451-456
35. Greene SA, Jefferson IG, Baum JD. Cerebral oedema complicating diabetic ketoacidosis. *Dev Med Child Neurol* **1990**;32:633-638
36. Rosenbloom AL. Intracerebral crises during treatment of diabetic ketoacidosis. *Diabetes Care* **1990**;13:22-33
37. Duck SC, Wyatt DT. Factors associated with brain herniation in the treatment of diabetic ketoacidosis. *J Pediatr* **1988**;113:10-14
38. Harris GD, Fiordalisi I, Harris WL, Mosovich LL, Finberg L. Minimizing the risk of brain herniation during treatment of diabetic ketoacidemia: a retrospective and prospective study. *J Pediatr* **1990**;117:22-31
39. Forman HP, Levin S, Stewart B, Patel M, Feinstein S. Cerebral vasculitis and hemorrhage in an adolescent taking diet pills containing phenylpropanolamine: case report and review of the literature. *Pediatrics* **1989**;83:737-741
40. Moinuddin M, Rockett J. Gallium scintigraphy in the detection of amiodarone lung toxicity. *AJR* **1986**;147:607-609
41. Yagupsky P, Gazala E, Safer S, Maor E, Abarbanel J. Fatal hepatic failure and encephalopathy associated with amiodarone therapy. *J Pediatr* **1985**;107:967-970
42. Costigan DC, Holland FJ, Daneman D, Hesslein PS, Vogel M, Ellis G. Amiodarone therapy effects on childhood thyroid function. *Pediatrics* **1986**;77:703-708
43. Schneider DL, Hebert LJ. Subcutaneous gas from hydrogen peroxide administration under pressure. *Am J Dis Child* **1987**;141:10-11
44. Osborne DR, Bohan T, Hodson A. CT demonstration of hyperdense cerebral vasculature due to bromide therapy. *J Comput Assist Tomogr* **1984**;8:982-984
45. Goldman IS, Winkler ML, Raper SE, et al. Increased hepatic density and phospholipidosis due to amiodarone. *AJR* **1985**;144:541-546
46. Aihara T, Fujioka M, Yamamoto K. Increased CT density of the liver due to cis-diaminedichloro platinum II. *Pediatr Radiol* **1987**;16:75-76
47. Taybi H, Capitanio MA. Tracheobronchial calcification: an observation in three children after mitral valve replacement and warfarin sodium therapy. *Radiology* **1990**;176:728-730

Book Review

Effective Choices for Diagnostic Imaging in Clinical Practice. Report of the WHO Scientific Group. (World Health Organization Technical Report Series, No. 795.) Albany, NY: WHO Publications Center USA, 131 pp., 1990. \$14.40

This is the report of the World Health Organization's scientific group on clinical diagnostic imaging, an international assembly of academicians, practitioners, scientists, and technologists. Their aim is "to provide clear and simple steps for the imaging of the most common clinical problems, taking into account the wide range of professional skills and facilities available in many parts of the world." They address disease-specific clinical concerns: In what specific clinical situations is imaging at all effective? What tests should be performed and in which order? The members of the group are aware that choosing the most effective imaging technique is often difficult and frequently controversial and that local factors governing such choices are often paramount.

The report is arranged anatomically and by diseases or complaints. Three levels of care of increasing complexity, cost, and sophistication are described. Level I is the minimum acceptable for good patient care (accounting for the most likely situation in much of the world). This includes standard radiography, general-purpose sonography, linear tomography, and fluoroscopy. Level II centers can perform all level I imaging studies plus sophisticated sonography and radiology, mammography, angiography, CT, and scintigraphy. Level III departments add MR imaging, positron emission tomography, and scintigraphy with monoclonal antibodies. For each disease category and clinical condition, the authors delineate what techniques at each level of care are helpful, not hesitating to dismiss many imaging techniques as being of no use. Much clinical wisdom is contained in the succinct pithy formulations. The accompanying reference lists are quite useful in themselves, concentrating on articles that critically evaluate imaging choices.

I could not agree entirely with the recommendations in some entries, or I could foresee frequent exceptions. Many North American and European practitioners might disagree with the scientific group in the areas of sonography and MR. These practitioners would see sonography recommended in situations in which, in their practice, CT would be more effective. Similarly, the scientific group relegates MR to tertiary care situations even for clinical situations in which MR has now supplanted CT. Of course, given the worldwide focus of the group, the greater availability of sonography as compared with CT, and the enormous cost of MR, the choices recommended in this report are understandable.

The report is interesting and well written and reflects a great deal of attention and care. Who will benefit most from it? Certainly practitioners and health care planners in the developing world will find it a useful guide for deploying their limited imaging resources. Medical students will find it a thought-provoking outline of imaging choices with a worldwide perspective. Most American practitioners would probably resist the limitations of choice that these guidelines mandate. I suspect that Western governments and third-party payers would be intrigued by the possibilities for more uniform and standardized imaging choices as outlined in the report. The members of the scientific group are to be commended for their efforts.

J. Eric Blum
Akron City Hospital
Akron, OH 44309

Review Article

Sonography of the Biliary Tract in Infants and Children

Jack O. Haller¹

Diseases of the gallbladder and biliary system are particularly well suited for investigation with sonography. As such, sonography has completely supplanted oral cholecystography in the evaluation of these disorders. Because it is easy to perform and does not expose the patient to radiation or contrast agents, sonography is being used more often in children to diagnose disorders of the gallbladder and biliary tract. Many of the sonographic signs of these diseases (e.g., cholelithiasis, cholecystitis) are well established in adults and are the same in children. However, the circumstances under which these diseases occur and their different causal factors are different in children and adults. This article reviews the distinctive aspects of gallbladder-biliary tract disease in children, concentrating on the role that sonography plays in its evaluation and therapy.

The Enlarged Gallbladder

Relatively few articles have described the normal gallbladder and given common bile duct measurements in children [1-5]. They provide normal volumes, lengths, and widths of the gallbladder, common bile duct, and common hepatic duct from infancy to adolescence. The reader is referred to these sources for exact age-measurement relationships.

The rate of diagnosis of gallbladder distension, whether acute or subacute, has increased dramatically in the past 10 years. This is especially true in premature neonates and infants, but more cases are being diagnosed in older children as well [6-9].

A problem has developed because of the interchangeable use of various poorly defined terms such as gallbladder distension [6], hydrops [7], acute dilatation [8], and acalculous

cholecystitis [9]. Despite the number of attempts by authors to establish normal and abnormal sonographic measurements, it is sometimes difficult to discern a difference between the normally distended gallbladder (e.g., owing to fasting) and the pathologically enlarged one (owing to inflammation) because some degree of overlap is expected. This makes diagnosis by sonography particularly difficult, especially when cystic duct obstruction is not shown. Most authors prefer the term acalculous cholecystitis when there is true inflammation of the gallbladder with appropriate clinical signs and symptoms. Gallbladder distension, acute dilatation, and hydrops are best reserved for acute noninflammatory enlargement of the gallbladder [10].

The causes of enlarged gallbladder in premature infants and neonates include infection, which causes biliary atony or lymph node enlargement that compresses the cystic duct. Total parenteral nutrition, severe vomiting, and starvation all result in lack of contraction, biliary stasis, and gallbladder enlargement.

Obstructive gallbladder enlargement can lead to true cholecystitis. In the neonate, this is most often caused by gallstones, inflammatory nodes, or congenital anomalies of the bile ducts.

In the older child, gallbladder distension is caused by a number of factors [9, 11-13]. At least 11 infectious agents have been implicated [9, 12, 13]. Infection is more common as a cause of gallbladder distension and inflammation than is trauma. Gastroenteritis from a variety of causes produces vomiting, which in turn causes dehydration leading to biliary stasis. The resulting hyperconcentrated bile interferes with

Received March 5, 1991; accepted after revision June 19, 1991.

¹ Department of Department of Radiology, State University of New York, Downstate Medical Center, Box 1208, 450 Clarkson Ave., Brooklyn, NY 11203. Address reprint requests to J. O. Haller.

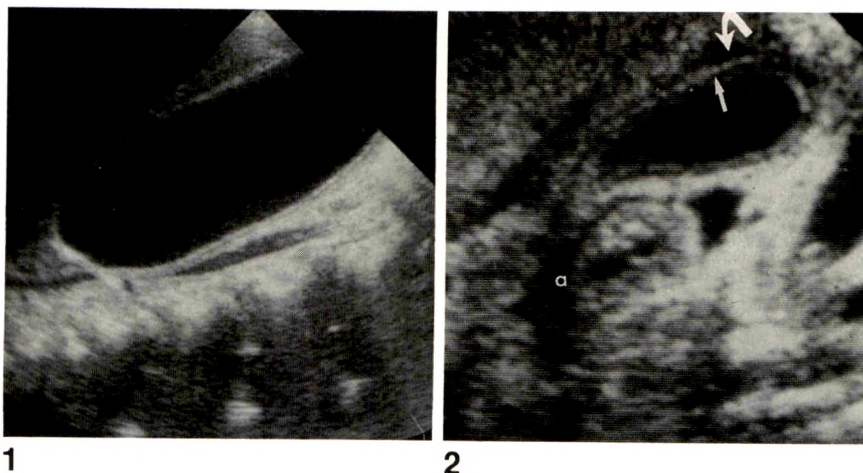


Fig. 1.—Kawasaki disease with gallbladder hydrops. Longitudinal sonogram with child supine shows markedly distended gallbladder.

Fig. 2.—Thickened gallbladder wall in child with nephrotic syndrome. Longitudinal sonogram with child supine shows ascites (a) surrounding bowel wall. Wall of gallbladder is surrounded by layers of increased and decreased echogenicity. Outermost hypoechoic layer represents ascitic fluid (curved arrow), and innermost hypoechoic layer represents edema (straight arrow).

drainage and ultimately produces gallbladder distension. Other diseases such as hepatitis, upper respiratory infections, and leptospirosis may produce lymphadenopathy that causes bile duct compression [14].

Often patients with Kawasaki disease have jaundice, direct hyperbilirubinemia, and acute distension of the gallbladder (Fig. 1). The cause of the jaundice is unclear because bile flow is not mechanically obstructed. The common and hepatic ducts are often normal, as shown by sonography and operative and postoperative cholangiography. The disease is believed to cause a nonspecific vasculitis. This vasculitis causes increased echogenicity of the kidney as well. These patients are treated medically, usually without sequelae [15, 16].

Acute and Chronic Cholecystitis

The sonographic signs of true cholecystitis in children are similar to those found in the adult. These include a thickened anechoic gallbladder wall, a hyperreflective irregular wall, and sludge or gallstones.

In children, the thickened gallbladder wall is defined as being greater than 3 mm, which is smaller than that found in the adult [10]. A thickened wall associated with a layer of anechoicity represents edema and/or necrosis. Patriquin et al. [17] described a number of causes of a thick gallbladder wall in children. These include hypoalbuminemia; ascites (the free fluid creates a halo effect around the extrahepatic gallbladder; Fig. 2); or a recent meal, causing physiologic thickening of the contracted gallbladder [18]. Pericystic inflammation occurs in cases of acute hepatitis. The venous drainage of the gallbladder may actually be decreased by a pericystic inflammation, thus resulting in edema of the wall. Systemic venous hypertension theoretically would have the same effect [17].

The hyperreflective wall is thought to correspond to fibrosis seen in pathology specimens in chronic cholecystitis. Stagnant bile, sludge, or stones in the gallbladder may be associated with it; this finding should always prompt the examiner to look for a thickened gallbladder wall [10].

Complications of cholecystitis include pericholecystic abscess, empyema, and perforation. These findings are extraor-

dinarily rare in children. Isolated case reports of complications of cholecystitis include empyema in a duplicated gallbladder and perforation in a premature infant with sepsis and in children with Kawasaki disease [14, 15, 19–21].

Cystic Fibrosis

Cystic fibrosis is the most common lethal inherited disorder in white children [22]. The gallbladder in many of these patients has a characteristic appearance on sonography, including stones and sludge, small gallbladder, obstruction of the cystic duct (either due to mucosal hyperplasia, inspissated mucus, or outright atresia), a thick gallbladder with trabeculations, and subepithelial cysts (Fig. 3A). Associated sonographic abnormalities include fatty or fibrotic changes in the pancreas (Fig. 3B), pancreatitis, pancreatic calcifications, splenic enlargement, and increased echogenicity as well as prominence of the portal venous system due to portal hypertension [23, 24].

Cholelithiasis

Cholelithiasis is a significant cause of right-upper-quadrant pain in children with or without hemolytic anemia. It is a disease predominantly of infants and adolescents. The number of risk factors found to be associated with pediatric cholelithiasis is rising [25–42].

Prenatal Gallstones

Prenatal gallstone formation is a distinctly uncommon entity; only a half dozen cases have been recorded in the literature [36–38]. Many of these stones may in fact represent echogenic sludge. Stones have not been detected by radiologic techniques, and the sludge often does not cause shadowing as stones would (Fig. 4).

The fetal gallbladder is easily identified in the right upper quadrant, and the only differential difficulty comes in identify-

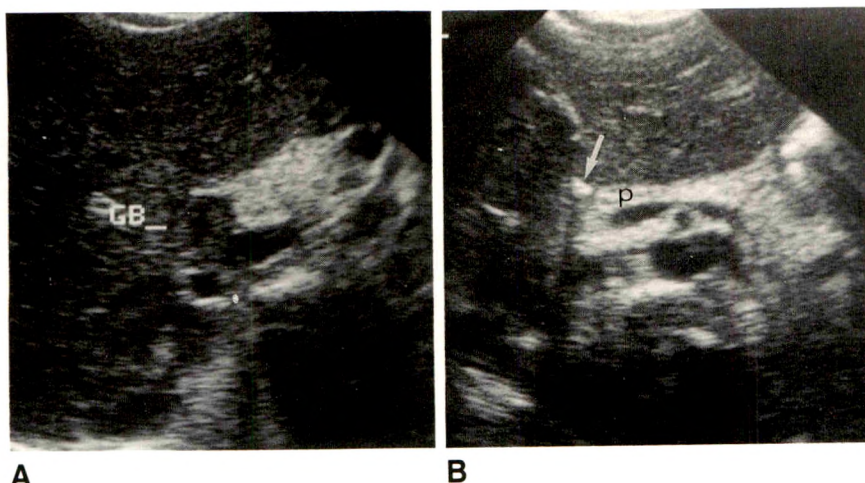


Fig. 3.—Cystic fibrosis.

A, Transverse sonogram with child supine shows thickened wall (GB) of a small gallbladder.

B, Transverse sonogram at slightly lower level shows pancreas (p) is small, fibrotic, and highly echogenic. Stone (arrow) with shadowing is seen next to pancreatic head.

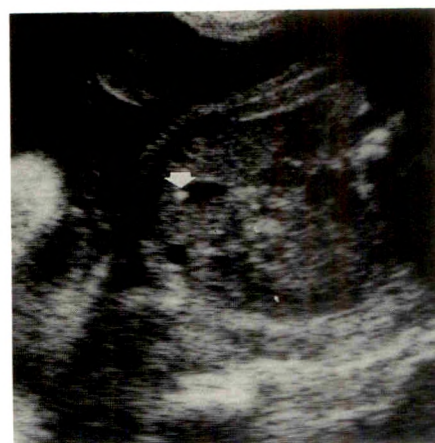


Fig. 4.—Prenatal gallstone. Prenatal sonogram of fetal abdomen shows echogenic shadowing focus in gallbladder (arrow). This stone was followed up postnatally until it ultimately resolved. Child had no associated risk factors for cholelithiasis. (Courtesy of M. Kirpekar, New York, NY.)

ing the umbilical vein as a separate structure. This can be accomplished with Doppler imaging.

Fetal abnormalities have not been shown in any of the cases of fetal gallstones. Fetal gallstones have not caused symptoms in neonates, and most have resolved spontaneously. However, these neonates must be closely monitored for the development of jaundice or biliary symptoms. As both hemolytic anemia and structural anomalies of the biliary tract predispose to stone formation, screening for these conditions should be done.

Infants

In the past 10 years, the frequency of diagnosis of gallstones in infants has increased dramatically. This is no doubt due to the increased use of sonography with new high-frequency transducers and to the increased number of premature infants and other infants on total parenteral nutrition. Cholestasis in neonates induced by total parenteral nutrition was initially described by Peden et al. [39] in 1971. Several hypotheses for gallstone formation resulting from total parenteral nutrition have been proposed. These include severe prematurity of the biliary system, cholestasis, abnormal content of parenteral fluid, and abnormal amino acid metabolism [26, 27].

The composition of most gallstones in infants and young children is primarily calcium bilirubinate pigment with calcium carbonate and cholesterol in various amounts. Often these stones are radiopaque on radiographs, but sonography remains the most reliable confirmatory study. The stones are movable echogenic structures that may or may not generate shadows (Fig. 5). Matos et al. (cited in [27]), in a prospective sonographic study of 41 neonates on total parenteral nutri-

tion, showed sludge developing after a mean of 10 days in 18 of 41 infants.

Once stones are detected, careful sonographic monitoring until their eventual resolution (usually in about 6 months) is in order [28, 40, 41].

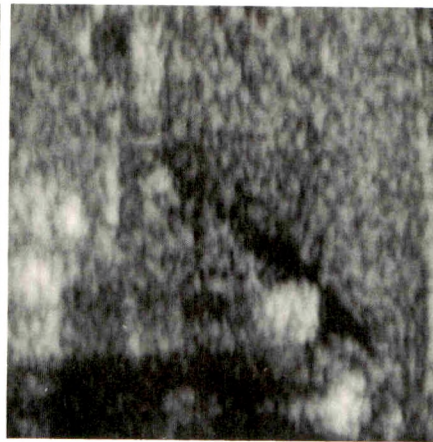
1- to 10-Year-Old Children

Friesen and Roberts [42] surveyed the literature of pediatric cholelithiasis up to 1989 and found that it is primarily a disease of adolescence and infancy. Children from 6 months to 5 years old, for example, accounted for only 5% of almost 700 published cases. Gallstones in 1- to 10-year-old children are mixtures of calcium bilirubinate (pigmented), calcium carbonate, and cholesterol. Starvation (malabsorption), hyperalimentation, and abdominal surgery seem to be the main causes. Because stones are uncommon in this age group, the diagnosis is often missed. Symptoms (the most common are abdominal pain and vomiting) are usually attributed to other diseases of the right upper quadrant. Only when jaundice develops is the differential diagnosis directed toward the hepatobiliary system. In this age group, some have reported the association of cardiac valve surgery and cholelithiasis. The prosthetic valves cause RBC destruction, which decreases bile salt-independent bile flow. Children who have had spinal fusion are also prone to stone formation [27].

Diseases causing bowel dysfunction become important contributors to gallstone formation as children get older. These include small-bowel resection, severe diarrhea, Crohn disease of the ileum, and cystic fibrosis [22, 29, 34, 42]. The stones result from an alteration of the bile acid pool, decreasing the ability to keep cholesterol in solution. The disease is found equally in boys and girls up to about 11 years of age; after that, it is more common in girls.



A



B

Fig. 5.—Gallstones in neonate receiving total parenteral nutrition. A and B, Longitudinal sonograms with child supine (A) and erect (B) show shadowing echogenic focus in gallbladder neck that fell toward fundus when child was erect.

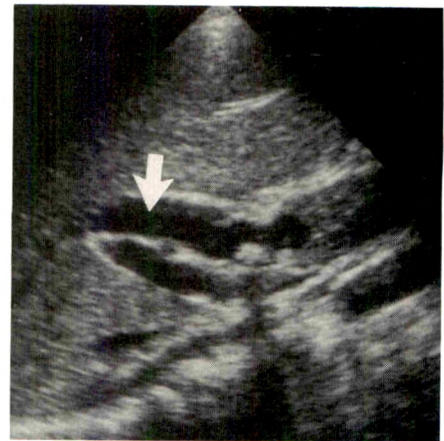


Fig. 6.—Sickle cell disease with choledocholithiasis. Oblique sonogram with child supine shows dilated common bile duct (arrow) with at least one stone creating a shadow in distal portion.

10- to 20-Year-Old Children

The demographic features of adolescents with gallstones are interesting. American black children are less likely to have nonhemolytic cholelithiasis than are American white children. Adolescents in the United States and Europe are more likely to have gallstones than adolescents in other parts of the world because their diet is higher in cholesterol and lower in fiber than the diet in the Eastern hemisphere. In Chile, 5–8% of adolescent girls and 25–30% of young women have gallstones, presumably caused by cholesterol hypersecretion [27, 43]. The number of girls with gallstones increases significantly with adolescence [11, 27, 42].

Several reports have pointed out the relationship between gallbladder disease and obesity [11]. Body weight in excess of 10% of normal for height and age has been found in 33% of teenagers with gallstones [27].

Anemia

Cholelithiasis in children with hereditary blood dyscrasias is well known. These children are all at increased risk of pigment stones owing to hemolysis. The proportion of children with hemolytic anemia and gallstones has been reported to be 20–80% of all children with gallstones [31, 33, 34].

Sonography is superb for showing gallstones and sludge in the gallbladders of these patients. Although many asymptomatic patients with hemolytic anemia have sludge and stones in their gallbladders, common bile duct enlargement and stones are uncommon. When detected in the proper clinical setting, these findings are diagnostic for bile duct obstruction.

The treatment in children with symptomatic gallstones who are under 20 years of age has usually been surgery [44, 45]. Nonoperative treatment with high doses of chenodeoxycholic acid or ursodeoxycholic acid has not been used in children. Extracorporeal shock-wave lithotripsy has been receiving

wide attention. Although some adolescents have been included in large series of patients, the use of extracorporeal shock-wave lithotripsy in the gallbladder in children has yet to be studied [27].

Gallstone pancreatitis, an unusual complication in children with gallstones, is for the most part benign, and the attacks seldom progress to chronic pancreatitis. Gallstones may pass through the common bile duct and the ampulla, causing a transient obstruction of the pancreatic duct orifice [46].

Choledocholithiasis

Choledocholithiasis in infants and children is uncommon. In one large series, common bile duct stones were reported in 12–21% of children with gallbladder stones [47, 48]. Stones migrate out of the gallbladder, and they become common bile duct stones. However, not all common bile duct stones originate in the gallbladder but, rather, in the intrahepatic and extrahepatic bile ducts. Congenital anomalies, choledochal cysts, or structural abnormalities (postsurgical or posttraumatic) of the bile ducts predispose to bile stasis and choledocholithiasis. Common bile duct stones have been implicated in the formation of choledochal cysts, perforation, hepatic damage, and pancreatitis.

Sonography is the most useful diagnostic method for imaging a dilated common bile duct and common bile duct stones (Fig. 6). The dilatation is easier to diagnose than the stones, which are detected with a 20–60% success rate. The stone is usually located in the distal duct above the sphincter. Dilatation of the common bile duct may be mild to moderate but often is not present [48].

Bile Plug Syndrome

Bile plug syndrome is defined as mechanical obstruction of the common bile duct by a plug of secretions and bile [48].

These plugs may pass spontaneously, but they have been known to cause cholangitis. Any sign of infection or biochemical cholestasis with associated dilatation of the intrahepatic ducts is thought to be an indication for treatment. Asymptomatic infants pose a treatment dilemma, because in many of the children the plug will resolve spontaneously. When treatment is needed, a variety of methods can relieve the obstruction. These include mucolytic agents and gallbladder washing (both are done with injection through a cholangiogram catheter into the gallbladder and bile ducts at laparotomy) and surgical exploration of the common bile duct [49, 50].

Congenital Bile Duct Dilatation

Choledochal Cyst

Vater [51] first described a choledochal cyst in 1723. It is a relatively rare lesion in the United States and other cultures in which most people are white. This disorder is three or four times more common in females than in males. No familial reports or other studies have implicated genetic factors [52]. Alonso-Lej et al. [53] devised a classification scheme of three major types. The type 1 choledochal cyst is a concentric dilatation of the common bile duct. It is often associated with proximal and/or distal atresia or obstruction. Type 2 choledochal cyst is a diverticular outpouching of the common bile duct. Type 3, a choledochocoele, is the rarest [54].

In 1974, Landing [55] hypothesized that neonatal hepatitis, biliary atresia, and choledochal cysts represented manifestations of what he called infantile obstructive cholangiopathy. He thought that a virus caused progressive scarring of the biliary tract, which resulted in panductular sclerosis of the biliary tree and the extrahepatic distal obstruction responsible for the formation of the choledochal cyst.

In 1973, Babbitt et al. [56] hypothesized an anomalous union between the common bile duct and the main pancreatic duct as the cause of the choledochal cyst. They demonstrated that the distal common bile duct inserts more proximally than usual into the pancreatic duct of Wirsung because of failure of normal separation. This anomaly results in refluxed pancreatic juice into the common bile duct, causing cholangitis with inflammation, weakening, and dilatation of the common bile duct wall (Fig. 7). This is apparently the mechanism in older children with choledochal cysts who have the typical triad of pain, mass, and jaundice. Apparently the choledochal cyst in the neonate with acholic stools and jaundice differs from the choledochal cyst of childhood and adolescence. The neonatal variety may in fact be due to a congenital abnormality in which an inherent weakness in the common bile duct in its developmental stages allows dilatation in response to the distal obstruction, as hypothesized by Landing [55]. This may account for the high association of choledochal cyst with biliary atresia in neonates [57].

The combination of hepatobiliary scintigraphy and sonography is diagnostic for choledochal cysts alone and those associated with extrahepatic biliary atresia. Visualization of radioactivity in the bowel excludes biliary atresia. Nonvisualization of radionuclide bowel activity signifies bile stasis or noncommunication of the biliary system with the intestinal

tract. Sonography will show the choledochal cyst as a cystic structure in the porta hepatis separate from the gallbladder and may show direct communication with a common hepatic duct into the cystic duct on real-time sonography (Fig. 8). Conversely, if a cystic structure is shown on sonography as the initial imaging study, nuclear medicine studies are performed to show that the cystic structure communicates with the biliary system and to determine the presence of distal obstruction.

In the older patient with nonobstructive choledochal cyst, the scintigraphic study classically shows the normal hepatic extraction and a filling defect in the region of the porta hepatis on the early images, with delayed accumulation of tracer in the region of the original filling defect indicating a communication with the cystic structure and biliary system.

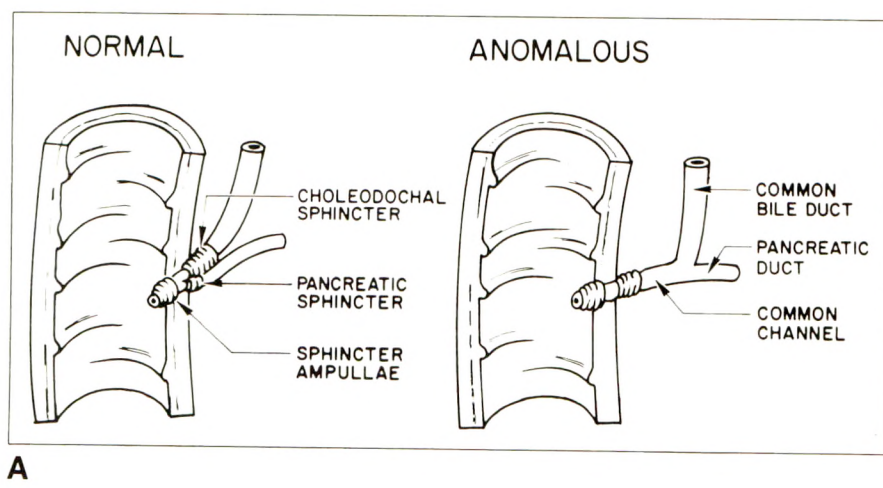
Rapid treatment of choledochal cyst is essential. Delay in surgical management may result in cirrhosis with portal hypertension, cholangitis, and pancreatitis [54, 58, 59]. Malignancy in choledochal cysts or their remnants is a recognized development in adults [60, 61].

A choledochocoele is a cystic dilatation of the distal intramural portion of the common bile duct typically protruding into the descending duodenum (also known as type 3 choledochal cyst). Forty cases have been reported worldwide since 1974. Ten of these patients were 21 years old or younger. An upper gastrointestinal series combined with ERCP correctly identified the lesion. Sonography was used predominantly to identify intrahepatic biliary dilatation or dilatation of the common bile duct [62].

Caroli Disease

Caroli and Couinaud [63] first described this condition, which is a biliary malformation and generalized cystic dilatation of the intrahepatic ducts, in 1958. It is thought to be autosomal recessive, although it has been reported in families [64]. This disorder is also being detected with increased frequency in children [65]. This disorder may in fact have two forms: the pure form (type 1), wherein there is an intrahepatic biliary duct dilatation, and type 2, which is associated with congenital hepatic fibrosis. Symptoms in type 1 are due to stone formation and cholangitis caused by biliary stasis, whereas in type 2, with congenital hepatic fibrosis, the clinical manifestations are mainly those of portal hypertension and varices. The etiology is still controversial, and theories are similar to those for choledochal cysts [56, 65]. Other disorders often diagnosed in patients with Caroli disease include recessive polycystic kidney disease, renal tubular ectasia, choledochal cyst, and biliary tract carcinoma [66].

Sonography is thought to be the best way to screen for this disorder, especially because IV contrast material can be a problem in patients with renal dysfunction [67]. Sonography enables the confirmation of communication of cystic lesions in the liver with the bile ducts. Bile stasis often leads to stone formation in these dilated ducts (Fig. 9). Enlarged echogenic kidneys indicative of concomitant renal disease can be diagnosed during the same sonographic examination.



A

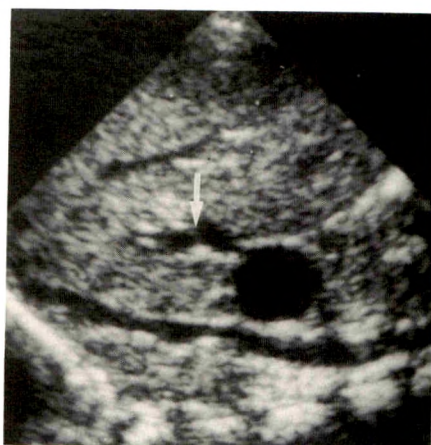


B

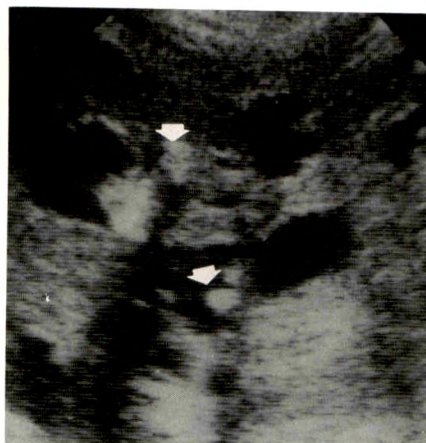
Fig. 7.—Anomalous bile duct-pancreatic duct union.

A, Diagram of normal and anomalous common bile duct-pancreatic duct union seen in older patients with choledochal cysts. Note that in anomalous situation, union of common bile duct and pancreatic duct is more proximal than normal, allowing reflux of pancreatic juice.

B, Operative cholangiogram in 9-year-old boy shows dilated bile ducts with common bile duct joining pancreatic duct anomalously (arrow). This child had repeated bouts of common bile duct obstruction and jaundice. Some authors believe this anomaly causes choledochal cysts.



8



9

Fig. 8.—Biliary atresia and choledochal cyst. Longitudinal sonogram with neonate supine shows cystic structure (choledochal cyst) in inferior aspect of liver with an echo-free tubular structure (common hepatic duct, arrow) leading to it. Choledochal cyst, atretic gallbladder, and biliary atresia were confirmed at surgery.

Fig. 9.—Caroli disease with intraductal stones. Transverse sonogram with boy supine shows multiple, focally dilated bile ducts containing hyper-echoic foci. Echogenic stones (arrows) cause shadowing.

Spontaneous Perforation of the Common Bile Duct

Although it is the second most common cause of jaundice amenable to surgical treatment in infants, spontaneous perforation of the common bile duct is a rare disorder [68]. Most authors have reported single cases [69, 70]. The presenting signs and symptoms of the disorder include vague abdominal distension, mild persistent hyperbilirubinemia, varying acholic stools, and occasionally a fluid-filled inguinal hernia [71, 72]. The pathogenesis of spontaneous perforation of the extrahepatic bile duct is not known, although various causes have been theorized: distal obstruction due to stones or actual ductal stenoses, mural malformation occurring during embryogenesis, weakness from pancreatic juice reflux caused by anomalies of the pancreaticobiliary system, and mural weakness caused by underperfusion at the anterior wall of the bile duct near its junction with the cystic duct [73–75].

Sonography shows free intraperitoneal and/or loculated subhepatic fluid. The preoperative sonographic findings of

ascites; pseudocyst in the porta hepatis; and an undilated biliary tree, with or without distal calculus, suggest the diagnosis. Hepatobiliary scintigraphy definitively shows that the intraperitoneal fluid originated from the biliary tract, without recourse to paracentesis. The combination of sonographic, scintigraphic, and clinical findings should lead to the correct preoperative diagnosis. Simple drainage is all that is usually required and results in spontaneous closure and subsequent cure [69].

Tumors

Rhabdomyosarcoma of the biliary tract is a rare type of cancer typically occurring in children between 1 and 5 years old who have obstructive jaundice. Jaundice is an atypical presenting sign for children with a hepatic mass. Palpable mass, anorexia, weight loss, and pain are more typical, but jaundice is classic for rhabdomyosarcoma [76–79]. The fact

that the jaundice is obstructive in nature, an unusual finding in a child, is the most important observation leading to definitive diagnostic studies [80].

Sonographically, a mass is detected that is either of a "Swiss cheese" appearance or solid with dilated bile ducts seen more proximally [80, 81]. The differential diagnosis includes malignant liver tumors, such as hepatoblastoma, hepatocellular carcinoma, or mixed mesenchymal sarcoma, and benign tumors, such as adenoma, hemangioma, or focal nodular hyperplasia [77, 78, 82]. Lymphoma/lymphosarcoma can also occur in the porta hepatis and cause obstructive jaundice.

The prognosis is generally poor, despite aggressive surgery, irradiation, and chemotherapy. Recently, long-term survivors have been reported [80, 83–85].

ACKNOWLEDGMENTS

I thank Gloria Jorge and Catherine Tripi for assistance in preparing the manuscript.

REFERENCES

- Palasciano G, Portincasa P, Vinciguerra V, et al. Gallstone prevalence and gallbladder volume in children and adolescents: an epidemiologic ultrasonographic survey and relationship to body mass. *Am J Gastroenterol* 1989;84:1378–1382
- McGahan JP, Phillips HE, Cox KL. Sonography of the normal pediatric gallbladder and biliary tract. *Radiology* 1982;144:873–875
- Sarniak S, Slovis TL, Corbett D, Emami A, Whitten CF. Incidence of cholelithiasis in sickle cell anemia using the ultrasonic gray-scale technique. *J Pediatr* 1980;96:1005–1008
- Witcombe JB, Cremin BJ. The width of the common bile duct in childhood. *Pediatr Radiol* 1978;7:147–149
- Carroll BA, Oppenheimer DA, Muller HH. High frequency real time ultrasound of the neonatal biliary system. *Radiology* 1982;145:437–440
- Peavy KJ, Weissman HJ. Gallbladder distention in septic neonates. *Arch Dis Child* 1982;57:75–76
- Goldthorn JF, Thomas DW, Ramos AD. Hydrops of the gallbladder in stressed premature infants. *Clin Res* 1980;28:122–123
- Bowen A. Acute gallbladder dilatation in a neonate: emphasis on ultrasonography. *J Pediatr Gastroenterol Nutr* 1984;3:304–305
- Dewan PA, Stokes KB, Solomon JR. Pediatric acalculous cholecystitis. *Pediatr Surg Int* 1987;2:120–121
- Greenberg M, Kangaroo H, Sachiko TC, Sample WF. The ultrasonographic diagnosis of cholecystitis and cholelithiasis in children. *Radiology* 1980;137:745–749
- Cheng ERY, Okoye MI. Cholecystitis and cholelithiasis in children and adolescents. *J Natl Med Assoc* 1986;78:1073–1078
- Cohen EK, Stringer DA, Smith CR, Daneman MD. Hydrops of the gallbladder in typhoid fever as demonstrated by sonography. *JCU* 1986;14:633–635
- Roca M, Sellier N, Mensire A, Kalifa G, Bennet J. Acute acalculous cholecystitis in *Salmonella* infection. *Pediatr Radiol* 1988;18:421–423
- Cunningham JJ. Empyema of a duplicated gallbladder: echographic findings. *JCU* 1980;8:511–512
- Suddleson BA, Reid B, Wooley MM, Takahashi M. Hydrops of the gallbladder associated with Kawasaki syndrome. *J Pediatr Surg* 1987;22:956–959
- Nardi PM, Haller JO, Friedman AP, Slovis TL, Schaffer RM. Renal manifestations of Kawasaki's disease. *Pediatr Radiol* 1985;15:116–118
- Patriquin HB, DiPietro M, Barber FE, Teele RL. Sonography of thickened gallbladder wall: causes in children. *AJR* 1983;141:57–60
- Banfield WF. Physiology of the gallbladder. *Gastroenterology* 1975;69:770–777
- Kane RA. Ultrasonographic diagnosis of gangrenous cholecystitis and empyema of the gallbladder. *Radiology* 1980;134:191–194
- Bergman AB, Neiman HL, Kraut B. Ultrasonographic evaluation of pericholecystic abscess. *AJR* 1979;132:201–203
- Smith R, Rosen JM, Alderson PO. Gallbladder perforation: diagnostic utility of cholescintigraphy in suggested subacute or chronic cases. *Radiology* 1986;158:63–67
- L'Heureux PR, Isenberg JN, Sharp HL, Warwick WJ. Gallbladder disease in cystic fibrosis. *AJR* 1977;128:953–956
- Willi UV, Reddish JM, Teele RL. Cystic fibrosis: its characteristic appearance on abdominal sonography. *AJR* 1980;134:1005–1010
- Phillips HE, Cox KL, Reid MH, McGahan JP. Pancreatic sonography in cystic fibrosis. *AJR* 1981;137:69–72
- Gorel L, Lallemand D, Montajne JP. The changing spectrum of cholelithiasis in children through a sonographic study. *Pediatr Radiol* 1981;11:75–79
- Callahan J, Haller JO, Cacciarelli AA, Slovis TL, Friedman AP. Cholelithiasis in infants: association with total parenteral nutrition and furosemide. *Radiology* 1982;143:437–439
- Holcomb GW Jr, Holcomb GW III. Cholelithiasis in infants, children and adolescents. *Pediatr Rev* 1990;2:268–275
- Williams HJ, Johnson KW. Cholelithiasis: a complication of cardiac valve surgery in children. *Pediatr Radiol* 1984;14:146–147
- Kassner EG, Klotz DH. Cholecystitis and calculi in a diverticulum of the gallbladder. *J Pediatr Surg* 1975;10:967–968
- Colon RF, Tolaymat N, Kao JCS. Gallbladder sludge and lithiasis in an infant born to a morphine user mother. *J Pediatr Gastroenterol Nutr* 1990;10:234–238
- Iachman BS, Lazerson J, Starshak RJ, Vaughters FM, Werlin SL. The prevalence of cholelithiasis in sickle cell disease as diagnosed by ultrasound and cholecystography. *Pediatrics* 1979;64:601–603
- Chittmittrapap S, Buachum V, Dharmklong-at A. Cholelithiasis in thalassemic children. *Pediatr Surg Int* 1990;5:114–117
- Bond LR, Hatty SR, Horn MEC, Dick M, Meire HB, Bellingham AJ. Gallstones in sickle cell disease in the United Kingdom. *BMJ* 1987;295:234–236
- Takiff H, Fonkalsrud EW. Gallbladder disease in childhood. *Am J Dis Child* 1984;138:565–568
- Buiumsohn A, Albu E, Gerst PH, Subbarao J. Cholelithiasis and teenage mothers. *J Adolesc Health Care* 1990;11:339–342
- Abbutt PL, McIlhenny J. Prenatal detection of gallstones. *JCU* 1990;18:202–204
- Beretsky I, Lankin D. Diagnosis of fetal cholelithiasis using real-time high resolution imaging employing digital detection. *J Ultrasound Med* 1983;2:381–383
- Klingsmith WC, Cioffi-Ragan DT. Fetal gallstones. *Radiology* 1988;167:143–144
- Peden V, Witzleben C, Skelton M. Total parenteral nutrition. *J Pediatr* 1971;78:180–181
- Schirmer WJ, Grisoni ER, Gauderer MWL. The spectrum of cholelithiasis in the first year of life. *J Pediatr Surg* 1989;24:1064–1067
- Keller MS, Markle BM, Laffey PA, Chawla HS, Jacir N, Frank JL. Spontaneous resolution of cholelithiasis in infants. *Radiology* 1985;157:345–348
- Friesen CA, Roberts CC. Cholelithiasis: clinical characteristics in children. *Clin Pediatr (Phila)* 1989;28:294–298
- Stockman JA III. Editor's comment. In: Oski FA, Stockman JA III, eds. *The year book of pediatrics*. Chicago: Year Book Medical, 1990:614–616
- Pappis CH, Galanakis S, Moussatos G, Keramidas D, Kattamis C. Experience of splenectomy and cholecystectomy in children with chronic hemolytic anemia. *J Pediatr Surg* 1989;24:543–546
- Bonadio WA. Clinical features of abdominal painful crisis in sickle cell anemia. *J Pediatr Surg* 1990;25:301–302
- Albu E, Buiumsohn A, Lopez R, Gerst PH. Gallstone pancreatitis in adolescents. *J Pediatr Surg* 1987;22:960–962
- Hanson BA, Mahour GH, Wooley MM. Diseases of the gallbladder in infancy and childhood. *J Pediatr Surg* 1971;6:277–283
- Lilly JR. Common bile duct calculi in infants and children. *J Pediatr Surg* 1980;15:577–580
- Brown DM. Bile plug syndrome: successful management with a mucolytic agent. *J Pediatr Surg* 1990;25:351–352
- Pfeiffer WR, Robinson LH, Balsara VJ. Sonographic features of bile plug syndrome. *J Ultrasound Med* 1986;5:161–163
- Vater A. *Dissertation in auguralis medica poes diss. qua. scirrhis viscerum*

- dissert. Edinburgh, Scotland: University Library, 1723;70:19
52. O'Neill JA Jr, Templeton JM Jr, Schnauffer L, Bishop HC, Ziegler MM, Ross AJ III. Recent experience with choledochal cyst. *Ann Surg* 1987;205:533-540
 53. Alonso-Lej F, Rever WB Jr, Pessagno DJ. Collective review. Congenital choledochal cyst, with a report of 2, and an analysis of 94 cases. *Int Abstr Surg* 1959;108:1-30
 54. Kirks DR, Coleman RE, Filston HC, Rosenberg ER, Merten DF. An imaging approach to persistent neonatal jaundice. *AJR* 1984;142:461-465
 55. Landing BH. Consideration of the pathogenesis of neonatal hepatitis, biliary atresia and choledochal cyst—the concept of infantile obstructive cholangiopathy. *Prog Pediatr Surg* 1974;5:113-139
 56. Babbitt DP, Starshak RJ, Clemett AR. Choledochal cyst: a concept of etiology. *AJR* 1973;199:57-62
 57. Torrisi JT, Haller JO, Velcek FT. Choledochal cyst and biliary atresia in the neonate. *AJR* 1990;155:1273-1276
 58. Papanicolaou N, Abramson SJ, Teele RL, Treves S. Specific preoperative diagnosis of choledochal cysts by combined sonography and hepatobiliary scintigraphy. *Ann Radiol (Paris)* 1985;28:276-282
 59. Fonkalsrud EW, Boles ET Jr. Choledochal cysts in infancy and childhood. *Surg Gynecol Obstet* 1965;121:733-742
 60. Todani T, Watanabe Y, Toki A, Urushihara N. Carcinoma related to choledochal cysts with internal drainage operations. *Surg Gynecol Obstet* 1987;164:61-64
 61. Ozawa K, Yamada T, Matsumoto Y, Tobe R. Carcinoma arising in a choledochocoele. *Cancer* 1980;45:195-197
 62. Manning PB, Polley TZ Jr, Oldham KT. Choledochocoele: an unusual form of choledochal cyst. *Pediatr Surg Int* 1990;5:22-26
 63. Caroli J, Couinaud C. Une affection nouvelle sans doute congenitale, des voies biliaires: la dilatation kystique unilobaire des canaux hepatoques. *Semin Hop Paris* 1958;34:496-502
 64. Iwafucai M, Ohsawa Y, Naito S, Naito M, Maruta Y, Saito H. Familial occurrence of congenital bile duct dilatation. *J Pediatr Surg* 1990;25:353-355
 65. Chang M, Wang T, Chen C, Hung W. Congenital bile duct dilatation in children. *J Pediatr Surg* 1986;21:112-117
 66. Takehara Y, Motoichiro T, Masaaki N, et al. Caroli's disease associated with polycystic kidney: its noninvasive diagnosis. *Radiat Med* 1989;7:13-15
 67. Marchal GJ, Desmet VJ, Proesmans WC, et al. Caroli disease: high frequency US and pathologic findings. *Radiology* 1986;158:507-511
 68. Lilly JR, Weintraub WH, Altman RP. Spontaneous perforation of the extrahepatic bile ducts and bile peritonitis in infancy. *Surgery* 1974;75:664-673
 69. Haller JO, Condon VR, Berdon WE, Oh KS, Price AP, Bowen A. Spontaneous perforation of the common bile duct in children. *Radiology* 1989;172:621-624
 70. Hoffman AD. Spontaneous perforation of the common bile duct in infancy. *AJR* 1984;142:1070-1072
 71. Marshall DG, Brabyn DG, Vezina WC. Spontaneous perforation of the common bile duct in infancy detected by ^{99m}TcHIDA scanning. *Can J Surg* 1984;27:590-591
 72. Fawcett HD, Hayden CK, Swischuk LE, Lobe TE. Spontaneous extrahepatic biliary duct perforation in infancy. *Can Assoc Radiol J* 1986;37:206-207
 73. Colver HD. Perforation of the biliary tract due to gallstones in infancy: an established clinical entity. *Ann Surg* 1964;2:226-231
 74. Pettersson G. Spontaneous perforation of the common bile duct in infants. *Acta Chir Scand* 1955;110:192-201
 75. Chen WJ, Chang C, Hung W. Congenital choledochal cyst: with observation on rupture of the cyst and intrahepatic ductal dilatation. *J Pediatr Surg* 1973;8:529-538
 76. Williams AG Jr, Sheward SE. Ultrasound appearance of biliary rhabdomyosarcoma. *JCU* 1986;14:63-65
 77. Exelby PR, Filler RM, Grossfeld JL. Liver tumors in children in the particular reference to hepatoblastoma and hepatocellular carcinoma. *J Pediatr Surg* 1975;10:329-337
 78. Markle BM, Potter BM, Madj M. The jaundiced infant and child. *Semin Ultrasound* 1980;1:123-133
 79. Clathworthy HW, Schiller M, Grossfeld JL. Primary liver tumors in infancy and childhood. *Arch Surg* 1974;109:143-147
 80. Ruymann FB, Raney RB Jr, Crist WM, Lawrence W Jr, Lindberg RD, Soule EH. Rhabdomyosarcoma of the biliary tree in childhood. *Cancer* 1985;56:575-581
 81. Witcombe JB. Biliary rhabdomyosarcoma of childhood. *Br J Radiol* 1979;52:1005-1006
 82. Takayanagi K, Issa M, Cook RCM. Obstructive jaundice in infancy due to compression of the bile ducts by malignant lymph nodes. *J Pediatr Surg* 1980;15:343-344
 83. Tiara Y, Nakayama I, Moriuchi A. Sarcoma botryoides arising from the biliary tract of children: a case report with review of the literature. *Acta Pathol Jpn* 1976;26:709-718
 84. Nagaraj HS, Kmetz DR, Leithmer C. Rhabdomyosarcoma of the bile ducts. *J Pediatr Surg* 1977;12:1071-1074
 85. Akers DR, Needham ME. Sarcoma botryoides (rhabdomyosarcoma) of the bile ducts with survival. *J Pediatr Surg* 1971;6:474-479

Perforation of the Augmented Urinary Bladder in Nine Children and Adolescents: Importance of Cystography

Richard M. Braverman^{1,2}
Robert L. Lebowitz¹

Augmentation of the urinary bladder is a popular surgical procedure for increasing the capacity and lowering the intraluminal pressure in patients whose bladder is small, noncompliant, or has high pressure. Among 250 augmentations performed at our hospital, nine patients have had 16 episodes of postoperative extravasation of urine from their augmented bladder. Thirteen episodes were studied by fluoroscopically monitored contrast cystography, which was diagnostic in 12. One patient's perforation was noted during an unrelated operation and the other two died of peritonitis before cystography could be performed. Four episodes occurred early, within 3 weeks of surgery. All were at a surgical anastomosis and presumably represented incomplete healing. Each patient with an early episode of extravasation had a perforation later. Nine perforations occurred from 1.0 to 6.5 months after the augmentation. Of these, three occurred at an anastomosis and four occurred in the augmenting segment. The locations of two were never fully documented. Three perforations occurred late, from 2.5 to 6.0 years after surgery, and all were in the augmenting segment. Three of the nine patients died of complications associated with perforation.

Perforation of the bladder is not rare and is a potentially fatal complication of augmentation. Whenever a patient who has undergone augmentation has signs or symptoms suggesting perforation, cystography can play a crucial role in diagnosis and should be performed without delay.

AJR 157:1059-1063, November 1991

Augmentation of the urinary bladder is currently widely used to fashion a large-capacity, low-pressure reservoir for urine in patients with a small-capacity, high-pressure, or noncompliant bladder [1]. Augmentation is performed by removing a portion of stomach or a segment of ileum or colon from the gastrointestinal tract and anastomosing it to the patient's bladder or a portion thereof. Leakage of urine from the augmented bladder into the peritoneal cavity is a life-threatening complication. This may occur from the surgical anastomoses or through the augmenting bowel or stomach segment and can happen weeks or months after surgery. Perforations have even occurred suddenly many years after surgery in patients who had been doing well [2-5]. We have found cystography crucial in the management of patients with an augmented bladder and report our experience with 16 episodes of extravasation occurring in nine patients.

Report of Cases

We reviewed our experience with 250 augmentations of the urinary bladder performed between 1977 and 1990. The most common indication, meningocele with bladder sphincter dyssynergia, accounted for nearly 40% of the surgeries. The next three most common indications were exstrophy/epispadias, chronic bladder dysfunction due to posterior urethral valves (the so-called valve bladder) [6], and decreased bladder compliance due to prior surgery. Together, these four indications accounted for more than 80% of the augmentations performed. Ileal, cecal, and sigmoid augmentations each accounted for approximately

Received March 21, 1991; accepted after revision July 16, 1991.

Presented at the Annual meeting of the American Roentgen Ray Society, Boston, MA, May 1991.

¹ Department of Radiology, Children's Hospital and Harvard Medical School, Boston, MA 02115. Address reprint requests to R.L. Lebowitz, Department of Radiology, Children's Hospital, 300 Longwood Ave., Boston, MA 02115.

² Present address: Department of Radiology, Texas Children's Hospital, 6621 Fannin St., Houston, TX 77030.

0361-803X/91/1575-1059
© American Roentgen Ray Society

25% of the total surgeries. Augmentation with stomach or ileocecum accounted for the remaining 25%.

We prospectively identified 16 episodes of extravasation occurring in nine patients, seven of whom were girls. All leaks were intraperitoneal. At the time of augmentation, the children ranged from 2 years 9 months to 14 years old. Eight had neurogenic dysfunction due to meningocele, and one had exstrophy of the bladder. After the immediate postoperative period, all drained their augmented bladder by intermittent catheterization. Six of the bladders were augmented with ileum and one each with ileocecum, sigmoid colon, and stomach.

Of the 16 episodes, 12 were diagnosed by fluoroscopically monitored contrast cystography. Two patients died before cystography could be performed, and one of the perforations was discovered during a subtotal colectomy. In only one case was the result of cystographic examination falsely reassuring.

Four episodes in three patients occurred within several weeks of surgery. These early leaks were all at the bladder-augmentation anastomosis and probably represented incomplete healing. Two of the leaks, one 9 days and the other 15 days after surgery, were asymptomatic and were noted on routine postoperative cystography. Both were simply and successfully treated by extending the usual period of suprapubic and urethral catheter drainage. Follow-up cystography in one case 12 days and in the other 15 days later showed that the anastomoses had healed. In the third patient, a marked decrease in urine output from her suprapubic tube and abdominal distension occurred 8 days after surgery. A cystogram showed extravasation, which was treated with surgery. She had a subsequent asymptomatic anastomotic leak 17 days later shown on a routine cystogram. This episode was treated by drainage of an intraperitoneal urinoma and continued bladder drainage. Findings on a cystogram 21 days later were normal. Each patient with an early episode of extravasation subsequently had a perforation later.

Nine perforations occurring from 1.0 to 6.5 months after augmentation were arbitrarily denoted intermediate. All were symptomatic. Three were anastomotic, four occurred through the augmenting bowel segment, and the locations of two were never fully documented. Of the three intermediate anastomotic perforations, two were diagnosed by cystography and were surgically repaired; the third patient died of this complication and her perforation was diagnosed at autopsy. Cystography was not performed in that case. Two of the four intermediate bowel-segment perforations were diagnosed cystographically and were surgically repaired. One of the four was diagnosed and repaired during an emergent subtotal colectomy for bleeding, and the last was diagnosed at autopsy. In these two cases, cystography was not performed. Of the intermediate perforations whose site was unknown, one patient was successfully treated nonoperatively by bladder drainage, and one died of sepsis 1.5 months after percutaneous drainage of an intrapelvic collection that probably resulted from a perforation.

There were three late perforations, all through the bowel segment, occurring 2.5, 4.0, and 6.0 years after augmentation. All were symptomatic and all had surgical repair. Each of the patients with a delayed perforation had suffered one or more earlier perforations as well.

Presenting signs and symptoms of perforation included abdominal pain, nausea, vomiting, lethargy, fever, and hypotension. Leukocytosis, bacteriuria, and bacteremia were often noted. Two of the patients complained of shoulder pain due to diaphragmatic irritation (Kehr sign). Several noticed decreased urine output either from a previously placed suprapubic tube or from intermittent catheterization.

Three of the patients with perforation died of overwhelming *Escherichia coli* sepsis. The remaining 13 episodes were successfully treated. Many of the patients who had a ventriculoperitoneal shunt required temporary externalization of the shunt because of perforation-induced peritonitis. Two patients required permanent revision of

their shunt, one to a ventriculoatrial system and another to a ventriculopleural system.

In the cases in which the site of perforation was analyzed pathologically, findings included local fibrosis, necrosis, muscular atrophy, mucosal disorganization, and inflammatory reaction. These nonspecific findings did not elucidate the cause of the perforations.

Discussion

For many years, urinary diversion was the standard treatment for children who had problems with storage or release of urine from their bladder. Although diversion often provided effective drainage of the upper urinary tract, it was cumbersome, unaesthetic, and fraught with complications.

In the past 15 years, bladder augmentation has emerged as an alternative to urinary diversion. This technique is designed to create a large-capacity, low-pressure reservoir. The leading indication for augmentation in children is meningocele with bladder-sphincter dyssynergia. Other indications include bladder exstrophy, cloacal exstrophy, prior bladder tumor, radiation fibrosis, postoperative bladder scarring, and so-called valve bladder.

A rare patient can empty the augmented bladder by normal voiding. Most patients, however, drain their bladder by clean intermittent catheterization [7, 8]. Patients requiring intermittent catheterization fall into two main categories: those with primary urinary retention, often due to neurologic disease, and those whose incontinence was treated with bladder neck or urethral procedures to produce continence (i.e., iatrogenic retention).

Complications of bladder augmentation include metabolic derangement caused by electrolyte reabsorption, vesicoureteral reflux, persistent incontinence, bladder calculi, bowel obstruction due to adhesions, and neoplasm [6, 9]. Perforation is another potentially life-threatening problem. We have seen nine patients who have had one or more perforations among 250 patients who have undergone bladder augmentation. This incidence is strikingly similar to that reported by Rink and Mitchell [5], who noted 16 spontaneous perforations (in 14 patients) in 231 augmentations or total bladder replacements. The fact that five of our nine patients suffered multiple perforations suggests a nonrandom distribution. Rushton et al. [2], Elder et al. [4], and Rink and Mitchell [5] have noted recurrent perforations in some of their patients as well. Early leakage at a surgical anastomosis [10] probably represents incomplete healing but may herald a patient at risk for a later perforation. The cause of delayed anastomotic leaks and of perforations through the augmenting bowel segments is not known, although there are many hypotheses.

Some have suggested that increased intraluminal pressure is partly responsible for perforations in augmented bladders. Notably in patients with increased outlet resistance, high pressure does not simply result in voiding, but instead, exerts substantial force on the walls of the reservoir. This force may cause perforation by stressing anastomoses and other preexisting areas of diminished mural integrity. Alternatively, high pressure may itself compromise mural strength by inducing ischemia [11, 12].

Increased intraluminal pressure develops for many reasons. It may occur because of peristaltic contraction of the applied bowel, a problem that has been largely solved by detubularizing the bowel segment before performing the augmentation [13]. All but one of the patients reported here had augmentation with a detubularized bowel segment. High pressure also may occur because of detrusor hyperreflexia [14]. Additionally, blunt external trauma can increase intraluminal pressure and cause perforation [15]. Finally, high pressures may develop when patients simply neglect to empty their bladder at reasonable intervals, or when mucus or other debris prevents complete emptying [11].

Some have postulated that delayed perforations result from direct catheter trauma at the time of intermittent catheterization. Elder et al. [4] have theorized that intraluminal adhesions, which develop while the augmented bladder heals in a non-distended state, can distort and fix the bladder so that a catheter might contact and traumatize the same region repeatedly [4]. The argument that these perforations are catheter induced is undermined by two facts: (1) such perforations have been reported in patients who are never catheterized, and (2) many of the perforations seen in patients who do undergo catheterization occur at remote sites within the bladder. Some believe that if catheterization plays any role at all, it does so by facilitating chronic infection which results in transmural inflammation predisposing to perforation [4].

Sheiner and Kaplan have suggested that perforation may occur when adhesions between the augmenting segment and the abdominal wall are avulsed as the bladder distends [3].

The causes of the perforations in the patients reported here are unknown. In several patients, increased intraluminal pressure was probably at least partly responsible. Four patients had significant detrusor hyperreflexia with high-pressure uninhibited contractions on urodynamic evaluation, which is now done routinely after augmentation. One boy failed to adhere to his catheterization schedule; overdistension probably caused at least two of his three perforations. Of note, in addition to augmentation, this patient had undergone the Kropp procedure, an operation that creates a continence mechanism that actually becomes progressively more effective as the bladder distends [16]. In several patients, thick mucus sometimes prevented complete bladder emptying. In none of the patients was blunt abdominal trauma implicated. As for the role of catheterization, we found that most of the perforations were in areas where direct catheter trauma was unlikely (Fig. 1). We could not, however, exclude a contribution from infection induced by catheterization because, despite the use of prophylactic antibiotics, most of the patients had nonsterile urine. These cases do not enable us to assess the validity of the avulsed adhesion theory [3].

Neurogenic dysfunction of the bladder, for some reason, appears to increase the risk of perforation after augmentation. Eight of the nine patients with perforation had meningocele, although this category comprised only 40% of the patients who had their bladder augmented. It is possible that the combination of the need for intermittent catheterization because of high outlet resistance and the tendency for overdistension of the bladder due to diminished sensation places these patients at special risk.

Aside from the cases of asymptomatic early leakage, all the patients in this series had acute illness. The presence of meningocele in many of them, however, complicated assessment of their history and physical findings. Symptoms of perforation were sometimes tempered by diminished pain sensitivity [2, 4], and in one patient, shoulder pain was a sign of perforation on two occasions but on a third occasion was simply related to irritation of the diaphragm by her ventriculoperitoneal shunt catheter.

Several authors have disparaged cystography in diagnosing perforation of the augmented bladder. Rink and Mitchell [5], for example, noted nine cystograms with falsely normal results in their 14 patients with spontaneous perforation. In the 10 patients with perforation reported by Rushton et al. [2], Sheiner and Kaplan [3], and Elder et al. [4], seven had normal findings on cystography. Elder et al. [4] have commented on the difficulty of distinguishing well-contained leaks from the markedly irregular contours of intact augmented bladders. Cases have also been reported in which leaks that were missed by cystography appeared during surgery to be sealed by adherent peritoneal or abdominal wall tissues [3].

We, on the other hand, have found fluoroscopically monitored contrast cystography invaluable for diagnosis, and we rely heavily on it to detect extravasation. It is a simple and direct method for identification and localization of perforation. By comparison, sonography can provide only indirect evidence of perforation (i.e., fluid in the peritoneal cavity), and in patients with a ventriculoperitoneal shunt (eight of the nine in this series) this finding is nondiagnostic because the fluid may simply be CSF.

We now routinely perform cystography several weeks after surgery to detect anastomotic leaks while bladder drainage catheters are still in place and to establish the baseline appearance of the augmented bladder. Thereafter, cystography is performed without delay in any patient with an augmented bladder who has signs or symptoms suggesting perforation.

We empty the patient's bladder before cystography to avoid dilution of the administered contrast agent. Then we instill 17% iodinated contrast material into the bladder by drip infusion under fluoroscopic monitoring with the contrast reservoir placed approximately 1 m above the bladder [17]. The bladder is filled until the flow spontaneously ceases, the patient experiences discomfort, or a leak is fluoroscopically identified. Knowing the volume used during earlier cystograms or the volume obtained by prior catheterization often enables us to estimate the capacity of the augmented bladder. Filming is performed in frontal, lateral, and oblique projections so that a posterior or anterior leak will not be obscured by contrast material in the augmented bladder (Figs. 1 and 2). The diagnosis of perforation is made when contrast material is actually seen to be leaking from the augmented bladder (Figs. 1-4) or when the administered contrast agent is otherwise detected in the peritoneal cavity. In one case the diagnosis was made because of relative lucency of the liver after cystography (Fig. 5), that is, the liver was outlined by faintly opacified peritoneal fluid [18].

We have encountered only one examination in which results of cystography were falsely reassuring. This patient had

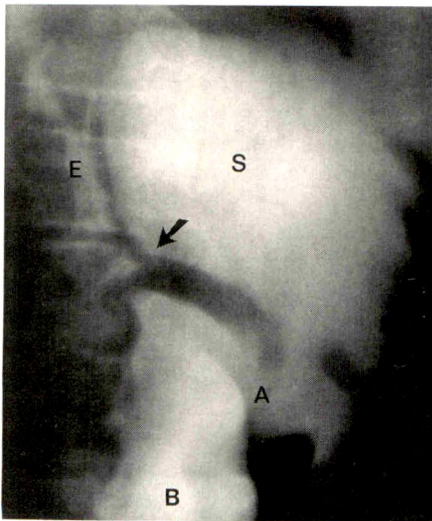


Fig. 1.—10-year-old boy with bladder exstrophy. Cystogram (frontal view) shows late postoperative perforation through augmenting segment of colon (arrow) at a site unlikely to have been subjected to catheter trauma. This was not visible on lateral view (not shown). E = extravasated contrast material; S = sigmoid colon segment; A = region of anastomosis; B = bladder.

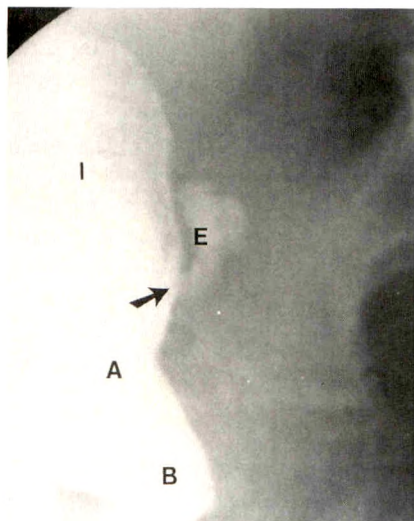


Fig. 2.—10½-year-old girl with meningocele. Cystogram (lateral view) shows late postoperative perforation through augmenting segment of ileum (arrow). This was not visible on frontal view (not shown). I = ileal segment; E = extravasated contrast material; A = region of anastomosis; B = bladder.

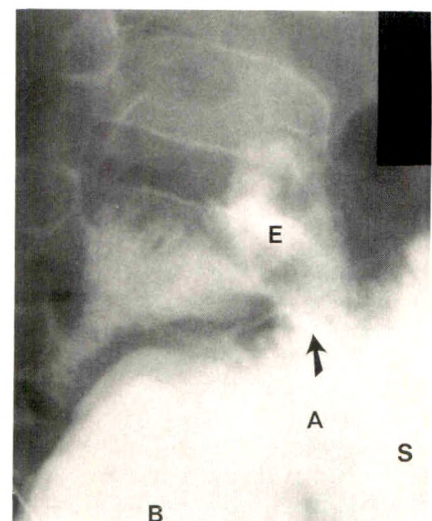
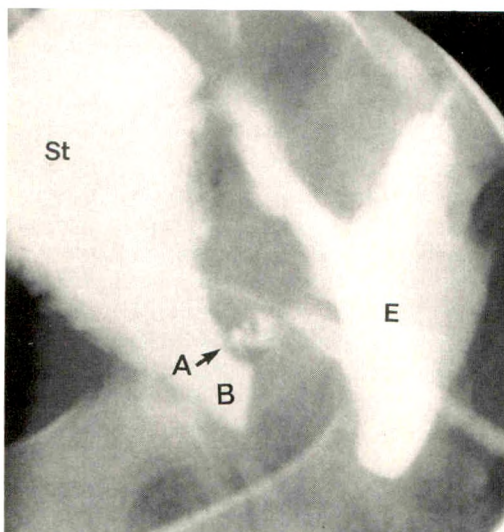


Fig. 3.—6-year-old boy with bladder exstrophy (same patient as Fig. 1, 4 years earlier). Cystogram (frontal view) shows early postoperative extravasation through anastomosis between augmenting sigmoid colon segment and bladder. E = extravasated contrast material; A = region of anastomosis; S = sigmoid colon segment; B = bladder.

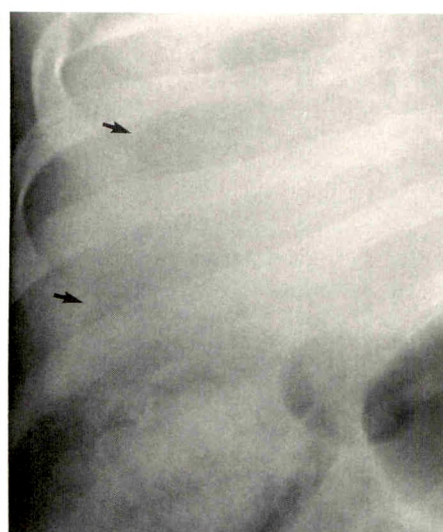
sepsis, but a cystogram showed no leak. Sonography, CT, and a labeled leukocyte scintigram showed a complex mass in the pelvis, perhaps related to an old sealed perforation. Although percutaneous drainage of the collection resulted in clinical improvement and discharge from the hospital, the patient died less than 2 months later, and two small anastomotic leaks were identified at autopsy.

In summary, perforation of the augmented bladder is not rare and can be life threatening. In our experience, extravasation in the first few postoperative weeks is usually asymptomatic, occurs at anastomoses, and may identify patients at

risk for later perforations. Perforations in the first several months after surgery are symptomatic and occur either at an anastomosis or through the augmenting bowel segment. Late perforations, occurring years after surgery, are symptomatic and occur through the augmenting segment. The diagnosis of perforation should be considered in any patient with augmentation of the bladder who has abdominal pain, fever, shoulder pain, or decreased urine output. Patients with meningocele seem to be at special risk. Cystography with fluoroscopy is the imaging study of choice, should be performed immediately, and is usually diagnostic.



4



5

Fig. 4.—8-year-old girl with meningocele. Cystogram (lateral view) shows intermediate postoperative perforation through anastomosis between augmenting stomach segment and bladder (arrow). St = segment of stomach; E = extravasated contrast material; A = region of anastomosis; B = bladder.

Fig. 5.—14-year-old boy with meningocele. View of right upper quadrant of abdomen after cystography shows that lateral margin of liver (arrows) is outlined by peritoneal fluid that is faintly opacified by extravasated contrast material.

ACKNOWLEDGMENTS

Stuart B. Bauer and N. Thorne Griscom made many helpful suggestions. Elaine Donnelly and Paulette Fontaine typed the manuscript, and Donald Sucher prepared the illustrations.

REFERENCES

1. Smith RB, Van Caugh P, Skinner DG, Kaufman JJ, Goodwin WE. Augmentation enterocystoplasty: a critical review. *J Urol* **1977**;118:35-39
2. Rushton HG, Woodard JR, Parrott TS, Jeffs RD, Gearhart JP. Delayed bladder rupture after augmentation enterocystoplasty. *J Urol* **1988**;140:344-346
3. Sheiner JR, Kaplan GW. Spontaneous bladder rupture following enterocystoplasty. *J Urol* **1988**;140:1157-1158
4. Elder JS, Snyder HM, Hulbert WC, Duckett JW. Perforation of the augmented bladder in patients undergoing clean intermittent catheterization. *J Urol* **1988**;140:1159-1162
5. Rink RC, Mitchell ME. Role of enterocystoplasty in reconstructing the neurogenic bladder. In: Gonzalez ET, Roth D, eds. *Common problems in pediatric urology*. St. Louis: Mosby-Year Book, **1991**:192-204
6. Gonzales ET Jr. Alternatives in the management of posterior urethral valves. *Urol Clin North Am* **1990**;17:335-342
7. Lapides J, Diokno AC, Silber SJ, Lowe BS. Clean intermittent self-catheterization in the treatment of urinary tract disease. *J Urol* **1972**;107:458-461
8. Mitchell ME, Kulb TB, Backes DJ. Intestinocystoplasty in combination with clean intermittent catheterization in the management of vesical dysfunction. *J Urol* **1986**;36:288-291
9. Filmer RB. Bladder augmentation problems in neurovesical dysfunction (malignancy following bladder augmentations). *Dialogues Pediatr Urol* **1987**;10:7-8
10. Kuss R, Bitker M, Camey M, Chatelain C, Lassau JP. Indications and early and late results of intestinocystoplasty: a review of 185 cases. *J Urol* **1970**;103:53-63
11. Crane JM, Scherz HS, Billman GF, Kaplan GW. Ischemic necrosis: a hypothesis to explain the pathogenesis of spontaneously ruptured enterocystoplasty. *J Urol* **1991**;146:141-144
12. Essig KA, Sheldon CA, Brandt MT, Wacksman J, Silverman DG. Elevated intravesical pressure causes arterial hypoperfusion in canine colocolocystoplasty: a fluorometric assessment. *J Urol* **1991**;146:551-553
13. Sidi AA, Reinberg Y, Gonzalez R. Influence of intestinal segment and configuration on the outcome of augmentation enterocystoplasty. *J Urol* **1986**;136:1201-1204
14. Anderson PAM, Rickwood AMK. Detrusor hyper-reflexia as a factor in spontaneous perforation of augmentation cystoplasty for neuropathic bladder. *Br J Urol* **1991**;67:210-212
15. Hendren WH. Discussion of papers on bladder augmentation. *J Urol* **1988**;140:1164
16. Kropp KA, Angwafo FF. Urethral lengthening and reimplantation for neurogenic incontinence in children. *J Urol* **1986**;135:533-536
17. Koff SA, Fischer CP, Poznanski AK. Cystourethrography: the effect of reservoir height upon intravesical pressure. *Pediatr Radiol* **1979**;8:21-22
18. Colodny AH, Griscom NT. Clue to diagnosis of neonatal urinary ascites: relative radiolucency of liver shadow. *Urology* **1978**;11:295-299

Videotape Review

RSNA Today Video, Vol. 4, No. 6. Oak Brook, IL: The Radiological Society of North America, 1990. \$55; by subscription, 6 issues annually at \$185 for RSNA members and \$225 for nonmembers (videotape)

This issue of *RSNA Today Video* covers four topics. The running time of the tape is approximately 1 hr, and physicians who view the entire tape can complete and return an accompanying postcard for 1 credit hour in category 1 of the Physicians Recognition Award of the American Medical Association.

The first topic is sonographic and CT evaluation of pain in the right lower quadrant. R. Brooke Jeffrey, Jr., discusses sonographic findings, and a large part of his discussion is about the diagnosis of appendicitis. He stresses the necessity of seeing large numbers of correctly diagnosed cases as a means of gaining confidence with this technique because of the significant steepness of the learning curve and the well-known operator dependency of sonography. Although the images shown are of excellent quality, little time is spent on technique. Jeffrey reports on 300 cases of patients with pain in the right lower quadrant. Most (177) did not have appendicitis and did not have surgery. The findings were falsely negative in 10 cases and falsely positive in seven. In only nine cases were the results of the study nondiagnostic. Alec J. Megibow then follows with CT findings, essentially reporting 24 proved cases of appendicitis studied by CT. He clearly defines the criteria for diagnosing the abnormal appendix and the technique for examining patients who have pain in the right lower quadrant. He then goes into an excellent differential diagnosis of other pathologic changes in this area that can cause similar clinical features.

The second topic is a discussion of MR findings in multiple sclerosis. Meredith A. Weinstein gives an excellent description of the typical findings on both unenhanced and gadolinium-enhanced MR images and also covers the differential diagnosis of these findings. Images of both brain and spinal cord are shown. This is followed by Alisa D. Gean-Marton discussing recent work on changes in the callosal-septal interface that appear to be distinctive for multiple sclerosis. In 42 patients with multiple sclerosis, these changes were present in 93%. Conversely, in patients without multiple sclerosis, such changes were seen in only 1.5%. Although the images are

generally of excellent quality, a more generous use of arrows would help the viewer grasp these changes.

The third section of the tape addresses the bowler hat sign. Although this sign was originally described in 1965 as a reliable indicator of colonic polyps, Wallace T. Miller, Jr., presents 37 cases, clearly showing that the sign is not specific for polyps and that the orientation of the bowler hat can be used to differentiate between diverticula and polyps. The images presented are excellent, and the time devoted to this topic is appropriate.

The final segment of the tape addresses the sonographic diagnosis of hypertrophic pyloric stenosis. Excellent use of real-time and static sonograms with many arrows clearly shows the appearance of the pylorus and the method of measuring it. Sjirk J. Westra reports that measurements of pyloric diameter and length result in some overlap between a normal pylorus and one that is hypertrophic. However, he gives a formula for measurement of pyloric volume that results in no overlap between the two conditions.

Overall, the material presented on this tape is based on recent clinical research and provides imaging information useful to practicing radiologists. Obviously, the factual information can be gleaned from a review of the literature, but the videotape format is excellent for showing the imaging techniques and findings in the disease processes that are covered. Regular viewing of this series therefore provides an excellent update on a limited number of current topics and is recommended. The major problems that I see with the use of videotapes are the limited number of topics that can be covered in a reasonable time and the difficulty in quickly reviewing these topics on tape as opposed to referring to journals or texts, which usually are immediately available in the office or department.

E. Stephen Amis, Jr.
Columbia-Presbyterian Medical Center
New York, NY 10032

Case Report

Fetal Abdominal Wall Mass Detected on Prenatal Sonography: Gastroschisis vs Omphalocele

Rita R. Perrella,¹ Nagesh Ragavendra,¹ Franklin N. Tessler,¹ Ines Boechat,¹ Barbara Crandall,² and Edward G. Grant¹

The prenatal sonographic differentiation of a gastroschisis from an omphalocele is not always clear, even though the two entities are reported to be embryologically distinct and to have characteristic sonographic findings. We report a case of a ventral wall mass that at first had the sonographic characteristics of an omphalocele but later had distinct characteristics of a gastroschisis. The gastroschisis then disappeared. Coinciding with the disappearance of the gastroschisis was the onset of bowel obstruction.

This intriguing sequence of events supports a theory put forth in 1975 [1] that the embryogenesis of a gastroschisis is not distinct from that of other umbilical cord masses but is, in fact, the result of rupture of the amniotic membrane at the base of the umbilical cord in a fetus with a small umbilical cord mass.

Case Report

A 20-year-old primigravid woman who had had juvenile-onset insulin-dependent diabetes since she was 9 years old had a pregnancy complicated by hypertension and episodes of poorly controlled levels of blood glucose. The initial sonography was performed at another hospital. A 12.7-week fetus was detected that had an umbilical cord mass (Figs. 1A and 1B) diagnosed as an omphalocele. The woman was referred to our institution because of her high-risk pregnancy. Sonography showed a 16.5-week intrauterine gestation.

A 14-mm soft-tissue extracoelomic mass was detected to the right of a normal umbilical cord near the cord's insertion into the fetal abdomen. This mass was sonographically consistent with a gastroschisis (Fig. 1C). The volume of amniotic fluid was normal. No other abnormalities were detected. Amniocentesis showed a normal fetal karyotype of 46,XX. The amniotic fluid had a markedly elevated level of alpha-fetoprotein (AFP) (9.73 mg/ml), and a test for acetylcholinesterase (AChE) was weakly positive.

The mass was again detected sonographically at 18.8 weeks' gestation (Fig. 1D). It had become slightly smaller. However, multiple dilated loops of bowel were now evident in the fetal abdomen. On follow-up sonography performed at 22.6 weeks' gestation (Fig. 1E), no trace of the extraabdominal mass could be found despite exhaustive scanning. Likewise, further follow-up at 23.5 and 32.3 weeks' gestation failed to show the extraabdominal mass. On each subsequent follow-up sonogram, however, the fetal bowel was progressively more distended (Fig. 1F). Fetal growth parameters remained otherwise appropriate.

At 36 weeks' gestation, the patient had a cesarean delivery of a 3500-g female neonate with Apgar scores of 9 at 1 min and 9 at 5 min. The neonate had a grossly distended abdomen with no defects in the ventral wall. Gross and pathologic examination of the placenta and umbilical cord revealed no abnormalities. The results of gastrointestinal studies with contrast material were consistent with complete malrotation, shortening of the midgut, and a microcolon. At surgery, no abnormalities of the ventral wall were detected. Complete malrotation, nearly a 70% jejunoileal absence of the small bowel with proximal obstruction, and a microcolon were confirmed. A jejunostomy was performed.

Received April 4, 1991; accepted after revision June 12, 1991.

¹ Department of Radiological Sciences, University of California, Los Angeles, School of Medicine, 10833 Le Conte Ave, Los Angeles, CA 90024. Address reprint requests to R.R. Perrella.

² Department of Pediatrics, University of California, School of Medicine, Los Angeles, CA 90024.

AJR 157:1065-1068, November 1991 0361-803X/91/1575-1065 © American Roentgen Ray Society

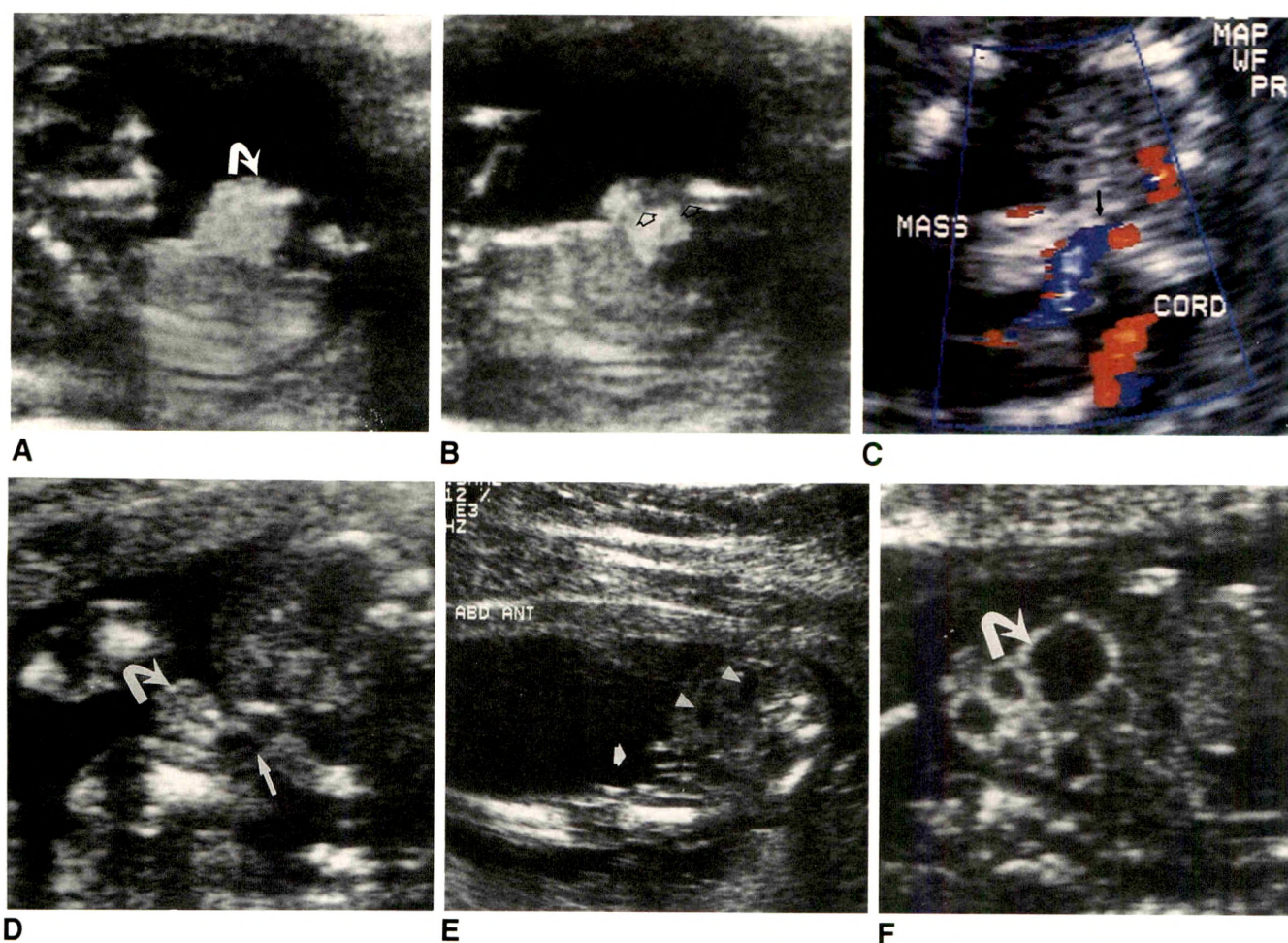


Fig. 1.—A, Sagittal sonogram of 12.7-week fetus with large omphalocele (arrow).
 B, Magnified sonogram of 12.7-week fetus shows umbilical vessels (arrows) coursing through omphalocele.
 C, Color Doppler sonogram of 16.5-week fetus with gastroschisis shows a paraumbilical mass with cord vessels (arrow) inserting normally. Umbilical arteries are red; umbilical vein is blue.
 D, Transverse sonogram of 18.8-week fetus shows normal insertion of umbilical cord (straight arrow) and small paraumbilical mass at base of cord (curved arrow).
 E, Sonogram of 22.6-week fetus shows disappearance of extracoelomic mass, normal insertion (arrow) of umbilical cord, and dilated loops of bowel (arrowheads).
 F, Sonogram of 32.3-week fetus shows progressively dilated bowel (arrow).

Discussion

Because the mother's diabetes necessitated frequent examinations during her pregnancy, we were able to document the transformation and subsequent disappearance of a ventral wall mass in the fetus. Three cases of disappearing ventral wall masses have been described in the literature [2]. In each case, the fetus had either a patent urachus or a vesicoallantoic mass in the abdominal wall that disappeared in the third trimester so that no abnormalities of the abdominal wall or umbilical cord were detected sonographically. At delivery, however, the base of the neonate's umbilical cord in each of these three cases had a defect.

Unlike the neonates in these cases, our neonate had absolutely no defect in the umbilical cord on physical and pathologic examinations, and no abnormalities of the abdominal wall were seen at delivery or subsequent surgery. The initial sonogram at 12.7 weeks' gestation showed a large mass in the umbilical cord "one half the diameter of the abdomen,"

approximately 11 mm (Fig. 1A). A mass larger than 7–10 mm at 8–12 gestational weeks or persistence of the bowel in the cord beyond 12 weeks is an omphalocele [3]. The significantly elevated levels of AFP and the presence of AChE in amniotic fluid at 16.5 weeks' gestation confirmed that a defect in the ventral wall had been present. Although AFP and AChE can become elevated with both a gastroschisis and an omphalocele, extremely high levels of AFP (9.73 mg/ml) are consistent with a gastroschisis because bowel comes directly in contact with the fluid.

In 1975, Shaw [1] published an article describing gastroschisis as the result of rupture of the amniotic membrane that occurred at the base of the umbilical cord in an embryo whose umbilical ring closure had been delayed or perhaps earlier at the time of normal physiologic umbilical herniation. Embryologically, somatization of the anterior abdominal wall is normal, and formation of the umbilical ring by the cephalic, caudal, and lateral folds is normal also. Failure of closure of the

umbilical ring in some embryos, however, results in a small isolated omphalocele or an umbilical cord hernia. Although Shaw and others have used the terms *small omphalocele* and *hernia of the umbilical cord* interchangeably, we define a small omphalocele (containing bowel only) as that resulting from failure of all or some of the intestines to return. We reserve umbilical cord hernia for those cases in which all of the intestines have returned normally, but some loops later prolapse through a patent umbilical ring. The key point is that these small isolated omphaloceles form as a result of mechanical rather than teratogenic events and therefore are rarely associated with abnormal karyotypes or non-bowel-related malformations. Shaw believes that the right umbilical vein, which normally disappears during embryogenesis, leaves an area of potential weakness where rupture may occur. The remaining left umbilical vein and omphalomesenteric vessels are to the left of this weak area, so that rupture would position eviscerated bowel to the right side. After rupture, the defect appears separate from the umbilical cord, because once the membrane has ruptured in utero, skin grows in from the edges, decreasing the size of the defect and forming a skin bridge. Infarction and atresia may ensue as a result of strangulation by a contracting umbilical defect or strangulation associated with volvulus.

In 1980, a similar theory was put forth again. DeVries [4] postulated that rather than an area of potential weakness at the base of the umbilical cord, an area of weakness in the paraumbilical abdominal wall was present as a result of abnormal circulation to the somatopleure during involution of the right umbilical vein. Interestingly, DeVries points out that in gastroschisis, "a portion of the medial wall of the defect usually includes the umbilical cord." If true, this tends to support Shaw's theory. Others [5] have postulated that the vascular pathogenesis of a gastroschisis does not involve the right umbilical vein, but ischemia of the omphalomesenteric artery leads to infarction and necrosis at the base of the umbilical cord, resulting in herniation of gut through this infarcted area and subsequent healing and resorption of tissue on the margins. Although the cause of the defect in the base of the cord is said to be arterial, this theory also supports Shaw's early theory that gastroschisis is the result of rupture at the base of the umbilical cord. In 1985, the first documented prenatal sonographic confirmation of Shaw's theory was reported [6].

This case has several important implications. The findings support the theory that gastroschisis may be the result of in utero rupture of the amniotic membrane at the base of the umbilical cord and that the concept of a separate embryogenesis for gastroschisis distinct from that of other small umbilical cord masses should be reevaluated. Seashore [7] reported that Shaw's theory is a unifying concept that explains many of the observed differences between an omphalocele and a gastroschisis. Seashore stated, however, that Shaw's theory failed to explain why neonates with a gastroschisis have malrotation, whereas in omphaloceles, malrotation occurs in those with the largest defects. Although malrotation does occur in large omphaloceles, likewise, the small omphaloceles, or so-called celosomia, which result when the umbilical orifice remains open, are occupied by midgut, which is fre-

quently malrotated [8]. This would explain why neonates with a gastroschisis have malrotation.

The theory that small omphaloceles containing only bowel may have an embryogenesis separate from that of more severe types is also supported [6-9]. During normal embryogenesis, the cephalic, caudal, and lateral folds converge to form the ventral wall. Body closure is complete by the fourth week except for the body stalk, which will contain physiologically herniated gut [7]. During the 10th through 12th weeks, the gut returns and the body stalk constricts to become the umbilical cord [7]. If a mechanical failure occurs in the final stages of closure of the abdominal wall resulting in a patent umbilical ring, all or some of the gut may fail to return, forming a small omphalocele. Liver is never extracorporeal during development, and, therefore, the presence of liver in an omphalocele suggests a separate cause [8]. Because these small, isolated omphaloceles are not the result of a teratogenic injury, a gastroschisis formed from a rupture at the base of the umbilical cord would rarely be associated with chromosomal abnormalities or nongastrointestinal anomalies. Recent studies reporting that omphaloceles containing only bowel are associated with an underlying chromosomal abnormality [10, 11] seemingly contradict our theory. A review of these two articles, however, shows that most [10], if not all [11], of the fetuses with omphaloceles containing only bowel did not have isolated omphaloceles such as we are describing but had severe associated malformations such as holoprosencephaly, cystic hygroma, and cardiac defects. In these studies, fetuses that had small omphaloceles plus other associated malformations were more likely to have abnormal karyotypes. These omphaloceles form, not as isolated malformations resulting from mechanical injury, but as part of a major teratogenic injury that produces a multitude of concurrent abnormalities, which are all probably caused by the chromosomal defect. Therefore, while it has been shown that a small omphalocele accompanied by other malformations has a higher association with an underlying chromosomal disorder [10, 11], it has not been shown that an isolated small omphalocele will have a higher association with an underlying chromosomal disorder, and any such generalization is misleading. In contrast to small omphaloceles containing only bowel, in which mesodermalization of the anterior abdominal wall is normal (apparently even with a chromosomal defect), large omphaloceles are the result of a teratogenic injury that has disrupted mesodermalization of the anterior abdominal wall. Abdominal muscles, fascia, and skin are absent at or surrounding the junction of the umbilical cord with the abdomen [4]. There is a widely open umbilical orifice through which contents may extrude. In these omphaloceles, nature has already provided a "rupture." Omphaloceles containing liver and gut result from early arrested development of the lateral folds in the third or fourth gestational week [7, 8] with normal development of the cephalic folds. Large thoracoabdominal omphaloceles result from arrested development of the cephalic folds, as well as the lateral folds [8, 11]. This explains associated anomalies such as ectopia cordis, intracardiac malformations, and defects of the sternum or diaphragm.

Finally, the sequence of events occurring in our neonate supports the theory that resorption of a devitalized segment

of bowel may be the genesis of intestinal atresia [1, 7, 9, 12]. At birth, our neonate had no signs that a defect in the ventral wall had ever been present. She was born, however, with significant atresias and complete malrotation. The disappearance of the mass on sonography coincided temporally with the appearance of bowel obstruction. The solid appearance of the mass suggested infarcted bowel, perhaps due to strangulation by a contracting umbilical defect or to strangulation caused by volvulus associated with abnormal mesenteric attachment [1]. It follows, and is supported in the literature [1, 7, 9, 12], that the disappearance of the mass in our case was associated with resorption of infarcted bowel. Strangulation, infarction, and subsequent resorption of this extruded bowel resulted in intestinal atresia that was seen on sonograms as progressively dilated bowel.

REFERENCES

1. Shaw A. The myth of gastroschisis. *J Pediatr Surg* **1975**;10:235-244
2. Persutte WH, Lenke RR. Disappearing fetal umbilical cord masses: are these findings suggestive of urachal anomalies? *J Ultrasound Med* **1990**;9:547-551
3. Brown DL, Emerson DS, Shulman LP, Carson SA. Sonographic diagnosis of an omphalocele during the tenth week of gestation (case report). *AJR* **1989**;153:825-826
4. DeVries PA. The pathogenesis of gastroschisis and omphalocele. *J Pediatr Surg* **1980**;15:245-251
5. Hoyme HE, Higginbottom MC, Jones KL. The vascular pathogenesis of gastroschisis: intrauterine interruption of the omphalomesenteric artery. *J Pediatr* **1981**;98:228-231
6. Glick PL, Harrison MR, Adzick NS, Filly RA, deLorimier AA, Callen PW. The missing link in the pathogenesis of gastroschisis. *J Pediatr Surg* **1985**;20:406-409.
7. Seashore JH. Congenital abdominal wall defects. *Clin Perinatol* **1978**;5:61-77
8. Duhamel B. Embryology of exomphalos and allied malformations. *Arch Dis Child* **1963**;38:142-147
9. Moore TC. Gastroschisis and omphaloceles: clinical differences. *Surgery* **1977**;82:561-568
10. Nyberg DA, Fitzsimmons J, Mack LA, et al. Chromosomal abnormalities in fetuses with omphalocele: significance of omphalocele contents. *J Ultrasound Med* **1989**;8:299-308
11. Benacerraf BR, Saltzman DH, Estroff JA, Frigoletto FD Jr. Abnormal karyotype of fetuses with omphalocele: prediction based on omphalocele contents. *Obstet Gynecol* **1990**;75:317-319
12. Barnard CN. The genesis of intestinal atresia. *Surg Forum* **1956**;7:393-396

Technical Note

MR Angiography of Vascular Grafts in Children

David J. Fillmore,¹ E. Kent Yucel,¹ Susan E. Briggs,¹ Fred L. Steinberg,² and Arthur C. Waltman¹

Peripheral arterial occlusion in children, although not frequent, may result in growth disturbances in the affected extremity [1]. Arterial occlusion in children is usually due to trauma, either iatrogenic or environmental. MR angiography provides a new means of noninvasive vascular imaging that can be used to complement existing techniques for assessing graft patency such as Doppler sonography, segmental pressure measurements, and evaluation of limb growth. We report our experience with this technique in four children.

Subjects and Methods

MR Angiography Techniques

All studies were performed on a Signa 1.5-T MR scanner (General Electric Medical Systems, Milwaukee, WI). Time-of-flight MR angiography was performed in all cases. Axial sequential gradient-echo images were obtained with inferior presaturation and first-order flow compensation (Fig. 1A). Other parameters were 36–53/9.5–15.0 (TR/TE), one or two excitations, 3- to 5-mm slice thickness, 24- to 40-cm field of view (FOV), flip angle 30–50°, and 128 phase-encoding steps. In five of the six studies, the presaturation slab was applied inferior to the imaged volume. In the sixth study, an inferior presaturation pulse that tracks 5 mm behind the slice being imaged was applied (Fig. 1B) [2]. Up to 60 slices were obtained per acquisition and reprocessed by using a maximum-intensity-projection (MIP) algorithm to form anteroposterior and oblique MR angiograms.

Population of Patients

Four patients between 5 and 14 years old were evaluated. Two of the patients required vascular grafts as the result of acquired mycotic

pseudoaneurysms that developed during long-term arterial monitoring. One patient was treated for thrombosis of a posttraumatic pseudoaneurysm of the popliteal artery. One patient was treated for occlusion of the popliteal artery due to a land-mine blast injury. This patient underwent repeated examination after replacement of the occluded graft. A total of three iliofemoral and three superficial femoral to popliteal/tibial grafts were evaluated.

Correlative Studies

Comparative examinations were available for all six grafts studied. All four patients had one or more arterial plethysmography studies. Three patients had duplex and color Doppler sonography. Results of intraoperative contrast angiography were available for correlation in one patient, obtained on two separate occasions during graft revision. Routine diagnostic contrast angiography was available for correlation in one patient. Surgical correlation was available in two patients.

Results

With MR angiography, we accurately assessed graft patency and the status of the inflow and outflow vessels in five of the six grafts examined. All five graft occlusions were successfully identified (Figs. 1 and 2). One of the six grafts examined, thought to be occluded on the basis of arterial plethysmography, was obscured by magnetic susceptibility artifact due to metallic clips at the operative site. The inflow and outflow vessels to this graft were shown to be patent. Duplex Doppler sonography subsequently showed patency of this graft. Clinically, this graft was thought to have become relatively stenotic because of the patient's growth. In two

Received April 1, 1991; accepted after revision June 18, 1991.

¹ Departments of Radiology and Surgery, Massachusetts General Hospital, Boston, MA 02114. Address reprint requests to E. K. Yucel.

² Department of Radiology, Cedars-Sinai Hospital, Los Angeles, CA 90048.

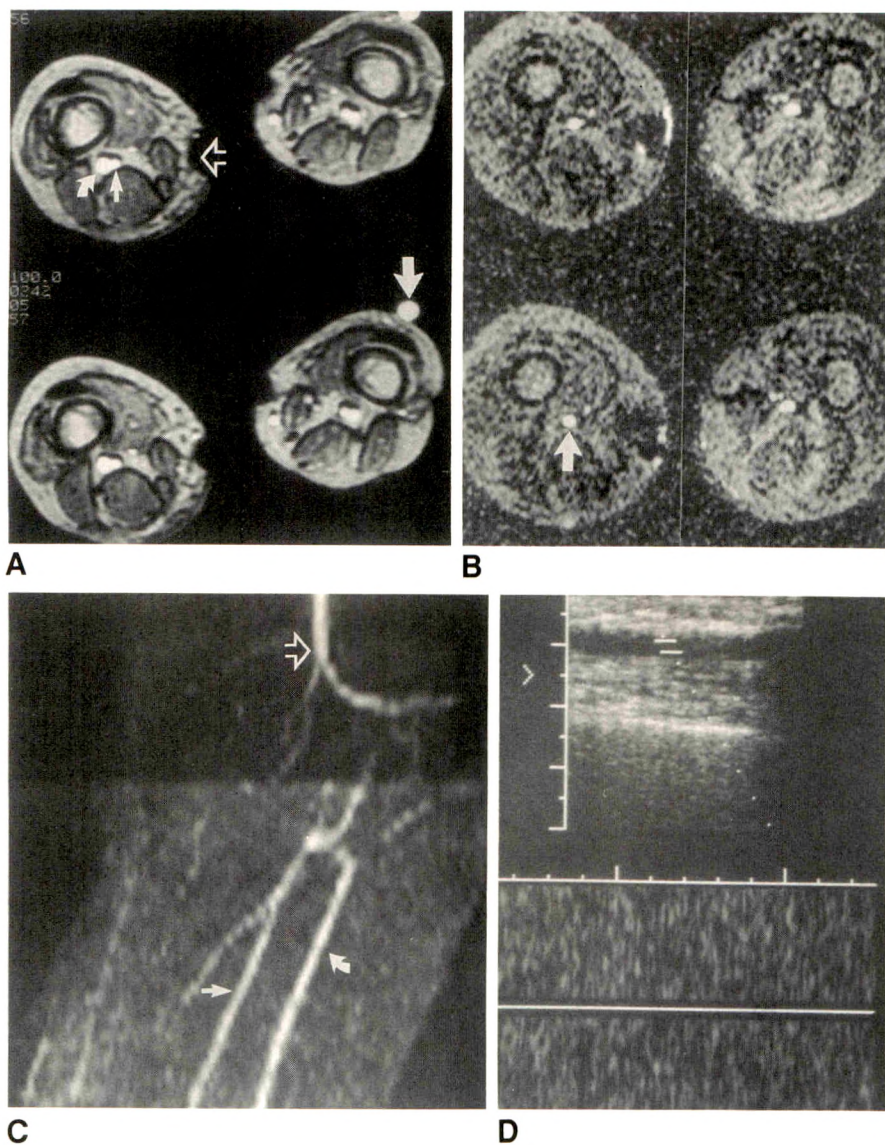


Fig. 1.—A, Axial gradient-echo (36/13/30°) MR images through distal thigh with saturation band below imaged volume. Femoral vein (curved arrow) is not adequately suppressed. Small straight solid arrow = superficial femoral artery; open arrow = clip artifact from saphenous vein harvesting; large straight solid arrow = gadolinium marker.

B, Axial gradient-echo (50/9.5/50°) MR images with tracking presaturation pulse with signal from artery only (arrow). Vein signal is completely suppressed. Clip artifact from previous contralateral vein harvesting is again seen.

C, Projection angiogram shows occlusion of popliteal artery (open arrow) and popliteal bypass graft with reconstitution of posterior (straight solid arrow) and anterior (curved arrow) tibial arteries.

D, Longitudinal duplex Doppler sonogram of popliteal bypass graft confirms graft occlusion.

cases, surgery was performed on the basis of the MR angiographic findings, and the MR findings were confirmed.

Discussion

Series of children with vascular injury reported in the surgical literature document that most of these injuries are due to iatrogenic trauma, including arterial catheterization for diagnostic arteriography, transcatheter therapeutic procedures, and invasive hemodynamic monitoring [3–5]. Arterial occlusion occurs in 3–5% of diagnostic cardiac catheterizations in children [6] and is more common in interventional cardiac catheterizations in children [3, 4]. It also occurs in peripheral and umbilical arterial catheterization performed for hemodynamic monitoring [5] and diagnostic arteriography for noncardiac indications.

Methods used to evaluate these vascular injuries in children have been quite variable. Catheter angiography is frequently

used in the acute setting, particularly if the injury is seen before the catheterization is completed. Serial evaluation of the peripheral pulses is routinely used with the addition of Doppler techniques to complement physical examination. Use of duplex Doppler and color Doppler techniques to evaluate the puncture site has been reported [7, 8]. IV digital subtraction angiography has also been used to image vascular injury in children [3].

MR angiography reliably shows the status of the inflow vessels supplying the vascular graft, the status of the graft, and the status of the outflow vessels supplied by the graft in standard anteroposterior and oblique projections, which are readily comparable to standard contrast angiograms. By using tracking spatial presaturation pulses, venous flow signal can be suppressed throughout the imaging volume, facilitating identification of the arterial anatomy in the reprojected images. A stationary venous saturation pulse outside the imaging volume may result in recovery of venous signal with overlap

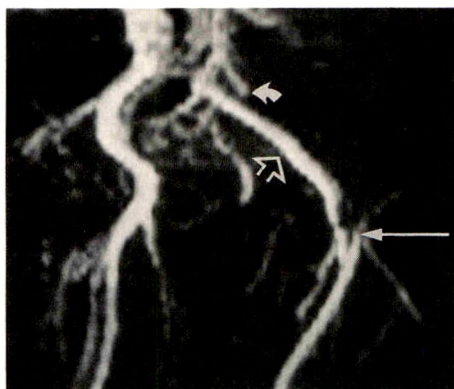


Fig. 2.—Left posterior oblique projection angiogram (36/13/45°) shows occlusion of left external iliac artery and iliofemoral bypass graft. Distal end of patent common iliac artery (curved arrow) and reconstituted common femoral artery (long arrow) can be identified. Open arrow = left iliac vein. Right iliac artery and vein are overlapped in this projection.

of venous structures in the subsequent reprojections. Figures 1A and 1B, with and without a tracking presaturation pulse, respectively, show the dramatic improvement in venous signal suppression when this technique is used. The presence of metallic clips immediately adjacent to the graft in one patient precluded adequate evaluation of the graft itself, although the inflow and outflow vessels were readily shown. Despite the presence of thrombus in the occluded graft shown in Figure 1, the signal intensity of the clot was insufficient on these flow-sensitive sequences to appear on the MIP reconstructions.

In this group of children, we have shown that MR angiography can accurately and noninvasively show vascular graft patency. We were able to characterize five of six grafts

completely by showing the status of the graft and the inflow and outflow vessels. MR angiography can supplant catheter angiography in the follow-up of many of these patients. In conjunction with impedance plethysmography, a completely noninvasive physiologic and anatomic assessment of this population can be done. Continued improvement in MR angiographic techniques, including shorter echo times and more rapid imaging (e.g., turboFLASH and echoplanar) may substantially shorten imaging times in the near future. These data can provide vascular surgeons and cardiologists caring for these children with a better understanding of the natural history of this problem and a better means of gauging the need and effectiveness of operative intervention in these patients.

REFERENCES

1. Bloom JD, Mozersky DJ, Buckley CJ, et al. Defective limb growth as a complication of catheterization of the femoral artery. *Surg Gynecol Obstet* 1974;138:524-526
2. Keller PJ, Drayer BP, Fram EK, Williams KD, Dumoulin CL, Souza SP. MR angiography with two-dimensional acquisition and three-dimensional display. *Radiology* 1989;173:527-532
3. Burrows PE, Bensen LN, Williams WG, et al. Iliofemoral arterial complications of balloon angioplasty for systemic obstructions in infants and children. *Circulation* 1990;82:1697-1704
4. Fellows KE, Radtke W, Keane JF, Lock JE. Acute complications of catheter therapy for congenital heart disease. *Am J Cardiol* 1987;60:679-683
5. Flanigan DP, Keifer TJ, Schuller JJ, et al. Experience with iatrogenic pediatric vascular injuries: incidence, etiology, management and results. *Ann Surg* 1983;198(4):430-439
6. Stanger P, Heymann MA, Tarnoff H, et al. Complications of cardiac catheterization of neonates, infants, and children: a three-year study. *Circulation* 1974;50:595-608
7. Taylor LM, Troutman R, Feliciano P, et al. Late complications after femoral artery catheterization in children less than five years of age. *J Vasc Surg* 1990;11:297-306
8. Sacks D, Robinson ML, Perlmutter GS. Femoral arterial injury following catheterization: duplex evaluation. *J Ultrasound Med* 1989;8:241-246

Book Review

Three-Dimensional Neuroimaging. Edited by Arthur W. Toga. New York: Raven, 317 pp., 1990. \$98

This exceptional work will be of interest to a cross section of scientists engaged in computational methods in several aspects of neurobiology. The outstanding contributions range from basic to clinical research. The primary thrust is digital imaging used to solve questions in research on the nervous system. The field of neuroimaging is so broad that this book is limited only to those disciplines that use physical sections of brain tissue and in which the imaging data are derived from analyses of serial sections. Although three-dimensional neuroimaging is a form of computational neuroscience, positron emission tomography and MR imaging are excluded. The contributors show the ways in which they use computers to facilitate their research.

The book is divided into three sections. Part I on instrumentation and procedures addresses image acquisition, frame processing, data presentation, high-resolution large-area analysis, neuronal arbor recording, and quantitative imaging. This section is valuable to both beginners and experts. Understanding it is essential for designing research projects that use these approaches. Knowledge needed is detailed here, and overviews are presented that allow novice investigators a close look at the issues. Common errors in image quantification are pointed out, and methods of system evaluation are suggested. Processing and management of data are carefully addressed in each chapter. Part II on methodologic applications deals with receptor binding, development of a digital brain atlas, and three-dimensional images of brain function. Neuroimaging techniques used to analyze histologic sections and autoradiographs, correlation of structure to function, and mapping and measurements are presented

in detail. The illustrations in this section are beautiful. With the exception of concept drawings, graphs, diagrams, and autoradiographs, the remaining 62 or so illustrations are in color. Color illustrations here and in the other sections give great value to the book. Limitations in each of the methods are carefully documented, and future directions are suggested. Part III contains selected topics on neuroimaging. The six chapters in this section include morphometrics, three-dimensional reconstruction, distortion correction, surface rendering, and an extensive data base of brain information.

Receptor-binding techniques offer expanded ways to study the action of neurotransmitters and drugs in the brain in order to understand mechanisms of function in health and disease. In chapter 5, loci of function is shown in three dimensions. Electronic integration of neuroanatomic information is presented in chapter 6 to show the development of a digital brain atlas in the rat. This method allows quantitative data matching unrestricted by sampling problems or section plane and results in three-dimensional comparisons.

All the chapters are well written, and the exquisite illustrations are often in color. An extensive subject index is included. The book is an excellent reference for those beginning or expanding into research that correlates structure and function in three dimensions by using neuroimaging techniques.

A. Basil Harris
University of Washington
Seattle, WA 98195

Review Article

Proton MR Spectroscopy in Multiple Sclerosis: Value in Establishing Diagnosis, Monitoring Progression, and Evaluating Therapy

Todd L. Richards¹

MR imaging is currently the technique of choice for evaluating brain lesions in patients with multiple sclerosis (MS). In addition to MR imaging, proton MR spectroscopy has shown potential in diagnosing MS and monitoring the progression of treatment. Spatially localized proton spectroscopy has been used to evaluate changes in choline, creatine, *N*-acetyl aspartate (NAA), lipids, and lactate in MS patients and in animal models of MS. The main spectroscopic findings are a decrease in the NAA:creatine ratio and an increase in the choline:creatine ratio in brain regions that include plaques defined by MR imaging. Proton MR spectroscopy along with MR imaging may be helpful in distinguishing those early lesions that might respond to therapy from late irreversible lesions. Preliminary evidence suggests that although the proton spectra acquired from patients with various brain diseases are similar (high choline, low NAA), there are differences in other resonances (lipids, lactate, glutamate, inositol) that could potentially help in diagnosing MS. Changes in proton metabolites potentially can be used to differentiate between the different stages of the MS lesion (hyperacute and edematous lesions, demyelinated lesions, and subacute to chronic plaques). It is hypothesized that successful treatment of demyelination and neuronal damage will be accompanied by changes in the proton spectrum (high choline:creatine ratio will lower to normal values and low NAA:creatine values will rise to normal values).

MR imaging is extremely sensitive to changes in water characteristics of tissue (i.e., edema, hemorrhage) and has been used to delineate focal abnormalities in multiple sclerosis (MS) [1]. Significant changes in T1 and T2 relaxation times

during the evolution of the disease have been reported [2]. Although conventional MR imaging is sensitive for detecting lesions, it cannot be used to characterize MS lesions chemically. The factors that influence image intensity in conventional MR imaging are complex, and image intensity changes cannot be used to infer specific pathologic events [3]. However, MR images enhanced with gadopentetate dimeglumine can be used to differentiate acute from chronic lesions in MS patients [4]. Information concerning the permeability of the blood-brain barrier obtained from these studies has provided insights about the pathogenesis and behavior of MS lesions [4].

In vivo MR spectroscopy can be used to measure relative concentrations and mobilities of different low-molecular-weight chemicals [5]. Proton MR spectroscopy can be used to monitor metabolites such as choline, creatine, *N*-acetyl aspartate (NAA), mobile lipids, and lactic acid [6, 7]. The purpose of this review is to discuss the value of proton MR spectroscopy in diagnosing MS, monitoring its progression, and evaluating its response to treatment.

Localized Proton Spectroscopy of the Brain

Recent developments in spatial localization techniques have allowed noninvasive acquisition of high-quality proton spectra from human and animal brains. These techniques rely on magnetic field gradients to spatially localize the MR spectroscopic signal. Proton spectroscopy is complicated by large

Received April 8, 1991; accepted after revision June 21, 1991.

This work was supported in part by National Institutes of Health grant R29NS24622 and the Regional Primate Center National Institutes of Health core grant RR00166.

¹ Department of Radiology, RC-05, University of Washington, Seattle, WA 98195. Address reprint requests to T. L. Richards.

AJR 157:1073-1078, November 1991 0361-803X/91/1575-1073 © American Roentgen Ray Society

unwanted signals from water and lipid. A proton spectrum of the brain in which the water signal is not suppressed (Fig. 1) contains a large water resonance that is at least 200 times more intense than the resonances of the proton metabolites (choline, creatine, NAA). Intense lipid signals from the scalp and adipose tissues around the head need to be suppressed by either active suppression or selective excitation of the brain tissue. Although many techniques have been used for volume-selective spectroscopy, studies in patients with MS have mainly used echo-generating pulse sequences such as single-voxel techniques [8, 9] and spectroscopic imaging (chemical-shift imaging) techniques [10]. Single-voxel techniques use pulse sequences in which three spatially selective RF pulses (either 90°-90°-90° pulses [8] or 90°-180°-180° pulses [9]) are used to produce an echo. As each of the three spatially selective RF pulses excites a different plane, the resultant echo signal arises from the intersection of the three planes. The spectroscopic imaging techniques acquire the proton signal from multiple voxels by using phase-encoding gradients [11]. Protocols that use localized spectroscopy must control for the fact that different regions of the brain have different concentrations of metabolites [12]. Technical challenges arise from variable water suppression, poor magnetic field homogeneity, nonreproducibility of position [13], the presence of eddy currents [14], and incomplete suppression of nonecho signals (gradient crusher amplitude too low). These factors can result in uninterpretable spectra.

In all studies mentioned in this review, proton spectra were quantified by dividing the peak area of the metabolite of interest by the peak area of another resonance in the spectrum. This procedure does not give an absolute measurement of metabolite concentration. Absolute concentration measurements are feasible but technically different because of the

calibration procedures with reference standards that are required. Absolute concentrations would be useful in detecting changes in metabolite concentration when metabolite ratios do not change.

It is now feasible to integrate a proton MR spectroscopic examination along with a conventional MR imaging examination. The MR imaging examination can be performed in the first 30 min to acquire scout views and standard T2-weighted images, and then the proton MR spectroscopic study can be done in the next 30 min with the same instrumentation (RF head coil, amplifier, etc.). The spectroscopic study also can use the MR images to prescribe the spectroscopic localized volume. The MR imaging technician can be taught to obtain the spectroscopic data as long as the software is fairly automated. Procedures in shimming the magnetic field and spectroscopic data processing would be new to the MR technician. As far as magnetic field strength is concerned, good spectra from the human brain can be obtained at 1.5 T in about 5 min; however, the spectroscopic localized volumes are large (20–100 cm³). The signal-to-noise ratio of the MR signal improves with increasing field strength, and preliminary results at 4 T have shown that higher field strength can be used to reduce the localized volume size or acquisition time [15].

MR Spectroscopy of Proton Metabolites In Vivo

Lipids

The lipid-methylene protons resonate at 1.2 ppm in the proton spectrum (Fig. 1) and contain mainly contributions from triglycerides and other mobile lipids. Lipid metabolism is important in the study of demyelination because the myelin sheath (which is damaged in demyelination) is composed of a lipid-bilayer membrane. Histopathologic techniques have allowed researchers to study lipid changes during demyelination because the lipids stain differently depending on their structural and biochemical state [16, 17]. These studies have shown that abnormal lipid droplets that form during demyelination are a sign of an irreversible lesion. Histopathologic techniques can be used only once per animal and, therefore, cannot be used to follow changes in the same animal. The signal intensity of membrane lipids in MR spectroscopy is influenced by the fluidity of the membrane structure, which depends on temperature, cholesterol content, lipid composition, lipid-water interactions, and membrane proteins [18, 19]. The proton spectrum of normal brain has little (if any) lipid signal [20] because the phospholipids in cell membranes and in myelin have limited mobility. However, it is hypothesized that as myelin degrades and the membrane structure changes, the lipids become less ordered and thus able to give a detectable MR spectroscopic signal.

Several technical challenges must be overcome to make a proper MR spectroscopic lipid measurement of the brain. Intense lipid signals that arise from the scalp and other adipose tissue outside the brain can easily contaminate the much less intense brain spectrum. Imperfections in the selective RF pulses and gradient-spoiler pulses may result in lipid contamination from outside tissues. Another challenge is the short T2 relaxation time of lipids, which may make detection

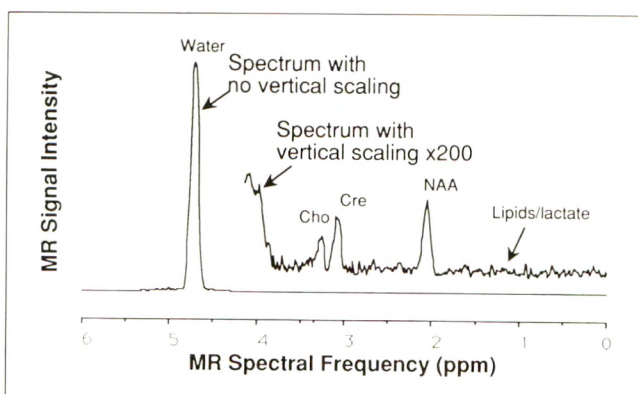


Fig. 1.—Graph shows in vivo proton MR spectrum obtained from normal brain of monkey (*Macaca fascicularis*). Spatial localization was achieved by using a stimulated-echo technique [8], which allows proton spectra to be acquired from individual cubic tissue regions (15 × 15 × 15 mm). Pulse sequence did not use any active water suppression; however, long echo time did passively suppress water peak. Spectra were acquired with a pre-delay of 1500 msec, TE of 250 msec, T1 relaxation delay of 20 msec, digital resolution of MR signal of 2048 complex points, sweep width of ± 1000 Hz, spectral frequency of 85.6 MHz, magnetic field strength of 2 T, 60 averages, and phase cycling. Acquisition delay was adjusted to collect most of the echo. Spectrum with no vertical scaling has large water resonance that is usually suppressed in proton spectroscopy of brain. Offset spectrum is vertically scaled by a factor of 200 so that proton metabolites can be seen. Cho = choline, Cre = creatine, NAA = N-acetyl aspartate.

of MR spectroscopic signals difficult. For this reason, it is important to closely evaluate claims of lipid changes within the brain.

Choline

The *N*-methyl groups of choline resonate at 3.2 ppm in the proton spectrum in vivo (Fig. 1) and contain contributions mainly from phosphorylcholine and glycerophosphorylcholine (GPC) [7], which are involved in lipid metabolism [21]. Phosphorylcholine is a precursor molecule that is incorporated into the polar head group of phosphatidylcholine and sphingomyelin [22, 23]. These phospholipids are then incorporated into cell and myelin membranes of the CNS [23]. GPC is a metabolite of the breakdown of phosphatidylcholine [22]. Unfortunately, all the *N*-methyl groups from the choline-containing compounds resonate at the same frequency. The contribution of phosphatidylcholine to this resonance is unknown. Phosphorylcholine and GPC are small molecules with long T2 relaxation times, whereas phosphatidylcholine is a large molecule with a relatively short T2 relaxation time that is made even shorter by being incorporated into the highly ordered myelin membrane [24]. However, recent evidence suggests that phosphatidylcholine contributes to the proton MR choline signal [25].

N-Acetyl Aspartate

The methyl group of *N*-acetyl aspartate (NAA) has a sharp resonance at 2.0 ppm in the proton spectrum (Fig. 1) of the brain [6]. The exact role of NAA in brain tissue is still unclear. Most researchers agree that NAA is a marker for neurons and may have a role in neuronal metabolism ([26] and references cited therein). Although some researchers claim that NAA is involved in myelin production, this seems to be contradicted by the fact that NAA is at much higher concentration in the neurons than in the glial cells [26, 27]. The NAA resonance has been of interest in the study of MS and other brain diseases because of the decrease in NAA:creatine and NAA:choline ratios localized to brain lesions. This decrease in NAA has been attributed to axonal loss [28], active degradation of NAA in injured neurons [29], and gliosis [30]. Although MS is primarily a demyelinating disease, injury to neurons becomes more apparent with decades-long progression of the illness, possibly because of the metabolic relationship between axons and myelin-forming oligodendroglia [31]. Along with the injured neurons, the normal-appearing "healthy neurons" may be influenced by the pathologic materials arising from inflammatory foci and the altered blood-brain barrier [31].

MR Spectroscopy in Animal Models of MS

By correlating the MR spectroscopic signal observed in vivo with histologic and biochemical measurements, animal models of MS can be used to elucidate the biologic and biochemical meaning of MR spectroscopic signals. Experimental allergic encephalomyelitis (EAE) is a model of the human demyelinating disease MS [32, 33]. EAE is induced in animals by the injection of myelin-basic protein in complete

Freund's adjuvant. Sensitization to myelin-basic protein causes a cell-mediated delayed type of hypersensitivity reaction to myelin in the CNS that is manifested microscopically by various degrees of inflammation, edema, demyelination, and necrosis [34, 35]. Previous invasive biochemical studies of EAE have shown changes in CNS lipids [36] and 2',3'-cyclic nucleotide 3'-phosphodiesterase (CNPase) activity [37, 38] and changes in proteolipid proteins isolated from myelin subfractions. CNPase activity was decreased in the brains of animals with EAE before any clinical or histologic alterations were detected [38]. A decrease in the absolute number of circulating lymphocyte subsets also has been detected before the onset of clinical signs and symptoms [39].

In EAE, the older lesions contain a higher degree of demyelination than acute lesions [32] and more closely approximate the chronic lesions of multiple sclerosis. The acute EAE lesions begin within the first 2–3 weeks after sensitization and are usually fatal if not successfully treated. These lesions are inflammatory and necrotizing and are not the same pathologically as an MS plaque. However, remitting-relapsing disease (similar to that of MS patients) can be induced in EAE animals by administering a suboptimal amount of antibody (causing only partial remission of disease) [33, 34] after the animals have been sensitized to myelin-basic protein. On the basis of these facts, older or chronic EAE lesions should behave spectroscopically like the MS demyelinated plaque.

With in vivo proton spectroscopy, increases in choline:creatine ratios [40] (Richards TL, unpublished data) have been measured in brain regions containing EAE lesions. However, changes in choline:creatine and choline:NAA ratios have been observed in brain regions *before* the development of large lesions detectable on MR images (Fig. 2) (Richards TL, unpublished data). Decreases in choline:NAA have also been measured in rats with EAE [41] and in rats after irradiation of the brain [42]. In a rat model of demyelination, Ford et al. [43] were able to measure changes in lipid signals at the rim of a brain lesion. They measured the proton image before and after lipid suppression and observed a change in image intensity at the lesion rim. They suggested that the signal change may be related to mobile lipids resulting from myelin membranes [43].

MR Spectroscopy in Patients with MS

MS patients have been studied with in vivo proton spectroscopic techniques in which the spectroscopic localized volume was placed over a region of brain that included a plaque defined by MR imaging. The main findings have been a decrease in NAA:creatine [10, 28, 30, 44–48] and an increase in choline:creatine [10, 44, 47–49]. An example of the decrease in NAA:creatine is shown in Figure 3. In some cases, the decrease in NAA did not depend on relative plaque volume inside the spectroscopic localized volume, suggesting that the disease extended into normal-appearing white matter surrounding the active chronic MS plaques [30]. Acute (edema, inflammation) and chronic (demyelination, gliosis) MS plaques appear to have different proton spectra, potentially allowing the number of irreversible chronic plaques in a patient to be determined spectroscopically [28]. The hypothesis is that metabolite ratios are unchanged in hyperacute (edema

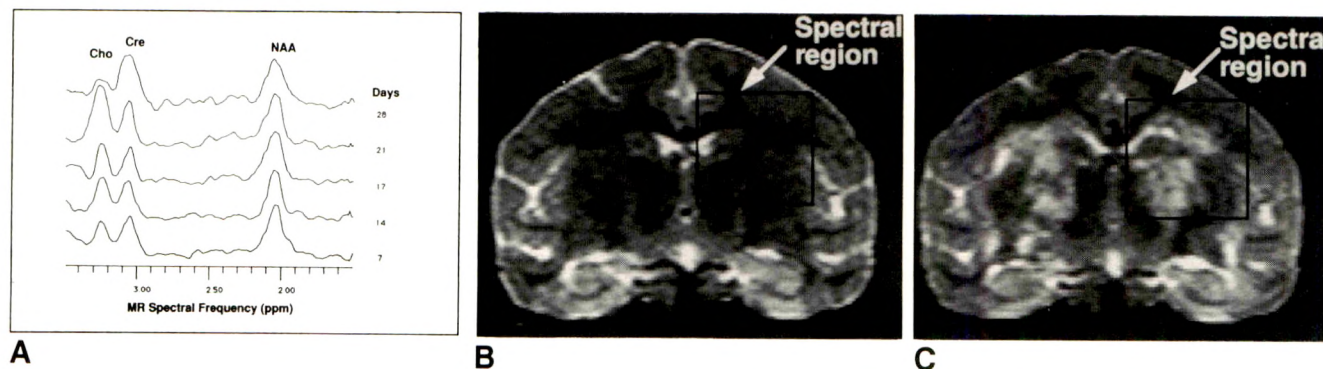


Fig. 2.—A, Graphs show in vivo proton spectra acquired from region of monkey brain shown in B during initial stages of experimental allergic encephalomyelitis (7–28 days after sensitization with myelin basic protein). Spectra were acquired by using stimulated-echo technique [8] with same parameters as in Fig. 1. Changes in choline (Cho) resonance on days 21 and 28 occurred before onset of large lesions (day 35). Cre = creatine, NAA = N-acetyl aspartate.

B, Coronal T2-weighted MR image, 3000/80 (TR/TE, 2-mm slice thickness), of monkey brain obtained before onset of lesions (28 days after sensitization with myelin basic protein). No lesions are visible. Black box outlines localized brain region for spectra shown in A.

C, Coronal T2-weighted MR image (3000/80, 2-mm slice) of monkey brain obtained after onset of lesions (35 days after sensitization). Lesions are visible in white matter. Black box outlines localized brain region for spectra shown in A. Animal was sacrificed after this scan, and histologic examination showed an acute inflammatory lesion with edema.

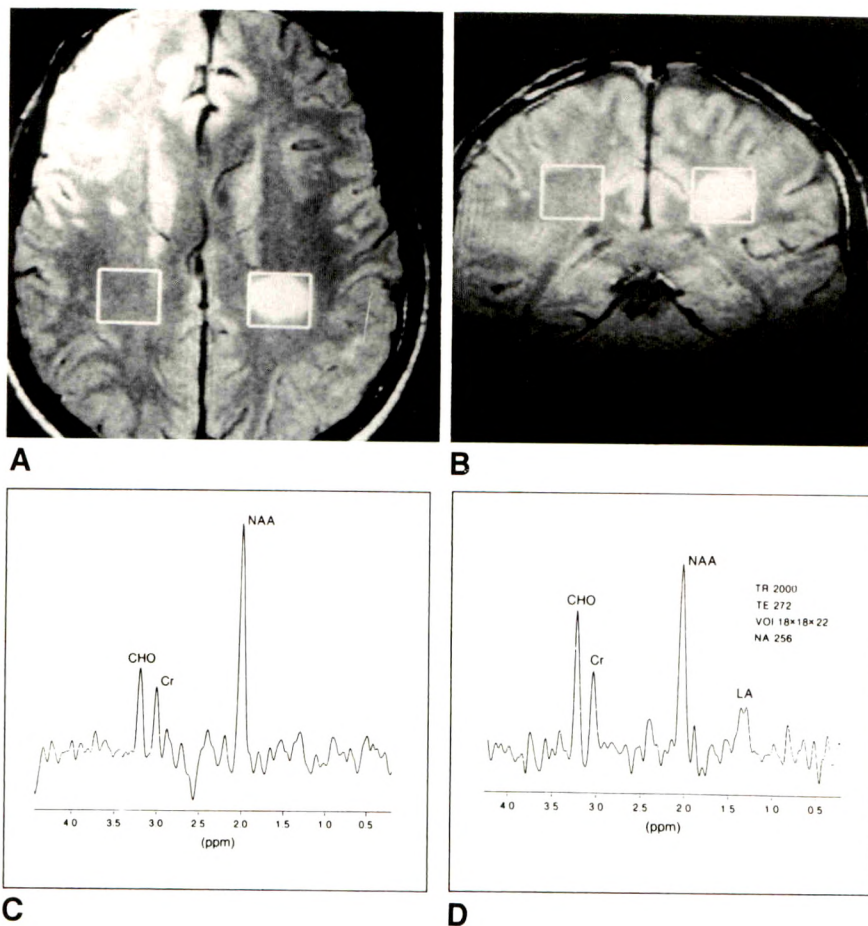


Fig. 3.—A, Axial MR image, 2100/30 (TR/TE), of patient with multiple sclerosis shows lesion in left hemisphere. Boxes outline volume of interest for proton spectra shown in C and D.

B, Coronal MR image (2100/30).

C, Proton MR spectrum (2000/272) localized to volume of interest in normal-appearing white matter contralateral to active plaque shown in D.

D, Proton MR spectrum (2000/272) localized to active plaque in left hemisphere. Volume of interest is outlined in A and B. Note relatively high choline (CHO); creatine (Cr) and low N-acetyl aspartate (NAA); Cr in plaque as compared with normal-appearing white matter (C) and also prominent lactate resonance in plaque spectrum. LA = lactate.

(Reprinted with permission from Matthews et al. [50].)

only) plaques, that demyelination in acute plaques is accompanied by an increased choline:creatine ratio, and that irreversible plaques in the subacute to chronic stage have a decreased NAA:creatine ratio [49].

Some claims have been made of lipid increases in MS plaques [45, 47, 51]; however, one of these investigators

admits the possibility of lipid contamination from scalp and bone marrow [45]. Other proton metabolites that have been reported to change in MS are lactate [10] and inositol [48].

It is now possible to measure the proton metabolites in patients with MS with spectroscopic imaging techniques [10]. These studies have added insight into the distribution of

metabolite concentration within a brain lesion. Den Hollander et al. [10] reported that NAA and choline are not uniform over the whole area of the MS plaque and that certain plaques have foci of high concentrations of choline or lactate. They hypothesized that these foci may indicate different stages of the disease.

The ability to differentiate between early reversible lesions and irreversible lesions would be useful in planning treatment of MS. Some MS lesions are purely edematous or inflammatory and should respond to corticosteroids [33, 35]. These early lesions should be detectable by an increased intensity on T2-weighted MR images and no changes in proton metabolites on MR spectroscopy. However, as MS progresses and the lesions become demyelinated with the appearance of lipids in macrophages [35], increases in mobile lipids and choline should be detected with MR spectroscopy. Many months or years later, myelin lipids are lost (no lipid spectrum) and are replaced by astrocytic gliosis (decrease in NAA). These older lesions most likely will not respond to any current medical treatment. Thus, proton MR spectroscopy along with MR imaging could be helpful in distinguishing those early lesions that might respond to therapy from late lesions, which probably will not respond.

MR Spectroscopy of Brain Tissue In Vitro

Brain tissue from MS patients and EAE animals also has been studied by using in vitro MR techniques. Magic-angle sample spinning (MASS) is a technique that can be used to enhance the MR spectroscopic signal from tissue constituents that otherwise would be invisible because of restricted mobility. Carbon-13 MASS was used to study myelin phospholipids, sphingolipids, and cholesterol in diseased human myelin. An increase in the cholesterol signal was observed, which would imply either an increased concentration of cholesterol or an altered membrane fluidity [52].

In vivo measurements of metabolites on MR spectroscopy are hindered by magnetic field inhomogeneity and broad line widths caused by electromagnetic interactions with large macromolecules. However, MR measurements of tissue extracts in vitro have the advantage of extremely high spectral resolution (narrower lines) because all of the large macromolecules are taken out of the tissue and the sample can be placed in a high-resolution test tube. The MR signal obtained from proton metabolites under these conditions is simplified by using a one-pulse technique in which there are no magnetic field gradients and the complicating factors of T1 and T2 are minimized by using a repetition time of five times T1 and essentially zero echo time. Also, the tissue extract techniques provide a way to assign the resonances in the spectrum accurately because resonances are sharper and less overlapping than in the spectrum obtained in vivo. In one study [53], brain samples from mice induced to develop chronic relapsing EAE were prepared as perchloric acid extracts and were measured with proton spectroscopy at 500 MHz. A reduction in inositol:creatine and NAA:creatine and an increase in taurine:creatine were observed. The depletion of inositol in the spinal cord of acute-phase and relapsing animals appears to correlate with periods of demyelination. Inositol phospholipids are mobile myelin components, and the resynthesis of inositol phospholipid might deplete tissue levels of free inositol [53]. In another study, analysis of white matter samples from MS

patients showed a significant decrease in phospholipids (measured by ^{31}P MR) and cholesterol (measured by proton MR) content [54]. These in vitro MR spectroscopic studies add insight to the biological meaning of the complex signal observed in vivo.

Summary

Proton MR spectroscopy offers a noninvasive way to observe biochemical changes that may provide new insights into demyelinating diseases such as MS. Although the role and importance of some of these proton metabolites (e.g., choline, NAA) in brain function and disease are not fully understood, the specificity of these changes may provide information about the stage and reversibility of the brain lesions. Animal studies are particularly insightful when the MR spectroscopic signals are correlated with histologic and biochemical techniques. Clinical application of proton MR spectroscopy could arise from the capability to differentiate between early lesions that might respond to therapy and older irreversible lesions. Although the focus of this review is in the use of MR spectroscopy in the study of MS, proton MR spectroscopy has also shown potential in the study of brain tumors [55] and stroke [29]. Although the proton spectra acquired from patients with brain tumors, stroke, and MS have some similarities (high choline, low NAA), there may be differences (lipids, lactate, glutamate, glutamine, inositol) that could help in diagnosing the disease. Although more data need to be obtained, proton MR spectroscopy shows promise for aiding in the differential diagnosis of various brain diseases [25], monitoring progression of MS, and evaluating therapy.

ACKNOWLEDGMENTS

I thank Ellsworth Alvord, Jr., and Grant Steen for helpful comments.

REFERENCES

1. Paty DW. Magnetic resonance imaging in demyelination. In: Kim SU, ed. *Myelination and demyelination: implications for multiple sclerosis*. New York: Plenum, 1989:259-272.
2. Larsson HBW, Frederiksen J, Petersen J, et al. Assessment of demyelination, edema, and gliosis by in vivo determination of T1 and T2 in the brain of patients with acute attack of multiple sclerosis. *Magn Reson Med*. 1989;11:337-348.
3. Karlik SJ, Gilbert JJ, Wong C, Vandervoort MK, Noseworthy JH. NMR studies in experimental allergic encephalomyelitis: factors which contribute to T1 and T2 values. *Magn Reson Med* 1990;14:1-11.
4. Kermode AG, Tofts PS, Thompson AJ, et al. Heterogeneity of blood-brain barrier changes in multiple sclerosis: an MRI study with gadolinium-DTPA enhancement. *Neurology* 1990;41:229-235.
5. Gadian DG. *NMR and its application to living systems*. New York: Oxford University Press, 1982.
6. Behar KL, den Hollander JA, Stromski ME, et al. High-resolution ^1H nuclear magnetic resonance study of cerebral hypoxia in vivo. *Proc Natl Acad Sci U S A* 1983;80:4945-4948.
7. Arus C, Chang Y, Barany M. Proton nuclear magnetic resonance spectra of excised rat brain: assignment of resonances. *Physiol Chem Phys Med NMR* 1985;17:23-33.
8. Frahm J, Merboldt KD, Hancic W. Localized proton spectroscopy using stimulated echoes. *J Magn Reson* 1987;72:502-508.
9. Bottomley PA. *Selective volume method for performing localized NMR spectroscopy*. U. S. Patent 4 480 228. Washington, DC: U.S. Patent Office, 1984.
10. Den Hollander JA, 's-Gravenmade EJ, Marien AHJ, et al. Detection of focal abnormalities of cerebral metabolism in patients with multiple sclerosis by means of ^1H NMR spectroscopic imaging. In: *Book of abstracts. Society of Magnetic Resonance in Medicine*, 1990, vol. 2. Berkeley, CA: Society

- of Magnetic Resonance in Medicine, **1990**:1116
11. Brown TR, Kincaid BM, Ugurbil K. NMR chemical shift imaging in three dimensions. *Proc Natl Acad Sci U S A* **1982**;79:3523-3526
 12. Frahm J, Bruhn H, Gyngell ML, Merboldt KD, Hanicke W, Sauter R. Localized proton NMR spectroscopy in different regions of the human brain in vivo: relaxation times and concentrations of cerebral metabolites. *Magn Reson Med* **1989**;11:47-63
 13. Van Zijl PCM, Moonen CTW, Gillen J, et al. Proton magnetic resonance spectroscopy of small regions (1 ml) localized inside superficial human tumors: a clinical feasibility study. *NMR Biomed* **1990**;3:227-232
 14. Klose U. In vivo proton spectroscopy in presence of eddy currents. *Magn Reson Med* **1990**;14:26-30
 15. Barfub H, Fischer H, Hentschel D, et al. Hydrogen spectroscopy of the human brain with a 4 tesla whole-body MR system. In: *Book of abstracts. Society of Magnetic Resonance in Medicine*, 1990, vol. 2. Berkeley, CA: Society of Magnetic Resonance in Medicine, **1989**:445
 16. Adams CWM, Ibrahim MZM, Leibowitz S. Demyelination. In: Adams CWM, ed. *Neurohistochemistry*, New York: Elsevier, **1965**:437-487
 17. Adams CWM, Leibowitz S. *Research on multiple sclerosis*. Springfield, IL: Thomas, **1972**
 18. Chan SI, Bocian DF, Petersen NO. Nuclear magnetic resonance studies of the phospholipid bilayer membrane. In: Grell E, ed. *Membrane spectroscopy: molecular biology, biochemistry, and biophysics*. New York: Springer-Verlag, **1981**:1-50
 19. Govil G, Hosur RV. *Conformation of biological molecules: new results with NMR*. New York: Springer-Verlag, **1982**:155-199
 20. Frahm J, Bruhn H, Gyngell ML, Merboldt KD, Hanicke W, Sauter R. Localized high-resolution proton NMR spectroscopy using stimulated echoes: initial applications to human brain in vivo. *Magn Reson Med* **1989**;9:79-93
 21. Stryer L. *Biochemistry*. San Francisco: Freeman, **1975**
 22. Pettegrew JW, Kopp SJ, Minshew NJ, et al. ^{31}P nuclear magnetic resonance studies of phosphoglyceride metabolism in developing and degenerating brain: preliminary observations. *J Neuropathol Exp Neurol* **1987**;46:419-430
 23. Tunggal B, Hofmann K, Stoffel W. In vivo ^{13}C nuclear magnetic resonance investigations of choline metabolism in rabbit brain. *Magn Reson Med* **1990**;13:90-102
 24. Joffe S, Block RE. Nuclear magnetic resonance studies suggestive of a lipid population tightly bound to myelin structural proteins. *Brain Res* **1972**;46:381-390
 25. Miller BL. A review of chemical issues in ^1H NMR spectroscopy: *N*-acetyl-L-aspartate, creatine, choline. *NMR Biomed* **1991**;4:47-52
 26. Birken DL, Oldendorf WH. *N*-acetyl-L-aspartic acid: a literature review of a compound prominent in ^1H -NMR spectroscopic studies of brain. *Neurosci Biobehav Rev* **1989**;13:23-31
 27. Gill SS, Small RK, Thomas DGT, et al. Brain metabolites as ^1H NMR markers of neuronal and glial disorders. *NMR Biomed* **1989**;2:196-200
 28. Arnold DL, Matthews PM, Francis G, Antel J. Proton magnetic resonance spectroscopy of human brain in vivo in the evaluation of multiple sclerosis: assessment of the load of disease. *Magn Reson Med* **1990**;14:154-159
 29. Bruhn H, Frahm J, Gyngell ML, Merboldt KD, Hanicke W, Sauter R. Cerebral metabolism in man after acute stroke: new observations using localized proton NMR spectroscopy. *Magn Reson Med* **1989**;9:126-131
 30. VanHecke P, Marchal G, Johannik K, et al. Human brain proton localized NMR spectroscopy in multiple sclerosis. *Magn Reson Med* **1991**;18:199-206
 31. Huszak I. Biochemical aspects of multiple sclerosis. In: Lajtha A, ed. *Handbook of Neurochemistry*, vol. 5. *Pathological chemistry of the nervous system*. New York: Plenum, **1972**:47-91
 32. Alvord EC, Kies MW, Sucking AJ. *Experimental allergic encephalomyelitis: a useful model for multiple sclerosis*. New York: Liss, **1984**
 33. Rose LM, Richards TL, Petersen R, Peterson J, Hruby S, Alvord EC. Remitting-relapsing EAE in nonhuman primates: a valid model of multiple sclerosis. *Clin Immunol Immunopathol* **1991**;59:1-15
 34. Shaw CM, Alvord EC, Hruby S. Chronic remitting-relapsing experimental allergic encephalomyelitis in monkeys with homologous myelin basic protein. *Ann Neurol* **1988**;24:738-748
 35. Alvord EC, Rose LM, Hruby S, et al. Experimental allergic encephalomyelitis in non-human primates: an excellent model of multiple sclerosis. In: Jonker M, ed. *Biomedical research in primates*. Rijswijk, the Netherlands: TNO Primate Center. **1988**:31-50
 36. Maggio B, Cumar FA. Experimental allergic encephalomyelitis: dissociation of neurological symptoms from lipid alterations in brain. *Nature* **1975**;253:364-365
 37. Salvati S, D'Urso D, Devirgiliis LC, Crescenzi GS. Biochemical changes in central nervous system membranes in experimental allergic encephalomyelitis. *J Neurochem* **1986**;47:239-244
 38. Clemons CS, Fan K. 2':3'-Cyclic nucleotide 3'-phosphodiesterase activity in brain of acute experimental allergic encephalomyelitis. *Brain Res* **1979**;169:620-624
 39. Rose LM, Richards TL, Alvord EC. Magnetic resonance imaging and peripheral blood abnormalities in experimental allergic encephalomyelitis. *Biomed Pharmacother* **1989**;43:347-350
 40. Williams SCR, Hawkins C, Barker GJ, Munro P, McDonald WI. In vivo NMR spectroscopy of experimental allergic encephalomyelitis. In: *Book of abstracts. Society of Magnetic Resonance in Medicine*, 1990, vol. 2. Berkeley, CA: Society of Magnetic Resonance in Medicine, **1990**:1237
 41. VanVaals JJ, 's-Gravenmade EJ, Bergman AH, et al. Localized ^1H brain spectroscopy and microimaging of rats with experimental allergic encephalomyelitis. In: *Book of abstracts. Society of Magnetic Resonance in Medicine*, 1989, vol. 1. Berkeley, CA: Society of Magnetic Resonance in Medicine, **1989**:480
 42. Richards T, Budinger TF. NMR imaging and spectroscopy of the mammalian central nervous system after heavy ion radiation. *Radiat Res* **1988**;113:79-101
 43. Ford CC, Ceckler TL, Karp J, Herndon RM. Magnetic resonance imaging of experimental demyelinating lesions. *Magn Reson Med* **1990**;14:461-481
 44. Miller DH, Austin SJ, Connelly A, Youl BD, Gadian DG, McDonald WI. Proton magnetic resonance spectroscopy of an acute and chronic lesion in multiple sclerosis. *Lancet* **1991**;337(8732):58-59
 45. Koopmans RA, Zhu G, Li DKB, Allen PS, Javidan M, Paty DW. In-vivo proton MRS of the acute and chronic lesion of multiple sclerosis. In: *Book of abstracts. Society of Magnetic Resonance in Medicine*, 1990, vol. 2. Berkeley, CA: Society of Magnetic Resonance in Medicine, **1990**:1205
 46. Van der Knaap MS, van der Grond J, Luyten PR, den Hollander JA, Valk J. MR spectroscopy in degenerative cerebral disorders: differentiation between gray and white matter disorders. In: *Book of abstracts. Society of Magnetic Resonance in Medicine*, 1990, vol. 2. Berkeley, CA: Society of Magnetic Resonance in Medicine, **1990**:1051
 47. Christiansen P, Larsson HBW, Frederiksen J, Jensen M, Henriksen O. Localized in vivo proton spectroscopy in the brain of patients with multiple sclerosis. In: *Book of abstracts. Society of Magnetic Resonance in Medicine*, 1990, vol. 1. Berkeley, CA: Society of Magnetic Resonance in Medicine, **1990**:109
 48. Bruhn H, Frahm J, Merboldt KD, et al. Metabolic alterations in children with multiple sclerosis as detected by localized proton MRS. In: *Book of abstracts. Society of Magnetic Resonance in Medicine*, 1990, vol. 2. Berkeley, CA: Society of Magnetic Resonance in Medicine, **1990**:1209
 49. Arnold DL, Matthews PM, Mollevarger L, Luyten P, Francis G, Antel J. In vivo localized proton magnetic resonance spectroscopy allows plaque characterization in multiple sclerosis. In: *Book of abstracts. Society of Magnetic Resonance in Medicine*, 1990, vol. 1. Berkeley, CA: Society of Magnetic Resonance in Medicine, **1990**:110
 50. Matthews PM, Francis G, Antel J, Arnold DL. Proton magnetic resonance spectroscopy for metabolic characterization of plaques in multiple sclerosis. *Neurology* **1991**;41:1251-1256
 51. Wolinsky JS, Narayana PA, Fenstermacher MJ. Proton magnetic resonance spectroscopy in multiple sclerosis. *Neurology* **1990**;40:1764-1769
 52. Husted C, Montez B, Oldfield E. C-13 magic angle sample spinning NMR dynamic studies of normal and diseased myelin membrane. In: *Book of abstracts. Society of Magnetic Resonance in Medicine*, 1990, vol. 2. Berkeley, CA: Society of Magnetic Resonance in Medicine, **1990**:1058
 53. Preece NE, VanBruggen N, Gadian DG, Baker D, O'Neill JK, Turk JL. H-1 NMR studies of CNS metabolism in an animal model of multiple sclerosis. In: *Book of abstracts. Society of Magnetic Resonance in Medicine*, 1990, vol. 2. Berkeley, CA: Society of Magnetic Resonance in Medicine, **1990**:1231
 54. Sappey MD. High-resolution NMR spectroscopy of cerebral white matter in multiple sclerosis. *Magn Reson Med* **1990**;15:229-239
 55. Luyten PR, Marien AJ, Heindel W, et al. Metabolic imaging of patients with intracranial tumors: H-1 MR spectroscopic imaging and PET. *Radiology* **1990**;176:791-799

Pictorial Essay

Sonography of the Eye

Peter L. Munk,¹ A. Dale Vellet,¹ Morris Levin,¹ David T. C. Lin,² and Robert T. Collyer³

Real-time sonography of the eye is a technique that is rapidly performed and readily available in most sonography departments. It is less expensive than CT and MR imaging and, if necessary, may be performed at the patient's bedside. This essay demonstrates a few of the large number of clinical entities that may be successfully examined with this technique.

Sonography has been used in the investigation of eye disorders since the 1950s. In spite of this, most radiologists are unfamiliar with ocular anatomy and disease as depicted sonographically, largely because ophthalmic sonography has principally been the domain of ophthalmologists. With the widespread availability of high-resolution, gray-scale, real-time sonography and high-frequency transducers, a gradually increasing interest in ophthalmic sonography by radiologists has become evident. Surprisingly, little has appeared in the literature on the use of nondedicated high-resolution sonographic applications to eye disease [1-8]. The purpose of this essay is to demonstrate a number of different pathologic entities that may readily be discerned and evaluated by using standard sonographic equipment available in most modern radiology departments.

Technique

The technique we use to examine the eye is relatively simple. A high-frequency probe is selected, preferably 7.5-10 MHz, although some linear-array 5-MHz probes will produce diagnostically adequate images. A standoff pad or thick layer

of commercially available sonographic gel is then placed over the patient's closed eyelid with the patient in the supine position. We have not found contact lenses to be a problem when scans are obtained, although we usually ask that they be removed prior to the examination. The entire eye should be scanned transaxially and sagittally. Selected oblique images are often useful in showing any abnormalities to advantage. Observing the eye as it is moved from side to side or up and down is often useful in demonstrating movement of membranes and other structures and may aid in identification of those structures [3, 5]. In most instances, this will complete the examination; however, when necessary. Doppler imaging or standardized A-mode scanning may provide additional information [1, 6, 9].

The severely traumatized eye must be scanned with great care, and an effort to avoid applying pressure is important. Likewise, patients who have had recent surgery should be treated with delicacy. Open wounds of the eye and surrounding tissues or severe inflammation are contraindications for sonography.

Anatomy

The eye is traditionally divided into three chambers: anterior, posterior, and vitreous (Fig. 1). The posterior chamber is located between the posterior aspect of the lens and the ciliary body and usually is not well visualized with sonography; it will not be discussed further. The anterior chamber is defined as extending from the cornea to the anterior aspect

Received April 1, 1991; accepted after revision May 17, 1991.

¹ Department of Diagnostic Radiology and Nuclear Medicine, University Hospital and University of Western Ontario, P.O. Box 5339, 339 Windermere Rd., London, Ontario N6A 5A5, Canada. Address reprint requests to P.L. Munk.

² Department of Ophthalmology, Vancouver General Hospital and University of British Columbia, 855 W. 12th Ave., Vancouver, B.C. V5Z 1M9, Canada.

³ Department of Ophthalmology, St. Joseph's Hospital and University of Western Ontario, 268 Grosvenor St., London, Ontario N6A 4V2, Canada.

AJR 157:1079-1086, November 1991 0361-803X/91/1575-1079 © American Roentgen Ray Society

of the lens. The iris plane includes the iris, ciliary body, and lens. Behind the lens is the large vitreous chamber, which occupies the bulk of the globe. At the posterior aspect of the vitreous chamber, the optic nerve may be seen exiting from the posterior foramen and is often visible as a hypoechoic band surrounded by the markedly echogenic retroorbital fat. Normally, both the anterior and vitreous chambers are virtually echo free. The normal lens is defined by anterior and posterior boundary echoes, but the lens itself is usually echo free. The iris plane is seen as a thin, echogenic line in continuity with the lens. The lateral and posterior boundaries of the vitreous chamber are seen as an echogenic line of modest thickness, extending from the iris plane posteriorly to the optic nerve. This echogenic line actually consists of three layers. The outermost layer is the sclera, which has the choroid applied to its inner surface. A thin, usually not visible layer on the internal aspect of the choroid is the retina. The retina extends from the optic nerve to the ora serrata, the anterior-most extent of the retina, which extends approximately three quarters of the way from the optic nerve to the iris plane. In the normal eye, these three layers are adherent; however, under certain pathologic conditions, they may separate and form potential spaces.

Anterior Chamber and Iris Plane

It is unusual to be able to observe abnormalities of the cornea, which is typically seen as a thin, echogenic, curved

line immediately adjacent to the moderately echogenic overlying soft tissues of the eyelid.

The anterior chamber may show marked echogenicity with hyphema, or hemorrhage in the anterior chamber. After intraocular hemorrhage, the normal drainage patterns of fluid may be deranged, and the anterior chamber may increase in depth (normal depth is approximately 4 mm). At times after trauma, the chamber may collapse completely, with the cornea almost opposed to the anterior surface of the iris plane.

Infrequently, abnormalities of the iris may be observed. Examples of this include benign nevi, which may be seen as small nodular echogenic lesions (Fig. 2). These are rarely of clinical significance. Occasionally, melanomas may form and can reach a large size (Fig. 3).

The most common abnormality of the lens is, as might be expected, the senile cataract. Usually a cataract is clinically obvious before any sonographic manifestation is apparent. As the cataract matures, the boundary echoes of the lens become increasingly prominent, and the substance of the lens becomes echogenic (Fig. 4). Sonographic examination is often routinely performed before cataract extraction in order to rule out the presence of possible contraindications to surgery, such as a tumor or chronic irreducible retinal detachment. Cataracts may form after trauma also, and at times dislocation of the lens is apparent. Most dislocations are posterior and may be subtle, or very obvious, with the lens dislocated into the posterior aspect of the vitreous chamber (Figs. 5 and 6).

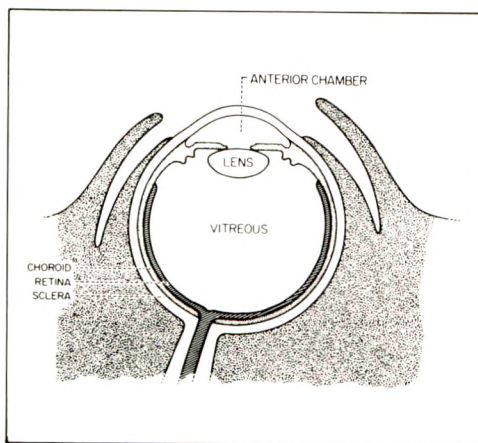
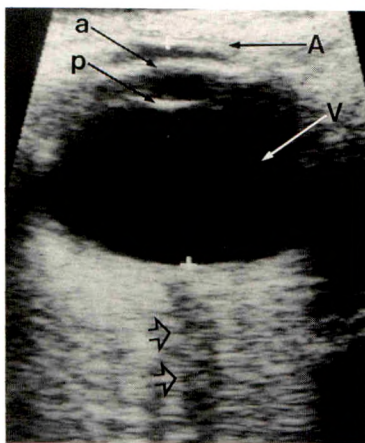
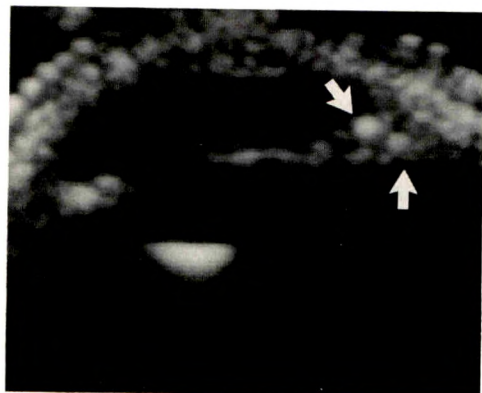
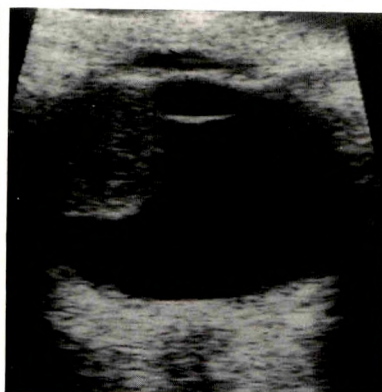


Fig. 1.—A, Sonogram of normal eye. Top caliper (cursor) is placed on cornea. Immediately posterior, anterior chamber is seen as an echo-free space (A). Anterior (a) and posterior (p) boundary echoes define lens. Vitreous chamber (V). Optic nerve surrounded by echogenic fat (open arrows). B, Schematic of normal eye anatomy.



2



3

Fig. 2.—Benign nevus of iris. Sonogram clearly shows small, echogenic nodule measuring slightly more than 1 mm in diameter (arrows) on anterior aspect of iris plane. Bright echo posterior and to the left of the image represents posterior boundary of lens.

Fig. 3.—Ciliary body melanoma. Sonogram shows large, echogenic mass, with its origin in ciliary body of iris plane, extending posteriorly into vitreous chamber.



Fig. 4.—Posttraumatic cataract. Within 3 months of a severe blow to eye, a dense cataract that precluded funduscopy developed in this 27-year-old man. On sonogram, boundary echoes are more prominent and whole contour of lens is seen easily. Small amount of echogenic debris is present in posterior aspect of vitreous chamber from an old vitreous hemorrhage.

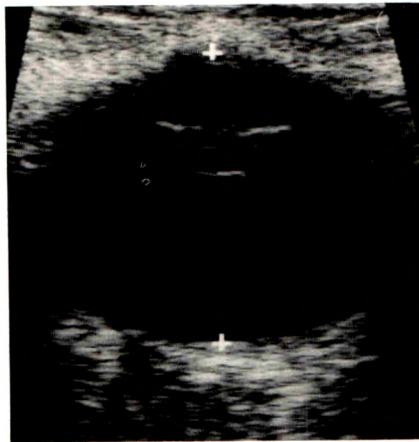


Fig. 5.—Posterior dislocation of lens. Sonogram obtained after blow to eye shows lens is situated more posteriorly than normal relative to iris plane, which makes anterior chamber unusually deep.



Fig. 6.—Free lens in vitreous chamber. Sonogram shows markedly echogenic, cataractous lens tumbling freely in posterior aspect of vitreous chamber several months after this 62-year-old patient was kicked in eye.

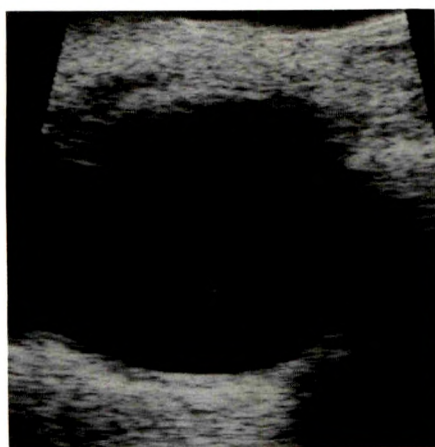
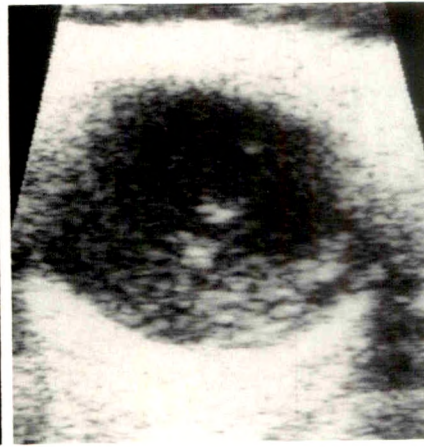


Fig. 7.—Acute hemorrhage in a diabetic patient. Despite dense hemorrhage in vitreous chamber that precluded visualization of fundus, only a few low-amplitude echoes are seen on sonogram obtained approximately 12 hr after onset of bleeding.



A



B

Fig. 8.—Importance of increasing gain settings to visualize hemorrhage. A, Sonogram shows only a few low-amplitude echoes at posterior aspect of vitreous chamber at normal gain settings. B, When gain is increased, hemorrhage becomes readily apparent.

Lens fragmentation may occur, and at times individual fragments are discernible.

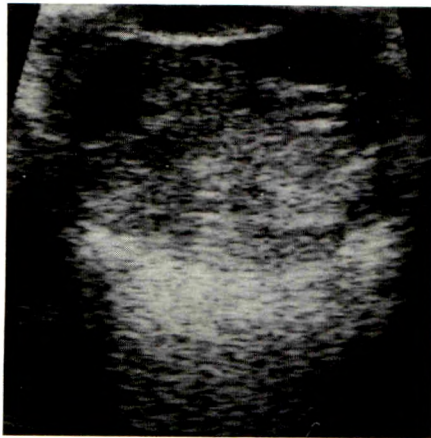
Vitreous Chamber and Its Layers

Although the vitreous chamber is usually described as being echo free, it is not unusual to see a few low-amplitude mobile echoes often referred to as "floaters." Thin, veil-like membranes can be observed also, which on eye movement are seen to be freely mobile with sinuous movements.

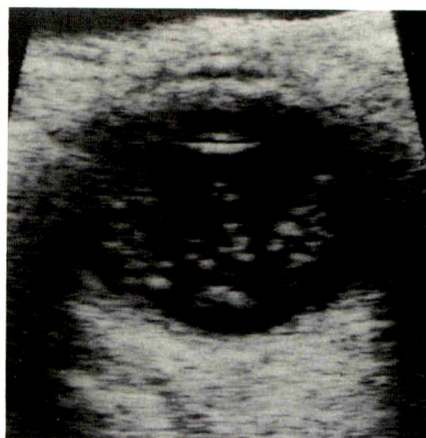
Probably the most common abnormality of the vitreous chamber is vitreous hemorrhage. It is most often caused by trauma and hemorrhage from diabetic retinopathy. In its early phase (up to a few days), hemorrhage, even if clinically very extensive, may be almost impossible to detect by sonography, with only a few very low amplitude echoes apparent (Figs. 7 and 8). As the hemorrhage matures and organizes, echogenicity increases dramatically. With time, the hemor-

rhage will resorb, often producing an extremely heterogeneous appearance in the vitreous chamber, with numerous thick, but usually mobile, membranes (Fig. 9). With eye movement, this hemorrhagic debris will show extensive movement and will settle dependently within the chamber. With time, usually 2–8 weeks, the hemorrhagic debris will gradually disappear, but vitreous membranes will often form and remain permanently. If extensive, they may retract with time, and if adherent to the retina, produce traction retinal detachment.

A less frequently seen, but very dramatic, echogenic lesion of the vitreous is asteroid hyalosis, a condition in which numerous, highly reflective bodies are present throughout the vitreous body, consisting of conjugates of calcium and fatty acid (Fig. 10). These reflective bodies produce a sparkling appearance on real-time sonography. The condition seldom produces significant visual impairment, and its origin is obscure.



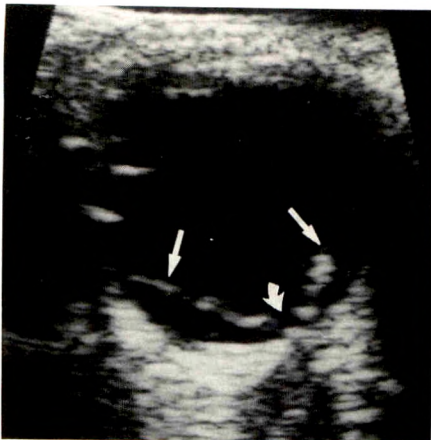
9



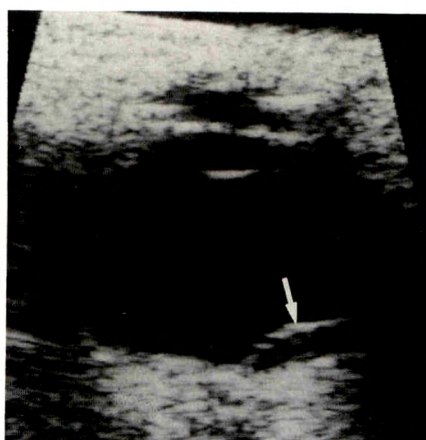
10

Fig. 9.—Vitreous hemorrhage. Sonogram of diabetic patient who had massive vitreous hemorrhage about 1 week before. Markedly echogenic, heterogeneous blood fills most of vitreous chamber.

Fig. 10.—Asteroid hyalosis. Sonogram shows numerous markedly echogenic bodies within vitreous chamber. Real-time observation showed a twinkling or sparkling appearance. This condition is frequently bilateral.



A



B

Fig. 11.—Acute retinal detachment.

A, Sonogram shows extensive detachment. Thin, echogenic retinal leaves (*straight arrows*) are attached near equator of eye and posteriorly (*curved arrow*), at head of optic nerve.

B, Sonogram of diabetic patient shows a small focal detachment immediately adjacent to nerve head (*arrow*). In both A and B, subretinal debris is seen as low-amplitude echoes.

A commonly encountered abnormality in the vitreous chamber is retinal detachment. The retina adheres relatively firmly to the optic nerve head posteriorly and to the ora serrata anteriorly. When the retina detaches, the retinal layer will remain attached at these two points, with fluid, sometimes containing echogenic blood, accumulating between the retina and the subjacent choroid. The retina may become detached along its entire surface or just focally (Fig. 11). The retinal layer is thin and highly reflective in acute retinal detachment. As the detachment becomes increasingly chronic, the retina will become thick, and the retinal leaves will move to the center to produce a funnel-shaped configuration. Eventually, cysts may form within the retinal leaf (Fig. 12). Not unusually, membranes will extend between the retinal leaves, making the retinal attachment essentially irreducible. Mobility of the detached retina also changes with time. In acute detachment, the retinal leaf is easily mobile; however, a chronically detached retina becomes increasingly stiff. Retinal detachments are common in patients with diabetic retinopathy because adhesions form between the organizing hemorrhage in the vitreous body and the underlying retina, and as the hemorrhage retracts, traction retinal detachments occur.

Choroidal detachments are encountered less frequently (Fig. 13). The typical situations in which they are seen include trauma, surgery for glaucoma, and after lens extraction for

cataracts. Classically, choroidal detachments have a more convex appearance than retinal detachments and are much thicker. In addition, the detached choroid does not typically extend as far posteriorly as the optic nerve head, and may extend farther anteriorly than the ora serrata.

Another frequently encountered detachment is the hyaloid detachment (Fig. 14). In the normal eye, the vitreous chamber is filled by a gelatinous structure known as the hyaloid body. At times, the hyaloid body may shrink, and a potential space is opened between the hyaloid body and the underlying retina. This is the subhyaloid space. A hyaloid detachment is not always associated with symptoms and is encountered as an incidental finding. Because adhesions may form between the posterior hyaloid face and the optic nerve head, these hyaloid detachments may be mistaken for retinal detachments. Color Doppler flow imaging has been reported as useful in differentiating between these two [6]. Because the retina is vascular and the hyaloid face is not, demonstration of blood flow in a membrane is strong evidence for retinal rather than vitreous detachment.

Orbital Lesions

The region of the orbit is difficult to investigate with sonography owing in part to poor penetration of high-frequency

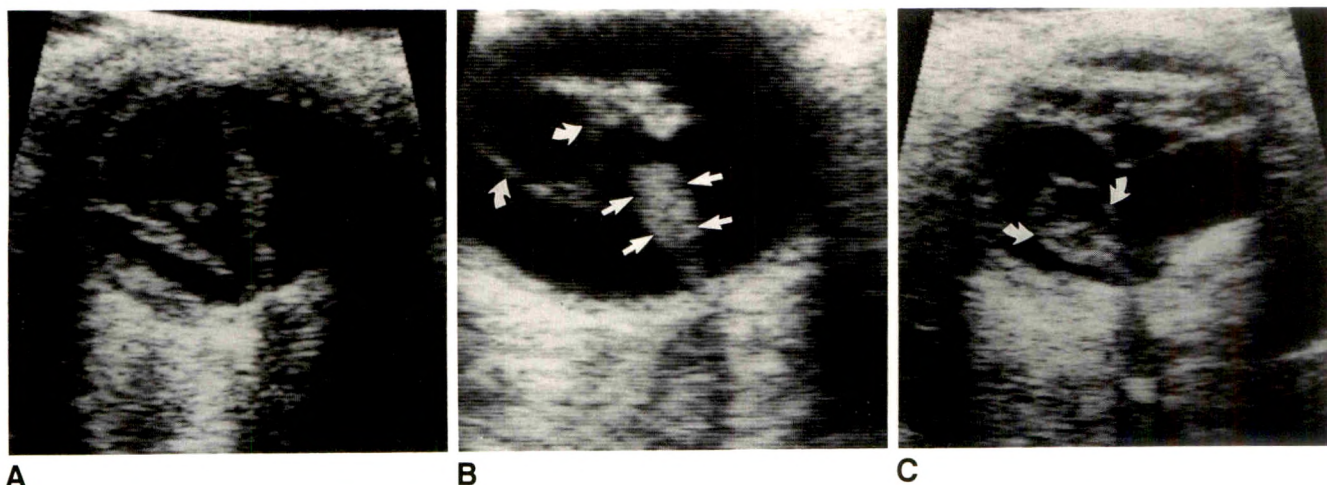
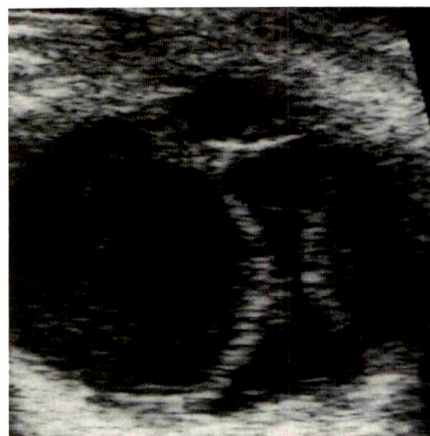


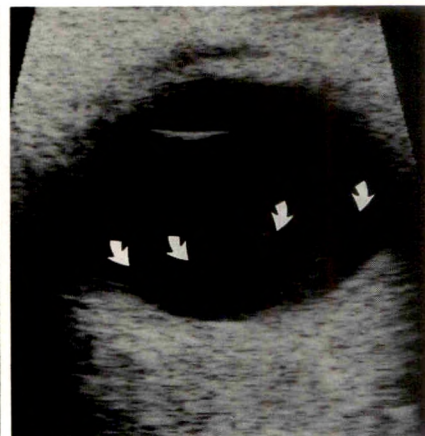
Fig. 12.—Chronic retinal detachment.

A, Sonogram of posttraumatic chronic retinal detachment shows retinal leaves much thicker than in Fig. 11A. Note also thickened sclera.
 B, In another patient, retinal leaves are adherent and form a closed-funnel configuration (*straight arrows*). Complex membranes are seen in anterior vitreous chamber (*curved arrows*).
 C, In another patient, a large cyst has formed (*arrows*) not far from retinal insertion into optic nerve head.

Fig. 13.—Choroidal detachment. Sonogram clearly shows choroidal membranes as two thick, echogenic convexities occupying most of vitreous chamber and almost touching. An echogenic sub-choroidal effusion is present.



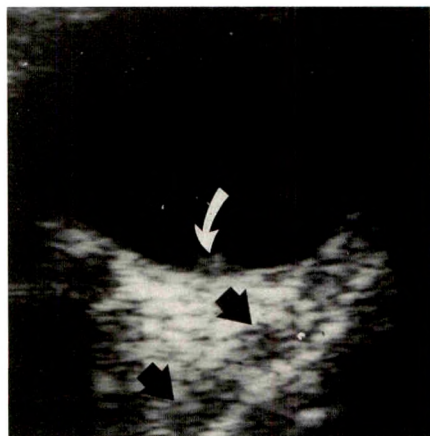
13



14

Fig. 14.—Detached posterior hyaloid face. Sonogram shows vitreous body retracted from posterior pole of eye, producing an interface with mildly echogenic subhyaloid effusion (*arrows*).

Fig. 15.—Extraocular muscle enlargement due to hyperthyroidism is easily seen on sonogram as a hypoechoic band outlined by echogenic fat (*straight arrows*). Occasionally, normal-sized muscles may be seen. Note macular degeneration found incidentally, manifested as a small echogenic lesion at posterior pole (*curved arrow*).

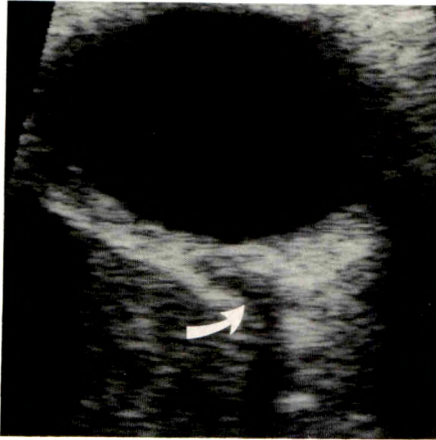


15



16

Fig. 16.—Orbital lymphangioma. Sonogram shows large mass of inhomogeneous echogenicity behind globe. Numerous small cystic spaces within lymphangioma provide innumerable interfaces.



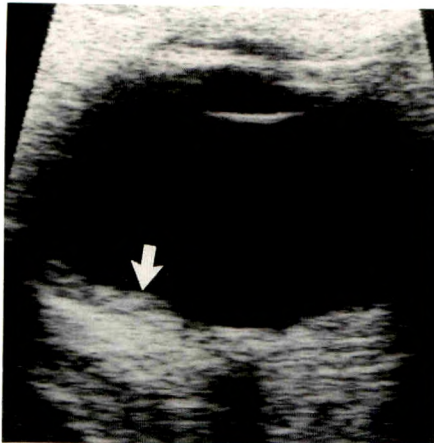
17



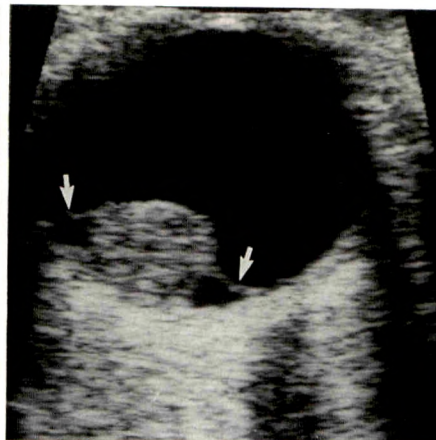
18

Fig. 17.—Metastasis from skin melanoma to extraocular muscle. Sonogram shows large mass within orbit displacing optic nerve (arrow).

Fig. 18.—Drusen. Sonogram shows an elevated, echogenic lesion at nerve head. Drusen is a collection of cholesterol-laden cells that often calcify and then show marked acoustic shadowing.



A



B



C

Fig. 19.—Choroidal melanoma.

- A, Small en plaque melanoma is seen on sonogram as a small, echogenic area of thickening of vitreous chamber wall (arrow).
 B, Sonogram shows typical "collar-button" melanoma with shallow retinal detachments on either side (arrows).
 C, Sonogram shows hypoechoic melanoma with choroidal excavation, which refers to posterior displacement of sclera (arrow). This is an artifact rather than true choroidal invasion, due to time delays while sound penetrates tumor.



Fig. 20.—Choroidal metastasis from bronchogenic carcinoma. Sonogram shows a large, echogenic lesion filling most of vitreous chamber.

ultrasound waves, and to the presence of a large amount of echogenic fat, which makes visualization of structures such as the extraocular muscles difficult. At times, the extraocular muscles can be visualized as echo-poor bands traversing the fat. These muscles may be enlarged in conditions such as hyperthyroidism (Fig. 15) [7, 8]. Orbital tumors may be identified, such as hemangiomas (Fig. 16), varices, optic nerve meningiomas or gliomas, and metastases (Fig. 17). Occasionally, a small, slightly raised lesion will be seen at the optic nerve head, which may be calcified. This is called a drusen and is usually of little clinical significance (Fig. 18).

Ocular Tumors

The most commonly encountered ocular tumor in clinical practice is the choroidal melanoma. Choroidal melanomas vary greatly in size and shape, ranging from large tumors, which may almost fill the vitreous chamber, to small en plaque

Fig. 21.—Ocular foreign bodies.

A, Sonogram shows echogenic, nonshadowing plastic foreign body adjacent to posterior wall of vitreous chamber (arrow).

B, Glass foreign body is seen embedded in sclera anteriorly (arrow). Acoustic shadowing is prominent.

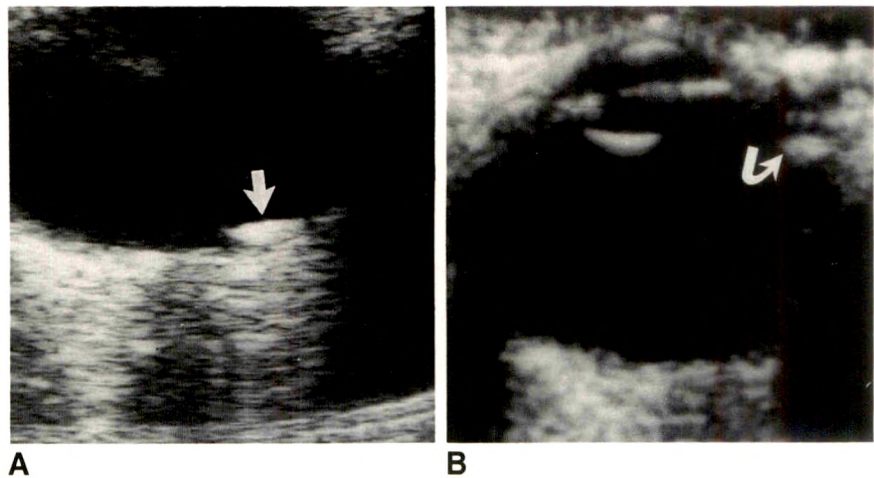


Fig. 22.—Phthisis bulbi. Sonogram shows small, deformed eye from a severe blow about 20 years before.



22

Fig. 23.—Staphyloma. Sonogram shows eye with an unusually long axis due to outpouching of posterior pole. Because eye is so long, this patient was markedly myopic.



23

melanomas, which can be extremely difficult to detect with real-time sonography (Fig. 19). The classic description is of a "collar-button" melanoma. Pathologic examination shows that virtually all melanomas have associated retinal detachments, and these are often shown with sonography (Fig. 19). Small melanomas characteristically have a relatively uniform echo texture; however, larger melanomas may be heterogeneous with areas of necrosis and/or hemorrhage.

Metastatic tumors may occasionally be encountered and may be more common than choroidal melanomas; however, they are rarely the first manifestation of a primary tumor (Fig. 20). On real-time sonography, it is virtually impossible to differentiate between metastatic lesions and choroidal melanomas; in this situation, standardized A-mode scanning may be helpful, as the spike amplitude pattern seen with this technique reputedly differentiates between the two types of lesions.

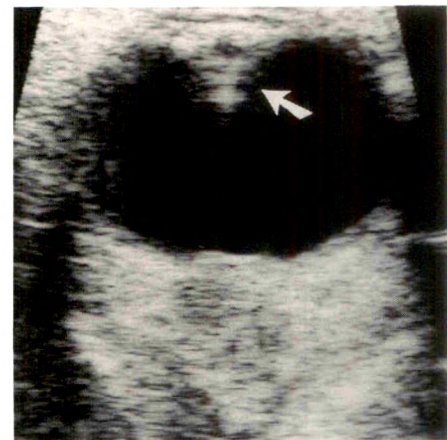
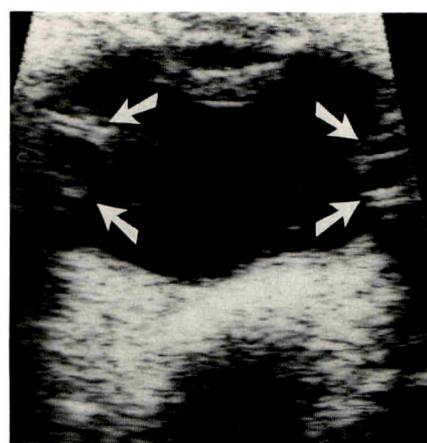
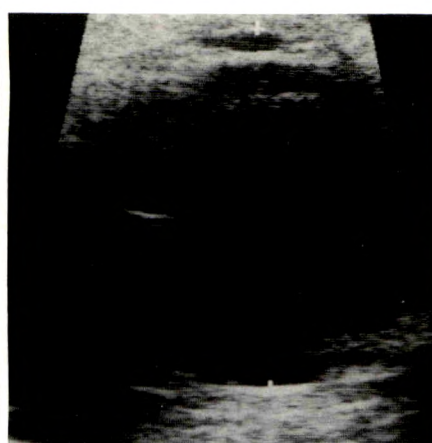


Fig. 24.—Intraocular lens implantation is almost always performed after cataract extraction. Sonogram shows characteristic reverberation artifact behind iris plane (arrow).



A



B

Fig. 25.—Treatment of retinal detachment.

A, Placement of a scleral buckle is one of the more common treatments for large retinal detachments. Globe is usually deformed by buckle, which is shown on sonogram as an echogenic interface on either side of globe (arrows).

B, Occasionally, silicon oil is injected into vitreous chamber to tamponade retinal detachment. Ultrasound waves penetrate oil with difficulty, obscuring detail on sonogram.

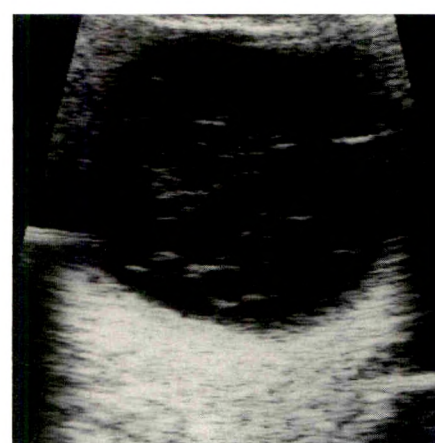


Fig. 26.—Endophthalmitis. After surgery for cataract extraction, an infection developed in the vitreous of this elderly diabetic patient. Sonogram shows distended globe filled with coarse echoes.

Trauma

Many of the manifestations of trauma are nonspecific, such as retinal and/or choroidal detachment and vitreous hemorrhage. Penetrating injury may introduce air into the chambers of the eye, which is recognized as highly echogenic areas with smudgy areas of shadowing posteriorly. Metallic foreign bodies are seen as small, bright areas with marked reverberation artifacts posteriorly. Foreign bodies that become embedded in the sclera, or in the retroorbital fat, are more difficult to visualize than those within the vitreous chamber (Fig. 21). With trauma, the eye may become misshapen, and in chronic injury, the globe may lose volume, show scleral thickening and/or calcification, and become generally deformed (Fig. 22). This is referred to as phthisis bulbi. At times, a small eccentric outpouching of the sclera may exist, usually at the posterior aspect of the vitreous chamber. This is a congenital variant and is called a staphyloma. This should not be mistaken for a posttraumatic lesion (Fig. 23).

Postoperative Eye

The most commonly seen postoperative change is the presence of an intraocular lens implant (Fig. 24). In this situation, the iris plane is noted to be markedly echogenic, and no lens can be seen. Normally, reverberation artifact is seen within the vitreous chamber behind the iris plane.

Another common procedure is scleral buckling (Fig. 25). This procedure consists of placing a band of material, usually Silastic, around the globe to reduce a retinal detachment. This produces some deformity of the globe, which is usually seen easily. At times, the buckle itself may be seen. Silicon oil is sometimes instilled into the vitreous chamber to reduce

retinal detachments. It produces severe artifacts that prevent adequate assessment of the posterior aspect of the vitreous chamber (Fig. 25).

Not infrequently, air may be seen within the vitreous chamber immediately postoperatively. This makes visualization of the posterior chamber difficult unless the patient's head is turned to one side or the other in order to displace the air from the anterior aspect of the vitreous chamber. Rarely, endophthalmitis (infection of the vitreous) may ensue, a dreaded complication. In this situation, the vitreous chamber is filled with low-amplitude echoes (Fig. 26).

REFERENCES

1. Erickson SJ, Hendrix LE, Massaro BM, et al. Color Doppler flow imaging of the normal and abnormal orbit. *Radiology* 1989;173:511-516
2. Munk PL. Coloboma: evaluation with real-time sonography. *AJR* 1990;154:391-392
3. Fielding JA. Ultrasound imaging of the eye through the closed lid using a non-dedicated scanner. *Clin Radiol* 1987;38:131-135
4. Lin DTC, Munk PL, Maberley AL, Cooperberg PL, Rootman J. Ultrasonography of pathologically proven choroidal melanoma with a high resolution small parts scanner. *Can J Ophthalmol* 1987;22:161-164
5. Munk PL, Lin DTC, Gibney RG, Kidney MR. Introduction to high resolution real-time ultrasonography of the eye. *Perspect Radiol* 1989;2:163-175
6. Wong AD, Cooperberg PL, Ross WH, Araki DN. Differentiation of detached retina and vitreous membrane with color flow Doppler. *Radiology* 1991;178:429-431
7. Given-Wilson R, Pope RM, Michell MJ, Cannon R, McGregor AM. The use of real-time orbital ultrasound in Graves' ophthalmopathy: a comparison with computed tomography. *Br J Radiol* 1989;62:705-709
8. Willinsky RA, Arenson AM, Hurwitz JJ, Szalai J. Ultrasonic B-scan measurement of the extra-ocular muscles in Graves' orbitopathy. *Can Assoc Radiol J* 1984;35:171-173
9. Byrne SF. Standardized echography of the eye and orbit. *Neuroradiology* 1986;154:391-392

MR Imaging of Malignant Uveal Melanoma: Role of Pulse Sequence and Contrast Agent

Futoshi Mihara¹
 Kundan L. Gupta¹
 Sadayuki Murayama^{1, 2}
 Nam Lee^{3, 4}
 J. Brent Bond⁵
 Barrett G. Haik⁵

To determine the most sensitive pulse sequence and to clarify the role of each pulse sequence in the MR diagnosis of uveal malignant melanoma, noncontrast T1- and T2-weighted, and postcontrast T1-weighted, spin-echo images were compared blindly and independently by two experienced observers. Thirty uveal malignant melanomas, preselected by ophthalmoscopy and sonography for size greater than 2 mm, were examined with a 1.5-T superconducting MR unit with an orbital surface coil. Fifteen tumor studies were done after the patient was injected with gadopentetate dimeglumine. Postcontrast T1-weighted images were the most sensitive in detecting melanomas, demonstrating tumors 2 mm in height accurately on axial planes and 1.6 mm in height on combined orthogonal planes. The contrast-to-noise ratio between melanoma and vitreous fluid was greatest on postcontrast T1-weighted images (average, 72.1), followed by noncontrast T1-weighted images (average, 32.9), and then by T2-weighted images (average, -21.2). Postcontrast T1-weighted images also proved useful in differentiating melanomas from subretinal fluid collections when combined with noncontrast images.

We conclude that postcontrast T1-weighted images are most helpful in detecting small uveal melanomas and in differentiating melanomas from subretinal fluid collections.

AJNR 12:991-996, September/October 1991; *AJR* 157:1087-1092, November 1991

Received August 22, 1990; revision requested December 5, 1990; revision received February 20, 1991; accepted April 21, 1991.

Presented at the annual meeting of the American Society of Neuroradiology, Los Angeles, March 1990.

This work was supported in part by the St. Giles Foundation, Brooklyn, NY, and by an unrestricted grant from Research to Prevent Blindness, New York, NY.

¹ Department of Diagnostic Radiology, University of Maryland Medical System, 22 So. Greene St., Baltimore, MD 21201. Address reprint requests to F. Mihara.

² Present address: Department of Radiology, Faculty of Medicine, Kyushu University, Fukuoka 812, Japan.

³ Tulane University Medical Center, New Orleans, LA 70112.

⁴ Present address: Department of Radiology, University of Florida Health Science Center, Jacksonville, FL 32209.

⁵ Department of Ophthalmology, Tulane University Medical Center, New Orleans, LA 70112.

0361-803X/91/1575-1087

© American Roentgen Ray Society

Malignant uveal melanoma is the most common ocular tumor in adults [1]. Diagnosis is confirmed by ophthalmoscopy [1, 2], fluorescein angiography [1], sonography [1-4], and CT [2-4]. Although accuracy of clinical diagnosis is high [5], misdiagnoses occur occasionally [6-9]. Recent studies have shown MR to be useful in evaluating uveal melanoma [4, 10] and to be facilitated by the use of a higher magnetic field strength and surface coils [11-14]. Peyster et al. [14] compared MR and CT in the evaluation of intraocular tumors and concluded that MR is superior in both detection and differential diagnosis. Mafee et al. [13] also showed superiority of MR over CT and demonstrated that sonography may be more accurate in detecting small tumors. However, these studies only used unenhanced MR imaging.

To further assess the potential of MR imaging and to determine the value of different pulse sequences in the detection and characterization of uveal melanoma, this study evaluated precontrast T1- and T2-weighted spin-echo (SE) MR images and postcontrast T1-weighted SE images using a surface coil at 1.5 T.

Materials and Methods

Thirty patients with malignant uveal melanoma were preselected to include only patients with tumors greater than 2 mm in size as determined by ophthalmoscopy and sonography (Tables 1 and 2). Twenty-nine tumors were melanotic and one was amelanotic by ophthalmoscopy. A 1.5-T superconducting MR unit (Sigma, General Electric, Milwaukee, WI) with a 12.5-cm-diameter receive-only surface coil (General Electric, Milwaukee, WI) was used for all

TABLE 1: Uveal Melanoma on Unenhanced MR Images

Case No.	Sex	Age (yr)	Location	Size ^a (mm)	Tumor Detection		Comments
					T1-Weighted	T2-Weighted	
1	F	75	OD/P	2 × 3	+	—	
2	M	76	OS/P	2 × 6	+	+	
3	M	64	OD/PM	2 × 7	+	+	
4	F	56	OD/P	2 × 10	+	+	
5	F	41	OS/P	4 × 6	+	+	SF
6	F	64	OD/P	4 × 10	+	+	
7	M	76	OD/PM	6 × 10	+	+	
8	F	58	OS/PM	8 × 8	+	+	SF ^b
9	M	66	OD/PL	8 × 12	+	+	SF ^b
10	M	79	OD/P	9 × 10	+	+	SF ^b
11	M	35	OD/AL	10 × 10	+	+	
12	F	80	OD/L	10 × 14	+	+	SF ^b
13	M	65	OD/AM	12 × 18	+	+	SF
14	F	66	OS/P	12 × 24	+	+	
15	F	72	OD/L	14 × 18	+	+	SF ^b

Note.—+ = detected; — = not detected; OD = right eye; OS = left eye; A = anterior; P = posterior; M = medial; L = lateral; SF = subretinal fluid collection.

^a Height × base diameter.

^b Detected by MR.

cases. T1-weighted images were obtained with sequences of 500,600/20,30/2 (TR/TE/excitations); T2-weighted images were obtained with 2000/70/2. Examination planes for T1-weighted images were axial, coronal, and oblique sagittal; for T2-weighted images, only the axial plane was used. Imaging parameters were 256 × 128 matrix, 18-cm field of view, 3-mm slice thickness, and 1.5-mm slice gap. In 15 studies, 0.1 mmol/kg of gadopentetate dimeglumine (Magnevist, Berlex, Cedar Knolls, NJ) was administered.

Tumor detection rate was compared among unenhanced T1- and T2-weighted axial images, and postcontrast T1-weighted SE images. Image evaluation was performed blindly and independently by two experienced neuroradiologists. Tumors not identified by both radiologists were considered to be undetected.

In the 15 cases in which gadopentetate dimeglumine was administered, signal intensity (SI) [15] of both tumor and vitreous fluid and standard deviations (SD) of noise were obtained by region-of-interest (ROI) calculations on the image that showed maximal tumor size. Measurements from two areas of tumor and vitreous fluid and four areas of noise were averaged. Contrast-to-noise ratios (CNR) were calculated by the formula [16]

$$\text{CNR} = (\text{SI of tumor} - \text{SI of vitreous fluid}) / \text{SD of noise.} \quad (1)$$

Subretinal fluid collection associated with tumor was also evaluated in regard to gadopentetate dimeglumine enhancement, which provided further information. MR findings were correlated with sonographic findings.

Results

Melanotic melanomas showed a characteristic pattern of contrast enhancement and of signal hyperintensity on T1-weighted images and signal hypointensity on T2-weighted images relative to the signal of vitreous fluid (Fig. 1). One small amelanotic melanoma showed slight hyperintensity relative to vitreous fluid on T1-weighted images, which was not detected on T2-weighted images. All cases in which contrast material was administered showed increased tumor SI compared with noncontrast T1-weighted images.

Tumor detection is summarized in Tables 1 and 2. Of the total number of 30 uveal melanomas, T1-weighted imaging detected 27, whereas T2-weighted imaging detected 22. Of the 15 cases in which gadopentetate dimeglumine was administered, postcontrast T1-weighted imaging detected 14

cases, noncontrast T1-weighted imaging detected 12 cases, and T2-weighted imaging detected eight cases. Tumor height of 2 mm was the lower limit for accurate detection on non-contrast images, and 1.6 mm was the lower limit on postcontrast images. Small discoid melanomas were detected in two patients only on postcontrast T1-weighted images owing to tumor enhancement (Figs. 2 and 3). One tumor was not evident on any of the axial images; however, it was easily detected on both coronal and sagittal postcontrast T1-weighted images (Fig. 4).

CNR on postcontrast T1-weighted images (average, 72.1) was greater than on either noncontrast T1-weighted images (average, 32.9, $p < .01$) or T2-weighted images (average, -21.2, $p < .001$) (Table 2).

By sonography, 13 patients had subretinal fluid collections associated with tumor. These were identified in 10 cases by a combination of T1- and T2-weighted MR imaging, while three small subretinal fluid collections could not be detected on MR images. Six of the 10 patients with subretinal fluid collections seen on MR images were studied with contrast-enhanced imaging. In three of these cases the fluid collections were apparent on noncontrast images and in two cases they were equivocal; one small subretinal fluid collection could not be detected on either pre- or postcontrast images. In the two equivocal cases, the subretinal fluid collections were clearly demonstrated on postcontrast images. One subretinal fluid collection was almost isointense with vitreous fluid on both T1- and T2-weighted images. This was apparent on postcontrast images because of marked retinal or choroidal enhancement (Fig. 5). Another subretinal fluid collection was isointense with tumor on noncontrast T1-weighted images with equivocal findings on T2-weighted images, but postcontrast T1-weighted images clearly separated tumor from fluid because of tumor enhancement (Fig. 6).

Discussion

Accurate and early diagnosis of choroidal melanoma by any means is important because of the direct correlation between tumor size and mortality. Shammas and Blodi [17] reviewed a series of 293 cases of choroidal melanoma and found that tumor diameter was the single most important prognostic factor.

Tumor size not only influences prognosis but may also determine subsequent management. Newer treatment methods, such as radioactive plaque therapy, proton beam irradiation, and en bloc resection, now offer an alternative to enucleation. However, successful implementation of therapy is dependent on early identification and complete delineation.

Although MR imaging is superior to CT in the detection and differentiation of most melanomas [4, 14], neither CT nor unenhanced MR imaging has been accurate in detecting tumors smaller than 2–3 mm in height [3, 13]. Although CT is faster than MR, it adds the risk of IV administration of iodinated contrast material [3, 4] and radiation exposure to the lens [18]. Increased SI after injection of gadopentetate dimeglumine facilitates accurate detection of small tumors on MR images by offsetting partial volume averaging and providing bright signal on T1-weighted images.

Gadopentetate dimeglumine shortens both T1 and T2 relaxation times in tissue, which results in contrast enhancement on T1-weighted images [19–22]. The paramagnetic

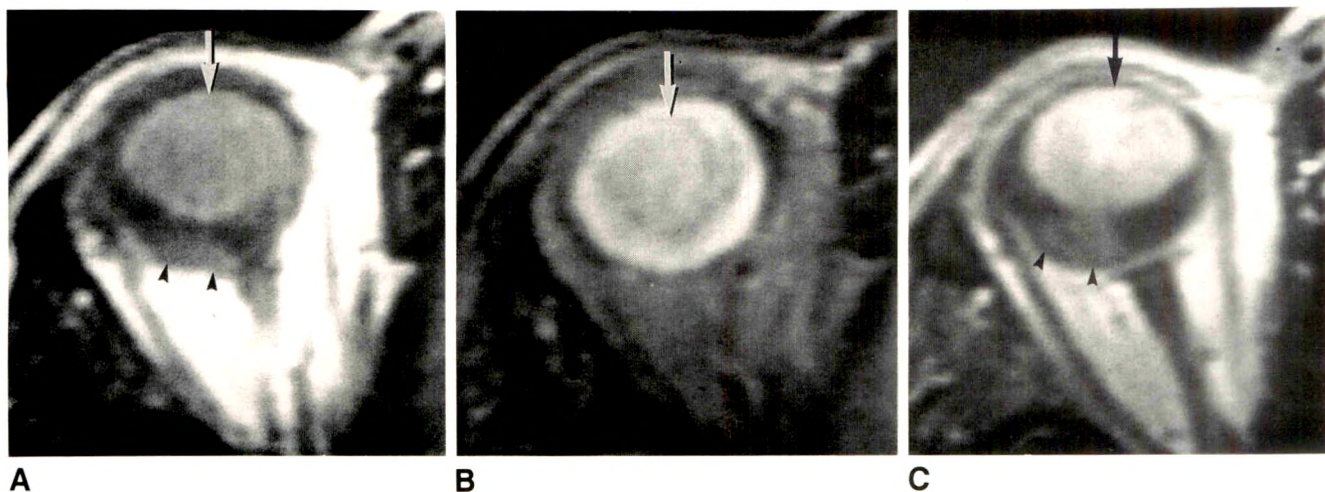


Fig. 1.—Choroidal melanoma with subretinal fluid collection.
A, Axial noncontrast T1-weighted spin-echo MR image. Tumor (arrow) demonstrated hyperintensity relative to vitreous fluid. Subretinal fluid (arrowheads) demonstrated slight hyperintensity.
B, Axial noncontrast T2-weighted spin-echo MR image. Tumor (arrow) demonstrated hypointensity relative to vitreous fluid. Subretinal fluid demonstrated isointensity.
C, Axial postcontrast T1-weighted spin-echo MR image. Tumor (arrow) demonstrated increased signal intensity whereas subretinal fluid (arrowheads) did not show enhancement.

TABLE 2: Uveal Melanoma on Contrast-Enhanced MR Images

Case No.	Sex	Age (yr)	Location	Size ^a (mm)	Tumor Detection/CNR			Comments
					Precontrast		Postcontrast	
					T1-Weighted	T2-Weighted	T1-Weighted	
1	M	62	OD/I	1.6 × 2.1	-/3.1	-/-2.7	-/35.6	
2	M	69	OD/P	1.6 × 6.5	-/15.0	-/-29.3	+18.4	
3	F	77	OD/PL	2.0 × 8.0	-/7.5	-/-15.0	+156.9	
4	F	50	OS/A	2.0 × 9.4	+44.8	-/-5.6	+148.0	
5	M	82	OD/PL	2.0 × 10.4	+10.0	-/-12.7	+33.0	
6	F	25	OD/P	2.1 × 7.8	+23.3	-/-35.6	+54.1	
7	M	71	OS/P	2.5 × 8.2	+41.0	+/-20.5	+55.5	
8	F	81	OS/PM	3.5 × 7.0	+51.5	+/-12.7	+92.1	SF
9	F	36	OS/AL	6.1 × 7.5	+54.4	-/-6.9	+89.5	
10	F	50	OD/AL	7.5 × 11.5	+40.0	+/-21.0	+41.6	
11	F	43	OD/AL	9.0 × 12.0	+25.0	+/-37.1	+73.5	SF ^b
12	M	60	OS/P	11.6 × 14.9	+15.3	+/-66.7	+60.0	SF ^b
13	F	78	OD/PM	12.7 × 16.9	+38.7	+/-31.7	+65.8	SF ^b
14	M	33	OD/PS	13.4 × 18.3	+60.8	+/-12.6	+90.8	SF ^b
15	F	72	OS/PL	13.4 × 15.6	+62.7	+/-8.2	+67.3	SF ^b

Note.—CNR = contrast-to-noise ratio; + = detected; - = not detected; OD = right eye; OS = left eye; A = anterior; P = posterior; M = medial; L = lateral; S = superior; I = inferior; SF = subretinal fluid collection.

^a Height × base diameter.

^b Detected by MR.

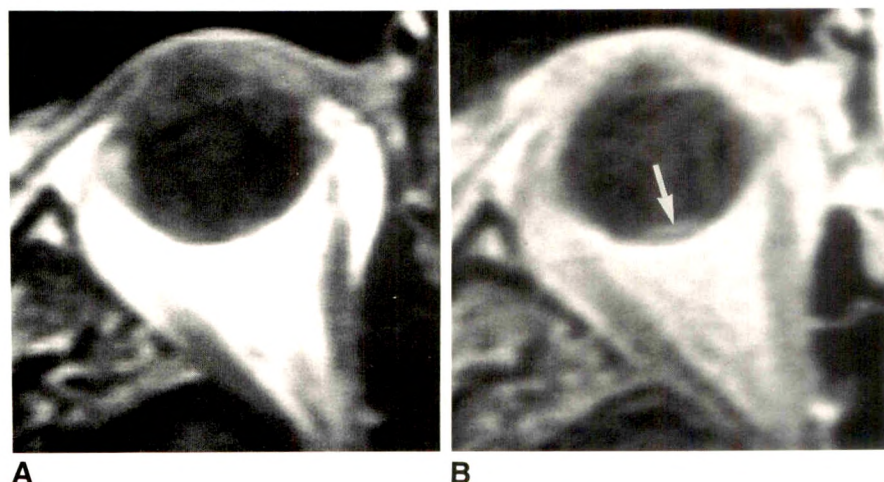


Fig. 2.—A, Axial noncontrast T1-weighted spin-echo MR image did not detect the lesion accurately.
B, Axial postcontrast T1-weighted spin-echo MR image detected discoid choroidal melanoma (arrow). Tumor size was 1.6 × 6.5 mm.

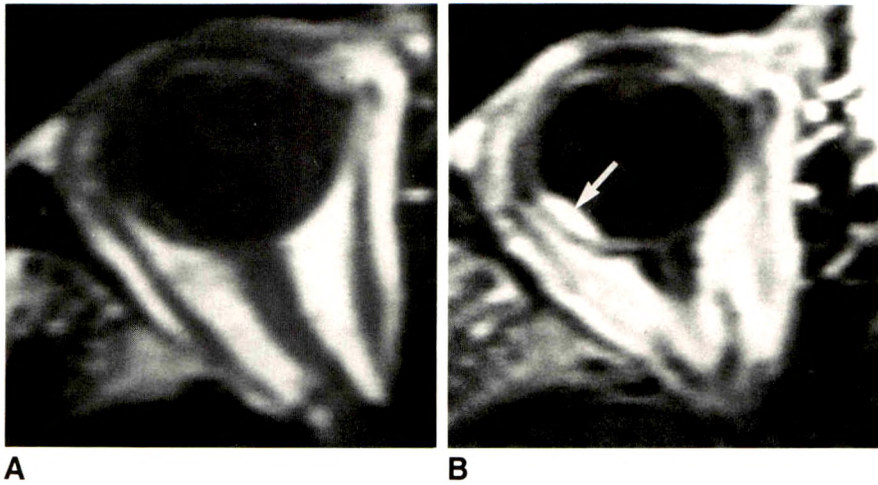


Fig. 3.—A, Axial noncontrast T1-weighted spin-echo MR image did not detect the lesion accurately.

B, Axial postcontrast T1-weighted spin-echo MR image detected discoid choroidal melanoma (arrow). Tumor size was 2.0 × 8.0 mm.

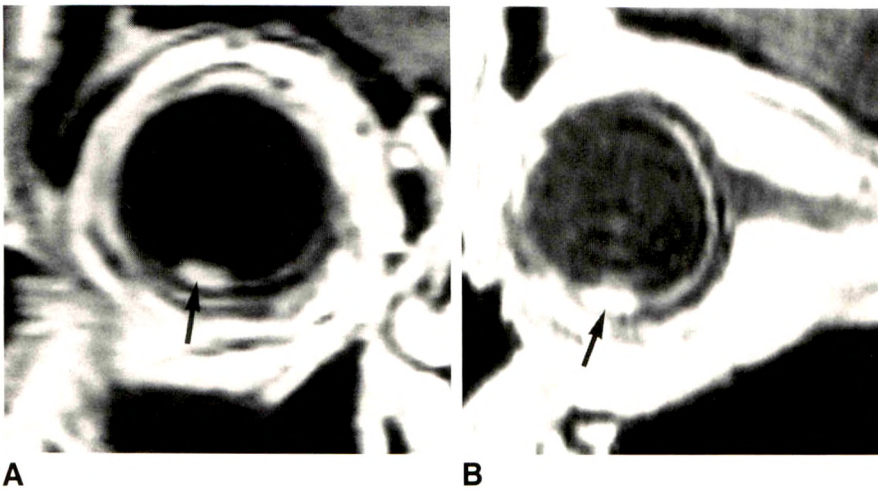


Fig. 4.—A and B, Coronal (A) and sagittal (B) postcontrast T1-weighted spin-echo MR images detected enhanced tumor (arrows) clearly.

effect seen with melanoma also decreases T1 relaxation time [4, 10, 13, 23, 24], which leads to increased SI on T1-weighted images.

Gomori et al. [24] measured the T1 and T2 relaxation times of uveal melanoma using nuclear MR spectroscopy. Moderately pigmented melanomas had average T1 and T2 relaxation times of 596 msec and 68 msec, respectively.

The observed relaxation times after administration of paramagnetic contrast agent are calculated by the formula [19, 21]

$$\frac{1}{T_{\text{obs}}} = \frac{1}{T_0} + R \times [C], \quad (2)$$

where T_{obs} is the measured relaxation time (sec), T_0 is T1 relaxation time (sec) of material without the contrast agent, R is the relaxivity, and $[C]$ is the concentration of paramagnetic contrast material (mmol/l). If the R of gadopentetate dimeglumine is $5 \text{ mmol}^{-1}\text{s}^{-1}$ [19], the observed T1 and T2 relaxation times are 457 msec and 65.7 msec at a gadopentetate dimeglumine concentration of 0.1 mmol/l, and 239 msec and 58.1 msec at a gadopentetate dimeglumine concentration of 0.5 mmol/l, respectively. These gadopentetate dimeglumine concentrations are theoretically calculated for enhancement on T1-weighted SE images after a routine dose of 0.1 mmol/kg [20–22].

The SI of tissues in SE imaging when $TR \gg TE$ is calcu-

lated by the formula [25]

$$SI = k \times N(H) (e^{-TE/T_2}) (1 - e^{-TR/T_1}), \quad (3)$$

where k is a constant expressing system gain, $N(H)$ is the mobile proton density, and T_1 and T_2 are relaxation times.

On the basis of the foregoing formulas and assumptions, noncontrast T1-weighted (500/20) SE images of moderately pigmented tumors show a relative SI of 0.426, 0.491 at 0.1 mmol/l of gadopentetate dimeglumine concentration and 0.621 at 0.5 mmol/l of gadopentetate dimeglumine concentration. Therefore, moderately pigmented melanoma shows increased signal after gadopentetate dimeglumine administration. It may be possible that a markedly pigmented melanoma does not increase in SI after contrast administration because shortening of the T2 relaxation time may cancel the effect of a short T1 relaxation time. However, with very short T1, highly pigmented tumors should show markedly high intensity on noncontrast T1-weighted images, facilitating detection.

T2-weighted images were least effective in detecting uveal melanoma owing to (1) low signal-to-noise ratio [13], (2) low contrast between tumor and vitreous fluid, (3) low spatial resolution [13], and (4) sensitivity to motion because of prolonged examination time [26]. This pulse sequence is better used to characterize lesions as to melanoma or other tumor, or to demonstrate subretinal fluid collection or hemorrhage.

In this study, all tumors detected by sonography were

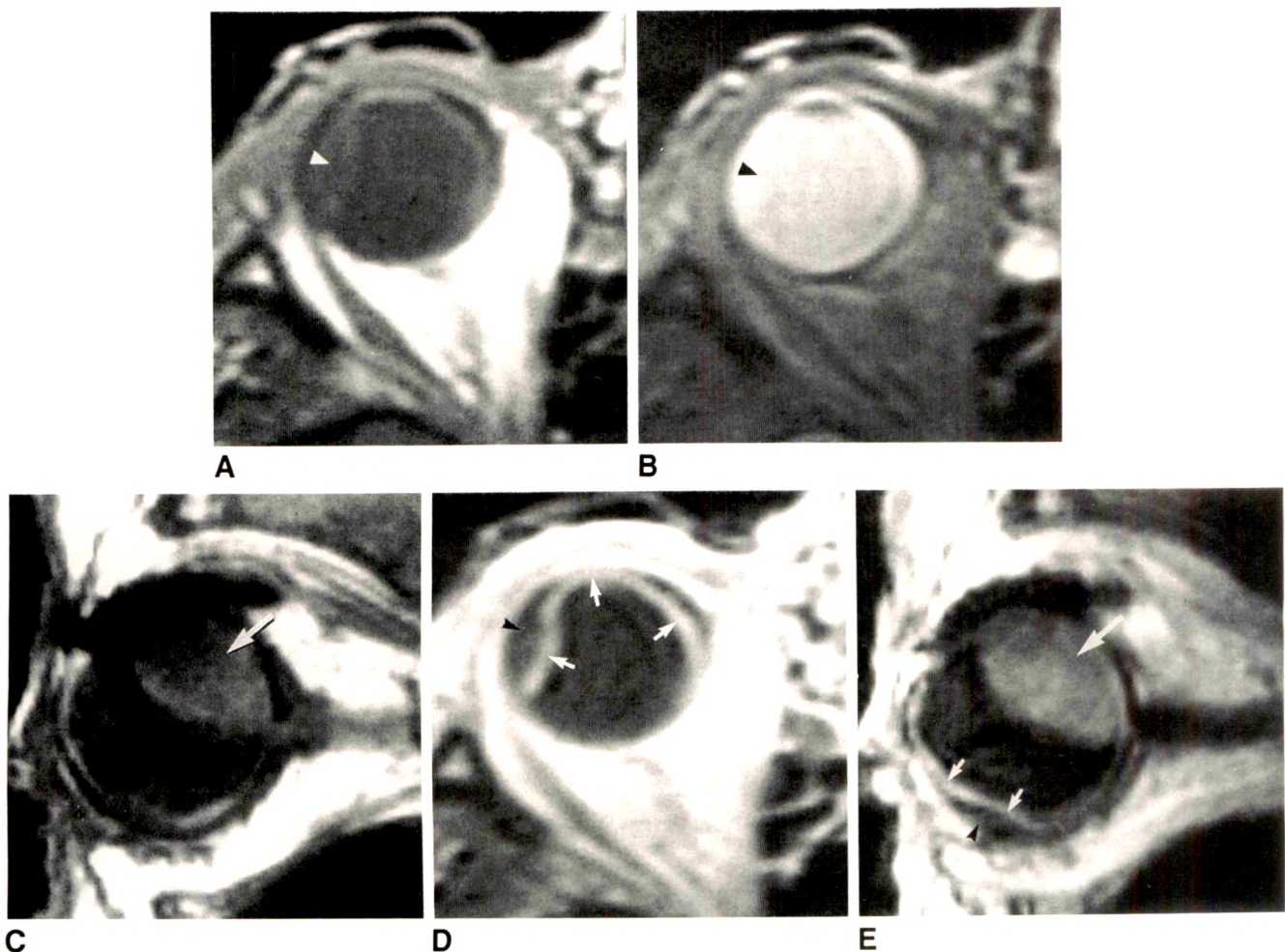


Fig. 5.—Choroidal melanoma with sudden deterioration of right-sided vision.
 A and B, Axial noncontrast T1-weighted (A) and T2-weighted (B) spin-echo MR images demonstrated subretinal fluid (arrowheads) almost isointense with vitreous fluid.
 C, Sagittal noncontrast T1-weighted spin-echo MR image demonstrated a large choroidal melanoma in posterosuperior portion of right globe (arrow).
 D and E, Postcontrast axial (D) and sagittal (E) T1-weighted spin-echo MR images clearly delineated subretinal fluid (arrowheads) because of retinal or choroidal enhancement (short arrows). A large choroidal melanoma demonstrated appreciable enhancement (long arrow in E).

demonstrated on postcontrast T1-weighted images when orthogonal examination planes were used. Therefore, postcontrast T1-weighted images were as sensitive as sonography in demonstrating melanomas more than 1.6 mm in height. However, one small subretinal fluid collection adjacent to a small melanoma was not detected even on postcontrast MR images. Therefore, detection of such small lesions may still require a combination of imaging techniques. However, sonography is not ideal for detecting lesions of the ciliary body or for patients with painful eyes, and it increases the risk of inflammation [3]. Ophthalmoscopy may be limited in cases of opaque ocular media, vitreous hemorrhage, or large amounts of subretinal effusion [27]. In these cases, MR examination becomes even more valuable.

In this study, all MR examinations were performed with a slice thickness of 3 mm and slice gap of 1.5 mm. Reduction in slice thickness and gap is probably advantageous for detecting small tumors [12], but this can be questioned since the CNR decreases as spatial resolution increases [28, 29].

Use of a smaller matrix (i.e., 192 or 256) may help to detect small lesions because of increased spatial resolution; however, this effect will be somewhat limited by decreased CNR and increased examination time [28]. Chemical shift techniques combined with contrast enhancement may also improve detection. However, small melanomas are usually confined to the globe [17]. Consequently, they are surrounded by vitreous fluid anteriorly and demarcated by sclera posteriorly. Both structures are hypointense on T1-weighted images in contrast to melanoma. Therefore, fat suppression would not be extremely helpful in detecting small intraocular melanomas. Furthermore, use of the fat-suppression technique has the additional disadvantages of decreased signal intensity and increased artifacts [30].

In conclusion, postcontrast T1-weighted images were most sensitive in detecting uveal melanoma by MR examination. This pulse sequence was helpful in differentiating tumor from subretinal fluid collection when combined with noncontrast T1-weighted images. Findings from contrast-enhanced MR

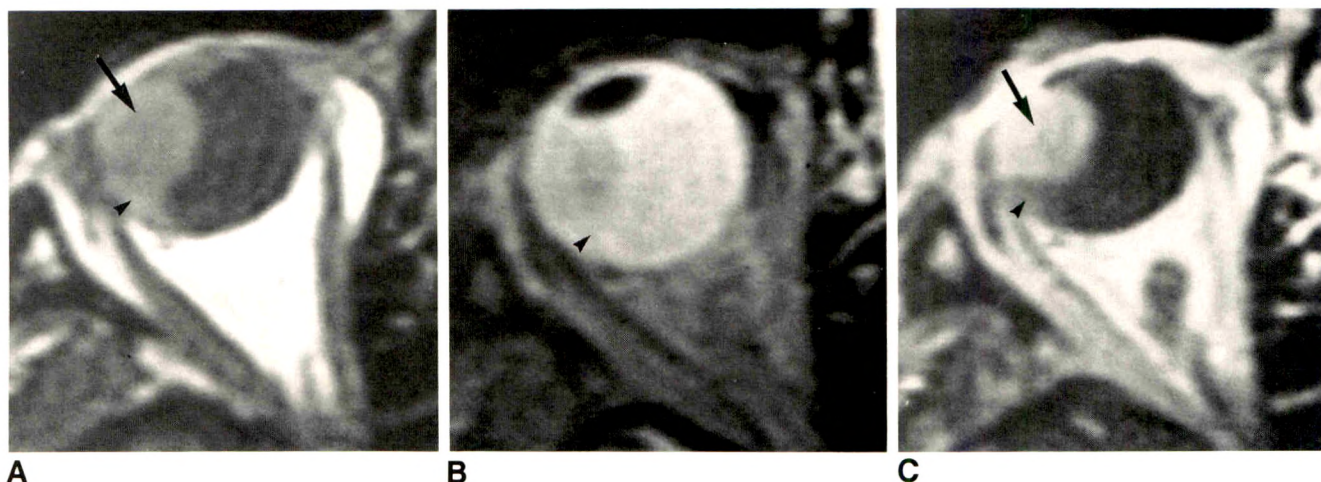


Fig. 6.—A, Axial noncontrast T1-weighted spin-echo MR image. Choroidal melanoma (arrow) and subretinal fluid collection (arrowhead) could not be clearly separated.

B, Axial noncontrast T2-weighted spin-echo MR image demonstrated equivocal findings of subretinal fluid collection (arrowhead).

C, Axial postcontrast T1-weighted spin-echo MR image separated tumor tissue (arrow) from subretinal fluid (arrowhead) because the former showed enhancement.

imaging, added to clinical data and results from other imaging techniques, provide further diagnostic information and allow confirmative diagnosis, thereby obviating unnecessary interventional procedures.

ACKNOWLEDGMENTS

We acknowledge the invaluable assistance of Arvin E. Robinson in preparing this manuscript, the patience and technical skill of Morris Francis, the professional photographs taken by Richard Hutton, and the secretarial assistance provided by Terry McGuckin.

REFERENCES

- Shields JA. Current approaches to the diagnosis and management of choroidal melanomas. *Surv Ophthalmol* 1977;21:443-463
- Peyster RG, Augsburger JJ, Shields JA, et al. Choroidal melanoma: comparison of CT, funduscopy, and US. *Radiology* 1985;156:675-680
- Mafee MF, Peyman GA, McKusick MA. Malignant uveal melanoma and similar lesions studied by computed tomography. *Radiology* 1985;156:403-408
- Mafee MF, Peyman GA, Grisolan JE, et al. Malignant uveal melanoma and simulating lesions: MR imaging evaluation. *Radiology* 1986;160:773-780
- Char DH, Stone RD, Irvine AR, et al. Diagnostic modalities in choroidal melanoma. *Am J Ophthalmol* 1980;89:223-230
- Rones B, Zimmerman LE. An unusual choroidal hemorrhage simulating malignant melanoma. *Arch Ophthalmol* 1963;70:30-32
- Ferry AP. Lesions mistaken for malignant melanoma of the posterior uvea: a clinicopathologic analysis of 100 cases with ophthalmoscopically visible lesions. *Arch Ophthalmol* 1964;72:463-469
- Shields JA. Lesions simulating malignant melanoma of the posterior uvea. *Arch Ophthalmol* 1973;89:466-471
- Mauriello JA Jr, Zimmerman LE, Rothstein TB. Intrachoroidal hemorrhage mistaken for malignant melanoma. *Ann Ophthalmol* 1983;15:282-284
- Haik BG, Louis ST, Smith ME, Ellsworth RM, Deck M, Friedlander M. Magnetic resonance imaging in choroidal tumors. *Ann Ophthalmol* 1987;19:218-238
- Bilaniuk LT, Schenck JF, Zimmerman RA, et al. Ocular and orbital lesions: surface coil MR imaging. *Radiology* 1985;156:669-674
- Sullivan JA, Harms SE. Surface-coil MR imaging of orbital neoplasms. *AJNR* 1986;7:29-34
- Mafee MF, Peyman GA, Peace JH, Cohen SB, Mitchell MW. Magnetic resonance imaging in the evaluation and differentiation of uveal melanoma. *Ophthalmology* 1987;94:341-348
- Peyster RG, Ausberger JJ, Shields JA, Hershey BL, Eagle R Jr, Haskin ME. Intraocular tumors: evaluation with MR imaging. *Radiology* 1988;168:773-779
- Enzmann DR, O'Donohue J. Optimizing MR imaging for detecting small tumors in the cerebellopontine angle and internal auditory canal. *AJNR* 1987;8:99-106
- Mano I, Yoshida H, Nakabayashi K, Yashiro N, Iio M. Fast spin echo imaging with suspended respiration: gadolinium enhanced MR imaging of liver tumors. *J Comput Assist Tomogr* 1987;11:73-80
- Shammas HF, Blodi FC. Prognostic factors in choroidal and ciliary body melanomas. *Arch Ophthalmol* 1977;95:63-69
- Mafee MF, Linder B, Peyman GA, Langer BG, Choi KH, Capek V. Choroidal hematoma and effusion: evaluation with MR imaging. *Radiology* 1988;168:781-786
- Weinmann HJ, Brasch RC, Press WR, Wesbey GE. Characteristics of gadolinium-DTPA complex: a potential NMR contrast agent. *AJR* 1984;142:619-624
- Weinmann HJ, Laniado M, Mutzel W. Pharmacokinetics of GdDTPA/dimeglumine after intravenous injection into healthy volunteers. *Physiol Chem Phys Med NMR* 1984;16:167-172
- Weinmann HJ, Gries H, Speck U. Gd DTPA and low osmolar Gd chelates. In: Runge VM, ed. *Enhanced magnetic resonance imaging*. St. Louis: Mosby, 1989;74-86
- Elster AD, Sobol WT, Hinson WH. Pseudolayering of Gd-DTPA in the urinary bladder. *Radiology* 1990;174:379-381
- Damadian R, Zaner K, Hor D. Human tumors by NMR. *Physiol Chem Phys* 1973;5:381-402
- Gomori JM, Grossman RI, Shields JA, Augsburger JJ, Joseph PM, DeSimeone D. Choroidal melanomas: correlation of NMR spectroscopy and MR imaging. *Radiology* 1986;158:443-445
- Hendrick RE, Newman FD, Hendee WR. MR imaging technology: maximizing the signal-to-noise ratio from a single tissue. *Radiology* 1985;156:749-752
- Atlas AW, Grossman RI, Axel L, et al. Orbital lesions: proton spectroscopic phase-dependent contrast MR imaging. *Radiology* 1987;164:510-514
- Peyman GA, Mafee MF. Uveal melanoma and similar lesions: the role of magnetic resonance imaging and computed tomography. *Radiol Clin North Am* 1987;25:471-486
- Wehrli FW, Kanal E. Orbital imaging: factors determining magnetic resonance imaging appearance. *Radiol Clin North Am* 1987;25:419-427
- Kucharczyk W, Crawley AP, Kelly WM, Henkelman RM. Effect of multislice interference on image contrast in T2- and T1-weighted MR images. *AJNR* 1988;9:443-451
- Hendrix LE, Kneeland JB, Houghton VM, et al. MR imaging of optic nerve lesions: value of gadopentetate dimeglumine and fat-suppression technique. *AJNR* 1990;11:749-754

Optimization of Techniques in Screening CT of the Sinuses

Robert Babbel¹
H. Ric Harnsberger
Brent Nelson
Jerry Sonkens
Steven Hunt

The number of screening examinations of the sinuses performed with CT has markedly increased owing to the widespread and increasing use of endoscopic sinonasal surgery. We reviewed scans from 500 patients who had screening CT examinations of the sinuses for preendoscopic evaluation of inflammatory sinonasal disease to better define an optimal imaging protocol. Three aspects of direct coronal imaging of the paranasal sinuses were investigated: (1) preparation of the patient prior to the examination; (2) technical factors of the CT study, including positioning of the patient, optimal coronal angle, slice thickness, and CT exposure factors; and (3) data display. Our experience indicates that pretreatment of the patient with maximal medical therapy enables the best preendoscopic definition of anatomy, disease pattern, and nonreversible disease component for the treating surgeon. CT technical factors are optimized with scanning in the prone position with thin (3-mm) sections obtained through the anterior paranasal sinuses. This allows optimal visualization of the ostiomeatal unit. The remaining posterior portions of the sinuses are adequately imaged with thicker slices (5 mm). The coronal scan angle used is less critical. Exposure factors (mAs) can be reduced dramatically without image compromise. Data display is optimized when the bone algorithm is used to acquire the data and with image display at intermediate window center and width level.

Use of the techniques outlined in this article results in a cost-effective yet diagnostic scan of the sinuses with decreased radiation exposure to the patient.

AJNR 12:849-854, September/October 1991; *AJR* 157:1093-1098, November 1991

Functional endoscopic sinonasal surgery has resulted in a dramatic increase in the use of CT as a presurgical screening study of the sinuses [1-3]. In this report, we describe a limited preendoscopic CT examination of the sinuses performed in a single plane, without IV contrast material and at a reduced cost. Various techniques and approaches to the screening CT study have been described [1-9]. However, no well-documented studies defining optimal techniques were found in the literature. We examined the various aspects of the screening sinonasal CT examination to document optimal techniques for preendoscopic evaluation. Three general features of the screening examination were analyzed: preparation of the patient, CT technique, and display of the acquired data. This article describes our findings and summarizes our experience with a list of recommendations for the optimal preendoscopic CT screening examination of the sinuses.

Direct coronal imaging is especially well suited for radiologic evaluation of the sinonasal region prior to endoscopic surgery owing to the similar anatomic orientations of imaging and endoscopy [1-5, 10]. Coronal imaging also affords an optimal view of the components of the ostiomeatal unit (OMU), including the maxillary ostium, infundibulum, uncinate process, ethmoid bullae, and middle meatus [2-5, 10]. The OMU is a critical area in endoscopic sinonasal surgery and the most frequent site of disease in the paranasal sinuses [10-14]. Besides the OMU, the other bony and soft-tissue structures of the sinonasal region are

Received November 19, 1990; returned for revision February 25, 1991; revision received March 26, 1991; accepted April 22, 1991.

¹ All authors: Department of Radiology, University of Utah Medical Center, 50 N. Medical Dr., Salt Lake City, UT 84132. Address reprint requests to H. R. Harnsberger.

0361-803X/91/1575-1093
© American Roentgen Ray Society

visualized superbly on coronal CT. Although the coronal imaging plane is assumed in this study to provide ideal visualization of the OMU for the surgeon, other facets of the CT examination were critically evaluated for this report.

Subjects and Methods

Investigational methods included analysis of two study groups. Group 1 consisted of routine screening CT scans of the sinuses in 500 consecutive patients scanned for preendoscopic evaluation of inflammatory sinonasal disease. Group 2 included an additional 44 patients whose scans were used in both a prospective and retrospective analysis. All scans were obtained with a General Electric 9800 Quickscan CT unit or a Picker 1200 SX CT unit by using bone algorithm with direct coronal scanning. Patients in group 1 were scanned with a slice width and interval of 3 mm anteriorly and 5 mm posteriorly. Patients in group 2 were scanned with a 5-mm slice width and interval throughout. All scans were reviewed by at least two of the authors.

To evaluate the relative merits of prone vs supine positioning, coronal scanning was attempted in both positions in each of 34 consecutive patients in group 2. The CT gantry was maximally angled in an attempt to obtain a true coronal plane of imaging in both positions. Factors assessed for each position were ease of patient positioning, diagnostic quality, demonstration of disease, and adequacy of visualization of the OMU.

In 10 group 1 patients, CT technical factors were varied to test the hypothesis that when the bone algorithm is used, high-quality CT scans can be obtained despite the use of significantly reduced CT exposure factors (mAs). In each case, one slice location was selected where repeated images were obtained with incremental decreases in mAs, while maintaining a constant kVp. The acquired images were photographed by using identical window levels and widths. These were compared for image quality and diagnostic utility.

The ability of patients to hyperextend their necks varied, often resulting in scans that were not truly coronal in angle. This resulted in scans with variable coronal angles, which allowed the retrospective analysis of the actual coronal angle used and the relationship, if any, of the scan angle to visualization of the OMU. The coronal scan angle was measured on each scan of the 40 patients in group 2, including 30 patients scanned in both supine and prone positions. The lateral scout localizer image, with annotated slices, was used to make the measurements in relationship to the hard palate. The angle of the

scan was correlated with adequacy of visualization of the OMU. Visualization of the OMU was graded on a scale of 1–4. A grade of 1 was assigned when the OMU was not visualized, grade 2 was assigned when the OMU area could be identified but the OMU anatomy was poorly defined, grade 3 was assigned for good visualization, and grade 4 was assigned when visualization was excellent.

The importance of CT slice thickness and interval in visualizing the OMU was evaluated by determining the frequency with which these structures were seen optimally (good to excellent visualization) on 5- vs 3-mm contiguous scans. The 40 patients in group 2 were scanned with the 5-mm technique, and the 1–4 grading system was used to assess image quality on the coronal scans. This was compared with visualization of the OMU in the 500 patients in group 1 scanned with the 3-mm technique. Scans showing severely diseased OMUs were excluded to avoid introduction of uncontrollable factors.

The filming technique was appraised in five patients in group 1 with sinonasal disease to determine if multiple filming formats are necessary to evaluate the sinuses on CT. The bone algorithm was used in all cases [15]. The data were displayed at soft-tissue (450 H, 50 H), bone (4000 H, 1100 H), and intermediate (2500 H, 250 H) window widths and levels, respectively. The images were evaluated for ease of perception of soft-tissue and bone disease, and for ability to visualize normal structures.

Difficulty in study design precluded an adequate objective analysis of patient preparation before scanning. However, subjective evaluation of our experience with use of a sympathomimetic nasal spray, nose-blowing immediately prior to the scan, and use of a prescan course of antibiotics [2] was performed.

Results

Patient Position

Of 34 consecutive patients, 30 were able to assume both the supine and prone positions. Two were unable to assume either position, while two were unable to assume the prone position but were able to assume the supine position. In the 30 patients able to assume both positions, 21 (70%) were adequately evaluated in either position. In six patients (20%), the studies were complementary and allowed a more accurate assessment than did either study alone (Fig. 1). This was particularly true for determining if an air/fluid level was present

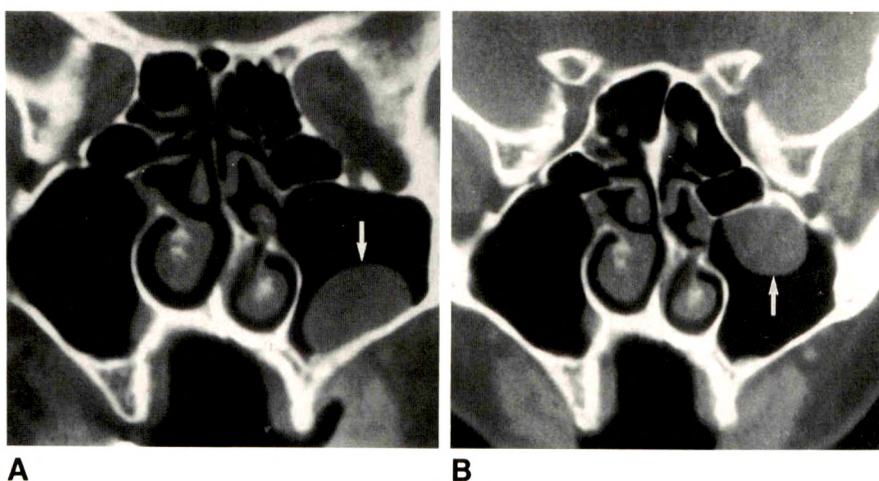


Fig. 1.—A and B, Free migrating ball of debris within left maxillary sinus (arrows) is seen in different locations on direct coronal images with patient prone (A) and supine (B). On either image alone, debris has the appearance of a mucous retention cyst or polyp. In order to categorize abnormality correctly, both images are necessary to document that lesion is not attached to sinus wall.

(Fig. 2). In three of the cases (10%), assessment was superior with the prone study, where the OMU was clearly visualized, whereas in the supine position, free fluid occluded the OMU. In no case was the supine position superior to the prone position in terms of image quality.

CT Technical Factors

In 10 patients imaged with the bone algorithm, but with decreasing mAs, there was no significant decline in image quality or diagnostic usefulness of the scan until exposures below 140 mAs (70 mA at 2 sec) were reached. Below this level, overall image sharpness and quality were diminished owing to quantum mottle (Fig. 3).

Excluding cases in which the OMU was severely diseased, visualization of the OMU was good to excellent (grade 3–4)

in 45% of scans with slice thickness and interval of 5 mm. With slice thickness and interval of 3 mm, visualization of the OMU was good to excellent in 100% of the patients.

In 40 patients assessed for optimal coronal angle, 30 were scanned in both supine and prone positions. Another 10 were scanned only in a single position. The actual coronal angle of the scan varied significantly between the prone and supine positions of each individual and between all individuals in the group. This allowed correlation between the angle and visualization of the OMU. In the prone position, the average angle of scans where OMU visualization was good to excellent (grade 3–4) was 119° (range, $100\text{--}140^\circ$), while scans with poor or nonvisualization of the OMU (grade 1–2) had an average angle of 124° (range, $97\text{--}140^\circ$). In the supine position the respective average angles were 114° (grade 3–4; range, $102\text{--}130^\circ$) and 113° (grade 1–2; range, $92\text{--}134^\circ$). Comparing angles of examinations where the OMU was poorly or inade-

Fig. 2.—A and B, Direct coronal images through sphenoidal sinuses obtained in prone (A) and supine (B) positions in patient with sinonasal polyposis. Air/fluid level is well seen on image obtained with patient prone, suggesting possibility of acute sinusitis (arrows). Supine images failed to reveal an air/fluid level, despite imaging completely through sphenoidal sinuses.

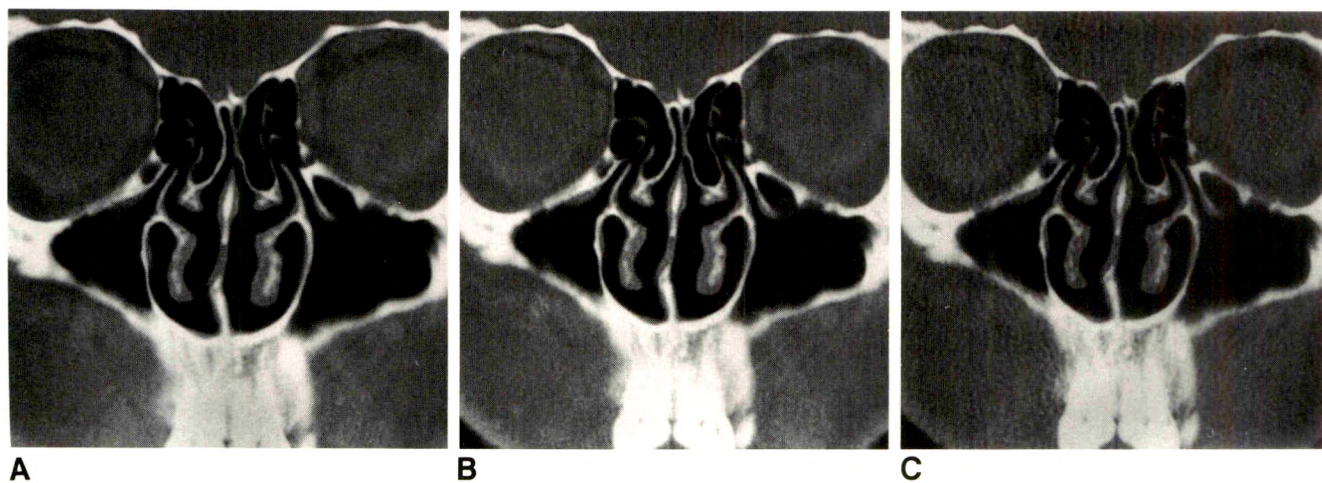
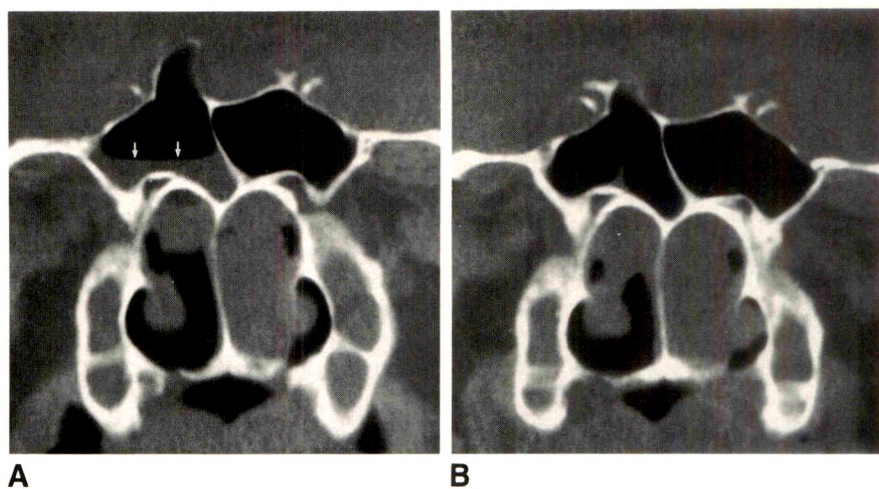


Fig. 3.—A–C, Images obtained with bone algorithm, all through same slice location, but with mAs decreasing from 400 (A) to 200 (B) to 40 (C) mAs. Even with dramatic reduction in exposure technique, image quality remains excellent. At 40 mAs (C), there is moderate aesthetic compromise owing to quantum mottle.

quately visualized with examinations where visualization was good to excellent, there was no statistically significant range of angles that resulted in consistently optimal visualization of the OMU.

Data Display

Of the five cases of noncomplicated inflammatory sinonasal disease filmed at three different window widths and levels (soft tissue, bone, and intermediate), none demonstrated significant disease on either bone or soft-tissue images that was not apparent on intermediate images. Image quality was excellent on the intermediate images, allowing superb visualization of bone and soft-tissue anatomy (Fig. 4).

Discussion

The results of our investigation enable delineation of a preendoscopic screening CT protocol with optimal techniques. The goals of a cost-effective, expeditious, low-radiation-dose preendoscopic examination are best attained when these techniques are used in performing the examination. Our recommendations and their justifications follow.

Patient Preparation

One of the goals of the screening CT examination of the sinuses is to define nonreversible disease; that is, the disease component that has not responded to conservative medical therapy and requires endoscopic sinonasal surgery [1-3]. Zinreich et al. [2] emphasized the importance of proper pre-scan patient preparation to eliminate as much reversible disease as possible. This can be accomplished by several measures, including administration of a course of antibiotics prior to the scan, thus eliminating any acute sinusitis component [2]; use of a sympathomimetic nasal spray 15 min before the scan in association with vigorous nose blowing immediately

prior to scanning to eliminate reversible nasal congestion and mucous; continued use of previously prescribed oral antihistamines and decongestants to eliminate nasal congestion and mucous; and consideration of administration of a short course of steroids in cases of nasal polyposis or other suspected allergic sinonasal disease. Although objective data documenting the necessity of prescan preparation are difficult to obtain, our experience suggests that use of these techniques allows optimal delineation of the chronic, nonreversible disease component (Fig. 5).

CT Technique

It has been suggested that the total amount of radiation (mAs) used in screening CT of the sinuses could be significantly reduced if a bone algorithm were used (Akiya F, personal communication). Advantages of reducing exposure techniques include decreased radiation exposure to the patient, extended CT tube life, and reduced expense. On the basis of the results of our study, we have reduced our exposure factor from 420 mAs (140 mA at 3 sec) to 200 mAs (100 mA at 2 sec) without image compromise.

Delineation of the individual components of the OMU is critical to the correct interpretation of inflammatory disease of the nose and sinuses. Direct coronal CT imaging with the patient in the prone position affords an optimal view of these components, with dependent fluid layering away from the OMU. Supplemental coronal scans with the patient supine occasionally are helpful for complete pathologic characterization. Coronal imaging with the patient supine can also be used for the rare patient who is unable to assume the prone position.

Scan angle might at first seem important to the optimal definition of the structures of the OMU. However, the OMU structures are seen well with a variety of coronal and oblique coronal planes. An optimal scan angle for visualization of the

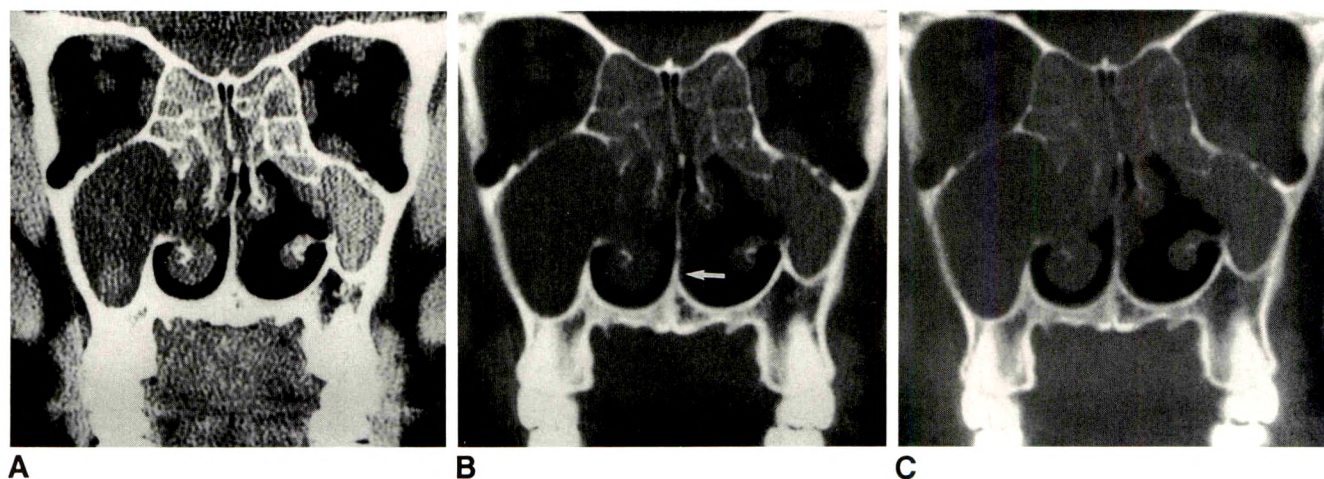


Fig. 4.—A-C, Single slice, obtained with bone algorithm, photographed at three different window levels and widths, respectively: 450 and 50 H (A), 2000 and 250 H (B), and 4000 and 1100 H (C). Note how even subtle soft tissues remain clearly visible on intermediate images (arrow), yet bone detail is also visualized accurately (B).

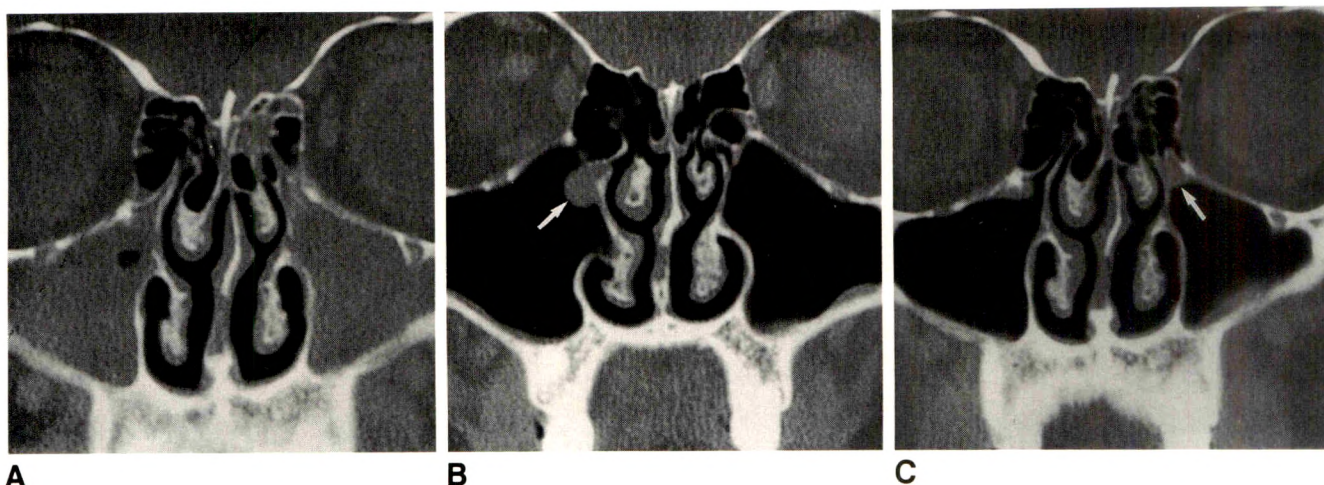


Fig. 5.—A–C, Dramatic example of usefulness of prescanning preparation of patient. A, Image obtained before preparation in a patient with recurrent sinusitis shows diffuse sinus opacification. B and C, Images obtained 10 days later, after maximal medical therapy, illustrate striking resolution of acute disease. This allows delineation of actual cause of sinus disease, endoscopically confirmed bilateral infundibular polyps (arrows). Posttreatment scanning permits specific guidance to endoscopic sinonasal surgeon.

OMU does not appear to exist. Instead, thin (3-mm) slice thickness is critical for optimal visualization. With 3-mm slices, the actual coronal angle is not significant, as good to excellent visualization of the OMU will be seen in all patients, regardless of angle used. We currently use a 3-mm contiguous scan technique through the anterior half of the paranasal sinuses (where the OMU is found) and a 5-mm contiguous scan technique through the posterior half. The scan technique changes at the anterior wall of the posterior ethmoid to ensure 3-mm scanning through the OMU (Fig. 6). This compromise allows optimal visualization of the OMU with a decrease in the total number of required slices.

As absolute coronal scan angle is not critical, the imaging angle may be set to maximally avoid dental amalgam [3, 8]. Zinreich et al. [2] demonstrated that direct coronal images, even with artifacts from dental amalgam, were superior to reformatted coronal images obtained from axial data. Consequently, coronal images are attempted in all patients initially, with supplemental axial images through the lower maxillary sinus obtained only in the rare circumstances where dental amalgam artifacts are severe. Full axial images with coronal reconstructions are used only in those few patients who are physically unable to assume either coronal scanning position.

Data Display

Chow and Mafee [3] documented the usefulness of photographing with a wide window technique for display of screening CT scans of the sinuses, and Chakeres [15] recommended the use of high-resolution bone-algorithm technique. Our experience confirms the usefulness of these techniques. In 500 patients studied by screening CT of the sinuses, display and filming of the acquired bone-algorithm data were sufficient when using a single intermediate window center and level (around 2500 and 250 H, respectively). In the vast majority of patients evaluated in this manner, diagnostic

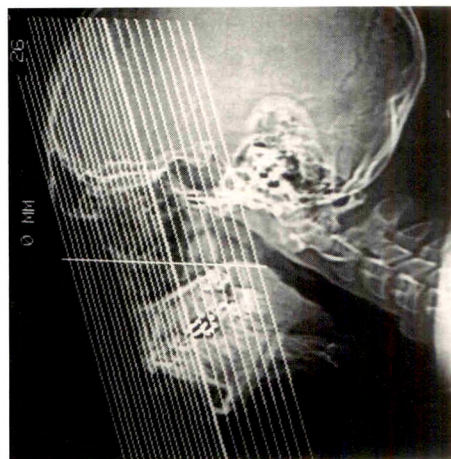


Fig. 6.—Scout view with image slice locations annotated to show technique of scanning with 3-mm slices through anterior one half of paranasal sinuses, including ostiomeatal unit, and 5-mm slices through posterior one half. Prescribed technique is prospective and does not slow the examination. This combination reduces the number of films and cost, but still affords an optimal view of ostiomeatal unit.

scans are obtained. We are aware of only a single case in which disease was not adequately assessed with this protocol. Therefore, these cases are sufficiently rare that the use of the single intermediate windowing technique only is warranted, thus limiting the number of displayed images and photographic films required.

Inflammatory sinonasal disease studied preendoscopically is adequately assessed without the use of IV iodinated contrast material [5, 16]. The screening CT study of the sinuses is ideal for preendoscopic evaluation of inflammatory disease. The protocol is not adequate for other disease processes [5, 6]. When initial images or clinical symptoms suggest tumor or intracranial complications of inflammatory sinus disease, a

TABLE 1: Protocol and Technique for Screening CT Evaluation of the Sinuses

Protocol	Description
Patient preparation	Key for eliminating reversible disease. Permits better delineation of anatomy and definition of chronic disease requiring endoscopic surgery. Preparation includes (1) completion of course of antibiotics; (2) continuation of oral antihistamines and decongestants; (3) sympathomimetic nasal spray 15 min before examination, followed by vigorous nose blowing; and (4) consideration of steroid use in allergic patients.
CT technique	
Patient position	Coronal imaging with patient in prone position with head hyperextended, resting on chin (keeps free fluid out of infundibulum). In patients unable to maintain prone position or when images obtained in prone position are inconclusive, the supine position with head hyperextended over the edge of the table is used for coronal imaging.
Gantry angle	Perpendicular to hard palate to obtain direct coronal images; actual coronal angle is not critical.
Scan extent	Posterior margin of sphenoid sinus to anterior margin of frontal sinus.
Section thickness	Posterior one half (posterior margin of sphenoid sinus to anterior margin of posterior ethmoid) scanned with 5-mm contiguous slices. Anterior one half (anterior margin of posterior ethmoid to anterior margin of frontal sinus) scanned with 3-mm contiguous slices; anterior thin sections are critical to ensure optimal visualization of ostiomeatal unit.
kVp	120
mAs (dose per slice)	200 (100 mA × 2-sec scan time); low exposure can be used because of bone-algorithm technique with filming at intermediate window.
Imaging algorithm	Bone (maximum-edge-enhancement program).
Photography	Window width: 2000–2500 H; window center: 100–300 H. Both bone and soft tissues are visualized on the single set of images.
Contrast material	Not used.

Note.—These recommendations are for the screening CT examination of the sinuses in evaluating inflammatory disease. In cases of noninflammatory disease, or in cases of extensive or complicated inflammatory disease, a full CT examination of the sinuses should be considered. This includes IV contrast material with axial and coronal images and multiple filming techniques.

full sinonasal CT protocol is indicated. This includes use of IV contrast material, axial and coronal imaging of the sinuses and intracranial structures, and photography to emphasize both soft-tissue and bone detail.

In conclusion, our recommended approach to the screening CT examination of the sinuses is summarized in Table 1. With these guidelines, maximal diagnostic information is obtained with reduced cost and radiation exposure to the patient. In addition, a clear presurgical picture of the irreversible inflammatory changes of the sinonasal region is provided to the endoscopic surgeon.

REFERENCES

1. Kennedy DW, Zinreich SJ, Rosenbaum AE, Johns ME. Functional endoscopic sinus surgery. *Arch Otolaryngol Head Neck Surg* **1985**;111:576–582
2. Zinreich SJ, Kennedy DW, Rosenbaum SE, et al. Paranasal sinuses: CT imaging requirements for endoscopic surgery. *Radiology* **1987**;163:769–775
3. Chow JM, Mafee MF. Radiologic assessment preoperative to endoscopic sinus surgery. *Otolaryngol Clin North Am* **1989**;22(4):691–701
4. Schatz CJ, Becker TS. Normal CT anatomy of the paranasal sinuses. *Radiol Clin North Am* **1984**;22(1):107–118
5. Pollei SR, Harnsberger HR. The radiologic evaluation of the sinonasal region. *Postgrad Radiol* **1989**;9:242–264
6. Som PM. CT of the paranasal sinuses. *Neuroradiology* **1985**;27:189–201
7. Unger JM, Shaffer K, Duncavage JA. Computed tomography in nasal and paranasal sinus disease. *Laryngoscope* **1984**;94:1319–1324
8. Sataloff RT, Grossman CB, Gonzales C, Naheedy MH. Computed tomography of the face and paranasal sinuses: Part I. Normal anatomy. *Head Neck* **1984**;7:110–122
9. McAlister WH, Lusk R, Muntz HR. Comparison of plain radiographs and coronal CT scans in infants and children with recurrent sinusitis. *AJR* **1989**;153:1259–1264
10. Harnsberger HR. The sinuses and nose. In: Harnsberger HR, ed. *Handbooks in radiology, head and neck imaging*. Chicago: Year Book Medical, **1990**:377–419
11. Drettner B. The obstructed maxillary ostium. *Rhinology* **1967**;51:100–104
12. Stammberger H. Endoscopic endonasal surgery—concepts in treatment of recurring rhinosinusitis. I. Anatomic and pathophysiologic considerations. *Otolaryngol Head Neck Surg* **1986**;94(2):143–146
13. Stammberger H. Endoscopic endonasal surgery—concepts in treatment of recurring rhinosinusitis. II. Surgical technique. *Otolaryngol Head Neck Surg* **1986**;94(2):147–156
14. Proctor DF. The mucociliary system. In: Proctor DF, Andersen IHP, eds. *The nose: upper airway physiology and the atmospheric environment*. New York: Elsevier, **1982**:245–278
15. Chakeres DW. Computed tomography of the ethmoid sinuses. *Otolaryngol Clin North Am* **1985**;18(1):29–42
16. Rice DH. Basic surgical techniques and variations of endoscopic sinus surgery. *Otolaryngol Clin North Am* **1989**;22(4):713–726

The reader's attention is directed to the commentary on this article, which appears on the following pages.

Commentary

Endoscopic Sinus Surgery: Role of the Radiologist

Mahmood F. Mafee¹

Endoscopic sinus surgery has become an increasingly popular procedure since Messerklinger [1] and Wigand et al. [2] described the advantages of the intranasal endoscope and its surgical application. The concept of "functional endoscopic sinus surgery" [3] evolved from the work of Hilding [4, 5], Proctor [6, 7], and Messerklinger [8–10] on mucociliary clearance and air flow in the paranasal sinuses and on the importance of establishing drainage and preserving the mucosa of the sinuses. Functional endoscopic sinus surgery is based on the hypothesis that the ostiomeatal complex (maxillary sinus ostium, anterior and middle ethmoid ostia, frontal recess, infundibulum, and middle meatal complex) is the key area in the pathogenesis of chronic sinus diseases [3, 8–17]. Minor pathologic changes in the nasal mucosa in the vicinity of the ostiomeatal complex may interfere with mucociliary clearance or with the ventilation of the maxillary, ethmoidal, and frontal sinuses. The underlying principle of functional endoscopic sinus surgery is that the *sinus mucosa will return to normal if adequate drainage can be established* [13]. No attempt is made to remove the sinus mucosa; rather, it is allowed to return to normal and to resume its normal function.

In their article, Babbel et al. [18] attempt to establish an optimal imaging protocol for preendoscopic screening CT of the sinuses, including preparation of the patient, CT technique, and data display (filming). I agree with the authors that pretreatment of patients with appropriate medical therapy and adequate preparation of patients enable the best CT assessment of mucosal disease of the nasal and paranasal sinuses. Coronal CT scanning with the patient in a prone position and the head hyperextended currently affords the best preoperative evaluation for endoscopic anterior ethmoidectomy, frontal

sinusotomy [14, 17], and for posterior endoscopic total sphenoidectomy [12]. The anterior and posterior walls of the frontal sinuses and the anatomic relationship between the posterior ethmoidal and sphenoidal sinuses are best evaluated in the axial plane [16]. In terms of filming, Babbel et al. recommend an intermediate (2500 H/250 H) window width/level technique. I prefer CT images filmed with extended window width-bone technique (4000 H/700–800 H). I also require that the technicians provide a set obtained by using a soft-tissue technique. The soft-tissue technique allows better evaluation of inspissated mucosal debris, microcalcifications, and incidental findings in the orbit and eyeball, as well as in the parts of the face and cranium included in the study.

I would like to discuss three issues related to the article by Babbel et al.: the concepts of functional endoscopic sinus surgery, the important role of the radiologist in preoperative assessment for endoscopic sinus surgery, and the increasing rate of significant and serious complications associated with endoscopic sinus surgery.

The paranasal sinuses, like other parts of the upper respiratory system, are lined with a pseudostratified columnar ciliated epithelium under which is a tunica propria, which contains mucous and serous glands [13, 14]. The secretions of these glands form surface films of mucus and fluid (mucus blanket) that cover the epithelium. Cilia of the upper respiratory mucosa beat with a wavelike, synchronous rhythm that continuously propels a surface coat of mucus, containing entrapped particles, toward the pharynx [20]. In the paranasal sinuses and nasal cavity, the ciliated epithelium and the mucus blanket form the so-called mucociliary system that protects the sinuses and nasal cavity [13, 14]. It is important to realize

This article is a commentary on the preceding article by Babbel et al.

¹ Department of Radiology and MR Center, The University of Illinois at Chicago, Box 6998, Chicago, IL 60680. Address reprint requests to M. F. Mafee.

that the mucus blanket is moved by the cilia toward the natural ostium of the individual sinus. This occurs regardless of any other openings that may or may not be present in the sinus [14]. In the maxillary sinus, mucociliary movement originates from the floor and radiates along the walls of the sinus to propel the mucus blanket toward the ostium [16], which is located in the posterosuperior portion of the medial wall of the sinus. This mucociliary system captures 80% of inspired particles larger than 3–5 μm and 60% of those larger than 2 μm and exposes them to mast cells, polymorphonuclear leukocytes, eosinophils, lysozyme, immunoglobulin G, and interferon while sweeping them into the pharynx to be swallowed [13]. Each sinus has its own specific pattern of movement of its mucociliary blanket going toward, and ending at, the natural ostium. Placement of an ostium in another location is ineffective, as the cilia continue to move the mucus blanket toward the natural ostium [14, 16]. Chronic or chronically recurrent sinusitis therefore implies a breakdown in the function of the mucociliary system [14, 16]. Most frequently, this breakdown involves the anterior ethmoidal sinuses because they are ideally located to suffer chronic obstruction. The majority of inspired particles are deposited on the anterior ends of the middle and inferior turbinates and in the anterior middle meatus where their effect will be greatest on the anterior ethmoidal air cells.

Knowledge of the pathophysiologic mechanisms that cause the chronic changes in the ostiomeatal region is still incomplete. The etiologic factors include a variety of exogenous factors such as aeroallergens, microorganisms (fungi, viruses, bacteria), toxic inhalants, and endogenous factors such as immunologic disorders [11]. Proctor [6] and later on Messerklinger [10] introduced the principle that chronic or recurrent bacterial sinusitis is most often caused by unappreciated, untreated anterior ethmoidal disease [6, 10]. Inasmuch as they must drain through this drainage site of the anterior ethmoid, the maxillary and frontal sinuses are often secondarily infected and may produce the dominant signs and symptoms. A necessary conclusion is that relief of the obstruction caused by the anterior ethmoidal air cells will permit resolution of disease in the maxillary and frontal sinuses.

The anatomy of the ethmoid bone, nasal cavity, ostiomeatal complex, natural ostium of the maxillary sinus, and exact drainage system of the frontal sinus is of considerable importance in this operative technique. A successful outcome of endoscopic sinus surgery is based on a clearly defined diagnostic evaluation of the disease in the ostiomeatal complex in patients with chronic sinusitis [3, 14, 16, 17]. This evaluation includes a good medical history; careful physical examination, including intranasal endoscopy; and, after medical therapy, a CT scan to examine the ostiomeatal complex [3, 16, 17]. Familiarity with the anatomy of the paranasal sinuses, particularly the ethmoidal sinuses, is critical for interpreting imaging studies of the paranasal sinuses. In the endoscopic approach, the most important landmarks are the agger nasi cells, frontal recess, middle turbinate, middle meatus, uncinate process, ethmoid infundibulum, hiatus semilunaris, bulla ethmoidalis, natural ostium of the maxillary sinus, basal lamella, and sphenoidal recess (Figs. 1–3).

The ostiomeatal complex or unit has been referred to as

the maxillary sinus ostium and infundibulum [16] and also as the normally aerated channels, providing airflow and mucociliary clearance for the maxillary, ethmoidal, frontal, and sphenoidal sinuses [21]. However, this term is often used to refer to the maxillary sinus ostium, anterior and middle ethmoidal air cells' ostia, frontonasal duct (frontal recess), infundibulum, and middle meatal complex. Also, in many otolaryngologic communications, the anterior and middle ethmoidal air cells are collectively referred to as anterior ethmoidal air cells. Recognition of the importance of the ostiomeatal complex has given the radiologist an important role in the examination of patients who are scheduled for functional endoscopic sinus surgery. Radiologists should be familiar with the principles of this operation, and make a careful evaluation of the paranasal sinuses, in particular, the ethmoid bone and the middle meatus region of the nasal cavity. The ethmoid bone is a delicate and complex structure. It articulates with 13 other bones: the frontal, sphenoid, nasals, maxillae, lacrimals, palatines, inferior nasal conchae, and vomer [22, 23]. The ethmoid bone consists of four parts: a horizontal lamina, called the cribriform plate; a perpendicular plate; and two lateral masses, called the labyrinths. Each ethmoidal labyrinth consists of thin-walled highly variable air cells, arranged in three groups: anterior, middle, and posterior clusters. These ethmoidal air cells are closed everywhere, except at their apertures or ostia of communication with the nasal cavity. (It is important to realize that the ostia of these ethmoidal air cells cannot be detected on CT images.) Some air cells are not entirely enclosed by the ethmoid bone (extramural cells); instead the ethmoid bone may be perforated so that the air-cell mucosa extends upward against the ethmoidal notch of the frontal bone, anteriorly against the lacrimal and maxillary bones and posteriorly against the sphenoid and palatine bones. The orbital plate of the ethmoid bone (lamina papyracea) covers the middle and posterior ethmoidal air cells. The anteriormost intramural ethmoidal air cells are the frontal recess cells, which extend toward the frontal bone anterosuperiorly. The frontal sinus arises from these cells, as do the supraorbital ethmoidal air cells [13]. The next most anterior group is the infundibular cells. From these arise the most anterior extramural cells, the agger nasi cells, which pneumatize the lacrimal bone and frontal process of the maxilla [13, 24]. The agger nasi cells are located on the lateral nasal wall immediately anterior to the anterior end of the middle turbinate [14]. These cells drain into the ethmoid infundibulum.

The medial surface of the labyrinth forms a part of the lateral wall of the corresponding half of the nasal cavity. Within the nasal cavity, scrolls of bone on the lateral walls, the conchae, project medially to divide the passageway into meatuses, or channels for air [22, 23]. The superior and middle conchae are parts of the ethmoid bone, but the inferior nasal conchae (a turbinate is a concha, meaning a soft-tissue complex) are a separate pair of bones. The superior, middle, and inferior meatuses (air channels), which are formed under the respective conchae, have increased contact with the nasal surfaces to permit more effective warming and moistening of inspired air [23].

The sphenoidal sinus ostium is located at the anterosuperior portion of the sphenoidal sinus. The sphenoidal ostium

Fig. 1.—A, Anatomy of lateral nasal wall. Middle turbinate in this dry skull has been removed, allowing visualization of left nasal wall. Note anteroinferior (*large arrows*) and posterosuperior (*open arrows*) borders of uncinate process. B = bulla ethmoidalis. Passage (*dashed line*) between posterosuperior border of uncinate process and anteroinferior border of bulla is semilunar hiatus (hiatus semilunaris). Hiatus courses around outer anteroinferoposterior border of bulla to reach middle meatus.

B, Direct parasagittal CT scan showing inferior turbinate (1), middle turbinate (2), bulla ethmoidalis (B), sinus lateralis (sl), and posterior ethmoidal air cells (p). Basal lamella is bony partition between bulla ethmoidalis and posterior ethmoidal air cells. Basal lamella is also between sinus lateralis and bulla ethmoidalis. A partial volume of the uncinate process (*white arrowheads*) is seen in this section. Note its anterior attachment (*long white arrow*) to ethmoidal process of inferior concha. Just superior and anterior to the uncinate process are the agger nasi cells. The infundibulum is a curved passage below bulla and above uncinate process (*short white arrow*). Area between posterosuperior border of uncinate process and anteroinferior border of bulla ethmoidalis is semilunar hiatus (*dashed line*), which courses around inferoposterior border of bulla to connect infundibulum with middle meatus. Note opacification of sphenoid sinus by a surgically proved mucous retention cyst. This image clearly explains why nasolacrimal duct (*black arrowhead*) or sac are injured during endoscopic anterior ethmoidectomy.

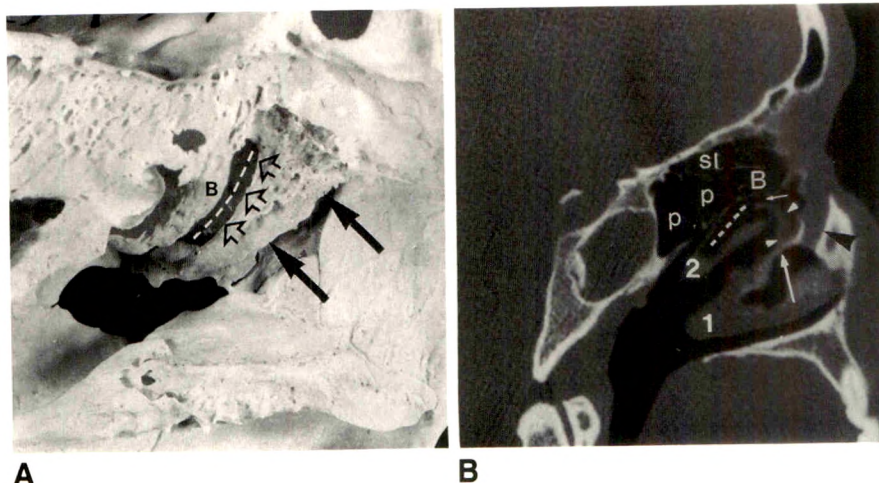
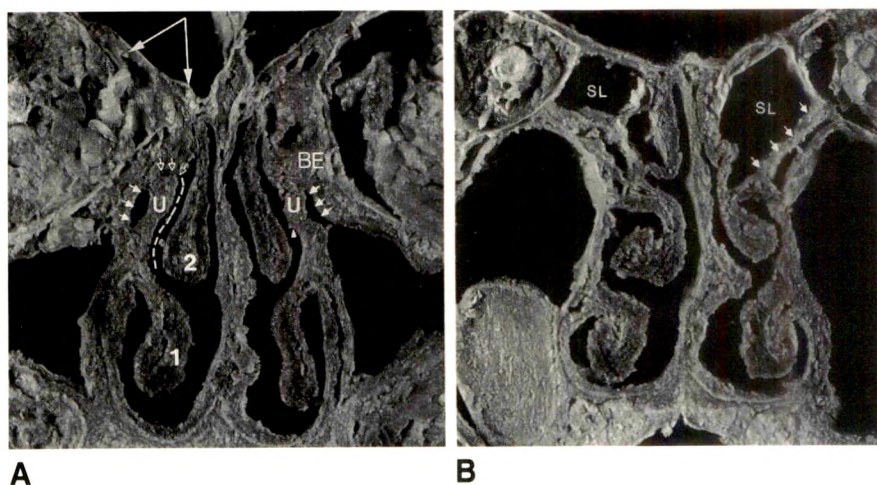


Fig. 2.—A, Coronal section through ostiomeatal complex of cadaveric head shows inferior turbinate (1), middle turbinate (2), uncinate process (U), and bulla ethmoidalis (BE). Note attachment of uncinate process (*arrowhead*) to the ethmoidal process of inferior concha. Infundibulum (*three solid arrows*) is passage between uncinate process and inferior border of bulla. Three open arrows indicate communication of middle meatus (*dashed line*) with infundibulum through semilunar hiatus. As seen, hiatus (*three open arrows*) is a passage between inferior aspect of bulla and superior aspect of uncinate process. Long arrows at top of photograph indicate fovea ethmoidalis (roof of the lateral masses of ethmoid bone). Note attachment of middle turbinate to junction of fovea ethmoidalis and cribriform plate.

B, Coronal section posterior to A and taken just posterior to bulla ethmoidalis. Note lateral attachment of middle turbinate, so-called basal or ground lamella (*arrows*). Basal lamella separates posterior ethmoidal air cells from bullar air cells. Sinus lateralis (SL) is posterior and superior to basal lamella. Note retention cyst along floor of right maxillary sinus.



and the posterior ethmoidal air cells drain into the superior meatus (sphenoethmoidal recess). The middle meatus connects via various ostia with the anterior and middle ethmoidal air cells and the frontal and maxillary sinuses. The frontal sinuses communicate with the middle meatus of the corresponding half of the nasal cavity by means of a passage called the frontonasal canal. This communication between frontal sinus and nasal cavity is not strictly a duct [16], but an internal channel positioned between the sinus and the anterior middle meatus referred to as the frontal recess.

Just anterior to the superior attachment of the middle

turbinate and anterior to the frontal recess is the agger (ridge) nasi [24]. This prominence on the lateral nasal wall represents the most anterior of the anterior ethmoidal cells. These cells (agger nasi cells) can invade the lacrimal bone or the ascending process of the maxilla. Because of their closeness to the frontal recess, they are excellent surgical landmarks. Opening these agger cells provides a good view of the nasofrontal duct.

Just posterior and inferior to the agger nasi cells lies the ethmoidal uncinate process (Fig. 1B), the starting point in an anterior-to-posterior endoscopic procedure [13]. The uncinate

process is a thin, curved bar of bone from the lateral side of the ethmoidal labyrinth that forms a portion of the lateral nasal wall (Figs. 1–3). It projects downward and backward and is subject to considerable variation in size. It ranges in height from 1 to 4 mm and is 14 to 22 mm long [14]. Anteriorly, it articulates with the lacrimal bone and ethmoidal process of the inferior nasal concha (Figs. 1B and 2). The superior edge of this process is free and forms the medial boundary of the hiatus semilunaris (Figs. 1 and 2) in the middle meatus of the nose [22]. As it progresses posteroinferiorly, it forms the inferior border of the semilunar hiatus (Fig. 1) and the medial wall of the infundibulum (Fig. 2).

The semilunar hiatus is a curvilinear opening of the lateral nasal wall that lies above the uncinate process and below the bulla ethmoidalis (Figs. 1 and 2A). This opening separates the uncinate process from the ethmoidal bulla and serves as a connection between the infundibulum and the middle meatus (Fig. 2A). The middle ethmoidal air cells produce a rounded swelling, called the bulla ethmoidalis, on the lateral wall of the middle meatus (Fig. 2A), whose lateral border forms a portion of the medial orbital wall. These cells open into the ethmoid

infundibulum or onto the medial wall of the bulla into the middle meatus.

The ethmoidal infundibulum is a trough-shaped cavity (deep curved passage) that is below the bulla and above and lateral to the uncinate process (Figs. 1–3). It potentially receives drainage from the anterior and middle ethmoidal air cells and the frontal and maxillary sinuses. In more than 50% of crania, the infundibulum is continued superiorly as the frontonasal duct into the frontal sinus [22]. Kasper [25] found that in 62% of cases the ethmoidal infundibulum and nasofrontal connections were discontinuous channels anatomically.

The exact drainage system of the frontal sinus depends on its embryologic development. The drainage usually occurs by way of rudimentary ethmoidal cells into the frontal recess [25] or directly into the frontal recess [13].

Medial to the bulla ethmoidalis and the uncinate process is the middle turbinate. Anteriorly, it attaches to the medial wall of the agger nasi and the superoanterior edge of the uncinate process [21]. Superiorly, it attaches to the cribriform plate. The attachment of the middle turbinate changes direction at its most posterior extent. Instead of running in an anteropos-

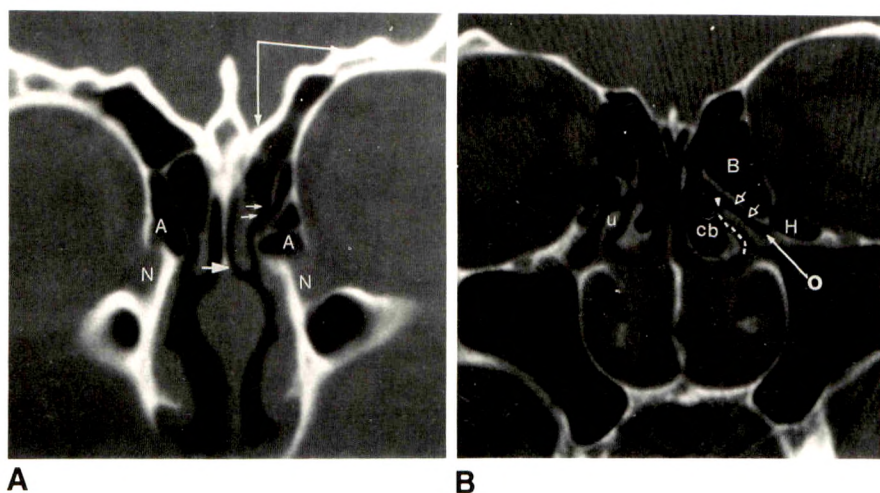


Fig. 3.—A, Coronal CT scan shows agger nasi cells (A), frontal recess (two small arrows), supraorbital anterior ethmoidal air cells, nasolacrimal canal (N), perpendicular plate of ethmoid bone (single short arrow), and fovea ethmoidalis (long arrows).

B, Coronal CT scan posterior to mid-portion of bulla ethmoidalis (B) shows uncinate process (u), bilateral concha bullosa (cb), orifice of maxillary sinus (O), and infraorbital ethmoidal air cells, the so-called Haller cells (H). Ethmoid infundibulum is the passage (two open arrows) between uncinate process and bulla. Arrowhead = hiatus semilunaris, which is the communication passage between middle meatus (dashed line) and infundibulum.

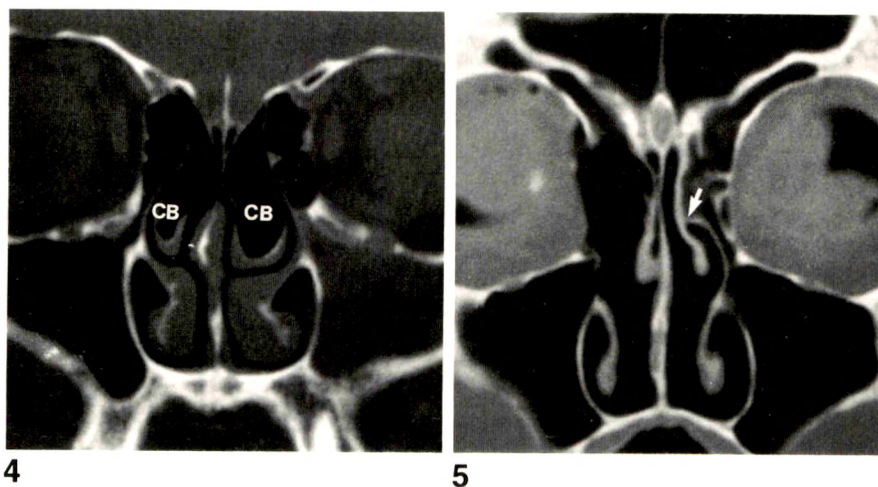


Fig. 4.—CT scan shows bilateral concha bullosa (CB). Note narrowing of left middle meatus and infundibulum and associated thickening of left maxillary mucosal lining.

Fig. 5.—CT scan of cadaveric head shows medial attachment (arrow) of left uncinate process to middle turbinate. Right uncinate process and anterior ethmoidal air cells have been removed, and natural ostium of right maxillary sinus has been widened.

terior direction, it curves laterally, and the final lateral attachment of the middle turbinate is oriented in the frontal plane and is called the basal or ground lamella (Fig. 2B) [16, 21, 24].

The posterior ethmoidal air cells are between the basal lamella and the sphenoidal sinus. The basal lamella is an excellent landmark for separating the anterior and middle ethmoidal air cells from the posterior ethmoidal air cells [24]. An airspace is usually found between the ground lamella and the bulla ethmoidalis, which may extend superiorly to the bulla. This is called the sinus lateralis (Figs. 1B and 2B). This sinus lateralis, unlike the other posterior ethmoidal air cells that open into the superior meatus, may communicate with the frontal recess [21] or may open directly and independently into the middle meatus.

The natural ostium of the maxillary sinus is important in endoscopic sinus surgery. This ostium is located in the superior portion of the medial wall and drains into the posterior aspect of the ethmoid infundibulum as the sinus funnels into it, usually posterior to the midpoint of the bulla ethmoidalis (Fig. 3B) [13]. The posterior extent of the uncinate process points to the position of the ostium and is an excellent imaging and endoscopic landmark for its localization. Accessory ostia are present in 15–40% of cases, usually in the membranous medial sinus wall, the so-called fontanelles. The fontanelles are two areas along the medial aspect of the maxillary sinus where a double layer of mucosa with no intervening bone forms the nasoantral wall inferior to the uncinate process.

Certainly, individual structural differences in ethmoidal and ostiomeatal complexes and other paranasal sinuses are to be expected, and the reader ought not to be discouraged should certain illustrations in the literature fail to be identical with the images he or she will review for any individual patient. Certain anatomic variations are observed more commonly and should be included in the imaging report. These are as follows. (1) *Concha bullosa*, a pneumatized middle turbinate. The otolaryngologist is interested to know whether the concha bullosa has compromised the middle meatus or even the ethmoid infundibulum (Fig. 4). (2) *Low position of fovea ethmoidalis* (the roof of the ethmoid labyrinth). A low position of the cribriform plate and fovea ethmoidalis is a potentially dangerous anatomic variation, which can be penetrated easily unless the surgeon is aware of the finding. (3) *Bulging of the optic canal into the posterior ethmoidal complex*. In rare instances, the internal carotid artery may be exposed in the posterior ethmoidal sinus [26]. An important observation is extensive lateral pneumatization of the posterior ethmoidal air cells, which can increase the vulnerability of the optic nerve. In addition, identification of an asymmetric intersphenoid septum is important because the posterior extension of this partition usually marks the location of the internal carotid artery. (4) *Deviation of the uncinate process*. The superior edge of the uncinate process may deviate medially to obstruct the middle meatus (Fig. 5) or, more importantly, may deviate laterally to obstruct the infundibulum. Marked lateral deviation or even fusion of the uncinate process to the medial orbital wall may endanger the orbit and hence the optic nerve while the uncinectomy is performed during anterior endoscopic sinus surgery. (5) *Haller cells*. These are ethmoidal air cells extending along the medial floor of the orbit (infraorbital air cells)

(Fig. 3B), which may cause narrowing of the infundibulum. Other anatomic variations include deviation of the nasal septum, paradoxical middle turbinate, uncinate process bulla, and posttraumatic or congenital deformity of the medial wall or floor of the orbit.

In summary, CT scanning and endoscopy are complementary in the diagnosis and treatment of disorders of the nasal cavity and paranasal sinuses. Endoscopic nasal sinus surgery, like traditional sinus surgery, is associated with serious risks. Complications such as blindness, ocular motility dysfunction, orbital hematoma, CSF leak, anterior cranial fossa brain and/or vascular damage, brain abscess, pneumocephalus, carotid-cavernous sinus fistula, and death have been reported [27–31]. Buus et al. [30] reported bilateral blindness in a 39-year-old woman following endoscopic ethmoidectomies. Pathologic specimens from both sides revealed optic nerve tissues. As an entire generation of otolaryngologists learns these new techniques, complications will continue to evolve. Prevention begins with proper endoscopic and CT preoperative evaluation and surgical preparation [28]. The study of Babbal et al. [18] supplements the radiologic data reported by Zinreich et al. [16], Chow and Mafee [17], and others by pointing out some useful technical clues that are helpful in the presurgical diagnosis of sinonasal inflammatory disease and by providing essential information for functional endoscopic sinus surgery [3].

REFERENCES

1. Messerklinger W. *Endoscopy of the nose*. Baltimore: Urban and Schwarzenberg, 1978
2. Wigand ME, Steiner W, Jaumann MP. Endonasal sinus surgery with endoscopic control: from radical operation to rehabilitation of the mucosa. *Endoscopy* 1978;10:255–260
3. Kennedy DW, Zenrich J, Rosenbaum AE, Johns ME. Functional endoscopic sinus surgery: theory and diagnostic evaluation. *Arch Otolaryngol* 1985;111:576–582
4. Hilding AC. The physiology of drainage of nasal mucus. IV. Drainage of the accessory sinuses in man. *Otolaryngol Rhinol Laryngol* 1944;53:34–41
5. Hilding AC. Physiologic basis of nasal operations. *Calif Med* 1950;72:103–107
6. Proctor DF. The nose, paranasal sinuses and pharynx. In: Waters W, ed. *Lewis-Walters practice of surgery*, vol. 4. Hagerstown, MD: Prior, 1966:1–37
7. Proctor DF. The mucociliary system. In: Proctor DF, Anderson IHP, eds. *The nose: upper airway physiology and the atmospheric environment*. New York: Elsevier, 1982
8. Messerklinger W. On the drainage of the normal frontal sinus of man. *Acta Otolaryngol* 1967;673:176–181
9. Messerklinger W. Über die Drainage der Menschlichen Nasennebenhöhlen unter normalen und pathologischen Bedingungen. II. Mitterlung: Die Stirnhöhle und ihr Ausführungssystem. *Monatsschr oxrenheild* 1967;101:313
10. Messerklinger W. *Endoscopy of the nose*. Baltimore: Urban and Schwarzenberg, 1978
11. Winther B, Gross CW. Introduction and indications for functional endonasal (endoscopic) sinus surgery. *Operative Techniques in Otolaryngol Head Neck Surg* 1990;1:92–93
12. Schaefer SD. Endoscopic sinus surgery: posterior approach. *Operative Techniques in Otolaryngol Head Neck Surg* 1990;1:104–107
13. Rice DH. Basic surgical techniques and variations of endoscopic sinus surgery. *Otolaryngol Clin North Am* 1989;22:713–726
14. Rice DH. Endoscopic sinus surgery: anterior approach. *Operative Techniques in Otolaryngol Head Neck Surg* 1990;1:99–103
15. Stammberger H. Endoscopic endonasal surgery: concepts in treatment of recurring rhinosinusitis. I. Anatomic and pathologic considerations. *Otolaryngol*

- ngol Head Neck Surg* **1986**;94:143-146
16. Zinreich SJ, Kennedy DW, Rosenbaum AE, Gayler BW, Kumar AJ, Stammberger H. Paranasal sinuses: CT imaging requirements for endoscopic surgery. *Radiology* **1987**;163:709-775
 17. Chow JM, Mafee MF. Radiologic assessment preoperative to endoscopic sinus surgery. *Otolaryngol Clin North Am* **1989**;22:691-701
 18. Babbel R, Harnsberger HR, Nelson B, Sonkens J, Hunt S. Optimization of techniques in screening CT of the sinuses. *AJNR* **1991**;12:849-854, *AJR* **1991**;151:1093-1098
 19. Schaefer SD. Endoscopic frontal sinusotomy. *Operative Techniques in Otolaryngol Head Neck Surg* **1990**;1:128-130
 20. Wheeler RR, Burkitt HG, Daniels VG. *Functional histology*. New York: Churchill Livingstone, **1979**:49-63
 21. Zinreich SJ, Abidin M, Kennedy DW. Cross-sectional imaging of the nasal cavity and paranasal sinuses. *Operative Techniques in Otolaryngol Head Neck Surg* **1990**;1:94-98
 22. Warwick R, Williams PL, eds. *Gray's anatomy*. Philadelphia: Saunders, **1973**:300-302
 23. Zemlin WR, Stople SC. *The structure of the human skull*. Champaign, IL: Stipes, **1967**:30-33
 24. Becker SP. Anatomy for endoscopic sinus surgery. *Otolaryngol Clin North Am* **1989**;22:677-682
 25. Kasper KA. Nasofrontal connections: a study based on one hundred consecutive dissections. *Arch Otolaryngol* **1936**;23:322-343
 26. Kennedy DW, Zinreich SJ, Hassab MH. The internal carotid artery as it relates to endonasal sphenoethmoidectomy. *Am J Rhinol* **1990**;4:7-12
 27. Stankiewicz JA. Blindness and intranasal endoscopic ethmoidectomy. *Laryngoscope* **1987**;97:1270-1273
 28. Stankiewicz JA. Complications of endoscopic sinus surgery. *Otolaryngol Clin North Am* **1989**;22:749-758
 29. Maniglia AJ. Fatal and major complications secondary to nasal and sinus surgery. *Laryngoscope* **1989**;99:276
 30. Buus DR, Tse DT, Farris BK. Ophthalmic complications of sinus surgery. *Ophthalmology* **1990**;97:612-619
 31. Neuhaus RW. Orbital complications secondary to endoscopic sinus surgery. *Ophthalmology* **1990**;97:1512-1518

Call for Papers on Neuroradiology

On January 1, 1992, The American Roentgen Ray Society and the American Society of Neuroradiology will terminate their agreement whereby manuscripts on neuroradiology submitted to the *AJR* are forwarded to the *AJNR* and selected *AJNR* papers are republished in the *AJR*.

To avoid any lag in the publication of neuroradiologic articles in the *AJR*, the Journal requests authors to submit neuroradiologic manuscripts effective immediately. We plan to expedite publication of these papers. Authors will receive an initial editorial decision in 3-4 weeks, and accepted papers will be published 3 months after revised manuscripts are accepted. This is more than twice as fast as most other journals.

The advantages of this rapid publication time and the *AJR*'s large circulation (24,000) are now available to all authors of neuroradiologic papers. An expanded section on neuroradiology, including review articles, pictorial essays, and commentaries, will accommodate more than the limited number of papers published under the previous agreement.

We invite authors of neuroradiologic articles to submit their papers for original publication in the *AJR* so that the Journal may continue to fulfill its commitment to supply timely and important original information about neuroradiology to general radiologists as well as to those who subspecialize in the field.

Robert N. Berk
Editor-in-Chief

Maternal Cocaine Abuse: The Spectrum of Radiologic Abnormalities in the Neonatal CNS

Linda A. Heier¹
 Carmela R. Carpanzano²
 Joelle Mast²
 Paula W. Brill³
 Patricia Winchester³
 Michael D. F. Deck¹

The purpose of this study was to determine the pattern and frequency of CNS abnormalities in the offspring of cocaine-abusing mothers. The study group consisted of a retrospective review of all neonates born or admitted to our neonatal intensive care unit over a 1-year period who met criteria for maternal cocaine abuse (43 patients). A control group (62 patients) was obtained from patients seen during the same interval and the cases were matched for gestational age and race. The radiologic studies were analyzed by two independent reviewers, and CNS abnormalities were assessed by means of sonography, CT, or MR. By matching the study and control groups for gestational age, we eliminated the higher frequency of prematurity. This allowed us to determine if maternal cocaine use was associated with any intracranial abnormalities other than those seen with prematurity. The frequency of intracranial hemorrhage, ventricular enlargement, and periventricular leukomalacia was not significantly different between the study and control groups. The frequency of cortical infarction was 17% in the study group and 2% in the control group. The frequency of major congenital malformations was 12% in the study group and 0% in the control group. All five of the congenital malformations seen were midline CNS abnormalities, particularly neural tube defects.

It is postulated that the higher statistically significant frequency of stroke and congenital malformations in the babies of maternal cocaine abusers is related to vasospasm caused by cocaine when used in the third and first trimesters, respectively.

AJNR 12:951-956, September/October 1991; *AJR* 157:1105-1110, November 1991

In the last year, an unusual constellation of midline CNS malformations were noted in neonates born or admitted to our institution. Maternal cocaine abuse was found to be a common denominator among these cases. The unusual irritability of babies born to cocaine-abusing mothers also prompted further radiologic investigation of the infants' CNS. The purpose of our study was to determine the pattern and frequency of CNS abnormalities in the offspring of maternal cocaine abusers.

Materials and Methods

The study group consisted of a retrospective review of all neonates born or admitted to our neonatal intensive care unit from January 1, 1988, to January 31, 1989, who met one of the following criteria for maternal cocaine abuse: (1) the mother confessed to cocaine use during the pregnancy, (2) the mother had a positive cocaine screen at delivery, or (3) the baby had a positive cocaine screen at birth. A control group was obtained from the same admission interval and the cases were matched for gestational age and race. An attempt was also made to match the urban geographic area from which the cases originated. There were 43 babies in the study group and 62 babies in the control group.

The entry criteria are summarized in Table 1. All the mothers in our study group used crack (i.e., cocaine free-based). All the mothers confessed to first trimester use and the majority continued drug use throughout the pregnancy. The maternal population consisted mainly of indigent crack addicts with a history of regular use (e.g., three patients were found

Received September 24, 1990; revision requested December 7, 1990; revision received March 28, 1991; accepted April 1, 1991.

¹ Department of Neuroradiology, New York Hospital-Cornell University Medical Center, 525 E. 68th St., New York, NY 10021. Address reprint requests to L. A. Heier.

² Department of Pediatric Neurology, New York Hospital-Cornell University Medical Center, New York, NY 10021.

³ Department of Pediatric Radiology, New York Hospital-Cornell University Medical Center, New York, NY 10021.

0361-803X/91/1575-1105

© American Roentgen Ray Society

using crack in the delivery room). Actual dosages were not available. Mothers who admitted to or were found to have physical evidence of IV drug abuse were excluded from the study. The frequency of recreational marijuana and alcohol use as well as cigarette smoking was not significantly different between the study and control groups. The cocaine screen was a urine assay performed according to the enzyme-mediated immunoassay technique (Syva EMIT d.a.u. kits) for benzoylecgonine, the major metabolite of cocaine. Any sample that was initially tested positive was confirmed with gas chromatography-mass spectrometry (GC-MS). Unfortunately, all the urine samples were tested for phenobarbital first, and the specimen volume was often insufficient for confirmation by GC-MS. Thus, even if the initial screen was positive on the first 3 ml of urine, if there was not a further 5 ml to confirm with GC-MS the assay would be called negative. Cocaine metabolites persist for only approximately 3 days, so occasionally it was a problem to obtain enough urine from a premature infant within such a short time.

Table 2 illustrates the demographic data and the match obtained between the study and control groups. The gestational age was matched between the study group and control group to within 1 week of both the mean and median gestational age. Since the study and control groups consisted of neonatal intensive care unit admissions, most (see Table 3) had sonography on a routine basis. Irritability, seizures, and structural abnormalities were other indications for study. Suspected cortical/subcortical infarctions on sonography were confirmed with CT. All congenital malformations were confirmed with CT and/or MR.

The radiologic CNS examinations of the study and control groups were collected and analyzed by two blinded independent reviewers. The following specific abnormalities were assessed whether they were found on sonograms, CT scans, or MR images: subependymal and intraventricular hemorrhage (SEH, IVH); intraparenchymal hemorrhage (IPH); ventricular dilatation; periventricular leukomalacia (PVL); porencephaly; infarcts; and congenital anomalies.

The cerebral sonograms were obtained on a real-time scanner with a 5-MHz transducer (Acuson, Mountain View, CA). CT studies were done on a third-generation scanner with 7-mm-thick axial images through the entire brain. MR imaging was performed on a 0.6-T Technicare unit using standard spin-echo pulse sequences, including short TR/short TE sequences in both the axial and sagittal planes and long TR/double-echo TE sequences in the axial plane or, alternatively, in the sagittal plane when a spine examination was being performed. A 7.5-mm slice thickness, a 2.5-mm interslice gap, a 256 × 128 matrix size, a 25-cm field of view, and two excitations were used. The effective pixel size was 1.9 × 1.0 mm.

A Fischer exact test was performed on the data obtained from the study and control groups for each type of abnormality to determine if cocaine abuse was associated with a higher frequency of these abnormalities. All results were reported as statistically significant if $p < .05$.

Results

The radiologic data are summarized in Table 3. Cerebral sonography was performed in 93% of the study group and 87% of the control group. By matching the study and control groups for gestational age, we eliminated the higher rate of occurrence of prematurity. This allowed us to determine if maternal cocaine use is associated with intracranial abnormalities other than those seen with prematurity (e.g., germinal matrix hemorrhage).

The frequency of the various forms of intracranial hemorrhage, PVL, porencephaly, and ventricular enlargement was

TABLE 1: Entry Criteria

	Study Group	Control Group
Maternal history of cocaine use	(n = 42, 1 set twins)	(n = 61, 1 set twins)
Yes	90% (38)	0% (0)
No	10% (4)	100% (61)
Urine cocaine screen maternal	(n = 42)	(n = 61)
Positive	21% (9)	0% (0)
Negative	5% (2)	8% (5)
Insufficient quantity/not done	74% (31)	92% (56)
Urine cocaine screen neonate	(n = 43)	(n = 62)
Positive	58% (25)	0% (0)
Negative	35% (15)	24% (15)
Insufficient quantity/not done	7% (3)	76% (47)

TABLE 2: Demographic Data

	Study Group (n = 43)	Control Group (n = 62)
Race		
Black	84% (36)	76% (47)
Hispanic	5% (2)	6% (4)
White	11% (5)	15% (9)
Other	0% (0)	3% (2)
Sex		
Male	44% (19)	47% (29)
Female	56% (24)	53% (33)
Gestational age (weeks)		
Mean	31.4 (24-41)	30.4 (24-41)
Median	31	31

TABLE 3: Imaging Data

Type of Examination	Study Group (n = 43)	Control Group (n = 62)
Sonography	93% (40)	87% (54)
CT	57% (23)	10% (6)
MR	16% (7)	6% (4)

TABLE 4: Radiologic Abnormalities

Abnormality	Study Group (n = 43)	Control Group (n = 62)	p Value
Subependymal hemorrhage	35% (15)	34% (21)	NS
Intraventricular hemorrhage	22% (10)	21% (13)	NS
Intraparenchymal hemorrhage	12% (5)	3% (2)	NS
Ventricular dilatation	14% (6)	16% (10)	NS
Periventricular leukomalacia	14% (6)	6% (4)	NS
Porencephaly	19% (8)	8% (5)	NS
Infarction	17% (7)	2% (1)	$p < .05$
Congenital abnormalities	12% (5)	0% (0)	$p = .02$
			$p < .05$
			$(p = .01)$

Note.—NS = not significant.

not significantly different between the study and control groups although the frequency of IPH, PVL, and porencephaly was higher in the study group (Table 4). The frequency of infarctions and congenital abnormalities was clearly higher than in the control group and statistically significant (Table 4). Sonography identified seven cortical infarctions in the study group within 72 hr of birth compared with one in the control group. All seven infarcts were confirmed on CT (four bland, Fig. 1; three hemorrhagic, Fig. 2) and two also had MR. Neonatal and/or maternal cocaine screens were positive in six of the seven cases of infarction. Maternal use within 48

Fig. 1.—32-week gestational age male infant with a right temporoparietal infarct.

A, Axial unenhanced CT scan. Note lucency of right temporoparietal lobe (arrows), which involves the cortical mantle.

B, Real-time sonogram in coronal plane. Arrow marks hyperechoic area of ischemia in right temporoparietal lobe.

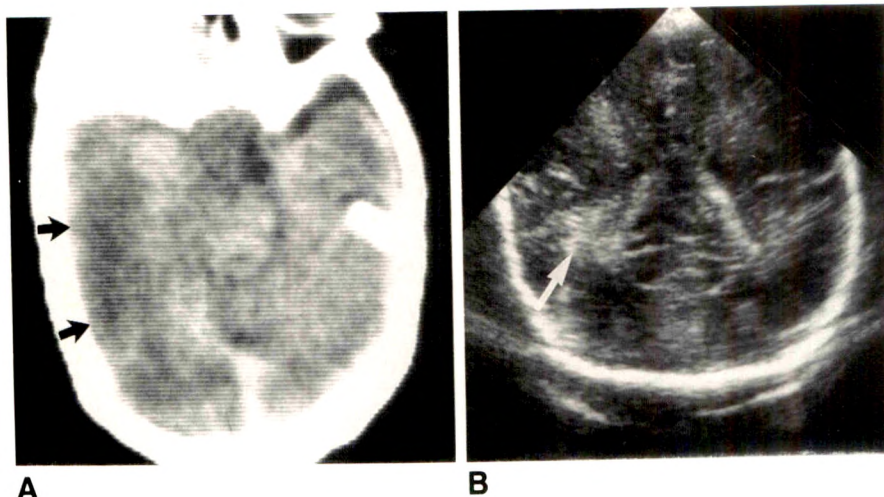
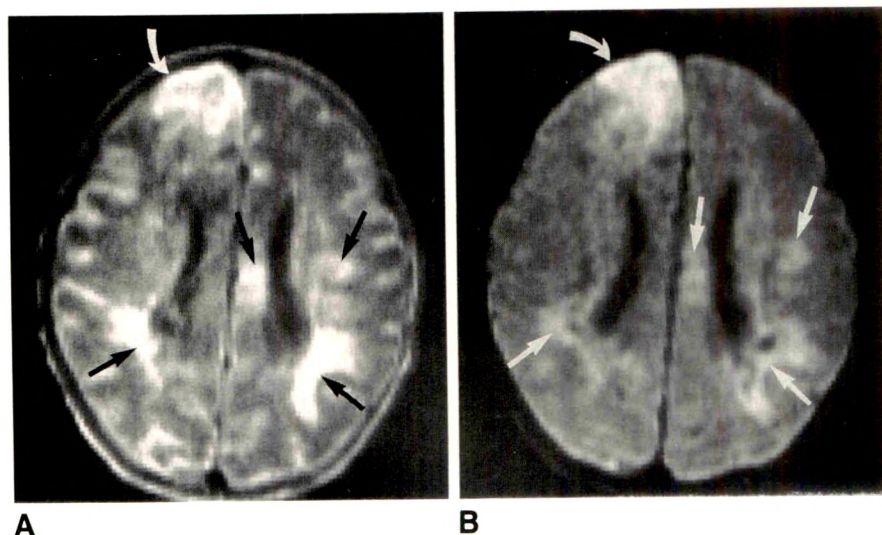


Fig. 2.—37-week gestational age female infant with a hemorrhagic right frontal infarct.

A and B, Axial spin-echo T1-weighted, 500/20 (A), and T2-weighted, 2000/60 (B), MR images. Curved arrows show hemorrhagic right frontal cortical infarct. Straight arrows indicate bilateral hemorrhagic periventricular leukomalacia (which was bland on the initial CT scan done 4 days before). The cortical mantle of gray matter is particularly bright on this sequence owing to the window settings.



hr of delivery was confirmed by history in all cases. No major congenital malformations (only one case of syndactyly) were found in the control group. Five major congenital malformations confined to the CNS were found in the study group. The most unique was a form of towering encephalocele (Fig. 3). A more conventional posterior encephalocele (Fig. 4) as well as a case of holoprosencephaly also occurred. Another unusual midline CNS malformation consisted of an intraspinal lipoma that communicated with a cutaneous ectopic penis at the level of the lower thoracic spine (Fig. 5). The last anomaly was a hypoplastic cerebellum. A nasofacial hemangioma (Fig. 6) developed after birth in one case.

Discussion

Many authors have reported on the apparent deleterious effects of maternal cocaine use on the fetus. The abnormalities have included increased rates of spontaneous abortion,

abruptio placenta, prematurity, intrauterine growth retardation, low birth weight, and decreased length and head circumference [1–9]. A higher frequency of congenital malformations was also reported by several authors [1, 3–5, 10].

Conflicting reports of the teratogenicity of cocaine has been found in experimental animal studies. Mahalik et al. [11] found nontoxic doses of cocaine to be teratogenic in mice who exhibited midline skull defects such as exencephaly, split supraoccipital bones, anophthalmia, and malformed lenses as well as non-CNS defects such as cryptorchidism. The work of Fantel and Macphail [12], also with mice, did not support the hypothesis that cocaine possesses teratogenic potential. Church et al. [13] found both cephalic hemorrhages and CNS anomalies (unilateral anophthalmia and microcephaly) in cocaine-exposed rat fetuses that did not occur in the nonexposed group.

Bingol et al. [10] noted that cocaine abuse in humans significantly reduced the weight of the fetus, increased the

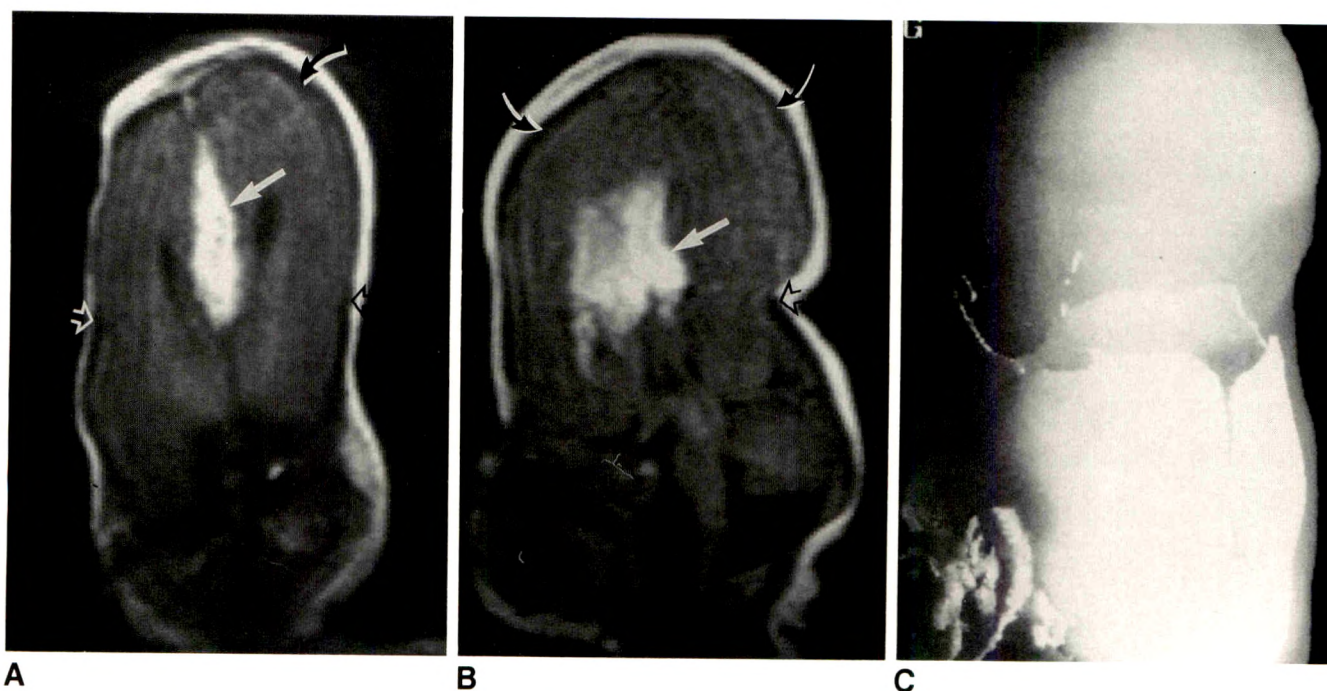


Fig. 3.—36-week gestational age female infant with a towering encephalocele, agenesis of the corpus callosum, and a midline lipoma. A and B, Coronal (A) and sagittal (B) T1-weighted (500/20) spin-echo MR images. Large white arrows indicate hyperintense lipoma, which occupies the space of the absent corpus callosum. Note elevation of contents of posterior fossa as most of the supratentorial brain has herniated out through the skull defect. Open arrows indicate the hypointense edge of the termination of the skull. The hypointense rim about the herniated brain (curved arrows) is caused by CSF.

C, 3-D CT reconstruction image shows large skull defect from a posterior aspect.

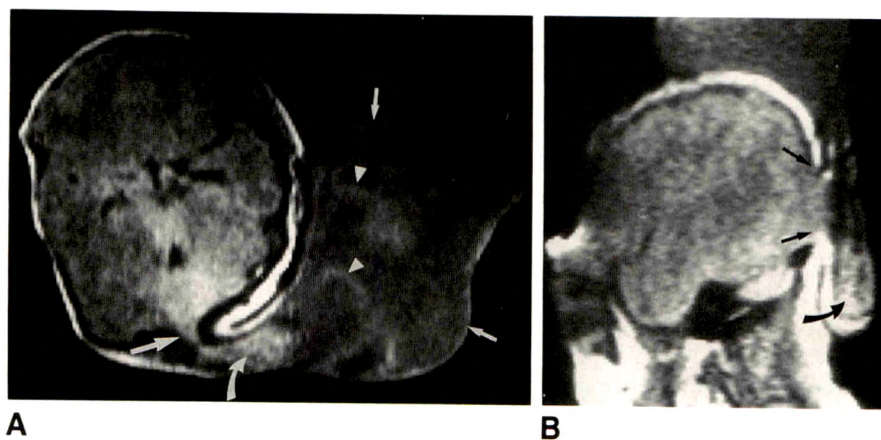


Fig. 4.—40-week gestational age female infant with a large posterior encephalocele.

A and B, Axial T1-weighted, 950/35 (A), and sagittal T1-weighted, 750/35 (B), spin-echo MR images. Large straight arrow indicates dehiscence in skull. Curved arrows indicate herniated cerebellum. The sac (small straight arrows) contains CSF and meninges (arrowheads).

still-birth rate related to abruptio placenta, and was associated with a higher frequency of congenital malformations (10% versus 2% for the control group). The malformations were all midline CNS abnormalities, specifically, one case of exencephaly, one parietal encephalocele, and one case of skull dysraphism with parietal bone defects. Our findings were similar, with five congenital malformations (12% versus 0% for the control group, $p = .01$) confined to the CNS, including an unusual towering encephalocele (Fig. 3), a posterior encephalocele (Fig. 4), holoprosencephaly, a hypoplastic cerebellum, and a spinal teratoma (Fig. 5). Other authors who

compared cocaine-exposed and nonexposed control groups found the rate of congenital malformations to be 5% versus 1.4% [1], 12.3% versus 0.8% [3], and 14% versus 0% [4, 5]. Many of these malformations involved the genitourinary tract.

Cerebrovascular events have been well documented in cocaine abusers [14–17] but have rarely been identified in the neonate after maternal use. A perinatal cerebral infarction was seen in a term infant after maternal cocaine use in the 72 hr before delivery [18], and an intracranial hemorrhage was identified by sonography in a term infant with a positive urine cocaine screen [19]. Seven cortical infarctions (four

Fig. 5.—39-week gestational age male infant born with an ectopic penis protruding from lower thoracic spine.

A and B, Axial T1-weighted, 750/35 (A), and sagittal T1-weighted, 500/35 (B), spin-echo MR images. Curved arrows indicate ectopic penis. Straight arrows indicate associated intraspinal lipoma. The extra- and intracanalicular components were removed in toto and the pathology was consistent with a teratoma.

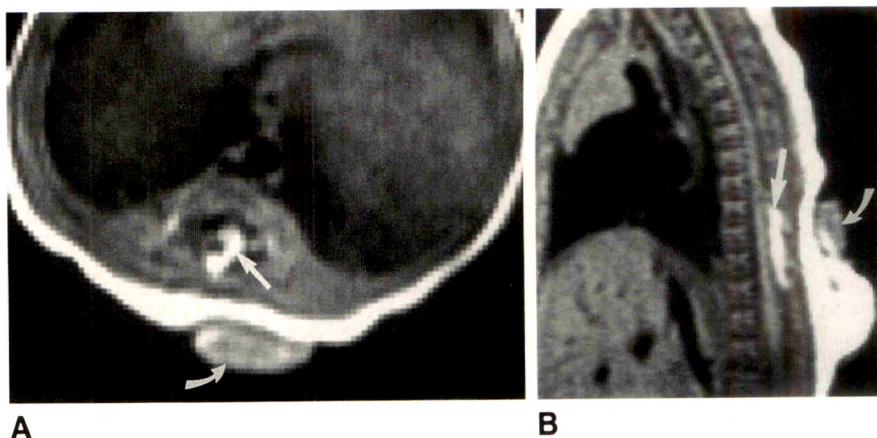
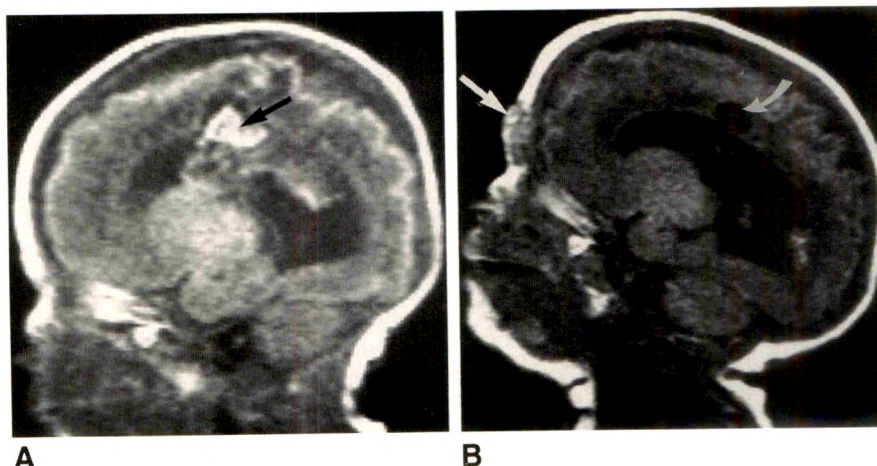


Fig. 6.—30-week gestational age female infant with subependymal, intraventricular, and intraparenchymal hemorrhages.

A, Sagittal T1-weighted (750/35) spin-echo MR image shows subependymal hemorrhage (arrow).

B, Sagittal T1-weighted (600/35) spin-echo MR image obtained 2 months later shows nasal hemangioma, which has developed in the interim (straight arrow). Curved arrow points to cystic area, which has resulted from prior hemorrhage.



bland, three hemorrhagic) were found in our study group (Figs. 1 and 2) compared with one in the control group ($p = .02$). Six of these cases had positive neonatal and/or maternal cocaine screens, and in each case the mother had a history of cocaine use in the 48 hr before delivery.

Cocaine raises catecholamine levels by inhibiting the reuptake of catecholaminergic neurotransmitters at the synaptic junction [11]. The excess catecholamines can cause vasospasm either in the placenta or the neonatal brain itself. Studies in pregnant ewes found that maternally administered cocaine produced dose-dependent increases in maternal blood pressure and decreases in uterine blood flow, reflecting uterine vasoconstriction. This resulted in fetal hypoxemia, hypertension, and tachycardia [20]. Cocaine has been shown to cause vasoconstriction of cerebral arteries in cats [21]. Hypoxia resulting from vascular constriction has been implicated in the pathogenesis of congenital malformations [22–25], usually causing an area of hemorrhage that involutes leaving behind a focal defect. This appears to be a likely cause of the anomalies seen with fetal cocaine exposure [26]. All the mothers in the study group were using cocaine at the

time of conception through the first trimester. The neural tube develops during the third and fourth weeks of gestation so the potential for its involvement existed. It is postulated that placental or cerebral artery vasoconstriction from cocaine use in the first trimester resulted in the congenital malformations while vasospasm of the cerebral vessels at or near the time of birth accounted for the higher occurrence of ischemic events.

Although this study is retrospective and urine cocaine screens were not universally obtained, the findings support the work of other authors. Cocaine has a teratogenic potential and a tendency to cause cerebral vascular events in the neonate. In view of the current crack epidemic, the investigation of neonatal stroke and neural tube defects should include a history of drug use and urine screening.

ACKNOWLEDGMENTS

We thank Ronald F. Gautieri, Temple University School of Pharmacy, for his support, and Martin Lesser for the statistical analysis.

REFERENCES

1. McGregor SN, Keith LG, Chasnoff IJ, et al. Cocaine use during pregnancy: adverse perinatal outcome. *Am J Obstet Gynecol* **1987**;157:686-690
2. Oro AS, Dixon SD. Perinatal cocaine and methamphetamine exposure: maternal and neonatal correlates. *J Pediatr* **1987**;111:571-578
3. Zuckerman B, Frank DA, Hingson R, et al. Effects of maternal marijuana and cocaine use on fetal growth. *N Engl J Med* **1989**;324:762-768
4. Chasnoff IJ, Burns WJ, Schnoll SJ, Burns KA. Cocaine use in pregnancy. *N Engl J Med* **1985**;313:666-669
5. Chasnoff IJ, Chisum GM, Kaplann WE. Maternal cocaine use and genitourinary tract malformations. *Teratology* **1988**;37:201-204
6. Ryan L, Ehrlich S, Finnegan L. Cocaine abuse in pregnancy: effects on the fetus and newborn. *Neurotoxicol Teratol* **1987**;9:295-299
7. Frank DA, Zuckerman BS, Maro H, et al. Cocaine use during pregnancy: prevalence and correlates. *Pediatrics* **1988**;82:888-895
8. Acker D, Sachs BP, Traciey KJ, Wyse WE. Abruptio placentae associated with cocaine use. *Am J Obstet Gynecol* **1983**;146:220-221
9. Madden JD, Payne TF, Miller S. Maternal cocaine abuse and effect on the newborn. *Pediatrics* **1986**;77:209-210
10. Bingol N, Fuchs M, Diaz V, Stone RK, Gromisch DS. Teratogenicity of cocaine in humans. *J Pediatr* **1987**;110:93-96
11. Mahalik MP, Gautieri RF, Mann DE. Teratogenic potential of cocaine hydrochloride in CF-1 mice. *J Pharm Sci* **1980**;69:703-706
12. Fantel AG, Macphail B. The teratogenicity of cocaine. *Teratology* **1982**;26:17-19
13. Church MW, Dintcheff BA, Gessner PK. Dose-dependent consequences of cocaine on pregnancy outcome in the Long-Evans rat. *Neurotoxicol Teratol* **1988**;10:51-58
14. Jacobs IG, Roszler MH, Kelly JK, Klein MA, Kling GA. Cocaine abuse: neurovascular complications. *Radiology* **1989**;170:223-227
15. Klonoff DC, Andrews BT, Obana WG. Stroke associated with cocaine use. *Arch Neurol* **1989**;46:989-993
16. Mody CK, Miller BL, McIntyre HB, Cobb SK, Goldberg MA. Neurologic complications of cocaine abuse. *Neurology* **1988**;38:1189-1193
17. Levine SR, Brust JCM, Futrell N, et al. Cerebral vascular complications of the use of the "crack" form of alkaloidal cocaine. *N Engl J Med* **1990**;323:699-704
18. Chasnoff IJ, Bussey ME, Savich R, Stack CM. Perinatal cerebral infarction and maternal cocaine use. *J Pediatr* **1986**;108:456-459
19. Spires MC, Gordon EF, Choudhuri M, Maldonado E, Chan R. Intracranial hemorrhage in a neonate following prenatal cocaine exposure. *Pediatr Neurol* **1989**;5:324-326
20. Woods JR, Plessinger MA, Clark KE. Effect of cocaine on uterine blood flow and fetal oxygenation. *JAMA* **1987**;257:957-961
21. Powers RH, Madden JA. Vasoconstrictive effects of cocaine, metabolites and structural analogues on cat cerebral arteries (abst). *FASEB J* **1990**;4:A1095
22. Grabowski CT. The etiology of hypoxia-induced malformations in the chick embryo. *J Exp Zool* **1964**;157:307-326
23. Franklin JB, Brent RL. The effect of uterine vascular clamping on the development of rat embryo 3-14 days old. *J Morphol* **1964**;115:273-290
24. Leist KH, Grauwiler J. Fetal pathology in rats following uterine-vessel clamping on day 14 of gestation. *Teratology* **1974**;10:55-68
25. Van Allen MI. Fetal vascular disruptions: mechanisms and some resulting birth defects. *Pediatr Ann* **1981**;10:219-233
26. Hoyne HE, Jones KL, Dixon SD, et al. Prenatal cocaine syndrome and fetal vascular disruption. *Pediatrics* **1990**;85:743-747

Chronic Acquired Hepatic Failure: MR Imaging of the Brain at 1.5 T

James A. Brunberg¹⁻³
Emanuel Kanal^{2,3}
William Hirsch^{2,3}
David H. Van Thiel⁴

The results of MR imaging of the brain at 1.5 T in 42 adults with non-Wilsonian chronic hepatic failure are reported. T1-weighted images demonstrated increased signal in the globus pallidus in 30 patients and in the putamen in 21, while T2-weighted images demonstrated no corresponding alteration in signal intensity. Symmetric low intensity in the central portion of the globus pallidus on spin-density and T2-weighted images in two patients correlated with regions of calcification on CT scans. Increased intensity on T1-weighted images also occurred in the mesencephalon surrounding the red nucleus (17/42) and in the quadrigeminal plate (4/42). Three patients demonstrated increased intensity in the pons on T2-weighted images unassociated with clinical brainstem dysfunction. Increased intensity on T1-weighted images was seen in the anterior pituitary in 28 of 35 patients. Alterations in signal intensity were not demonstrated in the cerebral cortex or cerebellum. MR findings did not correlate with laboratory indices of hepatic or thyroid function, with histologic liver diagnosis, or with neurologic status at the time of MR evaluation.

Increased signal intensity in the basal ganglia, pituitary gland, and mesencephalon surrounding the red nuclei is characteristic of chronic hepatocellular dysfunction. Deposition of an as yet unidentified paramagnetic substance or altered intracellular water relaxation associated with the proliferation of astrocyte cytoplasmic organelles is postulated as the likely mechanism for this previously undescribed MR manifestation of chronic acquired hepatic failure.

AJNR 12:909-914, September/October 1991; *AJR* 157:1111-1116, November 1991

Received December 26, 1990; revision requested February 21, 1991; revision received March 22, 1991; accepted March 28, 1991.

Presented in part at the annual meeting of the American Society of Neuroradiology, Chicago, May 1988.

¹ Department of Radiology, Division of Neuroradiology, University of Michigan Medical Center, Ann Arbor, MI 48105-0030. Address reprint requests to J. A. Brunberg.

² Department of Radiology, University of Pittsburgh, Pittsburgh NMR Institute, Pittsburgh, PA 15213.

³ Department of Radiology, University of Pittsburgh, Presbyterian-University Hospital, Pittsburgh, PA 15213.

⁴ Department of Surgery, University of Pittsburgh, Presbyterian-University Hospital, Pittsburgh, PA 15213.

0361-803X/91/1575-1111
© American Roentgen Ray Society

Histologic alteration occurring in the CNS of patients with chronic non-Wilsonian hepatocellular dysfunction has been well described [1-3]. Characteristic findings include the appearance of type II Alzheimer astrocytes within gray matter of the cortex and basal ganglia, the occurrence of nerve cell degeneration or loss, and the presence of laminar or pseudolaminar necrosis of the cerebral cortex with polymicrocavitation at the gray-white junction.

Neuroradiologic alterations occurring in association with chronic hepatic failure have been less well characterized. Early in the course of hepatic dysfunction, at a time when the presence of clinical hepatic encephalopathy may be detectable only on the basis of formal neuropsychological testing, CT imaging may demonstrate cortical atrophy, cerebral edema, or be entirely normal [4]. Similar CT changes occurring in patients with chronic liver failure due to processes other than alcohol toxicity have been described [5, 6]. MR findings in the brain associated with chronic hepatic failure, other than Wilson disease, have only briefly been reported [7, 8]. Our purpose is to describe the results of MR imaging of the brain in a prospective series of patients with chronic, severe non-Wilsonian hepatic failure and to correlate these findings with the etiology of the hepatic failure and with laboratory indices of hepatic function at the time of imaging. We also correlate these MR alterations with anatomic regions of known neuropathologic alteration occurring with chronic non-Wilsonian hepatocellular dysfunction.

Subjects and Methods

Our study population consisted of 42 patients undergoing evaluation (including MR imaging of the brain) preparatory to possible orthotopic liver transplantation. Laboratory studies obtained within 2 weeks of the time of MR imaging were available for each of the 42 patients and included determination of serum direct bilirubin (42/42 patients), total bilirubin (41/42), alkaline phosphatase (41/42), GCTP (39/42), SGPT (39/42), SGOT (41/42), NH_3 (41/42), phosphorus (33/42), magnesium (23/42), serum albumin (31/42), total protein (26/42), ceruloplasmin (34/42), iron (36/42), total iron binding capacity (36/42), ferritin (37/42), zinc (29/42), PT (40/42), PTT (40/42), T4 (36/42), T3 resin uptake (34/42), and TSH (30/42). A history and physical examination documenting the presence or absence of encephalopathy at the time of MR imaging were available in all patients. The presence or absence of indicators of portacaval shunting—including splenomegaly, ascites, or endoscopic evidence of varices—was recorded in 38 patients.

CT studies of the abdomen were available in all 42 patients. Data utilized for this study included the presence or absence of ascites or varices. Liver volume calculated from contiguous axial CT images through the liver was available in 36/42 patients.

Spin-echo MR images of the brain at 1.5 T utilized T1-weighted images at 600/20 (TR/TE) and long TR sequences at 2500/25, 100. Images were 5 mm thick with a 1-mm gap or were contiguous. The matrix was 128×256 or 256×256 , with two excitations and a 20-cm field of view in coronal and axial planes. MR images were graded perceptually, with scoring of alterations in intensity and volume of anatomic regions, which included cerebral cortex, globus pallidus, putamen, caudate, thalamus, mesencephalon, pituitary gland, pons, cerebellum, and lateral and third ventricles. The size of subarachnoid spaces over the cerebral and cerebellar convexities was also scored. In 35/42 patients, coronal T1-weighted images were obtained through the anterior lobe of the pituitary with slice placement satisfactory for characterizing signal intensity without partial volume effect from the neurohypophysis. Alterations in MR signal were graded 0, +1, or +2, respectively, for normal intensity or mildly or markedly increased intensity. Alterations in volume were graded 0, -1, or -2, respectively, for normal volume or mild or marked volume loss. CT studies of the brain obtained within 4 weeks of MR imaging were available for correlation in 38 patients.

Statistical evaluation was done to correlate the laboratory data, etiologic diagnosis, liver volume, and MR findings. A two-way cross tabulation of data was completed by using the Fisher exact test for data sets divided into four groups consisting of normal and abnormal imaging and laboratory data. A chi square test was used to compare normal vs abnormal imaging data with laboratory data, etiologic diagnoses, or liver volume when grouping into more than two fields was required.

Results

T1-weighted images in 30/42 patients demonstrated symmetrically increased signal intensity throughout the globus pallidus, which was mild (24/42) or marked (6/42) in severity (Figs. 1–4). Signal intensity in the putamen was mildly (17/42) or markedly (4/42) increased and was bilaterally symmetric (Figs. 1, 3, 4). Increased signal in the putamen only occurred when there was increased signal intensity in the globus pallidus. No patient with increased signal in the globus pallidus or putamen on T1-weighted images demonstrated altered intensity in a similar distribution on T2-weighted sequences. In two patients focal regions of low intensity in the globus pallidus

on T1- and on T2-weighted images correlated with calcification shown on CT scans (Fig. 2).

T1-weighted images demonstrated increased signal intensity surrounding the red nuclei in 17/42 patients (Figs. 1 and 3). This pattern, with one exception, occurred when there was increased intensity in both the globus pallidus and putamen. T1-weighted images demonstrated increased intensity in the quadrigeminal plate in four patients (Fig. 3). One patient who had mildly increased intensity in the caudate nuclei (Fig. 4) also had markedly increased signal intensity in the globus pallidus, putamen, and mesencephalon surrounding the red nuclei. This patient was one of three who had increased signal intensity on long TR short TE sequences in the globus pallidus, putamen, and caudate (Fig. 4).

Increased intensity of the anterior pituitary was seen in 23/35 patients (Fig. 1). In 6/28 this alteration was unassociated with increased signal intensity on T1-weighted images in other scored anatomic regions. Thyroid function was normal in all 35 of these patients.

Cortical volume loss manifested by prominence of cerebral sulci was seen in 19/42 patients involving frontal (18/19), parietal (14/19), temporal (6/19), and occipital (3/19) lobes. Severe volume loss was demonstrated only in frontal (8/18) and parietal lobes (2/14). Cerebellar volume loss occurred in 9/42 patients, with five of the nine occurring in the eight patients with Laennec cirrhosis. In no patient was altered signal intensity demonstrated in the cerebral or cerebellar cortex. There was prominence in size of the lateral ventricles in 8/42 (3/8 severe), of the third ventricle in 5/42 (2/5 severe) and of the fourth ventricle in 1/42 patients. Increased intensity in the central pons was seen on T2-weighted images in 3/42 patients. Three had increased signal in the globus pallidus and two in the putamen on T1-weighted images. None had symptoms of brainstem dysfunction.

The cause of chronic hepatic failure was determined in all patients (Table 1). Increased intensity on T1-weighted images occurred with cholestatic disease (12/13), chronic active hepatitis (13/21), and Laennec cirrhosis (5/8). The difference was not statistically significant. Laboratory indices of hepatic function and the presence or absence of varices or ascites did not correlate at a statistically significant level with the occurrence of regions of altered signal intensity. Altered liver volume did not statistically correlate with altered intensity in the basal ganglia on T1-weighted images when the sample of 36 patients was examined simultaneously. All eight patients with liver volumes less than 1000 cm^3 , however, had increased signal in the globus pallidus on T1-weighted images and six had increased intensity in the putamen.

Discussion

Hepatic encephalopathy may initially be subclinical, may be manifested as altered mental status, or may present as a combination of tremor, asterixis, incoordination, rigidity, myoclonus, seizures, or incontinence [9]. These findings occur with hepatocellular insufficiency of any cause, and may relate to either hepatocellular disease or to portasystemic shunting where portal blood bypasses the hepatocyte. In hepatic encephalopathy, ingested toxic agents and substances pro-

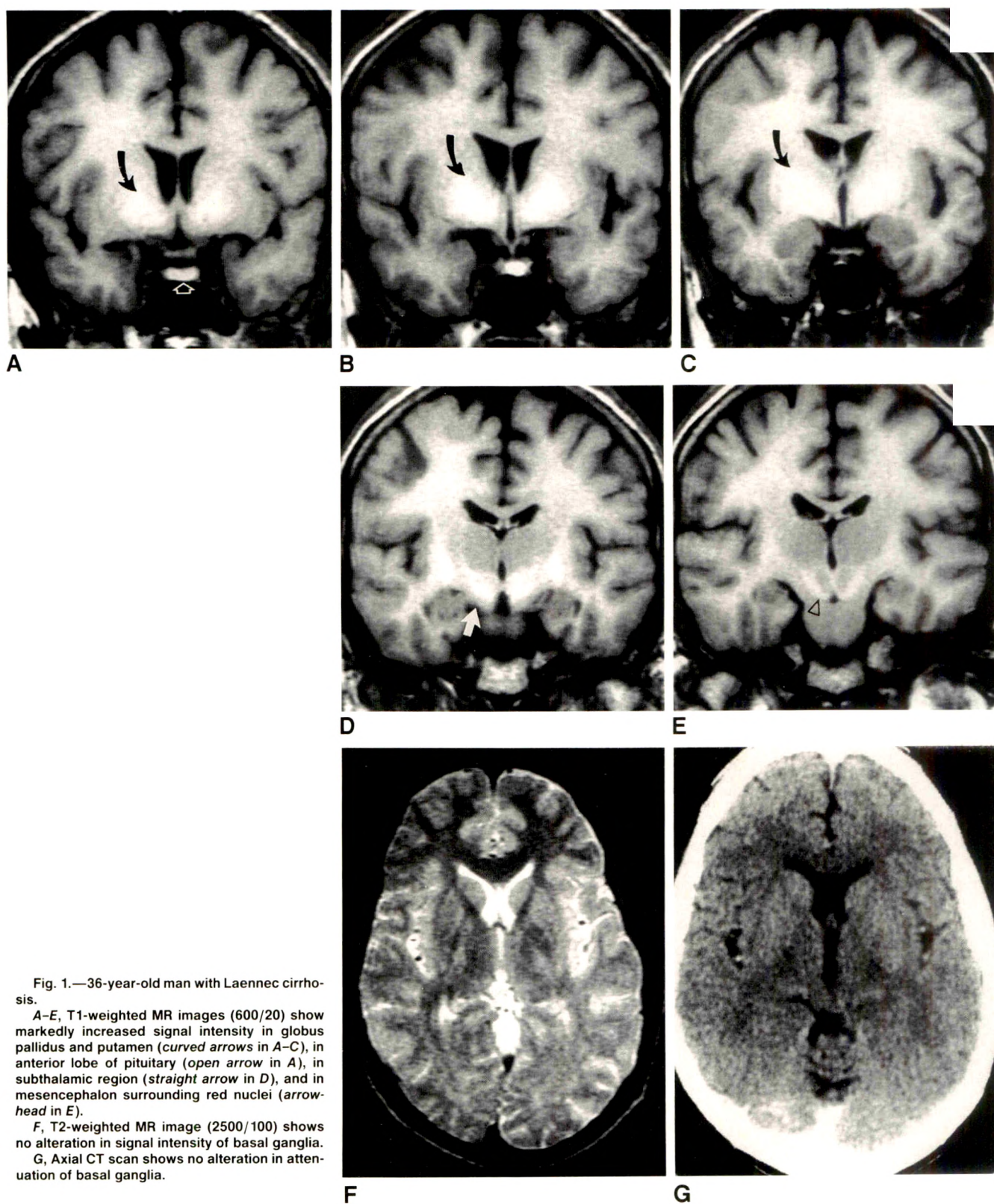


Fig. 1.—36-year-old man with Laennec cirrhosis.

A–E, T1-weighted MR images (600/20) show markedly increased signal intensity in globus pallidus and putamen (*curved arrows* in A–C), in anterior lobe of pituitary (*open arrow* in A), in subthalamic region (*straight arrow* in D), and in mesencephalon surrounding red nuclei (*arrowhead* in E).

F, T2-weighted MR image (2500/100) shows no alteration in signal intensity of basal ganglia.

G, Axial CT scan shows no alteration in attenuation of basal ganglia.

duced by intestinal bacteria enter the systemic circulation to alter cerebral metabolism, neuron membrane function, or neurotransmitter concentration. Major factors responsible for the development of hepatic encephalopathy appear to be

elevated levels of ammonia, gamma-aminobutyric acid, and aromatic amino acids [9, 10].

Neuropathologic findings in chronic non-Wilsonian liver failure are characteristic but not specific. Their severity varies

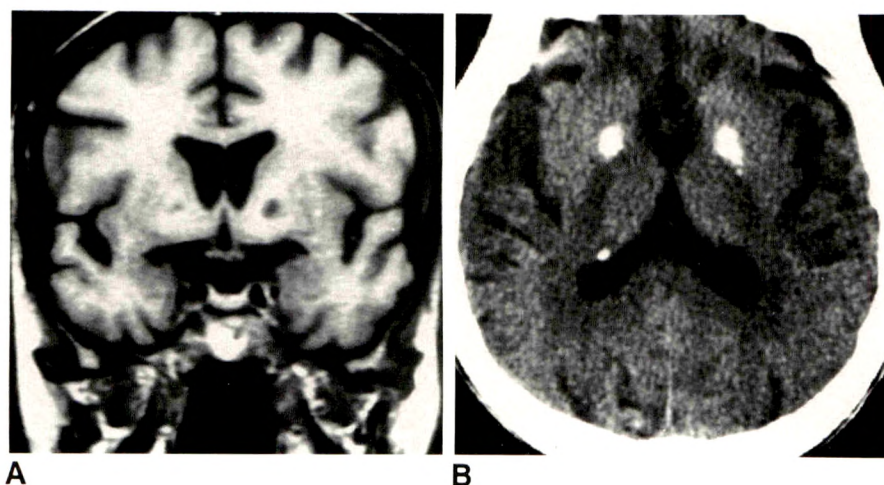


Fig. 2.—65-year-old man with primary biliary cirrhosis.

A, T1-weighted MR image (600/20) shows focal regions of low signal intensity in globus pallidus surrounded by a more diffuse slightly increased signal intensity.

B, CT scan shows foci of dense calcification in globus pallidus correlating with regions of low intensity on the MR image.

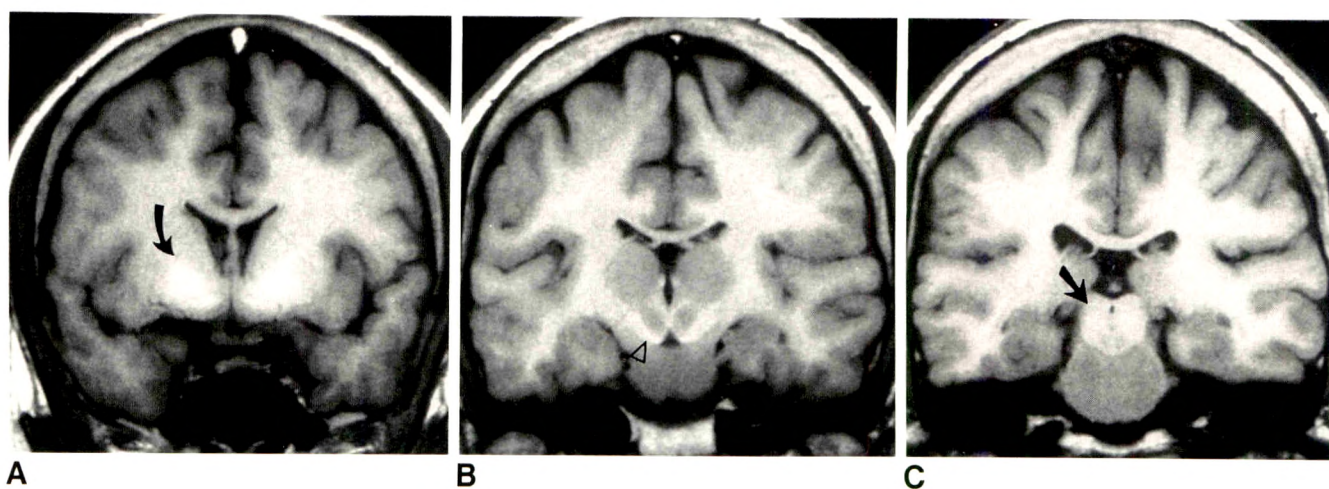


Fig. 3.—27-year-old man with chronic hepatitis.

A–C, T1-weighted MR images (600/20) show markedly increased signal intensity in globus pallidus and putamen (curved arrow in A), in mesencephalon surrounding red nuclei (arrowhead in B), and in quadrigeminal plate (straight arrow in C).

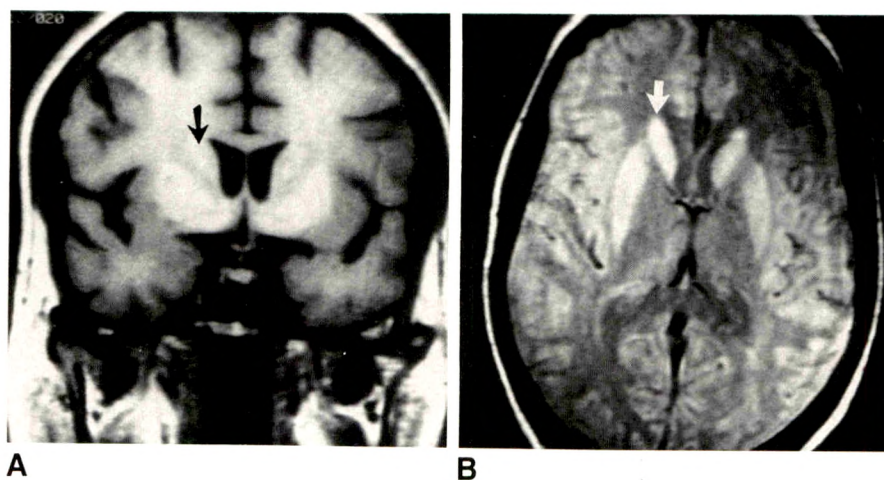


Fig. 4.—53-year-old man with postoperative biliary obstruction.

A, T1-weighted MR image (600/20) shows increased signal intensity in caudate (arrow), globus pallidus, and putamen.

B, At 3000/25 there is increased signal intensity in the heads of the caudate nuclei (arrow) and in putamen. T2-weighted images were normal.

TABLE 1: Causes of Hepatic Failure in 42 Patients

Finding (No. of Cases)
Laennec cirrhosis (8)
Cholestatic liver failure (13)
Sclerosing cholangitis (7)
Primary biliary cirrhosis (5)
Congenital biliary atresia (1)
Hepatocellular dysfunction (21)
Chronic active hepatitis (18)
Hemochromatosis (1)
Cryptogenic (1)
Alpha-1 antitrypsin deficiency (1)

with the duration and extent of hepatocyte dysfunction or portasystemic shunting [1-3], but not with the cause. With chronic hepatic failure the predominant finding is the conversion of protoplasmic astrocytes into Alzheimer II cells. This most likely relates to the astrocyte's function as the site of cerebral NH₃ metabolism to glutamate and glutamine [10, 11]. Alzheimer II cells have large pale nuclei with prominent nucleoli and marginated chromatin. The cytoplasm, relative to that of the astrocyte from which it is derived, is markedly distended by membrane-bound vacuoles, by a three- to fourfold increase in mitochondria, and by an increase in rough endoplasmic reticulum and lysosomes. Alzheimer II cells are found in the lenticular nuclei, caudate nuclei, thalamus, substantia nigra, red nucleus, dentate nuclei, pontine nuclei, and deep layers of the cerebral cortex [1-3].

In our series of 42 patients with chronic hepatic failure, T1-weighted images demonstrated symmetrically increased intensity in the globus pallidus in 30, in the putamen in 21, and in the mesencephalon surrounding the red nucleus in 17. Increased intensity was seen in the anterior pituitary in 28 of 35. In no patient was intensity alteration demonstrated in the cerebral cortex.

The cause of the increased intensity on T1-weighted images remains undetermined. The deposition of a paramagnetic substance that has bypassed the detoxification mechanisms of the liver due to portacaval shunting or hepatocyte dysfunction can be postulated but has not been demonstrated. In previous studies the presence of high signal intensity on T1-weighted images has been demonstrated in association with cerebral parenchymal calcification, possibly reflecting the incorporation of paramagnetic ions or altered effects of hydration [12]. Although CT studies in our patients demonstrated no change to correlate with regions of high MR signal intensity, the presence of increased calcium or other metal ions cannot be excluded. Analysis of postmortem tissue, not available in our series of patients, would have been useful in evaluating these possibilities.

Biologic membranes and macromolecules accentuate water proton relaxation both by the exchange of protons between water and the macromolecule and by a cross relaxation between water protons and protons within the membrane. These membrane effects appear to be responsible for the high signal intensities of myelin and of the posterior pituitary on T1-weighted images [13, 14]. They are also most likely responsible for the increased signal intensity seen within the basal ganglia on T1-weighted images in patients with

neurofibromatosis [15]. The abundant mitochondria and cell organelles of Alzheimer II cells may, by increasing intracellular membrane content, similarly promote relaxation of intracellular water protons, accounting for the increased signal intensity on T1-weighted sequences seen with chronic hepatocellular dysfunction. Saturation transfer techniques are being developed in our laboratory to test this hypothesis [16].

Oxygen radicals within reactive macrophages have been postulated as the cause of T1 shortening at sites of cerebritis or abscess formation [17]. In chronic hepatic failure significant cerebral macrophage accumulation does not occur and the presence of free radicals would not appear to be a likely explanation.

Since the occurrence of coagulopathy is well described in chronic liver failure, the presence of methemoglobin from recent petechial hemorrhage could theoretically account for the increased intensity on T1-weighted images and for the absence of markedly decreased intensity on T2-weighted sequences [18]. Although sequential studies are not available in our patients, the presence of petechial hemorrhage is thought unlikely because of the focal nature and symmetry of the findings, and because of the frequency of occurrence of the finding in clinically stable patients. The absence of signal loss on T2-weighted sequences also suggests that a prolonged process of petechial hemorrhage with hemosiderin deposition has not occurred.

The second major neuropathologic alteration occurring in chronic non-Wilsonian hepatic dysfunction is neuronal alteration. Changes included patchy pseudolaminar degeneration and loss of neurons deep in the cortex; polymicrocavitation of white matter at the gray-white junction; patchy neuronal degeneration in the basal ganglion, thalamus, and red nuclei; and neuronal degeneration of the cerebellar cortex [1, 3]. Laminar necrosis is patchy and most evident in the parietal, occipital, and frontal cortex [1]. Cortical neuronal alteration is generally more prominent than that seen in the basal ganglia [3, 19]. MR alterations in signal intensity to correlate with cortical laminar or pseudolaminar necrosis and with polymicrocavitation at the gray-white junction were not demonstrated in this study. We are unable to determine whether our patients, free of symptoms of extensive encephalopathy at the time of imaging, had less severe neuropathologic alteration or whether such changes, though present, were not imaged.

Alterations consistent with cortical volume loss, manifested by prominence of cerebral sulci, were demonstrated in 19/42 patients. Changes were most prevalent in the frontal and parietal regions. Cerebellar cortical volume loss was demonstrated in 9/42 patients with five of these occurrences in the eight patients with Laennec cirrhosis, possibly representing the effect of both ethanol toxicity and chronic hepatic dysfunction.

Although myelinated fibers have demonstrated histologic degeneration with fragmentation of axis cylinders in chronic hepatocellular dysfunction, prominent neuropathologic lesions of the cerebral or cerebellar white matter have not been reported. Other than in one patient with previous infarction, MR imaging in our series did not demonstrate alterations in cerebral or cerebellar white matter. Three patients did dem-

onstrate increased signal intensity limited to the pons on T2-weighted images, consistent with central pontine myelinolysis [20, 21]. Two had Laennec cirrhosis, and one had primary biliary cirrhosis. The possibility that the MR changes relate to spongy degeneration of pontine white matter associated with hepatic encephalopathy cannot be excluded [22]. None of our patients had symptoms of brainstem dysfunction.

Since our recognition of the correlation of T1 shortening within the globus pallidus and putamen in association with hepatic dysfunction, two patients undergoing MR imaging of the brain have been prospectively diagnosed as having underlying hepatic disease on the basis of this MR finding. Increased intensity in the lenticular nuclei on T1-weighted images is not specific for hepatic dysfunction and has been found in three additional patients with systemic lupus erythematosus. Two of these patients have had no clinical or laboratory indices of hepatic dysfunction, although liver biopsies have not been accomplished. The third has been subsequently diagnosed as having lupus hepatitis.

The presence of symmetrically increased intensity on T1-weighted images in the lenticular nuclei, in the mesencephalon surrounding the red nuclei, and in the anterior lobe of the pituitary gland has been found in the majority of our patients with chronic hepatocellular dysfunction. This finding appears to be characteristic of but not specific to chronic liver dysfunction or portosystemic shunting, and should prompt prospective consideration of such diagnoses when it is encountered. It is postulated that this finding may relate to deposition of a paramagnetic substance or may relate to altered intracellular water relaxation associated with the proliferation of astrocyte cytoplasmic organelles.

REFERENCES

- Victor M, Adams RD, Cole M. The acquired (non-Wilsonian) type of chronic hepatocerebral degeneration. *Medicine* 1965;44:365-396
- Laursen H. Cerebral vessels and glial cells in liver disease. A morphometric and electron microscopic investigation. *Acta Neurol Scand* 1982;65:381-412
- Finlayson MH, Superville B. Distribution of cerebral lesions in acquired hepatocerebral degeneration. *Brain* 1981;104:79-95
- Berenthal P, Hays A, Tarter RE, Van Thiel D, Lecky J, Hegedus A. Cerebral CT scan abnormalities in cholestatic and hepatocellular disease and their relationship to neuropsychologic test performance. *Hepatology* 1987;7:107-114
- Tarter RE, Hays AL, Sandford SA, Van Thiel DH. Cerebral morphological abnormalities with non-alcoholic cirrhosis. *Lancet* 1986;i:893-895
- Toda C, Chiba T, Matsuda Y, Inatome T, Inoh T, Fujita T. A case of brain atrophy after fulminate hepatic failure. *Am J Gastroenterol* 1983;78:446-448
- Hanner JS, Li KCP, Davis GL. Acquired hepatocerebral degeneration: MR similarity with Wilson disease. *J Comput Assist Tomogr* 1988;12:1076-1077
- Uchino A, Miyoshi T, Ohno M. Case report: MR imaging of chronic persistent hepatic encephalopathy. *Radiat Med* 1989;7:257-260
- Rothstein JD, Herlong HF. Neurologic manifestations of hepatic disease. *Neurol Clin* 1989;7:563-578
- Farmer PM, Mullakkan T. The pathogenesis of hepatic encephalopathy. *Ann Clin Lab Sci* 1990;20:91-97
- Norenberg MD. The astrocyte in liver disease. *Adv Cell Neurobiol* 1981;2:303-352
- Dell LA, Brown MS, Orrison WW, Eckel CG, Matwyloff NA. Physiologic intracranial calcifications with hypertension on MR imaging. *AJNR* 1988;9:1145-1148
- Kucharczyk W, Lenkinski RE, Kucharczyk J, Henkelman RM. The effect of phospholipid vesicles on the NMR relaxation of water: an explanation for the MR appearance of the neurohypophysis? *AJNR* 1990;11:693-701
- Koenig SH, Brown III RD, Spiller M, Lundbom N. Relaxometry of brain: why white matter appears bright on MRI. *Magn Reson Med* 1990;14:482-495
- Mirowitz SA, Sartor K, Gado M. High-intensity basal ganglia lesions on T1-weighted MR images in neurofibromatosis. *AJNR* 1989;10:1159-1163, *AJR* 1990;154:369-373
- Wolff SD, Balaban RS. Magnetization transfer contrast (MTC) and tissue water proton relaxation in vivo. *Magn Reson Med* 1989;10:135-144
- Haines AB, Zimmerman RD, Morgello S, et al. MR imaging of brain abscess. *AJNR* 1989;10:279-291
- Gomori JM, Grossman RI, Hackney DB, et al. Variable appearance of subacute intracranial hematoma on high field spin echo MR. *AJNR* 1987;8:1019-1026
- Graham DI, Adams JH, Caird FI, Lawson JW. Acquired hepatocerebral degeneration: report of a typical case. *J Neurol Neurosurg Psychiatry* 1970;23:656-662
- Miller GM, Baker HL, Okazaki H, Whishant JP. Central pontine myelinolysis and its imitators: MR findings. *Radiology* 1988;168:795-802
- Koci TM, Chiang F, Chow P, et al. Thalamic extrapontine lesions in central pontine myelinolysis. *AJNR* 1990;11:1229-1233
- Thornberry DS, Itabashi HH. Pontine spongy degeneration of white matter with hepatic encephalopathy. *Arch Pathol Lab Med* 1984;108:564-566

Computer Page

A PC-Based Semiautomated Reporting System

Lawrence H. Schwartz,¹ Paula W. Brill, and Patricia Winchester

A computerized reporting system was developed to speed dictation and typing of repetitive radiology reports. A popular word processing program was used with an IBM-compatible personal computer. The system was designed to be easily integrated into the standard dictating practices of radiologists. The system was created so that it would not be limited to preprogrammed or "canned" reports.

Materials and Methods

Hardware included an IBM-AT personal computer with 640K random access memory, a 1.2-megabyte floppy disk drive, a 40-megabyte hard disk drive, and a monochrome graphics adaptor and monitor. Output was printed on multipart radiology report forms with an IBM Proprinter. Wordperfect Version 5.0 (Wordperfect Corp., Orem, UT) was used as the word processing program. Wordperfect's macro programming language allows a group of keys (words, phrases, sentences, etc.) or keystrokes to be assigned to a single command or letter. Basically, a "macro" can be thought of as similar to the recall or programmable button on modern electronic telephones. Multiple keystrokes (i.e., letters or words) can be combined into one letter [1].

Radiographs from the pediatric intensive care unit (PICU) and the neonatal intensive care unit (NICU) were selected because of their repetitive nature and unique findings. Radiographs and their reports were carefully analyzed for several weeks, and repetitive items found within the dictations were noted. Macros were assigned to replace phrases or whole sentences indicating the positions of tubes and catheters and to describe the findings of common clinical entities.

Tube positions were assigned a mnemonic letter for the name of the tube and a second mnemonic letter for its position. If the position of the tube was uncommon, the first mnemonic letter would be

followed by free text, dictated by the radiologist. Additional free text could be placed at any position in a report. The mnemonic letters were selected for ease of pronunciation and recognition. The codes and translations were posted in the dictating areas for quick reference.

Results

Table 1 lists six of the common mnemonic letters used to begin the description of tube or catheter positions. Table 2 lists the choices of second mnemonic letters to complete the sentence describing the positions of endotracheal tubes and umbilical artery catheters. Table 3 lists the mnemonic letters used for complete sentences describing the findings of common clinical entities.

To dictate the findings in a typical patient with hyaline membrane disease, an endotracheal tube, an umbilical artery catheter, and a normal bowel-gas pattern, the radiologist would dictate "Alt H. Alt ET. Alt AT7. Alt B." The word "Alt" is used to alert the typist to press the ALT key on the

TABLE 1: Mnemonic Letter Codes for Phrases Indicating the Presence of Indwelling Catheters and Tubes

ALT N	A Nasogastric tube is seen with its tip
ALT E	An Endotracheal tube is
ALT F	A Feeding tube is seen with its tip
ALT V	The tip of an umbilical Venous catheter is in the
ALT A	The tip of an umbilical Artery catheter is in the
ALT S	The tip of a Swan-Ganz catheter is at the level of the

Received April 1, 1991; accepted after revision June 4, 1991.

¹ All authors: Department of Radiology, The New York Hospital-Cornell Medical Center, 525 E. 68th St., New York, NY 10021. Address reprint requests to P. W. Brill, Division of Pediatric Radiology.

AJR 157:1117-1118, November 1991 0361-803X/91/1575-1117 © American Roentgen Ray Society

TABLE 2: Mnemonic Letter Codes for Phrases Used in Conjunction with Table 1 to Indicate Locations of Endotracheal Tube and Umbilical Artery Catheter

ALT-E: An Endotracheal tube is	
C	at the level of the C ervical trachea.
T	at the level of the T horacic inlet.
U	at the level of the U pper thoracic trachea.
M	at the level of the M id thoracic trachea.
A	at the cA rina.
S	S lightly above the carina.
R	in the R ight main bronchus.
L	in the L eft main bronchus.
ALT-A: The tip of an umbilical artery catheter is in the	
M	M id thoracic aorta
L	aorta at the level of L ____ (radiologist dictates vertebral body level).
T	aorta at the level of T ____ (radiologist dictates vertebral body level).
A	aortic A rch.
B	aortic B ifurcation.

TABLE 3: Mnemonic Letter Codes for Frequently Used Sentences

ALT C	The C ardiomyic image and pulmonary vasculature are normal. The lungs are clear.
ALT B	The B owel gas pattern is normal. There is no evidence of pneumatosis intestinalis or free air.
ALT H	The lungs are finely granular with air bronchograms consistent with H yaline membrane disease. The cardiomyic image is normal.
ALT X	There is no evidence of pneumothorax X .

keyboard to activate the macro. The typist would type exactly what the radiologist dictated, and a full report would be generated on the screen.

The system was evaluated by having four radiologists dictate and two typists transcribe the reports for a selected series of 60 radiographs on two occasions 3 weeks apart. The radiologists, who were already familiar with the macro system, decreased their dictating time by an average of 17%, and the time for typing was decreased by 48%. The average dictating time for the four radiologists was 19.4 min (range, 17.0–21.5 min) using standard dictation and 16 min (range, 12.5–19.5 min) with the use of macros. The two typists took an average of 58–60 min for each of the series of 60 reports without macros and 29–33 min when macros were used.

Discussion

Many computerized systems have been designed for radiology reporting and transcribing. They include touch-sensitive screens, sense forms, bar coding, and voice recognition [2–4]. Many of the touch-sensitive screens and mark-sense forms are expensive and inflexible, and radiologists tend to be unhappy with the added burden of data entry. Similar problems have been encountered with bar-coding and voice-recognition systems. Although many advances have been made in voice-recognition systems, the radiologist must still check the screen to verify the output, and the speed of the dictation is significantly slower. As a result, these various computerized systems require the radiologist to spend additional time per radiograph on data entry tasks, in addition to viewing and dictating a report on each radiograph.

With these factors in mind, we set out to design a system that would allow the radiologist to use both abbreviated dictations and standard dictating practices. It was our goal to shorten both the dictating time of the radiologist and the transcribing time of the typist. In addition, the system was designed to be flexible and to allow the radiologist to ad lib free text.

This method differs from other available computerized systems in its ability to integrate an automated reporting system with standard dictation in the same report and even in the same sentence, while decreasing dictating and typing time. Both radiologists and typists found the system easy to learn and use. The final report was not perceived as different by the dictating radiologists or the referring physicians. With this system, radiologists can design their own set of macros for any number of reporting environments. In addition, if there is no macro for a phrase that the radiologist wishes to use, then standard dictating practices can be used. No additional time is needed for data entry by the radiologist. A small amount of dictating time and a large amount of typing time are saved, so that reports are produced significantly faster.

REFERENCES

1. WordPerfect for the IBM Personal Computers: Version 5.0. Orem, UT: WordPerfect Corp., 1988:224–228
2. Adams HG, Campbell AF. Automated radiographic report generation using barcode technology. *AJR* 1985;145:177–180
3. Robbins AH, Horowitz DM, Srinivasan MK, et al. Speech-controlled generation of radiology reports. *Radiology* 1987;164:569–573
4. Jost GR. Radiology reporting. *Radiol Clin North Am* 1986;24:19–26

Commentary

Understanding Receiver-Operating-Characteristic Curves: A Graphic Approach

Jan Brismar¹

Receiver-operating-characteristic (ROC) curves describe the relationship between signal and noise and were developed to compare different radar devices [1, 2]. ROC curves have gained increasing popularity in radiology for comparing different test and tester combinations [3]. In an earlier issue of *AJR* [4], a graphic definition of the commonly used efficacy terms sensitivity, specificity, accuracy, positive predictive value, and negative predictive value was presented. A similar graphic approach can be used to explain ROC curves.

The diagram in Figure 1 defines sensitivity and specificity. The horizontal axis (x-axis) denotes the outcome of a test from normal to abnormal. The outcome in the diseased group is plotted above the x-axis, and the outcome in the normal group is plotted below the x-axis.

Decision Threshold and Efficacy Terms

If only the two alternatives normal or abnormal are given, the diagnostician can place the *decision threshold*, which separates normal from abnormal, anywhere along the x-axis. All tests may be called normal (Fig. 1, point A) or all may be called abnormal (Fig. 1, point B); usually a decision threshold is selected somewhere in between (Fig. 1, point C). An "overreader" tends to place the threshold too far to the left, whereas an "underreader" places the threshold too far to the right. The decision threshold divides the *normal* population into a true-negative (TN) and a false-positive (FP) group, and the *diseased* population into a true-positive (TP) and a false-negative (FN) group.

As the decision threshold moves to the right along the x-axis, *sensitivity* (defined as $TP/[TP + FN]$) ranges from one, when all tests are read as abnormal (no false negatives), to zero, when all are called normal (no true positives) (Fig. 2). Maximal sensitivity is achieved when all tests are reported as abnormal. However, *specificity*, defined as $TN/[TN + FP]$, moves in concert from zero (all tests called abnormal, no true negatives) to one (all tests read as normal, no false positives). Maximal specificity consequently is gained by blindly reporting all tests as normal. Obviously, a sensitivity value given without a corresponding specificity value (or the reverse) is meaningless.

Not Only Normal or Abnormal Test Outcome

When evaluating a test (e.g., interpreting a chest radiograph), the radiologist works with more possibilities than just normal and abnormal, such as definitely abnormal, probably abnormal, equivocal, probably normal, and definitely normal. Depending on the consequences of a positive test, radiologists move their decision threshold (consciously or unconsciously).

Consider a chest radiograph in a 20-year-old boy with a "vague, nodular opacity projecting over the left apex." Now consider two possible clinical histories:

History of osteosarcoma with previously resected pulmonary metastasis; recent hemoptysis. In this case, the prior probability of a new metastasis is high, and the consequences of missing a lesion may be significant. Therefore, the rational

Received February 26, 1991; accepted after revision June 28, 1991.

¹Department of Radiology, King Faisal Specialist Hospital and Research Centre, P.O. Box 3354, Riyadh 11211, Saudi Arabia. Address reprint requests to J. Brismar.

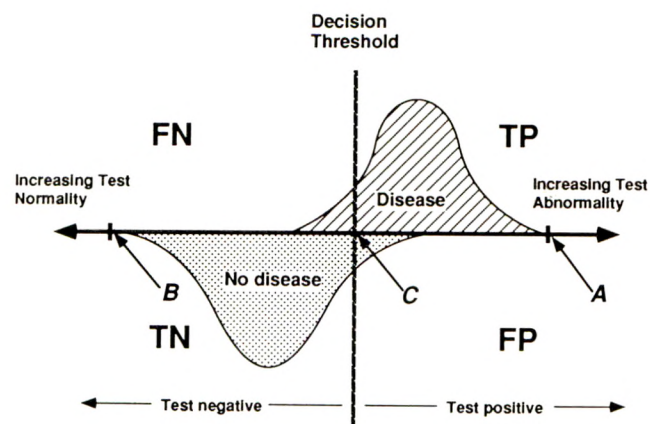


Fig. 1.—Graphic explanation of efficacy terms. Decision threshold separates normal from abnormal test results; it can be placed anywhere along test outcome axis (e.g., points A, B, and C). This threshold divides group with disease (above horizontal axis) into true-positives (TP) and false-negatives (FN) and group without disease (below axis) into true-negatives (TN) and false-positives (FP).

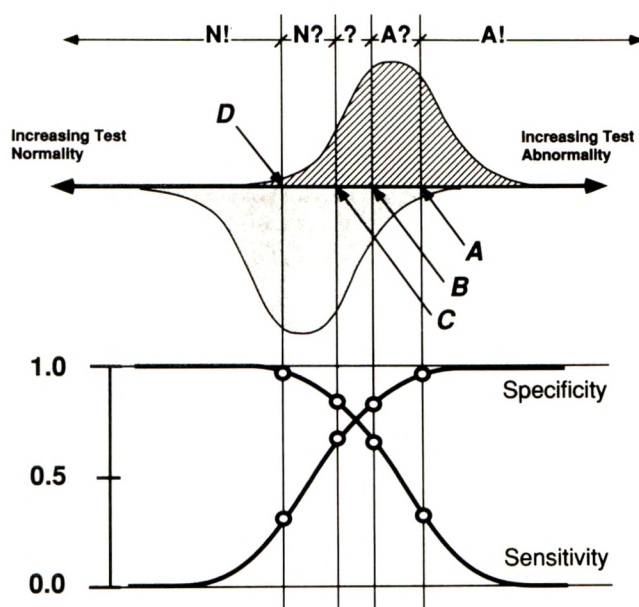


Fig. 2.—Decision threshold can be placed anywhere along outcome axis. At position A, only definitely abnormal test results (A!) are classified as abnormal; at position B, both probably (A?) and definitely abnormal results are read as abnormal; at position C, also equivocal results (?) are called abnormal, whereas in position D, only definitely normal outcomes are read as normal. Lower part of diagram shows how sensitivity and specificity change as decision threshold is moved. Each position of threshold gives a unique pair of sensitivity and specificity values.

radiologist adjusts the decision threshold to emphasize sensitivity (i.e., overreads the film). Interpretation of the chest film: "nodular pulmonary opacity; must exclude metastatic lesion; suggest CT with possible biopsy."

Inguinal hernia, routine preoperative chest radiograph. In this case, the prior probability of serious chest disease is low, as is the consequence of a false-negative interpretation. Therefore, the decision threshold should be adjusted to em-

phasize specificity (i.e., the film should be underread). Interpretation of the chest film: "vague nodular opacity of unknown chronicity, may represent confluence of normal structures; suggest comparison with prior films and attention on follow-up films."

For tests that have consequences when either positive or negative, the choice probably should be a threshold in the vicinity of equivocal test findings (Fig. 2, points B or C).

The Sensitivity-Specificity Curve

As seen from Figure 2, a unique combination of sensitivity and specificity values is obtained for each position of the decision threshold. Each sensitivity value can be plotted against its corresponding specificity value to create the diagram in Figure 3. The points 1.0, 0.0 (left lower corner) and 0.0, 1.0 (right upper corner) in this diagram represent positions of the decision threshold at the extreme left and the extreme right on the outcome axis in Figure 2, respectively.

The Receiver-Operating-Characteristic Curve

The traditional ROC axes have been altered, with the horizontal axis pointing to the left (Fig. 3). Normally ROC curves are presented with the horizontal axis representing false-positive fraction, that is $(1 - \text{specificity})$, whereas the vertical axis denotes true-positive fraction (i.e., sensitivity). The sensitivity-specificity curve presented in this way is thus, except for the names of the axes, identical to the ROC curve. As the phrase ROC curve to most readers is an acronym without meaning, it perhaps should be discarded. A term such

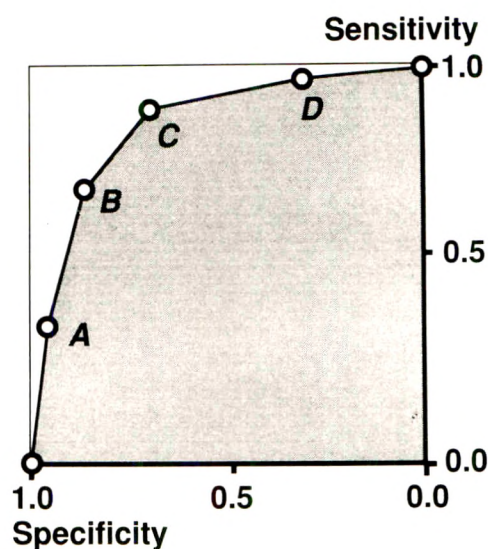


Fig. 3.—If, for each of four positions (A, B, C, and D) of decision threshold in Figure 2, each sensitivity value is plotted against its corresponding specificity value and points are connected, a sensitivity-specificity curve (receiver-operating-characteristic [ROC] curve) is obtained. Direction of x-axis is chosen to correspond to usual presentation of ROC curves. Size of shadowed area, covered by curve, is a measure of efficacy of test.

as *sensitivity-specificity curve (S-S curve)* better describes the curve.

Construction of a Receiver-Operating-Characteristic Curve

In order to construct an ROC curve, for example, for comparing CT and MR studies to detect liver metastases, patients are examined with both techniques, and the true diagnosis (metastasis or no metastasis) is established by a separate gold standard. The observer is asked to interpret each study as either definitely abnormal, probably abnormal, equivocal, probably normal, or definitely normal. Sensitivity and specificity are then calculated for each of four alternatives (Fig. 2): (1) only those read as definitely abnormal are regarded as positive tests; (2) those read as probably abnormal or definitely abnormal are classified as positive; (3) those read as equivocal, probably abnormal or definitely abnormal are regarded as positive; and finally (4) all but the definitely normal tests are considered positive. With these four sensitivity-specificity value pairs and the two corners (sensitivity = 1 for specificity = 0, and specificity = 1 for sensitivity = 0), an ROC curve is plotted.

Interpreting the Receiver-Operating-Characteristic Curve

The curve in Figure 3 gives the sensitivity-specificity combination for every possible placement of the decision threshold. An ideal test, clearly separating normal subjects from diseased ones (Fig. 4, A), gives a sensitivity-specificity (i.e., ROC) curve at the left upper corner of the diagram. A test/tester combination without any discrimination between normal and abnormal (Fig. 4, C) (e.g., reading mammograms blindfolded) would give a curve running straight from the left lower to the right upper corner. In most situations, the curve would run somewhere in between (Fig. 4, B); the better the test/tester combination is, the closer to the left upper corner the curve would run, or, more correctly, the larger area the curve would cover (shadowed in Fig. 3). The ROC curve thus can be used to compare the efficacy of different tests (or different equipment) used by the same tester, as well as the skill of different testers that use the same test material.

Construction of an ROC curve requires extra effort from the researcher, as compared with simply calculating sensitiv-

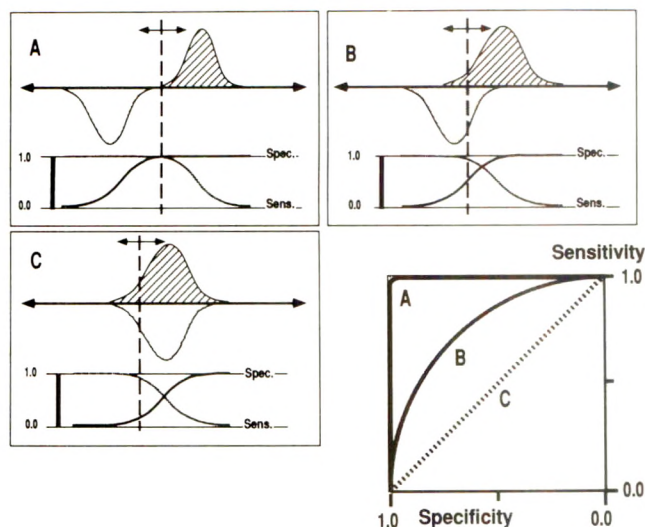


Fig. 4.—A–C, Three different tests. An ideal test (A), which clearly separates those with disease from those without disease, gives a sensitivity-specificity curve passing close to upper left-hand corner of diagram. Test without any discrimination (C) gives a curve running straight from lower left-hand to upper right-hand corner. Usually, curve runs somewhere in between (B).

ity and specificity values. However, for a serious comparison of different diagnostic tests, no approach is available to replace the ROC curve. For readers who wish to pursue a more in-depth analysis of ROC curves, several excellent articles are available [5, 6].

REFERENCES

1. van Meter D, Middleton D. Modern statistical approaches: reception in communication theory. *IRE Trans* 1954;PIGT-4:119–141
2. Peterson WW, Birdsall TG, Fox WC. The theory of signal detectability. *IRE Trans* 1954;PIGT-4:171–212
3. Metz CE. ROC methodology in radiological imaging. *Invest Radiol* 1986;21:720–733
4. Brismar J, Jacobsson B. Definition of terms used to judge the efficacy of diagnostic tests: a graphic approach. *AJR* 1990;155:621–623
5. Hanley JA, McNeal BJ. The meaning and use of the area under a receiver operating characteristic (ROC) curve. *Radiology* 1982;143:29–36
6. Hanley JA. Receiver operating characteristic (ROC) methodology. The state of the art. *Crit Rev Diagn Imaging* 1989;29:307–334

Forthcoming Articles

SPECIAL ARTICLE

Acute reactions to intravascular contrast media: types, risk factors, recognition, and specific treatment. *Bush WH, Swanson DP*

REVIEW ARTICLES

Clinical value of high-resolution CT in chronic diffuse lung disease. *Müller NL*

Masses of the anterior mediastinum: CT and MR imaging. *Brown LR, Aughenbaugh GL*

PULMONARY RADIOLOGY

CT bronchus sign in peripheral carcinoma of the lung: value in predicting results of transbronchial biopsy. *Gaeta M, Pandolfo I, Volta S, et al.*

Case report. Tuberculous bronchial stenosis: treatment with balloon bronchoplasty. *Nakamura K, Terada N, Ohi M, Matsushita T, Kato N, Nakagawa T*

GASTROINTESTINAL RADIOLOGY

Complications after total gastrectomy and esophagojejunostomy: radiologic evaluation. *Levine MS, Fisher AR, Rubesin SE, Laufer I, Herlinger H, Rosato EF*

Low-attenuation periportal collar in transplanted livers is not reliable CT evidence of acute allograft rejection. *Stevens SD, Heiken JP, Brunt E, Hanto DW, Flye MW*

Endosonography of the anal sphincter: findings in normal volunteers. *Nielsen MB, Pedersen JF, Hauge C, Rasmussen OØ, Christiansen J*

Case report. Chronic intestinal bleeding due to mesenteric vascular insufficiency. *Pollak JS, Bennick M, Denny DF Jr, Markowitz D*

Pictorial essay. Imaging of gallbladder variants. *Meilstrup JW, Hopper KD, Thieme GA*

Percutaneous drainage of hepatic abscesses: comparison of results in abscesses with and without intrahepatic biliary communication. *Do H, Lambiase RE, Deyoe L, Cronan JJ, Dorfman GS*

Technical note. Percutaneous drainage of hydatid cysts: use of a new cutting device to avoid leakage. *Saremi F*

GENITOURINARY RADIOLOGY

Cancer of the endometrium: value of MR imaging in determining depth of invasion into the myometrium. *Lien HH, Blomlie V, Tropé C, Kaern J, Abeler VM*

Case report. Sonographic appearance of primary testicular lymphoma. *Moorjani V, Mashankar A, Goel S, Khandelwal K, Patange V, Merchant N*

Case report. Gelatin sponge mimicking a pelvic neoplasm on MR imaging. *Hoeffner EG, Soulen RL, Christensen CW*

MUSCULOSKELETAL RADIOLOGY

Do asymptomatic marathon runners have an increased prevalence of meniscal abnormalities? An MR study of the knee in 23 volunteers. *Shellock FG, Deutsch AL, Mink JH, Kerr R*

Myositis ossificans: MR appearance with radiologic-pathologic correlation. *Kransdorf MJ, Meis JM, Jelinek JS*

Case report. Bacillary angiomatosis causing soft-tissue and osseous lesions: unusual manifestation of cat-scratch fever in patients with AIDS. *Herts BR, Rafii M, Spiegel G*

VASCULAR AND INTERVENTIONAL RADIOLOGY

Dye laser-assisted angioplasty with multifiber catheters: short-term results in the treatment of 29 peripheral arterial occlusions. *Huppert PE, Duda SH, Seboldt H, Claussen CD*

Anatomic relationship between the popliteal artery and vein: a guide to accurate angiographic puncture. *Trigaux J-P, Van Beers B, Dewispelaere J-F*

Percutaneous dilatation of benign biliary strictures: single-session therapy under general anesthesia. *Lee MJ, Mueller PR, Saini S, Hahn PF, Dawson SL*

PEDIATRIC AND FETAL RADIOLOGY

Vascularity of tumors in children: evaluation with color Doppler imaging. *Taylor GA, Perlman EJ, Scherer LR, Gearhart JP, Leventhal BG, Wiley J*

Case report. Fibroepithelial polyp of the ureter in a child. *Liddell RM, Weinberger E, Schofield DE, Pelman RS*

Sonographic prediction of gestational age: accuracy of second- and third-trimester fetal measurements. *Benson CB, Doubilet PM*

NEURORADIOLOGY

The prevalence and location of metastases from ocular melanoma: an imaging study in 110 patients. *Lorigan JG, Wallace S, Mavligit GM*

Pictorial essay. Intraventricular mass lesions of the brain: CT and MR findings. *Tien RD*

Stroke associated with coronary artery bypass surgery. *Hise JH, Nipper ML, Schnitker JC*

Commentary. A new role for radiologists in the development of cardiac surgery. *Moody DM*

Commentary. Neuroimaging of cerebral infarction associated with coronary revascularization. *Sila CA*

Assessment of carotid artery patency on routine spin-echo MR imaging of the brain. *Lane JL, Flanders AE, Doan HT, Bell RD*

Commentary. Re: Assessment of carotid artery patency on routine spin-echo MR of the brain. *Brant-Zawadzki M*

Angiographic diagnosis and management of head and neck schwannomas. *Abramowitz J, Dion JE, Jensen ME, et al.*

The morphologic correlate of incidental punctate white matter hyperintensities on MR images. *Fazekas F, Kleinert R, Offenbacher H, et al.*

Nonaneurysmal perimesencephalic subarachnoid hemorrhage: CT and MR patterns that differ from aneurysmal rupture. *Rinkel GJE, Wijdevicks EFM, Vermeulen M, et al.*

TELERADIOLOGY

Perspective. A dial-up digital teleradiology system: technical considerations and clinical experience. *Templeton AW, Dwyer SJ III, Rosenthal SJ, Eckard DA, Harrison LA, Cook LT*

RADIOLOGY PRACTICE

Productivity of radiologists: estimates based on analysis of relative value units. *Conoley PM, Vernon SW*

Radiology practices' contracts with hospitals, 1989-1990: a representative sample survey. *Sunshine J, Chan WC, Kassing PJ*

Letters

Use of CT for Evaluation of Possible Traumatic Aortic Injury

In their recent article [1], Richardson et al. advocate the use of CT in the examination of patients with blunt decelerating thoracic trauma who may have aortic injury. The authors are affiliated with a flagship trauma center, where experience with the management of such patients is optimal for a protocol such as the one presented.

In institutions that treat large numbers of trauma patients, delays may be encountered in obtaining urgent CT scans of the chest. Furthermore, in some institutions, radiologists may refuse to perform angiography unless the thoracic CT shows abnormalities that suggest aortic injury [2]. Advocacy of the use of CT as a screening test for aortic injury should be tempered by these facts, and Richardson et al. do acknowledge that the applicability of CT may vary with the institution. Our concern is that the widespread adoption of the protocol of Richardson et al. will lead to inappropriate use of CT as a screening examination, thus introducing critical delays in the treatment of patients with aortic injuries, including delay of nonselection of the accurate standard examination, aortography.

The risk of death in the hours after aortic injury is well known and should influence the choice of imaging techniques; it is a major cause of our concern with the use of CT. Is this concern valid? We think it is. In the series presented by Miller et al. [2], two patients became so unstable during angiography that the procedure was terminated. In our own experience, a patient with an aortic injury died en route to the operating room from the CT suite after having abdominal CT.

Two recent articles [2, 3] from the surgical literature illustrate the complexity of this issue. Miller et al. [2] prospectively evaluated 153 patients with suspected aortic injury, a larger series than that of Richardson et al. Patients had contrast-enhanced CT followed by angiography. In five patients, two with a transected aorta and three with injuries to a major aortic branch, the results of CT falsely showed no indications of aortic trauma. Richardson et al. appear to dismiss that experience because only two cases involved the aorta—in one patient, IV contrast medium was not used, and in the other, CT retrospectively showed a mediastinal hematoma. Nevertheless, this experience was important because it included clinically significant examples in which CT showed no evidence of aortic trauma. In a recent article, Fenner et al. [3] recommend CT “for the evaluation of widened mediastinum in the stable patient,” even though (1) only four patients in their series had both CT and angiography, and (2) the authors admit that small, “subclinical” intimal injuries could not be ruled out in their patients on the basis of CT findings.

A major concern with CT as a screening tool is the selection of too many patients with a high probability of aortic injury for CT rather than angiography, thus introducing inordinate delay in the diagnosis and treatment of these injuries. Four (4%) of 90 patients in the series of Richardson et al. who had chest CT had subsequent demonstration of aortic injury; the authors do not state whether they consider this an acceptable percentage. What is the authors' current definition of an equivocal chest radiograph? Many of the reasons cited for the inability to decide whether the mediastinum was normal (Table 2 in [1]) are signs of possible aortic injury listed by the authors, from the same institution as Richardson et al., of an earlier paper [4] on the value of chest radiography in excluding traumatic aortic rupture. Indeed, in that earlier publication [4], several of these reasons were listed among those criteria most discriminating of aortic rupture. Is any abnormal chest radiograph now to be considered equivocal for purposes of selection for CT examination?

Richardson et al. advocate the use of contrast-enhanced CT in their protocol. However, they fail to confirm that contrast enhancement is critical and indicate that CT is performed mainly to look for mediastinal hematoma, which does not require use of IV contrast medium. The use of IV contrast medium to study the mediastinum limits the option of high-dose bolus reinjection of contrast medium to study the abdomen and could have an effect on subsequent aortography, especially when digital subtraction angiography is not available, and higher doses of contrast material are required.

In patients suspected of having aortic injury, many of whom are less than 40 years old [2, 4], mediastinal hematoma could be interpreted incorrectly as residual thymus or a vascular structure, and needed angiography not be performed. What are the appearances of mediastinal hematoma that allow it to be distinguished from such normal structures? Richardson et al. allude to six equivocal studies resulting from thymic tissue or pulmonary artery averaging but do not indicate how to avoid confusion with mediastinal hematoma. Also, evaluation of the mediastinum may be complicated by artifacts due to a nasogastric tube or to motion in patients who are restless and in pain. A paucity of mediastinal fat in younger patients may contribute further to problems with interpretation.

Finally, long-term radiographic follow-up, which may be a better indicator of overlooked traumatic aortic injury than clinical follow-up alone, was available in less than one half (27/63) of the patients in the series of Richardson et al.

In summary, at our level 1 trauma center, we continue to discourage the use of chest CT for suspected aortic injury. We concur with the conclusions presented by Miller et al. [2] in the largest series

published to date that "chest CT has no screening role in the evaluation of blunt trauma patients with possible major vascular injury." In this instance, CT may be fool's gold, and its glitter should not distract us from choosing the gold standard: thoracic angiography.

John S. Wills
James F. Lally
Medical Center of Delaware
Newark, DE 19718

REFERENCES

1. Richardson P, Mirvis SE, Scorpio R, Dunham CM. Value of CT in determining the need for angiography when findings of mediastinal hemorrhage on chest radiographs are equivocal. *AJR* 1991;156:273-279
2. Miller FB, Richardson JD, Thomas HA, Cryer HM, Willing SJ. Role of CT in diagnosis of major arterial injury after blunt thoracic trauma. *Surgery* 1989;106:596-603
3. Fenner MN, Fisher KS, Sergel NL, Porter DB, Metzmaker CO. Evaluation of possible traumatic thoracic aortic injury using aortography and CT. *Am Surg* 1990;56:497-499
4. Mirvis SE, Bidwell JK, Buddemeyer EU, et al. Value of chest radiography in excluding traumatic aortic rupture. *Radiology* 1987;163:487-493

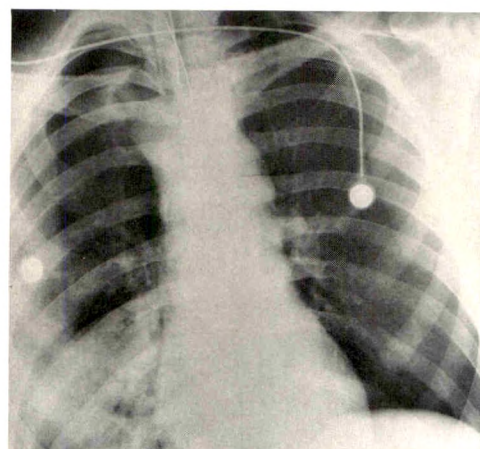
Reply

We appreciate the thoughtful comments of Drs. Wills and Lally. We share their genuine concern that CT might be applied inappropriately in evaluation of the thorax in patients with significant decelerating trauma and potential injury to the great vessel. In our article [1], we and our coauthors attempted to emphasize several caveats for the use of thoracic CT in this clinical setting.

First, when an institution has a large number of patients with blunt trauma who may have major arterial thoracic injury, the chest radiograph, specifically the appearance of the mediastinal contour, should be evaluated. As in all aspects of diagnostic imaging, the interpretation of the chest radiograph and evaluation of mediastinal anatomy depends on training and experience. Although some [2] advocate mandatory thoracic arteriography in all patients with a history of significant thoracic decelerating trauma, we think this is an impractical and unreasonably costly approach when a large number of such patients are treated at a given institution. In general, patients with normal mediastinal contours should not have further workup for thoracic vascular injury, unless indicated by clinical findings such as a significant pulse deficit. At the Maryland Shock-Trauma Center, 85-87% of patients with a history of blunt chest trauma are spared further workup on this basis.

Patients with obvious abnormality of the mediastinal contour, as shown by erect chest radiographs, should have prompt thoracic angiography. In our experience, one third to one fifth of these patients will have an injury of a great vessel, depending on whether the diagnosis of mediastinal hemorrhage is based on findings on the supine or the erect chest radiograph [3].

In several situations, the chest radiograph, supine or erect, may not show a sharply defined aortic contour without additional findings of mediastinal hematoma. Some of these situations include (1) patients with multisystem injury, particularly spinal fractures or pelvic ring disruption, for whom an erect chest radiograph is not safe; (2) patients in whom technically satisfactory chest radiographs cannot be acquired because of the patients' body habitus or lack of cooperation for the study; and (3) patients whose chest radiographs show a "near normal" mediastinum but who may have vascular ectasia, pulmonary contusion, aspiration, pleural effusion, or atelectasis that obliterates a portion of the mediastinal border and therefore does not permit an unequivocal interpretation of the mediastinum as normal.



A



B

Fig. 1.—Equivocal radiograph and CT scan of thoracic aortic rupture.

A, Admission erect chest radiograph of a young man who had fallen 30 ft (9 m) was initially interpreted as showing no evidence of mediastinal hemorrhage, but some concern about aortic arch region was raised.

B, Dynamic contrast-enhanced thoracic CT scan shows an intimal flap (solid arrow) and pseudoaneurysm (open arrows) of proximal descending aorta, which were confirmed immediately by arteriography.

Some may elect to perform thoracic arteriography on all patients who fall into these categories. However, our experience to date supports the use of dynamic contrast-enhanced CT as an ancillary screening procedure to detect mediastinal hemorrhage in these selected patients (CT was performed in 7% of our patients admitted because of blunt chest trauma [1]).

In our center, CT scanning is immediately available, which should be the case in all major trauma care facilities. In this circumstance, CT scanning usually is performed before arteriography for all trauma patients who require urgent CT evaluation, even when arteriography is indicated, simply because CT is generally available more rapidly. The dynamic thoracic CT study for detection of mediastinal hemorrhage requires less than 10 min and is almost always performed along with other required CT examinations. In circumstances in which our traumatologists think that the mechanism of injury indicates a high probability of thoracic arterial injury, angiography may be performed regardless of the appearance of the admission chest radiograph, although this has been distinctly rare.

As described in our article [1], we do not think that the experience of Miller et al. [4] significantly negates our recommendations about the appropriate use of CT. We think that excellent enhancement of the vascular structures of the mediastinum is needed to optimize the accuracy of interpretation. Equivocal CT studies, seen early in our experience, often were related to hand-injected and poorly timed boluses of contrast medium. Although direct visualization of a vascular injury is not required for a positive CT study, the presence of IV contrast medium may make this possible (Fig. 1) nonetheless. If the abdomen also is to be studied by CT, we do not give the patient another bolus of contrast medium but continue the scan dynamically through the abdomen with a continuous IV infusion. Parenchymal enhancement within the abdomen is not significantly degraded when

this protocol is used. In order to decrease the total dose of contrast medium administered, enhanced thoracic CT should be used only as an ancillary screening test for mediastinal hemorrhage, if intraarterial digital subtraction angiography is available, which requires less contrast material than conventional cut-film thoracic arteriography.

Our experience to date has shown that the proper selection of patients for contrast-enhanced dynamic CT to exclude mediastinal hemorrhage is safe, if used in the circumstances as described here, and will eliminate many unnecessary thoracic arteriograms. We strongly urge the use of immediate thoracic arteriography when the admission chest radiograph reveals evidence of mediastinal hemorrhage.

Stuart E. Mirvis
C. Michael Dunham
University of Maryland Medical Systems
Baltimore, MD 21201

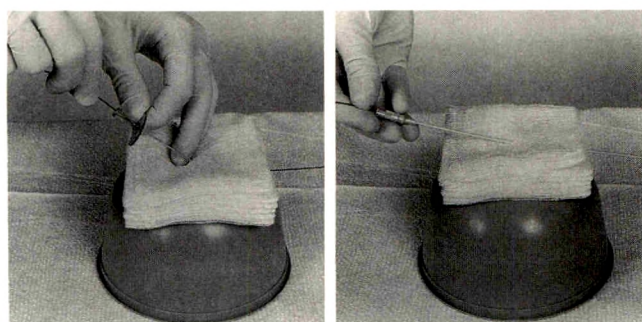
REFERENCES

1. Richardson P, Mirvis SE, Scorpio R, Dunham CM. Value of CT in determining the need for angiography when findings of mediastinal hemorrhage on chest radiographs are equivocal. *AJR* 1991;156:273-279
2. Jackson DH. Of TRAs and ROCs. *Chest* 1984;85:595-597
3. Mirvis SE, Bidwell JK, Buddemeyer, et al. Value of chest radiography in excluding aortic rupture. *Radiology* 1987;163:487-493
4. Miller FB, Richardson JD, Holis AT, Cujer HM, Willig SR. Role of CT in diagnosis of major arterial injury after blunt thoracic trauma. *Surgery* 1989;106:596-603

In Vitro Method for Teaching Percutaneous Vascular Catheterization

We describe a simple in vitro method for teaching residents how to perform percutaneous vascular catheterization and exchange over a guidewire.

A 2.5-cm stack of 4 × 4 in. (10.2 × 10.2 cm) gauze sponges is placed on an overturned plastic bowl. A Seldinger needle is introduced firmly into the middle of the stack at the proper angle and is inserted until the needle hits the bowl, which mimics the periosteum. The needle is withdrawn slowly, and a 15-mm J guidewire 0.038 in. (0.10 cm) in diameter is introduced through the needle in the standard fashion. The guidewire advances easily between the layers of the



A

B

Fig. 1.—In vitro method for teaching percutaneous vascular catheterization.

A, 15-mm J guidewire 0.038 in. (0.10 cm) in diameter passes easily through stack of 4 × 4 in. (10.2 × 10.2 cm) gauze sponges after stack is punctured with a Seldinger needle.

B, Exchanges over guidewire, such as placement of 6-French dilator shown here, can be practiced.

gauze stack and beyond (Fig. 1). Next, the needle is withdrawn while control of the guidewire and puncture site is maintained. Residents can practice exchanging dilators and catheters over the guidewire [1]. The gauze sponges remain stationary while allowing easy passage of wires, dilators, and catheters.

Manual dexterity and familiarity with basic angiographic techniques of percutaneous catheterization are essential to the successful performance of arteriograms. By using this simple method, residents can practice the Seldinger technique [1] and learn to exchange catheters before they perform an arteriogram. Although the tactile sensation of arterial puncture is not reproduced by this method, residents can practice exchanges and manipulations of guidewires and catheters.

David J. Eschelman
Alan J. Greenfield
Douglas T. Gibbens
Boston University Medical Center
Boston, MA 02118

REFERENCE

1. Seldinger SI. Catheter replacement of the needle in percutaneous angiography. *Acta Radiol* 1953;39:368-376

Subclavian Vein and Dialysis Access Planning

We read the article by Surratt et al. [1] with great interest. In our series [2], we had similar findings: a 50% prevalence of subclavian stenosis after temporary placement of a dialysis catheter in the subclavian vein. We think additional points should be made that were not in the paper of Surratt et al.

The length of time the subclavian vein is catheterized is important. In our series of 30 patients who had had catheterization of the subclavian vein and in whom 36 subclavian venograms were performed, the duration of catheterization was significantly longer ($p < .05$) in the group of patients with abnormal venograms (mean, 61 days; range, 13-180 days) than in the group with normal venograms (mean, 28 days; range, 8-60 days). The mere fact that the patient has had a catheter in the subclavian vein is not in itself a risk factor for stenosis, but the duration of placement of the catheter most certainly is. Surratt et al. make no reference to how long the subclavian veins that they studied had been catheterized.

It is also of interest that in our series, none of the six black patients studied had a normal venogram after catheterization of the subclavian vein, although this was not statistically significant. The two patients in whom clinical subclavian stenosis developed and on whom venography could not be performed (one patient was allergic to iodine, and the other had no peripheral veins for injection) also were black. This racial difference in the prevalence of subclavian stenosis has not been previously described and may explain the various prevalences of stenosis reported in previous studies [3, 4]. It would be interesting to know the ethnic origin of the patients studied in the series of Surratt et al. to see if any correlation exists between stenosis of the subclavian vein and ethnic origin.

We agree with the conclusions of Surratt et al. that the subclavian vein should be imaged by subclavian venography before placement of vascular access grafts in all patients who have a history of or have indwelling catheters in the subclavian vein and that the subclavian vein need not be imaged in asymptomatic patients who have never had lines in place in the subclavian vein.

Nigel K. Barrett
Edwina Brown
James McIvor
Charing Cross Hospital
London W6 8RF, England

REFERENCES

1. Surratt RS, Picus D, Hicks ME, Darcy MD, Kleinoffer M, Jendrisak M. The importance of preoperative evaluation of the subclavian vein in dialysis access planning. *AJR* 1991;156:623-625
2. Barrett NK, Spencer S, Brown E, McIvor J. Subclavian stenosis: a major complication of subclavian dialysis catheters. *Nephrol Dial Transplant* 1988;3:423-425
3. Venherwegher J-L, Yassine J, Goldman M, et al. Subclavian vein thrombosis: a frequent complication of subclavian vein cannulation for haemodialysis. *Clin Nephrol* 1986;26:235-238
4. Van Holder R, Lamiere N, Verhart J, et al. Complications of subclavian catheter haemodialysis: a 5 year prospective study in 25 patients. *Int J Artif Organs* 1982;5:297-303

Reply

We appreciate the letter of Barrett et al. Their comments on the length of time of catheterization and on possible racial differences are interesting. We did not match our patient populations with regard to race, so we cannot draw any conclusions about the effect of race on the prevalence of stenosis of the subclavian vein.

Although Barrett et al. put strong emphasis on the duration of catheter placement, they did note abnormal subclavian venograms in patients as few as 13 days after catheterization. Therefore, their data substantiate our fundamental recommendation: that imaging of the subclavian vein should be performed before dialysis access placement in all patients who have had catheterization of the subclavian vein.

Daniel Picus
Steve Surratt
Marshall Hicks
Michael Darcy
Mallinckrodt Institute of Radiology
Washington University School of Medicine
St. Louis, MO 63110

Outcome of Sonography for Deep Venous Thrombosis

In recent years, sonography has been replacing venography for the diagnosis of deep venous thrombosis in the lower extremity. This has led to the question of what effect this is having on patients. In a recent study [1] at Brown University, the outcomes of more than 1000 normal sonographic examinations were analyzed. My colleagues and I have just finished a similar study, although on a much smaller scale.

During the first 10 months (April 1988-January 1990) that we performed sonography for deep venous thrombosis, we completed 109 examinations on 103 patients. Eighteen of these patients also had venography. We saw a mixture of inpatients and outpatients at a tertiary-care Veterans Affairs medical center. Routine compression and augmentation of the femoral and popliteal veins were performed. All charts were reviewed, and 87 patients had follow-up—up to 2 years in some patients (average, 9 months).

No patient had complete heparinization for deep venous thrombosis or pulmonary embolism after normal findings on sonography. Twenty patients had abnormal sonograms, and only two did not receive heparin. Also, seven patients received heparin solely because of abnormal findings on sonography; no venography was performed.

The false-negative rate was 5.5%, from one patient with a clot in the calf that was not seen on sonography. No false-positive findings were observed on sonography in seven patients who also had venography. Almost 7% of sonograms were read as indeterminate.

These results support our use of sonography for the diagnosis of deep venous thrombosis in the lower extremity, as no negative outcome was seen in our population of patients. We will continue to use sonography as our primary examination and venography when the results of the first examination are indeterminate. The use of venography is becoming less frequent as we become more experienced with sonography.

James R. Grantham
Gainesville Veterans Affairs Medical Center
Gainesville, FL 32602

REFERENCE

1. Vaccaro JP, Cronan JJ, Dorfman GS. Outcome analysis of patients with normal compression on US examinations. *Radiology* 1990;175:645-649

Visualization of Meniscomemoral Ligaments on Coronal MR of the Knee

Singson et al. [1] recently described the appearance of bucket-handle tears of the medial meniscus and discussed the differentiation of low-signal-intensity structures in the intercondylar notch that might be mistaken for a displaced bucket-handle fragment. They maintain that the meniscomemoral ligament of Humphry should be considered in this process but state that it can be differentiated from a bucket-handle fragment by its relatively small size and its close relationship to the posterior cruciate ligament. Furthermore, they state that the ligament of Humphry "is never seen in the coronal plane." We disagree with this statement. We have seen coronal MR images of both the meniscomemoral ligaments of Humphry and Wrisberg in the literature [2, 3] and at the view box. Although visualization of an entire meniscomemoral ligament on a single coronal image is not common, the appearance of this structure is distinctive and should be recognized and differentiated from a bucket-handle fragment or loose body on either sagittal or coronal images (Fig. 1).

Russell C. Fritz
Clyde A. Helms
University of California, San Francisco
San Francisco, CA 94143

REFERENCES

1. Singson RD, Feldman F, Staron R, Kiernan H. MR imaging of displaced bucket-handle tear of the medial meniscus. *AJR* 1991;156:121-124
2. Watanabe AT, Carter BC, Teitelbaum GP, Seeger LL, Bradley WG Jr. Normal variation in MR imaging of the knee: appearance and frequency.

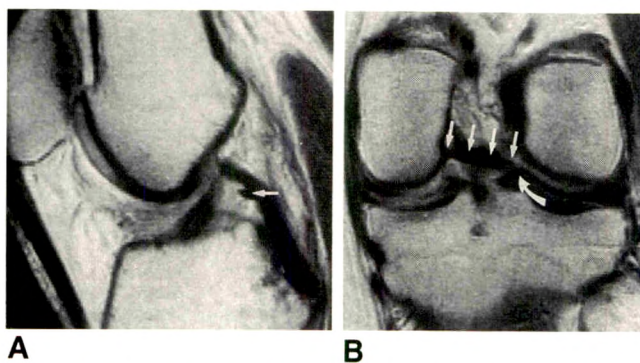


Fig. 1.—A and B, Sagittal (A) and coronal (B) T1-weighted MR images show course of meniscomemoral ligament of Humphry (straight arrows) arising from medial aspect of intercondylar notch and extending to posteromedial aspect of lateral meniscus (curved arrow).

AJR 1989;153:341-344

- Watanabe AT, Carter BC, Teitelbaum GP, Bradley WG Jr. Common pitfalls in magnetic resonance imaging of the knee. *J Bone Joint Surg [Am]* 1989;71-A:857-862

Reply

We thank Drs. Fritz and Helms for their comment and this opportunity to clarify the statement in our recent article [1] that the ligament of Humphry is never seen in the coronal plane. Our statement should have read, "We have not seen it in its entirety on a single coronal section in our material." As indicated, the ligament may be difficult to visualize on a single coronal image because of its obliquity and its thin diameter. It may therefore have a blunted or ovoid appearance. Tracing it in sequential coronal sections and checking with the sagittal view will lead to positive identification.

Conversely, as we noted, a bucket-handle fragment or loose body cannot be traced as a linear low-signal band on the coronal plane and therefore can be distinguished from the ligament of Humphry. In the articles [2, 3] cited by Fritz and Helms, only the ligament of Wrisberg is illustrated on coronal view.

Rolando D. Singson
St. Luke's/Roosevelt Hospital Center
New York, NY 10019
Frieda Feldman
Ronald Staron
Howard Kiernan
Columbia-Presbyterian Medical Center
New York, NY 10032

REFERENCES

- Singson RD, Feldman F, Staron R, Kiernan H. MR imaging of displaced bucket-handle tear of the medial meniscus. *AJR* 1991;156:121-124
- Watanabe AT, Carter BC, Teitelbaum GP, Seeger LL, Bradley WG Jr. Normal variation in MR imaging of the knee: appearance and frequency. *AJR* 1989;153:341-344
- Watanabe AT, Carter BC, Teitelbaum GP, Bradley WG Jr. Common pitfalls in magnetic resonance imaging of the knee. *J Bone Joint Surg [Am]* 1989;71-A:857-862

Cervical Spondylolysis

We read with interest the article by Forsberg et al. [1] on 12 cases of cervical spondylolysis. We would like to report another case, not mentioned by these authors, and to specify certain points.

A 26-year-old man was seen for neck pain, which had started 3 years earlier, after minor trauma. The pain was associated with bilateral brachialgia in the C8 and T1 dermatomes without neurologic deficit. Conservative treatment (cervical collar, nonsteroidal antiinflammatory drugs, physical therapy) was ineffective. Physical examination showed no limitation of movement of the cervical spine and no neurologic deficit. On conventional radiographs, frontal views showed a hypoplastic bilateral articular mass and spina bifida of the sixth cervical vertebra, and lateral views showed spondylolisthesis of C6 on C7 of 3 mm, hypoplastic spinous process, and pedicles of the sixth cervical vertebra (Fig. 1A). These abnormalities had also been present on radiographs obtained 3 years before. Dynamic radiographs showed a flexion angle of C6 on C7 of 22° (normal, 12-25°) and a restricted flexion of C5 on C6 (angle, 12°; normal, 16-29°). CT showed dysplastic changes: hypoplasia of the pedicles and lamina of the sixth cervical vertebra, spina bifida, and absence of closure of the left transverse canal (Fig. 1B). The diagnosis was congenital cervical spondylolisthesis. Because of the potential instability, the

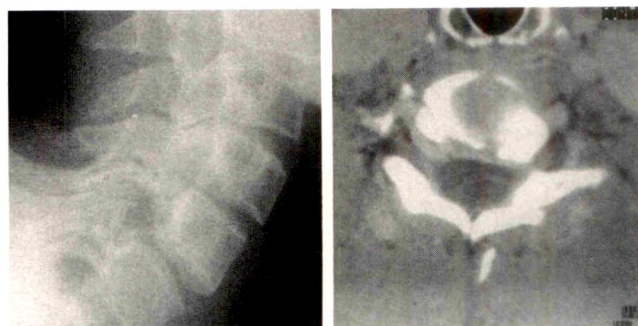


Fig. 1.—Cervical spondylolysis in a 26-year-old man.
A, Lateral radiograph of cervical spine shows spondylolisthesis of C6 on C7, hypoplastic spinous process, and pedicles of sixth cervical vertebra.
B, CT scan of C6 shows hypoplasia of pedicles and lamina of C6, spina bifida, and absence of closure of left transverse canal.

patient had anterior fusion of C5-C6 and C6-C7. On follow-up examination 3 months later, the movement of his neck was full and painless, and he had no pain or other symptoms.

We agree with Forsberg et al. [1] on several points, as noted in our review [2] of the literature in 1988 (33 cases): the preponderance of involvement of C6 (76%); age range of patients 5 to 60 years, with a mean of 32 years and 12 patients less than 20 years old; the preponderance of men (75%); a history of previous minor trauma (8/33); the rarity of neurologic signs and symptoms (3/33); a mild anterolisthesis less than 3 mm; and dysplastic changes on radiographs. The treatment is conservative (nonsteroidal antiinflammatory drugs, cervical collar, physical therapy) if no instability is seen on dynamic radiographs [3]. If conservative treatment is ineffective or if spinal instability occurs, then surgical treatment should be considered. Anterior fusion is the best method, and the course is favorable in all operative cases.

Awareness of congenital cervical spondylolisthesis will help prevent inappropriate explorations and treatment.

Philippe Goupille
Bernard Fouquet
Philippe Cotty
Jean-Pierre Valat
C. H. U. Trousseau
37044 Tours, France

REFERENCES

- Forsberg DA, Martinez S, Vogler JB III, Wiener MD. Cervical spondylolysis: imaging findings in 12 patients. *AJR* 1990;154:751-755
- Goupille P, Fouquet B, Asquier P, et al. Spondylolisthésis cervical de nature congénitale: a propos d'un cas, revue de la littérature. *Rev Rhum Mal Osteoartic* 1988;55:611-614
- Niemeyer T, Penning L. Functional roentgenographic examination in a case of cervical spondylolisthesis. *J Bone Joint Surg [Am]* 1963;45-A:1671-1678

Reply

We and our coauthors appreciate the report of an additional case of cervical spondylolysis illustrated by Goupille et al. We agree that increased awareness of the entity will help in the appropriate treatment of these patients. It is important to reiterate that most of these patients require only conservative therapy. If dynamic radiographs of the cervical spine show instability, then fusion is certainly warranted.

The most interesting case we found in the literature was that of a patient with bilateral pars interarticularis defects at C3–C5 who required surgical fusion because of instability [1].

Salutario Martinez
David Forsberg
Duke University Medical Center
Durham, NC 27705

REFERENCE

1. Prioleau GR, Wilson CB. Cervical spondylolysis with spondylolisthesis. *J Neurosurg* 1975;43:750–753

MR Imaging of the Knee in Rheumatoid Arthritis and Other Rheumatic Diseases

The article by Björkengren et al. [1] reported MR imaging of the knee in acute rheumatoid arthritis. Their results suggest that gadolinium–tetra-azacyclododecane tetraacetic acid (Gd-DOTA) is taken up by inflamed synovium and that Gd-DOTA-enhanced MR images can be useful in detecting acute synovitis in patients with rheumatoid arthritis.

Recently, we reported a study [2] of MR imaging of the knee in 10 patients with rheumatoid arthritis or psoriatic arthritis and two patients with osteoarthritis. All 12 patients had symptoms of inflammation of the knee. We performed MR before and after IV administration of Gd-DOTA. Then, each patient had classic arthrography. Our results confirmed that synovial hypertrophy with acute inflammation is responsible for high-intensity signal after injection of Gd-DOTA. This finding seems to be nonspecific for inflammatory involvement such as that seen in rheumatoid arthritis or other inflammatory rheumatic diseases. The same finding is seen on MR images of osteoarthritis (Fig. 1). Otherwise, synovial hypertrophy and joint effusion, especially in palpable joints like the knee, are clinical findings, and it would be excessive to suggest that MR imaging can be helpful in current rheumatology or therapeutic indications. However, in three patients, MR imaging showed small osteochondral ulcerations not seen on plain radiographs or arthrograms. Other studies are needed to confirm if MR imaging of the knee is helpful before surgical therapy.

Marc Pages
Claude Poey
Slim Lassoued
Bernard Fournie
Jean-Jacques Railhac
C. H. U. Purpan
31059 Toulouse, France

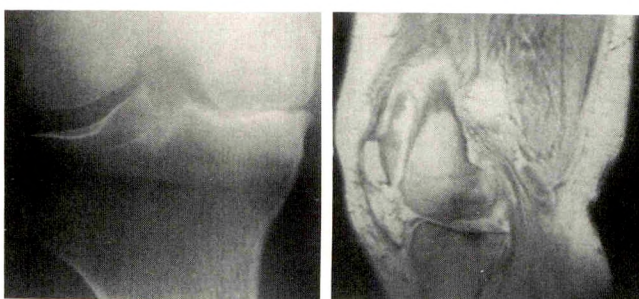


Fig. 1.—MR imaging of osteoarthritis of knee.
A, Tunnel view shows osteoarthritis of internal compartment.
B, Gadolinium-enhanced T1-weighted image shows high-intensity signal in synovium with low-intensity signal in joint effusion and area of low intensity in femoral condyle.

REFERENCES

1. Björkengren AG, Geborek P, Rydholm U, Holtås S, Petterson H. MR imaging of the knee in acute rheumatoid arthritis: synovial uptake of gadolinium-DOTA. *AJR* 1990;155:329–332
2. Sixou L, Poey C, Assoun J, et al. Imagerie par résonance magnétique avec injection de gadolinium dans les rhumatismes inflammatoires chroniques. *Rev Rhum Mal Osteoartic* 1990;57:722(E 43)

Vascular Erosion of a Cervical Neural Foramen: Diagnosis with MR Angiography

A 42-year-old woman complained of pain radiating to the left middle finger, paresthesia in both hands, and a sensibility disorder of the left upper extremity. Radiographs of the cervical spine showed a sharply margined widening of the right C4–C5 neural foramen, with erosion of the C4 vertebral body extending anteriorly and superiorly (Fig. 1A). MR angiography was performed because the plain film findings were more suggestive of a vascular erosion than of a neurinoma. A fast imaging by steady-state precession (FISP) sequence was used with a repetition time of 40 msec, a flip angle of 20°, and an echo time of 10 msec. The unit used was a superconductive 1.5-T magnetome. In the vicinity of the broadened neural foramen, we detected a tortuous right vertebral artery coiling medially and anteriorly at the intervertebral C4–C5 level (Fig. 1B).

Arterial expansion or lengthening can cause erosion of the posterolateral aspects of the vertebral bodies [1]. Most patients with this abnormality are asymptomatic, and vascular erosion of a cervical neural foramen may be regarded as a normal variant. Postmortem studies [2] found that the fourth cervical vertebra seems to be eroded most often, preferentially on the left side. The anomaly is more common in women. Usually the tortuous loop of the vertebral artery extends medially, anteriorly, and slightly superiorly. The neural foramen is then eroded in the anterior-superior direction. MR angiography in the sagittal and/or coronal plane provides sufficient detail to diagnose the tortuous malformation of the vertebral artery.

Plain film radiographs of an erosion with a smooth contour and a slightly sclerotic margin involving the posterolateral aspect of a cervical vertebral body should suggest a vascular cause. Cervical vertebral erosion has been shown in several cases to be caused by tortuosity of the vertebral artery. Our case is interesting for two reasons. First, this is an example of a normal vascular variant that can mimic disease, that is, enlargement of the neural foramen. Second, MR angiography is valuable as a noninvasive technique to

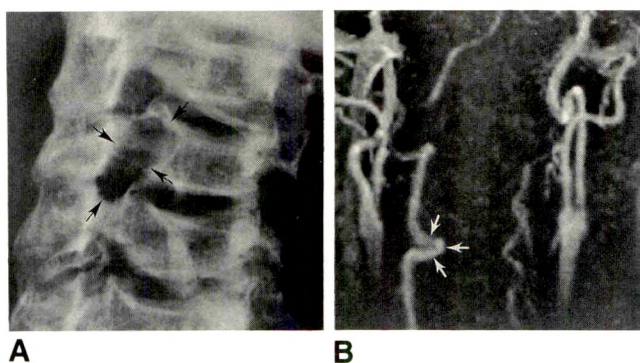


Fig. 1.—Vascular erosion of cervical neuralforamen.
A, Left oblique radiograph of cervical spine shows erosion of posterolateral surface and part of pedicle of C4 (arrows).
B, Sagittal MR angiographic image shows medially and anteriorly deviated (arrows) tortuous right vertebral artery.

delineate tortuosity of the vertebral artery. This letter shows that the invasive techniques of angiography and cervical myelography are no longer necessary to determine the cause of this type of cervical vertebral erosion.

Luc van Fraeyenhoven
Michael Baeyaert
University Hospitals
B-3000 Leuven, Belgium
Christopher Sweet
Marnix van Holsbeeck
Henry Ford Hospital
Detroit, MI 48202-2689

REFERENCES

1. Slover WP, Kiley RF. Cervical vertebral erosion caused by tortuous vertebral artery. *Radiology* 1965;84:112-114
2. Zimmerman HB, Farell WJ. Cervical erosion caused by vertebral artery tortuosity. *AJR* 1970;108:767-770

Focal High Signal on MR Images of the Midbrain

We read with great interest the article [1] in which Elster and Richardson correlate the MR and histologic findings of focal high signal on MR images of the midbrain. However, we have some comments:

First, the authors do not present or mention proton density-weighted images. In a differential diagnosis that includes enlargement of the perivascular spaces and lacunar lesions of the brain, proton density-weighted images are helpful. Both conditions cause hyperintense signals on T2-weighted images. Enlarged perivascular spaces have isointense signals similar to those of brain on proton density-weighted images [2], whereas lacunar infarcts remain hyperintense.

Second, the CSF-filled perivascular spaces (of Virchow-Robin) normally surround, to a variable extent, the perforating arteries that enter the medial temporal lobe, basal ganglia, and thalamus. The spaces often have areas of relative dilatation in contrast to the tapering blood vessel inside [3]. Some authors [4] consider perivascular spaces around perforating arteries a type of lacunae. In the area of the midbrain presented [1], it is difficult to correlate the linear foci seen on the MR images with the gross anatomic direction of the perivascular spaces accompanying the perforating branches of the collicular and accessory collicular arteries: They are perpendicular (as shown in Fig. 3 in [1]). Perhaps the punctuate and circular high-signal foci are due to enlargement of the perivascular space, but the linear hyperintense focus may not even be due to "slowly flowing blood in satellite veins," as the satellite veins also would be perpendicular to the longitudinal axis of the linear focus.

H. D. Tran-Dinh
Y. S. Soo

Cumberland College of Health Sciences, University of Sydney
Lidcombe NSW 2141, Australia

REFERENCES

1. Elster AD, Richardson DN. Focal high signal on MR scans of the midbrain caused by enlarged perivascular spaces: MR-pathologic correlation. *AJNR* 1990;11:1119-1122, *AJR* 1991;156:157-160
2. Kucharczyk W. *MR: central nervous system*. Philadelphia: Lippincott, 1990:1.40-1.41
3. Jungreis CA, Kanal E, Hirsch WL, Martinez AJ, Moosy J. Normal perivascular spaces mimicking lacunar infarction: MR imaging. *Radiology* 1988;169:101-105
4. Benhaïem-Sigaux AM, Gray F, Gherardi R, Roucayol AM, Poirier J. Expanding cerebellar lacunae due to dilatation of the perivascular space associated with Binswanger's subcortical arteriosclerotic encephalopathy. *Stroke* 1987;19:1087-1092

Reply

My coauthors and I thank Drs. Tran-Dinh and Soo for their comments on our recent article [1]. The signal intensity of the midbrain perivascular spaces we have described follows that noted in perivascular spaces elsewhere, remaining approximately isointense to CSF on all sequences. On proton density-weighted images, the contrast between brain and CSF is relatively poor, and consequently these perivascular spaces are poorly visualized. Although we obtained proton density-weighted images in all our patients, we did not publish any of these images in our article because the relevant structures are so difficult to see. To satisfy skeptics, we now submit a typical example (Fig. 1).

We appreciate the readers' difficulty in correlating the anatomic course and radiologic appearance of these vessels. The collicular arteries are indeed generally linear in course and lie in a plane approximately perpendicular to the main axis of the midbrain. However, routine transverse and coronal MR imaging planes are usually angulated 30°-50° relative to the anatomic axis of the midbrain. In the imaging frame of reference, therefore, the collicular vessels typically course obliquely through two or more slices. They are thus visualized segmentally as dots, ovals, and short arcs rather than as long straight lines as the anatomic drawing would suggest.

Allen D. Elster
Bowman Gray School of Medicine
Winston-Salem, NC

REFERENCE

1. Elster AD, Richardson DN. Focal high signal on MR scans of the midbrain caused by enlarged perivascular spaces: MR-pathologic correlation. *AJNR* 1990;11:1119-1122, *AJR* 1991;156:157-160

Disappearance of the Basivertebral Vein: A New MR Imaging Sign of Bone Marrow Disease

A 10-year-old child with osteosarcoma of the left femur had resection of the distal femur and rotation plasty. Six months later, paralysis of both legs and disturbances in micturition developed. In order to evaluate the cause of compressive myelopathy, bone scanning with technetium-99m methylene diphosphonate and MR of the spine were performed. The bone scan showed a normal accumulation of the radionuclide in the skeleton and did not show hot spots suggestive of spinal metastases. MR imaging performed the same day as the

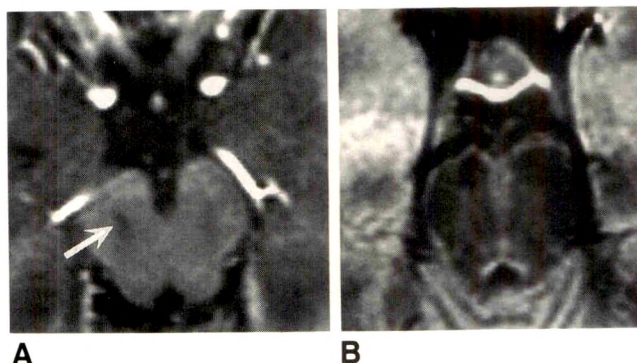


Fig. 1.—Signal intensity of midbrain perivascular spaces.
A, T1-weighted enhanced MR image through midbrain of a 34-year-old patient with no evidence of midbrain symptoms or cerebrovascular disease shows unilateral nonenhancing enlarged perivascular space (arrow) in its characteristic location.
B, On spin-density MR image (2800/30), structure is difficult to see because it is essentially isointense to CSF.

bone scan showed a large epidural metastasis compressing the distal part of the spinal cord. The bone marrow of L1 showed a subtle decreased signal intensity on T1-weighted (500/30 [TR/TE]) MR images (Fig. 1A) and a slightly increased signal intensity on T2-weighted (2000/100) images (Fig. 1B). In addition, the outline of the basivertebral vein in L1 was absent on both T1- and T2-weighted images. The basivertebral veins in the remaining vertebral bodies were clearly visible.

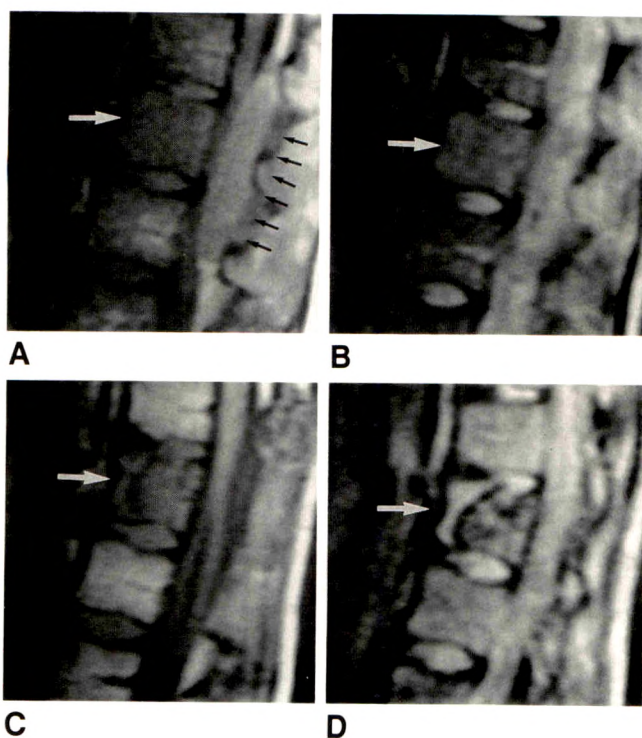


Fig. 1.—Disappearance of basivertebral vein in bone marrow disease. A and B, T1-weighted (500/30, A) and T2-weighted (2000/100, B) pre-operative MR images of spine show large epidural metastasis causing compressive myelopathy (black arrows, A). T1-weighted image (A) shows subtle loss of signal of bone marrow in L1, and T2-weighted image (B) shows slightly increased signal intensity. Note striking loss of outline of basivertebral vein in L1 (white arrows) on both A and B. Central bone marrow fat shows subtle loss of normal high signal intensity on A. C and D, Follow-up T1-weighted (500/30, C) and T2-weighted (2000/100, D) postoperative MR images show laminectomy at T12–L2 and loss of height of L1 vertebral body (arrows). Bone marrow in L1 has markedly decreased signal intensity on T1-weighted image (C) and marked high signal intensity on T2-weighted image (D). Findings are consistent with progressive metastatic disease.

After decompressive laminectomy at T12–L2, follow-up MR imaging showed a marked decrease in signal intensity on T1-weighted (500/30) images (Fig. 1C) and a marked increase in signal intensity on T2-weighted (2000/100) images (Fig. 1D). These images also showed a loss of height of the vertebral body L1. The results of a bone biopsy at L1 showed metastatic tumor.

In this case, MR imaging showed bone marrow invasion at a time that bone scintigraphy did not. The high sensitivity of MR imaging compared with bone scintigraphy in the detection of bone marrow metastases is well known [1, 2]. In our case, the loss of visibility of the basivertebral vein in the affected vertebral body is far more conspicuous than the subtle loss of normal signal intensity of the bone marrow.

On T1-weighted images, the normal basivertebral vein is a distinctive linear or triangular low-signal-intensity structure outlined by central bone marrow fat. The central bone marrow fat in our case was infiltrated by metastatic tumor, which diminished the outline of the basivertebral vein. T2-weighted images show the normal basivertebral vein as a structure of high signal intensity. The loss of normal outline of the basivertebral vein on T2-weighted images in our case might have been caused by clogging up of this venous structure by metastatic tumor.

Because the basivertebral vein has close connections with the valveless internal vertebral plexuses and intervertebral veins [3], it can serve as an entry site for hematogeneous spread of tumor. Experimental studies have shown that the blood flow in these valveless veins can be reversed [4]. This explains how neoplasms draining on these veins may lead to metastases in vertebral bodies.

Visibility of basivertebral veins can be inconsistent in healthy control subjects. However, when the basivertebral vein in one of the vertebral bodies is not visualized on MR imaging, but the basivertebral veins in the remaining vertebral bodies are visualized, we suggest that bone marrow disease such as metastases should be considered.

Paul R. Algra
Free University Hospital Amsterdam
Amsterdam, the Netherlands
Johannes L. Bloem
University Hospital Leiden
Leiden, the Netherlands
Jaap Valk
Free University Hospital Amsterdam
Amsterdam, the Netherlands

REFERENCES

1. Daffner RH, Lupetin AR, Dash N, Deeb ZL, Sefczek RJ, Schapiro RL. MRI in the detection of malignant infiltration of bone marrow. *AJR* 1986;146:353–358
2. Frank JA, Ling A, Patronas NJ, et al. Detection of malignant bone tumors: MR imaging vs scintigraphy. *AJR* 1990;155:1043–1048
3. Batson OV. The function of the vertebral veins and their role in the spread of metastases. *Ann Surg* 1940;112:138–149
4. Batson OV. The vertebral vein system. *AJR* 1957;78:195–212

Letters are published at the discretion of the Editor and are subject to editing.

Letters to the Editor must not be more than two double-spaced, typewritten pages. One or two figures may be included. Abbreviations should not be used. Limit the number of authors to four, or we will list only the first three and add "and colleagues" to the end of the list. See Authors Guidelines, page A5.

Material being submitted or published elsewhere should not be duplicated in letters, and authors of letters must disclose financial associations or other possible conflicts of interest.

Letters concerning a paper published in the *AJR* will be sent to the authors of the paper for a reply to be published in the same issue. Opinions expressed in the Letters to Editor do not necessarily reflect the opinions of the Editor.

Review of Current Literature

Initials and addresses of corresponding authors are provided in parentheses for each article so that the reader can obtain reprints directly. Abstracts are printed verbatim from each journal.

The New England Journal of Medicine

Prophylactic sclerotherapy for esophageal varices in men with alcoholic liver disease: a randomized, single-blind, multicenter clinical trial. The Veterans Affairs Cooperative Variceal Sclerotherapy Group (Gregory PB, Office of the Vice President and Dean, School of Medicine, Rm. M-121, Stanford University Medical Center, Stanford, CA 94305-5302). *N Engl J Med* 324:1779-1784, 1991

Background. Sclerotherapy is an effective treatment for bleeding esophageal varices in patients with alcoholic liver disease. It has also been suggested that sclerotherapy might be effective in preventing initial episodes of bleeding and improving survival among such patients.

Methods. We conducted a prospective, randomized trial comparing prophylactic sclerotherapy and sham therapy in 281 men with alcoholic liver disease who had at least three variceal channels and no history of variceal bleeding. All the patients underwent endoscopy; 143 received sclerotherapy, and 138 received sham therapy.

Results. The two patient groups were well matched at entry with respect to the extent of liver disease and other clinical indexes, except that other medical illnesses were significantly more common in the sclerotherapy group. The study's data-monitoring board terminated the trial 22.5 months after it began because the rate of mortality from all causes was significantly higher in the sclerotherapy group (32.2 percent) than in the sham-therapy group (17.4 percent, $P = 0.004$), despite the fact that the men who received sclerotherapy had significantly fewer episodes of esophageal variceal bleeding. The causes of death varied, and there is no obvious explanation for the excess mortality in the sclerotherapy group. After the termination of treatment, the excess mortality rate in the sclerotherapy group promptly declined. There were 53 episodes of upper gastrointestinal bleeding (including 10 from esophageal varices and 9 from esophageal ulcers) in the sclerotherapy group and 40 episodes (including 19 from esophageal varices) in the sham-therapy group. Complications of sclerotherapy were frequent but seldom life-threatening.

Conclusions. For unknown reasons, prophylactic sclerotherapy is associated with increased mortality among men with moderate-to-severe alcoholic liver disease and esophageal varices. Sclerotherapy should not be performed until after an initial episode of bleeding from esophageal varices has occurred.

Chest

Expiratory computed tomography for assessment of suspected pulmonary emphysema. Knudson RJ, Standen JR, Kaltenborn WT,

et al. (RJK, Division of Respiratory Sciences, University of Arizona College of Medicine, Tucson, AZ 85724). *Chest* 99(6):1357-1366, June 1991

Results of computed tomography of the lung performed at two levels in upper lung zones at full inspiration and full expiration were compared with results of tests of ventilatory function, lung mechanics, and single breath carbon monoxide diffusing capacity in 64 subjects, many of whom had some form of airflow obstruction. From the CT scans, the mean percentage of pixels in the range -900 to -1,024 Hounsfield units, or pixel index, was determined for each subject. The highest correlations of pixel index with physiologic variables consistent with a diagnosis of emphysema were observed for CT taken at full expiration. In some subjects, the inspiratory CT would give a "false positive" for emphysema when the hyperaeration observed at inspiration was not observed at expiration. We believe that the CT scan taken at full expiration can effectively reveal the abnormal permanent enlargement of airspaces which defines emphysema and provides a noninvasive method of assessing lung morphology in the living human subject.

Spontaneous pneumomediastinum: a report of 25 cases. Abolnik I, Lossos IS, Breuer R (IA, Pulmonary Unit, Hadassah University Hospital, Hebrew University, Jerusalem, Israel). *Chest* 100(1):93-95, July 1991

Spontaneous pneumomediastinum (SPM) is a relatively uncommon, infrequently reported entity. To determine the clinical presentation and sequelae of SPM, data were obtained from 25 patients: 14 from Hadassah University Hospital, and 11 from other medical institutions. The mean age was 18.5 ± 5.2 years (\pm SD), with a range of 8 to 31 years. The most common presenting complaint was retrosternal pain in 22 patients (88 percent), dyspnea in 15 (60 percent), dysphagia in 10 (40 percent), and weakness in 10 (40 percent). Predisposing factors for the development of SPM could be identified in 18 patients (72 percent). Information on the sequelae of SPM during a mean period of 87.4 ± 38.0 months following the initial SPM episode was obtained from 23 patients. Recurrent SPM occurred in 1 patient at 18 months, and another patient experienced 4 episodes of recurrent spontaneous pneumothorax. No other long-term sequelae were reported. We conclude that SPM is a benign self-limited disease with diverse clinical manifestations. Although uncommon, recurrences of SPM may be observed.

Circulation

Histopathologic validation of angioscopy and intravascular ultrasound. Siegel RJ, Ariani M, Fishbein MC, et al. (RJS, Cedars-Sinai Medical Center, 8700 Beverly Blvd., Cardiology, Rm. 5314, Los Angeles, CA 90048-0750). *Circulation* 84:109-117, 1991

Background. To establish a histopathologic basis for angioscopic and ultrasound image interpretation we studied 70 postmortem human arterial segments in vitro.

Methods and Results. We used 7- to 9-French fiber-optic angioscopes and 20- to 30-MHz intravascular ultrasound imaging catheters. Three observers assigned an angioscopic and ultrasound image classification to each vessel segment. The image and histological classification categories were then compared. The sensitivity, specificity, and accuracy of both methods separately or in combination for normal vessels were each greater than or equal to 95%. The predictive value was better for angioscopy than for ultrasound due to incorrect ultrasound interpretations of normal anatomy in the presence of thrombus. For stable atheroma the sensitivity, specificity, and accuracy of the individual methods were each greater than 90%. However, both angioscopy and ultrasound had classification errors in that disrupted atheroma was identified and classified as stable atheroma. Consequently, the predictive value was 74% for angioscopy and 78% for ultrasound. For disrupted atheroma the sensitivities for angioscopy and ultrasound were only moderate (73% and 81%, respectively), whereas the specificity, accuracy, and predictive value were each high (greater than 90%). For thrombus detection, the specificity, accuracy, and predictive value were high (greater than 93%) for each method. The sensitivity of angioscopy was 100%. However, sensitivity was lower for ultrasound (57%) due to false-negative interpretation of laminar clots in normal vessels and an inability to distinguish disrupted or stable atheroma from intraluminal thrombus.

Conclusions. Contingency analyses showed that each imaging method alone or combined had significant agreement with the results obtained from histology ($p < 0.001$). When assessing all cases in which angioscopy and ultrasound were concordant, there was a 92% agreement with the histological classification.

Gastroenterology

Abnormal esophageal motility: an analysis of concurrent radiographic and manometric findings. Massey BT, Dodds WJ, Hogan WJ, Brasseur JG, Helm JF (BTM, Dept. of Medicine, Medical College of Wisconsin, Milwaukee, WI). *Gastroenterology* 101:344-354, 1991

The findings of concurrent esophageal videofluoroscopy and manometry in 15 patients with major disturbances of esophageal motor function were evaluated and the data were analyzed from a fluid mechanical perspective. Each of 153 fluoroscopic barium swallow sequences was analyzed on a swallow-by-swallow basis. Two distinct pressure domains were identified: intrabolus pressure and pressure within a bolus-free contracting esophageal segment. Analyses in terms of these pressure domains showed specific and consistent correlations between the radiographic and manometric findings. Radiography was insensitive to contractions occurring in esophageal segments devoid of bolus fluid, whereas manometry was insensitive to contractions that did not occlude the lumen. It is concluded that using fluid mechanical principles of bolus transport allows meaningful comparison of esophageal motility as recorded by radiography and intraluminal manometry. However, the inherent limitations in the range of physical phenomena recorded by each modality make these techniques complementary for evaluating esophageal motor function.

Reprinted with permission by the American Gastroenterological Association.

Digestive Diseases and Sciences

Lithotripsy versus cholecystectomy for management of gallstones: a decision analysis by Markov process. Sonnenberg A, Derfus GA, Soergel KH (AS, VA Medical Center, 111-C, Milwaukee, WI). *Dig Dis Sci* 36(7):949-956, July 1991

Extracorporeal shock-wave lithotripsy is a new treatment method that effectively disintegrates radiolucent gallstones and is associated with a low complication rate. Using the model of a Markov process for decision analysis, survival and costs under four possible strategies to treat gallstones were compared: expectant management with

cholecystectomy (EC) or lithotripsy (EL) reserved for symptomatic gallstones; prophylactic cholecystectomy (PC) or lithotripsy (PL) for all gallstones. Life expectancy for the different strategies varies by a few days. Only if high annual rates of pain and complication occurred in subjects with silent gallstones would both prophylactic procedures marginally increase life expectancy. Prophylactic cholecystectomy then would be more cost-effective than prophylactic lithotripsy. Expectant strategies remain much cheaper than prophylactic management over a broad range of probability values and procedural costs. Expectant use of lithotripsy costs less than cholecystectomy. A low success rate of lithotripsy would raise the direct costs of lithotripsy above those of cholecystectomy but leave total costs of both strategies in the same order of magnitude. Lithotripsy appears to be a feasible alternative to treat symptomatic but not asymptomatic gallstones.

The Journal of Bone and Joint Surgery

Evaluation of the painful shoulder: a prospective comparison of magnetic resonance imaging, computerized tomographic arthrography, ultrasonography, and operative findings. Nelson MC, Leather GP, Nirschl RP, Pettrone FA, Freedman MT (MCN, Georgetown University Medical Center, 3800 Reservoir Rd. N.W., Washington, DC 20007-2197). *J Bone Joint Surg [AM]* 73-A(5):707-716, June 1991

Twenty-one patients who had had pain in the shoulder for more than three months were evaluated with ultrasonography and magnetic resonance imaging followed by computerized tomographic arthrography. The results of the imaging studies were then compared with the operative findings. Magnetic resonance imaging was found to be the most useful modality for establishment of the etiology of pain in the shoulder due to disease of the rotator cuff, instability associated with abnormality of the glenoid labrum, subacromial impingement, stenosis of the coracoacromial arch, and osteoarthritis of either the glenohumeral or the acromioclavicular joint.

The accuracy of magnetic resonance imaging was found to depend on both the operator and the technique and was decreased in extremely obese patients, due to difficulties in positioning, and in patients who had had a previous operation. Magnetic resonance imaging was more accurate than either computerized tomographic arthrography or ultrasonography in identifying partial-thickness tears (intrasubstance changes in the rotator cuff). Magnetic resonance imaging provided the same level of accuracy as computerized tomographic arthrography in the detection of abnormalities of the glenoid labrum.

Clinical Orthopaedics and Related Research

Nonunion and pseudarthrosis of fracture healing: a histopathologic study of 95 human specimens. Milgram JW (JWM, Northwestern University Medical School, 303 E. Chicago Ave., Chicago, IL 60611). *Clin Orthop* 267:203-213, July 1991

Forty-one human tissue specimens from fracture nonunions in extraarticular locations demonstrated a spectrum of clefts at the site of nonunion ranging from tiny microscopic spaces within the soft tissue of the nonunion to dominant clefts that completely separated the ends of the fracture. These latter specimens were examples of frank pseudarthrosis. The soft tissues lining the large clefts were often considerably eroded. Pseudarthrosis of fracture healing may be a late manifestation of more mobile nonunions that progressively tear apart. Fifty-four additional nonunion or pseudarthrosis specimens from former intraarticular fractures demonstrated the same sequence of changes occurring in 24 of the cases. However, 30 of the intraarticular fractures demonstrated no tissues of a fibrous nonunion, which could indicate that in such locations pseudarthrosis may exist from the date of the original fracture.

The Journal of Urology

Efficacy of transrectal ultrasound for identification of clinically undetected prostate cancer. Terris MK, Freiha FS, McNeal JE,

Stamey TA (Dept. of Urology (S287), Stanford University Medical Center, 300 Pasteur Dr., Stanford, CA 94305-5118). *J Urol* 146:78-84, July 1991

A total of 51 patients underwent transrectal ultrasound of the prostate before radical cystoprostatectomy for transitional cell carcinoma of the bladder. Each had a normal prostate by digital rectal examination, no history of prostatic adenocarcinoma and no invasion of the prostate by transitional cell carcinoma. Real-time and step-sectioned ultrasound images were interpreted at the time of sonography and results were compared to pathological examination of the step-sectioned prostate specimen. When adenocarcinoma was identified in the specimen, cancer volume was determined. Positive ultrasound scans consisted of those exhibiting hypoechoic lesions. Hypoechoogenicity due to transurethral resection defects, benign hyperplasia, vascular structures or shadowing from calcifications was not considered positive. Of 51 patients 27 (52.9%) exhibited no abnormality on ultrasound and were free of cancer in the prostate specimen, while 8 (15.7%) demonstrated a hypoechoic lesion that was proved to be prostate cancer. Seven patients (13.7%) with normal transrectal ultrasound scans had adenocarcinoma of the prostate, while 9 (17.6%) had lesions on ultrasound but no cancer. Based on these results, transrectal ultrasound has a sensitivity of 53.3% and a specificity of 75%. Further analysis reveals that transrectal ultrasound is more accurate in the detection of cancers of greater than 0.20 cc in volume than those of 0.20 cc or less. Transrectal ultrasound also is more accurate in the detection of peripheral zone than transition zone cancers.

The Journal of Nuclear Medicine

Indium-111-labeled B72.3 monoclonal antibody in the detection and staging of breast cancer: a phase I study. Lamki LM, Buzdar AU, Singletary SE, et al. (LML, Nuclear Medicine, Dept. of Radiology, University of Texas Medical School at Houston, 6431 Fannin, Houston, TX 77030). *J Nucl Med* 32(7):1326-1332, July 1991

Sixteen patients with primary breast cancer were studied with a pancarcinoma monoclonal antibody B72.3, an IgG₁ molecule directed against tumor-associated glycoprotein (TAG-72) present in several tumors. Five millicuries of ¹¹¹In was used to label 0.2 mg (six patients), or 2 mg (six patients), or 20 mg using the site-directed bifunctional DTPA method (at carbohydrate moiety). Digital, planar, and SPECT images were obtained at 2, 48, 72 and 96 hr when possible. HAMA levels were obtained before the Mab infusion and at 1, 3, and 6 wk postinfusion. Fourteen of 14 known primary breast lesions were detected by imaging (100% sensitivity). Two fibrocystic lesions were negative. Seven of 14 patients had lymph node metastases by histologic methods, but all were missed by radioimmunoscintigraphy. Tumor uptake of Mab ranged 0.00054%-0.0038% of the ID/g. The tumor-to-normal breast tissue ratio was 4.3 ± 0.91 (mean \pm s.e.m.). Lymph nodes localization of ¹¹¹In-B72.3 by tissue analysis was similar for tumor-bearing and normal nodes (0.0039 ± 0.0023 versus 0.0025 ± 0.0019). Pharmacokinetics revealed mean plasma half-life of 33.3-41.2 hr for the different doses. There was no statistical difference between any of the pharmacokinetic parameters of different doses. HAMA was positive only in 17% of the patients. The study suggests that this antibody has 100% sensitivity for primary breast cancers, but very poor detection rate of metastatic lesions in axillary lymph nodes; thus making it of questionable value in the initial staging process of this disease.

Gastrointestinal Radiology

Transrectal ultrasound and computed tomography in preoperative staging of lower rectal adenocarcinoma. Goldman S, Arvidsson H, Norring U, Lagerstedt U, Magnusson I, Frisell J (SG, Dept. of Surgery, Södersjukhuset, S-10064 Stockholm, Sweden). *Gastrointest Radiol* 16:259-263, 1991

A comparison of transrectal ultrasound (TRUS) and computed tomography (CT) for staging of rectal carcinoma was performed.

Thirty-two patients were examined by TRUS and 30 by CT. The results of these preoperative examinations were compared with postoperative histopathological findings. TRUS had an accuracy of 81% and it predicted perirectal tumor growth with a sensitivity of 90% and a specificity of 67%, whereas the corresponding figures for CT were 52%, 67%, and 27%. These findings indicate that TRUS is more efficient than CT in staging local tumor growth in rectal cancer. Neither technique, however, can reliably identify lymph node metastases, since no correlation was found between lymph node size as observed on CT and TRUS and tumor involvement as evaluated histopathologically.

Immunoscintigraphy of colorectal carcinoma utilizing ¹¹¹In-labeled monoclonal antibody conjugate CYT-103. Neal CE, Swan TL, Baker MR, Ellis RL, Katterhagen JG (CEN, Dept. of Radiology, Memorial Medical Center, 800 N. Rutledge Ave., Springfield, IL 62781). *Gastrointest Radiol* 16:251-255, 1991

Twelve presurgical patients with colorectal carcinoma received a single intravenous infusion of 0.5-20.0 mg of the radiolabeled monoclonal antibody conjugate CYT-103. This product is an immunoconjugate of B72.3 labeled with Indium-111 (¹¹¹In). Patients underwent preoperative gamma camera imaging and computed tomographic (CT) scanning of the abdomen and pelvis. Fifteen intraabdominal sites of tumor were found at surgery. Monoclonal antibody imaging detected 87% of these lesions, whereas CT of the abdomen and pelvis detected 47%. Monoclonal antibody imaging identified tumor in 27% of the patients in which CT did not identify any sites of tumor. The results of this study indicate that monoclonal antibody imaging using [¹¹¹In]CYT-103 is useful for the preoperative evaluation of colorectal carcinoma patients and the results are complimentary to CT of the abdomen and the pelvis.

Journal of Ultrasound in Medicine

Sonographic recognition of major malformations and aberrant fetal growth in trisomic fetuses. Dicke JM, Crane JP (JMD, Dept. of Obstetrics and Gynecology, The Jewish Hospital of St. Louis, Washington University School of Medicine, 216 S. Kingshighway Blvd., St. Louis, MO 63110). *J Ultrasound Med* 10:433-438, Aug. 1991

Structural malformations and growth retardation are commonly observed in chromosomally abnormal newborns. This study assesses the sensitivity of ultrasound for detecting aberrant fetal growth patterns and chromosome-related major malformations. The study population consisted of 74 trisomic fetuses (trisomy 13, 9; trisomy 18, 22; trisomy 21, 43). Overall, 63% (38 of 60) of trisomic fetuses had at least one major malformation on postnatal examination. One or more major anomalies were identified by prenatal sonography in 68% (26 of 38) of these malformed fetuses and 43% (26 of 60) of the entire trisomic population. Midtrimester onset growth retardation was evident in 43% of fetuses with trisomy 13 and 59% of fetuses with trisomy 18. These findings suggest that a systematic fetal anatomic survey can be a powerful screening tool for the prenatal detection of chromosome abnormalities.

Reprinted with permission by the American Institute of Ultrasound in Medicine.

Journal of Computer Assisted Tomography

CT of the normal appendix. Grosskreutz S, Goff WB II, Balsara Z, Burkhard TK (WBG II, Clinical Investigation Dept., Naval Hospital, San Diego, CA 92134-5000). *J Comput Assist Tomogr* 15(4):575-577, July/Aug. 1991

We conducted a prospective evaluation of the normal vermiform appendix in 203 patients. Conventional CT techniques were utilized with an 8 mm slice thickness and 10 mm slice interval. The normal appendix was definitely identified in 51% of the patients studied. Computed tomographic appearance of the normal appendix is demonstrated, and potential pitfalls are described.

1991-1992 Sterling Winthrop Visiting Professorship and Guest Lectureships at the AFIP

Sterling Drug, Inc., through its diagnostic imaging divisions of Winthrop Pharmaceuticals and Sterling-Winthrop, and Sterling Research Group will again support the Sterling Winthrop Visiting Professorship in Diagnostic Imaging and the Sterling Winthrop National Guest Lectureships in the Dept. of Radiologic Pathology at the Armed Forces Institute of Pathology. Anne G. Osborn, University of Utah, will continue as the Sterling Winthrop Visiting Professor in Diagnostic Imaging. The Sterling Winthrop National Guest Lecturers for 1991-1992 are Marc S. Levine, Hospital of the University of Pennsylvania; H. Ric Harnsberger, University of Utah; Joseph K. T. Lee, University of North Carolina; Nestor L. Muller, University of British Columbia; Thomas H. Berquist, Mayo Medical School; and James C. Reed, Bowman Gray School of Medicine, Wake Forest University.

Mammographically Detected Early Breast Cancer

The University of Alabama at Birmingham will present Mammographically Detected Early Breast Cancer, Jan. 6-9, 1992, at the Ritz-Carlton Resort Hotel, Naples, FL, and Feb. 10-13, 1992, at the Ritz-Carlton Rancho Mirage, Rancho Mirage, CA. Program directors: Eva Rubin and Peter J. Dempsey. Category 1 credit: 18 hr. Fee: physicians, \$450; residents, fellows, and technologists, \$300. Information: Dawne Ryals, Ryals and Associates, P. O. Box 1925, Roswell, GA 30077-1925; telephone: (404) 641-9773; fax: (404) 552-9859.

Advanced Seminars in Diagnostic Imaging

The University of California, San Diego, will present Advanced Seminars in Diagnostic Imaging, Jan. 10-12 and Feb. 27-March 1, 1992, at the Ritz-Carlton Resort Hotel, Laguna Niguel, CA, and Feb. 4-7, 1992, at Le Meridien Hotel, Coronado (San Diego), CA. Program director: David S. Feigin. Category 1 credit: January course, 15 hr; February courses, 20 hr. Fee: physicians: January course, \$400; February courses, \$500; physicians in training and technologists, \$300. Information: Dawne Ryals, Ryals and Associates, P. O. Box 1925, Roswell, GA 30077-1925; telephone: (404) 641-9773; fax: (404) 552-9859.

Updates on Diagnostic Imaging

Stanford University Medical Center is sponsoring Diagnostic Imaging Update, Jan. 12-16, 1992, at the Ritz-Carlton Palm Beach,

Palm Beach, CA, and Feb. 24-28, 1992, at the Ritz-Carlton Mauna Lani, Mauna Lani, HI. The January seminar will cover body imaging, mammography, neuroradiology, and pediatrics. The February program will deal with body imaging, mammography, MR imaging, and interventional radiology. Program director: R. Brooke Jeffrey. Category 1 credit: 23.5 hr. Fee: physicians, \$550; residents, fellows, and technologists, \$300; Stanford alumni (January meeting), \$500. Information: Dawne Ryals, Ryals and Associates, P. O. Box 1925, Roswell, GA 30077-1925; telephone: (404) 641-9773; fax: (404) 552-9859.

OB/GYN and Ultrasound

The University of California, San Diego, is sponsoring OB/GYN and Ultrasound, Jan. 16-19, 1992, at the Hotel Del Coronado, San Diego, CA. Program directors: Barbara B. Gosink and Sandra Hagen-Ansert. Category 1 credit: 20 hr (pending). Fee: physicians, \$450; residents, fellows, and technologists, \$300. Information: Dawne Ryals, Ryals and Associates, P. O. Box 1925, Roswell, GA 30077-1925; telephone: (404) 641-9773; fax: (404) 552-9859.

Seminars in MRI

The Medical College of Wisconsin is sponsoring Seminars in MRI, Jan. 18-25, 1992, at Marriott's Mark Resort and Conference Center, Vail, CO. The program will concentrate on the common and complex problems encountered in MR imaging of the body and neurologic system. Faculty: M. Brant-Zawadzki, E. K. Fram, V. M. Haughton, H. Hricak, T. L. Lawson, M. M. Pathria, D. D. Stark, and J. C. Weinreb. Category 1 credit: 33 hr. Fee: \$500. Information: Thomas L. Lawson, M.D., Dept. of Radiology, Milwaukee County Medical Complex, 8700 W. Wisconsin Ave., Milwaukee, WI 53226; telephone: (414) 257-6024; fax: (404) 257-8129.

Thoracic Imaging 1992

The Society of Thoracic Radiology will present Thoracic Imaging 1992, Jan. 19-23, 1992, at the Ritz-Carlton Resort Hotel, Laguna Niguel, CA. Program director: W. Richard Webb. Category 1 credit: 30 hr (pending). Fee: physicians, \$570; residents, fellows, and technologists, \$325. Information: Dawne Ryals, Ryals and Associates, P. O. Box 1925, Roswell, GA 30077-1925; telephone: (404) 641-9773; fax: (404) 552-9859.

Practical Aspects of Diagnostic Radiology and Medical Imaging

Vanderbilt University Medical Center will present Practical Aspects of Diagnostic Radiology and Medical Imaging V, Feb. 1-7, 1992, at Snowmass Village Conference Center, Snowmass Village, CO. Emphasis will be on everyday problems, approached from the point of view of diagnostic radiology and medical imaging. Even when other imaging techniques are presented, an effort will be made to include presentation of conventional radiographs when appropriate. Category 1 credit: 26 hr. Fee: physicians (through Dec. 2, 1991/after Dec. 2, 1991), \$535/\$550; residents and fellows, \$350 (letter required). Information: Sherri Culp, Vanderbilt Division of CME, D-8211 Medical Center North, Nashville, TN 37232-2337; (615) 322-4030.

MRI: Present and Future

The George Washington University Medical Center, University of Toronto, will present the 2nd annual MRI: Present and Future, Feb. 3-7, 1992, at the Ritz-Carlton Resort Hotel, Naples, FL. Program directors: Edward Kassel and David O. Davis. Category 1 credit: 20 hr (pending). Fee: physicians, \$540; residents, fellows, and technologists, \$350. Information: Dawne Ryals, Ryals and Associates, P. O. Box 1925, Roswell, GA 30077-1925; telephone: (404) 641-9773; fax: (404) 552-9859.

Intermountain Imaging Conference

The Medical College of Wisconsin is sponsoring the 13th annual Intermountain Imaging Conference, Feb. 8-15, 1992, at the Sheraton Steamboat Hotel and Resort, Steamboat Springs, CO. The program will cover CT, MR, and sonography of the chest, abdomen, and pelvis. The focus will be on integrated imaging and the advantages of various radiologic techniques and problem solving. Special mini-courses on mammography and orthopedic MR imaging will be presented also. Faculty: L. Bassett, N. R. Dunnick, L. R. Goodman, T. L. Lawson, A. J. Megibow, R. C. Nelson, S. J. Pomeranz, and E. A. Zerhouni. Category 1 credit: 33 hr. Fee: \$500. Information: Thomas L. Lawson, M.D., Dept. of Radiology, Milwaukee County Medical Complex, 8700 W. Wisconsin Ave., Milwaukee, WI 53226; telephone: (414) 257-6024; fax: (414) 257-8129.

Computed Body Tomography 1992: The Cutting Edge

The Johns Hopkins University School of Medicine is sponsoring Computed Body Tomography 1992: The Cutting Edge, Feb. 13-16, 1992, at the Peabody Orlando Hotel, Orlando, FL. The seminar will provide a comprehensive review of recent advances in CT of the chest and abdomen, including the spine, with some correlation with MR imaging. Program directors: Elliot K. Fishman and Stanley S. Siegelman. Guest faculty: J. P. Heiken, C. A. Helms, R. A. Holliday, D. P. Naidich, and D. R. Resnick. Category 1 credit: 22 hr. Fee: physicians, \$500; residents and fellows (letter required), \$375; technologists, \$375. Information: Program Coordinator, Johns Hopkins Medical Institutions, Office of Continuing Education, Turner Bldg., 720 Rutland Ave., Baltimore, MD 21205; (301) 955-2959.

MRI Update: 1992

Vanderbilt University Medical Center will present MRI Update: 1992, Feb. 17-22, 1992, at the Grand Hyatt Wailea Resort and Spa,

Maui, HI. The course will provide a review of current results and clinical potential of MR imaging. Guest faculty: S. E. Harms, H. Y. Kressel, and M. T. Modic. Category 1 credit: 21.5 hr. Fee: physicians (through Dec. 1, 1991/after Dec. 1, 1991), \$600/\$700; residents and Vanderbilt alumni, \$500; technologists, \$300. Information: Brenda Boner, Coordinator, Vanderbilt Division of CME, D-8211 Medical Center North, Nashville, TN 37232-2337; (615) 322-4030.

Musculoskeletal Imaging

Boston University School of Medicine is sponsoring Musculoskeletal Imaging for Orthopedic Surgeons and General Radiologists, March 2-6, 1992, at the Frenchman's Reef Hotel, St. Thomas, Virgin Islands. Course director: Peter D. Franklin. Category 1 credit: 21 hr. Fee: physicians, \$435; residents, \$300. Information: Boston University School of Medicine, Continuing Medical Education, 80 E. Concord St., Boston, MA 02118; (617) 638-6405.

Principles and Practice of Clinical MRI

The Dept. of Radiology, Division of Magnetic Resonance Imaging, The Johns Hopkins University School of Medicine, is sponsoring Principles and Practice of Clinical MRI, March 5-8, 1992, at the Walt Disney World Swan, Orlando, FL. Category 1 credit will be offered. Fee: physicians, \$550; residents, fellows, and technologists, \$375. Information: Program Coordinator, Johns Hopkins Medical Institutions, Office of Continuing Education, Turner Bldg., 720 Rutland Ave., Baltimore, MD 21205; (301) 955-2959.

Practical Pediatric Imaging

The Dept. of Radiology, Children's Hospital Medical Center, Cincinnati, OH, will present Practical Pediatric Imaging, March 15-20, 1992, at the Resort Center Lodge and Inn, Park City, UT. Information: Cathy Laine, International Meeting Managers, Inc., 4550 Post Oak Pl., Ste. 248, Houston, TX 77027; telephone: (713) 965-0566; fax: (713) 960-0488.

Radiology in Southeast Asia and China

The Dept. of Radiology, University of California, San Diego School of Medicine, is sponsoring Radiology in Southeast Asia and China, March 18-April 7, 1992. The course will be in Singapore, March 18-22; Bangkok, Thailand, March 22-25; Hong Kong, March 25-29; Beijing, China, March 29-April 2; Shanghai, April 2-4; Guilin, April 4-6; and Hong Kong, April 6. Category 1 credit: Singapore and Bangkok, 21 hr; Hong Kong and China, 17 hr; China, 16 hr; complete course, 37 hr. Fee: Physicians: complete course, \$695; Singapore and Bangkok, \$525; Hong Kong and China, \$525; China, \$475; residents, fellows, and technologists, \$375. Information: Dawne Ryals, Ryals and Associates, P. O. Box 1925, Roswell, GA 30077-1925; telephone: (404) 641-9773; fax: (404) 552-9859.

International Symposium on Diagnostic Imaging

The Dept. of Radiology, University of Florida, is sponsoring the 6th International Symposium on Diagnostic Imaging, May 18-22, 1992, in Barcelona, Spain. Topics to be covered will include MR imaging, CT, sonography, nuclear medicine, digital subtraction angiography, and positron emission tomography. The official languages of the symposium will be Catalan, Spanish, and English. Course directors:

C. Sanpons and Pablo Ros. Category 1 credit: 28 hr. Fee (through April 1, 1992/after April 1, 1992): physicians, \$495/\$595; residents, \$250/300 (letter required). Information: Loles Casserras, Centro Radiológico Computarizado, Tavern, 82, 08006-Barcelona, Spain; telephone: 34-3-201.68.69; fax: 34-3-201.51.49.

Advances in Cardiopulmonary Imaging

The Johns Hopkins University School of Medicine and the European Association of Radiology are sponsoring Advances in Cardiopulmonary Imaging, June 11–13, 1992, in Salzburg, Austria. Recent advances in the diagnosis and treatment of various disease entities and newer technology will be discussed. Category 1 credit: 16.5 hr. Information: Program Coordinator, Johns Hopkins Medical Institutions, Office of Continuing Education, Turner Bldg., 720 Rutland Ave., Baltimore, MD 21205; (301) 955-2959.

The American Board of Radiology Examinations

Written examinations for the American Board of Radiology (ABR) are scheduled for Oct. 1–2, 1992, and Oct. 14–15, 1993. Oral examinations will be held at the Executive West Hotel in Louisville, KY, June 1–5, 1992. The ABR will accept applications for admission to the examinations after July 1, but not later than Sept. 30, in the year *preceding* the year in which the examination is to be taken. For application forms and further information: Office of the Executive Director, The American Board of Radiology, 2301 W. Big Beaver Rd., Ste. 625, Troy, MI 48084.

Swallowing Center Preceptorship, times arranged, Baltimore (Jan)

Imaging Fellowship, times arranged, Miami Beach, FL (Jan)

Preceptorships in Ultrasound at Johns Hopkins, times arranged, Baltimore (June)

Practicum in Breast Imaging, times arranged, Baltimore (Aug)

San Diego Postgraduate Radiology Course, Oct. 28–Nov. 1, Coronado (San Diego), CA (June)

Magnetic Resonance Imaging and CT Update, Oct. 28–Nov. 1, Cambridge, MA (Aug)

Interventional Radiology Course, Nov. 1–3, Coronado (San Diego), CA (July)

MR Imaging Fellowships at LAC/USC Imaging Science Center, Nov. 4–8, Los Angeles (Feb)

Practical Training in Interventional Radiology, Nov. 4–8, Lund, Sweden (July)

Computed Body Tomography for the Technologist, Nov. 7–10, Orlando, FL (Sept)

Seminar on Bone and Joint Diseases, Nov. 15–17, Scottsdale, AZ (July)

Advanced Seminars in Diagnostic Imaging, Nov. 15–17, Laguna Niguel, CA (Aug)

Diagnosis and Treatment of Bone and Soft-Tissue Tumors, Nov. 21–23, Sacramento, CA (May)

Nuclear Medicine Update, Dec. 9–11, Atlanta (Oct)

MR Visiting Fellowships at UCLA, Dec. 9–13, 1991; Feb. 3–7, 1992; March 9–13, 1992; April 6–10, 1992; Sept. 14–18, 1992; Oct. 5–9, 1992; and Dec. 7–11, 1992; Los Angeles (Sept)

Current Topics in Nuclear Medicine Technology, Dec. 11–13, Atlanta (Oct)

Asian Oceanian Congress of Radiology, Dec. 14–18, New Delhi (July)

CT/MRI Head to Toe, Dec. 15–20, New York City (Sept)

Caribbean Cruise—Breast Imaging and MRI at Sea: breast imaging, Jan. 11–18, 1992; MR imaging, Jan. 18–25, 1992 (Sept)

Uroradiology 1992, Jan. 13–17, 1992, Scottsdale, AZ (Sept)

Park City 1992: MRI, Jan. 25–29, 1992, Park City, UT (Oct)

Course on Positron Emission Tomography, Jan. 26–29, 1992, Dana Point, CA (Oct)

Diagnostic Imaging in Puerto Rico, Jan. 26–31, 1992, Cerromar Beach Hotel, Puerto Rico (Sept)

Society of Gastrointestinal Radiologists Annual Meeting, Feb. 16–21, 1992, Orlando, FL (Oct)

Advanced Clinical Magnetic Resonance Imaging, Feb. 17–21, 1992, Hawaii (Oct)

MR Angiography and Imaging of the Head, Spine, and Musculoskeletal System, Feb. 17–21, 1992, Tucson, AZ (Oct)

Sun Valley Imaging Meeting, Feb. 23–29, 1992, Sun Valley, ID (Oct)

AFIP Neuroradiology Review Course, Feb. 29–March 1, 1992, Bethesda (Oct)

International Symposium on Recent Advances in Diagnostic Imaging and Radiation Oncology, March 24–27, 1992, Kathmandu, Nepal (June)

European Symposium on Uroradiology, Aug. 24–27, 1992, Herlev, Denmark (Aug)

AJR carries announcements of courses, symposia, and meetings of interest to its readers if received a minimum of 5 months before the event. There is no charge; receipt of items by the *AJR* Editorial Office is not acknowledged. Submit items for publication typed double-spaced. Provide title, date, location, brief description, sponsor, course directors, fees, category I credit, and address and telephone number for additional information. Faculty from the host institution will not be listed. Guest faculty names will appear **only** if initials are provided. Mail news items to *AJR* Editorial Office, 2223 Avenida de la Playa, Suite 103, La Jolla, CA 92037-3218.

American Roentgen Ray Society: Officers, Committees, and Membership Information

Officers

President: John A. Kirkpatrick, Jr.
President-elect: A. Everette James, Jr.
1st Vice-president: Andrew K. Poznanski
2nd Vice-president: George R. Leopold
Secretary: Joseph T. Ferrucci, Jr.
Treasurer: Beverly P. Wood

Executive Council: R. N. Berk, M. P. Capp, W. J. Casarella, N. R. Dunnick, R. G. Evens, J. T. Ferrucci, Jr., A. E. James, Jr., J. A. Kirkpatrick, Jr., A. M. Landry, Jr., G. R. Leopold, J. E. Madewell, T. C. McLoud, A. A. Moss, A. K. Poznanski, R. J. Stanley, J. H. Thrall, K. H. Vydareny, N. O. Whitley, B. P. Wood, R. J. Alfidi, chairman

Committees

Editorial Policy: R. N. Berk, E. Buonocore, Melvin M. Figley, C. R. B. Merritt, K. Valji, C. A. Rohrmann, Jr., W. J. Casarella, chairman

Education and Research: R. R. Hattery, C. B. Higgins, B. J. Hillman, R. J. Stanley, W. M. Thompson, N. O. Whitley, chairman

Finance and Budget: R. K. Gedgaudas-McClees, A. A. Moss, J. R. Thornbury, K. H. Vydareny, J. H. Thrall, chairman

Nominating: R. G. Evens, P. J. Fritzsche, A. A. Moss, chairman

Publications: E. Buonocore, C. R. B. Merritt, C. A. Rohrmann, Jr., W. J. Casarella, chairman

Membership: J. E. Madewell, T. C. McLoud, A. A. Moss, K. H. Vydareny, chairman

Representatives to Other Organizations

American Board of Radiology: W. J. Casarella, J. A. Kirkpatrick, Jr., L. F. Rogers

American College of Radiology: R. A. Gagliardi, J. E. Madewell, B. L. McClennan, R. J. Stanley

American Medical Association: S. F. Ochsner, delegate; K. L. Krabbenhoft, alternate; K. L. Kidd, CPT Advisory Committee

American National Standards Institute: M. E. Haskin

National Council on Radiation Protection and Measurements: F. D. Miraldi, E. L. Saenger

Armed Forces Institute of Pathology: J. E. Madewell

Meeting Arrangements

Annual Meetings: May 10–15, 1992, Marriott's World Center, Orlando, FL; April 25–30, 1993, Marriott San Francisco, San Francisco, CA

Annual Meeting Committee: J. K. Crowe, N. R. Dunnick, R. R. Lukin, N. H. Messinger, R. J. Stanley, R. D. Steele, Jr., A. M. Landry, Jr., chairman

Instructional Courses: Bruce L. McClennan, associate chairman; R. J. Stanley, chairman

Scientific Program: P. H. Arger, T. B. Hunter, D. Kushner, T. C. McLoud, L. B. Talner, J. H. Thrall, A. E. James, Jr., chairman

Scientific Exhibits: J. R. Haaga, D. S. Hartman, R. G. Ramsey, N. R. Dunnick, chairman

ARRS Membership

An application form is printed in the September issue of the Journal. For consideration at the 1992 ARRS meeting, send completed forms before February 1, 1992, to American Roentgen Ray Society, 1891 Preston White Dr., Reston, VA 22091. Active members are graduates of an approved medical or osteopathic school or hold an advanced degree in an allied science. They must practice radiology or work in an associated science in the United States or Canada and be certified by the American Board of Radiology, American Osteopathic Board of Radiology, or Royal College of Physicians of Canada or otherwise adequately document training and credentials. International members are foreign radiologists or scientists who are active in radiology or an allied science. Members-in-training are residents or fellows in radiology or postgraduate students in an allied science. Additional application forms can be obtained from the ARRS offices in Reston, VA.

Business Office

Paul Fullagar, Executive Director, American Roentgen Ray Society, 1891 Preston White Dr., Reston, VA 22091; (703) 648-8992.

American Roentgen Ray Society 92nd Annual Meeting May 10–15, 1992, Orlando, FL Marriott's Orlando World Center

Registration and Hotel Reservations

Forms for advance registration and hotel reservations will be in the February and March 1992 issues of the *AJR*.

Scientific Program

Abstracts of papers to be considered for the program must be submitted by November 1, 1991. Forms on which to submit abstracts are in this issue of the *AJR*. The ARRS Program Committee will select papers and notify authors in early January. The *AJR* has first rights to all papers accepted for presentation at the ARRS meeting. Mail original and five copies to

A. Everette James, Jr., M.D.
c/o Paul Fullagar
American Roentgen Ray Society
1891 Preston White Drive
Reston, VA 22091
Telephone (703) 648-8992

Scientific Exhibits

Proposals for scientific exhibits must reach the Chairman of Exhibits by November 1, 1991. Forms, which may be photocopied, are in this issue of the *AJR*. Send completed form to

N. Reed Dunnick, M.D.
c/o Paul Fullagar
American Roentgen Ray Society
1891 Preston White Drive
Reston, VA 22091
Telephone (703) 648-8992

Refresher Course Program

A summary of the refresher courses will appear in the *AJR* in February along with advance registration forms. Early registration is an advantage in ensuring preferred courses in this popular program.

Local Program

A program of sightseeing, shopping, and entertainment will be developed by the Local Arrangements Chairman. Information and advance registration forms will be in the February issue of the *AJR*.

Residents' Award Papers

The society offers several cash awards for the best scientific papers prepared by residents in radiology. The President's Award has a \$2000 prize. There are two Executive Council awards of \$1000 each. All are presented at the annual meeting. Papers should be submitted by February 15, 1992, for consideration in this competition. Send entries to

Nancy O. Whitley, M.D.
Dept. of Radiology
University of Maryland Medical Systems Hospital
22 S. Greene St.
Baltimore, MD 21201

Deadlines

Abstracts of papers: November 1, 1991
Scientific exhibit proposals: November 1, 1991
Residents' Award papers: February 14, 1992

Call for Papers

American Roentgen Ray Society
1992 Annual Meeting:
May 10–15, 1992, Orlando, FL

ADDRESS OF PRESENTING AUTHOR	
Department	
Institution	
Street	
City, State	Zip
Phone:	

Type title, authors, and abstract in the space provided below. (Instructions are on reverse side of this page. Abstract should not exceed 300 words.)

Select one category: ☐ Angio/Interventional ☐ Breast ☐ Chest ☐ CT ☐ Gastrointestinal Tract ☐ Genitourinary Tract
☐ MR ☐ Neuroradiology ☐ Skeletal ☐ Sonography ☐ Pediatric

Projection Requirements: ☐ 35 mm, single or double (circle one) ☐ 16 mm silent film ☐ 1/2" VHS ☐ 3/4"

Has this been presented elsewhere? ☐ yes ☐ no. If yes, please describe on reverse side of this page.

Instructions for Scientific Abstracts

1. Type the information single-spaced. Underline the name of the presenting author. Append as a last line of the abstract any research grant support, if applicable (e.g., Supported by USPHS Grant HE-80144). If the abstract is accepted, it will not be proof-read; it will appear exactly as typed. Use the following format:

MR IMAGING OF THE SPINE AND NECK
F. S. Lau, M.D., A. N. Kirk, M.D., and R. A. Beck, Ph.D.
University of California, Bakersfield, Bakersfield, CA 92338
2. Abstracts should include four paragraphs devoted sequentially to the following topics: (1) object or purpose of the study, (2) materials, methods, and procedures, (3) results, (4) significance of the results and conclusions. The text should not exceed 300 words. Specific data are essential. The abstract should be a succinct summary of work done rather than a promissory note.
3. The Program Committee will grade each abstract and determine acceptance. Further information will be forwarded to those whose abstracts are accepted for presentation.

Deadline for submission of abstract is November 1, 1991. Mail abstract and four copies to

A. Everette James, Jr., M.D.
c/o Paul R. Fullagar
American Roentgen Ray Society
1891 Preston White Dr.
Reston, VA 22091
Telephone (703) 648-8992

Call for Scientific Exhibits
American Roentgen Ray Society
1992 Annual Meeting:
May 10–15, 1992, Orlando, FL

FOR COMMITTEE USE ONLY

Date Received_____ Application No. _____
Subject_____ Score_____

Rejected_____ Accepted_____

Assigned_____ Space No. _____

Principal Exhibitor's Mailing Address

Name_____ Institution_____

Department_____ Street Address_____ City_____

State_____ Zip Code_____ Telephone: office () home ()

Names of Exhibitors (List principal exhibitor first and telephone number of each person.)

Last	First	Middle	Telephone	Degree (one only)	Member ARRS?
_____	_____	_____	_____	_____	_____
_____	_____	_____	_____	_____	_____
_____	_____	_____	_____	_____	_____
_____	_____	_____	_____	_____	_____
_____	_____	_____	_____	_____	_____

Title of Exhibit_____

Type abstract single-spaced in the space provided below. (See instructions on the reverse side of this page.)

Instructions for Abstract

The abstract should be a brief paragraph that states the purpose, principal information, and conclusions of the exhibit. Promissory statements are not acceptable. Type single-spaced in the space provided on the reverse side. Brevity is desirable but not at the expense of specific information. **The abstract will appear in the program book as submitted.** Please use typewriter and complete the application form on both sides. List space requirements.

What Type of Exhibit Is Proposed? (Check one and fill in all appropriate blanks.)

_____ **Free-standing.** This is a self-contained display created in total by the exhibitor. It may be a fold-open unit, a unit shipped in cases and assembled on site, or a tabletop unit. Linear feet required _____.

_____ **Poster Board (backboard panels).** Backboard panels are 4 × 8 ft. (1.2 × 2.5 m). Number of panels required _____. If two panels are needed, there will be a 1/4-in. frame separating the panels, thus requiring a separation in the presentation.

_____ **Viewbox.** Mounted materials (radiographs and other transparencies) for display on the society's illuminators. Each illuminator is 39.5 × 59.5 in. (100 × 151 cm). Number of illuminators required _____. Materials should not be glass mounted.

Please Indicate Most Appropriate Category.

_____ Bone _____ Cardiovascular _____ Chest _____ Gastrointestinal _____ Genitourinary _____ Breast _____ Medical physics
 _____ Neuroradiology _____ Nuclear medicine _____ Pediatric _____ Radiation oncology _____ Sonography

Exhibits will be chosen on the basis of the quality of the abstract and space available. Poster board and computer-based exhibits are encouraged, as they do not require a viewbox.

Signature of Principal Exhibitor _____

Exhibitors will receive instructions for exhibit preparation.

Applications must be received no later than November 1, 1991. Mail original and five copies to

N. Reed Dunnick, M.D.
 c/o Paul R. Fullagar
 American Roentgen Ray Society
 1891 Preston White Dr.
 Reston, VA 22091
 Telephone: (703) 648-8992

Classified Advertisements

Positions Available

PENN STATE UNIVERSITY, THE MILTON S. HERSHEY MEDICAL CENTER, FACULTY POSITION IN RADIOLOGY—The Penn State University, Dept. of Radiology is recruiting an additional faculty member with training or experience in diagnostic ultrasound, MRI, and CT for July 1, 1992. The position is open to physicians who have fulfilled the ABR requirements for certification and who have subspecialty training or experience in body imaging. Substantial experience in obstetrical ultrasound is desirable. The Penn State University Hospital is a 500-bed, tertiary-care facility in Hershey, PA, near Harrisburg, the state capital. Medical student education, resident training, and research are integral components of the health-care mission of the university. The Dept. of Radiology has 24 faculty and 20 residents. The ultrasound, MRI, and CT sections perform over 6000 exams, 3300 exams, and 8300 exams/yr, respectively. New equipment for 1991 includes a fifth ultrasound unit, a second MRI system, and a third CT scanner. Applicants may respond with a letter of interest and CV to Dr. Richard Moser, Chief, Diagnostic Radiology, Dept. of Radiology, The Milton S. Hershey Medical Center, Penn State University, P.O. Box 850, Hershey, PA 17033; (717) 531-8044. Penn State University is an affirmative action, equal opportunity employer. Women and minorities are encouraged to apply. 11xa

THE DEPT. OF RADIOLOGY AT NORTH SHORE UNIVERSITY HOSPITAL-CORNELL UNIVERSITY MEDICAL COLLEGE IN MANHASSET is seeking a BC/BE radiologist to fill the position of director of body CT. Fellowship experience, a strong interest in teaching, and collaborative clinical and basic research are desirable. Academic rank and salary are commensurate with experience. North Shore University Hospital is a 705-bed, tertiary-care teaching hospital approximately 20 mi. from New York City and Cornell University Medical College, with which it is affiliated. The dept. consists of 29 attending staff, 16 residents, 6 fellows, and does approximately 160,000 exams/yr. The dept. is well-equipped with 3 Picker 1200 SX CT scanners, 10 ultrasound scanners with color Doppler, transvaginal and transrectal capabilities, etc. Two new 1.5-T GE MRI scanners will be installed in Dec. 1991. A whole-body PET scanner and space for a small-bore magnet are located in a free-standing research facility on campus. The hospital is a major trauma center and has, on campus, a 250-bed extended-care facility. For further information, contact Dr. Harry L. Stein, Chairman, Dept. of Radiology, North Shore University Hospital-Cornell University Medical College, 300 Community Dr., Manhasset, NY. NSUH-CUMC is an equal opportunity/affirmative action employer. 11ap

DIAGNOSTIC RADIOLOGIST with skills in CT, MR, interventional, ultrasound, and nuclear medicine needed to join group of 17 board-certified radiologists. Practice is located in southwestern Ohio and provides services at 2 500-bed hospitals, an imaging center, and a private office. Excellent salary, vacation, and benefits leading to early partnership. Send inquiries with CV to Michael R. Carroll, M.D., Medical Radiologists, Inc., 111 W. First St., Ste. 918, Dayton, OH 45402. 11xa

DIAGNOSTIC RADIOLOGIST sought to join a fee-for-service group practice at 2 mid-Bronx hospitals. Board certification with expertise in imaging and special procedures/interventional radiology preferred. Please send CV to Arthur Avenue Radiology, P.C., P.O. Box 4332, Great Neck, NY 11027. 11-4ap

THE DEPT. OF RADIOLOGY AT NORTH SHORE UNIVERSITY HOSPITAL-CORNELL UNIVERSITY MEDICAL COLLEGE IN MANHASSET is seeking a BC/BE radiologist to fill the position of director of MRI. Fellowship experience, a strong interest in teaching, and collaborative clinical and basic research are desirable. Academic rank and salary are commensurate with experience. North Shore University Hospital is a 705-bed, tertiary-care teaching hospital approximately 20 mi. from New York City and Cornell University Medical College, with which it is affiliated. The dept. consists of 29 attending staff, 16 residents, 6 fellows, and does approximately 160,000 exams/yr. The dept. is well-equipped, with 3 Picker 1200 SX CT scanners, 10 ultrasound scanners with color Doppler, transvaginal and transrectal capabilities, etc. Two new 1.5-T GE MRI scanners will be installed in Dec. 1991. A whole-body PET scanner and space for a small-bore magnet are located in a free-standing research facility on campus. The hospital is a major trauma center and has, on campus, a 250-bed extended-care facility. For further information, contact Dr. Harry L. Stein, Chairman, Dept. of Radiology, North Shore University Hospital-Cornell University Medical College, 300 Community Dr., Manhasset, NY. NSUH-CUMC is an equal opportunity/affirmative action employer. 11ap

PEDIATRIC RADIOLOGIST—The Dept. of Radiological Sciences of the University of Oklahoma Health Sciences Center has an opening for a pediatric radiologist. Faculty rank and remuneration will depend on credentials and experience. Work site is Children's Hospital of Oklahoma (Oklahoma City) in a well-equipped radiology service performing approximately 75,000 studies/yr. Responsibilities include general diagnosis, ultrasound, body CT, and body MR. If interested, please contact J.J. Vanhoutte, M.D., Radiology Service, Children's Hospital of Oklahoma, P.O. Box 26307, Oklahoma City, OK 73126. 11-1a

BOARD-CERTIFIED RADIOLOGIST—The Dept. of Veterans Affairs Medical and Regional Office Center at Wichita, KS, is actively recruiting a board-certified radiologist. This medical center provides primary and secondary levels of care in medicine, surgery, psychiatry, and tertiary surgical care and is affiliated with the University of Kansas School of Medicine at Wichita. State-of-the-art equipment includes cardiology ultrasound, angiography, and CT. Incumbent will join active, multidisciplinary, teaching medical staff structured to facilitate academic growth. Competitive salary with the recent enactment of Physician Pay Comparability Bill. Send CV to Edward J. Huycke, M.D., Chief of Staff (11), VAM&ROC, 5500 E. Kellogg, Wichita, KS 67218; (316) 651-3603. EOE. 11-12a

ABDOMINAL IMAGING RADIOLOGIST—The University of California, Davis, School of Medicine has a full-time position available in the diagnostic division of the Dept. of Radiology. Appointment will be at the assistant, associate, or full professor level. Candidates must be board-certified in diagnostic radiology, eligible for licensure in California, and have an academic and clinical background in abdominal imaging (ultrasound, CT, and MRI). Please forward a CV, a letter outlining background and interests in teaching/research, and the names and addresses of 5 references to Richard W. Katzberg, M.D., Chairman, Dept. of Radiology, University of California, Davis, 2516 Stockton Blvd., TICON II Bldg., Sacramento, CA 95817. This position will be "open until filled," but not later than Jan. 31, 1992. The University of California is an equal opportunity/affirmative action employer and encourages applications from members of minority groups and women. 11-1a

BRIDGEPORT RADIOLOGY ASSOCIATES, P.C., is seeking a board-certified radiologist to join our group of 11. We provide imaging and therapy service for Bridgeport Hospital, a 525-bed community hospital, and 2 large private offices. All imaging modalities exist throughout the practice, including an outpatient 1.5-T MRI. Applicant must share office duties and night and weekend call for the practice, and must participate in teaching for the hospital-based, ABR-approved residency program. Subspecialty training is desirable. Salaried position leads to full partnership. Send letters of inquiry and CV to Anthony J. Bravo, M.D., Chairman, Dept. of Radiology, Bridgeport Hospital, 267 Grant St., Bridgeport, CT 06610. 11-1ap

MAMMOGRAPHY—Immediate opening for board-certified/eligible radiologist in the section of mammography. Large screening and diagnostic program performing approximately 13,000 exams/yr. Mobile unit and outpatient screening program, needle localization, cyst aspiration, and ultrasound. Program very interactive with patients and referring physicians. Academic rank commensurate with experience. Yale University is an equal opportunity/affirmative action employer. Applications from women and minority group members are encouraged. Send current CV or phone Carol Lee, M.D., Yale University School of Medicine, Dept. of Diagnostic Radiology, 333 Cedar St., New Haven, CT 06510; (203) 785-2425. Application deadline is Nov. 30, 1991. 11-12a

PACIFIC NORTHWEST DIAGNOSTIC RADIOLOGY, MRI, CT, AND ULTRASOUND—Progressive group of 4 radiologists seeks a board-certified radiologist with subspecialty interest and expertise in MRI, CT, and ultrasound. Busy, dynamic practice with regional medical center hospital, MRI center, and outpatient office. The practice is located in the beautiful recreation area of the inland northwest. This area offers world-class lakes for boating and sailing as well as excellent skiing, hunting, and fishing. Family-oriented environment only 30 min from Spokane, WA. Competitive salary with full partnership in 2 yr. Send CV to Doug Bruce, M.D., Radiology Associates of North Idaho, 1104 Ironwood Dr., Coeur d'Alene, ID 83814; (208) 667-0686. 11-1ap

VASCULAR/INTERVENTIONAL/DIAGNOSTIC RADIOLOGIST—Outstanding opportunity for a board-certified radiologist to join an established 12-member, hospital-based, and free-standing diagnostic imaging and radiation oncology practice. Affiliation with 2 major hospitals with over 600 beds and located on Staten Island in the New York metropolitan area. Fellowship training in vascular/interventional procedures to complement section chief in busy interventional service. Candidate can expect up to 50% of time involved with procedures or patient care. Should also have an interest in all facets of diagnostic radiology. Immediate availability. Attractive compensation and benefit package leading to full partnership after second yr. For more information, contact Orlando L. Manfredi, M.D., Director, or Mr. V. James Senatore, Business Manager; (718) 876-2010, or write to Regional Radiology, 360 Bard Ave., Staten Island, NY 10310. 11a

RADIOLOGIST, WASHINGTON—Prominent, 100-physician multispecialty clinic in Pacific Northwest is recruiting a diagnostic radiologist. Interventional fellowship training and/or individual with extensive experience in interventional radiology desired. Guaranteed salary and partnership track available. Excellent benefit package. Abundant 4-season recreational opportunities. Family-oriented community rated the 4th best metropolitan area in the U.S. Send CV to Fred Bockenstedt, M.D., P.O. Box 489, Wenatchee, WA 98807; (509) 663-8711, ext. 5590. 11-1a

CONSULTANT DIAGNOSTIC RADIOLOGISTS, DUNEDIN HOSPITAL: THE OTAGO AREA HEALTH BOARD, NEW ZEALAND—Applications are invited from fully trained radiologists holding medical qualifications registrable in New Zealand. Dunedin Radiology performs 97,000 exams/yr, including diagnostic radiography, CT, digital subtraction angiography, nuclear medicine, and ultrasound. The positions offered are full-time and preference will be given to applicants who are willing to provide a strong general radiological service and develop their own area of specialist interest. Applications from those with experience in neuroradiology, angiography, and interventional radiology would be particularly welcomed. A short term (12 mo) or permanent appointment may be offered, depending on applicant's preference. For application forms, please contact Staffing Administration, Dunedin Hospital, Dunedin, New Zealand; (64) 3 4747961, fax (64) 3 4747639. 11a

DIAGNOSTIC RADIOLOGIST—The Dept. of Radiology of St. Luke's-Roosevelt Hospital Center in New York City is seeking a BC/BE radiologist with expertise in ultrasound. This position offers a full range of clinical involvement in all aspects of abdominal, obstetrical, and vascular ultrasound. The candidate should also be interested in the interpretation of general diagnostic films. An active clinical practice, strong teaching program, as well as stimulating research opportunities are provided at this 1315-bed university hospital of Columbia University College of Physicians and Surgeons. Academic rank will be commensurate with candidate's qualifications and experience. Excellent facilities and remuneration. Please send inquiries with CV to Ronald C. Ablow, M.D., Dept. of Radiology, SLRHC, Amsterdam Ave. and 114th St., New York, NY 10025. Columbia University takes affirmative action to ensure equal opportunity. 11-12ap

SECTION CHIEF, ABDOMINAL CT AND MR IMAGING—St. Luke's-Roosevelt Hospital Center's Dept. of Radiology in New York City has a position at its St. Luke's site for a BC radiologist to be in charge of the abdominal and pelvic imaging performed on its GE Signa Advantage 1.5-T MRI and 2 CTs (GE 9800 HiLight Advantage and Siemens Somatom DRH). This 1315-bed hospital center is in the midst of a \$467 million building program. In addition to clinical expertise, a strong interest and ability in teaching is required for a program that includes residents, fellows, and medical students. Research opportunities are also available in this university hospital of Columbia University College of Physicians and Surgeons. Academic rank depends on qualifications. Excellent remuneration and benefits. Please send inquiries with a CV to Ronald C. Ablow, M.D., Dept. of Radiology, SLRHC, Amsterdam Ave. and 114th St., New York, NY 10025. Columbia University takes affirmative action to ensure equal opportunity. 11-12ap

TWO POSITIONS AVAILABLE—Fellowship training in body MRI with emphasis on orthopedics and ultrasound-fellowship-trained physician needed to join expanding group of 20 diagnostic radiologists (4 neuroradiologists and 5 interventional radiologists) in Orlando, FL. Postfellowship experience preferred. Three hospitals (total 1100 beds), 3 outpatient offices, 7 CT units, 5 MRI units, and 3 angiography suites. Central Florida offers a pleasant climate for year-round outdoor recreation and a dynamic growing economy. Please contact and forward a CV to Len W. Morris, M.D., 1403 Dolive Dr., Orlando, FL 32803; (407) 896-0764. 11-12ap

BOSTON—Expanding private-practice group. No night or evening call. Need experience in mammography. Great life style. Salary leading to equal partnership. Send letter and CV to Box E49, *AJR* (see address this section). 11-4a

DIAGNOSTIC RADIOLOGIST—A 3-member radiology group seeks a fourth radiologist with interventional skills to join them in a suburban community hospital practice in northern Ohio, 20 min from the boating and fishing pleasures of Lake Erie and its islands. Interested applicants please call or write to Dr. Matthew F. Gutowicz, Jr., 23 Patrician Dr., Norwalk, OH 44857; (419) 668-8101 ext. 6205 or 6208. 11-4ap

COLORADO—Immediate opening for board-certified radiologist to join 4-member group in Denver suburb of Aurora, CO. Candidates should be competent in all aspects of diagnostic radiology. Practice includes busy, 220-bed community hospital with active spine, interventional service, CT, ultrasound, nuclear medicine, mammography, MRI, as well as general radiology. Fellowship training and/or special expertise in 1 or more of these areas is desirable. Please send inquiries and CV to Jonathan D. Ain, M.D., Radiology Consultants, P.C., 2260 S. Xanadu Way, Ste. 235, Aurora, CO 80014; (303) 695-2643. 11ap

DIAGNOSTIC RADIOLOGIST, CONNECTICUT—Opening in July 1992 for BC/BE radiologist with expertise in general radiology and mammography. Additional training or experience preferred. No angiography/interventional experience required. Nine-radiologist practice includes a 435-bed, university-affiliated community hospital and a 54-physician multispecialty clinic. Approximately 107,000 exams/yr including MRI, CT, nuclear medicine, ultrasound, and an active interventional service. Excellent salary and benefits leading to full partnership after second yr. For more information, send CV to Paul C. Lakin, M.D., Dept. of Radiology, New Britain General Hospital, 100 Grand St., New Britain, CT 06050. 11-2ap

CROSS-SECTIONAL RADIOLOGIST—Excellent opportunity to join 8 subspecialized radiologists in New York state capital district and further develop a well-established, cross-sectional imaging section in a well-established community hospital and imaging center-based practice. Potential for a leadership responsibility in this subsection of the dept. State-of-the-art equipment includes 2 Siemens CT scanners, 2 Siemens 1.0-T MRI units, and 5 ultrasound units including color Doppler capability. Candidate should be BC/BE, fellowship trained, or academically experienced. Excellent compensation commensurate with experience leading to full lucrative partnership. Send CV to Michael E. Berlow, M.D., Director, Dept. of Medical Imaging, 600 Northern Blvd., Albany, NY 12204. 11-12ap

STAFF RADIOLOGIST—Samuel S. Stratton Dept. of Veterans Affairs Medical Center, Albany, NY, is seeking a board-certified/eligible, full-time staff radiologist. The SVAMC is a 514-bed, general medical and surgical hospital affiliated with Albany Medical College. Albany, the capital of New York, is located upstate and is only a 3-hr drive to New York City, Boston, and Montreal. New equipment located within the service includes a new Siemens Angiostar digital angiography suite, Philips 0.5-T superconductive MRI unit, upgraded Picker 1200 CT scanner, and Acuson color Doppler. Experience in MRI and/or angiography preferred. Interested radiologists please send CV to A. Fermin, M.D., Chief, Radiology Service (114), Stratton VA Medical Center, 113 Holland Ave., Albany, NY 12208. EOE. 11-1a

FULL-TIME DIAGNOSTIC RADIOLOGIST, LAS CRUCES, NM—Seeking a radiologist to work in an outpatient imaging center. No nights, weekends, or holidays. General radiography, CT, ultrasound, nuclear medicine, and mammography. Salary with insurance negotiable. Contact C. L. Chapman, 755 Telshor, Bldg. S/T, Ste. 101, Las Cruces, NM 88001; (505) 522-6236. 11-12ap

VETERANS AFFAIRS MEDICAL CENTER, AUGUSTA, GA, is seeking a physician, board-eligible/certified in radiology. Subspecialty interest in chest, skeletal, GI, or interventional radiology is desirable but not essential. This 1142-bed, tertiary-care medical center is affiliated with the Medical College of Georgia. Faculty appointment commensurate with qualifications and experience. Augusta enjoys a moderate climate, reasonable cost of living, numerous recreational facilities, and institutions of higher learning. An equal opportunity employer. For additional information, contact George T. Jamarik, M.D., Chief, Radiology Service; (404) 823-2236. 11a

DIAGNOSTIC RADIOLOGIST, BODY IMAGING—Large radiology group in western Massachusetts seeks board-certified radiologist with fellowship and/or experience in MRI, CT, and ultrasound. Neuroradiology expertise and/or interest desirable, but not required. Primary assignment with 330-bed community hospital. Practice includes 3 other hospitals with 6 private offices. Full partnership after 1 yr. Start on or around March 1, 1992. Send CV to W. M. Cloud, M.D., Radiology & Imaging, Inc., P.O. Box 2250, Springfield, MA 01101. 11-1ap

NEURORADIOLOGIST—Seeking a board-certified, fellowship-trained, ASNR-member neuroradiologist with training and/or experience in interventional procedures for non-tenure track faculty position, assistant to associate professor. Active, university-based neuroradiology fellowship training program in place. Salary and rank commensurate with faculty rank and experience. Applications will be accepted until Jan. 31, 1992. Please contact David O. Davis, M.D., Professor and Chairman, Dept. of Radiology, The George Washington University Hospital, 901 23rd St., N.W., Washington, DC 20037. The George Washington University is an affirmative action/equal opportunity employer. 11a

RADIOLOGISTS—The Beth Israel Medical Center, Dept. of Radiology, in New York City has positions available in 2 specialties. This newly renovated dept. has a staff of 20 full-time radiologists and offers an active clinical practice, a strong teaching program, and stimulating research activities within our 955-bed teaching hospital, affiliated with The Mount Sinai School of Medicine. Neuroradiologist — This section features state-of-the-art equipment including 3 GE 9800 CT scanners, a GE 1.5-T MRI, and a new angiography suite. Pulmonary radiologist — The BC diagnostic radiologist we seek will have expertise in chest radiography. Both positions require a strong interest and ability in teaching. Academic rank for these positions will be commensurate with candidates' qualifications and experience. Excellent remuneration and benefits. Please send inquiries with CV to Michael M. Abiri, M.D., Dept. of Radiology, Beth Israel Medical Center, First Ave. at E. 16th St., New York, NY 10003. An equal opportunity employer committed to a smoke-free environment. 11a

FACULTY POSITION IN ABDOMINAL IMAGING—Dartmouth-Hitchcock Medical Center is seeking a faculty member at the senior assistant or full professor level with experience and interest in abdominal imaging. Clinical responsibility will be in an entirely new 420-bed clinical facility opening in Oct. 1991 with state-of-the-art instrumentation. Position will involve responsibility for residency training in GI/GU area. Proven record of academic performance including research and teaching with an interest in providing academic guidance for energetic staff of younger radiologists. Interested candidates write with CV to Peter K. Spiegel, M.D., Chairman, Dept. of Diagnostic Radiology, Dartmouth-Hitchcock Medical Center, Hanover, NH 03756. AA/EOE. 11xap

PEDIATRIC RADIOLOGIST—Children's Hospital and Medical Center (CHMC) and the University of Washington School of Medicine, Seattle, have a faculty opening for an academic pediatric radiologist. Applicants must have completed at least 1 yr of pediatric radiology fellowship beyond a 4-yr residency and must be board-certified. CHMC is a 208-bed medical center that performs approximately 53,000 exams/yr in all phases of pediatric imaging. The successful applicant will join 8 full-time pediatric radiologists, 2 fellows, and 5 residents. The institution is committed to clinical and research excellence, and radiology faculty are encouraged and supported in clinical and basic research efforts. Compensation and fringe benefits are competitive. CHMC and UW are equal opportunity/affirmative action employers. Inquire for additional details to Eric L. Effmann, M.D., Director, Dept. of Radiology, Children's Hospital and Medical Center, P.O. Box C-5371, Seattle, WA 98105; (206) 526-2166. 11-1a

PEDIATRIC NEURORADIOLOGIST—Children's Hospital and Medical Center (CHMC) and the University of Washington School of Medicine, Seattle, have a faculty opening for an academic pediatric neuroradiologist. Applicants must have completed a 4-yr residency in radiology, be board-certified, and have completed an approved ACGME neuroradiology training program. Additional or prior training in pediatric radiology is desirable. CHMC is a 208-bed medical center that performs approximately 53,000 exams/yr in all phases of pediatric imaging. Successful applicants will join 8 full-time pediatric radiologists, 2 fellows, and 5 residents. The institution is committed to clinical and research excellence, and radiology faculty are encouraged and supported in clinical and basic research efforts. Compensation and fringe benefits are competitive. CHMC and UW are equal opportunity/affirmative action employers. Inquire for additional details to Eric L. Effmann, M.D., Director, Dept. of Radiology, Children's Hospital and Medical Center, 4800 Sand Point Way, N.E., Seattle, WA 98105; (206) 526-2166. 11-1a

IMMEDIATE OPENING—BE/BC general diagnostic radiologist to join 4-person group in Wilson, NC. This 366-bed hospital has state-of-the-art facilities including MRI. Imaging skills mandatory; interventional skills desirable. Excellent salary and benefits leading to early partnership. Contact James H. Melvin, M.D., Dept. of Radiology, Wilson Memorial Hospital, 1705 S. Tarboro St., Wilson, NC 27893. 11-1ap

RADIOLOGIST, MARYLAND—BC/BE to join 9-physician radiology dept. Special skills in angio/interventional and MRI desired. Fellowship training preferred. Must be willing to do most aspects of diagnostic radiology. Part of a larger, multispecialty group providing care for BC/BS-affiliated HMO as well as growing FFS practice. Excellent benefits and salary. Located in Columbia, MD, near cultural advantages and medical schools of the Baltimore-Washington, DC, area. Direct CV to Patuxent Medical Group, Inc., 2 Knoll North Dr., Ste. 401, Columbia, MD 21045, Attn: Physician Recruiter. EOE/MFHV. 11-12ap

UNIVERSITY OF CHICAGO, ANGIOGRAPHY/INTERVENTIONAL RADIOLOGIST—The University of Chicago Hospital's exceptionally active clinical and academic programs provide a wide variety of case material. A second new biplane digital room was just installed as well as a 5-bed recovery ward. Interested applicants should call or forward their CVs to Dr. Martin J. Lipton, Chairman, Dept. of Radiology—Box 429, 5841 S. Maryland Ave., Chicago, IL 60637; (312) 702-6024, fax (312) 702-1161. Affirmative action/equal opportunity employer. 11-1ap

LONG BEACH, CA—The VA Medical Center, Long Beach, CA, is seeking applications for full- and part-time radiologist positions in CT, ultrasound, and neuroradiology. Interest in MRI and intervention desirable. Board-certification/eligibility required. May be licensed in any state. U.S. citizenship is required. Responsibilities include teaching and supervision of residents in conjunction with the affiliated program, University of California, Irvine. Please send CV to Chief, Radiology Service, VAMC, 5901 E. 7th St., Long Beach, CA 90822; (213) 494-2611, or ext. 4787. The DVA is an equal opportunity employer. 11-2a

UNIVERSITY OF CHICAGO, CHIEF OF ABDOMINAL IMAGING—Excellent opportunity for a dynamic person who is interested in building an outstanding clinical and research program in abdominal imaging at the University of Chicago. During the past 3 yr, almost all of our diagnostic imaging equipment has been replaced and new rooms opened. Exciting clinical and research opportunities are available with new state-of-the-art CT, MRI, and ultrasound equipment. Four new CT units have been purchased, including a GE 9800 and an Imatron C-1000 (ultrafast CT). A Siemens 1.5-T MRI unit and a new GE 1.5-T Signa MRI unit are in operation, and an Instrumentarium 0.1-T MRI unit (the first in the U.S.) has recently been installed in the diagnostic area. Another new 1.5-T unit is on order for delivery in 1992. An additional small horizontal-bore, high-field 4.7-T MRI/MRS unit dedicated to research has been purchased and awaits installation. Interested applicants should call or forward their CVs to Dr. Martin J. Lipton, Chairman, Dept. of Radiology—Box 429, 5841 S. Maryland Ave., Chicago, IL 60637; (312) 702-6024, fax (312) 702-1161. Affirmative action/equal opportunity employer. 11-1ap

UNIVERSITY OF CHICAGO, CHIEF OF PEDIATRIC RADIOLOGY—The University of Chicago is seeking a pediatric radiologist at the rank of associate or professor who is interested in building an outstanding clinical and research program. Current workload approximately 30,000 exams/yr. Clinical facilities include fluoroscopy, ultrasound, CT, and MRI. Excellent opportunity for a dynamic person. Interested applicants should call or forward their CVs to Dr. John Fennessy, Chairman, Search Committee, Dept. of Radiology—Box 429, 5841 S. Maryland Ave., Chicago, IL 60637; (312) 702-6024, fax (312) 702-1161. Affirmative action/equal opportunity employer. 11-1ap

UNIVERSITY OF CHICAGO, CHIEF OF ANGIOGRAPHY/INTERVENTIONAL—Excellent opportunity for a dynamic person who is interested in building an outstanding clinical and research program. Our current chief is nearing retirement, and we are seeking a person with potential to succeed him. The University of Chicago Hospital's exceptionally active clinical and academic programs provide a wide variety of case material. A second, new biplane digital room was just installed as well as a 5-bed recovery ward. Interested applicants should call or forward their CVs to Dr. Martin J. Lipton, Chairman, Dept. of Radiology—Box 429, 5841 S. Maryland Ave., Chicago, IL 60637; (312) 702-6024, fax (312) 702-1161. Affirmative action/equal opportunity employer. 11-1ap

UNIVERSITY OF CHICAGO, PEDIATRIC RADIOLOGIST—The University of Chicago is seeking a pediatric radiologist for an academic position. Workload approximately 30,000 exams/yr. Clinical facilities include fluoroscopy, ultrasound, CT, and MRI. Candidate should be a member of the Society of Pediatric Radiology. Interested applicants should call or forward their CVs to Dr. Martin J. Lipton, Chairman, Dept. of Radiology—Box 429, 5841 S. Maryland Ave., Chicago, IL 60637; (312) 702-6024, fax (312) 702-1161. Affirmative action/equal opportunity employer. 11-1ap

UNIVERSITY OF CHICAGO, ABDOMINAL IMAGING—The University of Chicago is seeking a diagnostic radiologist for an academic position to participate in clinical service, medical student and resident teaching, and research projects. The major area of clinical responsibility will be abdominal imaging, which includes GI/GU, CT, ultrasound, and mammography. Applicants should be eligible or certified by the ABR. Interested applicants should call or forward their CVs to Dr. Martin J. Lipton, Chairman, Dept. of Radiology—Box 429, 5841 S. Maryland Ave., Chicago, IL 60637; (312) 702-6024, fax (312) 702-1161. Affirmative action/equal opportunity employer. 11-1ap

RADIOLOGISTS—Eight-member group seeking board-certified/eligible radiologist to join progressive hospital/clinic practice in scenic western Arkansas town of approximately 100,000. All modalities represented in practice. Competitive salary leading to early full partnership. Liberal fringe benefits and vacation. Interested parties, please send CV to Gary A. Plymale, P.O. Box 3887, Ft. Smith, AR 72913; (501) 452-9416 (collect). 11-1ap

CHAIRPERSON, DEPT. OF RADIOLOGY—Applications are being accepted for the position of professor and chairperson of the Dept. of Radiology, State University of New York at Buffalo. Applicants should have an M.D. degree, should have successfully completed a residency in radiology approved by the ACGME, and be certified by the American Board of Radiology or have equivalent qualifications. Applicants should demonstrate evidence of leadership and achievement in academic radiology with significant accomplishments in clinical, educational, administrative, managerial, and investigative endeavors. Candidate must qualify as professor with tenure. SUNY-Buffalo is an affirmative action/equal opportunity employer. SUNY-Buffalo is particularly interested in identifying prospective minority and women candidates. No person, in whatever relation with SUNY-Buffalo, shall be subject to discrimination on the basis of age, creed, color, handicap, national origin, race, religion, sex, marital, or veteran status. Please send letter of application and CV to Ronald L. Stempowski, Executive Vice-President, Diversified Health Search, 2005 Market St., Ste. 3300, Philadelphia, PA 19103. Application deadline is Dec. 31, 1991. 11a

MAINE—Board-certified radiologist, preferably with imaging fellowship, wanted for 13-member group based in Bangor. Strong skills in MRI, CT, and ultrasound highly desirable. Excellent vacation, CME, and fringe benefit package. Three yr to partnership. Great quality of life with ocean, mountains, cultural activities, and university easily accessible. Contact Peter Holman, Administrator, Andrews, Lynch & Field, Radiologists, P.A., 276 State St., Bangor, ME 04401; (207) 945-6877. 11a

LOUISIANA STATE UNIVERSITY is seeking a chairperson for the Dept. of Radiology. An M.D. degree with a minimum of 5 yr experience in an academic university dept. with an approved residency program is required. The dept. is equipped with the latest radiologic and nuclear technology. A biomedical research building is being built that will contain a PET scanner and cyclotron. The anticipated date for completion is Dec. 1993. The residency program was recently surveyed and is on provisional approval for 12 residents. LSUMC is an equal opportunity/affirmative action employer. Please address all inquiries to the Office of the Dean, Attn: Ike Muslow, M.D., P.O. Box 33932, Shreveport, LA 71130. 11a

CODY, WY has an immediate position available for a board-certified radiologist. Live and work in the beautiful Rocky Mountain region, located only 50 mi. from Yellowstone Park. Abundant fishing, hunting, and outdoor sports. No state income tax! For more information, call (307) 578-2488 or send CV to Gary Bishop, CEO, West Park Hospital, 707 Sheridan Ave., Cody, WY 82414. 11-1a

A MULTISPECIALTY MEDICAL GROUP has an immediate need for a radiologist. Excellent benefit package, guaranteed salary with incentive, all expenses paid first yr, with partnership opportunity for the future. Direct inquiries or send CV to Penny Phillips, Malone and Hogan Clinic, 1501 W. 11th Pl., Big Spring, TX 79720; (915) 267-6361. 10-3a

INTERVENTIONAL RADIOLOGIST—Well-established community hospital and imaging center-based practice in New York capitol district seeks fellowship-trained interventional radiologist. Individual should have expertise and interest in all aspects of interventional radiology including thrombolytic therapy. Ultramodern-equipped practice with state-of-the-art new biplane angiography suite. Practice emphasizes subspecialty expertise in all aspects of diagnostic imaging, performing 100,000 exams/yr. Excellent compensation package leading to lucrative full partnership. Send CV to Michael E. Berlow, M.D., Dept. of Medical Imaging, Albany Memorial Hospital, 600 Northern Blvd., Albany, NY 12204. 10-11ap

NEURORADIOLOGIST—Well-established community hospital and imaging center-based practice in Albany, NY, seeks fellowship-trained neuroradiologist. Applicants should have expertise and interest in all aspects of neuroradiology with particular emphasis on MRI. Interests in other aspects of radiology, particularly cross-sectional imaging, desirable. Ultramodern-equipped practice including 2 high-field Siemens MRI units and MRA capability, new biplane angiography suite, and 2 Siemens CT scanners. Practice emphasizes subspecialty expertise in all aspects of diagnostic imaging, performing 100,000 exams/yr. Capitol district community with abundant cultural, recreational, and educational opportunities. Excellent compensation package leading to lucrative full partnership. Send CV to Michael E. Berlow, M.D., Dept. of Medical Imaging, Albany Memorial Hospital, 600 Northern Blvd., Albany, NY 12204. 10-11ap

CALIFORNIA CENTRAL COAST—Established group has an opening for a general radiologist skilled in angiography, CT, MRI, and ultrasound to practice in 2 community hospitals, an MRI center, and a multispecialty clinic. Pediatric radiology experience a plus. Competitive compensation with opportunity for advancement to full partner. This is an excellent opportunity to join an expanding practice in a beautiful community along California's central coast. Please contact Managing Partner, Radiology Associates of SLO, P.O. Box 8129, San Luis Obispo, CA 93403-8129. 10-11ap

DIAGNOSTIC RADIOLOGIST—A 5-person group seeks a BC/BE diagnostic radiologist. MRI available. Located in northwest Indiana (greater Chicago metropolitan area). 80,000 diagnostic imaging procedures/yr. Excellent compensation commensurate with qualifications. Reply to Box P80, *AJR* (see address this section). 10-11ap

OPENING FOR BC/BE RADIOLOGIST with cross-sectional imaging (MRI/CT/ultrasound) fellowship or equivalent experience to join 8-member hospital-based group in Pensacola, FL. Position open Jan. 1992 (possible to hold open until July 1992). Teaching involved. 380-bed hospital/100,000+ procedures/yr. Send CV to Harry Cramer, M.D., P.O. Box 9210, Pensacola, FL 32513-9210. 10-11ap

NORTHWEST ROCKY MOUNTAINS—Highly respected, 8 person group with strong subspecialty interests seeks highly qualified radiologist. Fellowship or academic experience preferred. Body imaging/MRI, nuclear medicine with boards, or ABR special competency strongly desired. Position includes all aspects of radiology. Practice is located in Boise, ID, which has many recreational and cultural amenities. Reply to Paul Traugher, M.D., or J. Tim Hall, M.D., Dept. of Radiology, St. Alphonsus Regional Medical Center, 1055 N. Curtis Rd., Boise, ID 83706; (208) 378-2161. 10-1ap

THE DEPT. OF RADIOLOGY OF THE CHILDREN'S MEMORIAL HOSPITAL, CHICAGO, is seeking a third pediatric neuroradiologist. The Division of Neuroradiology has 3 positions including the director. There is 1 fellowship position per yr as well as a fellow rotating from Northwestern Memorial Hospital. The dept. has an active clinical service with state-of-the-art equipment as follows: 2 CT scanners (a GE 9800 Quick CT scanner, and a Philips LX), a 1.5-T GE Signa MRI, Acuson ultrasound units, and Siemens Angiostar with biplane digital imaging. Applicants must be certified by the American Board of Radiology and have completed a fellowship in neuroradiology. Duties include clinical services, teaching, and research. The institution has very active neurosurgery and neurology services with 4 full-time neurosurgeons. The Children's Memorial Hospital is affiliated with Northwestern University Medical School, and the candidate selected would have an appointment in the Dept. of Radiology at Northwestern University. Please send CV to Andrew K. Poznanski, M.D., Radiologist-in-Chief, Children's Memorial Hospital, 2300 Children's Plaza, Chicago, IL 60614. For inquiries, please call (312) 880-3520. Children's Memorial Hospital and Northwestern University are affirmative action/equal opportunity employers. Hiring is contingent on medical licensure in Illinois. 10-11a

NORTHERN CALIFORNIA—The Permanente Medical Group, Inc., is seeking a BC radiologist with multimodality interests and fellowship training in MR to join a 12-person group serving a 337-bed, acute-care hospital and 2 outpatient clinics. Teaching opportunities are available with residents of subspecialty services on rotation from Stanford University Hospital, as well as our own medical residents. We have sited a GE 1.5-T MRI system. Competitive salary and excellent benefits. Please send inquiries and CV to Bruce Baker, M.D., Chief, Dept. of Radiology, Kaiser Permanente Medical Center, 900 Kiely Blvd., Santa Clara, CA 95051; (408) 236-4444. EOE. 9-11a

DIAGNOSTIC RADIOLOGIST IMMEDIATE OPENING AT ROSE MEDICAL CENTER (RMC), DENVER, CO—An 8-person radiology group is recruiting an additional radiologist with fellowship training in MR and CT. The practice involves all imaging modalities. Highly competitive first yr salary and generous fringe benefit package. Position leads to offer of equal shares in the professional corporation after 1 yr., if mutually agreed upon. RMC is affiliated with the University of Colorado. Contact David W. Wilder, M.D., or Jeffrey A. Levy, M.D.; (303) 320-2256. 9-11ap

RADIOLOGISTS—An innovative health care organization is seeking radiologists to serve communities in rural southern West Virginia. Competitive salary and fringe benefits are offered. A desire and willingness to meet challenges of present-day health care delivery in rural settings is a must. Part- or full-time positions are available. Arrangements may also be made to accommodate continued residence outside West Virginia. Send confidential resume and inquiries to Box O9, *AJR* (see address this section). 10-11ap

COASTAL NORTHERN CALIFORNIA/SAN FRANCISCO BAY AREA—A progressive, diversified group of 16 board-certified diagnostic radiologists, 5 radiation oncologists, and 2 medical oncologists seeks a board-eligible/certified radiologist with some training in MRI and/or neuroradiology. The group serves 4 small- to medium-sized hospitals and a large, outpatient imaging center. The imaging center includes a GE 1.5-T MRI, 9800 Advantage CT, and Acuson ultrasound, as well as CGR mammography, and 3 RF rooms. Competitive salary, 2 yr to full partnership, and excellent benefits. Fast-growing, suburban community 50 min north of downtown San Francisco with sunny Mediterranean climate and very mild winters in the heart of the wine country. Excellent outdoor recreational opportunities. Please send initial inquiry and CV to John J. McGovern, M.D., 121 Sotoyome St., Santa Rosa, CA 95405; (707) 546-4062. 9-2ap

TEXAS, DIAGNOSTIC RADIOLOGIST—Excellent, private-practice opportunity for BC/BE radiologist seeking professional satisfaction and quality of life. Noninvasive procedures; all other modalities except MRI. New equipment in new hospital. Well-trained, congenial medical staff eager to work with radiologist. Great outdoor recreation; hunting and lakes; easy access to stream fishing and snow skiing. Contact Jim Truitt, Physician Resource Network, P.O. Box 37102, Fort Worth, TX 76117-8102; (800) 525-6055. 9-11ap

ONCOLOGIC RADIOLOGY/MAMMOGRAPHY The Dana-Farber Cancer Institute and Brigham and Women's Hospital, teaching affiliates of Harvard Medical School, seek a full-time diagnostic radiologist with interests in oncologic radiology and mammography. The 2 hospitals are in close proximity and the radiology dept. at Dana-Farber Cancer Institute is staffed by Brigham and Women's Hospital faculty and residents. The Dana-Farber Cancer Institute is one of the world's leading cancer treatment and research facilities and many opportunities exist for collaborative clinical research in cancer imaging. Please contact Jack E. Meyer, M.D., Director of Diagnostic Radiology, Brigham and Women's Hospital and Dana-Farber Cancer Institute, 75 Francis St., Boston, MA 02115; (617) 732-6269. Brigham and Women's Hospital/Dana-Farber Cancer Institute/Harvard Medical School is an affirmative action/equal opportunity educator and employer. 9-2a

RADIOLOGIST, TYLER, TX—The University of Texas Health Center at Tyler invites applications for a clinical faculty position in the Dept. of Radiology. Some teaching is required, but not publishing or research. A progressive, 4-person dept. practices general radiology (including interventional, MRI, and SPECT) and performs approximately 27,000 exams/yr. New equipment, flexible work hours, very light call, and no weekend schedule. Year-round tennis, golf, and boating are available in addition to excellent schools. Competitive first-yr salary and an unsurpassed benefits package are offered. Send CV to J. R. Shepherd, M.D., University of Texas Health Center at Tyler, P.O. Box 2003, Tyler, TX 75710; (903) 877-7100. The University of Texas Health Center at Tyler is an affirmative action, equal opportunity employer. Minorities are encouraged to apply. 9-11a

DIAGNOSTIC RADIOLOGIST—Immediate opening leading to partnership in expanding 4-member, hospital-based practice near Boston. Seeking recently trained BC/BE radiologist with skills and experience in general radiology, ultrasound, mammography, CT, and angio/interventional. Interested persons should contact Steven Sitzman, M.D., The Malden Hospital, One Hospital Rd., Malden, MA 02148; (617) 322-7560. 9-11ap

NEURO/GENERAL RADIOLOGIST—Exceptional private-practice opportunity created by involuntary departure of neuroradiologist. 350-bed community hospital with all modalities including 1.5-T MRI and new DSA. Full benefits, 1 yr to partnership, excellent salary, and liberal time off. Contact John Lacika, M.D., 1406 N. 6th Ave., St. Cloud, MN 56303; (612) 255-5619. 10-12ap

LARGE, DYNAMIC RADIOLOGY PRACTICE in central New Jersey and adjacent Pennsylvania region seeks diagnostic radiologist with expertise in 1 or more of the following: CT/ultrasound, angio/interventional, or nuclear medicine with cardiac emphasis. Outstanding opportunity for well-qualified person. Send resume to E. Tarasov, M.D., 838 W. State St., Trenton, NJ 08618. 10-12a

FLORIDA, NUCLEAR MEDICINE AND DIAGNOSTIC RADIOLOGISTS needed for a well-established and progressive group of 14 radiologists in Tampa Bay covering 2 hospitals and outpatient imaging centers. Busy nuclear division with single- and triple-headed SPECT. Nuclear boards or additional fellowship training in interventional radiology or sonography required. Candidate must be willing to cover other areas of diagnostic imaging as well. Competitive first yr salary followed by equitable partnership route. Send CV to Box O11, *AJR* (see address this section). 9-11ap

ULTRASOUND/CT/MRI—Opportunity for board-certified radiologist specializing in ultrasound, body CT, and body MRI to pursue an academic career at The New York Hospital-Cornell Medical Center. The dept. provides state-of-the-art equipment, including Acuson ultrasound, GE 9800 CT, and GE Signa 1.5-T MR. A wide variety of ultrasound exams are performed, including abdominal, OB-GYN, color Doppler, small parts, neonatal head, transvaginal, and transrectal. A candidate with prior fellowship in sectional imaging or ultrasound is preferred. Responsibilities include clinical practice, teaching, and research. Position available 9/1/91. Please send CV to Elias Kazam, M.D., Dept. of Radiology, the New York Hospital-Cornell Medical Center, 525 E. 68th St., New York, NY 10021. 9-12a

PHYSICIAN/RADIOLOGIST—Large radiology group with multiple private offices seeks a board-certified radiologist interested in a full-time position. Responsibilities include general radiography. Special training in CT, ultrasound, and nuclear medicine is preferred. Excellent southern New Jersey location. Competitive salary and benefit package. Send CV to RABC, P. O. Box 729, Mt. Holly, NJ 08060. 9-11ap

HOSPITAL-BASED, BC/BE RADIOLOGIST needed to join newly laid plans for a subregional medical center (campus). Must be proficient in general diagnostic radiology, ultrasound, nuclear medicine, CT, and MRI. Excellent opportunity plus attractive financial package. Located in east, central Montana along the Yellowstone River. Great outdoors for recreation, hunting, and fishing. Excellent education system. Lifestyle is rural and family-oriented. Send CV to Vice-President, Business Services, Holy Rosary Hospital, 2101 Clark, Miles City, MT 59301. 9-11ap

NORTHERN CALIFORNIA—BC diagnostic radiologist sought for medical imaging dept. in a large, multispecialty group practice. Facility features new state-of-the-art equipment, including Phillips CT, SPECT, color Doppler, and mobile 0.5-T MR. Beautiful community in the heart of the wine country, 50 mi. north of San Francisco. Excellent salary and benefits package leading to eligibility for shareholder status. Send CV to Alan Larocque, M.D., Ph.D., Dept. of Medical Imaging, Kaiser Permanente Medical Center, 401 Bicentennial Way, Santa Rosa, CA 95401-2192. EOE. 9-11a

FACULTY RADIOLOGIST, BODY MRI DIVISION, THOMAS JEFFERSON UNIVERSITY HOSPITAL—The Dept. of Radiology at Thomas Jefferson University Hospital has an opening for a radiologist in an active, body MRI section that encompasses a clinical mix of approximately 50% musculoskeletal and 50% chest/abdomen/pelvis cases. Equipment includes 4 1.5-T GE Signa systems with state-of-the-art and advanced prototype hardware and software. A full-yr body MRI fellowship and/or 1 yr of academic MRI experience is preferred. Clinical cross coverage in ultrasound and/or general radiology also can be incorporated depending on the interests and qualifications of the candidate. Dedicated, non-clinical research time is provided, and the dept. has excellent research facilities and support, including 2 MRI physicists, a radiology animal facility, radiology research funding, and a team of research assistants. Excellent faculty incomes and benefits are offered within a financially secure dept. and university hospital. This is a unique opportunity for an academically oriented MRI radiologist to join a dynamic and rapidly growing dept. Interested candidates should contact Donald G. Mitchell, M.D., Director of MRI, Dept. of Radiology, 1032 Main Bldg., Thomas Jefferson University Hospital, Philadelphia, PA 19107; (215) 955-4809. Jefferson is an equal opportunity/affirmative action employer. 11xa

SOUTHERN OREGON—Opportunity for BC/BE, general diagnostic radiologist to join group of 5 board-certified radiologists. Experience in all modalities desired. Practice includes 2 hospitals and own private office. Competitive starting salary with early full partnership. Excellent lifestyle with many outdoor activities from Pacific Coast to Oregon Cascades. Send CV to Larry Strickland, Administrator, Roseburg Radiologists, P.C., P. O. Box 1547, Roseburg, OR 97478. 8-1ap

DIAGNOSTIC RADIOLOGIST—Board-certified/eligible radiologist with skills in CT, MRI, ultrasound, nuclear medicine, and mammography needed for position with group of 12 young radiologists. Expanding practice is hospital-based, fee-for-service with 2 private-practice offices. Hospital-based practice in 400-bed hospital includes MRI, 2 CT units, modern interventional suite, satellite outpatient imaging center, and breast care center. Private-practice offices include MRI facility and full-service radiology office. Position available July 1992. Interested applicants should submit letter and CV to G. Edward Streubert, M.D., MRI of Bethlehem, Inc., Ste. 105, 95 Highland Ave., Bethlehem, PA 18017. 9-11ap

THE DEPT. OF RADIOLOGY AT TRIPLER ARMY MEDICAL CENTER, HONOLULU, HI. is recruiting academic radiologists for several divisions of the dept. including ultrasound, chest radiology, skeletal, neuroradiology, general diagnostic radiology, MRI, interventional radiology, and mammography. Our dept. offers a fully accredited residency program with 21 residents and 16 attending full-time staff. Numerous consultants from across the country lecture on a continuing and regular basis. The hospital is a modern, tertiary-care center serving Hawaii and the entire Pacific Basin. A strong residency program, diverse and interesting patient population, excellent equipment, and tropical lifestyle are positive aspects of the practice. Academic credentials and/or experience are necessary. Recently graduated fellows are encouraged to apply. Board certification is mandatory. Candidates should be particularly interested in patient care, teaching, and research. Salary and benefits are competitive and generous. Tripler is an EO/EEO employer. Please contact Dr. Mark F. Hansen, Col., MC, Chief, Dept. of Radiology, TAMC, HI 96859-5000; (808) 433-6393. 7-6a

SAN FRANCISCO BAY AREA, DIAGNOSTIC RADIOLOGY—Full-time position available as of July 1992 for BC/BE radiologist to join established group based in growing SF Bay area communities. Competence in all modalities including MRI and angiography required; fellowship training desirable. Contact J. Fish, M.D., c/o Walnut Creek Radiology, 1844 San Miguel Dr., #302, Walnut Creek, CA 94596; (415) 947-0560. 11-1xa

ISRAEL, DIAGNOSTIC RADIOLOGY. Opportunities for 3-4 week or longer working vacations in a number of Israeli medical centers, on a volunteer basis. Positions varied, arrangements flexible. For information contact: Jonathan H. Fish, M.D., 1844 San Miguel Dr., #302, Walnut Creek, CA 94596; (415) 947-0560. 11-1xa

THE NATIONAL INSTITUTES OF HEALTH is seeking an interventional radiologist with fellowship training. Resources include 20 fully equipped angiographic rooms and extensive research opportunities with laboratory support available. Would share duties with 2 other senior angiographers. Generous benefit package and appointment at Georgetown University Hospital is included. Interested candidates should contact John L. Doppman, M.D., Dept. of Radiology, National Institutes of Health, Bldg. 10, Rm. 1C-660, Bethesda, MD 20892; (301) 496-5080. 9-11ap

POSITION OPEN IMMEDIATELY—A 40-physician, multispecialty clinic serving central and western Kansas, seeks a board-eligible/certified radiologist. Excellent facilities include diagnostic radiography, CT scan, diagnostic ultrasound, nuclear medicine, and MR services. Very competitive salary and benefits. No night or weekend call. An excellent opportunity in a dynamic practice setting. Please send CV to Administrator, Hutchinson Clinic, 2102 N. Waldron, Hutchinson, KS 67502; (316) 669-2626 (collect). 9-11ap

DIAGNOSTIC RADIOLOGIST—Mallinckrodt Institute of Radiology, Washington University, seeks an additional board-certified radiologist with academic interest to staff a satellite hospital of Barnes Hospital in St. Louis. This satellite radiology facility in St. Louis county performs all aspects of diagnostic radiology, including CT, MRI, ultrasound, and nuclear medicine. Equipment is brand new and state-of-the-art. Candidates must be competent in all aspects of diagnostic radiology and must be able to do cross-sectional interventional procedures. Academic rank and salary are dependent on qualifications and previous experience. The institute is conducting research in teleradiology and outcomes research at the satellite facility. Washington University is an equal opportunity employer. Applications from women and minority group members are encouraged. Send CV to R. Gilbert Jost, M.D., Chief of Diagnosis, Mallinckrodt Institute of Radiology, 510 S. Kingshighway Blvd., St. Louis, MO 63110. 9-11ap

IMMEDIATE OPENING FOR BE/BC RADIOLOGIST in a regional hospital with a patient base of 25,000 located in a scenic western Wyoming community. Great outdoor recreation area. Competitive reimbursement. Ultrasound/CT/general radiology. Interested persons contact Paul Sonntag, M.D., P. O. Box 629, Ogden, UT 84402; (801) 625-2092. 8-1ap

DIAGNOSTIC RADIOLOGIST, NEW MILFORD, CT—A third radiologist is sought for a busy, private practice located in 1 of the most beautiful areas of Connecticut. We provide the full range of diagnostic services for a modern, well-equipped, community hospital. Choice environment; excellent compensation. Send inquiries and CV to Jules White, M.D., New Milford Hospital, 21 Elm St., New Milford, CT 06776; (203) 355-2611, ext. 235. 8-11ap

IMMEDIATE OPENING FOR BC/BE GENERAL RADIOLOGIST with experience in interventional and vascular radiology. Join a group of 4 radiologists in a 160-bed hospital located in Allentown, PA, about 60 mi. northwest of Philadelphia. The daily practice includes all aspects of general radiology, CT, ultrasound, and nuclear medicine. Please call or send CV to Asad Shohadai, M.D., Allentown Osteopathic Medical Center, 1736 Hamilton St., Allentown, PA 18104; (215) 770-8700. 11xa

VASCULAR/INTERVENTIONAL RADIOLOGIST, LONG ISLAND, NY—Board-certified radiologist with fellowship training or equivalent experience in vascular/interventional radiology needed to join a 5-member group starting July 1992. Angio suite currently being upgraded to latest state-of-the-art equipment. Must be willing to do most aspects of diagnostic radiology. This well-established practice includes a 325-bed community hospital, a private diagnostic radiology office, and a 1-yr-old MRI facility. Generous salary leading to full partnership. Contact Ira Langer, M.D., 250 Hospital Rd., Patchogue, NY 11722; (516) 475-1030. 8-11ap

CHEST RADIOLOGIST, THOMAS JEFFERSON UNIVERSITY HOSPITAL—The Dept. of Radiology at Jefferson has an opening for a thoracic radiologist at either the junior or senior level. The position encompasses plain film radiography, CT, and percutaneous thoracic interventions. Involvement in mammography, other general diagnostic areas, and ultrasound can also be incorporated, depending on the interests of the candidate. Dedicated, nonclinical research time is provided, and the dept. has excellent research facilities and support. Our chest radiology practice is expanding rapidly and close working relationships are maintained with pulmonary medicine and thoracic surgery. Teaching is also emphasized, with a large residency program and a thoracic radiology fellowship. Excellent faculty income and benefits. This is a fine opportunity for a radiologist with academic interests to join a dynamic and rapidly growing dept. Interested candidates should contact David C. Levin, M.D., Chairman, Dept. of Radiology, Thomas Jefferson University Hospital, Philadelphia, PA 19107; (215) 955-7264. Jefferson is an equal opportunity/affirmative action employer. 11xa

OREGON—Opportunity for BC/BE radiologist to join 7 BC radiologists in growing practice in the Portland metropolitan area. Training/expertise in all aspects of radiology including MRI is required. The practice includes 2 suburban hospitals, an outpatient clinic, and a new multimodality outpatient imaging clinic. Competitive compensation with generous fringe package and partnership in 2 yr. Send letter and CV to Jon C. Sewell, M.D., P.O. Box 227, Oregon City, OR 97045; (503) 655-1439. 11xa

RADIOLOGIST/ANGIOGRAPHER—There is an opportunity to join a progressive group of 11 board-certified radiologists practicing at the Lehigh Valley Hospital Center, a 500-bed, university-affiliated hospital. The position requires angiographic/interventional skills and an interest in general radiology including CT and ultrasound. The radiology dept. has state-of-the-art equipment including 2 angiographic suites, 3 CT scanners, color flow Doppler, and MRI. The hospital is an acute-care facility and a state-designated Level 1 Trauma Center, located 1 hr from Philadelphia and 1½ hr from New York. The radiology dept. offers a postresidency fellowship program that includes training in angiography. The position offers a competitive salary and benefit package that leads to full partnership. For further information, contact Robert Kricun, M.D., Dept. of Radiology, Lehigh Valley Hospital Center, P.O. Box 689, Allentown, PA 18105; (215) 776-8088. 11-1ap

HARTFORD, CT—Position available for board-certified radiologist to join an established group of 8. Practice includes hospital and 4 private offices, all fully equipped, including CT. Mammography and nuclear medicine experience is essential. Competitive starting salary and benefits. Please enclose CV with initial correspondence to Jeffrey Blau, M.D., 40 Hart St., New Britain, CT 06052; (203) 229-2059. 11ap

BC DIAGNOSTIC RADIOLOGIST—Affluent practice. Excellent salary, benefits, and early partnership. Investigate now before socialized medicine becomes a reality! Practice at a 395-bed hospital, the second largest in the beautiful state of Delaware, centrally located on the east coast. This is a rapidly expanding, high-powered, group practice. Subspecialty training in interventional, imaging, or neuro desired. Open to F-M with 1-2 yr of postgrad experience. Send resume to or contact Ben Hollander, M.D., Dept. of Radiology, St. Francis Hospital, 7th and Clayton Sts., Wilmington, DE 19805; (302) 421-4300. 9-2ap

THE DEPT. OF RADIOLOGY AT WALTER REED ARMY MEDICAL CENTER is recruiting academic radiologists. We need board-certified radiologists to work in this famous and modern health-care center. Our dept. has a residency program consisting of 24 residents and several fellows. Subspecialists are needed in ultrasound, chest, mammography, genitourinary, gastrointestinal, pediatric, CT, MRI, and interventional radiology, as well as general radiology. Excellent opportunity to live in the nation's capital and also become an integral part of a large teaching program. Salaries are competitive and generous. Highly motivated applicants should contact Col. Mark F. Hansen, Radiology Consultant to the Army Surgeon General, Dept. of Radiology, TAMC, HI 96859-5000; (808) 433-6393. 8-7a

THE RADIOLOGY DEPT. AT DWIGHT DAVID EISENHOWER ARMY MEDICAL CENTER is recruiting academic radiologists. The dept. provides a full range of services including angiography, ultrasound, CT (with a new GE 9800 Advantage system), and MRI (with a new 1.5-T GE Signa system). Development is underway for the installation of a digital teleradiology link to area medical facilities. The dept. is also beginning a radiology residency program in affiliation with the program at the Medical College of Georgia in Augusta. With this growth, the dept. has generated a need for several academic diagnostic radiologists. Board-certified diagnostic radiologists with academic credentials and/or experience are urged to apply. Fellowship training is desired, especially in interventional radiology and/or angiography, however candidates at all levels will be considered. Candidates should be particularly interested in patient care, teaching, and research. The medical center is located on Fort Gordon, GA, adjacent to Augusta and is the tertiary-care hospital supporting 9 Army community hospitals of the southeastern region and Puerto Rico. The hospital supports fully accredited residency programs in family practice, general surgery, medicine, orthopedics, pathology, and psychiatry. Salary and benefits are competitive and generous. The medical center is an EO/EEO employer. Please contact Dr. Thomas M. Ralston, LtC, Chief, Radiology Dept., Eisenhower Army Medical Center, Fort Gordon, GA; (404) 791-6245. 8-7a

ALASKA AREA NATIVE HEALTH SERVICE—Public-service-oriented radiologists needed for cross-cultural health care in Anchorage and Sitka, AK. Salary \$85-\$95K+, excellent benefits. Medical school loan repayment up to \$25K/yr additional. Contact Ken Bartline, RN, (907) 257-1457, collect. Indian Health Service. An equal opportunity employer. 8-1a

MRI/ABDOMINAL IMAGING NEW YORK/NEW JERSEY METROPOLITAN AREA—Board-certified/eligible radiologist needed for a position beginning July 1, 1991. Must have fellowship training in MRI and training in CT, ultrasound, and GI studies. Private practice with 400-bed hospital and outpatient imaging center located in northern New Jersey, near New York City. Send inquiries to James A. Heimann, M.D., Dept. of Radiology, Clara Maass Medical Center, 1 Franklin Ave., Belleville, NJ 07109. 7-12ap

IMMEDIATE OPENING IN PALM SPRINGS, CA Radiologist with MRI expertise/specialization needed to join 10-person group in community hospital/office practice. Contact Marvin J. Friedenbergh, M.D., Dept. of Radiology, Desert Hospital, 1150 N. Indian, Palm Springs, CA 92262. 11xa

IMMEDIATE OPENING IN PALM SPRINGS, CA Radiologist with mammography expertise/specialization needed to join 10-person group in community hospital/office practice. Contact Marvin J. Friedenbergh, M.D., Dept. of Radiology, Desert Hospital, 1150 N. Indian, Palm Springs, CA 92262. 11xa

DIAGNOSTIC RADIOLOGIST, IMMEDIATE OPENING—Ten-person radiology group seeks a diagnostic radiologist with fellowship training, including body MRI/body imaging, to join a busy, hospital-based practice located in rapidly growing north Dallas. GE 1.5-T magnet, Toshiba midfield magnet, 2 GE 9800 scanners, Acuson 128 with color flow Doppler, and new special procedures suite with DSA. Please send CV to Box K54, AJR (see address this section). 11xa

THE DEPT. OF RADIOLOGY AT BROOKE ARMY MEDICAL CENTER, SAN ANTONIO, TX, is recruiting academic radiologists for several divisions of the dept., including ultrasound, chest, skeletal, neuroradiology, general diagnostic, interventional radiology, and mammography. Our dept. offers a fully accredited residency program with 24 residents and 16 attending full-time staff. Numerous consultants from across the country lecture on a continuing and regular basis. The hospital is a modern, tertiary-care center serving Texas, Oklahoma, and Louisiana. A strong residency program, interesting patient population, excellent equipment, teleradiology and digital radiology implementations underway, coupled with a south Texas lifestyle are positive aspects of the practice. Academic credentials and/or experience are necessary. Recently graduated fellows are encouraged to apply. Board certification is mandatory. Candidates should be particularly interested in patient care, teaching, and research. Salary and benefits are competitive and generous. Brooke is an EO/EEO employer. Please contact Dr. Billy E. Cunningham, COL, MC, Assistant Chief, Dept. of Radiology, Brooke Army Medical Center, Fort Sam Houston, TX 78234-6200; (512) 221-8418/8218. 8-7a

NEURORADIOLOGIST—Senior ASNR member needed for excellent hospital and imaging center position in Tucson, AZ. Early partnership opportunity. Send CV to Arizona State Radiology, 7250 E. Ventana Canyon Dr., Tucson, AZ 85715. 8-7ap

MUSCULOSKELETAL RADIOLOGIST, UNIVERSITY OF ARKANSAS FOR MEDICAL SCIENCES, LITTLE ROCK—Join a busy group serving 2 hospitals covering CT, MRI, arthrography, and occasional biopsies, with additional coverage in mammography and some general radiology. Excellent rapport with orthopedic dept. Little Rock gives many large city amenities without the crowded, hectic lifestyle. Send CV to Richard L. FitzRandolph, M.D., or Ernest J. Ferris, M.D., University of Arkansas for Medical Sciences, 4301 W. Markham, Slot #556, Little Rock, AR 72205. 11-12a

CHIEF, AMBULATORY CARE CLINIC, UNIVERSITY OF ARKANSAS FOR MEDICAL SCIENCES—We are seeking a person with excellent general radiology experience with special interest and competence in bone radiology and mammography to oversee a busy outpatient clinic immediately attached to the hospital and the Arkansas Cancer Research Center. Excellent lifestyle opportunities afforded by both large-city amenities and multiple outstanding outdoor recreational opportunities. Send CV to Richard L. FitzRandolph, M.D., or Ernest J. Ferris, M.D., University of Arkansas for Medical Sciences, 4301 W. Markham, Slot #556, Little Rock, AR 72205. 11-12a

DIAGNOSTIC RADIOLOGIST with skills in CT, MR, interventional, ultrasound, and nuclear medicine needed to join group of 8 board-certified radiologists. Growing practice in eastern Washington at a 228-bed hospital, a new multimodality imaging center, and 2 private offices. Potential for long-term practice is excellent. Top-notch school system, including 3 first-rate universities. Excellent hunting, fishing, boating, and skiing. Contact L. E. Creelius, M.D., N. 5901 Lidgerwood, Ste. 18B, Spokane, WA 99207; (509) 482-2385. 11xa

DALLAS, TX—A 12-member, subspecialty group seeks a board-certified, general radiologist for an immediate opening. Fellowship training preferred, but will consider qualified individual with special expertise. CT/ultrasound, MRI, nuclear medicine, or angiography background particularly helpful. All imaging modalities available (state-of-the-art CT, angio, ultrasound, R & F, SPECT nuclear medicine, and MRI center). Salary and bonuses are excellent. Health and malpractice paid. No buy-in to partnership. Send CV to H. Stuart Peake, M.D., P.O. Box 814129, Dallas, TX 75381; (214) 888-7055. 11-4ap

Positions Desired

EXPERIENCED, YOUNG, FACULTY INTERVENTIONALIST (ABR, SCVIR) seeks private-practice position leading to full partnership. Can perform general radiology, including MRI, ultrasound, and CT. Prefer medium-sized to large hospital in urban or suburban location. Available March 1992. Reply Box P82, AJR (see address this section). 10-11bp

RADIOLOGIST, UNIVERSITY TRAINED—Previous angiographic interventional fellowship. Extensive angio/interventional experience (25 yr). Over 1000 angioplasties. Reasonable proficiency in modern imaging modalities. Presently holding responsible position in university-affiliated hospital. Please reply to Box P84, AJR (see address this section). 10-12bp

Fellowships and Residencies

ANGIO/INTERVENTIONAL FELLOWSHIP—The University of Chicago has an unexpected opening in our angio/interventional fellowship (instructorship) program for July 1992. The University of Chicago Hospital's exceptionally active clinical and academic programs provide a wide variety of case material. A second new biplane digital room was just installed as well as a 5-bed recovery ward. Interested applicants should call or forward their CVs to Dr. Chien-Tai Lu, Dept. of Radiology—Box 429, 5841 S. Maryland Ave., Chicago, IL 60637; (312) 702-1607, fax (312) 702-1161. Affirmative action/equal opportunity employer. 11-1cp

MUSCULOSKELETAL RADIOLOGY FELLOWSHIP—Applications are now being accepted for a musculoskeletal fellow position for 1993 at the Cleveland Clinic Foundation (CCF). CCF is a 1000-bed, tertiary-care teaching medical center with a large radiology residency program. Local, national, and international patients provide for an interesting and varied mix of bone pathology. Training includes all aspects of musculoskeletal radiology, including MR, CT, arthrography, biopsy, bone densitometry, and a large plain film experience. Fellowship includes patient care, teaching, and research. There is a close working relationship with the orthopedic, rheumatology, and endocrinology depts. There are presently 4 musculoskeletal staff in the section. For further information, please contact Bradford J. Richmond, M.D., Head, Section of Musculoskeletal Radiology, Desk A-21, 9500 Euclid Ave., Cleveland, OH 44195; (216) 444-3931. 11-4cp

FELLOWSHIP IN BODY IMAGING (CT/MR/ULTRASOUND)—The Dept. of Radiology, University Hospital at Stony Brook, offers a 1-yr fellowship in body CT/MR/ultrasound beginning July 1, 1992. The University Hospital at Stony Brook is a 480-bed, tertiary-care facility with a Level 1 trauma center located on Long Island's scenic North Shore with highly competitive salary/benefits. Training covers all aspects of body cross-sectional imaging including obstetric, pediatric and neurosonography, CT and MRI, and guided interventional procedures. State-of-the-art equipment includes 2 9800 GE CT scanners, a 1.5-T GE Signa unit with MRA capability, and Acuson and ATL ultrasound units with both pulsed and color flow Doppler. Involvement with new or ongoing research projects is encouraged. Requirements include satisfactory completion of an accredited 4-yr radiology residency. Candidates must be board-certified/eligible in diagnostic radiology and must obtain a New York medical license. Address inquiries and CV to G. Lucy van de Vegte, M.D., Dept. of Radiology, HSC L-4, SUNY at Stony Brook, Stony Brook, NY 11794-8460. An equal opportunity/affirmative action employer. 11cp

PEDIATRIC RADIOLOGY FELLOWSHIP—The Section of Pediatric Radiology at the University of Rochester Medical Center offers an ACGME-accredited, 1-yr fellowship in pediatric radiology beginning July 1, 1992. All imaging modalities are represented, including conventional radiology, CT, ultrasound, MRI, neuroradiology, interventional procedures, neonatal neurosonography, and nuclear imaging. Opportunities in clinical and basic imaging research are offered. Candidates must be board-certified/eligible in diagnostic radiology. Interested candidates should contact Dr. M. A. Manuli, Chief, Pediatric Radiology Section, University of Rochester Medical Center, 601 Elmwood Ave., Rochester, NY 14642-8648; (716) 275-5100, fax (716) 271-8698. EOE, M/F. 11-1c

MAMMOGRAPHY FELLOWSHIP—The University of Chicago has a fellowship (instructorship) position available for 1 yr beginning July 1, 1992. Facilities include 3 dedicated screen-film units at the hospital and 1 at a clinic. Space is being renovated for a comprehensive breast care center. A Fisher Mammotest is available for stereotactic breast biopsy. The University of Chicago has pioneered the stereotactic technique in this country. We also have a large research group involved in digital mammography/CAD (computer assisted diagnosis). Interested BC/BE applicants should call or forward their CVs and 3 letters of recommendation to Dr. Robert Schmidt, Dept. of Radiology—Box 429, 5841 S. Maryland Ave., Chicago, IL 60637; (312) 702-3282, fax (312) 702-1161. Affirmative action/equal opportunity employer. 11-1cp

CARDIOVASCULAR/INTERVENTIONAL RADIOLOGY FELLOWSHIPS, THE JOHNS HOPKINS HOSPITAL—The Johns Hopkins Hospital will offer 4 positions for its 2-yr CVIR training program beginning July 1993. The program has been redesigned to provide strong clinical experience in a wide variety of vascular and nonvascular interventional procedures, including angiography; angioplasty; percutaneous atherectomy; intravascular ultrasound; thrombolytic therapy; varicocele, tumor, and AVM embolization; caval filters; percutaneous central venous catheter placement; percutaneous abscess drainage; and complex urologic and biliary intervention including percutaneous biliary endoscopy and biliary atherectomy for biopsy. The first yr is a fellowship position during which basic techniques and fundamental elements of patient care are emphasized. In addition, daily morning conferences, a private CVIR patient admitting service, and a weekly vascular clinic strengthen the total patient care concept of this program. Elective clinical rotations with both the vascular surgery and general surgery services help to facilitate an understanding of the evaluation, care, and treatment of CVIR patients outside the dept. Generous research time for both clinical and laboratory sciences is an integral part of the training program. The candidate will also participate in resident and medical student teaching. The second yr is a faculty position (instructor level) with commensurate compensation and benefits. Responsibilities during the second training yr will include case planning and supervision of residents and first-yr fellows, laboratory and clinical research, and vascular MR and ultrasound. Our dept. is currently undergoing major renovations, with planned upgrades including a new room with a Siemens Angiostar, giving us 3 dedicated CVIR rooms and 2 shared rooms. Our division includes 6 full-time staff, 19 dedicated technologists, and 5 full-time RNs performing over 12,000 exams/yr. Interested candidates should contact Floyd A. Osterman, Jr., M.D., Chief, Division of CVIR, The Johns Hopkins Hospital, 600 N. Wolfe St., Baltimore, MD 20205; (301) 955-5687. 11-2cp

FELLOWSHIP IN CROSS-SECTIONAL IMAGING—The Dept. of Radiology, Dartmouth-Hitchcock Medical Center has an opening in July 1992 for a 1-yr fellowship in MRI/CT/ultrasound. Training includes experience in all aspects of MRI (including neuro and body), CT, and ultrasound (including obstetric and vascular imaging). Imaging-guided biopsies and drainage procedures will be an integral part of the program. The medical center has a completely new 420-bed, tertiary-care hospital with state-of-the-art imaging equipment opening in the fall of 1991. Protected research time will be available for the fellow. There is ample opportunity for clinical radiologic research as well as technology assessment and outcome analysis in collaboration with Dartmouth Medical School Center for Evaluative Sciences. For further information, contact Robert D. Harris, M.D., Dept. of Radiology, Dartmouth-Hitchcock Medical Center, Hanover, NH 03756; (603) 646-5686. 11xcp

MRI FELLOWSHIP—The University of Chicago, Dept. of Radiology, is seeking candidates for a new 1-yr fellowship (instructorship) program in clinical MRI to start July 1992. Six mo in all aspects of MRI, 2 mo neuro MRI, and 4 mo practical experience in CT/UTS. Equipment includes 1.5-T GE Signa and Siemens units and 0.1-T Instrumentarium scanner. Interested BC/BE applicants should forward their CVs and 3 letters of recommendation to Dr. David N. Levin, Director of MRI, Dept. of Radiology—Box 429, 5841 S. Maryland Ave., Chicago, IL 60637; (312) 702-6200, fax (312) 702-1161. Affirmative action/equal opportunity employer. 11-1cp

FELLOWSHIP POSITION—The Dept. of Radiology, Division of Cardiovascular/Interventional Radiology of the Brigham and Women's Hospital/Harvard Medical School has an opening for 1- or 2-yr position beginning July 1992. We are also considering applications for 1- and 2-yr fellowships starting July 1993. The Division of Cardiovascular/Interventional Radiology is a state-of-the-art training program in peripheral angiographic techniques, vascular and nonvascular interventions of all types, vascular ultrasound, and cardiovascular MRI. Some cardiac catheterization and coronary angiography is included. Research time is available for participation in original or ongoing clinical and/or laboratory projects. Please send CV to Kris Kandarpa, M.D., Ph.D., Co-Director, Division of Cardiovascular/Interventional Radiology, Dept. of Radiology, Brigham and Women's Hospital, 75 Francis St., Boston, MA 02115. Brigham and Women's Hospital/Harvard Medical School is an affirmative action/equal opportunity educator and employer. 11-4c

FELLOWSHIP IN DIAGNOSTIC IMAGING (CT/ULTRASOUND/MRI)—The University of Texas Southwestern Medical Center in Dallas, Dept. of Radiology, has 3 imaging fellowships available beginning July 1, 1992. Fellows receive extensive clinical training on state-of-the-art diagnostic imaging systems installed this year in CT, ultrasound, and MRI. Training in obstetric ultrasound is included. Fellows are based at Parkland Memorial Hospital, a 1025-bed trauma center. The Dept. of Radiology operates 3 CT scanners, including a Toshiba 900S installed in 1991, and 4 ultrasound rooms, including 2 Philips Platinum with color Doppler installed in 1991, as well as 2 MR imagers within Parkland. Additional case material is available at Zale Lipshy University Hospital, a 160-bed tertiary-care center opened in 1989 with a state-of-the-art radiology dept. The new Meadows Advanced Imaging Center, opened July 1991, houses 2 1.5-T MRI devices serving patients at Parkland and Zale Lipshy Hospitals, and UT Southwestern outpatients. The Rogers Magnetic Resonance Center at UT Southwestern operates a 0.5-T Toshiba MRI system for clinical studies and several MR devices dedicated to research. Candidates must be board-certified or eligible in diagnostic radiology and be eligible for Texas medical licensure. For further information, contact George Curry, M.D., Chief, Diagnostic Radiology, The University of Texas Southwestern Medical Center, 5323 Harry Hines Blvd., Dallas, TX 75235-8896; (214) 688-8020. An equal opportunity/affirmative action employer. 11-12c

IMMEDIATE OPENING, PEDIATRIC RADIOLOGY FELLOWSHIP—Position available for a 1- or 2-yr fellowship in pediatric radiology beginning July 1, 1992, or July 1, 1993. Full training with abundant hands-on experience with all imaging modalities. Supported by strong Dept. of Pediatrics with a good mixture of patient material. Excellent teaching on a 1-to-1 basis and ample opportunity for pursuing academic interests. Apply to Leonard E. Swischuk, M.D., Dept. of Radiology, The University of Texas Medical Branch, Child Health Center, C-65, Galveston, TX 77550; (409) 772-2096. UTMB is an equal opportunity M/F/H/V affirmative action employer. UTMB hires only persons authorized to work in the U.S. 11-1c

FELLOWSHIP IN ULTRASOUND, BODY CT, AND MRI—July 1992 and July 1993. One-yr program featuring ultrasound, body CT, body MRI, and noninvasive vascular diagnosis. Send CV to, or for information contact, William Zwiebel, M.D., Dept. of Radiology, University of Utah Hospital, Salt Lake City, UT 84132; (801) 581-7553. 11-4c

FELLOWSHIP IN CARDIOVASCULAR/INTERVENTIONAL RADIOLOGY—A 1-yr fellowship in cardiovascular/interventional radiology is available at the Dartmouth-Hitchcock Medical Center in Hanover, NH, beginning July 1992. DHMC is the major teaching component of Dartmouth Medical School and is situated in a classic northern New England town. Training includes all aspects of diagnostic angiography (including neuro and pulmonary) and vascular and nonvascular interventional techniques. This includes IVC filter placement, atherectomy, thrombolysis, biliary and urologic interventions, and biopsy and drainage procedures using multiple imaging modalities. We have a close working relationship with the depts. of vascular and general surgery. Approximately 2000 diagnostic and interventional procedures are performed per yr. The dept. will be moving to a new, tertiary-care, 429-bed hospital in fall 1991, equipped with 2 new, state-of-the-art, digital interventional suites and a 4-bed recovery room. Candidates must have completed an accredited diagnostic radiology residency program, must be certified or eligible by the ABR, and must be eligible for medical licensure in the state of New Hampshire. For further information, please contact Louis I. Juravsky, M.D., FRCPC, Dept. of Diagnostic Radiology, Dartmouth-Hitchcock Medical Center, 2 Maynard St., Hanover, NH 03756. Dartmouth College is an equal opportunity/affirmative action educator and employer. 11xc

NEURORADIOLOGY FELLOWSHIP—An unexpected opening for a neuroradiology fellow is available in the Dept. of Radiology at Thomas Jefferson University Hospital beginning July 1992. The Division of Neuroradiology has close clinical and research relationships with Jefferson's very active neurology, neurosurgery, orthopedic surgery, and otolaryngology depts. Complete training in ENT radiology is part of this program. Six full-time faculty members currently staff this division. Clinical facilities include 2 dedicated CT scanners, a myelography room, a biplane angiography room with DSA, and 4 GE 1.5-T MRI units. Contact Carlos Gonzalez, M.D., Director of Neuroradiology, 1009 Main Bldg., Thomas Jefferson University Hospital, Philadelphia, PA 19107; (215) 955-5447. Jefferson is an affirmative action/equal opportunity employer. 11-6c

WOMEN'S IMAGING FELLOWSHIP—A 1-yr fellowship is available at Oregon Health Sciences University, Portland, OR. Training includes hysterosalpingography, fallopian tube recanalization, mammography and breast procedures, obstetric ultrasound, pelvic ultrasound including vaginal ultrasound, and pelvic and breast MRI. Please contact Amy Thurmond, M.D., Director of Women's Imaging, Oregon Health Sciences University, L340, 3181 S.W. Sam Jackson Park Rd., Portland, OR 97201-3098; (503) 494-7576. 11-1c

RESEARCH FELLOWSHIP IN INTERVENTIONAL RADIOLOGY—A 2-yr position is available at Allegheny General Hospital, a 746-bed teaching hospital in Pittsburgh, for a research fellow in an innovative program in interventional radiology research beginning July 1992. The fellow will participate in imaging studies directed at ablation of tumors in the liver, prostate, lung, and brain. Percutaneous methods of removing herniated disks also are being pursued. Clinical responsibilities will be included as well as opportunities to pursue individual research interests. Candidates must be board certified/eligible in radiology. Please send CV to Dr. Gary Onik, 320 E. North Ave., Pittsburgh, PA 15212. 11-4cp

IMAGING FELLOWSHIP (CT, ULTRASOUND, MRI)—William Beaumont Hospital, a 970-bed, modern, tertiary-care teaching and academic institution in southeast Michigan, offers a 1-yr fellowship in sectional body imaging. The fellowship will provide extensive clinical experience in body CT, ultrasound, and MRI, including CT and ultrasound-guided procedures, conventional and color flow Doppler exams, and prostatic and endovaginal sonography. Ample elective time is also provided for other rotations of individual interest. Candidates must be board-certified/eligible in diagnostic radiology and have a valid Michigan medical license. Four positions are available for July 1993. Salary and fringe benefits are highly competitive. For further information, write to Ali Shirkhoda, M.D., Chief, Imaging Division, William Beaumont Hospital, 3601 W. 13 Mile Rd., Royal Oak, MI 48073; (313) 551-1001. 11-1c

ABDOMINAL IMAGING FELLOWSHIP—The University of Chicago has a fellowship (instructorship) position available July 1992. Training will include 6 mo of CT and ultrasound, with the remaining 6 mo as elective, and will consist of subspecialties such as MRI, GI/GU, mammography, or other subspecialties in radiology arranged with the approval of the program director. Interested BC/BE applicants should call or forward their CVs and 3 letters of recommendation to Dr. Elizabeth Holland, Dept. of Radiology—Box 429, 5841 S. Maryland Ave., Chicago, IL 60637; (312) 702-6200, fax (312) 702-1161. Affirmative action/equal opportunity employer. 11-1cp

FELLOWSHIP IN NEURORADIOLOGY—A fellowship position in neuroradiology is available July 1, 1992, in the Dept. of Radiology at New England Medical Center Hospitals, Boston, MA. The Boston Floating Hospital for Children is an integral part of the New England Medical Center Hospitals. The center is the teaching unit of Tufts University School of Medicine. The program is for 1 or 2 yr and includes both adult and pediatric case material. The fellow will be trained in the technique and interpretation of carotid and vertebral angiography as well as myelography. CT and MRI of the head and spine form major components of the neuroradiology service as does interventional neuroradiology. The facilities include state-of-the-art MRI and CT scanners. Neuroradiologic services at the New England Medical Center Hospitals are carried out in liaison with the Depts. of Neurology, Neurosurgery, and Pediatric Neurology. Joint radiologic and clinical conferences are held frequently, and within a short time, the applicants will have considerable exposure to an array of neuroradiologic material. The Dept. of Neuropathology also runs conferences, allowing correlation to be made between radiologic interpretation and pathology. The fellowship program is accredited by the Accreditation Council for Graduate Medical Education. Interested applicants should call (617) 956-6333 or write to Samuel M. Wolpert, M.D., Professor of Radiology and Neurology, Director, Neuroradiology Fellowship Program, Dept. of Radiology, 750 Washington St., Boston, MA 02111. 10-11cp

FELLOWSHIP IN ULTRASOUND/CT/ANGIO-INTERVENTIONAL—A 1-yr fellowship program is available beginning July 1992 at Lehigh Valley Hospital Center (LVHC) in Allentown, PA. LVHC is a 492-bed, acute-care, university-affiliated hospital. The fellowship program offers training in CT (head and body), ultrasound, angiography (neuro and visceral), and interventional radiology. MRI experience is also available. For further information, contact Robert Kricun, M.D., Dept. of Radiology, Lehigh Valley Hospital Center, P.O. Box 689, Allentown, PA 18105. 10-12cp

FELLOWSHIP IN NEURORADIOLOGY, JULY 1, 1992—The Dept. of Radiology, University of Massachusetts Medical Center offers a 1-yr fellowship position in neuroradiology starting July 1, 1992. Training is offered in neuroangiography, CT, myelography, and MRI. The position involves teaching of medical students and residents with opportunity for research. The University of Massachusetts Medical Center is a 370-bed, university hospital and medical school located in Worcester, 40 mi. west of Boston. The dept. consists of 22 staff, 14 residents, 2-4 fellows, and does approximately 130,000 exams/yr. The hospital is a major trauma center and is serviced by 2 Life Flight helicopters. The dept. is well-equipped with 2 state-of-the-art CT scanners, 2 1.5-T GE MR scanners, as well as 2.0-T small-bore units for animal research. The University of Massachusetts Medical Center is very active academically. Numerous radiologic, clinical, and basic science conferences are scheduled on a daily basis, and there is ample time during the course of the yr to attend many of these presentations. There are many on-going research projects. The fellowship position carries the title of instructor in radiology. For further information, contact Ronald L. Ragland, M.D., Chief, Division of Neuroradiology, University of Massachusetts Medical Center, 55 Lake Ave., N., Worcester, MA 01655; (508) 856-2215. The University of Massachusetts Medical Center is an affirmative action/equal opportunity employer. 11xc

FELLOWSHIP IN BODY MRI, THOMAS JEFFERSON UNIVERSITY HOSPITAL—The Dept. of Radiology at Thomas Jefferson University Hospital has an unexpected opening for a 1-yr MRI fellow beginning July 1, 1992. This is an active body MRI section that encompasses a clinical mix of approximately 50% musculoskeletal and 50% chest/abdomen/pelvis cases. Equipment includes 4 1.5-T GE Signa systems with state-of-the-art and advanced prototype hardware and software. Ample opportunity for research is provided. The dept. has excellent research facilities and support, including 2 MRI physicists, a radiology animal facility, radiology research funding, and a team of research assistants. Interested candidates should contact Donald G. Mitchell, M.D., Director of MRI, Dept. of Radiology, 1032 Main Bldg., Thomas Jefferson University Hospital, Philadelphia, PA 19107; (215) 955-4809. Jefferson is an equal opportunity/affirmative action employer. 8-1c

RADIOLOGY RESIDENCY POSITION—Unexpected immediate opening for an R3- or R4-radiology resident commencing July 1991 at Sacred Heart Medical Center (SHMC) in Spokane, WA. SHMC is a large, 650-bed tertiary-care hospital with a state-of-the-art radiology dept. The 11-member faculty are all fellowship trained. Residency program currently includes 2 residents/yr. Please direct all inquiries to Royce L. Zobell, M.D., Program Director, Dept. of Radiology, Sacred Heart Medical Center, W. 101 8th Ave., TAF-C9, Spokane, WA 99220; (509) 455-3020. 11xc

FELLOWSHIP IN MAMMOGRAPHY—The Emory University, Dept. of Radiology, offers a 6- or 12-mo fellowship in mammography. Approximately 17,000 mammograms are performed annually through a 600-bed university hospital, a 900-bed county hospital, and an outpatient clinic. Clinical activities would include extensive training in all aspects of mammography, breast ultrasound, stereotactic fine-needle aspirations, and biopsy. Candidates should be eligible for Georgia medical licensure. Contact Beth Kruse, M.D., Section of Radiology, The Breast Imaging Center, 1327 Clifton Rd. N.E., Atlanta, GA 30322; (404) 248-4446. Emory University is an equal opportunity/affirmative action employer. 10-1cp

VASCULAR AND INTERVENTIONAL RADIOLOGY FELLOWSHIP—The University of Arkansas for Medical Sciences is offering a 1-yr fellowship in vascular and interventional radiology starting July 1, 1992. Training includes all aspects of angiography and vascular and nonvascular interventions. Ample clinical material is available at a university hospital, a large veterans' hospital, and a children's hospital. Active vascular and nonvascular research programs are in place. Stipend and fringe benefits are competitive. Candidates must be board-certified or eligible in diagnostic radiology. Applications should include a current CV and 3 letters of reference. For further information, please contact David R. McFarland, M.D., Dept. of Radiology/556, University of Arkansas for Medical Sciences, 4301 W. Markham, Little Rock, AR 72205; (501) 686-6910. The University of Arkansas for Medical Sciences is an equal opportunity educator and employer. 10-12c

A FELLOWSHIP IN ULTRASOUND AND BODY CT/MRI is available July 1, 1992, to June 30, 1993, at The New York Hospital-Cornell Medical Center. The dept. provides state-of-the-art equipment, including Acuson ultrasound, GE 9800 CT, and GE Signa 1.5-T MR. Wide variety of ultrasound exams include abdominal, OB-GYN, color Doppler, small parts, neonatal head, transvaginal, and transrectal. Applicants should be ABR-eligible or certified. Send CV to Elias Kazam, M.D., Dept. of Radiology, The New York Hospital-Cornell Medical Center, 525 E. 68th St., New York, NY 10021. 10-1c

FELLOWSHIPS AT THOMAS JEFFERSON UNIVERSITY HOSPITAL—The Dept. of Radiology at Thomas Jefferson University Hospital in Philadelphia offers the following fellowship programs each yr. (1) Ultrasound/CT/MRI — Jefferson's ultrasound division is 1 of the largest in the world and performs all currently available exams including obstetric, vascular, lithotripsy, invasive, and endoluminal. We also operate 4 GE 1.5-T MRI units and 3 CT scanners. Contact Barry Goldberg, M.D., regarding this program. (2) Cardiovascular/interventional — this division is housed in a new suite containing Philips angio units with DSA and performs the full range of vascular and nonvascular interventional procedures. Contact Geoffrey Gardiner, Jr., M.D. (3) Neuro/ENT radiology — very active clinical services supply a wealth of material to this division, which is housed in a neurosciences imaging center containing all imaging modalities. Contact Carlos Gonzales, M.D. (4) Breast Imaging — Jefferson's new breast-imaging center performs approximately 85 studies/day including ultrasound and needle localizations. Contact Stephen Feig, M.D. (5) Chest — includes biopsies and CT. Contact Robert Steiner, M.D. (6) MRI — a dedicated body MRI program including excellent research opportunities in addition to a large clinical case load. Contact Donald Mitchell, M.D. (7) Ultrasound — a dedicated ultrasound program. Contact Barry Goldberg, M.D. (8) Musculoskeletal — includes MRI of the musculoskeletal system. Contact David Karasick, M.D. All program directors listed above can be contacted at the Dept. of Radiology, Thomas Jefferson University Hospital, Philadelphia, PA 19107. Jefferson is an equal opportunity/affirmative action employer. 11xc

NEURORADIOLOGY FELLOWSHIP—Two yr beginning July 1, 1992. Exposure to all aspects of clinical/academic neuroradiology. Participation in research/training. Send cover letter/CV to John R. Jenkins, M.D., Director, Neuroradiology Section, The University of Texas Health Science Center, 7703 Floyd Curl Dr., San Antonio, TX 78284-7800. The University of Texas Health Science Center at San Antonio is an affirmative action/equal opportunity employer. 10-12cp

FELLOWSHIP IN ABDOMINAL IMAGING AND INTERVENTIONS—The Dept. of Radiology, Massachusetts General Hospital and Harvard Medical School, offers a 2-yr fellowship in abdominal imaging and interventions beginning July 1, 1993. Training covers all aspects of abdominal imaging (radiography, fluoroscopy, ultrasound, CT, and MR) and nonvascular interventions in the GI and GU tracts. Research is active and participation is encouraged. Candidates should be ABR-eligible or certified. Address inquiries to Peter R. Mueller, M.D., or Nicholas Papanicolaou, M.D., Dept. of Radiology, Massachusetts General Hospital, Boston, MA 02114. An equal opportunity employer. 11-1cp

ACCREDITED FELLOWSHIPS IN PEDIATRIC RADIOLOGY AND PEDIATRIC NEURORADIOLOGY—Dept. of Radiology, Children's Hospital Medical Center, Cincinnati, OH, offers 1- or 2-yr accredited (Residency Review Committee for Radiology of ACGME) fellowships in pediatric radiology beginning July 1, 1993. A 1-yr pediatric neuroradiology fellowship program is also offered and may be taken separately or combined with 2 yr of adult neuroradiology fellowship at the University of Cincinnati Medical Center. Children's Hospital Medical Center (CHMC) is a 355-bed institution. The dept. performs over 105,000 radiologic exams/yr in the largest children's hospital and ambulatory practice in the U.S. The dept. has 14 full-time faculty pediatric radiologists, 6 fellows, and many resident trainees. Five pediatric radiology and 2 pediatric neuroradiology fellowship positions are available annually. Training includes all aspects of pediatric imaging including neonatal radiology, neuroimaging, oncologic imaging, ultrasonography, nuclear medicine, CT, MRI, and vascular/interventional procedures. The dept. has an active clinical service with state-of-the-art equipment including digital fluoroscopy; Acuson, AI, and ATL ultrasound units with Doppler and color-flow Doppler capabilities; planar SPECT gamma cameras; GE 9800 Quick CT scanner, 1.5-T GE MRI with spectroscopy; and cardiac catheterization/angiographic suite with digital vascular imaging. The fellowship provides a broad clinical experience in pediatric radiology as well as numerous opportunities to participate in both clinical and basic research. Candidates must be board-certified or qualified in diagnostic radiology and must obtain an Ohio medical license. Salary and fringe benefits are highly competitive. Applications are due before Jan. 1992, with interviews scheduled during the fall and winter of 1991-1992. There are numerous career opportunities in pediatric radiology in both academic and private practice settings. To receive more information about the fellowships at CHMC or careers in pediatric radiology, please contact Donald R. Kirks, M.D., Director, Dept. of Radiology, Children's Hospital Medical Center, Cincinnati, OH 45229-2899; (513) 559-8058. Children's Hospital Medical Center and the University of Cincinnati College of Medicine are affirmative action/equal opportunity employers. 9-5cp

FELLOWSHIP IN BODY CT/MRI AND ULTRASOUND—The Dept. of Radiology of Loyola University Medical Center has 2 1-yr fellowship positions available July 1, 1992. The dept. performs more than 180,000 exams/yr. Fellowship training in all aspects of ultrasound is available. All imaging equipment is state-of-the-art and includes 4 GE 9800 CT scanners, 4 Acuson units, and 2 GE 1.5-T magnets. Candidates must be board-certified/eligible in diagnostic radiology and have an Illinois medical license. For further information, contact Mary Olson, M.D., Dept. of Radiology, Loyola University Medical Center, 2160 S. First Ave., Maywood, IL 60153. 8-11cp

FELLOWSHIP IN MUSCULOSKELETAL IMAGING

—A position is available July 1, 1991, to June 30, 1992, for a board-certified radiologist to obtain advanced training and undertake research in musculoskeletal imaging at the Johns Hopkins Hospital. The experience includes MRI, CT, 3-D imaging, and conventional studies. Johns Hopkins Hospital has an active emergency service and serves as a regional pediatric trauma center. The fellow may participate in and extend ongoing research projects in 3-D imaging, using the Pixar Imaging Computer, and studies of osteoporosis and bone remodeling using the latest dual energy X-ray absorptiometry. MRI equipment includes high-field-strength research units as well as 2 1.5-T General Electric units for clinical studies. Body CT studies are performed on Siemens DR H and PLUS scanners, with over 14,000 body studies done yearly. The fellow will work closely with 2 experienced musculoskeletal radiologists. Interested parties should contact George Saba II, M.D., The Johns Hopkins Hospital, Dept. of Radiology, 600 N. Wolfe St., Baltimore, MD 21205; (301) 955-7700. 10-12c

ONCOLOGY/MAMMOGRAPHY FELLOWSHIP

The Dept. of Radiology at the Dana-Farber Cancer Institute and Brigham and Women's Hospital, Harvard Medical School affiliates, offers a 1-yr fellowship position beginning July 1, 1992. All imaging modalities involved in the diagnosis, staging, and follow-up of patients with malignant disease are integrated into this program. An additional feature is a concentrated experience in the performance of interventional breast diagnostic procedures. Please contact Jack E. Meyer, M.D., Director of Diagnostic Radiology, Brigham and Women's Hospital and Dana-Farber Cancer Institute, 75 Francis St., Boston, MA 02115; (617) 732-6269. Brigham and Women's Hospital/Dana-Farber Cancer Institute/Harvard Medical School is an affirmative action/equal opportunity educator and employer. 9-2c

MUSCULOSKELETAL IMAGING FELLOWSHIP

The Dept. of Diagnostic Radiology and Medical Imaging is offering a 1-yr fellowship in musculoskeletal imaging. The Division of Skeletal Radiology is an integral part of the Henry Ford Bone and Joint Specialty Center. This center represents a unique multispecialty program for clinical and academic excellence in the diagnosis and treatment of musculoskeletal disorders. It comprises the Dept. of Orthopedic Disorders, Dept. of Orthopedic Surgery, Division of Rheumatology, Division of Bone and Mineral Metabolism, Physics Section of the Dept. of Radiology, and the Division of Skeletal Radiology. The group includes recognized experts working closely in the investigation and clinical care of musculoskeletal disorders, providing a fertile environment for education and research. The Division of Skeletal Radiology consists of 3 dedicated osteoradiologists and state-of-the-art imaging technology including polytomography, 3D CT imaging, MRI, musculoskeletal sonography, and arthrography. Ongoing research in imaging includes high-resolution CT, sonography, and other clinical projects. Interested applicants should include CV with letter of inquiry to either Burton I. Ellis, M.D., or Marnix van Holsbeeck, M.D., Dept. of Diagnostic Radiology and Medical Imaging, Division of Musculoskeletal Radiology, Henry Ford Hospital, 2799 W. Grand Blvd., Detroit, MI 48202. 9-11ap

FELLOWSHIP IN VASCULAR/INTERVENTIONAL RADIOLOGY 1992

—The University of New Mexico has an unexpected opening for a 1-yr fellowship in vascular/interventional radiology beginning July 1, 1992. We perform all noncardiac diagnostic angiography, including neuroangiography, as well as a wide variety of vascular and nonvascular interventional procedures, with state-of-the-art equipment at the University Hospital (a level 1 trauma center) and the VA/Air Force Hospital. Applicants must have passed the ABR written exam, be eligible for ABR certification, and be eligible for medical licensure in the state of New Mexico. We are an equal opportunity employer. Contact Jerry King, M.D., Dept. of Radiology, University of New Mexico School of Medicine, 915 Camino Salud, N.E., Albuquerque, NM 87131; (505) 272-2439. 10-12c

VASCULAR AND INTERVENTIONAL RADIOLOGY FELLOWSHIP

—The University of South Florida, Dept. of Radiology, will offer a 1-yr fellowship in vascular and interventional radiology beginning July 1, 1992. Clinical experience will include the full range of interventional procedures including vascular, biliary and endourologic procedures, as well as abscess drainage and percutaneous biopsy. The fellow will rotate between the H. Lee Moffitt Cancer Center and Research Institute, the James A. Haley VA Hospital, and the Tampa General Hospital. There is active, ongoing clinical research. Interested candidates contact Steven Morse, M.D., Associate Professor of Radiology, University of South Florida, Director of Vascular Radiology, Moffitt Cancer Center and Research Institute, P. O. Box 280179, Tampa, FL 33682-0179; (813) 972-8425. 9-11cp

Tutorials/Courses**CARIBBEAN CRUISE—BREAST IMAGING AT SEA**

—Jan. 12-19, 1992. Faculty: Drs. Dorit Adler and Terry Silver. CME I. Medical Seminars International, 18981 Ventura Blvd., Ste. 303, Tarzana, CA 91356; (818) 774-9077. 9-12d

CARIBBEAN CRUISE—MRI AT SEA

—Jan. 19-26, 1992. Faculty: Drs. William G. Bradley, Rosalind Dietrich, and Ronald J. Friedman. CME I. Medical Seminars International, 18981 Ventura Blvd., Ste. 303, Tarzana, CA 91356; (818) 774-9077. 9-12d

AJR Classified Advertisements Information

Box Responses and Address for Ad Placement

Write Box _____, *AJR*, 2223 Avenida de la Playa, Suite 103, La Jolla, CA 92037-3218; Phone: (619) 459-2229; FAX: (619) 459-8814.

AJR Classified Advertisements Information

Box Responses and Address for Ad Placement

Write Box _____, *AJR*, 2223 Avenida de la Playa, Suite 103, La Jolla, CA 92037-3218; Telephone: (619) 459-2229; FAX: (619) 459-8814.

How to Place an Ad

AJR accepts classified advertising for Positions Available, Positions Desired, Fellowships and Residencies, and Tutorials/Courses. Ads are accepted by mail or FAX.

Rates: \$6.00/line with a \$30 minimum charge. Box service is \$10 additional for each month the ad appears. There are discounts for multiple insertions: 10% for 2-3 insertions; 20% for 4 or more. To estimate lines, count all words and divide by 7.

Billing: Ads *must* be prepaid, or advertisers will be billed after the ad appears *providing* a purchase order number is submitted with the advertising copy. Terms are net 30 days.

Deadlines: 6 weeks prior to issue date. For specific deadlines, telephone the *AJR* editorial office.

Estimating Ad Charges

Line charge: divide total words by 7 and multiply by \$6.00	\$
Multiple insertions? If so, multiply by number	x
Subtotal	\$
Discount applies to two or more insertions. Subtract 10% if ad appears 2-3 months; 20% if 4 months or more	-
Subtotal	\$
Box response requested? If so, multiply number of months by \$10.00	+
Approximate advertising charge	\$



UltiMATM

The Ultimate Image of Confidence.

Fuji introduces UltiMA... the ultimate imaging systems for mammography.

Here are the mammography systems you have been waiting for. Fuji has created UltiMA to provide you and your patients with the assurance that ultimate imaging technology is employed for every breast exam.

No other system can surpass the image quality and diagnostic information delivered by the unique combination of UltiMA films, intensifying screens, cassettes and Computed Radiography.

Fuji's UltiMA Quality Assurance Management Program provides further confidence that the UltiMA systems deliver the ultimate in image quality.

For further details, contact your
Fuji representative today,
or call 1-800-431-1850,
(In CT 353-0300).



A *... feeling thing*

SPECIAL ARTICLES

- 911 Perspective. AIDS risk and risk reduction in the radiology department. Wall SD, Olcott EW, Gerberding JL
- 919 Commentary. AIDS risk and risk reduction in the radiology department. Williams DM, Marx MV, Korobkin M

REVIEW ARTICLES

- 923 Radiologic assessment of impotence: angiography, sonography, cavernosography, and scintigraphy. Rosen MP, Schwartz AN, Levine FJ, Greenfield AJ
- 932 Commentary. The arteriolar component in impotence: a possible paradigm shift. Bookstein JJ, Valji K
- 935 Percutaneous biopsy of skeletal lesions. Kattapuram SV, Rosenthal DI

CARDIOPULMONARY RADIOLOGY

- 943 Pictorial essay. Defects of the interventricular septum of the heart: en face MR imaging in the oblique coronal plane. Yoo S-J, Lim T-H, Park I-S, Hong CY, Song MG, Kim SH
- 947 Case report. Bronchopulmonary sequestration: dynamic, ultrafast, high-resolution CT evidence of air trapping. Stern EJ, Webb WR, Warnock ML, Salmon CJ

GASTROINTESTINAL RADIOLOGY

- 951 The radiologic diagnosis of Barrett esophagus: importance of mucosal surface abnormalities on air-contrast barium studies. Glick SN, Teplick SK, Amenta PS
- 955 Disseminated histoplasmosis: abdominal CT findings in 16 patients. Radin DR
- 959 Primary sclerosing cholangitis: value of cholangiography in determining the prognosis. Craig DA, MacCarty RL, Wiesner RH, Grambsch PM, LaRusso NF
- 965 Case report. Color Doppler sonography in a case of splenic hemangioma: value of compressing the tumor. Niizawa M, Ishida H, Morikawa P, Naganuma H, Masamune O
- 967 Transfemoral venous catheterization through inferior vena caval filters: results in seven cases. Hansen ME, Geller SC, Yucel EK, Eggin TK, Waltman AC
- 971 Case report. Multiple intrahepatic portohepatic venous shunts: treatment with steel-coil embolization. Okada Y, Endo T, Kusano S, Yoshida M

GENITOURINARY RADIOLOGY

- 975 Detection of renal stones with real-time sonography: effect of transducers and scanning parameters. Kimme-Smith C, Perrella RR, Kaveggia LP, Cochran S, Grant EG
- 981 Imaging of the renal arteries: value of MR angiography. Debatin JF, Spritzer CE, Grist TM, et al.
- 991 Arteriovenous malformations of the kidneys: diagnosis and follow-up with color Doppler sonography in six patients. Takebayashi S, Aida N, Matsui K
- 997 Case report. Nonobstructing periureteric venous ring: diagnosis with conventional and three-dimensional reconstruction CT. Dillon EH, Computaro C
- 999 Transitional cell carcinoma of the bladder: patterns of recurrence after cystectomy as determined by CT. Ellis JH, McCullough NB, Francis IR, Grossman HB, Platt JF
- 1003 Case report. Testicular microlithiasis: sonographic features with pathologic correlation. Smith WS, Brammer HM, Henry M, Frazier H

MUSCULOSKELETAL RADIOLOGY

- 1005 Perspective. Hemorrhage associated with pelvic fractures: causes, diagnosis, and emergent management. Ben-Menachem Y, Coldwell DM, Young JWR, Burgess AR

- 1015 MR imaging of the labral-capsular complex: normal variations. Neumann CH, Petersen SA, Jahnke AH
- 1023 Dialysis-related amyloid arthropathy: MR findings in four patients. Cobby MJ, Adler RS, Swartz R, Martel W
- 1029 Pictorial essay. Hallux rigidus deformity: radiologic assessment. Karasick D, Wapner KL
- 1035 Case report. Skeletal lymphoma in a patient with Castleman disease. Buckley JG, Sundaram M

PEDIATRIC RADIOLOGY

- 1039 Review. Drug-related complications in infants and children: imaging features. Kassner EG
- 1051 Review. Sonography of the biliary tract in infants and children. Haller JO
- 1059 Perforation of the augmented urinary bladder in nine children and adolescents: importance of cystography. Braverman RM, Lebowitz RL
- 1065 Case report. Fetal abdominal wall mass detected on prenatal sonography: gastroschisis vs omphalocele. Perrella RR, Ragavendra N, Tessler FN, Boechat I, Crandall B, Grant EG
- 1069 Technical note. MR angiography of vascular grafts in children. Fillmore DJ, Yucel EK, Briggs SE, Steinberg FL, Waltman AC

NEURORADIOLOGY

- 1073 Review. Proton MR spectroscopy in multiple sclerosis: value in establishing diagnosis, monitoring progression, and evaluating therapy. Richards TL
- 1079 Pictorial essay. Sonography of the eye. Munk PL, Vellet AD, Levin M, Lin DTC, Collyer RT
- 1087 MR imaging of malignant uveal melanoma: role of pulse sequence and contrast agent. Mihara F, Gupta KL, Murayama S, Lee N, Bond JB, Haik BG
- 1093 Optimization of techniques in screening CT of the sinuses. Babbal R, Harnsberger HR, Nelson B, Sonkens J, Hunt S
- 1099 Commentary. Endoscopic sinus surgery: role of the radiologist. Mafee MF
- 1105 Maternal cocaine abuse: the spectrum of radiologic abnormalities in the neonatal CNS. Heier LA, Carpanzano CR, Mast J, Brill PW, Winchester P, Deck MDF
- 1111 Chronic acquired hepatic failure: MR imaging of the brain at 1.5 T. Brunberg JA, Kanal E, Hirsch W, Van Thiel DH

COMPUTER PAGE

- 1117 A PC-based semiautomated reporting system. Schwartz LH, Brill PW, Winchester P

COMMENTARY

- 1119 Understanding receiver-operating-characteristic curves: a graphic approach. Brismar J

OTHER CONTENT

- 918 Call for papers on neuroradiology
- 922 History page
- 950 Radiologic-pathologic conference
- 970 List of book and videotape reviews
- 973 ARRS 1992 residents' award papers information
- 974 Medicine in American art
- 1122 Forthcoming articles
- 1123 Letters
- 1131 Review of current literature
- 1134 News
- 1137 American Roentgen Ray Society information
- 1138 ARRS 1992 meeting announcement, calls for papers and exhibits
- 1143 Classified advertisements
- A13 Guidelines for authors
- A20 AJR business and subscriber information



UltiMATM

The Ultimate Image of Confidence.

Fuji introduces UltiMA... the ultimate imaging systems for mammography.

Here are the mammography systems you have been waiting for. Fuji has created UltiMA to provide you and your patients with the assurance that ultimate imaging technology is employed for every breast exam.

No other system can surpass the image quality and diagnostic information delivered by the unique combination of UltiMA films, intensifying screens, cassettes and Computed Radiography.

Fuji's UltiMA Quality Assurance Management Program provides further confidence that the UltiMA systems deliver the ultimate in image quality.

For further details, contact your
Fuji representative today,
or call 1-800-431-1850,
(In CT 353-0300).



SPECIAL ARTICLES

- 911 Perspective. AIDS risk and risk reduction in the radiology department. Wall SD, Olcott EW, Gerberding JL
- 919 Commentary. AIDS risk and risk reduction in the radiology department. Williams DM, Marx MV, Korobkin M

REVIEW ARTICLES

- 923 Radiologic assessment of impotence: angiography, sonography, cavernosography, and scintigraphy. Rosen MP, Schwartz AN, Levine FJ, Greenfield AJ
- 932 Commentary. The arteriolar component in impotence: a possible paradigm shift. Bookstein JJ, Valji K
- 935 Percutaneous biopsy of skeletal lesions. Kattapuram SV, Rosenthal DI

CARDIOPULMONARY RADIOLOGY

- 943 Pictorial essay. Defects of the interventricular septum of the heart: en face MR imaging in the oblique coronal plane. Yoo S-J, Lim T-H, Park I-S, Hong CY, Song MG, Kim SH
- 947 Case report. Bronchopulmonary sequestration: dynamic, ultrafast, high-resolution CT evidence of air trapping. Stern EJ, Webb WR, Warnock ML, Salmon CJ

GASTROINTESTINAL RADIOLOGY

- 951 The radiologic diagnosis of Barrett esophagus: importance of mucosal surface abnormalities on air-contrast barium studies. Glick SN, Teplick SK, Amenta PS
- 955 Disseminated histoplasmosis: abdominal CT findings in 16 patients. Radin DR
- 959 Primary sclerosing cholangitis: value of cholangiography in determining the prognosis. Craig DA, MacCarty RL, Wiesner RH, Grambsch PM, LaRusso NF
- 965 Case report. Color Doppler sonography in a case of splenic hemangioma: value of compressing the tumor. Niizawa M, Ishida H, Morikawa P, Naganuma H, Masamune O
- 967 Transfemoral venous catheterization through inferior vena caval filters: results in seven cases. Hansen ME, Geller SC, Yucel EK, Eggin TK, Waltman AC
- 971 Case report. Multiple intrahepatic portohepatic venous shunts: treatment with steel-coil embolization. Okada Y, Endo T, Kusano S, Yoshida M

GENITOURINARY RADIOLOGY

- 975 Detection of renal stones with real-time sonography: effect of transducers and scanning parameters. Kimme-Smith C, Perrella RR, Kaveggia LP, Cochran S, Grant EG
- 981 Imaging of the renal arteries: value of MR angiography. Debatin JF, Spritzer CE, Grist TM, et al.
- 991 Arteriovenous malformations of the kidneys: diagnosis and follow-up with color Doppler sonography in six patients. Takebayashi S, Aida N, Matsui K
- 997 Case report. Nonobstructing periureteric venous ring: diagnosis with conventional and three-dimensional reconstruction CT. Dillon EH, Computaro C
- 999 Transitional cell carcinoma of the bladder: patterns of recurrence after cystectomy as determined by CT. Ellis JH, McCullough NB, Francis IR, Grossman HB, Platt JF
- 1003 Case report. Testicular microlithiasis: sonographic features with pathologic correlation. Smith WS, Brammer HM, Henry M, Frazier H

MUSCULOSKELETAL RADIOLOGY

- 1005 Perspective. Hemorrhage associated with pelvic fractures: causes, diagnosis, and emergent management. Ben-Menachem Y, Coldwell DM, Young JWR, Burgess AR

- 1015 MR imaging of the labral-capsular complex: normal variations. Neumann CH, Petersen SA, Jahnke AH
- 1023 Dialysis-related amyloid arthropathy: MR findings in four patients. Cobby MJ, Adler RS, Swartz R, Martel W
- 1029 Pictorial essay. Hallux rigidus deformity: radiologic assessment. Karasick D, Wapner KL
- 1035 Case report. Skeletal lymphoma in a patient with Castleman disease. Buckley JG, Sundaram M

PEDIATRIC RADIOLOGY

- 1039 Review. Drug-related complications in infants and children: imaging features. Kassner EG
- 1051 Review. Sonography of the biliary tract in infants and children. Haller JO
- 1059 Perforation of the augmented urinary bladder in nine children and adolescents: importance of cystography. Braverman RM, Lebowitz RL
- 1065 Case report. Fetal abdominal wall mass detected on prenatal sonography: gastroschisis vs omphalocele. Perrella RR, Ragavendra N, Tessler FN, Boechat I, Crandall B, Grant EG
- 1069 Technical note. MR angiography of vascular grafts in children. Fillmore DJ, Yucel EK, Briggs SE, Steinberg FL, Waltman AC

NEURORADIOLOGY

- 1073 Review. Proton MR spectroscopy in multiple sclerosis: value in establishing diagnosis, monitoring progression, and evaluating therapy. Richards TL
- 1079 Pictorial essay. Sonography of the eye. Munk PL, Vellet AD, Levin M, Lin DTC, Collyer RT
- 1087 MR imaging of malignant uveal melanoma: role of pulse sequence and contrast agent. Mihara F, Gupta KL, Murayama S, Lee N, Bond JB, Haik BG
- 1093 Optimization of techniques in screening CT of the sinuses. Babbal R, Harnsberger HR, Nelson B, Sonkens J, Hunt S
- 1099 Commentary. Endoscopic sinus surgery: role of the radiologist. Mafee MF
- 1105 Maternal cocaine abuse: the spectrum of radiologic abnormalities in the neonatal CNS. Heier LA, Carpanzano CR, Mast J, Brill PW, Winchester P, Deck MDF
- 1111 Chronic acquired hepatic failure: MR imaging of the brain at 1.5 T. Brunberg JA, Kanal E, Hirsch W, Van Thiel DH

COMPUTER PAGE

- 1117 A PC-based semiautomated reporting system. Schwartz LH, Brill PW, Winchester P

COMMENTARY

- 1119 Understanding receiver-operating-characteristic curves: a graphic approach. Brismar J

OTHER CONTENT

- 918 Call for papers on neuroradiology
- 922 History page
- 950 Radiologic-pathologic conference
- 970 List of book and videotape reviews
- 973 ARRS 1992 residents' award papers information
- 974 Medicine in American art
- 1122 Forthcoming articles
- 1123 Letters
- 1131 Review of current literature
- 1134 News
- 1137 American Roentgen Ray Society information
- 1138 ARRS 1992 meeting announcement, calls for papers and exhibits
- 1143 Classified advertisements
- A13 Guidelines for authors
- A20 AJR business and subscriber information

A black and white photograph of a woman lifting a baby into the air. They are positioned in front of a window with lace curtains. The woman is seen from the side, looking up at the baby. The baby is upside down, with its legs and arms outstretched. The lighting is soft, coming from the window.

UltiMA™

**The Ultimate Image
of Confidence.**

**Fuji introduces UltiMA...
the ultimate imaging
systems for mammography.**

Here are the mammography systems you have been waiting for. Fuji has created UltiMA to provide you and your patients with the assurance that ultimate imaging technology is employed for every breast exam.

No other system can surpass the image quality and diagnostic information delivered by the unique combination of UltiMA films, intensifying screens, cassettes and Computed Radiography.

Fuji's UltiMA Quality Assurance Management Program provides further confidence that the UltiMA systems deliver the ultimate in image quality.

For further details, contact your
Fuji representative today,
or call 1-800-431-1850,
(In CT 353-0300).



A new way of seeing things.

SPECIAL ARTICLES

- 911 Perspective. AIDS risk and risk reduction in the radiology department. *Wall SD, Olcott EW, Gerberding JL*
- 919 Commentary. AIDS risk and risk reduction in the radiology department. *Williams DM, Marx MV, Korobkin M*

REVIEW ARTICLES

- 923 Radiologic assessment of impotence: angiography, sonography, cavernosography, and scintigraphy. *Rosen MP, Schwartz AN, Levine FJ, Greenfield AJ*
- 932 Commentary. The arteriolar component in impotence: a possible paradigm shift. *Bookstein JJ, Valji K*
- 935 Percutaneous biopsy of skeletal lesions. *Kattapuram SV, Rosenthal DI*

CARDIOPULMONARY RADIOLOGY

- 943 Pictorial essay. Defects of the interventricular septum of the heart: en face MR imaging in the oblique coronal plane. *Yoo S-J, Lim T-H, Park I-S, Hong CY, Song MG, Kim SH*
- 947 Case report. Bronchopulmonary sequestration: dynamic, ultrafast, high-resolution CT evidence of air trapping. *Stern EJ, Webb WR, Warnock ML, Salmon CJ*

GASTROINTESTINAL RADIOLOGY

- 951 The radiologic diagnosis of Barrett esophagus: importance of mucosal surface abnormalities on air-contrast barium studies. *Glick SN, Teplick SK, Amenta PS*
- 955 Disseminated histoplasmosis: abdominal CT findings in 16 patients. *Radin DR*
- 959 Primary sclerosing cholangitis: value of cholangiography in determining the prognosis. *Craig DA, MacCarty RL, Wiesner RH, Grambsch PM, LaRusso NF*
- 965 Case report. Color Doppler sonography in a case of splenic hemangioma: value of compressing the tumor. *Niizawa M, Ishida H, Morikawa P, Naganuma H, Masamune O*
- 967 Transfemoral venous catheterization through inferior vena caval filters: results in seven cases. *Hansen ME, Geller SC, Yucel EK, Eglin TK, Waltman AC*
- 971 Case report. Multiple intrahepatic portohepatic venous shunts: treatment with steel-coil embolization. *Okada Y, Endo T, Kusano S, Yoshida M*

GENITOURINARY RADIOLOGY

- 975 Detection of renal stones with real-time sonography: effect of transducers and scanning parameters. *Kimme-Smith C, Perrella RR, Kaveggia LP, Cochran S, Grant EG*
- 981 Imaging of the renal arteries: value of MR angiography. *Debatin JF, Spritzer CE, Grist TM, et al.*
- 991 Arteriovenous malformations of the kidneys: diagnosis and follow-up with color Doppler sonography in six patients. *Takebayashi S, Aida N, Matsui K*
- 997 Case report. Nonobstructing periureteric venous ring: diagnosis with conventional and three-dimensional reconstruction CT. *Dillon EH, Computaro C*
- 999 Transitional cell carcinoma of the bladder: patterns of recurrence after cystectomy as determined by CT. *Ellis JH, McCullough NB, Francis IR, Grossman HB, Platt JF*
- 1003 Case report. Testicular microlithiasis: sonographic features with pathologic correlation. *Smith WS, Brammer HM, Henry M, Frazier H*

MUSCULOSKELETAL RADIOLOGY

- 1005 Perspective. Hemorrhage associated with pelvic fractures: causes, diagnosis, and emergent management. *Ben-Menachem Y, Coldwell DM, Young JWR, Burgess AR*

- 1015 MR imaging of the labral-capsular complex: variations. *Neumann CH, Petersen SA, Jahnke A*
- 1023 Dialysis-related amyloid arthropathy: MR findings in four patients. *Cobby MJ, Adler RS, Swartz R, McEneaney J*
- 1029 Pictorial essay. Hallux rigidus deformity: radiologic assessment. *Karasick D, Wapner KL*
- 1035 Case report. Skeletal lymphoma in a patient with Kaposi's disease. *Buckley JG, Sundaram M*

PEDIATRIC RADIOLOGY

- 1039 Review. Drug-related complications in infants and children: imaging features. *Kassner EG*
- 1051 Review. Sonography of the biliary tract in infants and children. *Haller JO*
- 1059 Perforation of the augmented urinary bladder in children and adolescents: importance of cystography. *Braverman RM, Lebowitz RL*
- 1065 Case report. Fetal abdominal wall mass detected on prenatal sonography: gastroschisis vs omphalocele. *Perrella RR, Ragavendra N, Tessler FN, Boechat I, Dall B, Grant EG*
- 1069 Technical note. MR angiography of vascular growth in children. *Fillmore DJ, Yucel EK, Briggs SE, Stein FL, Waltman AC*

NEURORADIOLOGY

- 1073 Review. Proton MR spectroscopy in multiple sclerosis: value in establishing diagnosis, monitoring progression, and evaluating therapy. *Richards TL*
- 1079 Pictorial essay. Sonography of the eye. *Munk PL, AD, Levin M, Lin DTC, Collyer RT*
- 1087 MR imaging of malignant uveal melanoma: role of sequence and contrast agent. *Mihara F, Gupta RK, Murayama S, Lee N, Bond JB, Haik BG*
- 1093 Optimization of techniques in screening CT of the sinuses. *Babbal R, Harnsberger HR, Nelson B, Scott J, Hunt S*
- 1099 Commentary. Endoscopic sinus surgery: role of the radiologist. *Mafee MF*
- 1105 Maternal cocaine abuse: the spectrum of radiologic abnormalities in the neonatal CNS. *Heier LA, Cuzzocrea CR, Mast J, Brill PW, Winchester P, Deck M*
- 1111 Chronic acquired hepatic failure: MR imaging of the brain at 1.5 T. *Brunberg JA, Kanal E, Hirsch V, Thiel DH*

COMPUTER PAGE

- 1117 A PC-based semiautomated reporting system for CT. *Schwartz LH, Brill PW, Winchester P*

COMMENTARY

- 1119 Understanding receiver-operating-characteristic curves: a graphic approach. *Brisman J*

OTHER CONTENT

- 918 Call for papers on neuroradiology
- 922 History page
- 950 Radiologic-pathologic conference
- 970 List of book and videotape reviews
- 973 ARRS 1992 residents' award papers information
- 974 Medicine in American art
- 1122 Forthcoming articles
- 1123 Letters
- 1131 Review of current literature
- 1134 News
- 1137 American Roentgen Ray Society information
- 1138 ARRS 1992 meeting announcement, calls for papers and exhibits
- 1143 Classified advertisements
- A13 Guidelines for authors
- A20 AJR business and subscriber information

12 11/92

15

AJR

11/24/91 (clinical)

American
Journal of
Roentgenology



December 1991

At last! Lavage with 'La Taste'!

NuLYTELY[®]

PEG 3350, Sodium Chloride, Sodium Bicarbonate
and Potassium Chloride for Oral Solution

A double-blinded multicenter study¹ comparing
NuLYTELY[®] and GoLYTELY[®] demonstrates:

**Preference. Patients prefer
the taste of NuLYTELY 3 to 1.¹**

Manufactured for Braintree Laboratories, Inc., Braintree, MA 02184
by Lyne Laboratories, Inc., Stoughton, MA 02072.

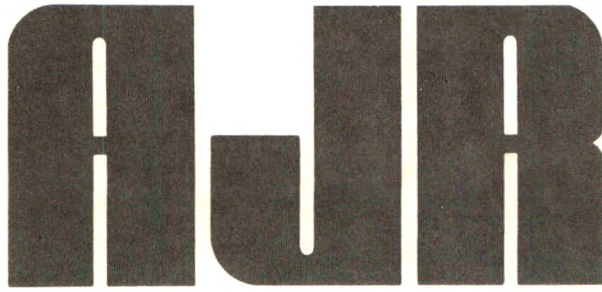
Reference: 1. Gastrointest Endosc 1990; 36: 285-289

LABORATORIES • INC

Braintree

© 1991 BRAINTREE LABORATORIES, INC. TRE-1080

Official Journal of the American Roentgen Ray Society



American Journal of Roentgenology
Diagnostic Imaging and Related Sciences

Editor-In-Chief	Robert N. Berk, <i>La Jolla, California</i> <i>University of California, San Diego</i> <i>School of Medicine and Medical Center</i>
Editor Emeritus	Melvin M. Figley, <i>Seattle, Washington</i>
Associate Editor	Karim Valji, <i>San Diego, California</i>
Consulting Editor	A. James Barkovich, <i>San Francisco, California</i>
Consulting Editor	Edward A. Sickles, <i>San Francisco, California</i>
Statistician	Charles C. Berry, <i>San Diego, California</i>

Editorial Board

John R. Amberg	John R. Hesselink	Peter
Ithamar Aviad	Charles B. Higgins	Sjef I
Mark E. Baker	Melvyn T. Korobkin	Stua
Lawrence W. Bassett	Faye C. Laing	David
Michael A. Bettmann	Thomas L. Lawson	Stefa
Felix S. Chew	Robert G. Levitt	Willia
N. Reed Dunnick	Bruce L. McClennan	Barry
David K. Edwards	Richard P. Moser	David
Ronald G. Evens	Albert A. Moss	Edwa
David S. Feigin	Jeffrey H. Newhouse	Mura
Sandra K. Fernbach	Donald L. Resnick	Eric
Richard H. Gold	Stewart R. Reuter	Robe
William R. Hendee	Charles A. Rohrmann, Jr.	

Editorial Staff: Margaret Levene, *managing editor*; Katie L. Spi
Barbara L. Halliburton, and Janine Anderson, *manuscript editors*; Na
manager; Sheri Smith, *administrative assistant*; Linda J. Waggo
secretary

AJR, AMERICAN JOURNAL OF ROENTGENOLOGY (ISSN 0361 803X) is the official journal of the American Roentgen Ray Society and is published monthly by Williams & Wilkins, 428 E. Preston St., Baltimore, MD 21202. Second-class postage paid at Baltimore, MD, and at additional mailing offices. Postmaster: send address changes (Form 3579) to AJR, 428 E. Preston St., Baltimore, MD 21202. Subscription rates \$125 (\$150 foreign); in training \$25 (\$80 foreign); single copy \$18 (\$22 foreign). The GST number for Canadian subscribers is R12307 6709. Airmail rates furnished on request. Indexed by *Current Contents* and *Index Medicus*. Copyright © 1997 American Roentgen Ray Society.



media currently available inhibit blood coagulation, in vitro, less than ionic contrast media. Clotting has been reported with the use of nonionic contrast media. Therefore, caution is indicated when using nonionic contrast media in patients with a history of bleeding disorders or those on anticoagulant therapy.

Nonionic OMNIPAQUE is used for more procedures than any other nonionic or low osmolar contrast agent.*

The reason is simple. Nonionic OMNIPAQUE offers more than any other contrast agent.

After more than 900 clinical studies worldwide, the superior safety profile of nonionic OMNIPAQUE is a fact.*

Nonionic OMNIPAQUE provides consistently excellent image quality.¹⁻³ And that's just one more reason why so many radiologists make nonionic OMNIPAQUE their first choice.


Nonionic OMNIPAQUE has the widest range of adult and pediatric indications. So there's less concern about limited use.

With more concentrations and more packagings, nonionic OMNIPAQUE offers greater convenience, the best possible dosing flexibility, and the least waste.

Nonionic OMNIPAQUE provides what you deserve in a contrast agent—superior safety, outstanding images, unsurpassed flexibility.

In fact, every ten seconds in this country, nonionic OMNIPAQUE is the contrast agent of choice.

No wonder.

NONIONIC
OMNIPAQUE® 
(IOHEXOL)

When it comes to safety, one image stands out.

*Data on file, Winthrop Pharmaceuticals.

Administration technique is necessary to minimize thromboembolic events. See next page for important product information concerning

OMNIPAQUE® 140 240 300 350

INJECTION (IOHEXOL) INTRAVASCULAR

PLEASE CONSULT FULL PRODUCT INFORMATION BEFORE USING. A SUMMARY FOLLOWS:

DESCRIPTION: OMNIPAQUE is a sterile, pyrogen-free and preservative-free, nonionic, water-soluble radiographic contrast medium for intravascular administration in concentrations of 140, 240, 300, and 350 mgI/mL. OMNIPAQUE 140 contains 302 mg of iohexol equivalent to 140 mg of organic iodine per mL; OMNIPAQUE 240 contains 518 mg of iohexol equivalent to 240 mg of organic iodine per mL; OMNIPAQUE 300 contains 647 mg of iohexol equivalent to 300 mg of organic iodine per mL; and OMNIPAQUE 350 contains 755 mg of iohexol equivalent to 350 mg of organic iodine per mL. Each milliliter of iohexol solution contains 1.21 mEq tromethamine and 0.1 mEq edetate calcium disodium with the pH adjusted between 6.8 and 7.7 with hydrochloric acid or sodium hydroxide. Unused portions must be discarded. Iohehexol solution is sensitive to light and should be protected from exposure.

CONTRAINDICATIONS: OMNIPAQUE should not be administered to patients with a known hypersensitivity to iohehexol. **WARNINGS—General:** Nonionic iodinated contrast media inhibit blood coagulation, in vitro, less than ionic contrast media. Clotting has been reported when blood remains in contact with syringes containing nonionic contrast media.

Serious, rarely fatal, thromboembolic events causing myocardial infarction and stroke have been reported during angiographic procedures with both ionic and nonionic contrast media. Therefore, meticulous intravascular administration technique is necessary, particularly during angiographic procedures, to minimize thromboembolic events. Numerous factors, including length of procedure, catheter and syringe material, underlying disease state, and concomitant medications, may contribute to the development of thromboembolic events. For these reasons, meticulous angiographic techniques are recommended including close attention to guidewire and catheter manipulation, use of manifold systems and/or three-way stopcocks, frequent catheter flushing with heparinized saline solutions and minimizing the length of the procedure. The use of plastic syringes in place of glass syringes has been reported to decrease but not eliminate the likelihood of in vitro clotting.

OMNIPAQUE should be used with extreme care in patients with severe functional disturbances of the liver and kidneys, severe thyrotoxicosis, or myelomatosis. Diabetics with a serum creatinine level above 3 mg/dL should not be examined unless the possible benefits of the examination clearly outweigh the additional risk. OMNIPAQUE is not recommended for use in patients with anuria.

Radiopaque contrast agents are potentially hazardous in patients with multiple myeloma or other paraproteinemia, particularly in those with therapeutically resistant anuria. Although neither the contrast agent nor dehydration has separately proven to be the cause of anuria in myeloma, it has been speculated that the combination of both may be causative factors. The risk in myelomatous patients is not a contraindication; however, special precautions are necessary. Partial dehydration in the preparation of these patients prior to injection is not recommended since this may predispose the patient to precipitation of the myeloma protein in the renal tubules. No form of therapy, including dialysis, has been successful in reversing the effect. Myeloma, which occurs most commonly in persons over age 40, should be considered before instituting intravascular administration of contrast agents.

Ionic contrast media, when injected intravenously or intra-arterially, may promote sickling in individuals who are homozygous for sickle cell disease.

Administration of radiopaque materials to patients known or suspected of having pheochromocytoma should be performed with extreme caution. If, in the opinion of the physician, the possible benefits of such procedures outweigh the considered risks, the procedures may be performed; however, the amount of radiopaque medium injected should be kept to an absolute minimum. The patient's blood pressure should be assessed throughout the procedure and measures for the treatment of hypertensive crisis should be readily available.

Reports of thyroid storm following the use of iodinated, ionic radiopaque contrast media in patients with hyperthyroidism or with an autonomously functioning thyroid nodule suggest that this additional risk be evaluated in such patients before use of any contrast medium.

Urography should be performed with caution in patients with severely impaired renal function and patients with combined renal and hepatic disease.

PRECAUTIONS—General: Diagnostic procedures which involve the use of radiopaque diagnostic agents should be carried out under the direction of personnel with the prerequisite training and with a thorough knowledge of the particular procedure to be performed. Appropriate facilities should be available for coping with any complication of the procedure, as well as for emergency treatment of severe reactions to the contrast agent itself. After parenteral administration of a radiopaque agent, competent personnel and emergency facilities should be available for at least 30 to 60 minutes, since severe delayed reactions have occurred (see ADVERSE REACTIONS: Intravascular—General).

Preparatory dehydration is dangerous and may contribute to acute renal failure in patients with advanced vascular disease, in diabetic patients, and in susceptible nondiabetic patients (often elderly with preexisting renal disease), infants, and small children. Dehydration in these patients seems to be enhanced by the osmotic diuretic action of urographic agents. It is believed that overnight fluid restriction prior to excretory urography generally does not provide better visualization in normal patients. Patients should be well hydrated prior to and following administration of any contrast medium, including iohehexol.

Acute renal failure has been reported in diabetic patients with diabetic nephropathy and in susceptible nondiabetic patients (often elderly with preexisting renal disease) following excretory urography. Therefore, careful consideration of the potential risks should be given before performing this radiographic procedure in these patients.

Immediately following surgery, excretory urography should be used with caution in renal transplant recipients. The possibility of a reaction, including serious, life-threatening, fatal, anaphylactoid or cardiovascular reactions should always be considered (see ADVERSE REACTIONS: Intravascular—General). It is of utmost importance that a course of action be carefully planned in advance for immediate treatment of serious reactions, and that adequate and appropriate personnel be readily available in case of any reaction.

The possibility of an idiosyncratic reaction in susceptible patients should always be considered (see ADVERSE REACTIONS: Intravascular—General). The susceptible population includes, but is not limited to, patients with a history of a previous reaction to contrast media, patients with a known sensitivity to iodine per se, and patients with a known clinical hypersensitivity: bronchial asthma, hay fever, and food allergies.

The occurrence of severe idiosyncratic reactions has prompted the use of several pretesting methods. However, pretesting cannot be relied upon to predict severe reactions and may itself be hazardous for the patient. It is suggested that a thorough medical history with emphasis on allergy and hypersensitivity, prior to the injection of any contrast media, may be more accurate than pretesting in predicting potential adverse reactions.

A positive history of allergies or hypersensitivity does not arbitrarily contraindicate the use of a contrast agent where a diagnostic procedure is thought essential, but caution should be exercised (see ADVERSE REACTIONS: Intravascular—General). Premedication with antihistamines or corticosteroids to avoid or minimize possible allergic reactions in such patients should be considered and administered using separate syringes. Recent reports indicate that such pretreatment does not prevent serious, life-threatening reactions, but may reduce both their incidence and severity.

Even though the osmolality of OMNIPAQUE is low compared to diatrizoate- or iohalamate-based ionic agents of comparable iodine concentration, the potential transitory increase in the circulatory osmotic load in patients with congestive heart failure requires caution during injection. These patients should be observed for several hours following the procedure to detect delayed hemodynamic disturbances.

General anesthesia may be indicated in the performance of some procedures in selected adult patients, however, a higher incidence of adverse reactions has been reported in these patients and may be attributable to the inability of the patient to identify untoward symptoms, or to the hypotensive effect of anesthesia, which can reduce cardiac output and increase the duration of exposure to the contrast agent.

Angiography should be avoided whenever possible in patients with hemocystinuria, because of the risk of inducing thrombosis and embolism.

In angiographic procedures, the possibility of dislodging plaques or damaging or perforating the vessel wall should be borne in mind during the catheter manipulations and contrast medium injection. Test injections to ensure proper catheter placement are recommended.

Selective coronary arteriography should be performed only in those patients in whom the expected benefits outweigh the potential risk. The inherent risks of angiocardiology in patients with chronic pulmonary emphysema must be weighed against the necessity for performing this procedure.

When OMNIPAQUE is to be injected using plastic disposable syringes, the contrast medium should be drawn into the syringe and used immediately.

If nondisposable equipment is used, scrupulous care should be taken to prevent residual contamination with traces of cleansing agents.

Parenteral products should be inspected visually for particulate matter and discoloration prior to administration. If particulate matter or discoloration is present, do not use.

Information for Patients: Patients receiving injectable radiopaque diagnostic agents should be instructed to:

1. Inform your physician if you are pregnant.
2. Inform your physician if you are diabetic or if you have multiple myeloma, pheochromocytoma, homozygous sickle cell disease, or known thyroid disorder (see WARNINGS—General).
3. Inform your physician if you are allergic to any drugs, food, or if you had any reactions to previous injections of dyes used for x-ray procedures (see PRECAUTIONS—General).
4. Inform your physician about any other medications you are currently taking, including nonprescription drugs, before you are administered this drug.

Drug/Laboratory Test Interaction: If iodine-containing isotopes are to be administered for the diagnosis of thyroid disease, the iodine-binding capacity of thyroid tissue may be reduced for up to 2 weeks after contrast medium administration. Thyroid function tests which do not depend on iodine estimation, eg, T₃ resin uptake or direct thyroxine assays, are not affected. Many radiopaque contrast agents are incompatible in vitro with some antihistamines and many other drugs; therefore, no other pharmaceuticals should be admixed with contrast agents.

OMNIPAQUE® injection (iohexol)

Carcinogenesis, Mutagenesis, Impairment of Fertility: No long-term animal studies have been performed to evaluate carcinogenic potential, mutagenesis, or whether OMNIPAQUE can affect fertility in men or women.

Pregnancy Category B: Reproduction studies have been performed in rats and rabbits with up to 100 times the recommended human dose. No evidence of impaired fertility or harm to the fetus has been demonstrated due to OMNIPAQUE. There are, however, no studies in pregnant women. Because animal reproduction studies are not always predictive of human response, this drug should be used during pregnancy only if clearly needed.

Nursing Mothers: It is not known to what extent iohehexol is excreted in human milk. However, many injectable contrast agents are excreted unchanged in human milk. Although it has not been established that serious adverse reactions occur in nursing infants, caution should be exercised when intravascular contrast media are administered to nursing women. Bottle feedings may be substituted for breast feedings for 24 hours following administration of OMNIPAQUE.

Pediatric Use: Pediatric patients at higher risk of experiencing adverse events during contrast medium administration may include those having asthma, a sensitivity to medication and/or allergens, congestive heart failure, a serum creatinine > 1.5 mg/dL, or those less than 12 months of age.

ADVERSE REACTIONS

Intravascular—General: Adverse reactions following the use of OMNIPAQUE are usually mild to moderate in severity. However, serious, life-threatening, and fatal reactions, mostly of cardiovascular origin, have been associated with the administration of iodine-containing contrast media, including OMNIPAQUE. The injection of contrast media is frequently associated with the sensation of warmth and pain, especially in peripheral angiography; pain and warmth are less frequent and less severe with OMNIPAQUE than with many contrast media.

Cardiovascular System: Arrhythmias including PVCs and PACs (2%), angina/chest pain (1%), and hypotension (0.7%). Others including cardiac failure, asystole, bradycardia, tachycardia, and vasovagal reaction were reported with an individual incidence of 0.3% or less. In controlled clinical trials involving 1,485 patients, one fatality occurred. A cause and effect relationship between this death and iohehexol has not been established.

Nervous System: Vertigo [including dizziness and lightheadedness] (0.5%), pain (3%), vision abnormalities [including blurred vision and photomas] (2%), headache (2%), and taste perversion (1%). Others including anxiety, blurred vision, fever, motor and speech dysfunction, convulsion, paresthesia, somnolence, stiff neck, hemiparesis, syncope, shivering, transient ischemic attack, cerebral infarction, and nystagmus were reported, with an individual incidence of 0.3% or less.

Respiratory System: Dyspnea, rhinitis, coughing, and laryngitis, with an individual incidence of 0.2% or less.

Gastrointestinal System: Nausea (2%) and vomiting (0.7%). Others including diarrhea, dyspepsia, cramp, and dry mouth were reported, with an individual incidence of less than 0.1%.

Skin and Appendages: Urticaria (0.3%), purpura (0.1%), abscess (0.1%), and pruritus (0.1%).

Individual adverse reactions which occurred to a significantly greater extent for a specific procedure are listed under that indication in full prescribing information.

Pediatrics: In controlled clinical trials involving 391 patients for pediatric angiocardiology, urography, and contrast-enhanced computed tomographic head imaging, adverse reactions following the use of OMNIPAQUE 240, OMNIPAQUE 300 and OMNIPAQUE 350 were generally less frequent than with adults.

Cardiovascular System: Ventricular tachycardia (0.5%), 2:1 heart block (0.5%), hypertension (0.3%), and anemia (0.3%).

Nervous System: Pain (0.8%), fever (0.5%), taste abnormality (0.5%), and convulsion (0.3%).

Respiratory System: Congestion (0.3%) and apnea (0.3%).

Gastrointestinal System: Nausea (1%), hypoglycemia (0.3%), and vomiting (2%).

Skin and Appendages: Rash (0.3%).

General Adverse Reactions to Contrast Media: Physicians should remain alert for the occurrence of adverse effects in addition to those discussed above. The following reactions have been reported after administration of other intravascular iodinated contrast media, and rarely with iohehexol. **Reactions due to technique:** hematomas and ecchymoses. **Hemodynamic reactions:** vein cramp and thrombophlebitis following intravenous injection. **Cardiovascular reactions:** rare cases of cardiac arrhythmias, reflex tachycardia, chest pain, cyanosis, hypertension, hypotension, peripheral vasodilatation, shock, and cardiac arrest. **Renal reactions:** occasionally, transient proteinuria; and rarely, oliguria or anuria. **Allergic reactions:** asthmatic attacks, nasal and conjunctival symptoms, dermal reactions such as urticaria with or without pruritus, as well as pleomorphic rashes, sneezing, and lacrimation; and rarely, anaphylactic reactions. Rare fatalities have occurred due to this or unknown causes. **Signs and symptoms related to the respiratory system:** pulmonary or laryngeal edema, bronchospasm, dyspnea, or to the nervous system: restlessness, tremors, convulsions. **Other reactions:** flushing, pain, warmth, metallic taste, nausea, vomiting, anxiety, headache, confusion, pallor, weakness, sweating, localized areas of edema (especially facial cramps), neutropenia, and dizziness. Rarely, immediate or delayed rigors can occur, sometimes accompanied by hyperpyrexia. Infrequently, "iodism" (salivary gland swelling) from organic iodinated compounds appears 2 days after exposure and subsides by the sixth day.

In general, the reactions which are known to occur upon parenteral administration of iodinated contrast agents are possible with any nonionic agent. Approximately 95% of adverse reactions accompanying the use of water-soluble intravascularly administered contrast agents are mild to moderate in degree. However, severe, life-threatening anaphylactoid reactions, mostly of cardiovascular origin, have occurred. Reported incidences of death range from 6.6 per 1 million (0.00066%) to 1 in 10,000 (0.01%). Most deaths occur during injection or 5 to 10 minutes later, the main feature being cardiac arrest, with cardiovascular disease as the main aggravating factor. Isolated reports of hypotensive collapse and shock are found in the literature. The incidence of shock is estimated to be 1 out of 20,000 (0.005%) patients.

Adverse reactions to injectable contrast media fall into two categories: chemotoxic reactions and idiosyncratic reactions.

Chemotoxic reactions result from the physicochemical properties of the contrast media, the dose, and the speed of injection. All hemodynamic disturbances and injuries to organs or vessels perfused by the contrast medium are included in this category.

Idiosyncratic reactions include all other reactions. They occur more frequently in patients 20 to 40 years old. Idiosyncratic reactions may or may not be dependent on the amount of dose injected, the speed of injection, and the radiographic procedure. Idiosyncratic reactions are subdivided into minor, intermediate, and severe. The minor reactions are self-limited and of short duration; the severe reactions are life-threatening and treatment is urgent and mandatory.

The reported incidence of adverse reactions to contrast media in patients with a history of allergy is twice that in the general population. Patients with a history of previous reactions to a contrast medium are three times more susceptible than other patients. However, sensitivity to contrast media does not appear to increase with repeated examinations.

Most adverse reactions to injectable contrast media appear within 1 to 3 minutes after the start of injection, but delayed reactions may occur.

Regardless of the contrast agent employed, the overall estimated incidence of serious adverse reactions is higher with angiocardiology than with other procedures. Cardiac decompensation, serious arrhythmias, angina pectoris, or myocardial ischemia or infarction may occur during angiocardiology and left ventriculography. Electrocardiographic and hemodynamic abnormalities occur less frequently with OMNIPAQUE than with diatrizoate meglumine and diatrizoate sodium injection.

CONSULT PACKAGE INSERT FOR A MORE DETAILED DISCUSSION OF ADVERSE REACTIONS FOR INTRAVASCULAR USE OF OMNIPAQUE.

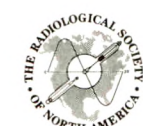
OVERDOSAGE: Overdosage may occur. The adverse effects of overdosage are life-threatening and affect mainly the pulmonary and cardiovascular systems. The symptoms include cyanosis, bradycardia, acidosis, pulmonary hemorrhage, convulsions, coma, and cardiac arrest. Treatment of an overdosage is directed toward the support of all vital functions and prompt institution of symptomatic therapy.

The intravenous LD₅₀ values of OMNIPAQUE (in grams of iodine per kilogram body weight) are 24.2 in mice and 15.0 in rats.

DOSAGE AND ADMINISTRATION: Details are provided in the package insert.

References:

1. Stake G. Contrast media in pediatric radiology: safety aspects. In: *Patient Safety and Adverse Events in Contrast Medium Examinations*. Amsterdam: Elsevier Science Publishers; 1989: 159-167.
2. Kolbenstvedt A. Iohexol in lower extremity, renal and visceral angiography: survey and present state. *Acta Radiol*. 1983; (suppl 366):153-157.
3. Kaye B, Howard J, Ford KD, Cumberland DC. Comparison of the image quality of intravenous urograms using low-osmolal contrast media. *Br J Radiol*. 1988;61:589-591.

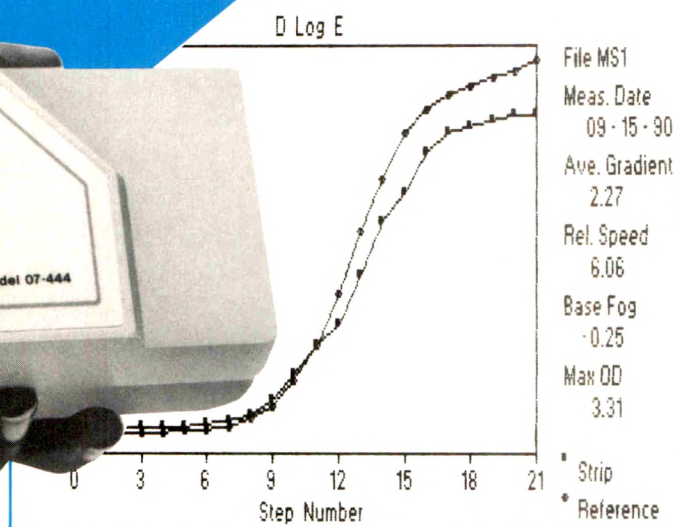


Vanguard Flagship
Scholar



DIAGNOSTIC IMAGING DIVISION
Winthrop Pharmaceuticals
Division of Sterling Drug Inc.
New York, NY 10016

IMAGINE...X-RAY FILM PROCESSOR QC IN THE PALM OF YOUR HAND!



*IMAGINE...performing daily film processor QC in seconds!
IMAGINE...a compact, lightweight, portable scanning QC
system that has more features and capabilities
than you ever dreamed were possible!*

MINISCAN

You can use it **WITH** or **WITHOUT** a Computer!

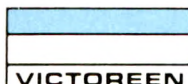
MINISCAN is a...

- Standard high quality transmission densitometer.
- Scanning QC densitometer to measure, analyze and store data for up to 20 independent sensitometric strips in its own built-in memory (no external computer or software needed)!
- Complete film processor QC system (when combined with the Film Processor QC Software Package) to track and monitor the performance of a virtually unlimited number of film processors. PLUS generate comprehensive reports, control charts, and corrective action forms, and more!

MINISCAN...More Than You Ever Imagined!

For more details,
request Bulletin 501-44

NUCLEAR ASSOCIATES



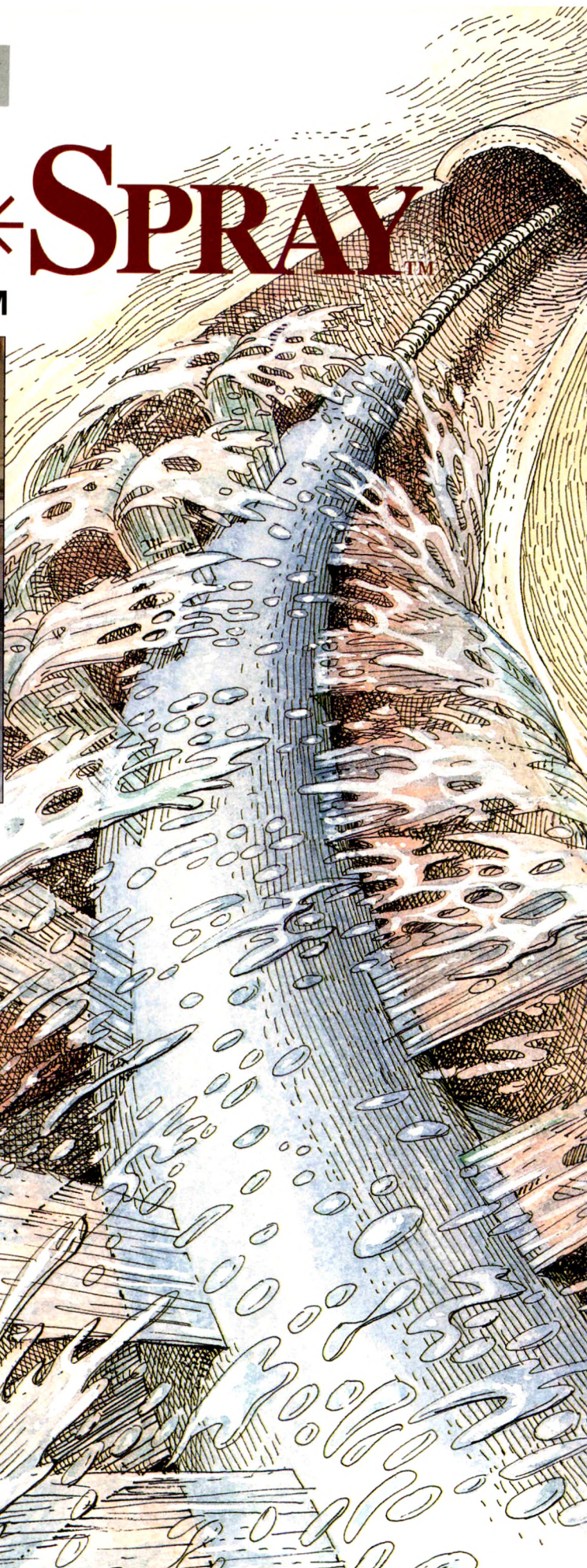
Division of VICTOREEN, INC.
100 VOICE ROAD • P.O. BOX 349
CARLE PLACE, NY 11514-0349 U.S.A.
(516) 741-6360
FAX (516) 741-5414



INTRODUCING

PULSE*SPRAY™

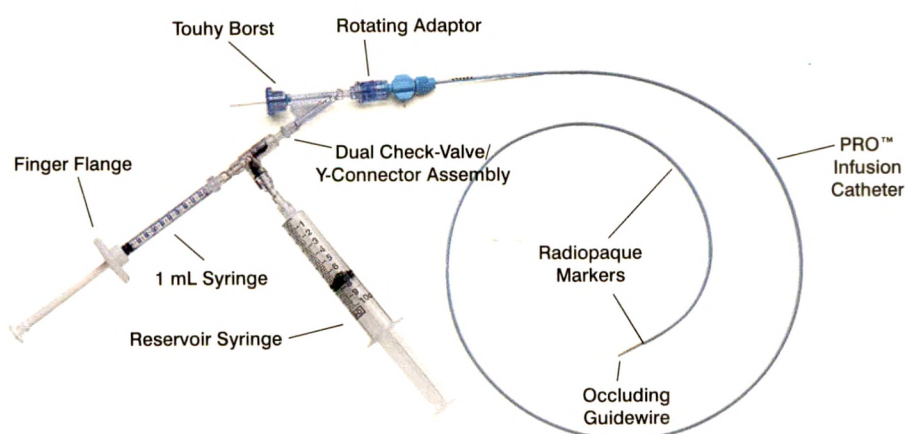
PULSED INFUSION SYSTEM



The PULSE*SPRAY™ System is contraindicated for use in the coronary vasculature.

A breakthrough from AngioDynamics specifically developed for the infusion of therapeutic solutions into the peripheral vasculature.

Developed in association with Joseph J. Bookstein, MD,
PULSE*SPRAY™ offers:



PRO™ Infusion Catheter (patent pending)

- 5F PRO™ (Pressure Responsive Orifice) Infusion Catheter features slits at 90° intervals around the axis of the catheter.
- Available in both 90 cm and 135 cm lengths, with infusion slit pattern variations of 10 cm and 20 cm.

Unique slit design

- Circumferential slit pattern provides uniform dispersion of the therapeutic solution.

Finger flange

- Conveniently designed finger flange incorporated with the 1 mL tuberculine syringe allows forceful and consistent injection, while offering comfort during the procedure.

Dual check-valve assembly

- Dual check-valve/Y-connector assembly simplifies aspiration and infusion of the therapeutic agent.

ANGIODYNAMICS™

Division of E-Z-EM, Inc.

AngioDynamics, Division of E-Z-EM, Inc. Glens Falls, NY 12801
1-800-77ANGIO

Distributed in Canada by THERAPEX
Division of E-Z-EM Canada, Inc. 1-800-465-5870

AJR Business and Subscriber Information

The American Roentgen Ray Society

AJR, *American Journal of Roentgenology*, is published monthly to disseminate research on current developments in the radiologic sciences and commentary on topics related to radiology. It is published by the American Roentgen Ray Society, 1891 Preston White Dr., Reston, VA 22091; (703) 648-8992. Inquiries regarding society business, the annual ARRS meeting, and membership should be addressed to the Society at the above address.

Correspondence Concerning the AJR

Correspondence regarding display (not classified) advertising, subscriptions, address changes, reprints, and permission requests should be addressed to Williams & Wilkins, 428 E. Preston St., Baltimore, MD 21202; (301) 528-4000.

Correspondence regarding editorial matters and classified advertising should be addressed to Editorial Office, *AJR*, 2223 Avenida de la Playa, Ste. 103, La Jolla, CA 92037-3218; telephone (619) 459-2229; FAX (619) 459-8814. For information on manuscript submission, see Guidelines for Authors, pages A21-A23.

Subscriber Information

Subscription requests and inquiries should be sent to Williams & Wilkins, 428 E. Preston St., Baltimore, MD 21202. ARRS annual dues include \$50 for journal subscription. Subscription rates are as follows: nonmembers, \$125/year (\$180 foreign); institutions, \$135 (\$190 foreign); nonmember in-training, \$25 (\$80 foreign). Single copies of the Journal may

be purchased for \$18 (\$22 foreign). Airmail rates will be furnished on request. The GST number for Canadian subscribers is 123394371.

Call toll-free, 1-800-638-6423 (in Maryland call 1-800-638-4007), with subscription questions or problems. Please have the mailing label from your latest issue available when you call.

If a subscriber receives a damaged copy of the *AJR* or fails to receive an issue, the subscriber should notify Williams & Wilkins (428 E. Preston St., Baltimore, MD 21202) within 60 days of publication (90 days for foreign subscribers) and that issue will be replaced.

Change of address information should be sent to Williams & Wilkins, 428 E. Preston St., Baltimore, MD 21202. Allow 90 days for address changes.

Copyrights, Permissions, and Reprints

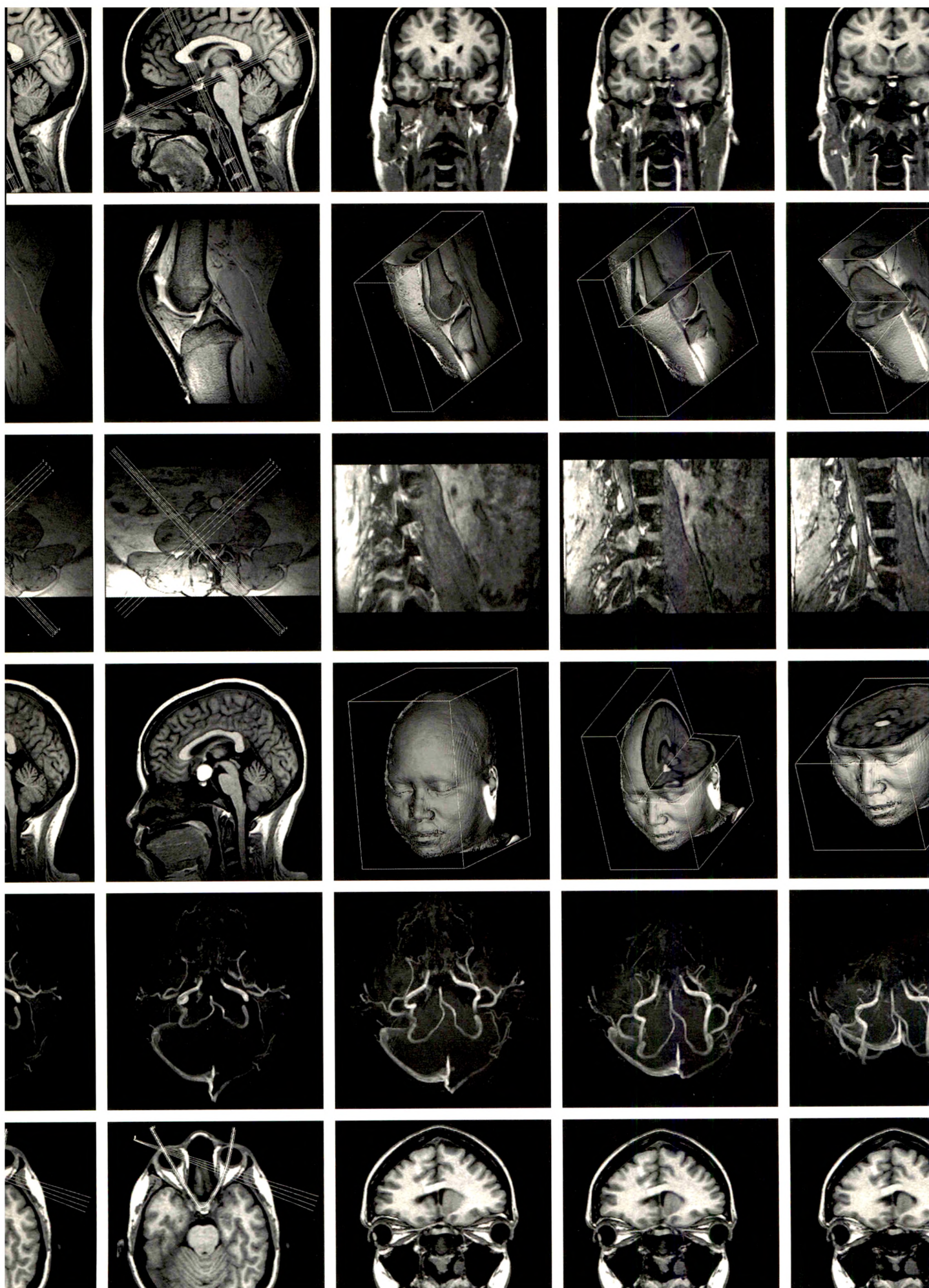
The American Roentgen Ray Society holds the copyright for all material published in the *AJR*. No part of this publication may be reproduced without permission from the ARRS. Requests for such permission should be addressed to Williams & Wilkins, 428 E. Preston St., Baltimore, MD 21202.

For reprints of a particular article, please contact the author designated in the footnotes for that article.

Indexes

The *AJR* provides volume and yearly indexes (subject and author) in the June and December issues each year. *AJR* articles are also indexed in *Current Contents*, *Index Medicus*, and the cumulative index published by *Radiology*.

WE
APPROACHED
THIS AD
FROM EVERY
POSSIBLE
ANGLE.





NOBODY'S LOOKING AT ANATOMY LIKE PICKER MR.

You've just seen it for yourself.

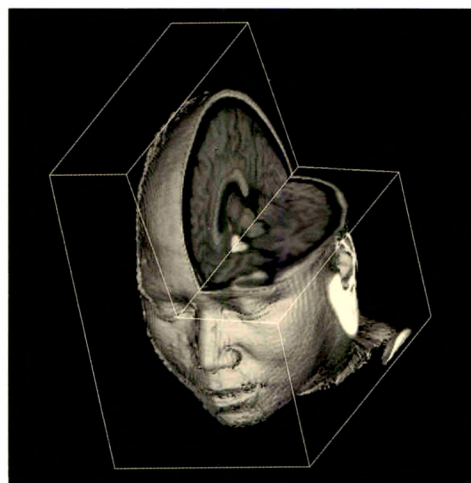
The images from our Vista® HPQ scanner are so clear they deserve a double take.

The high contrast and exceptional detail generated by our RF-Spoiled FAST™ acquisition technique let you capture entire parts of the body—for instance, a whole head—with submillimeter resolution. And submillimeter slice thickness. All in 10 minutes or less.

The ViStar™ supercomputer changes your viewpoint, too.

It allows you to instantly reformat Vista images—using multiple obliques, curved slices, surfaces and more—to precisely target the suspected pathology. And reveal anatomy as it's never been seen before.

Vista/ViStar from Picker. It's the



future of MR technology. No matter how you look at it.

For more information on Picker's Vista/ViStar at all field strengths, call us at 1 800 323-0550. Or write: Picker International, Inc., 595 Miner Road, Dept. CC, Cleveland, OH 44143.



PICKER

MORE THAN IMAGES. INSIGHT.

©1991 Picker International, Inc.

Visit us at RSNA booth 1557-East Hall.

6th SAN DIEGO SYMPOSIUM ON VASC

February 15 - 21, 1992

Sheraton Harbor Island I

SYMPOSIUM TOPICS

Real-time Doppler Color Flow Imaging Fundamentals

- Principles and pitfalls of real-time color flow imaging
- Strategies of color coding
- Doppler Artefacts
- Biologic effects of ultrasound

Cerebrovascular Sonography

- Real-time color flow imaging of the carotid bifurcation
- Aortic arch branches and vertebral arteries
- Carotid plaque morphology
- Intra-operative monitoring
- Late post-op monitoring

Transcranial Doppler Sonography

- Current status of TCD
- Prediction of stroke with TCD
- Intraoperative monitoring
- Extracranial Duplex vs. TCD

Peripheral Arterial Disease

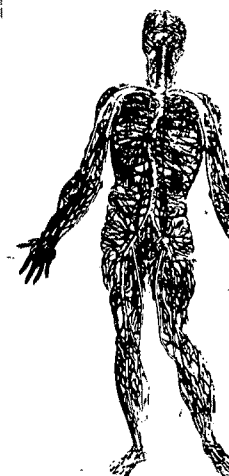
- Real-time color Doppler in peripheral arterial disease
- Scanning for aortoiliac occlusive disease
- Abdominal aneurysm

screening in the vascular lab

- Pre-angioplasty and pre-operative evaluation
- Evaluation of trauma and emergencies
- Quantitative plethysmography
- Evaluation of upper extremity ischemia
- Intra-operative and completion screening for PAD
- Angioscopy and angiography as completion alternatives
- Screening after surgery
- Quantitative diagnoses from Doppler information

Abdominal Sonography

- Renal artery
- Pitfalls in renal arterial studies
- Natural history of renal artery stenosis
- Renal parenchyma and transplantation
- Mesenteric and coeliac vessels
- Pitfalls in mesenteric and coeliac sonography
- Liver, incl. portal vein and transplantation



Venous Sonography

- Natural history of mini calf DVT
- DVT in the lower extremity with real-time color
- Significance of a negative duplex scan
- Quantitation of lower extremity venous disease
- Significance of free-flow

TUTORIALS AND BASIC WORKSHOPS

Each of the three half day tutorials will include a basic physician lecture, a basic technologist lecture, and a basic workshop.

Subjects include:

- Basic Cerebrovascular
- Basic Peripheral Arterial
- Basic Peripheral Venous

ADVANCED WORKSHOPS

Details of technical operation of instruments and interpretation of data with opportunities for discussion.

Symposium registration includes three advanced workshops.

INSTRUMENTATION EXPO

An exposition of the most modern and sophisticated new techniques for diagnostic studies of the vascular system.

SYMPOSIUM DIRECTOR

Eugene F. Bernstein*
Scripps Clinic
and Research Foundation

INVITED FACULTY

Rob G. A. Akerstaff
St. Antonius Hospital, Utrecht,
The Netherlands
James P. Bagian
NASA, Houston
Dennis F. Bandyk*
Medical College of Wisconsin
Kirk W. Beach
University of Washington
M. Gene Bond
Bowman Gray School of Medicine
John J. Cranley
Good Samaritan Hospital,
Cincinnati
David L. Dawson
University of Washington
Ralph B. Dille*
Scripps Clinic
and Research Foundation
Bernardus C. Elkelboom*
University Hospital, Utrecht,
The Netherlands
Arnost Fronck*
University of California, San Diego
William R. Flinn
Northwestern University

Seymour Glagov

University of Chicago
Edward G. Grant*
University of California,
Los Angeles
Lazer J. Greenfield
University of Michigan
Charles B. Higgins
University of California,
San Francisco
Jack Hirsh
McMaster University Medical Center,
Hamilton, Ontario
E. Meredith James
Mayo Clinic
Kaj Johansen
University of Washington
Richard F. Kempczinski
University of Cincinnati
Richard I. Kitney
Imperial College, London
Ted R. Kohler
University of Washington
Frederick W. Kremkau
Bowman Gray School of Medicine
Robert Mattrey
University of California, San Diego
Christopher R. B. Merritt*
Ochsner Clinic
Jay P. Mohr
College of Physicians and
Surgeons, New York

Marsha N. Neumyer

Pennsylvania State University
Andrew N. Nicolaides*
St. Mary's Medical School, Los Angeles
John W. Norris
University of Toronto
Shirley M. Otis
Scripps Clinic
and Research Foundation
John M. Porter
University of Oregon
Pravin Shah
Loma Linda University
D. Eugene Strandness*
University of Washington
David S. Sumner
Southern Illinois University
Kenneth J. W. Taylor
Yale University
Brian L. Thiele*
Pennsylvania State University
Paul S. Van Bemmelen
Southern Illinois University
James S. T. Yao*
Northwestern University
Paul G. Yock
University of California,
San Francisco
Brenda K. Zierler
University of Washington
R. Eugene Zierler*
University of Washington

FC

**Vascular Diagnosis
Meeting Management**
5665 Oberlin Drive,
Suite 110
San Diego, CA 921



I N C K R O D T

A water-loving medium. And the advantages it brings.

It has been suggested that water-loving contrast agents are less toxic than lipid-loving compounds.^{1,2}

Hydrophilic agents attract water when injected into the bloodstream and the body perceives them as "friendlier" molecules¹; they are less likely to cross the blood-brain barrier or to diffuse across the lipid bilayers of neural cell membranes.²

One measure of hydrophilicity is the octanol:water partition coefficient. By this standard, Optiray is the most hydrophilic of the nonionic media.

The ordering of LD₅₀ values is consistent with the ordering of octanol:water partition coefficients. The most hydrophilic agent, Optiray, demonstrates the least intracisternal toxicity.

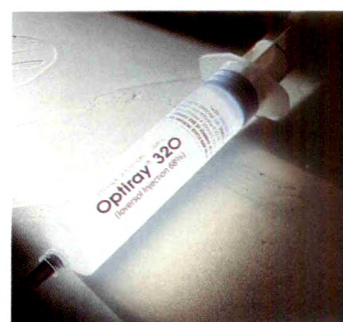
Relative Toxicity and Hydrophilicity of Nonionics^{3*}

Contrast Agents	LD ₅₀ Values† (mg I/kg)	Partition Coefficients§ (Octanol:Water)
Optiray	>1,200	4
Iohexol	977	8
Iopamidol	800	19

*Caution must be used to avoid drawing clinical conclusions based solely upon nonclinical data.
†Comparative acute intracisternal toxicity in rats.
§x10⁻¹.

(Higher LD₅₀ value indicates less toxicity; lower partition coefficient indicates greater hydrophilicity.)

With Optiray, you can expect a very low incidence of individual, drug-related adverse reactions.⁴ Optiray also offers the safety, convenience, and cost efficiency of the single-dose Ultraject® prefilled syringe. For more information, contact your Mallinckrodt Medical representative or call us toll free at (800) 325-3688.



All nonionic iodinated contrast media currently available inhibit blood coagulation, *in vitro*, less than ionic contrast media. Clotting has been reported when blood remains in contact with syringes containing non-ionic contrast media. Therefore, meticulous intravascular administration technique is necessary to minimize thromboembolic events.

References:

1. McClellan BL. Ionic and nonionic iodinated contrast media: evolution and strategies for use. *AJR*. 1990; 155: 225-233.
2. Hilal SK, et al. Development and evaluation of a new water-soluble iodinated myelographic contrast medium with markedly reduced convulsive effects. *Radiology*. 1978; 126:417-422.
3. Ralston WH, Robbins MS, Coveney J, Blair M. Acute and subacute toxicity studies of ioversol in experimental animals. *Invest Radiol*. 1989;24 (suppl 1):S2-S9.
4. Benamor M, Aten EM, McElvany KD, et al. Ioversol clinical safety summary. *Invest Radiol*. 1989;24 (suppl 1):S67-S72.

Nonionic
OPTIRAY®
(ioversol)

The friendlier molecule

OPTIRAY® 160 240 320
(Ioversol Injection)

DESCRIPTION: Each milliliter of OPTIRAY 160 (ioversol injection 34%) provides 339 mg of ioversol with 3.6 mg of tromethamine as a buffer and 0.2 mg of edetate calcium disodium as a stabilizer. OPTIRAY 160 provides 16% (160 mg/mL) organically bound iodine.

Each milliliter of OPTIRAY 240 (ioversol injection 51%) provides 509 mg of ioversol with 3.6 mg of tromethamine as a buffer and 0.2 mg of edetate calcium disodium as a stabilizer. OPTIRAY 240 provides 24% (240 mg/mL) organically bound iodine.

Each milliliter of OPTIRAY 320 (ioversol injection 68%) provides 678 mg of ioversol with 3.6 mg of tromethamine as a buffer and 0.2 mg of edetate calcium disodium as a stabilizer. OPTIRAY 320 provides 32% (320 mg/mL) organically bound iodine.

CONTRAINDICATIONS: None.

WARNINGS: Nonionic iodinated contrast media inhibit blood coagulation, in vitro, less than ionic contrast media. Clotting has been reported when blood remains in contact with syringes containing nonionic contrast media.

Serious, rarely fatal, thromboembolic events causing myocardial infarction and stroke have been reported during angiographic procedures with both ionic and nonionic contrast media. Therefore, meticulous intravascular administration technique is necessary, particularly during angiographic procedures, to minimize thromboembolic events. Numerous factors, including length of procedure, catheter and syringe material, underlying disease state and concomitant medications may contribute to the development of thromboembolic events. For these reasons, meticulous angiographic techniques are recommended including close attention to guidewire and catheter manipulation, use of manifold systems and/or three-way stopcocks, frequent catheter flushing with heparinized saline solutions and minimizing the length of the procedure. The use of plastic syringes in place of glass syringes has been reported to decrease but not eliminate the likelihood of in vitro clotting.

Serious or fatal reactions have been associated with the administration of iodine-containing radiopaque media. It is of utmost importance to be completely prepared to treat any contrast medium reaction.

As with any contrast medium, serious neurologic sequelae, including permanent paralysis, can occur following cerebral arteriography, selective spinal arteriography and arteriography of vessels supplying the spinal cord. A cause-effect relationship to the contrast medium has not been established since the patients' pre-existing condition and procedural technique are causative factors in themselves. The arterial injection of a contrast medium should never be made following the administration of vasopressors since they strongly potentiate neurologic effects.

Caution must be exercised in patients with severely impaired renal function, combined renal and hepatic disease, severe thyrotoxicosis, myelomatosis, or anuria, particularly when large doses are administered.

Intravascularly administered iodine-containing radiopaque media are potentially hazardous in patients with multiple myeloma or other paraproteinemias, particularly in those with therapeutically resistant anuria. Myeloma occurs most commonly in persons over age 40. Although neither the contrast agent nor dehydration has been proved separately to be the cause of anuria in myelomatous patients, it has been speculated that the combination of both may be causative. The risk in myelomatous patients is not a contraindication to the procedure; however, special precautions, including maintenance of normal hydration and close monitoring, are required. Partial dehydration in the preparation of these patients prior to injection is not recommended since this may predispose the patient to precipitation of the myeloma protein.

Administration of radiopaque materials to patients known or suspected of having pheochromocytoma should be performed with extreme caution. If, in the opinion of the physician, the possible benefits of such procedures outweigh the considered risks, the procedures may be performed; however, the amount of radiopaque medium injected should be kept to an absolute minimum. The blood pressure should be assessed throughout the procedure, and measures for treatment of a hypertensive crisis should be available.

Contrast media may promote sickling in individuals who are homozygous for sickle cell disease when administered intravascularly.

Reports of thyroid storm following the intravascular use of iodinated radiopaque agents in patients with hyperthyroidism or with an autonomously functioning thyroid nodule, suggest that this additional risk be evaluated in such patients before use of any contrast medium.

PRECAUTIONS: General: Diagnostic procedures which involve the use of iodinated intravascular contrast agents should be carried out under the direction of personnel skilled and experienced in the particular procedure to be performed. A fully equipped emergency cart, or equivalent supplies and equipment, and personnel competent in recognizing and treating adverse reactions of all types should always be available. Since severe delayed reactions have been known to occur, emergency facilities and competent personnel should be available for at least 30 to 60 minutes after administration.

Preparatory dehydration is dangerous and may contribute to acute renal failure in patients with advanced vascular disease, diabetic patients, and in susceptible non-diabetic patients (often elderly with pre-existing renal disease). Patients should be well hydrated prior to and following the administration of OPTIRAY.

The possibility of a reaction, including serious, life-threatening, fatal, anaphylactoid or cardiovascular reactions, should always be considered (See ADVERSE REACTIONS). Increased risk is associated with a history of previous reaction to a contrast medium, a known sensitivity to iodine and known allergies (i.e., bronchial asthma, hay fever and food allergies) or hypersensitivities.

The occurrence of severe idiosyncratic reactions has prompted the use of several pretesting methods. However, pretesting cannot be relied upon to predict severe reactions and may itself be hazardous to the patient. It is suggested that a thorough medical history with emphasis on allergy and hypersensitivity, prior to the injection of any contrast medium, may be more accurate than pretesting in predicting potential adverse reactions. A positive history of allergies or hypersensitivity does not arbitrarily contraindicate the use of a contrast agent when a diagnostic procedure is thought essential, but caution should be exercised. Premedication with antihistamines or corticosteroids to avoid or minimize possible allergic reactions in such patients should be considered. Reports indicate that such pretreatment does not prevent serious life-threatening reactions, but may reduce both their incidence and severity.

General anesthesia may be indicated in the performance of some procedures in selected patients; however, a higher incidence of adverse reactions has been reported in these patients, and may be attributable to the inability of the patient to identify untoward symptoms or to the hypotensive effect of anesthesia which can prolong the circulation time and increase the duration of exposure to the contrast agent.

In angiographic procedures, the possibility of dislodging plaques or damaging or perforating the vessel wall should be considered during catheter manipulations and contrast medium injection. Test injections to insure proper catheter placement are suggested.

Angiography should be avoided whenever possible in patients with hemocystinuria because of the risk of inducing thrombosis and embolism. Patients with congestive heart failure should be observed for several hours following the procedure to detect delayed hemodynamic

disturbances which may be associated with a transitory increase in the circulating osmotic load.

Selective coronary arteriography should be performed only in selected patients and those in whom the expected benefits outweigh the procedural risk. The inherent risks of angiocardiology in patients with chronic pulmonary emphysema must be weighed against the necessity for performing this procedure.

Extreme caution during injection of a contrast medium is necessary to avoid extravasation. This is especially important in patients with severe arterial or venous disease.

Drug Interactions: Renal toxicity has been reported in a few patients with liver dysfunction who were given oral cholecystographic agents followed by intravascular contrast agents. Administration of any intravascular contrast agent should therefore be postponed in patients who have recently received a cholecystographic contrast agent.

Other drugs should not be mixed with ioversol injection.

Drug Laboratory Test Interactions: The results of PBI and radioactive iodine uptake studies, which depend on iodine estimation, will not accurately reflect thyroid function for up to 16 days following administration of iodinated contrast media. However, thyroid function tests not depending on iodine estimations, e.g., T3 resin uptake and total or free thyroxine (T4) assays are not affected.

Carcinogenesis, Mutagenesis, Impairment of Fertility: No long term animal studies have been performed to evaluate carcinogenic potential. However, animal studies suggest that this drug is not mutagenic and does not affect fertility.

Pregnancy Category B: No teratogenic effects attributable to ioversol have been observed in teratology studies performed in animals. There are, however, no adequate and well controlled studies in pregnant women. It is not known whether ioversol crosses the placental barrier or reaches fetal tissues. However, many injectable contrast agents cross the placental barrier in humans and appear to enter fetal tissue passively. Because animal teratology studies are not always predictive of human response, this drug should be used during pregnancy only if clearly needed. X-ray procedures involve a certain risk related to the exposure of the fetus.

Nursing Mothers: It is not known whether ioversol is excreted in human milk. However, many injectable contrast agents are excreted unchanged in human milk. Although it has not been established that serious adverse reactions occur in nursing infants, caution should be exercised when intravascular contrast media are administered to nursing women because of potential adverse reactions, and consideration should be given to temporarily discontinuing nursing.

Pediatric Use: Safety and effectiveness in children have not been established.

ADVERSE REACTIONS: Adverse reactions following the use of OPTIRAY formulations are usually mild to moderate, of short duration and resolve spontaneously (without treatment). However, serious, life-threatening and fatal reactions, mostly of cardiovascular origin, have been associated with the administration of iodine-containing contrast media.

Injections of contrast media are often associated with sensations of warmth and pain. In controlled double-blind clinical studies, significantly less warmth and pain were associated with the injection of OPTIRAY than with iohalameglumine, diatrizoate meglumine, and diatrizoate meglumine and diatrizoate sodium.

When OPTIRAY 320 is used for coronary arteriography and ventriculography in double-blind clinical trials, electrocardiographic and hemodynamic changes occur with less frequency and severity with ioversol injection than with diatrizoate meglumine and diatrizoate sodium.

Following coronary artery and left ventricular injection, electrocardiographic parameters were affected less with OPTIRAY (ioversol injection) than with diatrizoate meglumine and diatrizoate sodium injection. These parameters included the following: bradycardia, tachycardia, T-wave amplitude, ST depression and ST elevation.

OPTIRAY has also been shown to cause fewer changes in cardiac function and systemic blood pressure than conventional ionic media. These include cardiac output, left ventricular systolic and end-diastolic pressure, right ventricular systolic and pulmonary artery systolic pressures and decreases in systolic and diastolic blood pressures.

The following table of incidence of reactions is based upon clinical trials with OPTIRAY formulations in over 1100 patients. This listing includes all adverse reactions which were coincidental to the administration of ioversol regardless of their direct attributability to the drug or the procedure. Adverse reactions are listed by organ system and in decreasing order of occurrence. Significantly more severe reactions are listed before others in a system regardless of frequency.

Adverse Reactions		
System	> 1%	≤ 1%
Cardiovascular	none	angina pectoris
		hypotension
		vascular spasm
		bradycardia
		conduction defect
		false aneurysm
		hypertension
		transient arrhythmia
		vascular trauma
		paresthesia
Digestive	none	nausea
		vomiting
Nervous	none	cerebral infarct
		headache
		blurred vision
		vertigo
		lightheadedness
		vasovagal reaction
		disorientation
		dysphasia
		paresthesia
		visual hallucination
Respiratory	none	laryngeal edema
		nasal congestion
		sneezing
		coughing
		hypoxia
		periorbital edema
Skin	none	urticaria
		facial edema
		flush
		pruritus
Miscellaneous	none	extravasation
		shaking chills
		bad taste
		general pain

Regardless of the contrast medium employed, the overall incidence of serious adverse reaction is higher with coronary arteriography than with other procedures. Cardiac decompensation, serious arrhythmias, myocardial ischemia or myocardial infarction may occur during coronary arteriography and left ventriculography.

General Adverse Reactions to Contrast Media

The following adverse reactions are possible with any parenterally administered iodinated contrast medium. Severe life-threatening reactions and fatalities, mostly of cardiovascular origin, have occurred. Most deaths

occur during injection or 5 to 10 minutes later; the main feature being cardiac arrest with cardiovascular disease as the main aggravating factor. Isolated reports of hypotensive collapse and shock are found in the literature. Based upon clinical literature, reported deaths from the administration of conventional iodinated contrast agents range from 6.6 per 1 million (0.00066 percent) to 1 in 10,000 patients (0.01 percent).

The reported incidence of adverse reactions to contrast media in patients with a history of allergy is twice that of the general population. Patients with a history of previous reactions to a contrast medium are three times more susceptible than other patients. However, sensitivity to contrast media does not appear to increase with repeated examinations.

Adverse reactions to injectable contrast media fall into two categories: chemotoxic reactions and idiosyncratic reactions.

Chemotoxic reactions result from the physicochemical properties of the contrast medium, the dose and the speed of injection. All hemodynamic disturbances and injuries to organs or vessels perfused by the contrast medium are included in this category.

Idiosyncratic reactions include all other reactions. They occur more frequently in patients 20 to 40 years old. Idiosyncratic reactions may or may not be dependent on the dose injected, the speed of injection, the mode of injection and the radiographic procedure. Idiosyncratic reactions are subdivided into minor, intermediate and severe. The minor reactions are self-limited and of short duration; the severe reactions are life-threatening and treatment is urgent and mandatory.

In addition to the adverse reactions reported for ioversol, the following additional adverse reactions have been reported with the use of other contrast agents and are possible with any water soluble, iodinated contrast agent.

Nervous: muscular spasm, convulsions, aphasia, syncope, paralysis, visual field losses which are usually transient but may be permanent, coma and death.

Cardiovascular: angioneurotic edema, peripheral edema, vasodilation, thrombosis and rarely thrombophlebitis, disseminated intravascular coagulation and shock.

Skin: maculopapular rash, erythema, conjunctival symptoms, ecchymosis and tissue necrosis.

Respiratory: choking, dyspnea, wheezing which may be an initial manifestation of more severe and infrequent reactions including asthmatic attack, laryngospasm and bronchospasm, pulmonary edema, apnea and cyanosis. Rarely these allergic-type reactions can progress into anaphylaxis with loss of consciousness, coma, severe cardiovascular disturbances and death.

Miscellaneous: hyperthermia, temporary anuria or other nephropathy.

Other reactions may also occur with the use of any contrast agent as a consequence of the procedural hazard; these include hemorrhage or pseudoaneurysms at the puncture site, brachial plexus palsy following axillary artery injections, chest pain, myocardial infarction, and transient changes in hepatorenal chemistry tests. Arterial thrombosis, displacement of arterial plaques, venous thrombosis, dissection of the coronary vessels and transient sinus arrest are rare complications.

In cerebral arteriography, cardiovascular reactions that may occur with some frequency are bradycardia and either an increase or decrease in systemic blood pressure. Neurological reactions that may occur are: seizures, drowsiness, transient paresis, and mild disturbances in vision.

Central nervous system reactions with OPTIRAY in controlled clinical studies in cerebral arteriography that occurred with frequencies greater than 1% were: vertigo (4%) and blurred vision (3%).

In aortography, depending on the technique employed, the risks of this procedure also include the following: injury to the aorta and neighboring organs, pleural puncture, renal damage including infarction and acute tubular necrosis with oliguria and anuria, retroperitoneal hemorrhage from the translumbar approach and spinal cord injury and pathology associated with the syndrome of transverse myelitis. Under conditions of slowed aortic circulation there is an increased likelihood for aortography to cause muscle spasm. Occasional serious neurologic complications, including paraplegia, have also been reported in patients with aortic iliac obstruction, femoral artery obstruction, abdominal compression, hypotension, hypertension, spinal anesthesia, and injection of vasopressors to increase contrast. In these patients the concentration, volume, and number of repeat injections of the medium should be maintained at a minimum with appropriate intervals between injections. The position of the patient and catheter tip should be carefully monitored.

Entry of a large aortic dose into the renal artery may cause, even in the absence of symptoms, albuminuria, hematuria, and an elevated creatinine and urea nitrogen. Rapid and complete return of function usually follows.

Cardiovascular system reactions with OPTIRAY in controlled clinical studies in coronary arteriography with left ventriculography that occurred with frequencies greater than 1% were: angina (1.2%) and nausea (1.2%).

PRECAUTIONS FOR SPECIFIC PROCEDURES:

Cerebral Arteriography

Extreme caution is advised in patients with advanced arteriosclerosis, severe hypertension, cardiac decompensation, senility, recent cerebral thrombosis or embolism, and migraine.

Peripheral Arteriography

Pulsation should be present in the artery to be injected. In thromboangiitis obliterans, or ascending infection associated with severe ischemia, angiography should be performed with extreme caution, if at all.

Coronary Arteriography and Left Ventriculography

Mandatory prerequisites to the procedure are specialized personnel, ECG monitoring apparatus and adequate facilities for immediate resuscitation and cardioversion. Electrocardiograms and vital signs should be routinely monitored throughout the procedure.

Venography

Special care is required when venography is performed in patients with suspected thrombosis, phlebitis, severe ischemic disease, local infection or a totally obstructed venous system. In order to minimize extravasation during injection, fluoroscopy is recommended.

OVERDOSAGE: The adverse effects of overdosage are life-threatening and affect mainly the pulmonary and cardiovascular system. Treatment of an overdosage is directed toward the support of all vital functions, and prompt institution of symptomatic therapy.

Ioversol does not bind to plasma or serum protein and is therefore, dialyzable.

The intravenous LD₅₀ values (g/kg) for ioversol in animals were: 17 (mice), and 15 (rats).

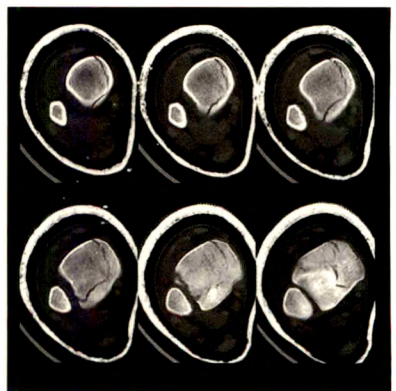
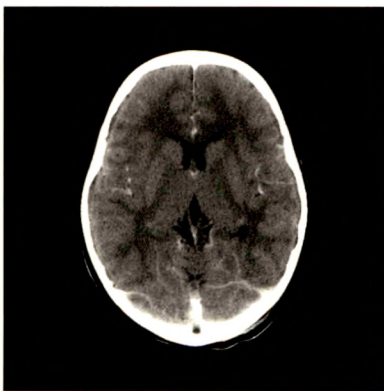
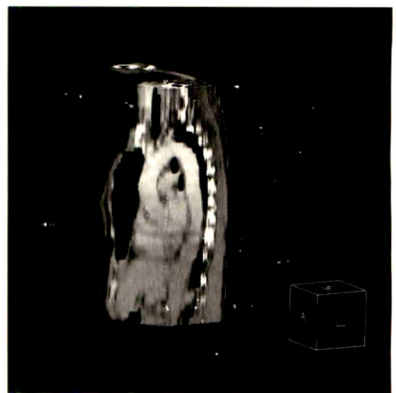
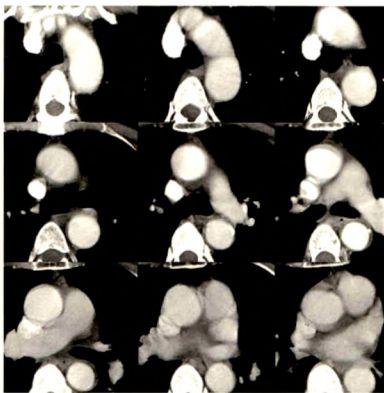
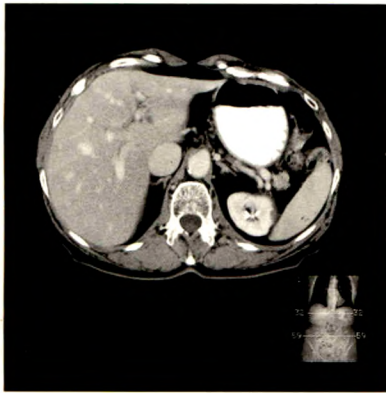
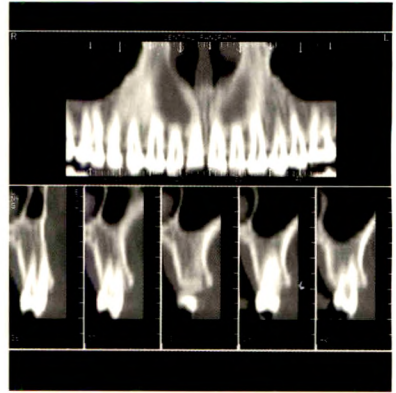
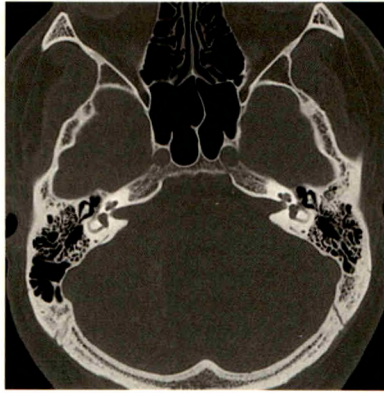
DOSAGE AND ADMINISTRATION: Details on dosage are provided in the package insert. CONSULT FULL PACKAGE INSERT BEFORE USE.

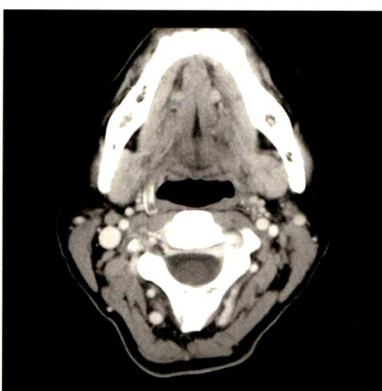
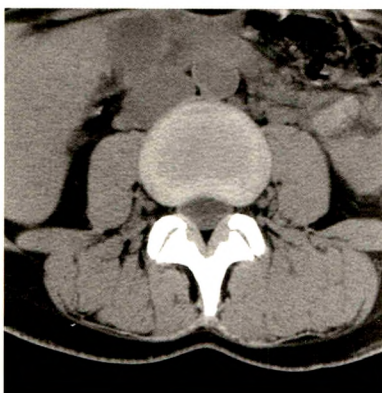
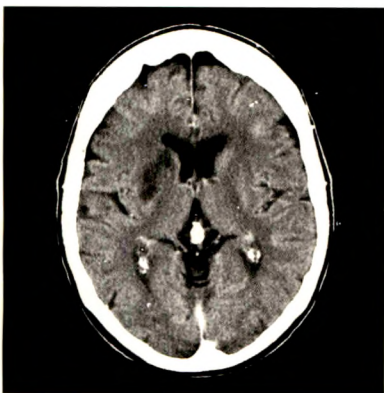
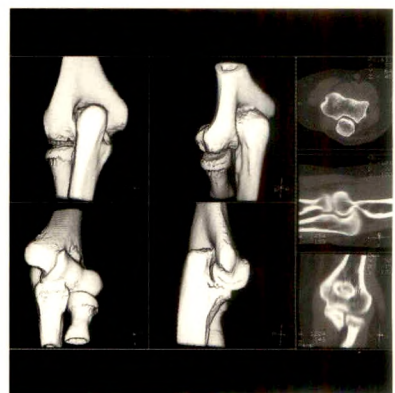
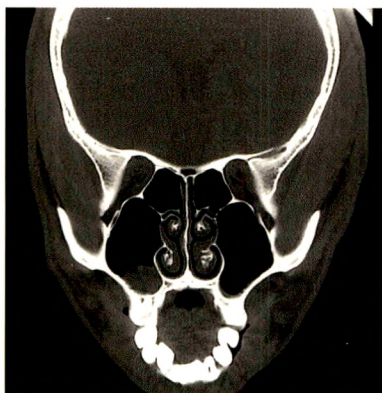
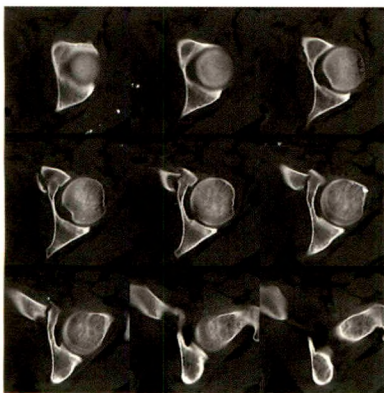
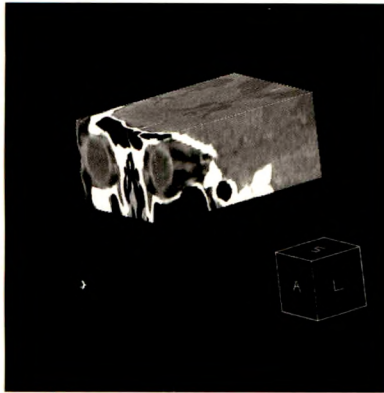


Changing the look of medicine.™

EVERY SIX SECONDS
WE COME UP WITH ANOTHER
IMPRESSIVE ARGUMENT
FOR OWNING THE PQ-2000.™







PQ-2000.
ANY
QUESTIONS?

 **PICKER**
MORE THAN IMAGES. INSIGHT.

Visit us at RSNA booth 1156 & 1556 - East Hall, or call us at 1-800-323-0550.

When you give blood
you give another birthday,
another anniversary,
another day at the beach,
another night under the stars,
another talk with a friend,
another laugh,
another hug,
another chance.



American Red Cross

Please give blood.

AJR Guidelines for Authors

Address new and revised manuscripts, correspondence, and classified ads to the Editor:

AJR Editorial Office
2223 Avenida de la Playa, Suite 103
La Jolla, CA 92037-3218

Telephone: (619) 459-2229; FAX: (619) 459-8814

Inquiries regarding subscriptions, display advertising, reprints, or permission to republish AJR material should be addressed to the publisher:

The Williams & Wilkins Co.
428 E. Preston St.

Baltimore, MD 21202 Telephone: 1-800-638-6423

The AJR publishes original contributions to the advancement of medical diagnosis and treatment. Submitted manuscripts should not contain previously published material and should not be under consideration for publication elsewhere.

Manuscript decisions are based on peer review. Reviewers receive manuscripts without title pages to ensure an unbiased review. Statements made in the article, including changes made by the Editor or manuscript editor, are the responsibility of the author and not of the AJR or its publisher. Authors will be sent the edited manuscript, galley proof, and proofs of illustrations. If the corresponding author will be unavailable to review galleys, arrangements should be made for a coauthor or colleague to read and return the proof.

The following guidelines are based on instructions set forth in the **Uniform Requirements for Manuscripts Submitted to Biomedical Journals** (*Ann Intern Med* 1988;108:258-265). Articles will be edited, however, to conform to the individual style of AJR.

General Guidelines for Major Papers

Abstract. Clearly state (in 200 words or less) the purpose, methods, results, and conclusions of the study. Include actual data.

Introduction. Briefly describe the purpose of the investigation and explain why it is important.

Methods. Describe the research plan, the materials (or subjects), and the methods used, in that order. Explain in detail how disease was confirmed and how subjectivity in observations was controlled.

Results. Present results in a clear, logical sequence. If tables are used, do not duplicate tabular data in text, but do describe important trends and points.

Discussion. Describe the limitations of the research plan, materials (or subjects), and methods, considering both the purpose and the outcome of the study. When results differ from those of previous investigators, explain the discrepancy.

AUTHOR'S CHECKLIST

For priority handling, complete the following checklist,

sign the copyright form on the reverse side of this page, and include both with the manuscript.

Two copies of the manuscript (the original and a photocopy) and two complete sets of figures are submitted. One copy has been retained by the author.

If appropriate, AJR Guidelines for case reports, technical notes, pictorial essays, or letters to the Editor have been followed. (See page A23.)

The manuscript, including references, figure legends, and tables, is typed double-spaced on 8½ × 11 in. (21.6 × 27.9 cm) *nonerasable* paper. Right-hand margins are not justified.

All manuscript pages are numbered consecutively beginning with the abstract. Authors' names do not appear on the manuscript pages.

The manuscript is organized as follows: title page, blind title page (title only), abstract, introduction, methods, results, discussion, acknowledgments, references, tables, figure legends, and figures.

Informed consent has been obtained from patients who participated in clinical investigations. If experiments were performed on animals, authors complied with NIH guidelines for use of laboratory animals.

Use of unfamiliar acronyms and abbreviations is kept to a minimum. When abbreviations are used they are defined at first mention, followed by the abbreviation in parentheses.

Metric measurements are used throughout, or the metric equivalent is given in parentheses.

Names and locations (city and state only) of manufacturers are given for equipment and nongeneric drugs.

Title Page

The following information is given: title of article; names and complete addresses (including zip code) of all authors; current addresses of authors who have moved since study; acknowledgment of grant or other assistance. The corresponding author is clearly identified, and a current address, phone number, and FAX number are given.

A blind title page is included in each copy of the manuscript, giving only the title (without the authors' names) for use in the review process.

Abstract

An abstract of approximately 200 words concisely states the purpose, methods, and results of the study in one paragraph. Actual data are included. Conclusions are stated in a second, summary paragraph.

No abbreviations or reference citations are used.

Case Reports

A case report is a brief description of a special case that provides a message that transcends the individual patient.

Format. There is no abstract. The introduction should be a short paragraph giving the general background and the specific interest of the case. No more than one case should be described in detail (similar ones can be mentioned briefly in the discussion). Emphasis should be on the radiologic aspects; clinical information must be limited to that necessary to provide a background for the radiology. The discussion should be succinct and should focus on the specific message and relevance of radiologic methods. A review of the literature is not appropriate.

Length. Maximum of five double-spaced, typewritten pages, including the references but not the title page or figure legends.

References. Maximum of eight.

Figures. Maximum of four, unless the text is shortened accordingly. Legends must not repeat the text.

Tables and Acknowledgments. Not appropriate in case reports.

Technical Notes

A technical note is a brief description of a specific technique or procedure, modification of a technique, or equipment of interest to radiologists.

Format. No abstract, headings, or subheadings are required. If headings are used, they should be a combination of "Case Report," "Materials and Methods," "Results," and "Discussion." A brief one-paragraph introduction should be included to give the general background. Discussion should be limited to the specific message, including the uses of the technique or equipment. Literature reviews and lengthy case reports are not appropriate.

Length. Maximum of five double-spaced, typewritten pages, including the references but not the title page or figure legends.

References. Maximum of eight.

Figures. Maximum of two, unless the text is shortened accordingly.

Tables and Acknowledgments. Not appropriate in technical notes.

Pictorial Essays

A pictorial essay is an article that conveys its message through illustrations and their legends. Unlike other *AJR* articles, which are based on original research, pictorial essays serve primarily as teaching tools, like exhibits at a scientific meeting. They are not encyclopedic book chapters. The abstract should be a short, introductory paragraph.

Length. Maximum of four double-spaced, typewritten pages, including the references but not the title page or figure legends.

References. Maximum of four.

Figures. Maximum of 30 figure parts. Number should be as few as necessary to convey the message of the paper.

Tables and Acknowledgments. Not appropriate in pictorial essays.

Letters to the Editor and Replies

Letters to the Editor and Replies should offer objective and constructive criticism of published articles. Letters may also discuss matters of general interest to radiologists. Do not end a letter with a hand-written signature.

Format. All letters should be typed double-spaced on nonletterhead paper, with no greeting or salutation. Name and affiliation should appear at the end of the letter. Titles for letters should be short and pertinent. The title for a reply is simply "Reply."

Length. Maximum of two double-spaced, typewritten pages, including references.

References. Maximum of four.

Figures. Maximum of two.

Tables and Acknowledgments. Not appropriate in Letters to the Editor and Replies.

Opinions, Commentaries, and Perspectives

Opinions, commentaries, and perspectives are special articles dealing with controversial topics or issues of special concern to radiologists.

Format. Include a title page but no abstract. Headings may be used to break up the text.

Length. Maximum of five double-spaced, typewritten pages.

References. Maximum of five.

Tables and Figures. Maximum of four.

Computer Page Articles

Articles published on the computer page deal with practical computer applications to radiology.

Format. Include a title page and an abstract.

Length. Maximum of eight double-spaced, typewritten pages.

References. Maximum of five.

Figures and Tables. Maximum of five. Computer printouts are not acceptable. Figures must be submitted as 5 × 7 in. glossy prints.

All submissions to the *AJR* must be accompanied by a completed copy of the Author's Checklist and the signed Copyright agreement.

References

References (not to exceed 35) are typed double-spaced starting on a separate page and are **numbered consecutively in the order in which they appear in the text**.

All references are cited in the text and are enclosed in brackets and typed on line with the text (not superscript).

Unpublished data are not cited in the reference list, but are cited parenthetically in the text, for example, (Smith DJ, personal communication), (Smith DJ, unpublished data). This includes papers submitted, but not yet accepted, for publication.

Papers presented at a meeting are not cited in the reference list, but are cited parenthetically in the text (e.g., Smith DJ et al., presented at the annual meeting of the American Roentgen Ray Society, May 1990). After first mention, use (Smith DJ et al., ARRS meeting, May 1990).

Inclusive page numbers (e.g., 333–335) are given for all references.

Journal names are abbreviated according to *Index Medicus*.

Style and punctuation of references follow the format illustrated in the following examples (all authors are listed when six or fewer; when seven or more authors, the first three are listed, followed by "et al."):

Journal article

1. Long RS, Roe EW, Wu EU, et al. Membrane oxygenation: radiographic appearance. *AJR* 1986;146:1257–1260

Book

2. Smith LW, Cohen AR. *Pathology of tumors*, 6th ed. Baltimore: Williams & Wilkins, 1977:100–109

Chapter in a book

3. Breon AJ. Serum monitors of bone metastasis. In: Clark SA, ed. *Bone metastases*. Baltimore: Williams & Wilkins, 1983:165–180

Tables

Each table is typed double-spaced on a separate page without vertical or horizontal rules; each has a short, descriptive title. Tables do not exceed two pages in length and contain at least four lines of data.

Tables are numbered in the order in which they are cited in the text.

Abbreviations are defined in an explanatory note below each table.

Tables are self-explanatory and do not duplicate data given in the text or figures.

All arithmetic (percentages, totals, differences) has been double checked for accuracy, and tabular data agree with data given in the text.

Figures and Legends

Two complete sets of original figures are submitted unmounted in labeled envelopes.

Figures are clean, unscratched, 5 × 7 in. (13 × 18 cm) glossy prints with **white borders**. A separate print is submitted for each figure *part*.

All figure parts relating to one patient have the same figure number.

Each figure is labeled on the back with the figure number and an arrow indicating "top." For black-and-white figures, labeling is done on a gummed label, which is then affixed to the back of the print. **Never** use labels on **color** figures, but write figure number on the back lightly in pencil. **Never** use ink on front or back of any figures.

Authors' names are *not* written on the backs of figures.

Only removable (rub-on) arrows and letters are used on the figures. Symbols are uniform in size and style and are not broken or cracked.

Images are uniform in size and magnification.

Line drawings are done in black ink on a white background. They are professional in quality, and all use the same size type. (Only glossy prints are acceptable.)

Written permission has been obtained for use of all previously published illustrations (and copies of permission letters are included), and an appropriate credit line is given in the legends.

Legends are typed double-spaced, and figure numbers correspond with the order in which the figures are cited in the text.

Transfer of Copyright Agreement, Conflict of Interest Acknowledgment, Certification of Coauthors, and Exclusive Publication Statement

Complete copyright to the article entitled: _____

is hereby transferred to the American Roentgen Ray Society (for United States government employees to the extent transferable), effective if and when the article is accepted for publication in the *American Journal of Roentgenology*. In the case of the authors who are officers or employees of the United States government, the American Roentgen Ray Society recognizes that works prepared by officers or employees of the United States government as part of their official government duties are in the public domain.

Authors reserve all proprietary rights other than copyright, such as patent rights and the right to use all or part of this article in future works of their own. The authors retain the right of replication, subject only to crediting the original source of publication and receiving written permission from the publisher.

Authors guarantee that this manuscript contains no matter that is libelous or otherwise unlawful, invades individual privacy, or infringes any proprietary rights.

Authors understand that they will receive no royalty or other compensation from the American Roentgen Ray Society or the publisher.

Authors guarantee that the editor has been or will be informed of any proprietary or commercial interest or conflicts of interest the authors may have that relate directly or indirectly to the subject of this article.

All authors certify that they have made substantive and specific intellectual contributions to the article and assume public responsibility for its content.

Finally, the authors certify that none of the material in this manuscript has been published previously or is currently under consideration for publication elsewhere.

First author/date

Second author

Third author

Fourth author

Fifth author

Sixth author

This agreement must be signed by all authors in order for the manuscript to be published.



G A D O

Advancing
to nonionic
MR contrast
media

IT'S USELESS, WITH

“Gadolinium.” It’s come to be a synonym for MR contrast. But without protective chelation, gadolinium would be, in effect, useless. Binding molecules—called ligands—permit otherwise toxic metals like gadolinium to be safely administered to patients.

The gadolinium chelate complex allows the favorable paramagnetic properties of the Gd^{3+} ion to be exploited for MR contrast enhancement. But since gadolinium alone is toxic, the choice of a ligand with high affinity for this metal is crucial. And if the chelate complex is also nonionic, its diagnostic utility can potentially be expanded.

Photomicrograph of gadolinium in solution (original magnification x40)

L I N I U M

OUT THE RIGHT LIGAND

Moving beyond the experience gained with ionic gadolinium chelates, our research effort is aimed at developing new, nonionic Gd-ligand complexes with greater in vivo stability. This research effort is committed to extending our tradition of leadership in nonionic contrast media into MR.

See us at RSNA Booth 7311, North Hall.

sanofi  WINTHROP

LEADERSHIP IN NONIONIC CONTRAST MEDIA SOON IN MR



No more bookkeeping headaches or medicare dictums. No worries about malpractice insurance. And a lot less paperwork.

As an FHP physician, you'll have more time to concentrate on what you really enjoy: practicing medicine. But that's not all.

Our predictable schedules mean more time for family and friends, too. And that time is truly your own — whether for quiet evenings at home or weekends camping against the backdrop of Utah's breathtaking Rocky Mountains.

Find out more by calling 1-800-283-8884, ext. 631.

Or send your C.V. to FHP, Professional Staffing, 35 West Broadway, Salt Lake City, UT 84101-9933. Opportunities also available in AZ, CA, NM and Guam. An equal opportunity employer.

"The reasons

for joining

FHP really start

to stack up."

—Joe Slattery, M.D.

*Giving Physicians More
of What They Want.*

FHP
HEALTH CARE

Gundersen Clinic: Because where you practice is as important as what you practice.

The Gundersen tradition: state-of-the-art medical care delivered by a highly qualified group of medical and dental specialists. And what sets our professionals apart from other medical staffs? Teamwork.

We are seeking General Radiologists to join our staff of 17 Radiologists who provide outreach services to those patients who visit our multiple branch community clinics in Iowa, Minnesota and Wisconsin, as well as provide care to patients in our full service main clinic in La Crosse. Last year, 139,412 radiographic examinations were performed throughout our system. It's the best of both worlds where you can combine sophisticated technology with one-on-one involvement in primary care.

Become part of the Gundersen tradition as we enter our second century serving the needs of 70,000 families through over 702,000 patient visits each year. You'll also enjoy an outstanding quality of life, competitive salaries and benefits, an excellent continuing education program and pension plan. Send your CV or call **Tim Skinner, Manager, Physician Recruitment, COLLECT, at 1-608-782-7300 ext. 6673**. An equal opportunity employer.

1891-1991



Gundersen Clinic, Ltd.

1836 South Avenue
Dept. KK-9
La Crosse, Wisconsin 54601

HAMAD MEDICAL CORPORATION DOHA, QATAR

Hamad Medical Corporation is a 1,065 bed referral facility with 4,100 staff and is the main health establishment in the country with its modern equipped facilities, is inviting highly qualified candidates to apply for the post of **Chairman of Radiodiagnosis**.

The required candidate must have FRCR or American Board and a minimum of 12 years experience after their postgraduate degree. The candidate should have experience with M.R.I. It is an ultra-modern department with the latest equipment including, CT, US, Angio and 1.5 Tesla M.R.I.

Salary is negotiable.

Send complete CVs, copies of certificates with contact telephone number/address and attach one recent photograph to:

**Head of Recruitment Section
Personnel Department
Hamad Medical Corporation
P.O. Box: 3050
Doha - State of Qatar
(Ad ref.# RS/AD/Rad.-1/Vol.2/91)**

How can the VESS Chair help you do a better Swallow Study?

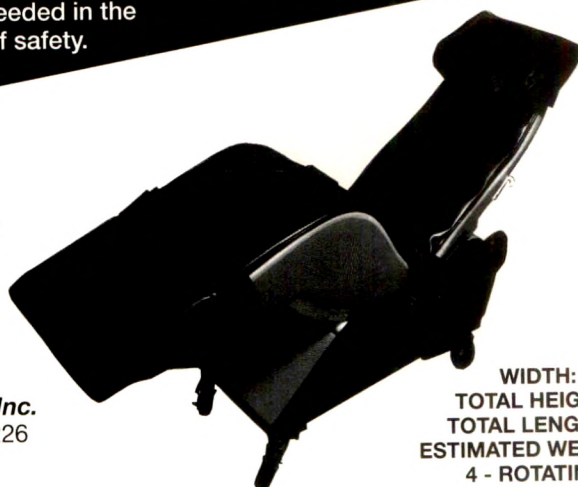
The VESS Chair is an adaptive seating device for the Modified Barium Swallow Study. For reliable Swallow Study outcomes, proper patient positioning and alignment of the head and neck is necessary. The VESS Chair provides Departments of Imaging and Speech/Language Pathology with positioning capability to effectively assess the more difficult or mobility-impaired patient.

The VESS Chair allows for both lateral and anterior-posterior viewing during videofluoroscopy. The VESS Chair's ergonomic design, narrow size, tilting flexibility and transportability will reduce the time needed in the fluoroscopy suite and contribute to patient and staff safety.



New Features Include -

- IV Stand Holder
- Chart Holder
- Oxygen Tank Holder
- Foley Bag Holder
- Removeable Arms



For More Information Call or Write To: **VESS Chairs, Inc.**
1033 N. Mayfair Road; Suite 200; Wauwatosa, WI 53226
(414) 476-2488 FAX (414) 259-0423
Demonstration Video Available.

WIDTH: 15-1/2 inches
TOTAL HEIGHT: 50 inches
TOTAL LENGTH: 52 inches
ESTIMATED WEIGHT: 110 lbs.
4 - ROTATING CASTERS

Musculoskeletal Radiology Fellowship

Beginning July 1, 1992. Training in US, CT, MRI, arthrography, myelography, discography, etc. Offered in multiple areas, including general and pediatric orthopedics, congenital dysplasias, joint replacement, spine and arthritis.

Competitive salary and excellent benefits. Send C.V. to: J. Beltran, M.D., Chairman, Department of Radiology.

Hospital for Joint Diseases Orthopaedic Institute

301 East 17 Street, New York, N.Y. 10003
an equal opportunity employer

Nuclear Radiologist

Hanover, New Hampshire 03756. Write to: Peter K. Spiegel, M.D., Chairman, Department of Diagnostic Radiology, Dartmouth-Hitchcock Medical Center, 2 Maynard Street. Permanent position. Department consists of 13 staff, 11 residents and 2 fellows with a full range of modern radiologic practice in a new Department in a new 420-bed Medical Center to be occupied in Fall of 1991. Seeking Nuclear Radiologist at senior assistant - full professor level to be member of a 200-physician academic multispecialty group which forms the clinical faculty of Dartmouth Medical School. ABR/ABNM preferred, experience in Nuclear Cardiology and SPECT essential. Interest in teaching essential. Research interest preferred with opportunity to develop academic program. AA/EOE.



**Dartmouth-Hitchcock
Medical Center**

The Hitchcock Clinic
Hanover, New Hampshire

The laser imager of choice is also the laser imager of choices

3M now has a laser imager to meet any user need

3M Laser Imager Systems have always been the imagers of choice of hospitals and original equipment manufacturers. After all, we were instrumental in introducing laser imaging to the medical community. And we have more placements than any other laser imager manufacturer.

But a 3M Laser Imager System is more than just the choice of those in the know, it's the only system that lets you be choosy. That's because 3M has not one, not two, but *three* models to choose from, each designed to fit your specific requirements.

The 3M Laser Imager is a fully-featured imager for single modality applications. The 3M Laser Imager Plus is a medium throughput, multi-modality-ready imager with enhanced features. And the 3M Laser Imager XL is a maximum throughput, fully integrated multi-modality system with high resolution imaging and high speed acquisition.

All accessories and options, like the 3M Laser Processor and the 3M Daylight Load Film Magazine, can be installed with any of the three systems. And there are now *four* 3M IR Laser Imaging Films, system-matched for high resolution and consistent, high quality imaging.

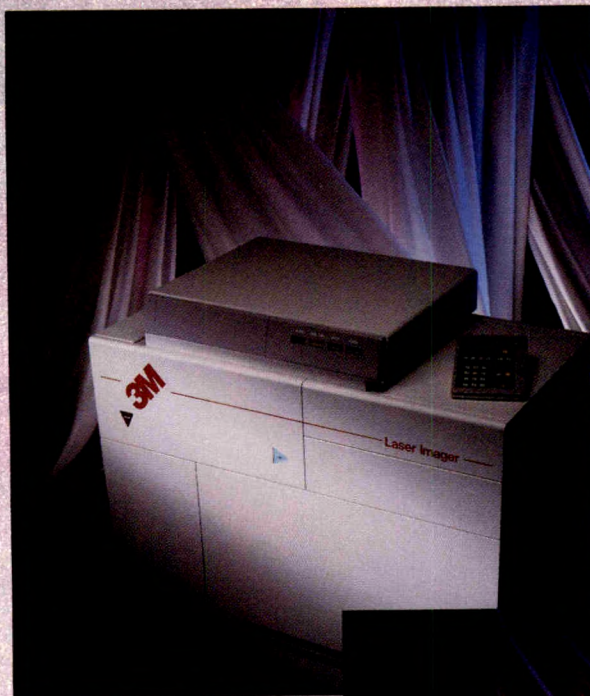
All of which means you can build a system that's precisely what you, your hospital and your patients need. For both today and in the future.

So make the right decision. Choose the laser imager of choice. And choices.

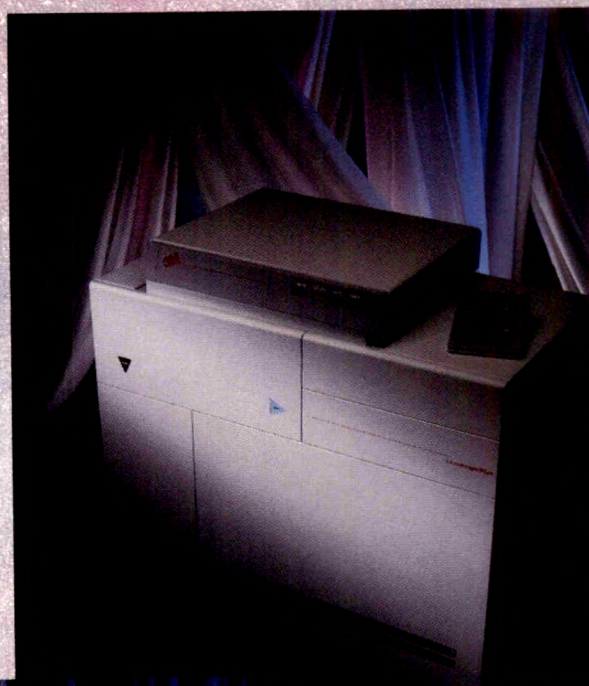
For more information call 1-800-328-1684 ext. 340. Or write: 3M Medical Imaging Systems Division, P.O. Box 33050, St. Paul, MN 55133-3050. In Canada, write: 3M Canada Inc., P.O. Box 5757 Terminal A, London, Ontario, Canada N6A 4T1.

Limited Time Offer!

*Purchase a 3M Laser Imager
for less than \$50,000*



The 3M Laser Imager



The 3M Laser Imager Plus



The 3M Laser Imager XL

No one ever said a lot of knowledge is a dangerous thing.

IN FACT, for radiologists, the only
danger is not keeping up with what's new.

AJR: American Journal of Roentgenology is
your monthly guide to the latest advances, with
articles that are timely, succinct, and relevant to
daily practice.

AJR
American Journal of Roentgenology

Published monthly

Robert N. Berk, M.D., Editor

The University of California, San Diego

Call toll-free to order: **1-800-638-6423**
from anywhere in the U.S. or Canada.
Or clip and mail this coupon.



Subscribe to **AJR** now. (Current rates available for
up to three years.)

- ☐ Individual \$125/year
- ☐ Institutional \$135/year
- ☐ In-training* \$25/year

(Add \$55/year outside the U.S.; in Canada, also add 7% GST.)

- ☐ 3 years ☐ 2 years ☐ 1 year

Maryland residents add 5% sales tax. Subscriptions outside the U.S.
must be prepaid in U.S. dollars. Rates valid through October 31, 1991.

Name

Address

City/State/Zip

*Please specify institution and training status

Payment Options:

- ☐ Check enclosed (payable to Williams & Wilkins)
- ☐ Bill me ☐ AmEx
- ☐ MasterCard ☐ VISA

Card # Exp. Date

Signature

Return coupon to:
Williams & Wilkins

P.O. Box 23291, Baltimore, MD 21203-9990

AJR: AMERICAN JOURNAL OF ROENTGENOLOGY is
the official journal of the American Roentgen Ray Society and is
published by Williams & Wilkins.

Clinical Medical Physics Residency Program

Two-year residency in Clinical Medical Physics offered by the Department of Diagnostic Radiology, Mayo Graduate School of Medicine. For individuals who recently received a doctorate in medical physics, physics or engineering and want a career in clinical diagnostic imaging.

Training includes experience in all clinical medical physics subspecialties, conferences, seminars, research and clinical assignments.

Rochester facilities include:

- Mayo Clinic: 280,000 patient registrations annually.
- Magnetic Resonance Research Laboratory: 1.5 T MRI system.
- Department of Diagnostic Radiology: 1,000,000 diagnostic imaging exams annually; 65 physicians, 6 clinical medical physicists, 1 radiopharmacist, 2 research medical physicists.
- Radiation Oncology: 6 medical physicists.
- Environmental Safety Office: 3 health physicists, 1 industrial hygienist.
- Imaging equipment: 220 X-ray tubes, 14 CT scanners, 9 MRI scanners, 13 ultrasound imagers, 21 gamma cameras, 8 SPECT systems.

Similar services provided at Mayo Clinic in Jacksonville, FL, and Scottsdale, AZ; short-term training available at both sites.

Stipend and generous benefits package offered.

Address inquiries to: Joel E. Gray, Ph.D.
Department of Diagnostic Radiology
Mayo Clinic, Rochester, MN 55905
(507) 284-4292

Mayo Foundation is an affirmative action and equal opportunity educator and employer.



King Faisal Specialist Hospital and Research Centre in Riyadh, Saudi Arabia

is inviting applications for
the position of

Chairman, Department of Radiology

The King Faisal Specialist Hospital and Research Centre in Riyadh, Saudi Arabia is inviting applications from suitably qualified physicians for the position of Chairman, Department of Radiology.

The hospital is the pre-eminent tertiary care referral centre for the Kingdom of Saudi Arabia and includes a research centre as an integral part of this rapidly expanding and superbly equipped facility. The medical staff consists of nearly two hundred carefully selected internationally qualified expatriate physicians. The Department of Radiology includes fifteen consultant specialists operating sections of general radiology, nuclear medicine, ultrasound, angiointerventional, MRI and computed tomographic imaging. More than 120,000 examinations are performed annually on state of the art equipment, including four CT scanners, and one high field MRI with a second unit under construction. The Department of Radiology supports many tertiary care programs throughout the hospital, including transplantation programs for kidney, heart and bone marrow. Department contributions to clinical research are strongly encouraged while basic research activities are supported by research centre programs in molecular biology, cytogenetics and pharmacokinetic programs.

A suitably qualified candidate for this position will be a mature physician with active clinical responsibilities and a full-time academic appointment at a major university medical centre. A record of significant accomplishments in clinical research, teaching and demonstrated capabilities in administration at the division or department head level are expected. A substantial bibliography of published work in referred medical journals is essential. The successful candidate will enjoy the full support of hospital administration and the medical staff to realize departmental aims in service, education and research.

The remuneration and benefits package for this position is well above the average for international expatriate physicians. Salary is individually negotiable according to qualifications and experience, and is free of local taxation. The compensation package is particularly attractive since living expenses are small. The hospital provides free, fully furnished single family accommodation, return airfares for the employee and dependents annually, comprehensive medical and dental care, educational assistance for dependent children and approximately sixty days of holiday and professional leave each year.

To obtain further information concerning this position, candidates are invited to send a curriculum vitae with full biographical information, professional experience and bibliography of published work, as well as the names of three professional referees, to:

The Chairman, Search Committee, MBC 53
King Faisal Specialist Hospital & Research Centre
Post Office Box 3354
Riyadh 11211, Kingdom of Saudi Arabia

CHANGE OF ADDRESS?

Please notify us eight weeks in advance. Send us your mailing label or your account number, along with your new address and the date the change of address is to take effect.

Williams & Wilkins
at your service.



For customer assistance,
call TOLL-FREE:
1-800-638-6423
(from anywhere in the U.S. or Canada)

Or write:
Subscription Fulfillment Department
428 East Preston Street
Baltimore, MD 21202-3993

AN IDEA OF WHAT TO EXPECT FROM OUR NEW CT SYSTEM.

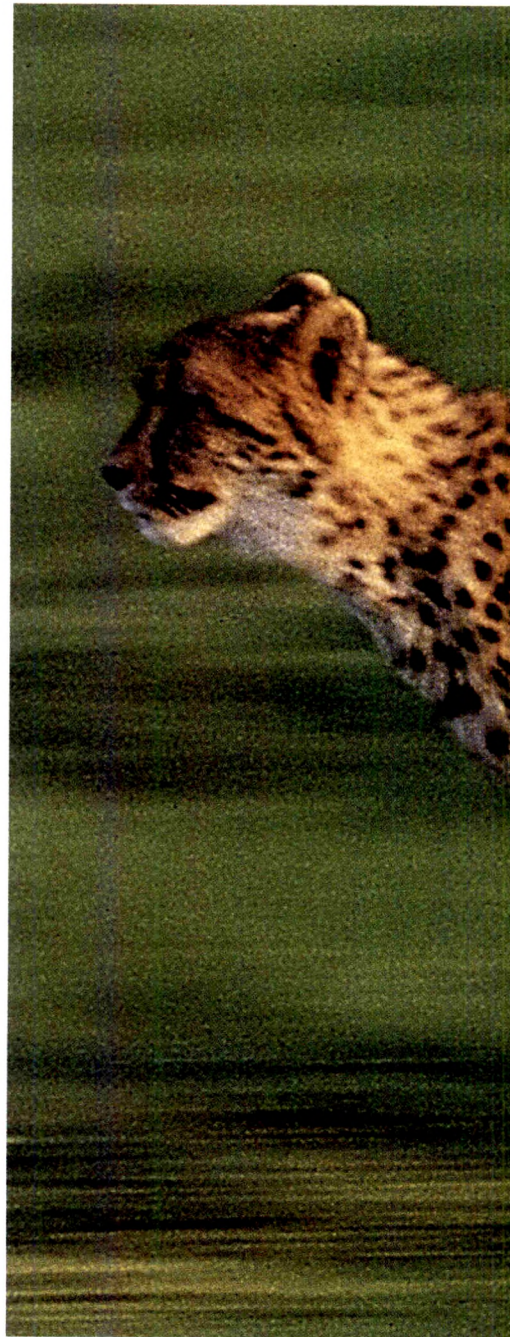
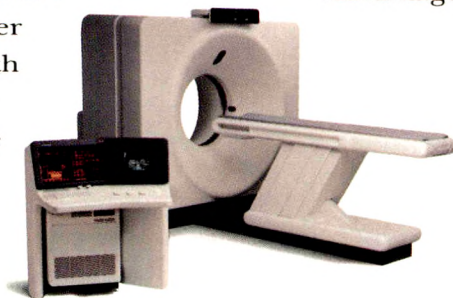
Quite simply, speed and power. Routine one second scans and a one second interscan delay — with no compromise in image quality. That's the kind of performance you can expect from the new CT HiSpeed Advantage.[™]

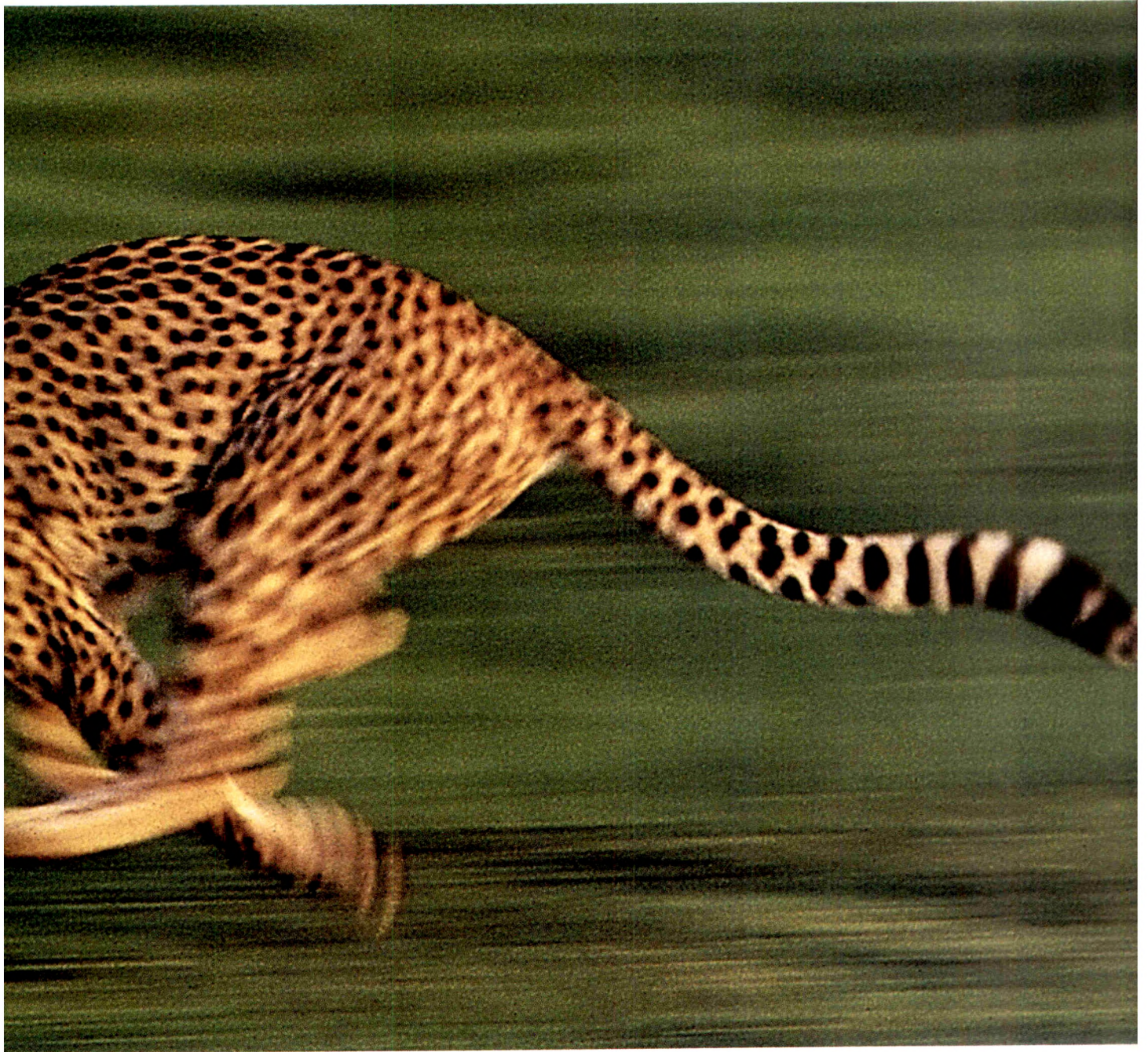
Slip-ring technology has made faster rotation possible, but in reality, slip rings are only a small part of the story. Our new 48 kW generator and x-ray tube provide the power needed to obtain these uncompromised one second images. This high power technology, coupled with the high quantum efficiency of GE's exclusive HiLight Detector, means new clinical capabilities such as cluster and helical

scanning will have even greater possibilities.

As with other GE CT systems, the HiSpeed Advantage is backed by our revolutionary Continuum philosophy. So your system can be cost-effectively upgraded to keep up with the latest clinical advancements. In fact, all CT 9800 series systems are upgradeable to the new HiSpeed Advantage.

So, if you're considering a fast CT scanner, only one choice is clear. The HiSpeed Advantage.





GE Medical Systems

We bring good things to life.

Full Coverage of Head and Spine Imaging in Adults and Children

Including MRA

Here's a resource that lets you compare the benefits of MRI and CT, so you can pick the best imaging technique for each case. **Magnetic Resonance Imaging and Computed Tomography of the Head and Spine** uses side by side correlation of CT and MR scans throughout the text for descriptive and comparative purposes to give you a unique perspective on the relative strengths of each technique. You get a full understanding of these "hi-tech" methodologies, the indications for their use, and the important new techniques that lead to the best possible results.

Here's what one of your colleagues had to say about this "formidable achievement":

"The strength of this book is the smooth integration of the CT, MR, and clinicopathologic findings of each entity discussed. Where pertinent, illustrations and tables on differential diagnosis enrich and emphasize the salient points...I think this is one book many have been looking for to tie together neuroradiology and the new technolo-

gies. It stands out among other books with similar titles and purposes as a standard for others to be compared with. I heartily recommend this book to all radiologists, neuroclinicians, and interested technologists. It is a worthwhile investment in time and money for the reader." —**AJR***

Magnetic Resonance Imaging And Computed Tomography Of The Head And Spine is filled with the timely, practical information you need to produce the best images and make the most precise diagnoses. Order today and see how this text can enhance your imaging skills.

1989/488 pages/882

illustrations/3768-4

To order call:

Toll Free 1-800-638-0672

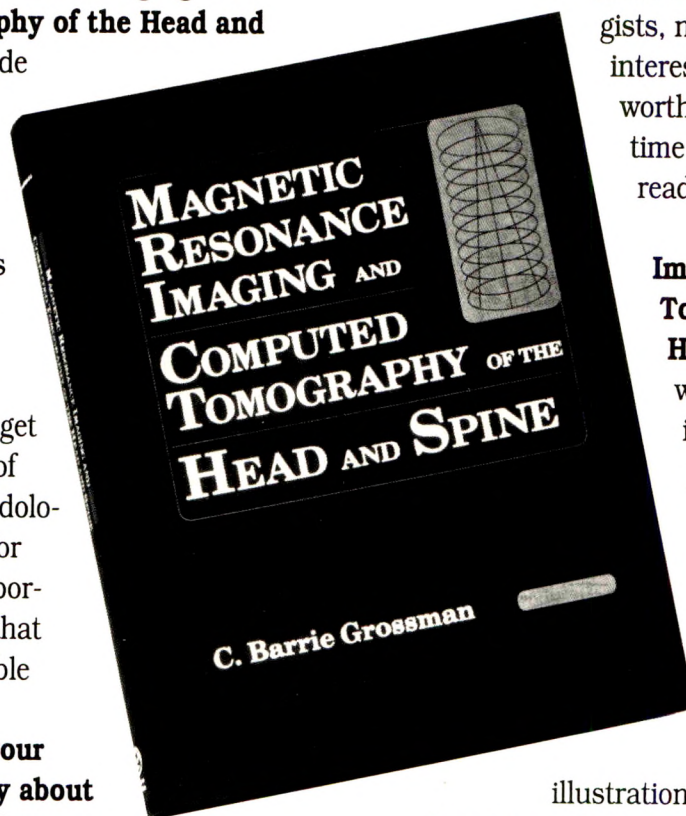
Fax 1-800-447-8438

Refer to #99069-0 when you order.

30 day approval for this book! (US only)



Williams & Wilkins
428 East Preston Street,
Baltimore, Maryland 21202



PERSONAL COMPUTER/LASER VIDEODISC SYSTEM

*to assist you in the
diagnosis of Skeletal Dysplasias*

*A unique collection of 400 Skeletal Syndromes
7000 Illustrations*

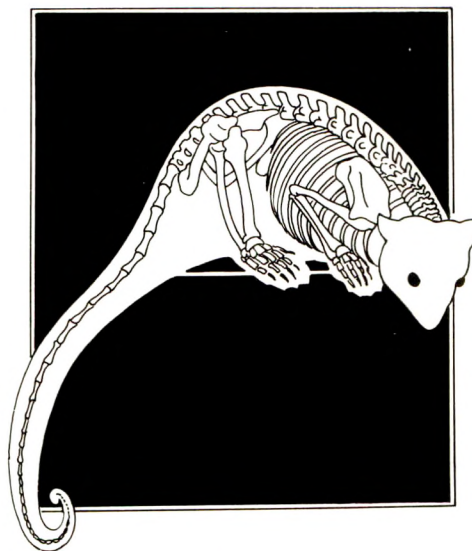
including

- *X-rays*
- *Clinical pictures*
- *Chondro-osseous histology*

O S S U M

AN ILLUSTRATED DATABASE OF SKELETAL DYSPLASIAS

**S
S
U
M**



at RSNA
Booth 8016

for further information contact:

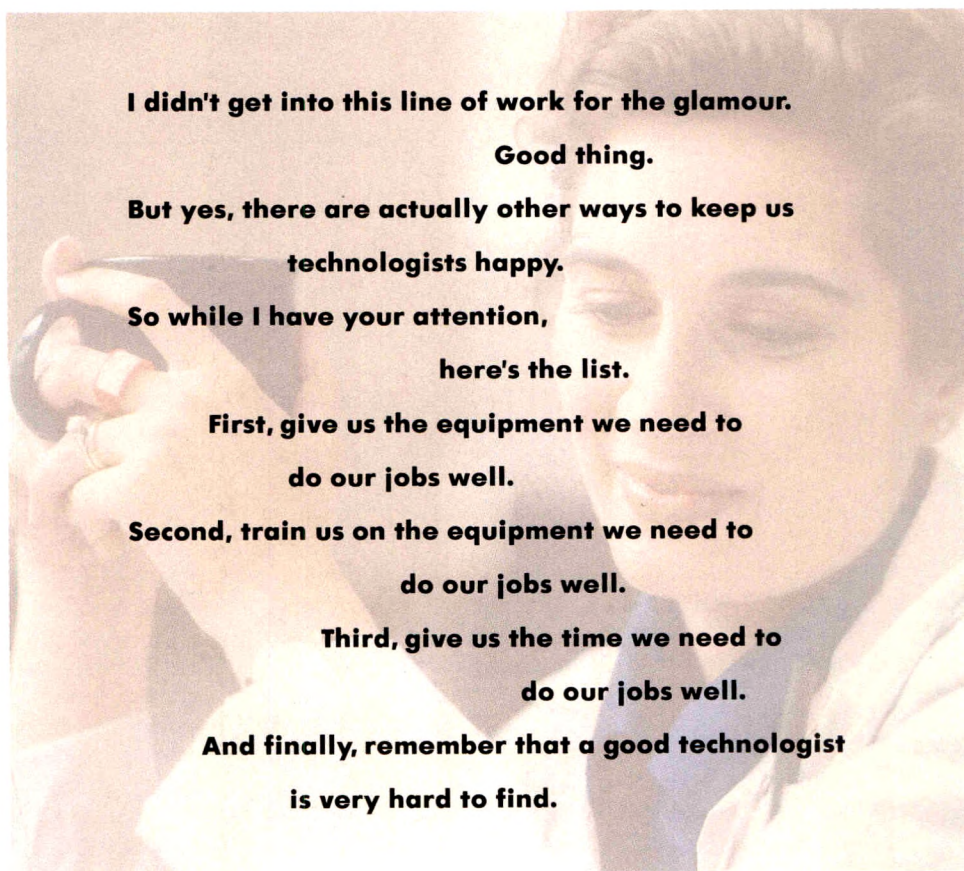
*Dr. Agnes Bankier – Medical Geneticist to the successful
related POSSUM system.*

PO Box 1100 Parkville Victoria 3052 Australia
Phone: (03) 345 5160 Fax: (03) 348 1391

Subject: Technology

Point of view: Technologist





I didn't get into this line of work for the glamour.

Good thing.

**But yes, there are actually other ways to keep us
technologists happy.**

**So while I have your attention,
here's the list.**

**First, give us the equipment we need to
do our jobs well.**

**Second, train us on the equipment we need to
do our jobs well.**

**Third, give us the time we need to
do our jobs well.**

**And finally, remember that a good technologist
is very hard to find.**

At Picker, our commitment is not only to developing technology. It's to developing technologists, as well. Which is why we were the first company to support the Summit on Manpower, a consortium of 18 radiological societies, in an effort to attract more technologists to the field.



Call for Papers on Neuroradiology

On January 1, 1992, The American Roentgen Ray Society and the American Society of Neuroradiology will terminate their agreement whereby manuscripts on neuroradiology submitted to the *AJR* are forwarded to the *AJNR* and selected *AJNR* papers are republished in the *AJR*.

To avoid any lag in the publication of neuroradiologic articles in the *AJR*, the Journal requests authors to submit neuroradiologic manuscripts effective immediately. We plan to expedite publication of these papers. Authors will receive an initial editorial decision in 3–4 weeks, and accepted papers will be published 3 months after revised manuscripts are accepted. This is more than twice as fast as most other journals.

The advantages of this rapid publication time and the *AJR*'s large circulation (24,000) are now available to all authors of neuroradiologic papers. An expanded section on neuroradiology, including review articles, pictorial essays, and commentaries, will accommodate more than the limited number of papers published under the previous agreement.

We invite authors of neuroradiologic articles to submit their papers for original publication in the *AJR* so that the Journal may continue to fulfill its commitment to supply timely and important original information about neuroradiology to general radiologists as well as to those who subspecialize in the field.

Robert N. Berk
Editor-in-Chief

Review Article

Acute Reactions to Intravascular Contrast Media: Types, Risk Factors, Recognition, and Specific Treatment

William H. Bush¹ and Dennis P. Swanson²

Acute, potentially life-threatening systemic reactions to contrast media are less frequent with lower osmolality, nonionic contrast agents, but they are not totally eliminated. Severe reactions remain a reality in all radiology departments. Typical reactions to contrast media include nausea and/or vomiting, scattered to extensive urticaria, bronchospastic reaction, hypotension (isolated) with compensating tachycardia, anaphylactoid reaction, vagal reaction, cardiovascular collapse, convulsion, and seizure. For each type of reaction, rapid recognition and initiation of specific corrective therapy enhance response and minimize side effects of drugs. Specific drugs for treating each reaction type are reviewed, including recommended dose, contraindications, and alternative choices. An approach to the high-risk patient and prevention of acute systemic reactions is discussed and pretreatment protocols are outlined.

It is estimated that the number of radiologic examinations incorporating the intravascular administration of a radiopaque contrast medium exceeds 10 million per year in the United States. Although the contrast media that have been used routinely for excretory urography, CT, and angiography for the past 30 years are relatively safe drugs, adverse reactions can be expected; the overall frequency is 5–8%. In one of every 1000–2000 examinations that use these agents, a reaction of life-threatening severity may occur.

Recent advances have resulted in the availability of agents that provide equal or improved X-ray opacification, but are more physiologic because of their lower osmolality. The rela-

tive risk of adverse reactions to these lower osmolality media may be a factor of five or more less than with conventional agents, but reactions, even fatal reactions, are not totally eliminated. Moreover, as a result of the substantially greater costs of these lower osmolality media, conventional contrast agents, with their attendant risks, continue to be used. Hence, severe adverse reactions to contrast agents remain a reality in all radiology departments.

Radiologists in charge of the administration of intravascular contrast media must be skilled in the emergent treatment of acute reactions even though such reactions are relatively infrequent. The objective of this review is to provide the radiologist with a basic approach for recognizing and treating adverse reactions to intravascular contrast media. Emphasis is placed on the appropriate use of a limited number of drugs to reverse the reaction or to stabilize the patient until more experienced personnel are available.

Background

Classification and Etiology of Adverse Reactions

Adverse reactions to intravascular contrast media are generally classified as either anaphylactoid (anaphylaxislike) or chemotoxic. Although most of the reactions appear to be anaphylactoid, the chemotoxic effects of these agents may account for the more severe adverse reactions, especially in

Received April 11, 1991; accepted after revision July 5, 1991.

¹ Department of Radiology, Virginia Mason Clinic and Hospital, Seattle, WA 98101. Present address: Department of Radiology (SB-05), University of Washington School of Medicine (RR 215), 1959 N.E. Pacific St., Seattle, WA 98195. Address reprint requests to W. H. Bush.

² School of Pharmacy, University of Pittsburgh, Pittsburgh, PA 15261.

AJR 157:1153–1161, December 1991 0361–803X/91/1576–1153 © American Roentgen Ray Society

debilitated or unstable patients. Both these types of reactions must be differentiated from intercurrent complications that may occur as a result of the patient's disease or other examination-related interventions (e.g., catheter placement).

Anaphylactoid (i.e., idiosyncratic, anaphylaxislike, allergic-like, or pseudoallergic) reactions to intravascular contrast media occur unpredictably and independently of the dose or concentration of the agent above a certain threshold level. Although these reactions typically resemble allergic or hypersensitivity reactions in the timing of their occurrence and symptoms, they do not appear to result from an antigen-antibody interaction. In fact, the exact cause of anaphylactoid reactions to intravascular contrast media remains uncertain [1]. Specific antibodies to the chemical constituents of the responsible contrast medium seldom can be detected in persons who have a reaction. Radiopaque contrast media can cause the direct release of histamine from mast cells and basophils, and systemic histamine produces reactions similar to those observed after the intravascular administration of contrast media. However, investigators have not been able to establish a correlation between the amount of histamine released in response to the contrast agent and the occurrence of adverse effects. Radiopaque contrast media also can activate directly or indirectly the complement, coagulation, fibrinolytic, and kinin systems, leading to the release of multiple mediators (e.g., histamine, lysosomal enzymes, fibrin-split products, bradykinin) capable of producing the adverse effects noted after injection of contrast media. However, again, the degree to which these systems are activated by a contrast medium does not appear to correlate with the production of observable reactions. In anaphylactoid reactions mediated by complement, an important consideration appears to be the extent to which the aforementioned systems are perturbed at the time the contrast medium is injected. Preexisting activation of these systems may make the patient susceptible to a contrast medium.

Chemotoxic reactions to intravascular contrast media are due to specific physicochemical effects of the injected agent on the organs or vessels that the agent perfuses [2]. Unlike anaphylactoid reactions, chemotoxic reactions are directly dependent on the dose and concentration of the administered agent. Hence, the rate and site of injection play important roles in the intensity and nature of resulting chemotoxic effects. Physicochemical factors responsible for the various effects include the medium's hyperosmolality, its potential for binding calcium ions, and the nature and concentration of its cations (i.e., sodium or meglumine) (Table 1).

Prevalence of Reactions and Classifications of Severity

Overall, acute adverse reactions occur in 5–8% of patients in whom conventional, ionic, higher osmolality contrast agents are administered intravascularly [3–6]. Most of these reactions are minor, and no treatment is required (Table 2). Approximately 1–2% of patients receiving these media will have a non-life-threatening, moderate reaction that requires treatment. Severe, life-threatening reactions occur with 0.05% to 0.10% of injections of conventional intravascular

TABLE 1: Selected Chemotoxic Effects of Intravascular Contrast Media

Effects	Responsible Physicochemical Properties
Vascular changes	
Increase in plasma osmolality	Hyperosmolality
Hypervolemia	
Increase in cardiac output	Hyperosmolality
Alteration in vascular permeability	
Inflammation or pain	Hyperosmolality
Formation of microthrombus	
Dilatation of vessels	
Increase in blood flow	
Decrease in blood pressure	
Pain	
Cerebral changes	
Dilatation of external carotid artery	Hyperosmolality
Stimulation of chemoreceptors	Hyperosmolality and sodium ion concentration
Alterations in systemic blood pressure	
Alterations in heart rate	Hyperosmolality
Tachypnea	
Alterations in permeability of the blood-brain barrier	Hyperosmolality
Alteration in neuroelectrical activity (with disruption of blood-brain barrier)	Presence and concentration of ions
Cardiac changes (during coronary angiography)	
Dilatation of coronary artery	Hyperosmolality
Electrocardiographic alterations	Hyperosmolality
Bradycardia	Calcium binding
Conduction delays	
Ventricular fibrillation	Calcium binding
Depression of myocardial contractility	
Renal changes	
Renovascular constriction (sustained)	Hyperosmolality
Decrease in renal blood flow	Hyperosmolality
Alteration in glomerular permeability	
Proteinuria	Concentration of nonreabsorbable solutes
Osmotic diuresis	
Renal tubular toxic effects	(?) Molecular toxicity

TABLE 2: Classification of Severity of Reactions to Contrast Media

Minor	Moderate	Severe
Nausea	Faintness	Hypotensive shock
Vomiting (limited)	Vomiting (severe)	Pulmonary edema
Urticaria (limited)	Urticaria (profound)	Respiratory arrest
Pruritus	Facial edema	Cardiac arrest
Diaphoresis	Laryngeal edema	Convulsions
	Bronchospasm (mild)	

contrast media. Reported mortality rates have varied from one in 10,000 [7] to one in 169,000 [8]; a commonly quoted mortality rate is one in 75,000 [6].

As a result of their reduced osmolality per given degree of

TABLE 3: Multicenter Surveillance Studies: Reactions to Contrast Media

Reference	Prevalence (%)		Relative Risk Conventional/Nonionic
	Conventional Media	Nonionic Media	
Overall prevalence of reactions			
Katayama et al. [8]	12.7	3.1	4.1
Palmer [11]			
Low risk	3.8	1.2	3.2
High risk	10.3	1.3	7.9
Wolf et al. [12]	4.1	0.7	5.9
Prevalence of severe reactions			
Katayama et al. [8]	0.22	0.04	5.5
Palmer [11]			
Low risk	0.09	0.00	(incalculable)
High risk	0.36	0.03	12.0
All	0.09	0.02	4.5
Wolf et al. [12]	0.04	0.00	(incalculable)

X-ray opacification and their reduced potential for binding calcium ions, the lower osmolality contrast media have been shown experimentally and clinically to produce fewer chemotoxic effects than conventional media do [2]. Preliminary experimental evidence also suggests that the lower osmolality, nonionic media have less potential to produce anaphylactoid reactions [1]. The results of large, multicenter surveillance studies [8–12] indicate that the relative risk of having a reaction to a lower osmolality, nonionic medium is a factor of five or more lower than the risk with a conventional agent (Table 3). However, to date, more controlled clinical studies have not shown a statistically significant difference between the lower osmolality and conventional media in causing certain clinically significant adverse effects, particularly renal effects [13–17].

Reactions to gadopentetate dimeglumine, an ionic paramagnetic contrast agent for MR imaging, are uncommon ($\leq 1\%$). However, a systemic anaphylactoid reaction can occur [18]. Nonionic versions of these agents are now undergoing clinical trials.

Factors Affecting the Risk of Adverse Reactions

Debililitated or unstable patients are inherently at increased risk for an adverse outcome associated with the chemotoxic effects of intravascular contrast media. Similarly, persons with allergic tendencies or allergic diatheses are at increased risk for an anaphylactoid reaction. It is generally accepted that for patients with a history of allergy, the relative risk of having an adverse reaction is approximately twice that for the general population; in patients with a history of asthma, this relative risk may be five times greater [1]. The expected prevalence of adverse reactions to conventional contrast media in patients who have had a previous reaction to a conventional agent and who have not received pretreatment is 17–35% [19, 20], or three to eight times greater than the risk for the general population. Subsequent administration of a lower osmolality, nonionic contrast medium to such patients appears to reduce the expected frequency of repeated reactions

to 5% (Siegle RL et al., presented at the annual meeting of the Radiological Society of North America, December 1989).

The overall prevalence of reactions appears to be greatest for persons 20–50 years old, less for persons older than 50 years old, and even less for persons younger than 20 years old. Katayama et al. [8] found no difference in reaction rates in patients less than 10 years old or more than 80 years old when conventional ionic contrast media were compared with the lower osmolality, nonionic contrast media [9]. However, adverse reactions to intravascular contrast media may be most severe in older persons [1]. Again, this pattern may reflect the difference between anaphylactoid and chemotoxic reactions. Persons in the second to fifth decades of life may have the most active immune systems, whereas elderly patients frequently are debilitated and unable to withstand a severe systemic reaction.

As addressed previously, total dose is likely to affect the prevalence of chemotoxic reactions but will have little influence on the prevalence of anaphylactoid reactions. This may account for the disparity in the literature about whether the occurrence of clinically significant adverse reactions is related to dose [1]. The overall prevalence of reactions is greater for IV than for intraarterial routes of administration; however, intraarterial injections appear to be associated with a higher percentage of severe reactions [1]. With IV administration, bolus injection produces fewer reactions than drip infusion does [7, 21].

Prevention of Adverse Reactions

Chemotoxic Reactions

Chemotoxic effects of intravascular contrast media are most likely to cause observable adverse reactions in patients who are debilitated or medically unstable. Hence, patients should be screened for the presence of clinically significant conditions (e.g., renal dysfunction, renovascular disease, severe cardiovascular disease, recent seizures) that may place them at high risk. In such patients, alternative diagnostic procedures that do not require intravascular administration of

a radiopaque contrast medium should be considered [22]. If administration of contrast medium is necessary, a lower osmolality agent should be used [23].

All patients should be well hydrated before the injection of any radiopaque contrast medium. In patients with renal insufficiency, nephrotoxic reactions to contrast medium can be mitigated by active hydration (e.g., 0.9% saline) IV [22]. If the intravascular administration of a contrast medium is required in a nonstabilized patient with recent seizures, pretreatment with diazepam (5–10 mg IV) may be advisable [24]. Adjunctive pretreatment with the α -adrenergic blocking agent, phentolamine (2–5 mg IV) is recommended in patients with pheochromocytoma who are receiving intravascular contrast media [1].

Anaphylactoid Reactions

Patients who have a history of multiple allergies, asthma, or previous reactions to radiopaque contrast media should be pretreated with corticosteroids and antihistamines (i.e., H_1 histamine blocker such as diphenhydramine) before injection of a conventional radiopaque contrast medium [25, 26]. If pretreatment cannot be accomplished, and the contrast examination is required, a lower osmolality, nonionic contrast agent should be administered. For patients who have previously had a severe reaction, consideration should be given to an alternative diagnostic procedure that does not require administration of contrast material. If the contrast study is necessary, such patients should be pretreated and then given a lower osmolality, nonionic contrast medium [27].

Incorporating a pretreatment regimen of prednisone and diphenhydramine (Table 4), Kelly et al. [25] found that the prevalence of repeated reactions to contrast medium decreased from 17–35% to approximately 5%. Using this same corticosteroid-antihistamine regimen, Greenberger et al. [26] saw a decrease in repeated reactions to approximately 11%. The addition of ephedrine sulfate (Table 4) to the regimen further reduced the occurrence of reactions to 5%; whereas the inclusion of cimetidine, an H_2 histamine blocker, increased the overall occurrence of reactions to 14%. Ephedrine should not be used in patients with a history of hypertension or cardiovascular disease. More recently, Greenberger and Patterson [27] found a significant further reduction in the occurrence of anaphylactoid reactions in patients who previously had an anaphylactoid reaction and were then pretreated with prednisone-diphenhydramine and were given a lower osmolality, nonionic contrast agent for a subsequent examination.

In a large prospective study, Lasser et al. [28] investigated the potential benefit of pretreating all patients with oral methylprednisolone, 32 mg 12 hr and 2 hr before intravascular administration of higher osmolality, conventional, ionic contrast media. Significant reductions in the number of reactions requiring treatment and the number of severe reactions were observed, but reactions were not totally eliminated. Additionally, in children with acute lymphoblastic leukemia and non-Hodgkin lymphoma, a tumor lysis syndrome is of sufficient concern that use of corticosteroids as prophylaxis against potential reactions to contrast media should be

TABLE 4: Effect of Pretreatment on the Prevalence of Reactions in Persons Who Previously Had Reactions to Intravascular Contrast Media

References	Pretreatment Regimen	Prevalence of Subsequent Reactions (%)
Witten [19], Fischer and Doust [20]	None	17–35
Kelly et al. [25], Greenberger et al. [26]	Prednisone, 50 mg, by mouth, every 6 hours for 3 doses (beginning 13 hr before ICM) <i>plus</i> Diphenhydramine, 50 mg by mouth or intramuscular (at 1 hr before ICM)	5–11
Greenberger et al. [26]	Prednisone/diphenhydramine (as per above) <i>plus</i> Ephedrine sulfate, 25 mg by mouth (at 1 hr before ICM)	5.0
Greenberger et al. [26]	Prednisone/diphenhydramine/ephedrine (as per above) <i>plus</i> Cimetidine, 300 mg by mouth (at 1 hr before ICM)	14.0
Lasser et al. [28]	Methylprednisolone (Medrol), 32 mg by mouth (at 12 and 2 hr before ICM)	5.0
Greenberger and Patterson [27]	Prednisone/diphenhydramine (as per above) <i>plus</i> Nonionic, lower osmolality contrast medium (iopamidol, iohexol)	0.5

Note.—ICM = intravascular contrast media.

avoided [29]. For most patients, this approach may be an alternative to routine use of the expensive lower osmolality media; however, issues of patient compliance arise. Moreover, although corticosteroid-antihistamine pretreatment appears beneficial in reducing the occurrence of anaphylactoid reactions, it is doubtful that it will have a substantial effect on chemotoxic reactions.

Treatment of Acute Reactions

Preparation and Planning

The key to treating a reaction to contrast medium effectively is being prepared to deal with the reaction should it occur. (1) Do not inject a contrast medium in an isolated setting, and have help immediately available and be able to summon additional assistance should a full-blown reaction or cardiac

arrest occur; (2) have equipment and drugs necessary to treat a reaction immediately available; (3) have basic knowledge about the patient's medical history, including risk factors and allergies; (4) have training in the treatment of various types of reactions: training in cardiopulmonary resuscitation (CPR) is necessary, and training in advanced cardiac life support (ACLS) protocols is recommended; (5) know how to recognize the specific type of reaction occurring so that appropriate, effective treatment can be started rapidly—with early treatment, lower doses of drugs can be used to reverse the reaction, thus minimizing the potential for drug-related side effects; (6) in order to ensure an available route for the administration of treatment drugs, IV access used for injection of the contrast medium should be maintained throughout the examination and until the potential for acute reactions has passed—in the series reported by Shehadi [30], all fatal reactions began within 15 min of the injection of contrast medium; (7) simple measures, such as releasing abdominal compression used for excretory urography or elevating the patient's legs to improve central vascular volume, must not be forgotten.

Typical Reactions to Contrast Media

The following types of acute reactions are associated with systemic administration of a contrast medium: (1) nausea and/or vomiting; (2) scattered to extensive urticaria (hives) without respiratory symptoms; (3) bronchospastic reaction: asthmatic symptoms without coexisting cutaneous or vascular manifestations; (4) hypotension (isolated) with normal sinus rhythm or compensatory tachycardia (note: compensatory tachycardia may be lacking in patients taking β -adrenergic receptor blockers); (5) anaphylactoid reaction: manifested by rapidly accelerating or severe bronchospasm with asthmatic wheezing, angioedema, laryngospasm, and developing or profound hypotension with compensatory tachycardia (note: compensatory tachycardia may be absent in patients taking β -adrenergic receptor blockers); (6) vagal reaction: hypotension with associated sinus bradycardia; (7) cardiovascular collapse, cardiac arrest: patient is unconscious, unresponsive, pulseless; (8) seizure or convulsions.

Treatment of Specific Reactions

The following sections and Table 5 list recommended treatment plans for the various reactions defined here. This information is an approach to deal with each reaction type; these recommendations are not the only methods or drugs that can be used [31, 32]. Each physician or department should develop a specific plan or protocol for dealing with the various reactions that may result from administration of a contrast medium, update the plan periodically, and be ready to implement it quickly and effectively should a reaction occur.

Nausea and vomiting.—Nausea and vomiting are typically minor, self-limited reactions that are not life-threatening. However, nausea and vomiting may be early signs of a more severe reaction; therefore, the patient should be watched closely for other systemic symptoms, and IV access should be maintained. (1) Stop or slow the rate of injection of the

contrast medium; (2) reassure the patient that a serious reaction is not occurring; (3) if nausea and vomiting persist, or become severe, without other systemic symptoms, an antiemetic drug (e.g., prochlorperazine, Compazine) can be administered.

Scattered to extensive urticaria with no respiratory symptoms.—If only a few scattered hives or pruritus develops, treatment most likely will not be necessary. (1) Observe the patient closely for other signs and symptoms and maintain IV access; (2) if scattered urticaria is the only sign and is protracted or troublesome to the patient, administration of an H_1 antihistamine (e.g., diphenhydramine, Benadryl) is often effective in providing relief—patients should be warned of potential drowsiness associated with the use of these drugs. Profound urticaria or diffuse cutaneous reactions may not respond completely to the administration of an H_1 antihistamine. In such situations, the addition of an H_2 blocker (e.g., cimetidine, ranitidine) may provide relief [33].

Bronchospastic reaction.—Sometimes bronchospasm is the primary manifestation of a reaction to contrast medium. For mild to moderate bronchospasm, when peripheral circulation remains adequate and profound hypotension has not developed, it is recommended that 0.1–0.2 ml (0.1–0.2 mg) of 1:1000 solution of epinephrine be administered subcutaneously. Alternatively, an inhaled β -agonist bronchodilator may be used.

Epinephrine is an agonist (stimulator) of both α - and β -adrenergic receptors [34]. The stimulation of α -adrenergic receptors results primarily in vasoconstriction. β -Adrenergic receptor agonists increase both the strength (inotropic) and rate (chronotropic) of myocardial contractions, and also the propensity for ventricular arrhythmias. Peripherally, the stimulation of β -adrenergic receptors results in smooth muscle relaxation, arteriolar vasodilatation, and, importantly, bronchiolar relaxation [35]. In the cellular energy cycle, the β -adrenergic effect raises the level of cyclic AMP, leading to less release of reactive mediators such as histamine and the more potent leukotrienes (slow-reacting substance of anaphylaxis [SR-A]). With slow subcutaneous release or slow IV injection, the β -adrenergic effects of epinephrine predominate; with rapid systemic administration, its α -adrenergic effects are more prominent.

Inhaled bronchodilators, such as albuterol (Proventil), metaproterenol (Alupent), and terbutaline (Brethaire), may be used instead of epinephrine for the treatment of mild to moderate bronchospasm (i.e., without coexisting cardiovascular symptoms) or for isolated wheezing. These potent β -adrenergic agonists, when inhaled, preferentially deliver medication to the airway tissue with minimal systemic effects. They are recommended for treating a bronchospastic reaction in a patient who has cardiac disease or is taking a noncardioselective drug that blocks β -adrenergic receptors. With the use of metered dose inhalers, appropriate doses of each of these agents are delivered with one to two deep inhalations. Their duration of action is 3–6 hr; hence, the dose should not be repeated for 4–6 hr.

Before inhaled β -adrenergic drugs were available, treatment for bronchospasm unrelieved by epinephrine was IV aminophylline. However, the onset of action of aminophylline is

TABLE 5: Guide for the Treatment of Acute Reactions to Contrast Media

Signs and Symptom	Treatment	Treatment Dose/Route of Administration		Treatment Interval	Treatment Precautions
		Adults	Children		
Nausea/vomiting					
Transient	Supportive				
Severe, protracted	Prochlorperazine injectable (Compazine)	5–10 mg/intramuscular, IV	>2 years old: 0.13 mg/kg/intramuscular <2 years old: not recommended	Every 3–4 hr	Observe patient IV—administer slowly; drowsiness
Urticaria					
Scattered, transient	Supportive				
Scattered, protracted	Diphenhydramine injectable (Benadryl)	25–50 mg/IV, intramuscular	1.25 mg/kg/IV, intramuscular	Every 2–3 hr	Observe patient Drowsiness
Profound	Cimetidine injectable (Tagamet) or Ranitidine injectable (Zantac)	300 mg (diluted—10 ml)/IV 50 mg (diluted—10 ml)/IV	5–10 mg/kg (diluted)/IV Use not established	Every 6–8 hr Every 6–8 hr	Administer slowly; drowsiness Administer slowly
Bronchospasm	Oxygen	3 l/min	3 l/min		
Mild-moderate	Subcutaneous epinephrine 1:1000	0.1–0.2 mg (0.1–0.2 ml)/subcutaneous	0.01–0.02 mg/kg to 0.2 mg maximum/subcutaneously	Every 10–15 min	Noncardioselective β -blockers
Accelerating, severe	IV epinephrine 1:10,000	0.1 mg (1 ml)/IV	0.01 mg/kg to 0.1 mg maximum/IV	Every 2–3 min	Administer slowly; β -blockers (especially noncardioselect)
Wheezing-protracted, isolated	Metaproterenol (Alupent) or Terbutaline (Brethaire) or Albuterol (Proventil)	Two deep inhalations (all)/metered dose inhaler	If possible: one to two deep inhalations (all)/metered dose inhaler	Every 4–6 hr	Proper inhalation technique (use of insert)
Hypotension					
Normal sinus rhythm, tachycardia	IV fluids (e.g., normal saline, Ringer's solution)	1–2 l/IV (rapid)	10–20 ml/kg/IV (rapid)	As per blood pressure, urine output	Fluid overload
Bradycardia	IV fluids (e.g., normal saline, Ringer's solution) plus Atropine injectable	1–2 l/IV (rapid) 1 mg/IV (push)	10–20 ml/kg/IV (rapid) 0.02 mg/kg to 0.60 mg (maximum)/IV	As per blood pressure, urine output Every 3–5 min to total 3 mg for adults or 2 mg for children	Fluid overload Monitor pulse rate
Seizures/convulsions					
Isolated	See hypotension				
Multiple, continuous	Diazepam injectable (Valium)	5–10 mg/IV	0.2–0.5 mg/kg/IV	Every 20 min	Respiratory depression

slow; thus it is less than optimal for treating acute reactions. Moreover, the required loading dose and the subsequent maintenance dose must be administered slowly and with caution to minimize hypotensive side effects.

In summary, the recommended treatment for a mild to moderate bronchospastic reaction includes the following: (1) oxygen (nasal prongs or mask, 3 l/min); (2) epinephrine

1:1000, subcutaneous, 0.1 mg (adult); or (3) inhaled bronchodilator, one to two inhalations.

Isolated hypotension with normal sinus rhythm or tachycardia.—Some patients will have reactions to contrast media that are manifested as profound hypotension with no respiratory symptoms, but with compensatory tachycardia. This last sign differentiates this reaction from a vagal reaction of

hypotension and bradycardia. In patients being treated with β -adrenergic blocking drugs (e.g., propranolol, atenolol), the compensatory tachycardia may not be observed.

Isolated, profound hypotension is treated most effectively and safely by the rapid infusion of large volumes of IV fluids. With a hand pump, up to 200 ml/min can be administered. A total volume of 3 l may be required to reverse the hypotension [36].

If the patient is markedly hypotensive, but without bradycardia or respiratory symptoms, administer IV fluids such as 0.9% sodium chloride injection (normal saline) or Ringer's solution.

Anaphylactoid reactions.—Anaphylactoid reactions that manifest as rapidly accelerating or severe bronchospasm, developing or profound hypotension (with compensatory tachycardia), laryngospasm, and angioedema require prompt treatment, including maintenance of airway patency, provision of supplemental oxygen, administration of adrenergic drugs, and rapid IV infusion of fluids.

For anaphylactoid reactions, epinephrine should be administered IV to provide a rapid effect and to avoid erratic or incomplete absorption from subcutaneous sites associated with hypotensive circulatory collapse. It is recommended that a *low dose* (1.0 ml, 0.1 mg) of 1:10,000 epinephrine be given at a slow infusion rate (e.g., 0.1 ml/min, 10 μ g/min) so as to maximize its β -adrenergic effects and reduce its α -adrenergic activity. When administered early in the reaction course and at low doses, IV epinephrine is safe and effective in reversing a potentially life-threatening situation.

IV epinephrine must be used cautiously in elderly patients or if hypoxia is present, as it can cause severe cardiac arrhythmias in those situations. Additionally, patients who are receiving noncardioselective β -blocking drugs (e.g., propranolol, Inderal) may respond adversely to IV epinephrine. In such patients, the β -adrenergic effects of epinephrine are blocked, and α -adrenergic effects may subsequently predominate. As a result of the unopposed α -agonist effects, the levels of cyclic AMP may decrease, resulting in increased release of histamine and leukotrienes. Moreover, antagonism of the bronchiolar β_2 -receptors by noncardioselective β -blocking drugs prevents the beneficial bronchodilatory effect of epinephrine in the treatment of bronchospasm. Hence, administration of IV epinephrine should be avoided, if possible, in these patients. These problems are of much less concern in patients taking cardioselective β_1 -blocking drugs (e.g., atenolol, Tenormin). In situations where initial use of epinephrine is inadvisable, bronchospasm can be treated effectively with a β_2 -agonist inhaler; IV fluids are given for hypotension; antihistamines, although less effective than epinephrine, may help with other systemic symptoms. Other patients who have been taking adrenergic medications for a long time (e.g., for asthma treatment) may be desensitized to effects of β -receptor agonists and require higher doses of epinephrine or β -agonist drugs for effective treatment.

As stated before, developing or profound hypotension is treated most effectively and safely by the rapid infusion of large volumes of IV fluids. If the hypotension is refractory to such treatment, consideration may be given to the adminis-

tration of an H_2 histamine receptor blocker such as cimetidine (300 mg diluted to 10 ml, IV) or ranitidine (50 mg diluted to 10 ml, IV) [35]. In patients with coronary artery disease, injection of an H_2 histamine-receptor blocker should be accompanied by the injection of an H_1 histamine-receptor blocker (e.g., diphenhydramine, Benadryl) because unopposed H_1 histamine-receptor stimulation will result in constriction of the coronary arteries. Also, histamine itself appears to act through the H_2 receptor to block further histamine release. Hence, blocking of the H_2 receptor with cimetidine or ranitidine may be counterproductive in mitigating the release of histamine.

The H_1 histamine-receptor blocker diphenhydramine (Benadryl) is used commonly in addition to IV epinephrine and fluids to treat an anaphylactoid reaction. The dose is 25–50 mg IV. The exact mechanism of the effect of diphenhydramine for this purpose is unclear. It most likely inactivates unbound circulating histamine; however, its effects on the clinical manifestations of a reaction already in progress are minimal. Presumably this is because diphenhydramine does not inactivate or block the action of leukotrienes, and the bronchoconstrictor activity of leukotrienes is several times greater than that of histamine. Diphenhydramine alone should not be used in place of IV epinephrine to treat an anaphylactoid reaction.

High doses of IV corticosteroids are often used in the treatment of anaphylactoid reactions. Although the exact mechanism of action remains undefined [37], the primary value of corticosteroid therapy is most likely related to its stabilizing effect on cell membranes, thereby preventing generation of arachidonic acid, leukotrienes, prostaglandins, and platelet-activating factor [38]. Onset of this effect is, however, slow, making the administration of corticosteroids of little value in the treatment of an acute reaction to a contrast medium.

If the patient has or is starting to have a severe, anaphylactoid reaction, the following treatment plan is recommended: (1) oxygen (nasal prongs or mask, 3 l/min); (2) IV fluids: 0.9% sodium chloride injection (normal saline) or Ringer's solution; (3) epinephrine 1:10,000, IV, 0.1 mg (adult); (4) diphenhydramine, IV, 50 mg (adult); (5) cimetidine or ranitidine, IV (only in the event of refractory hypotension); (6) corticosteroids, IV.

Vagal reaction.—Patients who have a vagal reaction after the injection of a contrast medium gradually become confused, apprehensive, and diaphoretic. Manifestations of increased vagal tone on the heart include depressed sinoatrial and atrioventricular node activity and inhibition of the atrioventricular conduction system; vasodilatation occurs peripherally [39]. Untreated, the reaction can progress in 10–20 min to unresponsiveness and cardiac arrest.

The cause of the vagal reaction is unknown. Not only is it observed after injections of contrast media, it also is encountered with injection, in general, and with other procedures such as manipulation of the common bile duct, proctoscopy, and barium enemas. Mild vagal reactions are frequently observed by anesthesiologists in the induction room, suggesting that this reaction is elicited or accentuated by anxiety.

The combination of prominent sinus bradycardia (pulse rate

<50 beats per minute) and hypotension (systolic pressure <80 mm Hg) characterizes the vagal reaction. Recognition of the bradycardia associated with a hypotensive adverse reaction is essential because treatment is specific and different from that for a hypotensive reaction with normal sinus rhythm or tachycardia. Treatment for a vagal reaction involves increasing intravascular fluid volume and reversing the bradycardia. Elevation of the patient's legs and the rapid infusion of IV fluids accomplish the former; IV atropine blocks vagal stimulation of the heart and corrects the latter. Atropine should be given in large doses, because small doses may accentuate cardiac arrhythmias [40]. It is therefore recommended that 1 mg be injected IV initially; the patient's pulse rate should be used to determine the need for further therapy. If bradycardia persists, repeated IV doses of 0.8–1.0 mg can be given every 3–5 min up to a total of 3 mg in adults. Despite resolution of the bradycardia, hypotension may continue, requiring further IV fluids.

Hence, for the treatment of an identified vagal reaction, the following are recommended: (1) IV fluids: 0.9% sodium chloride injection (normal saline) or Ringer's solution; (2) atropine, IV, 1 mg (adult).

Cardiovascular collapse, cardiac arrest.—If an anaphylactoid or severe vagal reaction has progressed to cardiovascular collapse, ventricular fibrillation, or cardiac arrest, standard cardiopulmonary resuscitative measures must be used. With immediate urgency, an airway must be established, ventilation started, cardiac massage instituted, and access for IV fluids ensured. Cardiac monitoring must be started, as defibrillation may be necessary. Although such severe reactions to intravascular contrast media are uncommon, resuscitative skills must be acquired and competency maintained, and appropriate equipment must be readily available. A complete discussion of the treatment of cardiovascular collapse and cardiac arrest is beyond the scope of this article. Hence, readers are referred to the ACLS (Advanced Cardiac Life Support) manual [41] for a detailed treatment plan in the event of cardiac arrest or other acute cardiac-related problems.

Seizures or convulsions.—The occurrence of a major convulsion or seizure after the injection of contrast medium may be the final result of a severe hypotensive episode or vagal reaction. If convulsions or seizures persist, an anticonvulsant such as diazepam (Valium) should be administered. (1) Protect the patient; (2) monitor pulse rate (treat hypotension or vagal reaction, if present); (3) administer diazepam, IV.

Conclusions

Acute adverse effects associated with the intravascular administration of contrast media include cutaneous, bronchospastic, hypotensive, anaphylactoid, vagal, and convulsive reactions. Each adverse effect most likely has more than one cause, and certain patients are at higher risk for each of these reactions.

Although acute adverse reactions appear to occur less often with use of lower osmolality contrast media than with use of higher osmolality conventional agents, adverse reactions are not totally eliminated. The radiologist must be able

to recognize and differentiate the various types of reactions to contrast media so that appropriate and specific treatment can be started rapidly and effectively. With such knowledge and a limited number of treatment drugs, adverse reactions to intravascular contrast media typically can be rapidly reversed and their progression to life-threatening severity or death avoided.

REFERENCES

1. Thrall JH. Adverse reactions to contrast media. In: Swanson DP, Chilton HM, Thrall JH, eds. *Pharmaceuticals in medical imaging*. New York: Macmillan, 1990:253–277
2. Swanson DP, Shetty PC, Kastan DJ, Rollins N. Angiographic contrast media. In: Swanson DP, Chilton HM, Thrall JH, eds. *Pharmaceuticals in medical imaging*. New York: Macmillan, 1990:13–39
3. Shehadi WH, Toniolo G. Adverse reactions to contrast media. *Radiology* 1980;137:299–302
4. Witten DM, Hirisch FD, Hartman GW. Acute reactions to contrast media: incidence, clinical characteristics and relationship to history of hypersensitivity states. *AJR* 1973;119:832–840
5. Ansell G, Tweedie MCK, West CR, Evans P, Couch L. The current status of reactions to intravenous contrast media. *Invest Radiol* 1980;15:532–539
6. Hartman GW, Hattery RR, Witten DM, Williamson B. Mortality during excretion urography: Mayo Clinic experience. *AJR* 1982;139:919–922
7. Shehadi WH. Adverse reactions to intravenously administered contrast media. *AJR* 1975;124:145–152
8. Katayama H, Yamaguchi K, Kozuka T, Takashima T, Seez P, Matsuura K. Adverse reactions to ionic and nonionic contrast media: a report from the Japanese Committee on the Safety of Contrast Media. *Radiology* 1990;175:621–628
9. Bettman MA. Ionic versus nonionic contrast agents for intravenous use: are all the answers in? *Radiology* 1990;175:616–618
10. Gerstman BB. Epidemiologic critique of the report on adverse reactions to ionic and nonionic media by the Japanese Committee on the Safety of Contrast Media. *Radiology* 1991;178:787–790
11. Palmer FJ. The R.A.C.R. survey of intravenous contrast media reactions: final report. *Australas Radiol* 1988;32:426–428
12. Wolf GL, Arenson RL, Cross AP. A prospective trial of ionic vs nonionic contrast agents in routine clinical practice: comparison of adverse effects. *AJR* 1989;152:939–944
13. Kinnison ML, Powe NR, Steinberg EP. Results of randomized controlled trials of low- vs high-osmolality contrast media. *Radiology* 1989;170:381–389
14. Foster CJ, Griffen JF. A comparison of the incidence of cardiac arrhythmias produced by two intravenous contrast media in coronary artery disease. *Clin Radiol* 1987;38:399–401
15. Schwab SJ, Hlatky MA, Peiper KS, et al. Contrast nephrotoxicity: a randomized controlled trial of a nonionic and an ionic radiographic contrast agent. *N Engl J Med* 1989;320:149–153
16. Denys BG, Reddy PS, Uretsky BF. Nephrotoxicity of a nonionic (iopamidol) versus an ionic (diatrizoate) contrast agent in the patient after cardiac transplant with moderate cyclosporine-induced renal insufficiency. *Am J Cardiol* 1989;64:405–406
17. McCullough M, Davies P, Richardson R. A large trial of intravenous Conray 325 and Niopam 300 to assess immediate and delayed reactions. *Br J Radiol* 1989;62:260–265
18. Salonen OLM. Case of anaphylaxis and four cases of allergic reaction following Gd-DTPA administration. *J Comput Assist Tomogr* 1990;14:912–913
19. Witten DM. Reactions to urographic contrast media. *JAMA* 1975;231:974–977
20. Fischer HW, Doust VL. An evaluation of pretesting in the problem of serious and fatal reactions to excretory urography. *Radiology* 1972;103:497–501
21. Ansell G. Adverse reactions to contrast agents: scope of the problem. *Invest Radiol* 1970;5:374–379
22. Bush WH. Management of adverse effects of contrast media. In: Bush

- WH, ed. *Urologic imaging and interventional techniques*. Baltimore: Urban & Schwarzenberg, 1989
23. McClennan BL. Ionic and nonionic iodinated contrast media: evolution and strategies for use. *AJR* 1990;155:225-233
 24. Pagani JJ, Hayman LA, Bigelow RH, Libshitz HI, Lepke RA, Wallace S. Diazepam prophylaxis of contrast media-induced seizures during computed tomography of patients with brain metastases. *AJR* 1983;140:787-792
 25. Kelly JF, Patterson R, Lieberman P, Mathison DA, Severson DD. Radiographic contrast media studies in high-risk patients. *J Allergy Clin Immunol* 1978;62:181-184
 26. Greenberger PA, Patterson R, Tapio CM. Prophylaxis against repeated radiocontrast media reactions in 857 cases. *Arch Intern Med* 1985;145:2197-2200
 27. Greenberger PA, Patterson R. The prevention of immediate generalized reactions to radiocontrast media in high-risk patients. *J Allergy Clin Immunol* 1991;87:867-872
 28. Lasser EC, Berry CC, Talner LB, et al. Pretreatment with corticosteroids to alleviate reactions to intravascular contrast media. *N Engl J Med* 1987;317:845-849
 29. Luna-Fineman S, Healy MV, Parker BR. Corticosteroid pretreatment for potential contrast reactions in children with lymphoreticular cancer: a word of caution. *AJR* 1990;155:357-358
 30. Shehadi WH. Death following intravascular administration of contrast media. *Acta Radiol Diagn* 1985;26:457-461
 31. Cohan RA, Dunnick NR. Treatment of reactions to radiologic contrast material. *AJR* 1988;151:263-267
 32. Bush WH. Treatment of systemic reactions to contrast media. *Urology* 1990;35:145-150
 33. Mayumi H, Kimura S, Asano M. Intravenous cimetidine as an effective treatment for systemic anaphylaxis and acute allergic skin reactions. *Ann Allergy* 1987;50:447-451
 34. Barach EM, Nowak RM, Tennyson GL, Tomlanovich MC. Epinephrine for treatment of anaphylactic shock. *JAMA* 1984;251:2118-2122
 35. Smith NT, Corbacio AN. The use and misuse of pressor agents. *Anesthesiology* 1970;33:58-101
 36. vanSonnenberg E, Neff CC, Pfister RC. Life-threatening hypotensive reactions to contrast media administration: comparison of pharmacologic and fluid therapy. *Radiology* 1987;162:15-19
 37. Lasser EC, Lang J, Sovak M, Kolb W, Lyon S, Hamlin AE. Steroids: theoretical and experimental basis for utilization in prevention of contrast media reactions. *Radiology* 1977;125:1-9
 38. Zipser RD, Laffi G. Prostaglandins, thromboxanes, and leukotrienes in clinical medicine. *West J Med* 1985;143:485-497
 39. Stanley RJ, Pfister RC. Bradycardia and hypotension following use of intravenous contrast media. *Radiology* 1976;121:5-7
 40. Fischer HW, Colgan FJ. Causes of contrast media reactions. *Radiology* 1976;121:223
 41. Grauer K, Cavallaro D. *ACLS: certification preparation and a comprehensive review*. St. Louis: Mosby, 1987



Food for thought...

Happy Holidays

To All Our
Readers, Authors, and Reviewers
From the AJR
Editorial Staff

Review Article

Clinical Value of High-Resolution CT in Chronic Diffuse Lung Disease

Nestor L. Müller¹

Chronic diffuse lung disease is demonstrated well on high-resolution CT, but the expense and the high dose of radiation associated with this technique make it inappropriate for every patient. This article compares the clinical usefulness of high-resolution CT with that of other diagnostic techniques. Specific indications for its use were determined after reviewing previously published reports.

Many conditions can cause chronic diffuse lung disease. These can be classified into chronic infiltrative lung diseases, chronic airway diseases, and emphysema. The definition of diffuse lung disease is somewhat arbitrary, as these conditions are often patchy in distribution or focal. Although chest radiography is a useful and inexpensive method for examining patients who have diffuse lung disease, the technique has well-known limitations. Findings on the radiograph are often normal in symptomatic patients with pathologically proved diffuse lung disease, they seldom allow a confident specific diagnosis, and they correlate poorly with clinical and functional impairment [1-5]. In the last 10 years, a number of studies have shown that CT, in particular, high-resolution CT (HRCT), can play a major role in the assessment of patients with diffuse lung disease. HRCT can show abnormalities in patients who have normal findings on radiographs, and because it provides an accurate assessment of the pattern and distribution of lung disease, it allows confident diagnosis in patients who have normal or nonspecific findings on conventional radiography [3, 6-19].

Several recent articles have reviewed the characteristic HRCT appearance of the various chronic diffuse lung diseases [18-26] but have made little mention of the specific clinical situations in which HRCT is likely to be most helpful and indicated [27]. Although HRCT has a number of advantages over conventional radiography, it is expensive and involves high doses of radiation. For these reasons, it clearly cannot be recommended for all patients with diffuse lung disease.

The aim of this article is to compare HRCT with other diagnostic techniques, summarize its clinical usefulness in patients with diffuse lung disease, and suggest specific indications based on a review of the literature. The clinical value of HRCT is assessed in terms of its ability to detect diffuse lung disease; its accuracy in the differential diagnosis; and when biopsy is required, its ability to determine the optimal type and site of lung biopsy. First, however, it is necessary to define what is meant by HRCT.

HRCT Technique and Radiation Dose

HRCT consists of thin-section CT (1- to 2-mm collimation) optimized by using a high-spatial-frequency reconstruction algorithm. Further improvement in spatial resolution can be obtained by targeting the image to a small field of view. Decreasing the field of view from 40 to 13 cm decreases pixel size from 0.78 to 0.25 mm but allows assessment of only a small area of lung [28]. Further decreases in field of view do not improve spatial resolution. Targeting allows better as-

Received June 19, 1991; accepted after revision July 19, 1991.

¹ Department of Radiology, University of British Columbia and Vancouver General Hospital, 855 W. 12th Ave., Vancouver, B.C., Canada V5Z 1M9.

AJR 157:1163-1170, December 1991 0361-803X/91/1576-1163 © American Roentgen Ray Society

assessment of focal abnormalities and fine parenchymal detail. However, it is time-consuming and not usually required in the assessment of diffuse lung disease.

The number of HRCT scans needed to assess patients with diffuse lung disease is controversial. Initially, HRCT was used as a complement to conventional CT [3]. More recently the use of HRCT alone has been recommended, without the need for conventional CT [7, 29–31]. Leung et al. [31] have shown that a limited number of HRCT scans provide a diagnostic accuracy in chronic infiltrative lung disease comparable to the accuracy associated with complete conventional CT scanning and that the combination of complete conventional CT plus HRCT does not significantly improve the diagnostic accuracy. In some centers, most patients being assessed for chronic infiltrative lung disease are scanned by using HRCT only at 4-cm intervals from the lung apices to bases (approximately five or six levels). This provides a representative sample of disease at different levels in the lung and can be done at a reduced cost [20, 30]. Obviously, with a small number of HRCT scans, focal parenchymal abnormalities may be overlooked, the patchy distribution of many diffuse infiltrative lung diseases may not be appreciated, and small nodules may be missed between high-resolution sections [3]. The optimal number of HRCT scans therefore depends on the clinical situation. In certain cases, a focused search strategy based on the known or suspected distribution of disease may be indicated. In the initial assessment of patients with suspected infiltrative lung disease or bronchiectasis, it is recommended that HRCT scans be obtained at 1-cm intervals through the chest. In patients with known or suspected occupational exposure to asbestos, scans of the prone patient are often necessary to distinguish reversible gravity-dependent density and atelectasis from fixed structural abnormalities in dependent portions of the lung bases, where pulmonary fibrosis is most likely to occur [7, 8].

One of the concerns about the use of HRCT has been the high dose of radiation. Radiation doses at the skin surface of the breast for patients undergoing conventional contiguous 10-mm collimation CT scanning of the chest are on the order of 20 mGy [32, 33]. These doses are approximately 100 times greater than those associated with posteroanterior chest radiographs, 40 times greater than those associated with lateral chest radiographs, and 10 times higher than those associated with mammographic examinations [32, 34]. Use of the high-spatial-frequency algorithm increases visualization of image noise. This can be reduced by increasing kilovolt peak or milliamperage settings [28]. However, the increased noise usually does not cause difficulty in clinical interpretation [28]. On the contrary, it has been shown that use of the high-resolution algorithm improves visualization of lung parenchymal detail not only on 1.5-mm collimation but also on conventional 10-mm scans [35]. Furthermore, Zwirewich et al. [36] have shown recently that in most patients equally diagnostic images can be obtained by using substantially less radiation. These authors compared 1.5-mm-collimation, 2-sec, 120-kVp scans obtained at 20 and 200 mA in 31 patients. Although image noise was greater with the low milliamperage technique, images acquired at 20 mA were judged to be as diagnostic as images at 200 mA in 97% of cases. These

results are similar to those of Naidich et al. [37], who were the first to show that diagnostic images of the lungs can be obtained at low radiation doses (120 kVp, 2-sec scan time, 10 mA) on conventional 10-mm-collimation CT scans. Therefore, when radiation exposure is a concern, particularly in young patients and when follow-up scans are obtained, scans should be obtained at lower radiation doses. The minimal dose required to produce a diagnostically adequate image depends on the type of scanner and on the thickness of the chest wall.

It is important to realize that the radiation dose to the patient is also affected by scatter and penumbra effects [32]. These are greater with contiguous slices than with interspaced scans. Whereas the radiation dose measured at the skin surface of the breast for 10-mm contiguous scans at 140 kVp and 200 mAs is approximately 20 mGy, the radiation dose with 3-mm-collimation scans at 10-mm intervals is only 8 mGy [32]. In the study by Mayo et al. [28], radiation dose was calculated for examinations that used contiguous sections. The CT dose index at 120 kVp and 300 mAs was 55 mGy for 10-mm-collimation scans and 61 mGy for HRCT with 1.5-mm-collimation scans. This calculation, therefore, represents the upper limit of the dose to the patient if contiguous HRCT sections are obtained and is considerably greater than the radiation dose when HRCT scans are obtained at 10-mm intervals [28, 32]. Conventional contiguous 10-mm-collimation scans through the chest are required to rule out focal lung disease and metastases. However, in patients with diffuse lung disease, contiguous scanning is usually not necessary, and HRCT scans should be obtained instead of conventional scans [29–32]. HRCT not only has a greater spatial resolution than does conventional CT but also results in less than half the radiation dose of conventional CT when kilovoltage, milliamperage seconds, and scanning intervals are kept constant.

Clinical Usefulness of HRCT

Detection of Lung Disease

The chest radiograph remains the first and foremost imaging technique used in the assessment of patients with suspected diffuse lung disease. However, radiographic findings are normal in 10–15% of patients with biopsy-proved infiltrative lung disease [1, 38], in 30–50% of patients with bronchiectasis [39, 40], and in 20–60% of patients with emphysema [41–43].

Abnormal findings on conventional CT or HRCT when findings on chest radiographs are normal have been reported in patients with a variety of chronic infiltrative lung diseases, including asbestosis [7–10], sarcoidosis [13, 14], lymphangioleiomyomatosis [12], fibrosing alveolitis [16], lymphangitic carcinomatosis [6], desquamative interstitial pneumonia [44], and extrinsic allergic alveolitis [44]. Abnormal and diagnostic CT scans in patients with normal radiographs have also been reported in bronchiectasis [17, 45] and in emphysema [46]. Therefore, CT is clearly indicated in the assessment of patients with normal findings on radiographs and clinical findings suggestive of diffuse lung disease.

HRCT is particularly helpful in the assessment of patients with suspected asbestosis. Findings on the radiograph are normal in 10–20% of patients with asbestosis [47], whereas the sensitivity of HRCT in the diagnosis of clinically suspected asbestosis approaches 100% [7–9]. Furthermore, the data of Epstein et al. [48] suggest a high percentage of false-positive diagnoses based on findings on radiographs. In their review of 200 hospital admission chest radiographs, Epstein et al. found that 22 patients without occupational exposure to asbestos (11%) had abnormalities that otherwise might have been interpreted as indicative of asbestosis. Friedman et al. [9] found that the positive predictive value of the chest radiograph in showing significant parenchymal disease in asbestosis was 79% as compared with 100% for HRCT. Aberle et al. [8] reported that HRCT was more sensitive than conventional CT for the diagnosis of parenchymal disease in asbestos-exposed persons, with a sensitivity of 96% as compared with 83%. Although the chest radiograph is undoubtedly the most important imaging technique used in the initial assessment of these patients, HRCT is indicated to assess symptomatic patients with normal findings on radiographs and to eliminate false-positive interpretations of findings on radiographs [49].

CT may also be helpful in determining what kind of parenchymal abnormality is responsible for the clinical and functional impairment in patients who have more than one diffuse lung disease. Kinsella et al. [50] have shown in patients with silicosis and abnormal results in pulmonary function tests that the clinical and functional impairment correlated with the presence and severity of emphysema rather than with that of silicosis. Dyspneic smokers with idiopathic pulmonary fibrosis may have marked impairment in gas transfer but normal or nearly normal lung volumes and spirometric measurements of lung function. Objective assessment of these patients is difficult because the radiograph may not show evidence of emphysema and the results of pulmonary function tests may be entirely misleading [51]. HRCT can show the presence and extent of emphysema and fibrosis and relative contributions of these conditions to the clinical and functional abnormalities, and therefore is valuable in the assessment of patients who have these entities [51, 52].

Although in the appropriate clinical setting the HRCT findings of pneumoconiosis may be diagnostic, in most chronic infiltrative lung diseases the specific diagnosis must be confirmed (this is discussed in the section on the usefulness of HRCT in the differential diagnosis). Conversely, in the other two diffuse lung diseases being discussed, namely, bronchiectasis and emphysema, definitive diagnosis usually can be made with HRCT.

Diagnostic Accuracy in Bronchiectasis

HRCT is the method of choice in the assessment of bronchiectasis. The clinical diagnosis of bronchiectasis is often difficult, as the typical symptom of chronic cough productive of large amounts of purulent sputum is frequently not present, and the findings on the chest radiograph are usually normal [39, 53]. The diagnosis is suspected clinically either because

of the presence of persistent cough or, less frequently, recurrent hemoptysis. In the past, the diagnosis was confirmed by bronchography. However, as bronchography is an unpleasant procedure and not without hazard, it has been replaced almost completely by CT. The accuracy of CT in the diagnosis of bronchiectasis depends on technique. Conventional CT with 10-mm-thick sections has a sensitivity of 60–80% [54–56]. Grenier et al. [57], using 1.5-mm-thick sections at 10-mm intervals, compared CT and bronchography in 44 lungs in 36 patients. The sensitivity of CT was 97% and the specificity was 93% in confirming a diagnosis of bronchiectasis [57]. In two lungs, the extent of disease was underestimated on the basis of HRCT, although in only one case with proved lower lobe disease were the HRCT findings interpreted as normal. On the other hand, in one case, bronchiectasis was detected on HRCT when bronchographic findings were equivocal because of incomplete opacification of mucus-filled airways.

HRCT is superior to bronchoscopy in the assessment of patients with chronic cough and clinically suspected bronchiectasis [17]. HRCT is also the method of choice for examining patients with hemoptysis in whom the clinical index of suspicion for underlying malignancy is low. Naidich et al. [17] compared CT with fiberoptic bronchoscopy in 58 patients with hemoptysis. Abnormalities involving the airways were shown on CT in 28 cases (48%). In 18 cases, CT showed focal abnormalities involving the central airways; 17 of these were subsequently proved to be malignant, and in 10 cases, CT showed bronchiectasis. In all cases in which fiberoptic bronchoscopy showed focal airway disease, CT findings were abnormal. Similarly, Millar et al. [45], using conventional CT in a study of 22 consecutive patients with hemoptysis and normal findings on chest radiographs, found that CT showed previously unsuspected abnormalities in 15 patients, three of whom had bronchiectasis. The authors concluded that CT should be considered an essential examination in all patients in whom findings on chest radiography and bronchoscopy are nondiagnostic. As proposed by Naidich et al. [17], optimal assessment of the airways in patients with hemoptysis is achieved by obtaining first, HRCT scans at 10-mm intervals from the thoracic inlet to the tracheal carina; second, 5-mm-thick sections at 5-mm intervals through the central airways; and third, HRCT scans at 10-mm intervals through the lung bases. This approach optimizes detection of central endobronchial lesions and bronchiectasis [17].

In summary, HRCT is the method of choice for confirming bronchiectasis when it is suggested by clinical or radiographic findings. Bronchography should be reserved for select cases in which HRCT findings are normal despite a strong clinical history.

Diagnostic Accuracy in Emphysema

HRCT is currently the most sensitive technique for the diagnosis of emphysema. The ability to make or exclude the diagnosis of emphysema correctly in symptomatic patients can greatly facilitate the management of patients [42]. Emphysema is strictly defined in pathologic terms as "a condition

of the lung characterized by abnormal permanent enlargement of air spaces distal to the terminal bronchiole, accompanied by the destruction of their walls, and without obvious fibrosis" [58]. It has been shown repeatedly that the results of pulmonary function tests correlate poorly with the pathologic severity of emphysema; the correlation coefficients between the results of various function tests and pathologic extent of emphysema range from .4 to .7 [59–63]. Emphysema may involve up to 30% of the lung parenchyma without obstructing air flow [42]. As emphysema is associated with destruction of lung parenchyma, it should be and is easiest to diagnose by using techniques that reflect the anatomic rather than the functional state of the lung.

The radiographic abnormalities in patients with emphysema include those related to hyperinflation (increase in retrosternal air space, flattening of the diaphragm) and those related to lung destruction and bulla formation leading to changes in the vascular pattern [42]. The most frequently quoted study claiming a low sensitivity for conventional radiography (40%) in the diagnosis of emphysema assessed the vascular pattern only [41]. When both signs of hyperinflation and lung destruction were assessed, the reported sensitivity of conventional radiography was 80% [42, 64]. The radiologic hallmark of emphysema, namely, hyperinflation, reflects the increase in total lung capacity as measured by pulmonary function tests. Several studies have shown that CT findings correlate better than the results of pulmonary function tests, including total lung capacity, with the pathologic severity of emphysema [61–63]. Two studies have shown that conventional CT is superior to conventional radiography in the diagnosis of emphysema [46, 65]. Hayhurst et al. [46] evaluated the usefulness of quantifying the number of pixels with abnormally low attenuation on CT by comparing CT with pathologic assessment of emphysema in 11 patients. Six patients had mild centriacinar emphysema, and five had no emphysema on pathologic examination. In five of the six patients with emphysema, CT showed that attenuation values of less than -900 H were characteristic of emphysema. Only one of these patients had radiologic evidence of emphysema. Sanders et al. [65], using decreased gas transfer and airway obstruction as functional criteria of emphysema, found that conventional CT was more sensitive than chest radiography in showing emphysema (96% vs 68%).

Using high-resolution CT and a state-of-the-art scanner, Hruban et al. [66] were able to detect even mild emphysema when they scanned 20 postmortem lung specimens. The correlation between the in vitro CT emphysema score and the pathologic grade was 0.91. Although it may be possible to obtain a nearly 1:1 correlation between CT and pathologic findings in vitro, it is not yet possible to obtain such a good correlation in vivo. Using a GE 9800 scanner, Miller et al. [67] obtained a CT-pathologic correlation of 0.81 when using 10-mm collimation scans and 0.85 when using 1.5-mm collimation scans. In this series, 33 of 38 patients had emphysema. Of these, four cases of mild centriacinar emphysema were missed on CT. Although mild emphysema may be missed even on HRCT, in most cases small localized areas of emphysema can be detected on HRCT, and no statistically significant difference exists between the HRCT emphysema

scores and the pathology scores [68]. CT also has a high specificity for emphysema; emphysema is rarely overdiagnosed in persons without lung disease or in patients with severe hyperinflation due to other causes [69].

Although highly accurate, in clinical practice HRCT is seldom indicated for the diagnosis of emphysema. Occasionally it may be requested for symptomatic patients with abnormal gas transfer (decreased carbon monoxide–diffusing capacity) without evidence of airway obstruction on pulmonary function tests [20]. In these patients, HRCT can be of great value in the clinical management by differentiating emphysema from pulmonary vascular disease [20].

Diagnostic Accuracy in Diffuse Infiltrative Lung Disease

The chest radiograph has well-known limitations in the differential diagnosis of patients with diffuse lung disease. McLoud et al. [2] found, in their evaluation of 365 cases of diffuse infiltrative lung disease proved by open biopsy, that an experienced chest radiologist was able to include the correct histologic diagnosis in the first two radiologic diagnostic choices in only 50% of cases. Moreover, interobserver agreement about the main type of abnormality and the severity of disease was only 70%. The authors concluded that although certain radiologic patterns may suggest a particular disease, a confident diagnosis can seldom be made.

Mathieson et al. [3] compared the accuracy of chest radiography and CT in the prediction of specific diagnosis in 118 consecutive patients with chronic diffuse infiltrative lung disease. The radiographs and CT scans were assessed independently by three observers without knowledge of clinical or pathologic data who listed the three most likely diagnoses in order of probability and recorded on a three-point scale the degree of confidence they felt in their first-choice diagnosis. Confidence level 1 (definite) was reached with 23% of radiographic and 49% of CT interpretations, and the correct diagnosis was made with 77% and 93% of those readings, respectively ($p < .001$). Thus, a confident diagnosis was made more than twice as often on the basis of CT scans than on the basis of chest radiographs, and the CT-based diagnosis was more often correct. The frequency and range of diseases in the study by Mathieson et al. [3] were similar to those in the study by McLoud et al. [2], and the observers, having no clinical information, were similarly at an unrealistic disadvantage as compared with radiologists in a clinical situation. The accuracy of the diagnoses made on the basis of the radiographs was also similar to that in the series by McLoud et al.

In the series by Mathieson et al. [3], 52 of 118 patients had conventional CT only, and 66 had additional high-resolution CT scans. The authors found that high-resolution CT was superior to conventional CT for the diagnosis of diseases characterized by irregular linear opacities, such as subtle reticulation in patients with usual interstitial pneumonia or thickening of the interlobular septa in patients with lymphatic spread of tumor.

Mathieson et al. [3] did not analyze the HRCT scans independently from the conventional CT scans but compared

the scans side by side and determined the ease with which the abnormalities could be seen. Because it was easier to distinguish nodular opacities from vessels on conventional CT scans than on HRCT scans, the authors recommended that both conventional and HRCT scans be obtained in the initial assessment of patients with chronic diffuse infiltrative lung disease [3]. More recently, Leung et al. [31] analyzed the HRCT and conventional CT scans separately and showed that although small nodular opacities were easier to distinguish from vessels on the conventional CT scans, the opacities were also clearly shown on the HRCT scans. This is in agreement with other studies that show that HRCT scans can be used to detect and characterize small nodular opacities in sarcoidosis [13] and various pneumoconioses [70, 71]. Remy-Jardin et al. [71] have suggested that HRCT may actually be more sensitive than conventional CT in the detection of small nodules in patients with pneumoconiosis. Leung et al. [31] found no significant difference in the diagnostic accuracy of HRCT and conventional CT in the assessment of patients with small nodular opacities such as those caused by sarcoidosis and silicosis. They did show that HRCT was significantly superior to conventional CT in the diagnosis of lymphangitic carcinomatosis. These results are similar to those of Stein et al. [6], who reported characteristic HRCT findings in two patients with lymphangitic carcinomatosis who had normal findings on radiographs and no evidence of interstitial disease on conventional CT scans.

Grenier et al. [72] compared the diagnostic accuracy of chest radiography and HRCT in 140 consecutive patients with chronic diffuse infiltrative lung disease. Three independent observers listed the three most likely diagnoses and recorded the degree of confidence they had in their choice on a 0–100% probability scale. The percentages of high-confidence diagnoses by each of the three observers that were correct on the basis of the chest radiograph were 29%, 34%, and 19%, respectively, as compared with 57%, 55%, and 47%, respectively, on the basis of the HRCT ($p < .001$ for each comparison). The interobserver agreement for the proposed diagnosis was also significantly better with HRCT than with conventional radiography.

On the basis of the results of these various studies, HRCT is clearly indicated in the assessment of patients with suspected infiltrative lung disease in whom the combination of clinical and radiologic findings does not allow a confident diagnosis. A more difficult question to address is whether a characteristic CT pattern can obviate lung biopsy in patients with chronic infiltrative lung disease. This decision will depend not only on the degree of confidence in the CT-based diagnosis but also on the specific infiltrative lung disease being diagnosed and on considerations such as clinical history, signs and symptoms, and age of the patient. When the CT features are highly suggestive of pneumoconiosis and the patient has a history of exposure, lung biopsy is seldom warranted. Likewise, when the CT findings are characteristic of hypersensitivity pneumonitis, the diagnosis usually can be confirmed on the basis of the clinical history and the results of serologic tests, precluding the need for lung biopsy. Also, particularly in the elderly, characteristic CT findings of idiopathic pulmonary fibrosis often obviate open lung biopsy. In

most other infiltrative lung diseases, however, a definitive histologic diagnosis is usually required.

The relative merits of conventional CT and HRCT for detecting small nodular opacities depend on the number, location, and size of the nodules. In patients with pneumoconiosis, subpleural nodules are visualized better on HRCT than on conventional CT, but more central nodules may be confused with vessels seen end on [71]. Furthermore, noncontiguous HRCT scans may miss nodules that would be detected on contiguous 10-mm sections. In patients with diffuse lung diseases such as sarcoidosis and various pneumoconioses, this does not decrease the diagnostic yield. However, in patients with neoplastic disease, contiguous 10-mm sections are required to determine the presence of pulmonary metastases.

HRCT as a Guide to the Type and Site of Lung Biopsy

Most chronic infiltrative lung diseases have a patchy distribution within the lung parenchyma; areas of normal parenchyma are interspersed between areas of active disease and areas with irreversible fibrosis. HRCT is helpful in determining the kind of diagnostic procedure most likely to yield a diagnosis and if biopsy is required, the area most likely to yield the correct diagnosis [3, 18, 19, 73].

The two chronic diffuse infiltrative lung diseases that can be consistently and reliably diagnosed on the basis of the findings of bronchial or transbronchial biopsy are lymphatic spread of tumor and sarcoidosis [74–76]. Diagnoses of interstitial pneumonia, fibrosis, chronic inflammation, nonspecific reaction, and normal lung that are based on the findings of transbronchial biopsy are unreliable and often entirely misleading [76]. Mathieson et al. [3] compared the accuracy of chest radiography and CT in the prediction of whether transbronchial biopsy was likely to yield a diagnostic-quality specimen. A transbronchial biopsy was considered to have been appropriately suggested when the first-choice radiologic diagnosis was correctly limited to either sarcoidosis or lymphangitic carcinomatosis. An open biopsy was considered to have been correctly suggested when the first-choice diagnosis avoided the erroneous inclusion of either sarcoidosis or lymphangitic carcinomatosis. Three independent observers correctly predicted that a transbronchial biopsy was indicated with 65% of radiographs and 87% of CT scans ($p < .001$). An open lung biopsy was correctly indicated on the basis of the radiographic findings in 89% of cases and on the basis of the CT findings in 99% of cases ($p < .001$).

When open lung biopsy is indicated, CT scanning is helpful in guiding the surgeon to the optimal biopsy site [73]. As pointed out by Gaensler and Carrington [38], the task of the surgeon at the time of open lung biopsy includes attempting to obtain representative tissue and avoiding areas of extensive honeycombing. This can be particularly difficult in cases of idiopathic pulmonary fibrosis because the most severe honeycombing is subpleural [77]. Also, disease distribution usually cannot be assessed adequately on the conventional radiograph, but it can be determined easily with CT.

HRCT in the Follow-up of Patients

Preliminary results also suggest that HRCT may play a role in the assessment of disease activity and response to treatment in patients with diffuse infiltrative lung disease [78–81].

In idiopathic pulmonary fibrosis, both long-term survival and response to treatment with corticosteroids correlate with the histologic changes. The best response to steroids is observed in patients with marked disease activity and little fibrosis [82–84]. Although open lung biopsy provides the gold standard for the estimate of the degree of alveolitis, it has two major limitations: It is invasive and it assesses only a small area of the lung that may not be representative of the overall process. Müller et al. [78] correlated the CT scans with pathologic determinants of disease activity in 12 patients with idiopathic pulmonary fibrosis. The hypothesis was that intraalveolar and interstitial cellularity would result in areas of opacification of air spaces (ground-glass density) on CT scans. All patients had open lung biopsy, and disease activity was assessed by using a pathologic grading system [85]. Seven patients had mild disease activity, and five had moderate to marked disease activity pathologically. Disease activity on CT scans was graded by two independent observers on a scale of 0–3 according to the relative density of the areas of air-space opacification compared with normal parenchyma. The pathologic score was significantly greater in the patients with high CT scores than in those with low CT scores ($p < .001$). Five patients with marked disease activity and five of seven patients with mild disease activity were categorized correctly by both observers. The two cases that were misdiagnosed had only conventional CT. All cases with high-resolution CT were correctly assessed. The capacity of HRCT for distinguishing irreversible fibrosis from acute alveolitis in most patients with idiopathic pulmonary fibrosis has been recently confirmed by Hansell et al. [79].

Lynch et al. [81] showed in a small number of patients with sarcoidosis that localized areas of hazy increased density (ground-glass opacities) correlated with active alveolitis as determined by using gallium-67 scans. Nodules on HRCT correlate with the presence of granulomata [14, 81]. Currently, it is thought that alveolitis rather than granuloma formation leads to fibrosis in these patients [86]. Follow-up HRCT in two patients who improved clinically with steroid therapy showed marked decrease in the ground-glass opacities and in the nodularity [81].

Although the results of these studies suggest a potential role of HRCT in the assessment of disease activity and in the follow-up of patients with known diagnoses, the studies are clearly preliminary. Further investigations are required to determine the role of HRCT in the assessment of disease activity, response to treatment, and follow-up of patients. Previously, the repeated performance of HRCT was worrisome because of the high doses of radiation. The study by Zwirwich et al. [36], who showed that diagnostic-quality HRCT scans can be obtained by using one tenth of the previously recommended radiation, has substantially expanded the potential role of HRCT in follow-up.

In patients with infiltrative lung disease, the presence of superimposed infection may be difficult or impossible to eval-

uate on the radiograph. Godwin et al. [87] reported the CT findings in nine patients with pulmonary alveolar proteinosis. In two cases, CT showed focal pneumonia that was not apparent on the radiograph. Hamper et al. [88] reported that CT was useful in the assessment of patients with pulmonary complications related to sarcoidosis, including bronchiectasis and cavitory lesions with and without air-fluid levels suggesting the possibility of superinfection. A correct diagnosis was made on the basis of CT findings in the majority of cases, and CT was also helpful for deciding on the most appropriate method to reach a definitive diagnosis (bronchoscopy, trans-tracheal biopsy, or percutaneous needle biopsy of a solitary mass).

The studies by Godwin et al. [87] and Hamper et al. [88] clearly show a role for CT in the assessment of patients with known infiltrative lung disease in whom a pulmonary complication is suspected clinically but is not evident on the radiograph. In these cases, as in all situations in which focal lung disease is being considered, HRCT scans should be based on the distribution of disease as assessed on the radiograph or be obtained in conjunction with conventional CT scans. In most patients, HRCT scans can be obtained at 10-mm intervals. However, if the focal abnormality is small, variations in the patient's breathing may make it difficult to obtain HRCT scans through the lesion. In these cases, five to seven HRCT scans at 1.5- to 5-mm intervals can be obtained through the area during a single breath hold by using a fast-scan technique [89].

Conclusions

The evidence from the various studies indicates that HRCT can play a major role in the assessment of diffuse lung disease. However, virtually all studies have been retrospective and have included a small number of patients. Prospective multicenter studies will be required to prove the diagnostic efficacy and cost-effectiveness of HRCT in diffuse lung disease. The evidence in the literature currently suggests that HRCT can be helpful and is indicated clinically (1) in patients with signs and symptoms suggestive of diffuse lung disease but normal or nonspecific findings on conventional radiography (these include patients with chronic cough or hemoptysis in whom bronchiectasis is suspected clinically, and patients with shortness of breath in whom emphysema or infiltrative lung disease is suspected), (2) in patients in whom the radiographic findings or the results of pulmonary function tests are not in keeping with the clinical history or symptoms, (3) before lung biopsy as a guide to the optimal type and site of biopsy in patients with infiltrative lung disease, and (4) in patients with infiltrative lung disease in whom complications (e.g., infection) are suspected.

REFERENCES

1. Epler GR, McLoud TC, Gaensler EA, Mikus JP, Carrington CB. Normal chest roentgenograms in chronic diffuse infiltrative lung disease. *N Engl J Med* 1978;298:934–939
2. McLoud TC, Carrington CB, Gaensler EA. Diffuse infiltrative lung disease: a new scheme for description. *Radiology* 1983;149:353–363

3. Mathieson JR, Mayo JR, Staples CA, Müller NL. Chronic diffuse infiltrative lung disease: comparison of diagnostic accuracy of CT and chest radiography. *Radiology* **1989**;171:111-116
4. McLoud TC, Epler GR, Gaensler EA, Burke GW, Carrington CB. A radiographic classification for sarcoidosis: physiologic correlation. *Invest Radiol* **1982**;17:129-138
5. Gaensler EA, Carrington CB, Couto RE, et al. Radiographic-physiologic-pathologic correlations in interstitial pneumonia. *Prog Respir Res* **1975**;8:223-241
6. Stein MG, Mayo J, Müller NL, Aberle DR, Webb WR, Gamsu G. Pulmonary lymphangitic spread of carcinoma: appearance on CT scans. *Radiology* **1987**;162:371-375
7. Aberle DR, Gamsu G, Ray CS. High-resolution CT of benign asbestos-related diseases: clinical and radiographic correlation. *AJR* **1988**;151:883-891
8. Aberle DR, Gamsu G, Ray CS, Feuerstein IM. Asbestos-related pleural and parenchymal fibrosis: detection with high-resolution CT. *Radiology* **1988**;166:729-734
9. Friedman AC, Fiel SB, Fisher MS, Radecki PD, Lev-Toaff AS, Caroline DF. Asbestos-related pleural disease and asbestosis: a comparison of CT and chest radiography. *AJR* **1988**;150:269-275
10. Staples CA, Gamsu G, Ray CS, Webb WR. High resolution computed tomography and lung function in asbestos-exposed workers with normal chest radiographs. *Am Rev Respir Dis* **1989**;139:1502-1508
11. Lenoir S, Grenier P, Brauner MW, et al. Pulmonary lymphangiomyomatosis and tuberous sclerosis: comparison of radiographic and thin-section CT findings. *Radiology* **1990**;175:329-334
12. Müller NL, Chiles C, Kullnig P. Pulmonary lymphangiomyomatosis: correlation of CT with radiographic and functional findings. *Radiology* **1990**;175:335-339
13. Brauner MW, Grenier P, Mompoin D, Lenoir S, DeCremeux H. Pulmonary sarcoidosis: evaluation with high-resolution CT. *Radiology* **1989**;172:467-471
14. Müller NL, Kullnig P, Miller RR. The CT findings of pulmonary sarcoidosis: analysis of 25 patients. *AJR* **1989**;152:1179-1182
15. Staples CA, Müller NL, Vedral S, Abboud R, Ostrow D, Miller RR. Usual interstitial pneumonia: correlation of CT with clinical, functional, and radiologic findings. *Radiology* **1987**;162:377-381
16. Strickland B, Strickland NH. The value of high definition, narrow section computed tomography in fibrosing alveolitis. *Clin Radiol* **1988**;39:589-594
17. Naidich DP, Funt S, Ettenger NA, Arranda C. Hemoptysis: CT-bronchoscopic correlations in 58 cases. *Radiology* **1990**;177:357-362
18. Müller NL, Miller RR. State of the art: computed tomography of chronic diffuse infiltrative lung disease. Part 1. *Am Rev Respir Dis* **1990**;142:1206-1215
19. Müller NL, Miller RR. State of the art: computed tomography of chronic diffuse infiltrative lung disease. Part 2. *Am Rev Respir Dis* **1990**;142:1440-1448
20. Webb WR. High-resolution CT of the lung parenchyma. *Radiol Clin North Am* **1989**;27:1085-1097
21. Noma S, Khan A, Herman PG, Rojas KA. High-resolution computed tomography of the pulmonary parenchyma. *Semin Ultrasound CT MR* **1990**;11:365-379
22. Webb WR. High-resolution computed tomography of the lung: normal and abnormal anatomy. *Semin Roentgenol* **1991**;26:110-117
23. Aberle DR. High-resolution computed tomography of asbestos-related diseases. *Semin Roentgenol* **1991**;26:118-131
24. Müller NL. Differential diagnosis of chronic diffuse infiltrative lung disease on high-resolution computed tomography. *Semin Roentgenol* **1991**;26:132-142
25. Naidich DP. High-resolution computed tomography of cystic lung disease. *Semin Roentgenol* **1991**;26:151-174
26. Takasugi JE, Godwin JD. The airway. *Semin Roentgenol* **1991**;26:175-190
27. Miller WT. Letter from the editor. *Semin Roentgenol* **1991**;26:99
28. Mayo JR, Webb WR, Gould R, et al. High-resolution CT of the lungs: an optimal approach. *Radiology* **1987**;163:507-510
29. Webb WR, Müller NL, Zerhouni EA. High-resolution CT of the lung: current clinical uses. *Perspect Radiol* **1989**;2:61-69
30. Gamsu G, Klein JS. High resolution computed tomography of diffuse lung disease. *Clin Radiol* **1989**;40:554-556
31. Leung AN, Staples CA, Müller NL. Chronic diffuse infiltrative lung disease: comparison of diagnostic accuracy of high-resolution and conventional CT (abstr). *Radiology* **1990**;177(P):113
32. Evans SH, Davis R, Cooke J, Anderson W. A comparison of radiation doses to the breast in computed tomographic chest examinations for two scanning protocols. *Clin Radiol* **1989**;40:45-46
33. Murphy F, Heaton B. Patient doses received during whole body scanning using an Elscint 905 CT scanner. *Br J Radiol* **1985**;58:1197-1201
34. Rueter FG, Conway BJ, McCrohan ML, Suleiman OH. Average radiation exposure values for three diagnostic radiographic examinations. *Radiology* **1990**;177:341-345
35. Zwirowich CV, Terriff B, Müller NL. High-spatial-frequency (bone) algorithm improves quality of standard CT of the thorax. *AJR* **1989**;153:1169-1173
36. Zwirowich CV, Mayo JR, Müller NL. Low-dose high-resolution CT of the lung parenchyma. *Radiology* **1991**;180:413-417
37. Naidich DP, Marshall CH, Gribbin C, Arams RS, McCauley DI. Low-dose CT of the lungs: preliminary observations. *Radiology* **1990**;175:729-731
38. Gaensler EA, Carrington CB. Open biopsy for chronic diffuse infiltrative lung disease: clinical, roentgenographic, and physiologic correlations in 502 patients. *Ann Thorac Surg* **1980**;30:411-426
39. Flower CDR, Shneerson JM. Bronchography via the fiberoptic bronchoscope. *Thorax* **1984**;39:260-263
40. Forrest JV, Safel SS, Omell GH. Bronchography in patients with haemoptysis. *AJR* **1976**;126:597-600
41. Thurlbeck WM, Simon G. Radiographic appearance of the chest in emphysema. *AJR* **1978**;130:429-440
42. Pratt PC. Role of conventional chest radiography in diagnosis and exclusion of emphysema. *Am J Med* **1987**;82:998-1006
43. Burki NK. Roentgenologic diagnosis of emphysema: accurate or not? *Chest* **1989**;1178-1179
44. Genereux GP. The Fleischner Lecture: Computed tomography of diffuse pulmonary disease. *J Thorac Imaging* **1989**;4:50-87
45. Millar AB, Boothroyd A, Edwards D, Hetzel MR. Value of computed tomography in unexplained haemoptysis (abstr). *Thorax* **1988**;43:811p
46. Hayhurst MD, Flenley DC, McLean A, et al. Diagnosis of pulmonary emphysema by computerised tomography. *Lancet* **1984**;2:320-322
47. Rockoff SD, Schwartz A. Roentgenographic underestimation of early asbestosis by International Labor Office classification: analysis of data and probabilities. *Chest* **1988**;5:1088-1091
48. Epstein DM, Miller WT, Bresnitz EA, Levine MS, Gefter WB. Applications of ILO classification to a population without industrial exposure: findings to be differentiated from pneumoconiosis. *AJR* **1984**;142:53-58
49. Naidich DP. Pulmonary parenchymal high-resolution CT: to be or not to be. *Radiology* **1989**;171:22-24
50. Kinsella M, Müller NL, Vedral S, Staples C, Abboud RT, Chan-Yeung M. Emphysema in silicosis: a comparison of smokers with nonsmokers using pulmonary function testing and computed tomography. *Am Rev Respir Dis* **1990**;141:1497-1500
51. Wiggins J, Strickland B, Turner-Warwick M. Combined cryptogenic fibrosing alveolitis and emphysema: the value of high resolution computed tomography in assessment. *Respir Med* **1990**;84:365-369
52. Galvin JR, Helmers RA, Schwartz DA, Mori M, Stanford W. High-resolution chest CT in the evaluation of dyspneic smokers with pulmonary fibrosis and normal spirometry (abstr). *Radiology* **1990**;177(P):113
53. Jones DK, Cavanagh P, Shneerson JM, Flower CDR. Does bronchography have a role in the assessment of patients with haemoptysis? *Thorax* **1985**;40:668-670
54. Müller NL, Bergin CJ, Ostrow DN, Nichols DM. Role of computed tomography in the recognition of bronchiectasis. *AJR* **1984**;143:971-976
55. Silverman PM, Godwin JD. CT/bronchographic correlations in bronchiectasis. *J Comput Assist Tomogr* **1987**;11:52-56
56. Phillips MS, Williams MP, Flower CDR. How useful is computed tomography in the diagnosis and assessment of bronchiectasis? *Clin Radiol* **1986**;37:321-325
57. Grenier P, Maurice F, Musset D, Menu Y, Nahum H. Bronchiectasis: assessment by thin-section CT. *Radiology* **1986**;161:95-99
58. Snider GL, Kleinerman J, Thurlbeck WM, Bengali ZH. The definition of emphysema: report of a National Heart, Lung, and Blood Institute, Division of Lung Diseases workshop. *Am Rev Respir Dis* **1985**;132:182-185
59. West WW, Nagai A, Hodgkin JE, Thurlbeck WM. The National Institutes of Health Intermittent Positive Pressure Breathing Trial—pathology studies. III. The diagnosis of emphysema. *Am Rev Respir Dis* **1987**;135:123-129

60. Thurlbeck WM. Aspects of chronic airflow obstruction. *Chest* **1977**; 72:341-349
61. Bergin CJ, Müller N, Nichols DM, et al. The diagnosis of emphysema: a computed tomographic-pathologic correlation. *Am Rev Respir Dis* **1986**;133:541-546
62. Morrison NJ, Abboud RT, Ramadan F, et al. Comparison of single breath carbon monoxide diffusing capacity and pressure-volume curves in detecting emphysema. *Am Rev Respir Dis* **1989**;139:1179-1187
63. Kinsella M, Müller NL, Abboud RT, Morrison NJ, DyBuncio A. Quantitation of emphysema by computed tomography using a "density mask" program and correlation with pulmonary function tests. *Chest* **1990**;97:315-321
64. Sutinen S, Christoforidis AM, Klugh GA, Pratt PC. Roentgenologic criteria for the recognition of nonsymptomatic pulmonary emphysema. *Am Rev Respir Dis* **1965**;91:69-76
65. Sanders C, Nath PH, Bailey WC. Detection of emphysema with computed tomography: correlation with pulmonary function tests and chest radiography. *Invest Radiol* **1988**;23:262-266
66. Hruban RH, Meziane MA, Zerhouni EA, et al. High resolution computed tomography of inflation-fixed lungs: Pathologic-radiologic correlation of centrilobular emphysema. *Am Rev Respir Dis* **1987**;136:935-940
67. Miller RR, Müller NL, Vedal S, Morrison NJ, Staples CA. Limitations of computed tomography in the assessment of emphysema. *Am Rev Respir Dis* **1989**;139:980-983
68. Kuwano K, Matsuba K, Ikeda T, et al. The diagnosis of mild emphysema: correlation of computed tomography and pathology scores. *Am Rev Respir Dis* **1990**;141:169-178
69. Kinsella M, Müller NL, Staples C, Vedal S, Chan-Yeung M. Hyperinflation in asthma and emphysema: assessment by pulmonary function testing and computed tomography. *Chest* **1988**;94:286-289
70. Akira M, Higashihara T, Yokoyama K, et al. Radiographic type p pneumoconiosis: high-resolution CT. *Radiology* **1989**;171:117-123
71. Remy-Jardin M, Degreffe JM, Beuscart R, Voisin C, Remy J. Coal worker's pneumoconiosis: CT assessment in exposed workers and correlation with radiographic findings. *Radiology* **1990**;177:363-371
72. Grenier P, Valeyre D, Cluzel P, Brauner MW, Lenoir S, Chastang C. Chronic diffuse interstitial lung disease: diagnostic value of chest radiography and high-resolution CT. *Radiology* **1991**;179:123-132
73. Miller RR, Nelems B, Müller NL, Evans KG, Ostrow DN. Lingular and right middle lobe biopsy in the assessment of diffuse lung disease. *Ann Thorac Surg* **1987**;44:269-273
74. Churg A. Lung biopsy: handling and diagnosing limitations. In: Thurlbeck WM, ed. *Pathology of the lung*. New York: Thieme Medical, **1988**: 67-78
75. Dahlquén P, Oberholzer M. Lung biopsy: methods, value, complications, timing, and indications. *Pathol Res Pract* **1979**;164:95-103
76. Wall CP, Gaensler EA, Carrington CB, Hayes JA. Comparison of trans-bronchial and open biopsies in chronic infiltrative lung diseases. *Am Rev Respir Dis* **1981**;123:280-285
77. Müller NL, Miller RR, Webb WR, Evans KG, Ostrow DN. Fibrosing alveolitis: CT-pathologic correlation. *Radiology* **1986**;160:585-588
78. Müller NL, Staples CA, Miller RR, Vedal S, Thurlbeck WM, Ostrow DN. Disease activity in idiopathic pulmonary fibrosis: computed tomographic-pathologic correlation. *Radiology* **1987**;165:731-734
79. Hansell DM, Wells AU, du Bois R, Corrin B. Disease activity in fibrosing alveolitis: assessment by high resolution CT with histological correlation (abstr). *Clin Radiol* **1990**;42:375
80. Klein JS, Webb WR, Gamsu G, Warnock M, Park CK. Hazy increased density in diffuse lung disease: high-resolution CT (abstr). *Radiology* **1989**;173(P):140
81. Lynch DA, Webb WR, Gamsu G, Stulberg M, Golden J. Computed tomography in pulmonary sarcoidosis. *J Comput Assist Tomogr* **1989**;13: 405-410
82. Carrington CB, Gaensler EA, Couto RE, FitzGerald MX, Gupta RG. Natural history and treated course of usual and desquamative interstitial pneumonia. *N Engl J Med* **1978**;298:801-809
83. Turner-Warwick M, Burrows B, Johnson A. Cryptogenic fibrosing alveolitis: response to corticosteroid treatment and its effect on survival. *Thorax* **1980**;35:593-599
84. Wright PH, Heard BE, Steel SJ, Turner-Warwick M. Cryptogenic fibrosing alveolitis: assessment by graded trephine lung biopsy histology compared with clinical, radiographic and physiologic features. *Br J Dis Chest* **1981**;75:61-70
85. Watters LC, King TE, Schwarz MI, Waldron JA, Stanford RE, Cherniack RM. A clinical, radiographic, and physiologic scoring system for the longitudinal assessment of patients with idiopathic pulmonary fibrosis. *Am Rev Respir Dis* **1986**;133:97-103
86. Hunninghake GW, Garrett KC, Richerson HB, et al. Pathogenesis of the granulomatous lung disease. *Am Rev Respir Dis* **1984**;130:476-496
87. Godwin JD, Müller NL, Takasugi JE. Pulmonary alveolar proteinosis: CT findings. *Radiology* **1988**;169:609-613
88. Hamper UM, Fishman EK, Khouri NF, Johns CJ, Wang PK, Siegelman SS. Typical and atypical CT manifestations of pulmonary sarcoidosis. *J Comput Assist Tomogr* **1986**;10:928-936
89. Shaffer K, Pugatch R. Small pulmonary nodules: dynamic CT with a single-breath technique. *Radiology* **1989**;173:567-568

Review Article

Masses of the Anterior Mediastinum: CT and MR Imaging

Larry R. Brown¹ and Gregory L. Aughenbaugh

CT and MR imaging allow earlier diagnosis and more specific characterization of anterior mediastinal masses than is possible with plain film radiographs. This review describes state-of-the-art CT and MR imaging of the anterior mediastinum. After a discussion of CT and MR imaging and indications for their use, normal and abnormal CT and MR findings in the anterior mediastinum are reviewed. Abnormalities include benign and malignant neoplasms, cysts, and mediastinal thyroid. Several masses such as thymolipomas, goiters, cysts, and lymphangiomas often do not require removal and now can be diagnosed with reasonable accuracy when imaging results are combined with clinical history. Detection, diagnosis, staging, and follow-up of malignant anterior mediastinal masses are important and have been improved with CT and MR imaging.

Since its advent in the mid 1970s, CT has emerged as the main technique used to evaluate the anterior mediastinum after plain film studies. A major advantage of CT over plain films is better contrast discrimination, which permits distinction between solid, fatty, cystic, calcified, and vascular structures. Also, cross-sectional imaging eliminates the problem of superimposition of mediastinal structures. Thus, CT is better at localizing and revealing the exact extent of anterior mediastinal abnormalities than is the plain film. CT is usually better at differentiating benign from malignant processes and can preclude the use of more invasive diagnostic procedures.

More recently, MR imaging has been found useful, usually as an adjunct to CT, for clarifying problems encountered with CT or for examining patients who cannot tolerate IV administration of contrast material. MR imaging can, at times, distinguish between some tissues that CT cannot. For in-

stance, in some cases, MR imaging can distinguish fibrosis from viable tumor. The ability to obtain sagittal and coronal images with MR imaging can add information on extent and localization of disease.

We review the efficacy of CT and MR imaging in the evaluation of the anterior mediastinum.

Indications

CT is used most often to evaluate the anterior mediastinum if a definite or possible abnormality is detected on chest radiography. Usually the abnormality is either diffuse widening of the mediastinum or a focal bulge or mass. CT improves diagnostic accuracy in determining whether a real abnormality is present in the mediastinum. CT also often can show the exact nature and extent of masses.

A second common indication for CT is to search for an anterior mediastinal abnormality that is clinically suspected but is not shown on chest radiographs. Examples of this include thymoma in patients with myasthenia gravis, thymic carcinoid in patients with ectopic corticotropin production, and mediastinal parathyroid adenoma in patients with ectopic parathormone production.

MR imaging is usually reserved for clarifying problems encountered on CT or to examine patients who cannot tolerate IV administration of contrast material. The flexible orientation of the plane of section allows MR to image mediastinal masses in virtually any projection, an advantage not shared by CT. The disadvantages of MR imaging of the mediastinum include decreased spatial resolution compared with that of

Received March 15, 1991; accepted after revision July 23, 1991.

¹ Both authors: Department of Diagnostic Radiology, Mayo Clinic and Mayo Foundation, 200 First St. S.W., Rochester, MN 55905. Address reprint requests to L. R. Brown.

AJR 157:1171-1180, December 1991 0361-803X/91/1576-1171 © American Roentgen Ray Society

CT and the inability to detect pathologic calcification accurately. Motion artifact, a problem in early MR imaging of the mediastinum, has been reduced considerably with ECG-gated sequences.

Technique

Our CT procedure is to obtain images of 10-mm slice thickness at 10-mm intervals from the level of the thyroid gland to the level of the adrenal glands in order to evaluate the entire chest, including the mediastinum. Window widths and levels of 400 and 20, respectively, are good for mediastinal imaging. One hundred thirty kilovolts and 110 mA with a 38- to 40-cm field of view are used. Targeted reconstruction with a 25-cm field of view is occasionally done to improve imaging of a particular region of interest.

Contrast material given IV is often unnecessary in evaluating the anterior mediastinum, because structures are usually separated by enough fat to eliminate confusion. If contrast material is to be used, an unenhanced study should be done first to evaluate high-attenuation features of certain mediastinal abnormalities: calcification of lymph nodes and neoplasms, milk of calcium in mediastinal cysts, high iodine content in goiters, and high hemoglobin content in recent hemorrhage [1]. Some lesions, however, are more easily diagnosed if IV contrast material is given.

Various techniques have been advocated for the administration of contrast material. Optimally, opacification should be sufficient for vascular structures to be identified easily, for enhancement of a mass to be evaluated, and for the various mediastinal structures to be distinguished confidently. The recent availability of programmable, high-volume, low-flow-rate injectors has permitted a more uniform and higher volume of contrast material to be delivered. This, combined with rapid or dynamic scanning with conventional scanners or use of ultrafast CT, permits excellent visualization of the entire mediastinum in a much shorter time.

The most common technique for MR imaging uses spin-echo pulse sequences. T1-weighted images are obtained to distinguish fat from nonfatty structures. In our practice, if findings on these images are normal, the examination can be terminated. If an abnormality is present, T2-weighted images are obtained to characterize tissues further. To decrease flow artifacts in vessels, we use a spatial presaturation technique. Ordered phase encoding is used to decrease respiratory artifacts, and cardiac gating is used to decrease cardiac motion artifacts. Although transverse sections are generally used, coronal or sagittal views are obtained when appropriate.

Normal CT and MR Findings

The anterior mediastinum is defined as that part of the mediastinum lying posterior to the sternum and anterior to the great vessels and pericardium. The mediastinal pleura in contact with the anteromedial aspect of each lung forms the lateral boundaries. The anterior mediastinum extends from the diaphragm inferiorly to the thoracic inlet superiorly [2] and

contains the thymus, mediastinal fat, lymph nodes, and internal mammary arteries and veins.

On axial CT images, the upper anterior mediastinum is triangular, with its apex pointing anteriorly toward the sternum. The apex continues anteriorly as the anterior junction line between the anteromedial aspects of the two lungs. This is a potential space that contains fat in patients more than 40 years old. The anterior junction line ends over the base of the heart, and below this level the anterior mediastinum represents the space between the heart and sternum. The thymus is usually visible in patients younger than 40 years. It is an arrowhead-shaped structure anterior to and molded by the great vessels (Fig. 1). It consists of two lobes, right and left, although the interface between the lobes can be distinguished in only one third of normal glands. Using CT, Baron et al. [3] showed thick and dense glands in patients younger than 19 years and progressive loss of thickness and density with advancing age. By about age 40 years, the thymus usually is almost completely replaced by fat. Residual glandular tissue is visible only as a slightly grainy appearance of the fat.

Mediastinal fat is the most signal-intense, solid tissue seen on T1-weighted MR images of the mediastinum. The thymus is more easily recognized on MR imaging than on CT. The shape, size, and signal intensity are age dependent. In children, the thymus has an intermediate intensity similar to that of muscle on T1-weighted images. As fatty replacement progresses in childhood, the thymus assumes a higher intensity. On T2-weighted images, however, the relaxation time of the thymus is similar to that of fat and does not change with age. The thymus appears larger and more discrete on MR imaging than on CT. On T2-weighted images, fluid and some neoplasms increase in signal intensity, whereas muscle and, to a lesser extent, fat decrease in signal intensity. The vessels of the mediastinum that contain flowing blood commonly have no evident signal, which allows easy distinction of solid structures from mediastinal vessels [4] (Fig. 2).

Abnormal CT and MR Findings

Differentiation by CT between a large, normal thymus and a thymic mass is sometimes difficult, particularly in younger patients with a large thymus. A thymic mass usually appears as a solid, oval or rounded density, with the bulk of the mass lateral to the midline. A mass does not conform to the normal contours of the mediastinum (Fig. 3). The presence of lobulation usually indicates a mass rather than a large gland. Obliteration of normal tissue planes indicates an infiltrating or invasive tumor. Occasionally, only one lobe of the thymus is visible and, if large, may be confused with a mass. In this circumstance, the lobe usually retains its elongated shape and drapes around the mediastinum rather than standing apart from mediastinal structures. The thymus undergoes atrophy and regrowth during various phases of chemotherapy for malignant disease. In patients younger than 35 years, regrowth of the volume of the thymus may exceed 50% after chemotherapy or after recovery from an illness. This is called thymic rebound. Sudden rebound of the thymus may be mistaken for a mass [5]. We have seen the thymus enlarge

Fig. 1.—30-year-old woman with normal thymus. Thin right and left lobes of thymus (arrows) form an arrowhead configuration on CT scan.

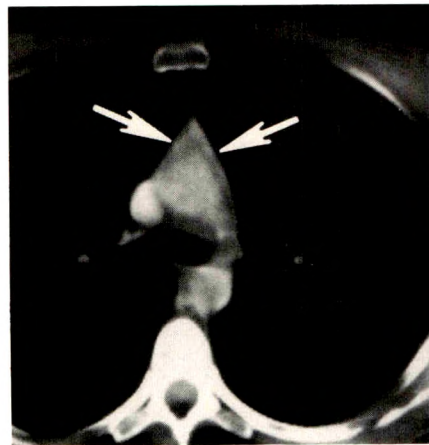
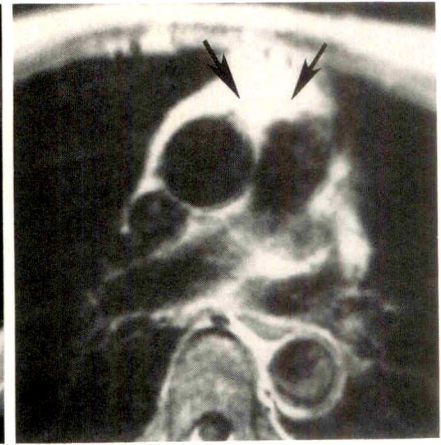


Fig. 2.—Spin-echo T1-weighted image of normal mediastinum in an adult. High signal intensity of normal thymus (arrows) is due to fatty replacement.



1

2

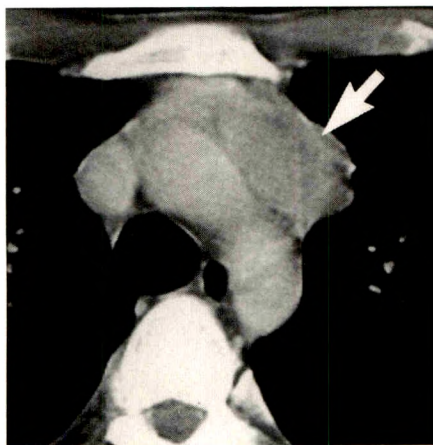


Fig. 3.—29-year-old man with recent onset of myasthenia gravis and thymoma that was seen to be invasive at surgery. CT shows oval mass (arrow) of left lobe of thymus consistent with diagnosis of thymoma.

in patients with acromegaly (Fig. 4) or Graves disease (Fig. 5), and it can resemble a thymic mass [6].

With MR imaging, most masses of the mediastinum are identified by their morphology, although fluid and fatty masses often have features that allow more specific tissue characterization [4].

Abnormalities of the middle mediastinum, such as an ascending aortic aneurysm or a pericardial cyst, can project anteriorly and simulate an anterior mediastinal mass. A mass in a cardiophrenic angle, such as a fat pad, enlarged lymph node, hernia of the foramen of Morgagni, or pericardial cyst, lies anteriorly, but these actually originate in the middle mediastinum. Discussion of these abnormalities is beyond the scope of this review.

Anterior Mediastinal Abnormalities

On plain films of the chest in an adult, any anterior mediastinal mass that involves the upper mediastinum and causes

the trachea to deviate is almost always of thyroid origin. Calcification within an upper mediastinal thyroid gland is a common finding. In children, a mass in this location is usually a cystic hygroma. Most anterior mediastinal masses below the level of the clavicles have a similar appearance on plain films; however, associated findings such as pleural nodules, pleural effusions, pulmonary nodules, or infiltration into the adjacent lung parenchyma can help in differential diagnosis. Clinical findings also can help in differentiating one lesion from another. Thymoma is the most common neoplasm of the anterior mediastinum in adults. The description of its features on plain films of the chest will apply to the other tumors discussed later. Once a mass is discovered on plain films of the chest, CT or MR imaging may show certain features that are unique to a specific lesion and often enable the radiologist to make a definitive diagnosis. This eliminates the need for resection or biopsy in some cases. The distinguishing features of several of these masses are described here.

Thymoma.—A thymoma is composed of benign-appearing neoplastic thymic epithelial cells mixed with lymphocytes. Thymomas may be encapsulated (with intact fibrous capsules), invasive (with benign-appearing cytologic characteristics but infiltrative growth), or metastasizing (with seeding of pleural surfaces and pulmonary parenchyma but with benign cytologic results and no extension outside the thoracic cavity). Cytologically, malignant thymomas are better described as thymic carcinomas than as malignant thymomas. Thymic carcinomas have a worse prognosis than thymomas [7].

The mean age at diagnosis is 52 years. The frequency in men and women is approximately equal. Almost half these patients have myasthenia gravis. An additional 10% have other paraneoplastic phenomena, including hypogammaglobulinemia and anemia due to erythrocyte hypoplasia. Myasthenia gravis not associated with thymoma is usually associated with thymic lymphoid follicular hyperplasia, which may or may not cause enlargement of the thymus. In general, symmetric, diffuse thymic enlargement in patients with myasthenia gravis indicates hyperplasia. However, 25–50% of patients with myasthenia gravis and histologic hyperplasia will show a normal-sized gland on CT.

Chest radiographs of patients with thymoma show a mass

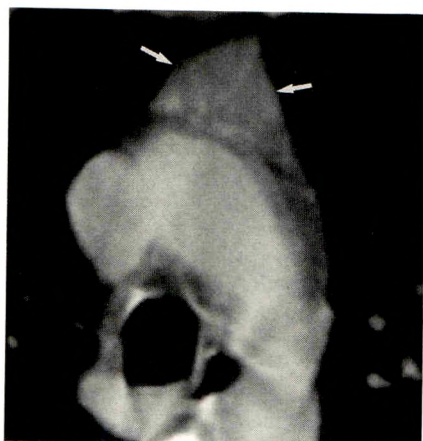
**A****B**

Fig. 4.—52-year-old man with acromegaly.
A, CT scan shows enlarged thymus gland or thymoma (arrows).
B, 4 months later, after resection of pituitary adenoma, thymus (arrows) has returned to its expected appearance for patient's age.

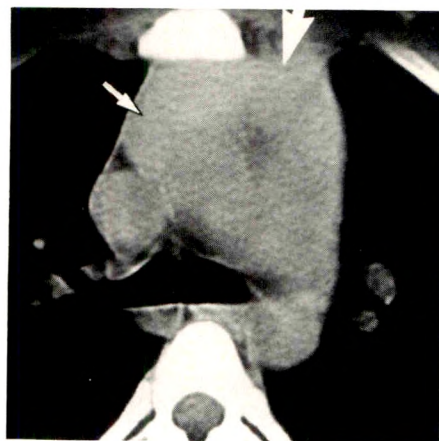


Fig. 5.—24-year-old woman with Graves disease and fullness of anterior mediastinum on chest radiograph. CT scan shows symmetrically enlarged thymus with thickened right and left lobes (arrows) related to Graves disease.

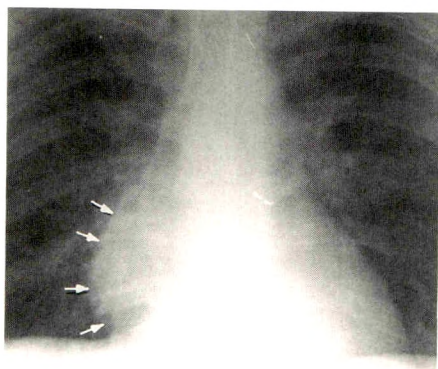


Fig. 6.—Posteroanterior chest radiograph shows enlargement and slight lobulation of right cardiac margin (arrows) due to large right anterior mediastinal thymoma.

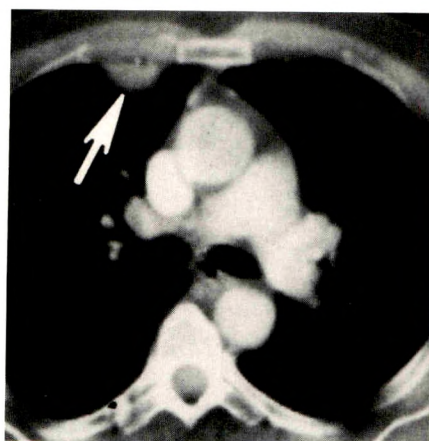
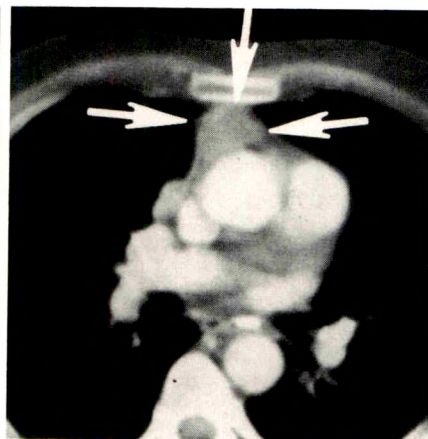
**A****B**

Fig. 7.—58-year-old man examined because of nodule seen on lateral chest radiograph.
A, CT scan at mid chest level shows it is a pleural nodule (arrow).
B, At a slightly lower level, CT scan shows small unsuspected invasive thymoma (arrows).
Diagnosis: thymoma with pleural metastasis.

projecting over some portion of the hilum in 50–80% of cases. These masses can be extremely small, subtle, oval opacities (17% of cases) [8]. Large masses projecting to the right or left of the cardiac margin are easily mistaken for the heart (Fig. 6). The presence of subtle lobulation and increased density of the heart in that area along with a normal cardiac configuration on the opposite side helps to identify the abnormality as a mass rather than an abnormal cardiac contour. Large thymomas that project to both sides of the mediastinum usually are malignant [9]. Calcification occurs in 7% of cases and can be coarse, dense, and irregular or ringlike. Calcification can occur in invasive or encapsulated tumors.

Nearly one fourth of thymomas in one series were not detected initially on the posteroanterior radiograph [8]. When thymomas were missed, the average delay in final diagnosis

was 41 months. This delay often allows extensive growth and infiltration of these tumors. Metastases from a thymoma usually involve the pleura, so that the presence of a pleural metastasis accompanying an anterior mediastinal mass makes thymoma likely (Fig. 7).

Smaller tumors can be detected by CT, which allows an accurate search for thymoma in patients with myasthenia gravis (Fig. 8). CT is helpful in judging the extent of tumor, but in some cases fibrous adherence of tumor without invasion may be confused with infiltration of tumor in the mediastinum. In general, preservation of fat planes around the tumor margins is strong evidence that the thymoma is not invasive. If the fat planes are completely obliterated, the tumor usually is invasive. When the fat planes are only partially preserved, only about half the tumors are invasive [10]. Attenuation is

Fig. 8.—36-year-old woman with myasthenia gravis and normal findings on chest radiograph. CT scan shows a 3-cm encapsulated thymoma (arrow) in anterior mediastinum.

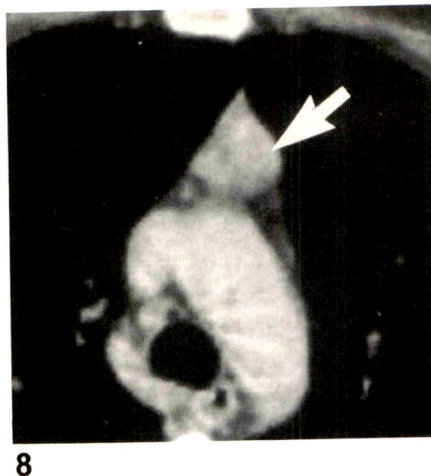
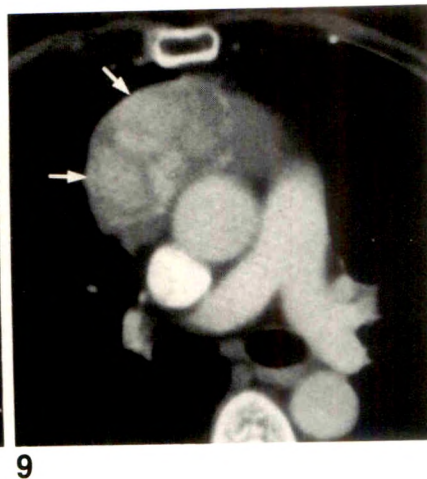


Fig. 9.—58-year-old woman with homogeneous anterior mediastinal mass on unenhanced CT scan. Enhanced CT shows thymoma (arrows). Mixed attenuation qualities of mass simulate interfaces. Pathologically, thymoma was found to be invasive.



often more heterogeneous in invasive thymoma after IV administration of contrast material (Fig. 9). Assessment of tumor during surgery is the most reliable means of determining invasiveness. A cystic component is present in one third of cases, but in our experience, a cyst is rarely seen by CT [8].

On MR images, thymomas appear as oval or lobulated masses with a signal intensity on T1-weighted images similar to that of muscle. Signal intensity increases and approaches that of fat on T2-weighted images. Sagittal images are useful, allowing another dimension of the tumor to be evaluated for invasion or adherence. However, CT has proved superior to MR imaging in the evaluation of thymomas because of better spatial resolution and thymic definition in a shorter time [11]. An anterior mediastinal mass accompanied by pleural metastasis, myasthenia gravis, anemia, or hypogammaglobulinemia in a patient 40–60 years old makes the diagnosis of thymoma a strong possibility.

Neuroendocrine tumors.—These tumors are usually composed of small, uniform round cells. A spectrum of malignancy is found in these tumors, from the well-differentiated mediastinal carcinoids to atypical carcinoids, and finally to the most malignant variety—the oat cell carcinoma of the thymus. Thymic carcinoid, which is thought to arise from the neural crest, is by far the most common neoplasm in this group, but among thymic tumors it is still relatively uncommon. As with other neuroendocrine neoplasms, such as pheochromocytoma, islet cell tumor of the pancreas, medullary carcinoma of the thyroid, and small-cell carcinoma of the bronchus, thymic carcinoid is often hormonally active. In cases of thymic carcinoid, ectopic corticotrophic hormone production, which causes Cushing syndrome, is found in 34–38% of patients [12].

Nonfunctioning carcinoids may be associated with other tumors, such as parathyroid adenoma, islet cell tumor of the pancreas, and pituitary adenoma when it is part of the multiple endocrine neoplasia (MEN), type I, syndrome.

Findings on plain films of the chest are often normal or equivocal [13]. A CT scan is often necessary for diagnosis because these tumors may be quite small and metastasize early (Fig. 10). Osteoblastic metastasis is typical of carcinoid.

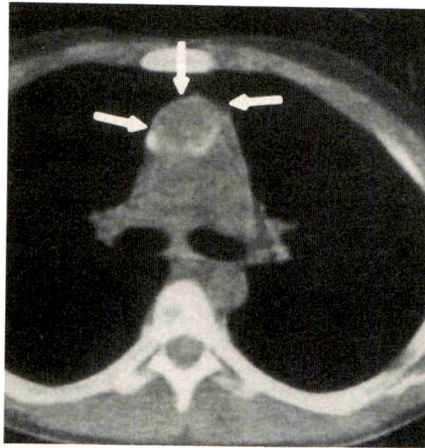
The presence of an anterior mediastinal mass in patients with clinical signs of Cushing syndrome or other tumors of the MEN I syndrome makes mediastinal carcinoid the most likely diagnosis.

Germ cell tumors.—These tumors arise from primitive cells that differentiate into embryonic and extraembryonic structures; the result is a spectrum of benign and malignant neoplasms. Histopathologic variants include teratoma, seminoma, embryonal cell carcinoma, yolk sac tumor, choriocarcinoma, and mixed types. Teratomas account for most mediastinal germ cell tumors. Teratomas can be further subdivided into (1) mature solid, (2) cystic (dermoid cyst), (3) immature, (4) malignant (teratocarcinoma), and (5) mixed. Mature teratomas account for 75% of mediastinal germ cell tumors. They are composed of several tissue elements that abnormally recapitulate the development of two or three embryonic layers (ectoderm, endoderm, and mesoderm) [14]. They usually contain mostly ectodermal elements such as sebaceous material, hair, calcification, and a large cystic component. They are more frequent in young adults, and the benign type is more common in females. The plain film appearance of teratoma is similar to that of thymoma.

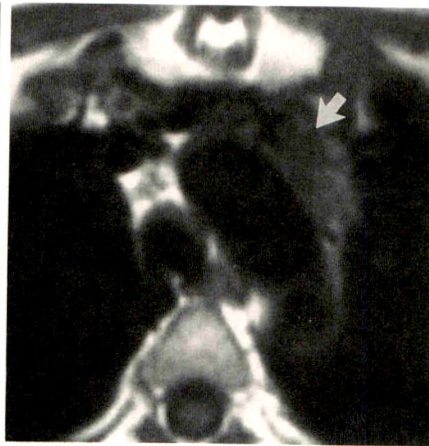
On CT, most teratomas contain a prominent cystic component, small dense localized areas of calcification or ossification, and, in up to half, either fat or mixed low-density material with an attenuation value nearer to that of fat than that of water [15, 16] (Fig. 11). Fat/fluid levels also have been reported [17]. Few teratomas are totally solid, although nearly all contain a solid component. In our experience, MR imaging has been helpful in detecting cystic, solid, and fatty areas within the tumor, which helps in differential diagnosis (Fig. 12).

Malignant germ cell tumors usually occur in young males, and more than half are seminomas. Seminomas are radiosensitive and are highly curable, whereas nonseminomatous malignant germ cell tumors are treated with a combination of surgery and chemotherapy and have a less favorable prognosis.

On CT, seminomas are large, bulky, uncalcified tumors with relatively homogeneous attenuation and smooth margins. If



A



B

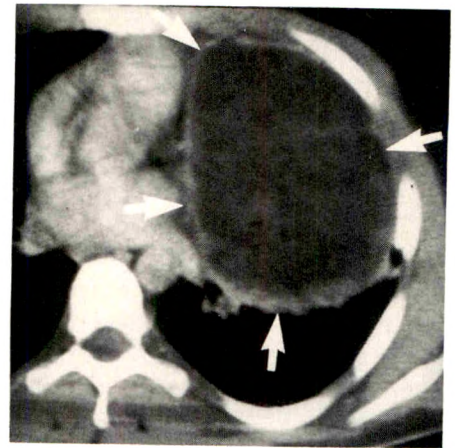
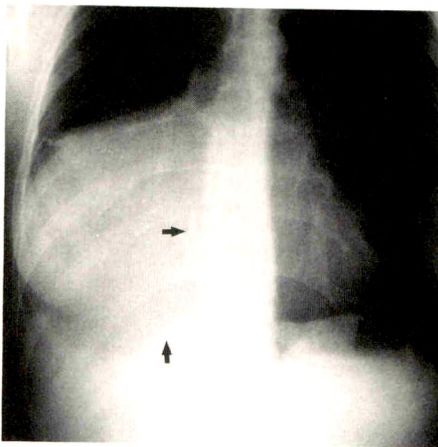


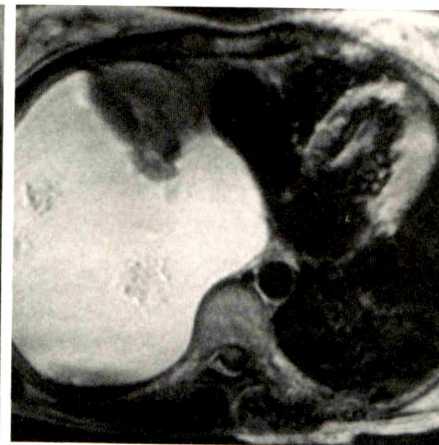
Fig. 10.—A, 28-year-old man with Cushing syndrome due to ectopic corticotrophic hormone production by thymic carcinoid. CT scan shows calcification within tumor (arrows). (Reprinted with permission from Brown et al. [13].)

B, 39-year-old woman with Cushing syndrome. MR image shows thymic carcinoid of left anterior mediastinum (arrow).

Fig. 11.—22-year-old man with left anterior mediastinal mass. CT scan shows encapsulated, cystic, mixed-attenuation mass (arrows) typical of benign cystic teratoma.



A



B



C

Fig. 12.—22-year-old woman with large anterior mediastinal teratoma.

A, Posteroanterior chest radiograph shows massive right anterior mediastinal mass containing curvilinear calcification in inferior medial wall (arrows). B and C, T1-weighted MR images in axial (B) and coronal (C) projections show large mass is predominantly high intensity, characteristic of fat. Note lower intensity soft-tissue elements within its structure.

cystic changes are present, they occupy 25% or less of the tumor. Nonseminomatous malignant germ cell tumors more commonly contain low-density cystic or necrotic areas, or both, with septated architecture that frequently occupy more than half the tumor. Calcification may be present [18, 19]. Fat planes are obliterated, indicating invasion. After treatment, malignant germ cell tumors tend to undergo necrosis and cyst formation. Residual masses may remain for years without tumor activity. Some masses may even enlarge as a result of benign factors, such as an enlarging benign teratoma component or necrosis when tumor markers indicate no activity [20, 21].

Lymphomas.—Adults with primary mediastinal lymphoma

usually have Hodgkin disease, nodular sclerosing type. Childhood mediastinal lymphoma is most commonly of the non-Hodgkin type. Nodular sclerosing Hodgkin disease is the most frequent form of lymphoma in the anterior mediastinum and is most common in women [14].

A primary mediastinal lymphoma confined to the anterior mediastinum has much the same appearance as any other type of anterior mediastinal mass on plain films. Secondary signs are common in Hodgkin disease but uncommon in other masses; these include pleural effusion and erosion of the sternum. Calcification is rare but does occur [22]. Harms and Brown (Harms G, Brown LR, presented at the annual meeting of the Society of Thoracic Radiology, February 1987) studied

the CT appearance of primary intrathoracic lymphoma in 95 patients before treatment and found CT to be helpful in the diagnosis. All but 14% of lymphomatous masses (that is, separate lesions 4.0 cm or larger) had associated adenopathy in some other region of the chest. Additionally, many of the lesions that appeared as masses on plain films were shown by CT to have discrete, well-defined interfaces within them, indicating matted lymph nodes (Fig. 13). Low-density areas presumed to be necrosis occurred in about half the patients (Fig. 14). Others have described associated thick-walled cysts. Lung invasion was present in one third of these patients: visible tumor grew along the bronchovascular sheaths.

Although patients with other diseases such as sarcoidosis, metastasis, or infection can have adenopathy in the anterior mediastinum, they seldom have the large bulky adenopathy found in lymphoma.

An anterior mediastinal mass that consists of a conglomeration of multiple lymph nodes or is associated with detectable adenopathy elsewhere should strongly suggest the diagnosis of lymphoma. Areas of low density that suggest necrosis, the presence of discrete thick-walled cysts within the mass, and lung invasion by tumor are additional helpful findings.

After adequate chemotherapy or radiation therapy for lymphoma, a residual mediastinal mass often is present and most often does not indicate active disease [23, 24]. The residual mass may be cystic or solid. MR imaging has shown promise in the differentiation of active from inactive residual masses. In one study involving mediastinal Hodgkin disease, the initial size of the mass seen on T2-weighted images paralleled the size of the residual mass. Inactive treated lymphomas had significantly lower signal intensity on T2-weighted images than did active lymphomas [25, 26].

Thymic enlargement may be present during staging. If the thymus is involved with lymphoma, accompanying mediastinal

adenopathy usually is present near the thymus. If smooth thymic enlargement is seen without accompanying adenopathy, an alternative diagnosis such as a large normal gland is more likely (Fig. 15). The thymus often enlarges after treatment as a result of thymic rebound, and this should not be mistaken for recurrence [27].

Thymic cysts.—These uncommon cysts are found anywhere along the embryologic course of the thymus. Krech et al. [28] divided thymic cysts into three groups: inflammatory, congenital, and neoplastic. Jaramillo et al. [29] described a fourth type, which is thymic cyst after thoracotomy. Most thymic cysts are probably congenital and derive from a persistently patent thymopharyngeal duct. They represent 1% of mediastinal masses [14]. They are symptomatic in 40% of cases [30]. Anterosuperior mediastinal cysts are most often found in children and are elongated, often extending from the neck. Anterior mediastinal cysts are not molded by the vascular structures and are usually round or ovoid. They may undergo hemorrhage and calcification.

Plain films show a nonspecific mediastinal mass, but CT reveals a thin-walled cystic structure in the mediastinum that has the density of water (Fig. 16). We have not found these to be associated with a soft-tissue component. Hemorrhage can cause a density greater than that of water on CT. Occasionally, one or more ringlike calcified structures are present as a result of previous hemorrhage. Although CT makes the diagnosis possible, opinion is still divided on whether or not surgery is required in these cases.

MR imaging is helpful in the diagnosis of mediastinal cysts and pseudocysts [31]. On T1-weighted MR images, cysts are low in signal intensity. On T2-weighted images, cysts are high in signal intensity. If the cyst contains blood, the T1-weighted signal is higher because of the T1 shortening effect of methemoglobin.

Cysts associated with neoplasms either before or after



Fig. 13.—17-year-old girl with nodular sclerosing Hodgkin disease limited to anterior mediastinum. Contrast-enhanced CT scan shows multiple discrete rounded opacities within mass, indicating massive adenopathy. This differs from thymoma shown in Fig. 9 in that interfaces in lymphomatous mass are due to multiple nodes that are present on scans before and after contrast enhancement.

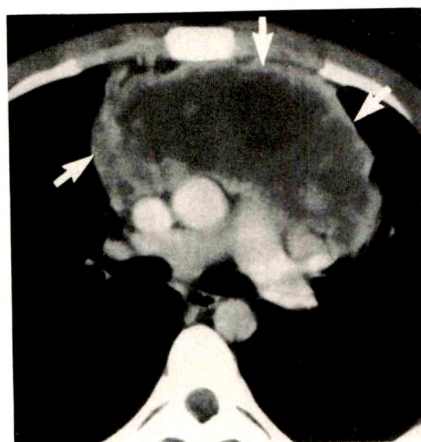


Fig. 14.—21-year-old man with non-Hodgkin lymphoma involving anterior mediastinum. Initial CT scan shows predominantly cystic/necrotic character of mass (arrows).

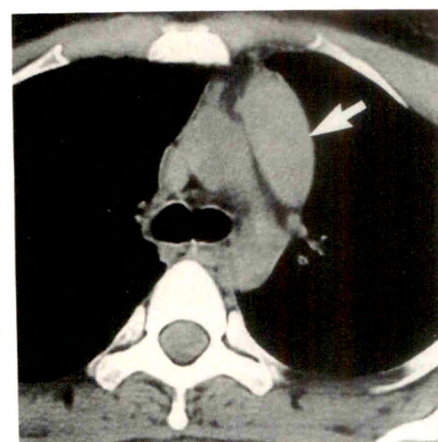


Fig. 15.—26-year-old woman with non-Hodgkin lymphoma who had extensive adenopathy of anterior mediastinum before treatment. After radiation therapy and remission, CT scan shows left lobe of thymus (arrow), which remained enlarged but unchanged during a 12-month interval.

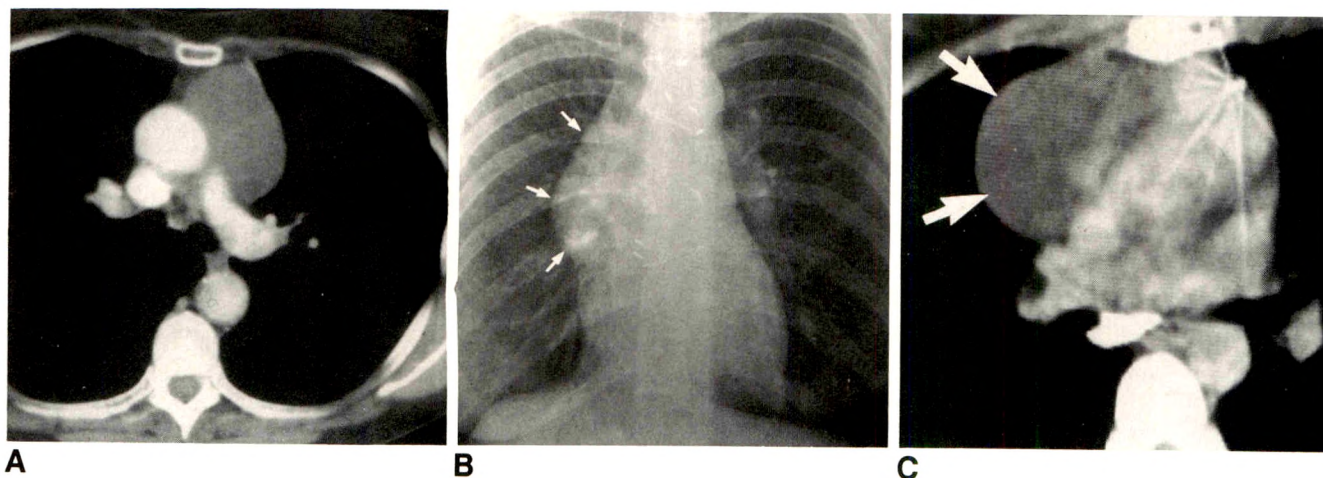


Fig. 16.—A, 72-year-old woman with anterior mediastinal mass of recent onset. Contrast-enhanced CT scan shows anterior mediastinal mass with low attenuation and density similar to that of water, typical of benign thymic cyst. Diagnosis was confirmed surgically.

B and C, 42-year-old woman who had thymoma resected 8 years earlier. Chest radiograph (B) shows slowly enlarging mediastinal mass (arrows). CT scan (C) shows benign cyst (arrows) of right thymic bed. Presumably, this developed postoperatively.

treatment with radiation or chemotherapy are not rare. They may occur with thymoma, teratoma, lymphoma, and lymphangioma. On CT, they usually show a fairly prominent soft-tissue component, but in some instances, the cyst predominates with little adjacent neoplastic soft tissue. These may resemble true congenital thymic cysts.

Thymolipoma.—These tumors often grow quite large before detection and are composed of lobules of fat and thymic tissue. They constitute 2–9% of all thymic neoplasms and are most common in adolescents and young adults. Because they are relatively soft, they frequently are asymptomatic. Occasionally they are associated with myasthenia gravis, Graves disease, aplastic anemia, or hypogammaglobulinemia.

Plain films show an anterior mediastinal mass, often of rather low density and quite large. The tumor may mimic an enlarged heart, enlarged fat pad, or a pericardial cyst. CT, however, usually shows a large bilobulated mediastinal mass with attenuation values approaching those of fat (Fig. 17). On spin-echo T1-weighted MR images, the mass has a strong signal intensity because of its fatty composition [32].

Mediastinal thyroid.—Most mediastinal thyroid masses are cervicomedial goiters extending from the neck into the anterosuperior mediastinum. About 75–80% of mediastinal goiters are situated anteriorly and 20–25% posteriorly, in the anterosuperior mediastinum. Multinodular or adenomatous goiters are characterized by a markedly enlarged gland distorted by multiple nodules and surrounded by a fibrous capsule. Areas of hemorrhage, calcification, and cystic degeneration within the mass are common.

On plain films, the mass is in the anterosuperior mediastinum, causing smooth displacement and often narrowing of the trachea. Areas of calcification frequently are present. These lesions are often identified on radioisotope scans because of their uptake of iodine-123.

Mediastinal thyroid masses also may be identified by CT scanning. Glazer et al. [33] described diagnostic CT findings in five representative cases: (1) anatomic continuity with the cervical portion of the thyroid gland, (2) focal calcification, (3) relatively high CT number on unenhanced CT scans, (4) increase in CT number after a bolus injection of contrast material, and (5) prolonged enhancement after administration of contrast material. Most also show a capsule, with the displaced mediastinal vessels arranged somewhat concentrically around the mass. We prefer CT to MR imaging in evaluating these lesions because of the specific CT appearance.

Ectopic parathyroid adenoma.—The parathyroid glands are derived from the third and fourth branchial pouches. Up to 25% of patients have more than four normal glands [34]. In patients with persistent hyperparathyroidism after adequate parathyroid surgery, an ectopic adenoma or hyperplastic gland located in the mediastinum must be considered. In one series [34], mediastinal parathyroid tumors occurred in 22% of patients operated on for hyperparathyroidism and 38% of those requiring further surgery for hyperparathyroidism. Eighty-one percent of these tumors were located in the anterior mediastinum, and 19% were located along the posterolateral wall of the esophagus or in the posterior mediastinum. Patients with profound hypercalcemia tended to have larger tumors.

Although some of these ectopic lesions are located within the thymus, most mediastinal extrathymic parathyroid adenomas can be recognized on CT as small rounded masses, 1–2 cm in diameter, in the upper portion of the anterior mediastinum (Fig. 18). Small isolated lymph nodes in this area can resemble an adenoma. Functioning mediastinal parathyroid cysts have been reported but are rare [35]. Some authors [34] prefer to use MR imaging to localize mediastinal parathyroid adenomas because no contrast material is required and

Fig. 17.—Asymptomatic 76-year-old man in whom anterior mediastinal mass was found incidentally on chest radiograph. Contrast-enhanced CT scan shows large, homogeneously fatty mass (arrow) typical of thymolipoma. Mass was not resected.



17

Fig. 18.—71-year-old man with persistent hyperparathyroidism after cervical exploration. Small mass (arrow) in anterior mediastinum was identified during surgery as a 1.2-cm ectopic parathyroid adenoma.



18

artifacts caused by the shoulders are not present. If hemorrhage into this vascular tumor occurs, both T1- and T2-weighted images show the lesion to have high signal intensity [31].

Lymphangioma and hemangioma.—Lymphangiomas and cystic hygromas are tumorlike congenital anomalies consisting of spaces that are lined with endothelial cells and can vary from capillary size to several centimeters in diameter. When these spaces contain chyle, the tumors are classified as lymphangiomas or cystic hygromas, depending on the size of the spaces. Many consider the two as variants of the same anomaly. In our experience [36], purely anterior mediastinal lymphangiomas occur in middle-aged patients, are usually asymptomatic, and have no specific characteristics on radiographs.

However, lymphangiomas and cystic hygromas in the anterosuperior portion of the mediastinum can be diagnosed more often. Most of these occur in young patients (average age, 11 years), extend from a cervical or supraclavicular location, recur postoperatively, cannot be removed completely surgically because of their proximity to vital structures in the neck, and become infected at some time before surgery.

Plain films show elongated masses extending through the thoracic inlet from the neck. The tumor usually causes tracheal deviation. CT scans are diagnostic, showing cervical mediastinal lesions of near water density. The combination of the clinical findings with CT findings makes diagnosis possible. Many lymphangiomas do not require surgery if they do not grow.

T2-weighted MR images usually show thin-walled, multiloculated cystic masses of high signal intensity. If the fluid in the mass has a high fat content, T1-weighted images show relatively high signal intensity [31].

In generalized lymphangiomatosis (cystic angiomas), lymphangiomas can coexist with hemangiomas, and they are difficult to distinguish histologically and with imaging techniques.

Pure hemangiomas of the anterior mediastinum can be diagnosed by CT if they contain calcified phleboliths.

Conclusions

Whereas many anterior mediastinal masses appear similar on plain films, the use of CT or MR imaging and knowledge of certain important details in the clinical history will allow correct diagnosis in many cases. In a patient 40–60 years old with an anterior mediastinal mass, pleural metastasis, myasthenia gravis, red cell hypoplasia, or hypogammaglobulinemia, thymoma is likely. A similar mass in a patient with Cushing syndrome or MEN I syndrome should be a mediastinal carcinoma. If the mass contains fatty material, dense calcification, cystic areas, or mixed low-attenuation contents, consider teratoma. Lymphomas often present as masses of lymph nodes with adenopathy elsewhere, and lung invasion along the bronchovascular sheaths is not uncommon. Masses purely cystic on CT or MR imaging may be thymic cysts, lymphangiomas, or cystic hygromas, and clinical history and anatomic position are helpful in separating them. On CT, a mass with high attenuation before and after contrast enhancement and arising in anatomic continuity with the lower pole of the thyroid represents a goiter. A mass situated in the anterior mediastinum of a young patient that is purely fatty on CT or MR imaging is usually a thymolipoma.

Although some anterior mediastinal masses will not lend themselves to a specific diagnosis, this review emphasizes that a specific diagnosis can be made in many cases, thus aiding in the surgical approach or nonsurgical clinical management.

REFERENCES

1. Glazer HS, Molina PL, Siegel MJ, Sagel SS. High-attenuation mediastinal masses on unenhanced CT. *AJR* 1991;156:45–50
2. Heitzman ER. *The mediastinum: radiologic correlations with anatomy and pathology*. St. Louis: Mosby, 1977:86–123

3. Baron RL, Lee JKT, Sagel SS, Peterson RR. Computed tomography of the normal thymus. *Radiology* **1982**;142:121-125
4. Spritzer C, Gamsu G, Sostman HD. Magnetic resonance imaging of the thorax: techniques, current applications, and future directions. *J Thorac Imaging* **1989**;4(2):1-18
5. Choyke PL, Zeman RK, Gootenberg JE, Greenberg JN, Hoffer F, Frank JA. Thymic atrophy and regrowth in response to chemotherapy: CT evaluation. *AJR* **1987**;149:269-272
6. Baron RL, Lee JKT, Sagel SS, Levitt RG. Computed tomography of the abnormal thymus. *Radiology* **1982**;142:127-134
7. Lewis JE, Wick MR, Scheithauer BW, Bernatz PE, Taylor WF. Thymoma: a clinicopathologic review. *Cancer* **1987**;60:2727-2743
8. Brown LR, Muhm JR, Gray JE. Radiographic detection of thymoma. *AJR* **1980**;134:1181-1188
9. Ellis K, Gregg HG. Thymomas—roentgen considerations. *AJR* **1964**;91:105-119
10. Chen J, Weisbrod GL, Herman SJ. Computed tomography and pathologic correlations of thymic lesions. *J Thorac Imaging* **1988**;3(1):61-65
11. Batra P, Herrmann C Jr, Mulder D. Mediastinal imaging in myasthenia gravis: correlation of chest radiography, CT, MR, and surgical findings. *AJR* **1987**;148:515-519
12. Rosai J, Higa E. Mediastinal endocrine neoplasm, of probable thymic origin, related to carcinoid tumor: clinicopathologic study of 8 cases. *Cancer* **1972**;29:1061-1074
13. Brown LR, Aughenbaugh GL, Wick MR, Baker BA, Salassa RM. Roentgenologic diagnosis of primary corticotropin-producing carcinoid tumors of the mediastinum. *Radiology* **1982**;142:143-148
14. Marchevsky AM, Kaneko M. *Surgical pathology of the mediastinum*. New York: Raven, **1984**
15. Suzuki M, Takashima T, Itoh H, Choutoh S, Kawamura I, Watanabe Y. Computed tomography of mediastinal teratomas. *J Comput Assist Tomogr* **1983**;7:74-76
16. Brown LR, Muhm JR, Aughenbaugh GL, Lewis BD, Hurt RD. Computed tomography of benign mature teratomas of the mediastinum. *J Thorac Imaging* **1987**;2:66-71
17. Fulcher AS, Proto AV, Jolles H. Cystic teratoma of the mediastinum: demonstration of fat/fluid level. *AJR* **1990**;154:259-260
18. Blomli V, Lien HH, Fosså SD, Jacobsen AB, Stenwig AE. Computed tomography in primary non-seminomatous germ cell tumors of the mediastinum. *Acta Radiol* **1988**;29:289-292
19. Lee KS, Im J-G, Han CH, Han MC, Kim C-W, Kim WS. Malignant primary germ cell tumors of the mediastinum: CT features. *AJR* **1989**;153:947-951
20. Fosså SD, Kullmann G, Lien HH, Stenwig AE, Ous S. Chemotherapy of advanced seminoma: clinical significance of radiological findings before and after treatment. *Br J Urol* **1989**;64:530-534
21. Panicek DM, Toner GC, Heelan RT, Bosl GJ. Nonseminomatous germ cell tumors: enlarging masses despite chemotherapy. *Radiology* **1990**;175:499-502
22. Panicek DM, Harty MP, Scicutella CJ, Carsky EW. Calcification in untreated mediastinal lymphoma. *Radiology* **1988**;166:735-736
23. Thomas F, Cosset JM, Cherel P, Renaudy N, Carde P, Piekarski JD. Thoracic CT-scanning follow-up of residual mediastinal masses after treatment of Hodgkin's disease. *Radiother Oncol* **1988**;11:119-122
24. Uematsu M, Kondo M, Tsutsui T, et al. Residual masses on follow-up computed tomography in patients with mediastinal non-Hodgkin's lymphoma. *Clin Radiol* **1989**;40:244-247
25. Nyman RS, Rehn SM, Glimelius BLG, Hagberg HE, Hemmingsson AL, Sundström CJ. Residual mediastinal masses in Hodgkin disease: prediction of size with MR imaging. *Radiology* **1989**;170:435-440
26. Webb WR. MR imaging of treated mediastinal Hodgkin disease. *Radiology* **1989**;170:315-316
27. Heron CW, Husband JE, Williams MP. Hodgkin disease: CT of the thymus. *Radiology* **1988**;167:647-651
28. Krech WG, Storey CF, Umiker WC. Thymic cysts: a review of the literature and report of two cases. *J Thorac Surg* **1954**;27:477-493
29. Jaramillo D, Perez-Atayde A, Griscom NT. Apparent association between thymic cysts and prior thoracotomy. *Radiology* **1989**;172:207-209
30. Merine DS, Fishman EK, Zerhouni EA. Computed tomography and magnetic resonance imaging diagnosis of thymic cyst. *J Comput Tomogr* **1988**;12:220-222
31. Molina PL, Siegel MJ, Glazer HS. Thymic masses on MR imaging. *AJR* **1990**;155:495-500
32. Shirkhoda A, Chasen MH, Eftekhari F, Goldman AM, Decaro LF. MR imaging of mediastinal thymolipoma. *J Comput Assist Tomogr* **1987**;11:364-365
33. Glazer GM, Axel L, Moss AA. CT diagnosis of mediastinal thyroid. *AJR* **1982**;138:495-498
34. Clark OH. Mediastinal parathyroid tumors. *Arch Surg* **1988**;123:1096-1099
35. Linos DA, Schoretsanitis G, Carvounis E. Parathyroid cysts of the neck and mediastinum: case report. *Acta Chir Scand* **1989**;155:211-216
36. Brown LR, Reiman HM, Rosenow EC III, Gloviczki PM, Divertie MB. Intrathoracic lymphangioma. *Mayo Clin Proc* **1986**;61:882-892

Bronchus Sign on CT in Peripheral Carcinoma of the Lung: Value in Predicting Results of Transbronchial Biopsy

Michele Gaeta¹
 Ignazio Pandolfo²
 Santi Volta¹
 Elvio G. Russi³
 Giovanni Bartiromo¹
 Gianfranco Girone²
 Francesco La Spada⁴
 Mario Barone⁴
 Giuseppe Casabianca⁴
 Anselmo Minutoli¹

The bronchus sign on CT represents the presence of a bronchus leading directly to a peripheral pulmonary lesion. We investigated the value of this sign in predicting the results of transbronchial biopsy and brushing in 33 consecutive cases of proved peripheral bronchogenic carcinoma studied with thin-slice CT (2-mm-thick sections). The bronchus sign was seen on CT in 22 patients and was absent in 11. Transbronchial biopsy and brushing showed peripheral carcinoma in 13 (59%) of 22 patients in whom the bronchus sign was seen on CT and in only two (18%) of 11 patients in whom it was not seen. The difference is statistically significant (Fisher's exact test, $p = .029$). When analyzed by the order of involved bronchus, a 90% success rate of transbronchial biopsy and brushing was found in patients in whom the bronchus sign was seen at a fourth-order bronchus ($p = .01$). This compared with a success of 33% when the bronchus sign was seen at fifth-, sixth-, or seventh-order branches.

Our results suggest that the bronchus sign at a fourth-order bronchus is valuable in predicting the success of transbronchial biopsy and brushing. The presence of the sign on CT may be useful in determining if the workup should include transbronchial biopsy and brushing or transthoracic needle aspiration in patients with peripheral lung lesions.

AJR 157:1181-1185, December 1991

Controversy exists about whether the first diagnostic procedure used to obtain a tissue sample of a peripheral lung mass or nodule should be via a percutaneous or transbronchial approach [1]. The bronchus sign on CT is the finding of a bronchus leading directly to a peripheral pulmonary mass [2]. We studied the value of this CT appearance in predicting the sensitivity of transbronchial biopsy and brushing in the diagnosis of peripheral carcinomas.

Materials and Methods

We retrospectively reviewed CT examinations and results of transbronchial biopsy and brushing in 33 patients (24 men and nine women 34-73 years old) with proved peripheral bronchogenic carcinomas (mean diameter, 3.2 ± 1.1 cm). Bronchogenic carcinoma was diagnosed in 15 patients by transbronchial biopsy and brushing, in 11 patients by transthoracic needle aspiration, in four patients by surgery, in two patients by biopsy of metastases after progression of disease, and in one patient by biopsy done with forceps of the bronchial wall. Histology revealed adenocarcinoma in 14 patients, squamous cell carcinoma in nine patients, small-cell carcinoma in four patients, large-cell carcinoma in four patients, and adenosquamous carcinoma in two patients.

According to Gibbs and Seal [3] and Hayata [4], a peripheral bronchogenic carcinoma is one that arises distal to a segmental bronchus.

CT examinations were done with a Somatom DR scanner with a 256×256 matrix. Scanning of 2-mm-thick sections was done from the hilum of the lung up to the lesion. Lesions were targeted by a zoom factor between 3 and 5, resulting in a pixel size of 0.66-0.40 mm. All scans were acquired with patients in suspended deep inspiration, and scanning times were 1.2-3.0 sec. For each patient, the CT study was evaluated by three radiologists

Received April 4, 1991; accepted after revision July 17, 1991.

¹ Diagnostic Imaging Service, Piemonte Hospital, via Spadafora 98124 Messina, Italy. Address reprint requests to M. Gaeta, via Sicilia 24, c/o fam. Sciabà, 98124 Messina, Italy.

² Institute of Radiologic Sciences, University of Messina, Policlinico Gazzi, 98100 Messina, Italy.

³ Satellite Unit of Biomedical Technology IST Genova, c/o Institute of Clinical Oncology, University of Messina, Messina, Italy.

⁴ Institute of Thoracic Surgery, University of Messina, c/o Piemonte Hospital, 98124 Messina, Italy.

0361-803X/91/1576-1181

© American Roentgen Ray Society

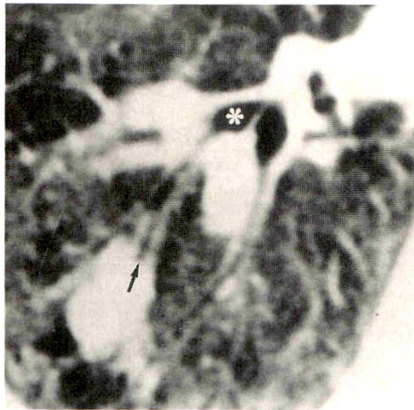
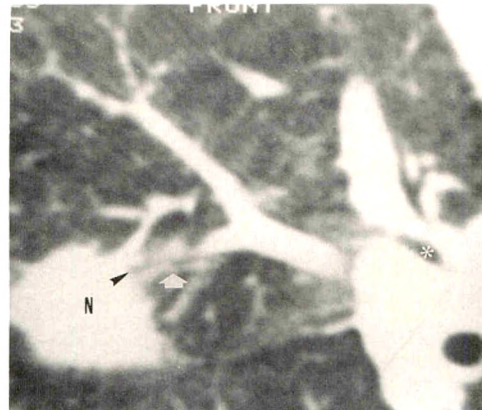
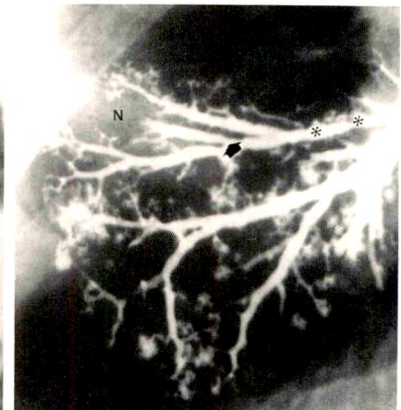


Fig. 1.—Bronchus sign on CT. CT scan through lower lobe of right lung shows fifth-order branch of lateral basal segmental bronchus (B9) (asterisk) leading to 16-mm nodule. Arrow shows point of bronchial obstruction. Transbronchial biopsy showed squamous cell carcinoma.



A



B

Fig. 2.—Bronchial stenosis causing false-negative findings on transbronchial biopsy. A, CT Scan through middle lobe of lung shows a 25-mm nodule (N). Fifth-order branch (arrow) of lateral segmental bronchus (B4) (asterisk) leads to and is obstructed by nodule (arrowhead). Fluoroscopy showed that endoscopic bioptic instruments failed to reach lesion. B, Selective bronchography of middle lobe of lung. Stenosis at origin of bronchus (arrow) leading to nodule (N) explains failure of transbronchial biopsy. Asterisks = lateral segment bronchus (B4).

for the presence of the bronchus sign, and a consensus interpretation was obtained.

We considered the CT finding of one or more bronchi leading directly to or contained within the nodule or mass to represent the bronchus sign, as defined by Naidich et al. [2]. The order of the bronchi leading to the lesion also was assessed. When two or more bronchi were involved, the order of the more proximal bronchus was tabulated. Moreover, we measured the greatest diameter of the lesions (at soft-tissue window setting) and assessed the relationship of the lesions to the nearest visceral pleural surface (pleurally based or not).

After the CT examinations, bronchoscopy was done under biplane fluoroscopic guidance. In two patients with suspected peribronchial-submucosal neoplastic spread, a deep biopsy of the bronchial wall also was done.

In nine patients who had the bronchus sign on CT but in whom transbronchial biopsy did not show peripheral carcinoma, selective bronchography was done to determine the cause of the false-negative biopsy. Bronchography was performed immediately after bronchoscopy in seven patients in whom the biopsy instruments failed to reach the lesion, as confirmed fluoroscopically. In the remaining two cases, bronchography was performed some days later, after histologic examination of the biopsy specimen failed to show carcinoma.

In 14 patients with false-negative biopsy results, CT-guided trans-thoracic needle aspiration was performed with a 19-gauge cutting needle.

Standard nomenclature and letter-number codes for the bronchi were derived from Ikeda [5].

Results

The bronchus sign was seen on CT in 22 (67%) of 33 patients (Fig. 1). The bronchus sign was seen at a fourth-order bronchus in 10 patients, at a fifth-order bronchus in eight, at a sixth-order bronchus in three, at a seventh-order bronchus in one. In 13 (59%) of 22 patients with the bronchus sign on CT, diagnosis was established by transbronchial biopsy. Conversely, in only two (18%) of 11 patients without

the bronchus sign on CT was the diagnosis made with transbronchial biopsy. Statistical analysis showed that the presence of the bronchus sign on CT is valuable in predicting the likelihood of transbronchial biopsy's showing peripheral carcinoma (Fisher's exact test, $p = .029$).

In nine (90%) of 10 patients with a bronchus sign at a fourth-order bronchus, carcinoma was shown by transbronchial biopsy, vs four (33%) of 12 patients with a bronchus sign at a fifth-, sixth-, or seventh-order bronchus ($p = .01$).

Transbronchial biopsy showed carcinoma in only 23% (three of 13 patients) when the greatest diameter of the lesion was 3 cm or less, vs 60% when the greatest diameter of the lesion was more than 3 cm ($p = .04$). Conversely, no significant correlation was found between the yield of transbronchial biopsy and the relationship of the neoplasms to the pleura ($p > .05$).

Selective bronchography was done in nine patients with the bronchus sign on CT but in whom carcinoma was not evident on transbronchial biopsy; the relationship between the tumor and the bronchial tree was confirmed in all cases. In two patients, bronchography showed bronchial stenosis unrelated to neoplasm as the cause of the false-negative biopsy results (Fig. 2).

We found three causes for the failure of the transbronchial biopsy in eight patients with the bronchus sign on CT: (1) bronchial stenosis unrelated to the neoplasm (two cases, Fig. 2), (2) the tumor-bronchus relationship prevented obtaining a sample of tumor by endoscopic bioptic instruments [6] (three cases, Figs. 3 and 4), and (3) neoplastic involvement of very small peripheral bronchi (three cases, Fig. 5). In the remaining patient with the bronchus sign on CT and false-negative results of transbronchial biopsy, the cause of biopsy failure could not be demonstrated.

In two patients who did not have the bronchus sign on CT, transbronchial biopsy showed bronchogenic carcinoma. The failure of CT to detect a bronchus leading to a lesion was due

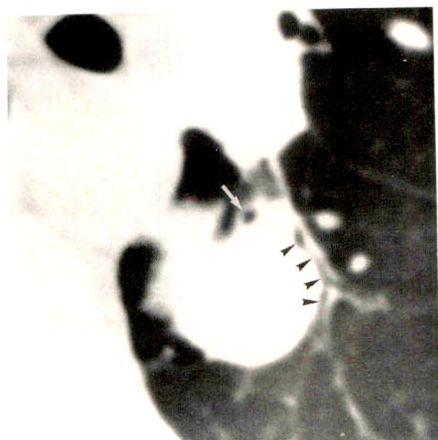
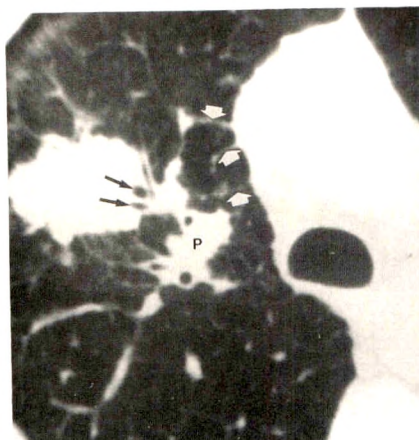
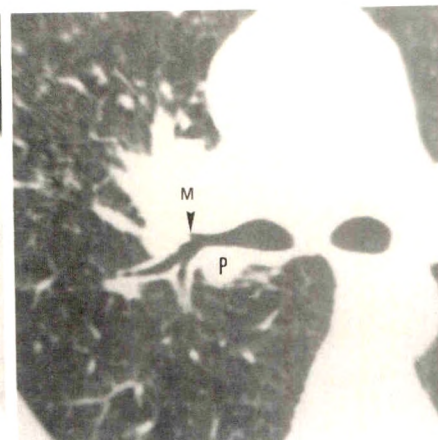


Fig. 3.—Tsuboi type 3 carcinoma [6]. CT scan through B6 segment shows medial (arrow) and lateral (arrowheads) branches of B6a bronchus contained in margin of 26-mm pulmonary nodule. Both fifth-order bronchi are patent, but lateral one is narrowed. Results of transbronchial biopsy and brushing did not show tumor, despite accurate cannulation of leading bronchi. Results of trans-thoracic needle aspiration revealed a large-cell carcinoma. At surgery, bronchi were compressed by tumor with no neoplastic infiltration of bronchial mucosa.



A



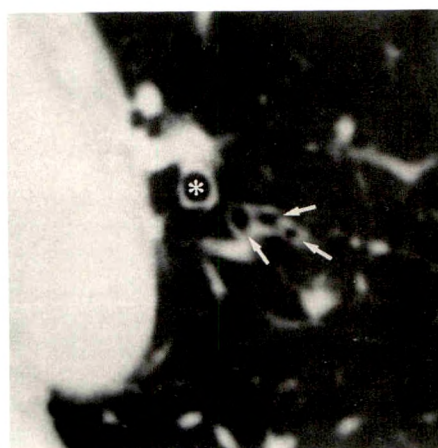
B

Fig. 4.—Tsuboi type 4 carcinoma [6].

A, CT scan shows 4- by 3-cm carcinoma with fifth-order bronchi (black arrows) leading to it (bronchus sign) in anterior segment of right upper lobe. Neoplastic spread along peribronchial lymphatics (P) is present. Kerley B lines probably result from neoplastic lymphangitis along interlobular septa (white arrows).

B, CT scan through right hilum shows peribronchial neoplastic extension (P) along posterior wall of right upper lobe and main bronchi. Anterior segmental bronchus (B3) (arrowhead) is compressed by nodal mass (M).

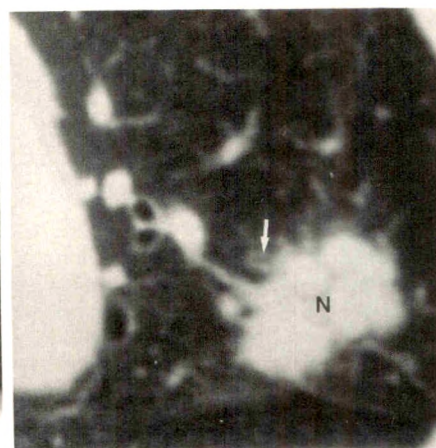
Bronchoscopy showed narrowing of anterior segmental bronchus (B3) with stretched but otherwise intact mucosa. Transbronchial biopsy was unsuccessful. Histologic specimen, obtained by biopsy with forceps, from wall of anterior segmental bronchus showed submucosal neoplastic spread with intact mucosa.



A



B



C

Fig. 5.—Unsuccessful transbronchial biopsy in carcinoma with bronchus sign at a sixth-order bronchus.

A, CT scan through upper lobe of left lung shows fourth- and fifth-order branches (arrows) of posterior segmental bronchus (B2). Asterisk = apical segmental bronchus (B1).

B, CT scan obtained 2 mm above A shows further bronchial bifurcation (arrows).

C, In a section 2 mm above B, subtle sixth-order bronchus (arrow) leads to 28-mm nodule (N).

Despite presence of bronchus sign of CT, fluoroscopy showed that endoscopic bioptic instruments were unable to reach lesion.

to peritumoral fibrosis and bullae in one patient and could not be explained in the other patient.

Discussion

The reported diagnostic accuracy of fluoroscopically guided transbronchial biopsy of peripheral bronchogenic carcinomas

varies from 40% to 75% [7–10]. Ono et al. [11] improved the diagnostic rate (98%) for peripheral cancer by first studying the location of pulmonary lesions with selective bronchography; however, fluoroscopically guided transbronchial biopsy cannot be performed immediately after bronchography and is not routinely done before transbronchial biopsy in patients with suspected bronchogenic carcinoma.

Transthoracic needle aspiration is a useful procedure with a high diagnostic efficacy. The reported success rate of transthoracic needle aspiration in peripheral lung carcinoma has exceeded 85% in recent series [12–14]. However, complications such as pneumothorax, hemorrhage, and air embolism can occur more commonly than with transbronchial biopsy [15].

The bronchus sign on CT is not pathognomonic of malignancy [16]. We have seen it in benign peripheral lung lesions (e.g., pulmonary infarct, inflammatory pseudotumor, tuberculoma).

In the study of Naidich et al. [2], 65 lung lesions were examined with 10-mm-thick CT sections; 35 (54%) of these were associated with a bronchus sign on CT. In 21 (60%) of these 35 lesions, the diagnosis was established by bronchoscopy. In the study of Naidich et al., the diagnostic yield of transbronchial biopsy in patients without the bronchus sign on CT was 30%, whereas in our study it was lower (18%). The different scanning techniques (10- vs 2-mm-thick sections) can explain the difference, because Naidich et al. [2] reported a transbronchial biopsy showing carcinoma in the absence of a bronchus sign on CT in only one (14%) of seven cases studied with 1.5-mm-thick sections. Therefore, we may assume that the bronchus sign can be overlooked on thicker CT sections in some cases.

Moreover, we attempted to correlate the order of the involved bronchi and results of transbronchial biopsy and brushing and to detect causes of false-negative results of transbronchial biopsy in patients with bronchus sign on CT. We found that the presence of the bronchus sign at a fourth-order bronchus is the best predictive factor of transbronchial biopsy's showing carcinoma. In nine (90%) of 10 patients in our study with the bronchus sign at a fourth-order bronchus, the diagnosis was established by transbronchial biopsy. Because of the higher complication rate from transthoracic needle aspiration, we think that the transbronchial approach should be used first in these patients. Conversely, transthoracic needle aspiration should be preferred in patients with a lower likelihood of transbronchial biopsy's showing carcinoma so that radiation exposure to both patient and operator that occurs during fluoroscopically guided transbronchial biopsy is avoided.

Furthermore, we determined the reasons for failure of transbronchial biopsy in eight of nine patients with the bronchus sign on CT. Preexisting bronchial diseases unrelated to neoplasm, particularly stenosis or distortion of the bronchus leading to the carcinoma, explained some cases of failure. Selective bronchography is the method of choice in diagnosing such a cause (Fig. 2).

The anatomic relationship between peripheral bronchogenic carcinomas and bronchi as well as its influence on the yield of transbronchial biopsy have been studied by Tsuboi et al. [6]. These authors classified the tumor-bronchi relationship into four types: (1) in type 1, the bronchial lumen is patent up to the tumor; (2) in type 2, the bronchus is contained in the tumor mass; (3) in type 3, the bronchus is compressed and narrowed by the tumor but the bronchial mucosa is intact; and (4) in type 4, the proximal bronchial tree is so narrowed

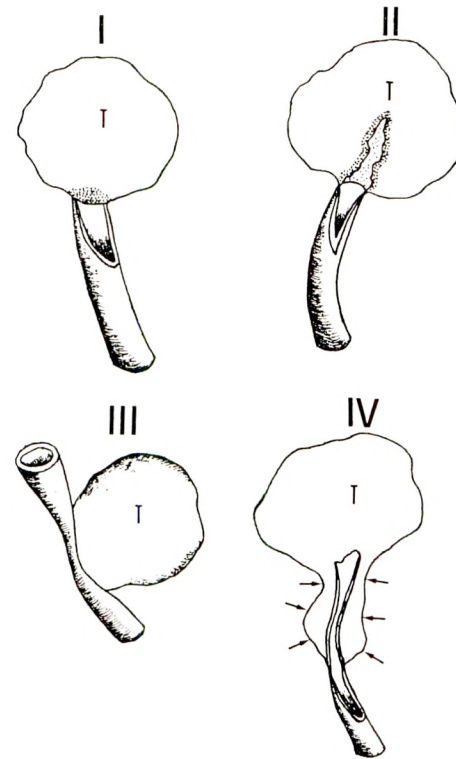


Fig. 6.—Schematic drawing shows four types of carcinoma defined by Tsuboi et al. [6]. I–IV represent Tsuboi types 1–4, respectively. T = tumor; arrows = peribronchial-submucosal neoplastic spread; stippling indicates neoplastic tissue that can be sampled by biopsy.

by peribronchial or submucosal spread of the tumor or by the enlarged nodes that endoscopic biopsy instruments cannot reach the lesion (Fig. 6). In their types 3 and 4, tumor cells cannot be obtained by transbronchial biopsy and brushing. CT and bronchoscopy can suggest peribronchial-submucosal neoplastic spread (Tsuboi type 4) (Fig. 4). This has significance when planning a biopsy with forceps of the bronchial wall or transbronchial needle aspiration [17–19]. We found one surgically demonstrated case of Tsuboi type 3 carcinoma (Fig. 3). Compressed but otherwise patent bronchi at the edge of the lesion and transbronchial biopsy that did not show carcinoma despite accurate cannulation of the leading bronchi were the features in this case. The potential role of thin-section CT in diagnosing Tsuboi type 3 carcinoma has yet to be evaluated in a larger series.

In our series, three cases in which transbronchial biopsy failed to show carcinoma involved small, peripheral sixth- or seventh-order bronchi leading to a subpleural carcinoma (Fig. 5). For cases such as these, Radke et al. [7] conclude that “cannulation of a single peripheral bronchus supplying a small lesion is a matter of fortuitous bronchial anatomy or chance.” Therefore, the bronchus sign on CT, when caused by small, peripheral bronchi, seems to have little value in predicting the diagnostic yield of transbronchial biopsy.

In conclusion, we think that thin-section CT of peripheral pulmonary lesions can be used to plan whether transbronchial biopsy or transthoracic needle aspiration should be done.

REFERENCES

- Cummings SR, Lillington GA, Richard RJ. Managing solitary pulmonary nodules. *Am Rev Respir Dis* **1986**;134:453-460
- Naidich DP, Sussman R, Kutcher WL, Aranda CP, Garay SM, Ettenger NA. Solitary pulmonary nodules: CT-bronchoscopic correlation. *Chest* **1988**;93:595-598
- Gibbs AR, Seal RM. The histological varieties of bronchial carcinoma. In: Bates M, ed. *Bronchial carcinoma: an integrated approach to diagnosis and management*. Berlin: Springer-Verlag, **1984**:129-145
- Hayata Y. *Lung cancer diagnosis*. Tokyo: Igaku-Shoin, **1982**:4
- Ikeda S. *Atlas of flexible bronchofiberscopy*. Tokyo: Igaku-Shoin, **1974**:58-71
- Tsuboi E, Ikeda S, Tajima M, Shimosato Y, Ishikawa S. Transbronchial biopsy smear for diagnosis of peripheral pulmonary carcinoma. *Cancer* **1967**;20:687-698
- Radke JR, Conway WA, Eyer WR, Kvale PA. Diagnostic accuracy in peripheral lung lesions. Factors predicting success with flexible fiberoptic bronchoscopy. *Chest* **1979**;76:176-179
- Cortese DA, McDougall JC. Biopsy and brushing of peripheral lung cancer with fluoroscopic guidance. *Chest* **1979**;75:141-145
- Zavala DC. Diagnostic fiberoptic bronchoscopy: techniques and results of biopsy in 600 patients. *Chest* **1975**;68:12-19
- Shiner RJ, Rosenman J, Katz I, Reichart N, Hershko E, Yellin A. Bronchoscopic evaluation of peripheral lung tumours. *Thorax* **1988**;43:887-889
- Ono R, Loke J, Ikeda S. Bronchofiberscopy with curette biopsy and bronchography in the evaluation of peripheral lung lesions. *Chest* **1981**;79:162-166
- Stanley JH, Fish GD, Andriole JG, et al. Lung lesions: cytologic diagnosis by fine-needle biopsy. *Radiology* **1987**;162:389-391
- Khoury NF, Stitik FP, Erozan YS, et al. Transthoracic needle aspiration biopsy of benign and malignant lung lesions. *ARJ* **1985**;144:281-288
- Johnston WW. Percutaneous fine needle aspiration biopsy of the lung: a study of 1015 patients. *Acta Cytol* **1984**;28:218-224
- Perlmutter LM, Johnston WW, Dunnick NR. Percutaneous transthoracic needle aspiration: a review. *AJR* **1989**;152:451-455
- Mori K, Saitou Y, Tominaga K, et al. Small nodular lesions in the lung periphery: new approach to diagnosis with CT. *Radiology* **1990**;177:843-849
- Naidich DP, Lee JJ, Garay SM, McCauley DI, Aranda CP, Boyd AD. Comparison of CT and fiberoptic bronchoscopy in the evaluation of bronchial disease. *AJR* **1987**;148:1-7
- Shure D, Fedullo PF. Transbronchial needle aspiration in the diagnosis of submucosal and peribronchial bronchogenic carcinoma. *Chest* **1985**;88:49-51
- Wang KB, Haponik EF, Britt EJ, Khouri N, Erozan Y. Transbronchial needle aspiration of peripheral pulmonary nodules. *Chest* **1984**;86:819-823

LIST OF BOOK REVIEWS

- 1186 **Cardiac Catheterization, Angiography, and Intervention**, 4th ed. Grossman W, Baim DS, eds
- 1220 **Magnetic Resonance in Experimental and Clinical Oncology**. Evelhoch JJ, Negendank W, Valeriote FA, Baker LH, eds
- 1238 **Radiology of Musculoskeletal Stress Injury**. Keats TE
- 1242 **Radiology of Syndromes, Metabolic Disorders, and Skeletal Dysplasias**, 3rd ed. Taybi H, Lachman RS
- 1252 **The Visible Human Body: An Atlas of Sectional Anatomy**. von Hagens G, Romrell LJ, Ross MH, Tiedemann K
- 1282 **MRI of the Brain II: Non-Neoplastic Disease**. Brant-Zawadzki M, Bradley WG Jr, eds
- 1324 **Magnetic Resonance Imaging of the Brain and Spine**. Atlas SW, ed

Book Review

Cardiac Catheterization, Angiography, and Intervention, 4th ed. Edited by William Grossman and Donald S. Baim. Philadelphia: Lea & Febiger, 698 pp., 1991. \$59.50

Cardiac Catheterization, Angiography, and Intervention is the fourth edition of William Grossman's textbook, whose earlier editions have become a popular introduction to the cardiac catheterization laboratory. Donald S. Baim has joined Dr. Grossman as a coeditor, and Dr. Baim's contributions have been extended to several chapters. In addition, six new authors have joined a new list of contributors.

The book is organized into eight parts. The first and second parts include well-written and comprehensive chapters on the general principles and techniques of cardiac catheterization. These chapters serve as a generally informative introduction to the imaging equipment, techniques, and the most frequent complications.

An unfortunate deficiency in this section is that less than two full pages is devoted to radiation safety, and the section on film badges from the third edition has been deleted. As most cardiac catheterizations are performed by nonradiologists, an expanded overview of health physics and radiation protection would be beneficial. Considering its importance in the catheterization laboratory, the discussion of contrast media is regrettably inadequate. The bibliography in this section has been updated but is incomplete.

Part 3 deals with hemodynamic principles and is the unchallenged strength of this text. The chapters are clearly written and logically organized. They provide excellent instruction for the uninitiated, yet are detailed enough to be useful as a reference for the more experienced operator. The text and illustrations are integrated in a straightforward manner that gives a unique degree of readability to a section dealing with the complex evaluation of various pressures and gradients. Dr. Grossman's chapter on pressure measurements is superb and should be required reading for anyone who is performing hemodynamic pressure measurements via a catheter in any part of the vascular tree.

Part 4 deals with the techniques used in coronary, pulmonary, and aortic angiography and in cardiac ventriculography. The chapter on coronary angiography is descriptive and well diagramed. However, the number and selection of coronary angiograms are inadequate for the reader to become comfortable with the interpretation of studies routinely performed in the various projections possible with modern equipment. Resolution of this deficiency would bring this book closer

to being the sole introductory text needed for the cardiac catheterization laboratory.

Part 5 is an introduction to the evaluation of cardiac function. The techniques of performing provocative tests used to evaluate the functional resilience of the myocardium and coronary circulation are described. Interpretation is provided, with abundant graphic illustrations, and a list of well-chosen references.

Parts 6 and 7 deal with special techniques such as endomyocardial biopsy and intraaortic balloon counterpulsation devices and interventional techniques such as angioplasty, balloon valvuloplasty, and pediatric interventions. They provide an informative introduction within the space allowed. The chapters on coronary angioplasty, atherectomy, and stents are especially comprehensive, with good quality illustrations and descriptions of the more modern devices in coronary revascularization.

Part 8 presents profiles of various pathologic entities that are likely to be seen in the catheterization laboratory. The format of these chapters is the second outstanding feature of this book. The authors dissect various hemodynamic and angiographic scenarios as the scenarios are related to particular pathologic conditions. They then integrate this information with case histories to illustrate how it is related to the clinical situation. This effective approach "puts it all together," emphasizing the inseparable relationship between quantitative measurements and the physical findings for formulating the correct diagnosis.

Drs. Grossman and Baim have succeeded in their stated objective to compile a book, aimed at cardiology fellows, that would be practical and bring together clear and concise descriptions of the major techniques used in the cardiac catheterization laboratory. This work does have deficiencies; however, its strengths as an introductory text are formidable. This book belongs on the reference shelf in radiology libraries and on the desk of cardiovascular radiology fellows training in the cardiac catheterization laboratory.

John E. Aruny
Brigham and Women's Hospital
Harvard Medical School
Boston, MA 02115

Case Report

Tuberculous Bronchial Stenosis: Treatment with Balloon Bronchoplasty

Kazuyoshi Nakamura,¹ Naohiro Terada, Maki Ohi, Tomohito Matsushita, Noriyuki Kato, and Tsuyoshi Nakagawa

We report two cases of tuberculous bronchial stenosis that were treated with balloon dilatation done through a flexible bronchoscope with the patient under local anesthesia. This procedure is much less invasive and expensive than open surgery and can be performed without the special instruments or sophisticated technique necessary in cryotherapy and laser therapy.

Case Report

A 58-year-old man with fever and dyspnea had pulmonary tuberculosis, for which he was being treated with antituberculous medications. Because of persistent dyspnea on exertion, he was referred to our hospital, where bronchoplasty was done to treat a stenosis in the left main bronchus. During the follow-up period of 16 months after the operation, the dyspnea on exertion was noted to increase and a concentric stenosis at the site of the bronchoplasty was revealed by a bronchoscopic examination. One month after that, balloon dilatation was done as follows: A flexible bronchoscope (Olympus, Tokyo) was inserted in the trachea through a mouthpiece. To determine the appropriate balloon size, we injected a contrast medium (15 ml of propyliodone) through the bronchoscope to outline the stenotic site and the bronchus beyond it. A 0.035-in. (0.09 cm) J guidewire (Terumo, Tokyo) was placed transbronchoscopically through the stenotic bronchus, and then the bronchoscope was withdrawn, leaving only the guidewire. A 7-French, 10-mm angioplastic balloon catheter (Medi-tech, Watertown, MA) was introduced over the wire and placed in the midportion of the stenosis. After that, under fluoroscopic observation, the balloon was inflated with a diluted contrast solution (amidotrizoic acid) from 10 sec to 2 min with a maximal pressure of 6 atm (6.1×10^5 Pa). The balloon inflations were

repeated after the balloon's position was adjusted until the stenosis disappeared. The dilatation of the stenotic bronchus was confirmed by injection of contrast medium through the catheter. Finally, bronchoscopic examination was repeated to check for local trauma or bleeding, and the bronchoscope was removed after aspirating the contrast medium in the bronchi.

For 3 days, the patient had a fever, which responded to broad-spectrum antibiotics. No other complications occurred. One week later, bronchoscopic and bronchographic examinations showed an increase from 4.6 to 6.0 mm in the diameter of the left main bronchus (Fig. 1). One month after balloon dilatation, pulmonary function tests showed improved lung volumes and large-airway obstruction. ^{81m}Kr ventilation scintigraphy performed after the bronchial dilatation showed improved ventilation in the left lung, which had been hypoventilated on the scintigram obtained before dilatation. After balloon dilatation, the patient was followed up for 8 months, and during that period he had no recurrence of dyspnea on exertion.

Discussion

Techniques used to treat bronchial stenosis include surgical resection, cryotherapy, laser photoresection, and balloon dilatation. Immediate cure of the stenosis after cryotherapy and laser photoresection has been reported. However, these procedures require expensive instruments and experienced personnel. Gruentzig balloon dilatation was introduced in 1974 for percutaneous transluminal angioplasty of the iliac and femoropopliteal arteries [1]. Balloon dilatation was first used to treat tracheobronchial stenosis by Cohen et al. [2] in 1984 and has been used in two children and five adults to treat

Received May 28, 1991; accepted after revision July 16, 1991.

¹ All authors: Department of Radiology, School of Medicine, Mie University, 2-174 Edobashi, Tsu City Mie 514, Japan. Address reprint requests to K. Nakamura.

AJR 157:1187-1188, December 1991 0361-803X/91/1576-1187 © American Roentgen Ray Society

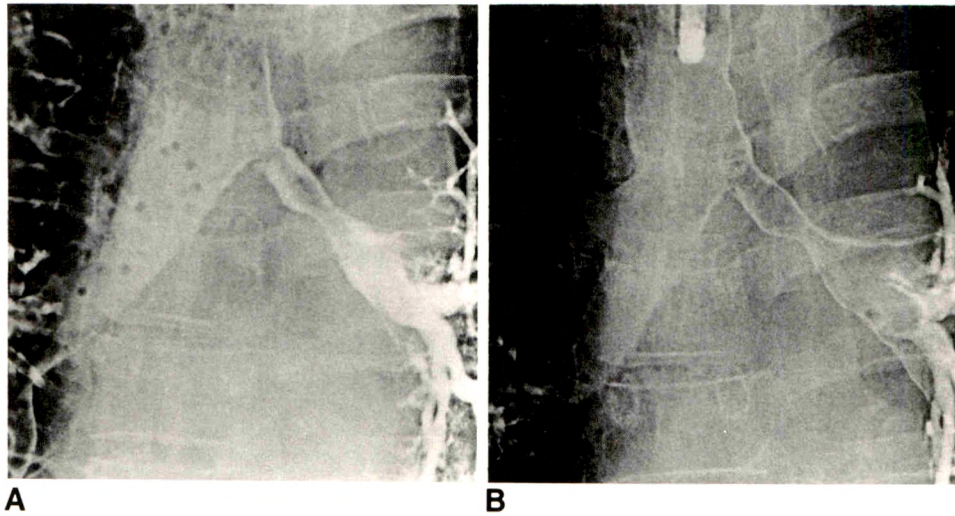


Fig. 1.—58-year-old man with stenosis of left main bronchus caused by pulmonary tuberculosis.

A, Bronchogram just before balloon dilatation shows narrowing of left main bronchus. Stenosis is most marked in proximal portion of bronchus at its origin.

B, Bronchogram after balloon dilatation shows improvement of stenosis, with smooth mucosa at original stenotic site.

bronchial stenoses of various causes: congenital stenosis, tracheal intubation, bronchoplasty to treat cancer, mediastinal fibrosis, aspiration of a pill, radiation therapy, and bronchial artery embolization [3]. All the cases had immediate good results, with follow-up study ranging from 2 to 14 months. We have found no English-language reports describing the use of balloon dilatation to treat tuberculous bronchial stenosis. We also performed balloon dilatation in a 46-year-old woman with stenosis of the left main bronchus caused by pulmonary tuberculosis, and her signs of wheezing and difficulty of coughing up sputum were relieved after the procedure.

All adults treated, except one, received general anesthesia. A balloon catheter was introduced through a rigid bronchoscope in all cases. Balloon dilatation was performed easily by using a flexible bronchoscope with the patient under local anesthesia. Bleeding and bronchial wall rupture are potential complications of this procedure; however, to our knowledge, no reports of these complications have been published. A few days of fever also may occur after this procedure, but this sign occurs after any kind of bronchoscopic procedure.

Involvement of the trachea and major bronchi is not rare in pulmonary tuberculosis. Bronchial obstruction has several pathologic mechanisms, including tuberculous constriction of the bronchial wall, impinging peribronchial nodes, occluding mural tuberculoma, and intraluminal caseous plug.

The balloon dilates the stenotic bronchus by stretching and expanding the bronchial wall [4]; therefore, we think this method is appropriate for the treatment of cicatric anular strictures such as tuberculous stenosis. Many reports have been published on treatment of bronchial stenosis by using laser photoresection with good results in cases of stenosis caused by tumors. In these cases, the stenosis is dilated by burning and resecting tumors. However, in the cases of cicatric stenosis, laser therapy may have a risk of bronchial

perforation. That is why we think that balloon dilatation is appropriate for cicatric anular strictures.

An expanding stainless steel stent originally used for vascular stenoses was modified for tracheobronchial use by Wallace et al. [5]. Although their preliminary findings showed good results with this technique, the disadvantage of this method is that the stent, once inserted, cannot be removed and, besides that, in some cases, the stent can be dislodged in the bronchus. That is why we do not use this technique as the first choice for the treatment of bronchial stenosis. However, we think that the stent should be used if restenosis occurs after several attempts with balloon dilatation.

We obtained immediate good results treating tuberculous bronchial stenosis with balloon dilatation performed with the patient under local anesthesia. This procedure is much less invasive and costly than open surgery. It is also easier and less costly than other interventions, such as cryotherapy and laser photoresection, and it can be done on an outpatient basis. Because of these advantages, we think balloon dilatation could be the first choice for treating cicatric bronchial stenosis.

REFERENCES

1. Gruntzig A, Hoff H. Perkutane Rekanalisation Chronischer Arterieller Verschlüsse mit einem neuen Dilatationskatheter. *Dtsch Med Wochenschr* 1974;99:2502-2510
2. Cohen MD, Weber TR, Rao CC. Balloon dilatation of tracheal and bronchial stenosis. *AJR* 1984;142:477-478
3. Girard P, Baldeyrou P, Lemoine G, Grunewald D. Left main-stem bronchial stenosis complicating bronchial artery embolization. *Chest* 1990;97:1246-1248
4. Castañeda-Zuñiga WR, Formanek A, Tadavarthy M, et al. The mechanism of balloon angioplasty. *Radiology* 1980;135:565-571
5. Wallace MJ, Charnsangavej C, Ozawa K, et al. Tracheobronchial tree: expandable metallic stents used in experimental and clinical applications. *Radiology* 1986;158:309-312

Complications After Total Gastrectomy and Esophagojejunostomy: Radiologic Evaluation

Marc S. Levine¹
 Adam R. Fisher¹
 Stephen E. Rubesin¹
 Igor Laufer¹
 Hans Herlinger¹
 Ernest F. Rosato²

Total gastrectomy and esophagojejunostomy is an increasingly common operation that is associated with a variety of early and late postoperative complications. Between 1980 and 1990, 26 patients at our hospital who underwent this surgery (19 Roux-en-Y esophagojejunostomies and seven loop esophagojejunostomies) had postoperative upper gastrointestinal studies with water-soluble contrast material or barium. The studies were performed during the early postoperative period (within 30 days after surgery) in seven patients, the late postoperative period (more than 30 days after surgery) in seven patients, or both in 12 patients. Five patients (19%) had anastomotic leaks, four involving the esophagojejunal anastomosis and one the blind-ending jejunal limb. Five patients (19%) had transient narrowing of the esophagojejunal anastomosis during the early postoperative period, probably due to acute postoperative edema and spasm. Six patients (23%) had narrowing of the esophagojejunal anastomosis during the late postoperative period due to anastomotic strictures (three patients) or recurrent tumor (three patients). Alkaline reflux esophagitis was found in three (43%) of seven patients who had a loop esophagojejunostomy. However, two (11%) of 19 patients with a Roux-en-Y esophagojejunostomy had relatively long strictures in the distal esophagus, apparently due to scarring from alkaline reflux esophagitis. Two patients (8%) had an afferent loop obstruction due to metastatic tumor and postsurgical scarring.

Radiologists need to be familiar with the normal postoperative radiologic appearances and the radiologic findings of early and late complications associated with this procedure.

AJR 157:1189-1194, December 1991

During the past decade, total gastrectomy and esophagojejunostomy has become an increasingly common operation for patients with gastric carcinoma or other benign or malignant conditions involving the stomach [1-3]. With advances in surgical technique, surgical mortality rates of 10% or less have been reported [2-4]. Nevertheless, this subject has received little attention in the radiologic literature. We therefore performed a retrospective study of 26 patients who experienced a variety of complications resulting from total gastrectomy and esophagojejunostomy to determine the normal postoperative radiologic appearances and the radiologic findings of early and late complications associated with this procedure.

Materials and Methods

A review of radiology records at our hospital between 1980 and 1990 revealed 26 patients who had undergone postoperative upper gastrointestinal contrast studies after total gastrectomy and esophagojejunostomy. Sixteen of the patients were men, and 10 were women. The mean age at the time of surgery was 60 years (range, 32-82 years). The indications for total gastrectomy were gastric carcinoma in 21 patients, complications associated with a Billroth II procedure in two patients, and breakdown of a vertical banded gastroplasty in one patient. In the remaining two patients, the indications for surgery were unknown.

Received June 3, 1991; accepted after revision July 23, 1991.

¹ Department of Radiology, Hospital of the University of Pennsylvania, 3400 Spruce St., Philadelphia, PA 19104. Address reprint requests to M. S. Levine.

² Department of Surgery, Hospital of the University of Pennsylvania, 3400 Spruce St., Philadelphia, PA 19104.

0361-803X/91/1576-1189
 © American Roentgen Ray Society

A total of 71 postoperative gastrointestinal contrast studies (33 water-soluble contrast studies, 22 single-contrast studies, and 16 double-contrast studies) were performed in these 26 patients. The average number of studies per patient was 2.8 (range, one–seven). Seven patients had contrast studies only during the early postoperative period (within 30 days after surgery), seven patients had contrast studies only during the late postoperative period (more than 30 days after surgery), and 12 patients had contrast studies during both the early and late postoperative periods. In all 19 patients who had radiologic examinations during the early postoperative period, the initial study was performed with water-soluble contrast material (i.e., Gastrografin, Squibb Diagnostics, Princeton, NJ) within 7–14 days after surgery. Seventeen patients had these studies as routine examinations to rule out clinically inapparent leaks before starting oral feeding. The remaining two patients had clinical signs of a leak. If no anastomotic leaks were shown on the initial postoperative study, future studies were performed with barium. Of the 19 patients who had radiologic examinations during the late postoperative period, 17 had reflux-related complaints, dysphagia, or other upper gastrointestinal symptoms. The remaining two had delayed clinical signs of a leak, so Gastrografin rather than barium was used as the contrast medium for those two patients.

The original radiologic reports, radiographs, and medical records were reviewed to determine how the gastrointestinal tract was reconstructed after total gastrectomy. The possibilities included simple loop esophagojejunostomy (Fig. 1A), loop esophagojejunostomy with distal jejunojejunostomy (Fig. 1B), Roux-en-Y esophagojejunostomy (Fig. 1C), and creation of a Roux-en-Y esophagojejunal pouch (Fig. 1D). The radiologic reports and radiographs also were reviewed to determine the radiologic findings of postoperative complications, including anastomotic leaks, anastomotic narrowing or obstruction, jejunoesophageal reflux, esophagitis, strictures, recurrent tumor, and abnormalities involving the small bowel.

Results

Postoperative Anatomy

A loop esophagojejunostomy was performed in all seven patients who underwent total gastrectomy between 1980 and 1983 (Fig. 2A). In three of those cases, a distal jejunojejunostomy also was performed. However, all 19 patients who underwent total gastrectomy after this period had a Roux-en-Y reconstruction with an end-to-side jejunojejunostomy about 40 cm distal to the esophagojejunal anastomosis to prevent reflux of bile or pancreatic secretions into the esophagus. A blind-ending jejunal limb was created in 16 patients (Fig. 2B) and an esophagojejunal pouch in three (Fig. 2C).

Early Complications

Anastomotic leaks.—Three patients (12%) had evidence of anastomotic leaks on water-soluble contrast studies performed during the early postoperative period (Table 1). In two patients who had leaks from the esophagojejunal anastomosis, the leaks appeared radiographically as thin, blind-ending tracks that extended several centimeters from the site of anastomosis (Fig. 3). The third patient had a leak from the blind-ending jejunal limb, appearing as an amorphous extraluminal collection of contrast material adjacent to the bowel (Fig. 4B). In the third patient, two earlier Gastrografin studies had failed to show the leak because of partial obstruction at the esophagojejunal anastomosis that prevented adequate filling of the jejunal limb (Fig. 4A). Two of the patients with

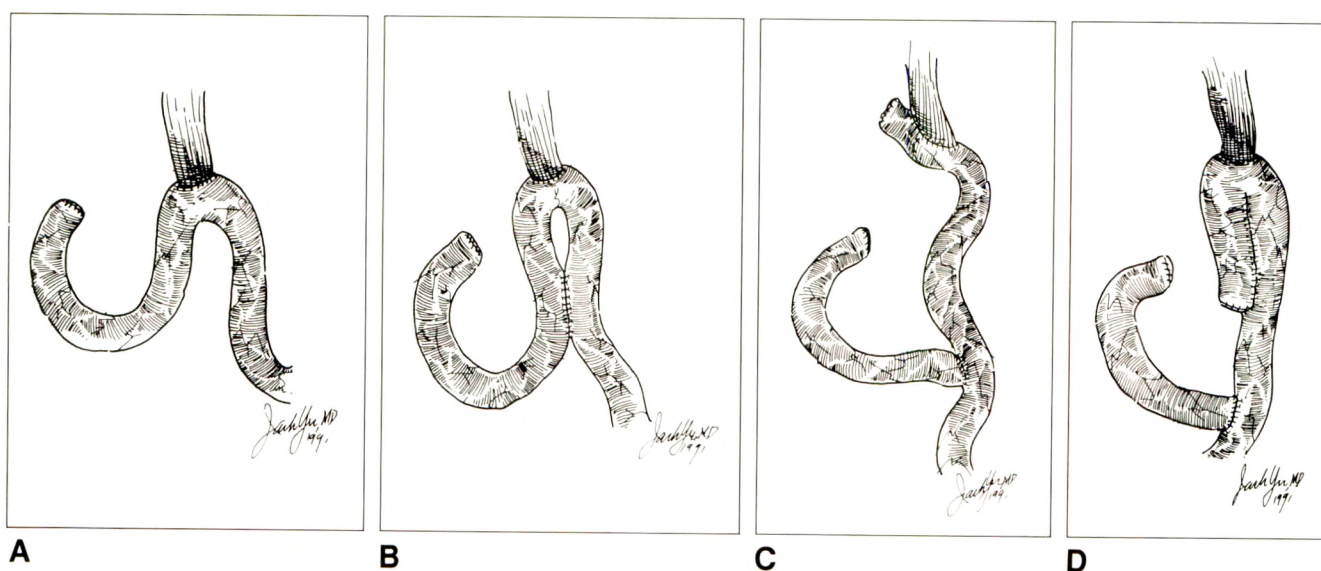


Fig. 1.—Line drawings of various types of total gastrectomy and esophagojejunostomy.

A, Simple loop esophagojejunostomy.

B, Loop esophagojejunostomy with distal jejunojejunostomy.

C, Roux-en-Y esophagojejunostomy.

D, Roux-en-Y esophagojejunal pouch.

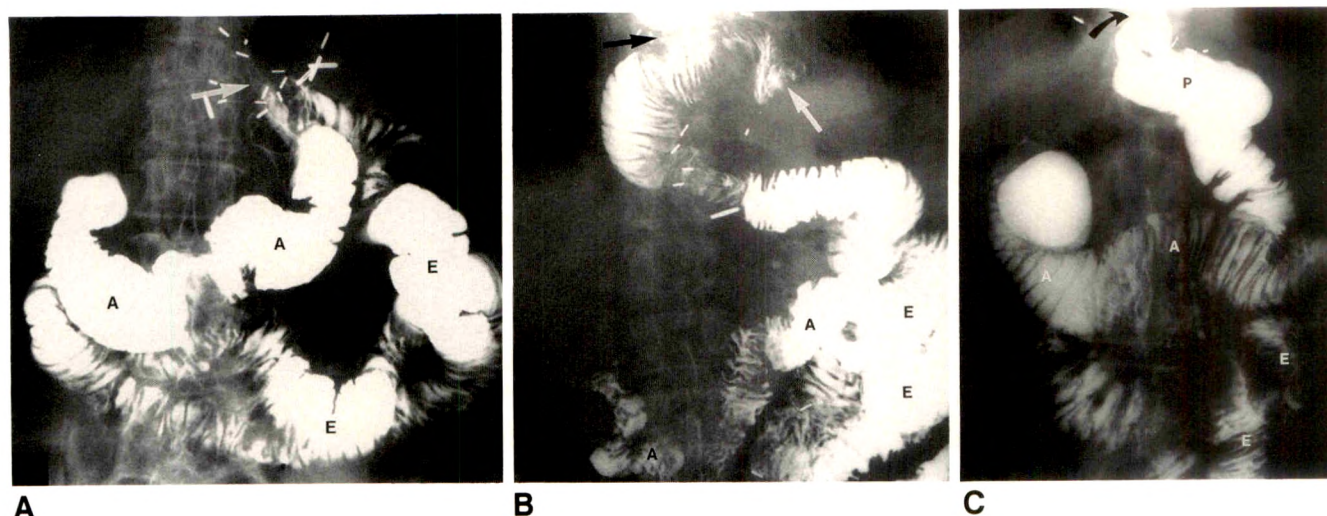


Fig. 2.—Contrast studies show various types of total gastrectomy and esophagojejunostomy.

A, Simple loop esophagojejunostomy. Although esophagus is collapsed, esophagojejunal anastomosis is denoted by arrow. Note barium in afferent (A) and efferent (E) loops of small bowel.

B, Roux-en-Y esophagojejunostomy. Note blind-ending jejunal limb (white arrow) adjacent to esophagojejunal anastomosis (black arrow). Also note afferent (A) and efferent (E) loops of small bowel, although actual site of distal jejunojejunostomy is obscured by overlying jejunum.

C, Roux-en-Y esophagojejunostomy pouch. Note how pouch (P) lies directly below esophagojejunal anastomosis (arrow). Also note Roux-en-Y reconstruction, with barium in afferent (A) and efferent (E) loops of small bowel.

TABLE 1: Summary of Radiologic Findings Associated with Early and Late Complications in 26 Patients After Total Gastrectomy and Esophagojejunostomy

Complications	No. of Patients (%)
Early	
Anastomotic leaks	3 (12)
Anastomotic narrowing or obstruction	5 (19)
Late	
Anastomotic leaks	2 (8)
Jejunoesophageal reflux	8 (31)
Alkaline reflux esophagitis	3 (12) ^a
Anastomotic narrowing	6 (23)
Benign strictures	3 (12)
Recurrent tumor	3 (12)
Esophageal strictures	2 (8) ^b
Recurrent tumor involving small bowel	4 (15)
Small-bowel obstruction	1 (4)
Afferent loop obstruction	2 (8)
Dilated jejunum without obstruction	4 (15)

^a All had simple esophagojejunostomy with or without distal jejunojejunostomy.

^b Both had Roux-en-Y esophagojejunostomy.

anastomotic leaks had fever, leukocytosis, and/or drainage of purulent material or intestinal contents from the surgical drains. In both cases, follow-up contrast studies showed complete healing of the leak on conservative treatment with antibiotics, tube drainage, and parenteral feedings. The third patient, who had a tiny leak from the esophagojejunal anastomosis, did well postoperatively without further radiologic evaluation, so that the leak presumably healed spontaneously.

Anastomotic narrowing or obstruction.—Five patients (19%) had transient narrowing of the esophagojejunal anastomosis during the early postoperative period, with anastomotic diameters from 1.0 to 1.5 cm. Two of the patients had radiologic evidence of obstruction at the esophagojejunal anastomosis, with proximal dilatation and delayed emptying of contrast material into the jejunum (Fig. 4A). Although none of the patients had dilatation procedures, additional contrast studies in all five during the late postoperative period showed that the esophagojejunal anastomosis had increased significantly in caliber with free emptying of contrast material into the jejunum.

Late Complications

Anastomotic leaks.—Two patients (8%) had leaks from the esophagojejunal anastomosis that were first shown on water-soluble contrast studies performed 3 months after surgery in one and 7 months after surgery in the other (Table 1). Both patients had tracks that extended laterally from the anastomosis into abscess cavities in the left upper quadrant of the abdomen (Fig. 5). Both patients were already being treated for a suspected anastomotic leak and an associated subphrenic abscess on the basis of the clinical findings. In one case, the leak healed spontaneously, but in the other, surgical revision of the esophagojejunal anastomosis was required.

Jejunoesophageal reflux and esophagitis.—According to the radiologic reports, jejunoesophageal reflux was observed at fluoroscopy in eight patients (31%). The degree of reflux was classified as marked in four patients, moderate in three, and mild in one. Two patients (8%) with marked jejunoe-

sophageal reflux had radiologic evidence of esophagitis, manifested by thickened folds in one and a nodular mucosa with superficial areas of ulceration in the other (Fig. 6). Both these patients had undergone a loop esophagojejunostomy with

distal jejunostomy. Endoscopy was not performed in either case. A third patient had severe esophagitis shown on endoscopy that had been missed on the barium study because of retained debris in the esophagus. That patient had

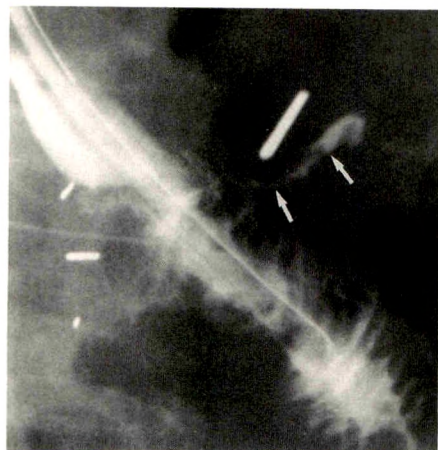
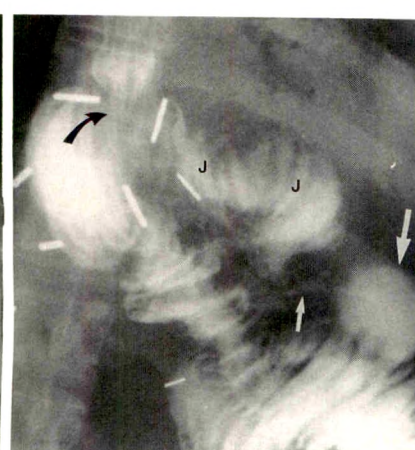


Fig. 3.—Water-soluble contrast study shows anastomotic leak during early postoperative period. Note tiny track (arrows) extending several centimeters laterally from esophagojejunal anastomosis.



A



B

Fig. 4.—Contrast studies of leak from blind-ending jejunal limb during early postoperative period. A, Initial water-soluble contrast study 7 days after Roux-en-Y esophagojejunostomy shows marked narrowing of esophagojejunal anastomosis (arrow), probably due to acute postoperative edema and spasm. Note how esophagus is dilated above anastomosis and how only a small amount of contrast material enters blind-ending jejunal limb (J).

B, Study repeated 5 days later shows widening of esophagojejunal anastomosis (black arrow) and better emptying of contrast material into proximal jejunum. A short track (small white arrow) is now seen extending laterally from blind-ending jejunal limb (J) into extraluminal collection (large white arrow) in left upper quadrant.

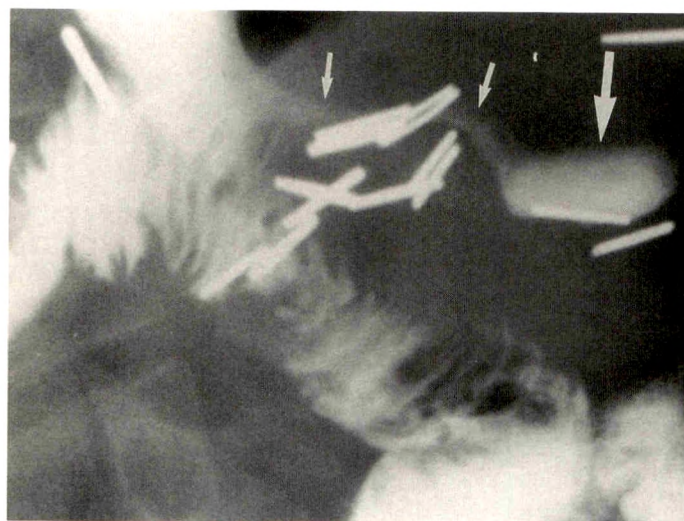


Fig. 5.—Water-soluble contrast study shows anastomotic leak during late postoperative period (i.e., 3 months after surgery). Note track (small arrows) extending laterally from esophagojejunal anastomosis into abscess cavity (large arrow) in left upper quadrant.

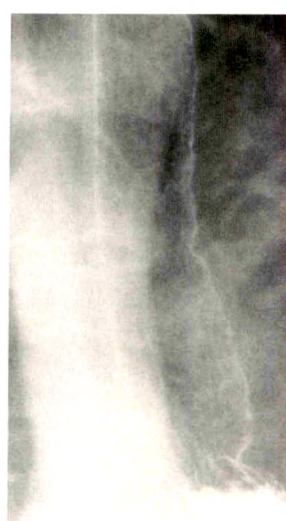


Fig. 6.—Esophagitis seen on double-contrast esophagogram 5 months after loop esophagojejunostomy. Note irregular mucosa and multiple shallow ulcers. Marked jejunoesophageal reflux was observed at fluoroscopy, so the diagnosis of alkaline reflux esophagitis is likely.

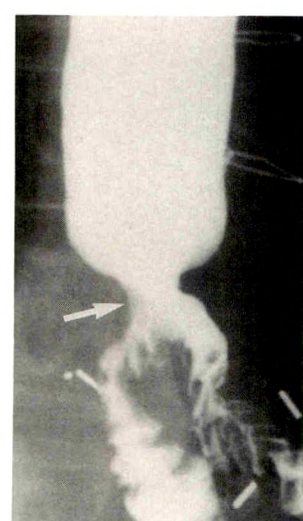


Fig. 7.—Barium study of benign anastomotic stricture with focal area of smooth, tapered narrowing (arrow) in region of esophagojejunal anastomosis. Note how esophagus is dilated above this level.

undergone a simple loop esophagojejunostomy. Esophagitis was therefore detected in three (43%) of seven patients with a loop esophagojejunostomy. As none of the three patients with radiologic or endoscopic evidence of esophagitis had undergone a Roux-en-Y reconstruction to prevent reflux of bile or pancreatic secretions into the esophagus, they all presumably had alkaline reflux esophagitis.

Anastomotic or esophageal strictures.—Six patients (23%) had radiologic evidence of strictures at the esophagojejunal anastomosis from 6 weeks to 7 years after surgery. Four of the patients had dysphagia, but the other two had no esophageal symptoms. The average width of the strictures was 1.3 cm (range, 0.7–2.0 cm).

Three patients had short (<1 cm long), smooth, tapered areas of narrowing in the region of the esophagojejunal anastomosis, probably as a result of postsurgical scarring and fibrosis (Fig. 7). One of these patients underwent endoscopy, which confirmed the presence of a benign-appearing stricture without evidence of tumor on brushings or biopsies from the anastomotic region. Two of the three patients with benign anastomotic strictures had partial obstruction at the esophagojejunal anastomosis with esophageal dilatation and delayed emptying of contrast material into the jejunum.

Three other patients had radiologic evidence of anastomotic strictures that were considered suggestive of recurrent carcinoma. Two had short (<1 cm long), irregular strictures at the esophagojejunal anastomosis, whereas the third had a longer (3 cm long) stricture with eccentric mass effect along one wall of the stricture (Fig. 8). In two of these patients, endoscopic biopsies from the anastomotic region revealed evidence of malignancy. Although the remaining patient did

not undergo endoscopy, the proximal margin of the surgical specimen contained tumor cells.

Two (11%) of 19 patients with a Roux-en-Y esophagojejunostomy had relatively long strictures in the esophagus that extended well above the esophagojejunal anastomosis. One patient had a smooth, tapered, 5-cm-long stricture in the distal third of the esophagus about 3 months after surgery (Fig. 9). The other patient had a short, smooth stricture at the esophagojejunal anastomosis that increased in length to about 3 cm on a follow-up barium study 5 months later. Both these patients had undergone a Roux-en-Y reconstruction to prevent reflux of bile and pancreatic secretions into the esophagus. Nevertheless, the smooth contour and length of the strictures suggest scarring from alkaline reflux esophagitis.

Jejunal abnormalities.—Four patients (15%) had areas of mass effect, nodularity, and/or tethering in the proximal jejunum, probably as a result of recurrent tumor. One of these patients had an associated jejunal obstruction. Two other patients (8%) had radiologic evidence of afferent loop obstruction. One patient with a simple esophagojejunostomy had a high-grade obstruction of the afferent loop near the esophagojejunal anastomosis. Subsequent endoscopy revealed severe stenosis of the opening of the afferent loop due to metastatic tumor at the esophagojejunostomy site. The other patient with a Roux-en-Y esophagojejunostomy had partial obstruction of the afferent loop at the jejunojejunal anastomosis due to postsurgical scarring.

Four patients (15%) had a dilated proximal jejunum (>4.5 cm in diameter) without evidence of obstruction. This jejunal dilatation may have represented an adaptive response of the proximal small bowel after total gastrectomy.



Fig. 8.—Barium study shows recurrent carcinoma at esophagojejunal anastomosis. Note irregular narrowing and eccentric mass effect (arrows) in region of anastomosis. Endoscopic biopsies confirmed presence of tumor.

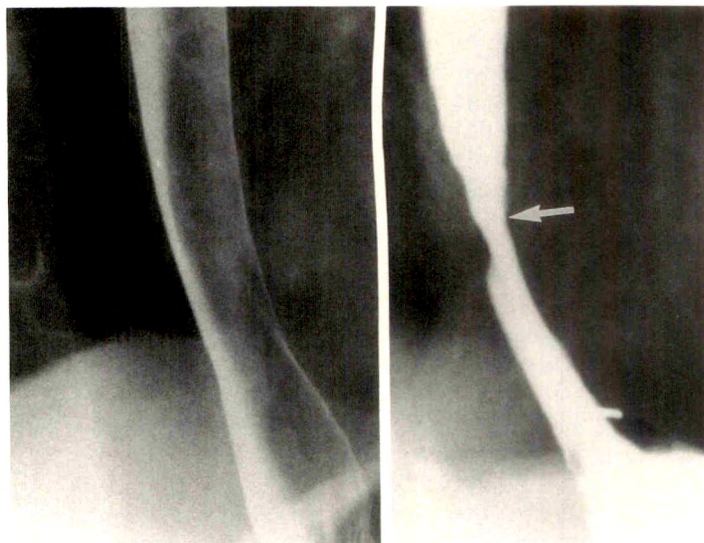


Fig. 9.—Contrast studies showing development of presumed alkaline reflux stricture.

A, Preoperative double-contrast study shows normal-appearing esophagus. However, other views of stomach revealed gastric carcinoma.

B, Study repeated 3 months after Roux-en-Y esophagojejunostomy shows relatively long, tapered stricture (arrow) in distal esophagus, presumably due to scarring from alkaline reflux esophagitis.

Discussion

The most important early complication after total gastrectomy and esophagojejunostomy is anastomotic breakdown, which is responsible for 35–65% of all operative and perioperative deaths [4, 5]. More than 90% of anastomotic breakdowns involve the esophagojejunal anastomosis [6]. However, other potential sites of anastomotic disruption after a Roux-en-Y reconstruction include the duodenal stump, blind-ending jejunal limb or pouch, and jejunojejunal anastomosis [6]. Anastomotic leaks may be manifested on water-soluble contrast studies by thin, blind-ending tracks that extend several centimeters or more from the site of anastomosis (Fig. 3) or by direct visualization of abscess cavities that communicate with the anastomosis via extraluminal tracks of various lengths (Figs. 4 and 5). Some anastomotic leaks may be detected during the late postoperative period (more than 30 days after surgery), as occurred in two of our patients (Fig. 5). It is unclear whether these leaks resulted from delayed anastomotic breakdown or delayed recognition of the breakdown. In any case, gross anastomotic disruptions may require immediate surgery, whereas tiny leaks can be managed conservatively without need for surgical intervention [7].

Anastomotic obstruction is also a frequent finding during the early postoperative period. In our study, water-soluble contrast examinations revealed transient narrowing or obstruction of the esophagojejunal anastomosis in five patients (19%), probably due to acute postoperative edema and spasm (Fig. 4). In contrast, anastomotic narrowing during the late postoperative period may be caused by postsurgical scarring and fibrosis or by recurrent tumor [1], as occurred in six of our patients (23%). Benign anastomotic strictures appeared on radiographs as smooth, tapered areas of narrowing at the esophagojejunal anastomosis (Fig. 7), whereas recurrent tumor was manifested by more irregular areas of narrowing, occasionally associated with areas of eccentric mass effect (Fig. 8). If the findings on radiographs are suggestive of recurrent tumor, endoscopy or CT may be required for a more definitive diagnosis. Although benign anastomotic strictures can be dilated endoscopically, the presence of recurrent tumor may necessitate more aggressive treatment with surgery, irradiation, or chemotherapy.

Because no anatomic sphincter is present at the esophagojejunal anastomosis, jejunoesophageal reflux is a frequent finding after total gastrectomy. It has been shown experimentally that refluxed bile salts and pancreatic enzymes in the esophagus can cause severe alkaline reflux esophagitis [8, 9]. As a result, patients who undergo a simple loop esophagojejunostomy often develop retrosternal burning, regurgitation of bile, or dysphagia due to esophagitis or stricture formation [10–12]. Thus, most surgeons now perform a Roux-en-Y reconstruction, placing the jejunojejunostomy about 40 cm distal to the esophagojejunal anastomosis to prevent reflux of bile and pancreatic secretions into the esophagus [2, 7]. In various series, esophagitis has been found in 25–90% of patients with a loop esophagojejunostomy [10–12] but in only 2–10% of patients with a Roux-en-Y esophagojejunostomy [6, 13, 14]. In our study, esophagitis was found in three (43%) of seven patients who had undergone a loop esophagojejunostomy (Fig. 6). However, two (11%) of

19 patients with a Roux-en-Y esophagojejunostomy had relatively long strictures in the distal esophagus, apparently due to scarring from alkaline reflux esophagitis (Fig. 9). Others also have emphasized that a Roux-en-Y reconstruction decreases the risk of esophagitis or strictures but does not completely eliminate these complications [14]. When strictures are caused by alkaline reflux disease, they tend to be rapidly progressive, increasing in length and severity within a relatively short period [11, 15]. Recent publications suggest that alkaline reflux esophagitis also predisposes to the development of Barrett esophagus [16, 17], but the significance of this observation is doubtful because of the limited life expectancy of most patients who undergo esophagojejunostomy.

In summary, a Roux-en-Y reconstruction seems to be the procedure of choice for patients undergoing total gastrectomy and esophagojejunostomy, because this surgery dramatically decreases the risk of alkaline reflux esophagitis developing. Water-soluble contrast studies can be performed during the early postoperative period to rule out anastomotic breakdown or obstruction, whereas barium studies may be helpful during the late postoperative period to rule out esophagitis, anastomotic or esophageal strictures, recurrent tumor, afferent loop obstruction, or other abnormalities. Radiologists need to be familiar with the normal postoperative radiologic appearances and the radiologic findings of early and late complications associated with this procedure.

REFERENCES

1. Paolini A, Tosato F, Cassese M, et al. Total gastrectomy in the treatment of adenocarcinoma of the cardia. *Am J Surg* 1986;151:238–243
2. Butler JA, Dubrow TJ, Trezona T, Klassen M, Nejdil RJ. Total gastrectomy in the treatment of advanced gastric cancer. *Am J Surg* 1989;158:602–604
3. Gustavsson S, Kelly KA. Total gastrectomy for benign disease. *Surg Clin North Am* 1987;67:539–550
4. Koga S, Kishimoto H, Tanaka K, et al. Results of total gastrectomy for gastric cancer. *Am J Surg* 1980;140:636–638
5. Papachriston DN, Fortner JG. Anastomotic failure complicating total gastrectomy and esophagogastrectomy for cancer of the stomach. *Am J Surg* 1979;138:399–402
6. Sanchez RE, Gordon HE. Complications of total gastrectomy. *Arch Surg* 1970;100:136–139
7. Saario I, Schroeder T, Tolppanen EM, Lempinen M. Total gastrectomy with esophagojejunostomy: analysis of 100 consecutive patients. *Am J Surg* 1986;151:244–246
8. Helsing N. Oesophagitis following total gastrectomy: a clinical and experimental study. *Acta Chir Scand [Suppl]* 1961;273:1–21
9. Salo JA, Kivilaakso E. Role of bile salts and trypsin in the pathogenesis of experimental alkaline esophagitis. *Surgery* 1983;93:525–532
10. Stensrud N. Late results after total gastrectomy for high gastric carcinoma. *Ann Surg* 1959;150:63–66
11. Helsing N. Oesophagitis following total gastrectomy: a follow-up study on 9 patients 5 years or more after operation. *Acta Chir Scand* 1960;118:190–201
12. Morrow D, Passaro ER. Alkaline reflux esophagitis after total gastrectomy. *Am J Surg* 1976;132:287–290
13. Olbe L, Lundell L. Intestinal function after total gastrectomy and possible consequences of gastric replacement. *World J Surg* 1987;11:713–719
14. Salo JA, Kivilaakso E. Failure of long limb Roux-en-Y reconstruction to prevent alkaline reflux esophagitis after total gastrectomy. *Endoscopy* 1990;22:65–67
15. Cox KR. Oesophageal stricture after partial gastrectomy. *Br J Surg* 1961;49:307–313
16. Meyer W, Vollmar F, Bar W. Barrett-esophagus following total gastrectomy. *Endoscopy* 1979;2:121–126
17. Sandvik AK, Halvorsen TB. Barrett's esophagus after total gastrectomy. *J Clin Gastroenterol* 1988;10:587–588

Low-Attenuation Periportal Collar in Transplanted Liver Is Not Reliable CT Evidence of Acute Allograft Rejection

Scott D. Stevens¹
 Jay P. Heiken¹
 Elizabeth Brunt²
 Douglas W. Hanto³
 M. Wayne Flye³

Recent reports indicate that the presence or absence of a periportal low-attenuation rim ("periportal collar" sign) on CT scans is of variable reliability in predicting rejection after liver transplantation. To study this matter further, we reviewed 178 CT scans in 68 patients (74 allografts) after hepatic transplantation. One hundred twenty-one scans were obtained within 7 days of liver biopsy. The presence or absence of a central or peripheral periportal collar on these scans was correlated with the presence or absence of acute rejection found at biopsy. A central periportal collar was defined as an abnormally large amount of low-attenuation material surrounding the main portal vein, the right portal vein, or the left portal vein. A peripheral periportal collar was defined as a low-attenuation area surrounding a portal vein branch distal to the left or right portal veins. A weak, but statistically significant correlation between the presence of a peripheral periportal collar and acute allograft rejection was shown in patients in whom CT scans were obtained within 3 days of biopsy. However, the sensitivity, specificity, accuracy, and positive predictive value of the presence of a peripheral collar in this group were 60%, 67%, 64%, and 63%, respectively. The sensitivity, specificity, accuracy, and positive predictive value of the presence of a central collar in patients scanned within 3 days of biopsy were 74%, 35%, 54%, and 52%, respectively. Negative predictive values of peripheral and central collars were 65% and 59%, respectively.

Our study shows that a periportal collar is seen more commonly in patients with recently transplanted allografts (mean interval after transplantation, 46 days for peripheral collars and 57 days for central collars) and in patients with ascites. The presence of a central or peripheral periportal collar on CT is not sufficiently sensitive, specific, or accurate to reliably diagnose or exclude acute allograft rejection.

AJR 157:1195-1198, December 1991

Orthotopic liver transplantation has become an accepted therapy for end-stage liver disease of various causes. Allograft rejection remains a major cause of morbidity and mortality after transplantation. Because of the need for early and aggressive treatment of acute allograft rejection, hepatic imaging studies have been evaluated for possible early signs of acute rejection that could obviate percutaneous liver biopsy [1, 2]. A region with a relatively low attenuation value approaching that of water commonly surrounds central or peripheral branches of the portal vein on CT scans of hepatic allografts [3]. This region of low attenuation has been called the periportal collar or periportal halo sign [4, 5]. Two recent papers [4, 5] report discordant results concerning the reliability of the periportal collar as a sign of acute allograft rejection. The purpose of this study was to examine a larger series of patients to determine better the reliability of the periportal collar as a sign of acute allograft rejection.

Materials and Methods

At our institution, 123 patients had orthotopic liver transplantation (149 allografts) between August 20, 1985, and June 12, 1990. One hundred eighty-one CT scans were obtained after

Received May 20, 1991; accepted after revision July 23, 1991.

¹ Mallinckrodt Institute of Radiology, Washington University School of Medicine, 510 S. Kingshighway Blvd., St. Louis, MO 63110. Address reprint requests to J. P. Heiken.

² Department of Pathology, Washington University School of Medicine, 660 S. Euclid Ave., St. Louis, MO 63110.

³ Department of Surgery, Washington University School of Medicine, 4960 Audubon Ave., St. Louis, MO 63110.

0361-803X/91/1576-1195
 © American Roentgen Ray Society

transplantation in 68 patients (74 allografts). The quality of three of these scans was technically poor, and they were excluded from further analysis. The remaining 178 scans in 68 patients (74 allografts) formed the basis of the study. Thirty-nine patients were male, and 29 were female. The patients were from 1 to 65 years old (mean, 37 years).

All CT scans were obtained on either a Siemens DRH or Somatom Plus scanner (Siemens Medical Systems, Inc., Iselin, NJ). One hundred fifty-six scans of the liver (88%) used 1-cm scan intervals, and 22 scans used 2-cm scan intervals. Slice thickness was 8–10 mm for all examinations. One hundred twenty-five scans (70%) were obtained without IV contrast material, and 53 scans (30%) were obtained with contrast material, administered as a rapid bolus (125–150 ml at 2.5 ml/sec) by power injector in nearly all cases. Scans were obtained both before and after administration of IV contrast material in 12 patients.

The CT examinations were evaluated retrospectively by two radiologists. Neither knew the biopsy findings on the presence or absence of acute rejection. The CT scans were evaluated for the presence or absence of central or peripheral periportal collars and for the presence of ascites. A central periportal collar was defined as an abnormally large amount of low-attenuation material surrounding the main portal vein, the right portal vein, or the left portal vein (Fig. 1A). A peripheral periportal collar was defined as a low-attenuation area surrounding a portal vein branch distal to the left or right portal veins (Figs. 1A and 1B). The diagnosis of a peripheral collar sign required the presence of two or more peripheral periportal collars. Correlation was made between CT presence of central or peripheral periportal collar and biopsy-proved acute rejection and between CT presence of ascites and central or peripheral periportal collar. Correlation was also made between central and peripheral collars and interval between transplantation and CT examination.

Of the total 178 scans, 121 were obtained within 7 days of liver biopsy (88 within 3 days). For these 121 scans, the pathologic diagnosis of the biopsy performed closest to the date of CT scanning was recorded. Two patients whose biopsies showed chronic rejection were excluded from further analysis. The histopathologic diagnosis of acute rejection was based on criteria that included the triad of mixed portal inflammation, destructive cholangitis, and portal or central venous endotheliitis. Chronic rejection (irreversible rejection) was diagnosed on the basis of a combination of zone 3 cholestasis, hepatocyte ballooning or necrosis, and paucity of bile ducts with or without inflammation [6].

The data were reviewed independently by a biostatistician. The relationship between central or peripheral periportal collars and acute

allograft rejection and the relationship between periportal collars and ascites were analyzed by using either a Chi-square test or Fisher's exact test. Analyses were done on the entire group of CT scans obtained within 7 days of liver biopsy and separately on (1) the group of CT scans obtained within 3 days of biopsy and (2) those done within 4–7 days of biopsy. The relationship between central and peripheral collars and interval between transplantation and CT examination was analyzed by using a nonparametric Wilcoxon rank-sum test. Sensitivity, specificity, accuracy, positive predictive value, and negative predictive value of the presence of peripheral or central periportal collar as a sign of acute allograft rejection were calculated.

Results

Fifty-three (44%) of the liver allografts evaluated on the 121 CT scans obtained within 7 days of liver biopsy were performed in patients who had histologically documented acute rejection. No statistically significant correlation between acute rejection and the presence of a central ($p = .850$) or peripheral ($p = .058$) periportal collar was seen (Table 1). The sensitivity, specificity, accuracy, positive predictive value, and negative predictive value of a peripheral periportal collar as a sign of acute rejection are shown in Table 2.

In the group of 88 scans obtained within 3 days of biopsy, the correlation between the presence of a peripheral periportal collar and acute allograft rejection was statistically significant ($p = .011$, correlation coefficient = .27; Table 3). No statistically significant correlation between acute rejection and a

TABLE 1: Correlation of Periportal Collar Sign and Acute Allograft Rejection on 121 CT Scans Obtained Within 7 Days of Liver Biopsy in Liver Transplantation Patients

Periportal Collar Sign	Rejection (<i>n</i> = 53)	No Rejection (<i>n</i> = 68)	<i>p</i> Value
Central	35 (66)	46 (68)	.850
Peripheral	27 (51)	23 (34)	.058
Central and Peripheral	27 (51)	23 (34)	.058
Not present	18 (34)	22 (32)	—

Note.—Numbers in parentheses are percentages.

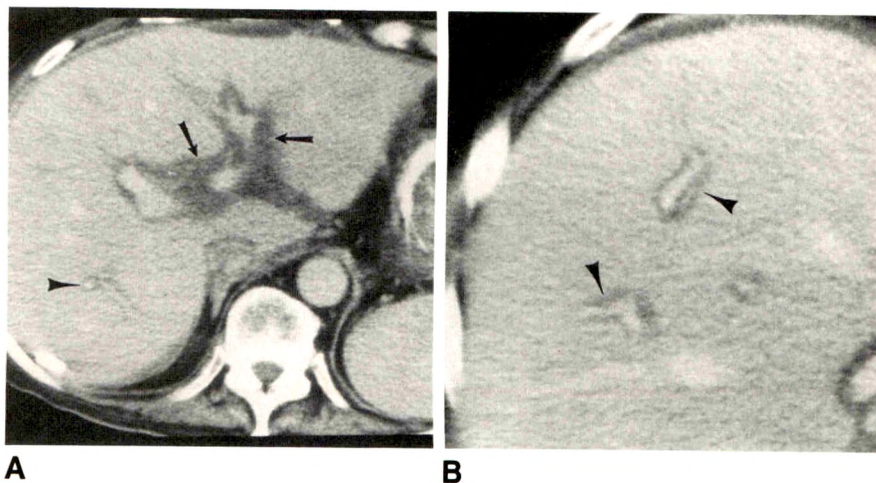


Fig. 1.—Low-attenuation periportal collar on CT scans of 61-year-old man, 3 weeks after hepatic transplantation.

A, Contrast-enhanced CT scan shows central (arrows) and peripheral (arrowhead) periportal collars.

B, A more cephalic section from same CT examination shows two additional peripheral periportal collars (arrowheads).

central periportal collar was shown ($p = .38$). Table 2 lists the sensitivity, specificity, accuracy, positive predictive value, and negative predictive value of a peripheral periportal collar as a sign of acute rejection in this group of patients.

Thirty-three of the 121 scans were obtained within 4–7 days of biopsy. No correlation between acute allograft rejection and either a central ($p = .065$) or a peripheral ($p = .43$) periportal collar was shown in this group (Table 4). The sensitivity, specificity, accuracy, positive predictive value, and negative predictive value of a peripheral periportal collar as a sign of acute rejection in this group are shown in Table 2.

The mean interval after transplantation of allografts with central periportal collars (109 scans, 56 allografts) was 57 days (range, 5–780 days; SD, 91 days). The mean interval after transplantation of those without central periportal collars (69 scans, 35 allografts) was 132 days (range, 5–900 days; SD, 170 days). The difference in mean interval after transplantation between those with and those without a central periportal collar was highly significant ($p = .0001$).

The mean interval after transplantation of allografts with peripheral periportal collars (68 scans, 38 allografts) was 46 days (range, 5–324 days; SD, 63 days). The mean interval after transplantation of those without peripheral periportal collars (110 scans, 53 allografts) was 110 days (range, 5–912 days; SD, 156 days). The difference in mean interval after transplantation between those with and those without a peripheral periportal collar was highly significant ($p = .0001$).

Ascites was present on 85 of 178 scans. Of the scans with ascites, central and peripheral periportal collars were present on 65 (77%) and 42 (49%), respectively. All scans that showed ascites and a peripheral periportal collar also had a central periportal collar. Ascites was absent on 93 of 178 scans. On

TABLE 2: Peripheral Periportal Collar Sign as a Predictor of Acute Rejection of a Hepatic Allograft

	Interval Between CT Scan and Liver Biopsy		
	0–7 days	0–3 days	4–7 days
Sensitivity (%)	51	60	18
Specificity (%)	66	67	64
Accuracy (%)	60	64	48
Positive predictive value (%)	54	63	20
Negative predictive value (%)	63	65	61

TABLE 3: Correlation of Periportal Collar Sign and Acute Allograft Rejection on 88 CT Scans Obtained Within 3 Days of Liver Biopsy in Liver Transplantation Patients

Periportal Collar Sign	Rejection ($n = 42$)	No Rejection ($n = 46$)	p Value
Central	31 (74)	30 (65)	.380
Peripheral	25 (60)	15 (33)	.011
Central and Peripheral	25 (60)	15 (33)	.011
Not present	11 (26)	16 (35)	—

Note.—Numbers in parentheses are percentages.

TABLE 4: Correlation of Periportal Collar Sign and Acute Allograft Rejection on 33 CT Scans Obtained Within 4–7 Days of Liver Biopsy in Liver Transplantation Patients

Periportal Collar Sign	Rejection ($n = 11$)	No Rejection ($n = 22$)	p Value
Central	4 (36)	16 (73)	.065
Peripheral	2 (18)	8 (36)	.430
Central and Peripheral	2 (18)	8 (36)	.430
Not present	7 (64)	6 (27)	—

Note.—Numbers in parentheses are percentages.

these 93 scans, 44 (47%) had a central periportal collar and 26 (28%) had a peripheral periportal collar. The relationship between the presence of ascites and a central or peripheral periportal collar was significant ($p < .001$).

Discussion

Various hepatic imaging techniques including CT have been evaluated for signs of hepatic allograft rejection that could obviate percutaneous liver biopsy [1, 2, 4, 5]. In a study of 17 liver transplantation patients, Wechsler et al. [4] reported that the peripheral periportal collar sign is a sensitive and moderately specific indicator of acute allograft rejection. Kaplan et al. [5] subsequently found that although a peripheral periportal collar does correlate with acute allograft rejection, the low sensitivity and relatively low accuracy of this finding limit its usefulness as a sign of allograft rejection.

Our data, collected from a larger group of patients, indicate that the presence of a central or peripheral periportal collar is not sufficiently sensitive, specific, or accurate to be reliable in diagnosing or excluding acute hepatic allograft rejection. Earlier studies evaluating the periportal collar sign have correlated biopsy results with findings on CT scans obtained within 7 days of liver biopsy. However, an interval greater than 3 days between CT scanning and biopsy may be too long to allow accurate correlation, particularly as most patients start anti-rejection therapy as soon as a biopsy-based diagnosis of rejection is made. In our study, we assessed the correlation between a peripheral periportal collar and acute rejection separately for CT scans obtained within 3 days of biopsy and for those obtained within 4–7 days of biopsy. A weak but statistically significant correlation was found for the group of CT scans obtained within 3 days of biopsy ($p = .011$), whereas no correlation was seen for the group of scans obtained within 4–7 days of biopsy ($p = .43$).

Although a statistical correlation was shown between acute allograft rejection and the presence of a peripheral periportal collar on scans obtained within 3 days of biopsy, the correlation was weak (correlation coefficient = .27). Furthermore, the low sensitivity, specificity, accuracy, and positive and negative predictive values of the peripheral periportal collar sign (all in the 60–67% range) indicate that this sign has little clinical usefulness in distinguishing patients with acute allograft rejection from those with hepatic dysfunction of other causes. Clinical and experimental studies [3, 7] suggest that

periportal low attenuation on CT scans is related to lymphedema. However, acute allograft rejection is only one cause of periportal lymphedema. Other causes include interruption of normal lymphatic drainage by the transplantation procedure, passive hepatic congestion, cholangitis, hepatitis, and graft necrosis [3, 4, 7]. The presence of peripheral and/or central periportal collars on a substantial percentage of scans of patients without acute rejection (34% and 68%, respectively) indicates that periportal low attenuation is a nonspecific finding. In addition to the many possible causes of periportal lymphedema, periportal low attenuation on CT also may be seen with traumatic liver injury, diffuse bile leakage caused by hepatic artery thrombosis, and tracking of ascitic fluid [5, 7, 8]. The fact that periportal collars are seen with greater frequency in patients with a shorter interval after transplantation and in those with ascites supports the role of generalized postoperative lymphedema, most likely caused by surgical interruption of periportal lymphatic vessels, in producing the sign.

REFERENCES

1. Dominguez R, Cuervas-Mons V, Van Thiel DH, Lecky JW, Starzl TE. Radiographic features of liver allograft rejection. *Gastrointest Radiol* **1986**;11:326-329
2. Letourneau JG, Day DL, Maile CW, Crass JR, Ascher NL, Frick MP. Liver allograft transplantation: post-operative CT findings. *AJR* **1987**;148:1099-1103
3. Marincek B, Barbier PA, Becker CD, Mettler D, Ruchti C. CT appearance of impaired lymphatic drainage in liver transplants. *AJR* **1986**;147:519-523
4. Wechsler RJ, Munoz SJ, Needleman L, et al. The periportal collar: a CT sign of liver transplant rejection. *Radiology* **1987**;165:57-60
5. Kaplan SB, Sumkin JH, Campbell WL, Zajko AB, Demetris AJ. Periportal low-attenuation areas on CT: value as evidence of liver transplant rejection. *AJR* **1989**;152:285-287
6. Snover DC. Liver transplantation. In: Sale GE, ed. *The pathology of organ transplantation*. Boston: Butterworths, **1990**:103-132
7. Koslin DB, Stanley JR, Berland LL, Shin MS, Dalton SC. Hepatic perivascular lymphedema: CT appearance. *AJR* **1988**;150:111-113
8. Campbell WL, Zajko AB. Radiology of liver transplantation. In: Taveras JM, Ferrucci JT, eds. *Radiology: diagnosis, imaging, intervention*. Philadelphia: Lippincott, **1988**:4-7

**American Roentgen Ray Society
Residents' Award Papers, 1992**

The ARRS announces competition for the 1992 President's Award and two Executive Council Awards for the best papers concerning the clinical application of the radiologic sciences.

Awards

The winner of the President's Award will receive a certificate and a \$2000 prize. The winners of the two Executive Council Awards will each be given a certificate and a prize of \$1000. The winners will be announced on March 16, 1992. Winning papers will be presented at the ARRS annual meeting at Marriott's Orlando World Center, Orlando, FL, May 10-15, 1992. Winning papers will be submitted for early publication in the *American Journal of Roentgenology*. All other papers will be returned to the authors.

Regulations

Eligibility is limited to residents or fellows in radiology who have not yet completed 4 years of approved training in a radiologic discipline. A letter from the resident's department chairman attesting to this status must accompany the manuscript. The resident must be the sole or senior author and be responsible for all or most of the project.

Submitted manuscripts must not exceed 5000 words and have no more than 10 illustrations. Four copies of the manuscript and illustrations are required. Submitted manuscripts should not contain previously presented or published material and should not be under consideration for publication elsewhere.

Deadline for submissions is February 14, 1992. Send papers to

Nancy O. Whitley, M.D.
Chairman, Committee on Education & Research
American Roentgen Ray Society
Department of Radiology
University of Maryland Medical Systems Hospital
22 S. Greene St.
Baltimore, MD 21201

Endosonography of the Anal Sphincter: Findings in Healthy Volunteers

Michael Bachmann Nielsen¹
 Jan Fog Pedersen¹
 Christina Hauge²
 Ole Ø. Rasmussen²
 John Christiansen²

Knowledge of the normal sonographic features of the anal canal is essential for the detection of anal carcinomas, anal sphincteric defects, or other anal abnormalities with endosonography. The anal sphincters consist of the circular smooth muscle fibers of the internal sphincter and the circular striated muscle fibers of the external sphincter together with the sling-shaped puborectalis muscle. Anal endosonography was performed in 14 healthy women with normal anophysiologic examinations. The procedure was performed during electromyographic registration in five. A radial 7-MHz probe and a multiplane 7-MHz probe were used, and transverse and longitudinal images were obtained. On transverse images, the internal anal sphincter was visualized as a circular hypoechoic band, which on longitudinal images was seen in continuity with the muscularis layer of the rectal wall. The external anal sphincter was seen as a thicker circular echogenic band just outside the internal sphincter. The puborectalis muscle sling, which is the medial part of the levator ani muscle, was visualized in the upper anal canal and had the same echogenic appearance as the external sphincter.

Our experience in volunteers provides information about the normal sonographic features of the anal canal as depicted on anal endosonography with high-frequency probes. The results suggest the procedure may be a useful diagnostic tool in detecting pathologic conditions in the anal canal.

AJR 157:1199-1202, December 1991

The anal sphincters consist of the circular smooth muscle fibers of the internal sphincter and the circular striated muscle fibers of the external sphincter together with the sling-shaped puborectalis muscle. Knowledge of the normal sonographic features of the anal canal is essential if sonography is to be used to detect carcinomas, sphincteric defects, or other abnormalities in the area. Anal endosonography with a rotating axial endoprobe has been described [1]. This technique provides a good overall view of the anal structures but gives no information on the anorectal junction. This, however, can be achieved by multiplanar imaging.

The junction between the lower rectum and the anal canal may be involved in diseases of both the rectum and anal canal. In our opinion, a complete examination should include multiplanar imaging of the anorectal junction and the anal canal. In this article, we describe the endosonographic findings in volunteers.

Received May 2, 1991; accepted after revision July 8, 1991.

The sonographic equipment used in this study was loaned by Brüel & Kjær, Nærum, Denmark.

¹ Department of Radiology and Ultrasound, University of Copenhagen, Glostrup Hospital, DK-2600 Glostrup, Denmark. Address reprint requests to M. B. Nielsen.

² Department of Gastroenterologic Surgery D, University of Copenhagen, Glostrup Hospital, DK-2600 Glostrup, Denmark.

0361-803X/91/1576-1199
 © American Roentgen Ray Society

Subjects and Methods

Fourteen women with no history of anorectal disease or surgery entered the study after informed consent was obtained. All volunteers had normal findings on anal manometry and electromyography (EMG) with an anal sponge electrode. Endosonography was performed with each patient in the left lateral decubitus position. No bowel preparation was used.

The volunteers were studied with a Brüel & Kjær (Nærum, Denmark) sonographic scanner, type 1846, with a 7-MHz rotating endoprobe, type 1850 (focus, 2-5 cm), covered with a hard

anechoic plastic cone (diameter, 17 mm) filled with degassed water. Serial axial images of the anal canal were obtained while this endoprobe was slowly withdrawn.

Next, all volunteers had multiplanar imaging with a Brüel & Kjær 7-MHz endoprobe, type 8551 (focus, 1–6 cm; sector, 112°; diameter, 23 mm). Transverse images were obtained at the 3, 6, 9, and 12 o'clock positions while the probe was slowly withdrawn. With both sphincters in view, the scanning plane was changed to longitudinal, and longitudinal images of the entire anal canal were obtained by rotating the probe.

Before scanning, a water-filled balloon was placed over the tip of the multiplane transducer. As the probe was withdrawn, the balloon remained in the rectum when the probe was in the anal canal. Thus, it was possible to obtain longitudinal images of the lower rectum and the upper anal canal at the same time. The tip of the probe, together with the balloon, can result in some deformation of the structures. However, the balloon is necessary to bring the rectal wall into the focal distance.

The thicknesses of the internal and external sphincters were measured in eight persons.

Four volunteers were scanned during an EMG procedure, with the EMG needle electrode positioned in the external anal sphincter. Under sonographic guidance, another volunteer had a specially designed longer EMG needle placed in the external anal sphincter with the use of the multiplane transducer and its built-in needle guide.

One resected specimen of the rectum and anal canal was examined endosonographically, first in the intact state, visualizing both the circular internal and external sphincters, and then after excising half the circumference of the external sphincter, leaving the internal sphincter intact.

Results

A schematic representation of the anal canal is shown in Figure 1. A transverse anal endosonogram showed the internal anal sphincter as a well-defined, circular, hypoechoic band (Figs. 2A and 2B) with a median thickness of 2 mm (range, 1–3 mm). With longitudinal scanning, the internal sphincter

could be traced to the muscularis layer of the rectal wall (Fig. 3A).

The external anal sphincter was located just outside the internal sphincter and was echogenic. It was visualized with both transverse and longitudinal imaging (Figs. 2 and 3). On a transverse image in the middle of the anal canal (Fig. 1, level 2), the circular muscle fibers of the external sphincter were seen as a broad echogenic band (Fig. 2B) with a median thickness of 6 mm (range, 5–8 mm). In the upper part of the anal canal (Fig. 1, level 1), the puborectalis muscle sling was visualized (Fig. 2A). At this level there was no external sphincter component in the anterior midline. In the lower part of the anal canal (Fig. 1, level 3), the internal sphincter was no longer present, and only the circular external anal sphincter could be seen as it came in close contact with the surface (Fig. 2C). This could also be demonstrated on longitudinal images (Fig. 3).

In all the volunteers scanned while EMG registration of the external sphincter was being done, the needle electrode could be seen positioned in the echogenic sphincteric mass (Fig. 4).

Examination of the resected specimen showed the echogenic band missing that corresponded to the site where the circular external sphincter had been removed, while the hypoechoic internal sphincter was intact.

Discussion

The external anal sphincter is composed of striated muscle fibers. There is no generally accepted descriptive subdivision of the external sphincter, but it is usually divided into deep and superficial compartments. The superficial compartment can be subdivided into subcutaneous and superficial parts. The deep compartment may be subdivided into the deep circular muscle fibers and, deep to them, the associated puborectalis muscle [2], which is also in close contact with

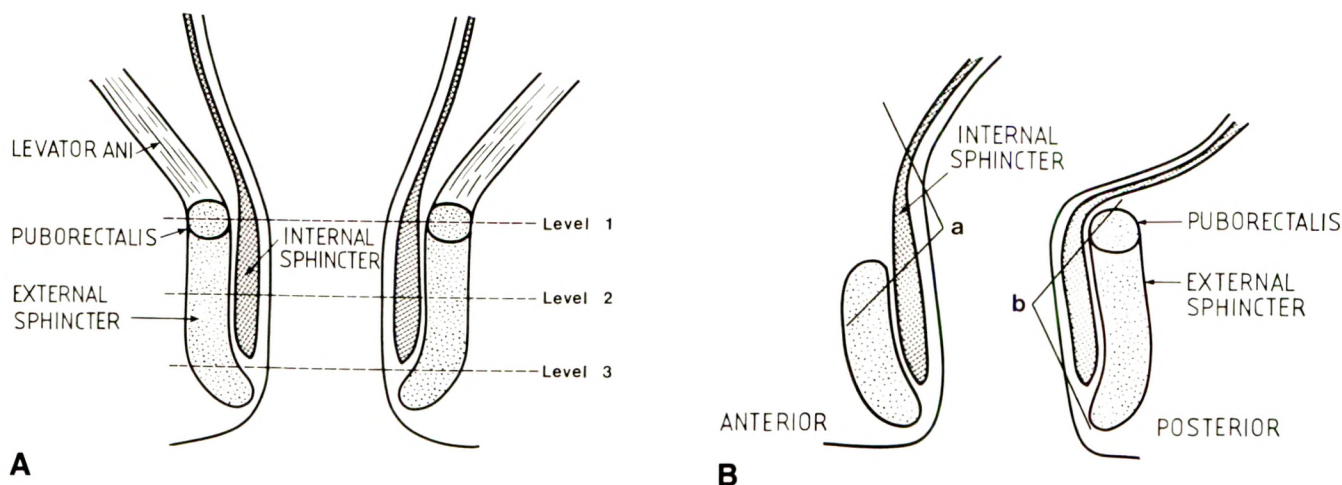


Fig. 1.—Schematic presentation of anal canal.

A and B, Frontal (A) and sagittal (B) sections show internal anal sphincter in continuity with muscularis propria layer of rectal wall. Deep to internal sphincter is circular external anal sphincter, which in lower part of anal canal is in contact with skin and proximally is in continuity with levator ani muscle. Upper part of external sphincter is sling shaped and is called the puborectalis muscle.

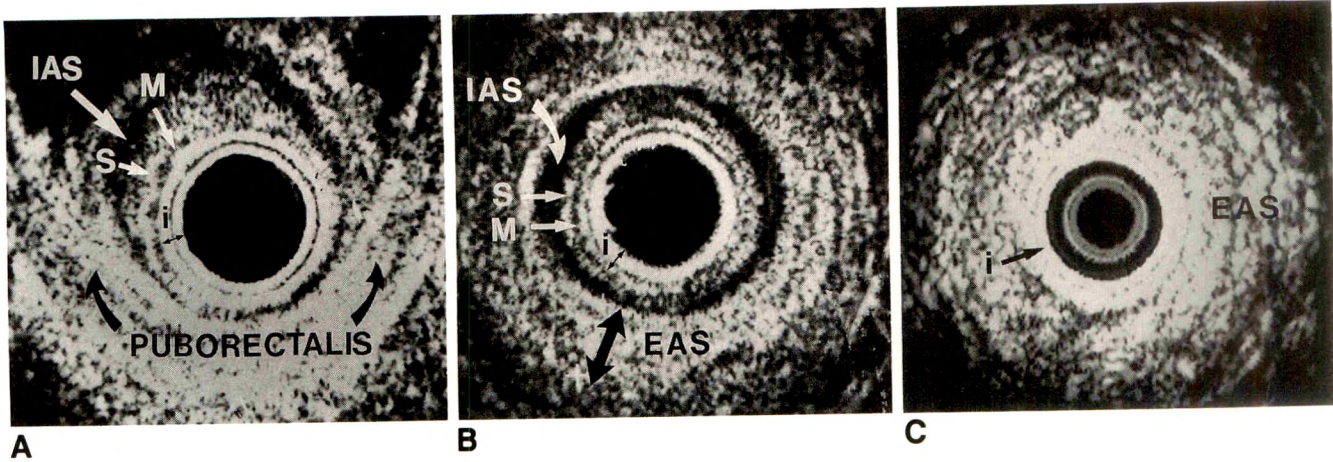


Fig. 2.—Endoluminal anal sonograms. Transverse images (seen from below, up is anterior).

A—C, A corresponds to level 1, B to level 2, and C to level 3 in Fig. 1A. Interface (i) between plastic cone, rubber balloon, and mucosa forms fairly thick echogenic ring sometimes seen as double interface with bright echoes from both the inside and the outside of the plastic cone. Mucosa (M), submucosa (S), and internal anal sphincter (IAS) form hypoechoic, echogenic, and hypoechoic layers, respectively, at levels 1 and 2 (A and B). External anal sphincter (EAS) is echogenic circular structure, at level 2, in contact with internal sphincter, and at level 3, in contact with skin. At level 1, external sphincter is sling shaped and called the puborectalis muscle.

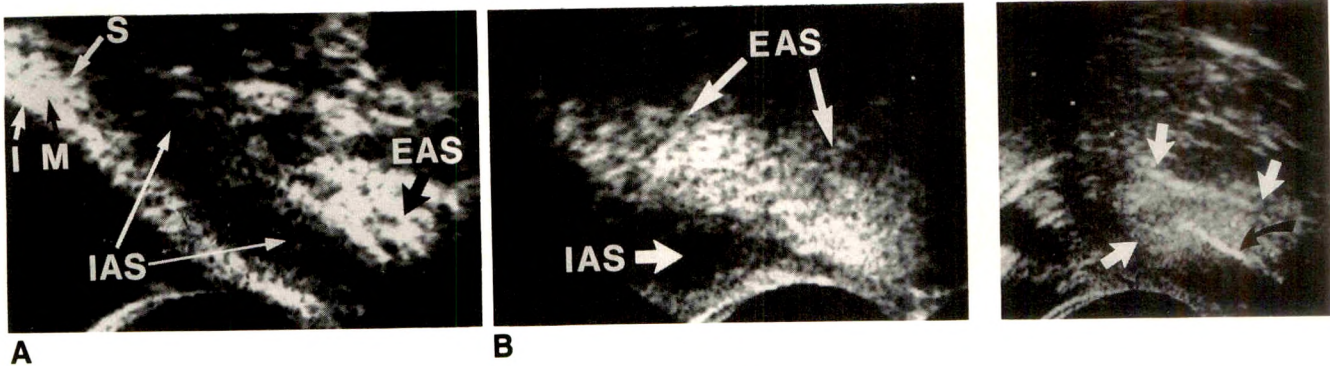


Fig. 3.—Endoluminal anal sonograms. Longitudinal images (left is toward patient's head).

A, Sonogram at upper and intermediate levels of anal canal (sector a in Fig. 1B) shows internal anal sphincter (IAS) in continuity with muscularis propria layer of rectal wall. Other layers include echogenic submucosa (S), hypoechoic mucosa (M), and echogenic interphase between balloon and mucosa (I).
B, Sonogram at intermediate and lower part of anal canal (sector b in Fig. 1B) shows echogenic external anal sphincter (EAS) deep to internal sphincter (at intermediate level) and in close contact to skin (lower level of anal canal). Part of external sphincter is also seen in A.

Fig. 4.—Longitudinal endosonogram shows echogenic external anal sphincter (white arrows). Under sonographic guidance, electromyographic electrode has been inserted into sphincter (black arrow).

the central part of the levator ani muscle [3]. The external sphincter extends farther downward than the internal sphincter, and the most distal part curves medially and comes in close contact with the skin (Figs. 1 and 3B).

Consequently, the sonographic appearance depends on the position and scanning plane of the probe and its level in the anal canal. Of the external anal sphincter, only the puborectalis component can be identified as a separate structure, whereas the remaining components cannot be distinguished from each other with endosonography. As there is no distinct fascia surrounding the external sphincter, the outer limit may sometimes be difficult to define, because the outer muscle fibers mix with the surrounding tissue.

With endosonography, the rectal wall has a typical five-layer structure, with three hyperechoic and two hypoechoic layers (Fig. 3A), as described in other reports [4, 5]. The first layer close to the lumen is hyperechoic and represents the

superficial mucosa and the balloon/surface interface. A similar layer can be seen with anal endosonography (Figs. 2 and 3). The second layer (hypoechoic) and third layer (hyperechoic) represent the mucosa and the submucosa, respectively. Similar layers can be identified in the anal canal (Fig. 2), but as they are in close contact with the endoprobe, they cannot be optimally focused. On longitudinal images, the fourth layer (hypoechoic) of the rectal wall, representing the muscularis propria, is seen in continuity with the internal anal sphincter, but only if the balloon is used to bring the anorectal junction into the focal distance (Fig. 3A). Anatomically, the circular smooth muscle fibers of the muscularis propria continue into the anal canal, where they thicken to become the internal sphincter.

With further retraction of the probe, the balloon remains in the rectum and is not visualized because of the limitation by the sector of 112°. On a longitudinal view at this level (Fig.

3B), the external sphincter is in the focal distance, whereas the internal sphincter is visualized poorly, partly because of the deformation of the structures by the probe. This can be seen by comparing the appearances of the internal sphincter in Figures 3A and 3B.

For imaging of the anal structures, we recommend that each examination begin with a rotating endoprobe. This is easy to use, and because of the 360° axial images it gives a good overall view of the structures. This should be followed by an examination with the multiplane transducer. With a sector of 112°, each quadrant must be examined separately, as previously described.

Anoscopy will reveal lesions that involve the epithelial surface, but is unable to show how deep a tumor penetrates, and it cannot detect perianal tumors if the surface is intact. By digital examination, involvement of deeper structures may be suspected, but anal endosonography will probably provide more exact information on the structures involved.

With anal endosonography, it is now possible to visualize the different layers of the anal canal and the anorectal junction in vivo. The anal endosonographic procedure causes no more discomfort than a digital rectal examination and can be completed in 10 min. Anal endosonography is safe and causes no ionizing radiation, and we think it can visualize more details of the anal structures than can CT, which will show only a homogeneous soft-tissue mass.

Few reports on anal endosonography of abnormalities have been published, and in those studies, only a rotating endoprobe was used (e.g., visualizing perianal abscesses and fistulas [6], mapping external sphincter defects [7], and stag-

ing anal carcinomas [8]). We have used the multiplane probe together with the rotating endoprobe to visualize perianal tumors (Hauge et al., unpublished data) and sphincteric defects (Nielsen et al., unpublished data) and have found the multiplane probe useful, although somewhat more difficult to use than the rotating endoprobe because of the limitations discussed earlier.

We believe that anal endosonography with high-frequency probes may prove to be a useful diagnostic tool for disorders of the anal canal.

REFERENCES

1. Law PJ, Bartram CI. Anal endosonography: technique and normal anatomy. *Gastrointest Radiol* 1989;14:349-353
2. Oh C, Kark AE. Anatomy of the external anal sphincter. *Br J Surg* 1972;59:717-723
3. Goligher JC. *Surgery of the anus, rectum and colon*, 5th ed. London: Ballière Tindall, 1984
4. Kimmey MB, Martin RW, Haggitt RC, Wang KY, Franklin DW, Silverstein FE. Histological correlates of gastro-intestinal ultrasound images. *Gastroenterology* 1989;96:433-441
5. Beynon J, Mortensen NJM, Rigby HS. Rectal endosonography, a new technique for the preoperative staging of rectal carcinoma. *Eur J Surg Oncol* 1988;14:297-309
6. Law PJ, Talbot RW, Bartram CI, Northover JMA. Anal endosonography in the evaluation of perianal sepsis and fistulas in ano. *Br J Surg* 1989;76:752-755
7. Law PJ, Kamm MA, Bartram CI. A comparison between electromyography and anal endosonography in mapping external anal sphincter defects. *Dis Colon Rectum* 1990;33:370-373
8. Goldman S, Glimelius B, Norming U, Pahlman L, Seligson U. Transanorectal ultrasonography in anal carcinoma. *Acta Radiol* 1988;29:337-341

Case Report

Chronic Intestinal Bleeding Due to Mesenteric Vascular Insufficiency

Jeffrey S. Pollak,¹ Michael Bennick,² Donald F. Denny, Jr.,¹ and David Markowitz¹

Standard imaging studies in patients with chronic intestinal bleeding are often unrevealing because of the intermittent nature of the bleeding or the slow rate of extravasation. Visceral angiography and small-bowel endoscopy are indicated when standard endoscopic and radiologic methods fail to identify the source. Recently, we encountered an unusual case of chronic, obscure intestinal hemorrhage that underscored the value of angiography even in patients with slow rates of blood loss.

Case Report

A 50-year-old woman with an 18-month history of chronic, occult intestinal bleeding was referred for angiography in August 1989. Her symptoms were limited to an occasional episode of throbbing epigastric pain 15 min after eating roughage, relieved by a bowel movement, and occasional heartburn. She required transfusions every 10–14 days and had received a total of 52 units of packed RBCs at the time of referral. Her medical history was notable for rheumatic heart disease, cigarette smoking that she had stopped 8 years earlier, and a weight loss of 19 lbs (8.6 kg).

Diagnostic work-up included several upper endoscopic examinations, which most recently showed a healing antral ulcer and bright red blood in the fourth part of the duodenum, believed to be coming from the more distal small bowel. Colonoscopy revealed blood in the ileum on at least one occasion. An abdominal CT scan, a gastrointestinal series, and scintigrams were unrevealing. Angiography was then planned, with the intention of performing a provocative study (with heparin and urokinase) if no cause was found on the conventional angiogram. After two severe proximal stenoses of the superior mes-

enteric artery (SMA) were discovered (Fig. 1A), the provocative maneuvers were not done because of concern about the possible difficulty in catheterizing beyond these lesions for superselective localization of a bleeding site and the potential risk of acutely occluding mesenteric blood flow. A subsequent lateral aortogram showed tight ostial stenoses of the celiac and inferior mesenteric arteries (Fig. 1B). At this time, consideration was given to an ischemic cause for the patient's blood loss and the possibility that she might have vasculitis; however, she did not have classic symptoms of mesenteric angina, her erythrocyte sedimentation rate was within normal limits, and the ostial location of the stenoses in the other two vessels suggested atherosclerosis as the cause.

Subsequently, she had an unrevealing exploratory laparotomy. At that time, the bowel was telescoped over a colonoscope to permit peroral "panendoscopy." Slight edema in the proximal small bowel and a small Meckel diverticulum (<1 cm) were seen. Because the patient continued to bleed, the proximal SMA stenoses were dilated with a 6-mm angioplasty balloon (Medi-tech, Watertown, MA; Fig. 1C) in anticipation of the possible need for superselective catheterization several weeks later, when she was to have a provocative bleeding test. However, after the angioplasty, the patient's intestinal bleeding ceased and her hematocrit rose from 28 to over 40. The antral ulcer also was noted to have healed on follow-up endoscopy. She continues to do well more than 1 year later and has gained 45 lbs (20.5 kg).

Discussion

Obscure gastrointestinal bleeding has been defined as bleeding for which no source has been determined by routine

Received May 9, 1991; accepted after revision June 25, 1991.

¹ Department of Radiology, Yale University School of Medicine, P.O. Box 3333, 333 Cedar St., New Haven, CT 06510. Address reprint requests to J. S. Pollak.

² Department of Internal Medicine, Yale University School of Medicine, 60 Temple St., Ste. 5A, New Haven, CT 06510.

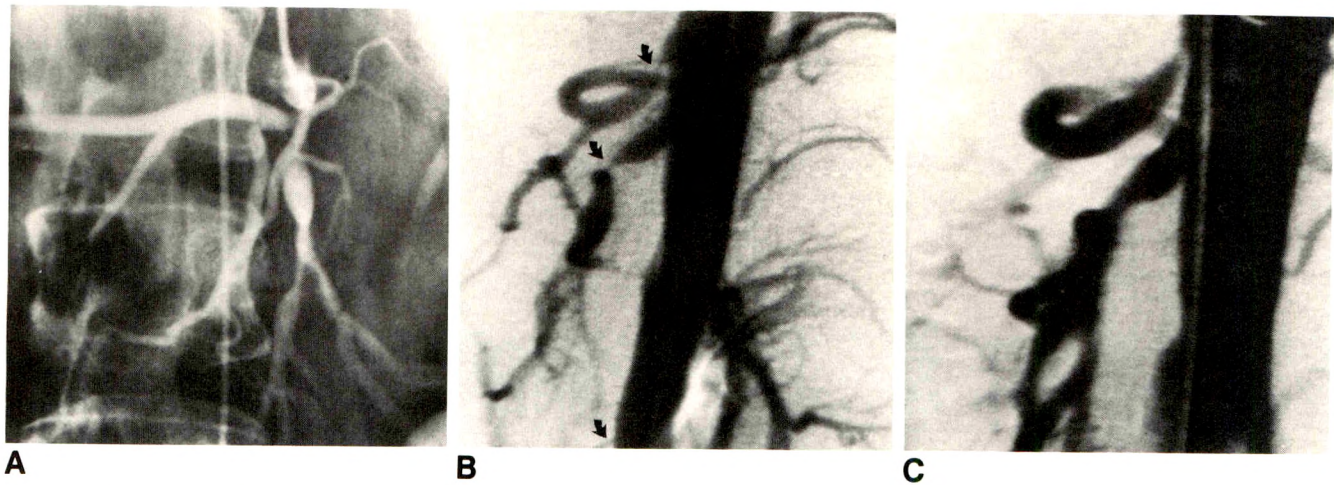


Fig. 1.—A, Angiogram after selective superior mesenteric injection shows two severe proximal stenoses in superior mesenteric artery (SMA), the first one at the level of a replaced right hepatic artery.
B, Lateral aortogram shows stenoses (arrows) in all three visceral vessels.
C, Lateral aortogram after angioplasty of SMA shows significant improvement in appearance of this vessel.

endoscopic and radiologic studies [1]. Such bleeding may be due to a lesion that is inaccessible to the endoscope or to one that is intermittently or slowly bleeding. Confounding factors may be the discovery of lesions that are of indeterminate significance with respect to the patient's current problem. The antral ulcer and Meckel diverticulum found in this patient are examples of this.

Lesions that cause obscure bleeding frequently lie in the small bowel or proximal colon. These include tumors, diverticula, ulcerations, and, more commonly, vascular abnormalities. Panendoscopy and arteriography are the most helpful studies [2, 3]. Although Peterson [1] mentions ischemia in the differential diagnosis of obscure bleeding, we have not been able to find a report of a patient with obscure bleeding as the primary sign of chronic vascular insufficiency.

Chronic mesenteric ischemia is clinically characterized by abdominal pain and weight loss [4]. Generally, at least two of the three intestinal vessels need to be severely diseased for symptoms to develop, but mesenteric angina with disease in only a single vessel has been reported [4]. Whereas intestinal bleeding is a well-known sign of acute mesenteric ischemia, this is not true of chronic arterial insufficiency, especially in the absence of any significant pain. Although the exact cause and location of bleeding were not shown in this patient, her dramatic improvement after treatment is indirect evidence that the bleeding was indeed due to ischemia, presumably caused by mucosal ulceration.

In reviewing the literature on chronic mesenteric ischemia, we found that only Stanton et al. [5] reported any patients with melena. Although two of their 17 patients did have bleeding, this occurred as a relatively recent sign (1 and 2 months) in patients with a more chronic history of postprandial pain (8 months and 1 year). Several other series make no mention of bleeding at all [6, 7]. Persistent gastric ulceration due to vascular insufficiency has been reported [8], but no mention is made of intestinal bleeding, and again, all these

patients had significant abdominal pain. Ischemic colitis frequently causes bleeding, and occasionally persistent colitis can develop, but this entity is generally considered an acute, localized syndrome and is usually associated with pain [4]. Of 36 patients with chronic obscure bleeding studied by Rollins et al. [3], none of the cases were attributed to mesenteric ischemia.

In conclusion, this patient appears to have had chronic intestinal bleeding related to mesenteric ischemia that was successfully treated with angioplasty. This sign has not been described before as the principal manifestation of chronic mesenteric vascular insufficiency and should be considered in the differential diagnosis in patients with chronic obscure bleeding.

REFERENCES

- Peterson WL. Obscure gastrointestinal bleeding. *Med Clin North Am* 1988;72:1169-1176
- Schwartz RW, Hagihara PF, Griffen WO. Intraoperative endoscopy for recurrent gastrointestinal bleeding. *South Med J* 1988;81:1106-1108
- Rollins ES, Picus D, Hicks ME, Darcy MD, Bower BL, Kleinhoffer MA. Angiography is useful in detecting the source of chronic gastrointestinal bleeding of obscure origin. *AJR* 1991;156:385-388
- Rogers AI, Cohen JL. Ischemic bowel disease. In: Berk JE, ed. *Bockus: gastroenterology*, 4th ed. Philadelphia: Saunders, 1985:1915-1936
- Stanton PE, Hollier PA, Seidel TW, Rosenthal D, Clark M, Lamis PA. Chronic intestinal ischemia: diagnosis and therapy. *J Vasc Surg* 1986;4:338-344
- Rapp JH, Reilly LM, Qvarfordt PG, Goldstone J, Ehrenfeld WK, Stoney RJ. Durability of endarterectomy and antegrade grafts in the treatment of chronic visceral ischemia. *J Vasc Surg* 1986;3:799-806
- Rheudasil JM, Stewart MT, Schellack JV, Smith RR III, Salam AA, Perdue GD. Surgical treatment of chronic mesenteric arterial insufficiency. *J Vasc Surg* 1988;8:495-500
- Cherry RD, Jabbari M, Goresky CA, Herba M, Reich D, Blundell PE. Chronic mesenteric vascular insufficiency with gastric ulceration. *Gastroenterology* 1986;91:1548-1552

Pictorial Essay

Imaging of Gallbladder Variants

Jon W. Meilstrup,¹ Kenneth D. Hopper, and Gary A. Thieme

A wide range of normal gallbladder variations are seen on gallbladder imaging. This essay illustrates the major variations that may be encountered, including anomalies in location, number, and form.

Routine imaging of the gallbladder demonstrates a wide array of imaging variants, including anomalies in location, number, and configuration [1–3]. An awareness of these normal variants may prevent misdiagnosis and will aid in evaluation of differential diagnostic possibilities.

Anomalies in Location

Normally, the gallbladder is situated adjacent to the under-surface of the liver, in the plane of the interlobar fissure, with the gallbladder neck maintaining a constant relationship to the porta hepatis. The gallbladder is routinely found in the right upper quadrant, but may be seen in any part of the abdomen. While anomalous positions are rare, the most common of these are (1) under the left hepatic lobe, (2)

intrahepatic, (3) transverse, and (4) retroplaced (retrohepatic or retroperitoneal) (Fig. 1).

A left-sided gallbladder location is seen in situs inversus totalis (Fig. 2). A gallbladder in the left upper quadrant without situs inversus is even more rare. Intrahepatic gallbladders have a subcapsular location along the anterior inferior right lobe of the liver. This poses a problem for scintigraphy, as an intrahepatic gallbladder can cause a focal defect; sonography can be helpful in these cases. The retroplaced gallbladder is rare and can be either congenital or acquired. Gallbladder rotation and/or displacement can be caused by hepatic lobe abnormalities (aplasia, hypoplasia, hypertrophy) and by abnormal mobility of the gallbladder itself.

From an imaging standpoint, it is important to realize that when the gallbladder is not visualized in its normal location, the possibility of an ectopic location must be considered.

Anomalies in Number

Agenesis of the gallbladder is rare, as are duplication anomalies. Imaging of multiple gallbladders is challenging, since the duplicated gallbladder(s) are difficult to detect on sonography, oral cholecystography (OCG), and scintigraphy.

Received May 17, 1991; accepted after revision July 24, 1991.

¹ All authors: Department of Radiology, The Milton S. Hershey Medical Center, The Pennsylvania State University, P.O. Box 850, Hershey, PA 17033. Address reprint requests to J. W. Meilstrup.

AJR 157:1205–1208, December 1991 0361–803X/91/1576–1205 © American Roentgen Ray Society

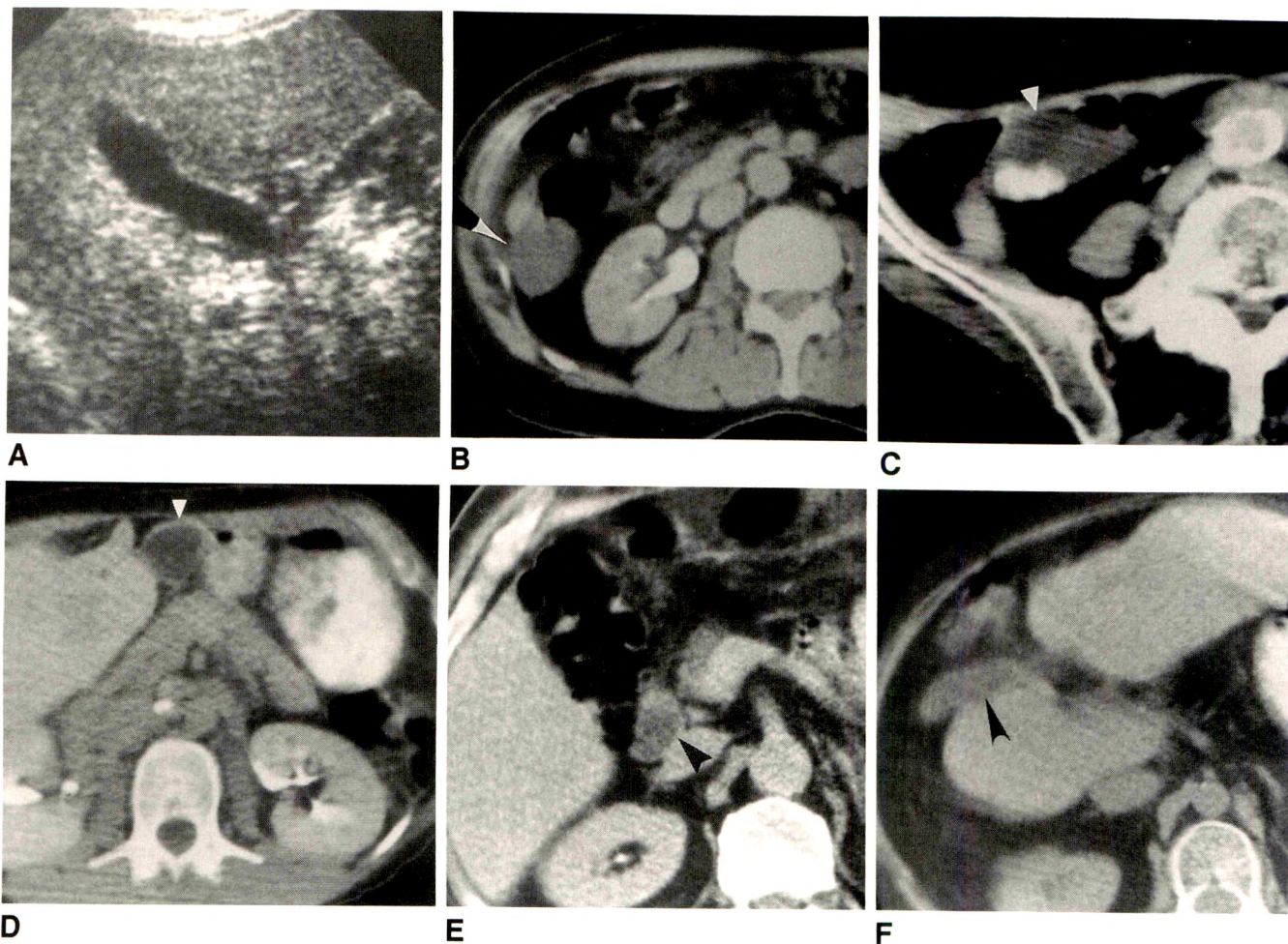


Fig. 1.—Ectopic locations of gallbladder. Gallbladder can be found in any part of abdomen.
A, Intrahepatic gallbladder on right longitudinal sonogram. This position poses a problem for scintigraphy in that a focal intrahepatic defect can mimic a mass. Sonography can be especially helpful when typical in appearance, as in this case.
B, Infrahepatic gallbladder. CT scan at midkidney level shows hanging gallbladder (*arrowhead*), which lies not only caudad to right lobe of liver but also lateral and posterior to ascending colon.
C, Pelvic gallbladder. CT scan shows that with a long mesentery, gallbladder (*arrowhead*) can even be located in pelvis. Multiple gallstones are noted incidentally.
D, Epigastric gallbladder. Gallbladder (*arrowhead*) is located in midabdomen in this CT scan of patient with hepatic inversion. (Reprinted with permission from Hopper [4].)
E, Hanging gallbladder. CT section shows gallbladder (*arrowhead*) with its body lying medial to hepatic flexure.
F, Lateral gallbladder. CT scan shows unusual gallbladder position (*arrowhead*) lateral to right lobe of liver.

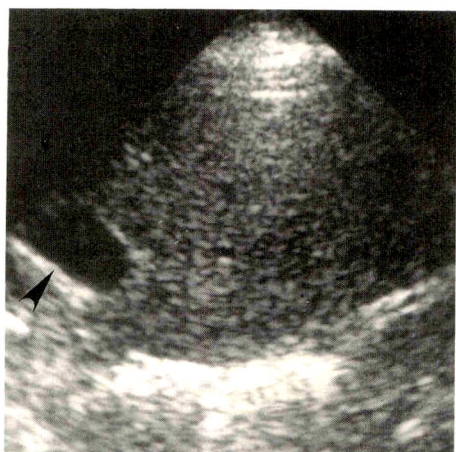


Fig. 2.—Gallbladder in left upper quadrant of abdomen. Transverse sonogram of left side shows liver with medially located gallbladder (*arrowhead*) in patient with situs inversus.

Anomalies in Form

Several variations in the radiologic appearance of gallbladder shape have been described. The so-called junctional fold is a kinking or folding of the gallbladder, usually of the posterior wall, but can occur anteriorly as well. Such junctional folds occur frequently, and are easily shown by sonography as well as by other imaging techniques. The gallbladder may show gross folding or bending, occasionally causing a bizarre or unusual shape (Fig. 3A). Careful analysis usually excludes adjacent disease (Figs. 3B and 3C).

The phrygian cap (Fig. 4) is a common normal variation. The name is derived from ancient Greek headgear, descriptive of this asymptomatic folding of the gallbladder fundus. This variant is readily identified with sonography, OCG, and CT. Scintigraphy of this variant may require delayed scans for visualization of the gallbladder fundus.

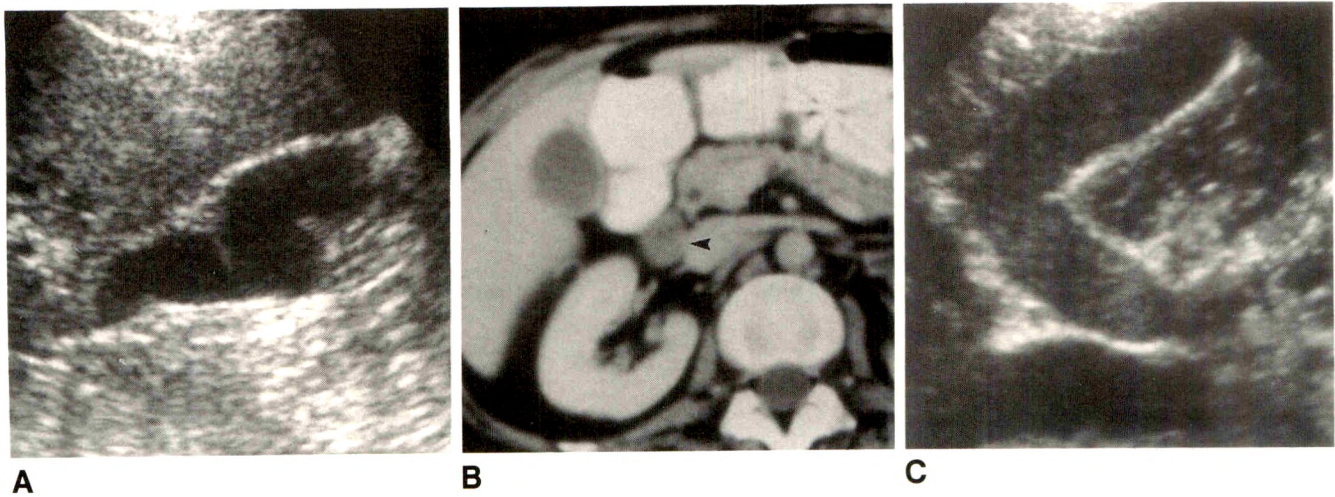


Fig. 3.—Unusual gallbladder shapes.
A, Multiple gallbladder folds on this longitudinal sonogram of right side give an undulating appearance to lumen.
B and C, “Boomerang” gallbladder. In another patient, CT scan (B) shows gallbladder and additional cystic “lesion” (arrowhead) lateral to head of pancreas. Longitudinal sonogram (C) shows boomerang shape of gallbladder, which proves cystic lesion is part of gallbladder. Low-level echoes in gallbladder are consistent with sludge.

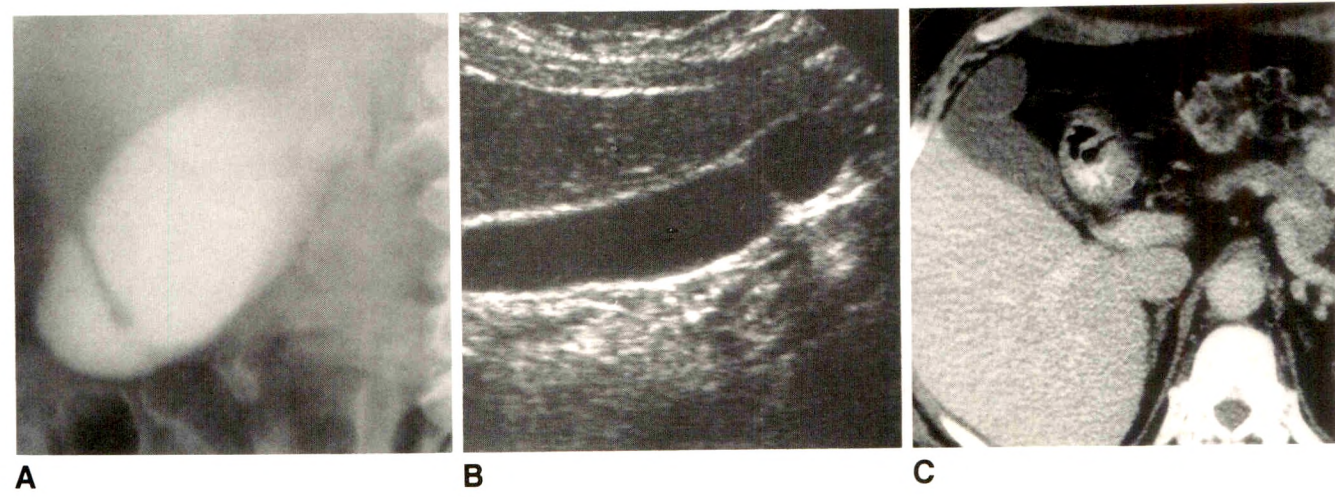


Fig. 4.—Phrygian cap anomaly. Prominent fundal fold in three different patients.
A, Oral cholecystography shows fold of phrygian cap.
B, Longitudinal sonogram shows this anomaly en face, simulating a septum.
C, Phrygian cap on CT scan.

Septa of the gallbladder (Fig. 5) can be either partial or complete. These can lead to stasis and stone formation. Multiseptate gallbladder is a rare anomaly, having a multi-chambered lumen with multiple septa, creating a honey-combed appearance. This is well demonstrated on OCG, which shows multiple locules formed by the septa. Differential

possibilities on sonography include desquamated gallbladder mucosa, extension of the spiral valves of Heister into the gallbladder neck region, and possibly polypoid cholesterosis. The spiral valves of Heister are small folds in the cystic duct that can be visualized with OCG and rarely with other imaging techniques.

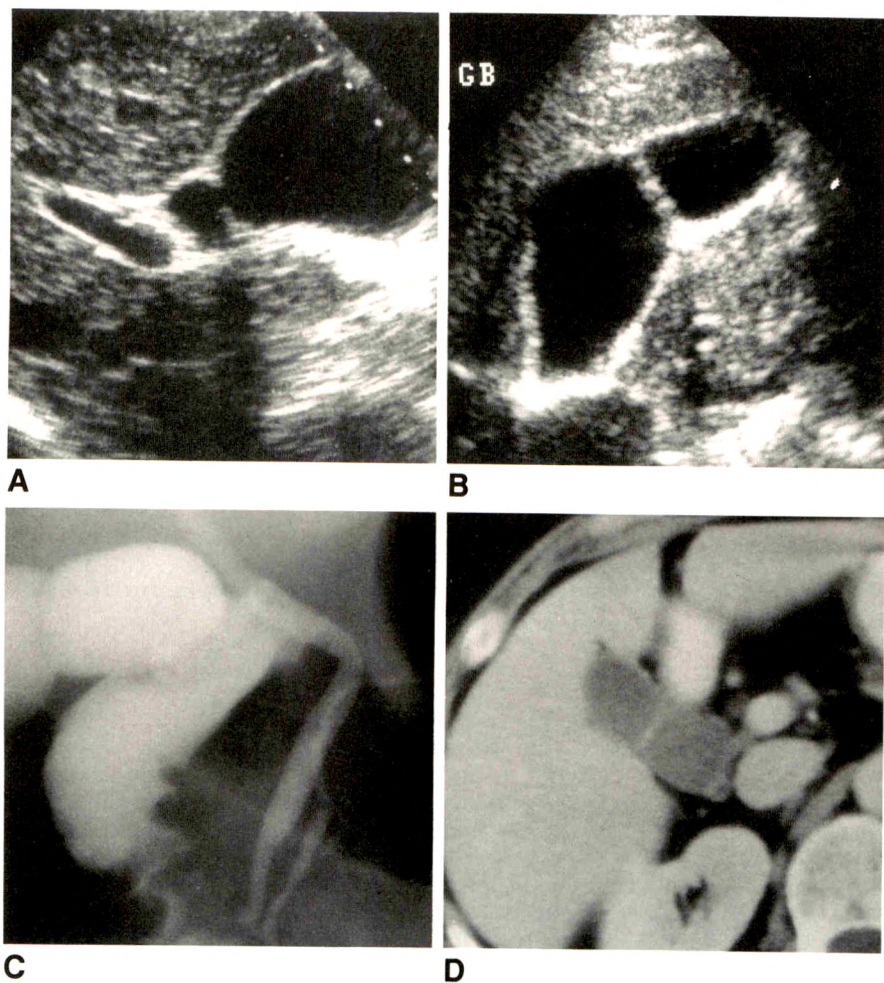


Fig. 5.—Gallbladder septation.

A and B, Longitudinal sonograms in two different patients show incomplete septation (**A**) and complete septation (**B**). A complete septum should cross lumen completely in both longitudinal and transverse views, as this does.

C and D, ERCP study in another patient (**C**) and CT in a fourth patient (**D**) show prominent septa.

REFERENCES

1. Gross RE. Congenital anomalies of the gallbladder. *Arch Surg* **1936**;32:131-162
2. Lev-Toaff AS, Friedman AC, Rindsberg SN, Caroline DF, Maurer AH, Radecki PD. Multiseptate gallbladder: incidental diagnosis on sonography. *AJR* **1987**;148:1119-1120
3. Smergel EM, Maurer AH. Phrygian cap simulating mass lesion in hepatobiliary scintigraphy. *Clin Nucl Med* **1984**;9:131-133
4. Hopper KD. Hepatic inversion with an epigastric gallbladder. *Gastrointest Radiol* **1988**;13:355-357

Percutaneous Drainage of Hepatic Abscesses: Comparison of Results in Abscesses With and Without Intrahepatic Biliary Communication

Huy Do¹
Robert E. Lambiase
Lane Deyoe
John J. Cronan
Gary S. Dorfman

Results of percutaneous drainage performed in eight patients with eight liver abscesses with intrahepatic biliary communication and 22 patients with 26 liver abscesses without biliary communication were analyzed to determine whether the presence of an intrahepatic biliary communication affected the outcome of treatment. The clinical features and response to treatment of both groups were compared. The presence or absence of biliary communication was determined by injection of contrast material into the abscess under fluoroscopic guidance either during or several days after initial drainage. Duration of drainage was longer ($p < .05$) in patients with communication (range, 7–44 days; mean, 22 days) than in patients without communication (range, 1–33 days; mean, 13 days). Percutaneous drainage was curative in five (63%) and palliative or temporizing in one (13%) of eight patients with communication. It was curative in 15 (68%) and palliative or temporizing in five (23%) of 22 patients without communication ($p = .317$). Liver abscesses with intrahepatic biliary communication did not require percutaneous transhepatic biliary diversion for cure.

Despite longer duration of drainage for abscesses with intrahepatic biliary communication, the cure rates of percutaneous drainage for both groups were similar. Patients in whom an intrahepatic biliary communication was shown did not require alternative interventional or surgical measures for cure.

AJR 157:1209–1212, December 1991

Pyogenic liver abscesses are serious disorders. Historically, they required surgical drainage for cure, although there are anecdotal reports of cure by antibiotic therapy alone [1, 2]. With advances in cross-sectional imaging techniques, more prompt diagnosis, improved drainage procedures, and increasingly effective antimicrobial chemotherapy, percutaneous drainage techniques have changed approaches to diagnosis and therapy of this disease [3–13]. Because percutaneous drainage has high success rates and minimal morbidity and mortality rates compared with older surgical procedures, it is widely held to be the first choice for treating hepatic abscess. However, none of the published series have compared results on the basis of the presence or absence of intrahepatic biliary communication. Additionally, the need for biliary diversion to effect cure has not been evaluated.

We reviewed the records of 30 patients with pyogenic liver abscesses treated percutaneously at our institution. The results of treatment in those patients whose abscesses showed intrahepatic biliary communication were compared with outcome in patients with abscesses without communication. The purpose was to determine whether liver abscesses with intrahepatic biliary communication required alternative interventional or surgical measures and if cure or palliation rates were different between the two groups.

Materials and Methods

We reviewed the medical records of 30 patients admitted to our institution between 1982 and 1988 who had percutaneous drainage of a hepatic abscess. The following data were

Received April 1, 1991; accepted after revision June 19, 1991.

¹ All authors: Department of Diagnostic Imaging, Rhode Island Hospital and Brown University Program in Medicine, 593 Eddy St., Providence, RI 02903. Address reprint requests to R. E. Lambiase.

0361-803X/91/1576-1209
© American Roentgen Ray Society

collected: age; sex; presenting signs and symptoms; medical history; history of recent surgery; diseases associated with immunosuppression, such as renal insufficiency (creatinine level > 2.0 mg/dl) or diabetes mellitus, known malignancy, immunosuppressive medication, human immunodeficiency virus (HIV) positive status, and absolute neutropenia (<500 granulocytes/ μ l); technique of radiologic diagnosis and drainage; type of catheter used; duration of drainage; presence of intrahepatic biliary communication; and results of treatment (cure, palliation/temporization, or failure).

Eight patients (six women and two men; age range, 28–77 years) with eight liver abscesses with intrahepatic biliary communication were compared with 22 patients (seven women and 15 men; age range, 9–90 years) with 26 liver abscesses with no biliary communication. Patients with liver abscesses communicating to the extrahepatic biliary tree (four patients) were excluded from the series.

A body temperature of 38.3°C (101°F) or greater, pain in the right upper quadrant or abdomen, and leukocytosis were the most common presenting signs and symptoms. Predisposing factors included recent surgery in 17 patients (six cholecystectomies, two left hepatic lobectomies, one splenectomy, one Whipple's operation, one gastrectomy, one appendectomy, one small-bowel reduction, and four colectomies) and immunosuppression in 17 patients (six with diabetes mellitus, seven with known malignancy, two on corticosteroid medications, one with renal insufficiency, and one with HIV-positive status). Nine of 17 postoperative patients had surgical procedures involving the biliary system (four [50%] of eight patients with abscess having biliary communication, five [23%] of 22 patients with abscess having no biliary communication). Six (46%) of the 13 postoperative patients with liver abscess without biliary communication had surgical procedures involving the gastrointestinal tract (Table 1). Four patients (one with and three without communication) had no recent surgery and were not immunosuppressed.

The cause of hepatic abscess was associated with pancreaticobiliary disease in six (75%) of eight patients with abscesses having communication, compared with five (23%) of 22 patients with abscesses without communication ($p < .014$). Pancreaticobiliary disease included patients with pancreatitis, pancreatic head carcinoma, cholangitis, or cholecystitis, and patients who recently had biliary or pancreatic surgery.

The radiologic diagnosis of liver abscess was made by sonography or CT in all patients. Percutaneous drainage was performed under CT guidance in 26 (87%) of the 30 patients and sonographic guidance in four (13%) of the 30 patients. Drainage catheters were placed over a guidewire most commonly, unless the superficial location of the abscess and safe access allowed use of the trocar method. Eight- or 10-French All-Purpose Drains (Boston Scientific Corp., Watertown, MA), or 12- or 14-French vanSonnenberg (Boston Scientific Corp.) catheters were used most often.

Follow-up sonograms, CT scans, or abscessograms were obtained without use of a specific protocol, predicated on clinical assessment.

When obtained, they were used specifically to evaluate the size of the abscess cavity and the position of the catheter, to ensure adequate drainage of all collections, and to search for evidence of biliary communication. Catheters were removed when clinical evidence of toxicity had resolved (normal temperature and WBC count, absence of abdominal tenderness), and catheter drainage had decreased to less than 10 ml/24 hr for 3 days.

Percutaneous management was defined as curative if complete resolution of clinical signs and symptoms occurred on long-term clinical follow-up (>2 years in all cases except for one patient who was lost to follow-up) and CT or sonography showed complete resolution of the abscess cavity. Palliation was defined as an improvement in signs and symptoms, with the patient clinically stable but not cured. Temporization was defined as clinical improvement but with the patient still in need of adjunctive surgery. An intrahepatic biliary communication was considered present if the intrahepatic and then the extrahepatic biliary system opacified when contrast material was injected into the abscess cavity via the drainage catheter either during or several days after initial drainage.

Differences in immunosuppression, recent surgery, cause of pancreaticobiliary disease, and cure rate between patients with abscesses having biliary communication and patients with abscesses without biliary communication were checked for statistical significance by using the chi-square test. The difference in mean drainage duration between the same two patient groups was tested for statistical significance with Student's *t* test.

Results

Duration of drainage in all patients ranged from 1 to 44 days (mean, 14 days); the most frequent duration was 1–2 weeks (14 patients, 47%). In three patients, duration of drainage was less than 7 days; in 10, 2–4 weeks; and in three, more than 4 weeks. Duration of drainage was longer on the average ($p < .05$) in patients with liver abscess and intrahepatic biliary communication (range, 7–44 days; mean, 22 days) when compared with patients with liver abscess without biliary communication (range 1–33 days; mean, 13 days).

In all patients, the cure rate was 67% (20/30) and the palliation/temporization rate was 20% (6/30). Percutaneous drainage alone was curative in five patients (63%) and temporizing in one patient (13%) who had a liver abscess with biliary communication. It was curative in 15 patients (68%) and palliative or temporizing in five patients (20%) who had liver abscess without biliary communication. The difference in rates between patients with biliary communication and those without was not statistically significant ($p = .317$).

TABLE 1: Population Characteristics

Factor	With Biliary Communication	Without Biliary Communication	Total
No. of patients	8	22	30
Mean age (yr)	57	57	—
Immunosuppressed ^a	4 (50%)	13 (59%)	17 (57%)
Recent surgery ^a	4 (50%)	13 (59%)	17 (57%)
Pancreaticobiliary cause ^b	6 (75%)	5 (23%)	11 (37%)
Other cause	2 (25%)	17 (77%)	19 (63%)

^a $p = .317$.

^b $p < .014$.

Four patients (two with and two without communication) died of generalized sepsis before resolution of the abscess could be documented.

One patient who had an abscess with biliary communication, in whom drainage was considered palliative, had an enterobiliary fistula after a left hepatic lobectomy for hepatic malignancy. On the 79th day of hospitalization, a liver abscess was drained percutaneously, and on the 102nd day the patient was transferred to another institution for management of the fistula.

Of five patients with abscess without biliary communication who improved after drainage, three required adjunctive surgery: one because of an accompanying loculated perihepatic pus collection that could not be adequately drained percutaneously, one because of an accompanying subphrenic abscess that was only incompletely drained percutaneously, and one because of the development of acute peritonitis. One patient with adenocarcinoma of the colon improved clinically after percutaneous drainage of a liver abscess, but died of cardiopulmonary arrest on the 19th day of hospitalization. One patient was lost to follow-up as an outpatient approximately 2 months after drainage.

Few complications of catheter placement occurred. Two patients (7%) had transient sepsis after initial catheter placement. Both stabilized after treatment with fluids and antibiotics only, with recovery to predrainage status in 10–12 hr. Neither of these patients had biliary communication. No deaths were directly related to catheter placement in this series.

Discussion

In our series the cure rates for patients with liver abscesses with biliary communication (63%) and for those without (68%) were similar. Age, sex, presenting signs and symptoms, and rates of recent surgery and immunosuppression were similar in both groups as well. A pancreaticobiliary cause of the abscess correlated significantly with the presence of biliary communication. The average duration of drainage was longer in patients with communication (22 days) than in patients without communication (11 days). This is most likely due to the continuous output of bile into the abscess cavity via the communicating tract, which required more time to close and heal.

Biliary communication was identified on initial drainage in only one patient. In the remaining seven patients, communication was shown 2–6 days later when contrast material was instilled directly into the abscess cavity via the drainage catheter under fluoroscopic observation (abscessogram). Suspicion of biliary communication was raised when bile-stained fluid that tested positive for bilirubin was within the collection bag, or when initial drainage outputs were persistently high (these invariably decreased with ongoing abscess therapy).

In all of our patients with communicating abscesses, the communication was to intrahepatic biliary radicles. None required diversion of bile flow for cure. We conjecture that this is because of the tamponading effect of hepatic parenchyma

and the low pressure of the unobstructed intrahepatic biliary system, as well as the relatively small volumes of bile involved. This is in contradistinction to abscesses showing communication to the extrahepatic biliary tree, where larger volumes of bile, lack of surrounding tissue for tamponade, and somewhat higher pressures often mandate biliary diversion for healing of the communication, particularly in cases of distal ductal stricture or obstruction [14–17]. The distinction between an abscess that has secondarily eroded into the biliary system and a primary biloma that becomes secondarily infected is, for therapeutic considerations, artificial.

We previously described a series of patients who had percutaneous treatment of abscesses that communicated with the extrahepatic biliary system [17]. These patients are not analogous to those in the present series, in whom the communication was intrahepatic in all cases. The fact that no patients required bile diversion for cure in the current series suggests that rents in the intrahepatic biliary radicles heal readily once the inciting inflammation is resolved or reduced. Cure/palliation occurred in six of eight patients with communicating abscess. The two who were not cured or palliated died of generalized sepsis. In both cases percutaneous management of the abscess appeared to progress satisfactorily, with no undrained collections by follow-up CT and with progressively decreasing drainages to a minimum (<10 ml/day). Lack of biliary fistula control was not a factor in the clinical failure in these cases. Instead, irreversible multiple organ failure was fatal despite satisfactory abscess management and response.

The overall cure rate for both communicating and noncommunicating abscesses in our series (67%) is somewhat lower than success rates reported in other patients with pyogenic hepatic abscesses, which range from 70% to 90% [10–13]. Explanations for this difference include differing indications for primary percutaneous drainage, a large percentage of immunocompromised patients in our population of patients, and our definition of cure, which includes a 1-year follow-up period [18].

It is unrealistic to anticipate a high long-term cure rate for any type of abscess drainage in patients who are immunosuppressed. If those patients with immunosuppression are excluded from our series, the cure rate increases to 84%, which agrees more with previously reported results.

In summary, results from this small series show that patients with pyogenic liver abscesses with an intrahepatic biliary communication require drainage for a longer time than do patients in whom the abscess does not communicate. However, the cure rate of percutaneous drainage in the two groups is not significantly different. Patients with an intrahepatic biliary communication do not require further alternative interventional or surgical measures to effect satisfactory abscess management.

REFERENCES

1. Ralph ED. Successful antimicrobial therapy of hepatic, intraabdominal and intrapelvic abscesses. *Can Med Assoc J* 1984;131:605–607
2. Herbert DA, Rothman J, Simmons F, Fogel DA, Wilson S, Ruskin J. Pyogenic liver abscesses: successful non-surgical therapy. *Lancet*

- 1982;1:134-136
3. Bertel CF, van Heerden JA, Sheedy PF. Treatment of pyogenic hepatic abscesses: surgical versus percutaneous drainage. *Arch Surg* 1986;121:554-558
 4. Farges O, Leese T, Bismuth H. Pyogenic liver abscess: an improvement in prognosis. *Br J Surg* 1988;75:862-865
 5. Falk KA, Angeras UJ, Friman VZ, Gamklou GR, Lukes PJ. Pyogenic liver abscesses: have changes in management improved the outcome? *Acta Chir Scand* 1987;153:661-664
 6. Gyorffy EJ, Frey CF, Silva J Jr, McGahan J. Pyogenic liver abscess: diagnostic and therapeutic strategies. *Ann Surg* 1987;206:699-705
 7. Lee JF, Block GE. The changing clinical pattern of hepatic abscesses. *Arch Surg* 1972;104:465-470
 8. Altemeier WA, Schowengerdt CG, Whiteley DH. Abscesses of the liver: surgical considerations. *Arch Surg* 1970;101:258-266
 9. Bernardino ME, Berkman WA, Plemmons M, Sones PJ Jr, Price RB, Casarella WJ. Percutaneous drainage of multiseptated hepatic abscess. *J Comput Assist Tomogr* 1984;8:38-41
 10. Johnson RD, Mueller PR, Ferrucci JT Jr, et al. Percutaneous drainage of pyogenic liver abscesses. *AJR* 1985;144:463-467
 11. Martin EC, Karlson KP, Fankuchen E, Cooperman A, Casarella WJ. Percutaneous drainage in the management of hepatic abscesses. *Surg Clin North Am* 1981;61:157-167
 12. Attar B, Levendoglu H, Cuasay NS. CT-guided percutaneous aspiration and catheter drainage of pyogenic liver abscesses. *Am J Gastroenterol* 1986;81:550-555
 13. Gerzof SG, Johnson WC, Robbins AH, Nabseth DC. Intrahepatic pyogenic abscesses: treatment by percutaneous drainage. *Am J Surg* 1985;149:487-494
 14. Zuidema GD, Cameron JL, Sitzmann JV, et al. Percutaneous transhepatic management of complex biliary problems. *Ann Surg* 1983;197:584-593
 15. Czerniak A, Thompson JN, Soreide O, Benjamin IS, Blumgart LH. The management of fistulas of the biliary tract after injury to the bile duct during cholecystectomy. *Surg Gynecol Obstet* 1988;167:33-38
 16. Kaufman SL, Kadir S, Mitchell SE, et al. Percutaneous transhepatic biliary drainage for bile leaks and fistulas. *AJR* 1985;144:1055-1058
 17. Vaccaro JP, Dorfman GS, Lambiase RE. Treatment of biliary leaks and fistulae by simultaneous percutaneous drainage and diversion. *Cardiovasc Intervent Radiol* 1991;14:109-112
 18. Fry DE, Garrison RN, Heitsch RC, Calhoun K, Polk HC Jr. Determinants of death in patients with intraabdominal abscess. *Surgery* 1980;88:517-523



The Radiology Outreach Foundation (ROF) is a nonprofit corporation whose goal is to help disadvantaged countries improve their health care by providing radiology equipment, books, consultation, education, and training to their practitioners. This assistance is on an application basis that is independent of political, ethnic, or religious orientation of the grantee. It depends on the need of the people and the ability of the ROF to meet that need. The ROF is approved by the U.S. Internal Revenue Service as a tax-exempt organization. It is endorsed by the following radiologic societies: American Association of Women Radiologists, American College of Radiology, American Roentgen Ray Society, Association of University Radiologists, Radiological Society of North America, Society of Chairmen of Academic Radiology Departments, Society for Pediatric Radiology, European Society of Pediatric Radiology.

All donations to the ROF are tax deductible. Persons who would like to contribute financially to the ROF, would be interested in being a visiting professor, would like to send books or journals to any of the institutions supported by the ROF, or would like further information about the ROF should write to Charles A. Gooding, M.D., President, Radiology Outreach Foundation, 3415 Sacramento St., San Francisco, CA 94118 USA.

Pictorial Essay

CT of Acquired Abnormalities of the Spleen

Andrew J. Taylor,¹ Wylie J. Dodds, Scott J. Erickson, and Edward T. Stewart

Imaging considerations and features when assessing acquired abnormalities of the spleen with CT are described. Indexes of normal size and the implications of splenomegaly are discussed, as well as the CT appearances and types of neoplasia, cysts, traumatic injuries, infarction, and inflammatory changes.

In a recent report, we described the radiologic features of splenic anatomy, embryology, and developmental anomalies [1]. In this essay, we describe CT findings of acquired abnormalities of the spleen.

General Considerations

The characteristics of the spleen on CT are determined largely by its underlying histologic anatomy. Covered by a tough capsule, the spleen consists of a lattice of lymphatic follicles and reticuloendothelial cells (white pulp) with interspersed vascular lakes (red pulp). On unenhanced CT scans, the spleen has an attenuation similar to that of the liver, approximately 40 H. Normally, the liver and spleen densities are within 15 H on unenhanced scans and within 25 H on dynamic contrast-enhanced scans. The spleen generally remains a constant reference point in CT attenuation values, as various metabolic states can decrease (fatty infiltration) or increase (hemochromatosis) the attenuation of the liver. Because of the difference in timing of enhancement of red and white pulp during the early phases of the dynamic contrast-enhanced CT, the spleen may be inhomogeneous initially (Fig. 1). These changes vary from subtly to markedly inhomogeneous. Repeating images of the spleen within minutes will show a homogeneous pattern.

Size

Although relatively large in children, the spleen progressively decreases in size with age. In middle-aged patients, the spleen is about the size of a fist, weighting approximately 150 g. A craniocaudal measure of 13 cm is frequently used as the upper limit of normal for splenic size. However, because of wide variation in shape, there is no direct correlation in the spleen's length to its overall volume as there is for other organs such as the kidney. A product of length (a craniocaudal measure of approximately 12 cm) times depth (an anteroposterior dimension of approximately 7 cm) times width (the thickness at the hilum of about 4 cm) has been used to define splenic size. Normal limits of this volume range up to 480 cm³ [2]. A more arduous measure of size is adding the volume of each slice on the CT scan. As a practical matter, judgment about the spleen size is usually based on visual inspection and experience.

The causes of splenomegaly are numerous. The most common cause of splenomegaly in our practice is cirrhosis with its attendant portal hypertension (Fig. 2). Approximately 30% of splenomegaly cases are caused by lymphoma. AIDS and IV drug abuse increasingly deserve consideration because they cause mild to moderate splenic enlargement either from reactive hyperplasia (Fig. 3) or from complications related to these disease complexes. Massive splenomegaly is usually caused by chronic myelogenous leukemia, lymphoma, polycythemia vera, myelofibrosis, or, in the appropriate population of patients, malaria. At times, spontaneous rupture may occur as a complication of splenomegaly, particularly with mononucleosis or leukemia.

Received May 6, 1991; accepted after revision July 2, 1991.

¹ All authors: Department of Radiology, Medical College of Wisconsin, Froedtert Memorial Lutheran Hospital, 9200 W. Wisconsin Ave., Milwaukee, WI 53226. Address reprint requests to A. J. Taylor.

AJR 157:1213-1219, December 1991 0361-803X/91/1576-1213 © American Roentgen Ray Society

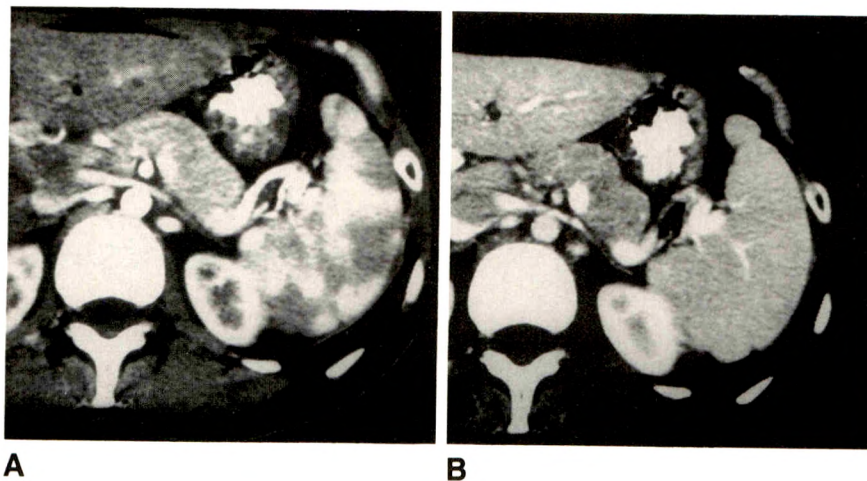


Fig. 1.—Normal spleen with marked inhomogeneity during early contrast enhancement.

A, CT image obtained early during single-level dynamic scanning shows variegated appearance of spleen. (Note lack of hepatic parenchymal and hepatic venous enhancement.)

B, On an image obtained 35 sec later, spleen is homogeneous.

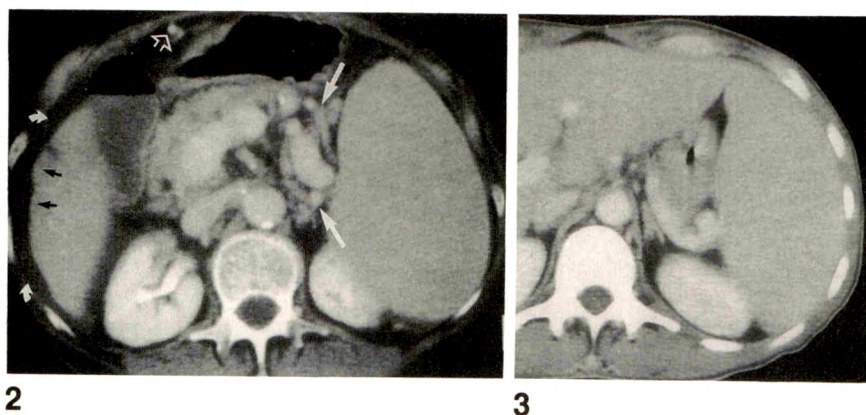


Fig. 2.—Cirrhosis. CT scan shows enlarged spleen with homogeneous parenchyma, a manifestation of portal hypertension. Also, note large splenic hilar varices (straight solid white arrows), recanalized periumbilical vein (open arrow), nodular liver edge (black arrows), and ascites (curved arrows).

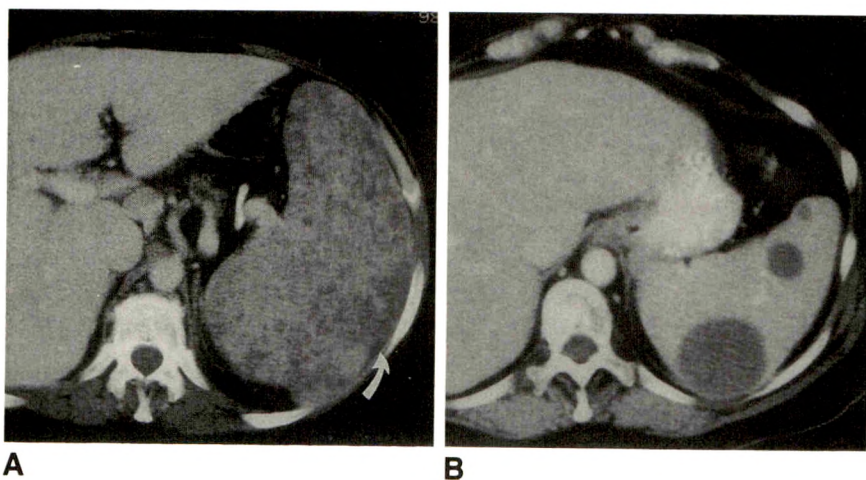


Fig. 4.—Lymphoma.

A, On this CT scan, non-Hodgkin lymphoma is manifested by numerous, small, low-attenuation areas representing nests of tumor. Laterally, these deposits are beginning to coalesce (arrow).

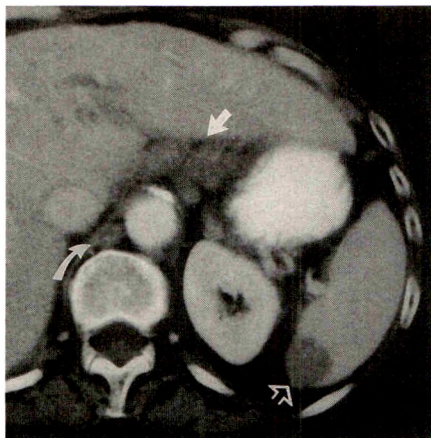
B, In another patient, CT scan shows a less common pattern of splenic lymphoma: discrete large masses within spleen.

Neoplasia

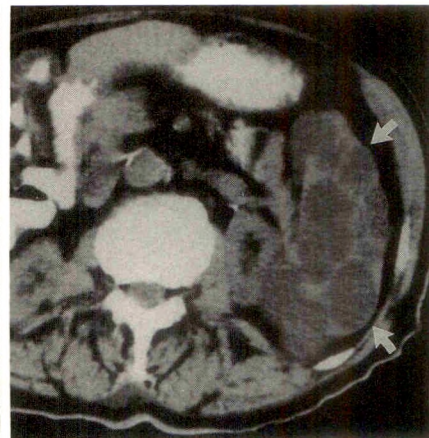
Both benign and malignant neoplastic involvement of the spleen occur, although a malignant cause is more frequent. Primary malignant tumors of the spleen, such as angiosarcoma, are rare. Much more common is hematologic malig-

nancy or metastatic disease. Lymphoma is the most common malignant tumor involving the spleen [2]. Approximately one third of all patients with lymphoma (Hodgkin disease and non-Hodgkin disease) have splenic involvement, usually with nests of cells smaller than 1 cm in diameter. This infiltrative pattern makes detection of disease difficult on CT (Fig. 4). Conversely,

Fig. 5.—Metastatic disease. CT scan shows well-circumscribed low-attenuation splenic mass (open arrow) in patient with ovarian carcinoma. This appearance is typical for splenic metastases. Other evidence of metastatic spread is usually present; in this case, adenopathy is present in retrocrural space (curved arrow) and gastrohepatic ligament (straight solid arrow).

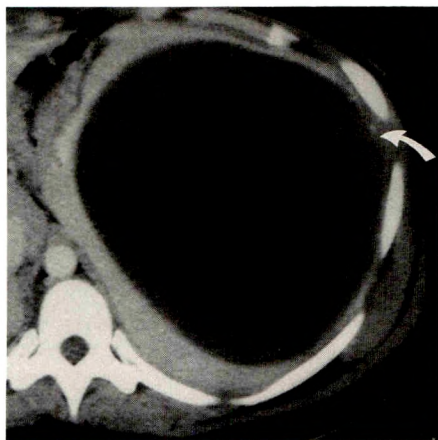


5

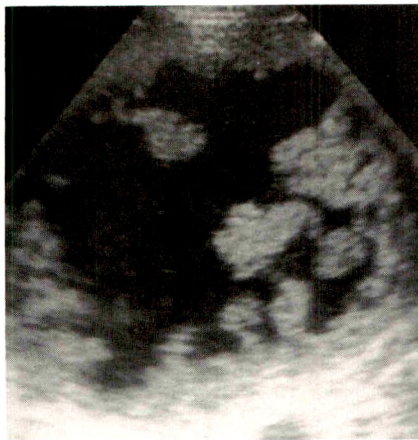


6

Fig. 6.—Lymphangioma. CT scan shows well-circumscribed, low-attenuation masses throughout spleen (arrows). These lesions correlated with cystic-appearing lesions seen on sonography. Having these typical findings of lymphangioma, this 85-year-old patient was treated conservatively.



A



B

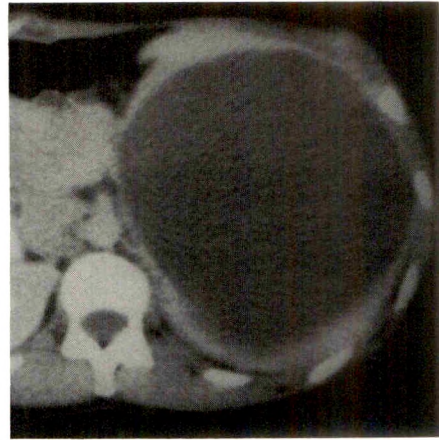


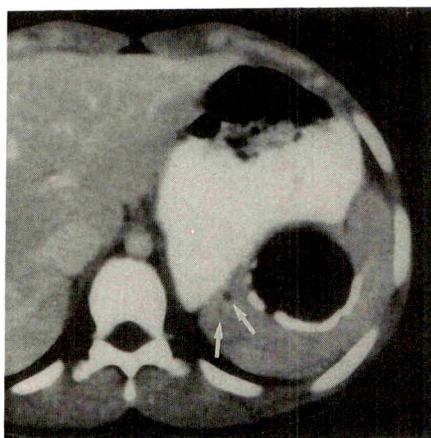
Fig. 7.—Traumatic cyst. This 23-year-old woman was in an auto accident 7 years earlier and now had increasing pain in left upper quadrant.

A, CT scan shows markedly enlarged spleen with low-attenuation mass replacing most of splenic substance. Internal architecture of cyst is relatively homogeneous, and borders appear fairly smooth. However, there is some subtle inhomogeneity, particularly along lateral aspect of cyst (arrow).

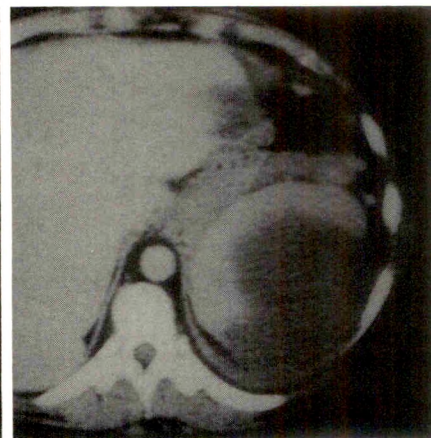
B, Sonogram obtained immediately after CT more accurately depicts architectural changes within this mass. Thickened, irregular septa are present. This case illustrates that traumatic cysts can show complex internal architecture similar to that associated with epidermoid cysts. Findings were confirmed at surgery.

Fig. 8.—Epidermoid cyst. CT scan through center of markedly enlarged spleen has an appearance similar to that seen in Fig. 7. An epithelial lining was found at surgery, however, making this a true or epidermoid cyst.

Fig. 9.—Echinococcal cyst. CT scan shows a cystic mass with a partially calcified rim in spleen. Adjacent tiny low-attenuation masses (arrows) represent daughter cysts. These findings suggest an echinococcal cyst, which was proved at surgery. (Courtesy of J. Sty, Milwaukee, WI.)



9



10

Fig. 10.—Splenic pseudocyst. Patient had a history of alcohol abuse. CT shows a lobulated cystic mass that was found at surgery to be an intrasplenic pseudocyst.

the enlargement of up to 30% of spleens in lymphoma patients is not due to lymphoma directly but is related to reactive hyperplasia or congestion [2].

Metastatic involvement of the spleen is seen in approximately 2–4% of routine autopsies in patients who died of cancer [3]. Melanoma is the most common source, followed by carcinoma of the lung, breast, gastrointestinal tract, and ovary (Fig. 5). Metastatic deposits to the spleen usually appear late in the course of malignant disease. These deposits may be single or multiple. As in lymphoma, reactive hyperplasia may be the cause of splenic enlargement in cancer patients.

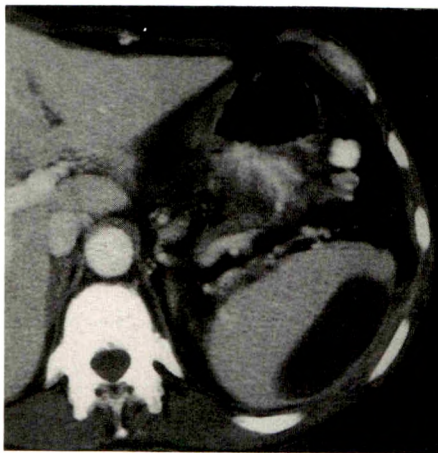
Benign tumors of the spleen are rare. The radiologic distinction between benign and malignant lesions is not always clear. Frequently, a splenectomy will be needed to make the final differentiation. The most frequent benign tumors of the spleen are hemangioma, hamartoma, lymphangioma, and epidermoid cyst. Hemangioma and hamartoma may appear as solid or complex masses on CT. The hemangioma will not necessarily show the typical enhancement pattern that is seen in its hepatic counterpart. The lymphangioma usually contains cystic masses, and, at times, septa may be seen within these cysts (Fig. 6).

Cysts

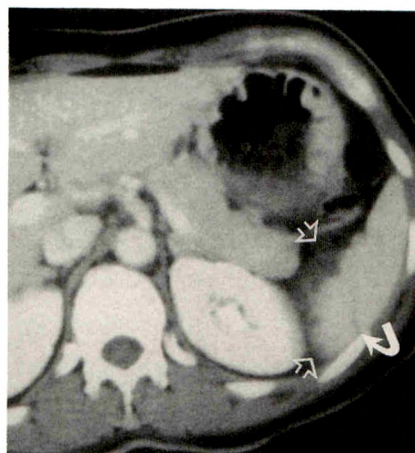
The majority of splenic "cysts" fall into one of three categories. Most cysts are false and do not have a true epithelial lining. Trauma is the presumed cause, although a supportive history is obtained in only a minority of cases. These cysts may have some calcification within their wall, and they may exhibit trabeculation (Fig. 7). A true cyst, or epidermoid cyst, is the second most common type of cyst (Fig. 8) and is probably developmental. Calcification within the cyst wall may be less prominent, but septa may be more prominent than in the traumatic cyst. The third type, the echinococcal cyst, usually has more prominent calcification, both within the wall and within the cyst itself (Fig. 9). Its margins may be more lobulated if daughter cysts are present. A fourth, and rarer, type of cyst is a pancreatic pseudocyst, which dissects into the splenic substance (Fig. 10).

Trauma

The spleen is the most frequently injured intraabdominal organ in blunt trauma. Owing to the current trend toward a more conservative approach to injury, there has been in-



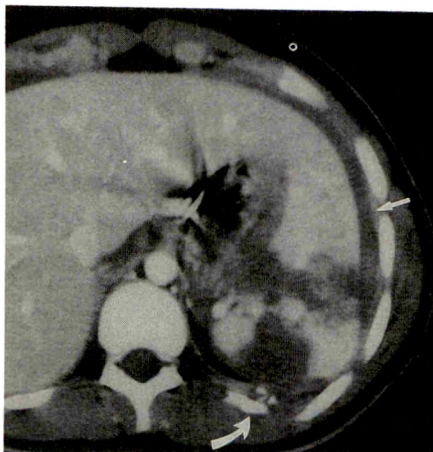
11



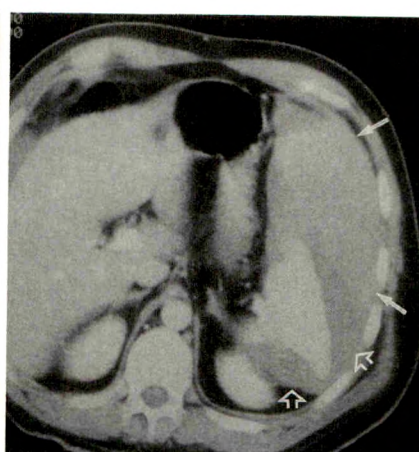
12

Fig. 11.—Subcapsular hematoma. CT scan shows subcapsular hematoma resulting from surgery on pancreatic tail. Typical lenticular shape is flattened medially as collection begins to recede during healing.

Fig. 12.—Laceration. This patient had blunt abdominal trauma hours earlier. On CT scan, a small linear parenchymal defect traversing capsule laterally (solid arrow) represents splenic laceration. Irregular posteromedial margin of spleen with associated perisplenic blood (open arrows) is another manifestation of splenic injury.



13



14

Fig. 13.—Fracture. CT scan shows relatively wide parenchymal defects, coursing from one capsular surface to another, constituting splenic fractures. These bands, representing blood, are oriented in different planes, thus segregating islands of enhancing spleen. Intraperitoneal blood (straight arrow) and left rib fracture (curved arrow) are also present.

Fig. 14.—Sequential hemorrhage causing an onion-skin appearance. On this CT image, layers of different-attenuation blood clot in perisplenic bed show differences in maturation of blood products after sequential episodes of hemorrhage. More peripheral, high-attenuation clot (solid arrows) in this patient represents mature blood clot. Fluid immediately surrounding spleen (open arrows) is from a more recent episode of hemorrhage.

creased emphasis on identifying, staging, and follow-up in imaging of splenic trauma. Dynamic contrast-enhanced CT scanning is very sensitive (95%) for detection of splenic injuries. The subcapsular hematoma is a peripheral, well-defined, lenticular, relatively low-attenuation mass that displaces the splenic parenchyma inwardly (Fig. 11). Rarely, an intrasplenic contusion or hematoma can be seen as a small, irregular, low-attenuation mass within the splenic parenchyma. Splenic laceration is seen as a cleft, usually with irregular borders, extending through the capsule into the parenchyma (Fig. 12). It is associated with perisplenic or intraabdominal fluid. The laceration traversing two capsular surfaces is designated a fracture (Fig. 13). Repeated episodes of bleeding may lead to a perisplenic clot with an onion-skin appearance (Fig. 14). More subtle signs of splenic trauma are a minor surface irregularity, or the presence of a perisplenic clot next to an otherwise normal-appearing spleen, the so-called sentinel clot sign [4]. All of the imaging abnormalities do not necessarily have a direct correlation with a patient's outcome, either with the need for surgery or with the subsequent development of delayed rupture. Pitfalls in the diagnosis of splenic trauma include clefts and a prominent left hepatic lobe (Fig. 15).

CT can be used to monitor healing also, evidenced by the sequential regression of intra- and perisplenic clots as well as the progressive diminution of laceration defects. On follow-up studies, an enlarging spleen is not necessarily an ominous sign; the spleen may transiently decrease in size shortly after the traumatic event because of the associated decrease in the patient's intravascular volume or because of the evoked adrenergic response [5]. Subsequent imaging studies will show an increase in splenic size, actually returning the splenic volume to normal (Fig. 16). Rarely, after abdominal trauma causing a severely damaged spleen, splenic tissue may be scattered about the abdomen, resulting in a condition called splenosis.

Infarction

Splenic infarction is a relatively common clinical consideration. At times, the acute event causes symptoms referable to the left upper quadrant. However, splenic infarction may be asymptomatic, with residual features seen on future imaging studies. Splenic infarction is usually the result of local vascular compromise. Frequently, it is caused by arterial emboli (usually from the heart), or from involvement of the local vascular

Fig. 15.—Pitfalls in CT of splenic trauma.
A, Lateral, low-attenuation crescent (arrows) could be confused with a subcapsular hematoma in this recently injured patient. Note fatty liver.
B, On a higher section, crescent is actually part of fatty liver that extends around spleen. Peripheral hepatic vessels (straight solid arrow) and a bridge of liver parenchyma (curved arrow) help to confirm crescent's true identity. Smooth, congenital splenic clefts (open arrows) are also seen at this level.

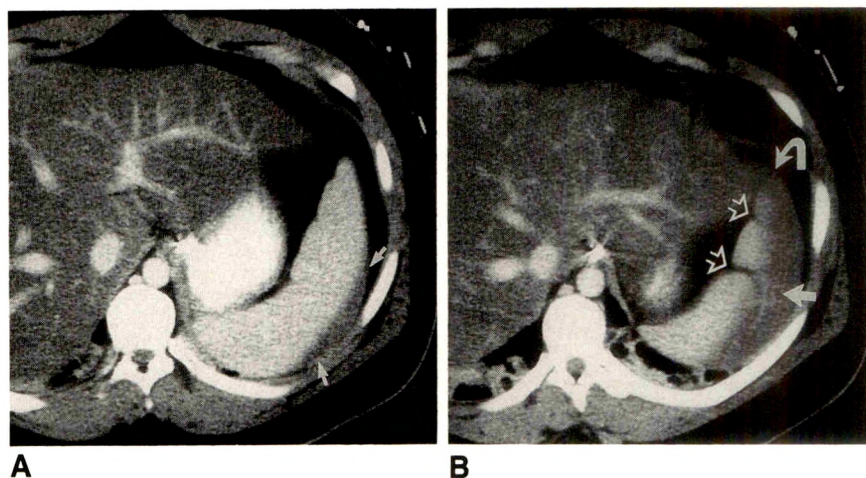
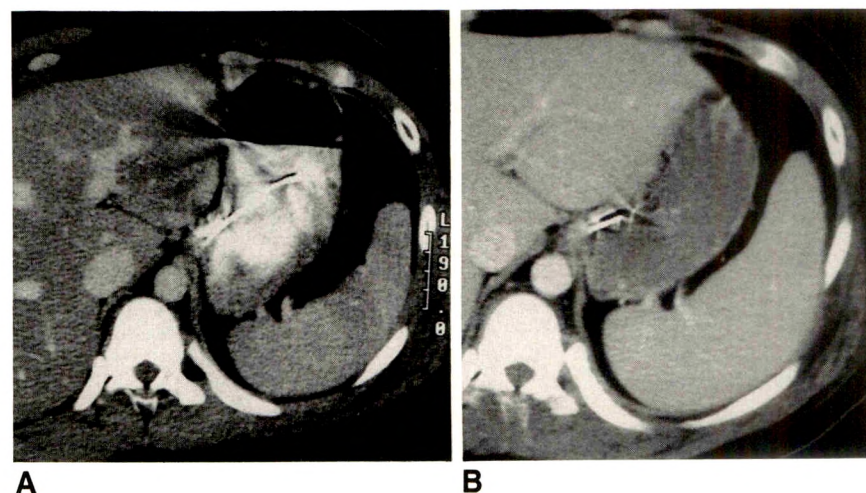


Fig. 16.—Physiologic change in size with trauma.
A, CT scan in a recently injured patient shows normal-appearing spleen.
B, With reversal of transient physiologic changes that may accompany trauma, spleen enlarges to original size 12 days later. There was a 10-mm increase in waist of spleen and a 12-mm increase in length from tip to tip.



bed by atherosclerosis, arteritis, or RBC sludging. Relative ischemia produced by splenomegaly may also cause infarction. Central inflammatory or neoplastic involvement of the splenic vasculature can also lead to infarction.

The classic peripheral, wedge-shaped, low-attenuation defect seen on CT causes no problem in diagnosis. However, the appearance of the infarct can vary. Attenuation can change during maturation; initially, a higher attenuation or a mottled appearance may be present, followed by a progressive decrease in attenuation with age [6]. The shape may vary from spherical or geographic areas of altered texture (Fig. 17). Rarely, the entire spleen may be infarcted, leaving only a rim of enhancing capsule (Fig. 18). Differentiation from splenic abscess, hematoma, or neoplasm usually requires clinical correlation or, if necessary, percutaneous fine-needle aspiration biopsy.

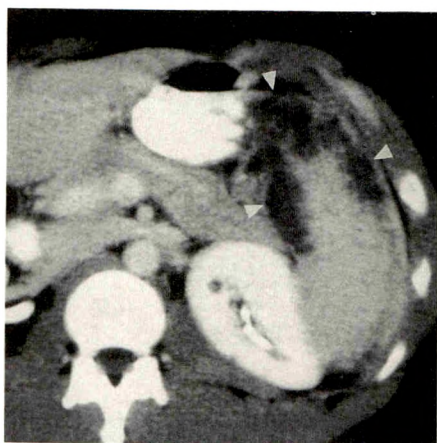
Inflammatory Changes

The spleen may be the primary focus of infection or be involved secondarily. Primary infections of the spleen with abscess formation are rare, reported in less than 1% of

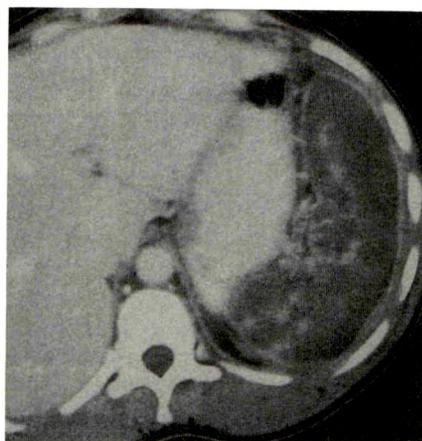
autopsy series [7]. Patients at risk frequently have a previously normal spleen with an underlying septic focus, such as bacterial endocarditis, seeding the spleen. Trauma, hematologic malignancy, hemoglobinopathy, IV drug abuse, alcoholism, and other forms of immunocompromised states are all risk factors as well. The study of choice for identification of inflammatory change is CT. Septic involvement of the spleen may occur as a single focus, which is seen as a low-attenuation area on a contrast-enhanced study. Peripheral rim enhancement may or may not be apparent when dynamic scanning techniques are used. Fluid levels, septa, or gas within the splenic mass may be present (Fig. 19). Alternatively, numerous, small, low-attenuation areas representing microabscesses may be present within the spleen (Fig. 20). Certain primary infections of the spleen, such as mononucleosis, show only mild to moderate splenomegaly without textural abnormality.

Percutaneous aspiration can be used to establish the diagnosis of splenic abscess. Although surgical splenectomy is the treatment of choice for splenic abscess, percutaneous treatment may be used in the unstable patient [7].

More commonly, the spleen is involved with a secondary disease such as pancreatitis. Pancreatitis may cause throm-



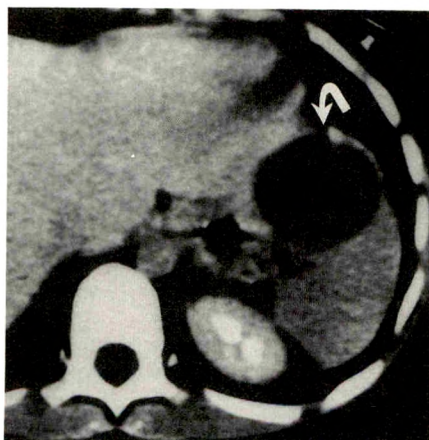
17



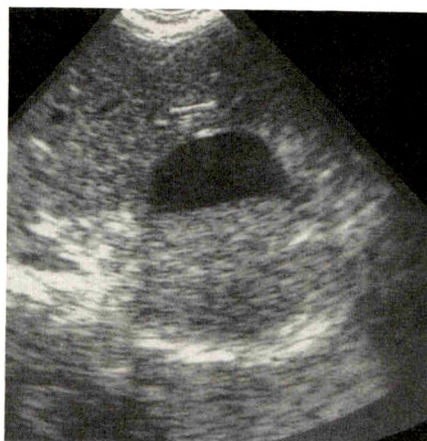
18

Fig. 17.—Infarction. A 33-year-old man with sickle cell-hemoglobin C disease had pain in left upper quadrant for 6 days. CT scan shows peripheral crescent of low attenuation with irregular borders (arrowheads). This geographic pattern is one appearance of infarction.

Fig. 18.—Global infarct. This 23-year-old IV drug abuser had upper quadrant pain. CT scan shows entire spleen is of abnormally low attenuation, except for an enhancing capsule and scattered central high-attenuation islands. This residual capsular enhancement is reminiscent of that seen in renal infarction. Having no septic symptoms, patient was managed conservatively and did well.



A



B

Fig. 19.—Abscess.

A, In this febrile patient, CT scan shows a well-circumscribed, apparently homogeneous mass (arrow) in anterosuperior spleen that could be mistaken for a splenic cyst.

B, Sonogram, obtained immediately after CT scan, shows fluid-fluid level. An abscess was confirmed at surgery. This illustrates importance of correlating imaging and clinical history of patient. (Courtesy of J. Sty, Milwaukee, WI.)

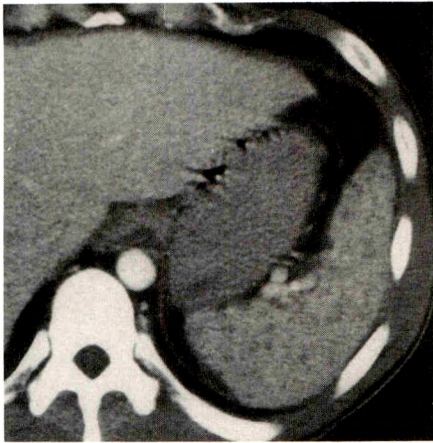


Fig. 20.—Abscess. Another manifestation of septic spleen is a myriad of tiny low-attenuation areas, as shown on this CT scan. In this immunocompromised patient, pattern of microabscesses suggests fungal infection. *Candida* was cultured from patient.

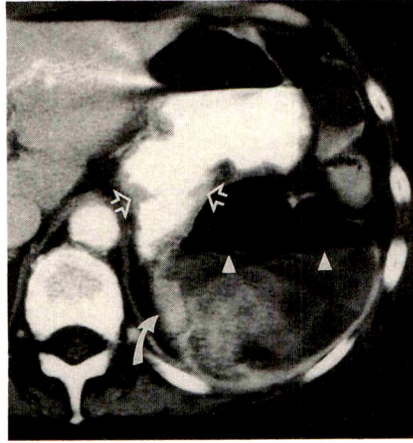


Fig. 21.—Abscess from local inflammatory process. A chronically ill man presented with sepsis. On CT scan, splenic parenchyma is replaced by infected collection with air-fluid level (arrowheads). This resulted from a benign posterior gastric ulcer (open arrows) that perforated spleen. High-attenuation material in splenic abscess (solid arrow) is oral contrast agent.



Fig. 22.—Sickle cell disease. End-stage spleen in sickle cell disease is usually small or absent. In this adult with sickle cell disease, a CT scan shows size of this diffusely calcified spleen is preserved. Note increased attenuation of liver from transfusion hemosiderosis.

basis of the splenic vein leading to development of collateral vessels or, less frequently, resulting in splenic congestion and enlargement. Rarely, splenic necrosis or hemorrhage occurs. A pseudocyst may extend from the pancreatic tail into the splenic hilum via the splenorenal ligament and eventually become intrasplenic (Fig. 10). Rarely, the spleen may become affected by other adjacent inflammatory processes in the abdomen (Fig. 21).

Miscellaneous

Splenic calcifications are a fairly frequent finding on abdominal CT. Most are granulomas, related to prior infections with histoplasmosis or tuberculosis. However, calcifications may occur as the result of a previous traumatic, infectious, or vascular insult. As previously mentioned, some tumors may contain calcifications. In AIDS patients, calcifications may be due to disseminated *Pneumocystis carinii* infection.

Certain hemoglobinopathies, classically, homozygous sickle cell disease, may lead to splenic calcification (Fig. 22). By age 5, the patient with sickle cell disease is functionally asplenic with only residual calcifications. However, sickle cell trait, or a combination of hemoglobinopathies (i.e., sickle cell-

hemoglobin C disease or sickle cell-thalassemia disease), may cause mild splenomegaly of normal texture. These spleens are at greater risk than those in patients without hemoglobinopathies for developing complications of infarcts (Fig. 17), abscesses, hemorrhage, or sequestration crises (sudden enlargement of the spleen with a concomitant drop in hematocrit). In hemoglobinopathies leading to severe anemia, the spleen becomes a site of extramedullary hematopoiesis.

REFERENCES

1. Dodds WJ, Taylor AJ, Erickson SJ, Stewart ET, Lawson TL. Radiologic imaging of splenic anomalies. *AJR* 1990;155:805-810
2. Shirkhoda A, Ros R, Farah J, et al. Lymphoma of the solid abdominal viscera. *Radiol Clin North Am* 1990;28:785-799
3. Morehouse HT, Thornhill BA. Splenic disease: a modern approach. *Postgrad Radiol* 1987;7:112-130
4. Orwig D, Federle MP. Localized clotted blood as evidence of visceral trauma on CT: the sentinel clot sign. *AJR* 1989;153:747-749
5. Goodman LR, Aprahamian C. Changes in splenic size after abdominal trauma. *Radiology* 1990;176:629-632
6. Balcar I, Seltzer SE, Davis S, Geller S. CT patterns of splenic infarction: a clinical and experimental study. *Radiology* 1984;151:723-729
7. Gleich S, Wolin DA, Herbsman H. A review of percutaneous drainage in splenic abscess. *Surg Gynecol Obstet* 1988;167:211-216

Book Review

Magnetic Resonance in Experimental and Clinical Oncology. Edited by Jeffrey J. Evelhoch, William Negendank, Frederick A. Valeriote, and Laurence H. Baker. Boston: Kluwer, 391 pp., 1990. \$90

This book contains the proceedings of the 21st annual Detroit Cancer Symposium, held April 13–14, 1989. The oral presentations from the symposium are given, accompanied by graphs, tables, MR spectra, and, in some cases, reproductions of MR images. The question-and-answer sessions that followed the presentations are included at the end of each chapter.

The primary focus of the text is the use of MR spectroscopy as an investigational tool in cancer research. Clinical oncology has a great need for a reliable method to predict the outcome and monitor treatment in individual patients. MR spectroscopy, with its unique ability to measure the flux of many metabolites noninvasively in vivo, has been cited as a potential means of fulfilling this need. Several studies in the text are about using MR spectroscopy to monitor the metabolic response of tumors to various forms of therapy. Investigations of animal tumor models and in vivo studies of human tumors are included. Additional topics include the measurement of tumor blood flow by deuterium MR spectroscopy, the use of MR spectroscopy for studying the effects of adriamycin cardiotoxicity, and the integration of MR imaging with MR spectroscopy of soft-tissue tumors in humans. The majority of the studies were performed with ^{31}P MR spectroscopy, with lesser emphasis on other nuclei such as

hydrogen-1 and carbon-13. The chapters on MR spectroscopy are generally concise, well written, and informative.

A relatively small portion of the text (less than 20%) is devoted solely to MR imaging. This section presents an overview of the role of MR imaging in clinical oncology, briefly covering some of the important anatomic sites of tumor involvement. Several reproductions of MR images of various tumors are included. These are limited in scope and are of variable quality. Although the individual chapters on MR imaging are quite good, this section of the text, taken as a whole, is superficial and incomplete. The role of MR imaging in clinical oncology is covered in greater depth in the standard MR imaging texts.

In summary, this text provides an excellent review of some interesting research on the use of MR spectroscopy as an investigative tool in clinical oncology and a brief overview of oncologic MR imaging. Its appeal will be limited to those who have a specific interest in the application of MR spectroscopy to cancer research.

Jeffrey J. Brown
Malinckrodt Institute of Radiology
St. Louis, MO 63110

Cancer of the Endometrium: Value of MR Imaging in Determining Depth of Invasion into the Myometrium

Hans H. Lien¹
Viggo Blomlie¹
Claes Tropé²
Janne Kærn²
Vera M. Abeler³

The depth of invasion into the myometrium correlates with the frequency of lymph node metastases in patients with cancer of the endometrium. A distinction between superficial invasion (<50% of the thickness of the myometrium) and deep invasion (>50%) is particularly important. The ability to distinguish between these two groups on MR was studied in 33 patients with endometrial cancer who had primary hysterectomy. The overall accuracy of MR in showing deep invasion was 82%, with a sensitivity of 91% and a specificity of 64%. The main limitation of MR was four false-positive results with regard to deep invasion. In all of these, the erroneous diagnosis was found at histologic examination to be due to a large polypoid tumor that distended the uterus so that a thin rim of myometrium was stretched over it rather than being deeply infiltrated by it.

Our experience shows that MR can be used to distinguish between superficial and deep invasion of the myometrium. However, degree of invasiveness may be overestimated in exophytic polypoid tumors with significant intraluminal extension.

AJR 157:1221-1223, December 1991

Most patients with early-stage endometrial cancer are cured. However, the prognosis is poor when the tumor has spread outside the uterus [1]. The prevalence of lymph node metastases is related to the stage of the disease, the grade of the tumor, and the depth of invasion into the myometrium [1-5]. Piver et al. [6] reported the prevalence of paraaortic lymph node metastases to vary from 3% among patients with tumor confined to the endometrium or superficial myometrium to 46% in patients with deep myometrial invasion. In a study of 1566 patients with endometrial adenocarcinoma, depth of myometrial invasion was the most important prognostic factor [7]. A distinction between superficial invasion (<50% of the thickness of the myometrium) and deep invasion (>50%) was of particular value.

The depth of invasion can be evaluated by abdominal [8-10] and vaginal sonography [11]. Earlier studies have shown that MR imaging is useful for showing endometrial carcinoma and assessing its size and invasiveness [10, 12-14]. In this prospective study of 33 patients who had hysterectomy, we compared the results of MR with the histologic findings of the surgical specimen. In particular, the reliability of MR for showing deep invasion of the tumor into the myometrium was investigated.

Subjects and Methods

The study included 33 consecutive patients admitted to our hospital because of endometrial cancer of clinical stage I (tumor confined to the uterine body, 22 patients) and II (tumor extending into the cervix, 11 patients). There were 28 carcinomas (21 adenocarcinoma, five adenosquamous carcinoma, one undifferentiated carcinoma, and one clear cell carcinoma) and five carcinosarcomas. The methods used were the same as those we used in an earlier study on tumor invasion in cervical carcinoma [15]. Each patient had a complete clinical

Received July 1, 1991; accepted after revision July 31, 1991.

¹ Department of Diagnostic Radiology, The Norwegian Radium Hospital, Montebello N-0310, Oslo 3, Norway. Address reprint requests to H. H. Lien.

² Department of Gynecologic Oncology, The Norwegian Radium Hospital, Montebello N-0310, Oslo 3, Norway.

³ Department of Pathology, The Norwegian Radium Hospital, Montebello N-0310, Oslo 3, Norway.

0361-803X/91/1576-1221
© American Roentgen Ray Society

workup consisting of a clinical staging examination under anesthesia, dilatation and curettage, cystoscopy, chest radiography, and excretory urography. All patients had hysterectomy. The patients' ages ranged from 37 to 80 (mean, 70) years. None of the patients were taking hormones.

Examinations were done on a 1.5-T Signa System (General Electric, Milwaukee, WI). Spin-echo (SE) pulse sequences were used, including a coronal localizer series followed by sagittal and axial T2-weighted series (2000/20–80[TR/TE]) and an axial T1-weighted series (600/20). All sequences but the localizer series used a 256 × 256 matrix and two excitations. Slice thickness was 5 mm, and 2.5-mm gaps were used. Field of view was 36 cm. Patients did not fast before the examinations, but were given two glasses of water 30–45 min before the study to fill the bladder.

The study was prospective and the MR images were evaluated by two radiologists who knew the diagnoses. The images were interpreted in conference and the findings were determined by consensus. The criteria used for evaluating extent of disease were widening of the endometrium and distortion of the zonal anatomy. The upper limit for normal endometrial width was 3 mm in postmenopausal women and 10 mm in premenopausal women [12].

The invasion of the tumor into the myometrium was measured with the cross-hair cursor on the monitor. The maximum infiltration was classified as less than 50% of the thickness of the myometrium (superficial invasion) or more than 50% (deep invasion).

All patients had total abdominal hysterectomy without lymphadenectomy. The surgical specimen was fixed in 5% formalin for 24–48 hr. The uterus was cut into approximately 5-mm-thick sagittal sections for evaluation of tumor size and gross extent of myometrial invasion. Sections for microscopic examinations were taken from those parts of the tumor that showed the deepest infiltration on gross examination. The pathologist did not know the MR findings.

Results

Histologic examination revealed deep invasion of the tumor into the myometrium in 22 patients. Twenty of these were correctly identified on MR images (Figs. 1 and 2). Superficial invasion was found at histologic examination in 11 patients. In four of these a deeply invasive tumor was erroneously suspected on MR imaging (Fig. 3). Thus, the overall accuracy in demonstrating deep invasion was 82%, with a sensitivity

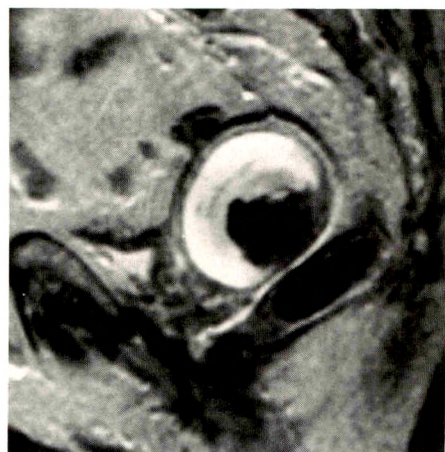
of 91% and a specificity of 64%. The positive and negative predictive values were 83% and 78%, respectively.

Discussion

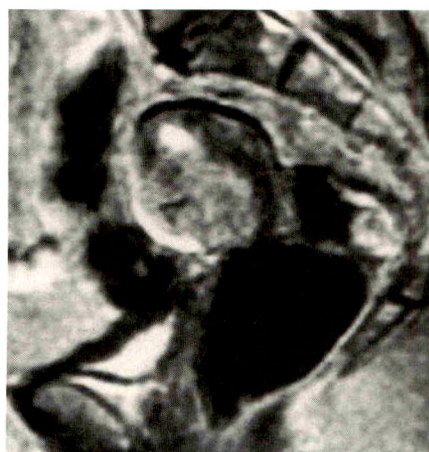
Our results show that MR imaging can provide valuable information about depth of tumor invasion into the myometrium. The overall accuracy of 82% in distinguishing between deep and superficial invasion is slightly lower than the 97% and 98% accuracies reported in earlier series [12, 13]. One limitation of MR was the four false-positive cases with regard to deep invasion. These accounted for the low specificity. In all of these, histologic examination disclosed a large intraluminal polypoid tumor that distended the uterus so that a thin rim of myometrium was stretched over it rather than being deeply infiltrated by it (Fig. 3). However, four false-positive results among a total of 24 positives are in accordance with two other series that reported one false-positive on MR among six positive results [10, 12]. On the other hand, Chen et al. [13] reported 17 positive findings with regard to deep invasion, all of which were true-positive. Some of the incorrect evaluations may be due to the technique, with a relatively large gap of 2.5 mm on a 5-mm slice thickness. The problem with overestimation of degree of invasiveness in cases of exophytic polypoid tumors has been reported with sonography also [8, 9].

The high prevalence of histologically proved deep invasion in the present series (22/33) differs from that reported in other MR series that reported deep invasion at histologic examination in five of 39 [12] and 18 of 50 patients [13]. In a clinical-pathologic correlative study, deep myometrial invasion was found in 29% [7]. Our patients therefore represent advanced cases treated with primary hysterectomy. This may be explained by the fact that most patients admitted to our hospital for hysterectomy as the primary treatment have carcinosarcomas, clinical stage II disease, or are older. All these conditions carry a high propensity for deep myometrial invasion [7].

Contrary to the situation in carcinoma of the uterine cervix, which usually has a relatively high signal on T2-weighted images [15, 16], endometrial carcinoma may have a highly



1

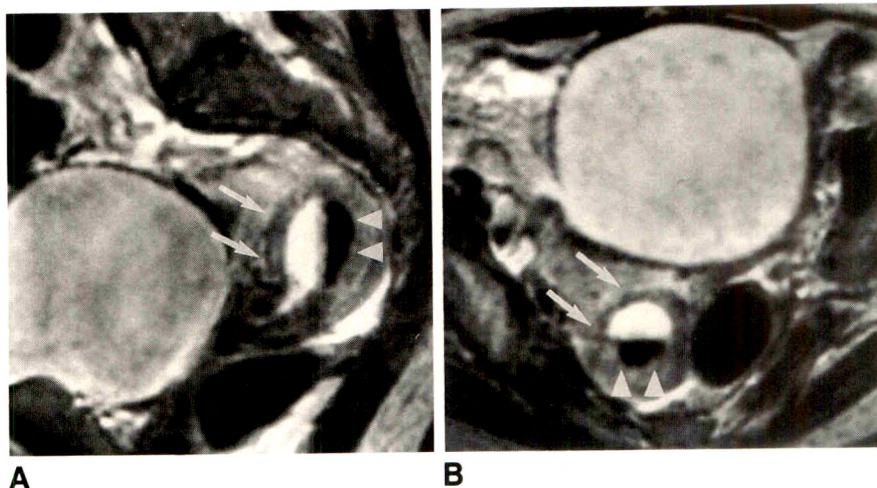


2

Fig. 1.—72-year-old woman with adenocarcinoma. T2-weighted (SE 2000/80) sagittal MR image shows mixed high and low signal intensity and deep invasion into myometrium. Invasion depth was confirmed at histologic examination.

Fig. 2.—79-year-old woman with carcinosarcoma. T2-weighted (SE 2000/80) sagittal MR image shows deep myometrial invasion (to serosa) of anterior wall. MR finding was confirmed at histologic examination.

Fig. 3.—A and B, 66-year-old woman with adenocarcinoma. Sagittal (A) and axial (B) T2-weighted (SE 2000/80) MR images show high signal intensity. MR was considered positive for deep myometrial invasion of anterior wall (arrows). Histologic examination disclosed a rim of myometrium stretched over the tumor and invasion depth less than half of myometrial thickness. Deoxyhemoglobin after curettage is seen posteriorly (arrowheads).

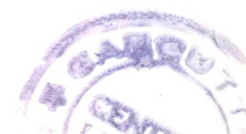


variable signal intensity [12]. Therefore, less-distinct criteria must be used in the interpretation of these tumors than when evaluating cervical carcinoma. As endometrial cancer is essentially a tumor of the postmenopausal woman, the potential changes in MR appearances at various times during the menstrual cycle seldom pose a problem [17]. In our series, only two of the 33 patients were of reproductive age. The absence of the junctional zone in postmenopausal women may create difficulties in differentiating a tumor confined to the endometrium from one with superficial myometrial infiltration. However, it does not influence the interpretation with regard to deep invasion of the myometrium.

There is a trend in gynecologic oncology centers to individualize the management of endometrial cancer. In this respect, selection of patients who are at a high risk for extrauterine disease is an important task. The grade of the tumor can be determined preoperatively by endometrial sampling. The present series indicates that MR imaging is a reliable method for distinguishing between superficial and deep myometrial invasion except in cases of polypoid, intraluminal tumors. Because of the correlation between depth of myometrial infiltration and frequency of paraaortic lymph node metastases [1–6], MR may be useful in selecting patients who might benefit from lymphadenectomy. Also, patients with cancer of the endometrium are often elderly and obese with additional medical problems that make them poor candidates for surgery. These patients are often treated with standard whole-pelvis irradiation. In this situation, MR may help depict deep myometrial invasion in patients in whom extended irradiation fields covering paraaortic lymph nodes could be beneficial.

REFERENCES

1. Boronow RC. Advances in diagnosis, staging, and management of cervical and endometrial cancer, stages I and II. *Cancer* 1990;65:648–659
2. Berman ML, Ballon SC, Lagasse LD, Watring WG. Prognosis and treatment of endometrial cancer. *Am J Obstet Gynecol* 1980;136:679–688
3. Boronow RC, Morrow CP, Creasman WT, et al. Surgical staging in endometrial cancer: clinical-pathologic findings of a prospective study. *Obstet Gynecol* 1984;63:825–832
4. Chen SS. Extrauterine spread in endometrial carcinoma clinically confined to the uterus. *Gynecol Oncol* 1985;21:23–31
5. Creasman WT, Morrow CP, Bundy BN, Homesley HD, Graham JE, Heller PB. Surgical pathologic spread patterns of endometrial cancer: a gynecologic oncology group study. *Cancer* 1987;60:2035–2041
6. Piver MS, Lele SB, Barlow JJ, Blumenson L. Para-aortic lymph node evaluation in stage I endometrial carcinoma. *Obstet Gynecol* 1982;59:97–100
7. Abeler VM, Kjørstad KE. Endometrial adenocarcinoma in Norway: a study of a total population. *Cancer* 1991;67:3093–3103
8. Fleischer AC, Dudley BS, Entman SS, Baxter JW, Kalemeris GC, James AE. Myometrial invasion by endometrial carcinoma: sonographic assessment. *Radiology* 1987;162:307–310
9. Cacciatori B, Lehtovirta P, Wahlström T, Ylöstalo P. Preoperative sonographic evaluation of endometrial cancer. *Am J Obstet Gynecol* 1989;160:133–137
10. Thorvinger B, Gudmundsson T, Horvath G, Forsberg L, Holtås S. Staging in local endometrial carcinoma: assessment of magnetic resonance and ultrasound examinations. *Acta Radiol* 1989;30:525–529
11. Cacciatori B, Lehtovirta P, Wahlström T, Ylänen K, Ylöstalo P. Contribution of vaginal scanning to sonographic evaluation of endometrial cancer invasion. *Acta Oncol* 1989;28:585–588
12. Hricak H, Stern JL, Fisher MR, Shapeero LG, Winkler ML, Lacey CG. Endometrial carcinoma staging by MR imaging. *Radiology* 1987;162:297–305
13. Chen SS, Rumancik WM, Spiegel G. Magnetic resonance imaging in stage I endometrial carcinoma. *Obstet Gynecol* 1990;75:274–277
14. Hricak H, Rubinstein LW, Gherman GM, Karstaedt N. MR imaging evaluation of endometrial carcinoma: results of an NCI cooperative study. *Radiology* 1991;179:829–832
15. Lien HH, Blomlie V, Kjørstad K, Abeler V, Kaalhus O. Clinical stage I carcinoma of the cervix: value of MR imaging in determining degree of invasiveness. *AJR* 1991;156:1191–1194
16. Hricak H, Lacey CG, Sandles LG, Chang YCF, Winkler ML, Stern JL. Invasive cervical carcinoma: comparison of MR imaging and surgical findings. *Radiology* 1988;166:623–631
17. Demas BE, Hricak H, Jaffe RB. Uterine MR imaging: effects of hormonal stimulation. *Radiology* 1986;159:123–126





Come to the
American Roentgen Ray Society

92nd

ANNUAL MEETING

Orlando, FL

Marriott's Orlando World Center
May 10–15, 1992

Scientific Program (200 papers)
Instructional Courses (60 hours)
Categorical Course on Neuroradiology
The Caldwell Lecture
Award Papers
Scientific Exhibits
Social, Golf, and Tennis Programs
Guest Programs

Case Report

Sonographic Appearance of Primary Testicular Lymphoma

Vijay Moorjani,¹ Anant Mashankar, Sanjay Goel, Kamlesh Khandelwal, Vijay Patange, and Nikhil Merchant

Since the first report of non-Hodgkin lymphoma manifesting as a testicular mass, described by Malassez in 1877 [1], primary testicular lymphoma has attracted attention because of its rarity and poor prognosis. Only a few reports of the sonographic appearance of testicular lymphoma have been published [2]. We describe the sonographic findings in two such cases.

Case Report

A 50-year-old man had an orchiectomy for malignant lymphoma (diffuse histiocytic type) of the right testis. He was referred to our hospital for further treatment. CT and sonographic examination of the abdomen and pelvis did not reveal enlarged nodes. The diagnosis of primary right testicular lymphoma was reached, and he began combination chemotherapy. A month later, nontender swelling of the left testis was noted. Sonograms obtained with a 7.5-MHz transducer with an attached water bath revealed an enlarged testis and a diffusely hypoechoic parenchyma (Fig. 1). In view of the patient's history, a preliminary diagnosis of malignant lymphoma of the testis was made. A biopsy was done with fine-needle aspiration, and the results were suggestive of lymphoma. An orchiectomy was performed, and final histopathology confirmed the diagnosis of malignant lymphoma (diffuse histiocytic type).

Discussion

A malignant lymphoma in which the tumor mass is limited to the testis at the time of clinical onset of the disease is rare. It is seen in approximately 1% of men with non-Hodgkin lymphoma, but can occur in up to 4% of cases of Burkitt lymphoma. It is practically nonexistent in Hodgkin disease [2].

Testicular lymphoma constitutes 1–7% of all testicular tumors [3] and is the most common testicular malignant tumor in men between 60 and 80 years old. Bilateral involvement is even rarer, constituting 23% of all cases of primary testicular lymphoma [4].

Pathologically, lymphomas appear as a diffuse, symmetric enlargement of the entire organ with involvement of epididymis and spermatic cord but without invasion through the tunica vaginalis. The hallmark of lymphoma is an infiltrative growth pattern that tends to surround and compress before destroying the seminiferous tubules. The histologic pattern is that of the poorly differentiated or large cell types [5].

The testis appears to provide a sanctuary for this disease, owing to an apparent "gonadal barrier" that inhibits concentration of chemotherapeutic agents [6]. This means that a patient can get an apparent primary lymphoma in the testis some time after he was apparently cured of primary lymphoma elsewhere.

The sonographic pattern of involvement includes focal or diffuse areas of decreased echogenicity in an enlarged testis [6]. The 50-year-old patient in the case described earlier had diffuse involvement of the testis by lymphoma. Sonograms of a second patient with primary testicular lymphoma revealed focal involvement. This was a 42-year-old man who had had abdominoperineal resection for adenocarcinoma of the rectum 5 years earlier and now had pain and swelling of the left testis. Sonographic examination of the scrotum revealed a well-defined, hypoechoic space-occupying lesion in the cranial aspect of the left testis (Fig. 2). Findings on sonographic and CT examinations of the abdomen and pelvis were normal. A left orchiectomy was performed. The histopathologic diagnosis was malignant lymphoma of the testis (histiocytic type).

Received May 15, 1991; accepted after revision July 8, 1991.

¹ All authors: Department of Radiodiagnosis, Tata Memorial Hospital, Dr. Ernest Borges Rd., Parel, Bombay 400 012, India.

AJR 157:1225–1226, December 1991 0361–803X/91/1576–1225 © American Roentgen Ray Society

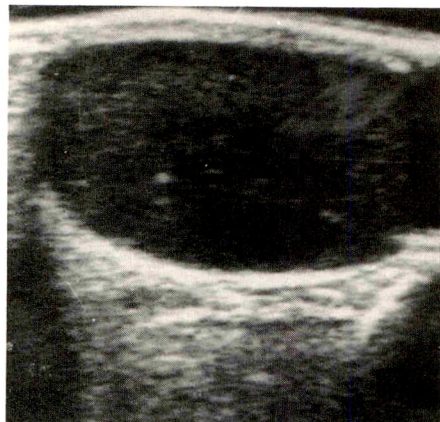
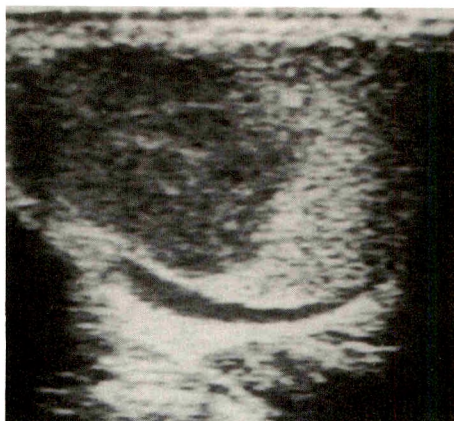
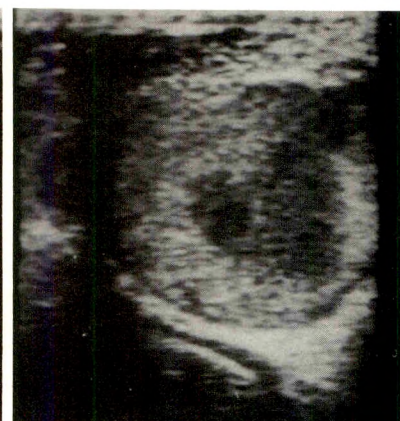


Fig. 1.—Longitudinal sonogram of 50-year-old man with nontender swelling of left testis shows an enlarged testis with generalized reduced echogenicity.



A



B

Fig. 2.—A and B, Longitudinal (A) and transverse (B) sonograms of 42-year-old man with pain and swelling of left testis show a focal hypoechoic area within testis.

The differential diagnosis of an enlarged testis with uniformly reduced echogenicity includes seminoma, leukemia, and orchitis. Occasionally, this disease is seen as an increased echogenic pattern or a focal area of increased echogenicity within a sonolucent testis. Some cases may have an accompanying hydrocele [7].

The prognosis for patients with testicular lymphoma is poor, because it is more lethal than testicular carcinomas [8]. Given the general biological aggressiveness of this disease, local treatment with orchiectomy and irradiation of regional nodes is insufficient, and in most cases chemotherapy is also given [3]. Early detection is important in the epidemiology of testicular lymphoma. The sonographic appearance is not specific for primary testicular lymphoma, but in the proper clinical setting, the diagnosis may be suspected and a biopsy suggested. Sonography plays a significant role in the detection of clinically occult cases and in following up patients with unilateral primary testicular lymphoma to detect dissemination and metachronous involvement of the contralateral testis.

Sonography also can serve as an index or marker in monitoring the effect of treatment.

REFERENCES

1. Malassez M. Cited by: Tepperman BS, Gospodarowicz MK, Bush RS, et al. Non-Hodgkin's lymphoma of the testis. *Radiology* **1982**;142:203-208
2. Charnsangavej C. Lymphoma of the genitourinary tract. *Radiol Clin North Am* **1990**;28:865-877
3. Baldetrop LA, Brunkwall J, Cavellin-Stahl E, et al. Malignant lymphoma of the testis. *Br J Urol* **1984**;56:525-530
4. Turner RR, Colby TV, Mackintosh FR. Testicular lymphomas: a clinicopathological study of 35 cases. *Cancer* **1981**;48:2095-2102
5. Damjanov I. Tumors of the testis and epididymis. In: Murphy WM, ed. *Urological pathology*. Philadelphia: Saunders, **1989**:314-379
6. Krone KD, Carroll BA. Scrotal ultrasound. *Radiol Clin North Am* **1985**;23:121-139
7. Finkelstein MS, Rosenberg HK, Snyder HM, Duckett JW. Ultrasound evaluation of scrotum in pediatrics. *J Urol* **1986**;27:1-9
8. Freeman C, Berg JW, Cutler SJ. Occurrence and prognosis of extranodal lymphoma. *Cancer* **1972**;29:252-260

Case Report

Gelatin Sponge Mimicking a Pelvic Neoplasm on MR Imaging

Ellen G. Hoeffner,¹ Renate L. Soulen,¹ and Carl W. Christensen²

Absorbable gelatin sponge is a commonly used hemostatic agent that is often left in surgical wounds at the time of closure. In animal experiments, gelatin sponge implanted in the CNS [1] and intraperitoneally [2, 3] was absorbed in 2–4 weeks. We report a case in which gelatin sponge mimicked residual or recurrent malignant ovarian teratoma on MR images obtained 6 weeks after the sponge was inserted.

Case Report

A 36-year-old woman had painful bowel movements 6 weeks after she had a hysterectomy and bilateral salpingo-oophorectomy for malignant ovarian teratoma stage 3C and three courses of chemotherapy. MR of the pelvis was performed on a 1.0-T imager (Magnetom, Siemens, Erlangen, Germany). Axial spin-echo (SE) images were obtained with a TR/TE of 700/23, a 256 × 192 matrix, two excitations, 10-mm slices, and an interslice gap of 2 mm. Sagittal SE images were obtained with a TR/TE of 2000/25, 90; a 256 × 192 matrix; one excitation; 7-mm slices; and a 1.8-mm gap.

The images showed an ovoid, 5.0 × 3.5 cm mass above the vaginal cuff. The mass appeared to be partially encapsulated, clearly separate from the bladder but adherent to the rectum without a clear cleavage plane. An irregular focus of low signal intensity characterized the center of the mass on all pulse sequences. The more peripheral portion was homogeneous and isointense with muscle on the T1-weighted images and progressively more hyperintense on spin-density and T2-weighted images (Fig. 1). Unfortunately, no preoperative MR had been performed. The mass was attributed to residual or recurrent neoplasm, and the central low intensity focus to calcification or fibrosis.

Because all gross tumor seen at the initial surgery had been removed and the interval since surgery was short for new growth of such size, the clinical diagnosis became probable abscess and the patient had exploratory surgery. The gross appearance of the mass at this time was described as resembling fetal brain; it was removed in fragments. Microscopic examination revealed the fragments to consist entirely of gelatin sponge with an acute inflammatory infiltrate. Four sheets (8 × 12.5 × 1 cm) of gelatin sponge had been used during the initial surgery to control diffuse bleeding that resulted from resection of multiple tumor implants.

Discussion

Gelatin sponge promotes hemostasis by forming an artificial clot and by providing a mechanical matrix that facilitates clotting. It can absorb up to 45 times its weight in whole blood. Histologic studies in rabbits have shown that gelatin sponge implanted intraperitoneally initially absorbs blood and becomes surrounded by an acute inflammatory reaction that is followed by infiltration of mononuclear and giant cells and fibrosis [1, 2]. In these animals, smaller pieces of sponge were absorbed by phagocytosis in 4–6 weeks; large implants (24 × 12 × 1.2 cm) persisted longer [2].

Gelatin sponge has been reported to mimic a spinal mass at the surgical site on MR images obtained 9–11 days after laminectomy. Dubin et al. [4] reported that such masses were inhomogeneous in signal intensity on both T1- and T2-weighted images, an appearance they attributed to a mixture of gelatin sponge, blood, exudate, and early granulation tis-

Received May 13, 1991; accepted after revision July 9, 1991.

¹ Department of Radiology, Vaitkevicius MR Center, Harper Hospital, 3990 John R. St., Detroit, MI 48201. Address reprint requests to E. G. Hoeffner.

² Department of Obstetrics and Gynecology, Wayne State University, Detroit, MI 48201.

AJR 157:1227–1228, December 1991 0361–803X/91/1576–1227 © American Roentgen Ray Society

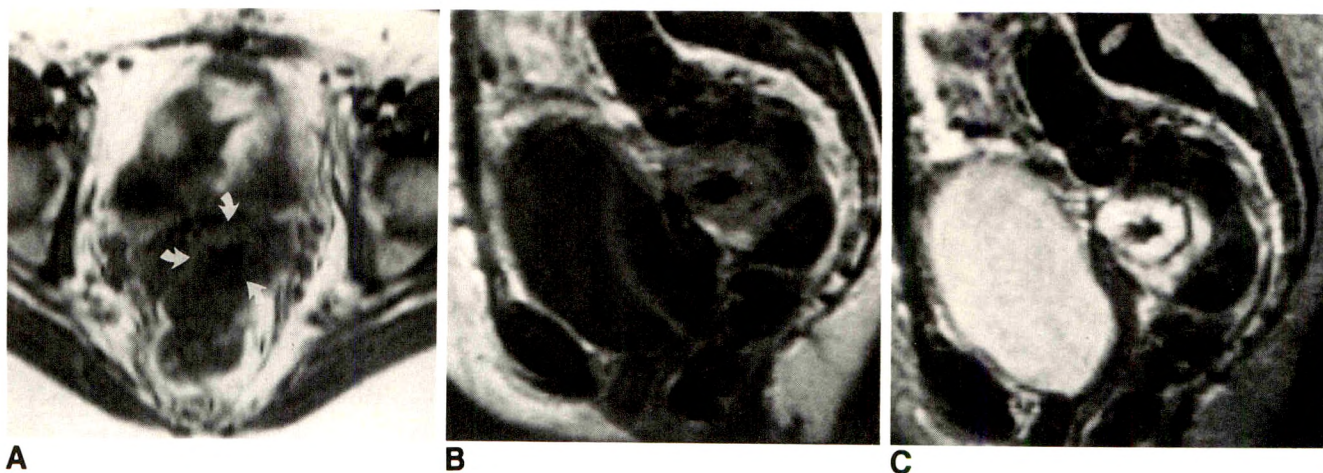


Fig. 1.—MR examination in a 36-year-old woman 6 weeks after hysterectomy and salpingo-oophorectomy for a malignant ovarian teratoma shows pelvic mass caused by gelatin sponge.

A, Axial image (700/23) shows mass (arrows) isointense with muscle except for a low-signal-intensity center.

B and C, Sagittal images (2000/25, 90) show persistently low-signal-intensity core with remainder of mass progressively increasing in signal intensity.

sue. They do not mention air. Intraabdominal bubbly air collections that could be confused with an abscess have been reported on plain films obtained postoperatively in patients in whom gelatin sponge was used [5].

Large volumes of gelatin sponge are thought to be absorbed slowly because phagocytic cells cannot reach the center of the sponge [2]. Persistence of some of this material 6 weeks later, as in our case, is in keeping with experimental results. The low-intensity "core," which we now attribute to air, and the homogeneity of the thick "rind" differ from the MR appearance reported for laminectomy sites, but the images of the latter were obtained much earlier in the postoperative period [4]. Likewise, the air reported on plain films was seen 7–10 days after surgery [5]. Our case shows that MR evidence of foci compatible with air, in the appropriate clinical

setting, should help differentiate gelatin sponge from residual or recurrent neoplasm.

REFERENCES

1. Light RU, Prentice HR. Surgical investigation of a new absorbable sponge derived from gelatin for use in hemostasis. *J Neurosurg* 1945;2:435–445
2. Blaine G. Absorbable gelatin sponge in experimental surgery. *Lancet* 1951;2:427–429
3. Bing J. Experimental observations on the use of a Danish gelatin sponge preparation ("Spongostan") as an absorbable haemostatic agent. *Acta Pharmacol* 1947;3:364–372
4. Dubin LM, Quencer RM, Green BA. A mimicker of a postoperative spinal mass: Gelfoam in a laminectomy site. *AJNR* 1988;9:217–218
5. Eklof O, Lebowitz RL. Localized intra- and retroperitoneal gas collections following intraoperative use of surgical gelatin sponge. *Pediatr Radiol* 1981;11:1–4

Review Article

Noninvasive Measurements of Bone Mass, Structure, and Strength: Current Methods and Experimental Techniques

Kenneth G. Faulkner,¹ Claus-C. Glüer, Sharmila Majumdar, Philipp Lang, Klaus Engelke, and Harry K. Genant

Current methods for assessing osteoporotic fracture risk involve measuring the content and/or density of bone at a number of skeletal sites and relating the measurement to that in either age-matched or young control subjects measured at the same site with the same technique. These densitometric methods have been used to predict several types of fractures; however, engineering principles verify that the bone structure and loading conditions also affect skeletal strength. Many densitometric measurements inherently contain information about skeletal structure and bone distribution, yet this information is not clinically used. In this paper, the currently available techniques for assessing bone content and density, namely, single-photon absorptiometry, dual-photon absorptiometry, dual-energy X-ray absorptiometry, and quantitative CT, and their usefulness in assessing fracture risk and distinguishing between patients with and without osteoporosis are reviewed. Extensions of conventional densitometry that have been developed by several researchers to include information in addition to bone mass also are presented. Results from recent studies using new applications of ultrasound techniques and MR imaging are reviewed. Preliminary studies show the value of these new techniques in noninvasive measurement of bone structure in order to estimate bone strength and assess fracture risk more accurately. However, to become clinically useful, many of these methods require further investigation to increase their ease of use and decrease their cost.

Considerable time and effort have been expended in search of the predominant risk factors for developing osteoporotic fractures. At the center of this research is the emerging field of bone densitometry, which is based on the theory that the amount of bone mineral at a particular skeletal site is directly

related to the strength either of the bone being measured or of the skeleton as a whole. Several studies have shown that bone mass is indeed one of the largest contributors to skeletal strength. However, basic engineering principles confirm that the strength of an object is a function of more than just the amount and the density of material present. Accurate estimates of strength require information about (1) the mechanical properties of the materials making up the structure, (2) the object's geometry, and (3) the loading conditions, in terms of magnitude, rate, and direction, to which the object is subject. For the skeleton, information regarding bone properties, structure, and loading can be inferred either by direct measurement or through empirical relations with measurable quantities. However, the relative contribution of each of these factors to overall bone strength is, for the most part, unknown.

Several techniques have been developed, on the basis of conventional radiographic and densitometric measurements, to include factors in addition to bone mass and density for the estimation of skeletal strength. We review clinically available conventional techniques for measuring bone content and density and show how these measurements relate to bone strength in vitro and the assessment of fracture risk in vivo.

Conventional Densitometric Techniques

The relationship of bone mineral density and content to bone strength has been verified by many researchers from biomechanical analyses of excised vertebral [1-6] and femoral [7-10] specimens. On the basis of this relationship, several

Received April 2, 1991; accepted after revision July 5, 1991.

¹ All authors: Department of Radiology, Osteoporosis Research Group, Box 0628, University of California, San Francisco, San Francisco, CA 94143. Address reprint requests to K. G. Faulkner.

AJR 157:1229-1237, December 1991 0361-803X/91/1576-1229 © American Roentgen Ray Society

techniques have been developed to measure bone mass noninvasively at several skeletal sites. Differences between techniques exist in terms of the type of bone measured (cortical vs trabecular), precision (based on the observed deviation in serial measurements), accuracy (defined as the difference of the measurement from a known standard), scanning time, and radiation dose (Table 1). These techniques have been evaluated both prospectively and cross-sectionally in time to determine their usefulness for assessing skeletal strength. Measurements of bone content in the appendicular skeleton made by using single-photon absorptiometry (SPA) have been shown to predict future forearm [11], spine [12], hip [13], and most appendicular [14] fractures. Dual-photon absorptiometry (DPA) measurements of the spine show results equivalent to appendicular SPA measurements in predicting both spinal and appendicular fractures [12, 15]. Although prospective data relating dual energy X-ray absorptiometry (DXA) and quantitative CT (QCT) measurements to risk of fracture have not yet been published, several cross-sectional studies have compared these densitometric techniques for distinguishing normal from osteoporotic patients. In general, the best sensitivity and specificity for distinguishing patients with spinal osteoporosis from subjects without it is provided by QCT, followed by DXA and DPA, and finally SPA [16–20]. For discriminating appendicular fractures, however, data from one study have shown that SPA measurements of the radius are superior to QCT measurements of the spine [17].

Some controversy exists over which of the currently available measurement techniques and sites is the most appropriate for evaluating risk of fracture, partially because of the lack of prospective data. Differences in cost, availability, ease of use, and radiation dose among the methods are the source

of some confusion among many clinicians. Some of this confusion is related to the different units derived from each technique to express bone mass, either in terms of the mineral content, linear density, real density, or “true” three-dimensional density (Fig. 1). Despite the differences in opinion regarding the method of bone-mass determination, a recent report from the American Society of Bone and Mineral Research [21] has stated that densitometric measurements of the skeleton are clinically indicated for the detection and assessment of osteoporosis and for the evaluation and monitoring of several diseases and therapies. These include (1) the detection of osteoporosis and assessment of its severity, (2) evaluation of perimenopausal women for the initiation of estrogen therapy, (3) evaluation of patients with metabolic diseases that affect the skeleton, and (4) monitoring of treatment and evaluation of disease course.

Noninvasive Structural Measurements

Although bone mineral density is one of the most important contributing factors to bone strength and risk of fracture, studies have shown that age-related factors, such as increased risk of falling and changes in bone quality and structure independent of bone mineral density, influence both bone strength and individual risk of fracture [5, 11, 13, 22–24]. The influence of these other factors is thought to explain at least partially the observed overlap in bone mineral measurements between patients with and without previous osteoporotic fractures, irrespective of measurement site or technique. However, because of the statistical nature of fractures and falling, and the fact that bone mass is continuously distributed throughout the population, densitometric measurements from

TABLE 1: Comparison of Currently Used Techniques for Measuring Bone Mineral Density

Technique	Cortical/ Trabecular Ratio	Precision in Vivo (%)	Accuracy Error (%)	Scanning Time (min)	Effective Dose Equivalent ^a (μSv)
Single-Photon Absorptiometry					
Distal third radius	95/5	1–2	4–6	10	<1
Ultradistal radius	60/40	1–2	4–6	10	<1
Os calcis	5/95	1–2	4–6	15	<1
Dual-Photon Absorptiometry					
Lumbar spine	50/50	2–4	5–10	30	5
Proximal femur	60/40	3–5	5–10	30	3
Total body	80/20	2–3	1–2	40	3
Dual Energy X-ray Absorptiometry (pencil beam)					
Lumbar spine					
Anteroposterior	50/50	1	4–8	5–10	1
Lateral	10/90	2–3	5–10	15–20	3
Proximal femur	60/40	1–2	4–8	5–10	1
Total body	80/20	1	1–2	20	3
Quantitative CT					
Single energy spine	0/100 ^b	2–4	5–15	20	50
Dual energy spine	0/100 ^b	4–6	3–6	25	100

^a Does not include dose due to localization radiographs such as spine films and computed radiographs. For comparison, a standard chest radiograph, depending on the technique, has an effective dose equivalent of 100–150 μSv.

^b Depends on region of interest. The vertebral core is essentially 100% trabecular bone.

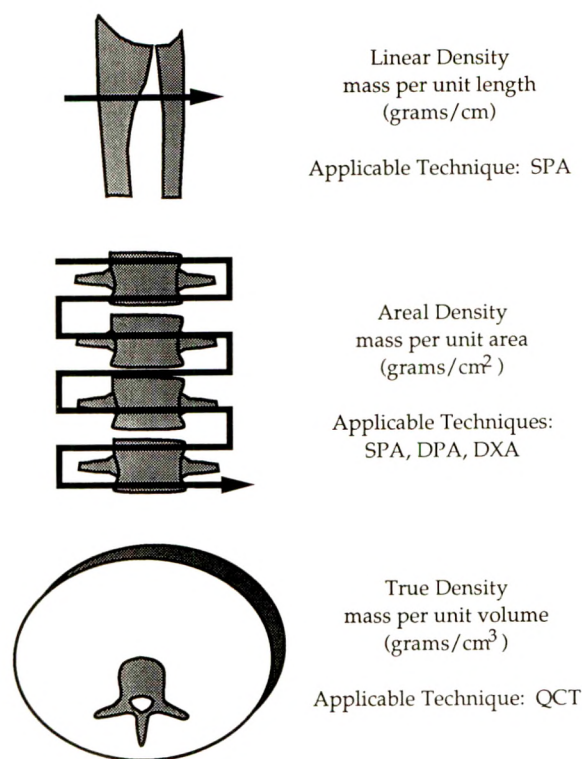


Fig. 1.—Various definitions used for the term *density* according to method of bone-mass measurement. SPA = single-photon absorptiometry, DPA = dual-photon absorptiometry, DXA = dual energy X-ray absorptiometry, QCT = quantitative CT.

patients with and without previous osteoporotic fractures will always overlap to some degree. In an attempt to improve the distinction between persons with and without osteoporosis and enhance determination of fracture risk by using bone mass measurements, several researchers have attempted to combine structural and densitometric information to estimate bone strength more accurately.

Most structural measurements of the skeleton are invasive (i.e., destructive). The most common measurement is of the iliac crest, where samples are taken with a bone-cutting needle and a local anesthetic and evaluated histomorphologically to determine parameters of bone formation and resorption. Earlier studies have shown a relationship between the mechanical strength of biopsy specimens from the iliac crest and that of the vertebral body [25, 26], although the relationship depends on the precise biopsy location [26]. However, the invasiveness of this procedure precludes its routine clinical use. As a result, iliac crest biopsies are used principally to define the nature of metabolic bone disease and not to assess the risk of osteoporotic fracture.

Several noninvasive techniques have emerged for combining bone densitometry with structural measurements to improve estimates of bone strength. Mathematical models based on plain radiographs and densitometric measurements from DPA, DXA, and QCT, which combine bone mass and geometry into a single model, have been developed. These range from relatively simple measures of cross-sectional area to complex patient-specific, three-dimensional, finite element

models. Besides radiographically based densitometric techniques, MR imaging and ultrasound measurements have been investigated as measures of bone density and structure, both on a macroscopic and microscopic level. We present several techniques for combining measures of bone density and distribution for the assessment of bone strength *in vivo*.

Direct Radiographic Measurements

Radiogrammetry was one of the first attempts to quantify the macroscopic structure from plain radiographs [27]. The technique involves measuring the cortical thickness of the metacarpals to assess skeletal status, but includes no direct quantitative measurement of bone mineral content or density. Recently a radiogrammetric approach has been advocated by Meema, which involves measurements of the combined cortical thickness at the second metacarpal bone and at the juxtametaphyseal radial shaft, showing good discrimination between persons with and without osteoporosis [28, 29]. However, when compared with bone mass measurements in the same population of patients, radiogrammetric measurements were clearly inferior to QCT measurements in distinguishing persons with and without osteoporosis [30]. A semi-quantitative measurement of trabecular bone structure for diagnosing osteoporosis has been proposed from radiographs of the hip [31] and calcaneus [32]. These techniques use a grading scheme that is related to the observed trabecular structures, but they provide no direct measure of bone mass. By the use of image processing and pattern recognition algorithms, trabecular structure can be quantified from radiographs [33] and high-resolution CT scans [34, 35]; however, these techniques have not seen much clinical use and remain primarily research tools.

Phillips et al. [36] have proposed a structural model of the proximal femur based solely on measurements made from an anteroposterior radiograph of the hip (Fig. 2). In this study, specimens from 39 cadavers were radiographed and various parameters of the femoral neck were measured. Estimates of the failure load were calculated from the femoral measurements by using cantilever beam theory. The specimens were then loaded to failure in a uniaxial testing machine, and the model's results were compared with actual fracture load *in vitro*. Good correlations were found between the predicted and experimental values, although the technique has not yet been applied to human subjects to assess fracture risk. In practice, the femoral measurements can be somewhat difficult to obtain from the radiograph; clinical application would most likely require an automated measurement scheme and a refinement of the measurement parameters. In addition, dual-energy densitometric techniques that provide equivalent structural information at a fraction of the radiation dose are readily available.

Dual-Photon Absorptiometry and Dual Energy X-ray Absorptiometry

DXA and its predecessor DPA have rapidly emerged in the field of bone densitometry as simple, low-radiation-dose tech-

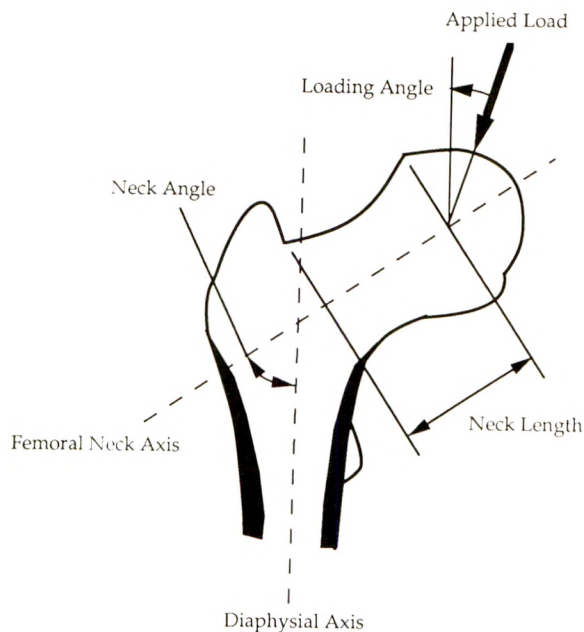


Fig. 2.—Femoral dimensions typically used for estimating strength of femoral neck.

niques for the noninvasive measurement of bone mass of the spine, hip, and total body. The X-ray-based DXA technology has essentially replaced the isotope-based DPA systems, owing to the increased precision and reduced radiation dose of the DXA systems without the need for frequent changes in radiation source. The increased output of the X-ray tube as compared with the isotope source has also greatly reduced the scanning time (Table 1), increased image resolution, and improved short- and long-term precision.

Several researchers have attempted to use DPA and DXA data for the assessment of femoral structure in predicting hip strength. Dalen and associates [37] scanned a group of 61 excised femora using a dual-energy spectrophotometric method that is similar to DXA. The specimens were loaded to failure, and the fracture load was defined as the maximum force obtained on the force/displacement curve. The fracture load was estimated on the basis of a few measurements of the femoral neck by using simple beam theory (Fig. 2). Dalen found that for the specimens obtained from females, the mechanically determined fracture loads correlated better with the noninvasively determined bone mineral content of the femoral neck ($r = .78$) than with the geometric estimates of strength ($r = .71$). However, both the mathematical model and the loading conditions for the fracture tests were highly simplified and may not accurately reflect behavior in vivo.

Gies et al. [38] have derived a similar mathematical model from dual-energy images of the femur. In this study, predicted failure loads based on nonhomogeneous beam theory correlated highly with actual fracture loads of excised femora ($r = .89$). In an extension of the method of Phillips [36], Beck et al. [7] have written an interactive computer program to extract geometric properties from DPA and DXA data of the proximal

femur. The program determines cross-sectional properties at various levels along the femoral neck and calculates strength estimates at each section. The use of computer software allows more rapid and precise measurements of the femur and also allows direct comparison with densitometry data.

On a sample of 20 excised femoral specimens subject to compression testing, Beck et al. showed an improved correlation of the fracture load with the geometric estimate of strength ($r = .89$) as compared with the bone mineral density of the femoral neck ($r = .79$). Refinements in the computer algorithm may improve this relationship further, and future improvements may permit its general clinical use. The technique has the advantage of being based on a readily available low-dose measurement and could be applied by using currently available DXA systems. Thus, for including macroscopic information on femoral structure, the technique has good potential. However, the usefulness of this method for distinguishing between those with and without osteoporosis or predicting future osteoporotic fractures has not been studied.

Quantitative CT

QCT is unique among the noninvasive methods of bone densitometry in that it can determine both the bone density and distribution in three dimensions at any skeletal site (Fig. 1). Currently QCT is performed primarily at the lumbar spine; however, some research has been done at the radius and tibia [39, 40] and at the proximal femur [9, 41–43]. On the basis of spinal QCT measurements, Jones et al. [44] compared the density of trabecular bone of the vertebral body to the total vertebral bone content in the lumbar spine of 19 patients with osteoporosis and 20 control subjects. They found a significant decrement in trabecular density of the vertebral body in patients with osteoporosis compared with the age-matched control subjects, even when total vertebral bone content was normal. The importance of the trabecular bone of the vertebral body to strength has been verified by other researchers [2, 45] and is most likely the reason behind the increased sensitivity and specificity of QCT for distinguishing between those with and without osteoporosis compared with other noninvasive methods [16–20].

Using QCT, Cody et al. [46] have developed a technique for the determination of trabecular mineral density in vivo of 18 regions of the vertebral body from scans of 1-mm-thick sections. The regions are chosen from the superior, central, and inferior vertebral body, six on each level. They then correlated the regional density measurements of excised human vertebrae with fracture loads of the entire vertebrae to determine how the trabecular distribution affects overall strength [47]. Correlation coefficients between the regional density measurements and fracture load among the 27 female patients ranged from .107 in the superoanterior region (representing a poor relationship) to .748 in one of the posterolateral regions (representing a good relationship). The highest correlations occurred in the posterior aspect of the vertebral body, which is not the region of observed fractures. They concluded that an architecture of trabecular bone directly affects the strength of the vertebral body. However, the

technique as used by Cody delivers a relatively high radiation dose compared with conventional QCT. As with any QCT measurement, practical application of the technique requires a well-maintained CT scanner equipped for quantitative measurements; specially developed analysis software also is required to define automatically and evaluate the various vertebral regions. As such, this technique is primarily a research tool.

Micro-CT, also termed microtomography, has recently been introduced as a new technique for the nondestructive assessment of the three-dimensional distribution of the bone structure of small objects [48–50]. Whereas conventional CT scanners have spatial resolutions of about 0.5–1.0 mm, images obtained on micro-CT devices offer resolution limits of up to 15 μm at slice thicknesses of about 25 μm [51]. Images of cortical bone clearly revealed Haversian canals [52] and local variations in mineralization [51]. Research with micro-CT may provide valuable answers regarding the role of trabecular structure in bone strength. However, this technique requires highly sophisticated machinery and extremely high radiation exposures and is limited to measuring excised specimens.

Finite Element Analysis

Engineers often use finite element analysis (FEA) to include structural information when assessing the strength of a new design. FEA has long been used by mechanical engineers to aid in the design of bridges, buildings, and other structures. FEA involves dividing a complex structure with unknown mechanical behavior into a series of geometrically simplified substructures or elements. The behavior of each individual element is determined from mathematical equations relating applied forces or stresses to the expected displacement or strain of the element. For a complete description of mechanical behavior of a structure, a finite element analysis requires knowledge of (1) the geometry, (2) the material properties, and (3) the loads acting on the object. Model geometry is usually obtained directly from the object, whereas loading conditions are measured or estimated according to the intended use of the structure. The mechanical properties are derived from compression tests of the materials making up the structure under appropriate loading conditions.

Finite element models based on three-dimensional QCT studies of contiguous slices of the spine [53, 54] and the hip [55, 56] have recently been created (Fig. 3). Results from the patient-specific FEA have been shown to agree with the observed mechanical behavior of vertebral and femoral specimens in vitro. In addition, estimates of vertebral strength from the patient-specific spinal FEA have been evaluated for the ability to distinguish between persons with and without osteoporosis [57]. Results showed a large variation in the FEA-estimated strength between models with virtually the same total bone content and trabecular mineral density. As these models contain the same amount of bone, the strength differences were attributed to the way the bone is distributed through the model, which is not reflected in the measurements of bone density and bone content. From these results it was concluded that vertebral FEA is a reasonably valid model for estimating vertebral strength.

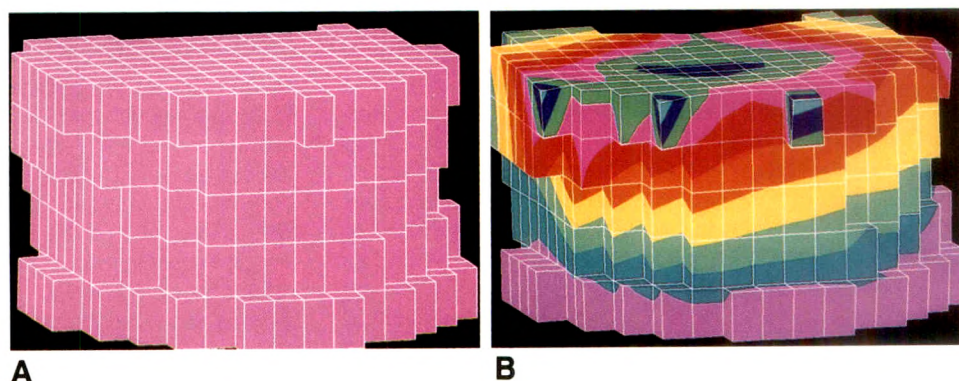
On the basis of a receiver-operating-characteristic analysis [58], the vertebral FEA strength estimates showed a slight but statistically significant improvement over the QCT trabecular density measurements for distinguishing between persons with and without osteoporosis (Fig. 4) [57]. Although the technique shows promise, the current implementation requires large amounts of computer time for analysis and is not yet applicable for general clinical use. Refinements are being made to improve precision and reduce the computing time of the vertebral and femoral models.

Ultrasound Techniques

Ultrasound techniques have recently been introduced as new tools for noninvasive assessment of skeletal status in osteoporosis without the need for ionizing radiation. The frequency dependence of ultrasound attenuation can be assessed at the os calcis (broadband ultrasound attenuation, or BUA approach), and the speed of sound can be measured both at the os calcis and the patella (speed of sound, or SOS approach) (Fig. 5). Ultrasound may potentially be suitable for measuring several of the various determinants of bone strength. Bone elasticity has been shown to have a close relationship to SOS [59–61] but appears not to be related to BUA [62]. Most in vitro studies have observed a relatively

Fig. 3.—A, Patient-specific finite element mesh of a vertebral body generated from three-dimensional quantitative CT data. In this case, the mesh is made of 575 rectangular solid elements.

B, Deformed mesh plot of A generated from analysis results. Banded displacement contours show regions of minimal displacement at inferior model surface (where model is constrained not to move) up to large displacement regions at superior surface of model. These results can be used to estimate strength of vertebral body [54].



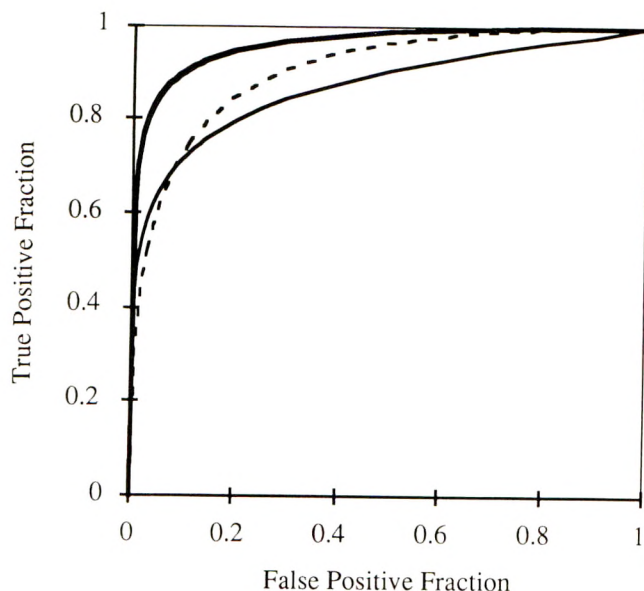


Fig. 4.—Receiver-operating-characteristic (ROC) curves for distinguishing control subjects from patients with osteoporosis on the basis of finite element analysis (FEA) estimated vertebral yield stress (*thick line*), quantitative CT (QCT) determined trabecular mineral density (*dashed line*), and the total vertebral body bone content (*thin line*). Curves are based on results from 28 control subjects and 15 patients with osteoporosis by using the computer program of Metz [58]. Area under the FEA ROC curve (0.964) is statistically larger ($p < .05$) than the areas under the density (0.907) and content (0.871) curves. (Reprinted with permission from Faulkner and Cann [57].)

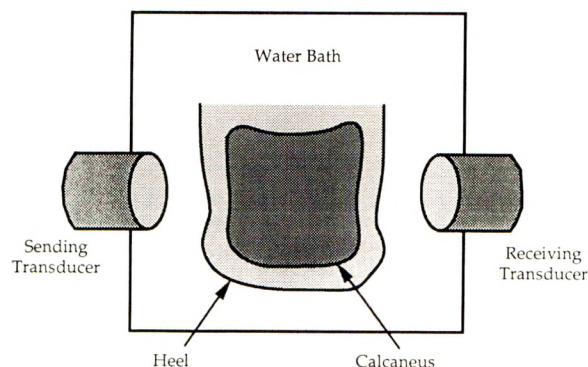


Fig. 5.—Schematic diagram shows method for measuring broadband ultrasound attenuation (BUA) and/or speed of sound (SOS) at heel. For heel measurement, water immersion is necessary to eliminate air between transducers and facilitate transmission of sound wave to measurement site.

close association of physical density and BUA [63, 64]. Preliminary efforts to correlate directly the parameters describing the trabecular structure and BUA have not been successful [62]. However, the anisotropic trabecular orientation was reported to be reflected by an orientational dependence of SOS [65] and BUA [62]. Fatigue damage has been shown to correlate with elasticity [66] and should also have a marked effect on SOS. However, this has not yet been demonstrated experimentally. The potential of SOS as a measure of anisotropy or porosity is supported by studies on nondestructive

testing of materials other than bone. SOS was found to be associated with porosity or anisotropy in dissimilar materials such as wood [67], ceramics [68], and sintered nickel [69].

McKelvie and Palmer have reported an assessment of the association of BUA and SOS with bone strength [70]. Measuring BUA on excised human vertebrae, they found a correlation of .46 between BUA and maximum compressive strength. The correlation improved markedly to .82 when four to five vertebrae obtained from the same cadaver were averaged, demonstrating the potential of BUA as a method for the direct assessment of bone strength. However, because vertebrae cannot be measured in vivo with the ultrasound devices currently available, it is unclear whether the association remains strong enough even if an accessible site such as the os calcis or the patella are measured in vivo. Finally, several reports also indicate that ultrasound may yield information about bone strength independently of bone mass [60, 62, 64, 71, 72]. However, this claim was mainly based on theoretical and statistical considerations and has not been thoroughly investigated experimentally. Clinical units have been developed for measuring SOS at the patella and BUA and SOS of the calcaneus; these units are being tested pending final government approval for clinical use. Ultrasound has great clinical potential because of its relative low cost and ease of use without the need for ionizing radiation. More research is needed to determine the optimal measurement method and to verify the usefulness of ultrasound for the assessment of fracture risk.

MR Imaging

MR imaging has recently emerged as a noninvasive imaging technique that provides quantitative information characterizing soft-tissue composition and function. To date, most MR imaging techniques have been restricted to study of soft tissue because the presence of compact bone in MR images results in a total absence of signal. However, recently developed MR techniques have been used to study trabecular bone. The presence of the trabecular bone matrix affects the signal intensity of bone marrow, an effect that is particularly enhanced in specific imaging sequences. The magnetic properties of trabecular bone and bone marrow are significantly different. These differences produce distortions of the magnetic lines of force, which make the local magnetic field within the tissue extremely inhomogeneous. Such inhomogeneities in the magnetic field in turn alter the relaxation properties of tissue, such as the apparent transverse relaxation time $T2^*$, in gradient-echo images. From theoretical considerations, such changes in $T2^*$ should directly relate to the density of the surrounding trabecular network and its spatial geometry. The resultant shortening of relaxation time becomes greater with an increase in the concentration of trabecular bone in the surrounding homogeneous marrow tissue. Thus, in a normal dense trabecular network, $T2^*$ shortening should be more pronounced than in rarefied osteoporotic trabeculae.

Recent experimental studies have confirmed the theoretical predictions, suggesting MR imaging as a promising tool for

studying trabecular bone architecture and assessing osteoporosis. Davis et al. [73] have shown a reduction in the in vitro $T2^*$ of both water and cottonseed oil in the presence of bone powder at 5.9 T. Recently, Rosenthal et al. [74] have measured a reduction in the $T2^*$ of water present in the trabecular spaces compared with extratrabecular water, using specimens of excised human vertebrae at 0.6 T. Investigators also have observed that the signal intensity [75] and relaxation decay curves [76] of bone marrow in the epiphysis are significantly different from those in the diaphysis. These relaxation effects and regional variations in the appearance of bone marrow in the appendicular skeleton have been attributed to the magnetic field inhomogeneities induced by the presence of trabecular bone. The variation in signal intensity in the appendicular skeleton due to a shortening of the relaxation time $T2^*$ by the presence of trabecular bone is visually apparent in gradient-echo images (Fig. 6).

Direct correlation between bone density and the relaxation time $T2^*$ has also been established, both in vitro and in vivo. In recent in vitro studies [77], correlation between vertebral bone density determined by quantitative CT and the inverse of $T2^*$ relaxation ($1/T2^*$) was strong ($r = .94$; $p \leq .001$). As it appears that $T2^*$ decay is influenced not only by trabecular density but also by trabecular geometry, gradient-echo MR imaging may provide unique morphologic information on trabecular structure and architecture, which may be of use in assessing bone strength and predicting fracture risk.

MR microscopy may be an additional MR-based technique to study trabecular microarchitecture. Wehri et al. [78] generated microscopic images of trabecular bone specimens with

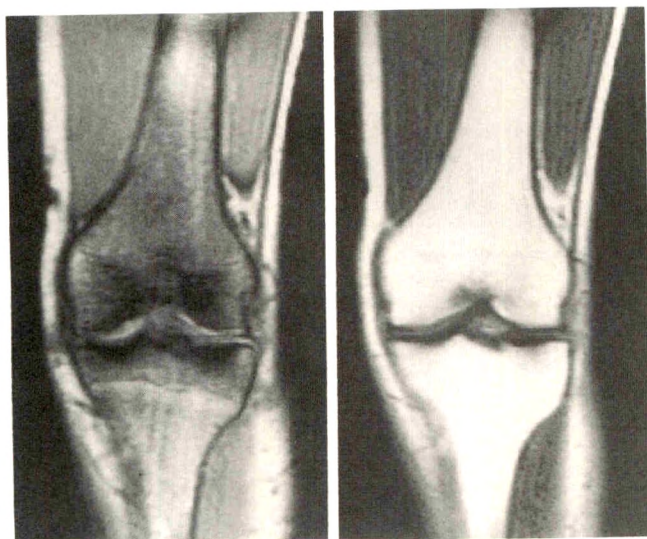
an in-plane resolution of $33 \times 33 \mu\text{m}$ to $66 \times 66 \mu\text{m}$. The resolution was sufficient to show individual trabeculae. However, the study was performed at a field strength of 9.4 T on specimens from which the marrow component had been removed in order to avoid chemical-shift artifact with resultant spatial misregistration. The same group has recently published preliminary data using MR interferometry to assess trabecular structure in vivo with promising results [79].

At present, quantitative MR imaging and MR microscopy appear to hold much potential for assessment of bone density and in particular bone structure. However, significant work remains to be done to develop these techniques to a stage where they are clinically usable. MR techniques are also inherently time consuming and costly; however, MR may provide significant information about the role of microscopic bone structure in skeletal strength.

Conclusions

Bone strength has been shown to depend on the amount and the density of bone present, which can be determined by using a number of radiation-based densitometric techniques. Several studies have shown a reduction in bone mass from normal values to indicate the relative risk for spine, hip, forearm, and most appendicular fractures. Bone mass measurements taken by using a variety of commercially available techniques have also shown the ability to distinguish accurately between persons with and without osteoporosis. In many of these studies, however, it was concluded that other factors significantly influence the risk for fractures. Basic engineering principles assure us that bone strength depends on the material properties (which are significantly influenced by density), the distribution of the material (related to the macroscopic and microscopic structure and quality of the bone), and the applied loads (which are related to the frequency and severity of falling).

The past several years have seen bone densitometry technology develop into a highly precise method for assessing bone mass. Even though these techniques inherently include information regarding both the amount and the distribution of bone, the structural information has not been widely used. Structural measurements based on conventional radiographs of the proximal femur have been proposed, but with the advent of DPA and DXA measurements of the hip, this method has seen little clinical use. Automated structural analysis developed on the basis of DPA and DXA images may hold promise for assessing risk of fracture, although the technique has not been clinically evaluated. Regional bone mineral analysis and more sophisticated finite element models based on three-dimensional QCT studies have been developed but currently exist only as research tools. Ultrasound techniques could provide information on bone mass and structure at a reasonable cost without the use of ionizing radiation; however, the clinical usefulness of the approach and its ability to predict future fracture need further investigation. Quantitative MR imaging also could be used to determine trabecular structure noninvasively, but it is presently limited to research because of the cost and time involved.



A

B

Fig. 6.—A, Coronal MR image through knee joint obtained by using a gradient-echo imaging sequence, obtained at a field strength of 1.5 T, 300/20, and a flip angle of 90 degrees. Note decrease in signal intensity of bone marrow from diaphysis to epiphysis in proximal tibia and distal femur due to increasing trabecular bone density.

B, Spin-echo, 300/30, MR image through same section does not show variations in marrow signal seen in gradient-echo image.

Although many of the techniques reviewed are currently limited in their clinical applicability, they can provide insights into the importance of regional bone distribution, as well as trabecular orientation and cortical structure, to overall skeletal strength. If significant relationships between bone strength, bone structure, and fracture risk are verified, the incentive will exist to improve and expand current techniques so that they can move from the research lab into clinical practice. However, as it is with all emerging technologies, researchers must first show efficacy of a technique before substantial amounts of time, energy, and financial support will be spent to improve the technology. To this end, we support further investigation of the noninvasive measurement of bone mass and structure to provide a more sensitive means for assessing risk of osteoporotic fracture.

REFERENCES

- Rockoff SD, Sweet E, Bluestein J. The relative contribution of trabecular and cortical bone to the strength of human lumbar vertebrae. *Calcif Tissue Res* 1969;3:163-175
- McBroom RJ, Hayes WC, Edwards WT, Goldberg RP, White AA. Prediction of vertebral body compressive fracture using quantitative computed tomography. *J Bone Joint Surg (Am)* 1985;67A:1206-1214
- Eriksson SAV, Isberg BO, Lindgren JU. Prediction of vertebral strength by dual photon absorptiometry and quantitative computed tomography. *Calcif Tissue Int* 1989;44:243-250
- Mosekilde L, Bentzen SM, Ørtoft G, Jørgensen J. The predictive value of quantitative computed tomography for vertebral body compressive strength and ash density. *Bone* 1989;10:465-470
- Mosekilde LI, Mosekilde LE, Danielsen C. Biomechanical competence of vertebral trabecular bone in relation to ash density and age in normal individuals. *Bone* 1987;8:79-85
- Hansson T, Roos B, Nachemson A. The bone mineral content and ultimate compressive strength of lumbar vertebrae. *Spine* 1980;5:46-55
- Beck TJ, Christopher BR, Warden KE, Scott WW, Rao GU. Predicting femoral neck strength from bone mineral data: a structural approach. *Invest Radiol* 1990;25:6-18
- Alho A, Høiseth A, Torstein H. Bone-mass distribution in the femur. *Acta Orthop Scand* 1989;60:101-104
- Esses SI, Lotz JC, Hayes WC. Biomechanical properties of the proximal femur determined in vitro by single-energy quantitative computed tomography. *J Bone Miner Res* 1989;4:715-722
- Lotz JC, Gerhart TN, Hayes WC. Mechanical properties of trabecular bone from the proximal femur: a quantitative CT study. *J Comput Assist Tomogr* 1990;14:107-114
- Hui SL, Slemenda CW, Johnston CC. Age and bone mass as predictors of fracture in a prospective study. *J Clin Invest* 1988;81:1804-1809
- Ross PD, Wasnich RD, Vogel JM. Detection of prefracture spinal osteoporosis using bone mineral absorptiometry. *J Bone Miner Res* 1988;3:1-11
- Cummings SR, Black DM, Nevitt MC, et al. Appendicular bone density and age predict hip fracture in women. *JAMA* 1990;263:665-668
- Seeley DG, Browner WS, Cummings SR, Genant HK. Which fractures are predicted with measurement of bone mineral density? *Radiology* 1990;177(P):128
- Wasnich RD, Ross PD, Heilbrun LK, Vogel JM. Prediction of postmenopausal fracture risk with use of bone mineral measurements. *Am J Obstet Gynecol* 1985;153:745-751
- Reinhold WD, Genant HK, Reiser UJ, Harris ST, Ettinger B. Bone mineral content in early-postmenopausal osteoporotic women and postmenopausal women: comparison of measurement methods. *Radiology* 1986;160:469-478
- Nordin BEC, Wishart JM, Horowitz M, Need AG, Bridges A, Bellon M. The relation between forearm and vertebral mineral density and fractures in postmenopausal women. *Bone Miner* 1988;5:21-33
- Heuck A, Block J, Glüer CC, Steiger P, Genant HK. Mild versus definite osteoporosis: comparison of bone densitometry techniques using different statistical models. *J Bone Miner Res* 1989;4:891-900
- Van Berkum FNR, Birkenhäger JC, Van Veen LCP, et al. Noninvasive axial and peripheral assessment of bone mineral content: a comparison between osteoporotic women and normal subjects. *J Bone Miner Res* 1989;5:679-685
- Pacifici R, Rupich R, Griffin M, Chines A, Susman N, Avioli LV. Dual energy radiography versus quantitative computer tomography for the diagnosis of osteoporosis. *J Clin Endocrinol Metab* 1990;70:705-710
- Johnston CCJ, Melton LJ, Lindsay R, Eddy DM. Clinical indications for bone mass measurements. *J Bone Miner Res* 1989;4[suppl 2]
- Cummings SR, Nevitt MC. A hypothesis: the causes of hip fractures. *J Gerontol Med Sci* 1989;44:107-111
- Melton LJ, Riggs BL. Risk factors for injury after a fall. *Clin Geriatr Med* 1985;1:525-539
- Parfitt AM. Trabecular bone architecture in the pathogenesis and prevention of fracture. *Am J Med* 1987;82[suppl 1B]:68-72
- Mosekilde LI, Viidik A, Mosekilde LE. Correlation between the compressive strength of iliac and vertebral trabecular bone in normal individuals. *Bone* 1985;8:79-85
- Britton JM, Davie MWJ. Mechanical properties of bone from iliac crest and relationship to L5 vertebral bone. *Bone* 1990;11:21-28
- Barnett E, Nordin BEC. The radiological diagnosis of osteoporosis: a new approach. *Clin Radiol* 1960;11:166-174
- Meema HE, Meema S. Postmenopausal osteoporosis: simple screening method for diagnosis before structural failure. *Radiology* 1987;164:405-410
- Meema HE. Improved vertebral fracture threshold in postmenopausal osteoporosis by radiographic measurements: its usefulness in selection for preventative therapy. *J Bone Miner Res* 1991;6:9-14
- Rosenthal DI, Gregg GA, Slovik DM, Neer RM. A comparison of quantitative computed tomography to four techniques of upper extremity bone mass measurement. In: Genant HK, ed. *Osteoporosis update 1987*. San Francisco, CA: Radiology Research and Education Foundation, 1987:87-93
- Singh YM, Nagrath AR, Maini PS. Changes in trabecular pattern of the upper end of the femur as an index of osteoporosis. *J Bone Joint Surg [Am]* 1970;52-A:457-467
- Aggarwal ND, Singh GD, Aggarwal R, et al. A survey of osteoporosis using the calcaneum as an index. *Int Orthop* 1986;10:147-153
- Rockoff SD, Scandrett J, Zacher R. Quantitation of relevant image information: automated radiographic bone trabecular characterization. *Radiology* 1971;101:435-439
- Henschke F, Kalender WA, Pesch HJ. Structural analysis of vertebral body spongiosa by computed tomography. *J Comput Assist Tomogr* 1982;6:205-206
- Bergot C, Preteux F, Laval-Jeantet AM. Quantitative image analysis of thin sagittal and transverse slices from autopsy specimens of L3 vertebrae. In: Christiansen C, Johansen JS, Riis BJ, eds. *Osteoporosis 1987*. Viborg, Denmark: Nørhaven A/S, 1987:338-340
- Phillips JR, Williams JF, Melick RA. Prediction of the strength of the neck from its radiological appearance. *Biomed Eng* 1975;10:367-372
- Dalen N, Hellstrom LG, Jacobson B. Bone mineral content and mechanical strength of the femoral neck. *Acta Orthop Scand* 1976;47:503-508
- Gies AA, Carter DR, Sartoris DJ, Sommer FG. Femoral neck strength predicted from dual energy projected radiography. In: *Proceedings of the 31st annual meeting of the Orthopaedic Research Society*. Las Vegas, NV: Orthopaedic Research Society, 1985:357
- Stebler B, Rueggsegger P. Special purpose CT system for quantitative bone evaluation in the appendicular skeleton. *Biomed Tech* 1983;28:196
- Schneider P, Börner W, Mazess RB, Barden H. The relationship of peripheral to axial bone density. *Bone Miner* 1988;4:279-287
- Sartoris DJ, Andre M, Resnick C, Resnick D. Trabecular bone density in the proximal femur: quantitative CT assessment. *Radiology* 1986;160:707-712
- Glüer CC, Genant HK. Quantitative computed tomography of the hip. In: Genant HK, ed. *Osteoporosis update 1987*. San Francisco: Radiology Research and Education Foundation, 1987:187-196
- Bhasin S, Sartoris DJ, Fellingham L, Zlatkin MB, Andre M, Resnick D. Three-dimensional quantitative CT of the proximal femur: relationship to vertebral trabecular bone density in postmenopausal women. *Radiology* 1988;167:145-149

44. Jones CD, Laval-Jeantet AM, Laval-Jeantet MH, Genant HK. Importance of measurement of spongy vertebral bone mineral density in the assessment of osteoporosis. *Bone* **1987**;8:201-206
45. Faulkner KG, Cann CE, Hasegawa BH. CT-derived finite element models to determine vertebral cortex strength. In: Loew MH, ed. *Medical imaging IV: image processing*. Newport Beach, CA: SPIE: **1990**:194-202
46. Dickie-Cody D, Flynn MJ, Vickers DS. A technique for measuring regional bone mineral density in human lumbar vertebral bodies. *Med Phys* **1989**;16:766-772
47. Dickie DL. *The determination of lumbar vertebral fracture characteristics using computed tomography* [Dissertation]. Ann Arbor: University of Michigan, **1987**
48. Elliott JC, Dover SD. X-ray microtomography. *J Microsc* **1982**;126:211
49. Grodzins L. Optimum energies for X-ray transmission tomography of small samples. *Nucl Instrum Methods* **1983**;206:541-545
50. Feldkamp LA, Goldstein SA, Parfitt AM, Jesion G, Kleerekoper M. The direct examination of three-dimensional bone architecture in vitro by computed tomography. *J Bone Miner Res* **1989**;4:3-11
51. Elliott JC, Dover SD. Three-dimensional distribution of mineral in bone at a resolution of 15 μ m determined by x-ray microtomography. *Metab Bone Dis Rel Res* **1984**;5:219-221
52. Elliott J, Dover S. X-ray microscopy using computerized axial tomography. *J Microsc* **1985**;138:329-331
53. Faulkner KG, Cann CE. Quantitative computed tomography and finite element modeling to predict vertebral fracture. *J Bone Miner Res* **1989**;4[suppl 1]:S234
54. Faulkner KG, Cann CE, Hasegawa BH. The effect of bone distribution on vertebral strength: assessment with patient-specific nonlinear finite element analysis. *Radiology* **1991**;179:669-674
55. Lotz JC. *Hip fracture risk predictions by x-ray computed tomography* [Dissertation]. Cambridge: Massachusetts Institute of Technology, **1988**
56. Keyak JH, Meagher JM, Skinner HB, Mote CD. Automated three-dimensional finite element modelling of bone: a new method. *J Biomed Eng* **1990**;12:389-397
57. Faulkner KG, Cann CE. ROC analysis of vertebral finite element models for fracture prediction: comparison with QCT. In: Christiansen C, Overgaard K, eds. *Osteoporosis 1990*. Copenhagen, Denmark: Osteopress, **1990**:1029-1031
58. Metz C. CLABROC: program to calculate statistical significance of the difference between two estimated ROC curves. Chicago: Department of Radiology, University of Chicago, **1988**
59. Floriani L, Debevoise N, Hyatt G. Mechanical properties of healing by the use of ultrasound. *Surg Forum* **1967**;18:468
60. Greenfield MA, Craven JD, Huddleston A, Kehrer ML, Wishko D, Stern R. Measurement of the velocity of ultrasound in human cortical bone in vivo. *Radiology* **1981**;138:701-710
61. Ashman RB, Corin JD, Turner CH. Elastic properties of cancellous bone: measurement by an ultrasonic technique. *J Biomech* **1987**;20:979-986
62. Langton CM, Evans GP, Hodgkinson R, Riggs CM. Ultrasonic, elastic and structural properties of cancellous bone. In: *2nd Conference on Osteoporosis and Bone Mineral Measurement*. Bath, UK: **1990**:10-11
63. McKelvie ML, Fordham J, Clifford C, Palmer SB. In vitro comparison of quantitative computed tomography and broadband ultrasonic attenuation of trabecular bone. *Bone* **1989**;10:101-104
64. McCloskey EV, Murray SA, Charlesworth D, et al. Assessment of broadband ultrasound attenuation in the os calcis in vitro. *Clin Sci* **1990**;78:221-225
65. Lipson SF. The relationship between elastic properties and microstructure of bovine cortical bone. *J Biomech* **1984**;17:231-240
66. Carter DR, Hayes WC. The compressive behavior of bone as a two-phase porous structure. *J Bone Joint Surg [Am]* **1977**;59-A:954-962
67. Bucur V. Bulk and surface waves for wood anisotropy characterization. *Mat Sci Eng* **1989**;A122:83-85
68. Dienst W, Zimmerman H. Investigation of the mechanical properties of ceramic breeder materials. *J Nucl Mat* **1988**;155-157:476-479
69. Stoimenov S, Stojanov Z. Influence of porosity on velocity of ultrasound and elastic moduli in sintered nickel. *Fizika* **1989**;21[suppl 1]:163-166
70. McKelvie M, Palmer S. The interaction of ultrasound with cancellous bone. In: *Ultrasonic studies of bone: meeting of the Physical Acoustics Group of the Institute of Physics and the Institute of Acoustics*. Hull: Institute of Physics, **1987** (IOP Short Meetings 6)
71. Langton CM, Palmer SB, Porter RW. The measurement of broadband ultrasound attenuation in cancellous bone. *Eng Med* **1984**;13:89-91
72. Heaney RP, Avioli LV, Chestnut CH, Lappe J, Recker RR, Brandburger GH. Osteoporotic bone fragility: detection by ultrasound transmission velocity. *JAMA* **1989**;261:2986-2990
73. Davis CA, Genant HK, Dunham JS. The effects of bone on proton NMR relaxation times of surrounding liquids. *Invest Radiol* **1986**;21:472-477
74. Rosenthal H, Thulborn KR, Rosenthal DI, Rosen BR. Magnetic susceptibility effects of trabecular bone on magnetic resonance bone marrow imaging. *Invest Radiol* **1990**;25:173-178
75. Sebag GH, Moore SG. Effect of trabecular bone on the appearance of marrow in gradient-echo imaging of the appendicular skeleton. *Radiology* **1990**;174:855-859
76. Ford JC, Wehrli FW, Gusnard DA. Quantification of the intrinsic magnetic field inhomogeneity of trabecular bone. *Magn Reson Imag* **1990**;8S1:37
77. Majumdar S, Thomasson D, Shimakawa A, Genant HK. Quantitation of the susceptibility difference between trabecular bone and bone marrow: experimental studies. *Magn Reson Med* **1991**;22 (in press)
78. Wehrli FW, Wehrli SL, Williams J. High-field MR microscopy of trabecular bone. *Radiology* **1990**;177(P):187
79. Wehrli FW, Ford JC, Attie M, Kressel HY, Kaplan FS. Trabecular structure: preliminary application of MR interferometry. *Radiology* **1991**;179:615-621

Book Review

Radiology of Musculoskeletal Stress Injury. By Theodore E. Keats. Chicago: Year Book Medical, 183 pp., 1990. \$74.95

This work is designed to be an all-inclusive book on the subject of musculoskeletal stress injuries. As stated by the author, this type of work is needed because of the increasing awareness of and emphasis on physical fitness in our society. The author has succeeded in creating a timely work.

The book is divided into four parts. A discussion of the general aspects of stress injury is found in the introduction (part 1). The discussion in this section is somewhat brief but to the point. The role of cross-sectional imaging procedures such as CT and MR in the evaluation of stress injuries could be discussed in greater detail. Part 2 (chapters 2–7) is a discussion of stress injury in the normal skeleton. This portion of the book is far and away the strength of this work. Individual sites of injury and specific stress-induced lesions in these sites are discussed lucidly in detail. Even normal variants related to stress are included (though this should come as no surprise to anyone familiar with Dr. Keats's previous publications). Another strength in this particular section is the abundance of well-selected illustrations. Some are unfortunately of lesser quality, but the author states in the preface that some illustrations had to come from photographs. I did not find this drawback distracting.

Stress injury in the abnormal skeleton is discussed in the next part

of the manuscript (chapters 8–10). The discussion focuses on insufficiency fractures associated with osteoporosis. My only complaint with this section concerns the introductory segment. For the importance of the topic, the brevity of this section is disappointing. The final section on overuse syndromes related to the musculoskeletal system is informative but again is lacking in its presentation of MR findings.

Overall, the book achieves its objective of providing a thorough review of stress injuries throughout the musculoskeletal system. At times, the discussion of individual entities is brief, but these entities are usually the more obscure lesions. The book is extremely well organized and is well worth the selling price.

In conclusion, I recommend this book to any radiologist or radiology resident. The book is dominated by plain film findings and, as such, has the feel of a large monograph, rather than a definitive textbook. Despite the lack of detailed discussion of MR findings, I found the book informative and a welcome addition to my library.

David W. Nelson
Oregon Health Sciences University
Portland, OR 97201-3098

Do Asymptomatic Marathon Runners Have an Increased Prevalence of Meniscal Abnormalities? An MR Study of the Knee in 23 Volunteers

Frank G. Shellock^{1,2}
 Andrew L. Deutsch¹
 Jerrold H. Mink^{1,2}
 Roger Kerr¹

Excessive repetitive musculoskeletal loads and stresses associated with intense physical activity may lead to deterioration of the menisci of the knee. Therefore, MR imaging was performed on the knees of 23 asymptomatic marathon runners (eight men, 15 women; average age, 40 years; average number of years training, 10; average training distance per week, 41 miles) to determine the prevalence of meniscal signal abnormalities. None of the runners had previous knee injuries or surgery and each of them regularly competes in 26-mile, 50-mile, or 100-mile marathon races. T1-weighted coronal MR images and proton density-weighted and T2-weighted sagittal images were obtained with a 1.5-T MR system and a transmit/receive extremity coil. The medial and lateral menisci were divided into four portions, or horns, and a total of 92 horns were evaluated (i.e., four horns per knee: medial posterior, medial anterior, lateral posterior, and lateral anterior). Two meniscal horns (2%) had grade 3 signal (grade 3 indicates a meniscal tear), 12 (13%) had grade 2 signal, 29 (32%) had grade 1 signal (grades 1 and 2 are indicative of meniscal degeneration), and 49 (53%) had grade 0 signal (grade 0 is normal). Overall, the prevalence of meniscal tears was 9% (two meniscal tears found in 23 runners). This is lower than the prevalence of MR signal abnormalities indicative of meniscal tears reported for asymptomatic, nonrunner athletes (20% of 20 athletes) and for asymptomatic nonathletes (16% of 74 subjects). Fifty-three percent of the meniscal horns of the nonrunner athletes had grade 1 or 2 signal, indicative of meniscal degeneration.

Our results indicate that the prevalence of meniscal tears in marathon runners is no higher than the prevalence reported for sedentary persons, and the runners have the same amount of meniscal degeneration as do nonrunner athletes.

AJR 157:1239–1241, December 1991

The increase in the popularity of running has seen a concomitant rise in the number of injuries related to this form of physical activity [1–3]. This is not surprising, as the forces generated during running have been calculated to be approximately one and one half to three times those experienced during normal walking [2–4]. Of particular concern is whether the excessive repetitive musculoskeletal loads and stresses associated with participation in intense activity, such as training for and competing in marathon races, cause the eventual deterioration of the menisci of the knee [4–6], a body part that normally absorbs lower-extremity forces [7–10].

A previous MR study [11] of the knees of 20 asymptomatic football and basketball players reported that 53% of the meniscal horns analyzed had grade 1 or 2 signal abnormalities (grades 1 and 2 are indicative of meniscal degeneration [12]), and 20% of these athletes had grade 3 signal abnormalities (grade 3 is indicative of a meniscal tear [12]) [11]. By comparison, a recent study [13] of five long-distance runners found that only 10% had grades 1 and 2 signal changes in the menisci and none of them had grade 3 signal, indicative of a meniscal tear. Because only a relatively small number of runners were involved in this study [13], we performed

Received July 2, 1991; accepted after revision July 31, 1991.

¹ Tower Musculoskeletal Imaging Center, Cedars-Sinai Medical Center, 8700 Beverly Blvd., Los Angeles, CA 90048. Address reprint requests to F. G. Shellock.

² Department of Radiological Sciences, University of California, Los Angeles, School of Medicine, Los Angeles, CA 90024.

0361-803X/91/1576-1239
 © American Roentgen Ray Society

MR examinations on a larger group of asymptomatic marathon runners to determine the prevalence of meniscal abnormalities.

Materials and Methods

The knees of 23 marathon runners (eight men, 15 women; average age, 40 years; age range, 25–55 years; average number of years training, 10; range of years training, 2–20; average training distance per week, 41 miles; range of training distance per week, 18–120 miles) were studied by MR imaging. These marathon runners were asymptomatic and had not had previous knee injuries or previous knee surgery. Twenty-two of these marathon runners regularly compete in at least two 26-mile marathon races each year, and one routinely competes in two or more 50- and 100-mile marathon races each year.

MR imaging of the knee was performed with a 1.5-T MR scanner (Signa, General Electric Company, Milwaukee, WI) and a transmit/receive extremity coil. The knee was positioned in the surface coil at an external rotation of approximately 20°. Routine MR images of the knee were obtained as follows: coronal T1-weighted (800/20 [TR/TE]) and sagittal proton density-weighted and T2-weighted (2000/20, 80) images were acquired with a 5-mm slice thickness, no interslice gap, a 128 × 256 matrix, and a 16-cm field of view [12, 13]. The same window widths and levels were used for the similar pulse sequences to optimize the depiction of anatomy, particularly the menisci (i.e., magnified, high contrast) and to compare images among subjects [12, 13].

MR images were reviewed by three musculoskeletal radiologists to identify increased intrameniscal signals and morphologic abnormalities of the meniscus. The entire medial and lateral menisci were divided into four portions, or horns—medial posterior, medial anterior, lateral posterior, and lateral anterior [12]—and a total of 92 meniscal horns were evaluated. Intrameniscal signal was categorized according to the scheme described by Mink et al. [12]: grade 0, normal; grade 1, intrameniscal globular focus of signal that is not adjacent to either the superior or inferior surface; grade 2, intrameniscal linear or wedge-shaped signal that does not extend to an articular surface; grade 3, linear or globular signal extending to an articular surface. Grades 1 and 2 are indicative of meniscal degeneration, whereas grade 3 indicates a tear [12]. The results were correlated with the subjects' ages and training distances.

Results

The findings are summarized in Table 1. Of the total 92 meniscal horns evaluated, grade 0 signal was seen in 49 (53%), grade 1 signal was seen in 29 (32%), grade 2 signal was seen in 12 (13%), and grade 3 signal (Fig. 1) was seen in two (2%). Overall, the prevalence of meniscal tears in these asymptomatic marathon runners was 9% (2/23). Forty-five percent of the meniscal horns analyzed had grade 1 or 2 signal abnormalities, indicating degeneration.

The prevalence of meniscal tears was 6% (1/16) in marathon runners less than 45 years old and 14% (1/7) in those 45 years old or older. No relationship was found between the age of the runner and the signal abnormalities in the meniscus. In addition, no relationship was found between signal abnormalities in the meniscus and the number of years training or the distance the marathon runners ran each week.

Discussion

Meniscal tears are extremely common and may exist without associated signs and symptoms [14–18]. Furthermore,

TABLE 1: Meniscal Signal on MR Images of Asymptomatic Marathon Runners

Meniscal Horn	Meniscal Signal (Grade)			
	0	1	2	3
Medial posterior	3	8	10	2
Medial anterior	22	1	0	0
Lateral posterior	8	13	2	0
Lateral anterior	16	7	0	0
Total	49	29	12	2

Note.—Grade 0, normal; grade 1, intrameniscal globular focus of signal that is not adjacent to either the superior or inferior surface; grade 2, intrameniscal linear or wedge-shaped signal that does not extend to an articular surface; grade 3, linear or globular signal extending to an articular surface, indicative of a definite meniscal tear. Grades 1 and 2 are indicative of meniscal degeneration, whereas grade 3 indicates a tear [12].

studies [15–18] have indicated that an apparent age-related degeneration of the meniscus occurs. Casscells [14] reported an 18% prevalence of meniscal tears in a study of 226 unselected cadavers with an average age at death of 71 years. In an investigation of 100 random necropsy samples by Noble and Hamblen [15], 60% of the subjects, with an average age at death of 65 years, had a meniscal tear. In another autopsy study of younger cadavers (average age at death, 44 years), the prevalence of meniscal tears was 19% [16].

Using MR imaging, Kornick et al. [17] examined the knees of asymptomatic nonathletes and found a 25% or greater prevalence of increased intrameniscal signals that were evident as early as the second decade of life. In addition, the authors found a direct correlation between signal abnormalities in the meniscus and the age of the study subjects. More recently, Boden et al. [18] reported that 16% of 74 asymptomatic, nonathletic subjects studied by MR had grade 3 signal, indicative of a meniscal tear, with a prevalence of 13% in those less than 45 years old and 36% in those more than 45 years old. Thirty percent of the subjects without tears had increased intrameniscal signals. Therefore, these studies show that there is a relationship between a person's age and abnormalities of the meniscus in asymptomatic nonathletes.

In an MR imaging study of the knees of asymptomatic athletes (five professional basketball players and 15 collegiate football players), Brunner et al. [11] found that 20% had meniscal tears (grade 3 signal was found in four of the 20 athletes) and 53% of remaining meniscal horns analyzed had grade 1 or 2 signal related to meniscal degeneration. With respect to these MR studies of meniscal signal abnormalities, it appears that asymptomatic athletic persons tend to have more signal abnormalities in the meniscus than less active subjects do, and grade 3 signal indicative of meniscal tears may be present without signs or symptoms in both groups.

In our investigation, the prevalence of meniscal tears in the knees of asymptomatic marathon runners was 9% (or 2% of the 92 meniscal horns evaluated), and 45% of the other meniscal horns evaluated had grade 1 or 2 signal abnormalities. These data indicate that the marathon runners had a prevalence of meniscal signal abnormalities similar to that in other asymptomatic (and supposedly younger) athletes and a



Fig. 1.—Sagittal proton density-weighted MR image of medial aspect of knee. Meniscal (high-contrast) windowed image shows grade 3 signal in posterior horn of medial meniscus (arrowheads), indicative of a meniscal tear.

prevalence of meniscal tears slightly lower than that in asymptomatic athletes and nonathletes of a comparable age.

The marathon runners in this study did not have a higher prevalence of meniscal tears than that reported for more sedentary persons, despite the runners' intense training (average length of time training, 10 years; average distance per week training, 41 miles) and advanced age (average age, 40 years).

If the menisci are unable to adapt or compensate for excessive loads and stress imposed by exercise, and if that is combined with the degeneration that occurs from the aging process, it may be presumed that a higher prevalence of meniscal tears (grade 3 signal in the meniscus) should be observed in athletes, particularly older ones, than in nonathletes. In addition, the older athletes should have a higher prevalence of meniscal degeneration (grades 1 and 2 signal) compared with younger athletes. However, this was not shown by our data. The menisci of these marathon runners may have adapted to the stresses imposed by their intense physical activity.

The adaptations of knee menisci to prolonged running exercise has been studied in rats by Vailas et al. [19]. Significant increases in the content of meniscal collagen, proteoglycans, and the concentration of calcium were observed [19]. Meniscal tissue is composed mostly of collagen (approximately 75%) and proteoglycans [7–9]. Collagen fibers, in association with proteoglycans, are particularly effective for resisting the forces of compression [7–9, 19]. Vailas et al. [19] also observed that the meniscus was capable of compensating for the stress from exercise training and that the anterior vs the posterior horns had distinctly different responses related to the different demands placed on them during exercise. These morphologic and structural alterations seen in rats were thought to be responsible for facilitating the ability of the meniscus to withstand the excessive mechanical stress from prolonged exercise [19].

In light of these data, we propose that our finding that marathon runners do not have a higher prevalence of grade 3 signal indicative of meniscal tears than that reported for more sedentary persons is possibly related to compensatory changes that occur in the menisci in response to prolonged

physical training, similar to what has been observed in the laboratory [19]. These data are compatible with those of other investigations of the musculoskeletal system of runners insofar as these other studies reported no greater preponderance of clinical or radiologic evidence of degenerative joint disease or premature osteoarthritis of the joints of the lower extremities than that found in nonrunners [3, 13, 20]. In addition, no relationship was found between a runner's age and the presence of meniscal degeneration (grade 1 or 2 signal) or tears (grade 3 signal), nor was there a higher prevalence of meniscal degeneration among runners (45% of the runners' meniscal horns had grade 1 or 2 signal) than in younger, nonrunner athletes (53% of the nonrunners' meniscal horns had grade 1 or 2 signal [11]). Thus, the adaptations experienced by the marathon runners may preserve the integrity of the menisci in these older athletes and delay degenerative meniscal changes that would normally occur.

ACKNOWLEDGMENTS

We are thankful for the involvement of Robert Scott and the L. A. Leggers in this research study and to Stacy Myers for her editorial assistance.

REFERENCES

1. Marti B, Vader JP, Minder CE, et al. On the epidemiology of running injuries. *Am J Sports Med* 1988;16:285–294
2. Sohn RS, Micheli LJ. The effect of running on the pathogenesis of osteoarthritis of the hips and knees. *Clin Orthop* 1985;198:106–109
3. Panush RS, Schmidt C, Caldwell JR, et al. Is running associated with degenerative joint disease? *JAMA* 1986;255:1152–1154
4. Cavanaugh PR, LaFortune MA. Ground reaction forces in distance running. *J Biomech* 1987;13:337–343
5. Radin EL, Paul IL, Rose RM. Role of mechanical factors in pathogenesis of primary osteoarthritis. *Lancet* 1972;1:519–521
6. Reimann I. Experimental osteoarthritis of the knee in rabbits induced by alteration of the load bearing. *Acta Orthop Scand* 1973;44:496–504
7. Brantigan OC, Voshell AF. The mechanics of the ligaments and menisci of the knee joint. *J Bone Joint Surg [Am]* 1941;23-A:41–66
8. Ghosh P, Taylor TKF. The knee joint meniscus: fibrocartilage of some distinction. *Clin Orthop* 1987;224:52–63
9. Henning CE, Lynch MA. Current concepts of meniscal function and pathology: symposium on the knee. *Clin Sports Med* 1985;4:259–265
10. Shrive N. The weightbearing role of the menisci of the knee. *J Bone Joint Surg [Br]* 1981;56-B:381–387
11. Brunner MC, Flower SP, Evancho AM, Allman FL, Apple DF, Fajman WA. MRI of the athletic knee: findings in asymptomatic professional basketball and collegiate football players. *Invest Radiol* 1989;24:72–75
12. Mink JH, Reicher MA, Crues JV. *Magnetic resonance imaging of the knee*. New York: Raven, 1987
13. Shellock FG, Mink JH. Knees of trained long-distance runners: MR imaging before and after competition. *Radiology* 1991;179:635–637
14. Casscells SW. A post mortem study of the changes encountered in the knee joint of the aged. *J Bone Joint Surg [Am]* 1969;51-A:1032
15. Noble J, Hamblen DL. The pathology of the degenerate meniscus lesion. *J Bone Joint Surg [Br]* 1975;57-B:180–186
16. Noble J. Lesions of the menisci: autopsy incidence in adults less than fifty-five years old. *J Bone Joint Surg [Am]* 1977;57-A:480–483
17. Kornick J, Trefeiner E, McCarthy S, Lange R, Lynch K, Joki P. Meniscal abnormalities in the asymptomatic population at MR imaging. *Radiology* 1990;177:463–465
18. Boden SD, Brown SD, Davis DO, Dina TS, Stoller DW. Incidence of abnormal magnetic resonance imaging scans of the knee in asymptomatic subjects: a prospective and blinded investigation (abstr). *Proc Am Acad Orthop Surg* 1991;1:139
19. Vailas AC, Zernicke RF, Matsuda J, Curwin S, Durivage J. Adaption of rat knee meniscus to prolonged exercise. *J Appl Physiol* 1986;60:1031–1034
20. Lane NE, Bloch DA, Jones HH, Marshall WH, Wood PD, Fries JF. Long-distance running, bone density, and osteoarthritis. *JAMA* 1986;255:1147–1151

Book Review

Radiology of Syndromes, Metabolic Disorders, and Skeletal Dysplasias, 3rd ed. By Hooshang Taybi and Ralph S. Lachman. Chicago: Year Book Medical, 932 pp., 1990. \$155

This is the third edition of a classic text originally written by Dr. Taybi that was published in 1970. A new author, Ralph S. Lachman, an authority on skeletal dysplasias, has been added to write on the subject of his expertise. The format of the third edition has been changed from that of the previous editions. The book now is divided into three sections: syndromes, metabolic disorders, and skeletal dysplasias. The first edition had descriptions of about 540 syndromes. The third edition has been expanded to include nearly 1000 entities. Common and rare disorders are described.

Each condition is concisely presented. For each disorder, the synonyms, clinical and radiologic manifestations, and, where known, the etiology, mode of inheritance, frequency, and differential diagnosis are listed. The most important aspects are printed in italics. An updated pertinent list of references follows each presentation. Many, but not all, of the disorders are illustrated. The illustrations include photographs, routine radiographs, isotope studies, sonograms, CT scans, and MR images.

At the end of the book are a "gamut" section, arranged according to organ systems; additional references; the International Nomenclature of Constitutional Diseases of Bone (May 1983 revision); and a brief index. The index is inadequate, as conditions are only partially listed. For example, the entry for caudal regression syndrome refers the reader to the main article on this syndrome but does not indicate that additional information on it is mentioned in the article on infants of diabetic mothers.

The descriptions of the syndromes and so forth are brief and to the point. If more information is desired, such as the natural course of the disorder, the references or one of the more voluminous texts, such as the *Birth Defects Encyclopedia* (1990, Buyse) or *Syndromes of the Head and Neck* (1990, Gorlin et al.), must be consulted.

In the past few years, new editions of many of the books on syndrome identification have been published. Among these, only the book by Taybi and Lachman emphasizes the radiologic manifestations. It could be improved by including normal values (e.g., facial

measurements) and a glossary of terms used for congenital anomalies.

The fourth edition (1988) of Smith's *Recognizable Patterns of Human Malformation* has more of an emphasis on the clinical aspects and has some longer discussions of the entities. It also has chapters on morphogenesis and dysmorphogenesis, genetics, approaches to problems of growth deficiency and minor anomalies as clues toward the recognition of malformation syndromes and a chapter that gives normal standards. This book supplements Taybi and Lachman's book but does not contain as many of the radiologic features of the conditions.

Syndromes of the Head and Neck has more detailed discussions than the books by Taybi and Lachman and Smith and a more complete reference list. The appendix contains normal cranial and facial measurements.

It is difficult to cite any one text for use in syndrome identification. For the radiologist, Taybi and Lachman's book is quite valuable in helping to identify possible syndromes when an abnormality is detected. Using the gamut system, the reader can find the abnormality listed and with it the syndromes or entities in which the abnormality may occur. Then, by consulting the description, the disorder can be classified.

I have always found *Radiology of Syndromes, Metabolic Disorders, and Skeletal Dysplasias* (from the first edition) valuable as a reference, and I have it in the bookcase near my film-reading area. This new edition maintains the excellence of the previous editions. Radiologists, especially those interested in pediatric radiology and skeletal radiology, will find this text valuable. I think that radiologists, geneticists, and pediatricians will find it a good addition to their libraries.

Melvin H. Becker
New York University Medical Center
New York, NY 10016

Myositis Ossificans: MR Appearance with Radiologic-Pathologic Correlation

Mark J. Kransdorf^{1,2}
 Jeanne M. Meis³
 James S. Jelinek^{2,4}

We reviewed retrospectively the MR images of eight histologically proved cases of myositis ossificans and correlated the MR appearance with the histologic findings, as well as with other radiologic studies. Patients with available MR images were chosen from a group of 326 cases in our radiologic archives of histologically proved and radiologically correlated myositis ossificans. In addition to MR images, all patients had plain radiographs, six had CT scans, and two had arteriograms. On T2-weighted spin-echo MR, the lesions were relatively well defined and inhomogeneous and had intermediate to high signal intensity. The latter corresponded to a central proliferating core of fibroblasts and myofibroblasts with a myxoid stroma resembling nodular fasciitis, rimmed by osteoblasts with bone production. Edema surrounded lesions less than a few months old. T1-weighted images of early lesions were normal or showed evidence of a mass by displacement of fat planes. Hemorrhage and fluid-fluid levels were seen in one lesion of intermediate duration. Mature lesions tended to be well defined with inhomogeneous signal intensity, similar to that of fat, representing areas of fat situated between bone trabeculae within the lesion.

We present the MR appearance of myositis ossificans and correlate it with other radiologic studies and the histologic findings. The varying appearance of myositis ossificans relates to the histologic changes that occur as the disorder progresses. Knowledge of the MR appearance of myositis ossificans is important in that the lesion has many of the MR imaging characteristics frequently associated with malignancy.

AJR 157:1243-1248, December 1991

Myositis ossificans is a benign, solitary, self-limiting, ossifying soft-tissue mass typically occurring within skeletal muscle. A history of trauma is often inapparent, and we make no distinction between lesions of atraumatic and traumatic origins. The pathogenesis of myositis ossificans is unknown, although the term myositis is a misnomer in that no primary inflammation of skeletal muscle is associated with the process [1]. Synonyms include pseudomalignant osseous tumor of soft tissue, extraosseous localized nonneoplastic bone and cartilage formation, myositis ossificans circumscripta, pseudomalignant myositis ossificans, and heterotopic ossification [1-4].

We describe the MR appearance of eight lesions of histologically proved myositis ossificans and correlate these findings with other radiologic and histologic studies.

Materials and Methods

The radiologic archives of the Armed Forces Institute of Pathology contain 326 cases of histologically proved and radiologically correlated myositis ossificans accumulated in consultation over 40 years. Through a retrospective review, we identified eight patients in whom MR images were available. The clinical histories and radiologic findings in these eight patients form the basis for this report. The study group consisted of five women and three men 12-73 years old (mean, 32 years). The thigh was the most common location; it was involved in five cases. One case each occurred in the popliteal fossa, proximal upper arm, and proximal forearm.

Received May 13, 1991; accepted after revision July 23, 1991.

The opinions or assertions contained herein are the private views of the authors and are not to be construed as official or as reflecting the views of the Department of the Army, the Department of Defense, or the Uniformed Services University of the Health Sciences.

¹ Department of Radiologic Pathology, Armed Forces Institute of Pathology, Washington, DC 20306-6000. Address reprint requests to M. J. Kransdorf.

² Department of Radiology and Nuclear Medicine, Uniformed Services University of the Health Sciences, Bethesda, MD 20814.

³ Department of Soft Tissue Pathology, Armed Forces Institute of Pathology, Washington, DC 20306-6000.

⁴ Department of Radiology, Washington Hospital Center, Washington, DC 20010.

0361-803X/91/1576-1243

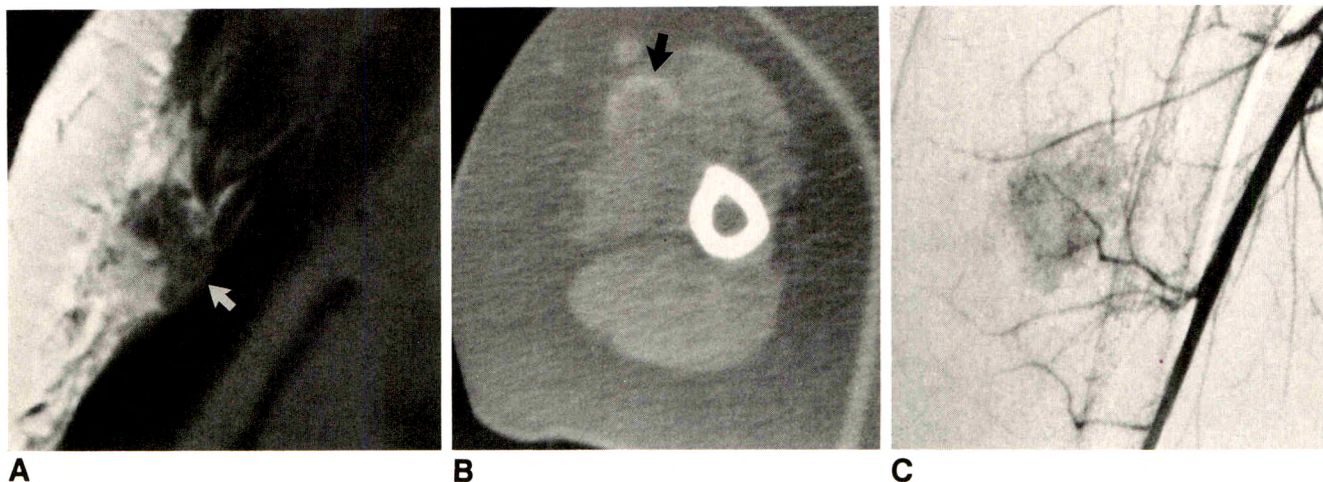


Fig. 1.—Early myositis ossificans in upper arm of 29-year-old woman.

A, Coronal T2-weighted SE MR image (2000/80) shows inhomogeneous mass in upper aspect of arm. Portions of margin are relatively well defined (arrow); others are obscured by diffuse surrounding edema and adjacent subcutaneous fat. Edema extends along fascial planes separating muscle and subcutaneous fat.

B, Axial CT scan (bone window) shows incomplete peripheral curvilinear calcification (arrow). Edema seen on A is not evident. Mineralization was not apparent on radiograph (not shown).

C, Digital subtraction arteriogram shows a diffuse tumor blush, indistinguishable from that of a malignant neoplasm.

MR examinations were performed with a variety of scanners. Scanning sequences included spin-echo (SE) T1-weighted, 300–650/20–40 (TR/TE), and T2-weighted, 2000–3000/60–90, pulse sequences. In addition, one patient was evaluated with gadopentetate dimeglumine-enhanced MR and another with inversion-recovery MR imaging. All lesions (except one) were imaged in at least two orthogonal planes and were evaluated for the following features: margin definition, intensity and homogeneity of the signal, and presence or absence of surrounding edema. When edema was present it was graded as diffuse or focal and as mild, moderate, or extensive. In addition to MR images, all patients had plain radiographs, six had CT scans, and two had arteriograms. All lesions were imaged before intervention; the time between MR imaging and biopsy or resection was 1–31 days (mean, 13 days). The clinical age of lesions was based on duration of symptoms in seven of eight cases. In one patient, the lesion was an incidental finding.

In all cases the diagnosis of myositis ossificans was verified histologically according to criteria previously described [1, 5–7]. Hematoxylin and eosin-stained slides were reviewed without previous knowledge of each lesion's duration, and the lesions were classified by the authors as early (recent), intermediate, or late (remote or fully mature) by using the following criteria. Early lesions consisted primarily of a nonossified central core of proliferating benign fibroblasts and myofibroblasts, with a minor component of osteoid and mature lamellar bone at the periphery; hyaline cartilage could be present as part of endochondral calcification. Intermediate lesions had either a minor or no proliferating fibroblastic core; they consisted almost entirely of osteoid rimmed by active osteoblasts and were surrounded by a shell of mature lamellar bone. Late lesions consisted exclusively of mature lamellar bone. The presence or absence of a zoning phenomenon, circumscription, intralesional inflammation, hemorrhage or hemosiderin deposition, hematopoiesis, entrapment or atrophy of skeletal muscle, intralesional vasculature, perilesional fibrosis or capsule formation, and edema or myxoid change in the surrounding connective tissue was assessed also.

The pathologic features of each lesion were then correlated with the patient's clinical history, MR images, and other radiologic images. One of these cases has been reported previously [2].

Results

MR Findings

In early and intermediate lesions, myositis ossificans appeared on T2-weighted SE MR images as a moderately to markedly inhomogeneous soft-tissue mass with increased signal intensity and extensive diffuse surrounding edema. Curvilinear and irregular areas of decreased signal intensity were seen surrounding and coursing through all intermediate lesions and through one of three early lesions, giving these lesions relatively well-defined margins. The margins of two early lesions were difficult to separate from the surrounding edema. Findings on corresponding T1-weighted images were normal, or showed evidence of a mass by displacement of fascial planes (Figs. 1 and 2). One patient with fluid-fluid levels had increased signal intensity in the muscle surrounding the lesion (Fig. 3). Imaging after administration of gadopentetate dimeglumine in one patient showed marked enhancement (Fig. 2). Changes compatible with marrow edema were also detected within the shaft of the femur adjacent to one lesion in the mid thigh.

Mature (late) lesions were well-defined inhomogeneous masses with a signal intensity approximating that of fat on both T2- and T1-weighted images without associated edema. On all pulse sequences, a rim of decreased signal intensity surrounded the lesion and similar areas of decreased signal intensity were apparent within the lesion (Fig. 4).

Other Radiologic Findings

CT scans were available for review in six patients. The marked edema detected on MR images was not detected on CT scans. In one early case, however, mild edema was seen in the subcutaneous adipose tissue adjacent to the lesion.

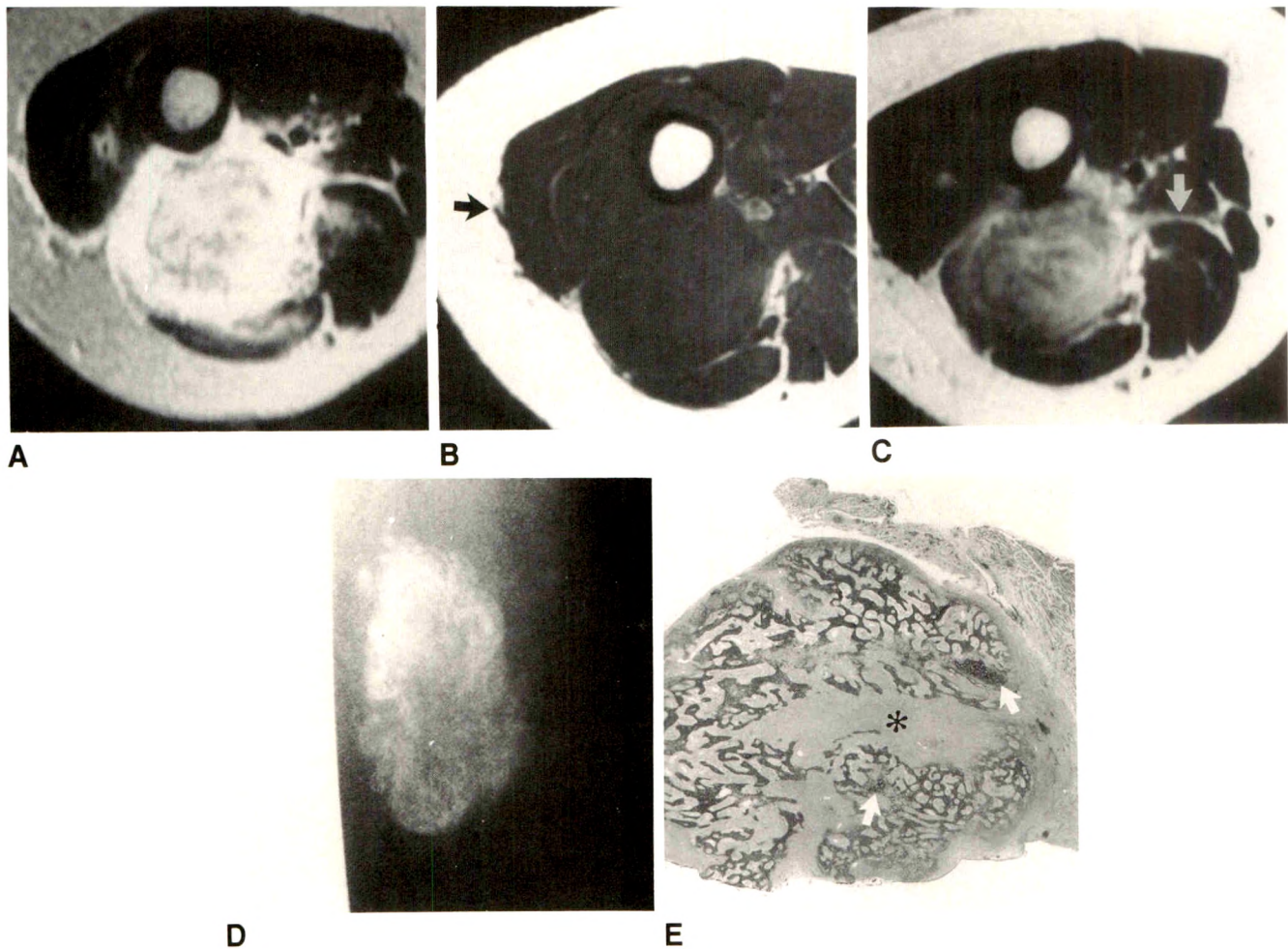


Fig. 2.—Early myositis ossificans in thigh of 24-year-old woman with pain for 3–4 weeks.

A, Axial T2-weighted SE MR image (2800/80) shows inhomogeneous, relatively well-defined mass surrounded by diffuse edema in posterior aspect of thigh. Edema extends along fascial plane separating muscle from subcutaneous fat.

B, Corresponding axial T1-weighted SE MR image (400/20) shows mass isointense with skeletal muscle. Area with signal intensity similar to that of skeletal muscle extends into subcutaneous fat laterally (arrow), matching area of increased signal intensity (edema) on A.

C, Axial T1-weighted SE MR image (400/20) obtained after IV gadopentetate dimeglumine at same level as A and B shows moderate inhomogeneous enhancement. Edema is seen enhancing along fascial planes (arrow).

D, Lateral radiograph shows densely mineralized mass in posterior aspect of thigh. Mineralized areas are present in A as curvilinear regions of decreased signal.

E, Low-power photomicrograph in another patient with similar early lesion shows characteristic zonation phenomenon with central cellular region (asterisk) and peripheral new bone formation. Scattered areas of cartilage formation (arrows) are also seen. Note compressed atrophic skeletal muscle adjacent to right of lesion. (H and E, original magnification $\times 7.5$)

Four cases had typical peripheral mineralization (Fig. 3), although it was irregularly shaped and somewhat convoluted in one case. In three of these cases, a narrow rim of decreased signal intensity could be seen retrospectively on MR scans. In an early lesion, the peripheral mineralization was incomplete and faint (Fig. 1). One mature lesion that had been clinically apparent for several years had diffuse mineralization (Fig. 4).

Arteriography was available in two cases. One early lesion showed a distinct tumor blush (Fig. 1). A second mature lesion was hypovascular.

Radiographs were available in all eight cases. In one early lesion, no mineralization was seen, and in another the mineralization was vague. The remaining early lesion was densely mineralized, more so peripherally, but the mineralization did

not demonstrate a definite bonelike character. A similar appearance was seen in one intermediate lesion. Two intermediate lesions were densely mineralized, with a distinct bonelike character, and were more mature peripherally. One mature lesion was densely mineralized diffusely, and the other had the appearance of heterotopic ossification. Periosteal reaction was detected adjacent to one intermediate lesion. In this case and one other, the mass was adjacent to but separate from bone.

Histologic Findings

Histologically, three cases were classified as early lesions, three as intermediate, and two as late. The central proliferat-

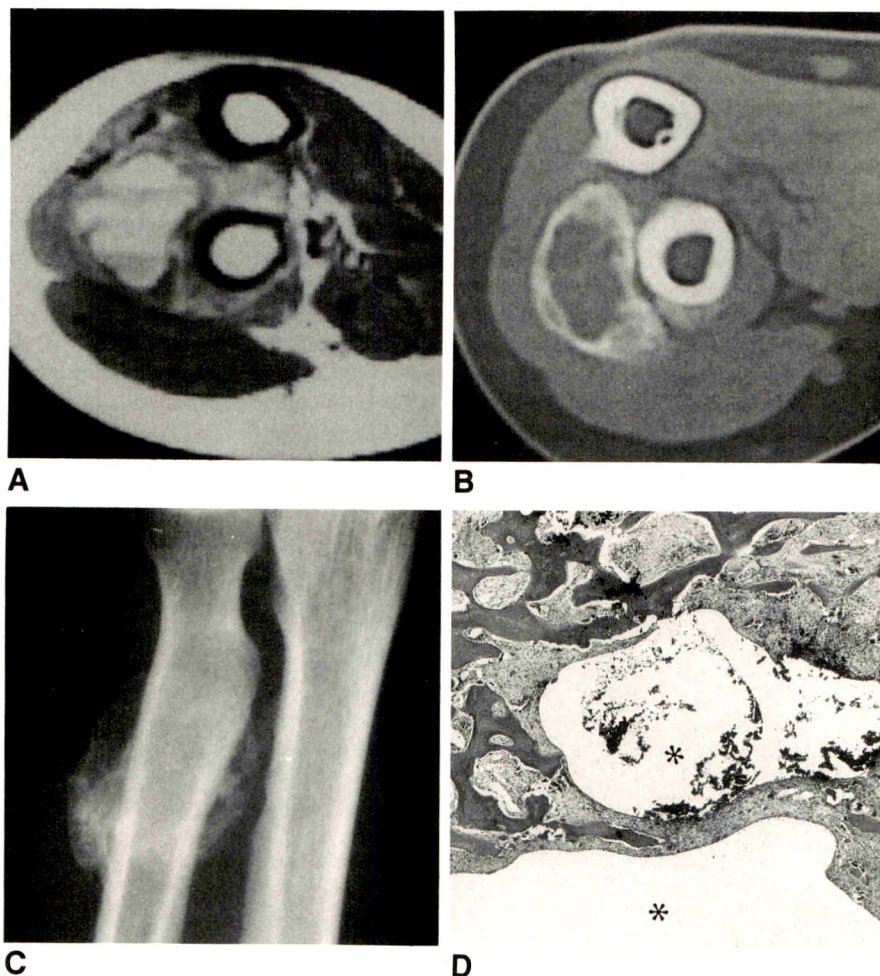


Fig. 3.—Myositis ossificans of intermediate age in forearm of 31-year-old woman.

A, Axial T1-weighted SE MR image (500/40) shows lesion with fluid-fluid levels adjacent to proximal radius. Areas of increased signal intensity adjacent to lesion may be related to hemorrhage.

B, CT scan (bone window) at level similar to that of A shows lesion's dense peripheral mineralization, less apparent on MR. Tissue attenuation within lesion is somewhat lower than that of surrounding soft tissue.

C, Radiograph shows densely mineralized mass overlying proximal radius. Peripheral mineralization is seen better on CT (B). Retrospective review of radiograph obtained 45 days earlier showed no mineralization.

D, Photomicrograph shows mature lamellar bone surrounding hemorrhagic cysts (asterisks). Regions between trabeculae consist of densely packed fibroblasts and myofibroblasts with occasional multinucleated giant cells. (H and E, original magnification $\times 30$)

ing fibroblastic and myofibroblastic core of tissue in early and intermediate lesions was extremely cellular and had a prominent myxoid stroma in some cases, resulting in a strong resemblance to nodular fasciitis, both histologically and radiologically. The nodular fasciitis-like areas merged with deposits of osteoid that were rimmed by osteoblasts; these areas in turn were surrounded by a rim of mature lamellar bone at the periphery of the lesions.

Five cases had a distinct zoning pattern in which lesional maturation progressed from central, nonossified cellular foci to osteoid to peripheral rims of mature lamellar bone. One of these was a multinodular lesion with zoning in multiple nodules. Another case (a biopsy) did not show a typical zoning pattern and consisted of nodular fasciitis-like areas with chondroosseous nodules; the other two were late lesions and were composed entirely of calcified, mature lamellar bone. Five cases had hyaline cartilage. One was a late lesion with a cartilaginous cap at the periphery; in the other four cases, the hyaline cartilage was associated with osteoid and undergoing endochondral calcification. All lesions were well circumscribed and rimmed by compressed fibrous connective tissue; most of these were surrounded by atrophic skeletal muscle, and, not infrequently, entrapped, atrophic skeletal

muscle fibers were seen within lesions. As lesions matured, the nodular fasciitis-like areas in the intertrabecular spaces became areas of delicate fibrosis containing thin-walled ectatic vascular channels that eventually became replaced by both adipose tissue and dense fibrosis in the most mature lesions.

In general, histologic stage correlated well with duration of symptoms, which usually were pain and/or soft-tissue mass. Early lesions were associated with 3–6 weeks of symptoms, intermediate lesions with symptoms of 6–8 weeks' duration, and late lesions with symptoms of up to 10 years' duration.

Discussion

On MR imaging, myositis ossificans was most often a relatively well-defined, inhomogeneous soft-tissue mass. Diffuse surrounding edema was quite prominent in lesions imaged within 8 weeks of the onset of symptoms (Figs. 1 and 2). This pattern of diffuse edema has been described previously, as has edema in the adjacent bone marrow [2]. The time required for resolution of the surrounding edema could not be determined; however, we speculate that the edema

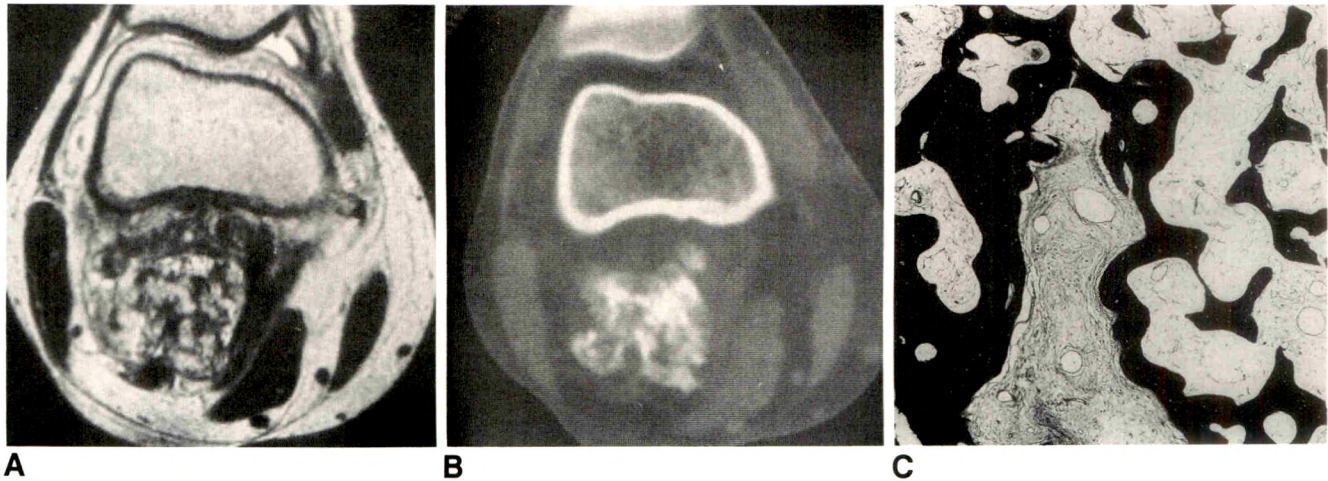


Fig. 4.—Mature myositis ossificans in popliteal fossa of 35-year-old man. Mass had been present for several years.

A, Axial T2-weighted SE MR image (2500/80) shows a well-defined inhomogeneous mass in popliteal fossa. Areas of increased signal within mass have about the same signal as subcutaneous fat. Similar findings were seen on T1-weighted image (not shown).

B, Axial CT scan (bone window) at level similar to that of A shows irregular diffuse mineralization throughout mass. Attenuation coefficient of nonmineralized area is difficult to assess, but may be similar to that of fat.

C, Photomicrograph shows mature lamellar bone corresponding to densely mineralized portions of mass. Regions between trabeculae consist of adipose tissue and delicate fibrous connective tissue. (H and E, original magnification $\times 30$)

could persist for several months. Edema was not detected in association with mature lesions.

MR images showed curvilinear and irregular regions of decreased signal intensity peripherally as well as within lesions, corresponding to mineralization seen on CT scans and radiographs. As expected, this was much less apparent on MR and was often best appreciated retrospectively (Figs. 2 and 3). It was not seen on MR in two early cases in which radiographs were normal or showed only faint mineralization. This mineralization delineated the lesion from the surrounding edema or tissue in all but two early cases.

The areas of increased signal intensity seen centrally within the early lesions on T2-weighted images are probably related to the extremely cellular central areas of proliferating fibroblasts and myofibroblasts within a myxoid stroma or extracellular matrix. These areas are histologically and radiologically similar in appearance to nodular fasciitis [8]. Areas of hyaline cartilage also may contribute to this appearance. The fluid-fluid levels detected in one case (Fig. 3) are consistent with previous hemorrhage [9], which is not an uncommon finding in the inner, most immature portion of the lesion. Fluid-fluid levels are a nonspecific finding and have been reported in other soft-tissue lesions including synovial sarcoma and hemangioma [9].

The areas of intermediate signal seen within late myositis ossificans on T2-weighted images reflect areas of fatty infiltration between bone trabeculae within the lesion. These same areas have a high signal intensity on T1-weighted images. The areas of decreased signal intensity on both pulse sequences represent the bone trabeculae of the lesion itself (Fig. 4). Areas of hemosiderin deposition from previous hemorrhage and fibrosis also may contribute to areas of decreased signal intensity on both pulse sequences.

The CT appearance of myositis ossificans has been well described [10–13]. CT usually will show a rim of mineralization around lesions after 4–6 weeks. Even when densely mineralized on CT, this rim is much less apparent on MR. The center of the mass may have decreased CT tissue attenuation [10, 13], again reflecting its similarity to nodular fasciitis [8], and corresponding to areas of increased signal intensity on T2-weighted SE MR imaging. Mature lesions may show diffuse ossification (Fig. 4), with corresponding regions of decreased signal intensity on all MR pulse sequences.

In the active phase of myositis ossificans, arteriography shows a diffuse tumor blush and fine neovascularity [14]. Although understanding of gadopentetate-dimeglumine enhancement is incomplete, this vascularity is likely responsible, at least in part, for the contrast enhancement identified within the lesion on MR [15]. Surrounding enhancement reflects associated edema [16]. Mature myositis will be avascular, reflecting the angiographic findings of normal bone [14], without associated edema, and we would expect no enhancement.

Plain radiographs in myositis ossificans show faint calcification within 2–6 weeks after onset of symptoms [1]. A sharply circumscribed mass is usually apparent by 6–8 weeks (although it may be seen much earlier), becoming smaller and mature by 5–6 months [13, 17, 18].

Although a discussion of the ability to reliably discriminate between benign and malignant lesions on the basis of MR imaging alone is clearly beyond the scope of this article, the spectrum of MR appearances in myositis ossificans serves to underscore the nonspecificity of MR imaging in many circumstances. Myositis ossificans, particularly in its early and intermediate phases, displays MR imaging characteristics frequently equated with malignancy.

REFERENCES

1. Ackerman LV. Extra-osseous localized non-neoplastic bone and cartilage formation (so-called myositis ossificans). *J Bone Joint Surg [Am]* **1958**; 40-A:279-298
2. Hanna SL, Magill HL, Brooks MT, Burton EM, Boulden TF, Seidel FG. Case of the day. Pediatric. Myositis ossificans circumscripta. *RadioGraphics* **1990**;10:945-949
3. Heinrich SD, Zembo MM, MacEwen GD. Pseudomalignant myositis ossificans. *Orthopedics* **1989**;12:599-602
4. Ogilvie-Harris DJ, Fornasier VL. Pseudomalignant myositis ossificans: heterotopic new-bone formation without a history of trauma. *J Bone Joint Surg [Am]* **1980**;62-A:1274-1283
5. Spjut HJ, Dorfman HD, Fechner RE, Ackerman LV. *Tumors of bone and cartilage: atlas of tumor pathology*, 2nd series fasc 5. Washington, DC: Armed Forces Institute of Pathology, **1971**:412-423
6. Johnson LC. Histogenesis of myositis ossificans. *Am J Pathol* **1948**;24:681-682
7. Angervall L, Stener B, Stener I, Ahren C. Pseudo-malignant osseous tumor of soft tissue: a clinical, radiological, and pathological study of five cases. *J Bone Joint Surg [Br]* **1969**;51-B:654-663
8. Meyer CA, Kransdorf MJ, Jelinek JS, Moser RP. Radiologic appearance of nodular fasciitis with emphasis on MR and CT. *J Comput Assist Tomogr* **1991**;15:276-279
9. Tsai JC, Dalinka MK, Fallon MD, Zlatkin MB, Kressel HY. Fluid-fluid level: a nonspecific finding in tumors of bone and soft tissue. *Radiology* **1990**;175:779-782
10. Amendola MA, Glazer GM, Agha FP, Francis IR, Weatherbee L, Martel W. Myositis ossificans circumscripta: computed tomographic diagnosis. *Radiology* **1983**;149:775-779
11. Heiken JP, Lee JKT, Smathers RL, Totty WG, Murphy WA. CT of benign soft-tissue masses of the extremities. *AJR* **1984**;142:575-580
12. Zeanah WR, Hudson TM. Myositis ossificans: radiologic evaluation of two cases with diagnostic computed tomograms. *Clin Orthop* **1982**;168:187-192
13. Hudson TM. *Radiologic-pathologic correlation of musculoskeletal lesions*. Baltimore: Williams & Wilkins, **1987**:589-604
14. Yaghamai I. Myositis ossificans: diagnostic value of arteriography. *AJR* **1977**;128:811-816
15. Pettersson H, Eliasson J, Egund N, et al. Gadolinium-DTPA enhancement of soft tissue tumors in magnetic resonance imaging—preliminary clinical experience in five patients. *Skeletal Radiol* **1988**;17:319-323
16. Erlemann R, Reiser MF, Peters PE, et al. Musculoskeletal neoplasms: static and dynamic Gd-DTPA-enhanced MR imaging. *Radiology* **1989**;171:767-773
17. Norman A, Dorfman HP. Juxtacortical circumscribed myositis ossificans: evolution and radiographic features. *Radiology* **1979**;96:301-306
18. Goldman AB. Myositis ossificans circumscripta: a benign lesion with a malignant differential diagnosis. *AJR* **1976**;126:32-40

Case Report

Soft-Tissue and Osseous Lesions Caused by Bacillary Angiomatosis: Unusual Manifestations of Cat-Scratch Fever in Patients with AIDS

Brian R. Herts,¹ Mahvash Rafii, and Gary Spiegel

Cat-scratch disease, caused by a pleomorphic Gram-negative rod known as the cat-scratch bacillus, has many rare and varied complications and unusual manifestations [1]. Recent reports [2–6] have described bacillary angiomatosis as a new manifestation of systemic cat-scratch disease seen in patients with AIDS who have cutaneous lesions, subcutaneous nodules, or osteolytic lesions. We report a case of bacillary angiomatosis that was manifested as a vascular soft-tissue mass in which cat-scratch bacilli were shown by electron microscopy. To our knowledge, no similar cases of soft-tissue masses in systemic cat-scratch disease have been reported. As our case illustrates, systemic cat-scratch disease has clinical and radiologic features that resemble both benign and malignant diseases. Although certain radiologic and clinical findings may suggest the diagnosis of systemic cat-scratch disease, a definitive diagnosis is made only on the basis of biopsy specimens examined by using either special stains or electron microscopy.

Case Report

A 42-year-old man with a history of IV drug use and bisexuality had had lower back pain for 6 days after an episode of mild trauma. He reported that he had fevers, night sweats, and generalized weakness. He also reported a "lump" in the left side of his chest wall that was occasionally painful and was first noticed about the time his fevers and night sweats began. His body temperature was 102.2°F

(39.0°C). A mobile, soft, and nontender 4 × 5 cm mass was palpated in the left side of the chest wall. Laboratory values on admission included an erythrocyte sedimentation rate of 90 mm/hr (normal, <15), a hemoglobin level of 11.9 g/dl (119 g/l), and a normal WBC count. The patient tested positive for antibodies to human immunodeficiency virus (HIV).

The mass in the chest wall showed enhancement on a contrast-enhanced CT (Fig. 1A) and abnormal uptake of radionuclide on gallium scintigraphy (Fig. 1B). An angiogram confirmed the vascular nature of the mass, which subsequently was resected for diagnosis; the provisional diagnosis was hemangiosarcoma.

Initial evaluation of the patient's lower back pain included radiographs, myelogram, and CT (after the myelogram) of the lumbosacral spine; findings on all were interpreted as normal. Two weeks into the hospitalization, a bone scan obtained because of continued back pain showed abnormal uptake of radionuclide at L3. Radiographs and CT images of the lumbosacral spine at this time showed an osteolytic lesion of the L3 vertebral body (Fig. 1C) that was thought to represent a metastatic focus of hemangiosarcoma.

Subsequent electron microscopic examination of the resected axillary mass showed benign vascular proliferation and multiple bacilli (Fig. 1D). The bacilli were consistent with cat-scratch bacilli, and the diagnosis of bacillary angiomatosis was established. CT-guided biopsy of L3 was performed; however, only necrotic tissue was obtained. The spinal lesion was thought to be due to disseminated cat-scratch disease, and the patient was treated with doxycycline. No recurrence of the axillary soft-tissue mass was seen, and follow-up CT of the L3 lesion showed partial resolution and sclerosis of the lesion consistent with healing. Retrospectively, the patient did not recall any exposure to cats.

Received May 20, 1991; accepted after revision July 17, 1991.

¹ All authors: Department of Radiology, New York University Medical Center, Bellevue Hospital 3W37, 27th St. and First Ave., New York, NY 10016.

AJR 157:1249–1251, December 1991 0361–803X/91/1576–1249 © American Roentgen Ray Society

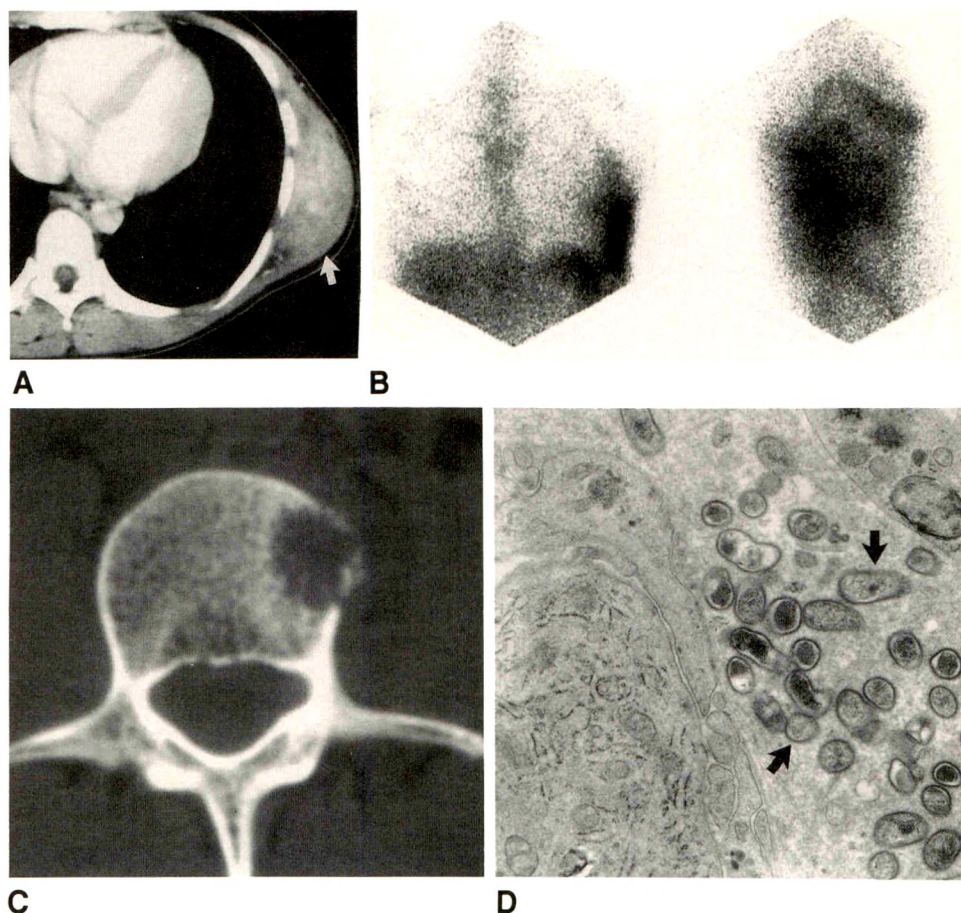


Fig. 1.—A, Contrast-enhanced CT scan shows a vascular heterogeneously enhancing mass (arrow) in left side of chest wall in patient positive for human immunodeficiency virus.

B, Anterior (left) and left lateral (right) views from ^{67}Ga scintigrams of chest show markedly abnormal uptake of radionuclide in left side of chest wall 120 hr after injection.

C, CT scan shows a well-marginated lytic lesion of third lumbar vertebral body with a small paraspinal soft-tissue component.

D, Electron micrograph of chest wall mass in A shows multiple cat-scratch bacilli (arrows) adjacent to a vascular endothelial cell.

Discussion

Before the discovery by Wear et al. [7] of the cat-scratch bacillus in 1983, cat-scratch disease was diagnosed solely on the basis of clinical criteria. The diagnosis of cat-scratch disease in non-AIDS patients is still based on clinical findings; specific histologic evaluation with Warthin-Starry silver staining or electron microscopy is necessary for confirmation. Clinical signs for the diagnosis of cat-scratch disease in non-AIDS patients were reviewed recently by Carithers [1] in a series of 1200 patients. He described the typical patient as being less than 18 years old and having a history of exposure to cats and often an identifiable inoculation site. Lymphadenopathy was usually present in a single lymph node chain referable to the site of inoculation. A diagnosis was made by exclusion of other potential causes for adenopathy and by a positive skin test reaction to cat-scratch disease antigen. Osteolysis in Carithers's series was extremely rare (two cases); bacillary angiomatosis was not described.

In contrast to Carithers's description, a different clinical presentation of systemic cat-scratch disease in patients positive for antibodies to HIV has been described recently [2–6]. These patients are young adults with anemia; cutaneous epithelial tumors referred to as bacillary angiomatosis; and systemic signs of infection, including an elevated erythrocyte

sedimentation rate. These cutaneous lesions are usually the presenting complaint and have not been reported to be due to cat-scratch disease in persons who are HIV-negative.

The patient described here has clinical signs and symptoms similar to those previously reported in cases of systemic cat-scratch disease, specifically, fevers, anemia, and an elevated erythrocyte sedimentation rate. However, our patient had no cutaneous lesions. He had a vascular soft-tissue mass that also showed increased uptake of gallium. Although Baron et al. [2] have described subcutaneous nodules, no report of a soft-tissue mass similar to the one described here has been published before. Our patient also had an osteolytic lesion with findings on radiographs and scintigrams that were similar to those in cases previously reported.

Kaposi sarcoma is the main consideration in the differential diagnosis of the typical cutaneous lesions seen due to cat-scratch disease in AIDS patients. As reported by Baron et al., the presence of osseous lesions can help in distinguishing cat-scratch disease from Kaposi sarcoma. The differential diagnosis of the vascular soft-tissue mass seen in our case might include angiosarcoma, melanoma, hemangioma, or metastatic thyroid carcinoma. However, these diagnoses have no particular association with AIDS.

Our case illustrates a manifestation of systemic cat-scratch disease not previously reported in patients with AIDS: a soft-

tissue mass due to bacillary angiomatosis that was proved by electron microscopy. The radiologic features of the reported soft-tissue and osseous lesions are nonspecific. However, when seen in conjunction with cutaneous lesions and signs and symptoms of systemic infection, the diagnosis of bacillary angiomatosis due to disseminated cat-scratch disease should be strongly considered, especially when the patient concerned is, or may be, HIV-positive.

REFERENCES

1. Carithers HA. Cat-scratch disease: an overview based on a study of 1,200 patients. *Am J Dis Child* **1985**;139:1124-1133
2. Baron AL, Steinbach LS, LeBoit PE, Mills CM, Gee JH, Berger TG. Osteolytic lesions and bacillary angiomatosis in HIV infection: radiologic differentiation from AIDS-related Kaposi sarcoma. *Radiology* **1990**;177:77-81
3. Cockerell CJ, Webster GF, Whitlow MA, Freidman-Kien AE. Epithelioid angiomatosis: a distinct vascular disorder in patients with the acquired immunodeficiency syndrome or AIDS-related complex. *Lancet* **1987**;2:654-656
4. Koehler JA, LeBoit PE, Egbert BM, Berger TG. Cutaneous vascular lesions and disseminated cat-scratch disease in patients with the acquired immunodeficiency syndrome (AIDS) or AIDS-related complex. *Ann Intern Med* **1988**;109:449-455
5. Knobler EH, Silvers DN, Fine KC, Lefkowitz JH, Grossman ME. Unique vascular skin lesions associated with the immunodeficiency virus. *JAMA* **1988**;260:524-527
6. LeBoit PE, Egbert BM, Stoler MH, et al. Epithelioid hemangioma-like vascular proliferation in AIDS: manifestation of cat-scratch disease bacillus infection? *Lancet* **1988**;2:960-963
7. Wear DJ, Margileth AM, Hadfield TL, Fischer GW, Schlagel CJ, King FM. Cat-scratch disease: a bacterial infection. *Science* **1983**;221:1403-1404

Book Review

The Visible Human Body. An Atlas of Sectional Anatomy. By Gunther von Hagens, Lynn J. Romrell, Michael H. Ross, and Klaus Tiedemann. Philadelphia: Lea & Febiger, 151 pp., 1991. \$37.50

This atlas of human anatomy is divided into seven anatomic parts: the head and neck, the upper and lower extremities, the chest and abdomen, and the pelvis. The anatomic sections include axial, coronal, and sagittal planes, and each part contains several CT scans or MR images that correlate with the anatomic sections. The pelvis is divided into two parts, one for the female and the other for the male.

The atlas consists of 120 anatomic sections that are displayed in large format, 10 × 14 in. (25.4 × 35.6 cm), and in color. The sections were prepared by using a new technique known as plastination. A frozen cadaver was sliced into sections 2.5 to 4.0 mm thick, and the sections were processed to remove water and lipids; the lipids were then replaced with an epoxy polymer. This process avoids the "collapse" and shrinkage, particularly of hollow structures (e.g., blood vessels, gastrointestinal tract), that is usually annoyingly apparent in most atlases of cadaveric sections. The result is amazing. These are the best anatomic sections that I have seen.

Each of the seven major anatomic regions is introduced with correlative CT scans and anatomic sections and a brief description of the important anatomic features shown on the images. The CT scans, MR images, and anatomic plates are labeled in detail around the periphery, and the corresponding anatomic structures are easy to identify. Each structure is indexed at the end of the book. The index is complete and easy to use.

The anatomic sections of the musculoskeletal system, particularly the shoulder, elbow, hand, wrist, hip, and knee, are particularly useful, as MR examination of these areas is now quite common. The

anatomic sections are presented in axial, coronal, and sagittal format. The addition of more correlative MR images would be useful here. The sections on the neck, chest, and abdomen are exceptional for their detail. For example, the heart is maintained in its normal configuration, and the valves can be seen perfectly; the mediastinal structures (e.g., esophagus, aorta, vena cava, azygos veins) are normally distended rather than collapsed, as is the usual case with cadaveric sections. Similar preservation of normal anatomic detail is apparent in the abdomen, especially the gastrointestinal tract and gallbladder.

Overall, this is an excellent atlas. It would benefit from and be even more useful with the addition of more correlative CT scans and MR images, particularly corresponding coronal and sagittal MR images and anatomic sections of the head, neck, chest, abdomen, and pelvis. Otherwise, the only fault that I found was the occasional use of outdated terminology (e.g., the use of quadrate lobe for the medial segment of the left lobe of the liver and suprarenal rather than adrenal gland) and one plate that labels the superior mesenteric vein-splenic vein confluence as the "portal vein." These are hardly worth worrying about when the atlas is viewed as a whole, and all for \$37.50! I strongly recommend the atlas to anyone in need of a detailed cross-sectional anatomy book.

Patrick C. Freeny
Virginia Mason Clinic
Seattle, WA 98111

Dye Laser-Assisted Angioplasty with Multifiber Catheters: Short-Term Results in the Treatment of 29 Peripheral Arterial Occlusions

Peter E. Huppert¹
 Stephan H. Duda¹
 Hartwig Seboldt²
 Claus D. Claussen¹

The use of pulsed dye laser energy for angioplasty offers the possibility of ablating atherosclerotic plaques without thermal damage to the adjacent arterial wall. However, to be of value, systems that deliver the energy safely and effectively are required. We tested multifiber catheters in 504-nm pulsed dye laser angioplasty for treatment of peripheral arterial occlusions. Flexible multifiber catheters consist of 12 (7-French) and 19 (9-French) concentrically arranged 200- μ m quartz fibers allowing guidewire-directed use. Laser-assisted angioplasty was performed in 2- to 13-cm- (mean, 7.5-cm) long occlusions of iliac (six) and femoropopliteal (23) arteries in patients with symptomatic occlusive vascular disease. Angiograms were obtained before and after laser ablation, after subsequent balloon dilatation, and if signs or symptoms indicated restenosis, during follow-up. The laser procedure was impossible to perform in three (10%) of 29 patients; this was related to unsuccessful passage of the wire in one patient and to inability to advance the laser catheter across the lesion in two patients. In one other patient, reocclusion occurred 1 day after angioplasty. Stand-alone laser angioplasty relieved residual stenosis of less than 30% in six (26%) of 23 femoropopliteal arteries, making balloon dilatation dispensable. Immediate clinical improvement was achieved in 26 (90%) of 29 patients. Laser treatment caused no perforation and no embolization, but minor dissections occurred in 36% of the patients.

Our experience suggests that pulsed dye laser angioplasty via multifiber catheters converts arterial occlusions into stenoses. With the exception of angioplasty in distal femoropopliteal arteries, additional balloon dilatation is necessary to complete recanalization.

AJR 157:1253-1257, December 1991

Previous studies have shown the value of pulsed dye laser light in the blue green spectral range for ablating atherosclerotic plaque with minimal thermal damage to the adjacent tissue [1-3]. Angioplasty with the pulsed dye laser has been performed by using single quartz fibers with a ball-tipped configuration [4, 5]. The fibers can be passed through occlusions in the femoral artery, but insufficient steerability of the device increases the risk of perforation and dissection when it is used in the distal femoropopliteal artery [5]. Multifiber catheters with circularly arranged thin quartz fibers around a central lumen can be directed over the wire. Multifiber catheters already have been used successfully in excimer laser angioplasty of coronary [6] and peripheral [7, 8] arteries.

The purpose of our study was to determine usefulness and safety of multifiber catheters for use in 504-nm pulsed dye laser angioplasty of occlusions of the femoropopliteal and iliac arteries.

Subjects and Methods

From August 1990 to January 1991, dye laser angioplasty was attempted in 29 patients, 20 men and nine women 45-83 years old (mean, 67 ± 12 years). All patients were recruited

Received April 22, 1991; accepted after revision July 19, 1991.

¹Department of Diagnostic Radiology, Eberhard-Karls-University Tübingen, Hoppe-Seyler-Str. 3, D7400 Tübingen-1, Germany. Address reprint requests to P. Huppert.

²Department of Cardiovascular Surgery, Eberhard-Karls-University Tübingen, D7400 Tübingen-1, Germany.

0361-803X/91/1576-1253
 © American Roentgen Ray Society

consecutively and had signs and symptoms of chronic ischemic peripheral vascular disease characterized by moderate intermittent claudication (19), rest pain (five), and minor tissue loss due to non-healing ulcers (five). Eight patients had diabetes, and 12 had a history of cigarette smoking. The study was approved by the local human research committee. Patients were informed in detail, and their consent was obtained. After initial clinical examination, all patients had diagnostic digital subtraction angiography.

Occlusions were located in six iliac arteries and 23 femoropopliteal arteries. The length of the occlusion varied from 2 to 13 cm (mean, 7.5 cm); 13 lesions were longer than 5 cm (Table 1).

A pulsed dye laser (Candela Corp., Wayland, MA) was used that emits light with a wavelength of 504 nm and a pulse width of 1.4 μ sec at a repetition rate of 10 Hz. Laser light was transmitted via commercially available multifiber catheters (Candela Corp.) coupled to the laser head. Catheters consist of 12 (7-French) or 19 (9-French) 200- μ m quartz fibers embedded in plastic material and concentrically arranged around a central channel for guidewire insertion. For the treatment of occlusions in iliac arteries, in femoral arteries, and in the proximal part of popliteal arteries, 9-French catheters, passed over 0.035-in. (0.09-cm) guidewires, were used. Two lesions located in the distal part of the popliteal artery were recanalized by using 7-French catheters, passed over 0.018-in. (0.05-cm) guidewires. Energy

transmitted via multifiber catheters was measured at the catheter tip by means of a power meter (Candela Corp.) before and after use.

For the treatment of femoropopliteal occlusions, 9- or 8-French introducer sheaths were placed into the superficial femoral artery percutaneously with the patient under local anesthesia. In patients with iliac lesions, 9-French sheaths were introduced into the external iliac artery. Road-map fluoroscopy was used for guidance, and a steerable guidewire (Terumo Corp., Tokyo, Japan) was passed through the occlusion. The laser catheter was gently advanced over the wire across the lesion while the laser continuously emitted energy. The catheter was withdrawn with continuous energy delivery at the same speed. Two, four, or a maximum of six passages were performed until no further luminal increase was obtained. The effect of each passage of the laser catheter was assessed angiographically; contrast material was injected via the introducer sheath after withdrawal of the catheter. The number of pulses applied and time needed for each passage were registered.

Balloon angioplasty was performed subsequently if a stenosis of more than 30% persisted after the laser procedure. The grade of stenosis was estimated visually by using two projections for iliac arteries and one projection for femoropopliteal arteries. Intravascular tantalum stents (Boston Scientific Corp., Watertown, MA) were implanted if residual stenoses of more than 50% remained after balloon dilatation and reocclusion was imminent.

Initially, 5000 U of heparin was administered. During the procedure, the introducer sheath was flushed with heparinized saline containing 20 mg of Tolazolin (Dispersa Corp., Germering, Germany) per 100 ml of solution. Heparinization was continued after the procedure by IV application of 1000 U/hr for 24 hr in patients with occlusions shorter than 5 cm and for 48 hr in patients with lesions 5 cm long or longer. Patients received 100 mg of aspirin per day starting 1 day before treatment and continuing for at least 6 months.

Recanalization was considered successful when the degree of residual stenosis was less than 30%. A clinical investigation, including determination of the ankle-brachial index (ABI), was performed 1 day

TABLE 1: Location and Length of Arterial Occlusions Treated by Pulsed Dye Laser Angioplasty

Length (cm)	Location		
	Iliac	Femoropopliteal	Total
2-5	5	11	16
6-10	0	9	9
11-13	1	3	4
Total	6	23	29

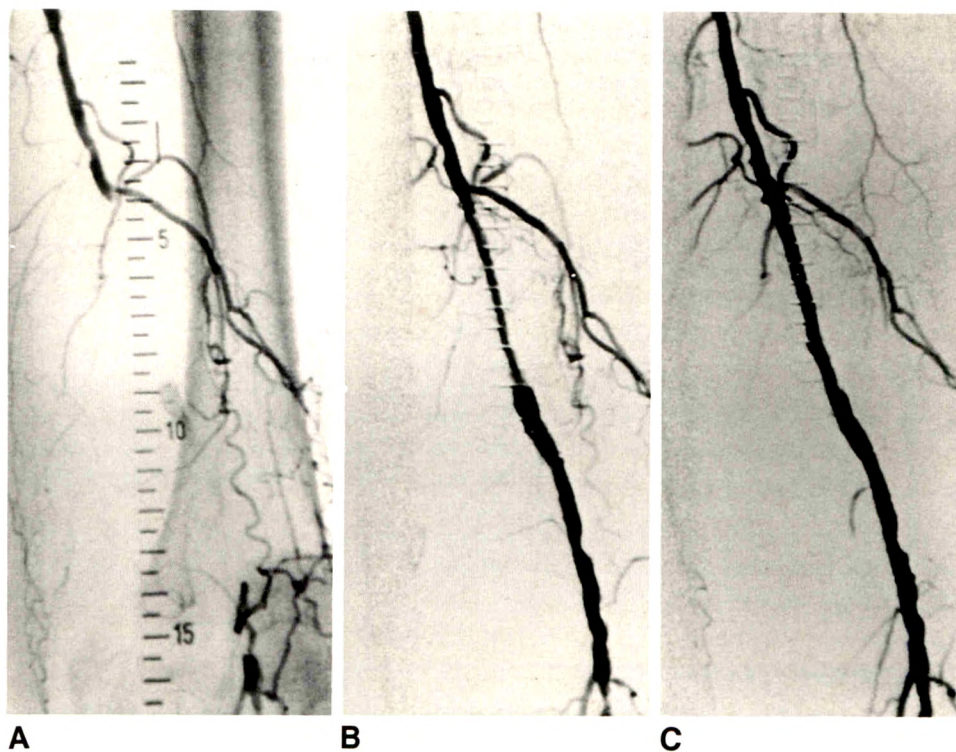


Fig. 1.—Dye laser-assisted balloon angioplasty of occluded femoral artery in a 65-year-old diabetic woman with pain in left leg when at rest.

A, Angiogram obtained before angioplasty shows 5-cm-long occlusion of distal femoral artery. Popliteal artery is not completely visible because collateral vessels branching from profunda femoral artery are not filled.

B, Angiogram obtained after four passages with a 9-French multifiber catheter (70 mJ per pulse) shows 50% residual stenosis with smooth margins.

C, Angiogram obtained after dilatation with a 6-mm balloon shows vessel diameter is now sufficient. In follow-up period of 7 months, the patient had a pain-free walking distance of 500 m.

before treatment, 2 days after treatment, and if signs or symptoms recurred. Immediate clinical results were classified according to recommendations by Rutherford [9]. A marked improvement was assumed if signs or symptoms disappeared and the ABI was greater than 0.90. Improvement was considered moderate if signs or symptoms decreased and the ABI increased by more than 0.10. Improvement was considered minimal if signs or symptoms decreased without significant increase of the ABI. Reocclusion was suspected if signs or symptoms recurred and the ABI decreased by more than 0.10 compared with the posttreatment status. Angiography was performed in all patients if reocclusion was suspected. Student's *t* test was used for statistical analysis.

Results

In 28 of 29 patients, passage of the guidewire succeeded as a prerequisite for the laser procedure. In one patient, placement of the guidewire across a 10-cm-long femoropopliteal occlusion failed. The multifiber catheter could be advanced across the lesion in 26 patients. Two distal femoropopliteal occlusions, one 5 cm long and one 13 cm long, could

be partially traversed with a 9-French laser catheter only. In these patients, balloon dilatation was performed successfully by using low-profile dilatation catheters (ultrathin balloon dilatation catheter, Boston Scientific Corp.). In another two patients, 12-cm-long femoropopliteal occlusions had been passed four times with the 7- or 9-French multifiber catheter, but no vessel patency was achieved. In these lesions, a sufficient lumen was produced by prolonged balloon dilatation.

In the remaining 24 (83%) of 29 patients, the laser procedure resulted in a partial reopening of the vessel. The mean grade of residual stenoses was 48% (SD = 17%). In 18 (62%) of 29 lesions, stenoses between 30% and 70% persisted after the laser procedure, and balloon dilatation was subsequently performed (Fig. 1). Stents were implanted in three iliac and two femoral lesions. In six occlusions (26%) of the distal femoral and proximal popliteal arteries (23 arteries) a lumen diameter of more than 70% was obtained after six passages of the 9-French multifiber catheter, and additional balloon dilatation was not necessary (Fig. 2).

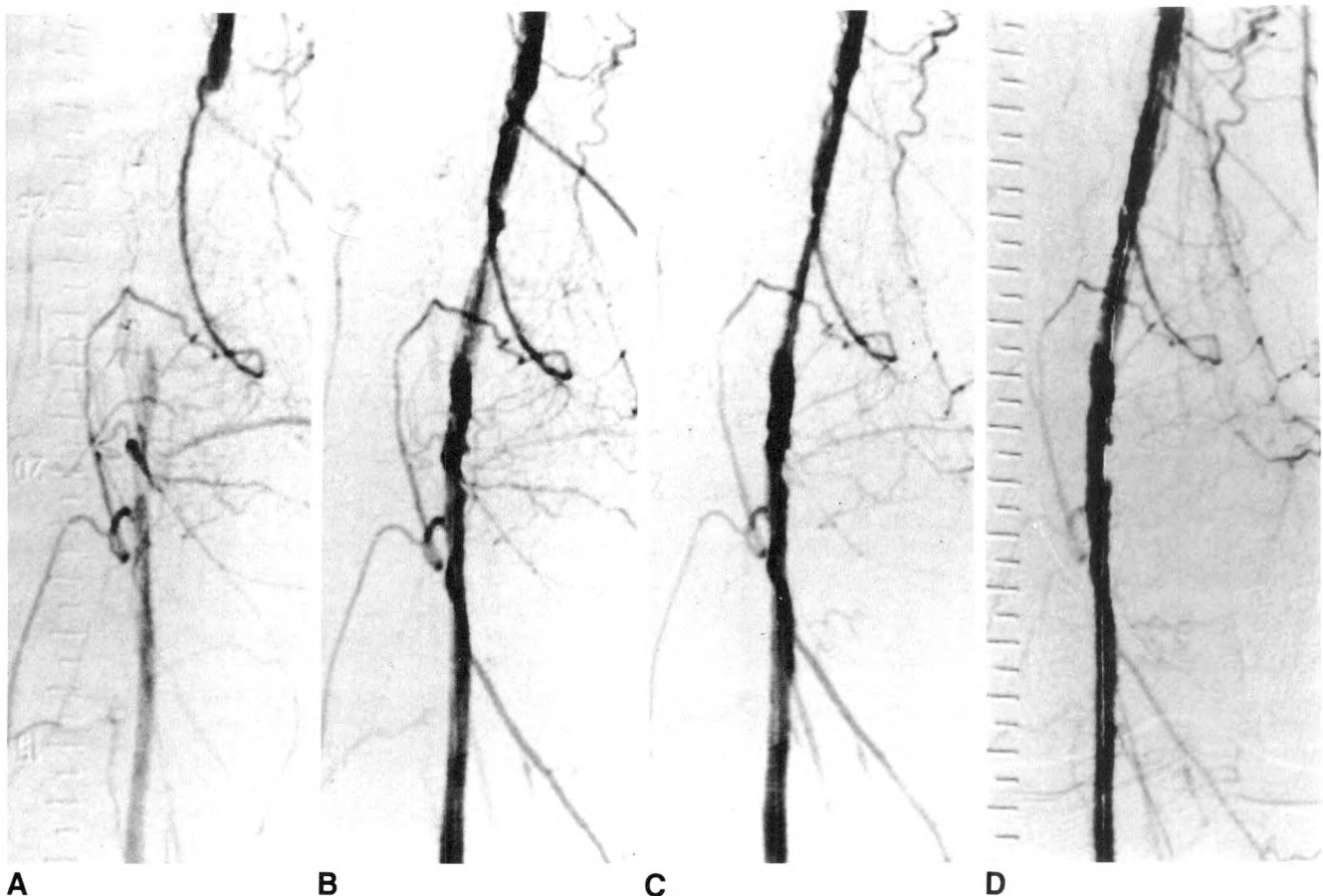


Fig. 2.—Stand-alone dye laser angioplasty of occluded distal femoropopliteal artery in a 66-year-old cigarette smoker with intermittent claudication of right leg.

A, Angiogram obtained before angioplasty shows 5-cm-long femoropopliteal occlusion.

B, Angiogram obtained after two passages with a 9-French multifiber laser catheter (100 mJ per pulse) shows small, irregular lumen has been created.

C, Angiogram obtained after four passages with laser catheter shows 50% residual stenosis.

D, Angiography obtained after six passages with laser catheter shows persistent residual stenosis of less than 30% and low-grade dissection in upper part of lesion. Balloon dilatation was not performed. After 4 months of follow-up, no symptoms indicating reocclusion have been seen.

During laser ablation, a mean number of 46 pulses per millimeter of occlusion was applied, resulting in a recanalization speed of 22 ± 8 mm/min. Level of energy measured before the laser procedure was 60–110 mJ per pulse (mean value, 78 ± 19 mJ) via the 9-French multifiber catheters and 50 and 60 mJ via the 7-French catheters used in two patients. After the procedure, transmitted energy was 66 ± 21 mJ per pulse in the 9-French catheters and 40 and 60 mJ, respectively, in the 7-French catheters. The differences between transmitted energy before and after the use of the 9-French catheters was not significant.

No major complications occurred, in particular, no perforation of a vessel wall and no embolization. In 10 patients, minor dissections of the arterial wall were noticed after the laser procedure (Fig. 2). The dissections were not obstructive. In five patients, luminal widening by balloon dilatation reduced the grade of dissection. Dissections were produced only by the use of 9-French multifiber catheters. In arteries showing dissections after laser ablation, a mean pulse energy of 87.5 ± 19 mJ (all but one 80 mJ or more) had been delivered, compared with 77.2 ± 11 mJ in those patients without dissections. This energy difference was not significant. Dissections were located in two iliac and eight femoropopliteal arteries. After the laser procedure, no damage to the coated guidewires was evident macroscopically.

Recanalization succeeded finally in 28 (97%) of 29 patients. The clinical improvement was marked in nine (31%) of 29 patients, moderate in 16 (55%) of 29 patients, and minimal in one patient (3%). Mean ABI increased significantly from 0.53 ± 0.12 before angioplasty to 0.91 ± 0.18 after angioplasty ($n = 29$; $p < .01$). The patient with minimal clinical improvement had a 10-cm-long femoropopliteal lesion that reoccluded 1 day after angioplasty. Reocclusion probably was due to a dissection produced by 6-mm balloon dilatation.

In a preliminary follow-up period of 1–7 months (mean, 2.8 months), three reocclusions (10%) occurred in femoropopliteal arteries. Two lesions, one 3 cm long and one 5 cm long, reoccluded 1 and 7 months, respectively, after stand-alone laser recanalization. In the third patient, a 12-cm-long lesion reoccluded 6 months after angioplasty. In this artery, acute reocclusion occurred after complete laser catheter passages, and patency was achieved by balloon dilatation. No reocclusion was seen in stented arteries.

Discussion

To examine the usefulness and limitations of multifiber catheters in dye laser angioplasty, we treated chronic peripheral arterial occlusions. During recanalization, catheters were advanced at a speed of 22 ± 8 mm/min. This rate is about four times higher than the rate reported for the advancement of multifiber catheters in peripheral laser angioplasty with a 308-nm XeCl-excimer laser with a pulse duration of 60 nsec [10]. Excimer laser systems with longer pulse durations of 120–160 nsec (Advanced Interventional Systems, Irvine, CA) ablate plaque more effectively, resulting in an increased speed of recanalization [11]. A shortening of the recanalization time is important for treatment of long femoropopliteal occlusions,

in which mechanical obstruction by the laser catheter itself increases the risk of thrombosis and embolization. Laser angioplasty prolonged the procedural time between 15 and 45 min. Preparation of the catheters and calibration required only a few minutes, but catheter passages through the occlusions were still time-consuming.

We could not use the dye laser in three (10%) of 29 patients. In one patient, placement of the guidewire across the lesion was impossible. To avoid perforation, the laser catheter was not used without wire guidance. In two patients, we could not maneuver the 9-French laser catheters across the femoropopliteal occlusions completely, and attempts to advance the catheter resulted in bending of the catheter. The pulse energy applied in these lesions was 70 and 90 mJ. This means an energy density of 0.12 and 0.15 J/mm², respectively. Energy densities required for ablation of atherosclerotic material depend considerably on plaque composition and exceed 1.5 J/mm² in dye laser angioplasty when calcifications are present [12]. Therefore, it is probable that failed passage of multifiber catheters was caused by insufficient plaque ablation. In contrast to the nontapered 9-French multifiber catheter, 5-French low-profile dilatation catheters could be advanced. In two more patients, reobstruction occurred immediately after laser angioplasty had been performed. We attribute this to recoil of incompletely removed plaque material into the vessel lumen after withdrawal of the laser catheter. In both cases, prolonged inflation of a 6-mm balloon was necessary to achieve sufficient vessel patency.

Murray et al. [5], who used a ball-tipped fiber for dye laser angioplasty, reported a 19% rate (5/26) of technical failures for recanalization of femoropopliteal arteries. Failures in three patients were due to insufficient steerability of the device, causing fiber-induced perforation, dissection by the fiber, and entrance of a side branch. In two patients, prograde penetration of the occlusion by the fiber was impossible. Eighty-one percent of lesions treated in this study were longer than 10 cm, compared with 13% in our study group. Angiographic evaluation of the laser effect after laser angioplasty with the ball-tipped fiber was not reported. Guidance of multifiber catheters over the wire is effective and reliably prevents perforation during recanalization of curved segments in long artery occlusions. However, the rate of insufficient penetration of the occlusion depends on the energy density applied and the composition of the ablated plaque and seems to be similar with both devices.

The laser procedure caused angiographically detectable dissections in 10 (36%) of 28 patients treated. All dissections were minor. In five of these patients, subsequent balloon dilatation was accompanied by a decrease in the grade of dissection. Our results suggest that the frequency of dissections caused by dye laser angioplasty depends on the energy fluency. Dissections were noted in eight (62%) of 13 patients when the pulse energy applied via 9-French laser catheters was 80 mJ or more but in only one (9%) of 11 patients when the pulse energy was 70 mJ or lower. The emission of 80 mJ per pulse via the 9-French multifiber catheter results in an energy density of 0.13 J/mm². This radiant exposure is about three times higher than that applied for excimer laser angioplasty [7, 10, 13]. Excimer laser-induced dissections were

not reported in these studies. This makes it probable that one factor causing these dissections is the shock wave generated during pulsed application of high-density energy. An additional factor might be a mechanical "Dotter" effect of the nontapered multifiber catheter, as dissections have not been reported in pulsed dye laser angioplasty, either with the ball-tipped fiber (energy density applied, about 0.45 J/mm²) or with the bare fiber (energy density applied, 1.1–1.6 J/mm²), in peripheral arteries [5, 12]. In order to reduce the frequency of dissections related to the use of multifiber catheters in dye laser angioplasty, it seems to be useful to start recanalization at a pulse energy of 70 mJ (50 mJ) when 9-French (7-French) catheters are used. If persistent resistance to catheter advancement indicates an increased threshold for tissue ablation, pulse energy should be raised in steps of 10 mJ. Withdrawing the catheter from the patient is necessary for energy measurement, and smaller steps of enlarging the energy would be too time-consuming.

Ablation of arteriosclerotic material when multifiber catheters were used in dye laser angioplasty converted arterial occlusions into stenotic lesions in most of our patients. Sufficient recanalization was achieved by using 9-French catheters in the distal femoral and proximal popliteal artery. In the proximal femoral artery and in iliac arteries, additional balloon dilatation was needed to achieve adequate luminal dimensions. The follow-up in these patients has been limited and does not yet allow us to draw any conclusion about whether treatment or pretreatment of arterial occlusions by dye laser angioplasty can provide improved long-term results compared with the results of balloon dilatation alone.

REFERENCES

1. Anderson RR, Jaenke KF, Parrish JA. Mechanism of selective vascular changes caused by dye lasers. *Lasers Surg Med* 1983;3:211–215
2. Prince MR, Deutsch TF, Shapiro AH, et al. Selective ablation of atheromas using a flashlamp-excited dye laser at 465 nm. *Proc Natl Acad Sci USA* 1986;83:7064–7068
3. Murray A, Basu R, Wells C, Wood RFM. Defining parameters for peripheral laser angioplasty. *Eur J Vasc Surg* 1989;3:31–36
4. Prince MR, LaMuraglia GM, Flotte T, Egglin TK, Gregory KW, Athanasoulis CA. Selective laser angioplasty at 480 nm with ball-tipped fibres in amputated human legs (abstr). *Radiology* 1989;173(P):148
5. Murray A, Mitchell DC, Grasty M, Wood RFM, Edwards DH, Basu R. Peripheral laser angioplasty with pulsed dye laser and ball-tipped optical fibres. *Lancet* 1989;2:1471–1474
6. Karsch KR, Haase KK, Voelker W, Baumbach A, Mauser M, Seipel L. Percutaneous coronary excimer laser angioplasty in patients with stable and unstable angina pectoris. *Circulation* 1990;81:1849–1859
7. Litvack F, Grundfest WS, Adler L, et al. Percutaneous excimer-laser and excimer-laser-assisted angioplasty of the lower extremities: results of initial clinical trial. *Radiology* 1989;172:331–335
8. Duda SH, Karsch KR, Haase KK, Huppert PE, Claussen CD. Laser ring catheters in excimer laser angioplasty. *Radiology* 1990;175:269–270
9. Rutherford RB. Standards for evaluating results of interventional therapy for peripheral vascular disease. *Circulation* 1991;83[suppl I]:I6–I11
10. Huppert PE, Duda SH, Seiboldt H, Karsch KR, Claussen CD. Periphere Excimer-Laserangioplastie: Indikationen, Methode und klinische Ergebnisse. *Dtsch Med Wochenschr* 1991;116:161–167
11. Cragg AH, Gardiner GA, Smith TP. Vascular applications of laser. *Radiology* 1989;172:925–935
12. Leon MB, Almagor Y, Bartorelli AL, et al. Fluorescence-guided laser-assisted balloon angioplasty in patients with femoropopliteal occlusions. *Circulation* 1990;81:143–155
13. Schwarten DE, Cutcliff WB. Use of excimer laser in the percutaneous management of peripheral atherosclerosis (abstr). *Radiology* 1987;165(P):276

Memorial

James A. Jagodzinski, 1939–1991



James A. ("Jag") Jagodzinski, a native of Toledo, received his medical degree from St. Louis University Medical School in 1964 and completed his specialty training in interventional radiology at the University of Michigan in 1971, with intervening duty in the U. S. Army Medical Corps. Jim was actively in-

involved in the medical staff affairs of The Toledo Hospital and was section head of interventional radiology. His expertise in angiography, percutaneous lung biopsies, and other percutaneous procedures was largely responsible for introducing and popularizing these procedures in the Toledo area.

Jim was very active in the medical community, serving as chairman of several commissions (mediation, judicial and internal affairs, education and professional affairs) and was secretary, vice-president, and in 1984, president of the Academy of Medicine of Toledo and Lucas County. He was president of his professional corporation, Toledo Radiological Associates, Inc., from 1977 to 1979 and served on its board of directors for 7 years. Jim was president of the Northwestern Ohio Radiology Society for one term; served 9 years as a delegate to the Ohio State Medical Association; and was involved in the formation of the Physicians Insurance Exchange (PIE Mutual Insurance Co.), where he served as board chairman. In 1985, he was honored by the Ohio House of Representatives with the Outstanding Citizen Award in

recognition of his many community activities, especially monetary gifts and his personal gratis services to the needy (chairman of the indigent care committee of the Community Planning Agency and the Mildred Bayer Health Care Clinic for the Homeless).

Jim's athletic skills and competitive spirit in golf and bowling were well known to his fellow physicians and to many people in the community and were superseded only by his other attributes of generosity, honesty, integrity, trustworthiness, and devotion to excellence. Jim personified the "A's" of medical practice: affable, available, accountable, affordable, and admirable.

His life ended prematurely on January 28, 1991, but the lasting effects of his achievements will continue to influence all who knew him or were associated with him to pursue those same standards of excellence with the same generous spirit. To his wife, Georgia; his children, Deborah, Joseph, and Anthony; and his mother, Constance, we extend our most heartfelt sympathy.

Leonard M. Heinz
Toledo, OH 43606

Anatomic Relationship Between the Popliteal Artery and Vein: A Guide to Accurate Angiographic Puncture

Jean-Paul Trigaux¹
Bernard Van Beers
Jean-François De Wispelaere

The anatomic relationship between the popliteal artery and vein means that an arteriovenous fistula can be created when a popliteal artery approach is used for endovascular interventions. To determine the best site for retrograde puncture of the popliteal artery, we studied six cadaveric specimens, CT scans of 31 patients at 280 levels, and 30 plain radiographs of the knee. In the cadaveric specimens, the vessels were enclosed in a common sheath. In 92% of all levels studied on CT, the artery was anterior to the vein (anterolateral in 9%, anteromedial in 43%, strictly anterior in 40%), and more than 25% of the diameter of the artery overlapped the vein in 87% of these levels. However, at the most cranial level analyzed (64 mm above the femorotibial joint space level), such an overlap occurred in only 60%, and the artery was medial in 25%, resulting in a relationship between the artery and the vein that involved less risk of fistula. On radiographic study, the popliteal crease was located above the level of the joint space (considered the most reliable landmark of the popliteal fossa anatomy) in 97% of cases, although the values were scattered (mean, 2.9 ± 1.5 cm).

In order to minimize the risk of creating an arteriovenous fistula, we recommend a skin incision be located 3–4 cm above the joint level as determined by fluoroscopy, and a puncture directed obliquely from caudal to cranial and from medial to lateral.

AJR 157:1259–1262, December 1991

Catheterization of the popliteal artery has been recently described as a useful procedure for endovascular interventions [1, 2]. Knowledge of the anatomic relationship between the popliteal artery and the popliteal vein is important so that the arterial puncture can be performed in the way least likely to result in arteriovenous fistula.

Most anatomy textbooks describe the popliteal artery as being medial and anterior to the popliteal vein [3, 4]. This relationship predisposes to puncture of both the artery and vein when posterior needle punctures of the artery are made. To determine the best technique for puncture of the popliteal artery, we studied the anatomic relationship between the artery and vein in six cadavers and on CT scans of 31 patients. Plain radiographs of the knee were also evaluated to calculate the distance of the femorotibial joint space to the popliteal skin crease, in order to determine the best site for skin incision.

Materials and Methods

To establish the anatomic relationships between the popliteal artery and vein, we dissected the popliteal spaces in six cadavers (12 specimens) and determined the anatomic relationship between the two vessels.

To study this relationship further, contrast-enhanced CT scans of the knee in 40 consecutive patients were reviewed. In 36 patients, both knees were imaged simultaneously, and in four patients, only the left knee was imaged; contiguous 4-mm axial images were obtained. The CT scans were excluded from the study if visualization of the popliteal vessels was poor

Received April 22, 1991; accepted after revision July 10, 1991.

¹ All authors: Department of Radiology, Université Catholique de Louvain, Cliniques Universitaires de Mont-Godinne, B-5530 Yvoir, Belgium. Address reprint requests to J.-P. Trigaux.

0361-803X/91/1576-1259
© American Roentgen Ray Society

because of the patient's body habitus ($n = 2$), if opacification of the vessels was inadequate ($n = 3$), or if an abnormality distorted the normal anatomy (cyst, $n = 3$; entrapment syndrome, $n = 1$; aneurysm, $n = 5$).

The CT studies finally included scans of 58 knees (31 left and 27 right) in 31 patients. The age range of the patients was 16–76 years (mean, 40 years). There were 21 men and 10 women. In all patients, the artery and the vein were easily differentiated on CT on the basis of the earlier opacification of the artery, the larger diameter of the vein, and occasionally the presence of calcifications along the arterial wall. The relationship of the vessels was evaluated on the CT scans at five levels: level 1 ($n = 58$) was at the femorotibial joint space; levels 2 ($n = 58$), 3 ($n = 58$), 4 ($n = 58$), and 5 ($n = 48$) were located 16, 32, 48, and 64 mm more cranially, respectively. The plane running through the posterior border of the two femoral condyles never diverged by more than 7° from the horizontal plane, thus minimizing the possible bias in the results due to leg rotation in relation to the sagittal plane. The location of the popliteal bifurcation into the tibial and/or peroneal arteries was noted and was considered high if the bifurcation occurred at or above the level of the femorotibial joint space.

Another part of the study involved 30 consecutive patients who had unilateral plain radiography of the knee. In these patients, the popliteal skin crease was marked with a metal clip before radiography. The anteroposterior radiographs were analyzed to determine the distance between the joint space and the metal clip. No corrections were made for parallax or magnification.

Frequencies of events were compared by using chi-square or binomial tests when appropriate.

Results

In eight of the 12 cadaveric knee specimens dissected, the popliteal artery was deep and anterior to the vein and crossed over it from medial to lateral and from cranial to caudal (Fig. 1). In two specimens, the artery was continuously anterior

and superimposed on the vein in the sagittal plane. In the other two specimens, the artery was continuously medial to the vein, without crossing over it. In all 12 cases, the artery and vein were intimately enclosed in a common sheath.

The data derived from the analysis of the CT scans are presented in Tables 1 and 2. The center of the artery was anterior (i.e., anterolateral, anterior, or anteromedial) to the vein in 95–100% of knees at levels 2–4; in contrast, at level 5, the artery was anterior to the vein in only 75%, and strictly medial in 25% ($p < .002$ between the configurations at levels 2–4 and level 5) (Fig. 2). In no case was the artery posterior to the vein at any level. When all levels were considered, the most common relationship (43%) was the artery anteromedial to the vein; in 9% only, the artery was anterolateral to the vein ($p < .001$). In addition, more than 25% of the diameter of the artery overlapped the vein in the anteroposterior plane in 92–98% of the vessel pairs analyzed at levels 2–4 but in only 60% of the vessel pairs at level 5 (Fig. 2, Table 2) ($p < .001$). A high bifurcation of the popliteal artery at the level of the joint (level 1) was observed in two (3%) of the 58 knees. Four duplications of the popliteal vein (7%) were suspected. No difference was noted between the older (>40 years) and the younger (≤ 40 years) age groups or between the left and right sides.

On plain radiographs, the popliteal skin crease was almost always (97%) cranial to the joint. Distance ranged from 1.8 cm below to 5.2 cm above the joint (mean, $2.9 \text{ cm} \pm 1.5 \text{ [SD]}$ above the joint).

Discussion

Our study revealed that the center of the popliteal artery is anterior to the popliteal vein 92% of the time (Table 1) and that more than 25% of the diameter of the artery overlaps the

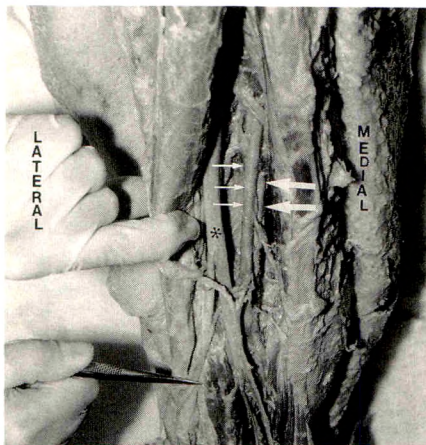
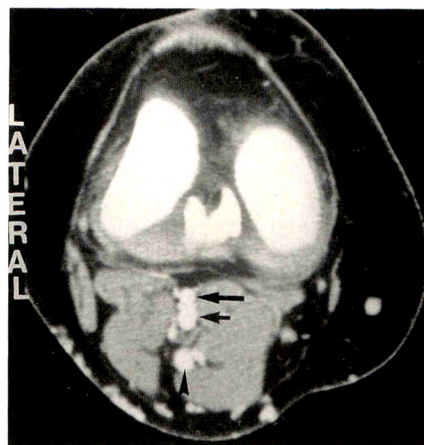
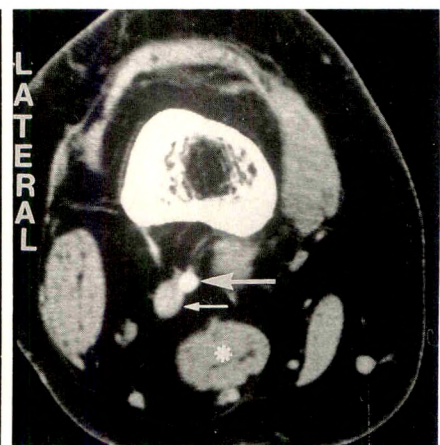


Fig. 1.—Photograph of popliteal fossa in a cadaver. In cranial part of fossa, artery (large arrows) is deep and anteromedial to vein (small arrows) and then crosses over vein from cranial to caudal; at level of femorotibial joint space, determined by forceps, artery is strictly anterior to vein. Tibial nerve (asterisk).



A



B

Fig. 2.—Contrast-enhanced CT scans of knee in a 37-year-old woman.

A, CT scan at level of femorotibial joint (level 1). Artery (large arrow) lies anterior to vein (small arrow), with an overlap of 75–100%. Short saphenous vein (arrowhead).

B, CT scan 64 mm above level of femorotibial joint (level 5). Artery (large arrow) is anteromedial to vein (small arrow), with an overlap of 0–25%. Note how diameter of vein is larger than diameter of artery. Semitendinous muscle (asterisk). Distance from artery to skin is 4.5 cm at level 1 and 5.0 cm at level 5.

TABLE 1: Anteroposterior and Mediolateral Relationships of Popliteal Artery to Popliteal Vein

Artery Location Relative to Vein	No. of Vessel Pairs at Each Anatomic Level					
	Level 1	Level 2	Level 3	Level 4	Level 5	All Levels
Lateral	3 (5)	0	0	0	0	3 (1)
Anterolateral	21 (36)	3 (5)	1 (2)	0	0	25 (9)
Anterior	26 (45)	45 (78)	29 (50)	8 (14)	3 (6)	111 (40)
Anteromedial	4 (7)	10 (17)	27 (46)	47 (81)	33 (69)	121 (43)
Medial	4 (7)	0	1 (2)	3 (5)	12 (25)	20 (7)
Total	58 (100)	58 (100)	58 (100)	58 (100)	48 (100)	280 (100)

Note.—Level 1 is level of femorotibial joint space; levels 2–5 are located 16, 32, 48, and 64 mm more cranially, respectively. Numbers in parentheses are percentages.

TABLE 2: Percentage of Popliteal Artery Overlapping Popliteal Vein in Anteroposterior Plane

Percent Overlap	No. of Vessel Pairs at Each Anatomic Level					
	Level 1	Level 2	Level 3	Level 4	Level 5	All Levels
0	4 (7)	1 (2)	2 (3)	2 (3)	10 (21)	19 (7)
1–25	4 (7)	0	0	3 (5)	9 (19)	16 (6)
26–50	2 (3)	1 (2)	1 (2)	2 (3)	3 (6)	9 (3)
51–75	6 (10)	3 (5)	6 (10)	16 (28)	16 (33)	47 (17)
76–100	42 (73)	53 (91)	49 (85)	35 (61)	10 (21)	189 (67)
Total	58 (100)	58 (100)	58 (100)	58 (100)	48 (100)	280 (100)

Note.—Percent overlap = the percentage of the diameter of the popliteal artery that overlapped the popliteal vein in the anteroposterior plane (measured from CT images, i.e., from axial planes). Level 1 is level of joint space; levels 2–5 are located 16, 32, 48, and 64 mm more cranially, respectively. Numbers in parentheses are percentages.

vein in 87% of the vessel pairs (Table 2). Thus, during the percutaneous puncture of the artery via a posterior approach, the needle is likely to pass through the superficially and posteriorly located vein; the overlapping of the artery and vein increases this risk [5]. Subsequent placement of a sheath or a percutaneous transluminal angioplasty catheter could lead to formation of an arteriovenous fistula. Catheterization via the popliteal artery has been described only recently, in 1988 [1]; thus, the real prevalence of arteriovenous fistulas with percutaneous punctures of the popliteal artery has not been documented yet in a large series. However, it appears from our anatomic study that the risk of an arteriovenous fistula should be kept in mind when the procedure is performed. In the groin, the femoral artery lies anterior and superficial to the vein, making creation of a fistula less likely than at the knee level when attempts are made to puncture the artery. On the contrary, the risk of an arteriovenous fistula at the femoral level exists theoretically when attempts are made to puncture the vein [5]; this complication is becoming more common because of the increase in interventional techniques, anticoagulation and thrombolysis, and the use of larger catheters during introduction of vena caval filters [6, 7] or cardiac catheterization [8].

On the basis of our results, the safest technique for percutaneous puncture of the popliteal artery is as follows. The entry site in the artery should be located at the level 5 described in our study, that is, 6–7 cm above the level of the femorotibial joint space. This is important because of the possible existence of a high bifurcation of the artery in 4.7% of cases [9]. We observed two cases of high division of the

artery in our series of 58 knees. Also, when the intent is to avoid creating an arteriovenous fistula, the relationship between the artery and the vein at level 5 means that a puncture here is safer than at levels 2–4; at level 5, the artery is strictly medial and not anterior to the vein in 25% of cases (0–5% at levels 2–4; $p < .002$) and less than 26% of the diameter of the artery overlaps the vein in the anteroposterior plane in 40% of the vessel pairs (2–8% at levels 2–4; $p < .001$). The level of the femorotibial joint space is a convenient landmark of the anatomy of the popliteal fossa. Because the popliteal skin crease is not a reliable indicator of the position of the joint, the level of the joint should be determined fluoroscopically. Depending on the amount of subcutaneous fat, a skin incision should be made about 3–4 cm above the level of the joint. When the needle is directed obliquely from caudal to cranial, the artery is then punctured 6–7 cm above the level of the joint, that is, approximately at level 5. The needle also should be directed upward in order to avoid the crossing of the semitendinous muscle, which is in front of the artery at level 5 (Fig. 2). It should be noted that the popliteal artery is located only minimally more deeply at level 5 than at level 1 (Fig. 2).

Our results show that the popliteal artery is anteromedial to the vein in 43% of the cases and is anterolateral in only 9% ($p < .001$). Consequently, the needle should be angled from medial to lateral (Dake MD et al., presented at the annual meeting of the Radiological Society of North America [RSNA] November 1990), and the skin incision should be made 1–2 cm medial to the midline in order to minimize the risk of a transvenous arterial puncture (Fig. 3).

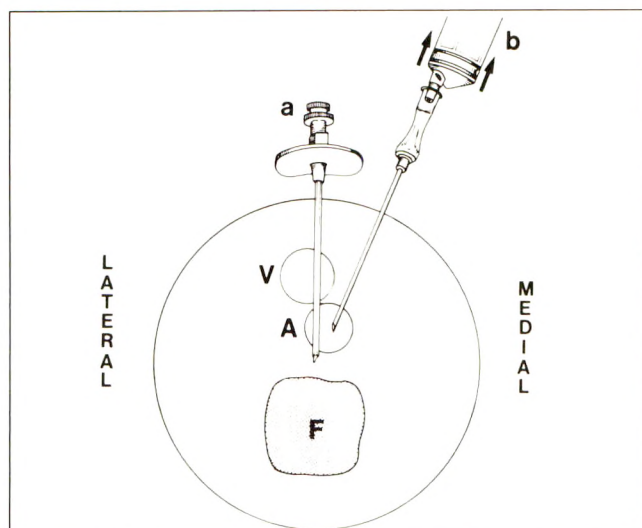


Fig. 3.—Diagram shows passage of needle (Seldinger type) (a) through vein (V) and artery (A) during a double-wall puncture. Needle (b) can be positioned to avoid vein by using a single-wall puncture oriented from medial to lateral. F = femur.

In addition, because of the close and variable relationships between the popliteal vessels, sonographic mapping before the procedure might be useful (Hunter V et al., RSNA, November 1990). Indeed, sonography is the imaging method of choice for the popliteal fossa, and sonographically guided puncture of the popliteal artery permits tailoring the puncture to the specific anatomy of the individual patient.

ACKNOWLEDGMENTS

We thank C. Gillet and J. Dulieu for valuable anatomic advice and J. Jamart for statistical assistance.

REFERENCES

1. Tonnesen KH, Sager P, Karle A, Henriksen L, Jorgensen B. Percutaneous transluminal angioplasty of the superficial femoral artery by retrograde catheterization via the popliteal artery. *Cardiovasc Intervent Radiol* 1988;11:127-131
2. Schroeder J. Catheter lysis and percutaneous transluminal angioplasty below the knee via the popliteal artery in a patient with femoral artery obstruction: technical note. *Cardiovasc Intervent Radiol* 1989;12:344-345
3. Patuere G. *Traité d'anatomie humaine*, tome II: membres supérieur et inférieur. Paris: Masson, 1951:933-989
4. Warwick R, Williams PL. *Gray's anatomy*, 35th ed. Edinburgh: Longman, 1973:588-744
5. Baum PA, Matsumoto AH, Teitelbaum GP, Zuurbier RA, Barth KH. Anatomic relationship between the common femoral artery and vein: CT evaluation and clinical significance. *Radiology* 1989;173:775-777
6. Rose BS, Simon DC, Hess ML, Vanaman ME. Percutaneous transfemoral placement of the Kimray-Greenfield vena cava filter. *Radiology* 1987;165:373-376
7. Grassi CJ, Bettmann MP, Rogoff P, Reagan K, Harrington DP. Femoral arteriovenous fistula after placement of a Kimray-Greenfield filter. *AJR* 1988;151:681-682
8. Altin RS, Flicker S, Naidech HJ. Pseudoaneurysm and arteriovenous fistula after femoral artery catheterization: association with low femoral punctures. *AJR* 1989;152:629-631
9. Ducksoo K, Orron DE, Skillman JJ. Surgical significance of popliteal arterial variants: a unified angiographic classification. *Ann Surg* 1989;210:776-781

Percutaneous Dilatation of Benign Biliary Strictures: Single-Session Therapy with General Anesthesia

Michael J. Lee¹
Peter R. Mueller
Sanjay Saini
Peter F. Hahn
Steven L. Dawson

Percutaneous biliary stricture dilatation (PBSD) is an uncomfortable procedure for patients that presently requires multiple dilatation sessions spread over many days. We evaluated the use of general anesthesia to enable PBSD to be performed in a single sitting in 14 patients with benign biliary strictures (11 anastomotic and three iatrogenic strictures). Four patients had multiple strictures, and the other 10 had a single stricture. Strictures were documented by transhepatic cholangiography (11 patients) or T-tube cholangiography (three); quantitative biliary perfusion studies were additionally performed in seven cases. Dilatation was performed transhepatically in 11 patients and via a T-tube track in three. Balloons ranged from 8 to 12 mm in diameter and were manually inflated for 3 min with an average of five inflations per stricture. Stenting catheters were left across the strictured areas in all patients for 6–21 days (mean, 10 days) before removal. The mean duration of hospital stay for all patients was 5.7 days, which could further be divided into means of 3.6 days (range, 1–6 days) for 11 patients without complications and 13.7 days (range, 13–14 days) for three patients who had complications. Complications included cholangitis; liver hematoma (which resolved with conservative therapy in both cases); and pseudoaneurysm of the hepatic artery, which necessitated angiographic embolization. PBSD achieved long-term patency in 13 (93%) of 14 patients with a follow-up period of 2.0 to 5.5 years (mean, 3.2 years). A stricture recurred in one patient 1.5 years after dilatation.

We conclude that PBSD with the patient under general anesthesia can be performed in a single visit to the radiology department with excellent long-term patency rates, a shorter hospital stay, and a pain-free procedure for the patient.

AJR 157:1263–1266, December 1991

Many previous reports have emphasized the importance of percutaneous biliary dilatation as an effective alternative to surgical management of benign biliary strictures [1–7]. Complications of this procedure are usually minimal, and the main complications of sepsis and bleeding are easily controlled. However, pain during the procedure, especially at the time of balloon inflation, can be severe and has remained problematic. Because of associated pain, biliary dilatation is often performed in several sessions, usually spread over 10 to 14 days. This necessarily increases the duration of hospital stay and absence from employment for most patients. Various solutions to the problem of pain during dilatation have been proposed and include (1) wide local infiltration with lidocaine or bupivacaine coupled with the liberal use of IV narcotics and sedatives, (2) direct installation of lidocaine or bupivacaine into the biliary tree [1, 8], or (3) administration of general anesthesia, if required.

We used to perform biliary dilatation in at least three sessions during a 5- to 8-day period and employed a combination of local anesthesia and IV sedatives and narcotics [3]. However, in the past 5 years we have used general anesthesia for control of pain. An added benefit of this approach is the freedom to perform the entire procedure from percutaneous transhepatic biliary drainage to biliary dilatation

Received May 30, 1991; accepted after revision July 26, 1991.

¹ All authors: Department of Radiology, Massachusetts General Hospital and Harvard Medical School, 32 Fruit St., Boston, MA 02114. Address reprint requests to P. R. Mueller.

0361-803X/91/1576-1263
© American Roentgen Ray Society

in one session. We report here our results and the complications we encountered in using this approach in 14 patients.

Materials and Methods

We retrospectively reviewed the records of all patients referred for percutaneous dilatation of benign biliary strictures in the last 5 years. Fourteen patients (eight male, six female; age range, 12–77 years; mean age, 44 years) had percutaneous biliary stricture dilatation (PBSD) under general anesthesia. The cause of the biliary strictures was previous surgery for benign disease with anastomotic strictures (choledochojejunostomy, hepaticojejunostomy) in 11 patients, and iatrogenic surgical trauma during cholecystectomy in three patients. Four patients had two strictures each while the rest had one stricture each. Twelve strictures were located in the common bile duct, and six were in the intrahepatic right or left main ducts. No patients with sclerosing cholangitis were treated during this period.

Eleven patients had recurrent episodes of cholangitis with or without jaundice, and three patients had a stricture seen at T-tube cholangiography. Alkaline phosphatase and bilirubin levels were measured in all patients before dilatation, and the levels were found to be elevated in eight. Alkaline phosphatase and bilirubin levels were elevated in the remaining six patients during episodes of cholangitis, but had returned to normal before PBSD. Sonography or CT was performed in all patients before dilatation and revealed mildly dilated biliary ducts in seven patients and normal nondilated ducts in the remaining seven. The presence of a stricture was documented in all patients by either transhepatic cholangiography (11 patients) or T-tube cholangiography (three patients). Provocative perfusion studies were used to make quantitative manometric determinations of functional biliary obstruction before dilatation in the first seven patients. Biliary pressures were measured and perfusion tests performed as described by previous investigators [9]. Quantitative pressure studies were not done in the remaining seven patients, because clinical and radiologic data convincingly proved the presence of significant biliary strictures.

In all cases, biliary dilatation was performed with the patient under general anesthesia. The transhepatic approach was used in 11 patients and a T-tube track was used in three patients. All strictures were between 1 and 5 mm in diameter and less than 2 cm in length. The entire procedure, from gaining access to the biliary tree (transhepatically or via a T-tube track) to stricture dilatation, was done in all cases with the patient under general anesthesia (Fig. 1). Biliary strictures were dilated by using techniques previously described [3]. Balloons varied between 8 and 12 mm in diameter and were reinforced to allow high inflation pressures. All balloons were manually inflated for 3 min during each inflation, with an average of five inflations per stricture (range, three to seven). Ten- to 12-French stenting catheters were left across the strictured areas in all patients after dilatation.

The end point for successful dilatation was established qualitatively in all patients by the disappearance of a balloon waist during inflation so that the strictured duct returned to the size of the adjacent normal duct. Quantitatively, the end point of dilatation was established in seven patients by recording biliary pressures after the procedure.

Long-term patency was determined by clinical follow-up and results of liver function tests in all patients for a mean of 3.2 ± 1.1 years (range, 2.0–5.5 years). Repeated physical examination and liver function tests were done, and episodes of cholangitis, jaundice, or sepsis were documented. Additionally, in two patients transhepatic cholangiography was repeated to assess patency.

Results

PBSD from initial transhepatic cholangiography to stricture dilatation with the patient under general anesthesia took an average of 1.7 hr. The length of hospital stay was short, with a mean of 5.7 ± 4.5 days for all patients. Eleven patients who did not experience any complications had a shorter hospital stay (mean, 3.6 days; range, 1–6 days) than did three patients who had complications (mean, 13.7 days; range, 13–14 days).

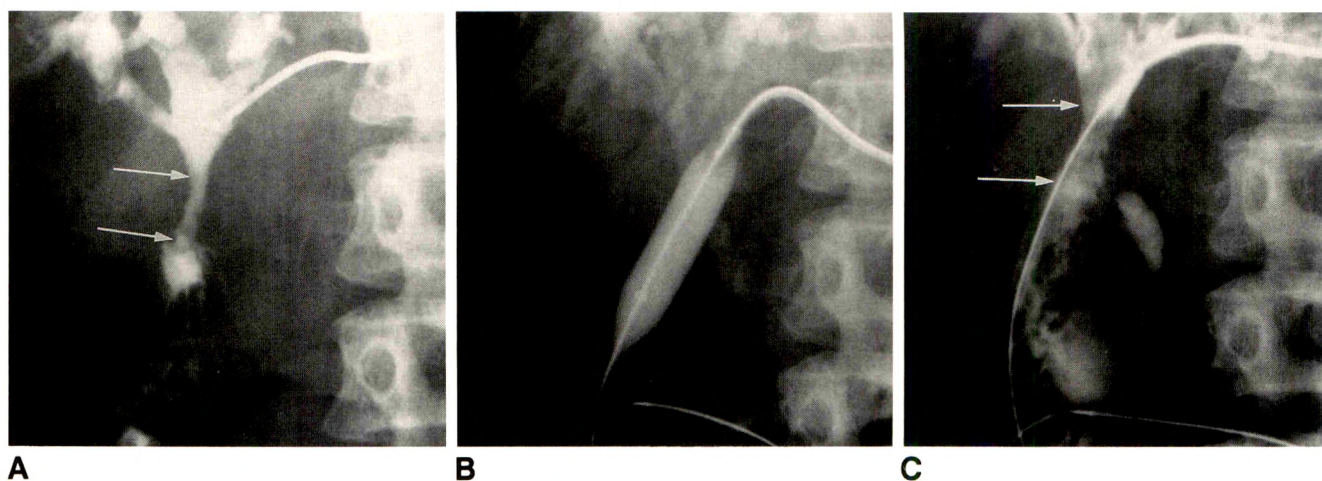


Fig. 1.—Cholangiograms of left-sided percutaneous biliary stricture dilatation (PBSD) in a 50-year-old man who had elevated alkaline phosphatase level and episodes of recurrent cholangitis. Patient had a choledochoduodenostomy 10 years earlier for benign disease. General anesthesia permitted whole procedure, from transhepatic cholangiography to PBSD, to be performed in a single 2-hr period.

A, Left-sided catheter injection shows dilated intrahepatic ducts and a slightly narrowed common bile duct over a length of 2 cm (arrows) at level of anastomosis. This patient was one of seven patients who had abnormal findings on a biliary perfusion test.

B, Dilatation with a 12-mm balloon shows no waist at level of stricture after third 3-min balloon inflation. Patient was discharged 2 days after dilatation with a 10-French catheter stenting stricture.

C, 2 weeks later, patient returned as an outpatient for catheter removal. Catheter injection shows a widely patent anastomosis (arrows). Catheter was removed, and patient remains asymptomatic 3 years later.

Complications included cholangitis in one patient, liver hematoma due to manipulation of the transhepatic track in another, and the development of a hepatic pseudoaneurysm in a third patient. Both the liver hematoma and the cholangitis resolved with conservative therapy and antibiotics, respectively. The hepatic pseudoaneurysm was treated with transcatheter embolization because of continued bleeding.

To date, 13 of 14 patients remain free of symptoms with normal results in liver function tests. In two of these 13 patients, liver function test results showed transient elevations 2 and 3 years after PBSD. However, findings on repeated transhepatic cholangiography and quantitative perfusion studies were normal. A stricture recurred in one patient, who initially had an iatrogenic stricture, 1.5 years after dilatation. The latter patient underwent further PBSD under general anesthesia and is now free of symptoms (12 months after dilatation).

Internal-external stenting catheters remained in situ for an average of 10 days after dilatation (range, 6–21 days). Most patients returned as outpatients for cholangiography through the indwelling catheter, followed by catheter removal. No residual stricture was seen in any patient at this time, as compared with radiographs taken before dilatation. In patients who had longer hospital stays, the stenting catheters were removed before discharge, again after findings on cholangiography were normal. Quantitative manometric pressure studies were performed in seven patients before and after dilatation. Resting biliary pressure recordings before dilatation were abnormal in seven patients (mean, 26 cm saline; normal, <20 cm) and returned to normal levels (mean, 12 cm saline), at perfusion rates of 5–7 ml/min for 5 min, after dilatation.

Discussion

Benign bile duct strictures can be difficult to treat, and it remains controversial whether percutaneous dilatation or surgical repair is the best treatment [10–13]. Pitt et al. [14], in a recent retrospective review of 25 patients treated with surgical repair compared with 20 patients treated by PBSD, claimed an 88% long-term success rate for surgery vs a 55% success rate for PBSD. Many other reports indicate that the long-term success rates for PBSD (80–90%) are equivalent to those for surgery [1–7]. This debate over surgical vs nonsurgical treatment of benign biliary strictures is unlikely to be resolved until a properly designed prospective, randomized study is performed.

Few previous reports on PBSD have emphasized that multiple sessions of balloon dilatation leading to a prolonged hospital stay are required to complete therapy and that the discomfort experienced by the patient during the procedure can be problematic. Indeed, a recent series [14], comparing PBSD with surgical repair, indicated that the total hospital stay (21.4 ± 1.7 days), when all visits for further dilatation were added, was not significantly different from the hospital stay associated with surgical repair (26.4 ± 2.5 days). In this series, we have used general anesthesia to overcome the problems of patients' discomfort, multiple treatment sessions, and long hospital stay.

The advantages of using general anesthesia for PBSD are threefold. First, the procedure is made pain-free and PBSD is performed in one session. In our experience, patients tolerate this much better than they do multiple painful sessions. In addition, single-session therapy reduces labor intensity for the interventional radiologist compared with multiple-session therapy. Second, because the patients' bile ducts are often not dilated or are minimally dilated (seven patients in the present series), resulting in difficult and time-consuming biliary manipulations [3], general anesthesia makes this part of the procedure more comfortable for the patient and subsequently makes the multiple manipulations and guidewire exchanges easier for the radiologist. Third, the length of hospital stay is considerably shortened (mean, 5.7 days), because the patient does not have to return to the radiology department for multiple treatment sessions. Indeed, our practice now is to admit patients to the hospital either the evening before or on the morning of the procedure and discharge them 1 or 2 days after the procedure, if there are no complications. The mean hospital stay in this study (5.7 ± 4.5 days) compares favorably with a mean hospital stay of 17 days reported in a recent series of 17 patients treated with PBSD [15]. Although no complications related to general anesthesia occurred in this series, general anesthesia is not without inherent risks, and a larger study would be required to evaluate possible complications related to general anesthesia.

Our results emphasize that it is possible to perform PBSD in a single session without sacrificing long-term patency. This is in large part due to the advantage, conferred by general anesthesia, of performing as many balloon inflations as necessary to dilate the stricture fully. In essence, the multiple treatments formerly used are condensed into a single session. In addition, more than one stricture can be dilated in a single session. Four patients in this series had two strictures that were accessed and dilated by using the same transhepatic or T-tube track in one session. Our long-term patency rate of 93% is comparable to that for PBSD reported in other series [1–7]. Two patients had transhepatic cholangiography for transient elevations shown in liver function test results 2 and 3 years after PBSD, respectively. No evidence of recurrent stricture was present in these patients either by morphologic appearance or by quantitative perfusion studies. One patient whose stricture did recur was free of symptoms for 1.5 years after dilatation. Because we arbitrarily define our long-term success rate as a symptom-free interval of 2 years, we deemed PBSD to have failed in this patient. However, a 1.5-year symptom-free interval might be considered a success in other series. Importantly, no early recurrences (<1 year) occurred with this approach.

The role of stenting after biliary dilatation remains controversial. Some authors [1, 2, 6, 7] advocate long-term stenting to enhance long-term patency rates. The rationale behind this approach is that if fibrosis occurs, the residual lumen will be no smaller than the size of the stent placed, which varied from 8.3- to 20-French. We have never adopted this approach at our institution and prefer to use short-term stenting because, theoretically, fibrotic reactions may be induced by long-term drainage catheters. Our results without stenting are

comparable to those from series in which long-term stenting has been used [1, 2, 6, 7].

The assessment of immediate technical success and the associated number of balloon inflations required to achieve successful dilatation varies from center to center. Our initial practice was to monitor the adequacy of inflations by performing quantitative pressure studies in order to measure the pressure gradients across the stricture. This technique was used to assess immediate success in our first seven patients in this series and in patients from our previous series [3]. However, we have found that disappearance of the balloon waist during balloon inflation correlates well with the normalizing of pressure gradients across the stricture. Hence, we no longer use quantitative pressure studies to monitor the number of balloon inflations. We do, however, use biliary perfusion tests in patients with questionable strictures before biliary dilatation.

Complications occurred in three (21%) of 14 patients, which is similar to reported complication rates (7–24.3%) [3, 7]. Two complications were self-limited (cholangitis and liver hematoma) and required only conservative management. The patient with cholangitis had episodes of biliary sepsis before biliary tract intervention. The PBSO procedure in the patient in whom the liver hematoma developed was prolonged because of difficulty in performing the initial biliary drainage in the presence of nondilated biliary ducts. Presumably, the hematoma was a result of the increased number of needle punctures required to gain access to the small ductal system. A third complication, formation of a hepatic artery pseudoaneurysm, occurred in a patient with dilated bile ducts, in whom access to the biliary tree was achieved with the first needle pass. This patient required angiographic embolization for continued bleeding from the pseudoaneurysm. These patients had a prolonged hospital stay because of the associated complications. There was no indication that any of these complications were related to the fact that PBSO was performed with the patient under general anesthesia.

Benign biliary strictures are likely to be seen more frequently with the advent of liver transplantation, extensive hepatic

trisegmentectomies, and the learning curve associated with laparoscopic cholecystectomy. PBSO will play an increasingly important role in the treatment of such patients. One-session biliary dilatation with the patient under general anesthesia will make PBSO more tolerable for patients, will shorten their hospital stay, and will reduce the intensity of labor for the radiologist by decreasing the number of treatment sessions.

REFERENCES

1. Gallagher DJ, Kadir S, Kaufman SL, et al. Nonoperative management of benign postoperative biliary strictures. *Radiology* **1985**;156:625–629
2. Moore AV, Illescas FF, Mills SR, et al. Percutaneous dilatation of benign biliary strictures. *Radiology* **1987**;163:625–628
3. Mueller PR, vanSonnenberg E, Ferrucci JT, et al. Biliary stricture dilatation: multicenter review of clinical management in 73 patients. *Radiology* **1986**;160:17–22
4. Morrison MC, Lee MJ, Saini S, Brink JA, Mueller PR. Percutaneous balloon dilatation of benign biliary strictures. *Radiol Clin North Am* **1990**;28:1191–1201
5. Russell E, Yrizarry JM, Huber JS, et al. Percutaneous transjejunal biliary dilatation: alternate management for benign strictures. *Radiology* **1986**;159:209–214
6. Salmonowitz E, Castañeda-Zúñiga WR, Lund G, et al. Balloon dilatation of benign biliary strictures. *Radiology* **1984**;151:613–616
7. Williams HJ, Bender CE, May GR. Benign postoperative biliary strictures: dilatation with fluoroscopic guidance. *Radiology* **1987**;163:629–634
8. Trambert JJ, Bron KM, Zajko AB, et al. Percutaneous transhepatic balloon dilatation of benign biliary strictures. *AJR* **1987**;149:945–948
9. vanSonnenberg E, Ferrucci JT, Neff CC, et al. Biliary pressure: manometric and perfusion studies at transhepatic cholangiography and percutaneous biliary drainage. *Radiology* **1983**;148:41–50
10. Pitt HA, Miyamoto T, Parapatis SK, et al. Factors influencing outcome in patients with postoperative biliary strictures. *Am J Surg* **1982**;144:14–21
11. Genest JF, Nanos E, Grundfest-Broniatowski S, et al. Benign biliary strictures: an analytic review (1970 to 1984). *Surgery* **1986**;99:409–413
12. Braasch JW, Bolton JW, Rossi RL. A technique of biliary tract reconstruction with complete follow-up in 44 consecutive cases. *Ann Surg* **1981**;194:635–638
13. Pelligrini CA, Thomas MJ, Way LW. Recurrent biliary stricture: patterns of recurrence and outcome of surgical therapy. *Am J Surg* **1984**;147:175–180
14. Pitt HA, Kaufman SL, Coleman J, White RI, Cameron JL. Benign postoperative biliary strictures: operate or dilate? *Ann Surg* **1989**;210:417–427
15. Citron SJ, Martin LG. Benign biliary strictures: treatment with percutaneous cholangioplasty. *Radiology* **1991**;178:339–341

Vascularity of Tumors in Children: Evaluation with Color Doppler Imaging

George A. Taylor^{1,2}
Elizabeth J. Perlman³
L. R. Scherer^{2,4}
John P. Gearhart^{2,5}
Brigid G. Leventhal⁶
Joseph Wiley⁶

Twenty-one tumors in 20 children were evaluated with duplex and color Doppler imaging to determine the value of the technique in assessing the origin and pattern of vascular supply and the degree of neovascularity. The origin of the vascular supply was detected correctly in 12 of 13 tumors that were subsequently resected. In five children, this aided in determining the organ from which the tumor originated, and in one child, it established the presence of a tumor by showing blood flow in the center of a suspected abscess. In 18 tumors, color Doppler imaging showed the pattern of the vascular supply. Eleven had a peripheral pattern, and seven had a central, branching pattern. Although individual tumor types appeared to have characteristic patterns of vascular supply, these were not specific enough to aid in making a specific diagnosis. When the degree of intratumor neovascularity was graded on the basis of the findings on color Doppler imaging, it agreed with the results of histologic evaluation in 16 of 19 tumors. In one tumor, neovascularity was overestimated, and in two, it was markedly underestimated.

Our experience suggests that color Doppler imaging is useful in detecting the origin and pattern of vascular supply and the degree of intratumoral blood flow in a variety of solid tumors in children.

AJR 157:1267-1271, December 1991

The development of a noninvasive, accurate method for assessing tumor vascularity may be useful in the initial differential diagnosis of tumors and in monitoring their response to therapy. Although recent studies have shown that color Doppler imaging can be used to detect tumor vascularization in a variety of human and experimental tumors [1-4], the usefulness of this technique for examining tumors in infants and children has not been evaluated. Accordingly, we studied the efficacy of duplex and color Doppler sonography in assessing the origin and pattern of vascular supply and the degree of intratumor neovascularity in a variety of tumors in children.

Subjects and Methods

Subjects

Infants, children, and adolescents up to 19 years old in whom physical examination revealed extraosseous extracranial solid tumors at least 1 cm in diameter were included in this study. Twenty children with 21 tumors were studied. Their age range was 1 week to 17 years (mean, 41 months). Diagnoses included neuroblastoma (five); rhabdomyosarcoma (three); Wilms tumor (two); germ cell tumor (two); hepatoblastoma (two); and one each of lymphoma, rhabdoid tumor of the liver (a poorly differentiated sarcoma with some histologic features of rhabdomyosarcoma), lipoblastomatosis, congenital myofibromatosis (chest wall), ganglioneuroma, ovarian sarcoma, and teratoma. The range of tumor volume (obtained on the basis of CT and sonographic measurements) was 37-1500 cm³ (mean, 412 cm³). The project was approved by the Institutional Review Committee, and informed consent was obtained for each patient.

Received February 21, 1991; accepted after revision July 26, 1991.

¹ Russell H. Morgan Department of Radiology and Radiological Science, The Johns Hopkins Medical Institutions, 600 N. Wolfe St., Baltimore, MD 21205. Address reprint requests to G. A. Taylor.

² Department of Pediatrics, The Johns Hopkins Medical Institutions, Baltimore, MD 21205.

³ Department of Pathology, The Johns Hopkins Medical Institutions, Baltimore, MD 21205.

⁴ Department of Pediatric Surgery, The Johns Hopkins Medical Institutions, Baltimore, MD 21205.

⁵ Division of Pediatric Urology, The Johns Hopkins Medical Institutions, Baltimore, MD 21205.

⁶ Division of Pediatric Oncology and The Oncology Center, The Johns Hopkins Medical Institutions, Baltimore, MD 21205.

0361-803X/91/1576-1267
©American Roentgen Ray Society

Doppler Studies

An Acuson 128 unit (Acuson, Mountain View, CA) was used for all studies. The choice of transducer was dictated by the size and location of the tumor and the size of the patient. Thirteen tumors were evaluated exclusively with a 7.0-MHz linear transducer, seven exclusively with a 3.5-MHz sector transducer, and one with a 5.0-MHz linear transducer. Twelve tumors were evaluated with both linear and sector transducers. Most studies were performed at the patient's bedside and videotaped for subsequent review. All Doppler studies were obtained within 24 hr of surgery.

The image was magnified electronically, and the color Doppler-encoded area restricted to maximize color sensitivity and frame rate. Color persistence was set at its maximum setting, the bandpass filter was set at its lowest setting (100 Hz), and color gain was adjusted dynamically during the examination. The color scale was set at its minimum. The lowest velocities detectable with the 3.5-, 5.0-, and 7.0-MHz transducers were 9, 6, and 3 cm/sec, respectively. Prolonged temporal averaging ("CD" capture mode) was not used because of the color flash artifacts frequently associated with respiratory motion with this technique. Each tumor was imaged in multiple planes and evaluated with color and duplex Doppler sonography with respect to the number and origin of vessels supplying the tumor, the pattern of vascular branching within the tumor, and the presence and degree of intratumoral blood flow. Each vessel supplying the tumor was traced to its origin whenever possible. The number and origin of feeder vessels were confirmed at surgery.

Intratumor vascularity was graded on a four-point scale: None = no intratumoral flow is detectable or vascular rim identified. Low = occasional pixels of color are transiently present within tumor parenchyma. A single feeder vessel at the hilum of the tumor may be present, but no other flow is detectable. Moderate = vascular rim or large feeder vessels are present in the periphery of the mass only; little or no flow is detectable in the central portions of the tumor. High = well-defined vascular rim surrounds the tumor; large feeder vessels are visible; flow is easily detectable throughout the tumor parenchyma.

Patterns of vascular branching within the tumor as seen on color Doppler imaging were characterized as either peripheral (basketlike) or central (branching) on the basis of the color Doppler appearance of tumor blood flow as described by Tanaka et al. [4].

Angle-corrected frequency spectra were obtained from intratumoral and peripheral feeder vessels and evaluated for the presence of disturbed or turbulent flow. Peak systolic and end-diastolic velocities were measured in vessels supplying the tumor and within it, and the degree of vascular impedance was estimated by calculating a resistive index (RI).

Doppler estimates of neovascular flow were correlated with histopathologic grading of tumor neovascularity and cellularity.

Histologic Grading

Biopsy and resection specimens were processed by using standard techniques. Each tumor was evaluated histopathologically for the presence and degree of tumor neovascularity. Tumor neovascularity was defined as the presence of thin-walled, sinusoidal spaces lacking a well-defined muscular wall and often composed of only endothelium and surrounding adventitia. Neovascularity was graded as follows: none = abnormal vessels not detected; minimal = abnormal vessels present only focally; moderate = abnormal vessels easily identified only in the tumor periphery, but not throughout the tumor; and marked = many dilated abnormal vessels present throughout the tumor parenchyma, appearing as a characteristic part of the tumor.

Results

Tumor Vascular Supply

Thirteen tumors in 12 children were completely resected. The origin and location of these vessels were determined correctly in 12 tumors. A single arterial feeder supplying a large, hypovascular fibrous tumor (congenital myofibromatosis) of the chest wall was missed with color Doppler imaging. In a second tumor (adrenal neuroblastoma), a moderate amount of venous bleeding was encountered in the peritumoral bed. However, no identifiable vessels were present surrounding the tumor.

In five children with large abdominal tumors, localization of the vascular supply aided in determining the organ from which the tumor originated. These included three ovarian tumors (Fig. 1) and two intrahepatic tumors (Fig. 2). In one child who had a poorly defined mass in the thigh after an intramuscular immunization, color Doppler imaging established the presence of a neoplasm (lipoblastomatosis) by showing an abnormal vessel supplying the center of the tumor (Fig. 3).

Pattern of Vascular Supply

The pattern of tumor vascularization could be visualized with color Doppler imaging in 18 tumors. Eleven tumors having a peripheral basket pattern included neuroblastoma, hepatoblastoma, Wilms tumor, germ cell tumor, rhabdoid tumor of the liver, and primitive sarcoma of the ovary (Fig. 4). Seven tumors having a central, branching pattern included rhabdomyosarcoma, Hodgkin lymphoma, ovarian teratoma, ganglioneuroma, and lipoblastomatosis (Fig. 3). Although different tumor types appeared to have characteristic patterns of vascularization, these were not specific enough to aid in the histologic diagnosis.

Intratumor Neovascularity

The degree of intratumoral blood flow was assessed in 19 of 21 tumors. One child with a large abdominal neuroblastoma had only biopsy confirmation of a distant lymph node metastasis before chemotherapy, and another had biopsy confirmation of a maturing ganglioneuroma several months before this study began. Color Doppler and histologic grading of neovascularity were in agreement in 16 of 19 tumors examined (Figs. 1, 2, 4, and 5). Marked discrepancy in grading was found in two tumors. Both had little or no flow detected by color Doppler imaging and moderate to high grades of neovascularity on microscopic examination. Both tumors were markedly echogenic because of extensive microscopic calcification or dense stromal tissue. A minor discrepancy was found in one tumor in which color Doppler imaging showed a pattern of low vascularity and microscopic examination showed no evidence of abnormal tumor vessels.

Pulse-Wave Doppler Findings

Doppler waveforms of intratumoral and feeder vessels were obtained in 17 of 21 tumors. Disorganized or turbulent flow

Fig. 1.—21-month-old girl with precocious puberty and granulosa-theca cell tumor of left ovary.

A, Transverse color Doppler sonogram through pelvis shows 8-cm adnexal mass on left side with many large vessels present throughout tumor.

B, More medial transverse sonogram through pelvis shows blood supply to tumor (arrow) arising from left adnexa. U = uterus, M = mass.

C, Histologic section shows thin-walled vascular spaces surrounding lobules of granulosa cell tumor. (H and E, original magnification $\times 75$)

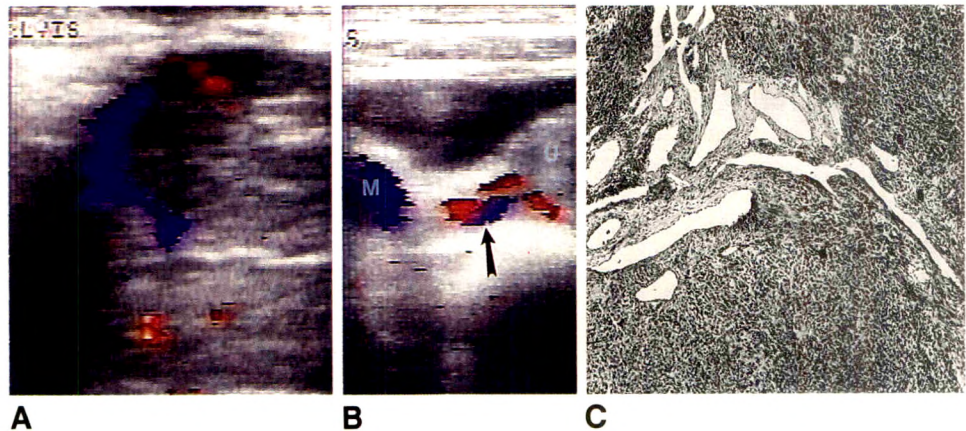
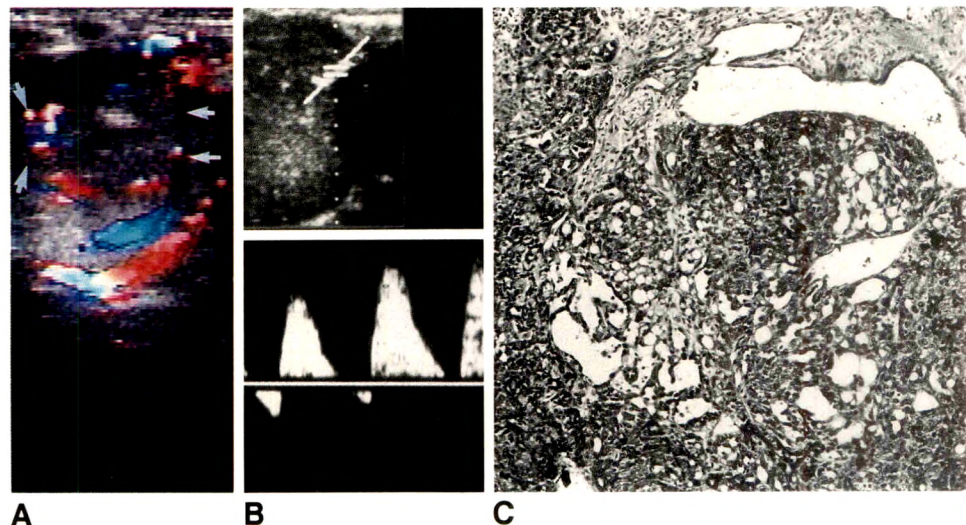


Fig. 2.—Tumor arising from anterior abdominal wall and appearing to originate from anterior surface of liver in 18-month-old girl with germ cell tumor.

A, Transverse color Doppler image shows 5-cm mass in anterior segment of right hepatic lobe. Flow is present in vessels incompletely surrounding mass (arrows) and throughout tumor parenchyma.

B, Duplex Doppler tracing shows high-impedance arterial flow in direction away from anterior abdominal wall. Waveform has been inverted and appears above baseline. Celiac arteriogram showed no tumor vessels arising from hepatic artery.

C, Histologic section shows numerous large and small thin-walled vascular spaces throughout endodermal sinus tumor. (H and E, original magnification $\times 180$)



compatible with arteriovenous shunting near the advancing edge of tumor was seen in only two patients (rhabdomyosarcoma of the bladder and Wilms tumor). Vascular impedance was quite variable even within different areas of the same tumor (Fig. 5). Low-impedance flow ($RI < 50\%$) was seen in only three tumors (granulosa-theca cell tumor of the ovary, hepatoblastoma, and adrenal neuroblastoma). The remaining tumors had RIs between 65% and 110%. Four tumors (metastatic rhabdomyosarcoma [two], lipoblastomatosis, and Hodgkin lymphoma) had extremely high impedance to flow, with RIs of 100–110%. Peak systolic velocities were also quite variable among all tumors, ranging from 9.3 to 50 cm/sec.

Discussion

The origin of the main blood vessel supplying the tumor was determined in most tumors evaluated with color Doppler imaging. Although this information was not considered critical for surgical planning, it helped in narrowing the differential diagnosis by establishing the organ from which the tumor originated in five children and by revealing the presence of a neoplasm in a child in whom a sterile abscess of the thigh

was suspected. Definition of small segmental branches and sectional hepatic anatomy was difficult to accomplish in children with large hepatic tumors because of the distortion of normal anatomic landmarks. We do not think that color Doppler imaging can replace arteriography or MR imaging in the assessment of tumor resectability of large hepatic masses.

Microangiographic studies have shown two basic patterns of tumor vascularization [5]: The first, described as a "peripheral" pattern, is present when the growing tumor continually incorporates within itself the vasculature it induces. The result is a fine network of vessels penetrating the tumor from the periphery. The second is a "central" pattern in which major vascular branches from host vessels supply the tumor via a hilum, resulting in a branching pattern with the largest trunks located in the center of tumor nodules. These patterns of vascular arborization appear to be tumor specific [6]. Tanaka et al. [4] were able to distinguish hepatocellular carcinoma from metastases and hemangiomas on the basis of the pattern of neovascular branching seen on color Doppler imaging. Although we were able to distinguish central and peripheral patterns of vascular branching with color Doppler imaging, and the pattern of vascularization remained similar within a given tumor type, a significant overlap in appearance between

tumors made specific tissue diagnosis virtually impossible. However, this study is limited by the small number of tumors studied, and further work is necessary to evaluate the usefulness of these findings in differential diagnosis.

Unlike the pattern of vascularization, the degree of tumor flow within tumors of the same histologic type was quite variable. Further, the distribution and hemodynamics of tumor flow were often different within different portions of the same tumor. These differences may have been due in part to differences in the phase of tumor growth. Rubin and Casarett [5] have shown that tumors compress their own vascular supply during rapid phases of growth. Eventually, the high metabolic expenditure of the tumor outstrips its available blood supply, energy stores are depleted, and central tumor cells die [7]. Other authors [8] have suggested that coexistent differences in Doppler signal in different parts of the same tumor may be due to vascular supply by different arteries. This situation may occur in tumors with a peripheral pattern of vascularization involving more than one vessel. Despite

careful searching, we could detect disorganized or turbulent flow characteristic of arteriovenous shunting in the periphery of only two malignant tumors. This is in contradistinction to the findings of Taylor et al. [8], who described this pattern in 86% of malignant tumors evaluated in adult patients. Whether these differences are due to technical or population differences remains unclear.

The relationship between degree of neovascular flow and prognosis in childhood tumors has not been fully explored. However, recent work by Weidner et al. [9] suggests that the degree of tumor neovascularization and the metastatic potential of breast carcinoma are strongly related. It is possible that a similar relationship exists in other tumors and that color Doppler imaging may be useful in predicting the metastatic behavior of tumors in children.

The correlation between color Doppler imaging and histologic grading of neovascularity was encouraging. However, color Doppler imaging did not show flow in two tumors in which histologic examination showed marked neovascularization. Both were quite echogenic and were composed of dense fibrous stroma or contained extensive microscopic calcification. Several other technical factors must be considered when little or no flow is detectable with color Doppler imaging. These include inappropriate selection of color Doppler scale or filter or gain settings and positioning the electronic focus outside the region of interest. In addition, many commercially available units are not capable of detecting low-amplitude, low-velocity flows that may be present within tumor parenchyma. In our study, five of 19 tumors for which histologic correlation was available were examined by using a 3.5-MHz sector transducer, which is relatively insensitive to low-velocity and low-amplitude flow. Intratumoral flow was graded as high in one, moderate in three, and absent in one. All cases were in agreement with histologic grading of neovascularity. Although every effort should be made to examine intratumoral flow with the highest frequency transducer available, at times the body habitus of the patient or location of the mass makes this impossible. Our data show that even in these situations, color Doppler imaging can be used to provide a qualitative assessment of tumor flow.

Although agreement was good between the results of color Doppler imaging and histologic grading of vascularity, it is

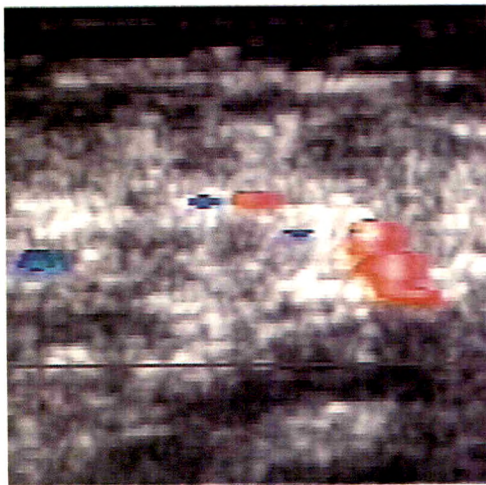


Fig. 3.—15-month-old boy with lipoblastomatosis of left thigh. Longitudinal color Doppler sonogram through middle of left thigh shows a single artery arising from superficial femoral artery supplying center of hypovascular tumor. Histologic examination showed a hypovascular tumor consisting of immature fat cells.

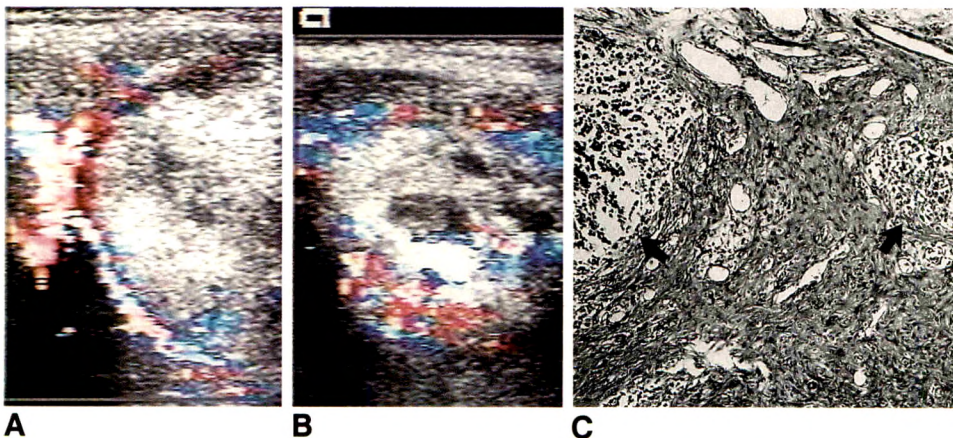


Fig. 4.—1-month-old boy with rhabdoid tumor of liver.

A and B, Transverse color Doppler sonograms show 5-cm heterogeneous mass in left lobe of liver surrounded by neovascular rind and deriving its blood supply from branches of hepatic artery in a basketlike pattern. Intratumoral flow could be detected only in periphery of tumor (A) and along its advancing edge inferiorly (B).

C, Histologic section of specimen from expanding edge of tumor shows tumor nodules (arrows) surrounded by large and small thin-walled vascular spaces. (H and E, original magnification $\times 110$)

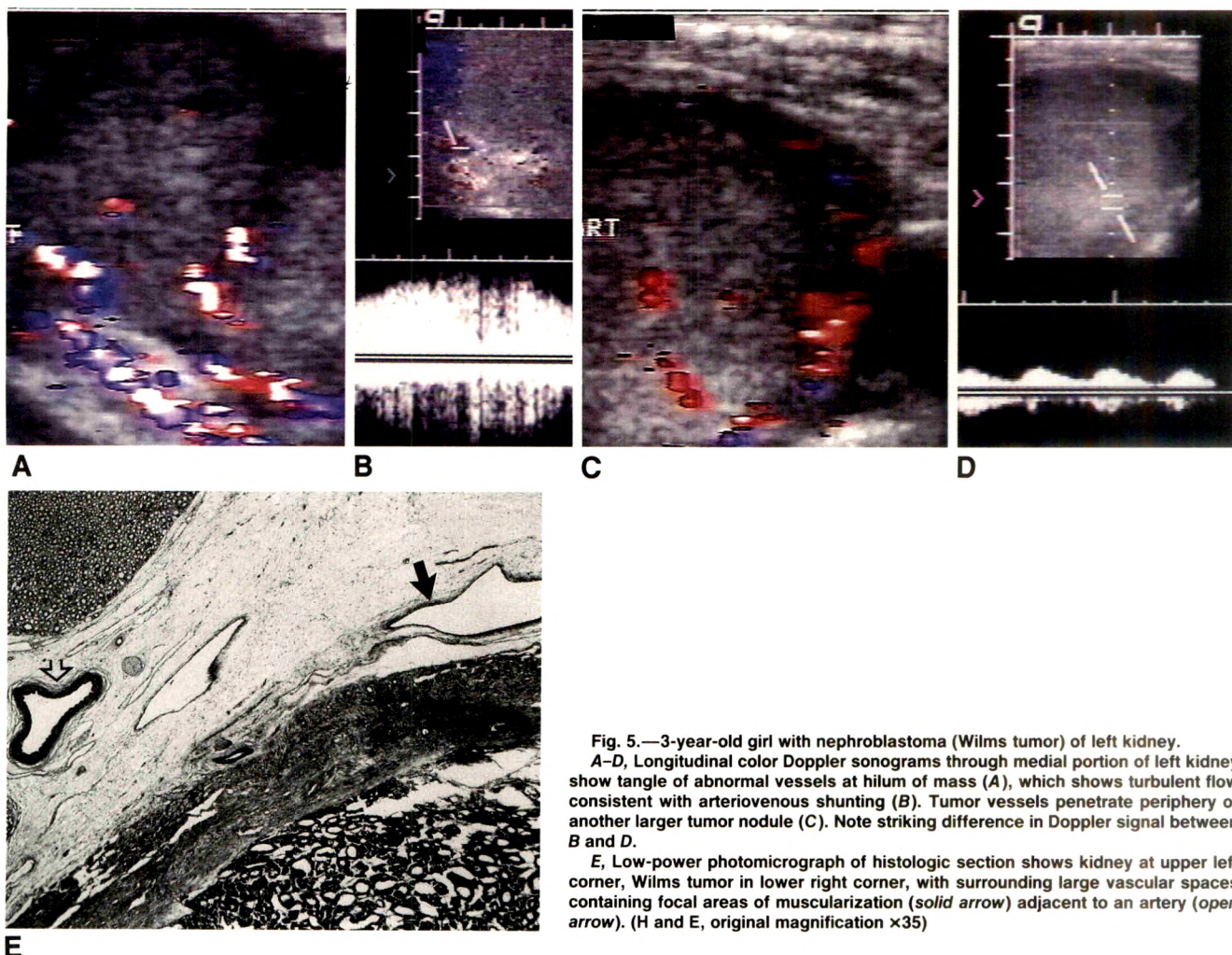


Fig. 5.—3-year-old girl with nephroblastoma (Wilms tumor) of left kidney.

A–D, Longitudinal color Doppler sonograms through medial portion of left kidney show tangle of abnormal vessels at hilum of mass (A), which shows turbulent flow consistent with arteriovenous shunting (B). Tumor vessels penetrate periphery of another larger tumor nodule (C). Note striking difference in Doppler signal between B and D.

E, Low-power photomicrograph of histologic section shows kidney at upper left corner, Wilms tumor in lower right corner, with surrounding large vascular spaces containing focal areas of muscularization (solid arrow) adjacent to an artery (open arrow). (H and E, original magnification $\times 35$)

unlikely that flow detected by color Doppler imaging corresponds directly to microscopic tumor neovascularity. Flow can be detected reliably with color Doppler imaging in relatively large (0.5 mm) vessels only. Considerable low-velocity and low-amplitude tumor flow in smaller vessels probably remains undetected with currently available equipment. Newer color flow procedures based on techniques other than frequency-shift estimates and the use of IV contrast agents such as perfluorooctylbromide may improve our ability to detect such low-level blood flow [10].

We conclude that color Doppler imaging can be used to detect the location and origin of blood supply, pattern of vascularization, and degree of intratumoral blood flow in a variety of solid tumors in infants and children.

REFERENCES

1. Rubin JM, Carson PL, Zlotecki RA, Ensminger WD. Visualization of tumor vascularity in a rabbit VX2 carcinoma by Doppler flow mapping. *J Ultra-sound Med* 1987;6:113–120
2. Shimamoto K, Sakuma S, Ishigaki T, Makino N. Intratumoral blood flow: evaluation with color Doppler echography. *Radiology* 1987;165:683–685
3. Cosgrove DO, Bamber JC, Davey JB, KcKinna JA, Sinnott HD. Color Doppler signals from breast tumors. *Radiology* 1990;176:175–180
4. Tanaka S, Kitamura T, Fujita M, Nakanishi K, Okuda S. Color Doppler flow imaging of liver tumors. *AJR* 1990;154:509–514
5. Rubin P, Casarett G. Microcirculation of tumors. Part I. Anatomy, function, and necrosis. *Clin Radiol* 1966;17:220–229
6. Shubik P. Vascularization of tumors: a review. *J Cancer Res Clin Oncol* 1982;103:211–222
7. Hoffer FA, Taylor GA, Spevak M, Ingber D, Fenton T. Metabolism of tumor regression from angiogenesis inhibition: ^{31}P magnetic resonance spectroscopy. *Magn Reson Med* 1989;11:202–208
8. Taylor KJW, Ramos I, Carter D, Morse SS, Snowere D, Fortune K. Correlation of Doppler US tumor signals with neovascular morphologic features. *Radiology* 1988;166:57–60
9. Weidner N, Semple JP, Welch WR, Folkman J. Tumor angiogenesis and metastasis—correlation in invasive breast carcinoma. *N Engl J Med* 1991;324:1–8
10. Mattrey RF. Sonographic enhancement of Doppler signals and perfused tissues with perfluorooctylbromide. *Invest Radiol* 1990;25:S158–S159

International Pediatric Radiology '91: Second Conjoint Meeting of the Society for Pediatric Radiology and the European Society of Pediatric Radiology, May 1991

Carol M. Rumack¹

International Pediatric Radiology '91 (IPR '91), the second conjoint meeting of the Society for Pediatric Radiology (SPR) and the European Society of Pediatric Radiology (ESPR), was held May 27–31, 1991, at the Bern's Congress Center in Stockholm, Sweden. This was the second conjoint meeting after the inaugural event in Toronto, Canada, in 1987. It was the first international pediatric radiology meeting to be held in Europe and was quite successful. It was truly an international event; the Australasian Society of Pediatric Imaging and the Latin American Society of Pediatric Radiology also joined the congress in Stockholm.

The meeting was officially opened by Hans Ringertz, president of the host ESPR and co-president of IPR '91, and Donald R. Kirks, president of the SPR and co-president of IPR '91. The total number of registrants was 810. Of these, 535 were pediatric radiologists: 175 SPR members from North America, 310 ESPR members from European countries, and 50 other pediatric radiologists from around the world.

Pediatric Imaging: Update '91, an 8.5-hr continuing educational symposium that presented an overview of advances in pediatric radiology, was chaired by Donald R. Kirks and Sven Laurin. The scientific program consisted of 88 scientific papers, 46 short presentations, and 36 poster presentations. The Jacques Lefebvre Award paper of the ESPR was presented to Jean Pierre Pracros for "Systematic Study of Superior Mesenteric Vessels in Abdominal Ultrasound."

The John Caffey Award paper of the SPR was "Juvenile Colonic Perforation: Experimental Results and Clinical Applications," by W. E. Shiels II, G. L. Keller, F. R. Ryckman, C. C. Daugherty, B. L. Specker, D. R. Kirks, and D. W. Summa. The Silver Award paper of the SPR was "MR Imaging of Growth Plate Disturbances Induced by Epiphyseal and Metaphyseal Injury," by D. Jaramillo, T. Laor, and D. J. Zaleske. The Bronze Award paper of the SPR was "Comparison of Radiographic and MRI Evaluation of the Craniocervical Junction in Down Syndrome," by K. S. White, W. S. Ball, E. C. Prenger, B. J. Patterson, and D. R. Kirks.

Two honored lectures were presented at IPR '91. The 21st Neuhauser Lecture of the SPR was given by D. C. Harwood-

Nash, Toronto, Ontario, Canada. This lecture was titled "Pediatric Neuroimaging: The Evolution and Revolution of a Subspecialty." The Swedish Society of Medicine Pediatric Radiology Lecture was given by Jan E. Lindsten, Stockholm, Sweden. His lecture was titled "Genes and Ethics at the Level of the Individual, Family and Population."

SPR Research and Education Fund Grants were awarded to five groups of investigators, for a total of \$20,000. These grants were given to the authors of the following: "Phosphorus-31 Magnetic Resonance Spectroscopy of Muscle Metabolism in Patients with Sickle Cell Disease Prior to and Following Isovolemic Exchange Transfusion," by G. S. Bisset III, A. A. Tzika, C. L. Morris, K. A. Kalinyak, and K. H. Caron (Cincinnati, OH); "Detection of Cerebral Vascular Disease in Patients with Sickle Cell Anemia Using Duplex Transcranial Doppler with MR Angiographic Correlation," by J. J. Seibert, C. A. James, C. M. Glasier, D. L. Becton, and D. H. Berry (Little Rock, AK); "Pulmonary Distribution of Endotracheally Administered Epinephrine in Pediatric Resuscitation," by M. S. Finkelstein, V. M. Nadkarni, M. S. Jasani, G. A. Mandell, and M. E. Norman (Wilmington, DE); "Changes in Bone Density in Children Undergoing Bone Marrow Transplantation," by V. S. Chakravarti, S. Mahboubi, N. R. Kamani, F. S. Kaplan, and C. S. August (Philadelphia, PA); and "Multiparameter Ultrasonic Tissue Characterization of the Immature Rat Brain: Normal Versus Disease States," by L. L. Barr, A. A. Tzika, and W. S. Ball, Jr. (Cincinnati, OH).

In 1981, the first discussions of an international pediatric radiology meeting seemed very complex with so many involved. However, the excellent scientific material, superb social events, and strong attendance by pediatric radiologists from around the world have made the IPR meeting an outstanding conference. With the initial success in Canada in 1987 and now the great success of the conjoint meeting in Europe, plans are being made for the third IPR meeting. IPR '96 will be held in Boston, May 26–30, 1996, and will be hosted by the SPR. Boston promises to be an excellent site to continue the success of the IPR meetings and to encourage the development of a truly international scientific community.

¹ Secretary, The Society for Pediatric Radiology, University of Colorado Health Sciences Center, 600 Grant St., 6th Fl., Denver, CO 80203-3527.

Case Report

Fibroepithelial Polyp of the Ureter in a Child

Robert M. Liddell,¹ Edward Weinberger,¹ Deborah E. Schofield,² and Richard S. Pelman³

Fibroepithelial polyp of the ureter is a benign mesodermal tumor that rarely occurs in children. Correct radiologic assessment is crucial to direct surgical management. We report a case of a fibroepithelial polyp of the ureter in a child in whom correct preoperative diagnosis was made by correlating the results of excretory urography, sonography, and CT.

Case Report

A 7-year-old boy had recurrent episodes of pain in the right flank. He had been in good health and had no history of trauma, infections, urinary tract stones, or bleeding diathesis. No abdominal mass was palpable on physical examination. Initial laboratory evaluation revealed microscopic hematuria without casts or pyuria. Urine cultures were sterile.

Sonography showed moderate right-sided hydronephrosis without hydroureter. A mildly echogenic structure with polypoid projections extended into the right renal pelvis from the ureter (Fig. 1A). There was no acoustic shadowing from this mass. The bladder, left kidney, and left ureter were normal. Excretory urography revealed a polypoid filling defect at the right ureteropelvic junction, causing a partial obstruction of the ureter (Fig. 1B). The preliminary scout radiograph did not show any calcifications. Unenhanced CT revealed soft tissue filling the right ureteropelvic junction and proximal ureter. No high attenuation, which would have suggested calculous disease, was seen (Fig. 1C). Because we found no evidence of a calculus, sloughed renal papilla, or blood clot to explain the filling defect, the right kidney and proximal ureter were surgically explored via an incision in the right flank. A 2-cm soft-tissue mass was excised with part of the proximal portion of the ureter, and the ureter was anastomosed to the renal pelvis. The patient recovered uneventfully and had no further

pain in the flank or hematuria. Histologically, the tumor was composed of loose fibrovascular connective tissue covered with a layer of normal urothelium, characteristic of a fibroepithelial polyp.

Discussion

Primary neoplasms of the ureter are characterized as epithelial or mesodermal [1]. The epithelial neoplasms are usually malignant, whereas the rare mesodermal neoplasms are almost always benign. The most common benign mesodermal ureteral tumor is the fibroepithelial polyp, which histologically has a core of loose fibrovascular stroma covered by a layer of normal urothelium [2, 3]. It is usually found in the proximal part of the ureter and is almost always solitary [3]. Although this tumor is usually found in adults, it also may occur in children and has even been reported in a neonate [2, 4]. Symptoms include pain in the flank and hematuria. The pain may be intermittent because of partial obstruction and may sometimes be associated with symptoms suggesting urinary tract infection [2].

Radiologic appearance is variable, depending on the gross appearance of the tumor. The tumor may be long and pedunculated with a smooth surface, or it may be relatively short and covered with multiple, thin, polypoid projections [5]. Excretory urography may show an intraluminal lesion that is smooth or polypoid, and does not cause marked dilatation of the urinary tract. Changing the patient's position may show mobility of a ureteral fibroepithelial polyp, unlike the fixation that is encountered with most malignant ureteral tumors. In

Received April 22, 1991; accepted after revision July 2, 1991.

¹ Department of Radiology, Children's Hospital and Medical Center, P.O. Box C-5371, Seattle, WA 98105. Address reprint requests to R. M. Liddell.

² Department of Pathology, Children's Hospital and Medical Center, P.O. Box C-5371, Seattle, WA 98105.

³ Department of Urology, University of Washington, Seattle, WA 98195.

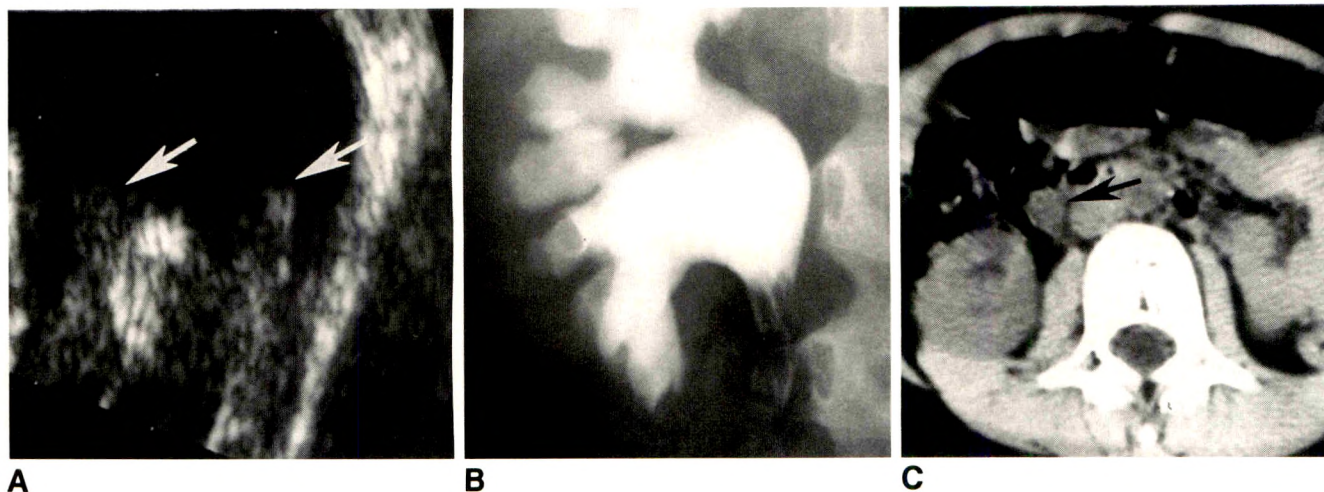


Fig. 1.—A, Coronal sonogram (rotated to align with B) shows soft-tissue fronds (arrows) floating in renal pelvis. There is no shadowing to suggest calculus.

B, Excretory urogram reveals well-defined filling defects at right ureteropelvic junction, with multiple frondlike projections arising from lesion.

C, CT scan reveals a mass expanding right ureter (arrow). CT attenuation is higher than that of urine but lower than that of a calculus, indicating it is of soft-tissue density.

our patient, mobility of the distal projections of the tumor was observed sonographically. Sonography and unenhanced CT are helpful in excluding a calculus and visualizing a soft-tissue mass.

In the child, congenital ureteropelvic junction obstruction and stone are much more likely causes of obstruction of the proximal portion of the ureter than is tumor. Nonetheless, a fibroepithelial polyp must be considered when imaging studies exclude the more likely causes of ureteral obstruction. The mobility of a portion of this lesion and the absence of findings of calculus are highly suggestive of the tumor. In children, a malignant ureteral tumor is unlikely. No reports of metastasizing or locally recurrent transitional epithelial tumors of the ureters in children have been published [6].

Preoperative radiologic examination was important in this patient because it directed the proper mode of therapy. If a stone had been found, extracorporeal shock-wave lithotripsy would have been attempted. The polyp found during surgery

was benign, and correct identification saved the patient from more radical surgery, such as nephroureterectomy.

REFERENCES

1. Van Poppel H, Nuttin B, Oyen R, Stessens R, Van Damme B, Verduyn H. Fibroepithelial polyps of the ureter. *Eur Urol* **1986**;12:174-179
2. Debruyne FMJ, Moonen WA, Daenekindt AA, Delaere KPJ. Fibroepithelial polyp of ureter. *Urology* **1980**;16:355-359
3. Fein AB, McClennan BL. Solitary filling defects of the ureter. *Semin Roentgenol* **1986**;21:201-213
4. Soderdahl DW, Schuster SR. Benign ureteral polyp in the newborn. *JAMA* **1969**;207:1714-1715
5. Banner MP, Pollack HM. Fibrous ureteral polyps. *Radiology* **1979**;130:73-76
6. Mydlo J, Reda E, Gill B, et al. Fibroepithelial polyp in a child. *Urology* **1988**;31:318-320

Sonographic Prediction of Gestational Age: Accuracy of Second- and Third-Trimester Fetal Measurements

Carol B. Benson¹
Peter M. Doubilet

We measured the accuracy of second- and third-trimester sonographic predictors of gestational age against highly reliable gold standard (crown-rump length) in a group of fetuses. Using a prospectively collected computerized data base, we selected 460 fetal sonograms obtained at 14–42 weeks of gestation in which age could be reliably established on the basis of crown-rump length in the first trimester. We used data obtained from these sonograms to compare several predictors of fetal age. The accuracy of all predictors worsened progressively as pregnancy proceeded. In the second trimester, corrected biparietal diameter and head circumference were more accurate predictors of gestational age than were biparietal diameter, femoral length, and abdominal circumference ($p < .05$, F test). In the third trimester, the corrected biparietal diameter, head circumference, and femoral length were the best predictors, significantly better than biparietal diameter and abdominal circumference ($p < .05$, F test).

Prediction of gestational age that relies on a single sonographic measurement should be based on the head circumference or corrected biparietal diameter in the second trimester and on one of these two predictors or the femoral length in the third trimester.

AJR 157:1275–1277, December 1991

Prediction of gestational age is an important component of obstetric sonography. Several sonographic fetal measurements during the second and third trimesters have been proposed for this purpose. These include biparietal diameter (BPD) [1], head circumference (HC) [2], corrected BPD [3], abdominal circumference (AC) [4], femoral length (FL) [5], length of other long bones [5], and binocular distance [6, 7]. Assessment of how accurate any of these measurements is for prediction of gestational age requires a large number of cases in which the relevant measurement is recorded and in which the true gestational age is known with a high degree of precision. Most studies have used the last menstrual period in women with regular cycles as the gold standard for true gestational age. This criterion has several potential sources of inaccuracy, including faulty memory, bleeding in early pregnancy, and use of oral contraceptives [8].

A highly reliable standard that is more objective than the last menstrual period is available for second- and third-trimester fetuses scanned in the first trimester: gestational age based on earliest measured crown-rump length (CRL). The low variability—and hence great precision—of the CRL, initially suggested by using last menstrual period as the gold standard [9], has recently been confirmed in infertility patients in whom the time of conception was known precisely [10, 11]. We used this first-trimester CRL measurement to assess the accuracy of a variety of measurements used to predict gestational age in the second and third trimesters.

Materials and Methods

From December 1987 to November 1988, data from all obstetric sonograms obtained at our institution were stored in a computer file. Data recorded for each case included the

Received June 20, 1991; accepted after revision August 14, 1991.

¹ Both authors: Departments of Radiology, Harvard Medical School, Brigham and Women's Hospital, 75 Francis St., Boston, MA 02115.

0361-803X/91/1576-1275
© American Roentgen Ray Society

patient's name and hospital identification number; date of examination; single vs multiple fetuses; CRL (in the first trimester); and the following fetal measurements in the second and third trimesters: BPD, occipitofrontal diameter (OFD) (if fetal position permitted its measurement), FL, and abdominal diameter (AD). The measurement recorded for each of these body parts was the mean value from two to three images of the structure. The AD recorded was the average of anteroposterior and transverse diameters. Sonograms were obtained with a variety of mechanical and electronic scanners, with both sector and linear formats. Each case was reviewed by a physician before the data were stored in the computer.

In every case in which the OFD could be measured, head circumference and corrected BPD were computed from the BPD and OFD by using the following formulas [3]:

$$HC = 1.57 \times (BPD + OFD + \text{skull-thickness factor})$$

$$\text{Corrected BPD} = \sqrt{\frac{BPD \times OFD}{1.265}}$$

Since BPD is measured from outer skull to inner skull, and OFD from mid-skull to mid-skull, a skull-thickness factor [3] is required for calculation of the outer-perimeter-based HC. Abdominal circumference was computed from AD by using the following formula [12]:

$$AC = 3.14 \times AD$$

Using computer-based search techniques, we selected 460 sonograms of singleton fetuses between 14 and 42 weeks of gestation in which the mother had had a sonogram in the first trimester and the fetus's CRL had been measured. Assignment of gestational age was based on the first sonogram in which a CRL could be measured. "True" gestational age for each of these 460 study cases was calculated as the sum of the age at the time of the patient's first sonogram as determined by CRL [9] plus the number of weeks elapsed between sonograms.

We used regression analysis to assess the variability of gestational age with respect to each of several measurements: BPD, corrected BPD, HC, FL, and AC. For each of these measurements, we generated polynomial regression equations: true gestational age = $a + bX + cX^2 + \dots$, where X represents the measurement and a, b, and c are regression coefficients computed via a statistical software package (SYSTAT, Evanston, IL). The SD, in weeks, of gestational age about the regression line, also computed by using SYSTAT, was used as the measure of the precision of each measurement as a predictor of gestational age. Nonpolynomial regression models, such as those involving exponentials or logarithms, were not considered because any such model can be closely approximated by a polynomial by using a Taylor series [13]. For each predictor, SDs were computed for four gestational age intervals: early second trimester (14–20

weeks), late second trimester (20–26 weeks), early third trimester (26–32 weeks), and late third trimester (after 32 weeks). Statistical comparisons among predictors were made by using the F test.

Results

The mean gestational age at the initial first-trimester sonogram was 10.6 ± 2.0 weeks (mean \pm SD). Gestational age for the second- and third-trimester study cases was assigned on the basis of the initial sonogram.

The variability of gestational age about the regression line for each predictor measured in the second and third trimester is shown in Table 1. Each value in the table equals two SDs, in weeks, as this corresponds closely to the commonly used 95% confidence range. The SDs are derived from second-degree polynomial regression models, as little change was seen in these values with higher-order polynomials.

Each predictor of gestational age became progressively less accurate as pregnancy proceeded, as shown by widening confidence ranges from the early second through the late third trimester. In the first half of the second trimester (14–20 weeks), predictors other than the AC had 95% confidence ranges of 1.2–1.4 weeks. This increased to 3.5–4.1 weeks in the latter parts of the third trimester (32–42 weeks).

The corrected BPD and HC were equivalent in accuracy and were significantly more accurate than the BPD was ($p < .05$, F test) throughout gestation. These two predictors were significantly more accurate than the FL was in both the early and late second trimester ($p < .05$, F test). In the third trimester, no statistically significant difference was seen among corrected BPD, HC, and FL. The AC was significantly less accurate than all other predictors in all four gestational age intervals ($p < .05$, F test).

Discussion

Previous studies of the accuracy of prediction of gestational age in the second and third trimesters have, in general, relied on a tarnished gold standard: age based on last menstrual period in women with regular cycle lengths. The fetuses of women who have had sonography in the first trimester can be assigned a more accurate gestational age on the basis of the CRL [9–11]. One study [14] used the CRL as a gold standard for gestational age to assess the accuracy of the BPD. That study was limited to the gestational ages of 20–

TABLE 1: Precision of Predictors of Gestational Age in the Second and Third Trimesters

Predictor	Gestational Age Interval (in Weeks)			
	14–20	20–26	26–32	32–42
BPD	1.4 (108)	2.1 (81)	3.8 (100)	4.1 (171)
Corrected BPD	1.2 (100)	1.9 (78)	3.3 (85)	3.8 (85)
FL	1.4 (100)	2.5 (79)	3.1 (104)	3.5 (174)
HC	1.2 (100)	1.9 (78)	3.4 (85)	3.8 (85)
AC	2.1 (98)	3.7 (83)	3.0 (101)	4.5 (166)

Note.—Numbers are two SDs (in weeks) for predicted gestational age based on number of patients (indicated in parentheses). BPD = biparietal diameter, FL = femoral length, HC = head circumference, AC = abdominal circumference.

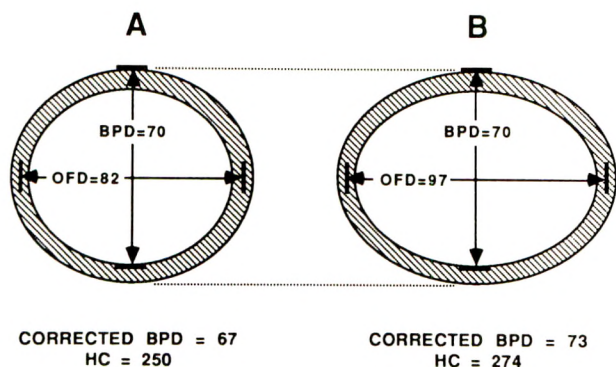


Fig. 1.—Diagram of two heads with different shapes and equal biparietal diameters (BPD). Head A is shorter and has a smaller corrected BPD and head circumference (HC) than head B. On basis of BPD, fetuses with heads A and B would be assigned same gestational age. On basis of corrected BPD or HC, fetus with head A would be assigned a younger gestational age than fetus with head B. OFD = occipitofrontal diameter. (All measurements in millimeters.)

24 weeks and 30–33 weeks and evaluated no measurement other than the BPD. We used the same reliable gold standard, the CRL, to assess the accuracy of several predictors of gestational age throughout the second and third trimesters.

Single and multiple sonographic measurements are used for gestational age prediction with a wide variety of published formulas and tables [1, 2, 4–7, 15, 16]. The intent of our study was not to evaluate specific formulas but instead to compare the accuracy of several sonographic measurements for age prediction by using an objective and reliable gold standard. Our method involved determining the variability about regression lines generated from our own data.

The following conclusions can be drawn from our study: (1) The accuracy of each predictor of gestational age worsens progressively as pregnancy proceeds. (2) The corrected BPD and the HC are equally accurate at all stages, and both are more accurate than is the BPD. The first two predictors take head shape into account, whereas BPD does not (Fig. 1). (3) In the second trimester, the corrected BPD and the HC are significantly more accurate in predicting gestational age than all other measurements. (4) In the third trimester, no significant difference in accuracy is seen among corrected BPD, HC, and FL.

Our findings suggest the following approach to assigning gestational age when using a single sonographic measurement after the first trimester. The BPD and FL should be measured in all cases, and the OFD should be measured whenever the position of the fetal head allows it. If a previous sonogram is available, calculate the age from the earliest sonogram (i.e., do not change dates on the basis of current

measurements). When the first sonogram is obtained in the second trimester, predict the age by using corrected BPD or HC if OFD is measurable and by using BPD or FL otherwise. When the first scan is obtained in the third trimester, use the FL, corrected BPD, or HC if the OFD is measurable and use the FL in preference to the BPD if the OFD is not measurable. All predictors are imprecise late in the third trimester, so gestational age assigned on the basis of a sonographic measurement made during this stage of pregnancy is not reliable.

ACKNOWLEDGMENTS

We thank Angela Treadwell and Naomi Davis for their secretarial assistance in preparing this manuscript.

REFERENCES

1. Kurtz AB, Wapner RJ, Kurtz RJ, et al. Analysis of biparietal diameter as an accurate indicator of gestational age. *JCU* 1980;8:319–326
2. Law RG, MacRae KD. Head circumference as an index of fetal age. *J Ultrasound Med* 1982;1:281–288
3. Doubilet PM, Greenes RA. Improved prediction of gestational age from fetal head measurements. *AJR* 1984;142:797–800
4. Hadlock FP, Deter RL, Harrist RB, Park SK. Fetal abdominal circumference as a predictor of menstrual age. *AJR* 1982;139:367–370
5. Jeanty PJ, Rodesch F, Delbeke D, Dumont JE. Estimation of gestational age from measurements of fetal long bones. *J Ultrasound Med* 1984;3:75–79
6. Jeanty P, Cantraine F, Cousaert E, Romero R, Hobbins JC. The binocular distance: a new way to estimate fetal age. *J Ultrasound Med* 1984;3:241–243
7. Mayden KL, Tortora M, Berkowitz RL, Bracken M, Hobbins JC. Orbital diameters: a new parameter for prenatal diagnosis and dating. *Am J Obstet Gynecol* 1982;144:289–297
8. Campbell S, Warsof SL, Little D, Cooper DJ. Routine ultrasound screening for the prediction of gestational age. *Obstet Gynecol* 1985;65:613–620
9. Robinson HP, Fleming JEE. A critical evaluation of sonar "crown-rump length" measurements. *Br J Obstet Gynecol* 1975;82:702–710
10. Chervenak FA, Brightman RC, Thornton J, Berkowitz GS, David S. Crown-rump length and serum human chorionic gonadotropin as predictors of gestational age. *Obstet Gynecol* 1986;67:210–213
11. Selbing A, Fjallbrant B. Accuracy of conceptual age estimation from fetal crown-rump length. *JCU* 1984;12:343–346
12. Greenes RA. OBUS: a microcomputer system for measurement, calculation, reporting, and retrieval of obstetric ultrasound examination. *Radiology* 1982;144:879–883
13. Abramowitz M, Segun IA. *Handbook of mathematical functions*. New York: Dover Publications, 1965
14. Smazal SF, Weisman LE, Hopper KD, Ghaed N, Shirts S. Comparative analysis of ultrasonographic methods of gestational age assessment. *J Ultrasound Med* 1983;2:147–150
15. Hadlock FP, Deter RL, Harrist RB, Park SK. Computer assisted analysis of fetal age in the third trimester using multiple fetal growth parameters. *JCU* 1983;11:313–316
16. Hadlock FP, Deter RL, Harrist RB, Park SK. Estimating fetal age: computer-assisted analysis of multiple fetal growth parameters. *Radiology* 1984;152:497–501

Ependymoma of the Fourth Ventricle

Martin R. Prince¹ and Felix S. Chew

The circumference of the head of a 17-month-old girl with lethargy, nausea, and irritability was above the 95th percentile for age. CT of the brain revealed a polypoid mass in the fourth ventricle with proximal hydrocephalus and decreased periventricular attenuation from trans-ependymal flow of CSF (Fig. 1). MR imaging showed the mass arising from the floor of the fourth ventricle and extending bilaterally through the foramina of Luschka into the cerebellopontine angle cisterns. IV administration of gadopentetate dimeglumine produced regional mass effect and minimal heterogeneous enhancement. The intraleSIONAL signal was heterogeneous on T2-weighted images. After surgical resection, gross examination revealed a solid tumor with regions of necrosis and hemorrhage. Microscopic findings were of a fairly cellular tumor with prominent perivascular pseudorosettes. The final pathologic diagnosis was ependymoma.

Ependymomas arise from the layer of differentiated ependymal cells that line the ventricles of the brain and the central canal of the spinal cord. Ependymomas constitute 8% of intracranial gliomas in children and 1–6% of intracranial gliomas in adults. Although they may occur at any age and anywhere along the ependymal portion of the neural axis, most are found in children in the first decade of life and are located on the floor of the fourth ventricle. Symptoms are usually the result of space-occupying effects; location in the fourth ventricle leads to obstructive hydrocephalus [1]. Most ependymomas grow slowly and are well-circumscribed. Soft and often frondlike,

they have a propensity for plastic growth and may protrude through the ventricular foramina into the subarachnoid space.

Approximately 50% of lesions appear as calcified on CT. On MR images, the mixed signal characteristics of solid portions of tumor can be due to hemorrhage, necrosis, tumor vascularity, or calcification; thus differentiation of ependymoma from other lesions is based on location and morphology rather than appearance [2].

Treatment includes surgery and irradiation, but the prognosis is generally poor because of the dangerous location and the technical difficulty in performing a complete resection [3]. Ependymomas can disseminate throughout the subarachnoid space and in rare instances can spread beyond the CNS. Cytologic features of malignancy are usually absent, but the histologic appearance does not correlate well with prognosis; one series reported a 100% mortality rate within 3 years of diagnosis [4].

REFERENCES

1. Rubinstein LJ. *Tumors of the central nervous system*. Washington, DC: Armed Forces Institute of Pathology, 1972:104–114
2. Spoto GP, Press GA, Hesselink JR, Solomon M. Intracranial ependymoma and subependymoma: MR manifestations. *AJNR* 1990;11:83–91
3. Shuman RM, Alvord EC, Leech RW. The biology of childhood ependymomas. *Arch Neurol* 1975;32:731–739
4. Ross GW, Rubenstein LJ. Lack of histopathological correlation of malignant ependymomas with postoperative survival. *J Neurosurg* 1989;70:31–36

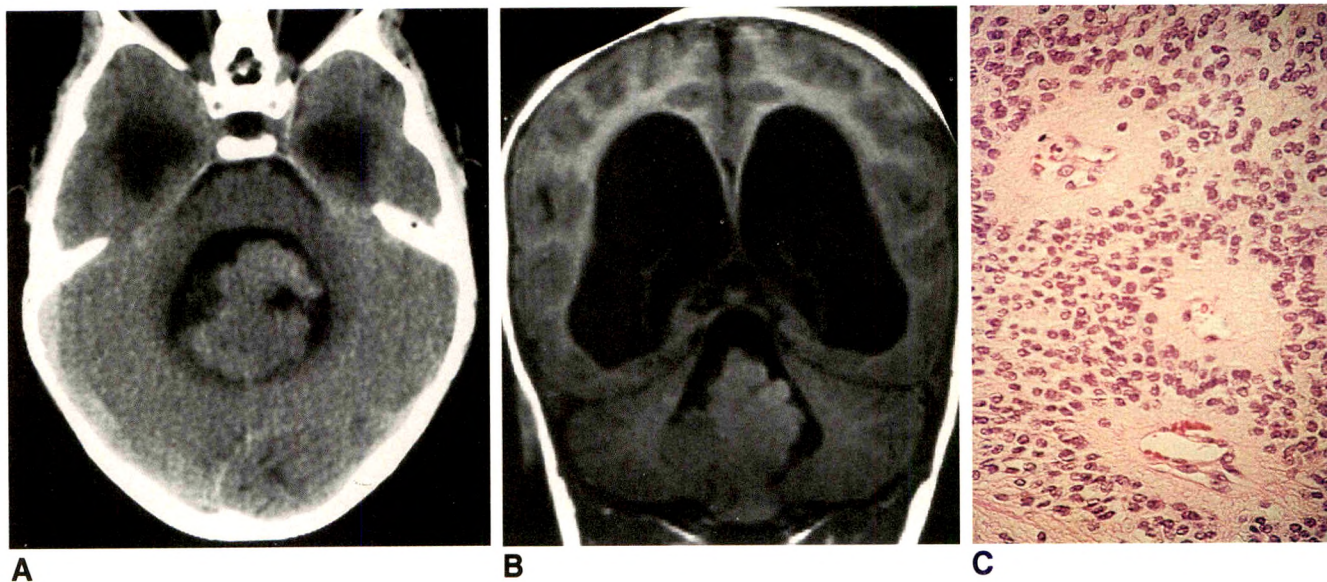


Fig. 1.—Ependymoma of fourth ventricle.

A, Axial CT scan shows polypoid lesion in fourth ventricle and hydrocephalus. Lesion is not calcified.

B, T1-weighted coronal MR image shows lesion arising from floor of fourth ventricle.

C, Photomicrograph of histologic specimen shows three blood vessels surrounded by eosinophilic cuffs of tumor cell cytoplasm separating nuclei of tumor cells from vessel walls (perivascular pseudorosettes). Nuclei are of uniform size and shape. (H and E, original magnification $\times 390$)

From the weekly radiologic-pathologic correlation conferences conducted by Jack Wittenberg. Pathology editor: Andrew E. Rosenberg. Radiology editors: Felix S. Chew, Daniel P. Barboriak, William E. Palmer, Daniel I. Rosenthal.

¹ Both authors: Department of Radiology, Massachusetts General Hospital and Harvard Medical School, 32 Fruit St., Boston, MA 02114. Address reprint requests to F. S. Chew.

The Prevalence and Location of Metastases from Ocular Melanoma: Imaging Study in 110 Patients

James G. Lorigan^{1,2}
 Sidney Wallace¹
 Giora M. Mavligit³

Ocular melanoma is characterized by an unpredictable clinical course, during which fulminant metastatic disease may occur after a prolonged disease-free interval. The purpose of this study was to determine the pattern of metastatic involvement in this disease. The clinical and radiologic findings in 110 patients with metastatic ocular melanoma were reviewed. The 54 men and 56 women were 24–79 years old (mean, 50 years) when the primary tumor was first diagnosed. Metastases were present in three patients at the time of first diagnosis and occurred in 107 patients 2 months to 36 years later (mean, 52 months). One hundred five patients died between 1 and 38 months after the onset of metastatic disease. Hepatic metastases developed in 101 patients (92%), and in 60 (55%) of these, the liver was the only organ involved initially. Pulmonary parenchymal metastases developed in 34 patients (31%), but in only four of them were metastases confined to the lungs. Twenty-five patients (23%) had bone involvement, mostly affecting the spine. Nineteen patients (17%) had skin or subcutaneous metastases, but in only two of them was this the initial finding. Nodal involvement was shown in 15 patients (14%), almost always associated with extensive hepatic metastases. Brain and adrenal metastases were seen in five and three patients, respectively.

Hepatic involvement occurs in almost all patients who develop metastatic ocular melanoma, and the liver is the most common initial site of metastatic involvement. Metastases may develop after a long disease-free interval.

AJR 157:1279–1281, December 1991

Ocular melanoma accounts for 3.5–6% of all melanoma patients at the University of Texas M. D. Anderson Cancer Center [1, 2]. These tumors are characterized by an unpredictable clinical course and a tendency for late metastases [3–5]. To our knowledge, the value of modern imaging techniques in the follow-up of these patients has not been studied. The purpose of this study was to evaluate the prevalence and location of metastases in ocular melanoma with the use of currently available imaging techniques.

Materials and Methods

We searched the data banks at our institution and found the records of 181 patients with ocular melanoma. These patients were first seen at this institution between October 1976 and November 1988. Of the total, 110 of them had metastases when first seen at the University of Texas M. D. Anderson Cancer Center, or developed them subsequently, and had sufficient follow-up to document the course of the disease. The 54 men and 56 women were 24–79 years old (mean, 50 years) when the primary tumor was diagnosed. The primary lesion was treated by enucleation in 87, by local irradiation in 13, by enucleation and irradiation in five, and by enucleation followed by orbital exenteration in two patients. In each case, the primary tumor had been treated elsewhere, prior to referral to our institution. The primary tumor was not treated in three patients who had metastases when first diagnosed.

The clinical records and radiology reports were reviewed to determine the prevalence and location of metastases. Metastases were considered proved if confirmed by biopsy, by

Received April 5, 1991; accepted after revision June 27, 1991.

¹ Department of Diagnostic Radiology, Division of Diagnostic Imaging, The University of Texas M. D. Anderson Cancer Center, 1515 Holcombe Blvd., Houston, TX 77030. Address reprint requests to S. Wallace.

² Present address: Department of Radiology, Cavan General Hospital, Cavan, Ireland.

³ Department of Clinical Immunology and Biological Therapy, Division of Medicine, The University of Texas M. D. Anderson Cancer Center, Houston, TX 77030.

0361-803X/91/1576-1279
 © American Roentgen Ray Society

change on serial radiologic studies, or by characteristic appearances on other imaging studies.

All patients had chest radiographs during follow-up at our institution. The abdomen was evaluated by CT in 72 patients, by sonography in 31, and by MR imaging in four. Hepatic angiography was done in 55 patients, usually before chemoembolization [6]. Fifteen patients had liver scintigraphy. The brain was evaluated by CT (49), scintigraphy (eight), or MR (one) in 58 patients. Thirty-three patients had bone scintigraphy.

Results

Three patients had metastases when the intraocular tumor was first diagnosed. In the other 107 patients, the metastases developed between 2 months and 36 years (mean, 52 months) after treatment of the primary tumor, and in 66 (62%) of these patients, the metastases developed within 5 years. One hundred five patients died between 1 and 38 months after development of metastatic disease (mean, 10 months). Three patients were alive with progressive disease 11, 19, and 21 months after metastases developed. The remaining two patients had stable disease 14 and 74 months after metastases were diagnosed.

The initial location and subsequent sites of metastatic involvement are shown in Table 1.

Hepatic metastases developed in 101 patients (92%) during the course of the disease. Of these, 94 patients (85%) had liver involvement when first seen at this institution, and 60 (55%) had no clinical or radiologic evidence of other metastatic disease at that time. Extrahepatic metastases developed in 10 of these 60 patients during follow-up, including eight with pulmonary parenchymal involvement, five with bone metastases, and four with adenopathy and skin or subcutaneous metastases. Diffuse disseminated metastases developed in one patient, with involvement of these organ systems, the adrenal glands, and the brain.

The lungs were involved in 34 patients (31%). Only four of these had localized disease at presentation, and nine additional patients had pulmonary and hepatic metastases when first seen. Six patients presented with pulmonary and hepatic metastases in addition to other sites of disease. Lung metastases developed in the other 15 patients during follow-up.

Bone involvement occurred in 25 patients (23%), but only

four patients had metastatic disease confined to bone. The spine was affected in 16 of these 25 patients; the calvaria in four; and the thoracic cage, pelvis, and long bones in three.

Nineteen patients (17%) had metastases to the skin and subcutaneous tissues, but only two patients were first seen with disease confined to the skin or subcutaneous tissues. The scalp or face was affected in 10 patients, including one lesion that eroded through the calvaria to involve the brain. The metastatic lesions in the other nine patients affected various sites on the trunk.

Fifteen patients (14%) had lymph node involvement. One of them presented with isolated mediastinal nodal disease; all of the other patients had additional sites of disease. Ten patients had upper abdominal adenopathy, always in association with extensive hepatic involvement. Three patients had metastases to the axillary nodes.

Brain metastases developed in five patients (4%). All of them had hepatic disease, and four had multisystem involvement. One patient who had tumor extension to the resection margin of the optic nerve at surgery returned 5 months later with locally recurrent disease and diffuse cerebral, cerebellar, hepatic, and bone metastases.

Adrenal metastases were seen in three patients, all of whom had diffuse upper abdominal disease. Stomach metastases developed in two patients and jejunal metastases in one. Two patients had splenic metastases.

Discussion

The incidence of ocular melanoma is six cases per million population per year [3]. It occurs in all age groups, but almost 70% of cases are identified in the fifth through seventh decades [4, 5]. The natural history of this disease is poorly understood, partly because the primary tumor is usually not diagnosed until it is large enough to cause visual disturbance or other ocular symptoms. The true prevalence of metastases in ocular melanoma is unknown, but the prognosis is determined by the tumor size and histology, and the presence or absence of extrascleral extension [5, 7, 8]. In an actuarial study of ocular melanoma, Paul et al. [5] calculated that the mortality was 29% within 5 years and 40% within 10 years of diagnosis of the primary tumor.

Enucleation has been the standard treatment for ocular melanoma and was used in most of our patients. However, it has been suggested that manipulation of the globe and the consequent fluctuations in intraocular pressure may actually cause dissemination of tumor cells [9]. Metastases from choroidal melanoma usually occur within 5 years of diagnosis [1, 2, 10, 11], as in our patients. However, late metastases are a well-recognized complication of this disease. One of our patients was free from disease for 36 years before diffuse hepatic metastases developed, and Shields et al. [12] reported a case of orbital recurrence and hepatic metastases 42 years after enucleation of the primary tumor.

In almost all of our patients, hepatic metastases developed, whereas lung or bone metastases developed in less than one third of them and only five patients had brain metastases. The brain and skeletal system were not routinely evaluated in

TABLE 1: Initial Location and Subsequent Sites of Metastatic Involvement in 110 Patients with Ocular Melanoma

Location of Metastases	No. (%)	
	Initial Location	Subsequent Sites
Liver	94 (85)	101 (92)
Lung	19 (17)	34 (31)
Bone	18 (16)	25 (23)
Skin and subcutaneous tissues	14 (13)	19 (17)
Lymph nodes	11 (10)	15 (14)
Brain	4 (4)	5 (4)
Adrenal gland	2 (2)	3 (3)
Stomach	2 (2)	2 (2)
Spleen	2 (2)	2 (2)

Note.—The follow-up after development of metastases was 1–74 months (mean, 11 months).

our patients, and because of this, it is possible that some clinically silent metastases remained undiagnosed. However, our findings are similar to those of Char [10] and Rajpal et al. [11].

Shirikhoda and Albin [13] reported hepatic involvement in 22%, nodal involvement in 40%, and adrenal gland involvement in 15% of patients in whom cutaneous melanoma was evaluated by abdominal CT. This pattern of metastatic involvement is different from that seen in our patients and suggests that ocular melanoma is biologically different from cutaneous melanoma. The reasons for the high prevalence of hepatic metastases compared with involvement of other organs in ocular melanoma have not been determined. The prevalence cannot be explained on the basis of lymphatic or venous drainage alone, and undoubtedly, many contributory factors exist.

Metastatic ocular melanoma is most likely to affect the liver initially, either in isolation or in combination with other sites. Liver involvement as the first site of metastatic disease implies a worse prognosis [2, 11] and should be suspected, clinically, in the presence of upper abdominal pain or "fullness" caused by irritation of the liver capsule. The predilection of ocular melanoma to metastasize to the liver must be remembered, even in patients who have been free from disease for many years.

REFERENCES

1. Einhorn LH, Burgess MA, Gottlieb JA. Metastatic patterns of choroidal melanoma. *Cancer* 1974;34:1001-1004
2. Bedikian AY, Kantarjian H, Young SE, Bodey GP. Prognosis in metastatic choroidal melanoma. *South Med J* 1981;74:574-577
3. Egan KE, Seddon JM, Glynn RJ, Gragoudas ES, Albert DM. Epidemiologic aspects of uveal melanoma. *Surv Ophthalmol* 1988;32:239-251
4. Campbell Wilder H, Paul EV. Malignant melanoma of the choroid and ciliary body: a study of 2,535 cases. *Milit Med* 1951;109:370-378
5. Paul EV, Parnell BL, Fraker M. Prognosis of malignant melanomas of the choroid and ciliary body. *Int Ophthalmol Clin* 1962;2:387-402
6. Mavligit GM, Charnsangavej C, Carrasco CH, Patt YZ, Benjamin RS, Wallace S. Regression of ocular melanoma metastatic to the liver after hepatic arterial chemoembolization with cisplatin and polyvinyl sponge. *JAMA* 1988;260:974-976
7. Ruiz RS. Malignant melanoma of the choroid and ciliary body. *Cancer Bull* 1985;37:6-12
8. Shammas HF, Blodi FC. Prognostic factors in choroidal and ciliary body melanomas. *Arch Ophthalmol* 1977;95:63-69
9. Zimmerman LE, McLean IW. The pathogenesis of metastases from uveal melanomas. *Ophthalmic Forum* 1983;1:28-29
10. Char DH. Metastatic choroidal melanoma. *Am J Ophthalmol* 1978;86:76-80
11. Rajpal S, Moore R, Karkousis CP. Survival in metastatic ocular melanoma. *Cancer* 1983;52:334-336
12. Shields JA, Augsburger JJ, Donosa LA, Bernardino VB, Portenar M. Hepatic metastases and orbital recurrence of uveal melanoma after 42 years. *Am J Ophthalmol* 1985;100:666-668
13. Shirikhoda A, Albin J. Malignant melanoma: correlating abdominal and pelvic CT with clinical staging. *Radiology* 1987;165:75-78

Book Review

MRI of the Brain II. Non-Neoplastic Disease. Edited by Michael Brant-Zawadzki and William G. Bradley, Jr. New York: Raven, 216 pp., 1991. \$60

This volume is one of a series of 10 that together make up The Raven MRI Teaching File. The neuroradiology section is contained in five volumes. Three volumes are devoted to the brain, one volume to the spine, and one volume to head and neck imaging. For complete coverage of neuroradiology, the five-volume set must be considered as a single unit. This volume on non-neoplastic disease emphasizes hydrocephalus, infarction, and demyelinating disease. Scattered throughout the text are additional topics, including developmental anomalies, infectious disease, and trauma.

The text is organized in the form of 100 separate unknown case presentations. Each case is an independent unit. A standard format is used throughout the text. On one page, an unknown case is presented. Three to 10 MR images of various T1 and T2 weightings are presented. Occasionally, use is made of gadolinium-enhanced and gradient-echo MR images and of CT scans. After the illustrations, a brief clinical history is given. From this information, readers are expected to develop a differential diagnosis.

On the facing page, the MR findings are summarized, and key findings are emphasized. The correct diagnosis is then given. A discussion follows. It is short, usually less than one third of a page, and highly focused to emphasize a few key teaching points. If the reader desires further information, available references are listed at the bottom of the page.

Emphasis is placed on the disease process. The text does not attempt to provide detailed discussion of MR physics or suggested imaging protocols. Rather, it begins with an abnormality on a clinical image. Basic MR physics and disease pathophysiology are then combined to explain the origin of this abnormality. The book, therefore, recreates the clinical environment, in which the goal is to analyze

an image and then determine the significance of the findings on that image.

The result is a teaching device rather than a reference text. The editor's stated intent is to "help the practicing radiologist rapidly acquire a storehouse of information." They have succeeded. The cases clearly present key teaching points without the use of excessive detail. The format is compatible with a busy practitioner's schedule. Each case requires only a few minutes to evaluate. This is a book that should be kept close at hand for use during those rare short segments of free time.

The quality of the images is variable. Many institutions contributed cases, and this may be the source of the variation. In general, the quality is good, and they are always adequate to illustrate the teaching point.

The book is valuable to a wide audience. For the resident or radiologist new to MR, key teaching points can be learned without the burden of excessive detail. The book offers experienced practitioners a vehicle they can use to evaluate their knowledge of MR imaging. They can thus identify weaknesses that require further study. The text would be extremely valuable to senior residents preparing for board examinations. It is a book that should be circulated. The reader should be tested by it, learn from it, and then pass it on. I therefore particularly recommend it to radiology residency programs, medical libraries, and large radiology groups. In summary, I think this is an excellent teaching device and is worth the purchase price.

Donald P. Mueller
University of Iowa Hospitals and Clinics
Iowa City, IA 52242

Pictorial Essay

Intraventricular Mass Lesions of the Brain: CT and MR Findings

Robert D. Tien^{1,2}

One tenth of all CNS neoplasms involve the ventricles of the brain. These mass lesions are located in areas that are difficult to reach surgically, and because they are intraventricular, spread via the CSF is common. CT and MR imaging have been useful in demonstrating these masses, but imaging characteristics are usually nonspecific. The location of the mass and the patient's age provide the most helpful information in the differential diagnosis.

Mass lesions within the ventricles of the brain represent 10% of all CNS neoplasms. This essay illustrates the CT and

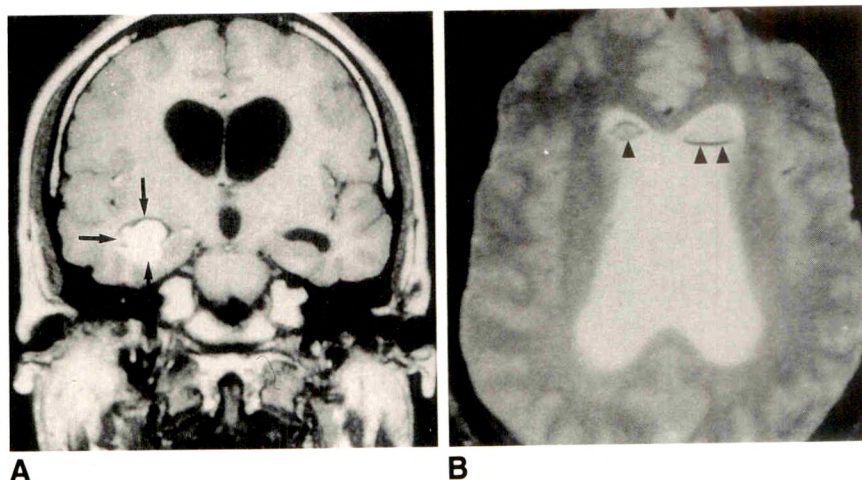
MR features of these lesions, emphasizing the features that aid in differential diagnosis. The MR images illustrating these features are T1 weighted (e.g., 600/20/2 [TR/TE/excitations]), T2 weighted (e.g., 2500/80/2), and proton-density weighted (e.g., 2500/30/2).

Intraventricular tumors are considered together because they are located in the ventricles, deep within the brain, where surgery is difficult. Because of their intraventricular location, they may obstruct the flow of CSF, leading to headache and hydrocephalus. In addition, metastases via the CSF are very common.

Fig. 1.—Ruptured dermoid cyst in temporal horn of 40-year-old man.

A, Coronal T1-weighted MR image (600/20/2) shows hyperintense mass (arrows) filling dilated right temporal horn. Lateral and third ventricles are enlarged.

B, Axial T2-weighted MR image (2500/80/2) shows masses isointense with gray matter at both frontal horns with dark edge (arrowheads) from chemical-shift artifact. MR signal of mass is compatible with that of fat.



Received May 15, 1991; accepted after revision July 17, 1991.

¹ Department of Radiology, University of California Medical Center, 225 Dickinson St., H756, San Diego, CA 92103-1990.

² Present address: Duke Medical Center, Durham, NC 27710. Address reprint requests to R. D. Tien.

AJR 157:1283-1290, December 1991 0361-803X/91/1576-1283 © American Roentgen Ray Society

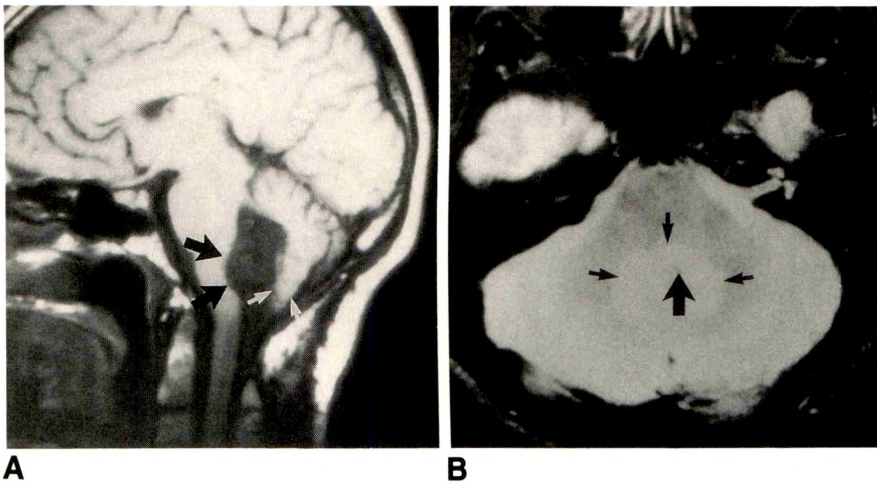


Fig. 2.—Epidermoid tumor in fourth ventricle of 33-year-old man.

A, Sagittal T1-weighted MR image (600/20/2) shows large mass filling fourth ventricle. Mass has slightly higher signal intensity than CSF on T1-weighted image. Brainstem is depressed by mass (black arrows). Tonsil and inferior vermis are elevated by mass (white arrows).

B, Axial T2-weighted MR image (2500/70/2) shows mass isointense with CSF (small arrows). Small, slightly hypointense area is noted within mass (large arrow).

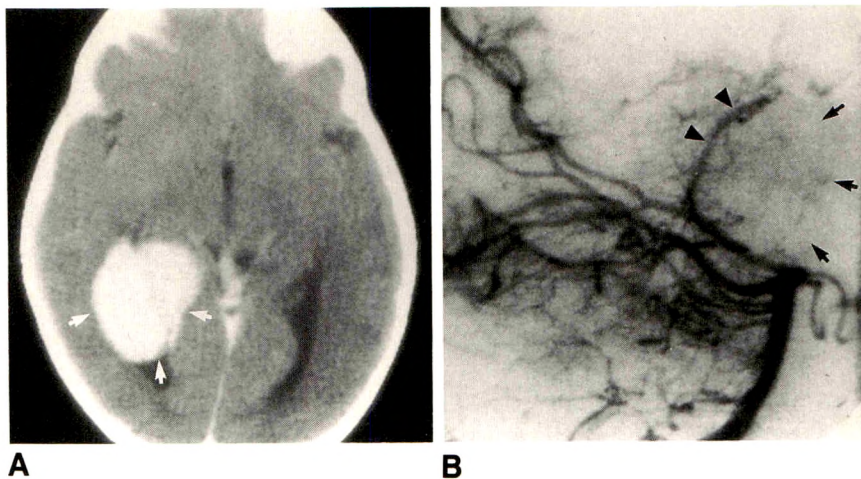


Fig. 3.—Choroid plexus papilloma affecting right trigone of 8-year-old boy.

A, Axial contrast-enhanced CT scan shows large enhancing mass in right trigone (arrows). Initial hydrocephalus was surgically shunted; thus, ventricles are normal in size.

B, Lateral angiogram shows marked tumor blush (arrows) from vascular supply via enlarged posterior choroidal arteries (arrowheads).

The various tumors of the ventricles have similar cell types histologically and have common clinical and anatomic features. Although nearly any CNS tumor can involve the ventricles, some tumors, such as choroid plexus papilloma and colloid cyst, occur almost exclusively intraventricularly.

CT and MR imaging are useful in the diagnosis of intraventricular tumors. In general, MR is superior to CT because of its multiplanar ability and superior spatial resolution. MR imaging is better for defining tumor location, tumor margins, and extent of disease. Both techniques, however, are relatively nonspecific in identifying the type of tumor. Occasionally, dermoid (signal intensity indicative of lipid, Fig. 1) or epidermoid (signal intensity similar to that of CSF, Fig. 2) cysts can be identified by MR imaging. The most useful indications of the specific tissue diagnosis are the anatomic location of the mass and the age of the patient [1–3]. The age divisions used in the essay are arbitrary. Some tumors occur throughout a wide range of ages, and overlap is inevitable. Nevertheless, the division by age is helpful in the differential diagnosis.

Tumors of the Lateral Ventricle

Atrial Lesions

Age less than 10 years: choroid plexus papillomas and carcinomas.—Choroid plexus papillomas (Fig. 3) have a rough, irregular surface and tend to involve the atria of the lateral ventricles. Excessive CSF production frequently causes hydrocephalus. Occasionally, the lesions are heavily calcified.

Carcinoma of the choroid plexus (Fig. 4) occurs mostly in infants and children; it is most common in children 2–4 years old. Direct extraventricular extension with surrounding edema and midline shift is common. Both papillomas and carcinomas frequently show intense contrast enhancement on imaging studies. However, MR signal characteristics of these tumors are nonspecific.

Age 10–40 years: astrocytoma, ependymoma, and vascular malformation.—Astrocytomas show no sex predilection. These tumors are hypovascular and usually enhance less

Fig. 4.—Choroid plexus carcinoma affecting right trigone of 1-year-old girl.

A, Axial unenhanced CT scan shows large, lobulated, hyperdense mass in right trigone with parenchymal invasion and marked edema.

B, Axial contrast-enhanced CT scan shows mass is inhomogeneously enhanced. Hemorrhagic mass was found at surgery.

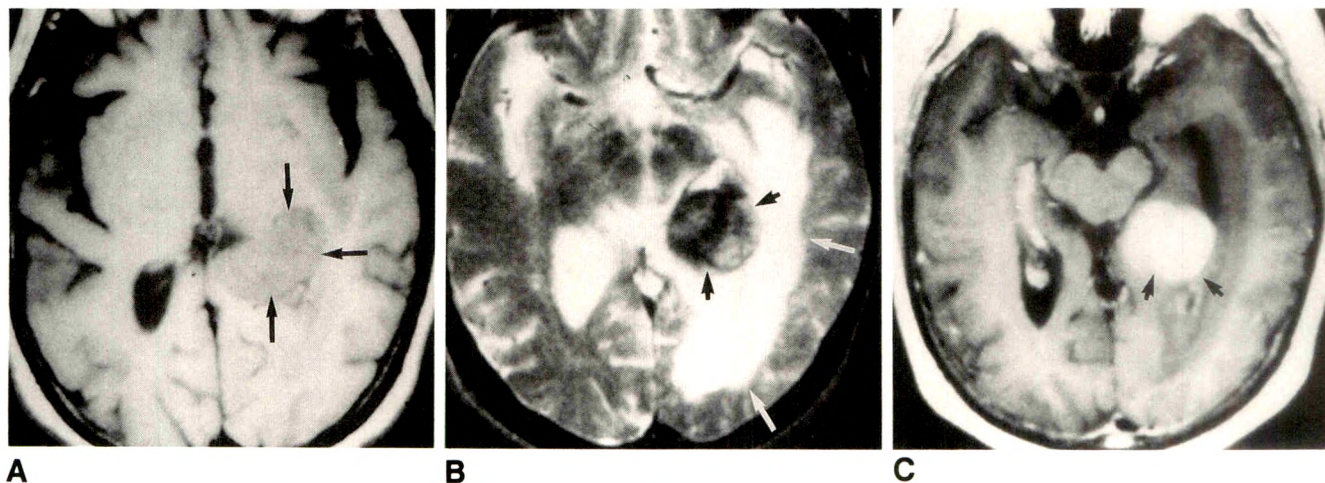
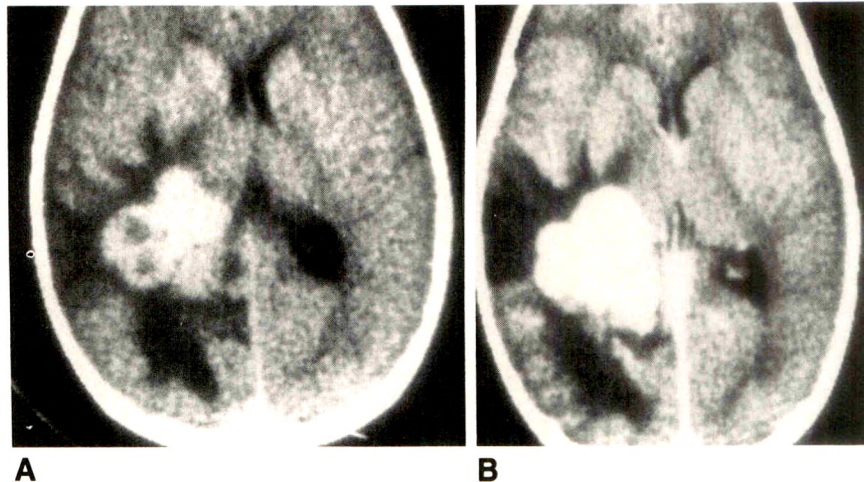


Fig. 5.—Meningioma in left trigone of 68-year-old woman.

A, Axial T1-weighted MR image (600/20/2) shows a 3-cm round mass (arrows) in left trigonal area. Mass is mildly hypointense on T1-weighted image.

B, Axial T2-weighted MR image (2500/80/2). Hypointensity of mass (black arrows) on T2-weighted image can be attributed to known calcification seen on CT images. Peritumoral edema is noted in left periventricular white matter (white arrows). MR T2 shortening effect is not uncommon in meningiomas.

C, Axial T1-weighted MR image (500/20/2) after administration of gadopentetate dimeglumine. Mass has enhanced intensely (arrows).

than other intraventricular mass lesions. Calcification is not uncommon.

Supratentorial ependymoma occurs throughout a wide distribution of ages. Cystic degeneration and inhomogeneous contrast enhancement are common. Calcification occurs in 10–20% of ependymomas.

Vascular malformations involving the choroid plexus are relatively common. Either angiography or MR imaging with flow-sensitive pulse sequences can suggest the diagnosis.

Age greater than 40 years: meningioma or metastasis.—Meningiomas (Fig. 5) constitute about 15% of all brain tumors, with a clear preponderance in older women. If calcification of the tumor occurs, the calcification can be easily seen on CT. The T2 shortening effect on MR images caused by calcification is not uncommon in meningiomas. Edema also is noted frequently around meningiomas. These tumors exhibit intense tumor blush on angiograms and reveal strong contrast en-

hancement. If meningioma is seen in a young patient, an underlying neurofibromatosis should be suspected.

Metastasis to the choroid plexus is rare but is a distinct possibility in older patients, especially in patients known to have cancer.

Lesions of the Body

Age less than 10 years: primitive neuroectodermal tumor, teratoma, and glioblastoma multiforme.—Most primitive neuroectodermal tumors (Fig. 6) are well circumscribed. Enhancement usually is intense and homogeneous. CSF metastasis is common. Cyst formation is not infrequent, especially in infratentorial tumors, often accounting for the large size of the neoplasm; the presence of cysts may signify a more favorable prognosis.

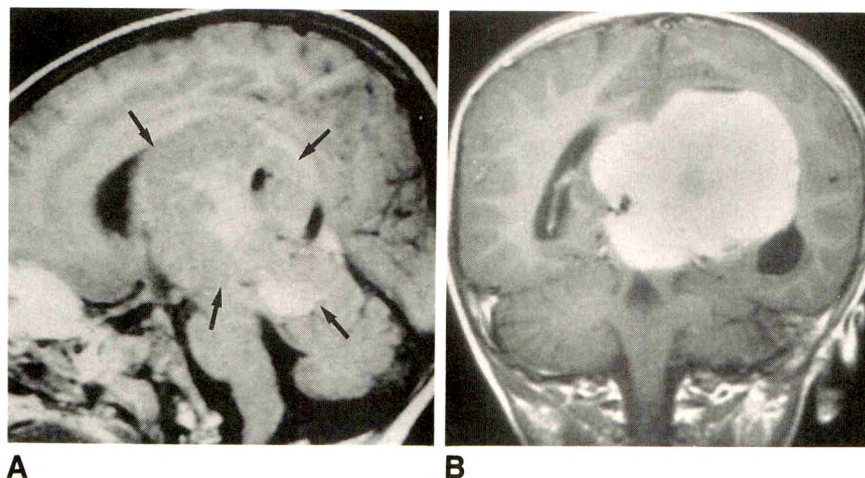


Fig. 6.—Primitive neuroectodermal tumor of lateral ventricle in a 7-month-old boy.

A, Sagittal T1-weighted MR image (800/20/2) shows a large, inhomogeneously isointense intraventricular mass (arrows) that fills entire body of left lateral ventricle and compresses third ventricle, midbrain, and upper vermis of cerebellum.

B, Coronal T1-weighted MR image (800/20/2) after administration of gadopentetate dimeglumine. Mass has enhanced intensely.

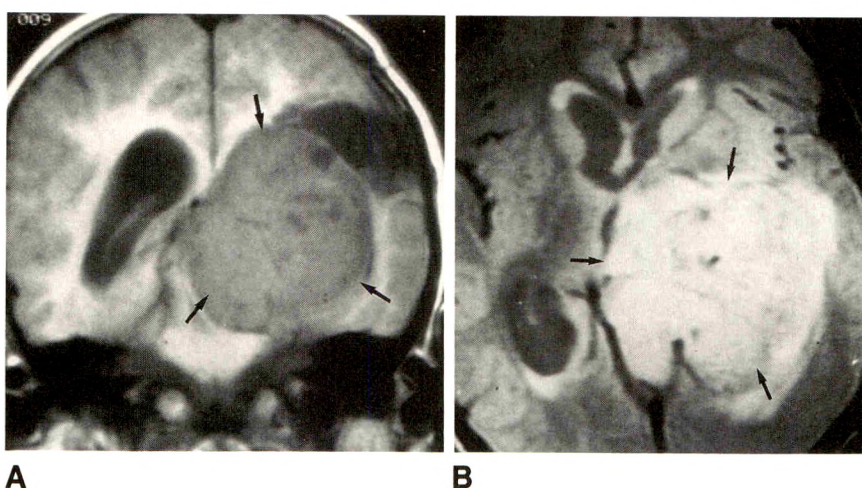


Fig. 7.—Malignant teratoma affecting left ventricle in a 2-year-old boy.

A, Coronal T1-weighted MR image (600/20/2) shows a large, irregular, lobulated mass (arrows) that is inhomogeneously hypointense on T1-weighted image. This mass occupies body and occipital horn of left ventricle.

B, Axial proton density-weighted MR image (2500/30/2) shows mass is hyperintense (arrows) relative to periventricular edema. α -Fetoprotein titer is abnormally high.

Teratomas occur in children less than 1 year old. Various epidermal components, such as fat and calcification, can be identified easily on CT and MR images. The presence of an elevated serum α -fetoprotein titer leads to a diagnosis of malignant teratoma (Fig. 7), endodermal sinus tumor, or embryonal carcinoma [4]. The calcification that is commonly seen in benign teratomas usually is not prominent in these malignant tumors.

Age 10–30 years: ependymoma, astrocytoma, ependymal cyst, and oligodendroglioma.—Oligodendrogliomas (Fig. 8) constitute 5% of intracranial gliomas. Most arise in the frontotemporal region. Recently, somewhat similar lesions have been described, presenting as intraventricular calcified neoplasms in adults. By light microscopy these tumors are virtually indistinguishable from oligodendrogliomas, but by electron microscopy they show evidence of neuronal differentiation, including the presence of synapses. The term central neurocytoma has been proposed for these exceptional tumors.

Age greater than 30 years: lymphoma, astrocytoma, glioblastoma multiforme, oligodendroglioma, and metastasis.—Primary CNS lymphoma (Fig. 9) was a rare brain tumor before

the AIDS epidemic. The number of cases reported has accelerated in the past few years. CNS lymphomas have a highly variable appearance. Many are solid, fairly well defined, space-occupying masses adjacent to lateral ventricles; others appear as a more diffuse infiltration of neural parenchyma. Intraventricular lymphoma is not rare. Lymphomas tend to be mildly hyperintense on unenhanced CT scans and enhance intensely with administration of contrast agent. The MR signal intensities of lymphoma vary, but most tumors are isointense or slightly hyperintense on T2-weighted images.

Lateral ventricular gliomas (Fig. 10) commonly arise from the corpus callosum or thalamus. The septum pellucidum is involved frequently.

Some tumors, such as dermoid (Fig. 1), are congenital lesions that can be detected in patients of any age. CT and MR imaging can show a dermoid's fatty component. A ruptured dermoid might cause leptomeningeal irritation.

Lesions Near the Foramen of Monro

Age less than 10 years: choroid plexus papilloma, ependymoma, teratoma, subependymal giant-cell astrocytoma.—All

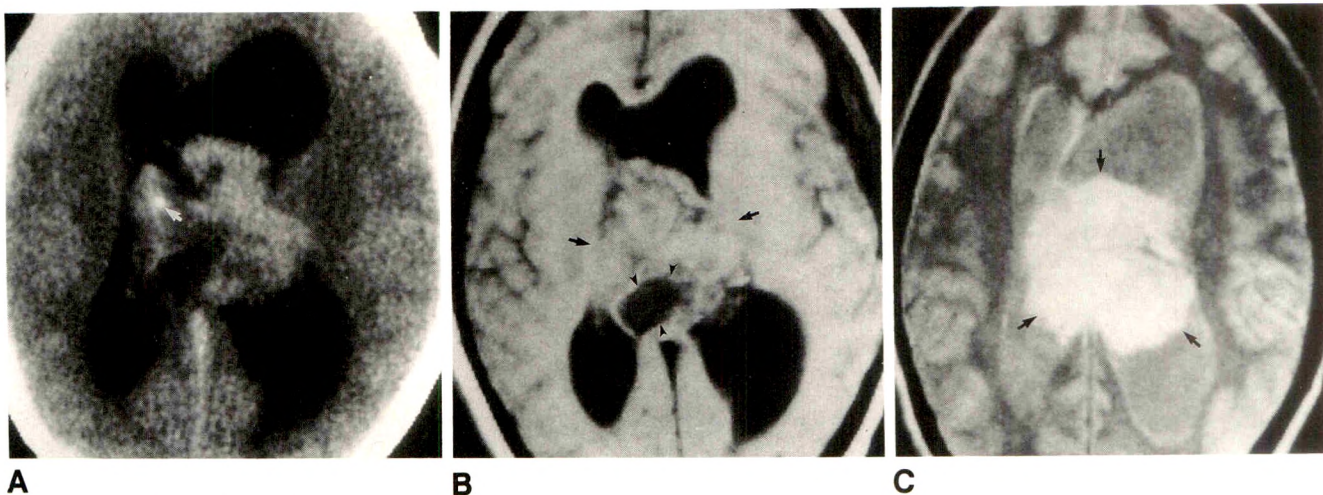


Fig. 8.—Oligodendroglioma affecting lateral ventricles in a 25-year-old man.
A, Unenhanced axial CT scan shows a large, lobulated mass involving septum pellucidum and bodies of lateral ventricles. Calcification was noted (arrow).
B, Axial T1-weighted MR image (600/20/2) shows mass is isointense (arrows) with cystic component (arrowheads).
C, Axial proton density-weighted MR image (2800/30/2) shows mass is hyperintense (arrows).

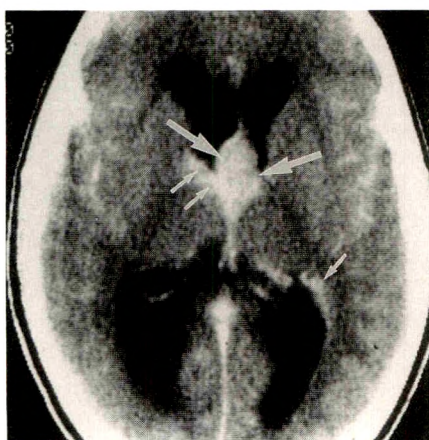
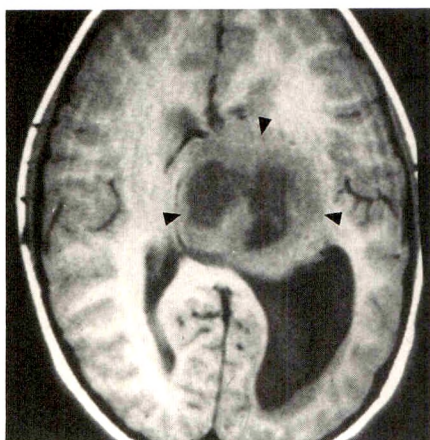
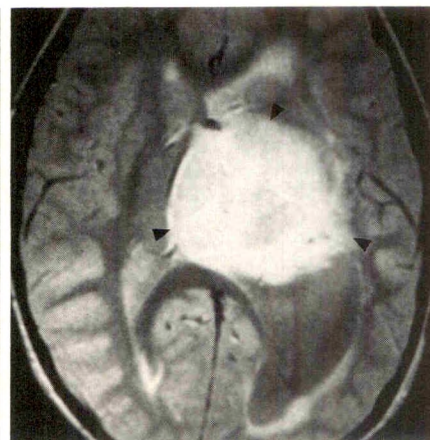


Fig. 9.—Primary CNS lymphoma affecting septum pellucidum in a 40-year-old man with AIDS. Axial contrast-enhanced CT scan shows a fusiform, enhanced mass involving septum pellucidum (large arrows) with subependymal spread (small arrows).



A



B

Fig. 10.—Anaplastic astrocytoma affecting lateral ventricles and septum pellucidum in a 53-year-old man.
A, Axial T1-weighted MR image (600/20/2) shows a bulky, inhomogeneously hypointense infiltrative mass (arrowheads) in lateral ventricles involving both thalamus and septum pellucidum. Left occipital horn is markedly dilated.
B, Axial proton density-weighted MR image (2500/30/2) shows mass to be hyperintense (arrowheads).

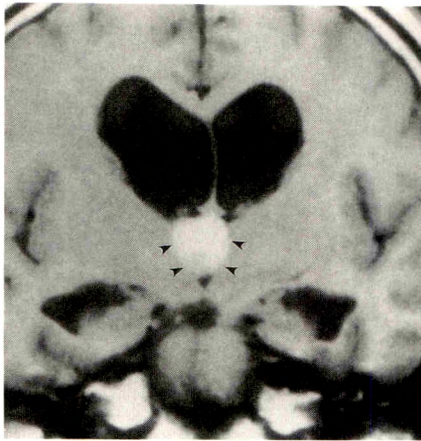
of these tumors can be seen in children less than 10 years old.

Age 10–40 years: colloid cyst, subependymal giant-cell astrocytoma, astrocytoma, and ependymoma.—Colloid cysts (Fig. 11), which are the most common lesions occurring near the foramen of Monro, are smooth and spherical, varying in size from 0.3 cm to 3.0–4.0 cm in diameter. The cysts are either isodense or hyperdense on unenhanced CT scans, and enhance inhomogeneously (usually with capsular enhancement) when contrast medium is used. The MR signal intensi-

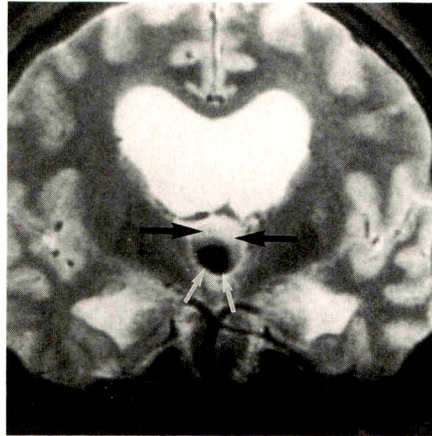
ties of colloid cysts are highly variable owing to their contents. Their characteristic location and morphology are the most useful clues for accurate radiologic diagnosis.

Subependymal giant-cell astrocytomas (Fig. 12) are slow-growing tumors frequently occurring in patients with tuberous sclerosis. Hydrocephalus due to blockage of the foramen of Monro by the mass is common. Cysts of various sizes may be present, and focal calcifications are frequent. Enhancement with contrast material is a common feature.

Age greater than 40 years: colloid cyst, subependymoma,



A

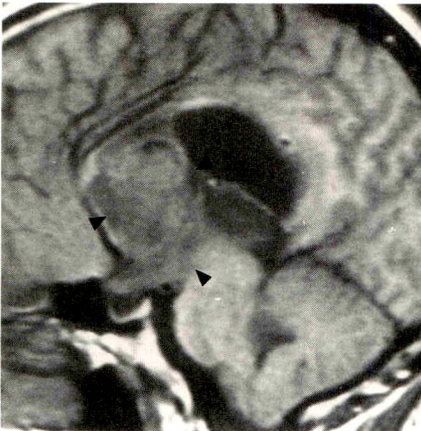


B

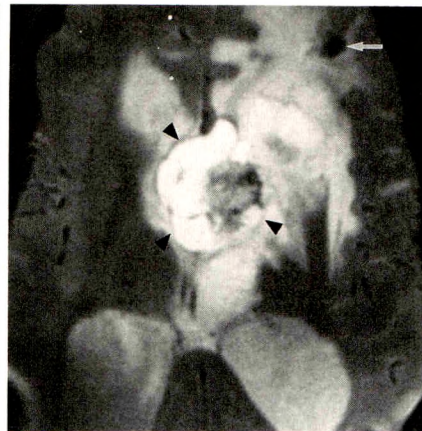
Fig. 11.—Colloid cyst at foramen of Monro in a 22-year-old man.

A, Coronal T1-weighted MR image (600/20/2) shows a well-circumscribed, round, hyperintense mass (arrowheads) about 1.5 cm in diameter located at foramen of Monro and upper third ventricle. Temporal horns of lateral ventricles are dilated.

B, Coronal T2-weighted MR image (2800/70/2) shows mass to be hyperintense (black arrows) with central hypointensity (white arrows).



A



B

Fig. 12.—Subependymal giant-cell astrocytoma near foramen of Monro in a 16-year-old boy with tuberous sclerosis.

A, Sagittal T1-weighted MR image (600/20/2) shows a large mass with irregular borders in region of foramen of Monro and third ventricle (arrowheads). Mass is inhomogeneously hypointense.

B, Axial T2-weighted MR image (2500/80/2) shows mass has mixed intensity (arrowheads) relative to periventricular edema. Lateral ventricles are dilated. Focus of hypointensity (arrow) at left frontal lobe probably represents a calcified tuber.

and metastasis.—Subependymomas (Fig. 13) usually are asymptomatic and are found only accidentally during autopsy, although a small number reach a large size and cause symptoms. These seem particularly likely to involve the septum pellucidum, foramen of Monro, aqueduct, fourth ventricle, and spinal cord. Contrast enhancement of subependymomas is usually mild. The larger ones frequently show cyst formation, focal calcifications, and hemorrhage.

Metastases (Fig. 14) can occur in any part of the ventricles. Twenty-five percent of patients who die of systemic cancer have CNS metastases at autopsy. Lung cancers, breast cancers, and malignant melanomas are the common neoplasms that metastasize to the ventricles.

Lesions of the Third Ventricle

Most patients with mass lesions of the third ventricle are children and young adults. Craniopharyngiomas arising from the hypothalamus with ventricular invasion and astrocytomas (including juvenile pilocytic astrocytoma) are the most com-

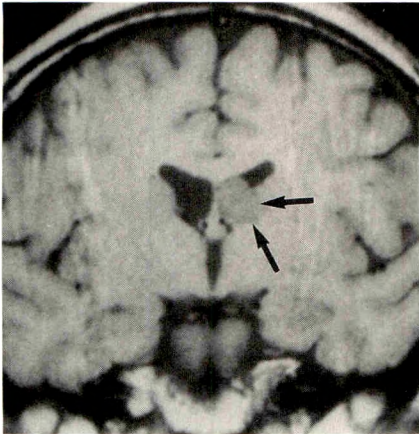
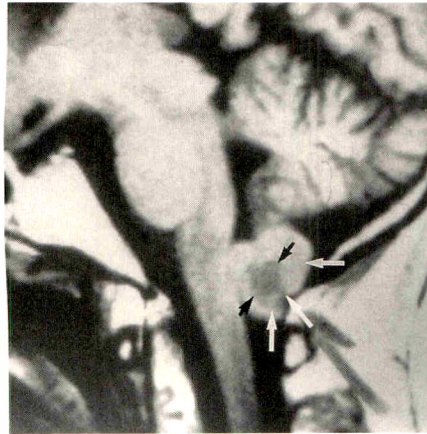
mon entities. Choroid plexus papilloma, ependymoma, and teratoma occasionally are seen in this location.

Craniopharyngiomas have a biphasic distribution with the second peak of occurrence in patients around 50 years old. Cystic degeneration and calcification can be seen in most cases. Unenhanced CT scans can show the calcification. The signal intensity of the mass on MR is highly variable, depending on the components of the cysts.

Juvenile pilocytic astrocytomas (Fig. 15) often are relatively circumscribed, except that those near the third ventricle are apt to infiltrate the optic chiasm and tracts. Cystic degeneration is a common feature. Total extirpation of the enhancing nodule results in a good prognosis or cure.

Lesions of the Fourth Ventricle

Age less than 30 years: medulloblastoma, astrocytoma, ependymoma, and choroid plexus papilloma.—Medulloblastoma (Fig. 16) and astrocytoma usually arise from the cere-

**A****B****Fig. 13.—Subependymoma.**

A, Subependymoma of left frontal horn in a 56-year-old man. Coronal T1-weighted MR image (600/20/2) shows a relatively well defined, isointense mass 1.8 cm in diameter at left frontal horn near foramen of Monro (arrows). Right frontal horn is slightly prominent.

B, Subependymoma of lower fourth ventricle in a 65-year-old man. Sagittal T1-weighted MR image (600/20/2) shows a lobulated mass 2 cm in diameter just beneath fourth ventricle (white arrows). Mass has a slightly hypointense center (center arrows). There is no evidence of hydrocephalus.

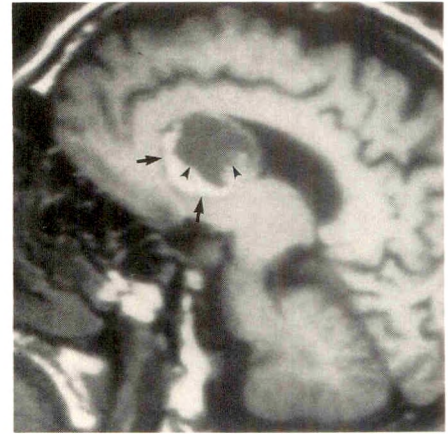
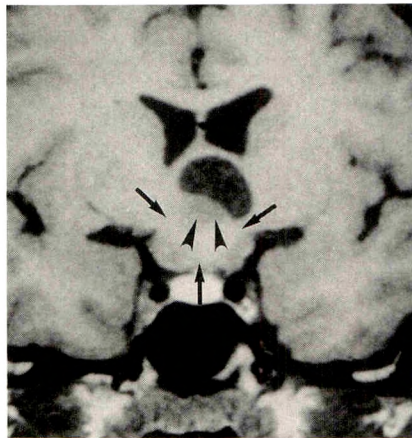
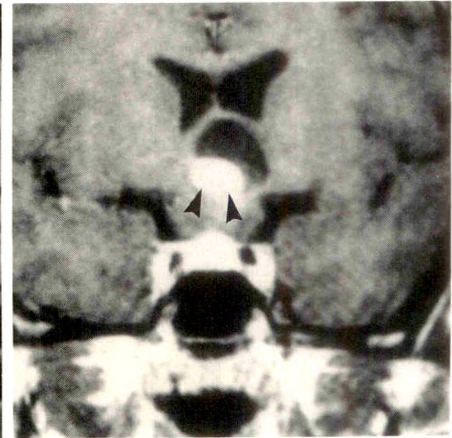


Fig. 14.—Hemorrhagic metastatic melanoma of left frontal horn in a 63-year-old man with systemic melanoma. Sagittal T1-weighted MR image (600/20/2) shows a 2.5-cm round mass filling left frontal horn near foramen of Monro. This mass has a hyperintense rim (arrows), most likely representing methemoglobin from hemorrhage, and a hypointense center (arrowheads). Corpus callosum is normal.

Fig. 15.—Juvenile pilocytic astrocytoma involving hypothalamus and third ventricle in a 14-year-old girl.

A, Coronal T1-weighted MR image (600/20/2) shows a hypothalamic mass involving floor of third ventricle that is largely isointense (arrows), with an area that is slightly hypointense (arrowheads). Third ventricle is markedly dilated.

B, Coronal T1-weighted MR image (600/20/2) after administration of gadopentetate dimeglumine shows intense enhancement in area that is hypointense on unenhanced image (arrowheads).

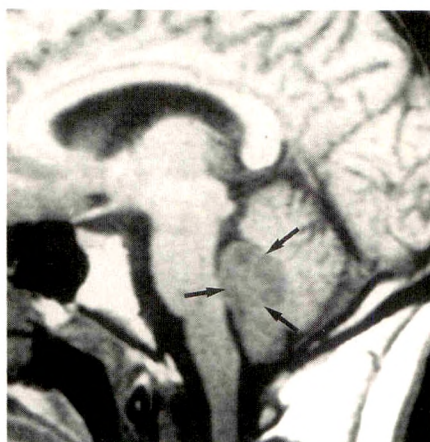
**A****B**

bellum or brainstem with intraventricular invasion. Medulloblastomas are solid and usually show strong contrast enhancement on CT and MR scans. Calcification and cystic change are rarely seen. On the other hand, astrocytomas can have various degrees of calcification, cystic change, and enhancement.

An infratentorially located ependymoma (Fig. 17) is noted in 60–70% of intracranial ependymomas. Frequently, tumors project into the foramen of Luschka, cerebellopontine angle, and even foramen magnum. Calcification and cystic change are common. Contrast enhancement of the solid portion of the tumor is the rule. CSF dissemination is common.

Age greater than 30 years: choroid plexus papilloma, subependymoma, ependymal cyst, epidermoid cyst, meningioma, and metastasis.—Choroid plexus papillomas (Fig. 18) can affect the fourth, lateral, and third ventricles, in that order of frequency. About 50% of choroid plexus papillomas arise in the fourth ventricle. In adults, these tumors are more likely to be infratentorial. The tumor frequently grows via the foramen of Luschka and presents as a cerebellopontine angle mass. Contrast enhancement is intense unless the mass is heavily calcified.

Lesions that are of low density on CT both before and after administration of contrast material include epidermoid (Fig.



A



B

Fig. 16.—Medulloblastoma involving fourth ventricle in a 22-year-old man.
A, Sagittal T1-weighted MR image (600/20/2) shows a mildly hypointense round mass (arrows) about 2 cm in diameter affixed to inferior vermis of cerebellum and protruding into fourth ventricle.
B, Sagittal T1-weighted MR image (600/20/2) after administration of gadopentetate dimeglumine shows no enhancement of mass (arrows); this is highly unusual in medulloblastoma.

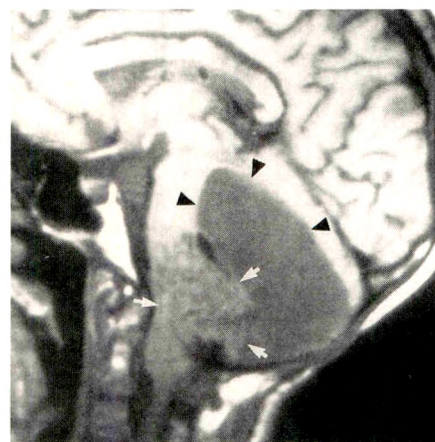
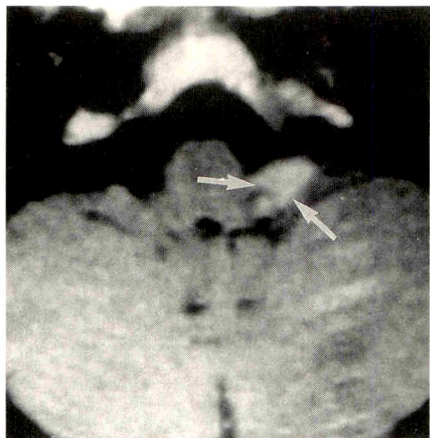
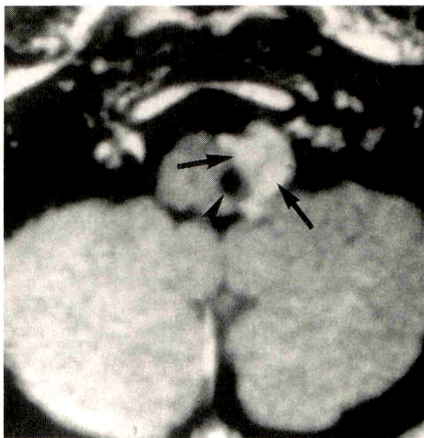


Fig. 17.—Ependymoma of fourth ventricle in a 17-year-old boy. Sagittal T1-weighted MR image (600/20/2) shows a hypointense, infiltrative fourth-ventricular mass (arrows) with large cystic component (arrowheads). This patient has CSF metastasis in spinal canal.



A



B

Fig. 18.—Choroid plexus papilloma involving foramen of Luschka in a 37-year-old man.

A, Axial T1-weighted MR image (600/20/2) after administration of gadopentetate dimeglumine shows a small, lobulated, enhancing mass at left foramen of Luschka of fourth ventricle (arrows).

B, Axial MR image from a level 10 mm above A again shows enhancing tumor (arrows). Mass has a small hypointense component (arrowhead). Tumor does not extend into fourth ventricle, which is normal in size.

2), cysticercosis cyst, and dermoid. MR imaging can help differentiate dermoid from epidermoid.

REFERENCES

1. Kendall B, Reider-Grosswasser I, Valentine A. Diagnosis of masses presenting within the ventricles on computed tomography. *Neuroradiology* 1983;25:11-22
2. Morrison G, Sobel DF, Kelley WM, Norman D. Intraventricular mass lesions. *Radiology* 1984;153:435-442
3. Jelinek J, Smirniotopoulos JG, Parisi JE, Kanzer M. Lateral ventricular neoplasms of the brain: different diagnosis based on clinical, CT, and MR findings. *AJR* 1990;155:365-372
4. Tien RD, Barkovich AJ, Edwards MSB. MR imaging of pineal tumors. *AJR* 1990;155:143-151

Stroke Associated with Coronary Artery Bypass Surgery

Joseph H. Hise¹
Michael L. Nipper
Jonathan C. Schnitker

Medical records and neuroimaging studies of 30 patients with major neurologic events after coronary artery surgery were reviewed. Two thousand and twenty-nine coronary artery bypass graft operations were performed in our institution between October 15, 1985, and December 27, 1989. Of these, there were 30 documented neurologic events suggesting acute ischemic injury during the intraoperative or the postoperative period. Clinical manifestations included hemiparesis, monoparesis, aphasia, bilateral cortical dysfunction, cortical and brainstem dysfunction, and left homonymous hemianopsia. There were five deaths directly attributable to neurologic injury. Twenty-two patients had a CT scan of the head, of which 15 showed evidence of acute infarction, two suggested watershed lesions from cerebral hypoperfusion, and the remainder showed findings consistent with multiple cerebral emboli or primary intracranial occlusion. Five carotid arteriograms and one digital subtraction arteriogram of the carotids were obtained. Angiographic findings revealed two common carotid artery occlusions, one callosal marginal artery occlusion, and two cases of bilateral high-grade internal carotid stenoses.

Our findings support the contention that in patients who suffer cerebral infarction associated with coronary artery bypass grafting, the main mechanism of injury is cerebral embolization rather than cerebral hypoperfusion.

AJNR 12:811-814, September/October 1991; *AJR* 157:1291-1294, December 1991

In the vascular and neurologic literature, there has long been interest concerning neurologic events after cardiac surgery. Shaw et al. [1] performed a prospective study of neuropsychological symptoms in patients after coronary artery surgery that showed neuropsychological symptoms and/or moderate or severe intellectual dysfunction in a significant number of patients (31% and 24%, respectively). Sotaniemi et al. [2] also evaluated neuropsychological, neurologic, cardiologic, and electroencephalographic findings in patients who had cardiac valve replacement and showed significant long-term neuropsychological consequences in a substantial percentage of these patients. Most recently, Kittner et al. [3] studied historical features relevant to the diagnosis of cardiac embolic strokes and pointed out the need for study of the radiologic features of cerebral vascular events with a possible cardiac source. Major neurologic events are a well-known complication in a small percentage of patients who have undergone coronary artery bypass graft procedures. The purpose of this study was to evaluate the radiologic findings in the CNS in this patient population and attempt to characterize the possible causes of major neurologic events in these patients.

Materials and Methods

The charts, postoperative CT scans, and postoperative cerebral angiograms were reviewed in all patients with clinically documented neurologic events occurring in the postoperative period following coronary artery bypass grafting. Nineteen of the 30 documented neurologic

Received November 16, 1990; revision requested February 11, 1991; revision received April 15, 1991; accepted April 23, 1991.

¹All authors: Department of Radiology, Scott and White Clinic, Texas A & M University College of Medicine, 2401 S. 31st St., Temple, TX 76508. Address reprint requests to J. H. Hise.

0361-803X/91/1576-1291
© American Roentgen Ray Society

events occurred within 24 hr of the surgical procedure. Seven occurred within 24–48 hr of surgery. The remaining four occurred between 48 hr and 11 days following surgery. The time interval between clinical symptoms or signs and the CT scan of the head in 20 of the 22 patients who had CT scans ranged from 2 hr to 96 hr, with a mean under 40 hr. The time interval between clinical signs and symptoms and CT scan in one of the 22 patients is not known, and in one patient was under 20 days.

Results

Of the 30 patients with neurologic deficits, 22 had head CT scans. The clinical presentations included hemiplegia or hemiparesis (19), monoparesis (one), aphasia (three), homonymous hemianopsia (one), "bioccipital stroke" (one), and diffuse cortical dysfunction or cortical and brainstem dysfunction (10). Two patients had head scans consistent with watershed infarction. In the first patient, the lesion was along the junction between the left anterior cerebral artery and the left middle cerebral artery distribution (Fig. 1). In the second patient, the lesion was located at the junction of the left middle cerebral artery and left posterior cerebral artery territories. An arteriogram obtained in this patient showed complete occlusion at the origin of the left internal carotid artery with ulceration. Of the remaining positive head scans, eight revealed infarctions within a single vascular territory while five had studies demonstrating infarction in more than one vascular territory (Fig. 2). Six of the patients in this group had angiographic studies, the results of which are summarized in Table 1. There were five deaths directly attributable to neurologic injury. Two of the patients had postmortem examinations. One of the two had a prior CT scan. The mortality rate associated with CNS infarction following bypass surgery was 16%.

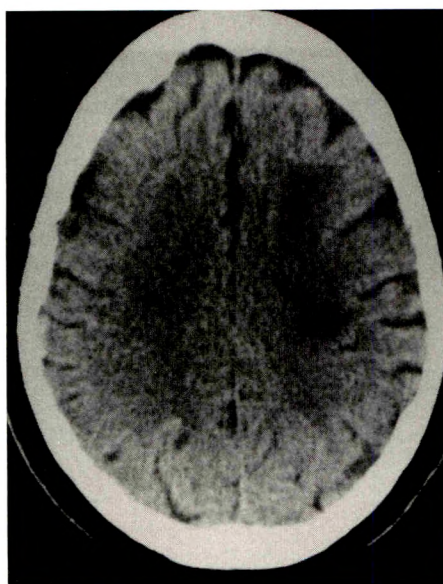
Discussion

Coronary artery bypass grafting is the most frequently performed cardiac surgery in the United States, with approximately 230,000 procedures performed in 1987 [4].

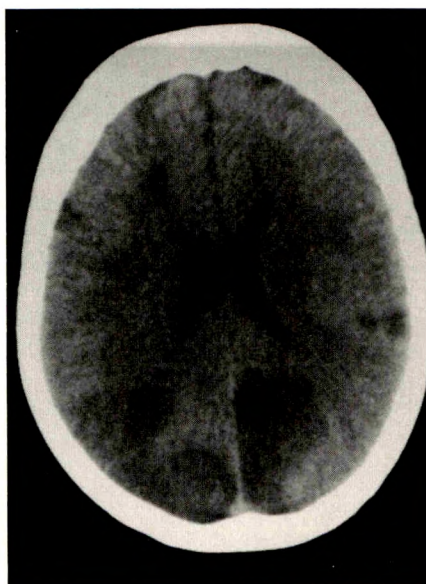
The frequency of stroke among patients undergoing coronary revascularization has been reported to be between 0.9% and 5.9%. Although the exact causes of stroke following coronary artery bypass graft are largely unknown, there has been extensive discussion of this complication in the surgical and neurologic literature [5–10]. Intraoperative hypotension, microemboli consequent to cardiopulmonary bypass apparatus, macroemboli from diseased heart valve, left ventricular thrombus, or an atheromatous aorta during cross clamping or cannulation have been implicated as causes of cerebral complications following bypass surgery [7]. Emboli forming at the proximal anastomosis of the vein graft have also been implicated as a cause of infarction following bypass. Inadvertent puncture of a carotid artery while attempting internal jugular vein cannulation, cardiac arrhythmias, and postoperative hypotension are other possible causes [6].

There is little information on this subject in the radiology literature and we found only a single reference in which CT scanning was used to search for the cause of bilateral visual field defects in a patient who had undergone a coronary artery bypass graft and excision of a myocardial aneurysm [11].

Of our patients with positive head scans, 13 showed evidence of injury suggesting an embolic source or, less likely, a primary intracranial occlusion. Five of the head scans were quite striking, with multiple acute infarctions in different vascular territories. Primary intracranial occlusion as a cause of infarction was considered less likely than embolism. All patients with single vascular territory occlusions presented in the immediate postoperative period and the occlusion pre-



1



2

Fig. 1.—CT scan of watershed infarction at boundary of left middle cerebral artery and left anterior cerebral artery.

Fig. 2.—CT scan of multiple infarctions in several internal carotid artery branch distributions, including right posterior cerebral artery, left posterior cerebral artery, right middle cerebral artery, and left middle cerebral artery, consistent with an embolic origin.

TABLE 1: Findings in 30 Patients with Cerebral Events After Coronary Artery Surgery

Case No.	Age (years)	Sex	Time to Clinical Signs or Symptoms	Time from Signs or Symptoms to CT Scan	Clinical Presentation	Cerebral CT Scan Findings	Cerebral Angiography or Postmortem Findings
1	53	M	<24 hr	<48 hr	Rt hemiplegia	Lt middle cerebral artery infarction	
2	66	F	<24 hr	<48 hr	Rt hemiparesis	Lt middle cerebral artery infarction, L lacunar infarction	Cerebral angiogram with 75% stenosis of the L internal carotid artery and 90% stenosis of the R internal carotid artery 10 days before coronary artery surgery
3	69	M	52.5 hr ^a	<96 hr	Lt homonymous hemianopsia	Rt posterior cerebral artery infarction	
4	72	M	22 hr	—	"Bioccipital stroke"		
5	70	M	24–48 hr	Unknown	Coma; death	Ventriculomegaly and Lt cerebellar infarction	Lt cerebellar hemorrhagic infarction and tonsillar herniation at autopsy
6	61	M	<12 hr	<12 hr	Coma; death	Infarctions in the Lt posterior cerebral artery, Lt middle cerebral artery, and Rt middle cerebral artery distributions	
7	61	F	<12 hr	60 hr	Coma	Infarctions in the Lt posterior cerebral artery, Lt middle cerebral artery, Rt posterior cerebral artery, Rt middle cerebral artery distributions	
8	70	M	Immediate post-operative period	—	Coma; death		
9	79	M	Immediate post-operative period	75 hr	Rt hemiplegia	Normal	
10	76	M	48 hr	26 hr	Rt hemiplegia; confusion	Atrophy	
11	69	M	24–48 hr	15 hr	Aphasia; Rt hemiparesis	Lt middle cerebral artery–Lt posterior cerebral watershed infarction	Cerebral angiography with Lt common carotid occlusion and ulceration
12	70	F	<24 hr	—	Death		Rt parietal and pontine infarctions at autopsy
13	66	M	11 days ^b	2 hr	Rt hemiparesis	Normal	Cerebral angiogram normal 2 days after coronary artery surgery
14	81	M	<48 hr	—	Lt hemiplegia		
15	65	M	<48 hr	<48 hr	Lt hemiparesis	New Rt posterior cerebral artery and Rt middle cerebral artery infarctions, old Lt middle cerebral artery and L posterior cerebral artery infarctions	Angiogram several years prior demonstrated minor bilateral arteriosclerotic disease
16	60	F	<24 hr	36 hr	Lt arm and Rt leg weakness; coma	Bilateral middle cerebral artery and Lt cerebellar infarctions	
17	89	M	24 hr	12 hr	Coma	Large Rt posterior cerebral artery infarction	
18	51	F	<24 hr	7 hr	Rt hemiplegia	Large Lt middle cerebral artery infarction	
19	66	F	<24 hr	<20 days	Rt hemiplegia	Lt anterior cerebral artery–Lt middle cerebral artery watershed infarction	
20	65	M	<24 hr	12 hr	Rt hand weakness	Subdural fluid collections	
21	69	M	<48 hr	<36 hr	Rt hemiparesis, coma; death	Small Lt anterior cerebral artery infarction	Postoperative angiogram demonstrated Lt callosal marginal artery occlusion
22	68	M	48–96 hr	6 hr	Aphasia	Normal	Digital subtraction angiogram demonstrated a Rt common carotid artery occlusion

TABLE 1: Continued.

Case No.	Age (years)	Sex	Time to Clinical Signs or Symptoms	Time from Signs or Symptoms to CT Scan	Clinical Presentation	Cerebral CT Scan Findings	Cerebral Angiography or Postmortem Findings
23	73	M	Immediate post-operative period	—	Lt hemiparesis		
24	69	M	<24 hr	<88 hr	Rt hemiplegia	Lt middle cerebral artery infarction	
25	70	M	<24 hr	56 hr	Lt hemiparesis	Atrophy	
26	76	M	5 days	<24 hr	Aphasia/Rt hemiparesis	Old Lt lacunar infarction	Postoperative angiogram demonstrated 50% stenosis in the Lt internal carotid artery, >50% stenosis in the Rt internal carotid artery, high-grade stenosis in the supraclinoid portion of the Lt internal carotid artery
27	72	F	Immediate post-operative period	—	Lt hemiparesis		
28	72	F	Immediate post-operative period	—	Lt hemiparesis		
29	68	M	<48 hr	—	Lt hemiparesis		
30	71	M	<24 hr	<84 hr	Coma	Lt posterior cerebral artery, Lt middle cerebral artery, and Rt middle cerebral artery infarctions	

Note.—Rt = right, Lt = left.
^a This was the first time the patient used his glasses.
^b This neurologic event may be unrelated to the coronary artery surgery.

sumably would have occurred during a time when the patient was anticoagulated. One of the two patients with a watershed pattern infarction on the CT scan had a carotid angiogram showing complete carotid occlusion. The patient with the watershed pattern infarction at the junction of the left anterior and middle cerebral artery territories had a CT scan showing a subcortical infarction in this distribution. Given the unilaterality of the finding and the positive correlation with the acute neurologic deficit, it is unlikely that this lesion could represent preexisting microangiopathic leukoencephalopathy. There were five patients with either a previous CT or MR examination of the brain available for review. This group's postoperative scan findings included two patients with single distribution infarctions, two patients with multiple distribution infarctions, and one patient with a watershed distribution infarction. None of these lesions was present on previous CT or MR examinations. Of the three remaining patients with positive head scans and postoperative cerebral arteriograms, one showed direct evidence of emboli with an abrupt cutoff of the left callosal marginal artery and clinical findings of diffuse cortical dysfunction suggesting multiple other emboli below the limits of angiographic resolution. Another patient had carotid angiograms in the postoperative period that showed stenoses at both common carotid artery bifurcations with 75% stenosis on the left and 90% stenosis on the right. The infarction in this patient occurred in the distribution of the left carotid artery. A single patient who did not have a CT scan of the head underwent an autopsy. The autopsy findings showed pontine and right parietal infarctions consistent with an embolic origin.

Although hypotension and watershed infarction play a sig-

nificant role in neurologic injury during and following coronary artery bypass surgery, our findings suggest that the majority of patients with severe neurologic dysfunction have suffered embolic infarctions.

REFERENCES

1. Shaw P, Bates D, Cartlidge N, et al. Neurologic and neuropsychological morbidity following major surgery: comparison of coronary artery bypass and peripheral vascular surgery. *Stroke* **1987**;18:700-707

2. Sotaniemi K, Mononen H, Hokkanen T. Long-term cerebral outcome after open-heart surgery: a five-year neuropsychological follow-up study. *Stroke* **1986**;17:410-416

3. Kittner S, Sharkness C, Price T, et al. Infarcts with a cardiac source of embolism in the NINCDS stroke data bank: historical features. *Neurology* **1990**;40:281-284

4. Killip T. Twenty years of coronary bypass surgery. *N Engl J Med* **1988**;319:366-368

5. Reed G, Singer D, Picard E, DeSanctis R. Stroke following coronary-artery bypass surgery. *N Engl J Med* **1988**;319:1246-1250

6. Breuer A, Furlan A, Hanson M, et al. Central nervous system complications of coronary artery bypass graft surgery: prospective analysis of 421 patients. *Stroke* **1983**;14:682-687

7. Shaw P, Bates D, Cartlidge N, et al. An analysis of factors predisposing to neurological injury in patients undergoing coronary bypass operations. *Q J Med* **1989**;267:633-646

8. Gravlee G, Hudspeth A, Toole J. Bilateral brachial paralysis from watershed infarction after coronary artery bypass. *J Thorac Cardiovasc Surg* **1984**;88:742-747

9. Coffey C, Massey E, Roberts K, Curtis S, Jones R, Pryor D. Natural history of cerebral complications of coronary artery bypass graft surgery. *Neurology* **1983**;33:1416-1421

10. Gardner T, Horneffer P, Manolio T, et al. Stroke following coronary artery bypass grafting: a ten-year study. *Ann Thorac Surg* **1985**;40:574-581

11. Smith J, Cross S. Occipital lobe infarction after open heart surgery. *J Clin Neuro Ophthalmol* **1983**;3:23-30

The reader's attention is directed to the commentaries on this article, which appear on the following pages.

Commentary

A New Role for Radiologists in the Development of Cardiac Surgery

Dixon M. Moody¹

Question: What iatrogenic situation will permanently injure the brain of more than 150,000 Americans this year and has never been the subject of an article in the radiologic literature?

Answer: Neurologic or neuropsychological complications of cardiac surgery. Hise et al. [1] deserve credit for bringing this matter to our attention.

The introduction of cardiopulmonary bypass (CPB) pump perfusion, the result of two decades of design and experimentation by Dr. John H. Gibbon at Massachusetts General Hospital and later Jefferson Medical College, has made cardiac surgery feasible. Its use has become widespread: 400,000 operations are performed yearly in the United States using this technology [2]. Putting this figure into perspective, the rate is nearly 30 times that of intracranial aneurysm surgery. One measure of a successful operation is that all of the noncardiac organs function at least as well after surgery as before. There is mounting evidence that one, the brain, does not. In a retrospective review of complications among cardiac surgery patients [3], the frequency of altered mental state was reported to be 3.4%, with a 1% reported rate of stroke. Hise et al. [1] have described the CT findings in a similar group of patients; that is, the 1% who will be found to have "stroke" retrospectively.

More recently, prospective testing has revealed a 24–34% rate of occurrence of permanent neurologic or neuropsychological deterioration after cardiac surgery [4–7]. One study [8] showed increased levels of a CSF enzymatic marker of brain injury (adenylate kinase) after heart surgery. (The disturbing issue of brain dysfunction in a smaller but significant

number of older patients undergoing major surgery apart from the heart [6] must be investigated further.)

Early CPB devices were reused, so that in spite of meticulous cleaning, many problems were caused by inadvertent injection of old blood products. There were and continue to be problems related to trauma to blood elements and foaming in the oxygenator. Filters have been developed for the system, but because they may cause trauma to blood elements if the filter size is below 40 μm , their value has been questioned [5]. Oily silicone antifoam agents were introduced into the system to remove air bubbles, but these agents were shown to embolize to the brain [9–11] and they are no longer used [12, 13]. Fat emboli have been documented after CPB [14, 15]. Air bubbles are known to embolize to the brain, but with the use of membrane oxygenators they are no longer considered to be a problem [13].

Focal neurologic deficits can occur in association with a large air embolism as a result of restarting cardiac pulsation without completely evacuating air in the cardiac chambers. Focal neurologic deficits can also occur in association with local hypoperfusion and particulate *macroemboli* (atherosclerotic plaque disruption at the site of aortic cannulation, calcium or vegetation fragments from valve manipulation, other exogenous debris from field-aspirated fat globules or blood clots). *Diffuse* neurologic and neuropsychological deficits are presumably due to *global* hypoperfusion or myriad *microemboli*. Microembolic agents could be platelet aggregates, chylomicrons, tiny air bubbles, glove powder, tube fragments, silicone, antifoam materials, or phospholipid remnants of dam-

This article is a commentary on the preceding article by Hise et al.

¹ Department of Radiology, Bowman Gray School of Medicine, The Wake Forest University, Medical Center Blvd., Winston-Salem, NC 27157-1088.

aged red blood cell membranes. Another source of emboli could be the fat globules that accumulate on the surface of field-aspirated blood.

In spite of recent improvements in CPB, there is evidence that emboli still occur. Blauth et al. [16] reported abrupt termination of blood flow in retinal vessels as seen by fundus fluorescein angiography during CPB, presumably resulting from small emboli. Using transcranial Doppler sonography, Padayachee et al. [17] noticed disturbances believed to be arterial microemboli with both membrane and bubble oxygenators during CPB. Moody et al. [18] demonstrated multitudinous small emboli in brain and other tissues in autopsy material from humans and research dogs following CPB. In that study histochemical staining of thick sections permitted visualization of long segments of the microvasculature on a single slide. In another study [19], investigators established that cerebral blood flow dramatically diminishes during CPB and does not return to normal levels at the end of the procedure. Some global phenomena—such as autoregulation, decreased metabolic requirement, or reaction to cooling—are thought to be the cause. Such a response is also compatible with multiple semipermanent microembolic events. In all four studies [16–19] the origin or composition of the microemboli was not determined conclusively. There may be several different varieties of these offending agents.

Recently, two groups of investigators have reported prospective MR imaging in cardiac surgery patients. First, Schmidt et al. [20] described findings in 10 patients before and after coronary artery bypass grafting (CABG). No change was found in the MR studies, but the three patients with postoperative neurologic complications had infarcts or basal ganglia lacunae prior to surgery. Therefore, it is possible that a subgroup exists, identifiable by MR imaging, that can be expected to have a poor neurologic outcome with heart surgery. Second, DeLaPaz et al. (paper presented at the annual meeting of the ASNR, Washington, DC, June 1991) reported findings in 16 patients who underwent cardiac valvular surgery. One half of the patients had new findings on MR studies after the operation, and two of these had appropriate neurologic deficits. Valvular surgery is believed to be more dangerous than CABG. My own judgment is that the conclusions of imaging studies purporting to establish the cause (hypoperfusion vs embolization, or embolism of “hard” products such as calcium vs “soft” products such as air or blood clots) of brain injury in this situation are questionable at best.

During cardiac surgery pulsatile perfusion is replaced most often by constant-pressure perfusion. It is possible that the pulsatile nature of flow has an as yet unknown salutary effect. Certain deep vascular beds of the brains of elderly patients may be irrigated only during the successive peaks of pulsatile perfusion [21].

Cardiac surgery has become safer, and further improvements can be anticipated. In the future, improved design of materials in the CPB apparatus may incite less inflammatory response and may be less traumatic to blood cells. Anesthesia protocols are also under investigation [2]. *N*-methyl-D-aspartate antagonists, calcium channel blockers, perfluorocarbons, blood glucose management, and other manipulations that might protect brain tissue during CPB are under consideration for clinical trials.

Sensitive new instruments for imaging alterations in brain

composition (MR) and metabolism (MR spectroscopy, PET, SPECT) will be instrumental in the next phase of the development of cardiac surgery. I believe there will be a role for radiologists in the development of modern cardiac surgery in the area of patient selection and outcome studies.

ACKNOWLEDGMENT

Special thanks to Donna McCain for manuscript preparation.

REFERENCES

1. Hise JH, Nipper ML, Schnitker JC. Stroke associated with coronary artery bypass surgery. *AJNR* 1991;12:811–814; *AJR* 1991;157:1291–1294
2. Reves JG, Croughwell N, Jacobs JR, Greeley W. Anesthesia during cardiopulmonary bypass: does it matter? In: Tinker JH, ed. *Cardiopulmonary bypass: current concepts and controversies*. Philadelphia: Saunders, 1989:41–67
3. Coffee CE, Massey EW, Roberts KB, et al. Natural history of cerebral complications of coronary artery bypass graft surgery. *Neurology* 1983;33:1416–1421
4. Sotaniemi KA, Mononen H, Hokkanen TE. Long-term cerebral outcome after open-heart surgery. A five year neuropsychological follow-up study. *Stroke* 1986;17:410–416
5. Aris A, Solanes H, Camará ML, et al. Arterial line filtration during cardiopulmonary bypass. *J Thorac Cardiovasc Surg* 1986;91:526–533
6. Shaw PJ, Bates D, Cartledge NEF, et al. Neurologic and neuropsychological morbidity following major surgery: comparison of coronary artery bypass and peripheral vascular surgery. *Stroke* 1987;18:700–707
7. Smith PLC, Treasure T, Newman SP, et al. Cerebral consequences of cardiopulmonary bypass. *Lancet* 1986;1:823–825
8. Aberg T, Ronquist G, Tyden H, et al. Adverse effects on the brain in cardiac operations as assessed by biochemical, psychometric, and radiologic methods. *J Thorac Cardiovasc Surg* 1984;87:99–105
9. Yates PO, Cassie AB, Dark JF, Jack GD, Riddell AG. The detection of antifoam emboli following perfusion with a heart-lung machine. *Lancet* 1959;1:130
10. Penry JK, Cordell AR, Johnston FR, Netsky MG. Cerebral embolism by antifoam A in a bubble oxygenator system: an experimental and clinical study. *Surgery* 1960;47:784–794
11. Thomassen RW, Howbert JP, Winn DF, Thompson SW. The occurrence and characterization of emboli associated with the use of a silicone antifoaming agent. *J Thorac Cardiovasc Surg* 1961;41:611–622
12. Govier AV. CNS complications after cardiopulmonary bypass. In: Tinker JH, ed. *Cardiopulmonary bypass: current concepts and controversies*. Philadelphia: Saunders, 1989:41–67
13. Edmunds LH, Williams W. Microemboli and the use of filters during cardiopulmonary bypass. In: Utley JR, Betleski R, eds. *Pathophysiology and techniques of cardiopulmonary bypass*. Baltimore: Williams & Wilkins, 1983:101–114
14. Miller JA, Fonkalsrud EW, Latta HL, Maloney JV. Fat embolism associated with extracorporeal circulation and blood transfusion. *Surgery* 1962;51:448–451
15. Ghatak NR, Sinneberg RJ, deBlois GG. Cerebral fat embolism following cardiac surgery. *Stroke* 1983;14:619–621
16. Blauth CI, Smith PL, Arnold JV, et al. Influence of oxygenator type on the prevalence and extent of microembolic retinal ischemia during cardiopulmonary bypass: assessment by digital image analysis. *J Thorac Cardiovasc Surg* 1990;99:61–69
17. Padayachee TS, Parsons S, Theobald R, Linley J, Gosling RG, Deverall PB. The detection of microemboli in the middle cerebral artery during cardiopulmonary bypass: a transcranial Doppler ultrasound investigation using membrane and bubble oxygenators. *Ann Thorac Surg* 1987;44:298–302
18. Moody DM, Bell MA, Challa VR, et al. Brain microemboli during cardiac surgery or aortography. *Ann Neurol* 1990;28:477–486
19. Prough DS, Rogers AT, Stump DA, et al. Hypercarbia depresses cerebral oxygen consumption during cardiopulmonary bypass. *Stroke* 1990;21:1162
20. Schmidt R, Fazekas F, Offenbacher H, et al. Results of pre- and postoperative MRI in coronary artery bypass surgery (CABS) (abstr). *Neurology* 1990; [suppl 1]:324
21. Moody DM, Bell MA, Challa VR. Regional cerebral vulnerability to perfusion deficits in the elderly. *Arch Neurol* (in press)

Commentary

Neuroimaging of Cerebral Infarction Associated with Coronary Revascularization

Cathy A. Sila¹

Coronary artery bypass surgery is the most frequently performed procedure that utilizes cardiopulmonary bypass. Most of the data pertaining to neurologic complications of open heart surgery have been derived from studies of this operation, but they are applicable generally to other forms of cardiac surgery not involving transplantation. Many technical improvements, including membrane rather than bubble oxygenators and in-line filtration, have decreased the risk of introducing macroemboli ($>25\ \mu\text{m}$) into the circulation, although they cannot protect against microemboli of air, fat, and particulate matter [1]. Since the advent of transcranial Doppler imaging as a simple and noninvasive technique for real-time monitoring of intracranial blood flow velocity, two recent studies have described the use of this technique for the intraoperative detection of air and particulate matter microemboli that migrate to the brain during coronary bypass surgery [2, 3]. Pathologic studies in patients and experimental animals following cardiopulmonary bypass surgery have revealed small capillary and arteriolar dilatations (SCADs) ranging from 10 to 40 μm in diameter, most commonly in the cortex and deep nuclei. The speculation that SCADs are sites of previous air or fat emboli needs to be confirmed and correlated with clinical neurologic manifestations [4].

Several retrospective studies on the complications of coronary artery bypass surgery have suggested that the rate of focal cerebral infarction in these patients is from 0.3–2% [5–9]. Prospective studies relying on clinical examination rather than chart review have suggested a higher rate of 4.7–5.2%, of which 2% of patients were severely affected [10, 11]. In

the prospective study by Breuer et al. [11] of 421 patients undergoing coronary artery bypass surgery at the Cleveland Clinic, the authors were unable to correlate a large number of preoperative, intraoperative, and postoperative variables with the risk of stroke. These variables included age, prior transient ischemic attack or stroke, carotid bruit, prior myocardial infarction or dysrhythmias, duration of pump time or aortic cross-clamp time, intraoperative hypertension, type of oxygenator, or reoperation within 48 hr. Although the small percentage of strokes may be a factor in limiting the demonstration of statistical significance of some of these variables, only a history of prior stroke approached statistical significance with an increased risk of stroke during coronary artery bypass surgery. However, potential mechanisms of stroke could be identified in 73% of the patients: these included intraoperative and perioperative cardiac arrhythmias, internal carotid artery atherosclerosis, air embolism, carotid artery trauma during internal jugular vein cannulation, aortic atherosclerosis at the site of aortic cross-clamping, and prolonged intraoperative hypotension [12].

Extracranial carotid artery atherosclerosis is often suggested as an important cause of stroke during coronary artery bypass surgery, which presupposes that severe carotid occlusive disease combined with intraoperative hypotension results in cerebral ischemia. However, most perioperative strokes occur in the absence of significant carotid occlusive disease or have a delayed onset in the postoperative period [13]. Intraoperative transcranial Doppler monitoring of ipsilateral middle cerebral artery blood flow during coronary artery

This article is a commentary on the article by Hise et al.

¹ Department of Neurology, Cleveland Clinic Foundation, One Clinic Center, Cleveland, OH 44195.

bypass surgery has failed to demonstrate significant velocity changes in patients with high-grade internal carotid artery stenosis [14]. In a retrospective study that identified 155 stenotic ($\geq 50\%$) or occluded carotid arteries in 144 patients who had coronary artery bypass surgery, ipsilateral cerebral infarction occurred in 1.1% of patients with 50–90% stenosis, 6.2% of patients with $>90\%$ stenosis, and 2% of patients with carotid occlusion [15]. In a recent study, Hertzner et al. [16] randomly assigned a group of 23 patients with symptomatic or bilateral $>70\%$ carotid stenosis to staged or simultaneous coronary artery bypass surgery and carotid endarterectomy. Among this small group of patients, who had undergone urgent coronary artery bypass grafting alone because of unstable coronary disease, only two (8.7%) developed a perioperative stroke. Although these small studies have too few patients to permit any statistical analysis, they suggest there is a subgroup of patients with carotid disease who are at a somewhat increased risk for stroke during coronary artery bypass surgery but that our ability to identify them preoperatively remains elusive.

In this issue of the *AJR*, Hise et al. [17] describe neuro-radiologic studies of patients suffering major neurologic events after coronary artery bypass surgery. Their data support the proposal that cerebral embolism is the main mechanism of cerebral infarction in the perioperative and postoperative periods. Cerebral hypoperfusion, as implied by a watershed pattern of cerebral infarction, was much less common and related to a complete ipsilateral internal carotid artery occlusion in at least one patient studied with angiography. Their data also support the observation that intracranial hemorrhage is a distinctly uncommon type of stroke after coronary artery bypass grafting.

Postoperative alteration in consciousness ranging from encephalopathy to prolonged coma is often multifactorial and may be related to drug effects, hypoxia, hemodynamic instability, metabolic derangements, sepsis, and intensive care psychosis. The frequency of clinically detectable diffuse encephalopathy ranges from 3–12% [8, 11, 18]. However, careful neuropsychological testing has demonstrated subtle but significant cognitive deficits occurring in up to 30% of patients [19, 20]. A prospective analysis of multiple preoperative, intraoperative, and postoperative variables [11] demonstrated a correlation with the use of intraaortic balloon pump counterpulsation and pressor agents in the postoperative period, which are both markers of severe hypotension. This suggests that in some individuals undergoing coronary artery bypass surgery, cerebral hypoperfusion may be a more important cause of encephalopathy than are focal neurologic deficits. Multifocal microemboli have also been implicated as a mechanism for diffuse encephalopathy, as suggested by the SCAD descriptions, although one recent study using intraoperative transesophageal echocardiography demonstrated that microbubbles, often detected during surgery, were not predictive of postoperative neurologic complications [21]. Further neuro-

radiologic investigation is desperately needed in this area, perhaps employing MR imaging as a high-resolution method for detecting microemboli.

REFERENCES

1. Brennan RW, Patterson RH, Kessler J. Cerebral blood flow and metabolism during cardiopulmonary bypass: evidence of microembolic encephalopathy. *Neurology* 1971;21:65–67
2. Albin MS, Bunegin L, Garcia C, McKay W. The transcranial Doppler can image microaggregates of intracranial air and particulate matter. *J Neurosurg Anesth* 1989;1:134–135
3. Albin MS, Hantler CB, Bunegin L, Grover FL, Cohen DJ, Mitzel H. Intracranial air embolism is detected by the transcranial Doppler (TCD) during cardiopulmonary bypass procedures (abstr). *J Neurosurg Anesth* 1990;2:223–224
4. Moody DM, Bell MA, Challa VR, Johnston WE, Praugh DS. Brain microemboli during cardiac surgery or aortography. *Ann Neurol* 1990;28:477–486
5. Hutchinson JE III, Green GE, Mekhjian HA, et al. Coronary bypass grafting in 376 consecutive patients, with three operative deaths. *J Thorac Cardiovasc Surg* 1974;64:7–16
6. Gonzalez-Scarano F, Hurtig HI. Neurologic complications of coronary artery bypass grafting: case control study. *Neurology* 1981;31:1032–1035
7. Loop FD, Cosgrove DM, Lytle BW, et al. An 11-year evolution of coronary arterial surgery (1967–1978). *Ann Surg* 1979;190:444–455
8. Coffey CE, Massey EW, Roberts KB, et al. Natural history of cerebral complications of coronary artery bypass graft surgery. *Neurology* 1983;33:1416–1421
9. Reed GL III, Singer DE, Picard EH, et al. Stroke following coronary artery bypass surgery: a case control estimate of the risk from carotid bruits. *N Engl J Med* 1988;319:1246–1250
10. Turnipseed WE, Berkoff HA, Belzer FO. Postoperative stroke in cardiac and peripheral vascular disease. *Ann Surg* 1980;192:365–368
11. Breuer AC, Furlan AJ, Hanson MR, et al. Central nervous system complications of coronary artery bypass graft surgery: prospective analysis of 421 patients. *Stroke* 1983;14:682–687
12. Furlan AJ, Breuer AC. Central nervous system complications of open heart surgery. *Stroke* 1984;15:912–915
13. Hart RG, Easton JD. Management of cervical bruits and carotid stenosis in preoperative patients. *Stroke* 1983;14:290–297
14. von Reutern G-M, Hetzel A, Birnbaum D, et al. Transcranial Doppler ultrasonography during cardiopulmonary bypass in patients with severe carotid stenosis or occlusion. *Stroke* 1988;19:674–680
15. Furlan AJ, Craciun AR. Risk of stroke during coronary artery bypass graft surgery in patients with internal carotid artery disease documented by angiography. *Stroke* 1985;16:797–799
16. Hertzner NR, Loop FD, Beven EG, et al. Surgical staging for simultaneous coronary and carotid disease: a study including prospective randomization. *J Vasc Surg* 1989;9:455–463
17. Hise JH, Nipper ML, Schnitker JC. Stroke associated with coronary artery bypass surgery. *AJNR* 1991;12:811–814; *AJR* 1991;157:1291–1294
18. Shaw PJ, Bates D, Cartledge NEF, et al. Early neurological complications of coronary artery bypass surgery. *Br Med J* 1985;291:1384–1387
19. Calabrese JR, Skwerer RG, Gullledge AD, et al. Incidence of postoperative delirium following myocardial revascularization: a prospective study. *Cleve Clin J Med* 1987;54:29–32
20. Sotaniemi KA, Mononen H, Hokkanen TE. Long-term cerebral outcome after open-heart surgery. A five-year neuropsychological follow-up study. *Stroke* 1986;17:410–416
21. Topol EJ, Humphrey LF, Borkon AM, et al. Value of intraoperative left ventricular microbubbles by transesophageal two-dimensional echocardiography in predicting neurologic outcome after cardiac operation. *Am J Cardiol* 1985;56:773–775

Assessment of Carotid Artery Patency on Routine Spin-Echo MR Imaging of the Brain

John I. Lane¹
Adam E. Flanders¹
Huynh T. Doan¹
Rodney D. Bell²

We retrospectively reviewed the routine spin-echo MR studies of the brain in 12 patients with 13 angiographically demonstrated occlusions and in 14 patients with 16 high-grade stenoses of the carotid arteries. Intraluminal signal that was isointense with adjacent brain on long TR/short TE and long TR/long TE images was 100% specific for atherosclerotic occlusion. Of the 13 proved occlusions, six (46%) had significant degrees of hyperintense intraluminal signal indistinguishable from that observed consequent to slow flow distal to high-grade stenoses. MR detected only five (31%) of the 16 proved high-grade stenoses.

Normal flow void does not exclude significant extracranial carotid stenosis. Occlusion cannot always be distinguished from high-grade stenosis when hyperintense intraluminal signal is encountered. However, a reliable diagnosis of atherosclerotic occlusion can be made when isointense intraluminal signal is observed.

AJNR 12:819-826, September/October 1991; *AJR* 157:1299-1306, December 1991

Several recent reports have described the loss of normal flow void within the proximal intracranial arteries distal to extracranial carotid or vertebral lesions on spin-echo (SE) MR imaging of the brain [1-6]. Hyperintense intraluminal signal has been interpreted as thrombus in an occluded vessel or, alternatively, slow flow distal to a high-grade stenosis. Katz et al. [2] recently reported seven cases of atherosclerotic occlusion that had an intraluminal signal that was predominantly isointense with adjacent brain, implying that this appearance is specific for occlusion. The rationale behind their statement was based on the pathologic nature of atherosclerotic occlusion, which is composed primarily of atherosclerotic plaque and fibrinous clot, containing a paucity of RBC thrombus. Disputing the claim that bright intraluminal signal represents thrombus, these authors suggested that markedly hyperintense signal should be interpreted as slow flow.

Heinz et al. [3] coined the term *partial flow void* to describe the intraluminal signal changes distal to extracranial high-grade carotid stenoses that they observed on routine SE sequences of the brain. Their report raised the hope that extracranial high-grade stenoses could be detected reliably on MR studies of the brain [7]. Brant-Zawadzki [4] subsequently reported a series that included six cases of internal carotid artery (ICA) stenoses with normal flow void and two cases of isointense intraluminal signal in the carotid siphon in the absence of complete occlusion.

It is difficult to ascertain the diagnostic value of these intraluminal signal changes without a critical assessment of their specificity and sensitivity in the detection of occlusive and preocclusive disease. Thus, the purpose of our study was to determine the utility of these signal changes in the diagnosis of compromised arterial flow. Our objectives were to determine whether angiography can be obviated in cases of suspected occlusion and to establish whether the presence of normal flow void can be used to exclude significant extracranial stenoses.

Received October 18, 1990; returned for revision December 17, 1990; revision received February 19, 1991; accepted February 27, 1991.

¹ Department of Radiology, Thomas Jefferson University Hospital, 10th and Sansom Sts., Room 1009 Main, Philadelphia, PA 19107. Address reprint requests to J. I. Lane.

² Department of Neurology, Thomas Jefferson University Hospital, Philadelphia, PA 19107.

0361-803X/91/1576-1299
© American Roentgen Ray Society

Materials and Methods

Two hundred thirty-six consecutive patients who had both carotid angiography and SE MR imaging of the brain between January 1987 and January 1990 were considered as candidates for this study. Patients were excluded if there was any significant change in their neurologic state between examinations or if either examination was technically unsatisfactory. Inclusion in this retrospective study required angiographically demonstrated total occlusion of the common carotid artery (CCA) or ICA or stenosis of either artery of greater than 90%. The 90% criterion was based on the degree of stenosis required to produce signal changes in an animal model developed by Heinz et al. [3]. A 90%-diameter stenosis was determined by comparing the narrowest diameter of the artery with the normal caliber of the vessel just distal to the lesion. Following the application of these inclusion criteria, 12 patients (13 vessels) with arteriographic occlusion and 14 patients (16 vessels) with high-grade stenosis were identified. Twenty age-matched control subjects with no hemodynamically significant disease were selected from the study population.

Angiograms were obtained by using intraarterial digital subtraction or conventional film-screen and subtraction techniques. For selective digital subtraction studies, the CCA was injected with 6 ml of 30% sodium diatrizoate at a rate of 4 ml/sec. For conventional studies, 12 ml of 60% sodium diatrizoate was injected at 10 ml/sec for CCA injections.

The MR studies were performed on a 1.5-T Signa scanner (General Electric, Milwaukee, WI). Pulse sequences consisted of short TR/short TE sagittal images, 600/20/1 (TR/TE/excitations), with a 256 × 192 matrix and dual-echo long TR axial and coronal images, 2000/20–80/1, with a 256 × 192 matrix. The slice thickness was 5 mm with a 2.5-mm interslice gap. No gradient-moment nulling or presaturation pulses were used in the studies performed at our institution. Gradient-moment nulling was used in two of three MR studies that had been submitted for consultation from outside institutions and included in our retrospective review. All studies were performed with cardiac gating.

The SE MR studies were reviewed independently of the angiographic studies by three neuroradiologists. Evaluation of the ICAs included assessment of the presence of normal flow void, the configuration of intraluminal signal when normal flow void was absent, and symmetry in the size of the ICAs. The ICAs were scrutinized from the skull base to the subclinoid segments. Any signal changes that were limited to entry or exit slices were excluded. All signal abnormalities had to be seen consistently from the skull base to the subclinoid segments in two orthogonal planes. By virtue of the sequences used, these observations were primarily made on dual-echo long TR images.

Each case was then classified as occlusion, high-grade stenosis, or normal on the basis of the observed intraluminal signal characteristics. The two cases of carotid dissection were excluded from this portion of the study in an effort to avoid potential confusion between intraluminal methemoglobin (consequent to dissection) and hyperintense intraluminal signal (slow flow) distal to a high-grade stenosis. Operating on the premise that atherosclerotic occlusion should appear as isointense intraluminal signal [2], the sole criterion for total occlusion was replacement of normal flow void with intraluminal signal that was predominantly isointense with adjacent brain. The MR criteria for high-grade stenosis included at least one of the following: (1) a reduction in vessel diameter with preservation of flow void; (2) a partial flow-void phenomenon, as described by Heinz et al. [3]; or (3) replacement of flow void with hyperintense intraluminal signal. If no intraluminal signal changes were noted, the study was considered normal.

To determine the reliability of these criteria, truth tables were

constructed for both carotid occlusions and carotid stenoses as diagnosed by SE MR imaging. Evaluating the criteria for carotid occlusion required that high-grade stenosis and normals be considered together in the nonoccluded category. Likewise, evaluating the criteria for high-grade stenosis required that occlusions and normals be considered together in the nonstenotic category.

Results

The occlusion group comprised seven men and five women 41–73 years old (median age, 62), the high-grade stenosis group comprised seven men and seven women 47–80 years old (median age, 60), and the control group comprised 12 men and eight women 33–80 years old (median age, 65). The mean interval between MR and angiography was 3 days. All occlusive and stenotic lesions had an atherosclerotic origin except for two that resulted from spontaneous carotid dissection. One lesion resulted in complete occlusion and the other in marked narrowing of the internal carotid lumen.

Nine of 13 occlusions and 15 of 16 high-grade stenoses were located in the proximal ICA. The distal CCA was the site of disease in four occlusions and one high-grade stenosis.

Intraluminal Signal Changes

The MR signal changes that we observed in both angiographically occluded and stenotic groups are listed in Table 1. A schematic display of the patterns of intraluminal signal observed is presented in Figure 1.

Normal intraluminal flow void was demonstrated in the ICAs of all 20 patients in the control group. The partial-flow-void phenomenon was identified in only three of 16 high-grade stenoses (Fig. 2). One case of an occluded left CCA also demonstrated a partial flow void in the left ICA (Fig. 3). Further review of the arteriogram revealed that the ICA reconstituted from retrograde flow through the left external carotid artery via left vertebral collaterals.

Intraluminal signal was predominantly isointense with brain in six (46%) of 13 occlusions (Figs. 4 and 5). This pattern was not identified in any of the cases of high-grade stenosis.

TABLE 1: Intraluminal Signal Changes on Spin-Echo MR Imaging of Angiographically Demonstrated Occlusion or Stenosis of the Carotid Artery

MR Signal	Angiographic Finding		
	Occlusion	High-Grade Stenosis	Normal
Partial flow void	1 (8)	3 (19)	0
Heterogeneous hyperintensity			
Hyperintense peripherally with central isointense focus	3 (23)	0	0
Central hyperintense focus with peripheral isointensity	3 (23)	1 (6)	0
Eccentric hyperintensity	0	1 (6)	0
Homogeneous hyperintensity	0	1 (6)	0
Isointensity	6 (46)	0	0
Normal	0	10 (63)	20 (100)
Total	13 (100)	16 (100)	20 (100)

Note.—Values represent no. (%) of vessels.

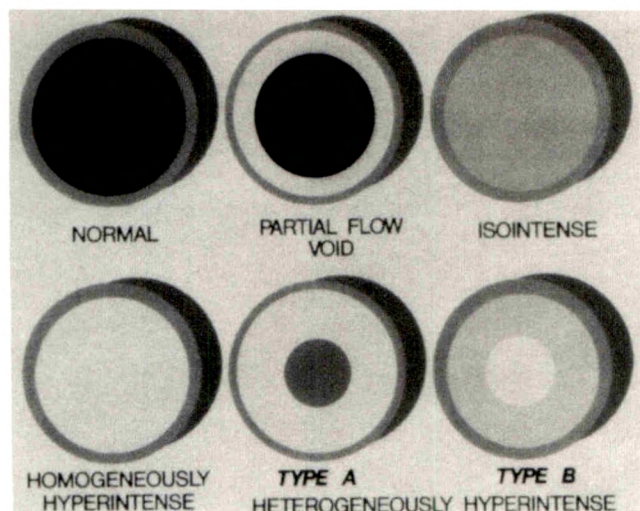


Fig. 1.—Schematic representation of observed intraluminal signal changes on long TR/short TE and long TR/long TE sequences (2000/20–80/1). Black represents flow void, white represents signal hyperintense relative to brain, and gray represents signal isointense with brain.

Hyperintense intraluminal signal had variable appearances on SE MR images; homogeneous and heterogeneous patterns of hyperintensity were observed (Figs. 6–8). These patterns of hyperintense signal were not pathognomonic for occlusion or for high-grade stenosis. One case of hyperintense intraluminal signal was eccentrically located within the vessel lumen.

The results of our effort to predict stenosis or occlusion on the basis of the MR appearance in those patients with atherosclerotic disease are listed in Table 2. The 20 normal control subjects are also included. Statistical analysis of these results is compiled in Table 3. Of particular note is the poor

sensitivity of MR in the detection of proximal high-grade stenoses (33%). When isointense intraluminal signal was used as the sole criterion for atherosclerotic occlusion, a specificity of 100% was obtained. Applying this criterion, however, resulted in a poor sensitivity (50%), since five atherosclerotic occlusions also demonstrated some degree of hyperintense intraluminal signal. There were no false-positive MR diagnoses of occlusion or stenosis in the control group.

Two cases of spontaneous ICA dissection were also included in this study. In one case, which resulted in total occlusion of the proximal ICA, heterogeneously hyperintense signal was seen that was indistinguishable from that produced by atherosclerotic disease on dual-echo long TR images. The second case of dissection, which resulted in marked stenosis of the proximal ICA, produced a partial flow void that also was indistinguishable from that produced by atherosclerotic stenosis.

Discussion

High-velocity signal loss (flow void) within the vessel lumen on SE sequences is a reliable indicator of vessel patency. When this signal loss is replaced by varying degrees of increased intraluminal signal, determination of vessel patency becomes more difficult. Several technical causes of intraluminal signal must be excluded before luminal compromise or occlusion should be considered; among these are flow-related enhancement, diastolic pseudogating, even-echo rephasing, and the use of flow-compensation techniques (gradient-moment nulling). Flow-related enhancement typically is encountered in the first few entry or exit slices of the imaged volume. Familiarity with the location and appearance of flow-related enhancement allows differentiation from pathologic signal changes [8]. Diastolic pseudogating can be eliminated with the use of cardiac gating. Even-echo rephasing can be eliminated by using odd rather than even TEs on long TR se-

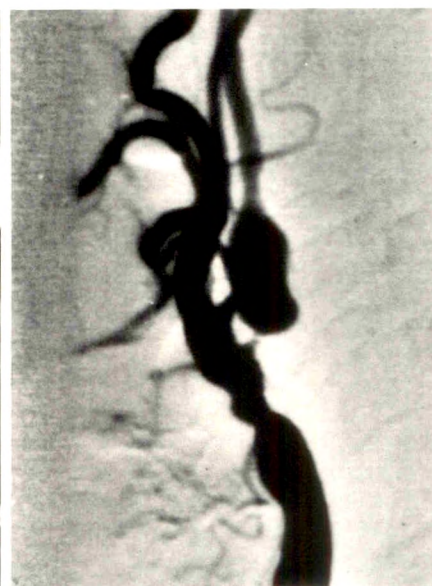
Fig. 2.—Partial flow void.

A, Long TR/short TE image (2000/20/1) shows decreased luminal diameter with peripheral rim of increased signal (partial flow void) in siphon (arrow) of proximal left internal carotid artery (ICA). Note normal flow void in contralateral ICA.

B, Selective injection of left common carotid artery reveals severe stenosis at origin of left ICA.



A



B

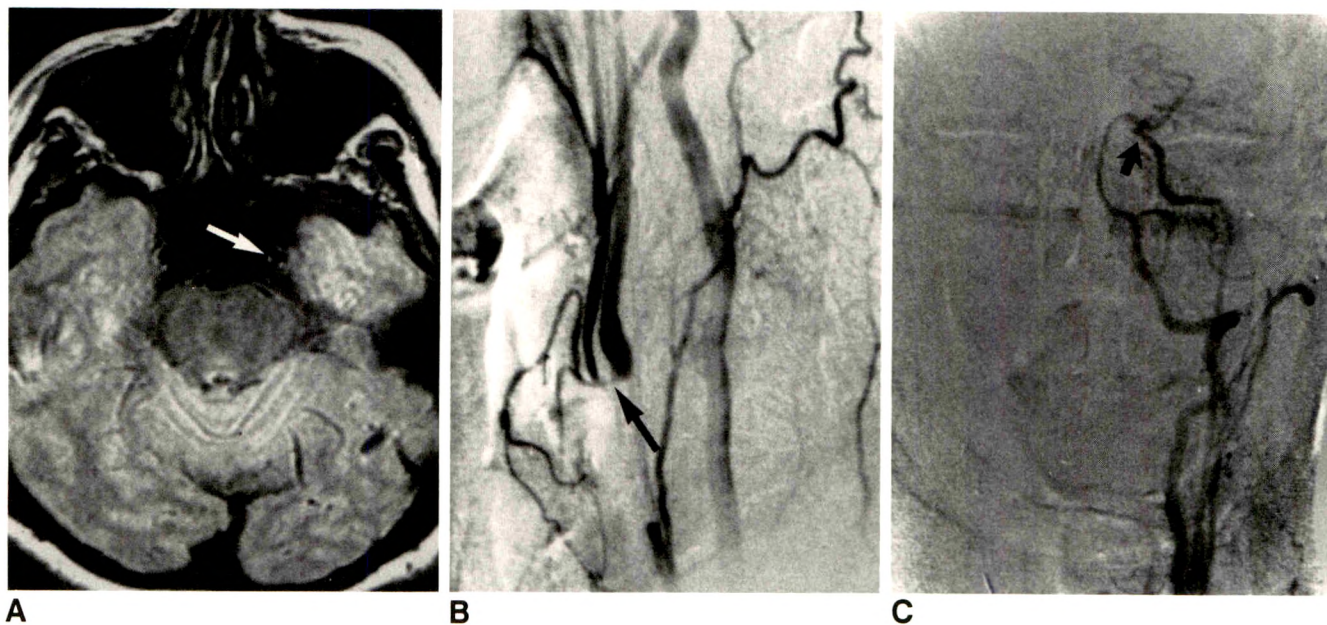


Fig. 3.—Partial flow void.

A, Long TR/short TE image (2000/20/1) shows partial flow void in siphon of proximal left internal carotid artery (ICA) despite angiographically demonstrated complete occlusion of left common carotid artery (CCA). Note similar but less dramatic changes in right ICA of patient studied 3 days after right carotid endarterectomy.

B, Lateral view of selective left vertebral injection shows collateralization to distal left CCA bifurcation and antegrade flow in left ICA (arrow).

C, Frontal view after selective injection of left vertebral artery shows opacification of left internal carotid siphon (arrow).

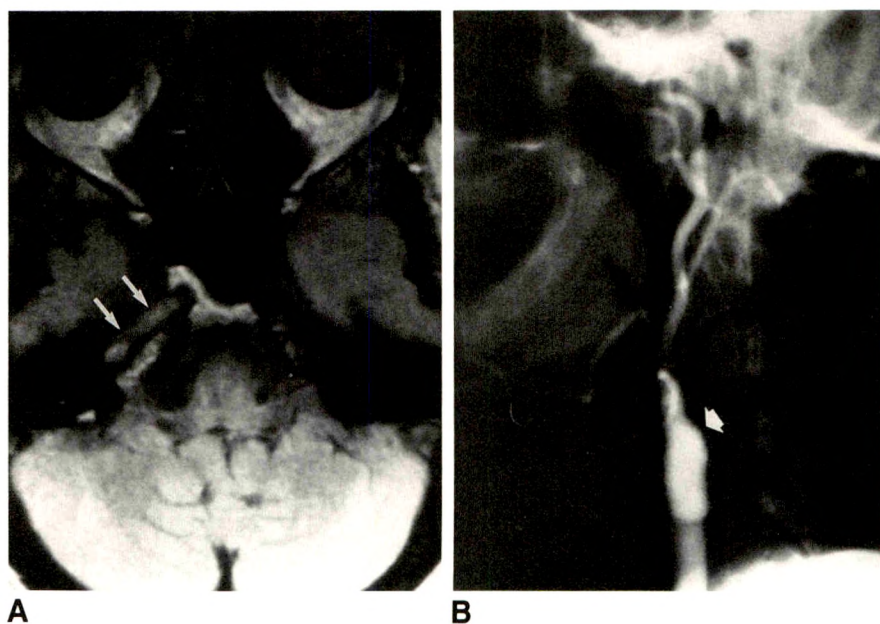


Fig. 4.—Isointense intraluminal signal.

A, Long TR/short TE image (2000/20/1) shows complete absence of flow void in horizontal portion of carotid canal (arrows) with intraluminal signal isointense with adjacent brain.

B, Selective injection of right common carotid artery shows complete occlusion at origin of right internal carotid artery (arrow).

quences. Gradient-moment nulling was used in only two of 46 studies reviewed in this investigation.

Intraluminal signal changes associated with extracranial ICA and vertebral stenosis and occlusion have been reported previously [1–6]. Alvarez et al. [1] first described the SE MR appearance of an ICA occlusion. They described absence of flow void and very intense intraluminal signal on all pulse

sequences in the cavernous portion of the ICA. Angiography demonstrated total occlusion just distal to the origin of the ICA. Katz et al. [2] reported a series of seven atherosclerotic occlusions, all of which contained intraluminal signal that was predominantly isointense with brain on both long TR and short TR sequences. They suggested that the isointense quality of the intraluminal signal was consequent to a paucity

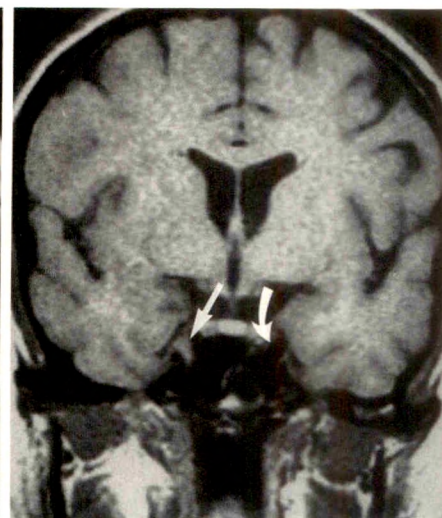
Fig. 5.—Isointense intraluminal signal in totally occluded right internal carotid artery.

A, Long TR/short TE axial image (2000/20/1) shows intraluminal signal isointense with adjacent brain (arrow).

B, Short TR/short TE coronal image (600/20/2) shows isointense intraluminal signal in proximal cavernous portion of right internal carotid artery (straight arrow). This appearance suggests a lack of methemoglobin within occluding thrombus; compare with normal flow void in left internal carotid artery (curved arrow).



A

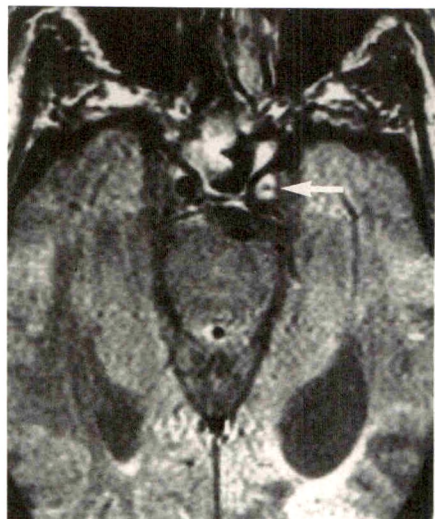


B

Fig. 6.—Patterns of heterogeneous hyperintensity in presence of total occlusion.

A, Long TR/short TE image (2000/20/1) shows hyperintense intraluminal signal peripherally with central focus of lower-intensity signal (arrow) in a patient with complete occlusion of left internal carotid artery.

B, Long TR/long TE image (2000/80/1) in a patient with a totally occluded right common carotid artery. Central focus of hyperintensity is surrounded by lower signal intensity (arrow).



A



B

of RBCs within the thrombus, which is composed predominantly of fibrin and platelets. They predicted that if markedly hyperintense intraluminal signal was encountered (as in the case reported by Alvarez et al.), this would be most consistent with slow flow (antegrade or retrograde) rather than atherosclerotic occlusion. Brant-Zawadzki [4] has disputed the specificity of isointense intraluminal signal. His series included two cases of isointense signal in the carotid siphon, reportedly produced by slow flow.

Several important differences in technique should be considered before comparing the results of our study with those of Brant-Zawadzki [4]. Of the 100 cases reviewed by Brant-Zawadzki, 22 studies had been performed on a 0.5-T magnet with a 10-mm slice thickness. The author did not specify which of the 14 studies in which carotid arteriograms were abnormal were obtained on the low-field unit. In our estimation, large voxel size could become a significant problem

when using a 10-mm slice thickness to evaluate the carotid canal and siphon. If this vessel were marginally patent, volume averaging could cause a small flow void to appear as isointense signal. A potentially more important difference in technique involves the use of motion-compensation gradients in studies performed on high-field units. A well-known disadvantage to the use of gradient-moment nulling is the replacement of normal flow void with hyperintense intraluminal signal in a slow-flow state. Although the use of spatial presaturation can reduce the amount of intraluminal signal produced by gradient-moment nulling, the signal is not always eliminated entirely by using this additional technique [9]. It is conceivable, therefore, that the combination of gradient-moment nulling and spatial presaturation could produce gray (isointense) intraluminal signal in a patent vessel [9]. Although this is not a problem with normal high-velocity flow in the carotid arteries, this technique may cause a marginally patent vessel to appear

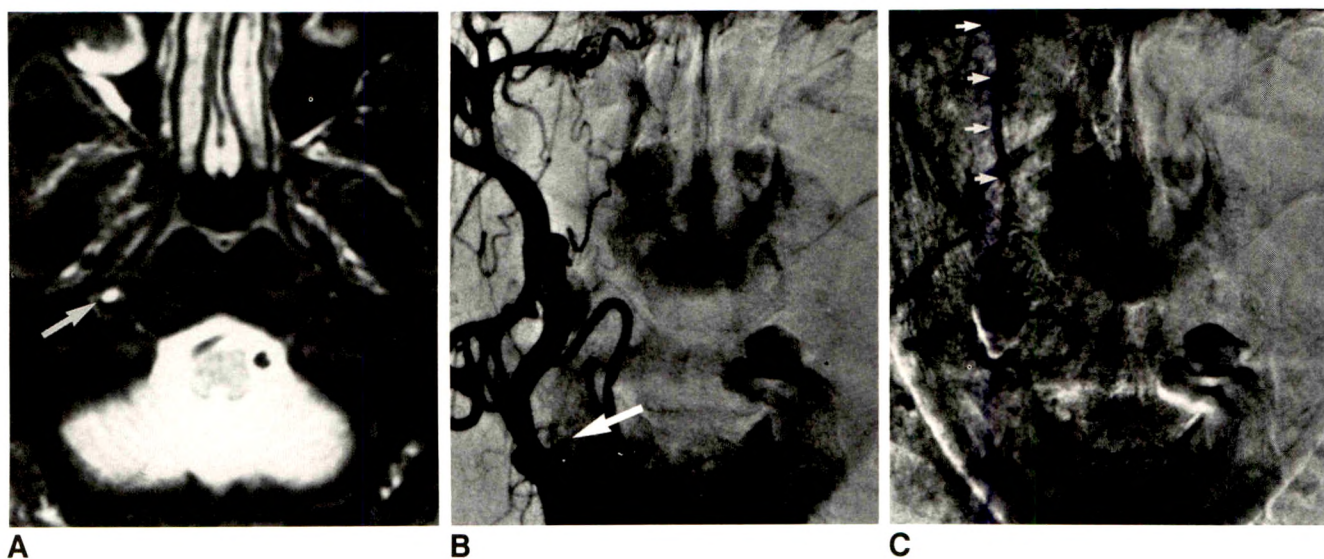


Fig. 7.—Homogeneous hyperintensity distal to severe stenosis.

A, Long TR/long TE image (2000/80/1) with gradient-moment nulling without presaturation shows markedly hyperintense intraluminal signal in distal cervical portion of right internal carotid artery (ICA) (arrow).

B, Early arterial phase of right common carotid injection suggests total occlusion of right ICA (arrow).

C, Late arterial phase shows slow antegrade flow of contrast material into right ICA (arrows).

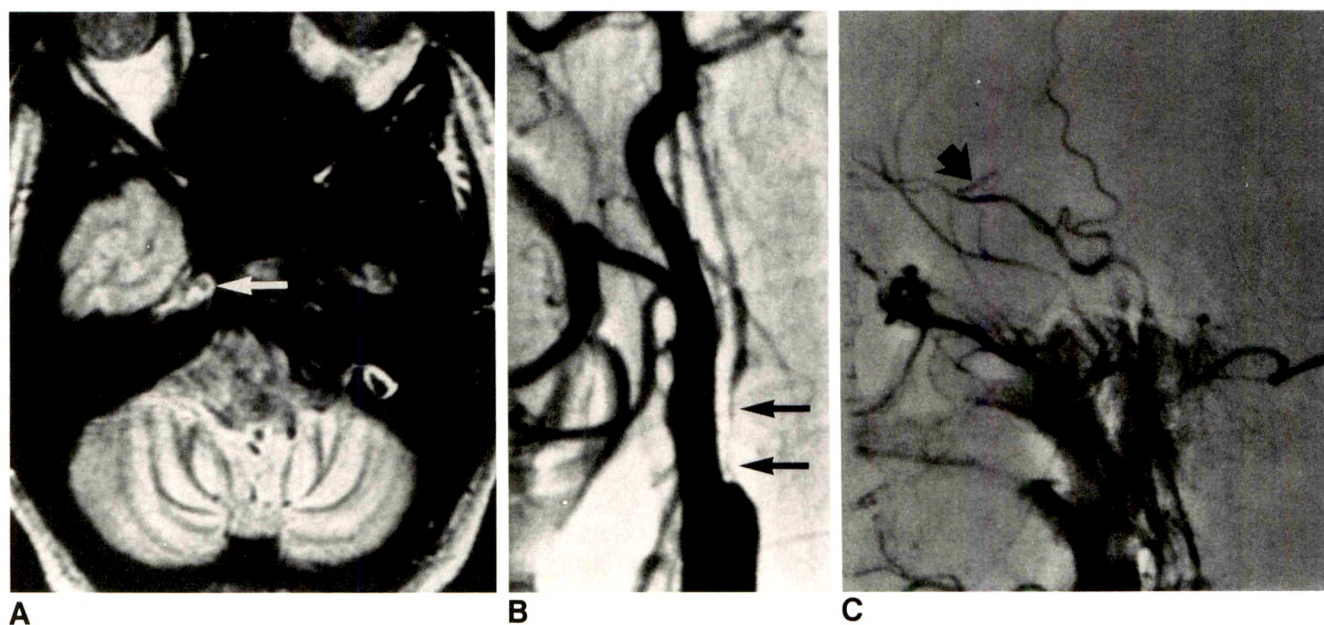


Fig. 8.—Heterogeneous hyperintensity in presence of high-grade stenosis.

A, Long TR/short TE presaturation image (2000/20/1) with gradient-moment nulling shows central focus of isointensity surrounded by hyperintense signal in distal petrous segment of right internal carotid artery (ICA) (arrow).

B, Selective injection of right common carotid artery shows angiographic "string sign" involving right ICA (arrows).

C, Lateral projection of late arterial phase shows opacification of right carotid siphon (arrow).

isointense. Our study included only two studies with gradient-moment nulling. We observed markedly hyperintense intraluminal signal in one case of angiographically demonstrated high-grade stenosis when MR was performed with gradient-moment nulling (without spatial presaturation) (Fig. 7). In a similar case of angiographic high-grade stenosis, MR per-

formed with gradient-moment nulling and spatial presaturation demonstrated heterogeneously hyperintense signal with a small central focus of isointensity (Fig. 8). The other three cases with a similar appearance on MR performed with cardiac gating appeared occluded only on angiography. Admittedly, the advantages of using gradient-moment nulling to

TABLE 2: Angiographic and MR Assessment of Patency of the Carotid Arteries in Occlusion and Stenosis

MR Interpretation	Angiographic Finding		
	Occlusion (n = 12)	Stenosis (n = 15)	"Normal" (n = 20)
Occlusion (n = 6)	6	0	0
Stenosis (n = 11)	6	5	0
Normal (n = 30) ^a	0	10	20

Note.—The two cases of spontaneous carotid dissection are not included in this table to avoid potential confusion between intraluminal methemoglobin consequent to dissection and hyperintense intraluminal signal (slow flow) distal to a high-grade stenosis.

^a Comprises 10 patients from the study group and 20 normal control subjects.

reduce or eliminate artifacts created by pulsatile flow far outweigh the disadvantages of artifactual intraluminal signal. If carotid occlusion is suspected on the basis of scans obtained with gradient-moment nulling and presaturation, additional MR angiographic sequences may be useful for confirmation.

In our experience, the partial-flow-void phenomenon was a reliable indicator of decreased flow within a partially collapsed lumen. Although Brant-Zawadzki [4] concluded that this appearance in the normal patient too often was simulated by volume averaging in the horizontal portion of the petrous segment, we did not find this to be an inconsistency, as we required the presence of the same signal abnormalities in the proximal intrapetrous and subclinoid segments. The use of a partial flow void as a criterion for diagnosing extracranial high-grade stenosis was quite insensitive, being present in only three of 16 cases. It should be remembered that partial flow void is not specific for high-grade stenosis, since it can also be seen within the reconstituted vessel distal to a total occlusion. Our results clearly indicate that the appearance of normal flow void on SE MR images of the brain by no means excludes significant (even preocclusive) atherosclerotic stenosis of the extracranial vessels. Brant-Zawadzki had reached a similar conclusion. No correlation was established between the quality of intraluminal signal changes and the degree of stenosis. This is not surprising, since the dynamics of blood flow are determined by more than the cross-sectional area of a stenotic lumen. Further in vivo studies correlating Doppler parameters, such as velocity and turbulence, with signal changes on SE MR are needed to clarify this relationship.

In our experience, the finding of isointense intraluminal signal from the skull base to the supraclinoid bifurcation on all pulse sequences is specific for complete occlusion. We concur with Katz et al. [2] that such an appearance can obviate invasive angiographic confirmation in the appropriate clinical setting. T1-weighted sequences in other than the sagittal plane were obtained in only one case of carotid occlusion in our series (Fig. 5). No evidence of intraluminal methemoglobin was evident in this single case. This would appear to support the contention expressed by Katz et al. that thrombus distal to an atherosclerotic occlusion is not composed of significant amounts of methemoglobin.

Six of the 12 atherosclerotic occlusive lesions had significant degrees of hyperintense intraluminal signal that prevented us from making the diagnosis of complete occlusion. It should be noted, however, that six of eight cases of heterogeneously hyperintense intraluminal signal proved to be atherosclerotic occlusions on angiography. Since the onset of atherosclerotic occlusion was not clinically apparent in any of the cases reviewed, no correlation was possible between the age of occlusion and the intraluminal signal pattern. This hyperintense intraluminal signal, which was identified in half of the atherosclerotic occlusions, may represent acute or subacute thrombus with a greater RBC component. Alternatively, small, angiographically occult channels of recanalization could produce areas of high signal consequent to slow flow.

Angiography remains the gold standard for the diagnosis of atherosclerotic stenosis and occlusion. However, this diagnostic test is not without its limitations. Several authors have reported their experiences with angiographically occluded ICAs that, on surgical exploration or repeat angiograms with large volumes of contrast material and prolonged injection times, have been noted to be marginally patent [10–13]. Retrograde flow via the ophthalmic artery into the carotid siphon and petrous and even cervical segments of the ICA has been documented with these modified techniques [11]. Only routine volumes and injection rates were used during the angiographic procedures reviewed in this study. Given these technical considerations, we cannot exclude the possibility that we failed to opacify the lumina distal to severely stenotic lesions that were included in the occlusion group, nor can we be sure that some totally occluded vessels did not reconstitute via small collaterals from the external carotid artery or contralateral ICA. Obviously, this amount of flow would be hemodynamically insignificant but might have important implications regarding intraluminal signal changes on

TABLE 3: Effectiveness of MR Imaging in the Diagnosis of Carotid Occlusion and High-Grade Stenosis

Disorder	No. of Studies				No. (%)				
	True Positive	False Positive	False Negative	True Negative	Sensitivity	Specificity	Positive Predictive Value	Negative Predictive Value	Accuracy
Carotid occlusion	6	0	6	35	50 ± 32 ^a	100 ± <1	100 ± <1	85 ± 11	87 ± 10
Stenosis	5	6	10	26	33 ± 27 ^a	81 ± 14	45 ± 33	72 ± 16	66 ± 14

Note.—Criteria for occlusion were complete absence of flow void and intraluminal signal isointense with brain on all pulse sequences. Other patterns of intraluminal signal were interpreted as not occluded. Criteria for high-grade carotid stenosis were demonstration of partial flow void or any of the patterns of hyperintense intraluminal signal interpreted as slow flow. In this table, all cases of isointense intraluminal signal and cases of normal flow void were considered nonstenotic.

^a Represents 95% confidence limits.

SE MR images of the brain. These possibilities may explain the inhomogeneously hyperintense signal that was encountered in approximately 50% of our angiographic occlusions.

Our own experience reflected the difficulties associated with the angiographic diagnosis of occlusion. Two cases in our review, one involving a critical ICA stenosis (Fig. 7) and the other a reconstituted CCA (Fig. 3), initially were misdiagnosed as total occlusions on angiography. Signal changes inconsistent with the angiographic diagnosis were observed on SE MR, prompting reevaluation of the angiographic studies, which subsequently demonstrated marginally patent vessels in both cases.

The MR appearance of carotid dissection was first described by Goldberg et al. [14]. The intraluminal signal changes observed in our two cases correlated well with the angiographic appearance. However, the intraluminal signal on axial and coronal long TR images was not specific, being indistinguishable from changes produced by atherosclerotic occlusion or stenosis. Axial short TR images through the area of dissection would allow a more specific diagnosis by demonstrating subintimal clot [15].

In summary, in our experience isointense intraluminal signal is specific for atherosclerotic occlusion. If this pattern is demonstrated consistently in two orthogonal planes on dual-echo sequences, we do not believe conventional angiography is necessary to confirm the diagnosis. However, atherosclerotic occlusion often contains varying degrees of hyperintense intraluminal signal that may prevent differentiation between occlusion and high signal produced by slow flow. Although a loss of flow void with variable hyperintense intraluminal signal is seen more commonly with occlusion than with high-grade stenosis, invasive angiography or MR angiography in combination with Doppler sonography will be needed to exclude marginal patency in these cases. The majority of high-grade stenoses produce no detectable signal changes on SE MR images of the brain. Partial flow void, although not a common finding, is a reliable indicator of proximal luminal compromise.

ACKNOWLEDGMENTS

We thank Sandra Ehrlich for assistance with statistics and Scott Faro for assistance in compiling the cases.

REFERENCES

1. Alvarez O, Edwards JH, Hyman RA. MR recognition of ICA occlusion. *AJNR* **1986**;7:359-360
2. Katz B, Quencer R, Kaplan J, Hinks RS, Post JD. MR imaging of intracranial carotid occlusion. *AJNR* **1989**;10:345-350
3. Heinz E, Yeates A, Djang W. Significant extracranial carotid stenosis: detection on routine cerebral MR images. *Radiology* **1989**;170:843-848
4. Brant-Zawadzki M. Routine MR imaging of the ICA siphon: angiographic correlation with cervical carotid lesions. *AJNR* **1990**;11:467-471
5. Uchino A, Ohnari N, Ohno M. MR imaging of intracranial vertebral artery occlusion. *Neuroradiology* **1989**;31:403-407
6. Knepper L, Biller J, Adams HP, Yuh W, Ryals T, Godersky J. MR imaging of basilar artery occlusion. *J Comput Assist Tomogr* **1990**;14:32-35
7. Russell EJ. Detection of significant extracranial carotid stenosis with routine cerebral MR imaging. *Radiology* **1989**;170:623-624
8. Bradley WG, Waluch V. Blood flow: magnetic resonance imaging. *Radiology* **1985**;154:443-450
9. Felmlee JP, Ehman RL. Spatial presaturation: a method for suppressing flow artifacts and improving depictions of vascular anatomy in MR imaging. *Radiology* **1987**;164:559-564
10. Clark OH, Moore WS, Hall AD. Radiographically occluded, anatomically patent carotid arteries. *Arch Surg* **1971**;102:604-606
11. Countess RW, Vijayanathan T. Reconstitution of "totally" occluded internal carotid arteries: angiographic and technical considerations. *Neurosurgery* **1979**;50:747-757
12. Gabrielsen TO, Seeger JF, Knake JE, Burke DP, Stilwell EW. The nearly occluded ICA: a diagnostic trap. *Radiology* **1981**;138:611-618
13. O'Leary DH, Mattie H, Potter JE. Atheromatous pseudo-occlusion of the ICA. *Stroke* **1989**;20:1168-1173
14. Goldberg HI, Grossman RI, Gomori JM, Asbury AK, Bilaniuk IT, Zimmerman RA. Cervical ICA dissecting hemorrhage: diagnosis using MRI. *Radiology* **1986**;158:157-161
15. Brugieres P, Castrec-Carpo A, Heran F, Goujon C, Gaston A, Marsault C. Magnetic resonance imaging in the exploration of dissection of the ICA. *J Neuroradiol* **1989**;16:1-10

The reader's attention is directed to the commentary on this article, which appears on the following pages.

Commentary

Re: Assessment of Carotid Artery Patency on Routine Spin-Echo MR Imaging of the Brain

Michael Brant-Zawadzki¹

In this issue, Lane et al. [1] provide additional data for the value of spin-echo MR imaging in assessing the patency of the internal carotid artery. A number of previous studies, including our own, have suggested that alteration of the normal signal void of the internal carotid artery should be viewed with suspicion [2-7]. The current study by Lane and his colleagues further categorizes the different types of signal alteration that may be encountered, specifically when the studies are performed with cardiac-gated spin-echo technique without the use of gradient-moment nulling (flow-compensation) software. These authors also verify our experience that a normal signal void may be present in the face of severe carotid stenosis (63% of their patients with stenosis greater than 90% exhibited normal signal void in the intracranial segment of the internal carotid artery).

Seemingly, only a minor discrepancy arises in the results of Lane et al. compared with our own. Namely, these authors place a high degree of confidence in the observation that a *completely* isointense signal within the intracranial carotid artery is indicative of atherosclerotic occlusion of that artery, whereas we reported two cases in which isointense signal was seen with severe stenosis but incomplete angiographic occlusion. Lane et al. explain the discrepancy in the different techniques employed. As noted earlier, their study was performed with cardiac gating instead of gradient-moment nulling to achieve reduction of flow-propagated phase-encoding artifacts (incidentally, the TR parameters quoted in their results obviously must have varied somewhat from the 600-msec and 2000-msec values given in their methods, as the heart

rate would determine the actual TR setting in any given individual).

It is highly likely that complete isointensity of the intracranial carotid artery may correspond to complete occlusion of the carotid artery angiographically in a high percentage of cases. Nevertheless, I would hold out the caveat that this is not likely to be 100% accurate. In our own observations, a slow rate of flow was noted angiographically in a carotid artery with isointense MR appearance. Serial frames from the angiogram demonstrated that the contrast propagation from the distal common carotid artery to the carotid siphon took 14 sec. I would submit that such a slow rate of flow is insufficient to induce the flow-related alterations of signal intensity observed by Lane et al. in their case material. I cannot totally dispute the fact that the combination of saturation pulses and gradient-moment nulling can combine to produce isointensity simulating complete occlusion in a slow-flow state. I would also predict that there may be instances in which a cardiac-gated technique is used where a combination of pseudogating and slow flow might induce an isointense picture.

Nevertheless, these are somewhat speculative points and one must bring the discussion back to the realm of the practical. Lane et al. state that their objectives "were to determine whether angiography can be obviated in cases of suspected occlusion. . . ." They also state that "a reliable diagnosis of atherosclerotic occlusion can be made when isointense intraluminal signal is observed." In their discussion, they state "such an appearance can obviate invasive angiographic confirmation in the appropriate clinical setting." The

This article is a commentary on the preceding article by Lane et al.

¹ Newport Harbor Radiology, 355 W. Placentia, Suite 207, Newport Beach, CA 92663. Address reprint requests to M. Brant-Zawadzki.

key phrase in all of this is *appropriate clinical setting*. I would suggest that any patient in whom transient ischemic attacks or fluctuating ischemic symptoms occur will undergo conventional angiography, even if isointense signal within the ipsilateral carotid artery is identified on MR. Such patients require evaluation of the entire cerebral circulation, including collateral flow, even if complete occlusion of the ipsilateral carotid artery is present. Therefore, the value of intracranial carotid artery isointensity in obviating conventional angiography wanes in "the appropriate clinical setting."

It might be pointed out that even the advent of MR angiography, with time-of-flight and phase-contrast techniques, may not allow us to completely obviate conventional angiography. It must be remembered that MR images of the vasculature relate strongly to *velocity* information rather than to true *anatomic* information of a contrast-filled lumen, which is provided by conventional angiography. These two phenomena are not equivalent. Even MR angiographic techniques have a threshold of flow velocity below which the observed signal intensity may simulate that of stationary hydrogen nuclei. The vagaries of MR artifacts at the skull base, effects from flow in the cavernous sinus, nuances of software manipulations such as gradient-moment nulling, saturation pulses, and so forth can befuddle the observer in any given case.

In summary, Lane and his colleagues have elegantly confirmed the observation that replacement of normal signal void

in the intracranial carotid artery should be viewed with suspicion. They also verify that the presence of normal signal void does not exclude significant carotid disease. Finally, we would all agree that although completely isointense signal within the carotid artery most often indicates occlusion of that vessel, in the appropriate clinical setting conventional angiography should still be performed to verify the complete occlusion (as pseudoocclusion can be treated surgically) and to provide additional information regarding pathways of collateral flow and possible compromise therein.

REFERENCES

1. Lane JI, Flanders AE, Doan HT, Bell RD. Assessment of carotid artery patency on routine spin-echo MR imaging of the brain. *AJNR* **1991**;12: 819-826; *AJR* **1991**;157:1299-1306
2. Alvarez O, Edwards JH, Hyman RA. MR recognition of ICA occlusion. *AJNR* **1986**;7:359-360
3. Katz B, Quencer R, Kaplan J, Hinks RS, Post JD. MR imaging of intracranial carotid occlusion. *AJNR* **1989**;10:345-350
4. Heinz E, Yeates A, Djang W. Significant extracranial carotid stenosis: detection on routine cerebral MR images. *Radiology* **1989**;170:843-848
5. Brant-Zawadzki M. Routine MR imaging of the ICA siphon: angiographic correlation with cervical carotid lesions. *AJNR* **1990**;11:467-471
6. Uchino A, Ohnari N, Ohno M. MR imaging of intracranial vertebral artery occlusion. *Neuroradiology* **1989**;31:403-407
7. Knepper L, Biller J, Adams HP, Yuh W, Ryals T, Godersky J. MR imaging of basilar artery occlusion. *J Comput Assist Tomogr* **1990**;14:32-35

Angiographic Diagnosis and Management of Head and Neck Schwannomas

Joshua Abramowitz¹
 Jacques E. Dion¹
 Mary E. Jensen²
 Mark Lones¹
 Gary R. Duckwiler¹
 Fernando Viñuela¹
 John R. Bentson¹

Schwannomas are tumors derived from nerve sheath cells, which are often located in the head and neck, including the CNS. Although a definitive vascular pattern has been previously characterized for these lesions, preoperative embolization of the more vascular schwannomas has not been described. In a review of eight patients with schwannomas who underwent angiography at our institution since 1987, a characteristic vascular pattern became apparent that helped distinguish these lesions from other lesions of the head and neck. The lesions were moderately vascular with tortuous tumor vessels. Scattered, small puddles of contrast medium seen in the mid-arterial, capillary, and venous phases were believed to be characteristic of these lesions. Multiple feeding vessels were noted in all but one case, but these were only minimally enlarged. No arteriovenous shunting or vascular encasement was identified. Six of eight lesions were embolized with significant devascularization and no morbidity or mortality.

In patients with head and neck tumors whose angiographic findings include a pattern of moderate hypervascularity, tortuous tumor vessels, and, in particular, scattered contrast puddles without arteriovenous shunting or vascular encasement, schwannoma should be suspected. Embolization is a useful and safe presurgical adjunct in the treatment of vascular schwannomas.

AJNR 12:977-984, September/October 1991; *AJR* 157:1309-1316, December 1991

In the era prior to the development and widespread use of cross-sectional imaging techniques, angiography played a major role in the diagnosis and work-up of head and neck tumors [1, 2]. The radiologic and surgical literature contains descriptions of characteristic vascular displacements that helped localize lesions to various compartments (i.e., Meckel cave) [3-6]. Much less is written about characteristic staining patterns of head and neck schwannomas at angiography.

The current radiologic work-up for head and neck schwannomas usually included CT and/or MR imaging. Angiography has been relegated to an ancillary role in those cases in which a highly vascular lesion is suspected (i.e., paraganglioma), critical adjacent arterial structures need to be assessed prior to surgery, or when preoperative embolization is planned. This latter indication is the most common at our institution; six of the eight patients presented here had therapeutic embolization at the time of angiography.

In a review of the eight patients with schwannomas who had angiography at our institution, a particular vascular pattern was noted that helped distinguish schwannomas from other lesions of the head and neck. We will define the vascular pattern seen in our cases and discuss preoperative embolization of these lesions.

Materials and Methods

We retrospectively reviewed the angiograms of eight patients with schwannomas of the head and neck, seven proved histologically and one presumed, performed over a 2-year period. All studies were done on a GE Fluoricon 5000 digital system (General Electric,

Received October 2, 1990; revision requested January 24, 1991; revision received April 5, 1991; accepted May 1, 1991.

¹ Department of Radiological Sciences, Endovascular Therapy Service, B2-188, CHS, UCLA Medical Center, 10833 Le Conte Ave., Los Angeles, CA 90024. Address reprint requests to J. E. Dion.

² Department of Pathology, UCLA School of Medicine, Los Angeles, CA 90024.

0361-803X/91/1576-1309
 © American Roentgen Ray Society

Milwaukee, WI). Embolization was performed with a coaxially placed Tracker-18 catheter (Target Therapeutics, San Jose, CA) through a standard 5.5-French diagnostic angiography catheter (Cook, Inc., Bloomington, IN). Polyvinyl alcohol (PVA) particles (Ingenor, Paris, France) were the main embolic material used in all the embolizations; Gelfoam pledgets (Upjohn, Kalamazoo, MI) were occasionally used, either distally for protection of potential anastomoses with internal carotid circulation, proximally to complete the occlusion, or both. In one case of balloon occlusion of the vertebral artery, two #16 Debrun latex Gold Valve balloons (Ingenor, Paris, France) were used, having been detached from a Tracker catheter introduced over a 7-French thin-wall introducer (Balt, Montmorency, France).

The tumor was removed surgically in six cases (1–4, 7, and 8), and the specimens were fixed in 10% buffered formalin and processed routinely with paraffin sections stained with hematoxylin and eosin. The histologic sections from these cases were reviewed to examine microscopic features of the vascular channels. Gross specimens were not available for review.

Results

Angiography was performed in eight cases of head and neck schwannomas at our institution over a 2-year period. Therapeutic embolization was performed in six of the eight cases. In case 1, the schwannoma was located within the left orbital cone and fed by branches of the left ophthalmic artery (Fig. 1). It was thought that this lesion could not be embolized safely.

In seven patients the tumors were surgically removed. In case 6, a 21-year-old woman with a history of right facial numbness and with a dumbbell-shaped lesion in the right Meckel cave, a diagnosis of presumed trigeminal schwannoma was made on the basis of imaging and angiographic findings (Fig. 2). Her 2-year follow-up examination revealed minimal growth of the lesion and no change in neurologic status.

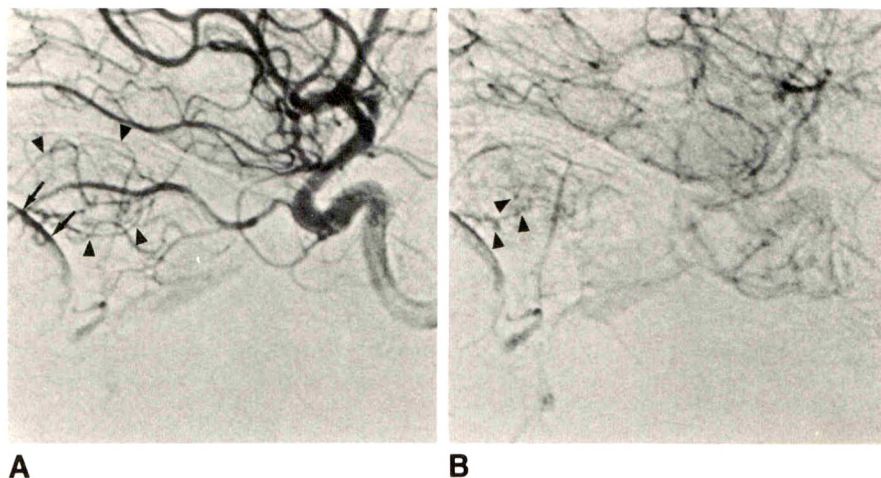


Fig. 1.—Case 1: Left orbital schwannoma.
A, Left internal carotid angiogram, lateral view. Left ophthalmic artery branches (arrowheads) are draped over an intraorbital mass indenting the posterior choroidal blush (arrows).
B, Left internal carotid angiogram, lateral view. Capillary phase reveals several small contrast puddles (arrowheads) within mass, characteristic of schwannomas.

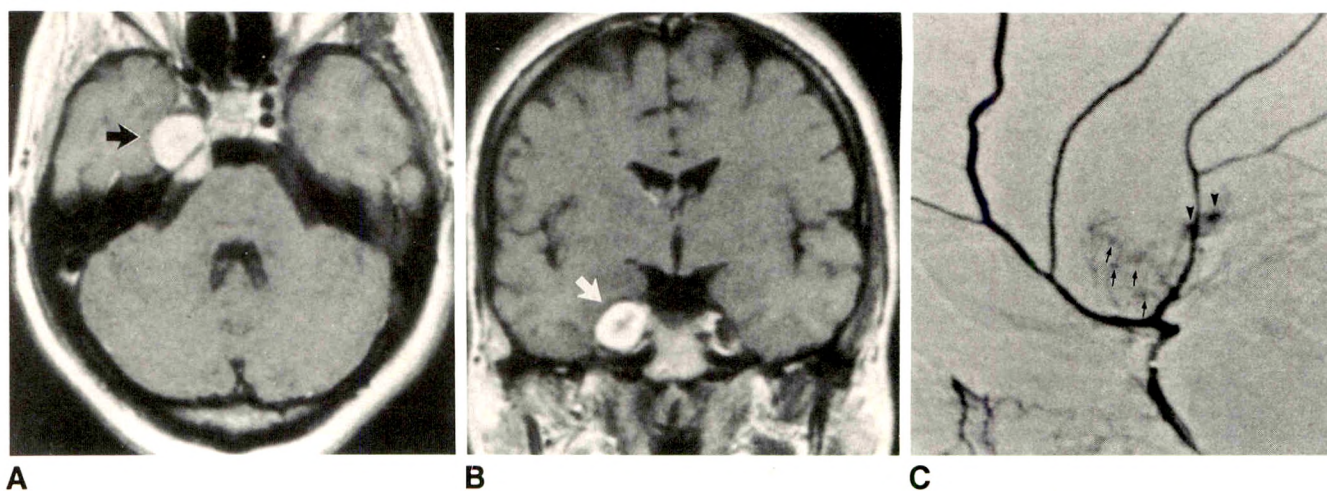


Fig. 2.—Case 6: Presumed right trigeminal schwannoma.
A, Contrast-enhanced axial T1-weighted (500/40/2) MR image shows enhancing mass (arrow) in right Meckel cave extending beyond dural reflection into posterior fossa.
B, Contrast-enhanced coronal T1-weighted (500/40) MR image shows mass (arrow) causing medial displacement of cavernous sinus structures.
C, Superselective right middle meningeal angiogram, lateral view. The moderately vascular tumor contains several small contrast puddles (arrows) as well as large ones (arrowheads).

A common angiographic pattern was apparent in these eight cases. Arterial feeders to the lesions were generally of normal caliber or only mildly enlarged. All except the orbital schwannoma had more than one feeding arterial pedicle. The lesions were generally moderately hypervascular with irregular, tortuous tumor vessels. Characteristic small contrast puddles were scattered randomly, appearing in the mid-arterial phase and persisting into the capillary and venous phase (Figs. 3 and 4). There was slight persistence of the capillary stain into the venous phase. No arteriovenous shunting, venous or arterial encasement, or vascular invasion was noted. In two cases, the lesions appeared smaller at angiography than on cross-sectional imaging studies; presumably, this was due to cystic degeneration (avascular) seen on the imaging studies.

The arterial supply to these lesions was variable, but generally from the external carotid branches as expected by location (Table 1). The orbital schwannoma was supplied exclusively by the ipsilateral ophthalmic artery from the internal carotid artery. In two cases of parapharyngeal space

schwannomas (cases 2 and 4), some supply was noted from the ipsilateral vertebral artery. In two cases of Meckel cave seventh nerve schwannomas (cases 5 and 6), some supply from the ipsilateral meningohypophyseal trunk was present on internal carotid injections. In case 7, there was sole supply from the left vertebral artery to a C2 neural foramen schwannoma.

Significant devascularization of these lesions was achieved in the six cases in which embolization was performed (Table 1). In all six, the supplying branches of the external carotid artery were superselectively catheterized with Tracker-18 catheters. In four of these cases small PVA particles (150–250 μ m) were used. Gelfoam pledgets, usually 2×4 mm, were used to protect distal territories, such as the neuromeningeal trunk of the ascending pharyngeal artery, as well as proximally to complete the occlusion of the embolized vessels. In case 3, a schwannoma of low-grade malignancy with extensive supply from branches of the internal maxillary artery, the main internal maxillary trunk was embolized with medium-size PVA particles (250–590 μ m) (Fig. 5). Medium-

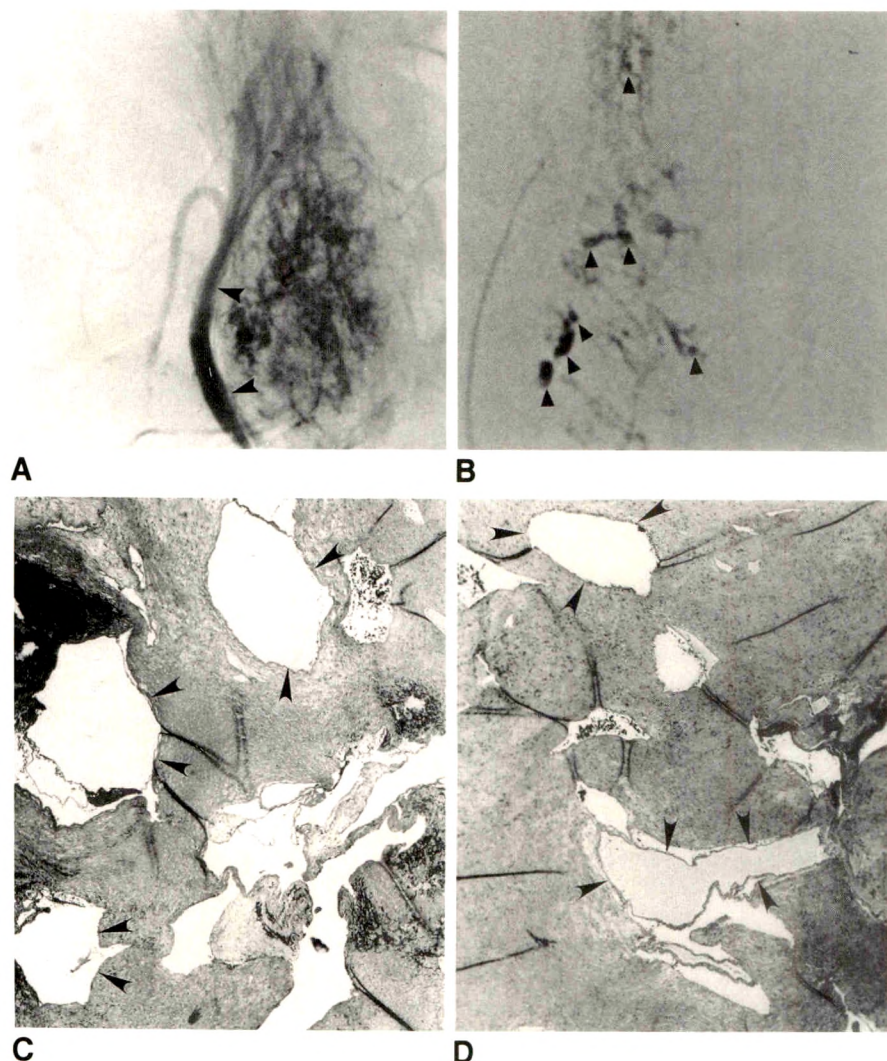


Fig. 3.—Case 4: Left carotid bifurcation schwannoma.

A, Left external carotid angiogram of a suspected paraganglioma, lateral view. Hypervascular mass with numerous contrast puddles displaces left external carotid artery anteriorly (arrowheads).

B, Superselective left ascending pharyngeal angiogram, lateral view. The numerous contrast puddles are more clearly identified (arrowheads) and are more characteristic of a schwannoma than a paraganglioma.

C and D, Representative histologic sections of left carotid bifurcation schwannoma. Larger sinusoidal vessels with thin walls (arrowheads) are surrounded by tumor. (H and E, original magnification $\times 50$)

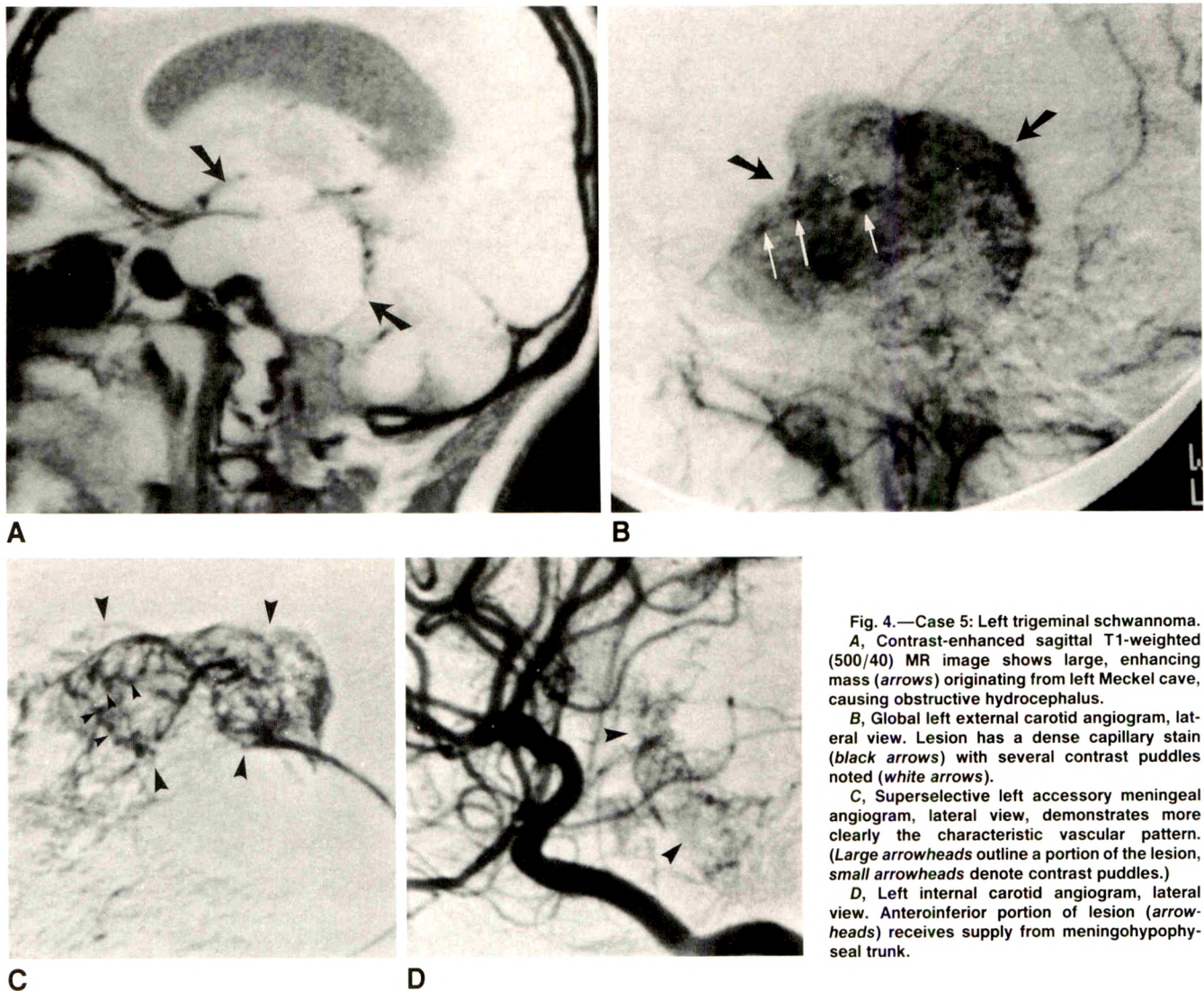


Fig. 4.—Case 5: Left trigeminal schwannoma. A, Contrast-enhanced sagittal T1-weighted (500/40) MR image shows large, enhancing mass (arrows) originating from left Meckel cave, causing obstructive hydrocephalus.

B, Global left external carotid angiogram, lateral view. Lesion has a dense capillary stain (black arrows) with several contrast puddles noted (white arrows).

C, Superselective left accessory meningeal angiogram, lateral view, demonstrates more clearly the characteristic vascular pattern. (Large arrowheads outline a portion of the lesion, small arrowheads denote contrast puddles.)

D, Left internal carotid angiogram, lateral view. Anteroinferior portion of lesion (arrowheads) receives supply from meningo-hypophyseal trunk.

size PVA particles were also used in case 8, a jugular foramen schwannoma of the vagus nerve.

In case 2, a left parapharyngeal space schwannoma of the vagus nerve, significant vascular supply was noted from the left vertebral artery. Right vertebral angiography revealed a dominant right vertebral system with reflux into the left vertebral artery. A test balloon occlusion of the left vertebral artery at the C1 level, above the level of the tumor feeders, under full systemic heparinization with 5000 units of heparin, was tolerated without ischemic symptoms for 20 min. At this point, the same balloon, filled with Iohexol-200 (Winthrop, New York, NY) was detached at C1. The tumor feeders proximal to the balloon were then embolized with small PVA particles and a second, similar balloon was finally detached more proximally at C3–C4 to trap the segment (Fig. 6).

In all cases embolization was tolerated very well without neurologic sequelae. Devascularization of 60–95% of the tumor bed was achieved, in most cases closer to 95%. In five cases in which both embolization and surgery were performed, surgical blood loss was thought to be diminished,

presumably due to the preoperative embolization. In case 4, the schwannoma was located at the cervical bifurcation; surgical blood loss was estimated at 25 ml, and the patient was able to be discharged on the second postoperative day. In the case of the low-grade malignant schwannoma with extensive internal maxillary artery supply, there was an estimated 1500 ml blood loss at surgery. Only 60% devascularization was achieved in this case. Additionally, a very extensive surgical procedure was performed in this case, including exploration of the infratemporal fossa and resection of a portion of the mandible that was invaded by tumor. Total operating time was 16 hr, but gross total removal of the lesion was achieved.

Pathology

The six cases in which histologic sections were examined microscopically included four schwannomas (cases 1, 2, 7, and 8), one neurilemmoma, ancient type (case 4), and one malignant schwannoma arising in a neurofibroma (case 3).

TABLE 1: Data and Findings in Eight Patients with Schwannomas of the Head and Neck

Case No.	Age (years)	Sex	Clinical Presentation	MR and CT Findings	Angiographic Findings	Estimated Blood Loss During Surgery
1	30	M	Left eye proptosis; decreased visual acuity with normal extraocular movement	3 × 2 cm bilobed intraconal left orbital mass that enhanced with contrast; mild bone remodeling	Arterial supply from left ophthalmic artery; no embolization	Minimal
2	40	F	2-year history of "lump in the throat"	4 × 5 cm low-density left parapharyngeal space mass obliterating left fossa of Rosenmüller, splaying the carotid bifurcation	Arterial supply by left ascending pharyngeal artery, left occipital artery, and muscular branch of left vertebral artery at C2; embolization of ascending pharyngeal and left occipital arteries; left vertebral segment "trapped" with balloons and muscular feeder embolized; 95% devascularized	150 ml
3	14	M	Several month history of right mandibular pain	5.5 × 6 cm right infratemporal fossa mass of heterogeneous MR signal and CT density distorting posterior maxillary sinus and pterygoid plates, with invasion of right mandible	Multiple arterial feeders including right middle meningeal, right accessory meningeal, right deep temporal, right posterior auricular, and right internal maxillary; embolization of right internal maxillary and right posterior auricular, 60% devascularization; right internal carotid test occlusion also performed	1500 ml
4	24	M	2-year history of left neck swelling	4 × 3 cm heterogeneously dense mass in left posterior styloid, parapharyngeal space, with central low density and thick rim	Arterial supply by left ascending pharyngeal and small muscular branch of left vertebral; embolization of left ascending pharyngeal; 95% devascularization	25 ml
5	20	F	6-month history of severe headaches, difficulty swallowing, and left facial numbness	4 × 6 cm dumbbell-shaped mass in left Meckel cave with posterior fossa extension compressing the brainstem causing obstructive hydrocephalus	Arterial supply by left accessory meningeal, left middle meningeal, and left meningohypophyseal trunk; embolization of left accessory meningeal and left middle meningeal; 90% devascularization	1500 ml
6	21	F	1-year history of right facial numbness; history of SLE	2 × 3 cm contrast-enhancing mass involving right Meckel cave with anterior and posterior extension; marked right masticator muscle atrophy	Arterial supply by right middle meningeal, right accessory meningeal, and right meningohypophyseal trunk; embolization of right middle meningeal and right accessory meningeal; 80% devascularization	No surgery or biopsy; 2-year follow-up
7	10	F	1-month history of right arm and leg weakness; 2-week history of left arm spasm	3 × 3 cm mass in left C2 neural foramen with marked cord compression	Arterial supply from muscular branches of left vertebral; no embolization	250 ml
8	28	F	High-pitched tinnitus in right ear; difficulty swallowing for 3 months	3 × 3 cm enhancing mass in right jugular foramen	98% of arterial supply from neuromeningeal trunk of right ascending pharyngeal, 1–2% from right AICA; neuromeningeal trunk completely embolized; 98% devascularization	350 ml

Note.—SLE = systemic lupus erythematosus, AICA = anterior inferior cerebellar artery.

The schwannomas exhibited characteristic features of an encapsulated tumor composed of spindle-shaped cells arranged in cellular Antoni A areas, hypocellular myxoid Antoni B areas, and occasional Verocay bodies. The neurilemmoma, ancient type, was similar except for marked hyalinization. The malignant schwannoma arising in a neurofibroma showed areas of marked nuclear pleomorphism, hyperchromaticity, and mitotic figures.

Tumor vessels were usually numerous with expanded sinusoidal-appearing spaces. The majority of these vessels had

thin walls. Occasional vessels were present singly or in clusters with hyalinized walls. Most vessels were less than 1 mm in diameter, and only a few were 1–2 mm in diameter. No regions of necrosis or large areas of hemorrhage were present. There were a few small foci of perivascular extravasated erythrocytes and rare foci of hemosiderin deposition. Several vessels of varying sizes showed thrombus formation. Isolated vessels contained PVA or Gelfoam, sometimes with thrombus or inflammatory cells or both. A representative section including some larger vessels is shown in Figure 3.

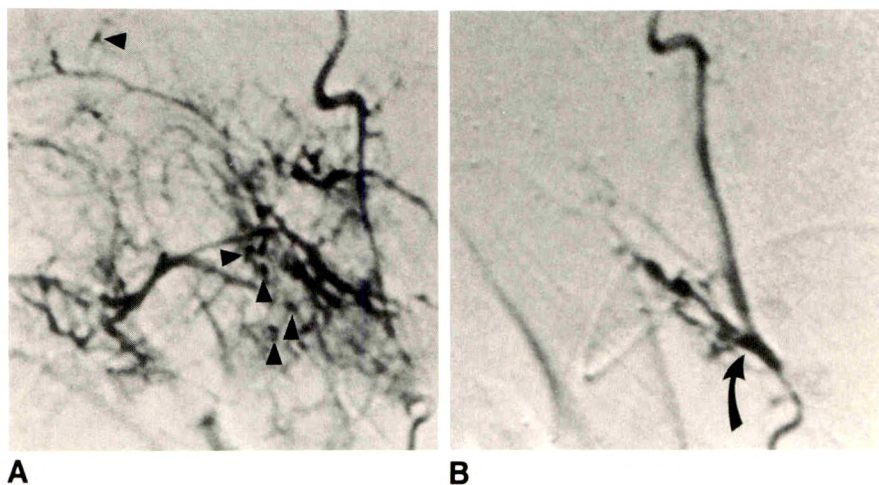


Fig. 5.—Case 3: Right infratemporal fossa low-grade malignant schwannoma.

A, Superselective right internal maxillary angiogram, lateral view, late arterial phase. Hypervascular tumor with irregular vascular channels and contrast puddles (arrowheads) is noted to have significant supply from internal maxillary artery branches.

B, Right internal maxillary angiogram, lateral view, after embolization with PVA particles and Gelfoam pledgets. The tumor is devascularized and the proximal internal maxillary artery is preserved (curved arrow).

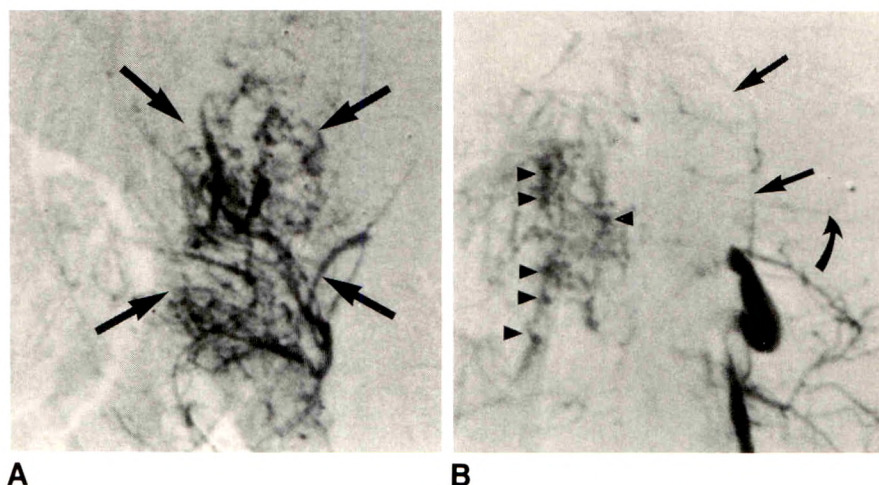


Fig. 6.—Case 2: Left parapharyngeal space schwannoma.

A, Left occipital artery angiogram, lateral view, capillary phase. Lesion exhibits characteristic tortuous tumor vessels and contrast puddles (arrows).

B, Left vertebral angiogram, lateral view, following balloon occlusion at C1 (curved arrow) shows C2 muscular branch (straight arrows) providing significant vascular supply to posterior aspect of tumor. (Arrowheads identify contrast puddles.) This tumor was embolized with PVA particles.

Variation in the size of vessels among the cases was most apparent with the neurilemmoma, ancient type, which contained numerous larger thin-walled vessels, and with the malignant schwannoma arising in a neurofibroma, which had relatively fewer smaller-size vessels.

Discussion

Schwannomas are most often solitary lesions that arise from the neural sheath of peripheral, spinal, or cranial nerves [7]. They are usually benign but in rare instances can be malignant, the latter occurring *de novo* or following radiation therapy for benign lesions.

The terminology used to classify nerve sheath tumors has been quite confusing. In the past, schwannomas have been alternatively called neurilemmomas, neuromas, neurinomas, and perineural fibroblastomas [8, 9]. Additionally, some authors [7, 9] have used the term schwannoma to encompass neurilemmoma and neurofibroma, both of which are com-

posed of Schwann cells to some degree. The current literature, however, distinguishes between neurilemmoma (schwannoma) and neurofibroma on a histologic bases [9]. Neither of these lesions should be confused with neuromas. The latter represents an exaggerated repair response to neuronal injury in which a tangle of regenerating axons, fibrous tissue, and Schwann cells form at the site of a severed nerve.

Schwannomas are relatively uncommon lesions; the head and neck, including the CNS, is by far their most common location. In early series, neurofibromas were included with schwannomas, leading to inaccurate estimates of the rate of occurrence of the latter. However, in one large series of 389 schwannomas reported by Gore et al. [10], in which neurofibromas were excluded, 65% of schwannomas were found to be in the CNS with another 13% outside the CNS in the head and neck. Inside the CNS, they most commonly arise from the eighth cranial nerve, followed by spinal nerves and the fifth cranial nerve in descending order of frequency [8]. In the head and neck (outside the CNS) they can occur in any anatomic site, but most frequently in the lateral cervical region.

Schwannomas most often occur in women in their third and fourth decades of life, but may occur at any age. Five of the eight patients reported here are female, ranging in age from 10 to 40 years old. Presentation can be quite variable depending on the size of the lesion, its location, the specific nerve involved, and the presence of anaplasia (malignancy).

Microscopic examination of these cases revealed a vascular pattern dominated by numerous, predominantly thin-walled sinusoidal spaces, in keeping with previously described cases [11–13], and in contrast to angiographic findings in peripheral neurilemmomas.

Angiographic findings revealed that the contrast puddles ranged in size from 1 mm to 4 mm in diameter and were distributed throughout the tumor mass in small clusters. Histologic sections showed only a few larger vessels within this size range. This incongruity between angiographic and histologic findings may be due to the small size and random selection of the tissue specimens from these tumors, which were obtained without angiographic localization. Also, vessel size as seen in histologic sections may appear smaller than angiographic measurements owing to formalin fixation of tissue and lack of vascular pressure.

CT and MR are the prime imaging techniques used in the radiologic work-up of these lesions [14, 15]. Angiography is no longer necessary to diagnose a mass in the head and neck but may be of help in distinguishing between lesions known to occur in certain locations. Additionally, with the ongoing development of interventional techniques in the head and neck, preoperative embolization can be performed on most of these lesions.

A typical angiographic pattern of schwannomas is not clearly established. The radiologic and surgical literature contains few references to the angiography of schwannomas, particularly since the advent of cross-sectional imaging techniques. Several case reports and small series make note of vascular displacements and the presence of tumor "blush" [2–6, 13–18]; in particular, Moscow and Newton [2] as well as Silver et al. [15] described the same characteristic puddles of contrast material at angiography as we have. The presence of prominent capsular veins in eighth nerve tumors has also been described [1]. In one series of 32 patients with "neurinomas" 22 were found to be hypervascular; however, some were considered to be indistinguishable angiographically from meningiomas. These authors described five cases as having irregular tortuous vessels and puddling of contrast material, as we found in our cases. It is unclear from that report whether "neurinoma" refers to schwannoma, neurofibroma, or both. Taveras and Ferrucci's text [19] claims that schwannomas are hypovascular on angiography. This was also noted in another series of 14 trigeminal neurilemmomas (schwannomas) in which eight were said to be avascular [16]. A pattern of nonshunting hypervascularity with tortuous tumor vessels and, in particular, contrast puddles was noted in each of the eight cases we have presented, and was believed to be characteristic. In our single case of malignant schwannoma, we were unable (even retrospectively) to observe distinguishing features that would have enabled us to predict the histology; this was also the experience of Moscow and Newton [2], who described "no correlation between angiographic

appearance of tumor vascularity within intracranial neurinomas and degree of malignancy."

Embolization would have no place in the treatment of avascular tumors; however, the hypervascularity of these schwannomas made them quite suitable for embolization. As with meningiomas, one may argue that these lesions could be operated on without prior embolization. In our experience, this varies from institution to institution. Our surgeons felt that the preoperative embolization had greatly contributed to the safety and efficacy of their procedure. The orbital lesion was the least vascular and also the least amenable to embolization on an anatomic basis (ophthalmic artery supply). In five of the six cases embolized, 80% or greater devascularization was achieved. PVA particles were the chosen embolic agents for obliterating the vascular bed of the tumor while avoiding embolization of potential anastomoses with internal carotid circulation. This resulted in uniformly good outcomes without neurologic sequelae, as well as a reduction in the amount of blood lost during surgery.

In cases of head and neck tumors that are examined angiographically, a pattern of moderate hypervascularity, irregular tumor vessels, and, in particular, scattered contrast puddles and lack of arteriovenous shunting should bring to mind the possibility of schwannoma. These lesions are safely amenable to preoperative embolization in cases in which the surgeon judges that this devascularization will enhance the efficacy and safety of the surgery.

ACKNOWLEDGMENT

We thank Apryl V. Howard for secretarial help and manuscript preparation.

REFERENCES

1. Newton TH, Potts DG. *Radiology of the skull and brain*, vol. 2. St. Louis: Mosby, 1974:2281
2. Moscow NP, Newton TH. Angiographic features of hypervascular neurinomas of the head and neck. *Radiology* 1975;114:635–640
3. Westberg G. Angiographic changes in neurinomas of the trigeminal nerve. *Acta Radiol [Diagn]* 1963;1:513–520
4. de Benedittis G, Berasconi V, Ettore G. Tumors of the fifth cranial nerve. *Acta Neurochir* 1977;38:37–64
5. Arseni C, Dumitrescu L, Constantinescu A. Neurinoma of the trigeminal nerve. *Surg Neurol* 1975;4:497–503
6. Palacios E, MacGee E. The radiographic diagnosis of trigeminal neurinomas. *J Neurosurg* 1972;36:153–156
7. Thawley SE, Panje WR. *Comprehensive management of head and neck tumors*, vol. 2. Philadelphia: Saunders, 1987:1253–1256
8. Rosenberg RN, Grossman RG, Schochet SS Jr, Heinz ER, Willis WD Jr. *The clinical neurosciences*, vol. 3. New York: Churchill Livingstone, 1983:151–153
9. Batsakis JG. *Tumors of the head and neck*, 2nd ed. Baltimore: Williams & Wilkins, 1979:313–326
10. Gore DO, Rankow R, Hanford JM. Parapharyngeal neurilemmoma. *Surg Gynecol Obstet* 1956;103:193
11. Kasantikul V, Glick AD, Netsky MG. Light and electron microscopic observations of blood vessels in neurilemmomas. *Arch Pathol Lab Med* 1979;103:683–687
12. Stener B, Angervall L, Nilsson L, Wickbom I. Angiographic and histologic studies of the vascularization of peripheral nerve tumors. *Clin Orthop* 1969;66:113
13. Berlin O, Stener B, Lindahl S, Irstam L, Lodding P. Vascularization of

- peripheral neurilemmomas: angiographic computed tomographic, and histologic studies. *Skeletal Radiol* **1986**;15:275-283
14. Mancuso AA, Hanafee WN. *Computed tomography and magnetic resonance imaging of the head and neck*. Baltimore: Williams & Wilkins, **1985**;179:441
 15. Silver AJ, Mawad ME, Hilal SK, et al. Computed tomography of the carotid space and related cervical spaces. Part II: neurogenic tumors. *Radiology* **1984**;150:729-735
 16. Pollack IF, Sekhar LW, Jannetta PJ, Janecka IP. Neurilemmomas of the trigeminal nerve. *J Neurosurg* **1989**;70:737-745
 17. Reinbold WD, Wimmer B, Adler CP, Genant HK. Radiologic findings in peripheral neurilemmoma. *Eur J Radiol* **1987**;7:268-273
 18. Allman MI, Frayer WC, Hedges TR Jr. Orbital neurilemmoma. *Ann Ophthalmol* **1977**;11:1409-1413
 19. Taveras JM, Ferrucci JT. *Radiology: diagnosis, imaging, intervention*, vol. 3. Philadelphia: Lippincott, **1986**: Ch. 56, 13

Call for Papers on Neuroradiology

On January 1, 1992, The American Roentgen Ray Society and the American Society of Neuroradiology will terminate their agreement whereby manuscripts on neuroradiology submitted to the *AJR* are forwarded to the *AJNR* and selected *AJNR* papers are republished in the *AJR*.

To avoid any lag in the publication of neuroradiologic articles in the *AJR*, the Journal requests authors to submit neuroradiologic manuscripts effective immediately. We plan to expedite publication of these papers. Authors will receive an initial editorial decision in 3-4 weeks, and accepted papers will be published 3 months after revised manuscripts are accepted. This is more than twice as fast as most other journals.

The advantages of this rapid publication time and the *AJR*'s large circulation (24,000) are now available to all authors of neuroradiologic papers. An expanded section on neuroradiology, including review articles, pictorial essays, and commentaries, will accommodate more than the limited number of papers published under the previous agreement.

We invite authors of neuroradiologic articles to submit their papers for original publication in the *AJR* so that the Journal may continue to fulfill its commitment to supply timely and important original information about neuroradiology to general radiologists as well as to those who subspecialize in the field.

Robert N. Berk
Editor-in-Chief

The Morphologic Correlate of Incidental Punctate White Matter Hyperintensities on MR Images

F. Fazekas¹
 R. Kleinert²
 H. Offenbacher¹
 F. Payer¹
 R. Schmidt¹
 G. Kleinert¹
 H. Radner²
 H. Lechner¹

Postmortem examinations were made of the brains of six patients, 52–63 years old, who exhibited incidental punctate white matter hyperintensities on MR images before death. Our aim was to unravel the morphologic correlate of such lesions. By repeating the MR study after fixation on four specimens, cutting the brain parallel to the MR imaging plane, and examining whole-hemisphere microscopic sections, we optimized lesion identification. The white matter signal abnormalities were better delineated on pre- than postmortem scans, and visual inspection of the brain slices was normal in all but one location. Histologically, we found areas of reduced myelination with atrophy of the neuropil around fibrohyalinotic arteries as well as different stages of perivenous damage. The latter ranged from spongiform transformation of the neuropil and scattered foci of demyelination to large perivenous areas with marked rarefaction of myelinated fibers. Edematous glial swelling in foci of ganglion cell heterotopia caused subcortical white matter hyperintensities in one case.

Our results suggest minor perivascular damage but not infarction as the most likely substrate of punctate MR white matter hyperintensities in elderly brains. Histologic correlations with MR images obtained during life or with studies of unfixed material are necessary to analyze such small lesions.

AJNR 12:915–921, September/October 1991; *AJR* 157:1317–1323, December 1991

Areas of white matter displaying clinically unsuspected high signal intensity on proton-density- and T2-weighted sequences are a frequent finding on MR images of elderly individuals, and their sizes range from discrete foci to large coalescent lesions. When subjects above 70 years of age with a history of brain ischemia are excluded, the majority of these abnormalities consists of small hyperintensities [1]. This is especially true for neurologically asymptomatic volunteers with punctate white matter hyperintensities (WMH) that increase in frequency from 11% in the fourth decade to 65% in the seventh decade [2]. These lesions are located in the deep and subcortical white matter, are usually multiple, and rarely exceed 5 mm in diameter [3]. A vascular origin is suggested by their preponderance in persons exhibiting stroke risk factors [1, 2, 4, 5].

Ultimately, histologic assessment of such lesions is needed to unravel their morphologic substrate. Studies to date have used different methodological approaches, have included WMH of various size in their analyses, and have come to different conclusions. Awad et al. [5] compared specimens excised from brain areas harboring incidental WMH on MR with sections from normal-appearing brain both shortly after death and after fixation. The WMH specimens always contained enlarged perivascular spaces and ectatic small arteries and veins. Small areas of infarction were rarely seen. Kirkpatrick and Hayman [6] examined serial, whole-brain microscopic sections from 15 healthy subjects in the Armed Forces Institute of Pathology Yakovlev Collection. Their findings suggested zones of atrophic perivascular demyelination as the most frequent cause of small white matter lesions. However, no imaging correlates were available to these authors. Finally, MR of

Received December 18, 1990; revision requested February 11, 1991; revision received April 24, 1991; accepted April 29, 1991.

¹ Department of Neurology and MR Institute, Karl-Franzens University, Auenbruggerplatz 9, A-8036 Graz, Austria. Address reprint requests to F. Fazekas.

² Institute of Pathology, Laboratory of Neuropathology, Karl-Franzens University, Graz, Austria.

0361-803X/91/1576-1317
 © American Roentgen Ray Society

fixed brains guided the pathologists' search for WMH histomorphology in two other groups [7, 8]. Both describe infarcts as their predominant finding, but state that smaller foci frequently had not been identified.

These divergent observations stimulated us to conduct a correlative study focusing on punctate WMH as the most frequent incidental MR signal abnormality of still unclear significance. We compared the histology of whole-brain microscopic sections to in vivo MR results. Repeat scans done before the brain was cut served to determine fixation-induced signal changes and to document possible death-related alterations.

Materials and Methods

In a series of 34 patients who had undergone MR imaging (1.5-T, Philips Gyroscan S 15, Philips Medical Systems, Eindhoven, the Netherlands) of the head before death, six exhibited WMH of the punctate type. These abnormalities had been the only finding in two patients and appeared to be unrelated to a brain tumor in four others. None of them had had radiotherapy to the brain. The pertinent data of these patients and the time intervals between MR and death are provided in Table 1. Proton-density-weighted and T2-weighted images, 2400–2600/30,60–80/2 (TR/TE/excitations), had been obtained in all patients; T1-weighted axial scans, 600/30/2, were available in four cases. Slice thickness was 5–6 mm.

At postmortem the brains were removed in toto and fixed in 10% formaldehyde solution for at least 3 weeks. After fixation, four brains were rescanned with the same technique used for the patient studies.

Guided by the sagittal MR localizing view, the fixed specimens were then cut in 5-mm-thick axial slices. After careful inspection by two neuropathologists and the neuro-MR staff, at least two of those slices exhibiting WMH on MR and unaffected by the primary disease process were selected for preparing whole-brain microscopic sections. These were stained with H and E, Masson's trichrome, and the Klüver Barrera technique for myelin.

Results

Three to 24 (mean, 15) punctate WMH were present on in vivo MR images of the brains selected for this study. While

hyperintense on both echos of the long TR sequence, they did not appear on corresponding T1-weighted scans, which were available in four cases (1, 3, 4, 6). The majority of these lesions could be identified on postmortem images of brains 2, 3, 4, and 6, but many of them would not have been identified without knowledge of the in vivo results. There was less contrast between the focal abnormalities and normal white matter on MR images of the fixed brains so that WMH often were sufficiently visualized only on T2-weighted postmortem scans. Otherwise, the isointensity of WMH with CSF on this sequence impaired the detectability of subcortical lesions (Figs. 1A and 1B). In contrast to the situation on MR performed during life, we noted a higher signal intensity ratio of gray to white matter structures on T1-weighted images of the fixed brains. This fact has already been observed by others [8, 9].

The gross inspection of all brain slices, although guided by MR images, allowed us to identify a WMH correlate in only one instance. Brain 5 harbored a group of small disseminated grayish foci in a subcortical location corresponding to scattered WMH (Figs. 2A and 2B). There was no evidence of infarcts or lacunae in the white matter of any of the brains examined. Arteriosclerosis of the circle of Willis was mild in two cases and moderate in four.

Microscopic sections revealed abnormalities corresponding to in vivo MR findings in about one third of WMH. These consisted predominantly of perivascular tissue changes and are listed in Table 2. Frequently, we encountered arteries surrounded by large fluid-filled spaces. In regions with WMH this état criblé was associated with a halolike area of demyelination extending from a zone of compressed tissue toward the periphery (Fig. 1D). Sometimes the reduction of myelinated fibers was even more impressive around venous structures and coexisted with periarterial changes (Fig. 1D). In one location we identified a zone of edema adjacent to a white matter vein leading to spongiform transformation of the tissue (Fig. 3A). Scattered foci of demyelination close to venous structures (Fig. 3B) were seen at the site of another WMH. Finally, an area of dense periarterial fibrosis was noted in specimen 1 (Fig. 4), and a focal rarefaction of the myelin could not be clearly assigned to vascular structures in brains 4 and 5.

TABLE 1: Pertinent Patient Data and MR–Autopsy Intervals

Case No.	Age (years)	Sex	Cerebrovascular Risk Factors	Cause for MR Study	Cause of Death	MR to Autopsy Interval
1	52	M	Hypertension hypercholesterolemia	Psychosis	Congestive heart failure	14 days
2	55	M	Hypercholesterolemia	Cerebellar metastasis	Congestive heart failure	13 mo
3	59	M	Hypertension	Oligoastrocytoma	Increased intracranial pressure	34 days
4	60	M	Hypertension, diabetes mellitus, atrial fibrillation	Glioblastoma	Increased intracranial pressure	6 days
5	63	M	Myocardial infarction	Cervical myelopathy	Cardiac arrest	3 days
6	63	M	Diabetes mellitus, smoking	Glioblastoma	Congestive heart failure	17 days

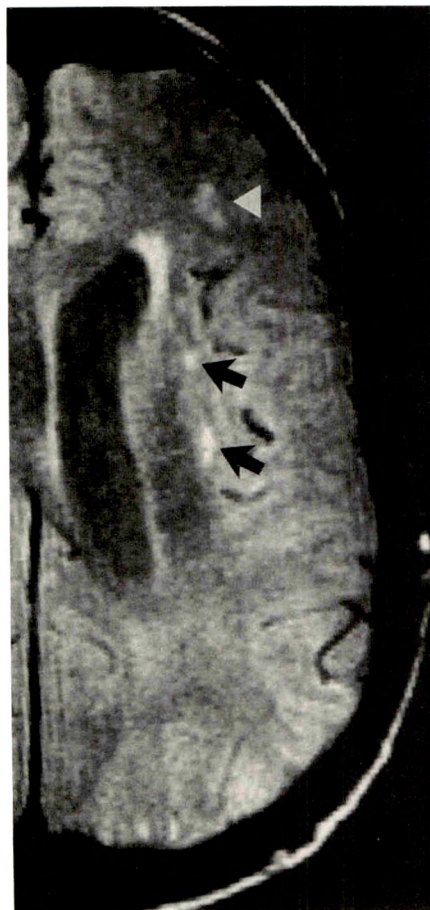
Fig. 1.—Case 4.

A, In vivo proton-density-weighted MR image (2500/30/2) shows two small hyperintensities in external capsule (arrows) and a less well defined hyperintensity in frontal white matter (arrowhead).

B, T2-weighted MR image (2500/80/2) after brain fixation shows only one of the lesions seen in vivo (arrow). It could not be unequivocally identified without knowledge of the premortem result.

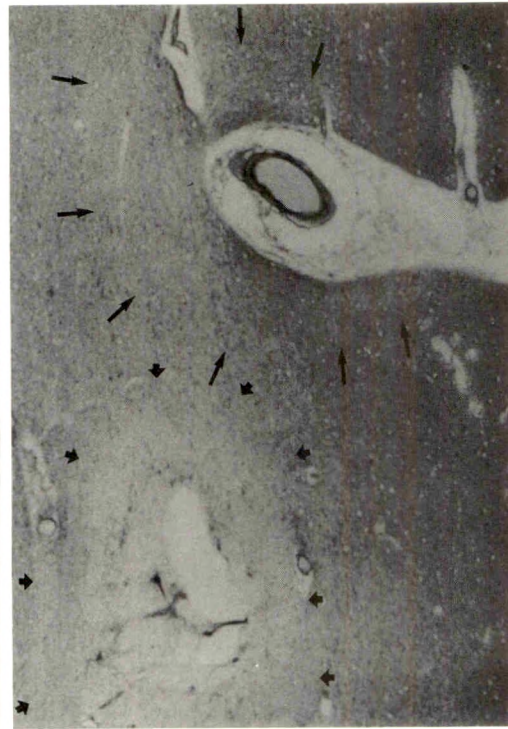
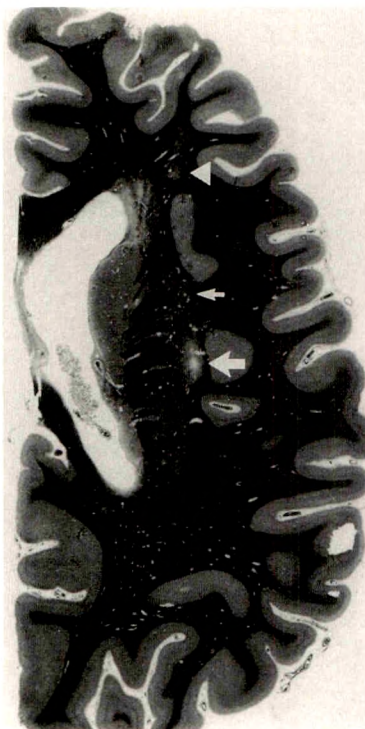
C, Myelin-stained whole-hemisphere microscopic section. Obvious correlate to white matter hyperintensities is delineated on both pre- and postmortem MR (large arrow), while more subtle changes correspond to those white matter hyperintensities present on in vivo MR only (small arrow and arrowhead). The latter was correlated to a circumscribed area of demyelination (not shown).

D, Histologic section of region indicated by large arrows in parts A–C. In upper right hand corner an artery with marked fibrohyalinosis is located within a large fluid-filled space bordered by a rim of compressed tissue (état criblé). The latter is surrounded by a halo of demyelination (short arrows). More extensive rarefaction of myelinated tissue is seen around a large vein (long arrows), whose wall was disrupted during preparation.



A

B



C

D

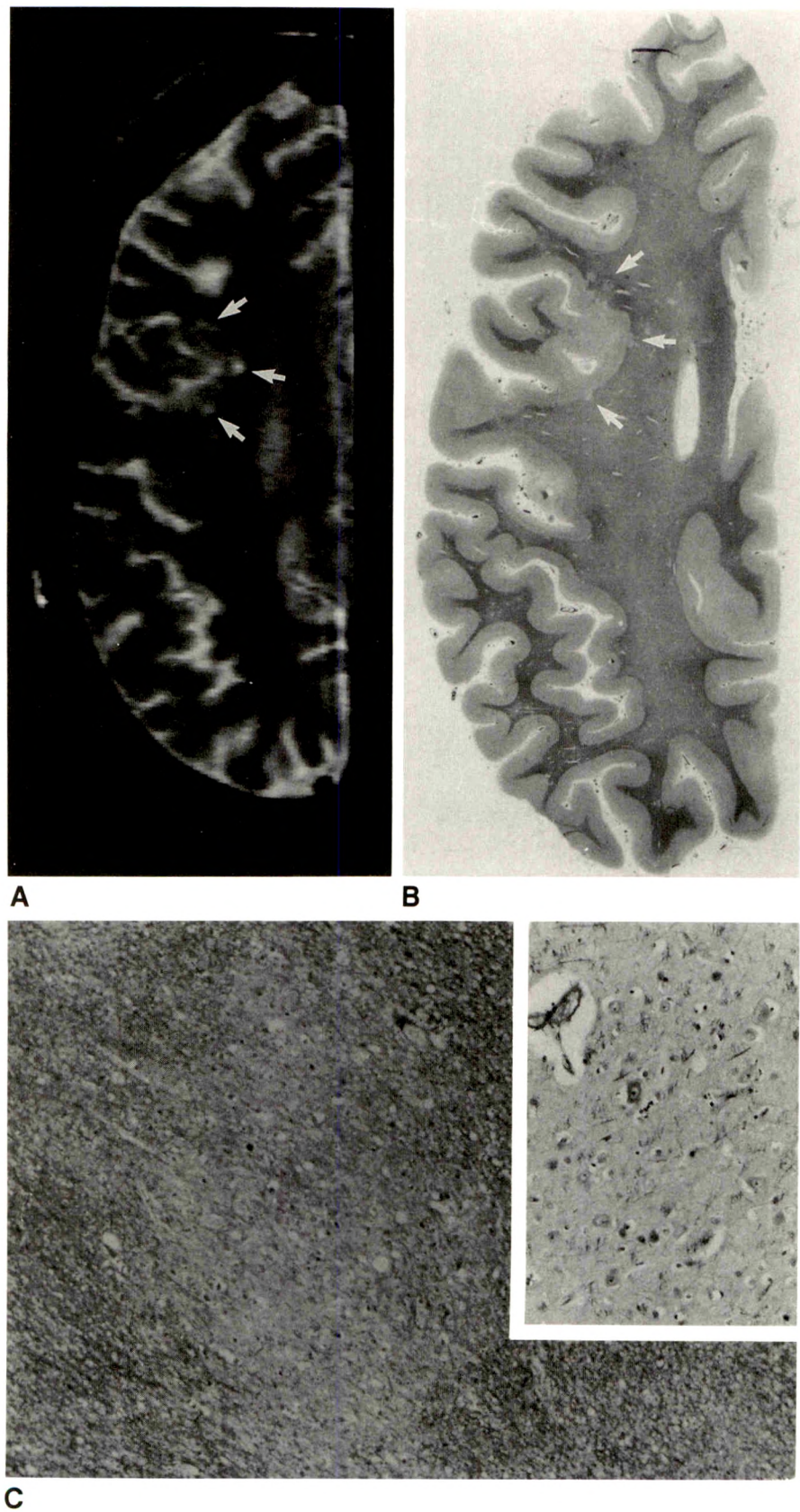
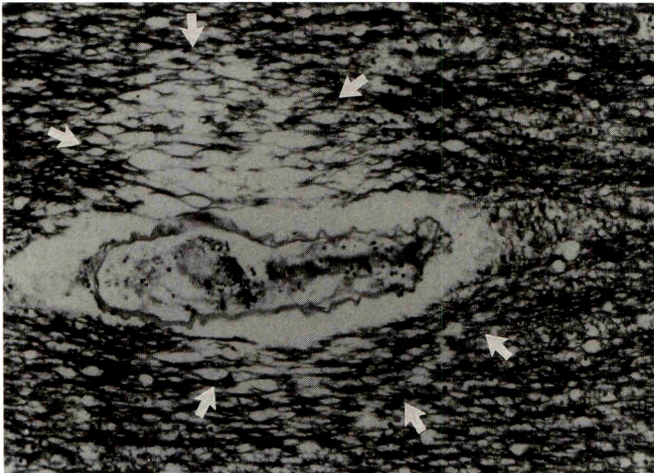


Fig. 2.—Case 5.
A, In vivo T2-weighted MR image (2500/60/2) shows discrete foci of high signal intensity in subcortical white matter (arrows).
B, Corresponding whole-hemisphere microscopic section reveals scattered grayish foci in this location (arrows).
C, Histologically, these gray foci consist of circumscribed ganglionic heterotopias (pale area) with edema of the neuropil. (Klüver Barera, original magnification $\times 75$; original magnification of inset $\times 256$)

TABLE 2: MR and Histopathologic Findings

Case No.	No. of White Matter Hyperintensities	No. of Lesions Identified/No. of White Matter Hyperintensities on Corresponding MR Scans	Type (No.) of Histopathologic Findings	Vessel-Wall Findings
1	24	3/14	Periarteriolar demyelination (2) and fibrosis (1)	Marked angiofibrosis and hyalinosis; mild arteriosclerosis
2	15	2/10	Perivenous edema (1) and demyelination (1)	Mild angiofibrosis and hyalinosis; moderate arteriosclerosis
3	6	0/3	None	Mild angiofibrosis and hyalinosis; moderate arteriosclerosis
4	7	5/6	Periarteriolar (2) and perivenous (2) demyelination; circumscribed area of demyelination (1)	Marked angiofibrosis and mild hyalinosis; mild arteriosclerosis
5	5	3/4	Ganglion cell heterotopia (2); circumscribed area of demyelination (1)	Mild angiofibrosis; moderate arteriosclerosis
6	3	1/2	Periarteriolar demyelination (1)	Marked angiofibrosis and moderate hyalinosis; moderate arteriosclerosis

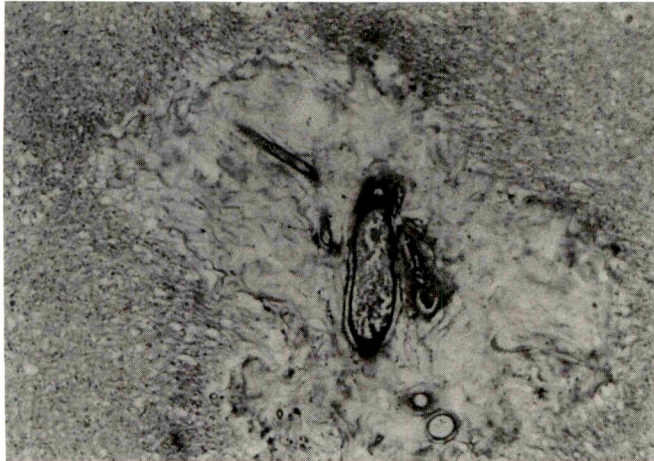


3A



3B

Fig. 3.—Case 2.
A, Focal perivenous edema adjacent to a white matter vein (arrows) causing spongiform tissue transformation. (Klüver Barrera, original magnification $\times 90$).
B, Scattered foci of reduced myelination and minimal edema in proximity to small veins tapering toward periphery. Arrows indicate border zone between area of tissue damage and almost normal-appearing white matter. (Klüver Barrera, original magnification $\times 75$).



4

Fig. 4.—Case 1. Sharply demarcated zone of dense periarterial fibrosis in deep white matter. No signs of inflammation. (Masson's trichrome, original magnification $\times 90$).

The small subcortical grayish foci observed visually in brain 5 appeared microscopically as clusters of heterotopic ganglion cells. However, the MR hyperintensity most likely resulted from the associated edematous glial swelling (Fig. 2C). Inflammatory cells were not seen in any of the lesions identified and there was no evidence of infarctions.

Discussion

Our histologic findings in areas corresponding to WMH on MR images consisted of a spectrum of perivascular tissue damage. Around arteries with walls thickened by hyalinosis and fibrosis we frequently observed large perivascular spaces bordered by atrophic neuropil. Extensive arterial pulsations have been implicated in their pathogenesis by initiating a water-hammer effect on the surrounding tissue. The resulting fluid-filled perivascular tunnels may not be enough, however, to explain the signal changes in question [5]. They should be iso- not hyperintense relative to CSF on a mixed sequence, as was described for the Virchow-Robin spaces over the high convexities, along the arteries entering the basal ganglia, and in the midbrain [10, 11]. Also, one might expect to notice such tunnels on subsequent cuts, which is not the case in MR signal abnormalities defined as WMH in this study. Additional tissue damage has to be the morphologic substrate for signal hyperintensity on both echos of a long TR sequence. In our study it consisted of a halolike rarefaction of myelinated fibers that surrounded the atrophic neuropil. It was only seen in correlation with WMH, while large perivascular spaces were present in MR negative regions as well. Focally decreased permeability of the vessel walls with subsequent malnutrition of the adjacent tissue was suggested as the underlying pathologic mechanism [6, 12].

These changes sometimes extended far beyond the vascular structures and were often seen better when looking at the myelin-stained section with the naked eye than with the microscope. This may be the reason why Awad et al. [5] attributed less importance to these findings than to the dilated perivascular spaces and to vascular ectasia. Foci of myelin loss that we identified remote from vascular structures appeared similar to demyelination around arteries, indicating that we may have sectioned a lesion border. Otherwise, one could suspect nutritive problems to occur in the border zones between small vessels as well.

WMH often appear to have been caused by tissue damage around white matter veins. The varying type and extent of changes observed histologically may reflect the gradual development of such lesions. As with arteries, signal abnormalities could start with episodes of perivascular edema caused by a temporary focal breakdown of the blood-brain barrier. Vessel-wall changes of both arteries and veins are known to occur with aging and are aggravated by the presence of cerebrovascular risk factors [13]. Astrocytes take up the extravasated serum proteins. Their intracellular water content increases and so-called "reactive" astrocytes develop. In the study of Marshall et al. [8] there was evidence of the presence

of such cellular changes at a great distance from small white matter infarcts. In addition, this form of chronic edema contributed to the actual MR lesion size. Concomitant damage to myelinated fibers would give rise to scattered rarefaction at first. With time, confluence of these foci might lead to the larger zones of perivenous demyelination present in two of the specimens examined. If, and to what extent, the cardiac situation or a chronically increased intracerebral pressure may have played some role in our cases is still unknown. Certainly the perivenous changes observed did not represent postmortem damage, since they corresponded to white matter signal abnormalities detected on MR images during life.

Scattered subcortical foci of heterotopic ganglion cells were an unexpected correlate of WMH in one of the specimens. Gray matter structures normally do not appear hyperintense on a T2-weighted sequence, but the high signal intensity can be explained by the associated edematous glial swelling.

We did not identify any complete infarct of the white matter in our series. This is in contrast to previous reports [7, 8] and, as suggested by one of the authors [7], methodological differences may account for it. We noticed a reduced likelihood of identifying small WMH on postmortem MR images compared with in vivo studies. The effects of formalin, brain shrinkage, and parenchymal alterations following death may all have contributed. Consequently, there is a skew toward detection of larger lesions when morphologic correlation is based only on WMH evidence from fixated brains, and an overestimation of the frequency of white matter infarcts underlying WMH in vivo is the result. The unexpectedly low number of WMH observed in those studies of fixed elderly brains further supports this assumption. Problems in identifying small histologic abnormalities on postmortem MR images were also noted in a more recent study evaluating fixed brains of AIDS patients [14]. Therefore, when analyzing small lesions, it is essential to perform correlative neuropathologic studies to MR images obtained during life or to images of unfixed specimens [5].

Unfortunately, this approach also has its disadvantages. If one uses for correlation only brains that have been studied by MR before death, one severely limits the number of specimens available and makes it necessary to include brains harboring other gross pathologic abnormalities. A consequent cerebral cause of death might mask or add some pathologic findings. Furthermore, there are serious problems in lesion localization. Brain cutting at an angle only slightly different from the imaging plane may be enough to miss small areas of damage. This does not occur when obtaining MR of fixed brain slices [15]. Therefore, some rarer causes for clinically unexpected punctate WMH will have remained undetected by our study. Nevertheless, our results support the vascular origin and subtle histologic nature of small incidental MR hyperintensities in the deep and subcortical white matter.

REFERENCES

1. Awad IA, Spetzler RF, Hodak JA, Awad CA, Carey R. Incidental subcortical lesions identified on magnetic resonance imaging in the elderly. I. Corre-

- lation with age and cerebrovascular risk factors. *Stroke* **1986**;17:1084-1089
2. Fazekas F. Magnetic resonance signal abnormalities in asymptomatic individuals: their incidence and functional correlates. *Eur Neurol* **1989**;29:164-168
 3. Fazekas F, Offenbacher H, Fuchs S, et al. Criteria for an increased specificity of MRI interpretation in elderly subjects with suspected multiple sclerosis. *Neurology* **1988**;38:1822-1825
 4. Lechner H, Schmidt R, Bertha G, Justich E, Offenbacher H, Schneider G. Nuclear magnetic resonance image white matter lesions and risk factors for stroke in normal individuals. *Stroke* **1988**;19:263-265
 5. Awad IA, Johnson PC, Spetzler RA, Hodak JA. Incidental subcortical lesions identified on magnetic resonance imaging in the elderly. II. Post-mortem pathological correlations. *Stroke* **1986**;17:1090-1097
 6. Kirkpatrick JB, Hayman LA. White-matter lesions in MR imaging of clinically healthy brains of elderly subjects: impossible pathologic basis. *Radiology* **1987**;162:509-511
 7. Braffman BH, Zimmerman RA, Trojanowski JQ, Gonatas NK, Hickey WF, Schlaepfer WW. Brain MR: pathologic correlation with gross and histopathology. 2. Hyperintense white-matter foci in the elderly. *AJNR* **1988**;9:629-636
 8. Marshall VG, Bradley WG, Marshall CE, Bhoopat T, Rhodes RH. Deep white matter infarction: correlation of MR imaging and histopathologic findings. *Radiology* **1988**;167:517-522
 9. Unger EC, Gado MH, Fulling KF, Littlefield JF. Acute cerebral infarction in monkeys: an experimental magnetic resonance study. *Radiology* **1987**;162:789-795
 10. Heier LA, Bauer CJ, Schwartz L, Zimmerman RD, Margello S, Deck MDF. Large Virchow-Robin spaces: MR-clinical correlation. *AJNR* **1989**;10:929-936
 11. Elster AD, Richardson DN. Focal high signal on MR scans of the midbrain caused by enlarged perivascular spaces: MR-pathologic correlation. *AJNR* **1990**;11:1119-1122
 12. Cervos-Navarro J, Iglesias K. The arteriole as a site of metabolic exchange. *Adv Neurol* **1978**;20:17-20
 13. Cervos-Navarro J, Schneider H. Pathologie des Nervensystems, volume 13/1. In: Doerr W, Seifert G, Uehlinger E, eds. *Spezielle pathologische Anatomie*. Berlin: Springer Verlag, **1980**:11-48
 14. Grafe MR, Press GA, Berthoty DP, Hesselink JR, Wiley CA. Abnormalities of the brain in AIDS patients: correlation of postmortem MR findings with neuropathology. *AJNR* **1990**;11:905-911
 15. Burger PC. Postmortem (specimen) MR. *AJNR* **1990**;11:912-913

Book Review

Magnetic Resonance Imaging of the Brain and Spine. Edited by Scott W. Atlas. New York: Raven, 1151 pp., 1991. \$165

Magnetic Resonance Imaging of the Brain and Spine consists of 28 chapters written by authors who have extensive personal experience with the topics on which they write. The text is comprehensive and for a work of this size with more than one contributor, has surprisingly little redundancy. The illustrations generally are of superior quality. A lack of cross-referencing is a general deficiency. The index would be better if it were more extensive.

Chapters 1–7 and chapters 26 and 28 are devoted to the basic physical principles and applications of clinical MR imaging techniques. Overall, they provide a good introduction to the technical aspects of medical MR imaging. As in any work that has many contributors, the quality of the various sections is somewhat uneven. The chapters on instrumentation, the basis of MR contrast, fast imaging, bioeffects and safety considerations, and MR spectroscopy present the subject matter in a lucid and concise manner that is entirely suitable for the intended audience. Other sections in this part of the book are sometimes sketchy and depend too much on text alone for the description of difficult concepts (e.g., principles of image formation); present information so dense and complex that it may inundate many in the intended audience (e.g., contrast agents and relaxation effects); or although providing good discussion of some topics, are unbalanced in other areas (e.g., the chapter on artifacts gives an excellent account of artifacts due to instrumentation errors whereas that on sampling artifacts is difficult to follow). The chapter on artifacts and the one on flow theory and MR techniques are examples of where cross-referencing would improve the book. The discussion of MR angiography in chapter 4 does not reflect the importance of the topic; however, this is somewhat compensated for by the excellent discussion of MR angiography given in chapter 27. The separation of these two interlinked topics and lack of cross-referencing is an indication of the difficulty in keeping a work of this magnitude from becoming outdated even as it is in preparation.

The remaining 19 chapters (8–25, 27) discuss, using traditional disease classification, the use of MR imaging in diagnosing diseases of the CNS and spine. These chapters provide a generally excellent discussion of the place of MR in the evaluation of CNS and spinal diseases. As with the physics portion of the book, however, the completeness and clarity of the various chapters are somewhat uneven. The sections on brain development, intracranial hemorrhage, intra- and extraaxial brain tumors, intracranial vascular malformations, trauma, white matter disease, the sella and parasellar region, base of the skull, the orbit and visual system, degenerative diseases of the spine, and congenital anomalies of the spine and spinal cord are noteworthy because of their completeness and the high quality of the illustrations. As with some of the chapters on the technical aspects of MR, some material in these chapters is either of questionable value to the intended audience or is presented with a conviction that does not reflect the reality of clinical practice (e.g., the discussion on the magnetic properties of matter given in chapter 9 and the statement in chapter 10 that necrosis can be identified with “near certainty” with appropriate pulse sequences).

In his preface to *Magnetic Resonance Imaging of the Brain and Spine*, Atlas says that his aim in preparing this text was to provide “a sophisticated, complete and accurate book on the science that was up-to-date on the technical and clinical topics.” From our perspective, full realization of such a goal in a field that is developing and evolving at the rate that MR is cannot be achieved in a hardcover volume. This difficulty and the expense of this otherwise excellent book are its major deficiencies.

James A. Sorenson
Charles M. Strother
University of Wisconsin Medical School
Madison, WI 53792

Nonaneurysmal Perimesencephalic Subarachnoid Hemorrhage: CT and MR Patterns That Differ from Aneurysmal Rupture

Gabriel J. E. Rinkel¹
 Eelco F. M. Wijdicks¹
 Marinus Vermeulen²
 Lino M. P. Ramos³
 Hervé L. J. Tanghe⁴
 Djo Hasan²
 Linda C. Meiners³
 Jan van Gijn¹

We describe a characteristic distribution of cisternal blood in 52 patients with nonaneurysmal subarachnoid hemorrhage proved by a normal angiogram. On CT, the center of the bleeding was located immediately anterior to the brainstem in all patients, which was confirmed in four patients who were studied with MR imaging. Extension to the ambient cisterns or to the basal parts of the sylvian fissures was common, but the lateral sylvian or anterior interhemispheric fissures were never completely filled with blood. Rupture into the ventricular system did not occur. MR demonstrated downward extension of the blood anterior to the brainstem as far as the medulla, but failed to detect the source of hemorrhage. Our aim was to determine whether this so-called nonaneurysmal perimesencephalic hemorrhage could be distinguished from aneurysmal subarachnoid hemorrhage on early CT scans. Two neuroradiologists were shown a consecutive series of 221 CT scans of patients with subarachnoid hemorrhage who subsequently underwent angiography. Only one patient with a basilar artery aneurysm on angiography was incorrectly labeled by both observers as having a nonaneurysmal perimesencephalic pattern of hemorrhage.

The high predictive value of the perimesencephalic pattern of hemorrhage for a normal angiogram (0.95 and 0.94, respectively, for the two observers) and the excellent interobserver agreement (κ 0.87) demonstrate that nonaneurysmal perimesencephalic hemorrhage can be distinguished on CT in the majority of patients. Recognition of this pattern of hemorrhage is important as patients with this subset of subarachnoid hemorrhage have an excellent prognosis.

AJNR 12:829-834, September/October 1991; *AJR* 157:1325-1330, December 1991

The distribution of extravasated blood on CT scans in patients with subarachnoid hemorrhage may predict the site of the ruptured aneurysm [1]. Half the patients with subarachnoid hemorrhage and a normal angiogram showed a predominance of blood in the cisterns around the midbrain [2, 3]. This contrasts with aneurysmal subarachnoid hemorrhage, in which hemorrhages resulting from posterior circulation aneurysms were found in only approximately 10% of the patients [1, 4].

The clinical picture of patients with perimesencephalic hemorrhage and a normal angiogram is characterized by an uncomplicated clinical course, without delayed cerebral ischemia or rehemorrhage [2], and with an excellent prognosis 18 months to 7 years after the hemorrhage [5]. These clinical features differ from the aneurysmal type of subarachnoid hemorrhage and strongly argue against an undetected aneurysm as the source of this type of hemorrhage.

We studied the radiologic characteristics in a large series of consecutive patients with this so-called nonaneurysmal perimesencephalic hemorrhage to gather radiologic criteria for its recognition. Using these criteria, we addressed the question of whether this pattern could be completely distinguished from that of aneurysmal subarachnoid hemorrhage on CT. Therefore, we conducted an interobserver study to determine the predictive value of identifying a perimesencephalic pattern of hemorrhage on CT for a normal angiogram.

Received October 19, 1990; revision requested January 14, 1991; revision received March 11, 1991; accepted March 22, 1991.

¹ University Department of Neurology, Heidelberglaan 100, 3584 CX Utrecht, The Netherlands. Address reprint requests to G. J. E. Rinkel.

² University Department of Neurology, Rotterdam, The Netherlands.

³ University Department of Radiology, Utrecht, The Netherlands.

⁴ University Department of Radiology, Rotterdam, The Netherlands.

0361-803X/91/1576-1325

© American Roentgen Ray Society

Subjects and Methods

We studied 52 consecutive patients with (1) signs and symptoms of subarachnoid hemorrhage, (2) a normal four-vessel angiogram, and (3) a CT study performed within 72 hr of the first clinical symptoms that showed a subarachnoid hemorrhage located predominantly in the posterior portion of the basal cisterns. Patients with a normal angiogram in which the center of the hemorrhage was located in the anterior portion of the basal cisterns, suggesting an anterior communicating–internal carotid or middle cerebral artery aneurysm, were excluded and will be the subject of a separate paper.

CT scanning was performed within 24 hr of the ictus in 45 patients and between 24 and 72 hr in seven patients. In 12 patients CT scanning was repeated 1 week after the hemorrhage. CT scans were performed on a Philips tomoscan 350 or 500 third-generation scanner. Contiguous slices of 3 mm were used in the region of the basal cisterns. In the supratentorial part of the brain noncontiguous slices of 5 mm were made. In none of the patients was contrast material used.

In four patients MR scans with detailed views of the brainstem were obtained within 5 days of the hemorrhage and again after 6 weeks to investigate the possibility of a small angioma being the source of bleeding in perimesencephalic hemorrhage. MR images were made on a Philips Gyroscan S15 (1.5-T) scanner. Slices of 4 mm thickness with a 0.8-mm gap were made in the area of the brainstem in both the transverse and sagittal planes. Both T1-weighted spin echo (SE) 500/30/2 (TR/TE/excitations) and T2-weighted SE 2000/50/2 and 2000/100/2 sequences were used. Additional T2-weighted SE 2000/50/1 and 2000/100/1 transverse slices of 8 mm thickness with a 1.6-mm gap were made of the entire brain. The MR examination was not performed with contrast agent.

All patients had selective bilateral internal carotid and bilateral vertebral angiography with frontal, lateral, and oblique projections. Subtraction films were obtained in most patients. Angiograms were usually made within 3 days of the hemorrhage. Angiography was repeated in 12 patients, in two because of narrowing of the basilar artery on the first angiogram and in one because of poor visualization of the posterior inferior cerebellar artery. In the remaining nine patients angiography was repeated 3 months after the hemorrhage. All repeated angiograms were completely normal.

After having detailed the blood distribution in these 52 patients, we outlined radiologic criteria for the pattern of perimesencephalic hemorrhage as follows: (1) center of the hemorrhage located immediately anterior to the midbrain, with or without extension of blood to the anterior part of the ambient cistern or to the basal part of the sylvian fissure; (2) no complete filling of the anterior interhemispheric fissure and no extension to the lateral sylvian fissure, except for minute amounts of blood; (3) absence of frank intraventricular hemorrhage. To test the validity of these criteria, we conducted an interobserver study with two neuroradiologists. From a consecutive series of patients with spontaneous subarachnoid hemorrhage admitted between 1983 and 1989 to the departments of neurology of the university hospitals in Utrecht and Rotterdam we selected patients who had blood visible on CT scans obtained within 72 hr of the ictus and who underwent selective four-vessel angiography. The CT scans of the 221 patients fulfilling these criteria form the basis of the present study. All CT scans were made on a Philips tomoscan 350 or 500 third-generation scanner. The results of angiography in the 221 patients were as follows. Thirty-one patients had a normal four-vessel angiogram. In the remaining 190 patients angiograms revealed aneurysms of the anterior cerebral artery in 72, the internal carotid artery in 55, the middle cerebral artery in 41, the pericallosal artery in seven, and the posterior circulation in 15, with 12 located at the basilar artery. Twenty-two of the 31 patients with a normal angiogram had

extravasated blood predominantly in the posterior portion of the basal cisterns, in the remaining nine patients the center of the bleeding was located in the anterior half of the basal cisterns.

The entire set of CT scans was shown separately to two experienced neuroradiologists. They were asked to distinguish between a nonaneurysmal perimesencephalic and an aneurysmal pattern of subarachnoid hemorrhage. The observers were unaware of the results of angiography at the time of the review. The degree of agreement between the two observers was measured by kappa statistics [6]. $\kappa = (P_o - P_e)/(1 - P_e)$, where P_o is the observed percentage of agreement and P_e is the percentage of agreement that is expected by chance. (κ is 0.0 when there is just chance agreement and 1.0 when there is perfect agreement.)

Results

The mean age of the patients was 53 years (range, 22–70 years). Thirty-two patients were men, 20 were women. All patients had a sudden onset of headache. Only two patients lost consciousness for a few minutes at the time of the ictus. All patients were found to have a normal level of consciousness on admission, and, except for neck stiffness, a normal neurologic examination corresponding with WFNS grade 1 [7].

Amount of Blood on CT Scan

There was a marked variation of the amount of cisternal blood within this series. In two patients only one of the basal cisterns was filled with blood, and then only partly. At the other extreme were four patients in whom all perimesencephalic cisterns were filled with blood, with extension to both basal parts of the sylvian fissures. In most other patients two or more cisterns were partly or completely filled with blood.

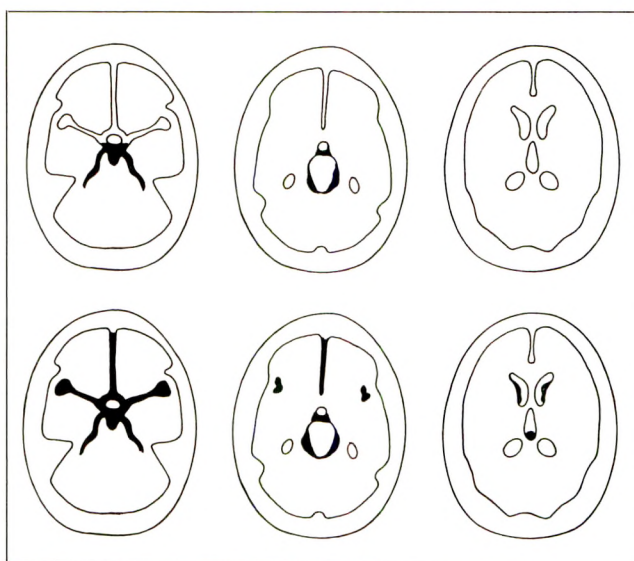


Fig. 1.—Line drawing shows axial views of characteristic pattern of blood distribution in nonaneurysmal perimesencephalic hemorrhage (upper row) compared with characteristic pattern of blood distribution in subarachnoid hemorrhage from a ruptured basilar artery aneurysm (lower row).

Fig. 2.—CT scan shows center of bleeding in interpeduncular fossa, with extension of blood into both ambient cisterns.

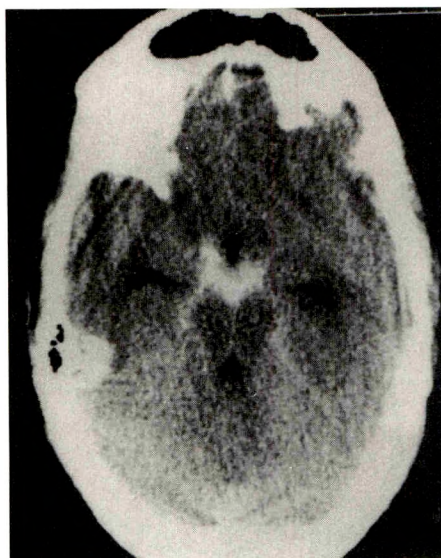


Fig. 3.—CT scan shows center of bleeding extending from interpeduncular fossa to left ambient cistern.



2

3

Sedimentation of blood in the posterior parts of the lateral ventricles occurred in 11 patients (21%), but frank intraventricular hemorrhage was not found.

Distribution of Blood on CT Scan

The characteristic pattern of blood distribution in nonaneurysmal perimesencephalic subarachnoid hemorrhage is illustrated in Figure 1.

In 45 (87%) of the 52 patients the center of the bleeding was located immediately anterior to the midbrain and pons (Fig. 2). In the remaining seven patients (13%) the center of

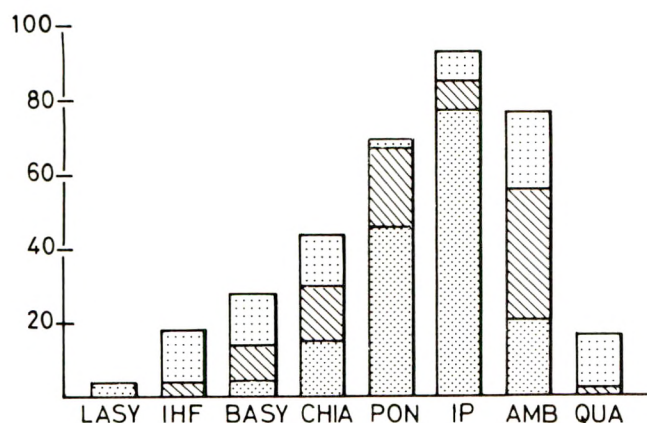


Fig. 4.—Graph shows distribution of cisternal blood in 52 patients with perimesencephalic hemorrhage. Bars represent percentage of patients in whom the cistern in question contained blood. Densely dotted areas = completely filled (grade 3); hatched areas = partly filled (grade 2); sparsely dotted areas = blood barely visible (grade 1). LASY = lateral part of sylvian fissures; IHF = anterior interhemispheric fissure; BASY = basal part of sylvian fissures; CHIA = chiasmatic cisterns; PON = prepontine cistern; IP = interpeduncular cistern; AMB = ambient cisterns; QUA = quadrigeminal cistern.

the bleeding extended from the interpeduncular cistern to the anterior part of one of the ambient cisterns (Fig. 3).

The distribution of cisternal blood is summarized in Figure 4. The prepontine cistern could be adequately visualized in 38 patients, in all of which it contained blood, most often contiguous with blood in the interpeduncular and suprasellar cisterns, either as a long, thin layer (Fig. 5) or as a more local clot. In some patients the blood extended to the lower pons. In two patients a prepontine clot was the only site of hemorrhage (Fig. 6). The interpeduncular cistern was filled with blood in 50 patients (96%), completely in 37 patients, and partly in 13. Blood extended to one or both chiasmatic cisterns in 24 patients (46%), but in only three patients were both chiasmatic cisterns completely filled with blood. In 46 patients (88%) blood was visible in one or both ambient cisterns, with extension into the quadrigeminal cistern in only 10 of these (19%). Blood in the quadrigeminal cistern not accompanied by blood in an ambient cistern did not occur in this study.

In 19 patients (37%) evidence of blood was present in the basal part of the sylvian fissure, invariably contiguous with blood in the chiasmatic cistern. In nine of these 19 patients both basal sylvian fissures contained blood, and in one of these patients the basal part of both fissures was completely filled with blood. In two patients a small amount of blood (grade 1) was found in the lateral sylvian fissure.

In nine patients (17%) the hemorrhage extended to the posterior part of the anterior interhemispheric fissure (Fig. 7). This fissure was never completely filled.

Repeated CT Scanning

In 12 patients CT scanning was repeated 1 week after the hemorrhage. In one patient a small amount of blood was still visible in the prepontine cistern, in all other patients the cisternal blood had completely disappeared.



Fig. 5.—CT scan shows long, thin layer of blood in prepontine cistern.

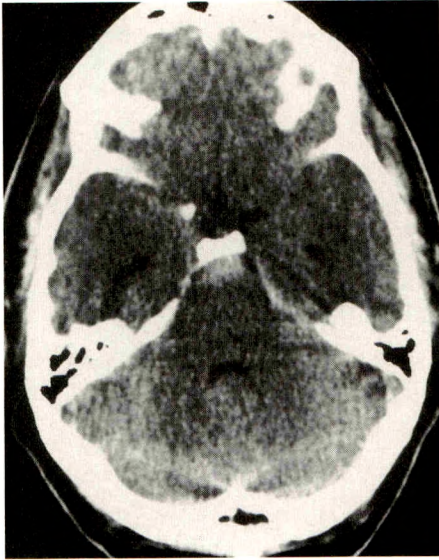


Fig. 6.—CT scan shows isolated clot in prepontine cistern.

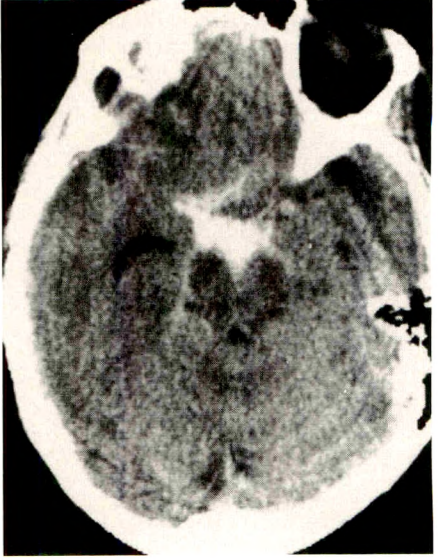
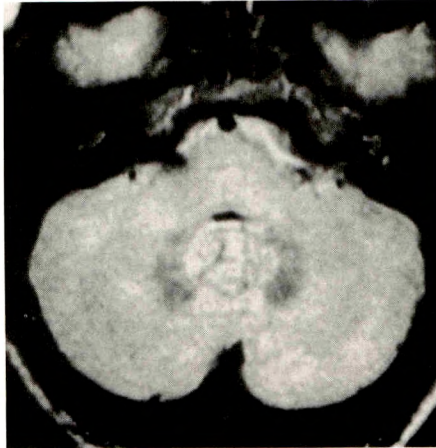


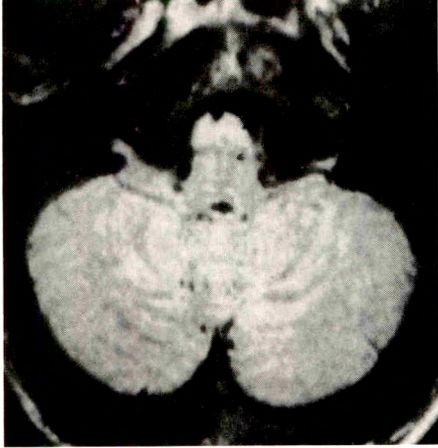
Fig. 7.—CT scan shows blood in interpeduncular fossa with extension to both ambient cisterns, chiasmal cistern, and basal part of sylvian fissure on the right, and to posterior part of anterior interhemispheric fissure.



A

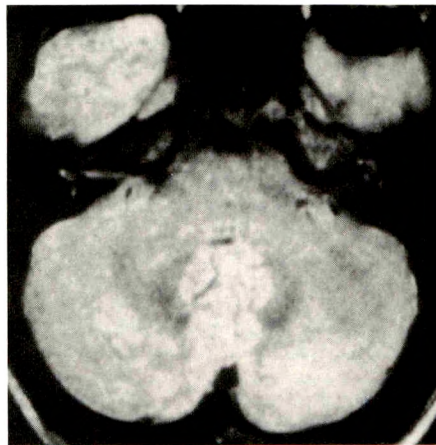


B

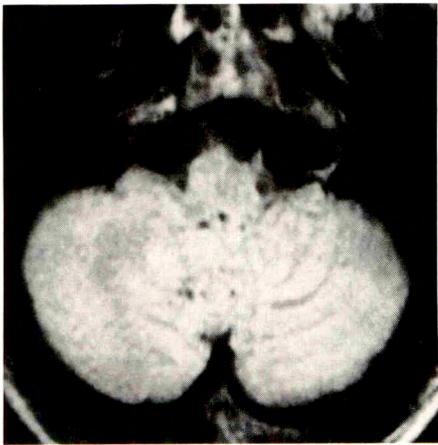


C

Fig. 8.—A-E, Blood in interpeduncular cistern on CT scan (A) and blood in front of pons (B) and medulla oblongata (C) on MR images (SE 2000/50) in same patient. MR images obtained 6 weeks later show that blood had disappeared (D and E).



D



E

		result of angiography		
		aneurysm	no aneurysm	total
prediction of observers	A			
	B			
aneurysm	aneurysm	14	7	21
	no aneurysm	1	15	16
total		15	22	37

Fig. 9.—Schematic shows observers' predictions of aneurysmal origin of subarachnoid hemorrhage in posterior circulation on the basis of CT scans (observer A = upper right half, observer B = lower left half) compared with the results of angiography.

MR Scanning

Within 5 days after the hemorrhage, subarachnoid blood was best visualized on the first echo of the T2-weighted sequence (2000/50). On this sequence the blood showed increased signal relative to the adjacent brainstem. The appearance of blood was hyperintense on the second echo of the T2-weighted sequence. The signal of the blood on the T1-weighted sequence was intermediate between the signal of the brainstem and the signal of CSF. In all patients examined, blood was demonstrated immediately anterior to the lower brainstem. In one case the hemorrhage extended from the pons to the medulla (Figs. 8A–8C). After 6 weeks blood could no longer be demonstrated in any of the patients (Figs. 8D and 8E). A vascular abnormality could not be visualized, either in the acute phase or after the blood had disappeared.

Interobserver Study

The strongest agreement between the two observers was found in patients who had a CT scan in which the center of

the bleeding was not predominantly in the posterior portion of the basal cisterns. All these patients were considered to have the aneurysmal pattern of hemorrhage by both observers. A compilation of the observers' predictions of the origin of hemorrhage in the 37 patients with a predominance of blood in the posterior portion of the basal cisterns (15 patients with a proved posterior circulation aneurysm and 22 patients with a normal angiogram) appears in Figure 9. A fair proportion of patients with a posterior hemorrhage were thought to have an aneurysm when in fact they did not: three of 17 by observer A (false-positive rate 18%; 95% confidence interval [CI] 0.04–0.43) and seven of 21 by observer B (false-positive rate 33%; 95% CI 0.15–0.57). In all these CT scans the relative amount of cisternal blood in front of the brainstem was comparatively great (Fig. 10).

The predictive value of a perimesencephalic pattern of hemorrhage for a normal angiogram (true-negative rate) was 0.95 (95% CI 0.75–0.99) for observer A and 0.94 (95% CI 0.70–0.99) for observer B. Both observers mislabeled one (the same) patient with a proved basilar artery aneurysm as a perimesencephalic pattern of hemorrhage (false-negative rate for observer A 0.05 (95% CI 0.01–0.25) and for observer B 0.06 (95% CI 0.01–0.30)). All 15 CT scans correctly labeled as nonaneurysmal perimesencephalic by observer B were also labeled as nonaneurysmal perimesencephalic by observer A. The CT scans of the remaining three patients with a posterior hemorrhage and a normal angiogram were not identified as nonaneurysmal perimesencephalic by either observer. Thus, the observers disagreed on four patients with a normal angiogram. The κ value for interobserver agreement was 0.87 (95% CI 0.75–0.99).

Discussion

In approximately 15% of patients with subarachnoid hemorrhage no aneurysm is found despite high-quality four-vessel angiography [8]. In patients with a normal angiogram, a high rate of hemorrhages originating in the posterior portion of the basal cisterns has been noted by several authors [2, 3, 9–11]. In the present series of patients with nonaneurysmal perimesencephalic hemorrhage we found that the CT pattern of subarachnoid bleeding suggested a site of origin immediately anterior to the brainstem, usually in the interpeduncular and prepontine cisterns. In a few cases the suggested site of origin extended to the anterior part of one of the ambient cisterns. Prepontine blood was always present when this region was properly visualized. In only a few patients, subarachnoid blood extended farther backward to the quadrigeminal cistern or anteriorly to the basal part of the sylvian fissure or the posterior part of the anterior interhemispheric fissure. MR studies in these patients showed blood immediately anterior to the lower part of the brainstem. We never found complete filling of the anterior interhemispheric fissure, and extension to the lateral sylvian fissure was extremely uncommon and then only minimal. Frank intraventricular hemorrhage did not occur.

We found that this pattern of cisternal hemorrhage could be differentiated from patterns of subarachnoid hemorrhage

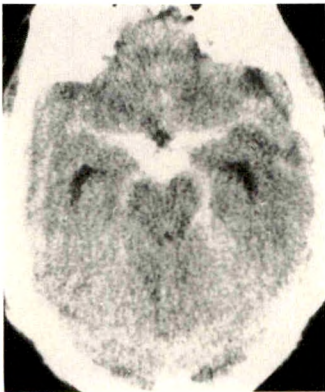


Fig. 10.—CT scan of a patient with nonaneurysmal perimesencephalic hemorrhage, mistaken for a ruptured basilar artery aneurysm.

caused by a ruptured aneurysm in most patients. The predictive value of a perimesencephalic pattern of hemorrhage for a normal angiogram was very high, but a serious source of error is that the occasional patient with a ruptured aneurysm of the basilar artery may show a pattern of hemorrhage on CT resembling that of nonaneurysmal perimesencephalic hemorrhage. In our series, 11 of the 12 basilar artery aneurysms could easily be distinguished from nonaneurysmal perimesencephalic hemorrhage by either extension of blood into the anterior interhemispheric or lateral sylvian fissures or by the presence of intraventricular hemorrhage. In the 12th case of basilar artery aneurysm, however, both features were absent and the pattern of extravasation could not be distinguished from a perimesencephalic pattern of hemorrhage by either observer. A careful reconsideration of this misjudged CT scan of the patient with a proved basilar artery aneurysm revealed one possible distinguishing feature. The slice through the suprasellar cisterns in this particular patient showed a homogeneous filling by blood of all suprasellar cisterns (interpeduncular as well as chiasmatic) and both ambient cisterns, rather than a clot remaining confined immediately anterior to the midbrain and pons, which is characteristic of a perimesencephalic pattern hemorrhage. Studies with even larger series of patients are needed to validate this potential discriminating feature.

Given that the rare patient with a ruptured aneurysm of the basilar artery but a nonaneurysmal pattern of hemorrhage will still occur in one of every 20 (observer A) or 16 (observer B) cases in which a negative angiogram is predicted, the risk of missing a basilar artery aneurysm by omitting angiography in patients with this type of hemorrhage is about 5–6% (95% CI 0–31%). The chance of a fatal rehemorrhage in patients with a ruptured basilar artery aneurysm after the second week has been found to be 48% [12]. This risk of fatal rehemorrhage after omitting angiography clearly outweighs complications of angiography in patients with a normal angiogram (0.7%) [13] even if combined with the mortality of operations on a ruptured basilar artery aneurysm (6%) [14]. Therefore, we still advocate angiography in all patients with a perimesencephalic pattern of hemorrhage, despite the many negative results.

The cause of perimesencephalic hemorrhage remains elusive. Angiograms with particular attention to the venous phase [2] and MR scans with detailed views of the brainstem and surrounding cisterns have, to date, failed to detect a cause for nonaneurysmal perimesencephalic hemorrhage. Nevertheless, not only the negative findings on angiography but also certain features that are common to all patients with nonaneurysmal perimesencephalic hemorrhage, strongly argue against an undetected basilar artery aneurysm. These are (1) the localized nature of the clot, quite different from the extension in aneurysmal patterns; (2) the uncomplicated clinical course without rehemorrhage or ischemia [2]; and (3) the excellent prognosis after a mean follow-up period of 4 years (range, 18–83 months) without deterioration or rehemorrhage

in a large series of patients with perimesencephalic hemorrhage [5], whereas basilar artery aneurysms usually carry a fatal rehemorrhage risk of almost 50% in the first 4 years after the initial hemorrhage [12]. These features favor a venous or capillary rupture. Rupture of one of the anterior longitudinal pontine veins in the prepontine cistern or of the interpeduncular and posterior communicating veins in the interpeduncular cistern [15, 16] may explain both the clinical picture and the peculiar CT scan pattern. Widespread awareness of this CT pattern of hemorrhage may eventually be useful in determining the cause of this separate entity of nonaneurysmal hemorrhage.

REFERENCES

1. van Gijn J, van Dongen KJ. Computed tomography in the diagnosis of subarachnoid haemorrhage and ruptured aneurysm. *Clin Neurol Neurosurg* 1980;82:11–24
2. van Gijn J, van Dongen KJ, Vermeulen M, Hijdra A. Perimesencephalic hemorrhage: a nonaneurysmal and benign form of subarachnoid hemorrhage. *Neurology* 1985;35:493–497
3. Alexander MSM, Dias PS, Uttley D. Spontaneous subarachnoid hemorrhage and negative cerebral panangiography. *J Neurosurg* 1986;64:537–542
4. Maurice-Williams RS. *Subarachnoid hemorrhage: aneurysms and vascular malformations of the central nervous system*. Bristol: Wright, 1987: 101–105
5. Rinkel GJE, Wijdeveld EFM, Vermeulen M, Hageman LM, Tans JTJ, van Gijn J. Outcome in perimesencephalic (nonaneurysmal) subarachnoid hemorrhage. *Neurology* 1990;40:1130–1132
6. World Federation of Neurological Surgeons. Report of World Federation of Neurological Surgeons committee on a universal subarachnoid hemorrhage grading scale. *J Neurosurg* 1988;68:985–986
7. Cohen J. A coefficient of agreement for nominal scales. *Educ Psychol Meas* 1960;20:37–46
8. Kassell NF, Torner JC, Jane JA, Haley EC, Adams HP. The international cooperative study on the timing of aneurysm surgery. Part 2: Surgical results. *J Neurosurg* 1990;73:37–47
9. Iwanaga H, Wakai S, Ochai C, Narita J, Inoh S, Nagai M. Ruptured cerebral aneurysms missed by initial angiographic study. *Neurosurgery* 1990;27:45–51
10. Cioffi F, Pasqualin A, Cavazzani P, Da Pian R. Subarachnoid hemorrhage of unknown origin: clinical and tomographical aspects. *Acta Neurochir* 1989;97:31–39
11. Stober T, Emde H, Anstätt T, Freier G, Metzger U. Blood distribution in computer cranial tomograms after subarachnoid hemorrhage with and without an aneurysm on angiography. *Eur Neurol* 1985;24:319–323
12. Troupp H. The natural history of aneurysms of the basilar bifurcation. *Acta Neurol Scand* 1971;47:350–356
13. Mani RL, Eisenberg RL. Complications of cerebral arteriography: analysis of 5000 procedures. II. Relation of complication rates to clinical arteriographic diagnosis. *AJR* 1978;131:867–869
14. Peerless SJ, Drake GG. Vertebro-basilar aneurysms. In: Wilson CB, Hoff JT, eds. *Current surgical management of neurological disease*. London: Churchill Livingstone, 1980:144–168
15. Yasargil GM, Kasdaglis K, Jain KK, Weber HP. Anatomical observations of the subarachnoid cisterns of the brain during surgery. *J Neurosurg* 1976;44:298–302
16. Braun JP, Tournade A, Ammerich H. Transverse anastomoses of the veins at the base of the brain. *Neuroradiology* 1976;12:165–169

Perspective

A Dial-Up Digital Teleradiology System: Technical Considerations and Clinical Experience

Arch W. Templeton,¹ Samuel J. Dwyer III, Stanton J. Rosenthal, Donald A. Eckard, Linda A. Harrison, and Larry T. Cook

Teleradiology transmits radiologic images and consultative text from one site to another [1]. A digital teleradiology system requires the integration of a wide area network (WAN) and local area networks (LANs) [2]. The WAN acquires digital images from the LAN at one site and transmits them to an LAN at one or more other sites. Connected sites can include hospitals, clinics, trauma centers, and subspecialty interpretation centers. Transmitted images can be used in emergency service, treatment planning, definitive diagnosis, subspecialty consultations, and backup.

The LANs at Munson and Irwin Army Community Hospitals and our radiology department at the University of Kansas Medical Center are each interfaced to a laser film digitizer, an interactive display, a computer system, and a WAN interface. In addition, the LAN at the University of Kansas Medical Center has a laser film printer. Transmitted images are displayed on either a gray-scale workstation or conventional view boxes by using the laser-printed hard copy. Digital imaging techniques that are interfaced to the LAN, such as CT, MR, sonography, nuclear medicine, and computed radiography, can have their image data transmitted directly.

We have implemented and clinically tested a teleradiology system that uses dial-up, multiple switched 56,000-bits/sec digital voice channels for the WAN. This article presents some of the technical considerations and our clinical experiences and perspectives in the use of the system.

Teleradiology Network

The University of Kansas Medical Center teleradiology system (Fig. 1) is a dial-up, full-duplex WAN interconnecting the Munson Army Community Hospital, the Irwin Army Community Hospital, and the University of Kansas Medical Center. The WAN uses a combination of copper T-1 service (1.544

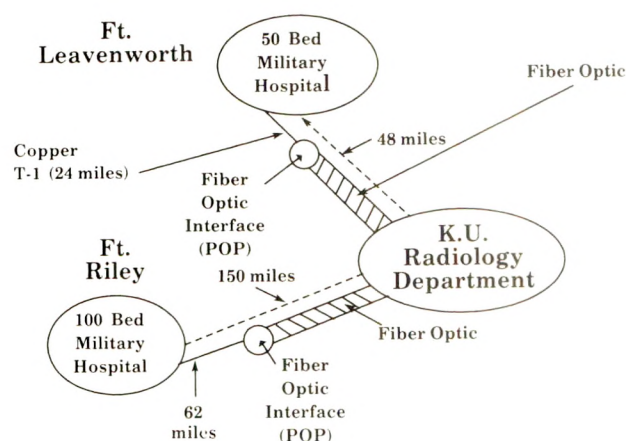


Fig. 1.—Drawing shows wide area network's communication links combining copper and fiber-optic cables of University of Kansas system. Point of presence (POP) is the interface onto fiber-optic cable.

Received June 28, 1991; accepted after revision August 5, 1991.

¹ All authors: Department of Diagnostic Radiology, University of Kansas Medical Center, 39th and Rainbow Blvd., Kansas City, KS 66103. Address reprint requests to A. W. Templeton.

megabits/sec) [3] and switched fiber-optic link DS-1 service (24 channels \times 56,000 bits/sec per channel = 1.344 megabits/sec). Access points onto the switched fiber-optic link service are the points of presence (POP, US Sprint, Kansas City, KS).

The LAN used at the three sites is Ethernet [4] (Siemens Gammasonics, Hoffman Estates, IL). The equipment interfaced to each LAN (Fig. 2) includes a laser film digitizer (DuPont, Wilmington, DE), an interactive gray-scale workstation (LiteBox, Siemens Gammasonics), a computer system (Siemens Gammasonics), a WAN bridge (CrossComm Corp., Marlboro, MA), and a multiple dial-up 56,000-bits/sec multiplexer (Digital Access, Reston, VA). The University of Kansas Medical Center radiology department also has a laser film printer (Siemens Gammasonics) and a diagnostic reporting console (DRC-20, Siemens Gammasonics).

LAN Ethernet image data packets are formatted into a high-speed serial bit stream of 1.344 megabits/sec by the WAN bridge. The bit stream is applied to the 56,000-bits/sec multiplexer (Fig. 3). This multiplexer dials up the requested num-

ber ($n = 1, 2, \dots, 24$) of digital voice channels and transmits the serial data over these channels in parallel. At the receiving destination, an identical $n \times 56,000$ -bit/sec multiplexer resynchronizes and reassembles the individual 56,000-bit/sec streams into a single serial stream. A WAN bridge at the receiving site reformats the serial bit stream into the original Ethernet packets for use by the LAN. The packets are reassembled into an image file by the LAN computer and recorded by the laser film digitizer and/or displayed on the gray-scale display workstation. The LAN's computer system controls the laser film digitizer and printer. Computer system software organizes digitized images by using a patient folder format and archives and transmits the images by using the ACR-NEMA data standard. The patient folder files at each site maintain the header block information such as the patient's name, identification number, and other relevant data.

A knowledge of the input-output characteristics of laser film digitizers and printers is essential to the successful transmission of radiologic image data. The laser film digitizers used in the University of Kansas Medical Center teleradiology system have a linear characteristic (Fig. 4) with a sampling quantization of 210- μ m pixels. The digital data matrix size is 1682 pixels/row \times 2084 rows \times 12 bits/pixel. The characteristics of the laser film printer are shown in Figure 5. A universal laser printer look-up table (LUT) was developed that enables all transmitted digital images to be printed automatically.

Use

More than 1000 cases have been digitized, transmitted, and printed on our teleradiology system. A carefully selected set of 150 formed a validation library. Cases from the validation library were used to detect any artifacts in the system that would affect hard copy quality and diagnostic accuracy. Some cases from the validation library have been digitized and transmitted many times to and from sites to establish the stability and constancy of the system.

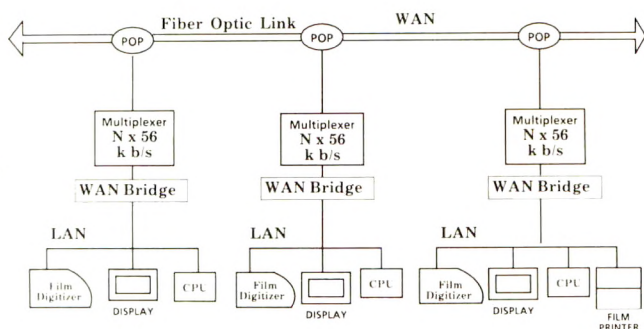


Fig. 2.—Drawing shows equipment located at each local area network (LAN) site of University of Kansas Medical Center teleradiology system. WAN = wide area network, k b/s = kilobits/sec; POP = point of presence.

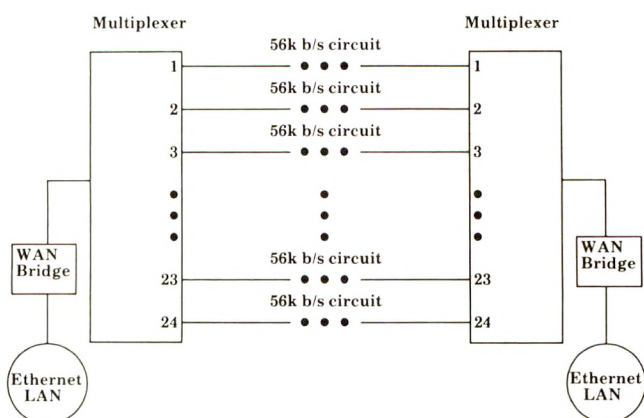


Fig. 3.—A multiplexer provides desired number of switched 56 kilobits/sec (k b/s) digital channels for transmitting digitized image data. Multiplexer processes high-speed serial bit stream from wide area network (WAN) bridge and transmits bit stream in increments over multiple dial-up 56 kilobit/sec circuits. Multiplexer at receiving site reassembles parallel transmitted increments into original high-speed serial bit stream. WAN bridge at receiving site places serial bit stream into local area network (LAN) Ethernet format.

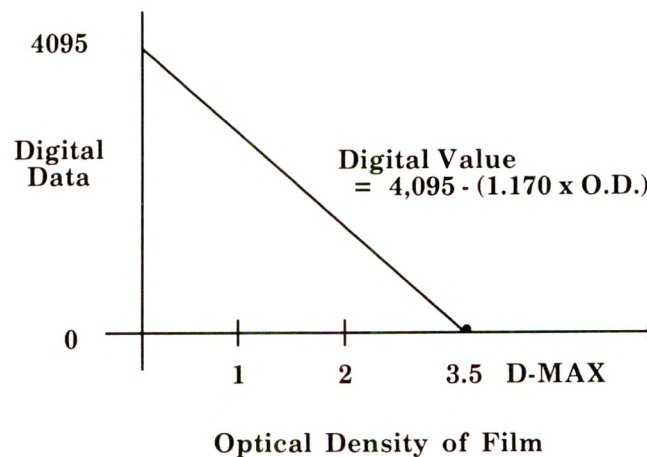


Fig. 4.—Graph shows input-output linear characteristic of laser film digitizer. Optical densities (O.D.) of radiographic film are digitized into digital data.

Teleradiology hard copy from the laser printer together with the universal LUT has been nearly equal to and occasionally better than the original predigitized film (Figs. 6 and 7). Actual measured throughput rates [5, 6] per digitized radiologic film

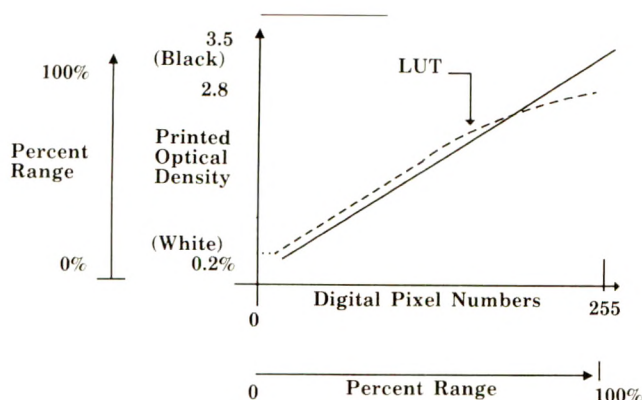


Fig. 5.—Graph shows laser film printer look-up table (LUT). LUTs are used to enhance contrast of anatomic sites represented by digital pixel number ranges.

on the University of Kansas Medical Center teleradiology system are presented in Table 1. Excluding the time (90 sec) required to develop the laser-printed latent image, the throughput per digitized radiologic image is 7.67 min ($n = 8$) or 6.17 min ($n = 24$). The universal LUT improves throughput because the time required to adjust window and level functions on an interactive display workstation are eliminated.

Discussion

Our experience with the University of Kansas Medical Center teleradiology system has shown that the film digitizing process is important in maintaining the quality of transmitted image hard copy. Calibration of the laser film digitizers to ensure linear input-output characteristics (Fig. 4) is required once each week. An image check of these devices has been accomplished by digitizing a film step wedge (Eastman photographic step tablet 3, optical density range of 0.05 to 3.05, Eastman Kodak, Rochester, NY), transmitting it, and reading out the received digital numbers by using the gray-scale workstation at the receiving site. Aliasing errors can be gen-

Fig. 6.—A, Original chest radiograph of 51-year-old man with 1.1-cm carcinoma in right upper lobe of lung.

B, Teleradiology hard copy of image shown in A. Lower maximum output optical density of laser printer film makes original radiograph less black. Carcinoma is easy to see.

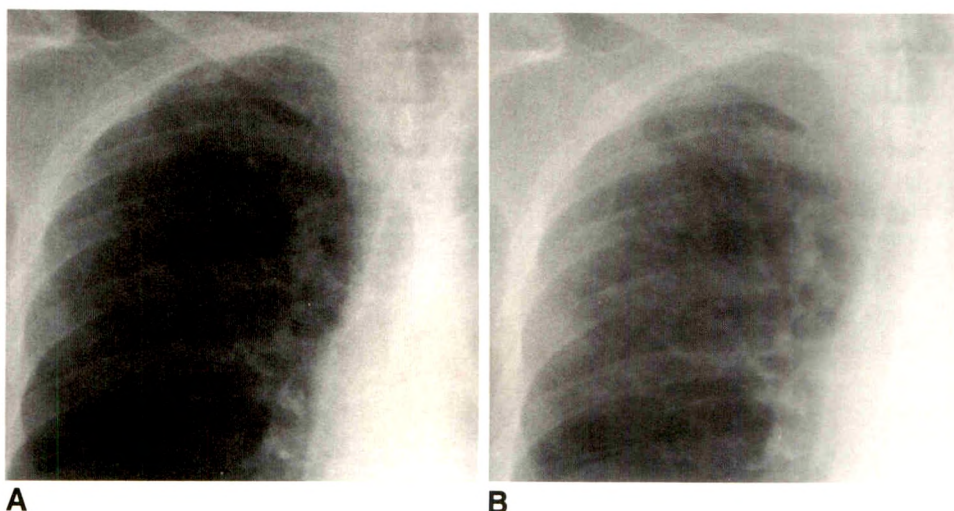
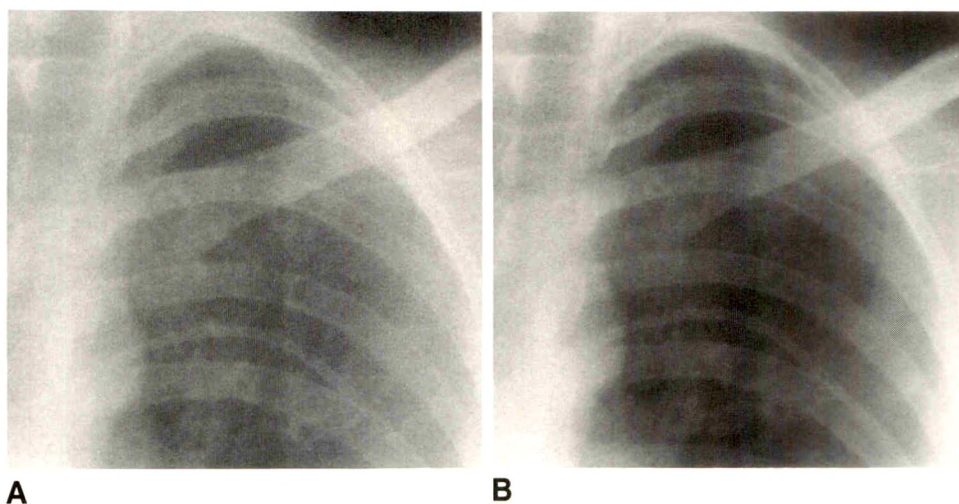


Fig. 7.—A, Original chest radiograph of 29-year-old woman with left apical pneumothorax. Small chest catheter is in place.

B, Teleradiology hard copy of A. Fixed maximum output optical density makes lighter original radiograph darker. Pneumothorax is more obvious.



erated by digitizing radiologic images made with fixed grids whose pitch is close to the sampling rate. The width of the laser digitizer spot size can be increased to avoid any aliasing errors, but this results in a reduction of spatial resolution. Dust on the optical mirrors or increased electronic noise in the transmitted laser light detector amplifiers results in a reduction in the signal-to-noise ratio of the digitized image data.

The digitized image array of 1682 pixels/row \times 2084 rows \times 12 bits/pixel (2.35 cycles/mm) has been adequate for representing the diagnostic information contained by conventional film-screen analog radiographs (Fig. 8). It is advantageous to digitize the laser-printed film recordings from CT and MR examinations. Transmission of the actual digital image data requires that a radiologist at the University of Kansas Medical Center must establish the proper window and level settings.

The stability of the laser film printer was critical for the successful operation of our teleradiology system. The universal LUT must faithfully record the optical densities represented by the transmitted digital data. It also must carefully map the desired gray-scale levels against the gamma curve of a specific laser-sensitive X-ray film. Variations occurring in the LUT over time will result in significant degradation of the printed images. Calibration is required each day to detect any drift in the range of printed optical densities. The laser printer in the University of Kansas Medical Center teleradiology system

uses the ACR-NEMA data format and maps the 12 bits from the digitized images into 8 bits by dividing the 12-bit range by 16 (truncation). The input digital value range is 0 to 255 (Fig. 5), and the printed output optical density range is 0.2 (D_{min}) to 3.5 (D_{max}). Although the laser recorder prints 12-bit LUTs, its input of 255 digital levels (8 bits) requires that D_{max} be set at about 2.8. This provides an increased number of gray levels for regions like the mediastinum in a chest image and the bones and soft tissues of a thick structure like the pelvis. The teleradiology hard copy closely approximates the original image (Figs. 9 and 10). The digital process of printing a lower D_{max} than the original radiograph with a fixed D_{min} has at times resulted in improved lesion detection (Fig. 7). The reduced D_{max} may also cause the black on CT or MR images to be less black (Fig. 11).

We have experimented with video-driven hard copy recordings as an alternative to laser-printed films. It appears that video-driven hard copy recordings are very useful for reviewing digitized and transmitted images. However, the image quality of a laser film printer remains superior.

The same wet-film processor should be used to develop the latent laser-printer image. A processor step wedge must be performed each day. Changes in fixer and/or developer or temperature strongly influence the optical density range of the laser printer.

The gray-scale workstations at each site enable interactive reviewing of digitized radiologic images before transmission. If a site is not equipped with a laser film printer, transmitted digital image data are displayed and reviewed on the gray-scale displays. Thus, the referring physician at one site can review additional examinations performed at another site. Images that are manipulated on gray-scale workstations cannot be faithfully reproduced by a laser film printer. The screen brightness of gray-scale monitors is limited to 50 or 60 foot-lamberts, whereas conventional view boxes have 400 foot-lamberts of luminescence. This difference in luminescence levels limits contrast detectability on the gray-scale monitors when compared with hard copies mounted on view boxes. Additionally, gray-scale monitors are driven by digital-to-ana-

TABLE 1: Measured Mean Throughput Rates of the University of Kansas Teleradiology System

Stage	Time
Laser film digitizing	12 sec
Formatting of image data	70 sec
Transmission	2.3 min ($n = 8$) 0.8 min ($n = 24$)
Reformatting of image data	70 sec
Transfer to laser film printer	2.3 min
Printing by laser film printer	32 sec
Developing of laser-printed film by wet processor	90 sec

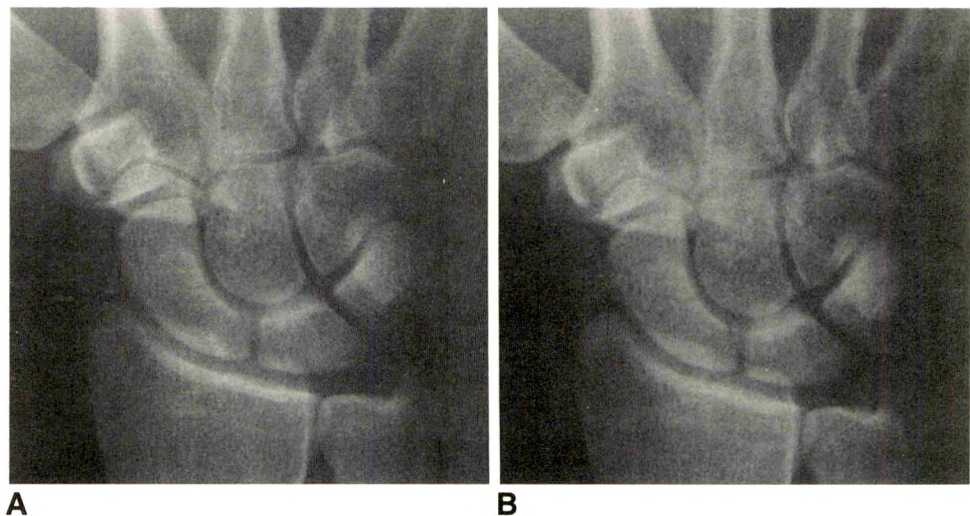


Fig. 8.—A, Original radiograph of wrist of 17-year-old boy with undisplaced, linear fracture of carpal navicular bone.
B, Teleradiology hard copy of A. Trabecular detail is good.

log converters with only 8-bit ranges. Electronic noise in gray-scale monitors video amplifiers actually limit the gray-level display range to less than 8 bits.

The costs of using the University of Kansas Medical Center teleradiology system have been estimated [7]. Hardware costs at each site are about \$110,000 per year for 3 years, decreasing to \$20,000 per year maintenance costs after 3 years. The University of Kansas Medical Center hardware costs approximate \$155,000 per year for 3 years, decreasing to \$36,000 per year for maintenance after 3 years. Equipment costs for teleradiology systems are rapidly declining, consistent with that of computer hardware.

Communication costs for the dial-up service consist of access charges (each site is provided with access to DS-1 service) and usage charges of \$0.06/min per 56,000-bits/sec digital voice channel. Access charges depend on available digital service provided by the local telephone carrier. These charges can be significant (\$1700 per month for Munson Army Community Hospital, \$354 per month for Irwin Army Community Hospital, and \$356 per month for the University

of Kansas Medical Center). The primary advantage of the dial-up switched 56,000-bits/sec digital voice channel method of communication is that user costs are based on \$0.06 per min per channel, irrespective of the distances between sites. The costs of using a dial-up, digital switched telephone system are decreasing because of the increased bandwidth available with installation of fiber-optic cables. Dedicated communication systems operate between fixed points, and their costs are based on distance. Increased user demand will further reduce the costs of implementing and operating any teleradiology system. Comparing the costs of the dial-up teleradiology service with dedicated point-to-point T-1 service shows that the dial-up service is less expensive for transmitting an average of 100 images per site per day.

The teleradiology system as currently configured is capable of transmitting 80–90 films per site per 8-hr day. Throughput can be improved by a factor of two to three by incorporating faster computer platforms, adding queuing software to each site on the WAN, and incorporating faster data transfers from the laser film digitizer and printer. Downtime on the WAN has

Fig. 9.—A, Original chest radiograph of 26-year-old woman with pneumonia in right lung base.

B, Teleradiology hard copy of A. Mediastinal structures are well shown.

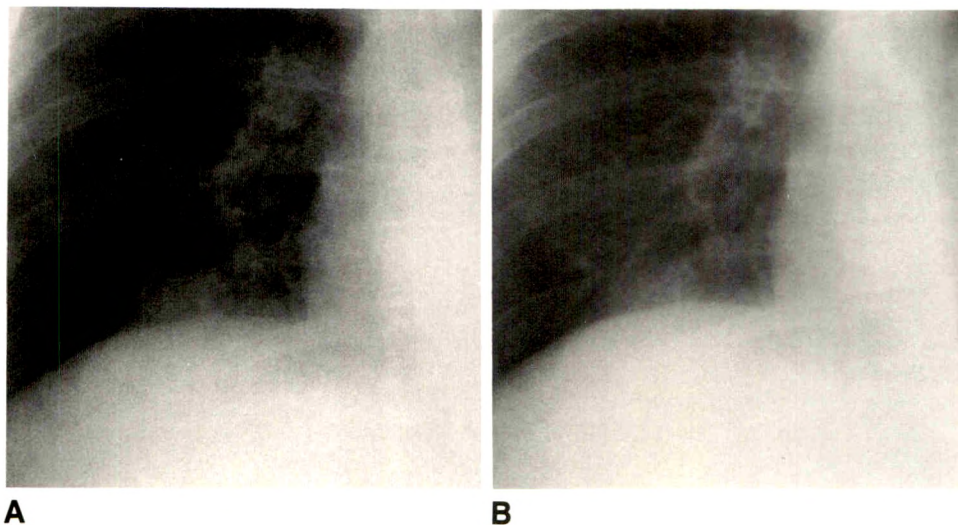
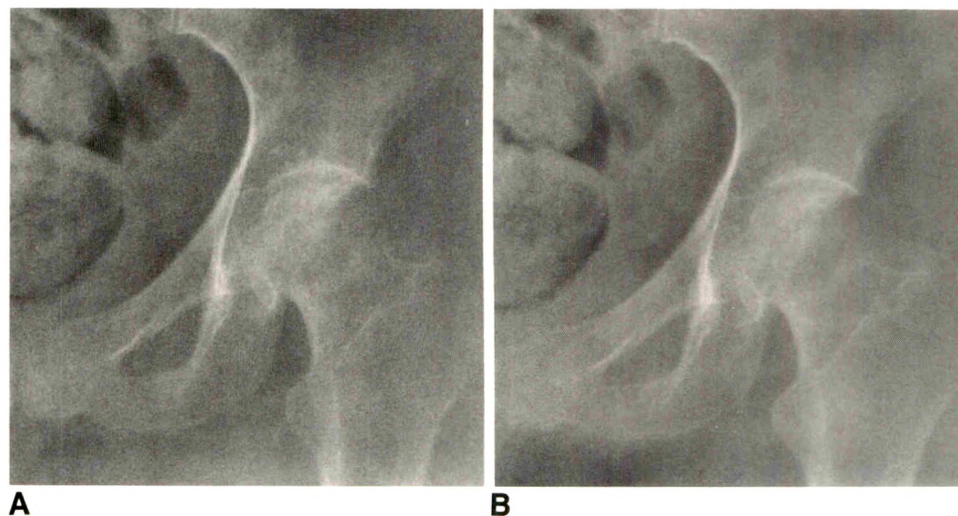


Fig. 10.—A, Original radiograph of pelvis of 32-year-old man with impacted fracture of neck of left femur.

B, Teleradiology hard copy of A. Bone and soft-tissue detail is equal to that on original.



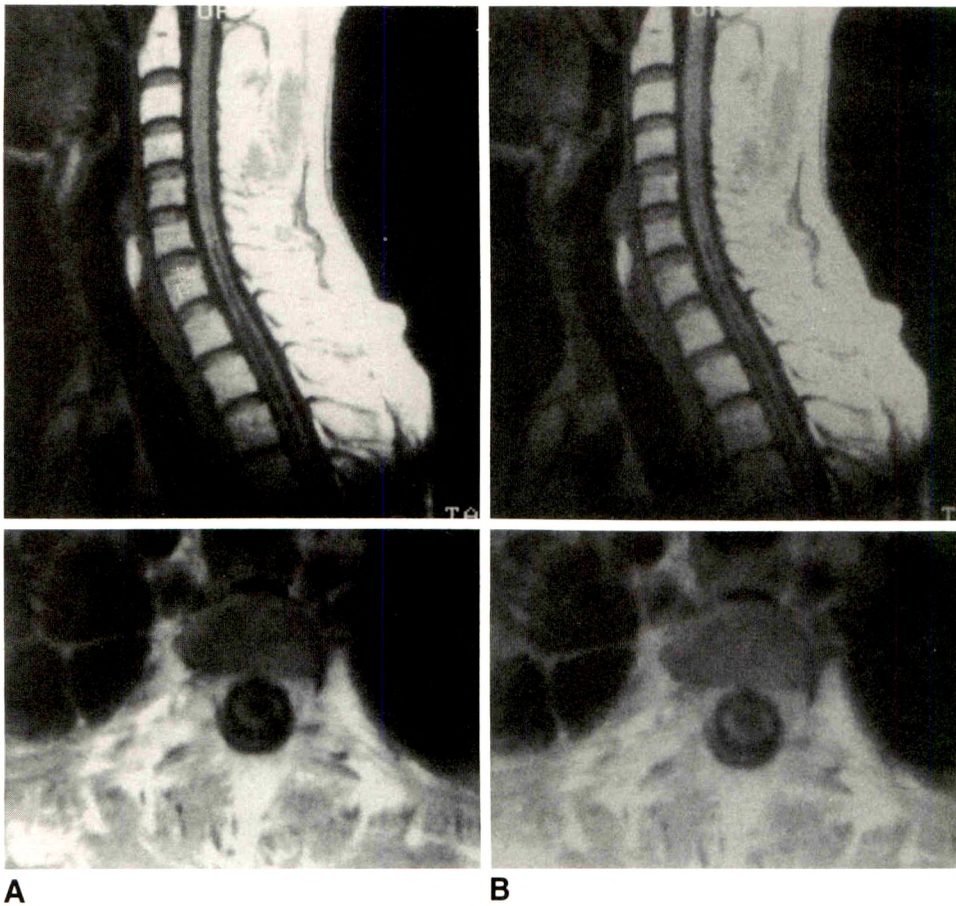


Fig. 11.—A, Original MR images of 21-year-old man with syrinx in lower cervical and upper thoracic spinal cord. B, Teleradiology hard copy of A. Black is less black and white is less white than on original. Image detail is still good.

been traced to outages caused by severe weather storms. No error bits have been detected during transmission. The reliability of the dial-up, switched DS-1 service has been excellent. Dial-up, multiple 56,000-bits/sec switched DS-3 service is being tested.

REFERENCES

1. Batnitzky S, Rosenthal SJ, Siegel EL, et al. Teleradiology: an assessment. *Radiology* 1990;177:11-17
2. Baxter KG, Wetzel LH, Murphey MD, et al. Wide area networks for teleradiology. *J Digital Imaging* 1991;4(1):51-59
3. Tanenbaum AS. *Computer networks*. Englewood Cliffs, NJ: Prentice-Hall, 1981:105-106
4. Shoch JF, Dalal YK, Redell DD, Crane RC. Ethernet. In: Kumemrle K, Tobagi FA, Limb JO, eds. *Advances in local area networks*. New York: IEEE, 1987:28-48
5. Jain R. *The art of computer system performance analysis*. New York: Wiley, 1991:507-569
6. Stuck BW, Arthurs E. *A computer and communications network performance analysis primer*. Englewood Cliffs, NJ: Prentice-Hall, 1985:141-187
7. Dwyer SJ III, Templeton AW, Batnitzky S. Teleradiology: costs of hardware and communications. *AJR* 1991;156:1279-1282

Productivity of Radiologists: Estimates Based on Analysis of Relative Value Units

Patrick M. Conoley¹
Sally W. Vernon²

Analysis of relative value units (RVUs) was used to quantify patient-care productivity of radiologists in 19 multispecialty group practices and to determine how productivity is affected by certain characteristics of the practices. The RVUs used in this study are the professional component RVUs developed by the American College of Radiology and the Health Care Financing Administration and published as the Radiology Relative Value Scale. An RVU workload was calculated by multiplying the number of times each procedure was performed by the procedure's corresponding RVU; the sum of these products gave the overall professional RVU workload. Five productivity indexes were calculated. The physician index denotes the ratio of the total number of physicians in the clinics to the total number of radiologists. The availability index denotes the fraction of radiologists who are available to perform clinical work after deductions are made for time away from clinical work. The difficulty index measures, in RVUs per examination, the level of complexity of the overall examination mix. The examination index measures examinations per available radiologist, and the RVU index measures RVUs per available radiologist. Altogether, the 19 clinics reported 3,234,451 examinations performed by 299 radiologists. The computed overall indexes were as follows: physician index = 20 physicians per radiologist; availability index = 0.77; difficulty index = 2.27 RVUs per examination; examination index = 14,098 examinations per year per available radiologist; RVU index = 32,065 RVUs per year per available radiologist. When the clinics were grouped according to characteristics of the practices, the RVU index was higher for single-site practices, high-prepaid practices, outpatient-only practices, and practices without radiology training programs. Fifty-two percent of the RVUs were in general radiology, 37% in sectional imaging, and 10% in special procedures.

The concept of RVU workload is timely because it undoubtedly will be used to compare workloads across medical subspecialties, and these workloads are likely to be related by third-party payers to compensation.

AJR 157:1337-1340, December 1991

The American College of Radiology (ACR) and Health Care Financing Administration have quantified radiology services for purposes of reimbursement by using relative value units (RVUs) [1]. The service of interpreting a posteroanterior chest radiograph was assigned the value of 1.00 RVU. All other procedures in the radiology section of the Current Procedural Terminology (CPT) coding system [2] were assessed in relation to the service of reading a posteroanterior chest radiograph, and each procedure was assigned a value in RVUs. The list of these values is the Relative Value Scale. The scale rates both technical and professional components of each procedure. In the assignment of the professional component, consideration was given to such factors as the training, knowledge, skill, stress, and time required of the radiologist to perform the procedure. Thus, the scale measures the overall reimbursable service provided by the radiologist during the procedure. The Relative Value Scale is analogous to the Resource-Based Relative Value Scale, which will be applied by Medicare to nonradiology physician reimbursement in 1992 [3].

Received March 21, 1991; accepted after revision July 24, 1991.

¹ Kelsey-Seybold Clinic, P. A., 6624 Fannin St., Ste. 1800, Houston, TX 77030. Address reprint requests to P. M. Conoley.

² University of Texas Health Science Center at Houston, School of Public Health, Houston, TX 77225.

0361-803X/91/1576-1337
© American Roentgen Ray Society

In this study, we used the RVU concept to quantify the productivity of radiologists in multispecialty group practices, to determine how productivity is affected by certain characteristics of the practices, and to provide a basis for analyzing secular trends in the distribution of radiologists' productivity among the various imaging techniques. The study accepts the Relative Value Scale as the measure of productivity. It should be noted, however, that only work devoted to the *care of patients* is included in the CPT and Relative Value Scale systems. Many other activities of radiologists do not have RVUs assigned to them; these include continuing education, research, didactic teaching, clinical instruction of residents, and administrative duties. In this paper, the radiologist resources allocated to these non-RVU efforts are removed from the staffing analysis through the concept of "available radiologists," defined in the Methods section.

The study of total professional RVU workload of radiologists is timely and relevant because the RVU workload undoubtedly will be compared with the total Resource-Based Relative Value Scale workload of other specialists, and these workloads will be related by third-party payers to compensation.

Methods

Twenty-two large, multispecialty clinics, scattered across the United States, that are members of the American Society of Clinic Radiologists were asked to provide a comprehensive list of the volume of procedures performed during a recent 12-month period for each of the CPT codes in the Diagnostic Radiology section of the Relative Value Scale [1, 2]. Nuclear imaging and radiotherapy procedures were not included in the study. New diagnostic radiology CPT codes for 1990 were included because some of the clinics were using these codes, even though RVUs have not yet been assigned to the procedures by ACR and the Health Care Financing Administration. We assigned the new codes RVUs equivalent to RVUs of similar techniques so that all reported examinations would be included in the RVU analysis. These new codes accounted for approximately 0.7% of the examinations and approximately 2% of the total RVUs in the study. No audit was performed to determine if the clinics used the CPT-coding system accurately or to ascertain whether examinations were underreported or overreported. This study assumes that differences between clinics in the use of the CPT-coding system have introduced only random error into the data.

Of the 22 clinics, 21 responded to the questionnaire, but only 19 provided a comprehensive list of CPT-code volumes. These 19 were included in the RVU analysis. Nine of the clinics were located in the Midwest, four in the South, three in the Northeast, and three in the West/Southwest. Data were submitted for 12-month periods with ending dates from as early as December 31, 1989, to as recent as September 30, 1990. Two practices estimated volumes for calendar-year 1990 on the basis of two thirds of the year's work.

An RVU workload was calculated by multiplying the number of times each procedure was performed by its corresponding professional-component RVU. The sum of these individual CPT workloads gave the entire professional RVU workload. The total RVU workload and the total number of examinations provided numerators for the productivity calculations.

Practice styles have considerable variation both in the amount of time off and in types of work that cannot be expressed in RVUs. In determining denominators for the calculations, an attempt was made to adjust for these differences by reducing the total number of radiologists in the practice by a self-reported amount of "radiologists not available for clinical work." "Not available" deductions were made for continuing medical education, vacations, academic activities, and

administrative duties. Residents were not included in the quantification of radiology staffing. Practices also were asked to report the total number of physicians in the multispecialty practice.

Five productivity indexes were calculated, as defined in Table 1. A physician index was calculated as the ratio of the total number of physicians ("headcount") in the multispecialty clinics to the total number of radiologists (headcount) in the clinics. An availability index was calculated as the ratio of the number of available radiologists to the total number of radiologists, indicating the fraction of time the radiologists were available to do clinical work. A difficulty index was calculated by dividing the total RVU workload by the total number of examinations to express in RVUs per examination the weighted level of "difficulty" of the procedures performed. Finally, two workload indexes were calculated: an examination index (the total number of examinations per year per available radiologist) and an RVU index (the total number of RVUs per year per available radiologist).

Other data were collected in the survey in order to categorize the clinics according to selected variables that might affect workload. The criteria and resultant clinic groupings are presented in Table 2. Productivity indexes were calculated on the combined data submitted by all the clinics and by clinic categories on the combined data of all the clinics within each category. The indexes also were calculated for each clinic to obtain mean values, standard deviations, and standard errors of the indexes among the clinics.

Each CPT-code was also categorized to permit analysis of the workload distribution among examination techniques. The categories were (1) general radiography and fluoroscopy (head and neck, chest, extremity, and spinal plain film radiography; genitourinary, gastrointestinal, musculoskeletal, and intrathecal contrast studies; and mammography), (2) sectional imaging (sonography, MR, and CT of the head and body), (3) specials (angiography, neuroangiography, and interventional), and (4) other (unlisted procedures, review of outside films). In a previous report, Johnson and Abernathy [4] provided a breakdown by imaging technique of projected national radiologic procedures in the United States for 1980 that we compared with our data. Nuclear procedures reported in their study were excluded in our analysis because that technique was not included in our survey. Although the Relative Value Scale did not exist in 1980, a weighted difficulty index calculated from the current data for each technique category was used to estimate the RVU workload that would have been attributed to that technique in 1980. Thus, the distribution of the 1980 RVU workload among techniques could be estimated.

Results

Altogether, these 19 practices reported 3,234,451 examinations, corresponding to 7,356,462 RVUs. These were performed by 299 radiologists among the total of 6055 physicians in the clinics. The productivity indexes are presented in Table 2. Based on the combined data of all clinics, the examination index is 14,098 examinations per year per available radiologist, and the RVU index is 32,065 RVUs per year per available radiologist. If the availability correction is omitted, there were 10,818 examinations and 24,604 RVUs per year per radiologist by "headcount."

The questionnaire did not ask for volumes of "injection codes," which should accompany procedures billed with "supervision and interpretation" CPT codes. Overall, 14,180 supervision and interpretation procedures were reported. Although RVUs have not yet been approved for injection codes, it is possible to estimate that approximately 90,000 RVUs have not been counted. Thus, in order to obtain a more accurate total RVU workload, the RVU index should be increased to 32,344 to correct for these lost RVUs.

As shown in Table 2, the physician index was high in the single-site practices, in the high-prepaid practices, and in the

outpatient-only practices. The availability index was higher for outpatient practices and practices without training programs. The difficulty index was quite low in the outpatient practices and slightly high in multiple-site practices, low-prepaid practices, inpatient practices, and very large practices, as well as in those with radiology training programs. The examination and RVU indexes were higher for single-site practices, high-prepaid practices, outpatient-only practices, the large as opposed to very large practices, and the practices without radiology training programs.

Table 3 presents the breakdown of the reported examinations and the distribution of RVUs by technique category. Also, the 1980 data from Johnson and Abernathy [4] are included in the table for comparison. Their examination categories have been grouped to correspond with our current groups. Sectional imaging represented 14% of all examinations in the clinics in 1989 compared with 6% of all national examinations in 1980, and general radiology represented 83% of all examinations in 1989 compared with 93% in 1980. The weighted difficulty index of sectional imaging of 5.86 RVUs per examination was higher than the difficulty index for general radiology of 1.44. This fourfold difference in difficulty

indexes accentuates the drop in general radiology from 74% of the national RVU workload in 1980 to 52% of the clinics' RVU workload in 1989. By percentage of examinations and RVUs, special procedures remained stable. The overall weighted difficulty index for all national procedures in 1980 was 1.82, whereas the overall weighted difficulty index in the clinic procedures in 1989 was 2.28, a 25% increase.

Discussion

The ACR research department was consulted to provide an external reference to compare with our data. According to ACR data (Sunshine J, Mabry M, personal communication), the examinations in this study represent approximately 1% of the total number of examinations performed by radiologists in the United States in 1989, and the radiologists in the study constitute approximately 1% of the radiologists estimated by the ACR to have been working in the United States in that year. The ACR reported a national mean of approximately 11,700 examinations per radiologist per year, but this estimate does not take availability into account. From the 1987 Medicare Part B Reimbursement data (Sunshine J, Mabry M, personal communication) consisting of 110,000,000 examinations, mostly diagnostic radiology, the ACR calculated a nationally weighted difficulty index of 2.31 RVU per examination for diagnostic radiology procedures performed on Medicare patients. By using the 1989 ACR examination index, the 1987 Medicare difficulty index as an estimate of the national difficulty index, and the 1989-1990 overall availability index from this survey as an estimate of national availability, a rough estimate of a national RVU index can be made: 35,100 RVUs per year per available radiologist. This calculated national figure is probably an overestimate because the difficulty index for the Medicare population undoubtedly is higher than the index for the general population, because of greater use of sectional imaging and special procedures in older patients. In

TABLE 1: Definitions of Productivity Indexes

Index	Definition
Physician	Total physicians
	Total radiologists
Availability	Available radiologists
	Total radiologists
Difficulty	Relative value units (RVUs)
	Number of examinations
Examination	Examinations per year
	Available radiologist
RVU	RVUs per year
	Available radiologist

TABLE 2: Productivity Indexes for Individual Clinics, All Clinics, and by Characteristics of Clinics

Type of Clinic or Characteristic	No.	Productivity Indexes				
		PI	AI	DI	EI	RI ^a
Individual clinics						
Mean	19	23	0.77	2.25	15,231	33,705
Standard deviation		7	0.07	0.24	4,577	7,855
Standard error		1.6	0.02	0.06	1,050	1,802
All clinics	19	20	0.77	2.27	14,098	32,065
Number of sites						
Single	6	24	0.77	2.15	16,410	35,268
Multiple	13	19	0.77	2.31	13,551	31,306
Prepaid fraction						
≤5%	7	17	0.76	2.31	13,440	31,017
>5%	12	24	0.77	2.24	14,750	33,104
Inpatient fraction						
0%	3	30	0.80	2.01	18,666	37,464
>0%	16	19	0.76	2.30	13,737	31,639
Radiology residency ^b						
≤1 Resident	11	23	0.79	2.22	15,374	34,114
>5 Residents	8	19	0.76	2.31	13,347	30,858
Size						
≤300,000 RVU (large)	10	22	0.75	2.19	14,843	32,564
>300,000 RVU (very large)	9	19	0.77	2.31	13,762	31,841

Note.—PI = physician index, AI = availability index, DI = difficulty index, EI = examination index, RI = RVU index.

^a Theoretically, $DI \times EI = RI$. Discrepancies in the products and in the standard errors are due to rounding error.

^b No practice had a radiology training program with two to four residents.

TABLE 3: Percentage Distribution of Examinations and of Professional Relative Value Units Among Examination Techniques

Technique	1989 (%)		1980 (%)	
	Examinations	RVUs	Examinations	RVUs
General (radiography and fluoroscopy)	83	52	93	74
Sectional imaging (CT, sonography, MR)	14	37	6	16
Specials (vascular, interventional)	1	10	1	10
Other (outside films, miscellaneous)	2	1	—	—

Note.—RVUs = relative value units. 1980 data from Johnson and Abernathy [4] are included for reference.

addition, almost two thirds of the radiologists in this study are involved in practices with radiology training programs, which is probably a higher proportion than in the general population of radiologists in the United States. Because as a group, practices with training programs have a lower RVU index than practices without training programs, the mean RVU index for our study is probably an underestimate of the national RVU index. When these two points are kept in mind and when the standard error of 23% is considered, this figure extrapolated from ACR and Medicare data is fairly close to the RVU index that we report.

In the analysis by clinic characteristics, the high examination and RVU indexes in the single-site clinics may indicate that these practices are more efficient, possibly because of the ease of scheduling work assignments, immediate availability of cross coverage, or less time spent in commuting. Likewise, the high physician, examination, and RVU indexes of high-prepaid practices corroborate the managed-care philosophy of high-volume, low-cost care. Of interest, the difficulty index is lower in the prepaid practices, possibly because utilization-review processes control access to the more advanced imaging procedures.

The higher difficulty index of practices with an inpatient component is due to the admixture of high RVU procedures such as interventional and angiographic work in the inpatient setting. However, the higher availability, physician, and examination indexes in the outpatient-only practices compensated for low difficulty, so that the workload as measured by RVU index was 18% greater in the outpatient-only setting compared with the inpatient setting.

The practices with radiology training programs had a higher difficulty index but lower examination and RVU indexes than practices without training programs. The lower productivity may be due to an intrinsic inefficiency in teaching residents during film interpretation; however, this teaching is a valid activity within the mission of the sponsoring organizations. It simply is not measured by RVUs.

Seven of the nine very large practices (>300,000 RVUs/year) have training programs, whereas only one among the 10 large practices (≤300,000 RVUs/year) does. Thus, the categorization by size largely duplicates the trends in the training/nontraining category, with difficulty indexes higher and workload indexes lower in the very large (training) clinics than in the large (nontraining) clinics.

The 1% of injection code RVUs not included in the survey data were spread fairly evenly among the practices (0.01–4.05%) and probably do not represent a systematic error. These “lost RVUs,” however, may also represent lost revenues to the practices if corresponding injection codes were not billed along with supervision and interpretation procedures.

Finally, Johnson and Abernathy’s study [4] was designed to project overall national volumes of examinations for 1980 and the distribution of examinations among techniques. Our data show actual examinations performed by a subset of practitioners in multispecialty clinics in 1989. Although extrapolation of our data to give an estimate of the 1989 national distribution is beyond the scope of this study, it is plausible to suggest that the dramatic shift of RVU workload from general radiology to advanced imaging techniques (Table 3) reflects trends in the national data.

Conclusions

This study attempted to quantify work devoted to the care of patients that is included in the CPT and Relative Value Scale systems. The results of this RVU analysis are similar to the results of extrapolations based on ACR and Medicare data. Many other non-RVU activities of radiologists do not have assigned RVUs but must be recognized as productive work. As third-party payers shift to RVU-based methods of reimbursement, accurate and complete coding will be essential to include all the billable RVUs; injection codes, in particular, must not be neglected. The RVU method allows analysis of the distribution of workload among the various imaging techniques, which can be used to study trends in utilization. Although this method was developed for comparing radiology practices within multispecialty groups, it can be used to evaluate other radiology practice settings, and it can serve as a model for making workload comparisons among specialties.

ACKNOWLEDGMENTS

We express appreciation to Michael Lenker of Kelsey-Seybold Clinic for helpful editorial suggestions, Virginia Heckel of Kelsey-Seybold Foundation Crump Cancer Center for statistical assistance, Mike Nelson of Park Nicollet Medical Center, Christopher Merritt of Ochsner Clinic, Reilly Kidd of Mason Clinic, Timothy Parker of Lovelace Medical Center for suggestions regarding the survey questionnaire and methods, and all respondents to the questionnaire.

REFERENCES

1. Medicare programs: fee schedules for radiologists’ services. *Federal Register*. March 2, 1989;54:8994–9023
2. American Medical Association. *CPT: Physician’s Current Procedural Terminology*. Chicago: American Medical Association, 1990
3. Hsiao WC, Braun P, Becker ER, et al. A national study of resource-based relative value scales for physician services: final report to the Health Care Financing Administration (Publication 17-C-98795/1-03). Cambridge, MA: Harvard School of Public Health. September 1988.
4. Johnson JL, Abernathy DL. Diagnostic imaging procedure volume in the United States. *Radiology* 1983;146:851–853

Radiology Practices and Their Contracts with Hospitals, 1989–1990: A Representative Sample Survey

Jonathan Sunshine¹
William C. Chan
Pamela J. Kassing

Because of concern about pressures from hospitals for changes in their contracts with radiology practices, the American College of Radiology undertook a stratified sample survey of radiology practices and their contracts with hospitals in late 1989 and early 1990. After three remailings, the survey obtained 904 valid responses for a 64% response rate. It found (weighting data to represent all radiology practices in the nation) that 91% of radiology practices provide services in hospitals. There are contracts at 57% of these hospital sites, and hospitals use tax-exempt bond financing in 54% of the sites with contracts. One year is the most common duration of contracts, and 90 days is the most common cancellation period (89% of contracts can be canceled during the contract's term). Eighty-six percent of contracts are exclusive; 73% are automatically renewable ("evergreen"). Separate billing exists in well over 90% of hospitals with contracts. Two percent of contracts require radiologists to provide equipment; 4% require them to provide support staff. There are fixed-fee arrangements in 9% of contracts and percent compensation arrangements in 3%. Hospitals share in radiologists' fees as a charge for contractual privileges in 5% of contracts. Twenty-seven percent of contracts require hospital approval for radiologists' fee increases; 19% require radiologists to participate with Blue Shield or Medicare. If a contract characteristic is predominant nationally, it is predominant in every region, for solo, small, medium, and large practices, and whether or not hospitals use tax-exempt bond financing. There is, however, some modest variation in frequency of contract provisions. Multivariate analysis shows that most such variation reflects true effects of region and other variables, not statistical artifacts. Region was a statistically significant determinant of 11 of 17 contract characteristics studied. Practice size was a statistically significant determinant of only about half as many characteristics.

The survey found some interference in the independence of radiology practices (e.g., required hospital approval of fee increases), questionable clauses (e.g., mandated provision of equipment), and even illegal ones (hospitals charging a fee for contract privileges). Knowledge of the survey findings can make individual radiology practices more effective in negotiations with hospitals and assist the profession in forming a strategy to oppose disadvantageous and illegal provisions.

AJR 157:1341–1347, December 1991

Contracts between radiologists and hospitals are an increasingly important issue for radiologists. Such contracts were once uncommon, but have become more frequent. At the same time, concern over their terms has increased for at least two reasons. First, in the context of legal concerns related to tax-exempt bond financing, some hospitals have recently sought more restrictive terms in their contracts with radiologists. Second, hospitals face growing financial pressures, and they may, in turn, be seeking contract changes that work to their advantage and, coincidentally, to the disadvantage of radiologists. The American College of Radiology (ACR), the principal professional organization of radiologists in the United States, has cautioned its members that having a contract, as compared with practicing without one, may be detrimental in important respects, particularly in loss of due process rights under medical staff bylaws [1].

Received March 21, 1991; accepted after revision July 10, 1991.

¹ All authors: Research Department, American College of Radiology, 1891 Preston White Dr., Reston, VA 22091. Address reprint requests to J. Sunshine.

0361-803X/91/1576-1341
© American Roentgen Ray Society

In response to concerns about contracts, the ACR undertook a survey of hospitals' contracts with radiologists. Its objective was to learn how common such contracts are, what provisions are typical, and what factors affect contract terms. In this report, we present findings of that survey.

Materials and Methods

Survey Methods

The survey questionnaire was designed by the ACR's research department with input from its center on economics and its legal department.

The survey questionnaire was mailed to 1455 practices selected from the ACR's master list of radiology practices in the United States, which includes both solo and group practices. The sample of practices was selected to contain an approximately equal number of practices in each of the four census regions (Northeast, Midwest, South, and West). The sample in each region was further stratified to contain approximately equal numbers of the smallest practices (typically one- or two-radiologist practices) and larger practices. Sampling was random within each stratum. An original mailing and three follow-up mailings took place between November 1989 and April 1990. Altogether, 904 valid responses were received. Returns indicated approximately 2% of the original sample was out of scope (principally physics practices and retired solo practitioners). Thus, the true response rate (valid responses divided by in-scope sample) was approximately 64%. Response rates of 60% or more are considered good in surveys of physicians, for physicians are notably busy and therefore prone not to respond [2].

Telephone follow-up was used to ensure that all valid respondents answered the survey's questions about practice size, number of hospitals in which the practice was active, and number of these hospitals with which it had contracts. For other questions, question-specific response rates are shown in Table 1.

Analytic Methods

We present data in three ways: as aggregate data, after single-variable analysis, and after multivariate analysis. The aggregate data cover all practices or all contracts in the United States. Single-variable analysis separates data according to individual variables thought possibly to have an important effect on the characteristics of contracts. Three variables are used in this fashion: whether or not the hospital uses tax-exempt bond financing, the region of the country, and practice size.

Tax-exempt bond financing raises legal concerns regarding some contract provisions—most notably contract duration and the cancellation period—but not others. As a case/control analytic strategy, we examined the effect of tax-exempt bond financing on all contract provisions, seeking to ascertain whether the analysis showed more of an effect on those contract provisions related to tax-exempt status than on other provisions.

After the single-variable analyses, we present multivariate analyses. Such analyses recognize that the characteristics of a contract may be the consequence of several factors acting simultaneously. These analyses attempt to estimate the *independent* effect of each factor separately, while controlling for the effects of all the other factors being considered. If the characteristic in question—for example, whether a contract is exclusive—takes on only two values (typically "yes" or "no"), logistic regression was the multivariate technique used. If the characteristic is a more or less continuous vari-

able—for example, contract duration—multiple regression was used. These are the usual multivariate analytic techniques of choice [3].

Numbers in the text and tables of this report are based on weighted tabulations and analyses. They thus represent what findings would be if every practice in the United States had been surveyed and had responded. Weighting was according to census region crossed by the two categories of practice size. For each of these eight sampling strata, the weight was the estimated total number of practices in the United States in the stratum divided by the number of valid responses. All valid responses were used in the analyses.

Statistical Significance and Standard Errors

Statistical significance of national aggregate statistics and of statistics in the single-variable analyses is readily assessed by using a simple formula: The difference between two statistics is regarded as statistically significant at the p percent level if the difference equals at least $Z_p(a^2 + b^2)^{1/2}$, where Z_p is the relevant statistic from a table of the normal distribution, a is the standard error of the first statistic, and b is the standard error of the second statistic. It is the usual practice to estimate the standard error of a survey statistic as if it were due to sampling variance alone; that is, to use the formula

$$\text{Standard error} = \text{approximately } [p(1-p)(1-n/N)/n]^{1/2},$$

where p is the observed probability (e.g., the probability that a contract is exclusive), n is the number of responses, and N is the size of the population from which the sample is drawn. The use of this formula indicates that, for national averages, the maximum standard error is approximately 0.7%. The standard error is approximately 1.0–1.3% for individual geographic regions, 0.6% for solo practices, 1.1–1.6% for various size categories of group practices, and 1.0% for the categories defined by whether a hospital does or does not use tax-exempt bond financing. These standard errors are computed for $p = .5$; for probabilities greater or smaller than 50%, standard errors are smaller. They can be approximated by multiplying the standard errors given by $[p(1-p)/0.25]^{1/2}$.

Statistical significance in the multivariate analyses is reported in the tables, which show the results of these analyses. In discussing findings of the multivariate analyses, a p value of .01 or less has been taken as the minimum significance level at which findings were considered statistically meaningful. Because the typical multivariate analysis involved approximately five independent variables, this significance test is approximately equivalent to the usual 5% significance level test applied to one variable at a time.

Results

National averages and the results of single-variable analysis are shown in detail in Table 1. The results of multiple regression analyses are detailed in Table 2. Detailed findings of the logistic regressions, which are more complex to present, may be obtained from the authors. We describe the most salient findings in this section.

National Averages and Single-Variable Analysis

Practice sites, contracts, and tax-exempt bond financing.—The survey found that of the approximately 3300 radiology practices in the United States, 9% did not practice in hospitals at all, 50% practiced in one hospital, 22% practiced in two hospitals, and 18% practiced in three or more hospitals. Not

TABLE 1: Characteristics of Hospital Practice Sites with Contracts

Characteristics	All Sites with Contracts	Practice Size				Region				Contract Sites Where Hospital Uses Tax-Exempt Financing	Contract Sites Where Hospital Does Not Use Tax-Exempt Financing	Item Response Rate
		Solo	2–4	5–7	≥8	Northeast	Midwest	South	West			
Hospital uses tax-exempt bond financing	54	45	49	57	59	60	53	53	52	100	0	90
Contract is exclusive	86	85	84	93	83	89	80	85	91	88	83	97
Contract is automatically renewable	73	67	79	72	68	73	78	76	65	78	69	95
Contract is cancelable mid-term	89	87	91	92	86	89	88	90	89	86	94	89
Hospital bills separately	94	90	94	95	95	94	96	94	94	95	94	98
Radiologists bill separately	92	86	90	95	95	90	94	95	90	92	93	98
Contract requires radiologists to purchase or maintain equipment	2	3	2	1	4	2	4	2	2	1	2	98
Contract requires radiologists to provide technologists, etc.	4	5	4	2	5	3	6	1	7	2	4	98
Practice shares in hospital profit	1	2	1	2	1	1	2	2	1	1	2	98
For privilege of contract, hospital shares in practice's fee	5	4	6	5	4	12	1	4	4	6	3	98
Fixed fee arrangement?	9	12	9	7	8	16	6	7	8	10	8	98
If yes, does fee vary with volume?	22	7 ^a	34 ^a	0 ^a	27 ^a	26 ^a	8 ^a	29 ^a	20 ^a	27	12	97 ^b
Compensation based on percentage contract	3	8	4	2	1	4	2	1	5	4	1	98
Contract requires prior hospital approval of fee increase	27	25	22	32	30	38	17	18	43	28	29	97
Contract requires hospital to act as practice's agent with HMOs and PPOs	8	10	8	12	5	13	5	4	14	10	6	96
Contract requires radiologists to "participate" with Blue Shield or Medicare	19	13	14	24	22	45	13	10	15	19	18	94
Contract requires practice to indemnify hospital for professional liability	43	50	38	45	47	46	33	42	56	42	46	94

Note.—Numbers in table are percentages of sites with given characteristics. HMO = health maintenance organization; PPO = preferred provider organization.

^a Reliability poor because of small sample size.

^b Response rate for practices with fixed-fee arrangement.

TABLE 2: Findings of Multiple Regression Analyses

Dependent Variable	Independent Variables							
	Increase of 1 FTE Radiologist in Practice Size	Northeast (Rather than Midwest)	South (Rather than Midwest)	West (Rather than Midwest)	Hospital Uses Tax- Exempt Financing	Contract Is Exclusive	Increase of 1 Year in Length of Contract	Contract Is Automatically Renewable
Number of hospitals in which a practice operates ^a	0.056 (.0001)	-0.828 (.0001)	-0.467 (.0003)	-0.598 (.0001)				
Number of hospitals with which a practice has contracts ^b	0.037 (.0001)	-0.449 (.001)	-0.402 (.001)	-0.288 (.034)				
Duration of the contract (in years)	0.023 (.057)	0.080 (.737)	0.009 (.965)	0.067 (.772)	0.331 (.035)	0.558 (.138)		
Length of the cancellation period (in days)	0.648 (.169)	1.55 (.841)	-16.26 (.023)	-17.49 (.023)	2.55 (.619)	-3.17 (.666)	3.81 (.029)	18.11 (.003)

Note.—Coefficients shown are the additive effect of each independent variable on the dependent variable (significance levels are in parentheses). Blanks indicate variable was not used in the regression. FTE = full-time equivalent.

^a Includes all practices, even those not operating in hospitals.

^b Includes only those practices that operate in hospitals.

surprisingly, the pattern depended on practice size. Almost 30% of solo practices did not practice in any hospitals, and less than 20% of them practiced in two or more hospitals. In contrast, only 1% of practices with eight or more radiologists did not practice in any hospitals, and 55% of these large practices operated in two or more hospitals. Regional differences were smaller. The most conspicuous regional difference was that only 5% of practices in the South and Midwest did not practice in any hospitals, compared with 12% in the Northeast and 18% in the West.

Altogether, the approximately 3000 practices that did function in hospitals reported operating in 5575 hospital sites, an average of approximately 1.9 sites each. The number of hospitals per practice varied with practice size, but by less than might be expected. The one-radiologist practices that functioned in hospitals averaged 1.5 hospitals each, while groups with eight or more radiologists that functioned in hospitals averaged 2.3 hospitals each. Of the practices that did function in hospitals, 30% reported having no contracts with any hospital, 49% reported one contract, 12% two contracts, and 9% three or more contracts. Surprisingly, there was relatively little practice-size-related variation in number of contracts per practice.

Altogether, approximately 3190 contracts were reported. This is approximately 57% of the total number of hospital practice sites, which means that in about 43% of practice sites, the radiology group had no contract with the hospital. Contracts were found in 64–66% of practice sites in the West and Northeast, compared with 52–53% in the South and Midwest.

In about 54% of the hospitals with contracts, the hospital was reported to use tax-exempt bond financing; in the other

46%, the hospital did not do so (Table 1). Tax-exempt bond financing was more common in hospitals with which large practices had contracts. There were also regional differences, with tax-exempt bonds used by 60% of hospitals with which radiologists in the Northeast had contracts compared with 52–53% in other regions.

Characteristics of contracts.—Eighty-six percent of contracts were exclusive (Table 1). The figure was somewhat higher in the West and Northeast and somewhat higher in hospitals that used tax-exempt bond financing.

The most common duration of a contract was 1 year. This was the duration of 46% of all contracts. Three percent ran for less than a year, 12% for 2 years, 19% for 3 years, and 20% for 4 years or more, mostly for 5 years. Contract lengths were quite similar regardless of whether the hospital used tax-exempt bond financing. The largest deviation from the national average pattern was found for solo practices; 59% of their contracts ran for 1 year and only 11% were for 4 years or more.

A large majority of contracts (73%) were automatically renewable ("evergreen") (Table 1). This was true of slightly more contracts with hospitals that used tax-exempt bond financing (78%) than of contracts with hospitals that did not (69%). Some differences related to region and practice size were found also.

Although the overwhelming majority of contracts could be canceled during their duration, 11% were noncancelable. Noncancelable contracts were more common (13–14%) for hospitals that used tax-exempt bond financing and for solo radiologists and large groups.

Ninety days was the most common cancellation notice period. Forty-nine percent of all contracts were cancelable on

90 days' notice, 18% on shorter notice (typically 30 or 60 days), and 22% on longer notice (typically 180 days, none over 1 year). For hospitals that used tax-exempt bond financing, only 14% of contracts could be canceled on less than 90 days' notice, while, for hospitals that did not use tax-exempt bond financing, 25% of contracts could be canceled this rapidly. Solo radiologists relatively often had contracts subject to cancellation on less than 90 days' notice (26% of their contracts), while groups of eight or more radiologists rather infrequently had contracts cancelable this quickly (10%).

Arrangements in which the hospital and the radiologists billed separately overwhelmingly predominated. The hospital billed separately for its services in 94% of sites where there was a contract, and the radiology practice reported billing separately for its services in 92% of these sites (Table 1). Separate billing was somewhat less common (by 5–10%) in hospitals where solo radiologists had contracts than in sites where multiple-radiologist groups had contracts.

Contracts rarely required radiologists to purchase or maintain equipment or to provide technologists or other support staff. Only 2% of contracts reported in the survey had any such requirements regarding equipment, and only 4% required radiologists to provide technologists or other support staff or services.

It was rare for radiology practices to share in the profits of hospitals with which they have contracts. This was reported for only 1% of contracts. It was somewhat less rare (5% of contracts) for hospitals to share in the practice's fees as a charge for contractual privileges.

Other financial links between hospitals and radiology practices were also uncommon in hospitals when there were contracts. In 9% of contracts, there was a fixed-fee arrangement; that is, the radiologist's compensation came from the hospital and was basically a flat, predetermined amount. Fixed-fee arrangements were more common than average for solo radiologists and for practices in the Northeast. In about 20% of contracts with a fixed-fee arrangement, the fee varied depending on volume. In 3% of contracts, the compensation to radiologists was based on a percentage contract with the hospital; 8% of solo radiologists' contracts had this arrangement.

Contracts with hospitals sometimes regulated business aspects of radiologists' practices. Twenty-seven percent of contracts required hospital approval before the practice could increase its fees. Such a requirement was twice as common in the West and Northeast as elsewhere. Less frequently, in 8% of contracts, the contract required the practice to use the hospital as its agent in negotiating with health maintenance organizations (HMOs) and preferred provider organizations (PPOs). Again, this was more common in the West and Northeast than elsewhere. Finally, 19% of contracts with hospitals required radiologists to be "participating" physicians with Blue Shield or Medicare. (A participating physician agrees in advance to accept the insurer's allowed charge as payment in full and not to bill the patient for any additional amount, even if the physician's usual charge is higher.) Required participation was more common in the Northeast and for large practice groups.

Forty-three percent of contracts required the radiology practice to indemnify the hospital and hold it harmless for professional liability. Such provisions were most common in the West and least common in the Midwest.

Multivariate Analysis

Multivariate analysis is designed to show the *separate* effect of each of several independent variables that may affect a dependent variable, and to measure the effect of each while controlling for the effects of all the others. Effects reported in this section and in Table 2 are measured on this basis.

Thus, for example, the single-variable analyses found that small practices operated in fewer hospitals than large ones, and that practices in the Northeast and West were more likely than others not to practice in any hospitals. Multivariate analysis answers the question of whether these are independent effects or occur only because of a concentration of small practices in the Northeast and West.

Table 2, which reports findings of multiple regression analyses, shows the relevant findings in its first two rows. Both practice size and region turn out to be important. Specifically, each increase of one radiologist in the size of a practice on average increased the number of hospitals in which it functioned by 0.056. (In other words, there was an increase of one hospital for every 18-radiologist increase in group size.) In addition, for any given size, practices in the Northeast on average functioned in 0.8 fewer hospitals than corresponding-sized practices in the Midwest, and practices in the West on average functioned in 0.6 fewer hospitals than corresponding-sized practices in the Midwest. (Throughout, the regressions use the Midwest as the base case to which other regions are compared.) All these effects are significant at the .0001 level; that is, the probability that the observed effects occurred by chance is less than .0001.

Interested readers can examine Table 2 further to see which factors had an independent, statistically significant effect on some other aspects of contracts. Overall, the multivariate analyses indicate that most of the effects found in the single-variable analyses are true effects, not statistical artifacts.

Discussion

An extensive examination of the published literature found no survey of the provisions of radiologists' contracts with hospitals nor any systematic examination of these provisions. Most of the literature consists of commentary, often from a legal perspective, on the desirability for radiologists and hospitals of specific contract provisions. An article by Gravely [4] is a fine example of this genre, covering several issues. However, most of this literature deals with only one point: antitrust implications of contract exclusivity.

The closest the literature comes to a report on what contract terms are most common is one business consultant's impressionistic description of typical terms [5]. He stated (generally correctly, we have found) that the typical contract is annual, renewable, exclusive, and has fee-for-service pay-

ment of the radiologists with no administrative fee paid to the radiologists by the hospital. The hospital provides facilities and equipment, pays departmental staff, and sometimes helps with malpractice coverage.

The ACR's survey thus constitutes the first systematic examination of the contract terms that are now in effect and how common each is. In brief, it found that 91% of radiology practices practice in hospitals, there are contracts in 57% of these practice sites, and hospitals use tax-exempt bond financing in 54% of the practice sites with contracts. Eighty-six percent of contracts are exclusive; 1 year is the most common duration of contracts and 90 days is the most common cancellation period. Seventy-three percent of contracts are automatically renewable (evergreen); 89% can be canceled during the term of the contract. Separate billing exists in well over 90% of hospitals with contracts. Only 2% of contracts require radiologists to provide equipment and only 4% require them to provide support staff. There are fixed-fee compensation arrangements in 9% of contracts and percent compensation arrangements in 3%. In 5% of contracts, hospitals share in radiologists' fees as a charge for contract privileges; 1% of contracts have the reverse arrangement, with radiologists sharing in the hospital's profits. Twenty-seven percent of contracts require hospital approval for radiologists to increase fees and 19% require the radiologists to participate with Blue Shield or Medicare.

Because survey follow-up was pursued to obtain a good response rate, these statistics probably are generally sound estimates for radiology practices in the United States. However, practices with arrangements considered inappropriate might have tended not to respond to the survey, and the frequency of such arrangements may therefore be underreported. This can particularly be a problem with uncommon arrangements. Thus, for example, there may be serious underreporting of contracts requiring radiologists to provide staff or equipment, or to pay the hospital for contractual privileges. Federal law regarding Medicare patients prohibits payments for contractual privileges, and requirements to provide staff or equipment often also contravene the law [6].

In addition to possibly severe response bias in measuring the frequency of uncommon, inappropriate arrangements, there may be relatively small response bias in other findings. By weighting the data by region and practice size, we have eliminated some such response bias. (For example, our surveys usually show radiologists' response rate below average in the Northeast and West. In this survey, we find regional differences in contract characteristics, and, without weighting, the differential response rate would cause errors.) However, some response bias may remain. For example, the response rate for busier practices may be lower than average, and the characteristics of their contracts may differ.

Another possible source of error, as in most surveys, consists of errors in the information supplied by respondents. Because this was a mail survey, respondents could gather information they did not have at hand and verify information about which they were unsure. We requested they check with their hospitals if they did not know whether the hospitals

used tax-exempt bond financing. However, some may not have checked the information they supplied. Also, deliberate misrepresentation may have occurred on sensitive issues despite our assurance that responses would remain anonymous.

As in all studies, omitted variables may be significant. For example, urban/rural differences may be significant. There may also be differences in contracts depending on the size of the hospitals involved and whether they are for profit, voluntary, publicly owned, and so forth.

In addition to reporting national averages, we have conducted an extensive analysis of factors associated with variation in contract terms, focusing particularly on region, practice size, and whether or not a hospital uses tax-exempt bond financing. Probably the dominant conclusion to emerge from this analysis is how limited variation is. If a provision is predominant nationally, it is predominant in every region, for every practice size, and whether or not hospitals use tax-exempt bond financing. There is, however, some modest variation in how common provisions are among the various regions, practice-size categories, and so on. The multivariate analyses indicate that most of the effects found in the single-variable analyses are true effects, not statistical artifacts.

Whether a hospital used tax-exempt bond financing was found to have relatively little effect on contract terms. Specifically, it was found to have statistically significant effects in only five of the 17 multivariate analyses of contract characteristics. Moreover, the use of tax-exempt bond financing did not have a significant effect on contract duration or the cancellation period, the two aspects of contracts to which rules regarding tax-exempt bond financing most clearly apply. Most likely, when the survey was conducted (late 1989 to early 1990), the response of hospitals to new legal provisions regarding tax-exempt bond financing had not yet resulted in widespread changes of contract terms. Also, although hospitals may refer to the tax-exempt bond financing issue in contract negotiations with radiologists, our impression is that the current objectives of hospitals for contract changes derive more from the general financial pressures they feel than from the tax-exempt bond financing issue *per se*. In any case, with the current survey as a baseline, future changes in contracts can be monitored through follow-up studies.

The multivariate analyses also showed that practice size had a significant effect on relatively few aspects of contracts. It was significant in only six of the 17 multivariate analyses of contract characteristics. This finding is important, for it means that small groups and solo radiologists have much the same contract terms as large groups, rather than being relatively disadvantaged.

Regional differences, in contrast, were often found significant. They showed a statistically significant effect in 11 of the 17 analyses of contract characteristics. Although regional differences are varied in character, some patterning seems present. Specifically, in the Northeast, and to a lesser extent in the West, hospitals seem especially involved in the business affairs of radiologists. For example, the odds are particularly high in the Northeast that a hospital receives a portion of

radiologists' fees or has a fixed-fee arrangement with them, that it must approve their fee increases or act as their agent in negotiating with HMOs and PPOs, and that it requires them to participate with Blue Shield or Medicare. Radiology practices in the Northeast may find it helpful in negotiating with hospitals to point out that these contractual arrangements are uncommon in the United States as a whole.

Indeed, knowing what is and is not usual may help radiology practices nationwide to resist pressures from hospitals to accept undesirable contract provisions that are now uncommon. Also, the radiology profession can use our findings to map a strategy for countering undesirable arrangements. We have confirmed the existence of apparently illegal provisions; this certainly merits attention. As well, since contracting is now a widespread mode of establishing the relationship between radiologists and hospitals, it may be appropriate to augment educational activities by informing radiologists of the potentially disadvantageous consequences of some of the contract provisions we have found.

More detailed data are available on request from the authors.

ACKNOWLEDGMENTS

We thank Dana Friedman for typing the many drafts of this manuscript and Thomas Greeson for providing advice on the questionnaire and explaining legal issues.

REFERENCES

1. American College of Radiology. *Digest of official council actions, 1980-1989*. Reston, VA: American College of Radiology, 1989
2. Maheux B, Legault C, Lambert J. Increasing response rates in physicians' mail surveys: an experimental study. *Am J Public Health* 1989;79: 638-639
3. Hosmer DW Jr, Lemeshow S. *Applied logistic regression*. New York: Wiley, 1989
4. Gravely SD. Pitfalls in negotiating hospital-based physician contracts. *Radiol Management* 1988;10(4):20-23
5. Carter K. Competition forcing changes in terms of radiology contracts. *Mod Healthcare* 1986;16(9):44
6. Kusserow RP. *OIG management advisory report. Financial arrangements between hospitals and hospital-based physicians*, OEI-09-89-00330. Washington, DC: Office of the Inspector General, U.S. Department of Health and Human Services, 1991

Forthcoming Articles

CALDWELL LECTURE

Respiratory problems of early life now allowing survival into adulthood: concepts for radiologists. *Griscom NT*

REVIEW ARTICLES

The scintigraphic diagnosis of osteomyelitis. *Schauwecker DS*
Computed radiography in musculoskeletal imaging: state of the art. *Murphey MD, Quale JL, Martin NL, Bramble JM, Cook LT, Dwyer SJ III*

Duplex sonography of the cerebral arteries: efficacy, limitations, and indications for the procedure. *Zwiebel WJ*

Commentary. The future of carotid sonography. *Merritt CRB, Bluth EI*

CHEST RADIOLOGY

Sclerotherapy of malignant pleural effusion through sonographically placed small-bore catheters. *Morrison MC, Mueller PR, Lee MJ, et al.*

BREAST RADIOLOGY

The British Columbia Mammography Screening Program: evaluation of the first 15 months. *Warren Burhenne LJW, Hislop TG, Burhenne HJ*

Design and implementation of a low-cost mammography screening project: experience of the American Cancer Society, Texas Division. *Vogel VG, Peters GN, Evans WP*

Commentary. Low-cost mass mammography screening for breast cancer. *Sickles EA*

GASTROINTESTINAL RADIOLOGY

Commentary. Colonic contour changes in chronic ulcerative colitis: reappraisal of some old concepts. *Gore MR*

Case report. Intestinal stricture due to lapbelt injury. *Shalaby-Rana E, Eichelberger M, Kerzner B, Kapur S*

Sonography with intraarterial infusion of carbon dioxide microbubbles (sonographic angiography): value in differential diagnosis of hepatic tumors. *Kudo M, Tomita S, Tochio H, et al.*

Case report. Splenic and hepatic peliosis: MR findings. *Maves CK, Caron KH, Bisset GS III, Agarwal R*

Case report. Intrahepatic cholangiocarcinoma: MR appearance. *Hamrick-Turner J, Abbitt PL, Ros PR*

Case report. Tiny echogenic foci in the liver and kidney in AIDS patients: not always due to disseminated *Pneumocystis carinii*. *Bray HJ, Lail VJ, Cooperberg PL*

Technical note. Delineation of surgical segmental liver anatomy: value of PRISE, an MRI fast scanning technique. *Meyer CA, Colon E, Provost T, Sherman JL*

Case report. Pleomorphic pancreatic sarcoma mimicking pancreatic pseudocyst: CT appearance. *Laverdiere JT, vanSonnenberg E, Strum WB, Kuster GGR*

GENITOURINARY RADIOLOGY

Symptomatic renal obstruction or urosepsis during pregnancy: treatment by sonographically guided percutaneous nephrostomy. *vanSonnenberg E, Casola G, Talner LB, Wittich GR, Varney RR, D'Agostino HB*

MR appearance of the normal and abnormal vagina after hysterectomy. *Brown JJ, Gutierrez ED, Lee JKT*

MUSCULOSKELETAL RADIOLOGY

Chondromalacia patellae: diagnosis with MR imaging. *McCauley TR, Kier R, Lynch KJ, Joki P*

Commentary. Chondromalacia patellae. *Hodler J, Resnick D*

Diagnosis of pelvic fractures in patients with acute pelvic trauma: efficacy of plain radiographs. *Resnik CS, Stackhouse DJ, Shanmuganathan K, Young JWR*

Unstable Jefferson variant atlas fractures: an unrecognized cervical injury. *Lee C, Woodring JH*

Pictorial essay. Hemophilia: evaluation of musculoskeletal involvement with CT, sonography, and MR imaging. *Hermann G, Gilbert MS, Abdelwahab IF*

PEDIATRIC AND FETAL RADIOLOGY

Benign gaseous distension of the bowel in premature infants treated with nasal continuous airway pressure: a study of contributing factors. *Jaile JC, Levin T, Wung JT, Abramson SJ, Ruzal-Shapiro C, Berdon WE*

Sonography of hypertrophic pyloric stenosis: frequency and cause of nonuniform echogenicity of the thickened pyloric muscle. *Spevak MR, Ahmadjian JM, Kleinman PK, Henriquez G, Hirsh MP, Cohen IT*

Correlation between omphalocele contents and karyotype abnormalities: sonographic study in 37 cases. *Getachew MM, Goldstein RB, Edge V, Goldberg JD, Filly RA*

Voiding cystourethrography in children: value of digital fluoroscopy to reduce radiation dose. *Cleveland RH, Constantinou C, Blickman JG, Jaramillo D, Webster E*

Pictorial essay. Hepatic masses in infants and children: CT evaluation. *Jabra AA, Fishman EK, Taylor GA*

NEURORADIOLOGY

Early angiographic and CT findings in patients with hemorrhagic infarction in the distribution of the middle cerebral artery. *Bozzao L, Angeloni U, Bastianello S, Fantozzi LM, Pierallini A, Fieschi C*

Commentary. Hemorrhagic infarction: guilt by association? *Pessin MS, Teal PA, Caplan LR*

Subacute necrotizing myelopathy: MR imaging in four pathologically proved cases. *Mirich DR, Kucharczyk W, Keller MA, Deck J*

Commentary. Necrotizing myelopathy. *Kim RC*

MR contrast enhancement in brainstem and deep cerebral infarction. *Elster AD*

Real-time sonography in ocular trauma. *Kwong JS, Munk PL, Lin DTC, Vellet AD, Levin M, Buckley AR*

MR IMAGING

MR lymphography using iron oxide particles: dose-response studies and pulse sequence optimization in rabbits. *Hamm B, Taupitz M, Hussmann P, Wagner S, Wolf K-J*

INTERVENTIONAL RADIOLOGY

The relationship between back pain and lead apron use in radiologists. *Moore B, vanSonnenberg E, Casola G, Novelline RA*

A new electronically enhanced biopsy system: value for improving needle-tip visibility during sonographically guided interventional procedures. *Perrella RR, Kimme-Smith C, Tessler FN, Ravagendra N, Grant EG*

Technical note. Use of hot-tip laser probes to recanalize occluded expandable metallic biliary endoprostheses. *Lossef SV, Druy E, Jelinger E, Fleischer D, Barth KH*

ADVICE TO AUTHORS

Preparation of manuscripts for radiology journals: advice to first-time authors. *Berk RN*



Recognition of Manuscript and Book Reviewers for 1991

The editors and the editorial staff wish to express their appreciation to the following colleagues, who as manuscript reviewers have spent many hours in 1991 helping to select only the most authentic, original, and useful articles for publication in the *AJR*, and to those responsible for book reviews.

Each manuscript received by the Journal is forwarded anonymously to two knowledgeable reviewers for their opinions concerning the worthiness of the paper for publication and/or their suggestions for improvement. The Journal receives 1500 manuscripts annually, of which only approximately 630 (42%) are published. The reviewers perform this service without compensation and with no recognition except for this acknowledgment.

The dedication of the reviewers is largely responsible for the exceedingly short mean time (3.9 weeks) between submission of manuscripts and notification of authors about the initial editorial decision. Initial editorial decisions are reached this quickly only because reviewers agree to judge manuscripts within 2 weeks, an enormous commitment considering the extent of their other responsibilities.

Book reviewers have been equally generous with their time, evaluating for the readers the burgeoning number of textbooks published each year.

These contributors have added immeasurably to the value, scientific merit, and relevance of the Journal. The quality of the Journal is in their hands. We are grateful for the erudite and conscientious manner in which they discharge these imposing responsibilities.

Robert N. Berk
Editor-in-Chief

Henry G. Adams
Alex M. Aisen
Abass Alavi
Philip O. Alderson
T. Noel K. Allan
Marco A. Amendola
Edward S. Amis
Gary M. Amundson
Dixie J. Anderson
James H. Anderson
Michael Andre
Jerry S. Apple
John D. Armstrong
John E. Aruny
William L. Ashburn
Gregory L. Aughenbaugh
John H.M. Austin
Leon Axel
Diane S. Babcock
Jeanne W. Baer
David H. Baker
Mark E. Baker
Stephen R. Baker
Dennis M. Balfe
William S. Ball
Emil J. Balthazar
Marc P. Banner
A. James Barkovich
Richard L. Baron
Royal J. Bartrum
Lawrence W. Bassett
Solomon Batnitzky
Stanley Baum
Bruce R. Baumgartner
Craig Beam
Gary J. Becker
Joshua A. Becker

Melvin H. Becker
Colin B. Begg
Javier Beltran
Beryl Benacerraf
Carol B. Benson
Paul Berger
Colleen J. Bergin
Michael E. Bernardino
Charles C. Berry
Michael A. Bettmann
Gayle H. Bickers
Jeffrey Bisker
George S. Bisset III
Ann Bjorkengren
William C. Black
M. Donald Blafox
Johan G. Blickman
J. Eric Blum
Stanley P. Bohrer
Nicole-Fr. Bolender
Joseph Bonn
Joseph J. Bookstein
Gregory P. Borkowski
William G. Bradley
Thomas J. Brady
Folke J. Brahme
Robert T. Bramson
Jeffrey C. Brandon
William E. Brant
Robert Brasch
Ethan M. Braunstein
Robert L. Bree
Alan S. Brody
Anne C. Brower
Jeffrey J. Brown
Patrick J. Bryan
Edward Buonocore

H. Joachim Burhenne
Linda Warren Burhenne
Anthony J. Buschi
William H. Bush
Rodney James Butch
Richard B. Buxton
John B. Campbell
William L. Campbell
Gary Caputo
David H. Carlson
Harley Carlson
Erik Carlsson
Barbara A. Carroll
William J. Casarella
Philip N. Cascade
Giovana Casola
Manuel Cerqueira
Arnold Chait
Vijay P. Chandnani
Paul Joseph Chang
Norman E. Chase
Charles H. Chesnut
Felix S. Chew
Judith L. Chezmar
Kyung J. Cho
Peter L. Choyke
Ross Christensen
Robert A. Clark
Robert H. Cleveland
W. Peter Cockshott
Alan M. Cohen
Harris L. Cohen
Jesse M. Cohen
Mervyn D. Cohen
Beverly G. Coleman
Dewey J. Conces
Virgil R. Condon

James J. Conway
William F. Conway
Peter L. Cooperberg
Constantin Cope
Philip Costello
Michael Crade
Lawrence E. Crooks
Harte C. Crow
John V. Cruces
Donald A. Cubberley
John T. Curnes
David J. Curtis
Horacio R. D'Agostino
Abraham H. Dachman
Richard H. Daffner
Michael D. Dake
Murray K. Dalinka
Michael David Darcy
Frederick L. Datz
Patricia C. Davis
Peter L. Davis
Sheila D. Davis
Steven L. Dawson
Arthur A. De Smet
James B. Dealy
Barbara E. Demas
Terrence C. Demos
Wilma C. Diner
Robert E. Dinsmore
Michael A. DiPietro
Jeffrey A. Dobkin
Karl T. Dockray
Gerald D. Dodd
James Donaldson
John L. Doppman
John P. Dorst
Peter M. Doubilet

Walter Drane
Edward M. Druy
N. Reed Dunnick
Andrew Dwyer
Samuel J. Dwyer
Steven Edell
Robert R. Edelman
David K. Edwards
Juri Eenmaa
Eric L. Effmann
Georges Y. El-Khoury
Kent Ellis
Allen D. Elster
Ronald G. Evens
Jacob I. Fabrikant
Joseph Fakhry
Michael P. Federle
Stephen A. Feig
David S. Feigin
Sandra K. Fernbach
Joseph T. Ferrucci
Melvin M. Figley
Hossein Firooznia
Dale W. Fitting
Arthur C. Fleischer
Barry D. Fletcher
L. Christopher Foley
W. Dennis Foley
John Forrest
Lee A. Forstrom
Lawrence R. Frank
Edmund A. Franken
Gerald S. Freedman
Patrick C. Freeny
Robert H. Freiburger
Irwin M. Freundlich
Donald G. Frey



Andrew M. Fried	Richard M. Heller	Robert A. Kubicka	Alec J. Megibow	Howard M. Pollack
Arnold C. Friedman	William R. Hendee	Jerald P. Kuhn	G. Leland Melson	Thomas Lee Pope
Paul J. Friedman	Mark Henkelman	Madan V. Kulkarni	Ellen B. Mendelson	M. Judith Donovan Post
J. James Frost	Robert Herfkens	Harold L. Kundel	Christopher R.B. Merritt	Barry M. Potter
Dennis G. Fryback	Hans Herlinger	Sevil Kursunoglu-Brahme	David F. Merten	Andrew K. Poznanski
Carl R. Fuhrman	George Hermann	Alfred B. Kurtz	Charles E. Metz	Leslie Preger
Gary D. Fullerton	Marta Hernanz-Schulman	David C. Kushner	Morton A. Meyers	David F. Preston
Raymond A. Gagliardi	John R. Hesselink	Ralph S. Lachman	Peter Meyers	Dolores H. Pretorius
Gordon Gamsu	Charles B. Higgins	Faye C. Laing	Reuben S. Mezrich	Anthony V. Proto
Stephen S. Gebarski	Saskia Hilton	Elvira V. Lang	Michael S. Middleton	Robert D. Pugatch
David W. Gelfand	Waldo S. Hinshaw	Erich K. Lang	William D. Middleton	Douglas J. Quint
Harry Genant	Charles P. Ho	Elliott C. Lasser	Linda M. Miketic	Jack G. Rabinowitz
Ajax E. George	Paul B. Hoffer	Igor Laufer	John R. Milbrath	Patricia Ann Randall
Gary G. Ghahremani	Alan D. Hoffman	Paul C. Lauterbur	Stephen W. Miller	Vassilios Raptopoulos
Thurman Gillespy	Marc J. Homer	Thomas L. Lawson	Lee Milner	Helen C. Redman
Louis A. Gilula	Steven Horii	Edward A. Lebowitz	Howard J. Mindell	Barbara S. Reid
John J. Gisvold	Brian A. Howard	Robert L. Lebowitz	Jerrold H. Mink	Robert R. Renner
Ronald B.J. Glass	Hedvig Hricak	Joseph K.T. Lee	Charles A. Mistretta	Donald L. Resnick
Seth N. Glick	H.K. Huang	John C. Leonidas	Donald G. Mitchell	Charles S. Resnik
Morton Glickman	David W. Hunter	George R. Leopold	Carol A. Mittlestaedt	Stewart R. Reuter
J. David Godwin	Douglas E. Hutchinson	Janis Gissel Letourneau	Harold A. Mitty	Todd Richards
Thomas C. Goergen	Nola M. Hylton	Anna S. Lev-Toaff	Roger E. Moe	Michael L. Richardson
Richard H. Gold	Gerald A.L. Irwin	Henry Levenson	Paul L. Molina	Matthew D. Rifkin
Richard P. Gold	Valerie P. Jackson	David C. Levin	Elizabeth H. Moore	Ernest J. Ring
Robert E. Gold	C. Carl Jaffe	Errol Levine	Sheila G. Moore	Barry Robbins
Barry B. Goldberg	Richard B. Jaffe	Marc S. Levine	William E. Moore	Anne C. Roberts
Marvin E. Goldberg	Edward Janon	Robert G. Levitt	Richard L. Morin	Shauna R. Roberts
Amy Beth Goldman	Paul F. Jaques	David K. Li	Thomas W. Morris	William D. Robertson
Harold S. Goldman	R. Brooke Jeffrey	King C. Li	Richard P. Moser	Arvin E. Robinson
Antoinette S. Gomes	James Jelinek	Herman I. Libshitz	Albert A. Moss	Maurice A. Robkin
Charles A. Gooding	Mary Ann Johnson	Joel E. Lichtenstein	Donald P. Mueller	Charles A. Rohrmann
Gretchen A.W. Gooding	Gordon C. Johnson	Karen K. Lindfors	Peter R. Mueller	Pablo R. Ros
Lawrence R. Goodman	Bronwyn Jones	Daniel P. Link	Nestor L. Muller	David M. Rosenbaum
Philip Goodman	R. Gilbert Jost	Joseph P. LiPuma	Peter L. Munk	Murray A. Rosenberg
Roy L. Gordon	Saadoon Kadir	Martin J. Lipton	Mark D. Murphey	Arthur Rosenfield
Richard M. Gore	Emanuel Kanal	Hing-Har Lo	William A. Murphy	Carl John Rosenquist
Antonio Govoni	Krishna Kandarpa	Gwilym S. Lodwick	Howard J. Naidech	Daniel I. Rosenthal
Edward G. Grant	Robert A. Kane	H. Esterbrook Longmaid	Harvey L. Neiman	Richard E. Rosenthal
Joel E. Gray	Hooshang Kangarloo	John W. Loop	David W. Nelson	Jeffrey S. Ross
Edward V. Grayson	Stephen A. Kanter	Ronald J. Lorig	Marvin D. Nelson	Alan H. Rowberg
Curtis E. Green	George W. Kaplan	Leon Love	Rendon C. Nelson	V. Allen Rowley
Reginald Greene	Phoebe Ann Kaplan	Robert B. Lufkin	Thomas Roy Nelson	Deborah Rubens
Robert A. Greenes	David Karasick	Kenneth H. Luk	Albert A. Nemcek	Stephen E. Rubesin
Adam Greenspan	Richard W. Katzberg	Caroline J. Lundell	Arthur H. Newberg	Jonathan M. Rubin
Guerdon Greenway	Barry T. Katzen	David A. Lynch	Jeffrey H. Newhouse	Carol M. Rumack
N. Thorne Griscom	Robert A. Kaufman	Robert L. MacCarty	Alex Norman	Anthony H. Russell
Julius Harry Grollman	Stephen L. Kaufman	Laurence A. Mack	Robert A. Novelline	Francis F. Ruzicka
Stuart A. Groskin	Chester Kay	Heber MacMahon	Stanley Novy	Stuart S. Sagel
David Gur	Jeremy J. Kaye	Nabil F. Maklad	Ray L. Nunnally	David J. Sahn
Jud Gurney	Theodore E. Keats	Michael L. Manco-Johnson	Michael J. O'Brien	Sanjay Saini
Marvin Guter	Frederick S. Keller	Frederick A. Mann	Anne G. Osborn	Colleen Sanders
Diana F. Guthaner	Frederick M. Kelvin	Stephen I. Marglin	David J. Ott	Carl M. Sandler
Michael T. Gyepes	James G. Kereiakes	Carroll Markivee	Theron W. Oviit	Martin P. Sandler
David B. Hackney	Pamela Kidd	Bruce M. Markle	Maer B. Ozonoff	E. Nicholas Sargent
Ferris Hall	Stephen A. Kieffer	Richard I. Markowitz	Julio C. Palmaz	David J. Sartoris
Robert A. Halvorsen	Thomas S. Kilcheski	William Martel	David M. Panicek	Mohammad Sarwar
William Hanafee	Ray F. Kilcoyne	David S. Martin	Bruce R. Parker	Stefan C. Schatzki
Roger K. Harned	E. Edmund Kim	John E. Martin	Suresh K. Patel	William Scheible
Donald P. Harrington	Carolyn Kimme-Smith	Myron Marx	Mini Nutan Pathria	William L. Schey
A. Basil Harris	Michael S. Kipper	Alan H. Maurer	Heidi Patriquin	Melvyn H. Schreiber
John H. Harris	John A. Kirkpatrick	Gerald R. May	James A. Patton	Scott J. Schulte
Ronald D. Harris	Donald R. Kirks	Richard B. Mazess	Sven J.K. Paulin	D. James Schumacher
David S. Hartman	Eugene C. Klatte	John G. McAfee	David M. Paushter	Jeno I. Sebes
Derek Harwood-Nash	Richard M. Klein	William H. McAlister	William Pavlicek	Arthur J. Segal
Robert R. Hattery	Paul K. Kleinman	Ronald W. McCallum	Alan S. Pearlman	Steven E. Seltzer
Irvin F. Hawkins	P. Ruben Koehler	Michael J. McCarthy	Wallace Peck	Jerome H. Shapiro
Curtis W. Hayes	Daniel B. Kopans	Bruce L. McClennan	Rita Perrella	Marcelle J. Shapiro
David R. Haynor	Kenyon K. Kopecky	John P. McGahan	Jerry P. Petasnick	Douglas R. Shearer
Linda A. Heier	Melvyn Korobkin	Richard A. McLeod	Warren C. Phillips	William H. Shehadi
Jay P. Heiken	Elissa L. Kramer	Theresa C. McLoud	Daniel Picus	William P. Shuman
Richard S. Heilman	Mark J. Kransdorf	H. Erik Meema	Joseph F. Polak	Edward A. Sickles

Barry A. Siegel
Hano Armin Siegel
Marilyn J. Siegel
Michael E. Siegel
Paul M. Silverman
Stuart G. Silverman
Allan L. Simon
Chris Siström
M. Leon Skolnick
Jovitas Skucas
Richard M. Slone
Thomas L. Slovis
James G. Smirniotopoulos
Edward H. Smith
Julius Smith
Tony P. Smith
Peter Som
F. Graham Sommer
Thomas A. Sos
Constantine Soter
Benigno Soto
Renate L. Soulen
Richard P. Spencer
Hugo Spindola-Franco
Beverly A. Spirt
David B. Spring
Charles E. Spritzer

Eugene L. St. Louis
Edward V. Staab
Robert C. Stadalnik
Philip Stanley
Robert J. Stanley
Tom W. Staple
David D. Stark
Paul Stark
Lynne S. Steinbach
Harvey V. Steinberg
Robert M. Steiner
David H. Stephens
Eric J. Stern
Giles Stevenson
Edward T. Stewart
Richard G. Stiles
William H. Straub
David A. Stringer
Charles M. Strother
David M. Stubbs
John R. Sty
Murali Sundaram
Henry A. Swett
Leonard E. Swischuk
Gordon Sze
Lee Talner
John P. Tampas

Robert D. Tarver
Juan M. Taveras
George A. Taylor
Kenneth J.W. Taylor
Sharlene A. Teehey
Rita Teele
George Teitelbaum
Phillip A. Templeton
Steven K. Teplick
Franklin N. Tessler
Ruedi F. Thoeni
F. Deaver Thomas
William M. Thompson
John R. Thornbury
M. Kristin Thorsen
Robert D. Tien
Jaime Tisnado
Irena Tocino
Ina L.D. Tonkin
William E. Torres
William G. Totty
Richard Towbin
Micahel Trambert
Theodore A. Tristan
Rosalind H. Troupin
David A. Turner
James A. Usselman

Karim Valji
Ronald L. Van Heertum
Michael W. Vannier
Eric vanSonnenberg
Robert R. Varney
C. Whitley Vick
Frederick Vines
Michael R. Violante
Robert L. Vogelzang
Kay H. Vydareny
Susan D. Wall
Sidney Wallace
William J. Walls
Joseph F. Walter
Arthur C. Waltman
Keith Y. Wang
Yen Wang
John F. Ward
W. Richard Webb
Michael W. Weiner
Jeffrey C. Weinreb
Barbara N. Weissman
Richard L. Wesenberg
Jack L. Westcott
John Wexler
Lewis Wexler
Joseph P. Whalen

E. Maureen White
Nancy O. Whitley
Mark H. Wholey
John S. Wills
Anthony J. Wilson
Stephanie Wilson
Gary G. Winzelberg
Jack Wittenberg
Gerhard Wittich
Gerald L. Wolf
John N. Wolfe
Michael K. Wolverson
Beverly P. Wood
Michael L. Wood
Peter Wootton
Kenneth C. Wright
David W. Yeung
Isabel C. Yoder
Jeremy W.R. Young
Lionel W. Young
William T. C. Yuh
Heun Y. Yune
Ronald J. Zagoria
Albert B. Zajko
Robert A. Zamenhof
Robert K. Zeman
Michael B. Zlatkin

Fate of Manuscripts Rejected for Publication in the *AJR*

Dr. Chew [1] did a follow-up on a cohort of scientific papers rejected by the *AJR* in 1986. He found that the majority of papers, more or less revised, appeared after some time in other journals.

Dr. Chew's conclusion that most scientific work, once submitted, will eventually be published is gratifying. It might suggest that publication bias is not a major problem. This bias occurs when certain papers, notably those with "negative" results, stand less chance of publication than papers that have "positive" results. As scientific consensus progresses on the basis of information from scientific journals, publication bias might be a seriously distorting factor.

I wonder, however, if a generalization based on *AJR* submissions is valid. As Dr. Chew points out, many papers are never submitted at all. In addition, scientists may perform some selection in choosing the journals they submit their papers to and usually will not submit a paper that they think stands little or no chance of being published in a particular journal. An author may wish to minimize the mental agony of too many rejections. Such a submission policy implies that the papers submitted to a prestigious journal such as the *AJR* are generally of high quality—perhaps not good enough for the *AJR*, but of sufficient quality to allow subsequent publication in another journal. However, papers submitted directly to less high ranking journals may not have a second chance after a first rejection and will indeed be lost.

In a study also cited by Dr. Chew, Dickersin et al. [2] found that a considerable publication bias exists. They wrote to authors of published papers on clinical trials about the authors' participation in other trials. Of a total of 1312 completed trials, information on 21% had never been published. Of the trials for which no articles were published, 86% had a negative result, whereas only 45% of those for which articles were published had a negative result. The cause of nonpublication was nonsubmission rather than rejection. Still, the investigators may have anticipated the policy of editorial boards of scientific journals. This policy was recently summarized by an editor of a leading medical journal who remarked that journals will not publish information on a trial that shows that penicillin does not cure cancer, but they will publish a paper on one that shows it does.

F. R. Rosendaal

Department of Clinical Epidemiology
University Hospital Leiden
2300 RC Leiden, the Netherlands

REFERENCES

1. Chew FS. Fate of manuscripts rejected for publication in the *AJR*. *AJR* 1991;156:627-632

2. Dickersin K, Chan S, Chalmers TC, Sacks HS, Smith H Jr. Publication bias and clinical trials. *Controlled Clin Trials* 1987;8:343-353

Reply

I appreciate Dr. Rosendaal's commentary on my paper about the fate of manuscripts rejected by the *AJR* [1]. His letter raises two issues: (1) does publication bias occur, and (2) can the results of my study of rejected *AJR* submissions be generalized to the rejected submissions of other journals?

Publication bias can be defined as a systematic difference in the likelihood of publication of submitted articles that is based on whether an article has specific characteristics. In the context of Dr. Rosendaal's query, the one criterion resulting in publication bias is that the results reported in the manuscript are positive. That is, all other things being equal, a paper that reports a study with a positive result is more likely to be published than a paper that does not. It is an artifact of the scientific method that in observational studies it is easier to show the presence of an association between two factors (assuming an association is present) than it is to show the absence of one (assuming no association is present). The weaker the association, the more difficult it is to show the association scientifically (the larger the necessary sample size). Studies that do not show the presence of a strong association may not have enough statistical power (large enough sample size) to show the presence of a weak association or to show the absence of an association. It is probably because of this artifact that many observational studies are abandoned at the point where failure to show a strong positive result is evident but before enough data are collected to show conclusively a negative result. It should be realized that the lack of positive results includes both negative results and inconclusive results. Inconclusive studies are unlikely to be submitted or to be published. It is uncertain how many unpublished studies that did not have positive results had results that were actually inconclusive rather than negative. In the descriptive studies common to radiologic research, the problem of inconclusive results generally does not occur. However, if the description is of normal radiologic examinations associated with some disease process or clinical presentation, it will not be of much interest unless the prevailing paradigm is that there are abnormalities that should be evident on radiologic examination.

I did not have available to me the data necessary to show if manuscripts submitted to journals other than the *AJR* were as likely to be published, either in the journal of initial submission or in some other journal, as were submissions to *AJR*. It is certainly possible that journals of "lower prestige" than the *AJR* have higher initial rates

of acceptance than *AJR* but that the manuscripts these journals reject have lower rates of acceptance elsewhere. It is my impression that authors decide to publish a particular research result before they write the paper and ponder where to submit it. Once a paper is submitted, authors are likely to have invested so much time and effort in a project that they usually see the paper through to publication, regardless of whether the manuscript initially is rejected.

Felix S. Chew
Massachusetts General Hospital
Harvard Medical School
Boston, MA 02114

REFERENCE

1. Chew FS. Fate of manuscripts rejected for publication in the *AJR*. *AJR* 1991;156:627-632

A Simple Program for Rapid Retrieval of ACR Diagnosis Codes

Often a researcher wishes to find all the radiologic examinations of patients with a specific disease or condition. Unfortunately, although cases in teaching files are routinely coded with American College of Radiology (ACR) diagnosis codes, most routine examinations remain uncoded and are therefore unavailable for retrieval according to diagnoses. We estimate that providing ACR diagnosis codes manually by looking them up in the *Index for Radiological Diagnosis*, would occupy 10-20% of a radiologist's total film-reading time. Thus, routine coding is impractical.

In an attempt to reduce the time required to find the desired code, my colleagues and I wrote a simple list management program that allows rapid access to the desired code by the use of a mouse and menu interface. The codes themselves are available in electronic form from the ACR. Basically, a code consists of two to four digits representing the anatomy code, a decimal point, and two to five digits specifying the pathology code. A short description follows each code. The program reads the data file and creates a tree structure containing the code information. Ten trees are available, one for each of the

10 principal anatomic fields. In the first version of this program, we only use one anatomy digit (the principal field), though we do use all the pathology digits. A leaf in the tree is a data structure that contains the short description of the digit in question and 10 pointers to other leaves that represent the possible digits to follow. As not all the possible codes are used, the tree is dynamically allocated so that empty leaves do not consume memory. Because the entire structure resides in memory, access to all 10 trees is extremely fast. On the other hand, because the tree is dynamically created each time the program is run, it does take a fraction of a second to start the program. We find that the memory and computational speed of a desktop workstation are not at all taxed by this program.

The user interface is based on the OpenWindows flavor of the MIT X11 Windowing system. The user is presented with a window containing six buttons and the short description appropriate for that button (Fig. 1). Selecting the list glyph (the small downward-pointing arrowhead) causes a list of the digits available for that decimal place to be specified. Each time a selection is made, the program updates the selections in the next lower list. A user thus starts with the top (anatomy) digit and progresses down through the list glyphs until he or she has reached the desired level of precision or until the fifth digit is reached.

The program also can be used to identify an unknown code. By clicking the mouse on the numbered buttons, the user can display a given code, and the description of that code is displayed on the screen to the right. Last, a "pick" button allows the displayed code to be sent to the Unix standard output to be used by another program in a Unix "pipe."

Having the user interface coded in variant of MIT X11 allows the program to be used from any workstation on the department network. Even suitably equipped personal computers can display X windows. We hope that this rapid method of coding will allow radiologists to code more of the daily film load and therefore make these cases available for retrieval according to diagnosis.

David S. Channin
The Pennsylvania State University College of Medicine
The Milton S. Hershey Medical Center
Hershey, PA 17033

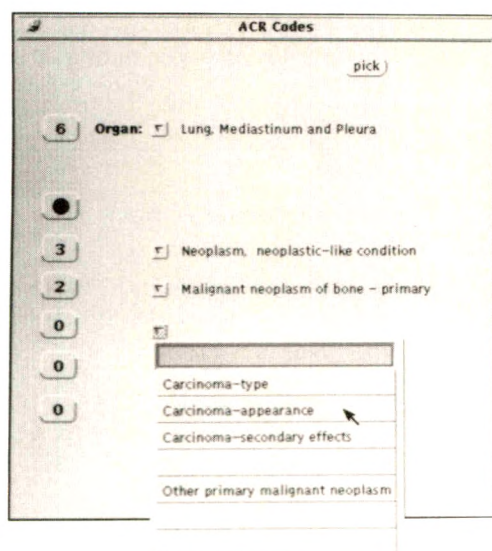


Fig. 1.—Example of a window display in a simple system for retrieving radiologic examinations according to American College of Radiology diagnosis codes.

Radiologic Findings in the Diagnosis of Hughes-Stovin Syndrome

Hughes-Stovin syndrome is the exceedingly rare combination of pulmonary arterial aneurysms and venous thrombosis [1-4]. Signs and symptoms are cough, dyspnea, hemoptysis, headache, intermittent fever, and papilledema as well as those due to peripheral phlebothrombosis. The most frequent cause of death is rupture of an aneurysm into the pulmonary airways. To our knowledge, fewer than 20 cases have been reported.

A 20-year-old male Romanian refugee with a history of two episodes of hemoptysis in Romania was admitted because of severe hemoptysis. A chest radiograph showed enlarged lower poles of the left and right hila (Fig. 1A). Phlebography showed partially thrombosed external and common iliac veins bilaterally and an incompletely thrombosed distal infrarenal inferior vena cava. Suprapubic and lumbar collateral vessels eventually filled the proximal inferior vena cava. Pulmonary angiography showed one aneurysm in the right lung and two smaller aneurysms in the left lung (Figs. 1B and 1C). The aneurysms corresponded to the lesions seen on the chest radiograph. All laboratory data, including the results of coagulation studies and tests for infectious and autoimmune diseases, were normal.

The obscure cause of the peripheral thrombotic events and the cryptic genesis of the pulmonary aneurysms in Hughes-Stovin syn-

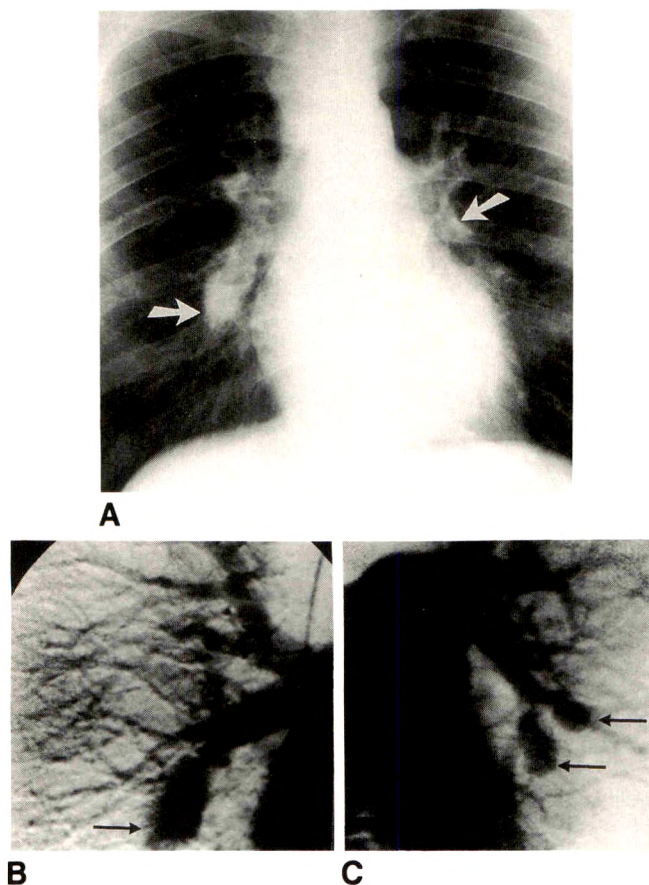


Fig. 1.—Hughes-Stovin syndrome.
A, Chest radiograph shows bilaterally enlarged lower poles of hila (arrows).
B and C, Pulmonary angiograms show large aneurysm (arrow, **B**) of pulmonary artery in right lower lobe and two moderately sized aneurysms (arrows, **C**) of pulmonary arterial branches to left lower lobe.

drome do not help in choosing a specific therapy. Coumadin (sodium warfarin), Persantine (dipyridamole), and cortisone have been given empirically to prevent thrombotic events and to stem a possibly autoimmune vasculitic component that might be present [3]. Our patient has received no specific therapy and, with the exception of another small episode of hemoptysis, is doing fine.

Markus E. Ammann
 Franz Karnel
 Friedrich Olbert
 AKH, Vienna University
 A-1090 Vienna, Austria
 Klaus Mayer
 AöKH Barmherzige Schwestern
 A-4060 Wels, Austria

REFERENCES

1. Beattie JM, Hall AJ. Multiple embolic aneurysms of pulmonary arteries from veins of the leg: death from rupture of aneurysm into lung. *Proc R Soc Med* 1911;5:147-155
2. Hughes JP, Stovin PGI. Segmental pulmonary aneurysms with peripheral venous thrombosis. *Br J Dis Chest* 1959;53:19-27
3. Wolpert SM, Kahn PC, Farbman K. The radiology of the Hughes-Stovin syndrome. *AJR* 1971;112:383-388
4. Teplick JG, Haskin ME, Nedwich A. The Hughes-Stovin syndrome. *Radiology* 1974;113:607-608

Mammography Quality Assurance

With the advent of radiologic quality assurance, our department has attempted to institute an efficient yet informative program for follow-up of women who have mammography at our hospital. Recently, the American College of Radiology (ACR) has required institutions to maintain appropriate records of patients' follow-up in order to obtain and maintain certification of the institutions' mammography units. To that end, we wish to share our department's system.

We use an ADAC Laboratory Computer System, but our method can be modified for radiology departments without computerization. All our patients are referred by physicians. After interpreting a mammogram, the radiologists dictate a "Code I" report if they think the mammogram is abnormal and additional follow-up is required. Our Code I reports might request a biopsy or another examination in 4 months and so forth.

Once a month, we obtain from the computer a list of those patients whose mammographic reports received a Code I the preceding month. The referring physician for each Code I patient is then sent a letter of notification about the abnormal findings and a self-addressed, stamped postcard. The physician is asked to sign and return the postcard to indicate that the notification was received.

This system has been in effect for several months and has been quite successful. A secretary collects all the returned postcards and checks the patients' names off a master list (produced by the computer). Any postcard not returned prompts a telephone call to the referring physician to whom it was sent. After the first few months, our return rate has been 100%.

All referring physicians have been participating, and only two have voiced any objection, claiming "harassment." However, we think these objections have been greatly outweighed by the physician who thanked us for bringing an abnormal mammogram to his attention. The original report apparently was filed before he was able to read it.

This system is easy to implement, and it meets the requirements for ACR mammography certification. More importantly, it provides a mechanism to ensure that a patient with an abnormal mammogram receives the appropriate follow-up. In addition, radiologists more and more are being held liable for the content of their interpretations and are expected to ensure that their reports are read and acted on. Our system addresses these conditions also.

Steven J. Zweig
 Paul Sylvester
 Alpena General Hospital
 Alpena, MI 49707

Pneumoperitoneum on Supine Abdominal Radiographs

In a recent article, Levine et al. [1] analyzed the radiologic signs of pneumoperitoneum on supine abdominal radiographs. The right-upper-quadrant gas sign was the most frequently observed sign, and the authors justly state the lack of attention this sign has received in the literature. In their series, Levine et al. had only one false-positive case with a linear lucency, probably representing fat rather than air, in the subhepatic space. We present another patient with a false-positive linear, right-upper-quadrant gas sign.

A 32-year-old man complained of severe, progressively exacerbating abdominal pain located mainly in the right iliac fossa and epigastrium. An abdominal radiograph showed a linear air collection in the right upper quadrant, probably in the subhepatic or hepatorenal space (Fig. 1A). A sonogram showed air anterior to the right kidney [2]. A CT scan showed the true nature of the air collection: a large, air-filled

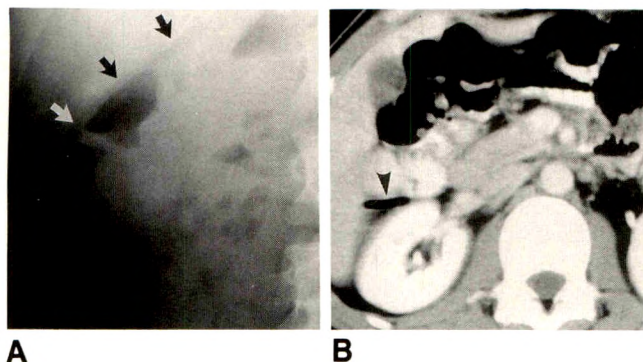


Fig. 1.—Right-upper-quadrant gas sign.
A, Plain supine radiograph shows linear air collection (arrows) in right upper quadrant, outside colon.
B, CT scan shows large, air-filled appendix (arrowhead) extending into hepatorenal space.

appendix lining the right kidney and extending into the hepatorenal space (Fig. 1B). No evidence of free air or inflammation was present. The final diagnosis was gastroenteritis, from which the patient recovered easily.

By showing a normal variant, that is, the atypical position and size of the appendix, mimicking the right-upper-quadrant gas sign, this case indicates that any hyperlucent area in the right upper quadrant must be viewed with suspicion [3].

W. P. Milants
 H. R. Degryse
 A. M. De Schepper
*University Hospital Antwerp
 B 2650 Edegem, Belgium*

REFERENCES

1. Levine MS, Scheiner JD, Rubesin SE, Laufer I, Herlinger H. Diagnosis of pneumoperitoneum on supine abdominal radiographs. *AJR* 1991;156:731-735
2. Lee DH, Lim JH, Ko YT, Yoon Y. Sonographic detection of pneumoperitoneum in patients with acute abdomen. *AJR* 1990;154:107-109
3. Kyunghee CC, Baker SR. Air in the fissure for the ligamentum teres: new sign of intraperitoneal air on plain radiographs. *Radiology* 1991;178:489-492

A Miraculous Cure: Spontaneous Disappearance of Abdominal Tumor After "Laying on of Hands"

Several reports [1-3] of intraabdominal pseudotumors (most commonly unopacified bowel and vascular anomalies) have appeared since the introduction of CT. Loculated ascites also can mimic an intraabdominal mass. Density measurements in the fluid range usually allow differentiation from tumor, but loculated ascites in which the fluid has a high concentration of blood or protein can pose a diagnostic dilemma.

A 50-year-old man had had increasing abdominal distension for 2-3 weeks. Physical examination revealed a tense, distended abdomen with a positive fluid wave and shifting dullness consistent with a large amount of ascitic fluid. Paracentesis shortly after admission, and before abdominal CT, produced clear transudative ascitic fluid. CT showed a 7.5 × 10.0 cm soft-tissue mass in the pouch of Morison between the liver and right kidney (Fig. 1A). The mass was hyperdense with respect to the liver before injection of IV contrast material

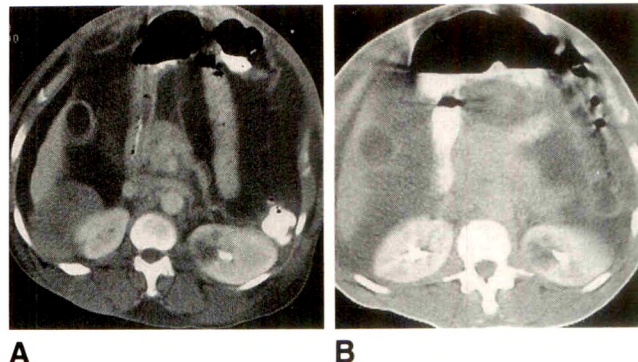


Fig. 1.—A and B, Contrast-enhanced CT scans show spontaneous disappearance of abdominal tumor. Initial scan (A) shows mass in Morison pouch; mass has no significant enhancement. Scan (B) obtained 5 days after A, before planned biopsy and after "laying on of hands," shows mass is no longer present.

and did not enhance after the injection. The differential diagnosis included benign or malignant hepatic neoplasm and, less likely, liver metastasis or retroperitoneal sarcoma. Five days after the initial study, CT was performed again in preparation for a percutaneous biopsy. The previously described abdominal mass was no longer present (Fig. 1B).

It was discovered that the patient had had a second paracentesis, which produced bloody ascitic fluid. Even more interesting was the report that the patient had been visited by members of his religious group the day before the planned biopsy and had undergone vigorous "laying on of hands" to his abdomen, a healing rite common in some fundamentalist groups.

We think that the mass seen on the initial CT scan was a loculated collection of bloody ascitic fluid that was ruptured by vigorous manual manipulation before the second paracentesis and the follow-up CT study. Although no pathologic correlation is available, the sequence of events as they miraculously unfolded would support this contention.

Gary M. Suhr
 J. Alex Lushington, Jr.
 B. G. Brogdon
*University of South Alabama Medical Center
 Mobile, AL 36617*

REFERENCES

1. Brady TM, Gross BH, Glazer GM, Williams DM. Adrenal pseudomasses due to varices: angiographic-CT-MRI-pathologic correlations. *AJR* 1985;145:301-304
2. Mitty HA, Cohen BA, Sprayregen S, Schwartz K. Adrenal pseudotumors on CT due to dilated portosystemic veins. *AJR* 1983;141:727-730
3. Silverman PM. Gastric diverticulum mimicking adrenal mass: CT demonstration. *J Comput Assist Tomogr* 1986;10:709-710

Malignant Brenner Tumor: MR Findings

Brenner tumors are uncommon, and the malignant form is extremely rare. Although the radiologic features of benign Brenner tumors have been described, those of malignant Brenner tumors have not been previously reported. We report the MR findings in a case of malignant Brenner tumor.

A 72-year-old postmenopausal woman had vaginal bleeding. Physical examination revealed a hard, greater than fist-sized pelvic mass. MR imaging with a 1.5-T superconducting scanner and spin-echo techniques showed a 10 × 9 cm mass of complicated cysts with a

solid component at one pole. On T1-weighted images, the cystic lesions appeared as low-signal-intensity masses with sharp margins (Fig. 1A). Administration of gadopentetate dimeglumine showed a smooth, thin wall and a solid component with an intermediate uptake of contrast material. On T2-weighted images, the signal intensity of the cystic lesions was similar to that of fat, and the solid component had medium to high signal intensity (Fig. 1B). No apparent invasion of adjacent organs was seen on either T1- or T2-weighted images. At surgery, a large cystic mass was found that had replaced the left ovary. The mass was removed, and bilateral salpingo-oophorectomy and total hysterectomy were performed. The mass was $10.5 \times 10.0 \times 8.0$ cm and had an essentially smooth outer surface. A solid area at one pole had small cystic spaces up to 1 cm in size containing mucoid material. The cystic areas were multiloculated and contained clear fluid. The solid area was composed of poorly differentiated cells. The pathologic findings indicated a malignant Brenner tumor. A uterine leiomyoma was found also.

Brenner tumors of the ovary are uncommon, accounting for 1–2% of all ovarian tumors. Brenner tumors arise from the surface epithelium of the ovary and are thus classified as epithelial neoplasms, along with serous and mucinous cystadenomas and cystadenocarcinomas, endometrioid carcinomas, and clear cell carcinomas [1–4]. The major pathologic variants are proliferative and malignant Brenner tumors. Proliferative Brenner tumors have epithelial cell atypia, but the prognosis generally is favorable [3, 4]. Benign Brenner tumors have been discovered in women of all ages (median age, 45–50 years) [1, 2]. For the malignant and proliferative Brenner tumors, the average age of the patient is 60 years [3, 4]. Although most Brenner tumors, both benign and malignant, are asymptomatic, abnormal uterine bleeding is the most common manifestation; nonspecific pain is next most common [1–4].

The benign Brenner tumor is typically a solid, round-to-ovoid tumor. Most have been smaller than 5 cm in diameter. On gross inspection, they resemble fibromatous thecomas, leiomyomas, Krukenberg tumors, and carcinoid tumors of the ovary. Approximately 30% of patients with Brenner tumors have a second neoplasm, usually a serous or mucinous cystadenoma or cystic teratoma, frequently in the ipsilateral ovary [1, 2]. Many of the malignant and all of the proliferative Brenner tumors are multicystic and partially solid, unilateral masses that are more than 8–10 cm in diameter on gross examination. For approximately one third of malignant Brenner tumors, evidence of spread beyond the confines of the ovary is seen at the time of the tumor's discovery, although diffuse peritoneal seeding is not a typical feature of the tumor [1, 3, 4].

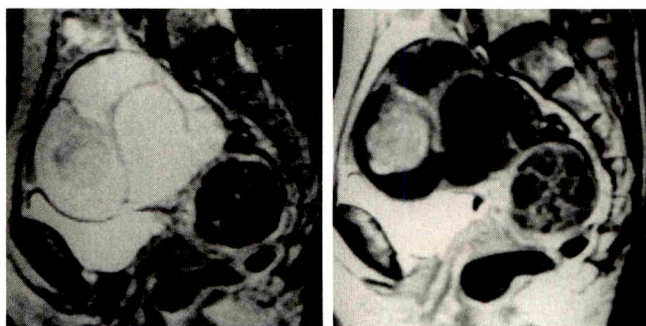


Fig. 1.—Malignant Brenner tumor.
A, Sagittal MR image (2200/70) shows high-signal-intensity cystic lesions.
B, MR image (600/20) obtained after administration of contrast material shows marked patchy enhancement of solid parts of lesions.

Previous reports of CT findings in a benign Brenner tumor describe a smoothly margined, solid, enhancing mass. However, the MR features of malignant Brenner tumor have not been reported. In our case, the tumor was composed of complicated cysts with a solid component at one pole. It resembled a mucinous or serous cystadenocarcinoma but clearly was not a typical benign Brenner tumor. MR can be used to distinguish malignant from benign Brenner tumors but not malignant Brenner tumors from proliferative Brenner tumors or mucinous or serous cystadenocarcinomas.

Kazuro Sugimura
Hiromi Okizuka
Izumi Imaoka
and colleagues
Shimane Medical University
Izumo 693, Japan

REFERENCES

1. Novak ER, Woodruff JD. *Novak's gynecologic and obstetric pathology*, 3rd ed. Philadelphia: Saunders, 1967:379–388
2. Yoonessi M, Abell M. Brenner tumor of the ovary. *Obstet Gynecol* 1979;54:90–96
3. Haid M, Victor TA, Weldon-Linne CM, Danforth DN. Malignant Brenner tumor of the ovary. *Cancer* 1983;51:498–508
4. Roth LM, Dallenbach-Hellweg G, Czernobilsky B. Ovarian Brenner tumors. I. Metaplastic, proliferating, and of low malignant potential. *Cancer* 1985;56:582–591

Vertebral Osteosclerotic Sarcoidosis

We report a case of vertebral osteosclerosis caused by sarcoidosis. A 32-year-old white man was referred to us for evaluation of ankle pain, weight loss, and myalgias. He also had mild chronic backache. Physical examination showed diffuse marked enlargement of lymph nodes and bilateral mild synovitis of both ankles. Chest radiographs showed bilateral hilar adenopathy and fine parenchymal

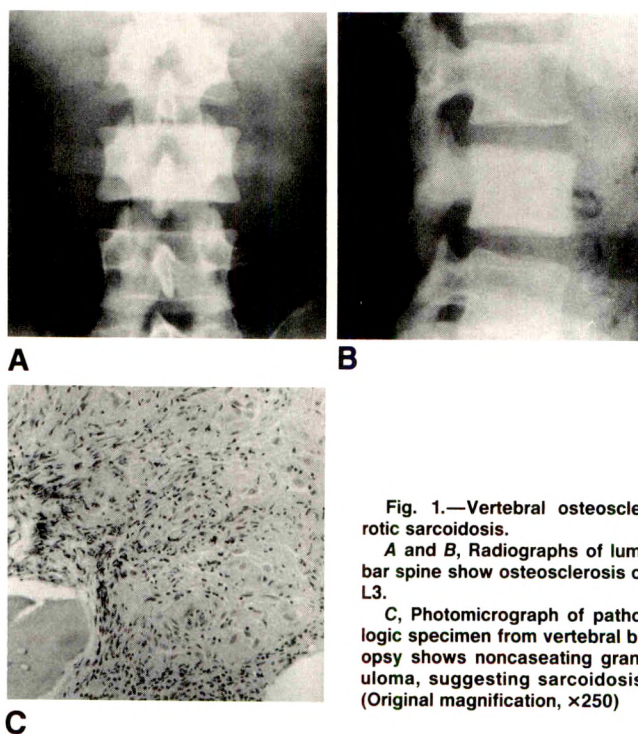


Fig. 1.—Vertebral osteosclerotic sarcoidosis.
A and B, Radiographs of lumbar spine show osteosclerosis of L3.
C, Photomicrograph of pathologic specimen from vertebral biopsy shows noncaseating granuloma, suggesting sarcoidosis. (Original magnification, $\times 250$)

densities. CT scans of the lungs showed bilateral adenopathy in the mediastinal, paratracheal, right and left hilar, and carinal regions, suggestive of sarcoidosis. The results of multiple biopsies (of skin, muscle, accessory salivary glands, bronchi) were normal. Radiographs of the lumbar spine showed a homogeneous osteosclerosis of the body and pedicles of L3 (Figs. 1A and 1B). Scintigraphy with technetium-99m pyrophosphate showed avid uptake of the radionuclide in L3, and findings on CT confirmed the osteosclerosis. A biopsy of the vertebra was performed. Histologic examination of the specimen showed thickened osseous lamellae, narrowing of medullary spaces, and noncaseating granulomata in the marrow (Fig. 1C), compatible with the diagnosis of sarcoidosis.

Michel De Bandt
Maggie Grossin
Marc Smadja
Marcel-Francis Kahn
Bichat Hospital
Paris 75018, France

Osteosarcoma of the Cervical Spine

Osteosarcoma of the cervical spine is rare; only 11 cases have previously been reported. In their review of more than 1000 cases of osteosarcoma, Shives et al. [1] found only 30 primary vertebral tumors, four of which began in the cervical region.

A 27-year-old man had had increasing pain and paresthesias in the upper extremities for 1 week. Bilateral ankle clonus, diminished strength in all four extremities, and reduced pin-prick sensation from C3 caudad were present. Radiographs (Fig. 1A) showed a lytic lesion in the C3 vertebral body, with preservation of the disk spaces. Cervical CT showed destruction of the C3 vertebral body by a noncalcified soft-tissue mass. On MR, the mass had decreased T1 signal relative to adjacent bone marrow and enhanced uniformly with gadolinium (Fig. 1B). Preoperative T2-weighted MR images were not obtained. The patient had surgery and subsequently was treated with radiation. He died of widespread metastatic disease 7 months after treatment.

This case is unusual because of the location and osteolytic appearance of the tumor. Purely osteolytic osteosarcomas are seen in only 10% of patients [2]. Nonetheless, such tumors should be considered in the differential diagnosis of lytic vertebral lesions, whether or not CT shows calcifications. In this case, radiographs showed an

aggressive, probably malignant mass that was causing destruction of a vertebral body but not of the adjacent disk spaces. This made infection unlikely, but the MR and CT findings were still not specific for tumor type, and a biopsy was performed. MR was useful to show the extent of the soft-tissue mass, its location in regard to the thecal sac and spinal cord, and the location of adjacent vessels. This information is useful for planning the approach and extent of surgery required and in determining the location and amount of subsequent bone grafting needed [1].

Mark T. Yoshino
Raymond F. Carmody
University of Arizona
Tucson, AZ 85724

REFERENCES

- Shives TC, Dahlin DC, Sim FH. Osteosarcoma of the spine. *J Bone Joint Surg [Am]* 1986;68-A:660-668
- DeSantos LA, Edeiken B. Purely osteolytic osteosarcomas. *Skeletal Radiol* 1982;7:1-7

Parasitization by Hepatocellular Carcinoma of Branches of the Superior Mesenteric Artery

In a study of 200 human cadavers, Michels [1] found 26 potential pathways for collateral arterial supply to the liver after ligation of the hepatic artery. Charnsangavej et al. [2] showed many of these pathways angiographically in patients who had ligation or embolization of the hepatic artery. These authors [2] point out that the extrahepatic collateral vessels can develop in the suspensory ligaments of the liver in the peritoneal cavity. Such arterial collateral vessels include the pancreaticoduodenal arcades, right and left gastric arteries, right and left inferior phrenic arteries, various periportal arteries, omental branches, intercostal or lumbar arteries, internal mammary arteries, superior epigastric arteries, and capsular branches of the right renal artery. In four of their patients who had peripheral embolization of hypervascular hepatic tumors, collateral vessels to the liver were shown to arise from the middle and right colic arteries [2]. Other articles [3, 4] have reported sources of collateral blood supply to hepatocellular carcinoma that included the right and left inferior phrenic, right and left gastric, pancreaticoduodenal, gastroduodenal, and omentoepiploic arteries, either before or after embolization or ligation of the hepatic artery or chemotherapy. To our knowledge, the English literature has no report of parasitic

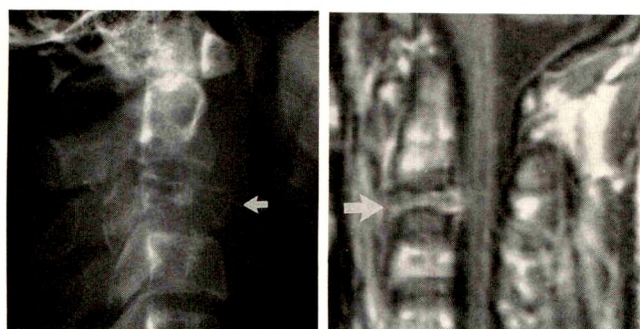


Fig. 1.—Osteosarcoma of cervical spine.
A, Radiograph shows C3 vertebral body is destroyed (arrow), but disk spaces are maintained.
B, Contrast-enhanced MR image shows soft-tissue mass replacing C3 (arrow) has increased signal intensity compared with findings on unenhanced images (not shown). Thecal sac, but not spinal cord, is compressed.

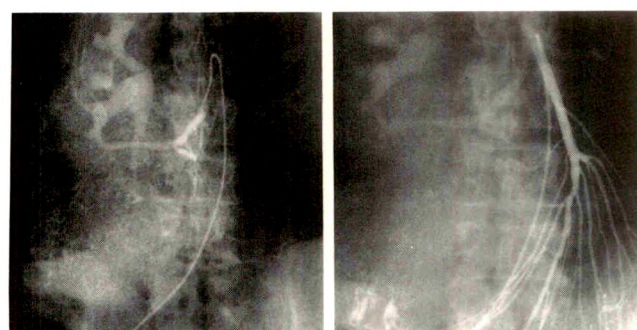


Fig. 1.—A, Celiac arteriogram shows a large hypervascular mass with features typical of a hepatocellular carcinoma in right lobe of liver.
B, Superior mesenteric arteriogram shows displacement of arterial branches by tumor and parasitization of ileocolic branches by inferior part of tumor.

blood supply to an untreated hepatic tumor from the ileocolic branches of the superior mesenteric artery. It is not certain if such a blood supply may result from local invasion of the ileum or colon by the tumor or from the abnormal proliferation and extension of collateral vessels toward the tumor.

A 71-year-old woman had weakness and a weight loss of 15 lb (6.8 kg). A hard mass was palpable in the right upper quadrant of the abdomen. The results of liver function tests were abnormal. The level of carcinoembryonic antigen was 0.4 ng/ml, and tests for antibodies to hepatitis A and B antigens were negative. The serum level of alpha-fetoprotein was zero. Liver biopsy results were consistent with hepatocellular carcinoma with positive staining for alpha-fetoprotein. Celiac and superior mesenteric arteriograms (Fig. 1) showed a large hypervascular mass occupying much of the right lobe of the liver. Angiographic features of the tumor included neovascularity, disorganization, and early venous filling and puddling. The inferior part of the tumor received its blood supply from several small ileocolic branches of the superior mesenteric artery, which also showed these features. Encasement of the gastroduodenal artery was evident, but the superior mesenteric, splenic, and main portal veins were patent.

In the evaluation of hepatocellular carcinoma, demonstration of all sources of blood supply is necessary before therapy is started. In order to maximize the potential benefits of ligation, intraarterial infusion of chemotherapeutic agents, or transcatheter arterial embolization, separate treatment of collateral vessels may be required. Angiographic evaluation of hepatocellular carcinoma should include catheterization of the superior mesenteric artery not only for evaluation of the superior mesenteric and portal veins but also for detection of possible parasitization by the tumor of branches of the superior mesenteric artery.

Nicholas W. Skezas
Dimitrios G. Spigos
Patrick M. Dunne
Bradley G. Langer
Cook County Hospital
Chicago, IL 60612

REFERENCES

1. Michels NA. Collateral arterial pathways to the liver after ligation of the hepatic artery and removal of the coeliac axis. *Cancer* 1953;6:708-724
2. Charnsangavej C, Chuang VP, Wallace S, Soo C, Bowers T. Angiographic classification of hepatic collaterals. *Radiology* 1982;144:485-494
3. Ohtome K, Furui S, Yoshikawa H, et al. CT and angiographic appearances of hepatocellular carcinoma partially feeded [sic] by right inferior phrenic artery. *Rinsho Hoshasen* 1983;28(4):449-452 (in Japanese, with English abstract)
4. Wang S, Chen X, Wang G. Selective angiography in 50 cases of primary hepatocellular carcinoma. *Chin Med J [Engl]* 1982;95(3):171-180

Technique for Conversion from Deep to Superficial Femoral Artery Catheterization

Antegrade catheterization of the common femoral artery is often used for interventional procedures that involve the ipsilateral superficial femoral artery or the popliteal or infrapopliteal arteries. Often the guidewire enters the deep femoral artery. A variety of methods have been described for redirecting the wire into the superficial femoral artery [1, 2]. The following is a description of a technique that has the advantages of direct visualization and maintenance of vascular access.

When a guidewire preferentially enters the profunda femoris during an antegrade approach, it is left in place, and the sheath is advanced over the guidewire into the deep femoral artery (Fig. 1A). With the original guidewire left in place, the sheath is withdrawn slowly under

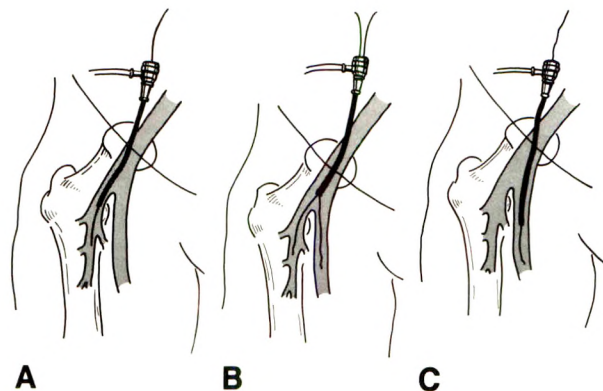


Fig. 1.—Drawings show conversion from deep to superficial femoral artery catheterization.

- A, Guidewire and sheath enter deep femoral artery.
B, Sheath is withdrawn to common femoral artery over initial guidewire, and directional guidewire is advanced into superficial femoral artery.
C, Initial guidewire is withdrawn from deep femoral artery, and sheath is introduced over directional guidewire into superficial femoral artery.

fluoroscopic control, with test injections of contrast material through the side port, until the distal end of the sheath is above the bifurcation of the common femoral artery (Fig. 1B). At this point, a second directional-type guidewire is inserted and directed into the superficial femoral artery. When the superficial femoral artery is entered successfully, the first guidewire is removed from the deep femoral artery, and the sheath is advanced into the superficial femoral artery (Fig. 1C) over the second guidewire.

This method of redirecting a guidewire into the superficial femoral artery has several advantages. The guidewire left in the deep femoral artery ensures vascular access if the sheath is withdrawn too far and leaves the vessel. As long as the puncture is made in the distal common femoral artery, the superficial femoral artery can usually be selected. The side port of the sheath allows (1) injection of contrast material to confirm the positioning of the sheath and (2) visualization of the vascular anatomy without removal of the guidewire. Inasmuch as we normally use sheaths for all angioplasties and vascular interventional work, the only extra expense is the second directional guidewire that may be needed during these procedures. We have found that this method is also helpful in retrograde approaches in attempts to enter the anteriorly placed end-to-side anastomosis of an aortofemoral graft when the first guidewire enters the native obstructive iliac segment.

Johannes Buiteweg
Robert A. Ellwood
Manfred T. Benson
William Beaumont Hospital
Royal Oak, MI 48073

REFERENCES

1. Ring EJ, Mclean GK, eds. *Interventional radiology principles and techniques*. Boston: Little, Brown, 1981:139-142
2. Saddekni S, Srur M, Cohn DJ, Rozenblit G, Wetter EB, Sos TA. Antegrade catheterization of the superficial femoral artery. *Radiology* 1985;157:531-532

Thrombosis of the Internal Jugular Vein: Findings on MR and Color Doppler Imaging

Thrombosis of the internal jugular vein (IJV) is associated with many conditions, including neoplasms of the head and neck, polycy-

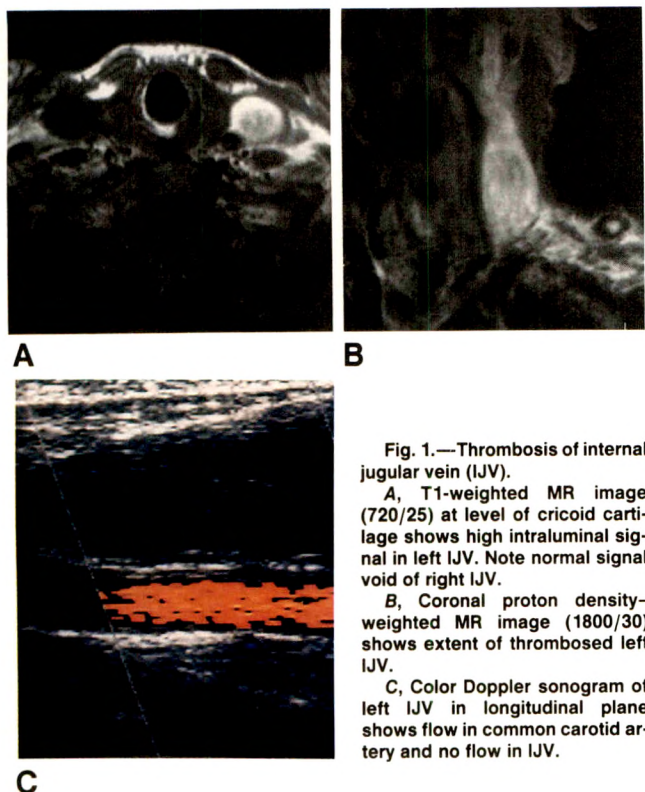


Fig. 1.—Thrombosis of internal jugular vein (IJV).

A, T1-weighted MR image (720/25) at level of cricoid cartilage shows high intraluminal signal in left IJV. Note normal signal void of right IJV.

B, Coronal proton density-weighted MR image (1800/30) shows extent of thrombosed left IJV.

C, Color Doppler sonogram of left IJV in longitudinal plane shows flow in common carotid artery and no flow in IJV.

themia, local inflammation, infective cervical lymphadenopathy, and venous access lines [1]. The thrombosis can be diagnosed by using any of several available imaging techniques. Catheter venography has been replaced by newer techniques such as CT, sonography, and MR [1–3]. The last two are noninvasive and require no IV contrast material.

We examined a 70-year-old man who had swelling of the left side of his neck. He had had an upper respiratory infection that was followed by a “fullness” in the left side of the neck. Broad-spectrum antibiotics were prescribed. The patient was referred for MR imaging 3–4 weeks after the initial onset of the persistent swelling. Transverse and coronal planes and T1- and T2-weighted pulse sequences were used. High signal intensity was seen within the lumen of the left IJV on the T1- and T2-weighted images in both imaging planes, with no significant difference in signal on the first and second echoes of the T2-weighted images. This appearance is consistent with subacute thrombus, with extracellular methemoglobin causing enhanced T1 relaxation. Pulsed and color Doppler imaging confirmed the presence of thrombus in the IJV by showing relatively low-level echoes in the vein, lack of compressibility, and the absence of flow.

Although slow flow also can increase intraluminal signal on MR images, it usually shows an increase in signal on the second echo of the T2-weighted images. In addition, the presence of increased intraluminal signal on images in more than one plane supports the diagnosis of thrombus. Gradient-echo and phase-contrast imaging, not performed in this case, can also help differentiate thrombus from slow flow.

IJV thrombosis has many causes. If this condition is suspected because of clinical findings, Doppler imaging is the most available and cost-effective way to make the diagnosis. MR also can be used

to diagnose IJV thrombosis and may provide additional information, such as the age and extent of the clot and the possible cause.

Donald S. Ostrum
Nazareth Hospital
Philadelphia, PA 19152

REFERENCES

1. Albertyn L, Alcock M. Diagnosis of internal jugular vein thrombosis. *Radiology* 1987;162:505–508
2. Wing V, Scheible W. Sonography of jugular vein thrombosis. *AJR* 1983;140:333–336
3. Braun IF, Hoffman JC, Malko JA, Pettigrow RI, Daniels W, Davis PC. Jugular vein thrombosis: MR Imaging. *Radiology* 1985;157:357–360

Kissing-Balloon Angioplasty of the Popliteal Artery Trifurcation

We read with interest the description of Mewissen et al. [1] of kissing-balloon angioplasty of the trifurcation vessels. We too have found the technique useful as a way of treating branch-point stenoses. We have successfully used kissing balloons in the trifurcation vessels and recently in the branch vessels of a renal transplant.

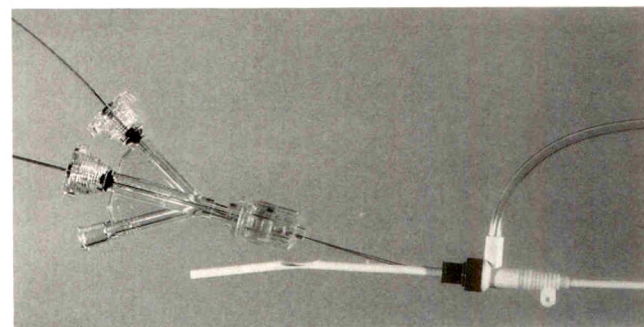


Fig. 1.—Instrument for kissing-balloon angioplasty. Both Tegtmeier guidewires are placed through hemostasis valve via a plastic peel-away introducer. Touhy-Borst adapter locks on to Luer ring at hemostasis valve.

We find it helpful to use a 6-French sheath that comes with a Luer-locking hemostasis valve (Argon Medical, Athens, TX). Both balloons can be introduced through the hemostasis valve as a unit by using a preslit introducer such as those packaged as tip-straighteners on certain pigtail catheters (Fig. 1). The balloons have been preloaded through a double-valved Touhy-Borst adapter (ACS, Temecula, CA), which is then attached to the Luer ring at the hemostasis valve. Use of this system produces minimal blood loss and allows independent maneuverability of the catheters.

Virginia McDonald
Terence A. S. Matalon
Rush-Presbyterian-St. Luke's Medical Center
Chicago, IL 60612

REFERENCE

1. Mewissen MW, Beres RA, Bessette JC, Lipchik EO. Kissing-balloon technique for angioplasty of the popliteal artery trifurcation. *AJR* 1991; 156:823–824

Reply

McDonald and Matalon and their colleagues have attached a double-valved Touhy-Borst adapter to the hemostasis valve of the 6-French sheath to maintain a fluid-tight seal around the protruding ends of both Tegtmeier guidewires in the TEGwire (Medi-tech, Watertown, MA) balloon angioplasty device. The added feature also allows independent maneuverability of the guidewires. Their system, as well as ours, is well suited for angioplasty at the popliteal trifurcation area, where the branching vessels are at obtuse angles, but it does not allow placement of TEGwire balloon devices without the guidance of a curved 6- or 7-French sheath in areas where vessels branch at acute angles. In our experience, use of TEGwire devices

in kissing-balloon angioplasty of branch vessels in a transplanted kidney would necessitate use of such guiding sheaths and would therefore be performed via bilateral puncture of the common femoral arteries.

Mark W. Mewissen
Robert A. Beres
Jeffrey C. Bessette
Elliot O. Lipchik
*Veterans Affairs Medical Center
Medical College of Wisconsin
Milwaukee, WI 53295*

Letters are published at the discretion of the Editor and are subject to editing.

Letters to the Editor must not be more than two *double-spaced*, typewritten pages. One or two figures may be included. Abbreviations should not be used. Limit the number of authors to four, or we will list only the first three and add "and colleagues" to the end of the list. See Author Guidelines, page A21.

Material being submitted or published elsewhere should not be duplicated in letters, and authors of letters must disclose financial associations or other possible conflicts of interest.

Letters concerning a paper published in the *AJR* will be sent to the authors of the paper for a reply to be published in the same issue. Opinions expressed in the Letters to the Editor do not necessarily reflect the opinions of the Editor.

Review of Current Literature

Initials and addresses of corresponding authors are provided in parentheses for each article so that the reader can obtain reprints directly. Abstracts are printed verbatim from each journal.

The New England Journal of Medicine

Differences in the use of procedures between women and men hospitalized for coronary heart disease. Ayanian JZ, Epstein AM (AME, Dept. of Health Care Policy, Harvard Medical School, 25 Shattuck St., Parcel B, 1st Fl., Boston, MA 02115). *N Engl J Med* 325(4):221-225, July 1991

Background and Methods. Previous studies at individual hospitals have reported differences in the use of major diagnostic and therapeutic procedures for women and men with coronary heart disease. To assess whether these differences can be generalized, we performed retrospective analyses of coronary angiography and revascularization (coronary-artery bypass surgery or percutaneous transluminal coronary angioplasty) in women and men hospitalized for coronary heart disease in 1987, using abstract data on 49,623 discharges in Massachusetts and 33,159 discharges in Maryland. We used multiple logistic regression to estimate the adjusted odds of the use of a procedure, controlling for principal diagnosis, age, secondary diagnosis of congestive heart failure or diabetes mellitus, race, and insurance status.

Results. The adjusted odds of undergoing angiography were 28 percent and 15 percent higher for men than for women in Massachusetts and Maryland, respectively (95 percent confidence intervals for the odds ratios, 1.22 to 1.35 and 1.08 to 1.22). The respective adjusted odds of undergoing revascularization were 45 percent and 27 percent higher for men than for women (95 percent confidence intervals, 1.35 to 1.55 and 1.16 to 1.40). Because these differences could be related to differing thresholds for hospital admission, we performed a second analysis limited to patients with diagnosed acute myocardial infarction (11,865 discharges in Massachusetts and 6894 discharges in Maryland), a group in which all patients would be expected to receive hospital care. The male-to-female odds ratios in both states remained similar in magnitude and were statistically significant for angiography and revascularization.

Conclusions. These findings demonstrate that women who are hospitalized for coronary heart disease undergo fewer major diagnostic and therapeutic procedures than men. These differences may represent appropriate levels of care for men and women, but it is also possible that they reflect underuse in women or overuse in men. Further study should assess the cause of these differences and their effect on patients' outcomes.

Sex differences in the management of coronary artery disease. Steingart RM, Packer M, Hamm P, et al. (RMS, Winthrop-University

Hospital, 259 First St., Mineola NY 11501). *N Engl J Med* 325(4):226-230, July 1991

Background. Despite the fact that coronary artery disease is the leading cause of death among women, previous studies have suggested that physicians are less likely to pursue an aggressive approach to coronary artery disease in women than in men. To define this issue further, we compared the care previously received by men and women who were enrolled in a large postinfarction intervention trial.

Methods. We assessed the nature and severity of anginal symptoms and the use of antianginal and antiischemic interventions before enrollment in the 1842 men and 389 women with left ventricular ejection fractions ≤ 40 percent after an acute myocardial infarction who were randomized in the Survival and Ventricular Enlargement trial.

Results. Before their index infarction, women were as likely as men to have had angina and to have been treated with antianginal drugs. However, despite reports by women of symptoms consistent with greater functional disability from angina, fewer women had undergone cardiac catheterization (15.4 percent of women vs. 27.3 percent of men, $P < 0.001$) or coronary bypass surgery (5.9 percent of women vs. 12.7 percent of men, $P < 0.001$). When these differences were adjusted for important covariates, men were still twice as likely to undergo an invasive cardiac procedure as women, but bypass surgery was performed with equal frequency among the men and women who did undergo cardiac catheterization.

Conclusions. Physicians pursue a less aggressive management approach to coronary disease in women than in men, despite greater cardiac disability in women.

Chest

Evaluation of ultrasonically guided biopsies of mediastinal masses. Yu CJ, Yang PC, Chang DB, et al. (PCY, National Taiwan University Hospital, No. 1 Chang-te St., Taipei, Taiwan, Republic of China). *Chest* 100(2):399-405, Aug. 1991

Eighty patients with roentgenographic evidence of mediastinal abnormalities were examined with ultrasonography. Fifty-four lesions were malignant, and 26 lesions were benign. The histologic diagnoses were confirmed by ultrasonically guided fine needle aspiration/cutting needle (Tru-Cut) biopsy, surgical specimens, or transbronchial biopsy. There were no unique ultrasonographic features for diagnosis of specific tumors. Ultrasonically guided aspiration biopsies (UGAB) were performed in 44 of the malignant lesions and in 14 of the benign lesions (nine of the noncystic lesions and five of the cystic lesions). Cytologic diagnosis of malignancies was obtained in 34 (77 percent) of these 44 malignancies; however, accurate histologic classifications of malignancies were achieved in only 24 (55 percent). Accurate

diagnoses were achieved in only three (33 percent) of the nine noncystic benign lesions. Ultrasonically guided cutting biopsies (UGCB) were performed in 24 malignant and five benign lesions. All attempts yielded satisfactory specimens for histologic diagnosis. Using UGAB and UGCB together, a positive diagnosis was achieved in 89 percent (39/44) of the malignancies, and accurate histologic diagnosis was achieved in 89 percent and 78 percent (7/9) in malignant and benign noncystic lesions, respectively. Correct histologic diagnosis with UGAB alone is lower in thymoma (55 percent [6/11]) and lymphoma (30 percent [3/10]) but higher in lung cancer (67 percent [8/12]) and metastatic cancer (78 percent [7/9]). There were no complications in this series. We conclude that ultrasonography with UGAB has a high diagnostic yield in diagnosing mediastinal tumors, and UGCB is necessary for thymic tumors, lymphoma, and benign lesions.

Circulation

Dipyridamole thallium-201 scintigraphy as a preoperative screening test: a reexamination of its predictive potential. Mangano DT, London MJ, Tubau JF, et al. (DTM, Dept. of Anesthesia (129), University of California, San Francisco, Dept. of Veterans Affairs Medical Center, 4150 Clement St., San Francisco, CA 94121). *Circulation* 84:493-502, 1991

Background. We examined the value of dipyridamole thallium-201 (^{201}Tl) scintigraphy as a preoperative screening test for perioperative myocardial ischemia and infarction.

Methods and Results. We prospectively studied 60 patients undergoing elective vascular surgery. We performed ^{201}Tl scintigraphy preoperatively and blinded all treating physicians to the results. Historical, clinical, laboratory, and physiological data were gathered throughout hospitalization. Myocardial ischemia was assessed during the intraoperative period using continuous 12-lead electrocardiography (ECG) and transesophageal echocardiography (TEE) and during the postoperative period using continuous two-lead ambulatory ECG. Adverse cardiac outcomes (cardiac death, myocardial infarction, unstable angina, severe ischemia, or congestive heart failure) were assessed daily throughout hospitalization. Twenty-two patients (37%) had defects that improved or reversed on delayed scintigrams (redistribution defects), 18 (30%) had persistent defects, and 20 (33%) had no defects on ^{201}Tl scintigraphy. There was no association between redistribution defects and adverse cardiac outcomes: 54% (seven of 13) of adverse outcomes occurred in patients without redistribution defects, and the risk of an adverse outcome was not significantly increased in patients with redistribution defects (relative risk 1.5, 95% confidence interval 0.6-3.9, $p=0.43$). Consistent with these findings, there was also no association between redistribution defects and perioperative ischemia: 54% (19 of all 35) of perioperative ECG and TEE ischemic episodes and 58% (14 of 24) of severe ischemic episodes occurred in patients without redistribution defects. The sensitivity of ^{201}Tl scintigraphy for perioperative ischemia and adverse outcomes ranged from 40% to 54%, specificity from 65% to 71%, positive predictive value from 27% to 47%, and negative predictive value from 61% to 82%.

Conclusions. These results differ from those of previous studies and suggest that the routine use of ^{201}Tl scintigraphy for preoperative screening of patients undergoing vascular surgery may not be warranted.

Gastroenterology

Acalculous biliary pain: cholecystectomy alleviates symptoms in patients with abnormal cholescintigraphy. Yap L, Wycherley AG, Morphet AD, Tooili J (LY, Dept. of Surgery, Flinders Medical Centre, Adelaide, South Australia, Australia). *Gastroenterology* 101:786-793, 1991

A 45-minute infusion of an octapeptide of cholecystokinin (Kinevac; Squibb Diagnostics, New Brunswick, NJ) was used to measure the gallbladder ejection fraction during cholescintigraphy in 40 normal volunteers. Cholecystokinin cholescintigraphy was shown to be a reproducible test. The maximum mean gallbladder ejection fraction occurred 15 minutes after cholecystokinin infusion and was $74.5\% \pm 1.9\%$ (mean \pm SEM). A gallbladder ejection fraction $> 40\%$ (mean $- 3\text{SD}$) was arbitrarily defined to be normal. The gallbladder ejection fraction test was then used to identify patients with acalculous biliary symptoms who may respond to cholecystectomy. A total of 103 patients was tested; 21 had abnormal gallbladder ejection fractions and were randomized into two groups, cholecystectomy or no operation. These patients were followed up symptomatically at 3-month intervals for 13-54 months (mean, 34 months). Of the 11 patients who underwent cholecystectomy, 10 (91%) lost their symptoms and 1 improved. Of the 10 patients in the group that did not undergo surgery, all continued to be symptomatic, 2 of whom requested cholecystectomy after 13 and 24 months, respectively. Of the 13 gallbladders obtained from surgery, 12 showed evidence of chronic cholecystitis, muscle hypertrophy, and/or narrowed cystic duct. A normal gallbladder ejection fraction was recorded in 82 patients, and further treatment was left to the discretion of their referring clinician. On follow-up, 50 patients were asymptomatic and 10 were symptomatic without specific treatment of the biliary tract; 14 underwent cholecystectomy, 8 of whom were asymptomatic. Pathological abnormalities were recorded in 6 of the removed gallbladders. It is concluded that the gallbladder ejection fraction obtained after a 45-minute infusion of cholecystokinin during cholescintigraphy is a reproducible measure of gallbladder emptying, and that cholecystectomy alleviates the biliary-type pain of patients with a reduced gallbladder ejection fraction.

Reprinted with permission by the American Gastroenterological Association.

The effects of chronic endoscopic variceal sclerotherapy on portal pressure in cirrhotics. Korula J, Ralls P (JK, Dept. of Medicine (Hepatology), University of Southern California School of Medicine, Los Angeles, CA). *Gastroenterology* 101:800-805, 1991

The effect of obliterating esophageal varices by endoscopic sclerotherapy on portal pressure was prospectively studied in 11 cirrhotic patients with variceal hemorrhage. Portal venous pressure gradient, determined as the difference between transhepatic portal and hepatic vein pressure, increased by a mean of $31.1\% \pm 14.5\%$ in 8 (73%) and decreased by a mean of $30.1\% \pm 11.7\%$ in 3 (27%) patients, with no statistically significant change overall ($P = 0.1$). These changes in portal venous pressure gradient occurred despite an improvement in the laboratory and clinical parameters of hepatic function. Deep abdominal sonography with color flow imaging at variceal obliteration showed patent paraumbilical veins in 6 (55%) patients, 3 of whom had decreases in portal venous pressure gradient (29%, 19%, 42.5%) at variceal obliteration. In 5 (45%) patients without patent paraumbilical veins, a statistically significant increase in portal venous pressure gradient between initial endoscopic variceal sclerotherapy and variceal obliteration was noted ($P = 0.008$). Rebleeding (single episode in all 4 patients, before obliteration in 3 patients) occurred in those with an increase in portal venous pressure gradient; all patients with portal venous pressure gradient decreases were nonbleeders. No correlation between changes in portal venous pressure gradient and time to variceal obliteration, number of sclerotherapy treatments, or rebleeding episodes was observed. Thus, an increase in portal venous pressure gradient was noted in the majority of patients at variceal obliteration. Although the portal venous pressure gradient decrease may be explained by a patent paraumbilical vein, the mechanism of portal venous pressure gradient increase is not clear. It is speculated that this portal venous pressure gradient increase may be caused by an increase in collateral resistance or flow or a combination of both, resulting from obliteration of esophageal varices by endoscopic sclerotherapy.

Reprinted with permission by the American Gastroenterological Association.

Digestive Diseases and Sciences

Successful shock-wave lithotripsy of bile duct stones using ultrasound guidance. Gordon SJ, Stampfl DA, Grimm IS, Dahnert W, Goldberg BB, Taglienti G (SJG, Jefferson Medical College, 1025 Walnut St., Rm. 901, Philadelphia, PA 19107-5083). *Dig Dis Sci* 36(8):1102-1109, Aug. 1991

Eighteen patients with 41 gallstones in the common bile duct, common hepatic, cystic, and intrahepatic ducts underwent shock-wave lithotripsy using the electrohydraulic Sonolith 3000 lithotripter. Lithotripsy was performed using ultrasound guidance alone under intravenous analgesia/sedation. All patients previously had failed stone extraction via retrograde endoscopy, T-tube, or cholecystostomy. Lithotripsy was performed according to an FDA-approved protocol allowing a maximum of two 2500 shock-wave treatments at a 48 hr interval. Following the final lithotripsy or cholangiographic evidence of stone fragmentation, residual fragments were removed via endoscopic or percutaneous route within 24-72 hr. Ultrasound localization of gallstones was aided by continuous infusion of the common bile duct with saline solution. In 15 of the 18 patients, complete fragmentation of the stones was accomplished, two had minimal fragmentation, and one with an encysted stone had no fracturing. No serious complications were encountered. Overall non-surgical stone-free success rate was 17 of 18 patients, indicating biliary duct stones can be successfully treated using an ultrasound-guided lithotripter and intravenous sedation alone.

Combined treatment of symptomatic gallbladder stones by extracorporeal shock-wave lithotripsy (ESWL) and instillation of methyl tert-butyl ether (MTBE). Holl J, Sauerbruch T, Sackmann M, Paulietzki J, Paumgartner G (TS, Medical Dept. II, Klinikum Grosshadern, University of Munich, Marchioninistrasse 15, 8000 Munich 70, Germany). *Dig Dis Sci* 36(8):1097-1101, Aug. 1991

Twenty-four patients with symptomatic gallbladder stones (12 radiolucent and 12 calcified) were treated by a combined approach of extracorporeal shock-wave lithotripsy (ESWL) and subsequent instillation of methyl tert-butyl ether (MTBE). The patients received a mean of 1500 ± 185 shock-wave discharges. The mean instillation time of MTBE was 13 ± 4.2 hr. Treatment was tolerated without major adverse effects. Within a time period of three to five days eight of 12 patients with pure radiolucent stones and four of 12 with calcified stones became stone-free. After a median follow-up of five months (range: one week to 26 months), a total of 11 patients (92%) with radiolucent stones and of eight patients (66%) of those with calcified stones were free of stones, fragments, or debris. These clearance rates appear high when compared with reports on monotherapy with ESWL or MTBE, suggesting a positive effect of a combined approach in selected patients. Two patients exhibited recurrent stones after six and seven months, respectively.

The Journal of Bone and Joint Surgery

Extraspinal causes of lumbosacral radiculopathy. Kleiner JB, Donaldson WF III, Curd JG, Thorne RP (JBK, Colorado Spine Center, Ste. 307, 1455 S. Potomac St., Aurora, CO 80012). *J Bone Joint Surg [Am]* 73-A(6):817-821, July 1991

Twelve of 12,125 patients who had been referred during a seven-year period to a specialist in spinal disorders were found to have an extraspinal cause of radiculopathy or neuropathy of the lower extremity. The records of these twelve patients were reviewed retrospectively.

The average age of the twelve patients was sixty-five years (range, forty-two to seventy-seven years). The cause of the symptoms was an occult malignant tumor in nine patients and a hematoma, an aneurysm of the obturator artery, or a neurilemoma of the sciatic nerve in the others. The average time from the onset of symptoms to the final diagnosis was eight months (range, one month to two years).

The most useful test for determination of the correct diagnosis was computed tomography or magnetic resonance imaging of the abdomen and pelvis. Computed tomography or magnetic resonance imaging of the spine and bone-scanning of the whole body were of little help in localizing the disease.

In four of the twelve patients, an operation was performed on the basis of an incorrect diagnosis. In dealing with elderly patients who have radiculopathy, one should be suspicious that the cause is outside the spine.

Clinical Orthopaedics and Related Research

Shoulder impingement syndrome: a critical review. Fu FH, Harner CD, Klein AH (FHF, The Albert B. Ferguson, Jr., M.D. Laboratory for Orthopaedic Research, 986 Scaife Hall, University of Pittsburgh School of Medicine, Pittsburgh, PA 15261). *Clin Orthop* 269:162-173, Aug. 1991

Impingement syndrome is an ill-defined term of a variety of disorders of the shoulder that manifest as anterior shoulder pain, especially during overhead activities. These disorders each have a common pathologic course that includes rotator cuff tendinitis (RCT), and, if untreated, may proceed to cuff rupture. RCT has at least two distinct etiologies. Primary impingement of the supraspinatus tendon on the coracoacromial arch is responsible in the majority of nonathletic cases. Overhead movements in sports are prone to developing secondary mechanical impingement because of an instability pattern that is common in this population. Information from this review and clinical practice permits differentiation of the two distinct etiologies of RCT which is important in treatment planning. Much work still needs to be done in defining the microscopic pathology of RCT.

The Journal of Urology

Sonographic visualization of the ureter in pregnancy. MacNeily AE, Goldenberg SL, Allen GJ, Ajzen SA, Cooperberg PL (AEM, 450-1144 Burrard St., Vancouver, B.C., Canada V6Z 2A5). *J Urol* 146:298-301, Aug. 1991

We describe a method of differentiating physiological from pathological dilatation of the renal collecting system in pregnant patients. In physiological hydronephrosis the dilated ureter extends down only to the level of the common iliac artery. In 2 patients with distal ureteral stones a dilated ureter was visualized past the vessels.

To determine the frequency and reliability of visualizing the ureters in pregnant patients 105 consecutive asymptomatic pregnant patients were examined. Hydronephrosis was found in 83 kidneys in 59 of the patients. The dilated ureter was visualized in 64 of the renal units. The anatomy was well demonstrated by color flow Doppler scanning and in all of these cases the dilated ureter was seen to taper where it crossed the common iliac artery. These results suggest that the presence of a dilated ureter past the iliac artery is strong evidence for pathological distal ureteral obstruction in pregnancy.

Pediatrics

Pediatric heart transplantation at Stanford: results of a 15-year experience. Baum D, Bertstein D, Starnes VA, et al. (DB, Dept. of Pediatrics, Stanford University School of Medicine, Stanford, CA 94305). *Pediatrics* 88(2):203-214, Aug. 1991

The long-term results of pediatric heart transplantation were evaluated in 53 patients, ages 0.25 to 18.94 years, who received transplants at Stanford University Medical Center between 1974 and 1989. Indications for transplantation were idiopathic cardiomyopathy (68%), congenital heart disease (21%), endocardial fibroelastosis (8%), and doxorubicin cardiomyopathy (3%). Immunosuppression was achieved with combinations of cyclosporine, prednisone, and azathioprine. Thirty-seven of 42 recipients leaving the hospital after transplantation

were alive and in New York Heart Association class I at study's end. Cumulative survival was 79% at 1 year, 76% at 3 years, and 69% at 5 years. Fourteen recipients have survived more than 5 years (5.1 to 12.4 years). Hospital readmission for illness has been infrequent, decreasing from 6.8 days to 0.9 days per year over 5 years. Eleven patients have required no rehospitalization. Posttransplant deaths were due to infection (19%), rejection (4%), pulmonary hypertension (4%), coronary artery disease (2%), and lymphoproliferative disease (2%). Retransplantation was required for intractable rejection in 4 patients and advanced coronary artery disease in 2. Hypertension and elevated blood urea nitrogen and creatinine levels were common in individuals receiving cyclosporine. Growth was often impaired in prepubertal children receiving daily prednisone. Based on this 15-year experience, it is concluded that heart transplantation represents a reasonable alternative for selected young patients with end-stage cardiac disease.

Reprinted by permission of PEDIATRICS © 1991.

The Journal of Pediatrics

Multicenter controlled trial comparing high-frequency jet ventilation and conventional mechanical ventilation in newborn infants with pulmonary interstitial emphysema. Keszler M, Donn SM, Bucciarelli RL, et al. (MK, Georgetown University Medical Center, 3800 Reservoir Rd. N.W., Washington, DC 20007). *J Pediatr* 119:85-93, 1991

One hundred forty-four newborn infants with pulmonary interstitial emphysema were stratified by weight and severity of illness, and randomly assigned to receive treatment with high-frequency jet ventilation (HFJV) or rapid-rate conventional mechanical ventilation (CV) with short inspiratory time. If criteria for treatment failure were met, crossover to the alternate ventilatory mode was permitted. Overall, 45 (61%) of 74 infants met treatment success criteria with HFJV compared with 26 (37%) of 70 treated with CV ($p < 0.01$). Eighty-four percent of patients who crossed over from CV to HFJV initially responded to the new treatment, and 45% ultimately met success criteria on HFJV. In contrast, only 9% of those who crossed over from HFJV to CV responded well to CV ($p < 0.01$), and the same 9% ultimately met success criteria ($p < 0.05$). Therapy with HFJV resulted in improved ventilation at lower peak and mean airway pressures, as well as more rapid radiographic improvement of pulmonary interstitial emphysema, in comparison with rapid-rate CV. Survival by original assignment was identical. When survival resulting from rescue by the alternate therapy in crossover patients was excluded, the survival rate was 64.9% for HFJV, compared with 47.1% for CV ($p < 0.05$). The incidence of chronic lung disease, intraventricular hemorrhage, patent ductus arteriosus, airway obstruction, and new air leak was similar in both groups. We conclude that HFJV, as used in this study, is safe and is more effective than rapid-rate CV in the treatment of newborn infants with pulmonary interstitial emphysema.

The Journal of Nuclear Medicine

False-negative dipyridamole-thallium-201 myocardial imaging after caffeine infusion. Smits P, Corstens FHM, Aengevaeren WRM, Wackers FJT, Thien T (PS, Division of General Internal Medicine, Dept. of Internal Medicine, University Hospital Nijmegen, Geert Grooteplein Zuid 8, P. O. Box 9101, 6500 HB Nijmegen, the Netherlands). *J Nucl Med* 32(8):1538-1541, Aug. 1991

The vasodilator effect of intravenously administered dipyridamole may be caused by an increase in endogenous plasma adenosine levels. We evaluated the effect of caffeine, an adenosine receptor antagonist, on the diagnostic results of dipyridamole- ^{201}Tl myocardial imaging in eight patients with coronary artery disease. Caffeine infusion significantly attenuated the dipyridamole-induced fall in blood pressure and the accompanied increase in heart rate. The infusion of dipyridamole alone resulted in chest pain and ST-segment depressions on the electrocardiogram in four patients, whereas none of these problems occurred when the tests were repeated after caffeine. In six of eight patients, caffeine was responsible for false-negative dipyridamole- ^{201}Tl tests. Semiquantitative scores of the dipyridamole-induced ^{201}Tl perfusion defects were decreased by caffeine from 9.0 ± 0.9 to 2.0 ± 1.1 points ($p < 0.05$). Computerized analysis revealed a caffeine-mediated reduction in the percent reversibility of the images from $46\% \pm 16\%$ to $6\% \pm 10\%$ ($p < 0.05$). We conclude that the use of caffeinated products prior to dipyridamole- ^{201}Tl testing may be responsible for false-negative findings.

Gastrointestinal Radiology

Transhepatic cholangiography in patients with suspected biliary disease and nondilated intrahepatic bile ducts. Teplick SK, Flick P, Brandon JC (SKT, Dept. of Radiology-Slot 556, University of Arkansas for Medical Sciences, 4300 W. Markham St., Little Rock, AK 72205). *Gastrointest Radiol* 16:193-197, 1991

Transhepatic cholangiography (THC) was performed in 107 patients who had nondilated intrahepatic bile ducts on computed tomography (CT) or ultrasound. The cholangiogram was diagnostic in 72 patients (67%). Thirty-one (43%) of the 72 diagnostic studies were abnormal and showed poor emptying, stones, or strictures. Twenty-three (21%) complications occurred, including two deaths. Sixteen patients experienced acute pain, requiring additional narcotics. There was one case of peritonitis and pancreatitis, and two of bacteremia. We compared our success and complication rates to those of endoscopic retrograde cholangiography (ERC) reported in the literature.

We conclude that when a bile duct abnormality is clinically suspected, the incidence of pathology is sufficiently high to warrant direct visualization of the ducts in order to make an anatomic diagnosis, even if the intrahepatic ducts are not dilated. However, ERC has a better success rate and fewer complications than THC and it should be the initial invasive procedure.

Journal of Ultrasound in Medicine

Transperineal sonography in second trimester to term pregnancy and early labor. Zilianti M, Azuaga A, Calderon F, Redondo C (MZ, P.O. Box 62320, Caracas, Venezuela). *J Ultrasound Med* 10:481-486, Sept. 1991

We studied the diagnostic potential of transperineal sonography in 184 pregnant women from midtrimester to term pregnancies and at early labor. In 65 patients in false labor, we established cervical effacement and dilatation. We confirmed the clinical diagnosis of premature rupture of the membranes (PROM) in 27 cases and assessed the placental relationship with the internal cervical os in 20 patients. In 61 women in early labor we measured cervical dilatation, and in 11 patients we looked for details of fetal anatomy. Adequate diagnostic information was obtained in 180 cases (97%). Our results and data from the literature suggest that transperineal sonography is the imaging technique of choice in the situations we studied.

Reprinted with permission by the American Institute of Ultrasound in Medicine.

News

Imaging, Malpractice, and the Law

The Postgraduate Division, University of Southern California School of Medicine, is sponsoring Imaging, Malpractice, and the Law: A Symposium on the Medical-Legal Issues in Radiology, Jan. 11, 1992, at the USC Health Sciences Campus, Los Angeles. The symposium will be devoted to current issues in medical malpractice and risk management in radiology. Course director: Yuri R. Parisky. Category 1 credit: 8.5 hr. Fee: physicians and attorneys, \$175; allied health specialists, \$95. Information: Donna Bowker, USC Postgraduate Medicine, 1975 Zonal Ave., KAM 307, Los Angeles, CA 90033; (213) 342-2555, (800) 421-6729 (nationwide), or (800) USC-1119 (in California).

Practical Radiology 1992

The Dept. of Radiology, University of British Columbia, is sponsoring the first Japanese-Canadian postgraduate course, Practical Radiology 1992, Jan. 19–24, 1992, at the Whistler Ski Resort, Whistler, B.C. The course is designed for practicing radiologists. Program director: Brian C. Lentle. Program chairman: H. Joachim Burhenne. Guest faculty: T. Ichikawa; R. Baron; H. Goldberg; J. P. Heiken; C. A. Rohrmann, Jr.; G. Stevenson; P. C. Freeny; R. M. Gore; A. A. Moss; D. H. Stephens; E. T. Stewart; and W. M. Thompson. Category 1 credit: 21 hr. Fee (\$U.S./\$Canadian): physicians, \$485/\$560; residents and fellows, \$385/\$445 (letter required). Information: H. Joachim Burhenne, M.D., Dept. of Radiology, University of British Columbia, 10th Ave. and Heather St., Vancouver, B.C., Canada V5Z 1M9; telephone: (604) 875-4355; fax: (604) 875-4319.

Midwinter Radiological Conference

The Los Angeles Radiological Society (LARS) is sponsoring the 44th annual Midwinter Radiological Conference, Jan. 31–Feb. 2, 1992, at the Century Plaza Hotel, Los Angeles. Four subject areas will be covered: MR imaging and neuroradiology, musculoskeletal imaging, emergency radiology, and breast imaging. A 1-day seminar on nuclear medicine and a 2-day seminar on cardiovascular and intervention radiology will be given concurrently. Faculty: T. Berquist, J. Crues, W. P. Evans, E. Fram, A. Hasso, C. Helms, V. Jackson, and A. van Breda. Category 1 credit: up to 17.25 hr. Fee (3 days/2 days/1 day): physicians, \$425/\$380/\$230; LARS members, \$200/\$150/\$100; residents and technologists, \$125/\$100/\$50; LARS resident members, \$100/\$70/\$35. Information: Los Angeles Radiological Society—MWRC, P. O. Box 91215, Los Angeles, CA 90009-1215; (213) 827-9078 or (800) LARS-013.

Mid-Pacific Radiological Conference

The Los Angeles Radiological Society (LARS) will sponsor the 18th annual Mid-Pacific Radiological Conference, Feb. 4–8, 1992, at the Hyatt Regency Waikoloa, Hawaii, HI. Topics will include breast imaging, sonography, neuroradiology, and MR imaging. Faculty: W. Bradley, P. Callen, R. Dietrich, V. Jackson, and D. Resnick. Category 1 credit: up to 18.5 hr. Fee: physicians, \$550; residents and technologists, \$295. Information: Los Angeles Radiological Society—MPRC, P. O. Box 91215, Los Angeles, CA 90009-1215; (213) 827-9078 or (800) LARS-013.

Current Topics in Diagnostic Imaging

The NYU Medical Center, Post-Graduate Medical School, is sponsoring Current Topics in Diagnostic Imaging, Feb. 10–14, 1992, at the Hyatt Regency Cerromar Beach, Puerto Rico. Topics to be covered include CT, sonography, MR imaging, neuroradiology, head and neck imaging, chest radiology, gastrointestinal radiology, urology, bone and joint radiology, and pediatric radiology. Category 1 credit: 20.5 hr. Fee: \$495. Information: NYU Medical Center, Post-Graduate Medical School, 550 First Ave., New York, NY 10016; telephone: (212) 263-5295; fax: (212) 263-5293.

Magnetic Resonance Imaging

The University of California, San Diego, will sponsor Magnetic Resonance Imaging, March 2–6, 1992, at the Hotel Del Coronado, San Diego, CA. Program director: John Hesselink. Category 1 credit: 27.25 hr (pending). Fee: physicians, \$540; residents, fellows, and technologists, \$340. Information: Dawne Ryals, Ryals and Associates, P. O. Box 1925, Roswell, GA 30077-1925; telephone: (404) 641-9773; fax: (404) 552-9859.

PET and SPECT Imaging of Living Brain Chemistry in Health and Disease

The Johns Hopkins University School of Medicine is sponsoring PET and SPECT Imaging of Living Brain Chemistry in Health and Disease, March 11–13, at the Johns Hopkins Medical Institutions, Baltimore. The course will present the latest uses of positron emission tomography, single-photon emission CT, and simple probe systems in the study of brain function and chemistry. Starting with basic principles, the course will describe clinical problems in neuropsychiatry and how these techniques can be used to approach solutions.

Specific examples of studies in patients will be presented and discussed. Category 1 credit: 19 hr. Fee: physicians, \$495; residents, \$395. Information: Program Coordinator or Julia W. Buchanan, Course Co-director, Johns Hopkins Medical Institutions, Office of Continuing Education, Turner Bldg., 720 Rutland Ave., Baltimore, MD 21205; (301) 955-2959 (coordinator) or (301) 955-8582 (Ms. Buchanan).

Advances in Diagnostic Radiology

The Dept. of Diagnostic Radiology, Mayo Clinic, will present Advances in Diagnostic Radiology, March 15–19, 1992, at the Cloister Resort, Sea Island, GA. The course will cover major advances and new trends in diagnostic radiology, including a comprehensive update on vascular imaging. Gastrointestinal, genitourinary, musculoskeletal, breast, chest, and neuroradiologic imaging will be emphasized also. Category 1 credit: 23 hr. Fee: physicians, \$525; residents, \$262.50. Information: Division of Continuing Medical Education, Mayo Clinic, Rochester, MN 55905; telephone: (800) 323-2688; fax: (507) 284-0532.

Head and Neck Surgery and Imaging

The Dept. of Otolaryngology—Head and Neck Surgery and the Dept. of Radiology, The Johns Hopkins University School of Medicine, are sponsoring Head and Neck Surgery and Imaging: An Interactive Problem-Solving Meeting, March 22–25, 1992, at the Silvertree Hotel, Snowmass Village, CO. The course will cover the diagnosis and treatment of otorhinologic and head and neck diseases. Audience participation, through case presentations, will be emphasized. Category 1 credit: 16 hr. Fee: physicians, \$475; residents and fellows, \$300. Information: Program Coordinator, Johns Hopkins Medical Institutions, Office of Continuing Education, Turner Bldg., 720 Rutland Ave., Baltimore, MD 21205; (301) 955-2959.

MRI Workshop in Hawaii 1992

MRI Workshop in Hawaii 1992 will be held at the Kea Lani Hotel, Wailea, Maui, March 22–27, 1992. Lecturers will describe their methods, review clinical disorders, and discuss developments in MR imaging. Participants are encouraged to bring interesting problem cases or curiosities for the Stump the Stars segment. Course directors: Marc Coel and Robert A. Bell. Faculty: W. Kelly, C. Schatz, E. Unger, K. Heithoff, J. P. Finn, A. L. Deutsch, M. Rafii, and R. A. Bell. Category 1 credit: 37 hr. Fee: \$595. Information: Ms. Susan Block, Dept. of Nuclear Medicine, Queen's Medical Center, 1301 Punchbowl St., Honolulu, HI 96813; (808) 547-4544.

National Council on Radiation Protection and Measurements Annual Meeting

The 28th annual meeting of the National Council on Radiation Protection and Measurements will be April 1–2, 1992, at the Crystal City Marriott, Washington, DC. The principal scientific session will be on radiation protection in medicine. Information: NCRP, 7910 Woodmont Ave., Ste. 800, Bethesda, MD 20814; telephone: (301) 657-2652; fax: (301) 907-8768.

AFIP Uroradiology Weekend

The Armed Forces Institute of Pathology (AFIP), the American Registry of Pathology, and the American College of Radiology are

sponsoring AFIP Uroradiology Weekend, April 4–5, 1992, at the Hyatt Regency Hotel, Capitol Hill, Washington, DC. The purpose of the course is to critically assess new developments in uroradiology and to review basic principles of radiologic-pathologic correlation in selected areas. Course directors: Alan J. Davidson and David S. Hartman. Category 1 credit: 13 hr. Fee: physicians, \$275; federal employees, \$100; residents and fellows, deduct 25% (letter required); Friends of the AFIP, deduct 10%. Information: telephone: (301) 427-5618 or 427-5620; fax: (301) 427-5001.

General Radiology Review Course

The Dept. of Radiological Sciences, University of California, Los Angeles School of Medicine, will present General Radiology Review Course, April 5–10, 1992, at the Miramar Sheraton Hotel, Santa Monica, CA. The course will include the basics of diagnostic radiology and will cover sonography, nuclear medicine, angiography, CT, and MR imaging. Course director: Poonam Batra. Category 1 credit: 40 hr. Fee: \$425. Information: Darryl Bailey, Program Coordinator, Dept. of Radiological Sciences, B2-170, UCLA Medical Center, Center for Health Sciences, Los Angeles, CA 90024-1721; telephone: (213) 825-8763; fax: (213) 206-5725.

Residents' Radiology Review Course

The University of California, San Diego, is sponsoring Residents' Radiology Review Course, April 19–24, 1992, at the Hotel Del Coronado, San Diego, CA. Program director: Folke J. Brahme. Category 1 credit: 39 hr (pending). Fee: \$470. Information: Dawne Ryals, Ryals and Associates, P. O. Box 1925, Roswell, GA 30077-1925; telephone: (404) 641-9773; fax: (404) 552-9859.

Interventional Radiology

The University of California, San Diego, is sponsoring Interventional Radiology, April 25, at the Hotel Del Coronado, San Diego, CA. Program director: Eric vanSonnenberg. Category 1 credit: 8.25 hr (pending). Fee: \$125. Information: Dawne Ryals, Ryals and Associates, P. O. Box 1925, Roswell, GA 30077-1925; telephone: (404) 641-9773; fax: (404) 552-9859.

Ghana Diagnostic Medical Project

The Ghana Diagnostic Medical Project is a publicly supported nonprofit organization whose sole purpose is to find and deliver donated diagnostic medical machines and other hospital equipment and educational materials to research groups and hospitals in Ghana. The project has already taken possession of some diagnostic medical and other hospital equipment valued at \$100,000. It needs more equipment and funds to transport procured items and to purchase spare parts for the equipment. For more information, contact Mohammed Bashiru, Chairman, Ghana Diagnostic Medical Project, 1487 Presidential Dr., Columbus, OH 43212; (614) 488-5562; or Abdul Brimah, 1525 E. Park Shore, East Ct., Chicago, IL 60637; (312) 752-1835.

NCRP Robert D. Moseley, Jr., Award

The National Council on Radiation Protection and Measurements (NCRP) invites applications for the Robert D. Moseley, Jr., Award in Radiation Protection in Medicine. The Award will be made for an

outstanding paper on radiation protection in medicine by a young investigator. The awardee will receive \$1,000 and travel expenses to attend the NCRP annual meeting in Washington, DC, April 1–2, 1992. Applications will be welcome from an eligible author or from colleagues or others on behalf of an eligible author who deem the paper worthy of consideration. Applications should be made by Jan. 15, 1992. Information: NCRP, 7910 Woodmont Ave., Ste. 800, Bethesda, MD 20814: (301) 657-2652.

The American Board of Radiology Examinations

Written examinations for the American Board of Radiology (ABR) are scheduled for Oct. 1–2, 1992, and Oct. 14–15, 1993. Oral examinations will be held at the Executive West Hotel in Louisville, KY, June 1–5, 1992. The ABR will accept applications for admission to the examinations after July 1, but not later than Sept. 30, in the year *preceding* the year in which the examination is to be taken. For application forms and further information: Office of the Executive Director, The American Board of Radiology, 2301 W. Big Beaver Rd., Ste. 625, Troy, MI 48064.

Meeting and Course Review

For the reader's convenience, a summary of upcoming meetings and courses is provided. Detailed listings are given in the *AJR* issue given in parentheses.

Swallowing Center Preceptorship, times arranged, Baltimore (Jan)
Imaging Fellowship, times arranged, Miami Beach, FL (Jan)
Preceptorships in Ultrasound at Johns Hopkins, times arranged, Baltimore (June)

Practicum in Breast Imaging, times arranged, Baltimore (Aug)

Nuclear Medicine Update, Dec. 9–11, Atlanta (Oct)

MRI Visiting Fellowships at UCLA, Dec. 9–13, 1991; Feb. 3–7, 1992; March 9–13, 1992; April 6–10, 1992; Sept. 14–18, 1992; Oct. 5–9, 1992; and Dec. 7–11, 1992; Los Angeles (Sept)

Current Topics in Nuclear Medicine Technology, Dec. 11–13, Atlanta (Oct)

Asian Oceanian Congress of Radiology, Dec. 14–18, New Delhi (July)

CT/MRI Head to Toe, Dec. 15–20, New York City (Sept)

Mammographically Detected Early Breast Cancer, Jan. 6–9, 1992, Naples, FL, and Feb. 10–13, 1992, Rancho Mirage, CA (Nov)

Advanced Seminars in Diagnostic Imaging, Jan. 10–12 and Feb. 27–March 1, 1992, Laguna Niguel, CA, and Feb. 4–7, 1992, San Diego (Nov)

Caribbean Cruise—Breast Imaging and MRI at Sea: breast imaging, Jan. 11–18, 1992; MR imaging, Jan. 18–25, 1992 (Sept)

Updates on Diagnostic Imaging, Jan. 12–16, 1992, Palm Beach, CA, and Feb. 24–28, Mauna Lani, HI (Nov)

Uroradiology 1992, Jan. 13–17, 1992, Scottsdale, AZ (Sept)

OB/GYN and Ultrasound, Jan. 16–19, 1992, San Diego (Nov)

Seminars in MRI, Jan. 18–25, 1992, Vail, CO (Nov)

Thoracic Imaging 1992, Jan. 19–23, 1992, Laguna Niguel, CA (Nov)

Park City 1992: MRI, Jan. 25–29, 1992, Park City, UT (Oct)

Course on Positron Emission Tomography, Jan. 26–29, 1992, Dana Point, CA (Oct)

Diagnostic Imaging in Puerto Rico, Jan. 26–31, 1992, Cerromar Beach Hotel, Puerto Rico (Sept)

Practical Aspects of Diagnostic Radiology and Medical Imaging, Feb. 1–7, 1992, Snowmass Village, CO (Nov)

MRI: Present and Future, Feb. 3–7, 1992, Naples, FL (Nov)

Intermountain Imaging Conference, Feb. 8–15, 1992, Steamboat Springs, CO (Nov)

Computed Body Tomography 1992: The Cutting Edge, Feb. 13–16, 1992, Orlando, FL (Nov)

Society of Gastrointestinal Radiologists Annual Meeting, Feb. 16–21, 1992, Orlando, FL (Oct)

Advanced Clinical Magnetic Resonance Imaging, Feb. 17–21, 1992, Hawaii (Oct)

MR Angiography and Imaging of the Head, Spine, and Musculoskeletal System, Feb. 17–21, 1992, Tucson, AZ (Oct)

MRI Update: 1992, Feb. 17–22, 1992, Maui, HI (Nov)

Sun Valley Imaging Meeting, Feb. 23–29, Sun Valley, ID (Oct)

AFIP Neuroradiology Review Course, Feb. 29–March 1, 1992, Bethesda (Oct)

Musculoskeletal Imaging, March 2–6, 1992, St. Thomas, Virgin Islands (Nov)

Principles and Practice of Clinical MRI, March 5–8, 1992, Orlando, FL (Nov)

Practical Pediatric Imaging, March 15–20, 1992, Park City, UT (Nov)

Radiology in Southeast Asia and China, March 18–April 7, 1992, Singapore, Bangkok, Hong Kong, Beijing, Shanghai, and Guilin (Nov)

International Symposium on Recent Advances in Diagnostic Imaging and Radiation Oncology, March 24–27, 1992, Kathmandu, Nepal (June)

International Symposium on Diagnostic Imaging, May 18–22, 1992, Barcelona (Nov)

Advances in Cardiopulmonary Imaging, June 11–13, 1992, Salzburg, Austria (Nov)

European Symposium on Uroradiology, Aug. 24–27, 1992, Herlev, Denmark (Aug)

AJR carries announcements of courses, symposia, and meetings of interest to its readers if received a minimum of 5 months before the event. There is no charge; receipt of items by the *AJR* Editorial Office is not acknowledged. Submit items for publication typed double-spaced. Provide title, date, location, brief description, sponsor, course directors, fees, category I credit, and address and telephone number for additional information. Faculty from the host institution will not be listed. Guest faculty names will appear **only** if initials are provided. Mail news items to *AJR* Editorial Office, 2223 Avenida de la Playa, Suite 103, La Jolla, CA 92037-3218.

American Roentgen Ray Society: Officers, Committees, and Membership Information

Officers

President: John A. Kirkpatrick, Jr.

President-elect: A. Everette James, Jr.

1st Vice-president: Andrew K. Poznanski

2nd Vice-president: George R. Leopold

Secretary: Joseph T. Ferrucci, Jr.

Treasurer: Beverly P. Wood

Executive Council: R. N. Berk, M. P. Capp, W. J. Casarella, N. R. Dunnick, R. G. Evens, J. T. Ferrucci, Jr., A. E. James, Jr., J. A. Kirkpatrick, Jr., A. M. Landry, Jr., G. R. Leopold, J. E. Madewell, T. C. McLoud, A. A. Moss, A. K. Poznanski, R. J. Stanley, J. H. Thrall, K. H. Vydareny, N. O. Whitley, B. P. Wood, R. J. Alfidi, chairman

Committees

Editorial Policy: R. N. Berk, E. Buonocore, Melvin M. Figley, C. R. B. Merritt, K. Valji, C. A. Rohrmann, Jr., W. J. Casarella, chairman

Education and Research: R. R. Hattery, C. B. Higgins, B. J. Hillman, R. J. Stanley, W. M. Thompson, N. O. Whitley, chairman

Finance and Budget: R. K. Gedgaudas-McClees, A. A. Moss, J. R. Thornbury, K. H. Vydareny, J. H. Thrall, chairman

Nominating: R. G. Evens, P. J. Fritzsche, A. A. Moss, chairman

Publications: E. Buonocore, C. R. B. Merritt, C. A. Rohrmann, Jr., W. J. Casarella, chairman

Membership: J. E. Madewell, T. C. McLoud, A. A. Moss, K. H. Vydareny, chairman

Representatives to Other Organizations

American Board of Radiology: W. J. Casarella, J. A. Kirkpatrick, Jr., L. F. Rogers

American College of Radiology: R. A. Gagliardi, J. E. Madewell, B. L. McClennan, R. J. Stanley

American Medical Association: S. F. Ochsner, delegate; K. L. Krabbenhoft, alternate; K. L. Kidd, CPT Advisory Committee

American National Standards Institute: M. E. Haskin

National Council on Radiation Protection and Measurements: F. D. Miraldi, E. L. Saenger

Armed Forces Institute of Pathology: J. E. Madewell

Meeting Arrangements

Annual Meetings: May 10–15, 1992, Marriott's World Center, Orlando, FL; April 25–30, 1993, Marriott San Francisco, San Francisco, CA

Annual Meeting Committee: J. K. Crowe, N. R. Dunnick, R. R. Lukin, N. H. Messinger, R. J. Stanley, R. D. Steele, Jr., A. M. Landry, Jr., chairman

Instructional Courses: Bruce L. McClennan, associate chairman; R. J. Stanley, chairman

Scientific Program: P. H. Arger, T. B. Hunter, D. Kushner, T. C. McLoud, L. B. Talner, J. H. Thrall, A. E. James, Jr., chairman

Scientific Exhibits: J. R. Haaga, D. S. Hartman, R. G. Ramsey, N. R. Dunnick, chairman

ARRS Membership

An application form is printed in the September issue of the Journal. For consideration at the 1992 ARRS meeting, send completed forms before February 1, 1992, to American Roentgen Ray Society, 1891 Preston White Dr., Reston, VA 22091. Active members are graduates of an approved medical or osteopathic school or hold an advanced degree in an allied science. They must practice radiology or work in an associated science in the United States or Canada and be certified by the American Board of Radiology, American Osteopathic Board of Radiology, or Royal College of Physicians of Canada or otherwise adequately document training and credentials. International members are foreign radiologists or scientists who are active in radiology or an allied science. Members-in-training are residents or fellows in radiology or postgraduate students in an allied science. Additional application forms can be obtained from the ARRS offices in Reston, VA.

Business Office

Paul Fullagar, Executive Director, American Roentgen Ray Society, 1891 Preston White Dr., Reston, VA 22091; (703) 648-8992.

Classified Advertisements

Positions Available

DIAGNOSTIC RADIOLOGIST POSITION AVAILABLE JULY 1992—Join 2 other radiologists in a 154-bed hospital with a superior medical staff and an excellent, stimulating practice. High income, early partnership, and generous vacation time. The community, which includes the headquarters of 2 large multinational corporations, is an ideal place to live. It has all the advantages of a small town (low crime rate, reasonable cost of living, and country atmosphere), many big city amenities (symphony, theater, etc.), and a population with a high level of education. Contact Gene Martin, M.D., Radiology Dept., Corning Hospital, Corning, NY 14830; (607) 937-7289; home (607) 962-2037. 12-3ap

MODESTO IMAGING CENTER needs additional radiologists trained in all facets of imaging. Modalities present are MRI (Signa Advantage), CT, color Doppler, x-ray, fluoroscopy, mammography, and soon nuclear medicine. All equipment is new and top-of-the-line G.E. (except Acuson ultrasound) in a yr-old outpatient imaging center. Tired of call, old equipment, outrageous time, or requirements to partnership? Would you like to work with the best technologists in a beautiful setting? Modesto is located only 90 min from San Francisco or the Yosemite area. Send your CV to Advanced Imaging Associates, 157 E. Coolidge Ave., Modesto, CA 95350; (209) 524-6800. 12ap

DIVISION HEADS IN ABDOMINAL IMAGING AND MUSCULOSKELETAL RADIOLOGY—The newly Unified Dept. of Radiology of Montefiore Medical Center/Albert Einstein College of Medicine is recruiting for the above positions at the level of professor or associate professor. Individuals selected will work at Montefiore, but have responsibility for developing clinical and teaching programs in their subspecialty at the 2 major teaching hospitals constituting the medical center. Please send CV to E. Stephen Amis, Jr., M.D., Professor and Chairman, Unified Dept. of Radiology, Montefiore Medical Center, 111 E. 210th St., Bronx, NY 10467. Montefiore/Einstein is an equal opportunity employer. 12ap

INTERVENTIONAL RADIOLOGIST CHARLOTTE, NC—Fellowship-trained interventional radiologist needed for July 1992. This subspecialized, 14-member group with 2 busy interventional radiologists performs all aspects of invasive radiology in a 600-bed, community/referred hospital. Great family-oriented community with warm 4-season climate centrally located between mountains and coast. Send CV to P. O. Box 221211, Charlotte, NC 28222. 12-1ap

RADIOLOGIST—Well-established group seeks a seventh radiologist for central Ohio area. BC or BE required. MRI experience desired. Practice includes 2 community hospitals, private office and clinics, and contracts. Limited call. 7 wk vacation. Excellent work schedule. Varied assignments. Salaried first yr then begin partnership track. Full partner at end of fourth yr. Metro area of 1,000,000+ with affordable housing, quality schools, major university and hospital, state capital, and many cultural events. Contact Thomas T. Fox, M.D., President, Mid-Ohio Radiology, Inc., 7239 Sawmill Rd., Ste. 111, Dublin, OH 43017; (614) 791-1300. 12ap

SAN FRANCISCO REGION—Growing 3-person radiology practice needs 2 new BC members, preferably with MR musculoskeletal and/or neuro fellowship training. Competitive salary and benefits leading to partnership. New hospitals and free-standing facilities with 1.5-T Picker Vista MR, Acuson ultrasound, Picker CT, and digital angio. Close to San Francisco, wine country, and Tahoe skiing. Serious applicants contact Box Q96, AJR (see address this section). 12-2ap

VETERANS AFFAIRS MEDICAL CENTER, AUGUSTA, GA, is seeking a physician, board-eligible/certified in radiology. Subspecialty interest in chest, skeletal, GI, or interventional radiology is desirable but not essential. This 1142-bed, tertiary-care medical center is affiliated with the Medical College of Georgia. Faculty appointment commensurate with qualifications and experience. Augusta enjoys a moderate climate, reasonable cost of living, numerous recreational facilities, and institutions of higher learning. An equal opportunity employer. For additional information, contact George T. Jamarik, M.D., Chief, Radiology Service; (404) 823-2236. 12a

CHIEF OF RADIOLOGY—St. Louis Regional Medical Center seeks an experienced radiologist to assume leadership of our dept. as we undertake a major upgrade in equipment and facilities. The dept. performs 70,000 exams annually in a teaching hospital with an extensive clinic system. Contact John Kissel, M.D., Vice-President Medical Affairs, 5535 Delmar Blvd., St. Louis, MO 63112; (314) 879-6363. 12-2ap

FACULTY POSITION IN ABDOMINAL IMAGING, THOMAS JEFFERSON UNIVERSITY HOSPITAL—This position includes responsibilities in GI and GU radiology, abdominal and pelvic ultrasound, and body CT. Jefferson has a large and well-equipped dept. that carried out over 208,000 studies last yr. There are 5 modern fluoroscopic rooms, 3 CT scanners, 21 ultrasound scanners, and 4 GE 1.5-T MRI units available to the staff. There is an excellent mix of stimulating clinical work, sizeable teaching programs at the residency and fellowship levels, and strong support for research. Every faculty member has dedicated academic time, and salaries and benefits are maintained at high levels. Interested candidates should contact David C. Levin, M.D., Chairman, Dept. of Radiology, or Robert M. Steiner, M.D., Director, General Diagnostic Radiology, Thomas Jefferson University Hospital, Philadelphia, PA 19107; (215) 955-7264. An equal opportunity/affirmative action employer. 12xa

UNIVERSITY-TRAINED, BC DIAGNOSTIC RADIOLOGIST WITH ANGIO/INTERVENTIONAL SKILLS needed for busy, quality-oriented, 16-member private group. Position includes 40-50% angiography/interventional, body imaging, and myelography. Group covers university-affiliated, tertiary, 940-bed cardiovascular-oriented and 350-bed pediatric hospitals, as well as 3 nearby outpatient facilities. Address inquiries with CV to Barry Toombs, M.D., or Clark L. Carroll, M.D., 6720 Bertner, Houston, TX 77030. 12ap

CHIEF INTERVENTIONAL RADIOLOGIST Exciting opportunity to join 8 radiologists in a community hospital and imaging center-based practice in the New York state capital district. High-quality practice emphasizes subspecialty expertise in all aspects of diagnostic imaging. Individual is to assume a leadership position to further develop an already well-established interventional radiology practice. Candidate must be BC/BE, fellowship trained or academically experienced, and should have expertise and interest in all aspects of interventional radiology, including thrombolytic therapy. State-of-the-art equipment includes a new biplane angiography suite, 2 CT scanners, and 2 MRI units performing 100,000 diagnostic procedures/yr. Cosmopolitan community boasts abundant cultural, recreational, and educational opportunities. This position is available immediately, however, starting date is flexible. Excellent compensation package leads to lucrative full partnership. Send CV to Michael E. Berlow, M.D., Dept. of Medical Imaging, Albany Memorial Hospital, 600 Northern Blvd., Albany, NY 12204. 12ap

ULTRASOUND SECTION HEAD—Position available in 17-member, diagnostic radiology dept. to manage an ultrasound section that produces nearly 10,000 studies annually, including abdominal, OB-GYN, prostate, interventional, and vascular studies. Up-to-date equipment includes color Doppler and intraoperative equipment. Teaching of 12 radiology residents is an important function. The position also includes the opportunity for experience in other areas of general radiology and cross-sectional imaging. The Dept. of Radiology is an integral part of a 260+ physician multispecialty clinic/hospital providing primary and tertiary care on the outskirts of Boston. All interested radiologists should contact Richard A. Baker, M.D., Dept. of Diagnostic Radiology, Lahey Clinic Medical Center, 41 Mall Rd., Burlington, MA 01805; (617) 273-8170, fax (617) 273-5232. 12a

INTERVENTIONAL RADIOLOGIST, ALBUQUERQUE, NEW MEXICO—Well-established, 14-physician group has immediate opening for fellowship-trained, vascular interventionalist. Initially, approximately 40-50% of work time will be devoted to interventional procedures; potential exists for additional interventional volume as senior physicians phase-down. Practice serves a major hospital within the metropolitan area, 2 MRI centers, 2 outpatient centers, and 3 outlying facilities. All vascular interventional work performed at 1 location. Candidates must have ability and desire to perform both interventional and general radiology procedures. Strong desire to live and work in the southwest is a must. Competitive compensation package. Send CV with references to J. R. Ellison, Executive Director, Radiology Associates of Albuquerque, P.A., 4001 Indian School Rd., N.E., Ste. #300, Albuquerque, NM 87110; (505) 262-1975. 12a

UCSD SCHOOL OF MEDICINE—The Dept. of Radiology is seeking an ultrasonologist to assist in clinical service, medical student and resident teaching, and research projects at the Veterans Affairs Medical Center/UCSD Medical Center. Participation in other diagnostic subspecialties is available. Qualifications required are board eligibility/certification, California medical license, and 1-yr fellowship in ultrasound. Title Series is assistant or associate professor (in-residence or clinical series—not currently a tenure-track position); level based on years experience; salary commensurate with rank and step of appointment based on the established salary schedule of the UCSD School of Medicine Faculty Compensation Plan. The University of California, San Diego, is an equal opportunity/affirmative action employer. All CVs received prior to Dec. 31, 1991, or thereafter, until position is filled, will be given full consideration. Send to Dolores Pretorius, M.D., Chief of Ultrasound, H-756, UCSD Medical Center, 225 Dickinson St., San Diego, CA 92103. 12a

DIAGNOSTIC RADIOLOGIST seeks board-certified radiologist to join established 2-person practice at 150-bed hospital on Virginia's eastern shore. Opening Jan. 1992. We offer radiologic services, including MRI, CT, mammography, and nuclear medicine. Competitive salary and good benefits. Send CV to Box Q100, AJR (see address this section). 12-1ap

FLORIDA, BC DIAGNOSTIC RADIOLOGIST Opening for board-certified radiologist with fellowship training in MRI to join our group of 3 board-certified radiologists in a hospital practice. We recently installed a GE 1.5-T MRI system. Candidate must be willing to cover other areas of diagnostic imaging as well. Competitive salary leading to early partnership. Please send inquiries and CV to David M. Mullin, M.D., Chief of Radiology, 1210 S. Old Dixie Hwy., Jupiter, FL 33458; (407) 744-4411. 12-1ap

BODY MR IMAGING—The Geisinger Medical Center and Clinic in Pennsylvania seeks an individual with training/interest in body MRI with emphasis on musculoskeletal applications. This is an expansion position due to the acquisition of a new scanner. Radiology dept. has 16 associates, 12 residents, and 72 techs. Equipment includes 3 Picker CT's and 2 virtually identical GE Signa 1.5-T Advantage MR systems. In 1990-91, radiology performed 151,000 exams; 4700 were MRI, using 1 stationary and 1 mobile unit. Call (no angiography) is shared with a resident and includes 6 weekends and 22 evenings/yr. Geisinger provides care for 2.5 million with 480+ physicians in 62 specialties and 200 residents/fellows in 21 training programs. The small-town setting and diverse recreational pursuits enhance family-oriented activities. Good schools abound; 3 nearby universities enrich cultural amenities. For details, call Carole Gregory directly (215) 640-3774 or 24-hr voice mail (800) 220-1556 or mail CV to MedQuest, P.O. Box MQ, Devault, PA 19432. 12a

UCSD SCHOOL OF MEDICINE—The Dept. of Radiology is seeking a diagnostic radiologist to participate in clinical service, medical student and resident teaching, and research projects in the subspecialty of osteoradiology. Qualifications required are board-eligibility/certification; California medical license; and 1-yr fellowship in osteoradiology. One-yr experience including MRI in osteoradiology in an academic program is preferred. Title Series is assistant professor (in-residence or clinical series—not currently a tenure-track position); level based on years experience; salary commensurate with rank and step of appointment based on the established salary schedule of the UCSD School of Medicine Faculty Compensation Plan. The University of California, San Diego, is an equal opportunity/affirmative action employer. All CVs received prior to Dec. 31, 1991, or thereafter, until position is filled, will be given full consideration. Send to Donald Resnick, M.D., Chief of Radiology, VA Medical Center, 3350 La Jolla Village Dr., San Diego, CA 92161. 12a

RADIOLOGIST(S), ULTRASOUND/CT/MRI—The Dept. of Radiology of New York Medical College has 2 immediate openings for radiologists with fellowship background in cross-sectional imaging. The positions offer academic status and faculty appointments at New York Medical College. Applicants will participate in medical student, resident, and fellow training as well as clinical services. Applicants sought should be board-certified or eligible and New York state licensed. Interested candidates should submit a CV to Michael S. Tenner, M.D., Professor and Chairman, Dept. of Radiology, New York Medical College, Valhalla, NY 10595; (914) 285-8546. 12-1a

NEURORADIOLOGIST—Well-established community hospital and imaging center-based practice in Albany, New York, seeks fellowship-trained neuroradiologist. Individual should have expertise and interest in all aspects of neuroradiology with particular emphasis on MRI. Interests in other aspects of radiology, particularly cross-sectional imaging, desirable. Ultramodern equipment including 2 high-field Siemens MRI units and MRA capability, new biplane angiography suite, and 2 Siemens CT scanners. Practice emphasizes subspecialty expertise in all aspects of diagnostic imaging, performing 100,000 exams/yr. Capital district community with abundant cultural, recreational, and educational opportunities. Excellent compensation package leading to lucrative full partnership. Send CV to Michael E. Berlow, M.D., Dept. of Medical Imaging, Albany Memorial Hospital, 600 Northern Blvd., Albany, NY 12204. 12ap

PEDIATRIC RADIOLOGIST—The Nemours Children's Clinic is seeking a BC/BE individual to join the expanding program in Jacksonville, Florida, as a staff radiologist. The Nemours Children's Clinic is a multidisciplinary pediatric medical and surgical specialty clinic. The radiology program is a rapidly expanding service providing community-wide service for a city of 800,000 with a large referral base in south Georgia and northeast Florida. The candidate will be offered a university appointment as an assistant professor/associate professor. Teaching and research are strongly encouraged and funded. Salary will be commensurate with experience. The recruiting deadline is Jan. 15, 1992. Interested applicants should send their CV to Ian T. Nathanson, M.D., Chairman, Search Committee, Nemours Children's Clinic, 807 Nira St., Jacksonville, FL 32207; (904) 390-3788. Academic status is offered by the University of Florida, an equal opportunity, affirmative action employer with whom Nemours is affiliated. 12a

PEDIATRIC RADIOLOGIST—The Nemours Children's Clinic is seeking a board-certified individual to join the expanding program in Jacksonville, Florida, as Chairman of the Dept. of Radiology. The Nemours Children's Clinic is a multidisciplinary pediatric medical and surgical specialty clinic. The radiology program is a rapidly expanding service providing community-wide service for a city of 800,000 with a large referral base in south Georgia and northeast Florida. The candidate will be offered a University appointment as an associate professor and chief/professor and chief. Teaching and research are strongly encouraged and funded. Salary will be commensurate with experience. The recruiting deadline is Jan. 15, 1992. Interested applicants should send their CV to Ian T. Nathanson, M.D., Chairman, Search Committee, Nemours Children's Clinic, 807 Nira St., Jacksonville, FL 32207; (904) 390-3788. Academic status is offered by the University of Florida, an equal opportunity, affirmative action employer with whom Nemours is affiliated. 12a

DIAGNOSTIC RADIOLOGIST, ABDOMINAL IMAGING—The University of Missouri-Columbia Hospital and Clinics is seeking a radiologist with expertise in abdominal imaging (GI, CT, ultrasound, and MRI). Board-certification required. Fellowship desirable. Tenured and nontenured tracks available at assistant and associate professor levels. Address inquiries to Robert J. Churchill, M.D., Dept. of Radiology, University of Missouri-Columbia Hospital and Clinics, One Hospital Dr., Columbia, MO 65212. An equal opportunity/affirmative action employer. 12-3a

PEDIATRIC NEURORADIOLOGIST—An opportunity is available for a qualified pediatric neuroradiologist certified by the American Board of Radiology and fully trained in general neuroradiology and pediatric neuroradiology. The candidate must be a senior member of the American Society of Neuroradiology. In addition, the individual must be qualified to practice and teach general diagnostic pediatric radiology, cross-sectional imaging, as well as all aspects of diagnostic and interventional pediatric neuroradiology. A solid knowledge of MR and an interest in neuroradiology research is required. Other duties include clinical service and teaching. Candidates must be qualified for faculty appointment at the George Washington University Medical Center with a future in academic pediatric neuroradiology. All applicants should apply to David C. Kushner, M.D., Chairman, Dept. of Diagnostic Imaging and Radiology, Children's National Medical Center, 111 Michigan Ave., N.W., Washington, DC 20010. Children's National Medical Center is an equal opportunity employer. 12-2a

THE LOUISIANA STATE UNIVERSITY MEDICAL CENTER, DEPT. OF RADIOLOGY, is seeking faculty members with experience or fellowship training in neuroradiology, emergency radiology, chest, bone, CT/MRI/ultrasound, angiography/interventional, nuclear medicine, pediatrics, and GI. The dept. practice is centered at Charity Hospital in New Orleans, a 700-bed general hospital with an active emergency room. 180,000 exams/yr. The residency program has 20 residents. Research, teaching, and clinical service are important. Certification by the American Board of Radiology or its equivalent is desired. Energetic persons are encouraged. Interested persons should submit CV and references to Dr. Jane Clayton, Acting Chairman, Dept. of Radiology, 1542 Tulane Ave., New Orleans, LA 70112. EOE/AA. 12-2a

CHIEF, RADIOLOGY SERVICE AND STAFF RADIOLOGIST POSITIONS—The Syracuse VA Medical Center is recruiting a Chief, Radiology Service, and has 3 other vacancies for staff diagnostic radiologists. The Syracuse VAMC is an active teaching hospital affiliated with the medical school at the State University of New York at Syracuse. For the position of Chief, Radiology Service, board certification with a minimum of 1-3 yr post-residency experience is desired. BE candidates with no post-residency experience will be considered for staff radiologist vacancies. All applicants must be licensed in a "state" and must qualify for academic appointment in the Dept. of Radiology at SUNY. All positions involve house staff responsibilities. Research opportunities are available. VA central office recently approved both scarce specialty and geographic pay, making salary and fringe benefits very competitive. Salary and academic rank commensurate with qualifications. U.S. citizenship required. Contact Richard Kazel, Chief of Staff's Office; (315) 476-7461, ext. 2230. The Syracuse VA Medical Center is an equal opportunity employer. 12xa

DIAGNOSTIC RADIOLOGIST ON THE ISLAND OF KAUAI needed to join 45 doctors in multi-specialty group. Three radiologists in clinic and hospital dept. BC radiologist to perform diagnostic radiology, CT scan, ultrasound, mammography, nuclear medicine, but no angiography. Strong FNA service. Island of 50,000 with moderate subtropical climate. All outdoor sports, including scuba, snorkeling, fishing, golf, tennis, and biking. Incentive formula on becoming stockholder after 1 yr; excellent benefits. Congenial group with quality-care emphasis. Send CV to, or call, Rex D. Couch, M.D., Medical Director, Kauai Medical Group, Inc., 3420-B Kuhio Hwy, Lihue, HI 96766; (808) 245-1077; fax (808) 246-1625 welcomed. 10-2a

MADISON, WISCONSIN—An excellent opportunity exists for a BE/BC general diagnostic radiologist to join a 12-person group. Our practice consists of a 400+ bed hospital and 5 outpatient clinics. The practice includes all diagnostic imaging modalities, however, interest in developing and participation in noninterventional modalities is desirable. Madison, the state capital and home of the University of Wisconsin, is located on 4 lakes and offers many recreational and cultural activities. This is a great opportunity for a congenial and motivated individual. Send letter of inquiry or CV to James G. Olson, M.D., Dept. of Medical Imaging, Meriter Hospital, 202 S. Park St., Madison, WI 53715. 12ap

COASTAL MAINE—Board-certified, experienced radiologist required to share relaxed but growing solo practice in picturesque seascape setting. Ample time off to enjoy it, with acceptable income. For details send CV to Paul D. Cray, M.D., Box 697, Boothbay Harbor, ME 04538; (207) 633-3385. 12-3ap

GENERAL RADIOLOGY, BERGEN COUNTY, NEW JERSEY—Lucrative home/office practice in gracious community conducive to family living. Solid middle-class patient population and referrals from nearby large institutions. Good schools, churches, and parks. Minutes from New York City. Elegant colonial building on half-acre lot includes 3-bedroom home with pool. Office has 3 lead-lined rooms. Contact Dr. Cosman, Medical Equity, Inc., 32 Knickerbocker at Oak, Tenafly, NY 07670; (800) 338-0208. 12ap

GENERAL RADIOLOGISTS desired to join established radiology group. Minimum \$200K first yr. 1:4 call, working out of regional facility with new radiology dept. featuring CT, MRI, angiography, mammography, ultrasound, and nuclear medicine. Beautiful midwestern community serving 300,000. Best schools in the region, low cost of living, and a great place to raise your family! Malls, arts, sports, all right in town. I've been there! For more information, send your CV to Thomas Schroth, Harris Kovacs Alderman, 4170 Ashford Dunwoody Rd., Ste. 500, Atlanta, GA 30319; (800) 347-7987, ext. #1-206. 12ap

BC/BE DIAGNOSTIC RADIOLOGIST wanted to join expanding practice of 12 radiologists in northeastern Pennsylvania. Practice includes 3 hospitals (720 beds) and a free-standing MRI. Candidate must have experience in cross-sectional imaging with an interest in ultrasonography and must be willing to cover other areas of diagnostic imaging. No angiography skills are necessary. Contact Paul M. Leiman, M.D., Dept. of Radiology, Moses Taylor Hospital, 700 Quincy Ave., Scranton, PA 18501; (717) 963-2601. 12-1ap

DIRECTOR OF EMERGENCY RADIOLOGY Emory University School of Medicine is seeking applicants for the position of Director of Emergency Radiology. This director will have clinical and teaching responsibilities at Grady Memorial Hospital, an Emory Hospital affiliate. Salary and faculty position are commensurate with experience. Please direct inquiries to William J. Casarella, M.D., Professor and Chairman, Dept. of Radiology, Emory University School of Medicine, 1364 Clifton Rd., N.E., Atlanta, GA 30322; (404) 727-4996, fax (404) 727-0899. Emory University is an AA/EEO employer. 12a

PENNSYLVANIA—The Geisinger Clinic seeks a diagnostic radiologist with solid skills to work with 5 others at Geisinger-Wyoming Valley Medical Center, its eastern cornerstone in the beautiful Pocono Mts. Busy practice has excellent pathology. Modern equipment includes MRI, CT, SPECT, and a new digital angio room. Call is shared equally. Compensation is competitive with private practice partnership; benefits include TSA's, insurances, 4 wk vacation/4 wk CME. The region boasts affordable housing, excellent schools, 12 colleges, and a family-oriented lifestyle that supports traditional values. For details, call Carole Gregory directly, (215) 640-3774 or 24-hr voice mail (800) 220-2168 or mail CV to MedQuest, P. O. Box MQ, Devault, PA 19432. 12a

BODY IMAGING DIAGNOSTIC RADIOLOGIST Young, progressive group in Washington, DC, area has position immediately available for a board-certified diagnostic radiologist in an expanding and diversified hospital and office-based practice with facilities in Maryland and Virginia. Our group covers 1 hospital, 5 full-service private offices, and 2 diagnostic centers for women. All imaging modalities represented, including 3 MRIs, 6 CTs, 9 ultrasound suites with color-flow, and an ISG 3-D imaging workstation. Very attractive practice setting. Commitment to leading edge technology. Address inquiries and CV to Grant McClure, Radiology Imaging Associates, 7801 Old Branch Ave., Ste. 300, Clinton, MD 20735; (301) 856-6718. 12-2ap

DIAGNOSTIC RADIOLOGIST, SALEM, OR Excellent opportunity for a BC/BE diagnostic radiologist to join Kaiser Permanente's 50-physician multispecialty group at our medical offices in Salem, located in the lush Willamette Valley, close to ocean beaches and mountains. Outpatient position requires no call and includes ultrasound, CT, mammography, and routine fluoroscopy. Full range of professional services provided for 38,000 plan members in area. Excellent salary/benefits, senior physician standing after 2 yr, paid liability coverage, and sabbatical leave. Forward CV and inquiry to Regional Medical Director, Northwest Permanente, P.C., 2701 N.W. Vaughn St., #300, Portland, OR 97210-5398. EOE. 12a

DIAGNOSTIC RADIOLOGISTS—Immediate openings for 2 recently trained BC/BE diagnostic radiologists with expertise in all modalities to join busy 2-person group in expanding, 222-bed hospital in northwest Arkansas. 40,000 exams/yr. New equipment includes GE Advantage MR, GE High-light Advantage CT, GE Starcam 3000 SPECT, and Acuson ultrasound. Excellent salary and early partnership. Robust local economy, no heavy industry, and mild climate. Near University of Arkansas. Excellent outdoor recreational opportunities. Contact David Rhodes, M.D., 28 Greenbriar Dr., Fayetteville, AR 72703. 12-1ap

DIRECTOR OF BREAST IMAGING CENTER Emory University School of Medicine is seeking applicants for the position of Director of the Division of Breast Imaging. The division is currently staffed by 3 full-time radiologists. The director will have clinical, administrative, and teaching responsibilities. Salary and faculty position are commensurate with experience. Please direct inquiries to William J. Casarella, M.D., Professor and Chairman, Dept. of Radiology, Emory University School of Medicine, 1364 Clifton Rd., N.E., Atlanta, GA 30322; (404) 727-4996, fax (404) 727-0899. Emory University is an AA/EEO employer. 12a

THE DEPT. OF RADIOLOGY, VIRGINIA COMMONWEALTH UNIVERSITY/MEDICAL COLLEGE OF VIRGINIA, AND THE MCGUIRE VA MEDICAL CENTER, RICHMOND, VIRGINIA, seek faculty for positions in diagnostic radiology (chest, GI, mammography, CT/ultrasound/MR, musculoskeletal, ER, angio/interventional, neuro-radiology), and radiologic physics. MCV is a 1058-bed facility and a Level I Trauma Center. The McGuire VAMC is an 800-bed facility. ABR certification or eligibility required. Individual should have experience working in a culturally diverse environment. Academic rank and salary commensurate with experience. For position description, or to submit CV, write or phone A. V. Proto, M.D., Dept. of Radiology, MCV Box 470, Richmond, VA 23298-0470; (804) 786-7212. VCU/MCV is an equal opportunity/affirmative action employer. Women and minorities are encouraged to apply. 12-1a

LONG BEACH, CA—The VA Medical Center, Long Beach, CA, is seeking applications for full- and part-time radiologist positions in CT, ultrasound, and neuroradiology. Interest in MRI and intervention desirable. Board-certification/eligibility required. May be licensed in any state. U.S. citizenship is required. Responsibilities include teaching and supervision of residents in conjunction with the affiliated program, University of California, Irvine. Please send CV to Chief, Radiology Service, VAMC, 5901 E. 7th St., Long Beach, CA 90822; (213) 494-2611, or ext. 4787. The DVA is an equal opportunity employer. 11-2a

BOSTON—Expanding private-practice group. No night or evening call. Need experience in mammography. Great life style. Salary leading to equal partnership. Send letter and CV to Box E49, AJR (see address this section). 11-4a

PENN STATE UNIVERSITY, THE MILTON S. HERSHEY MEDICAL CENTER, FACULTY POSITION IN RADIOLOGY—The Penn State University, Dept. of Radiology is recruiting an additional faculty member with training or experience in diagnostic ultrasound, MRI, and CT for July 1, 1992. The position is open to physicians who have fulfilled the ABR requirements for certification and who have subspecialty training or experience in body imaging. Substantial experience in obstetrical ultrasound is desirable. The Penn State University Hospital is a 500-bed, tertiary-care facility in Hershey, PA, near Harrisburg, the state capital. Medical student education, resident training, and research are integral components of the health-care mission of the university. The Dept. of Radiology has 24 faculty and 20 residents. The ultrasound, MRI, and CT sections perform over 6000 exams, 3300 exams, and 8300 exams/yr, respectively. New equipment for 1991 includes a fifth ultrasound unit, a second MRI system, and a third CT scanner. Applicants may respond with a letter of interest and CV to Dr. Richard Moser, Chief, Diagnostic Radiology, Dept. of Radiology, The Milton S. Hershey Medical Center, Penn State University, P. O. Box 850, Hershey, PA 17033; (717) 531-8044. Penn State University is an affirmative action, equal opportunity employer. Women and minorities are encouraged to apply. 12xa

PEDIATRIC RADIOLOGIST—The Dept. of Radiological Sciences of the University of Oklahoma Health Sciences Center has an opening for a pediatric radiologist. Faculty rank and remuneration will depend on credentials and experience. Work site is Children's Hospital of Oklahoma (Oklahoma City) in a well-equipped radiology service performing approximately 75,000 studies/yr. Responsibilities include general diagnosis, ultrasound, body CT, and body MR. If interested, please contact J.J. Vanhoutte, M.D., Radiology Service, Children's Hospital of Oklahoma, P. O. Box 26307, Oklahoma City, OK 73126. 11-1a

BOARD-CERTIFIED RADIOLOGIST—The Dept. of Veterans Affairs Medical and Regional Office Center at Wichita, KS, is actively recruiting a board-certified radiologist. This medical center provides primary and secondary levels of care in medicine, surgery, psychiatry, and tertiary surgical care and is affiliated with the University of Kansas School of Medicine at Wichita. State-of-the-art equipment includes cardiology ultrasound, angiography, and CT. Incumbent will join active, multidisciplinary, teaching medical staff structured to facilitate academic growth. Competitive salary with the recent enactment of Physician Pay Comparability Bill. Send CV to Edward J. Huycke, M.D., Chief of Staff (11), VAM&ROC, 5500 E. Kellogg, Wichita, KS 67218; (316) 651-3603. EOE. 11-12a

RADIOLOGIST, WASHINGTON—Prominent, 100-physician multispecialty clinic in Pacific Northwest is recruiting a diagnostic radiologist. Interventional fellowship training and/or individual with extensive experience in interventional radiology desired. Guaranteed salary and partnership track available. Excellent benefit package. Abundant 4-season recreational opportunities. Family-oriented community rated the 4th best metropolitan area in the U.S. Send CV to Fred Bockenstedt, M.D., P. O. Box 489, Wenatchee, WA 98807; (509) 663-8711, ext. 5590. 11-1a

FULL-TIME DIAGNOSTIC RADIOLOGIST, LAS CRUCES, NM—Seeking a radiologist to work in an outpatient imaging center. No nights, weekends, or holidays. General radiography, CT, ultrasound, nuclear medicine, and mammography. Salary with insurance negotiable. Contact C. L. Chapman, 755 Telshor Bldg. S/T, Ste. 101, Las Cruces, NM 88001; (505) 522-6236. 11-12ap

UNIVERSITY OF CHICAGO, ANGIOGRAPHY/INTERVENTIONAL RADIOLOGIST—The University of Chicago Hospital's exceptionally active clinical and academic programs provide a wide variety of case material. A second new biplane digital room was just installed as well as a 5-bed recovery ward. Interested applicants should call or forward their CVs to Dr. Martin J. Lipton, Chairman, Dept. of Radiology—Box 429, 5841 S. Maryland Ave., Chicago, IL 60637; (312) 702-6024, fax (312) 702-1161. Affirmative action/equal opportunity employer. 11-1ap

UNIVERSITY OF CHICAGO, ABDOMINAL IMAGING—The University of Chicago is seeking a diagnostic radiologist for an academic position to participate in clinical service, medical student and resident teaching, and research projects. The major area of clinical responsibility will be abdominal imaging, which includes GI/GU, CT, ultrasound, and mammography. Applicants should be eligible or certified by the ABR. Interested applicants should call or forward their CVs to Dr. Martin J. Lipton, Chairman, Dept. of Radiology—Box 429, 5841 S. Maryland Ave., Chicago, IL 60637; (312) 702-6024, fax (312) 702-1161. Affirmative action/equal opportunity employer. 11-1ap

UNIVERSITY OF CHICAGO, CHIEF OF PEDIATRIC RADIOLOGY—The University of Chicago is seeking a pediatric radiologist at the rank of associate or professor who is interested in building an outstanding clinical and research program. Current workload approximately 30,000 exams/yr. Clinical facilities include fluoroscopy, ultrasound, CT, and MRI. Excellent opportunity for a dynamic person. Interested applicants should call or forward their CVs to Dr. John Fennessy, Chairman, Search Committee, Dept. of Radiology—Box 429, 5841 S. Maryland Ave., Chicago, IL 60637; (312) 702-6024, fax (312) 702-1161. Affirmative action/equal opportunity employer. 11-1ap

RADIOLOGIST, MARYLAND—BC/BE to join 9-physician radiology dept. Special skills in angio/interventional and MRI desired. Fellowship training preferred. Must be willing to do most aspects of diagnostic radiology. Part of a larger, multispecialty group providing care for BC/BS-affiliated HMO as well as growing FFS practice. Excellent benefits and salary. Located in Columbia, MD, near cultural advantages and medical schools of the Baltimore-Washington, DC, area. Direct CV to Patuxent Medical Group, Inc., 2 Knoll North Dr., Ste. 401, Columbia, MD 21045, Attn: Physician Recruiter. EOE/MFHV. 11-12ap

UNIVERSITY OF CHICAGO, CHIEF OF ABDOMINAL IMAGING—Excellent opportunity for a dynamic person who is interested in building an outstanding clinical and research program in abdominal imaging at the University of Chicago. During the past 3 yr, almost all of our diagnostic imaging equipment has been replaced and new rooms opened. Exciting clinical and research opportunities are available with new state-of-the-art CT, MRI, and ultrasound equipment. Four new CT units have been purchased, including a GE 9800 and an Imatron C-1000 (ultrafast CT). A Siemens 1.5-T MRI unit and a new GE 1.5-T Signa MRI unit are in operation, and an Instrumentarium 0.1-T MRI unit (the first in the U.S.) has recently been installed in the diagnostic area. Another new 1.5-T unit is on order for delivery in 1992. An additional small horizontal-bore, high-field 4.7-T MRI/MRS unit dedicated to research has been purchased and awaits installation. Interested applicants should call or forward their CVs to Dr. Martin J. Lipton, Chairman, Dept. of Radiology—Box 429, 5841 S. Maryland Ave., Chicago, IL 60637; (312) 702-6024, fax (312) 702-1161. Affirmative action/equal opportunity employer. 11-1ap

FACULTY POSITION IN ABDOMINAL IMAGING Dartmouth-Hitchcock Medical Center is seeking a faculty member at the senior assistant or full professor level with experience and interest in abdominal imaging. Clinical responsibility will be in an entirely new 420-bed clinical facility opening in Oct. 1991 with state-of-the-art instrumentation. Position will involve responsibility for residency training in GI/GU area. Proven record of academic performance including research and teaching with an interest in providing academic guidance for energetic staff of younger radiologists. Interested candidates write with CV to Peter K. Spiegel, M.D., Chairman, Dept. of Diagnostic Radiology, Dartmouth-Hitchcock Medical Center, Hanover, NH 03756. AA/EOE. 12xap

DIAGNOSTIC RADIOLOGIST, BODY IMAGING Large radiology group in western Massachusetts seeks board-certified radiologist with fellowship and/or experience in MRI, CT, and ultrasound. Neuroradiology expertise and/or interest desirable, but not required. Primary assignment with 330-bed community hospital. Practice includes 3 other hospitals with 6 private offices. Full partnership after 1 yr. Start on or around March 1, 1992. Send CV to W. M. Cloud, M.D., Radiology & Imaging, Inc., P. O. Box 2250, Springfield, MA 01101. 11-1ap

PEDIATRIC RADIOLOGIST—Children's Hospital and Medical Center (CHMC) and the University of Washington School of Medicine, Seattle, have a faculty opening for an academic pediatric radiologist. Applicants must have completed at least 1 yr of pediatric radiology fellowship beyond a 4-yr residency and must be board-certified. CHMC is a 208-bed medical center that performs approximately 53,000 exams/yr in all phases of pediatric imaging. The successful applicant will join 8 full-time pediatric radiologists, 2 fellows, and 5 residents. The institution is committed to clinical and research excellence, and radiology faculty are encouraged and supported in clinical and basic research efforts. Compensation and fringe benefits are competitive. CHMC and UW are equal opportunity/affirmative action employers. Inquire for additional details to Eric L. Effmann, M.D., Director, Dept. of Radiology, Children's Hospital and Medical Center, P. O. Box C-5371, Seattle, WA 98105; (206) 526-2166. 11-1a

PEDIATRIC NEURORADIOLOGIST—Children's Hospital and Medical Center (CHMC) and the University of Washington School of Medicine, Seattle, have a faculty opening for an academic pediatric neuroradiologist. Applicants must have completed a 4-yr residency in radiology, be board-certified, and have completed an approved ACGME neuroradiology training program. Additional or prior training in pediatric radiology is desirable. CHMC is a 208-bed medical center that performs approximately 53,000 exams/yr in all phases of pediatric imaging. Successful applicants will join 8 full-time pediatric radiologists, 2 fellows, and 5 residents. The institution is committed to clinical and research excellence, and radiology faculty are encouraged and supported in clinical and basic research efforts. Compensation and fringe benefits are competitive. CHMC and UW are equal opportunity/affirmative action employers. Inquire for additional details to Eric L. Effmann, M.D., Director, Dept. of Radiology, Children's Hospital and Medical Center, 4800 Sand Point Way, N.E., Seattle, WA 98105; (206) 526-2166. 11-1a

DIAGNOSTIC RADIOLOGIST sought to join a fee-for-service group practice at 2 mid-Bronx hospitals. Board certification with expertise in imaging and special procedures/interventional radiology preferred. Please send CV to Arthur Avenue Radiology, P.C., P. O. Box 4332, Great Neck, NY 11027. 11-4ap

ABDOMINAL IMAGING RADIOLOGIST—The University of California, Davis, School of Medicine has a full-time position available in the diagnostic division of the Dept. of Radiology. Appointment will be at the assistant, associate, or full professor level. Candidates must be board-certified in diagnostic radiology, eligible for licensure in California, and have an academic and clinical background in abdominal imaging (ultrasound, CT, and MRI). Please forward a CV, a letter outlining background and interests in teaching/research, and the names and addresses of 5 references to Richard W. Katzberg, M.D., Chairman, Dept. of Radiology, University of California, Davis, 2516 Stockton Blvd., TICON II Bldg., Sacramento, CA 95817. This position will be "open until filled," but not later than Jan. 31, 1992. The University of California is an equal opportunity/affirmative action employer and encourages applications from members of minority groups and women. 11-1a

DIAGNOSTIC RADIOLOGIST with skills in CT, MR, interventional, ultrasound, and nuclear medicine needed to join group of 17 board-certified radiologists. Practice is located in southwestern Ohio and provides services at 2 500-bed hospitals, an imaging center, and a private office. Excellent salary, vacation, and benefits leading to early partnership. Send inquiries with CV to Michael R. Carroll, M.D., Medical Radiologists, Inc., 111 W. First St., Ste. 918, Dayton, OH 45402. 12xa

BRIDGEPORT RADIOLOGY ASSOCIATES, P.C., is seeking a board-certified radiologist to join our group of 11. We provide imaging and therapy service for Bridgeport Hospital, a 525-bed community hospital, and 2 large private offices. All imaging modalities exist throughout the practice, including an outpatient 1.5-T MRI. Applicant must share office duties and night and weekend call for the practice, and must participate in teaching for the hospital-based, ABR-approved residency program. Subspecialty training is desirable. Salaried position leads to full partnership. Send letters of inquiry and CV to Anthony J. Bravo, M.D., Chairman, Dept. of Radiology, Bridgeport Hospital, 267 Grant St., Bridgeport, CT 06610. 11-1ap

MAMMOGRAPHY—Immediate opening for board-certified/eligible radiologist in the section of mammography. Large screening and diagnostic program performing approximately 13,000 exams/yr. Mobile unit and outpatient screening program, needle localization, cyst aspiration, and ultrasound. Program very interactive with patients and referring physicians. Academic rank commensurate with experience. Yale University is an equal opportunity/affirmative action employer. Applications from women and minority group members are encouraged. Send current CV or phone Carol Lee, M.D., Yale University School of Medicine, Dept. of Diagnostic Radiology, 333 Cedar St., New Haven, CT 06510; (203) 785-2425. Application deadline is Nov. 30, 1991. 11-12a

PACIFIC NORTHWEST DIAGNOSTIC RADIOLOGY, MRI, CT, AND ULTRASOUND—Progressive group of 4 radiologists seeks a board-certified radiologist with subspecialty interest and expertise in MRI, CT, and ultrasound. Busy, dynamic practice with regional medical center hospital, MRI center, and outpatient office. The practice is located in the beautiful recreation area of the inland northwest. This area offers world-class lakes for boating and sailing as well as excellent skiing, hunting, and fishing. Family-oriented environment only 30 min from Spokane, WA. Competitive salary with full partnership in 2 yr. Send CV to Doug Bruce, M.D., Radiology Associates of North Idaho, 1104 Ironwood Dr., Coeur d'Alene, ID 83814; (208) 667-0686. 11-1ap

UNIVERSITY OF CHICAGO, CHIEF OF ANGIOGRAPHY/INTERVENTIONAL—Excellent opportunity for a dynamic person who is interested in building an outstanding clinical and research program. Our current chief is nearing retirement, and we are seeking a person with potential to succeed him. The University of Chicago Hospital's exceptionally active clinical and academic programs provide a wide variety of case material. A second, new biplane digital room was just installed as well as a 5-bed recovery ward. Interested applicants should call or forward their CVs to Dr. Martin J. Lipton, Chairman, Dept. of Radiology—Box 429, 5841 S. Maryland Ave., Chicago, IL 60637; (312) 702-6024, fax (312) 702-1161. Affirmative action/equal opportunity employer. 11-1ap

SECTION CHIEF, ABDOMINAL CT AND MR IMAGING—St. Luke's—Roosevelt Hospital Center's Dept. of Radiology in New York City has a position at its St. Luke's site for a BC radiologist to be in charge of the abdominal and pelvic imaging performed on its GE Signa Advantage 1.5-T MRI and 2 CTs (GE 9800 Hilight Advantage and Siemens Somatom DRH). This 1315-bed hospital center is in the midst of a \$467 million building program. In addition to clinical expertise, a strong interest and ability in teaching is required for a program that includes residents, fellows, and medical students. Research opportunities are also available in this university hospital of Columbia University College of Physicians and Surgeons. Academic rank depends on qualifications. Excellent remuneration and benefits. Please send inquiries with a CV to Ronald C. Ablow, M.D., Dept. of Radiology, SLRHC, Amsterdam Ave. and 114th St., New York, NY 10025. Columbia University takes affirmative action to ensure equal opportunity. 11-12ap

STAFF RADIOLOGIST—Samuel S. Stratton Dept. of Veterans Affairs Medical Center, Albany, NY, is seeking a board-certified/eligible, full-time staff radiologist. The SVAMC is a 514-bed, general medical and surgical hospital affiliated with Albany Medical College. Albany, the capital of New York, is located upstate and is only a 3-hr drive to New York City, Boston, and Montreal. New equipment located within the service includes a new Siemens Angiostar digital angiography suite, Philips 0.5-T superconductive MRI unit, upgraded Picker 1200 CT scanner, and Acuson color Doppler. Experience in MRI and/or angiography preferred. Interested radiologists please send CV to A. Fermin, M.D., Chief, Radiology Service (114), Stratton VA Medical Center, 113 Holland Ave., Albany, NY 12208. EOE. 11-1a

TWO POSITIONS AVAILABLE—Fellowship training in body MRI with emphasis on orthopedics and ultrasound-fellowship-trained physician needed to join expanding group of 20 diagnostic radiologists (4 neuroradiologists and 5 interventional radiologists) in Orlando, FL. Postfellowship experience preferred. Three hospitals (total 1100 beds), 3 outpatient offices, 7 CT units, 5 MRI units, and 3 angiography suites. Central Florida offers a pleasant climate for year-round outdoor recreation and a dynamic growing economy. Please contact and forward a CV to Len W. Morris, M.D., 1403 Dolve Dr., Orlando, FL 32803; (407) 896-0764. 11-12ap

IMMEDIATE OPENING—BE/BC general diagnostic radiologist to join 4-person group in Wilson, NC. This 366-bed hospital has state-of-the-art facilities including MRI. Imaging skills mandatory; interventional skills desirable. Excellent salary and benefits leading to early partnership. Contact James H. Melvin, M.D., Dept. of Radiology, Wilson Memorial Hospital, 1705 S. Tarboro St., Wilson, NC 27893. 11-1ap

CROSS-SECTIONAL RADIOLOGIST—Excellent opportunity to join 8 subspecialized radiologists in New York state capital district and further develop a well-established, cross-sectional imaging section in a well-established community hospital and imaging center-based practice. Potential for a leadership responsibility in this subsection of the dept. State-of-the-art equipment includes 2 Siemens CT scanners, 2 Siemens 1.0-T MRI units, and 5 ultrasound units including color Doppler capability. Candidate should be BC/BE, fellowship trained, or academically experienced. Excellent compensation commensurate with experience leading to full lucrative partnership. Send CV to Michael E. Berlow, M.D., Director, Dept. of Medical Imaging, 600 Northern Blvd., Albany, NY 12204. 11-12ap

DIAGNOSTIC RADIOLOGIST—The Dept. of Radiology of St. Luke's—Roosevelt Hospital Center in New York City is seeking a BC/BE radiologist with expertise in ultrasound. This position offers a full range of clinical involvement in all aspects of abdominal, obstetrical, and vascular ultrasound. The candidate should also be interested in the interpretation of general diagnostic films. An active clinical practice, strong teaching program, as well as stimulating research opportunities are provided at this 1315-bed university hospital of Columbia University College of Physicians and Surgeons. Academic rank will be commensurate with candidate's qualifications and experience. Excellent facilities and remuneration. Please send inquiries with CV to Ronald C. Ablow, M.D., Dept. of Radiology, SLRHC, Amsterdam Ave. and 114th St., New York, NY 10025. Columbia University takes affirmative action to ensure equal opportunity. 11-12ap

CODY, WY has an immediate position available for a board-certified radiologist. Live and work in the beautiful Rocky Mountain region, located only 50 mi. from Yellowstone Park. Abundant fishing, hunting, and outdoor sports. No state income tax! For more information, call (307) 578-2488 or send CV to Gary Bishop, CEO, West Park Hospital, 707 Sheridan Ave., Cody, WY 82414. 11-1a

A MULTISPECIALTY MEDICAL GROUP has an immediate need for a radiologist. Excellent benefit package, guaranteed salary with incentive, all expenses paid first yr, with partnership opportunity for the future. Direct inquiries or send CV to Penny Phillips, Malone and Hogan Clinic, 1501 W. 11th Pl., Big Spring, TX 79720; (915) 267-6361. 10-3a

THE DEPT. OF RADIOLOGY AT BROOKE ARMY MEDICAL CENTER, SAN ANTONIO, TX, is recruiting academic radiologists for several divisions of the dept., including ultrasound, chest, skeletal, neuroradiology, general diagnostic, interventional radiology, and mammography. Our dept. offers a fully accredited residency program with 24 residents and 16 attending full-time staff. Numerous consultants from across the country lecture on a continuing and regular basis. The hospital is a modern, tertiary-care center serving Texas, Oklahoma, and Louisiana. A strong residency program, interesting patient population, excellent equipment, teleradiology and digital radiology implementations underway, coupled with a south Texas lifestyle are positive aspects of the practice. Academic credentials and/or experience are necessary. Recently graduated fellows are encouraged to apply. Board certification is mandatory. Candidates should be particularly interested in patient care, teaching, and research. Salary and benefits are competitive and generous. Brooke is an EO/EEO employer. Please contact Dr. Billy E. Cunningham, COL, MC, Assistant Chief, Dept. of Radiology, Brooke Army Medical Center, Fort Sam Houston, TX 78234-6200; (512) 221-8418/8218. 8-7a

DIAGNOSTIC RADIOLOGIST, CONNECTICUT Opening in July 1992 for BC/BE radiologist with expertise in general radiology and mammography. Additional training or experience preferred. No angiography/interventional experience required. Nine-radiologist practice includes a 435-bed, university-affiliated community hospital and a 54-physician multispecialty clinic. Approximately 107,000 exams/yr including MRI, CT, nuclear medicine, ultrasound, and an active interventional service. Excellent salary and benefits leading to full partnership after second yr. For more information, send CV to Paul C. Lakin, M.D., Dept. of Radiology, New Britain General Hospital, 100 Grand St., New Britain, CT 06050. 11-2ap

DIAGNOSTIC RADIOLOGIST—A 3-member radiology group seeks a fourth radiologist with interventional skills to join them in a suburban community hospital practice in northern Ohio, 20 min from the boating and fishing pleasures of Lake Erie and its islands. Interested applicants please call or write to Dr. Matthew F. Gutowicz, Jr., 23 Patrician Dr., Norwalk, OH 44857; (419) 668-8101 ext. 6205 or 6208. 11-4ap

RADIOLOGISTS—Eight-member group seeking board-certified/eligible radiologist to join progressive hospital/clinic practice in scenic western Arkansas town of approximately 100,000. All modalities represented in practice. Competitive salary leading to early full partnership. Liberal fringe benefits and vacation. Interested parties, please send CV to Gary A. Plymale, P. O. Box 3887, Ft. Smith, AR 72913; (501) 452-9416 (collect). 11-1ap

OPENING FOR BC/BE RADIOLOGIST with cross-sectional imaging (MRI/CT/ultrasound) fellowship or equivalent experience to join 8-member hospital-based group in Pensacola, FL. Position open Jan. 1992 (possible to hold open until July 1992). Teaching involved. 380-bed hospital/100,000+ procedures/yr. Send CV to Harry Cramer, M.D., P. O. Box 9210, Pensacola, FL 32513-9210. 10-1ap

SOUTHERN OREGON—Opportunity for BC/BE, general diagnostic radiologist to join group of 5 board-certified radiologists. Experience in all modalities desired. Practice includes 2 hospitals and own private office. Competitive starting salary with early full partnership. Excellent lifestyle with many outdoor activities from Pacific Coast to Oregon Cascades. Send CV to Larry Strickland, Administrator, Roseburg Radiologists, P.C., P. O. Box 1547, Roseburg, OR 97478. 8-1ap

CHEST RADIOLOGIST, THOMAS JEFFERSON UNIVERSITY HOSPITAL—The Dept. of Radiology at Jefferson has an opening for a thoracic radiologist at either the junior or senior level. The position encompasses plain film radiography, CT, and percutaneous thoracic interventions. Involvement in mammography, other general diagnostic areas, and ultrasound can also be incorporated, depending on the interests of the candidate. Dedicated, nonclinical research time is provided, and the dept. has excellent research facilities and support. Our chest radiology practice is expanding rapidly and close working relationships are maintained with pulmonary medicine and thoracic surgery. Teaching is also emphasized, with a large residency program and a thoracic radiology fellowship. Excellent faculty income and benefits. This is a fine opportunity for a radiologist with academic interests to join a dynamic and rapidly growing dept. Interested candidates should contact David C. Levin, M.D., Chairman, Dept. of Radiology, Thomas Jefferson University Hospital, Philadelphia, PA 19107; (215) 955-7264. Jefferson is an equal opportunity/affirmative action employer. 12xa

UNIVERSITY OF CHICAGO, PEDIATRIC RADIOLOGIST—The University of Chicago is seeking a pediatric radiologist for an academic position. Workload approximately 30,000 exams/yr. Clinical facilities include fluoroscopy, ultrasound, CT, and MRI. Candidate should be a member of the Society of Pediatric Radiology. Interested applicants should call or forward their CVs to Dr. Martin J. Lipton, Chairman, Dept. of Radiology—Box 429, 5841 S. Maryland Ave., Chicago, IL 60637; (312) 702-6024, fax (312) 702-1161. Affirmative action/equal opportunity employer. 11-1ap

OREGON—Opportunity for BC/BE radiologist to join 7 BC radiologists in growing practice in the Portland metropolitan area. Training/expertise in all aspects of radiology including MRI is required. The practice includes 2 suburban hospitals, an outpatient clinic, and a new multimodality outpatient imaging clinic. Competitive compensation with generous fringe package and partnership in 2 yr. Send letter and CV to Jon C. Sewell, M.D., P.O. Box 227, Oregon City, OR 97045; (503) 655-1439. 12xa

RADIOLOGIST/ANGIOGRAPHER—There is an opportunity to join a progressive group of 11 board-certified radiologists practicing at the Lehigh Valley Hospital Center, a 500-bed, university-affiliated hospital. The position requires angiographic/interventional skills and an interest in general radiology including CT and ultrasound. The radiology dept. has state-of-the-art equipment including 2 angiographic suites, 3 CT scanners, color flow Doppler, and MRI. The hospital is an acute-care facility and a state-designated Level 1 Trauma Center, located 1 hr from Philadelphia and 1½ hr from New York. The radiology dept. offers a postresidency fellowship program that includes training in angiography. The position offers a competitive salary and benefit package that leads to full partnership. For further information, contact Robert Kricun, M.D., Dept. of Radiology, Lehigh Valley Hospital Center, P.O. Box 689, Allentown, PA 18105; (215) 776-8088. 11-1ap

CHIEF, AMBULATORY CARE CLINIC, UNIVERSITY OF ARKANSAS FOR MEDICAL SCIENCES—We are seeking a person with excellent general radiology experience with special interest and competence in bone radiology and mammography to oversee a busy outpatient clinic immediately attached to the hospital and the Arkansas Cancer Research Center. Excellent lifestyle opportunities afforded by both large-city amenities and multiple outstanding outdoor recreational opportunities. Send CV to Richard L. FitzRandolph, M.D., or Ernest J. Ferris, M.D., University of Arkansas for Medical Sciences, 4301 W. Markham, Slot #556, Little Rock, AR 72205. 11-12a

DALLAS, TX—A 12-member, subspecialty group seeks a board-certified, general radiologist for an immediate opening. Fellowship training preferred, but will consider qualified individual with special expertise. CT/ultrasound, MRI, nuclear medicine, or angiography background particularly helpful. All imaging modalities available (state-of-the-art CT, angio, ultrasound, R & F, SPECT nuclear medicine, and MRI center). Salary and bonuses are excellent. Health and malpractice paid. No buy-in to partnership. Send CV to H. Stuart Peake, M.D., P.O. Box 814129, Dallas, TX 75381; (214) 888-7055. 11-4ap

RADIOLOGIST—Second radiologist needed for a 54-physician, multispecialty clinic located in western Montana. Experience or formal training in mammography a must; general radiologic procedures excluding CT and MRI. Offered salary and benefits generous. Send CV to Administrator, Western Montana Clinic, P.O. Box 7609, Missoula, MT 59807. 12ap

IMMEDIATE OPENING IN PALM SPRINGS, CA Radiologist with mammography expertise/specialization needed to join 10-person group in community hospital/office practice. Contact Marvin J. Friedenberg, M.D., Dept. of Radiology, Desert Hospital, 1150 N. Indian, Palm Springs, CA 92262. 12xa

IMMEDIATE OPENING FOR BC/BE GENERAL RADIOLOGIST with experience in interventional and vascular radiology. Join a group of 4 radiologists in a 160-bed hospital located in Allentown, PA, about 60 mi. northwest of Philadelphia. The daily practice includes all aspects of general radiology, CT, ultrasound, and nuclear medicine. Please call or send CV to Asad Shohadai, M.D., Allentown Osteopathic Medical Center, 1736 Hamilton St., Allentown, PA 18104; (215) 770-8700. 12xa

THE RADIOLOGY DEPT. AT DWIGHT DAVID EISENHOWER ARMY MEDICAL CENTER is recruiting academic radiologists. The dept. provides a full range of services including angiography, ultrasound, CT (with a new GE 9800 Advantage system), and MRI (with a new 1.5-T GE Signa system). Development is underway for the installation of a digital teleradiology link to area medical facilities. The dept. is also beginning a radiology residency program in affiliation with the program at the Medical College of Georgia in Augusta. With this growth, the dept. has generated a need for several academic diagnostic radiologists. Board-certified diagnostic radiologists with academic credentials and/or experience are urged to apply. Fellowship training is desired, especially in interventional radiology and/or angiography, however candidates at all levels will be considered. Candidates should be particularly interested in patient care, teaching, and research. The medical center is located on Fort Gordon, GA, adjacent to Augusta and is the tertiary-care hospital supporting 9 Army community hospitals of the southeastern region and Puerto Rico. The hospital supports fully accredited residency programs in family practice, general surgery, medicine, orthopedics, pathology, and psychiatry. Salary and benefits are competitive and generous. The medical center is an EO/EEO employer. Please contact Dr. Thomas M. Ralston, LtC., Chief, Radiology Dept., Eisenhower Army Medical Center, Fort Gordon, GA; (404) 791-6245. 8-7a

FACULTY RADIOLOGIST, BODY MRI DIVISION, THOMAS JEFFERSON UNIVERSITY HOSPITAL—The Dept. of Radiology at Thomas Jefferson University Hospital has an opening for a radiologist in an active, body MRI section that encompasses a clinical mix of approximately 50% musculoskeletal and 50% chest/abdomen/pelvis cases. Equipment includes 4 1.5-T GE Signa systems with state-of-the-art and advanced prototype hardware and software. A full-yr body MRI fellowship and/or 1 yr of academic MRI experience is preferred. Clinical cross coverage in ultrasound and/or general radiology also can be incorporated depending on the interests and qualifications of the candidate. Dedicated, non-clinical research time is provided, and the dept. has excellent research facilities and support, including 2 MRI physicists, a radiology animal facility, radiology research funding, and a team of research assistants. Excellent faculty incomes and benefits are offered within a financially secure dept. and university hospital. This is a unique opportunity for an academically oriented MRI radiologist to join a dynamic and rapidly growing dept. Interested candidates should contact Donald G. Mitchell, M.D., Director of MRI, Dept. of Radiology, 1032 Main Bldg., Thomas Jefferson University Hospital, Philadelphia, PA 19107; (215) 955-4809. Jefferson is an equal opportunity/affirmative action employer. 12xa

ALASKA AREA NATIVE HEALTH SERVICE—Public-service-oriented radiologists needed for cross-cultural health care in Anchorage and Sitka, AK. Salary \$85-\$95K+, excellent benefits. Medical school loan repayment up to \$25K/yr additional. Contact Ken Bartline, RN. (907) 257-1457, collect. Indian Health Service. An equal opportunity employer. 8-1a

SAN FRANCISCO BAY AREA, DIAGNOSTIC RADIOLOGY—Full-time position available as of July 1992 for BC/BE radiologist to join established group based in growing SF Bay area communities. Competence in all modalities including MRI and angiography required; fellowship training desirable. Contact J. Fish, M.D., c/o Walnut Creek Radiology, 1844 San Miguel Dr., #302, Walnut Creek, CA 94596; (415) 947-0560. 11-1xa

ISRAEL, DIAGNOSTIC RADIOLOGY. Opportunities for 3-4 week or longer working vacations in a number of Israeli medical centers, on a volunteer basis. Positions varied, arrangements flexible. For information contact: Jonathan H. Fish, M.D., 1844 San Miguel Dr., #302, Walnut Creek, CA 94596; (415) 947-0560. 11-1xa

THE DEPT. OF RADIOLOGY AT TRIPLER ARMY MEDICAL CENTER, HONOLULU, HI is recruiting academic radiologists for several divisions of the dept. including ultrasound, chest radiology, skeletal, neuroradiology, general diagnostic radiology, MRI, interventional radiology, and mammography. Our dept. offers a fully accredited residency program with 21 residents and 16 attending full-time staff. Numerous consultants from across the country lecture on a continuing and regular basis. The hospital is a modern, tertiary-care center serving Hawaii and the entire Pacific Basin. A strong residency program, diverse and interesting patient population, excellent equipment, and tropical lifestyle are positive aspects of the practice. Academic credentials and/or experience are necessary. Recently graduated fellows are encouraged to apply. Board certification is mandatory. Candidates should be particularly interested in patient care, teaching, and research. Salary and benefits are competitive and generous. Tripler is an EO/EEO employer. Please contact Dr. Mark F. Hansen, Col., MC, Chief, Dept. of Radiology, TAMC, HI 96859-5000; (808) 433-6393. 7-6a

MRI/ABDOMINAL IMAGING NEW YORK/NEW JERSEY METROPOLITAN AREA—Board-certified/eligible radiologist needed for a position beginning July 1, 1991. Must have fellowship training in MRI and training in CT, ultrasound, and GI studies. Private practice with 400-bed hospital and outpatient imaging center located in northern New Jersey, near New York City. Send inquiries to James A. Heimann, M.D., Dept. of Radiology, Clara Maass Medical Center, 1 Franklin Ave., Belleville, NJ 07109. 7-12ap

IMMEDIATE OPENING IN PALM SPRINGS, CA Radiologist with MRI expertise/specialization needed to join 10-person group in community hospital/office practice. Contact Marvin J. Friedenberg, M.D., Dept. of Radiology, Desert Hospital, 1150 N. Indian, Palm Springs, CA 92262. 12xa

MUSCULOSKELETAL RADIOLOGIST, UNIVERSITY OF ARKANSAS FOR MEDICAL SCIENCES, LITTLE ROCK—Join a busy group serving 2 hospitals covering CT, MRI, arthrography, and occasional biopsies, with additional coverage in mammography and some general radiology. Excellent rapport with orthopedic dept. Little Rock gives many large city amenities without the crowded, hectic lifestyle. Send CV to Richard L. FitzRandolph, M.D., or Ernest J. Ferris, M.D., University of Arkansas for Medical Sciences, 4301 W. Markham, Slot #556, Little Rock, AR 72205. 11-12a

COASTAL NORTHERN CALIFORNIA/SAN FRANCISCO BAY AREA

A progressive, diversified group of 16 board-certified diagnostic radiologists, 5 radiation oncologists, and 2 medical oncologists seeks a board-eligible/certified radiologist with some training in MRI and/or neuroradiology. The group serves 4 small- to medium-sized hospitals and a large, outpatient imaging center. The imaging center includes a GE 1.5-T MRI, 9800 Advantage CT, and Acuson ultrasound, as well as CGR mammography, and 3 RF rooms. Competitive salary, 2 yr to full partnership, and excellent benefits. Fast-growing, suburban community 50 min north of downtown San Francisco with sunny Mediterranean climate and very mild winters in the heart of the wine country. Excellent outdoor recreational opportunities. Please send initial inquiry and CV to John J. McGovern, M.D., 121 Sotoyome St., Santa Rosa, CA 95405; (707) 546-4062. 9-2ap

ONCOLOGIC RADIOLOGY/MAMMOGRAPHY

The Dana-Farber Cancer Institute and Brigham and Women's Hospital, teaching affiliates of Harvard Medical School, seek a full-time diagnostic radiologist with interests in oncologic radiology and mammography. The 2 hospitals are in close proximity and the radiology dept. at Dana-Farber Cancer Institute is staffed by Brigham and Women's Hospital faculty and residents. The Dana-Farber Cancer Institute is one of the world's leading cancer treatment and research facilities and many opportunities exist for collaborative clinical research in cancer imaging. Please contact Jack E. Meyer, M.D., Director of Diagnostic Radiology, Brigham and Women's Hospital and Dana-Farber Cancer Institute, 75 Francis St., Boston, MA 02115; (617) 732-6269. Brigham and Women's Hospital/Dana-Farber Cancer Institute/Harvard Medical School is an affirmative action/equal opportunity educator and employer. 9-2a

ULTRASOUND/CT/MRI—Opportunity for board-certified radiologist specializing in ultrasound, body CT, and body MRI to pursue an academic career at The New York Hospital-Cornell Medical Center. The dept. provides state-of-the-art equipment, including Acuson ultrasound, GE 9800 CT, and GE Signa 1.5-T MR. A wide variety of ultrasound exams are performed, including abdominal, OB-GYN, color Doppler, small parts, neonatal head, transvaginal, and transrectal. A candidate with prior fellowship in sectional imaging or ultrasound is preferred. Responsibilities include clinical practice, teaching, and research. Position available 9/1/91. Please send CV to Elias Kazam, M.D., Dept. of Radiology, The New York Hospital-Cornell Medical Center, 525 E. 68th St., New York, NY 10021. 9-12a

NORTHERN CALIFORNIA—The Permanente Medical Group, Inc., is seeking a BC radiologist with multimodality interests and fellowship training in MR to join a 12-person group serving a 337-bed, acute-care hospital and 2 outpatient clinics. Teaching opportunities are available with residents of subspecialty services on rotation from Stanford University Hospital, as well as our own medical residents. We have sited a GE 1.5-T MRI system. Competitive salary and excellent benefits. Please send inquiries and CV to Bruce Baker, M.D., Chief, Dept. of Radiology, Kaiser Permanente Medical Center, 900 Kiely Blvd., Santa Clara, CA 95051; (408) 236-4444. EOE. 12-2a

NEURO/GENERAL RADIOLOGIST—Exceptional private-practice opportunity created by involuntary departure of neuroradiologist. 350-bed community hospital with all modalities including 1.5-T MRI and new DSA. Full benefits, 1 yr to partnership, excellent salary, and liberal time off. Contact John Lacika, M.D., 1406 N. 6th Ave., St. Cloud, MN 56303; (612) 255-5619. 10-12ap

BC DIAGNOSTIC RADIOLOGIST—Affluent practice. Excellent salary, benefits, and early partnership. Investigate now before socialized medicine becomes a reality! Practice at a 395-bed hospital, the second largest in the beautiful state of Delaware, centrally located on the east coast. This is a rapidly expanding, high-powered, group practice. Subspecialty training in interventional, imaging, or neuro desired. Open to F-M with 1-2 yr of postgrad experience. Send resume to or contact Ben Hollander, M.D., Dept. of Radiology, St. Francis Hospital, 7th and Clayton Sts., Wilmington, DE 19805; (302) 421-4300. 9-2ap

THE DEPT. OF RADIOLOGY AT WALTER REED ARMY MEDICAL CENTER

is recruiting academic radiologists. We need board-certified radiologists to work in this famous and modern health-care center. Our dept. has a residency program consisting of 24 residents and several fellows. Subspecialists are needed in ultrasound, chest, mammography, genitourinary, gastrointestinal, pediatric, CT, MRI, and interventional radiology, as well as general radiology. Excellent opportunity to live in the nation's capital and also become an integral part of a large teaching program. Salaries are competitive and generous. Highly motivated applicants should contact Col. Mark F. Hansen, Radiology Consultant to the Army Surgeon General, Dept. of Radiology, TAMC, HI 96859-5000; (808) 433-6393. 8-7a

LARGE, DYNAMIC RADIOLOGY PRACTICE in central New Jersey and adjacent Pennsylvania region seeks diagnostic radiologist with expertise in 1 or more of the following: CT/ultrasound, angio/interventional, or nuclear medicine with cardiac emphasis. Outstanding opportunity for well-qualified person. Send resume to E. Tarasov, M.D., 838 W. State St., Trenton, NJ 08618. 10-12a

NORTHWEST ROCKY MOUNTAINS—Highly respected, 8 person group with strong subspecialty interests seeks highly qualified radiologist. Fellowship or academic experience preferred. Body imaging/MRI, nuclear medicine with boards, or ABR special competency strongly desired. Position includes all aspects of radiology. Practice is located in Boise, ID, which has many recreational and cultural amenities. Reply to Paul Traugher, M.D., or J. Tim Hall, M.D., Dept. of Radiology, St. Alphonsus Regional Medical Center, 1055 N. Curtis Rd., Boise, ID 83706; (208) 378-2161. 10-1ap

ALASKA DIAGNOSTIC RADIOLOGIST, FULL-TIME—Managed Health Care, Ltd., operates radiology services at military hospitals throughout the U.S. and is currently seeking a radiologist at Ft. Wainwright, Fairbanks, AK. The position offers a full-time, \$210,000 compensation package. Board certification is required. Position is immediate. Licensure required in 1 of the 50 states to qualify. Please call collect for further information. David A. Descoteau, Managed Health Care, Ltd., 6140 Scarborough Way, Columbia, MD 21044; (301) 992-1443. 12-1ap

NEURORADIOLOGIST—Senior ASNR member needed for excellent hospital and imaging center position in Tucson, AZ. Early partnership opportunity. Send CV to Arizona State Radiology, 7250 E. Ventana Canyon Dr., Tucson, AZ 85715. 8-7ap

IMMEDIATE OPENING FOR BE/BC RADIOLOGIST in a regional hospital with a patient base of 25,000 located in a scenic western Wyoming community. Great outdoor recreation area. Competitive reimbursement. Ultrasound/CT/general radiology. Interested persons contact Paul Sonntag, M.D., P.O. Box 629, Ogden, UT 84402; (801) 625-2092. 8-1ap

DIAGNOSTIC RADIOLOGIST with skills in CT, MR, interventional, ultrasound, and nuclear medicine needed to join group of 8 board-certified radiologists. Growing practice in eastern Washington at a 228-bed hospital, a new multimodality imaging center, and 2 private offices. Potential for long-term practice is excellent. Top-notch school system, including 3 first-rate universities. Excellent hunting, fishing, boating, and skiing. Contact L. E. Crecelius, M.D., N. 5901 Lidgerwood, Ste. 18B, Spokane, WA 99207; (509) 482-2385. 12xa

Positions Desired

DIAGNOSTIC RADIOLOGIST—Dedicated, mature, board-certified radiologist seeks permanent, part-time position in general diagnostic radiology in southeastern U.S. Experiences include Dept. Director. Excellent references. Available on short notification. Reply to Box Q92, *AJR* (see address this section). 12bp

SECOND YR RADIOLOGY RESIDENT (PGY3) seeks PGY3 or PGY4 position. Enthusiastic, amiable, and hardworking. Desiring more challenge and diversity. Willing to relocate. Reply Box Q94, *AJR* (see address this section). 12xbp

RADIOLOGIST, UNIVERSITY TRAINED—Previous angiographic interventional fellowship. Extensive angio/interventional experience (25 yr). Over 1000 angioplasties. Reasonable proficiency in modern imaging modalities. Presently holding responsible position in university-affiliated hospital. Please reply to Box P84, *AJR* (see address this section). 10-12bp

Fellowships and Residencies

FELLOWSHIP IN ANGIOGRAPHY/INTERVENTIONAL RADIOLOGY OPENING—The Dept. of Radiology, The George Washington University Medical Center, Washington, DC, has an opening for a 1-yr fellowship in angiography/interventional radiology beginning July 1, 1992. The section consists of 2 adjoining state-of-the-art angio suites sharing a large common control room. The section is responsible for all non-neuro and non-cardiac diagnostic angiography, as well as all non-vascular imaging guided interventions with ultrasound, CT, or fluoro. Current ongoing research projects in male impotency and chemoembolization of liver tumors. Active vascular interventions, including thrombolytic therapy, laser-assisted angioplasty, and atherectomy. Cross-training in vascular ultrasound and vascular MRI also possible. Approximately 800 cases/yr. The section is staffed by 2 attendings and a physician assistant. Applicants must be graduates of an approved U.S. medical school or its equivalent, must have completed an approved residency in diagnostic radiology, be eligible for ABR certification, and be eligible for medical licensure in the District of Columbia. Please send inquiries with CV to Edward M. Drury, M.D., Dept. of Radiology, The George Washington University Medical Center, 901 23rd St., N.W., Washington, DC 20037. The George Washington University is an EEO/affirmative action employer. 12cp

FELLOWSHIP IN BREAST IMAGING AND SONOGRAPHY—The Dept. of Radiology, Albert Einstein College of Medicine/Montefiore Medical Center, is offering a 1-yr fellowship beginning July 1992 in breast imaging (including stereotactic aspiration) and ultrasonography. State-of-the-art equipment with color Doppler. Transvaginal and transrectal scanning as well as sonographically guided interventional techniques are performed. Address inquiries to Rosalyn Kutcher, M.D., Dept. of Radiology, Montefiore Medical Center, 111 E. 210th St., Bronx, NY 10467, or call (212) 920-4626 for further information. 12cp

MUSCULOSKELETAL RADIOLOGY FELLOWSHIP—Applications are now being accepted for a musculoskeletal fellowship position for 1993 at the Cleveland Clinic Foundation (CCF). CCF is a 1000-bed, tertiary-care, teaching medical center with a large radiology residency program. Local, national, and international patients provide an interesting and varied mix of bone pathology. Training includes all aspects of musculoskeletal radiology, including MR, CT, arthrography, biopsy, bone densitometry, and a large plain film experience. Fellowship includes patient care, teaching, and research. There is a close working relationship with the orthopedic, rheumatology, and endocrinology depts. There are presently 4 musculoskeletal staff in the section. For further information, please contact Bradford J. Richmond, M.D., Head, Section of Musculoskeletal Radiology, Desk A-21, 9500 Euclid Ave., Cleveland, OH 44195; (216) 444-3931. 12-5cp

FELLOWSHIP IN BODY CT/MRI AND ULTRASOUND—The Dept. of Radiology of New York Medical College has 2 openings for a 1-yr imaging fellowship starting in July 1992. Westchester County Medical Center is a 650-bed, tertiary-care facility offering advanced training with state-of-the-art equipment. Equipment includes 2 Siemens Hi-Q CT Scanners, GE Signa, 1.5-T MR, ISG 3-D reconstruction console, and 6 ultrasound imagers (Acuson and Dasonics). Applicants must have completed an approved residency in diagnostic radiology and must be board-eligible or certified. Please contact Michael S. Tenner, M.D., Professor and Chairman, Dept. of Radiology, New York Medical College, Valhalla, NY 10595; (914) 285-8546. 12-1c

FELLOWSHIPS IN PEDIATRIC RADIOLOGY The Dept. of Diagnostic Imaging and Radiology, Children's National Medical Center, Washington, DC, is soliciting applications for postgraduate fellowship training in pediatric radiology. The dept. performs over 70,000 exams annually in 1 of the 4 largest children's hospitals and ambulatory practices in North America. The dept. has 11 faculty, 4 fellows, and many resident trainees. Imaging services and training include state-of-the-art radiography, fluoroscopy, ultrasound, nuclear medicine, cardiovascular imaging, interventional radiology, CT, and MRI. There are many opportunities for rewarding careers in pediatric radiology in either academic or practice environments. If you wish to receive more information about the fellowship or careers in pediatric radiology, please contact David C. Kushner, M.D., Chairman, Dept. of Diagnostic Imaging and Radiology, Children's National Medical Center, 111 Michigan Ave., N.W., Washington, DC 20010; (202) 745-5080. 12c

MR FELLOWSHIP, SAN FRANCISCO REGION A 6-mo or 1-yr position is available. Primary instructor is nationally recognized expert. Neuro emphasis, musculoskeletal and body work as well. Picker 1.5-T Vista with Beta-site applications. Teaching responsibilities as desired. Close to San Francisco, wine country, and Tahoe skiing. Serious applicants contact Box Q96, *AJR* (see address this section). 12-2cp

PEDIATRIC RADIOLOGY FELLOWSHIP Egleston Children's Hospital at Emory University offers a 1-yr fellowship in pediatric radiology beginning July 1, 1992. Training includes conventional radiography, digital fluoroscopy, ultrasound (including color Doppler), CT, nuclear medicine, MRI, neuroradiology, and interventional techniques. Egleston Children's Hospital is a 225-bed, tertiary-care, pediatric hospital on the Emory University campus that performed 50,000 imaging studies in 1990. The dept. is staffed by 7 pediatric radiologists and 1 pediatric neuroradiologist. Two fellowship positions are available each yr. The application deadline is April 1, 1992. Candidates must be board-certified or eligible in diagnostic radiology. For additional information, please address inquiries to Dr. Turner Ball, c/o Radiology, Egleston Children's Hospital, 1405 Clifton Rd., N.E., Atlanta, GA 30322-1101. Egleston Children's Hospital is an equal opportunity/affirmative action employer. 12-3c

ANGIOGRAPHY/INTERVENTIONAL RADIOLOGY FELLOWSHIP—Because of an unexpected vacancy, New York Medical College offers a 1-yr fellowship to begin immediately. The program includes training in all phases of diagnostic angiography and interventional radiologic techniques. Training is based at Westchester County Medical Center, a 650-bed, tertiary-care center located on the medical college campus in a prestigious suburban setting only about 1/2 hr from New York City. Active participation in clinical management of patients is emphasized. Approximately 900 procedures were performed in 1990. Current research interests include transmesenteric sclerosis of portal varices and hepatic arterial chemoembolization. A new digital interventional suite was opened in 1990. A digital biplane imaging suite is anticipated in 1991. Applications are also being accepted for a 1-yr fellowship to begin July 1, 1992. For additional information and application, contact Stuart Katz, M.D., Dept. of Radiology, New York Medical College, Valhalla, NY 10595; (914) 285-8388. 12-1c

CARDIOVASCULAR/INTERVENTIONAL RADIOLOGY FELLOWSHIPS—The Johns Hopkins Hospital has a position open for its 1-yr CVIR training program beginning July 1993. The program has been redesigned to provide strong clinical experience in a wide variety of vascular and nonvascular interventional procedures including angiography; angioplasty; percutaneous atherectomy; intravascular ultrasound; thrombolytic therapy; varicocele, tumor, and AVM embolization; caval filters; percutaneous central venous catheter placement; percutaneous abscess drainage; and complex urologic and biliary intervention, including percutaneous biliary endoscopy and biliary atherectomy for biopsy. In addition, daily morning conferences, a private CVIR patient admitting service, and a weekly vascular clinic strengthen the total-patient-care concept of this program. Superb interaction with both the vascular surgery and general surgery services help to facilitate an understanding of the evaluation, care, and treatment of CVIR patients outside the dept. Research time for both clinical and laboratory sciences is available. The candidate will also participate in resident and medical student teaching. Our dept. is currently undergoing major renovations, with planned upgrades, including a new room with a Siemens Angiostar, giving us 3 dedicated CVIR rooms and 2 shared rooms. Our division includes 6 full-time staff, 19 dedicated technologists, and 5 full-time RNs performing over 12,000 exams/yr. Interested candidates should contact Floyd A. Osterman, Jr., M.D., Chief, Division of CVIR, The Johns Hopkins Hospital, 600 N. Wolfe St., Baltimore, MD 21205; (301) 955-5687. 12-3cp

FELLOWSHIP IN MAGNETIC RESONANCE IMAGING at Central Massachusetts Magnetic Imaging Center, July 1993 through June 1994. CMMIC is a consortium of 3 area teaching hospitals (The Medical Center of Central Massachusetts, St. Vincent Hospital, and the University of Massachusetts Medical Center) with clinical, research, and teaching responsibilities. CMMIC currently uses 2 state-of-the-art clinical 1.5-T GE Signa systems as well as a 2.0-T GE Fremont CSI research system. The fellowship includes thorough training in MRI physics, imaging principles, clinical applications, and image interpretation. Duties include interpretation of neuro, musculoskeletal, abdominal, pediatric, and cardiac studies, and participation in CMMIC's teaching and research activities. Requirements include satisfactory completion of a 4-yr accredited radiology training program and board-eligibility or certification. Please send inquiries to Ronald Ragland, M.D., Medical Director, CMMIC, Inc., 367 Plantation St., Worcester, MA 01605. 12-1cp

FELLOWSHIPS, DEPT. OF MEDICAL IMAGING, MEMORIAL SLOAN-KETTERING CANCER CENTER (MSKCC)—Excellent opportunity for intensive clinical training and research at the Memorial Sloan-Kettering Cancer Center (a Cornell University Medical College affiliate) located in New York City with competitive salary/benefits. Send inquiries to the following: Cross-Sectional Imaging—J. Caravelli, M.D., or R. Castellino, M.D. (MSKCC); Breast Imaging—D. Dershaw, M.D. (MSKCC); Nuclear Medicine—S. Larson, M.D. (MSKCC). Integrated fellowships are available based at both New York Hospital (NYH) and MSKCC, during which the fellows rotate between the 2 institutions. Selection of applicants is done conjointly. Send inquiries to the following: Neuroradiology—G. Krol, M.D., (MSKCC) or R. Zimmerman, M.D. (NYH); Vascular/Interventional—J. Botet, M.D. (MSKCC) or T. Sos, M.D. (NYH), 1275 York Ave., New York, NY 10021. 12-1cp

MUSCULOSKELETAL RADIOLOGY FELLOWSHIP—Applications are now being accepted for a musculoskeletal fellow position for 1993 at the Cleveland Clinic Foundation (CCF). CCF is a 1000-bed, tertiary-care teaching medical center with a large radiology residency program. Local, national, and international patients provide for an interesting and varied mix of bone pathology. Training includes all aspects of musculoskeletal radiology, including MR, CT, arthrography, biopsy, bone densitometry, and a large plain film experience. Fellowship includes patient care, teaching, and research. There is a close working relationship with the orthopedic, rheumatology, and endocrinology depts. There are presently 4 musculoskeletal staff in the section. For further information, please contact Bradford J. Richmond, M.D., Head, Section of Musculoskeletal Radiology, Desk A-21, 9500 Euclid Ave., Cleveland, OH 44195; (216) 444-3931. 11-4cp

IMMEDIATE OPENING, PEDIATRIC RADIOLOGY FELLOWSHIP—Position available for a 1- or 2-yr fellowship in pediatric radiology beginning July 1, 1992, or July 1, 1993. Full training with abundant hands-on experience with all imaging modalities. Supported by strong Dept. of Pediatrics with a good mixture of patient material. Excellent teaching on a 1-to-1 basis and ample opportunity for pursuing academic interests. Apply to Leonard E. Swischuk, M.D., Dept. of Radiology, The University of Texas Medical Branch, Child Health Center, C-65, Galveston, TX 77550; (409) 772-2096. UTMB is an equal opportunity M/F/H/V affirmative action employer. UTMB hires only persons authorized to work in the U.S. 11-1c

FELLOWSHIP IN DIAGNOSTIC IMAGING (CT/ULTRASOUND/MRI)—The University of Texas Southwestern Medical Center in Dallas, Dept. of Radiology, has 3 imaging fellowships available beginning July 1, 1992. Fellows receive extensive clinical training on state-of-the-art diagnostic imaging systems installed this year in CT, ultrasound, and MRI. Training in obstetric ultrasound is included. Fellows are based at Parkland Memorial Hospital, a 1025-bed trauma center. The Dept. of Radiology operates 3 CT scanners, including a Toshiba 900S installed in 1991, and 4 ultrasound rooms, including 2 Philips Platinum with color Doppler installed in 1991, as well as 2 MR imagers within Parkland. Additional case material is available at Zale Lipshy University Hospital, a 160-bed tertiary-care center opened in 1989 with a state-of-the-art radiology dept. The new Meadows Advanced Imaging Center, opened July 1991, houses 2 1.5-T MRI devices serving patients at Parkland and Zale Lipshy Hospitals, and UT Southwestern outpatients. The Rogers Magnetic Resonance Center at UT Southwestern operates a 0.5-T Toshiba MRI system for clinical studies and several MR devices dedicated to research. Candidates must be board-certified or eligible in diagnostic radiology and be eligible for Texas medical licensure. For further information, contact George Curry, M.D., Chief, Diagnostic Radiology, The University of Texas Southwestern Medical Center, 5323 Harry Hines Blvd., Dallas, TX 75235-8896; (214) 688-8020. An equal opportunity/affirmative action employer. 11-12c

ANGIO/INTERVENTIONAL FELLOWSHIP—The University of Chicago has an unexpected opening in our angio/interventional fellowship (instructorship) program for July 1992. The University of Chicago Hospital's exceptionally active clinical and academic programs provide a wide variety of case material. A second new biplane digital room was just installed as well as a 5-bed recovery ward. Interested applicants should call or forward their CVs to Dr. Chien-Tai Lu, Dept. of Radiology—Box 429, 5841 S. Maryland Ave., Chicago, IL 60637; (312) 702-1607, fax (312) 702-1161. Affirmative action/equal opportunity employer. 11-1cp

MAMMOGRAPHY FELLOWSHIP—The University of Chicago has a fellowship (instructorship) position available for 1 yr beginning July 1, 1992. Facilities include 3 dedicated screen-film units at the hospital and 1 at a clinic. Space is being renovated for a comprehensive breast care center. A Fisher MammoTest is available for stereotactic breast biopsy. The University of Chicago has pioneered the stereotactic technique in this country. We also have a large research group involved in digital mammography/CAD (computer assisted diagnosis). Interested BC/BE applicants should call or forward their CVs and 3 letters of recommendation to Dr. Robert Schmidt, Dept. of Radiology—Box 429, 5841 S. Maryland Ave., Chicago, IL 60637; (312) 702-3282, fax (312) 702-1161. Affirmative action/equal opportunity employer. 11-1cp

FELLOWSHIP IN MAMMOGRAPHY—The Emory University, Dept. of Radiology, offers a 6- or 12-month fellowship in mammography. Approximately 17,000 mammograms are performed annually through a 600-bed university hospital, a 900-bed county hospital, and an outpatient clinic. Clinical activities would include extensive training in all aspects of mammography, breast ultrasound, stereotactic fine-needle aspirations, and biopsy. Candidates should be eligible for Georgia medical licensure. Contact Beth Kruse, M.D., Section of Radiology, The Breast Imaging Center, 1327 Clifton Rd. N.E., Atlanta, GA 30322; (404) 248-4446. Emory University is an equal opportunity/affirmative action employer. 10-1cp

FELLOWSHIP IN CROSS-SECTIONAL IMAGING—The Dept. of Radiology, Dartmouth-Hitchcock Medical Center has an opening in July 1992 for a 1-yr fellowship in MRI/CT/ultrasound. Training includes experience in all aspects of MRI (including neuro and body), CT, and ultrasound (including obstetric and vascular imaging). Imaging-guided biopsies and drainage procedures will be an integral part of the program. The medical center has a completely new 420-bed, tertiary-care hospital with state-of-the-art imaging equipment opening in the fall of 1991. Protected research time will be available for the fellow. There is ample opportunity for clinical radiologic research as well as technology assessment and outcome analysis in collaboration with Dartmouth Medical School Center for Evaluative Sciences. For further information, contact Robert D. Harris, M.D., Dept. of Radiology, Dartmouth-Hitchcock Medical Center, Hanover, NH 03756; (603) 646-5686. 12xcp

MRI FELLOWSHIP—The University of Chicago, Dept. of Radiology, is seeking candidates for a new 1-yr fellowship (instructorship) program in clinical MRI to start July 1992. Six mo in all aspects of MRI, 2 mo neuro MRI, and 4 mo practical experience in CT/UTS. Equipment includes 1.5-T GE Signa and Siemens units and 0.1-T Instrumentarium scanner. Interested BC/BE applicants should forward their CVs and 3 letters of recommendation to Dr. David N. Levin, Director of MRI, Dept. of Radiology—Box 429, 5841 S. Maryland Ave., Chicago, IL 60637; (312) 702-6200, fax (312) 702-1161. Affirmative action/equal opportunity employer. 11-1cp

WOMEN'S IMAGING FELLOWSHIP—A 1-yr fellowship is available at Oregon Health Sciences University, Portland, OR. Training includes hysterosalpingography, fallopian tube recanalization, mammography and breast procedures, obstetric ultrasound, pelvic ultrasound including vaginal ultrasound, and pelvic and breast MRI. Please contact Amy Thurmond, M.D., Director of Women's Imaging, Oregon Health Sciences University, L340, 3181 S.W. Sam Jackson Park Rd., Portland, OR 97201-3098; (503) 494-7576. 11-1c

PEDIATRIC RADIOLOGY FELLOWSHIP—The Section of Pediatric Radiology at the University of Rochester Medical Center offers an ACGME-accredited, 1-yr fellowship in pediatric radiology beginning July 1, 1992. All imaging modalities are represented, including conventional radiology, CT, ultrasound, MRI, neuroradiology, interventional procedures, neonatal neurosonography, and nuclear imaging. Opportunities in clinical and basic imaging research are offered. Candidates must be board-certified/eligible in diagnostic radiology. Interested candidates should contact Dr. M. A. Manuli, Chief, Pediatric Radiology Section, University of Rochester Medical Center, 601 Elmwood Ave., Rochester, NY 14642-8648; (716) 275-5100, fax (716) 271-8698. EOE, M/F. 11-1c

RESEARCH FELLOWSHIP IN INTERVENTIONAL RADIOLOGY—A 2-yr position is available at Allegheny General Hospital, a 746-bed teaching hospital in Pittsburgh, for a research fellow in an innovative program in interventional radiology research beginning July 1992. The fellow will participate in imaging studies directed at ablation of tumors in the liver, prostate, lung, and brain. Percutaneous methods of removing herniated disks also are being pursued. Clinical responsibilities will be included as well as opportunities to pursue individual research interests. Candidates must be board certified/eligible in radiology. Please send CV to Dr. Gary Onik, 320 E. North Ave., Pittsburgh, PA 15212. 11-4cp

CARDIOVASCULAR/INTERVENTIONAL RADIOLOGY FELLOWSHIPS, THE JOHNS HOPKINS HOSPITAL—The Johns Hopkins Hospital will offer 4 positions for its 2-yr CVIR training program beginning July 1993. The program has been redesigned to provide strong clinical experience in a wide variety of vascular and nonvascular interventional procedures, including angiography; angioplasty; percutaneous atherectomy; intravascular ultrasound; thrombolytic therapy; varicocele, tumor, and AVM embolization; caval filters; percutaneous central venous catheter placement; percutaneous abscess drainage; and complex urologic and biliary intervention including percutaneous biliary endoscopy and biliary atherectomy for biopsy. The first yr is a fellowship position during which basic techniques and fundamental elements of patient care are emphasized. In addition, daily morning conferences, a private CVIR patient admitting service, and a weekly vascular clinic strengthen the total patient care concept of this program. Elective clinical rotations with both the vascular surgery and general surgery services help to facilitate an understanding of the evaluation, care, and treatment of CVIR patients outside the dept. Generous research time for both clinical and laboratory sciences is an integral part of the training program. The candidate will also participate in resident and medical student teaching. The second yr is a faculty position (instructor level) with commensurate compensation and benefits. Responsibilities during the second training yr will include case planning and supervision of residents and first-yr fellows, laboratory and clinical research, and vascular MR and ultrasound. Our dept. is currently undergoing major renovations, with planned upgrades including a new room with a Siemens Angiostar, giving us 3 dedicated CVIR rooms and 2 shared rooms. Our division includes 6 full-time staff, 19 dedicated technologists, and 5 full-time RNs performing over 12,000 exams/yr. Interested candidates should contact Floyd A. Osterman, Jr., M.D., Chief, Division of CVIR, The Johns Hopkins Hospital, 600 N. Wolfe St., Baltimore, MD 20205; (301) 955-5687. 11-2cp

ABDOMINAL IMAGING FELLOWSHIP—The University of Chicago has a fellowship (instructorship) position available July 1992. Training will include 6 mo of CT and ultrasound, with the remaining 6 mo as elective, and will consist of subspecialties such as MRI, GI/GU, mammography, or other subspecialties in radiology arranged with the approval of the program director. Interested BC/BE applicants should call or forward their CVs and 3 letters of recommendation to Dr. Elizabeth Holland, Dept. of Radiology—Box 429, 5841 S. Maryland Ave., Chicago, IL 60637; (312) 702-6200, fax (312) 702-1161. Affirmative action/equal opportunity employer. 11-1cp

IMAGING FELLOWSHIP (CT, ULTRASOUND, MRI)—William Beaumont Hospital, a 970-bed, modern, tertiary-care teaching and academic institution in southeast Michigan, offers a 1-yr fellowship in sectional body imaging. The fellowship will provide extensive clinical experience in body CT, ultrasound, and MRI, including CT and ultrasound-guided procedures, conventional and color flow Doppler exams, and prostatic and endovaginal sonography. Ample elective time is also provided for other rotations of individual interest. Candidates must be board-certified/eligible in diagnostic radiology and have a valid Michigan medical license. Four positions are available for July 1993. Salary and fringe benefits are highly competitive. For further information, write to Ali Shirkhoda, M.D., Chief, Imaging Division, William Beaumont Hospital, 3601 W. 13 Mile Rd., Royal Oak, MI 48073; (313) 551-1001. 11-1c

ONCOLOGY/MAMMOGRAPHY FELLOWSHIP

The Dept. of Radiology at the Dana-Farber Cancer Institute and Brigham and Women's Hospital, Harvard Medical School affiliates, offers a 1-yr fellowship position beginning July 1, 1992. All imaging modalities involved in the diagnosis, staging, and follow-up of patients with malignant disease are integrated into this program. An additional feature is a concentrated experience in the performance of interventional breast diagnostic procedures. Please contact Jack E. Meyer, M.D., Director of Diagnostic Radiology, Brigham and Women's Hospital and Dana-Farber Cancer Institute, 75 Francis St., Boston, MA 02115; (617) 732-6269. Brigham and Women's Hospital/Dana-Farber Cancer Institute/Harvard Medical School is an affirmative action/equal opportunity educator and employer. 9-2c

A FELLOWSHIP IN ULTRASOUND AND BODY CT/MRI

is available July 1, 1992, to June 30, 1993, at The New York Hospital-Cornell Medical Center. The dept. provides state-of-the-art equipment, including Acuson ultrasound, GE 9800 CT, and GE Signa 1.5-T MR. Wide variety of ultrasound exams include abdominal, OB-GYN, color Doppler, small parts, neonatal head, transvaginal, and transrectal. Applicants should be ABR-eligible or certified. Send CV to Elias Kazam, M.D., Dept. of Radiology, The New York Hospital-Cornell Medical Center, 525 E. 68th St., New York, NY 10021. 10-1c

FELLOWSHIP IN NEURORADIOLOGY, JULY 1, 1992

The Dept. of Radiology, University of Massachusetts Medical Center offers a 1-yr fellowship position in neuroradiology starting July 1, 1992. Training is offered in neuroangiography, CT, myelography, and MRI. The position involves teaching of medical students and residents with opportunity for research. The University of Massachusetts Medical Center is a 370-bed, university hospital and medical school located in Worcester, 40 mi. west of Boston. The dept. consists of 22 staff, 14 residents, 2-4 fellows, and does approximately 130,000 exams/yr. The hospital is a major trauma center and is serviced by 2 Life Flight helicopters. The dept. is well-equipped with 2 state-of-the-art CT scanners, 2 1.5-T GE MR scanners, as well as 2.0-T small-bore units for animal research. The University of Massachusetts Medical Center is very active academically. Numerous radiologic, clinical, and basic science conferences are scheduled on a daily basis, and there is ample time during the course of the yr to attend many of these presentations. There are many on-going research projects. The fellowship position carries the title of instructor in radiology. For further information, contact Ronald L. Ragland, M.D., Chief, Division of Neuroradiology, University of Massachusetts Medical Center, 55 Lake Ave., N., Worcester, MA 01655; (508) 856-2215. The University of Massachusetts Medical Center is an affirmative action/equal opportunity employer. 12xc

NEURORADIOLOGY FELLOWSHIP—An unexpected opening for a neuroradiology fellow is available in the Dept. of Radiology at Thomas Jefferson University Hospital beginning July 1992. The Division of Neuroradiology has close clinical and research relationships with Jefferson's very active neurology, neurosurgery, orthopedic surgery, and otolaryngology depts. Complete training in ENT radiology is part of this program. Six full-time faculty members currently staff this division. Clinical facilities include 2 dedicated CT scanners, a myelography room, a biplane angiography room with DSA, and 4 GE 1.5-T MRI units. Contact Carlos Gonzalez, M.D., Director of Neuroradiology, 1009 Main Bldg., Thomas Jefferson University Hospital, Philadelphia, PA 19107; (215) 955-5447. Jefferson is an affirmative action/equal opportunity employer. 11-6c

FELLOWSHIP POSITION

The Dept. of Radiology, Division of Cardiovascular/Interventional Radiology of the Brigham and Women's Hospital/Harvard Medical School has an opening for 1- or 2-yr position beginning July 1992. We are also considering applications for 1- and 2-yr fellowships starting July 1993. The Division of Cardiovascular/Interventional Radiology is a state-of-the-art training program in peripheral angiographic techniques, vascular and nonvascular interventions of all types, vascular ultrasound, and cardiovascular MRI. Some cardiac catheterization and coronary angiography is included. Research time is available for participation in original or ongoing clinical and/or laboratory projects. Please send CV to Kris Kandarpa, M.D., Ph.D., Co-Director, Division of Cardiovascular/Interventional Radiology, Dept. of Radiology, Brigham and Women's Hospital, 75 Francis St., Boston, MA 02115. Brigham and Women's Hospital/Harvard Medical School is an affirmative action/equal opportunity educator and employer. 11-4c

FELLOWSHIP IN ULTRASOUND, BODY CT, AND MRI

July 1992 and July 1993. One-yr program featuring ultrasound, body CT, body MRI, and noninvasive vascular diagnosis. Send CV to, or for information contact, William Zwiebel, M.D., Dept. of Radiology, University of Utah Hospital, Salt Lake City, UT 84132; (801) 581-7553. 11-4c

ACCREDITED FELLOWSHIPS IN PEDIATRIC RADIOLOGY AND PEDIATRIC NEURORADIOLOGY

Dept. of Radiology, Children's Hospital Medical Center, Cincinnati, OH, offers 1- or 2-yr accredited (Residency Review Committee for Radiology of ACGME) fellowships in pediatric radiology beginning July 1, 1993. A 1-yr pediatric neuroradiology fellowship program is also offered and may be taken separately or combined with 2 yr of adult neuroradiology fellowship at the University of Cincinnati Medical Center. Children's Hospital Medical Center (CHMC) is a 355-bed institution. The dept. performs over 105,000 radiologic exams/yr in the largest children's hospital and ambulatory practice in the U.S. The dept. has 14 full-time faculty pediatric radiologists, 6 fellows, and many resident trainees. Five pediatric radiology and 2 pediatric neuroradiology fellowship positions are available annually. Training includes all aspects of pediatric imaging including neonatal radiology, neuroimaging, oncologic imaging, ultrasonography, nuclear medicine, CT, MRI, and vascular/interventional procedures. The dept. has an active clinical service with state-of-the-art equipment including digital fluoroscopy; Acuson, AI, and ATL ultrasound units with Doppler and color-flow Doppler capabilities; planar SPECT gamma cameras; GE 9800 Quick CT scanner, 1.5-T GE MRI with spectroscopy; and cardiac catheterization/angiographic suite with digital vascular imaging. The fellowship provides a broad clinical experience in pediatric radiology as well as numerous opportunities to participate in both clinical and basic research. Candidates must be board-certified or qualified in diagnostic radiology and must obtain an Ohio medical license. Salary and fringe benefits are highly competitive. Applications are due before Jan. 1992, with interviews scheduled during the fall and winter of 1991-1992. There are numerous career opportunities in pediatric radiology in both academic and private practice settings. To receive more information about the fellowships at CHMC or careers in pediatric radiology, please contact Donald R. Kirks, M.D., Director, Dept. of Radiology, Children's Hospital Medical Center, Cincinnati, OH 45229-2899; (513) 559-8058. Children's Hospital Medical Center and the University of Cincinnati College of Medicine are affirmative action/equal opportunity employers. 9-5cp

FELLOWSHIP IN MUSCULOSKELETAL IMAGING

A position is available July 1, 1991, to June 30, 1992, for a board-certified radiologist to obtain advanced training and undertake research in musculoskeletal imaging at the Johns Hopkins Hospital. The experience includes MRI, CT, 3-D imaging, and conventional studies. Johns Hopkins Hospital has an active emergency service and serves as a regional pediatric trauma center. The fellow may participate in and extend ongoing research projects in 3-D imaging, using the Pixar Imaging Computer, and studies of osteoporosis and bone remodeling using the latest dual energy X-ray absorptiometry. MRI equipment includes high-field-strength research units as well as 2 1.5-T General Electric units for clinical studies. Body CT studies are performed on Siemens DR H and PLUS scanners, with over 14,000 body studies done yearly. The fellow will work closely with 2 experienced musculoskeletal radiologists. Interested parties should contact George Saba II, M.D., The Johns Hopkins Hospital, Dept. of Radiology, 600 N. Wolfe St., Baltimore, MD 21205; (301) 955-7700. 10-12c

MARYLAND FELLOWSHIPS

The University of Maryland School of Medicine at Baltimore is accepting applications for fellowships beginning July 1992. One-yr fellowships are available in angio/interventional, skeletal, CT/ultrasound/MR, neuroradiology, trauma and critical care, and pediatrics. The University of Maryland offers competitive salaries, ample time for academic pursuits, and funding for continuing medical education. Board certification in radiology is desired, board eligibility is required. Additional information regarding each fellowship is available by calling toll-free (800) 866-8667 ext. 3477 or direct (301) 328-3477. Send CV to Gerald S. Johnston, M.D., 22 S. Greene St., Baltimore, MD 21201. The University of Maryland is an affirmative action/equal opportunity employer who encourages applications from members of minority groups. 12xc

FELLOWSHIPS AT THOMAS JEFFERSON UNIVERSITY HOSPITAL

The Dept. of Radiology at Thomas Jefferson University Hospital in Philadelphia offers the following fellowship programs each yr. (1) Ultrasound/CT/MRI — Jefferson's ultrasound division is 1 of the largest in the world and performs all currently available exams including obstetric, vascular, lithotripsy, invasive, and endoluminal. We also operate 4 GE 1.5-T MRI units and 3 CT scanners. Contact Barry Goldberg, M.D., regarding this program. (2) Cardiovascular/interventional — this division is housed in a new suite containing Philips angio units with DSA and performs the full range of vascular and nonvascular interventional procedures. Contact Geoffrey Gardiner, Jr., M.D. (3) Neuro/ENT radiology — very active clinical services supply a wealth of material to this division, which is housed in a neurosciences imaging center containing all imaging modalities. Contact Carlos Gonzales, M.D. (4) Breast Imaging — Jefferson's new breast-imaging center performs approximately 85 studies/day including ultrasound and needle localizations. Contact Stephen Feig, M.D. (5) Chest — includes biopsies and CT. Contact Robert Steiner, M.D. (6) MRI — a dedicated body MRI program including excellent research opportunities in addition to a large clinical case load. Contact Donald Mitchell, M.D. (7) Ultrasound — a dedicated ultrasound program. Contact Barry Goldberg, M.D. (8) Musculoskeletal — includes MRI of the musculoskeletal system. Contact David Karasick, M.D. All program directors listed above can be contacted at the Dept. of Radiology, Thomas Jefferson University Hospital, Philadelphia, PA 19107. Jefferson is an equal opportunity/affirmative action employer. 12xc

VASCULAR AND INTERVENTIONAL RADIOLOGY FELLOWSHIP—The University of Arkansas for Medical Sciences is offering a 1-yr fellowship in vascular and interventional radiology starting July 1, 1992. Training includes all aspects of angiography and vascular and nonvascular interventions. Ample clinical material is available at a university hospital, a large veterans' hospital, and a children's hospital. Active vascular and nonvascular research programs are in place. Stipend and fringe benefits are competitive. Candidates must be board-certified or eligible in diagnostic radiology. Applications should include a current CV and 3 letters of reference. For further information, please contact David R. McFarland, M.D., Dept. of Radiology/556, University of Arkansas for Medical Sciences, 4301 W. Markham, Little Rock, AR 72205; (501) 686-6910. The University of Arkansas for Medical Sciences is an equal opportunity educator and employer. 10-12c

FELLOWSHIP POSITIONS—The Dept. of Radiology, University of Arkansas for Medical Sciences, Little Rock, AR, has openings for fellowships to begin July 1992. Positions are available in body imaging/intervention, neuroradiology, vascular and interventional radiology, and pediatric radiology. Eligible candidates must be board-certified or eligible for certification in diagnostic radiology and should be eligible for licensing in the state of Arkansas. Interested candidates should contact the program directors: imaging/intervention — Teresita L. Angtuaco, M.D., or Steven K. Teplick, M.D.; neuroradiology — Edgardo J. C. Angtuaco, M.D.; vascular and interventional radiology — Joanna J. Siebert, M.D. All program directors listed above can be contacted at the Dept. of Radiology, University of Arkansas for Medical Sciences, Slot 556, 4301 W. Markham St., Little Rock, AR 72205; (501) 686-5740. The University of Arkansas for Medical Sciences is an affirmative action/equal opportunity employer. 12xc

RADIOLOGY RESIDENCY POSITION—Unexpected immediate opening for an R3- or R4-radiology resident commencing July 1991 at Sacred Heart Medical Center (SHMC) in Spokane, WA. SHMC is a large, 650-bed tertiary-care hospital with a state-of-the-art radiology dept. The 11-member faculty are all fellowship trained. Residency program currently includes 2 residents/yr. Please direct all inquiries to Royce L. Zobel, M.D., Program Director, Dept. of Radiology, Sacred Heart Medical Center, W. 101 8th Ave., TAF-C9, Spokane, WA 99220; (509) 455-3020. 12xc

FELLOWSHIP IN VASCULAR/INTERVENTIONAL RADIOLOGY 1992—The University of New Mexico has an unexpected opening for a 1-yr fellowship in vascular/interventional radiology beginning July 1, 1992. We perform all noncardiac diagnostic angiography, including neuroangiography, as well as a wide variety of vascular and nonvascular interventional procedures, with state-of-the-art equipment at the University Hospital (a level 1 trauma center) and the VA/Air Force Hospital. Applicants must have passed the ABR written exam, be eligible for ABR certification, and be eligible for medical licensure in the state of New Mexico. We are an equal opportunity employer. Contact Jerry King, M.D., Dept. of Radiology, University of New Mexico School of Medicine, 915 Camino Salud, N.E., Albuquerque, NM 87131; (505) 272-2439. 10-12c

FELLOWSHIP IN CARDIOVASCULAR/INTERVENTIONAL RADIOLOGY—A 1-yr fellowship in cardiovascular/interventional radiology is available at the Dartmouth-Hitchcock Medical Center in Hanover, NH, beginning July 1992. DHMC is the major teaching component of Dartmouth Medical School and is situated in a classic northern New England town. Training includes all aspects of diagnostic angiography (including neuro and pulmonary) and vascular and nonvascular interventional techniques. This includes IVC filter placement, atherectomy, thrombolysis, biliary and urologic interventions, and biopsy and drainage procedures using multiple imaging modalities. We have a close working relationship with the depts. of vascular and general surgery. Approximately 2000 diagnostic and interventional procedures are performed per yr. The dept. will be moving to a new, tertiary-care, 429-bed hospital in fall 1991, equipped with 2 new, state-of-the-art, digital interventional suites and a 4-bed recovery room. Candidates must have completed an accredited diagnostic radiology residency program, must be certified or eligible by the ABR, and must be eligible for medical licensure in the state of New Hampshire. For further information, please contact Louis I. Juravsky, M.D., FRCPC, Dept. of Diagnostic Radiology, Dartmouth-Hitchcock Medical Center, 2 Maynard St., Hanover, NH 03756. Dartmouth College is an equal opportunity/affirmative action educator and employer. 12xc

FELLOWSHIP IN ABDOMINAL IMAGING AND INTERVENTIONS—The Dept. of Radiology, Massachusetts General Hospital and Harvard Medical School, offers a 2-yr fellowship in abdominal imaging and interventions beginning July 1, 1993. Training covers all aspects of abdominal imaging (radiography, fluoroscopy, ultrasound, CT, and MR) and nonvascular interventions in the GI and GU tracts. Research is active and participation is encouraged. Candidates should be ABR-eligible or certified. Address inquiries to Peter R. Mueller, M.D., or Nicholas Papanicolaou, M.D., Dept. of Radiology, Massachusetts General Hospital, Boston, MA 02114. An equal opportunity employer. 11-11c

FELLOWSHIP IN BODY MRI, THOMAS JEFFERSON UNIVERSITY HOSPITAL—The Dept. of Radiology at Thomas Jefferson University Hospital has an unexpected opening for a 1-yr MRI fellow beginning July 1, 1992. This is an active body MRI section that encompasses a clinical mix of approximately 50% musculoskeletal and 50% chest/abdomen/pelvis cases. Equipment includes 4 1.5-T GE Signa systems with state-of-the-art and advanced prototype hardware and software. Ample opportunity for research is provided. The dept. has excellent research facilities and support, including 2 MRI physicists, a radiology animal facility, radiology research funding, and a team of research assistants. Interested candidates should contact Donald G. Mitchell, M.D., Director of MRI, Dept. of Radiology, 1032 Main Bldg., Thomas Jefferson University Hospital, Philadelphia, PA 19107; (215) 955-4809. Jefferson is an equal opportunity/affirmative action employer. 8-1c

NEURORADIOLOGY FELLOWSHIP—Two yr beginning July 1, 1992. Exposure to all aspects of clinical/academic neuroradiology. Participation in research/training. Send cover letter/CV to John R. Jinkins, M.D., Director, Neuroradiology Section, The University of Texas Health Science Center, 7703 Floyd Curl Dr., San Antonio, TX 78284-7800. The University of Texas Health Science Center at San Antonio is an affirmative action/equal opportunity employer. 10-12c

FELLOWSHIP IN ULTRASOUND/CT/ANGIO-INTERVENTIONAL—A 1-yr fellowship program is available beginning July 1992 at Lehigh Valley Hospital Center (LVHC) in Allentown, PA. LVHC is a 492-bed, acute-care, university-affiliated hospital. The fellowship program offers training in CT (head and body), ultrasound, angiography (neuro and visceral), and interventional radiology. MRI experience is also available. For further information, contact Robert Kricun, M.D., Dept. of Radiology, Lehigh Valley Hospital Center, P. O. Box 689, Allentown, PA 18105. 10-12c

Tutorials/Courses

CARIBBEAN CRUISE—BREAST IMAGING AT SEA—Jan. 12-19, 1992. Faculty: Drs. Dorit Adler and Terry Silver. CME I. Medical Seminars International, 18981 Ventura Blvd., Ste. 303, Tarzana, CA 91356; (818) 774-9077. 9-12d

CARIBBEAN CRUISE—MRI AT SEA—Jan. 19-26, 1992. Faculty: Drs. William G. Bradley, Rosalind Dietrich, and Ronald J. Friedman. CME I. Medical Seminars International, 18981 Ventura Blvd., Ste. 303, Tarzana, CA 91356; (818) 774-9077. 9-12d

AJR Classified Advertisements Information

Box Responses and Address for Ad Placement

Write Box _____, AJR, 2223 Avenida de la Playa, Suite 103, La Jolla, CA 92037-3218; Phone: (619) 459-2229; FAX: (619) 459-8814.

Author Index Volumes 156-157

Authors of *AJR* articles are also included in the 5-year cumulative index published in *Radiology*.

A

Abbitt PL, 157:337
 Abcarian PW, 157:773
 Abécassis J-P, 156:981
 Abeler VM, 156:1191, 157:1221
 Aberle DR, 156:833
 Ablin DS, 156:635
 Abrahams JJ, 156:599
 Abramowitz J, 157:1309
 Abu-Yousef MM, 156:79
 Achong D, 156:407
 Acunaş B, 156:751
 Acunaş G, 156:751
 Adam A, 156:321, 157:291
 Adam G, 156:125
 Adams HG, 156:198
 Adcock LL, 157:37
 Adler DD, 157:711
 Adler RS, 157:1023
 Advani SH, 157:413
 Agatston S, 156:467
 Aggarwal SK, 157:198
 Agildere AM, 156:1113
 Aida N, 157:991
 Aikawa H, 157:19
 Aizpuru R, 156:1007
 Akhan O, 156:1113
 Akins EW, 156:875, 156:1155
 Alder DC, 157:385
 Alegret X, 156:931
 Alexander A, 156:99
 Alexandre JH, 156:1324
 Algra PR, 157:1130
 Al-Kawas F, 157:747
 Allard JC, 156:875
 Allen B, 156:471
 Allison JW, 156:255
 Alper A, 156:751
 Alperin JB, 156:1189
 Alpern MB, 156:1113
 Alquier P, 157:255
 Alurkar SS, 157:413
 Amenta PS, 157:951
 Amis ES Jr, 157:321, 157:1064
 Ammann ME, 157:1353
 Amplatz K, 156:1007, 156:1087
 Anderson DJ, 156:405, 157:181
 Antonucci F, 156:389
 Appen RE, 157:595
 Applegate G, 156:307
 Argy N, 156:849, 156:1295
 Arneson M, 157:461
 Arno LJ, 156:1110
 Aronson D, 156:527
 Aronson FR, 156:281
 Aronson J, 156:353
 Aruny JE, 157:1186

Asleson RJ, 157:389
 Atlas SW, 156:1229
 Aughenbaugh GL, 157:1171
 Auletta AG, 157:789
 Awh MH, 157:177

B

Babbal R, 157:1093
 Babcock DS, 157:793
 Babikian G, 157:341
 Bach DB, 156:520
 Baert AL, 156:640
 Baeyaert M, 157:1128
 Bagley D, 156:99
 Baillie J, 156:975, 157:281
 Bakal CW, 157:49, 157:59
 Baker LL, 156:1133
 Baker ME, 157:195, 157:281
 Baker S, 156:345
 Balduini FC, 156:769
 Balthazar EJ, 156:23
 Banna M, 157:867
 Bansal S, 157:609
 Bar MH, 156:281
 Baran DT, 156:1326
 Baran GA, 157:648
 Barbieri RL, 157:99
 Barboriak D, 156:474
 Barkovich AJ, 156:587, 156:791
 Barloon TJ, 156:579
 Barnes DA, 156:785
 Barnes PD, 157:559
 Baron RL, 156:945
 Barone GW, 156:639
 Barone M, 157:1181
 Barr LL, 157:793
 Barreda R, 156:199
 Barrett NK, 157:1125
 Barron PT, 156:1261
 Bartiromo G, 156:341, 157:1181
 Barzel E, 157:545
 Basch C, 157:799
 Bassett LW, 156:59, 156:449, 157:21, 157:25, 157:347
 Batnitzky S, 156:1052, 156:1279
 Beam CA, 156:1209, 157:981
 Beatrous TE, 156:407
 Becker C, 156:345
 Becker JM, 156:769
 Becker MH, 157:1242
 Beckett WW Jr, 157:200
 Beckwith JB, 157:549
 Belanger PL, 156:775, 156:781
 Belizon I, 157:49, 157:59
 Bell DG, 156:1081
 Bell RD, 157:1299
 Bellah RD, 157:119
 Beldegrun A, 156:833

Bellon EM, 156:807
 Belloni C, 156:753
 Beltran J, 156:457
 Benenati JF, 156:327
 Beningfield SJ, 156:1263, 157:646
 Benjamin IS, 156:321, 157:291
 Ben-Menachem Y, 156:1101, 157:1005
 Bennick M, 157:1203
 Benson CB, 157:1275
 Benson JE, 156:807
 Benson MT, 157:1358
 Benson RC, 156:1205
 Bentson JR, 157:1309
 Benzel EC, 156:801
 Berbaum KS, 156:177, 157:173
 Berdon WE, 157:549, 157:553
 Beres RA, 156:823
 Beres RR, 157:1360
 Berg P, 157:509
 Berk RN, 157:86, 157:614, 157:653
 Berkowitz JE, 156:638
 Bernardino ME, 156:1171
 Bernstein J, 157:721
 Bernstein RM, 156:864
 Bero L, 156:1109
 Berquist TH, 156:337
 Berry M, 156:1112
 Bertino RE, 156:404
 Bertrand Y, 156:1037
 Bessette JC, 156:823, 157:1360
 Bettmann MA, 157:66
 Beute BJ, 157:257
 Beyssen B, 156:389
 Bigler SA, 156:945
 Bisceglia M, 156:351
 Bisesi MA, 156:475
 Björgvinsson E, 157:539
 Blanc P, 156:281
 Bland PH, 156:511
 Blaser SI, 156:807, 157:819
 Blebea JS, 156:343
 Blinkhorn RJ, 156:870
 Bloem JL, 156:1017, 157:1130
 Blomlie V, 156:1191, 157:1221
 Blum JE, 156:58, 156:806, 157:784, 157:1050
 Boal DKB, 156:1219
 Boechar I, 157:1065
 Bohndorf K, 156:125
 Bohrer SP, 157:1034
 Bonagura V, 157:553
 Bond JB, 157:1087
 Bongartz G, 157:731
 Bonnin A, 156:981
 Bood B, 156:198
 Bookstein JJ, 156:617, 157:932
 Bornman PC, 156:1263
 Botet JF, 156:63
 Bouachour G, 157:255
 Bouillot JL, 156:1324
 Boulware SD, 156:599
 Bower BL, 156:385
 Bowie JD, 157:73
 Box LM, 156:1154
 Boyko OB, 156:1053
 Brady TM, 156:404
 Braha S, 157:49, 157:59
 Brahme FJ, 156:1244
 Brammer HM, 157:1003
 Brandon JC, 156:471, 157:235
 Brandser E, 156:201, 157:412
 Brant WE, 156:636, 157:544
 Brant-Zawadzki M, 157:1307
 Braun IF, 156:373
 Braun MA, 157:199
 Braunstein EM, 156:545, 157:608
 Braverman RM, 156:365, 157:1059
 Bree RL, 157:503
 Brenner RJ, 156:719
 Bressler EL, 157:200
 Briggs SE, 157:1069
 Brill PW, 156:561, 157:1105, 157:1117
 Brink JA, 156:1163
 Brismar J, 157:1119
 Brisson LJ, 156:639
 Broadwater R Jr, 157:235
 Brody AS, 157:341
 Brogan M, 156:161
 Brogdon BG, 157:1355
 Brooks BS, 156:1075
 Brown CEL, 156:523
 Brown DE, 156:333
 Brown E, 157:1125
 Brown JH, 157:318
 Brown JJ, 157:81, 157:1220
 Brown LR, 157:1171
 Brown ML, 157:527
 Brown WE, 156:871
 Browning M, 156:1155
 Brown-Jones C, 156:141
 Brunberg JA, 157:1111
 Brunt E, 157:1195
 Bryan RN, 157:133, 157:585
 Buchberger W, 157:715
 Buchbinder SS, 156:866
 Buck JL, 156:481, 157:160
 Buckley AR, 157:753
 Buckley JG, 157:1035
 Buckley KM, 156:467
 Buckner CB, 156:255
 Buiteweg J, 157:1358
 Bulas DI, 156:155, 156:571, 157:111
 Burger PC, 156:1053

Burgess AR, 157:1005
 Burhenne HJ, 156:73, 157:287,
 157:485, 157:753
 Burns MA, 157:465
 Burrell MI, 157:223
 Burrows PE, 157:819
 Burton DJ, 156:555
 Burton SS, 157:761
 Bush WH, 157:1153
 Busuttill RW, 157:293
 Buxton R, 156:307

C

Caballero-Saez A, 156:769
 Cáceres J, 156:931
 Cahill P, 157:87
 Camerino V, 157:93
 Cameron JL, 156:327
 Campbell WL, 157:29, 157:303
 Campeau RJ, 156:406
 Camputaro C, 157:997
 Capello W, 156:545
 Caputo GR, 157:9
 Cardoza JD, 156:725
 Carmody RF, 157:1357
 Caro JJ, 156:825
 Carpanzano CR, 157:1105
 Carpenter RJ Jr, 156:636
 Carrera GF, 156:131
 Carroll BA, 157:73
 Carty H, 156:635
 Casablanca G, 157:1181
 Casas JM, 156:1113
 Cascade PN, 157:777
 Caskey CI, 156:711
 Casola G, 157:33
 Cassady CI, 156:59
 Castañeda-Zúñiga WR, 156:1007,
 156:1087
 Castellino RA, 157:469
 Castillo M, 157:888
 Cataldo MF, 156:403
 Catena LM, 156:141
 Cattau EL Jr, 157:747
 Cavallino RP, 156:1253
 Cazenave FL, 156:395
 Çelik L, 156:751
 Cerqueira MD, 156:44
 Cervilla V, 157:523
 Chacko AK, 157:267
 Chakeres DW, 156:161
 Chan WC, 157:1341
 Chan WP, 157:799
 Chandnani V, 156:457
 Chang KH, 157:393
 Chang PJ, 157:412
 Channin DS, 157:1353
 Chapuis Y, 156:981
 Charboneau JW, 156:1081
 Charles HC, 156:105
 Charnsangavej C, 156:1025
 Chen HH, 156:858, 156:1314
 Chen MYM, 157:769
 Chen YM, 156:303
 Chetty N, 156:321, 157:291
 Chew FS, 156:200, 156:474,
 156:627, 156:724, 156:1016,
 156:1144, 157:44, 157:318,
 157:468, 157:792, 157:950,
 157:1278, 157:1352
 Chezmar JL, 157:885
 Chiang KS, 157:416
 Chisholm RJ, 157:873
 Choi H, 157:353
 Choi HY, 157:835
 Choyke PL, 156:407
 Christensen CW, 157:1227
 Christiansen J, 157:1199
 Christoph R, 156:125
 Chrousos GP, 156:39

Chu PK, 156:1059, 156:1245
 Cirkovic S, 156:408
 Clark D, 157:741
 Clark RA, 156:96, 157:490
 Clarke JTR, 157:819
 Claussen CD, 157:1253
 Cobby MJ, 157:1023
 Coblenz CL, 156:197
 Cochran S, 157:975
 Cogbill TH, 156:1105
 Cogen PH, 156:587, 156:791
 Cohen HL, 157:545
 Cohen L, 156:161
 Cohen MD, 156:345, 157:646
 Coldwell DM, 156:1101, 157:1005
 Colletti PM, 156:1205
 Collins MB, 157:199
 Collyer RT, 157:1079
 Compton CC, 157:499
 Conces DJ Jr, 156:717, 157:249
 Conner RT, 156:403
 Conoley PM, 157:1337
 Constantinou C, 157:721
 Conway WF, 157:789
 Cook LT, 156:1095, 157:1331
 Cooper CJ, 157:297, 157:747
 Cooper J, 157:545
 Cooperstein LA, 156:199
 Corson JD, 157:813
 Cory DA, 156:345
 Coscojuela P, 156:931, 156:1114
 Costello P, 156:1167
 Cotton PB, 156:975, 157:281
 Cotty P, 156:1327, 157:1127
 Cozzolluela R, 156:1113
 Cozzolino G, 157:886
 Crade M, 156:286, 157:480
 Cragg AH, 157:173
 Craig DA, 157:959
 Crain MR, 157:565, 157:575
 Crandall B, 157:1065
 Cronan JJ, 157:757, 157:1209
 Crow P, 156:559
 Cruz F, 156:405
 Cumming WA, 156:1227
 Cunningham JJ, 157:643
 Cunningham-Rundles S, 156:561
 Curnes JT, 156:1053
 Curry NS, 156:871
 Cutler GB Jr, 156:39
 Czervionke LF, 157:389

D

Dachman AH, 157:223
 Daffner RH, 156:332, 157:346
 D'Agostino HB, 157:33
 Dail DH, 156:985
 Dalinka M, 157:523
 Dalley RW, 157:837
 Damiano MA, 156:381
 Dammer M, 156:125
 Dang H, 156:471
 Dangman BC, 157:115
 Daniel TB, 156:875
 Daniels DL, 157:389
 Darcy MD, 156:385, 156:623,
 157:1126
 Daum-Kowalski R, 156:1321
 Davey DD, 156:287
 David CL, 156:1159
 Davis GB, 156:617
 Davis LM, 156:917
 Davis M, 157:647
 Davis PC, 156:1039, 156:1237,
 157:122, 157:200
 Davis S, 156:345
 Davros WJ, 156:493, 157:747
 Dawson SL, 157:491, 157:1263
 De Bandt M, 157:1356
 Debatin JF, 157:781, 157:981

Deck MDF, 157:1105
 Dee PM, 156:539
 Degryse HR, 157:1354
 DeLaPaz RL, 156:579
 Del Buono EA, 156:511
 DelMaschio A, 156:753
 DeMarco T, 157:851
 De Marcos JA, 156:931
 Demas BE, 156:989, 157:773
 Denaro CP, 157:851
 Denath FM, 156:1322
 Denny DR Jr, 157:1203
 Desai RK, 157:275, 157:787
 Desberg AL, 157:787
 De Schepper AM, 157:1354
 deSouza NM, 156:507
 Deutsch AL, 157:1239
 Deutsch L-S, 156:471
 De Wispelaere J-F, 157:1259
 Deyoe L, 157:1209
 Dicke KA, 157:461
 Dillon EH, 157:997
 Dillon WP, 156:689
 Dines KA, 157:25
 Dion JE, 157:1309
 Disler DG, 156:1016, 157:44
 Doan HT, 157:1299
 Dobben RL, 156:757
 Dobkin BL, 156:858, 156:1314
 Doda SS, 157:198
 Dodd GD III, 157:449
 Dodds WJ, 157:1213
 Do HM, 157:757, 157:1209
 Doi O, 156:921
 Dolenz K, 156:757
 Donald JJ, 157:287, 157:753
 Donaldson JS, 156:351
 Donoso L, 156:1114
 Doppman JL, 156:39
 Dorfman GS, 157:1209
 Doubilet PM, 157:1275
 Douek P, 156:1037
 Downey DB, 156:404
 Downey PR, 156:1199
 Doyle TB, 156:313
 Draganic M, 156:408
 Drane WE, 156:199
 Duberg A, 156:1245
 DuBrow RA, 156:1159
 Duckwiler GR, 157:1309
 Duda SH, 157:1253
 Dunham CM, 156:273, 157:1124
 Dunn RS, 156:1116
 Dunne PM, 157:1357
 Dunnick NR, 157:776, 157:781
 Dupuy D, 156:1167
 Duva-Frissora AD, 156:852,
 156:1301
 Dwyer AJ, 156:39
 Dwyer SJ III, 156:1279, 157:1331

E

Easter DW, 157:241
 Eckard DA, 157:1331
 Eckardt JJ, 157:347
 Edelstein G, 157:884
 Edgerton VR, 156:765
 Edwards DK III, 157:371
 Edwards MSB, 156:587, 156:791
 Effmann EL, 156:1209, 157:557
 Eggleston DE, 156:345
 Eggli KD, 157:539
 Egglin TK, 157:99, 157:727,
 157:967
 Ehara S, 156:1110
 Ehrlich SM, 156:367
 Eichelberger MR, 157:111
 Eidelman EM, 156:611
 Eidt JF, 156:639, 157:235
 Einstein DM, 157:275

Eisenberg P, 157:545
 Eisenberg RL, 156:944, 157:274
 Eisner DJ, 157:517
 Ekberg O, 156:293, 156:1181,
 157:647
 El Gammal T, 156:1075
 Elias ER, 157:549
 Elkadi T, 156:14
 El-Khoury GY, 156:1199, 157:685,
 157:813
 Ellis JH, 156:995, 157:999
 Ellis K, 156:669
 Ellwood RA, 157:1358
 El-Ramahi K, 157:867
 Elster AD, 156:157, 156:605,
 157:1129
 Embry RL, 156:1321
 Endo T, 157:971
 Engeler CE, 156:1087
 Engelke K, 157:1229
 Erickson SJ, 156:3, 156:131,
 156:539, 157:331, 157:1213
 Eschelman DJ, 156:846, 156:849,
 156:852, 156:854, 156:858,
 156:1288, 156:1295, 156:1301,
 156:1307, 156:1314, 157:1125
 Essinger A, 156:389
 Estes DN, 156:1328
 Ethier R, 157:843
 Evens RG, 156:400, 157:603
 Evens RG Jr, 157:603
 Evers K, 157:271
 Ezaki T, 156:868

F

Fache JS, 157:287, 157:485,
 157:753
 Faerber EN, 157:549
 Fagien M, 156:199
 Fallon M, 157:93
 Fanney D, 157:747
 Fatouros PP, 156:373
 Faulkner KG, 157:1229
 Fava M, 156:405
 Fay J, 156:467
 Fazekas F, 157:1317
 Federle MP, 157:303
 Feigin DS, 156:280, 157:1022
 Feinberg MJ, 156:293, 156:1181,
 157:647
 Feinstein KA, 156:1215
 Feld R, 156:737
 Feldman F, 156:121, 157:1127
 Fenke F, 156:125
 Fernandez MdP, 156:1171
 Fernbach SK, 156:137, 156:1215
 Ferrucci JT, 156:317, 156:867,
 156:869, 157:633
 Feuerstein IM, 156:39
 Fielding JR, 156:849, 156:1295
 Figley MM, 156:1100
 Figlin RA, 156:833
 Fillmore DJ, 157:1069
 Filly RA, 156:555
 Finberg HJ, 156:359
 Finch IJ, 157:179
 Findling JW, 156:39
 Fisher AR, 157:1189
 Fishman EK, 156:517, 156:711,
 156:715
 Fishman JE, 156:833
 Fishman M, 156:1005
 Fitz CR, 156:571
 Fitzgerald SW, 156:131, 157:307,
 157:331
 Flanders AE, 157:1299
 Fletcher BD, 157:825
 Flickinger FW, 156:1324
 Flower CDR, 156:1145
 Flye MW, 157:1195

Foley WD, 156:3, 157:331
 Foradori G, 156:405
 Forer LE, 157:747
 Formanek AG, 156:1033
 Fornage BD, 157:353
 Forrest JV, 156:1277, 157:47
 Forsberg DA, 156:200, 157:1127
 Foster E, 157:9
 Foster RG, 157:29
 Fouquet B, 156:1327, 157:1127
 Fournie B, 157:1128
 Francica G, 157:886
 Francis IR, 156:1113, 157:777, 157:999
 Franken EA, 156:177
 Frank JA, 156:407
 Frank RG, 156:865, 156:1326
 Franquet T, 156:1113
 Fraser RG, 157:630
 Frazier H, 157:1003
 Freeman NJ, 157:49, 157:59
 Freeny PC, 156:326, 157:1252
 Friedland GW, 157:330
 Friedman AC, 156:104, 157:49, 157:59, 157:516
 Friedman M, 156:1253
 Friedman PJ, 157:692
 Friloux L, 156:307
 Frisch RE, 157:99
 Fritz RC, 157:1126
 Fuchigami T, 156:741
 Fujishima M, 156:741, 156:965
 Fujita J, 156:1322
 Fujita M, 156:921
 Fukunaga T, 156:765
 Fullagar PR, 157:635
 Futerman C, 156:471

G

Gaeta M, 156:341, 157:1181
 Gagliardi RA, 157:922
 Galvin JR, 156:15
 Gamsu G, 156:281
 Gardner DJ, 157:403
 Garra BS, 156:493, 157:297, 157:747
 Garvin KL, 156:333
 Gatewood OMB, 156:638
 Gaux JC, 156:389
 Gavant ML, 157:415
 Gearhart JP, 157:1267
 Gebarski SS, 156:790, 156:1218
 Gehring BJ, 157:293
 Geisinger MA, 157:703
 Gelfand DW, 156:1, 156:303, 156:939, 157:196, 157:769
 Geller SC, 156:97, 157:967
 Gelman R, 156:51, 157:411
 Genant HK, 157:799, 157:1229
 Gens D, 156:51
 Gentry LR, 157:595
 Gerard EL, 157:99
 Gerard-McFarland EL, 156:724
 Gerard PS, 156:865, 156:1325
 Gerberding JL, 157:911
 Gerharter J, 157:523
 Gerscovich E, 156:1011
 Gervin AS, 157:789
 Ghose R, 156:1112
 Gianturco C, 156:757
 Giardina PJ, 156:561
 Gibbens DT, 156:849, 156:852, 156:854, 156:1295, 156:1301, 156:1307, 157:1125
 Gikas PW, 156:511
 Gilula LA, 157:105
 Ginals JM, 156:872
 Gindre T, 156:866
 Giorgio A, 157:886
 Girard MJ, 157:491

Giron G, 157:1181
 Giuliano AE, 157:21
 Glass P, 156:571
 Glass-Royal MC, 156:395, 156:493
 Glazer GM, 156:511
 Glazer HS, 156:45, 156:405, 157:181
 Glickman MG, 157:166
 Glick SN, 156:961, 157:311, 157:951
 Glover JR, 156:197
 Glüer C-C, 157:1229
 Goel S, 157:1225
 Goerg C, 156:949, 156:1185
 Goerg K, 156:949
 Gökmen E, 156:751
 Gold RH, 156:59, 157:21, 157:25, 157:365, 157:1028
 Goldberg BB, 156:99
 Goldberg HI, 156:1229
 Goldberg JA, 157:747
 Goldberg MA, 157:727
 Goldman MA, 157:545
 Goldberg ME, 157:1038
 Goldman SM, 157:517
 Golebiovski P, 156:916
 Gomes AS, 157:293
 Good BC, 156:1107
 Goodman P, 156:1189
 Goodman PC, 156:944, 157:274
 Gosink BB, 157:403
 Gotschall CS, 157:111
 Goupille P, 156:1327, 157:1127
 Gourley GR, 157:381
 Grambsch PM, 157:959
 Gramm HF, 156:748, 157:266
 Grant EG, 157:293, 157:975, 157:1065
 Grantham JJ, 156:501
 Grantham JR, 157:1126
 Grantmyre EB, 156:149
 Grassi CJ, 156:813
 Grattan-Smith JD, 156:785
 Graviss ER, 157:383
 Greene GM, 157:565, 157:575
 Greene R, 156:467
 Greenfield AJ, 157:923, 157:1125
 Greensite F, 156:307
 Greenspan A, 156:635, 156:1011
 Grenier N, 157:93
 Griscom NT, 156:371
 Grist TM, 156:105, 157:981
 Grix A, 156:635
 Gronemeyer SA, 157:861
 Groskin SA, 156:680, 156:960, 157:702
 Gross BR, 157:545
 Gross GW, 156:367
 Grossin M, 157:1356
 Grossman HB, 156:511, 157:999
 Grossman RI, 156:1229
 Guidici MAI, 157:817
 Guijo CG, 157:887
 Guimaraes AR, 157:99
 Guisto DF, 157:F789
 Gulliver DJ, 156:975, 157:281
 Günther RW, 156:125, 156:389, 157:883
 Gupta AK, 156:1257
 Gupta KL, 157:1087
 Gur D, 156:198, 156:1107
 Gurney JW, 157:461
 Gutierrez FR, 157:465
 Guzman S, 156:405
 Gyepes MT, 156:1208

H

Hackbarth DA, 156:539
 Hackney DB, 156:1074

Hadden TA, 156:801
 Hagler NG, 156:871
 Hahn PF, 156:235, 156:252, 156:317, 156:1163, 157:727, 157:1263
 Haik BG, 157:1087
 Haliloglu M, 156:1113
 Hall DA, 157:675
 Hall FM, 156:200, 156:637, 156:867, 156:872, 157:415, 157:644, 157:647, 157:883
 Haller JO, 157:553, 157:646, 157:1051
 Halvorsen RA Jr, 157:37
 Hamilton PA, 156:745
 Hamm B, 156:235, 156:245, 156:317
 Hammerman AM, 156:313
 Hamper UM, 156:401
 Han MC, 157:393, 157:697
 Han MH, 157:393
 Hanafee W, 156:1068, 157:768
 Hanna SL, 157:861
 Hansen ME, 157:967
 Hanto DW, 157:1195
 Harada K, 156:297
 Haramati N, 157:49, 157:59
 Harley JD, 157:807
 Harms GF, 156:925
 Harned RK, 156:481
 Harned RK II, 157:885
 Harnsberger HR, 157:147, 157:155, 157:161, 157:1093
 Harrell RS, 156:523
 Harris AB, 157:1072
 Harris HS, 156:875
 Harris MN, 156:866
 Harrison LA, 157:1331
 Harry P, 157:255
 Hart MN, 157:575
 Hasan D, 157:1325
 Hata K, 156:1115
 Hata T, 156:408, 156:636, 156:1115
 Hattery RR, 156:1081
 Hauge C, 157:1199
 Haughton VM, 157:389
 Hawkins IF Jr, 156:875
 Hawkins RA, 157:365
 Hayashi T, 156:1177
 Hayes CW, 157:789
 Hayes WS, 157:297, 157:747
 Hayman LA, 157:133
 Hazebrucq V, 156:981
 Heberger R, 156:343
 Hebrang A, 156:1091
 Heier LA, 157:1105
 Heiken JP, 157:1195
 Heim K, 157:715
 Heinz LM, 157:1258
 Heitmiller RF, 156:715
 Helms CA, 156:531, 157:1126
 Helvie MA, 157:711
 Hendee WR, 156:176, 156:1283
 Hendrick RE, 157:473
 Hendrix LE, 157:389
 Hennerici M, 156:873
 Henry M, 157:1003
 Henschke CI, 157:87
 Herlinger H, 156:731, 157:1189
 Herman TE, 156:151, 156:799, 157:375
 Hernandez RJ, 156:1029
 Hernigou A, 156:1324
 Herts BR, 157:1249
 Hertzberg BS, 157:73
 Hesselink JR, 156:1059, 156:1245
 Hessler C, 156:543
 Hicks ME, 156:385, 156:623, 157:1126
 Higashiyama M, 156:921

Higgins CB, 157:9
 Hillman BJ, 156:443
 Hilsenrath PE, 156:177
 Hirsch W, 157:1111
 Hise JH, 157:1291
 Hoeffner EG, 157:1227
 Hoefs J, 156:307
 Hofer HO, 156:113
 Hoffer FA, 157:559
 Hoffman AD, 156:1081
 Hoffman JC Jr, 156:1039, 156:1237, 157:200
 Hoffmann G, 156:265
 Hofmann AF, 157:33
 Hogg JC, 156:225
 Holder JC, 156:639
 Holland DG, 157:17
 Holthaus LH, 157:785
 Homer MJ, 157:645
 Honeyman JC, 156:1326
 Hong CY, 157:835, 157:943
 Hong R, 157:381
 Hopper DK, 157:1205
 Hopper KD, 156:1219
 Horii SC, 157:297, 157:747
 Houser OW, 156:1081
 Houssin D, 156:981
 Howard BA, 157:532
 Howards S, 157:337
 Howland WJ, 157:196
 Hricak H, 156:989
 Huang HK, 156:835
 Hubbard A, 157:119
 Hudgins PA, 156:1039, 156:1237
 Huijbregtse K, 157:495
 Hull JE, 156:403
 Hung W, 156:141
 Hunt S, 157:1093
 Hunter DW, 156:1007, 156:1087
 Hunter TB, 157:411
 Huppert PE, 157:1253
 Hutter RVP, 157:257

I

Idvall I, 156:634
 Iida M, 156:965
 Ikeda DM, 157:711
 Ikezoe J, 156:297
 Im J-G, 157:697
 Imaoka I, 157:1355
 Ingram JD, 156:571
 Inoue E, 156:921
 Irino S, 156:1322
 Irwin GAL, 156:486
 Irwin RS, 156:917
 Ishida H, 157:965
 Iwanaga S, 157:19
 Iwashita A, 156:741

J

Jackson JE, 157:291
 Jackson VP, 157:25, 157:481
 Jacobson AF, 157:807
 Jaeger Ph, 156:872
 Jafri SZH, 157:503
 Jahnke AH, 157:1015
 Jain R, 156:1112
 Jamshidian J, 156:1323
 Janney C, 157:648
 Janower ML, 157:196
 Jansen PLM, 157:495
 Javors BR, 156:1325
 Jeffrey RB Jr, 156:725, 156:749
 Jelinek JS, 157:1243
 Jendrisak M, 156:623
 Jenkins R, 156:1167
 Jensen ME, 157:1309
 Joffre F, 156:389
 Johnson CD, 156:93

Johnson JE, 156:131
 Johnson MB, 156:85
 Johnston DA, 157:353
 Johnston GS, 156:865
 Jones B, 156:517
 Jordan SG, 157:73
 Joseph S, 156:1257
 Jost RG, 157:81, 157:181

K

Kaalhus O, 156:1191
 Kadish EG, 157:49, 157:59
 Kaern K, 157:1221
 Kagetsu NJ, 157:645
 Kahn M-F, 157:1356
 Kalisher L, 157:257
 Kallman CE, 157:403
 Kamel F, 157:1353
 Kamenica S, 156:408
 Kamino K, 156:1177
 Kanal E, 157:850, 157:1111
 Kane NM, 157:777
 Kaneko M, 156:868
 Kanel GC, 156:91, 156:307
 Kang YS, 156:517
 Kaplan AS, 156:1109
 Kaplan PA, 156:333, 156:353, 157:650
 Kapoor DA, 157:509
 Karani J, 157:167
 Karasick D, 157:1029
 Karellas A, 156:781, 157:721
 Karnik S, 156:406
 Kartchner ZA, 156:406
 Kassing PJ, 157:1341
 Kassner EG, 157:1039
 Kathol MH, 156:1199, 157:813
 Kato N, 157:1187
 Kattan M, 156:866
 Kattapuram SV, 157:935
 Katz RD, 157:365
 Katz RL, 156:199
 Kaude JV, 156:199, 156:1326
 Kaveggia LP, 157:975
 Kazerooni E, 156:543
 Keefe B, 156:1195
 Keenleyside A, 157:648
 Kehler M, 156:345
 Kelsch RC, 156:1029
 Kennedy DN, 157:99
 Kerr R, 157:1239
 Kerut T, 156:367
 Kesaria AC, 157:885
 Kessler LS, 156:1326
 Khandelwal KC, 157:416, 157:1225
 Kiernan H, 156:121, 157:1127
 Kier R, 156:527
 Killian JM, 157:585
 Kim D, 156:173, 157:521
 Kim EE, 156:780, 156:1025, 157:352, 157:353
 Kim IO, 157:697
 Kim IY, 157:198
 Kim PN, 157:198
 Kim SH, 157:835, 157:943
 Kim SJ, 157:697
 Kimme-Smith C, 156:234, 156:449, 156:954, 157:408, 157:975
 Kimura K, 157:397
 Kimura Y, 156:965
 Kinard RE, 156:1321
 King AR, 156:1199
 King BF, 156:1081
 King JG, 156:287
 Kinoshita T, 156:69
 Kipper MS, 156:500
 Kirchhoff R, 156:874
 Kirk IR, 156:199
 Kirkpatrick JA Jr, 157:447, 157:630
 Kirshenbaum GL, 156:1253

Kirshenbaum KJ, 156:1253
 Kirshenbaum MD, 157:411
 Kitao M, 156:1115
 Kivelitz D, 157:731
 Kjørstad K, 156:1191
 Klein DS, 156:633
 Kleinert G, 157:1317
 Kleinert R, 157:1317
 Kleinhoffer MA, 156:385, 156:623
 Klein JS, 156:281
 Kleinman PK, 156:576, 156:775, 156:781
 Kliewer MA, 157:73
 Klukowicz A, 156:1110
 Knapp PH, 157:87
 Kneeland JB, 156:131
 Knudson GJ, 156:539
 Ko YT, 157:41
 Kobayashi K, 156:297
 Koch E, 156:113
 Koch P, 156:265
 Koch SR, 156:1001
 Kochhar R, 156:1111
 Kodama K, 156:921
 Koffman CG, 156:507
 Kogutt MS, 156:634
 Kolberg H, 157:119
 Kolin A, 156:745
 Kondo C, 157:9
 Korobkin M, 156:1113, 157:520, 157:777, 157:919
 Korula J, 156:85
 Koslow AR, 157:199
 Kosuge T, 156:69
 Kothari K, 157:267
 Kotlyarov E, 156:865
 Kotner LM Jr, 156:313
 Kozuka T, 156:297
 Krabbenhoft KL, 157:631
 Kraft KA, 156:373
 Krakowski FM, 157:196
 Kransdorf MJ, 157:684, 157:1243
 Krauthamer R, 156:763
 Kressel HY, 157:93
 Kricheff II, 156:611, 156:1110
 Krige JEJ, 156:1263
 Kroll SS, 156:1159
 Kromhout J, 156:202
 Kronthal AJ, 156:517, 156:715
 Kucharczyk J, 156:1133, 157:123
 Kucharczyk W, 157:123
 Kuhlman JE, 156:517, 156:715
 Kuhn JP, 157:341
 Kuipers D, 156:1017
 Kumar R, 156:1189
 Kumar S, 156:1257
 Kuriyama K, 156:921
 Kuroda C, 156:921
 Kursunoglu-Brahme S, 156:457
 Kurtz AB, 156:99, 156:737
 Kusano S, 157:971
 Kushner DC, 156:141

L

Lachman RS, 156:149
 Laine FJ, 156:373
 Laing FC, 157:469
 Lake JR, 157:851
 Lally JF, 157:1123
 Lamb MN, 156:1261
 Lambiase RE, 157:1209
 Lammert GK, 157:703
 Land P, 157:799
 Lane JL, 157:1299
 Lang EK, 156:870, 157:77
 Lang EV, 156:1225
 Lang NP, 157:235
 Lang P, 157:1229
 Langer BG, 157:1357
 Langston JW, 157:415, 157:861

Lantz PE, 156:1033
 Larcos G, 157:527
 LaRusso NF, 157:959
 La Spada F, 157:1181
 Lassoued S, 157:1128
 Laufer I, 156:731, 156:955, 157:223, 157:1189
 Lautin EM, 157:49, 157:59
 Lautin JL, 157:49, 157:59
 Lawson TL, 157:331
 Lebowitz RL, 156:365, 156:407, 157:115, 157:1059
 Lechner H, 157:1317
 Lecky JW, 157:29
 Lee DH, 157:41
 Lee G, 156:917
 Lee JH, 157:393
 Lee JKT, 157:81
 Lee KF, 156:1252
 Lee KP, 156:85
 Lee KS, 157:198, 157:697
 Lee KY, 157:29
 Lee MJ, 156:97, 156:317, 156:1163, 157:499, 157:1263
 Lee N, 157:1087
 Lee YY, 157:416, 157:888
 Leeba J, 156:636
 Leithiser RE, 156:255
 Leonidas JC, 157:553
 Leopold GR, 156:867
 Letourneau JG, 156:1087, 157:37
 Leung AN, 157:693
 Levenson H, 156:307
 Leventhal BG, 157:1267
 Levin M, 157:1079
 Levine D, 157:371
 Levine E, 156:501
 Levine FJ, 157:923
 Levine MS, 156:731, 156:955, 157:319, 157:1189
 Levy IM, 156:117
 Levy LM, 157:585
 Lew R, 156:917
 Lewis D, 156:1167
 Lewis ER, 156:711
 L'Hoste P, 157:255
 Libshitz HI, 156:199, 156:1159
 Lida M, 156:741
 Liddell RM, 157:1273
 Lieberman JM, 156:870
 Liem MD, 156:769
 Lien HH, 156:1191, 157:1221
 Lightdale C, 156:63
 Lillington GA, 156:404
 Lim JH, 157:1, 157:41
 Lim T-H, 157:943
 Lin DTC, 157:1079
 Linder J, 157:461
 Ling A, 156:39
 Linn MR, 157:533
 Lipchik EO, 156:823, 157:331, 157:1360
 Lipsky BA, 157:807
 Litt AW, 156:611
 Liu J-B, 156:99
 Liu T-H, 157:21
 Llewellyn CH, 157:785
 Llewellyn HJ, 156:467
 Loes DJ, 156:579, 157:565, 157:575
 Logan-Young W, 157:267
 Lones M, 157:1309
 Longmaid HE III, 156:492
 Longmate JA, 156:1326
 Loriaux DL, 156:39
 Lorigan JG, 157:1279
 Lossef SV, 157:882
 Lou SL, 156:835
 Loyer EM, 156:1159
 Lu C-T, 157:177
 Lucas D, 156:77

Luethke JM, 156:381
 Luisiri A, 157:383
 Lushington JA Jr, 157:1355
 Lycke G, 156:77

M

Mabry MR, 157:609
 MacCarty RL, 157:959
 MacEwan DW, 156:1188
 Mack LA, 156:359
 Macken MB, 156:149
 Madewell JE, 157:631
 Madrazo BL, 157:503
 Mafee MF, 157:1099
 Magaram DL, 156:863
 Magen AB, 157:817
 Majd M, 157:539
 Majoie CBLM, 157:495
 Majumdar S, 157:799, 157:1229
 Makuuchi M, 156:69
 Malchow SC, 157:81
 Malik AK, 156:1111
 Mallada JJ, 157:887
 Malt RA, 157:499
 Manaster BJ, 157:523
 Mandel FS, 157:545
 Mandel L, 157:553
 Mandell SH, 156:511
 Mann FA, 157:105, 157:533
 Mann R, 157:648
 Maravilla KR, 157:837
 Marchand T, 156:493
 Marcus ML, 156:15
 Marcuzzi DW, 157:873
 Marder DM, 156:636
 Marglin SI, 157:469
 Mari G, 156:408, 156:636
 Marincek B, 156:113
 Mark LP, 157:389
 Markowitz D, 157:1203
 Markowitz RI, 157:119
 Marks SC Jr, 156:775
 Marks TI, 156:1029
 Martel W, 157:1023
 Martin LC, 156:852, 156:858, 156:1301, 156:1314
 Martin TD, 156:1155
 Martineau BS, 156:863
 Martinez S, 156:200, 157:1127
 Martinez-Noguera A, 156:1114
 Marx M, 156:864
 Marx MV, 157:919
 Masamune O, 157:965
 Mashankar A, 157:1225
 Maskovic J, 156:1091
 Mast J, 157:1105
 Mata J, 156:931
 Matalon TAS, 157:1359
 Mathiesen TI, 156:634
 Mathieson JR, 157:33
 Matsuda M, 156:1110
 Matsui K, 157:991
 Matsui T, 156:741
 Matsumoto T, 156:965
 Matsushita T, 157:1187
 Matthews JG II, 156:1011
 Mattox HE, 157:769
 Mavligit GM, 157:1279
 Mawad ME, 157:416
 Mayer K, 157:1353
 Mayfield WR, 156:1155
 McCann SB, 157:197
 McCauley RGK, 157:549
 McClennan BL, 156:841, 156:866
 McClure RD, 156:989
 McCullough J, 156:903
 McCullough NB, 157:999
 McCuskey WH, 157:648
 McDonald V, 157:1359
 McDowell J, 156:870

McEwen KL, 157:824
 McGahan JP, 156:547, 156:636, 157:223
 McGeady SJ, 156:367
 McGhee RA Jr, 156:457
 McGorray SP, 157:761
 McGregor M, 156:825
 McIvor J, 157:1125
 McLachlan SJ, 156:611
 McLellan GL, 156:397
 McLelland R, 157:473
 McLeod RA, 156:337
 McLoud TC, 156:1145
 McNeely GF, 156:1321
 Mehta RC, 157:595
 Meilstrup JW, 157:1205
 Meiners LC, 157:1325
 Meis JM, 157:1243
 Melanson D, 157:843
 Menu Y, 157:413
 Merchant NH, 157:416, 157:1225
 Merchant S, 156:406, 157:201
 Merine D, 157:197
 Merritt TA, 157:371
 Merton DA, 156:99
 Mewissen MW, 156:823, 157:1360
 Meyer JS, 157:559
 Mezwa DG, 157:503
 Miers JF, 156:567
 Mihara F, 157:1087
 Milants WP, 157:1354
 Miller DL, 156:638
 Miller FH, 157:307
 Miller R, 156:343
 Miller RA, 156:1110
 Miller WJ, 157:29, 157:303
 Millmond SH, 157:517
 Millward SF, 156:1261
 Milne N, 157:412
 Milner LB, 156:948
 Mink JH, 156:765, 157:1239
 Mintonovitch J, 156:1133
 Minutoli A, 156:341, 157:1181
 Mirfakhraee M, 156:801
 Mirvis SE, 156:51, 156:273, 156:865, 157:411, 157:1124
 Mirza W, 156:605
 Mistry A, 157:201
 Mitchell CS, 157:385
 Mitchell SE, 156:327
 Mitchell SP, 156:404
 Mitnick JS, 156:866
 Mittelstaedt CA, 156:1195
 Miura K, 156:1177
 Miura T, 156:1177
 Miyake H, 157:19
 Mizushima A, 156:807
 Mochizuki T, 156:868
 Modic MT, 156:235, 156:239
 Mohan C, 157:413
 Moldawer NP, 156:833
 Molina PL, 156:45, 156:405, 157:181, 157:465
 Molpus WM, 156:353
 Monsees BS, 157:533
 Moody DM, 157:1295
 Moore TE, 156:1199, 157:813
 Moorjani V, 157:1225
 Morehouse HT, 156:117
 Mori H, 157:19
 Morikawa P, 157:965
 Morimoto S, 156:297
 Morin de Finfe C-H, 156:866
 Morin LRM, 156:1115
 Morin RL, 156:925
 Morparia H, 156:406
 Morrison MC, 156:1163
 Morton MJ, 156:337
 Moseley HS, 156:539
 Moseley ME, 156:1133

Moser RP, 156:481, 156:1010
 Moser RP Jr, 157:526, 157:817
 Moskos MM, 156:852, 156:1301
 Moumdjian R, 157:843
 Mrose HE, 156:467
 Muelenaer AA Jr, 156:1209
 Mueller DP, 157:1282
 Mueller PR, 156:97, 156:1163, 157:235, 157:491, 157:727, 157:1263
 Mukherjee M, 157:198
 Müller E, 157:715
 Müller NL, 157:693, 157:1163
 Mulligan SA, 156:930
 Mulliken JB, 157:559
 Munk PL, 157:471, 157:1079
 Murayama S, 157:1087
 Murphy WA Jr, 157:533
 Murray WT, 157:649
 Mussurakis S, 157:882
 Myers JL, 156:925

N

Nabhani HA, 156:871
 Nadel L, 156:373
 Nadel S, 156:957
 Nadimpalli SR, 156:1253
 Naganuma H, 157:965
 Nagi B, 156:1111
 Nahum H, 157:413
 Nakagawa N, 157:173
 Nakagawa T, 157:1187
 Nakamura K, 157:1187
 Nakao N, 156:1177
 Narumi Y, 156:921
 Nathan MH, 156:633
 Nelson B, 157:1093
 Nelson DW, 157:340, 157:1238
 Nelson NL, 156:333
 Nemcek AA Jr, 157:307
 Neumann CH, 157:1015
 Newell JD II, 156:381
 Newman GE, 157:981
 Newman KD, 157:111
 Neylan JF, 156:1171
 Nielsen MB, 157:1199
 Nieman LK, 156:39
 Nikolic G, 156:408
 Nino-Murcia M, 157:412
 Nipper ML, 157:1291
 Nisce L, 157:87
 Nishimura T, 156:868
 Nizawa M, 157:965
 Noguchi A, 157:383
 Nomura F, 156:707
 Norman A, 156:116
 Norman G, 156:198
 Northington FJ, 156:567
 Northway WH Jr, 156:681
 Novy SB, 156:774
 Nowels K, 156:77
 Nuruddin RN, 156:989

O

Oakes WJ, 156:1053
 Oakley GJ, 157:37
 Oates E, 156:407
 O'Brien MJ, 156:968
 O'Connor JF, 156:845, 156:846, 156:849, 156:852, 156:854, 156:858, 156:1287, 156:1288, 156:1295, 156:1301, 156:1307, 156:1314
 Offenbacher H, 157:1317
 O'Grady J, 157:167
 Ohi M, 157:1187
 Ohnishi M, 156:1177
 Okada Y, 157:971
 Okamoto E, 156:1177

O'Keeffe FN, 156:145
 Okizuka H, 157:1355
 Olbert F, 157:1353
 Olcott EW, 156:725, 157:911
 Olmsted WW, 156:481
 Olson RA, 156:1171
 Omae T, 157:397
 Onik G, 156:531
 Optican RJ, 157:557
 Osborn AG, 157:147, 157:584
 Osborn RE, 157:385
 Osterman FA Jr, 156:327
 Ostrum DS, 157:1358
 Oteo JA, 156:1113
 Ott DJ, 156:303, 156:939, 157:769
 Ott R, 156:471
 Owen DA, 156:177
 Ownby DR, 156:903
 Ozaki H, 156:69
 Ozonoff MB, 156:154

P

Pages M, 157:1128
 Palmer R, 156:1199
 Palmer WE, 156:724, 156:1144, 157:950
 Panaccione JL, 157:761
 Panageas E, 156:846, 156:1288
 Pandolfo I, 156:341, 157:1181
 Panushka C, 157:37
 Papanicolaou N, 157:315
 Parienté D, 156:981
 Park C, 157:119
 Park I-S, 157:835, 157:943
 Parker DR, 156:849, 156:852, 156:854, 156:1295, 156:1301, 156:1307
 Parker GD, 157:161
 Parsa MB, 156:1095
 Pashu-Cerecina V, 156:408
 Pass HI, 156:39
 Patange V, 157:1225
 Patel V, 156:406
 Patel VH, 157:201
 Patel YD, 157:199
 Patet JD, 156:1037
 Patriquin H, 156:364
 Patt RH, 157:297
 Patten RM, 156:359, 156:1101
 Patterson SK, 156:995
 Pavlicek W, 157:98
 Payer F, 157:1317
 Peck WW, 156:586, 157:523
 Pecoraro RE, 157:807
 Pedersen JF, 157:1199
 Peene P, 156:640
 Peix J-L, 156:866
 Pelc NJ, 157:139
 Pelman RS, 157:1273
 Penn-Jones K, 156:403
 Perlash I, 157:412
 Perlman EJ, 157:1267
 Perrella RR, 157:293, 157:975, 157:1065
 Pervulov S, 156:408
 Peterman SB, 156:1039
 Peters JJM, 156:202
 Peters ME, 157:381
 Peters PE, 156:265, 157:644, 157:731
 Petersen SA, 157:1015
 Petronis J, 157:517
 Pfeifer EA, 156:1324
 Philippe N, 156:1037
 Phillips WC Jr, 156:199
 Picus D, 156:385, 156:623, 157:1126
 Pinckney LE, 156:1225
 Pinna A, 157:29
 Pinto RS, 156:611

Pircher W, 157:731
 Plainfosse MCh, 156:1324
 Platt JF, 156:995, 157:999
 Platt LD, 156:1205
 Plewes DB, 157:359
 Poetter R, 156:265
 Poey C, 157:1128
 Pollak JS, 157:1203
 Pomeroy OH, 156:858, 156:1314
 Poon PY, 156:404
 Porter DH, 156:173, 157:521
 Porter FR, 157:195
 Posalaky IP, 157:69
 Posner M, 157:553
 Potchen EJ, 156:475, 157:883, 157:884
 Potchen JE, 156:475
 Pottmeyer A, 156:870
 Poulton TB, 156:201
 Pozniak MA, 156:874
 Pracros J-P, 156:866
 Prando A, 156:871
 Press HC Jr, 156:871
 Prewitt LH Jr, 157:549
 Preziosi TJ, 157:585
 Price DB, 156:1047
 Prince MR, 157:1278
 Pursell SH, 156:1001
 Putnam W, 157:281

Q

Quinn SF, 156:539
 Quint DJ, 156:200
 Quint LE, 156:511, 157:17, 157:777

R

Rabinov JD, 156:854, 156:1307
 Raby N, 157:167
 Radin DR, 156:91, 156:487, 157:45, 157:955
 Radner H, 157:1317
 Rafii M, 157:1249
 Ragavendra N, 157:293, 157:1065
 Railhac J-J, 157:1128
 Rak KM, 156:381
 Ralls PW, 156:85, 156:874, 156:1205, 156:874 Marinelli DL
 Ramos LMP, 157:1325
 Ramsey RG, 156:181
 Randall PA, 157:834
 Rao AS, 156:1257
 Rao VRK, 156:1257
 Rappaport DC, 156:1227, 157:761
 Raptopoulos V, 156:917, 157:721
 Rasmussen OQ, 157:1199
 Rattner DW, 156:1163, 157:235
 Ravimandalam K, 156:1257
 Rawat B, 156:73, 157:485
 Rawlinson KF, 157:545
 Raynaud A, 156:389
 Reale FR, 157:721
 Reaman G, 156:155
 Reddy PK, 157:69, 157:509
 Reed EC, 157:461
 Reeder JWAJ, 157:495
 Reers B, 157:731
 Reidy JF, 156:507
 Reinhart M, 156:635
 Reiser M, 157:731
 Reiter AA, 156:408
 Remley K, 156:1069
 Renfrew DL, 157:685
 Rennard SI, 157:461
 Rennie D, 156:1109
 Resch H, 156:1327
 Resnick D, 157:523
 Revenis ME, 156:571
 Reynolds HE, 157:25, 157:481
 Rice R, 157:281

Rice S, 156:85
 Rice TW, 157:703
 Richards TL, 157:1073
 Richardson DN, 156:157
 Richardson P, 156:273
 Richli WR, 156:1025
 Richmond JM, 156:775
 Riles TS, 156:611
 Rimo DL, 156:149
 Rinkel GJE, 157:1325
 Rissius B, 157:703
 Rivitz SM, 157:950
 Robbins RA, 157:461
 Roberts AC, 156:617
 Roddie ME, 156:321, 157:291
 Rohrmann CA Jr, 157:310
 Rollins ES, 156:385
 Romo LV, 156:846, 156:849, 156:1288, 156:1295
 Ros PR, 156:481, 156:1227, 157:761
 Rosario JA, 157:585
 Rosato EF, 157:1189
 Rose BS, 156:201
 Rosen BR, 157:99
 Rosen G, 157:347
 Rosen MP, 156:846, 156:1288, 157:923
 Rosenberg BF, 157:503
 Rosenberg HK, 157:119
 Rosenberg MA, 157:498
 Rosenburg MA, 156:456
 Rosendaal FR, 157:1352
 Rosenthal DI, 157:935
 Rosenthal RE, 157:602
 Rosenthal SJ, 157:1331
 Rothschild B, 157:415
 Rothstein RD, 156:955
 Rousseau H, 156:389
 Rozanes I, 156:751
 Rubens DJ, 156:343, 157:267
 Rubens JR, 156:467
 Rubesin SE, 156:731, 157:1189
 Rubin GD, 156:749
 Rubio G, 157:887
 Ruiz ME, 156:131
 Rumack CM, 157:1272
 Rummeny E, 156:265, 157:731
 Russi EG, 157:1181
 Ryals TJ, 157:565, 157:575
 Ryan T, 156:717

S

Sachs PB, 157:703
 Sack K, 157:799
 Sacks D, 156:873, 157:200
 Sadriah K, 156:1323
 Safirstein BH, 156:1110
 Sagel SS, 156:45, 156:181, 156:405, 157:181, 157:465, 157:643
 Sahn DJ, 156:14, 156:916
 Saini S, 156:97, 156:235, 156:236, 156:317, 156:1163, 157:491, 157:499, 157:727, 157:1263
 Saka H, 156:707
 Sakai S, 156:707
 Sakai T, 156:965
 Salazar J, 156:1328
 Salinas-Madrigal L, 157:383
 Salmon CJ, 157:947
 Saloner D, 157:139
 Sammons N, 156:903
 Samuels BI, 156:1025
 Sanders JB, 157:495
 Sargent SK, 156:559
 Sarr MG, 156:93
 Sarrafizadeh M, 157:199
 Sartoris DJ, 156:130, 156:784
 Sarwar M, 157:842

Sato K, 156:1322
 Sato Y, 156:579, 157:565, 157:575
 Savader BL, 156:401
 Savader SJ, 156:327
 Sawhney S, 156:1112
 Sax EJ, 156:858, 156:1314
 Saxon RR, 156:281
 Scanlan KA, 156:1267
 Schaefer KM, 156:467
 Schatzki SC, 156:554, 156:1024, 156:1180, 157:110, 157:280, 157:720, 157:974
 Scheiner JD, 156:731
 Scherer LR, 157:1267
 Schiebler ML, 157:93, 157:707
 Schlam BW, 157:521
 Schlesinger AE, 156:1029
 Schmalbrock P, 156:161
 Schmidt R, 157:1317
 Schnitker JC, 157:1291
 Schoenfeld AH, 157:49, 157:59
 Schofield DE, 157:1273
 Schröcksnadel H, 157:715
 Schteingart CD, 157:33
 Schultz DS, 156:199
 Schuttevaer HM, 156:1017
 Schwartz AN, 157:923
 Schwartz LH, 157:1117
 Schwartzberg St, 156:611
 Schweitzer ME, 157:523
 Schwerk WB, 156:949, 156:1185
 Scorpio R, 156:273
 Sebes JI, 157:415
 Seboldt H, 157:1253
 Secaf E, 156:989
 Seeger LL, 157:347
 Segal JL, 157:412
 Seibert JJ, 156:353, 156:567
 Seidel FG, 157:341
 Semelka R, 157:9
 Sen KK, 157:414
 Seneterre E, 156:317
 Setiawan AT, 156:523
 Sevik RJ, 156:1133
 Shah A, 157:449
 Shanley DJ, 156:1321
 Sharif H, 157:741
 Sharma B, 156:870
 Sharma OP, 157:413, 157:416, 157:414
 Sheffner SE, 156:995
 Shellock FG, 156:765, 157:1239
 Shereff MJ, 156:131
 Sherman JL, 156:1219
 Sheth S, 156:401
 Shiga M, 157:19
 Shigemitsu O, 157:19
 Shimakawa A, 157:9, 157:139
 Shimokata K, 156:707
 Shiozaki H, 156:297
 Shogen K, 156:297
 Sialer G, 156:113
 Siegel EL, 156:1095
 Siegel HA, 156:316, 157:380, 157:494
 Siegel JB, 156:173
 Siegel ME, 156:762
 Siegel MJ, 156:45, 156:151, 156:799, 157:375
 Sierra AE, 156:475
 Sila CA, 157:1297
 Silberstein MJ, 157:383
 Silva E, 156:307
 Silverman PM, 156:395, 157:297, 157:747
 Silverstone DZ, 156:173
 Sim FH, 156:337
 Simeone JF, 156:1163, 157:223
 Simon JH, 157:267
 Simon M, 157:517

Simpson W, 156:559
 Singer AM, 157:417
 Singson RD, 156:121, 157:1127
 Sironi S, 156:753
 Siviti CJ, 156:141, 157:111
 Skezas NW, 157:1357
 Skolnick ML, 156:984
 Skorton DJ, 156:15
 Skucas J, 156:730
 Slifer KJ, 156:403
 Slone RM, 156:863, 156:1155
 Slusher SL, 156:501
 Smadja M, 157:1356
 Smith AS, 156:807
 Smith C, 156:201
 Smith JA, 156:345
 Smith JW, 156:131
 Smith PL, 156:474
 Smith TP, 157:173
 Smith WL, 156:177
 Smith WS, 157:1003
 Smoker WRK, 157:155
 Snow RC, 157:99
 Soberman N, 157:553
 Solomon DJ, 157:645
 Solomon SL, 156:405, 157:181
 Soloway RD, 156:493
 Someshwar R, 156:406
 Sonda LP, 156:995
 Song MG, 157:835, 157:943
 Sonkens J, 157:1093
 Soo YS, 157:1129
 Sorensen AG, 157:99
 Sorenson JA, 157:1324
 Sostman HD, 156:105, 157:981
 Soto B, 156:930
 Souillet G, 156:1037
 Soulen RL, 157:1227
 Spencer RP, 156:798
 Spevak MR, 156:775, 156:781
 Spiegel G, 157:1249
 Spigos DG, 157:1357
 Sprayregen S, 157:49, 157:59
 Spring BI, 157:707
 Spritzer CE, 157:781, 157:981
 Stafford SA, 156:822
 Stallard D, 157:197
 Stanford W, 156:15
 Stanley MD, 156:403
 Stanley RJ, 156:1266
 Stanojevic M, 156:408
 Stansberry SD, 156:145
 Staples CA, 157:693
 Staron R, 156:121, 157:1127
 Steen RG, 157:243
 Steinberg FL, 157:1069
 Steinke W, 156:873
 Steinman RM, 157:761
 Stelling CB, 156:287
 Stephens DH, 156:93
 Stern EJ, 157:947
 Stevens MP, 157:799
 Stevens SD, 157:1195
 Stewart BK, 156:835
 Stewart ET, 157:1213
 Stewart IET, 157:646
 Stieber AC, 157:29
 Stigers KB, 156:287
 Stoller DW, 157:799
 Storella JM, 156:173
 Strasser K, 157:715
 Straub WH, 156:1107
 Stringer DA, 157:819
 Strong M, 157:341
 Strother CM, 157:866, 157:1324
 St. Ville EW, 157:503
 Sugimura K, 157:1355
 Sugisawa M, 156:1110
 Suhr GM, 157:1355

Sundaram M, 157:197, 157:648, 157:1035
 Sunshine JH, 157:609, 157:1341
 Surratt RS, 156:623, 157:1126
 Susman N, 156:400
 Sutton RT, 157:527
 Suzuki K, 157:19
 Svetkey LP, 157:981
 Swan JS, 156:545
 Swanson D, 156:77
 Swanson DP, 157:1153
 Swartz R, 157:1023
 Sweet C, 157:1128
 Sweet DE, 157:341
 Swensen SJ, 156:925
 Swischuk LE, 156:145
 Sylvester P, 157:1354
 Szabo RM, 156:1011
 Szapiro N, 157:255
 Szumowski J, 156:1059, 157:267

T

Taccagni GL, 156:753
 Tada S, 156:741
 Tagliabue JR, 157:275
 Takahashi M, 156:868
 Takashima S, 156:297
 Takayama T, 156:69
 Takayasu Y, 156:1177
 Takebayashi S, 157:991
 Takehara Y, 156:868
 Takeuchi N, 156:297
 Talner LB, 156:985, 156:1005
 Tampas JP, 156:938
 Tampieri D, 157:843
 Tanghe HLJ, 157:1325
 Tarazov PG, 157:887
 Tarr RW, 156:807
 Tart RP, 156:863
 Tarver RD, 156:717, 157:249
 Tateishi R, 156:921
 Taupitz M, 156:317
 Taylor AJ, 157:1213
 Taylor BJ, 156:567
 Taylor DB, 157:819
 Taylor FC, 157:177
 Taylor GA, 156:141, 156:571, 157:111, 157:1267
 Teefey SA, 156:945
 Teitelbaum GP, 156:395
 Tempany CMC, 156:517
 Templeton AW, 156:1279, 157:1331
 Teplick SK, 157:235, 157:951
 Terada N, 157:1187
 Terasaki K, 156:77
 Terblanche J, 156:1263
 Tersegno MM, 156:869
 Tessier FN, 157:293, 157:1065
 te Strake L, 157:741
 Thakur M, 157:414
 Thieme GA, 157:1205
 Thoeni RF, 156:909
 Thomas BM, 156:197
 Thomas P, 156:404
 Thomas S, 157:167
 Thompson R, 156:155
 Thorner P, 157:819
 Thrall JH, 156:1273
 Thurmond AS, 156:33, 157:415
 Tien RD, 156:1059, 156:1245, 157:123, 157:1283
 Tisnado J, 157:172
 Tobin GR, 156:1001
 Tomac B, 156:1091
 Tomiyama N, 156:297
 Tomlanovich M, 156:903
 Torres GM, 157:761
 Torres W, 157:223
 Torrisi J, 157:646
 Totterman SM, 156:343, 157:267

Totty WG, **157:81**
 Towbin R, **156:345**
 Towers MJ, **156:404, 156:745**
 Townsend RR, **156:969**
 Trackler RT, **156:622**
 Tran-Dinh HD, **157:1129**
 Tran-Minh VA, **156:866, 156:1037**
 Traugher PD, **157:649**
 Travelli R, **156:1105**
 Travis WD, **156:39**
 Trefelner E, **156:599**
 Trigaux J-P, **157:1259**
 Trindade E, **156:825**
 Tristan TA, **156:570**
 Tropé C, **157:1221**
 Troupin RH, **157:271**
 Truwit CL, **157:851**
 Tsuchiya T, **157:397**
 Tsuruda JS, **156:1069, 157:139**
 Tu RK, **156:1111, 157:381**
 Tublin ME, **157:449**
 Tucker MS, **156:1195**
 Tung GA, **157:315**
 Turner ML, **156:769**
 Twickler DM, **156:523**

U

Udani RJ, **157:416**
 Uflacker R, **157:885**
 Umali C, **156:917**
 Underberg-Davis S, **157:319**
 Unger JM, **156:1111**
 Unni KK, **156:337**
 Unni M, **156:1257**
 Usselman JA, **156:394**

V

Valat J-P, **156:1327, 157:1127**
 Valji K, **156:617, 157:932**
 Valk J, **157:1130**
 Valk PE, **156:689**
 Van Beers B, **157:1259**
 Van Blarcom ST, **156:1328**
 Vandermarck P, **156:587**
 Vandemark RM, **156:638**
 van der Heul RO, **156:1017**
 Van Erp JS, **156:511**
 van Fraeyenhoven L, **157:1128**
 van Gijn J, **157:1325**

van Holsbeeck M, **157:1128**
 Vannier MW, **157:81**
 vanSonnenberg E, **157:33, 157:223**
 Van Thiel DH, **157:1111**
 Varache N, **157:255**
 Varma DGK, **156:406, 156:1025, 157:353**
 Vassallo P, **156:265, 157:644, 157:731**
 Vaughan WP, **157:461**
 Vazquez MF, **156:866**
 Velez MA, **157:235**
 Vellet AD, **156:520, 157:471, 157:1079**
 Venbrux AC, **156:327**
 Verbeeten B Jr, **156:202**
 Vermeulen M, **157:1325**
 Vernon SW, **157:1337**
 Vilgrain V, **157:413**
 Vine HS, **156:154**
 Viñuela F, **157:1309**
 Vix VA, **157:249**
 Volta S, **156:341, 157:1181**
 von Schulthess GK, **156:1113**
 von Sinner W, **157:741**
 Vorwerk D, **156:389**

W

Wack JP, **156:864**
 Wagner ML, **156:785**
 Walker CW, **156:255, 156:353**
 Wall SD, **157:911**
 Wallace S, **156:757, 156:1025, 157:1279**
 Walling A, **156:539**
 Walmsley S, **156:745**
 Walter JF, **156:749**
 Walter R, **156:77**
 Waltman AC, **157:967, 157:1069**
 Wandtke JC, **157:359**
 Wapner KL, **157:1029**
 Warnock ML, **157:947**
 Warshaw DM, **156:1195**
 Warshaw AL, **156:97**
 Wasserman NF, **157:69, 157:509**
 Watanabe A, **156:707**
 Watson L, **157:337**
 Webb JAW, **156:985**
 Webb WR, **156:281, 157:254, 157:947**

Weber A, **156:957**
 Weber TM, **157:73**
 Weigle JB, **157:513**
 Weinberger E, **157:1273**
 Weinreb JC, **156:611**
 Weinstein JM, **157:595**
 Weisner KM, **156:1033**
 Weiss KL, **156:117**
 Weissleder R, **157:468, 157:792**
 Weissman BN, **156:120, 156:1036**
 Wernecke K, **156:265, 157:644, 157:731**
 Wessbecher FW, **157:837**
 Wetzel LH, **156:501**
 Whalen E, **156:189, 157:181, 157:615, 157:875**
 White KS, **156:1209, 157:557**
 White SJ, **156:345**
 Whitlow WD, **157:585**
 Widlus DM, **156:327**
 Widoff BE, **157:347**
 Wiechmann BN, **156:1155**
 Wiener SN, **156:1116**
 Wiesmann W, **157:731**
 Wiesner RH, **157:959**
 Wijdicks EFM, **157:1325**
 Wilcox PA, **157:473**
 Wiley C, **156:1245**
 Wiley J, **157:1267**
 Williams AL, **157:389**
 Williams DM, **157:919**
 Williams R, **157:167**
 Willing SJ, **156:1001**
 Wills JS, **157:1123**
 Wilms G, **156:640**
 Wilson AJ, **157:81, 157:105, 157:533**
 Winchester P, **156:561, 157:1105, 157:1117**
 Winzelberg GG, **157:286**
 Wise GJ, **156:1325**
 Withers CE, **156:745**
 Wittenberg J, **156:1273, 157:654**
 Witte RJ, **157:461**
 Wittich GR, **156:77**
 Wolber R, **156:73**
 Wong WK, **156:835**
 Woolsey EJ, **156:995**
 Woomert CA, **157:817**
 Wootton P, **156:688**

Wright CJ, **157:111**
 Wright KC, **156:757**
 Wu WC, **157:769**

Y

Yakes WF, **156:381**
 Yamaguchi T, **157:397**
 Yamamoto J, **156:69**
 Yancey JM, **156:1321**
 Yankelevitz DF, **157:87**
 Yao T, **156:741**
 Yasaka M, **157:397**
 Yedlicka JW Jr, **156:1007, 156:1087**
 Yeung E, **156:321**
 Yi Y, **157:87**
 Yoder IC, **157:315, 157:675**
 Yoo S-J, **157:835, 157:943**
 Yoshida M, **157:971**
 Yoshino MT, **157:1357**
 Young JWR, **156:1198, 157:1005**
 Young W, **156:559**
 Yousem DM, **156:1229**
 Yuan C, **156:161**
 Yucel EK, **157:967, 157:1069**
 Yuh WTC, **156:579, 157:565, 157:575, 157:813**

Z

Zachariah E, **157:267**
 Zafaranloo S, **156:865**
 Zajko AB, **157:29, 157:449**
 Zawacki JK, **157:721**
 Zegel HG, **156:639, 156:769**
 Zelch MG, **157:703**
 Zeman RK, **156:395, 156:493, 156:737, 157:223, 157:297, 157:747**
 Zeppa MA, **157:47**
 Zerhouni EA, **156:403**
 Zerin JM, **156:407, 156:1029**
 Zetti G, **157:29**
 Zhang G, **157:69, 157:509**
 Zimmon DS, **157:223**
 Zininger MD, **157:473**
 Zlatkin M, **157:93**
 Zollikofer ChL, **156:389**
 Zukerberg LR, **157:315**
 Zuurbier R, **156:395**
 Zweig SJ, **157:1354**
 Zwirewich C, **157:471**
 Zyed A, **157:133**

Subject Index Volumes 156–157

AJR articles are also included in the 5-year cumulative index published in *Radiology*.

Index Key: a = abstract, b = book review, e = editorial, l = letter, m = memorial, p = pictorial essay, v = videotape review

Subjects in this index are cataloged by body part where possible. Disease entities unique to a body part are listed by that part; other more general diseases have separate listings by name. Technical procedures are also listed by part, as appropriate. Because of general interest, subjects dealing with CT, MR imaging, sonography, radionuclide imaging, and pediatric radiology are listed under those headings as well as under appropriate body part and/or disease.

A

Abdominal aorta, coarctation, malignant hypertension and collateral mesenteric circulation (l), 156:201

Abscess, see specific organ or site

Absorptiometry

dual-photon, osteoporotic fracture risk assessment, 157:1229

single-photon, osteoporotic fracture risk assessment, 157:1229

X-ray, osteoporotic fracture risk assessment, 157:1229

Achalasia, elderly patients (a), 156:1331

Achilles tendon, rupture, polylactic acid implant for repair of, 156:769

Acquired renal cystic disease, dialysis patients, 156:501

Adamantinoma, vs fibrous dysplasia, tibia, 156:1017

Adenocarcinoma

colon and rectum, population-based study (a), 157:203

lower rectal, transrectal sonography and CT in (a), 157:1133

Adenoid cystic carcinoma, airway, MR (l), 156:1321

Adenomatous polyposis syndromes, extracolonic manifestations (p), 156:481

Adrenal cortex, macrocysts, Beckwith-Wiedemann syndrome, 157:549

Adrenal gland, Castleman disease, MR, 157:781

Adrenal hyperplasia, neonatal congenital, sonography, 156:141

Adrenal mass, percutaneous biopsy of, pancreatitis after, 157:777

Adrenal myelolipoma, 156:724

Adrenocorticotrophic hormone, bronchial carcinoid tumors produced by, MR vs CT, 156:39

AIDS

adenovirus colitis in (a), 157:202

benign lymphoepithelial parotid tumors in, CT and MR, 156:1253

cat-scratch fever in, unusual manifestation of, 157:1249

intraabdominal *Mycobacterium tuberculosis* vs *Mycobacterium avium-intracellulare*, CT, 156:487

lymphoma related to

CT (p), 156:969

infant, 156:1037

Pneumocystis carinii pneumonia

aerosolized pentamidine against (a), 156:409

oral therapy (a), 156:409

visceral calcification and, 156:745

primary aspergillosis in (a), 157:419

risk reduction, radiology department, 157:911,

157:919

Afferent loop syndrome, sonography, 157:41

Airway, adenoid cystic carcinoma, MR (l), 156:1321

Alkaline phosphatase, serum level, embolization of hepatic artery in liver cancer and (l), 157:887

Allergic reaction, Gd-DTPA and (a), 156:646

Alpha-1-antitrypsin, deficiency, liver disease (a), 156:882

Alpha-fetoprotein, maternal serum, elevated, normal sonography and (a), 156:410

American College of Radiology

diagnosis codes, retrieval of (l), 157:1353

Mammography Accreditation Program, 157:473

summit meeting—1990, 156:841, 156:1273,

156:1277

American Journal of Roentgenology

appointment of new associated editor, 157:86

manuscripts rejected (l), 157:1352

American Roentgen Ray Society

ARRS Presidential Address: Reflections on radiology as a career, 157:447

award-winning scientific exhibits, 1991, 157:636

information and application for membership, 156:214, 156:432, 157:214, 157:434,

157:640

1991 meeting, Boston, MA, 156:211, 157:623

administrative report, 157:635

instructional courses and symposium, 156:423, 156:659, 156:885

introduction to research seminar, 156:1266

invitation, 156:419, 156:651

local activities and tennis and golf tournaments, 156:425

scientific program, 156:888

secretary's report, 157:633

summary, 156:213, 156:421, 156:654, 156:884

1992 meeting, Orlando, FL, 156:1338, 157:208, 157:428, 157:660, 157:896, 157:1138

new members, 157:638

officers, committees and membership information, 156:210, 156:428, 156:653, 156:894,

156:1124, 157:213, 157:433, 157:659,

157:901, 157:1137

Amiodarone, lung, CT-pathology correlation (a), 156:206

Amniography, monoamniotic pair in a triplet pregnancy, 156:559

Amniotic band syndrome, sonography (p), 156:555

Amyloid arthropathy, dialysis-related, MR imaging, 157:1023

Amyloidosis

small intestine

barium meal study (a), 156:205

double-contrast radiographs, 156:741

systemic, scintigraphy evaluation (a), 156:410

Anal sphincter, endosonography, 157:1199

Anaphylaxis

barium enemas and latex balloons, 156:1

Gd-DTPA and (a), 156:646

latex allergy and, during barium studies, 156:903

latex balloons (l), 157:885

Angiocardiology, congenital heart malformations (b), 156:1208

Angiography

accurate puncture, popliteal artery and vein relations, 157:1259

coronary, predicting the appropriate use of (a), 156:642

digital subtraction, hemopericardium diagnosis (l), 157:645

enhanced 3-D MR, venous anatomy of brain, 156:161

gastrointestinal bleeding, obscure origin, 156:385

head and neck, schwannomas, 157:1309

iliac artery stenosis, renal allograft-mediated hypertension, 157:513

impotence, 157:923, 157:932

lower-extremity, midazolam/fentanyl for sedation in, 157:174

MR

- and contrast, diagnosis of carotid artery stenosis, **156:611**
 cerebrovascular disease in sickle cell anemia (a), **156:645**
 cervical neural foramen (l), **157:1128**
 renal arteries, **157:981**
 need for, mediastinal hemorrhage, **156:273**
 normal and variant anatomy (b), **157:172**
 pulmonary, upper lobe of lung after surgery, **157:471**
 stroke, coronary artery bypass surgery and, **157:1295**, **157:1297**, **157:1291**, commentary
 visceral, mesenteric vascular insufficiency, **157:1203**
- Angiomatosis**, bacillary, soft tissue and osseous lesions, **157:1249**
- Angioplasty**
 balloon
 after hepatic transplantation, **157:167**
 infrarenal portion of abdominal aorta, **156:1257**
 unsuccessful, iliac artery stenosis after, **156:389**
 dye laser-assisted, with multifiber catheters, **157:1253**
 kissing-balloon technique for, popliteal artery trifurcation, **156:823**, **157:1359** (l)
 percutaneous transluminal, subclavian arteries, **156:1091**
- Angioscopy**, histopathologic validation of (a), **157:1131**
- Ankle**
 acute injuries, radiography, **157:789**
 lateral collateral ligament, MR (p), **156:131**
- Anorectal tuberculosis**, CT (l), **156:870**
- Anorexia nervosa**, adolescent girls, decreased bone density in (a), **156:205**
- Antecubital vein**, insertion of Simon nitinol caval filter, **157:521**
- Anterior spinal artery syndrome**, infarction of conus medullaris (l), **156:1115**
- Antroduodenal motility**, real-time sonography (a), **156:880**
- Aorta**
 abdominal
 coarctation, malignant hypertension and collateral mesenteric circulation (l), **156:201**
 infrarenal portion, balloon angioplasty, **156:1257**
 descending, anomaly of, pediatric, **156:1033**
 translumbar access, CT, **156:395**
- Aortic thrombosis**, after umbilical artery catheterization, neonate, **156:567**
- Aortic valvular disease**, carotid duplex sonography in, **157:403**
- Aortitis**, nonaneurysmal bacterial, impending rupture of, CT (a), **156:645**
- Aortoenteric fistula**, manifested as intramural duodenal hematoma, **157:47**
- Aortography**, translumbar, uncommon complication of (l), **156:408**
- Aortopulmonary window**, Berry syndrome, MR imaging, **157:835**
- Appendix**, normal, CT (a), **157:1133**
- Arterial puncture technique**, standard, modification of (l), **156:864**
- Arterial sheath set**, embolized fragment, percutaneous retrieval, **157:873**
- Arteriography**
 coronary, techniques other than, **156:15**
 ipsilateral antegrade femoral (l), **157:199**
- Arteriosclerosis**, intravascular sonography in detection of, **156:1087**
- Arteriovenous fistulas**, biopsy of renal allografts and, **156:507**
- Arteriovenous malformations**, renal, color Doppler sonography, **157:991**
- Arthritis**
 rheumatoid, knee, enhanced MR, **156:125**
 septic, hip, pelvic fractures and, **157:817**
 septic, hip, infant (a), **156:412**
- Arthrography**, wrist, unidirectional joint communications, **157:105**
- Arthroplasty**, girdlestone, aspiration of hip in, **156:545**
- Artifacts**
 computed radiography (p), **157:181**
 magnetic susceptibility, MR, spine, **156:1069**
 motion, simulating aortic dissection, CT, **157:465**
 sonography, origins (p), **156:1267**
- Ascites**
 new sign of (l), **156:1325**
 peritoneal carcinomatosis with (p), **156:1185**
- Aspergillosis**
 paranasal, CT (l), **157:416**
 primary, AIDS (a), **157:419**
- Aspiration**, elderly patients, videofluoroscopy, **156:293**
- Aspiration cytology**
 breast lesions, **157:711**
 phylloides tumor, **157:715**
- Aspirin**, low-dose, heparin comparison, myocardial infarction (a), **156:1117**
- Atherectomy**, facilitated by long vascular sheaths, **156:173**
- Atherosclerotic plaque**, pulsed dye laser light and, **157:1253**
- Atrial septal defect**, surgical repair, long-term outcome (a), **156:1118**
- Audiovisual presentation**
 editorial, **157:614**
 effective, **156:181**
 proper citation of sources (l), **157:643**
- Autostapler**, urinary tract calculi on surgical staples, **157:115**
- Avascular necrosis**, femur, MR imaging, canine model, **157:341**
- Azygos lobe**, imaging (p), **156:931**
- B**
- Back pain**, lower, percutaneous procedures, review, **157:685**
- Balloon, latex**
 barium enema
 anaphylactic reactions and, **156:1**
 rectal tip, condom coverage of (l), **156:1323**
- Barium studies**
 air-contrast
 Barrett esophagus, **157:951**
 inverted colonic diverticulum, **156:961**
 amyloidosis, small intestine (a), **156:205**
 catheters for (l), **157:196**, **157:197**
 enema rectal tip, condom coverage of (l), **156:1323**
 E-Z-EM balloon enema tip, retained (l), **157:885**
 E-Z-EM balloon-retaining (l), **156:869**
 gastrointestinal, iohexol comparison, infants and children, **156:345**
 inadvertent vaginal filling (l), **157:197**
 latex balloons, anaphylactic reactions and, **156:1**, **903**
 normal volunteers, **157:761**
- Barrett esophagus**, radiologic diagnosis, **157:951**
- Basivertebral vein**, disappearance of, MR imaging of bone marrow disease (l), **157:1129**
- Beckwith-Wiedemann syndrome**, adrenocortical macrocytes, infants, **157:549**
- Behcet disease**, neurologic involvement, **157:867**
- Bile duct**
 diverticula, webs and, **157:281**
 malignant obstruction, self-expandable stainless steel endoprosthesis for, **156:321**
 obstruction, sinicalide-aided sonography (a), **156:412**
 papillomatosis, ampullary carcinoma and (l), **156:405**
 stones, endoscopic laser lithotripsy (a), **156:204**
- Bile flow**, choledochoduodenal, cholescintigraphy (a), **157:203**
- Bile-plug syndrome**, spontaneous resolution, **156:1225**
- Biliary atresia**, choledochal cyst and, neonate (l), **157:646**
- Biliary duct**, strictures, percutaneous transluminal biopsy, **156:77**
- Biliary endoprosthesis**
 metallic, placement via cholecystostomy, **157:491**
 occluded metallic self-expandable, **157:291**
 stainless steel self-expandable, malignant obstruction of bile duct, **156:321**
- Biliary obstruction**, liver transplants, **157:29**
- Biliary stents**, metal, cholangioscopic or transpapillary insertion (a), **156:1331**
- Biliary tract**
 imaging for the 1990s, **157:223**
 interventional radiology (b), **157:490**
 sonography, infants and children, **157:1051**
- Biopsy**
 breast, abnormalities caused by, mammographic findings (p), **156:287**
 endoscopic, larger mucosal samples (a), **157:892**
 fine-needle aspiration
 breast carcinoma (a), **156:206**
 breast lesions (a), **156:643**
 small hepatocarcinoma, fatal bleeding after (l), **156:1114**
 percutaneous
 CT-guided (l), **156:639**
 left adrenal mass, pancreatitis after, **157:777**
 needle aspiration, nonfluoroscopic, lung, patient with pneumonia (a), **156:410**
 skeletal lesions, **157:935**
 renal allografts, arteriovenous fistulas and, **156:507**
 stereotactic, breast (l), **156:634**
 transbronchial, prediction, bronchus sign on CT, **157:1181**
 transluminal, biliary strictures, biptome, **156:77**
 vs phase-contrast MR, fatty infiltration of liver, **156:307**
- Biptome**, percutaneous transluminal biopsy with, biliary strictures, **156:77**
- Bladder**
 augmented, perforation, children and adolescents, **157:1059**
 transitional cell carcinoma
 recurrence after cystectomy, CT, **157:999**
 stage D2 (l), **156:1325**
- Blood flow**
 velocity
 measurements with velocity-encoded cine MR, **157:9**
 transcranial real-time color flow Doppler sonography, **157:397**
- Blood supply**, systemic, lung, developmental abnormalities, **156:669**
- Blue medicine**, **157:110**
- Body coil**, MR imaging with, prostate carcinoma, **156:511**
- Body fat**, overall distribution, young women, MR, **157:99**
- Boerhaave syndrome**, intramural hematoma, esophagus (l), **157:197**
- Bone**
 diseases (b), **156:120**
 dysplasia, deferoxamine-induced, **156:561**
 imaging, scan equalization radiography, **157:359**
 language of fractures (b), **157:532**
 loss, spinal, ovulatory disturbances and (a), **156:642**
 radionuclide imaging, stress injury of anterior iliac crest (a), **156:413**
 scan, radioisotope, metastatic prostatic cancer patients (a), **156:203**
 scintigraphy, pelvic pain (l), **156:407**
- Bone marrow**
 thoracic and lumbar, radiation therapy effects, MR, **157:87**
 transplantation
 diffuse pulmonary alveolar hemorrhage after, **157:461**

- febrile patients, ultrafast chest CT in (a), 157:421
- Book reviews**
- aids to radiological differential diagnosis, 156:316
- angiocardiology of congenital heart malformations, 156:1208
- atlas of interventional radiology, 157:166
- atlas of oral diagnostic imaging, 157:768
- atlas of roentgenographic measurement, 6th ed, 157:498
- atlas to normal and variant angiographic anatomy, 157:172
- cancer imaging with radiolabeled antibodies, 156:798
- cardiac catheterization, angiography and intervention, 157:1186
- cardiothoracic trauma, 157:702
- cardiovascular application of Doppler ultrasound, 156:930
- cartilaginous tumors of the skeleton, 157:1034
- Christensen's physics of diagnostic radiology, 4th ed, 156:234
- clinical profiles of diffuse interstitial pulmonary disease, 156:680
- clinical radiology of the breast, 157:266
- comparative cardiac imaging, 157:, 157:834
- computed tomography, anatomy, and morphometry of the lower extremity, 156:1198
- computed tomography of the trunk, 156:326
- congenital heart disease, 156:1154
- control of radon in houses, 156:968
- creative medical teaching, 157:1022
- CT and MRI of the genitourinary tract, 157:330
- CT and MRI of the liver and biliary system, 156:492
- CT review, 156:486
- detection and treatment of early breast cancer, 157:480
- diagnosis of diseases of the chest, 157:692
- disorders of the patellofemoral joint, 2nd ed, 156:332
- Dr. Susan Love's breast book, 156:286
- duplex scanning in vascular disorders, 156:984
- Edeiken's roentgen diagnosis of diseases of bone, 4th ed, 156:120
- effective choices for diagnostic imaging in clinical practice, 157:1050
- essentials of neuroimaging, 157:866
- Fuch's principles of radiography exposure, processing and quality control, 156:954
- gamuts and pearls in MRI, 157:602
- imaging anatomy of the head and spine, 156:586
- imaging of the lumbar spine, 157:684
- imaging of the pelvis, 157:784
- magnetic resonance imaging of the pediatric brain, 157:122
- magnetic resonance imaging of the brain and spine, 157:1324
- magnetic resonance imaging of carcinoma of the urinary bladder, 157:516
- magnetic resonance in experimental and clinical oncology, 157:1220
- manual of clinical magnetic resonance imaging, 157:850
- maxillofacial imaging, 156:1068
- morphological and functional MR of the kidneys and adrenal glands, 157:776
- MRI. Central nervous system, 156:790
- MRI. Musculoskeletal system, 156:784
- MRI of the brain II, 157:1282
- MRI of the musculoskeletal system, 2nd ed, 157:526
- MRI of the musculoskeletal system, 156:456
- MRI of the wrist and hand, 157:340
- neuroradiology test and syllabus, 157:584
- nuclear cardiovascular imaging, 156:44
- nuclear medicine annual 1990, 156:780
- obstetrics and gynecology, 157:544
- optimization of image quality and patient exposure in diagnostic radiology, 156:176
- osteoporosis, 156:130
- physics and instrumentation of diagnostic medical ultrasound, 157:408
- pocket atlas of normal CT anatomy of the head and brain, 156:1244
- pocket atlas of pediatric ultrasound, 156:364
- practical echocardiography and Doppler, 156:916
- practical MRI atlas of neonatal brain development, 157:842
- practical nuclear medicine, 156:394
- primer of sectional anatomy with MRI and CT correlation, 156:570
- quantitative imaging, 156:762
- radiation protection, 156:688
- radiologic clinics of North America
- imaging of joints, 157:346
- imaging the lymphomas, 156:748
- interventional radiology of the biliary tract, 157:490
- lung cancer, 156:280
- metabolic bone diseases, 157:1028
- radiology in the management of cancer, 157:352
- radiology of musculoskeletal stress injury, 157:1238
- radiology of renal failure, 2nd ed, 156:104
- radiology of syndromes, metabolic disorders, and skeletal dysplasia, 157:1242
- radiology of the eye and orbit, 156:1218
- radiology review manual, 157:1038
- radionuclides in nephro-urology, 156:500
- review of radiology, 156:58
- skeletal radiology, 156:116
- textbook of clinical imaging, 157:608
- textbook of uro-radiology, 157:516
- the abdominal plain film, 156:730
- the language of fractures, 2nd ed, 157:532
- the lungs, 157:254
- therapeutic endoscopy and radiology of the gut, 157:310
- the visible human body, 157:1252
- the year book of diagnostic radiology, 1990, 156:806
- three-dimensional neuroimaging, 157:1072
- thyroid disease, 157:286
- tissue characterization in MR imaging, 157:98
- trauma of the spine, 156:1036
- trauma radiology, 156:774
- two-dimensional echocardiography and cardiac Doppler, 156:14
- Bottle cap ingestion** (I), 157:411
- Bowel**
- inflammatory disease
- epidemiology of (a), 156:1118
- familial (a), 156:1330
- small, enteroscopy (a), 156:1331
- Brain**
- CT and MR comparison, acute infarction, 157:585
- hemorrhagic lesions, contrast-enhanced MR imaging, 157:861
- intracranial vascular abnormalities, MR phase imaging, 156:373
- intraventricular mass lesions, CT and MR imaging (p), 157:1283
- metastases, diagnosis, CT vs MR, 156:1039
- migraine headaches, MR imaging, 157:385
- MR imaging
- cerebral ischemia, contrast-enhanced, 157:575
- cerebral ischemia, first 24 hours, 157:565
- diabetes insipidus patient, 157:123
- pediatric (b), 157:122
- paranasal sinus mucosal thickening, MR images, 156:381
- radiation injury, 156:689
- venous anatomy, enhanced 3-D MR angiography, 156:161
- white matter disease (v), 156:1074
- Brain stem**, MR (v), 156:1052
- Breast**
- biopsy, abnormalities caused by, mammography (p), 156:287
- cancer
- early (b), 157:480
- mass screening in Japan (a), 157:420
- self-referred mammography patients, 157:481
- carcinoma
- indium-111-labeled B72.3 monoclonal antibody in detection of (a), 157:1133
- palpable vs impalpable lesions on mammography, 157:21
- tumor angiogenesis and metastasis in (a), 156:1117
- ultrasound-guided fine-needle aspiration biopsy (a), 156:206
- chemical shift-MR imaging, 157:267
- clinical radiology (b), 157:266
- imaging, medicolegal aspects of, 156:719
- lesion
- fine-needle aspiration biopsy (a), 156:643
- needle aspiration, 157:711
- nonpalpable, transected wire localization (I), 156:877
- preoperative CT-guided percutaneous localization of, 157:179
- lobular carcinoma in situ, 157:257
- localization wire, inappropriate location of (I), 157:645
- mucocoele of, 156:199
- node-negative cancer, adjuvant chemotherapy in (a), 156:1330
- noncalcified mass, radiographic density of, 157:25
- reconstruction, mammographic and CT findings after (p), 156:1159
- sonography, 156:449
- stereotactic biopsy (I), 156:634
- Brenner tumor**, malignant, MR imaging (I), 157:1355
- Bronchial stenosis**, tuberculous, balloon bronchoplasty, 157:1187
- Bronchogenic cyst**, bilateral, 157:950
- Bronchograms**, air, small peripheral carcinoma of the lung, CT, 156:921
- Broncholithiasis**, CT, 157:249
- Bronchoplasty**, balloon, tuberculous bronchial stenosis, 157:1187
- Bronchopulmonary dysplasia**
- late pulmonary sequelae of (a), 156:1117
- research in diagnostic radiology, 156:681
- Bronchopulmonary sequestration**, intralobular, CT, 157:947
- Bronchus sign**, CT, peripheral carcinoma of the lung, 157:1181
- Brucellosis**, abdominal, CT (I), 156:1323
- Brunner glands**, hyperplasia (a), 157:204
- C**
- Calcium**, supplementation, postmenopausal women (a), 156:409
- Caliceal diverticula**, renal, stones and infection in, 156:995
- Cancer**
- radiolabeled antibodies (b), 156:798
- radiology in (b), 157:352
- see also specific type or site
- Carcinomatosis**, peritoneal, with ascites (p), 156:1185
- Cardiothoracic trauma**, management of (b), 157:702
- Carotid artery**
- patency, spin-echo MR imaging, brain, 157:1299, 157:1307
- retrieval of 4-French diagnostic catheter fragment from, 156:1105
- stenosis, angiography comparison, 156:611
- Case of the day**
- abdominal, 156:852, 156:1301
- chest, 156:846, 156:1295
- general diagnosis, 156:846, 156:1288
- neuroradiology, 156:854, 156:1307
- pediatric, 156:859, 156:1314

- Castleman disease**, skeletal lymphoma with, 157:1035
- Catheter**
balloon, hemorrhage from subclavian artery after catheter removal, 156:1261
barium studies (I), 157:196, 157:197
5-French, high-velocity jets from (I), 156:874
4-French, retrieval from common carotid artery, 156:1105
- Catheterization**
cardiac (b), 157:1186
percutaneous vascular, teaching (I), 157:1123
transfemoral venous, inferior vena caval filters, 157:967
- Cat-scratch fever**
AIDS patients, unusual manifestation of, 157:1249
disseminated hepatic and splenic lesions, imaging of, 156:1227
- Cavernosography**, impotence, 157:923
commentary, 157:932
- Celiac axis**, ligamentous compression, CT, 156:1101
- Central nervous system**, neonatal, maternal cocaine abuse and, 157:1105
- Centrilobular lesions**, staphylococcal pneumonia (I), 156:1322
- Cerebral arteries**, basal, transcranial real-time color flow Doppler sonography, 157:397
- Cerebral ischemia**, MR/spectroscopy, 156:1133
- Cerebral ventricles**
asymmetric growth of, posthemorrhagic ventricular dilation, infant (a), 156:1333
fourth, ependymoma of, CT and MR imaging, 157:1278
- Cerebrospinal fluid**, shunt function, evaluation, 156:801
- Cervix**
carcinoma, MR, 156:753
clinical stage I carcinoma, degree of invasiveness, MR, 156:1191
transperineal approach to sonography, third trimester of pregnancy, 157:73
uterine, third-trimester, translabial sonography (a), 156:883
- Chemotherapy**
adjuvant, node-negative breast cancer (a), 156:1330
osteosarcoma and Ewing sarcoma response to, 157:825
- Child abuse**
healing fractures
extension of growth plate cartilage into metaphysis, 156:775
normal metaphyseal radiologic variants confused with (p), 156:781
osteogenesis imperfecta differentiation (I), 156:634
- Cholangiography**
choledochal cyst appearance (p), 156:327
intraoperative, serum diatrizoate during (a), 156:204
orthotopic liver transplantation, 157:29
primary sclerosing cholangitis, 157:281, 157:495
transhepatic, biliary disease (a), 157:1364
value, primary sclerosing cholangitis, 157:959
- Cholangiohepatitis**, oriental, 157:1
- Cholangiopancreatography**, endoscopic retrograde, asymptomatic pancreatitis after (a), 156:206
- Cholangioscopy**, percutaneous, insertion of biliary metal stents (a), 156:1331
- Cholangitis**
primary sclerosing, 157:281
biliary tract strictures in (a), 156:1332
cholangiographic findings, 157:495, 157:959
history and prognosis (a), 157:651
ulcerative colitis with (a), 157:421
- Cholecystectomy**
biliary pain after (a), 157:203
laparoscopic (a), 156:1331
laparoscopic, 157:235
commentary, 157:241
lithotripsy vs. gallstones, analysis by Markov process (a), 157:1132
obstructive jaundice after (I), 157:197
vs extracorporeal shock-wave lithotripsy (a), 157:891
- Cholecystolithotripsy**, extracorporeal shock-wave, altered gallbladder contractility, 157:485
- Cholecystostomy**
metallic biliary endoprosthesis placement, 157:491
percutaneous, sepsis of unknown cause, 156:1163
- Choledochal cyst**, appearance, cholangiography (p), 156:327
- Cholelithiasis**
dissolution
methyl *tert*-butyl ether, morphology after (a), 157:651
methyl *tert*-butyl ether, thin-layer chromatography of, 157:33
fragmentation, biliary lithotripsy, 156:493
lithotripsy, 157:747
lithotripsy versus cholecystectomy, analysis by Markov process (a), 157:1132
medical dissolution of (a), 156:1331
nonsurgical therapies, laparoscopic cholecystectomy and, 157:235, 157:241
- Cholescintigraphy**
abnormal, cholecystectomy for alleviation of pain (a), 157:1362
gallbladder perforation (a), 156:1120
- Cholestasis**, severe, scintigraphic assessment (a), 156:643
- Cholesterol**, gallstone disease, gallbladder motility and (a), 156:643
- Chondrodysplasia**, Schmid-like metaphyseal, simulating child abuse, 156:576
- Chondrosarcoma**, MR, 156:1016
- Chromatography**, thin-layer, cholesterol gallstone dissolution by methyl *tert*-butyl ether, 157:33
- Chronic obstructive pulmonary disease**
lung transplantation and (a), 157:202
plain radiographic signs (a), 157:423
- Cirrhosis**
intraparenchymal regenerating nodules in, sonographic high-frequency transducers (a), 157:892
portal pressure in, endoscopic variceal sclerotherapy (a), 157:1362
- Claustrophobia**, MR-induced, alprazolam and (I), 156:633
- Clavicle**, condensing osteitis, 156:1011
- Clinoril**, esophageal ulcer due to, 156:955
- Colitis**
adenovirus, AIDS and (a), 157:202
collagenous, pathophysiology (a), 157:891
ulcerative
cancer surveillance in (a), 157:421
colorectal cancer and (a), 156:641
primary sclerosing cholangitis in (a), 157:421
- Collagen vascular diseases**, cervical paraspinal calcification in, 157:523
- Collateral mesenteric circulation**, malignant hypertension and, coarctation of abdominal aorta associated with (I), 156:201
- Colon**
adenocarcinoma, population-based study (a), 157:203
cancer, radiologic screening, economic implications, 156:939
inverted diverticulum, air contrast barium findings, 156:961
neoplasms, radiologic detection of, 156:303
- Colonoscopy**
large colorectal polyps (a), 157:422
screening, asymptomatic persons (a), 156:880
total (a), 157:422
- Colorectal cancer**
cross-sectional imaging, 156:909
immunoscintigraphy, indium-111-labeled monoclonal antibody conjugate CYT-103 (a), 157:1133
ulcerative colitis and (a), 156:641
- Computed radiographic systems**, artifacts in (p), 157:181
- Computer page**, PC-based semiautomated reporting system, 157:1117
- Contrast media**
atypical reactions, interleukin-2 therapy, 156:833
barium studies, normal volunteers, 157:761
cerebral ischemia imaging with, 157:575
CSF shunt function, 156:801
gadopentetate dimeglumine, MR imaging of intracranial lesions, 157:837
Gd-DTPA, anaphylaxis and allergic reaction (a), 156:646
hemorrhagic brain lesions, subtraction images in detection of, 157:861
high- vs low-osmolality, risks, 156:825
intraperitoneal, CT detection of peritoneal metastases, 157:37
intravascular
acute reactions to, 157:1153
noncardiogenic pulmonary edema and, 157:255
MR
advances in, 156:235
gastrointestinal agents, 156:252
nonionic, guidelines for (I), 156:865
renal dysfunction induced by, 157:49, 157:59, 157:66
vomiting induced by, prevention (I), 156:633
- Coronary artery**
bypass graft, patency, 156:15
bypass surgery, stroke with, 157:1291
disease, intensive lipid-lowering therapy and (a), 156:641
- Coronary vessels**, dipyridamole technetium-99m-2-methoxy isobutyl isonitrile tomoscintigraphic imaging for (a), 157:652
- Cricopharyngeal bars**, biomechanics (a), 156:411
- Crohn disease**
gastric carcinoma in, 157:311
lesions, rectum and sigmoid colon (a), 157:891
predictability of (a), 156:204
- Cryptococcosis**, intracranial, immunocompromised patients, CT and MR, 156:1245
- CT**
AIDS-related lymphoma (p), 156:969
cross-sectional, intravascular hematocrit effect in (a), 157:653
pyelonephritis (a), 156:204
quantitative, osteoporotic fracture risk assessment, 157:1229
review (b), 156:486
sectional anatomy (b), 156:570
- CT, abdomen**
active intraabdominal arterial hemorrhage, 156:725
acute pancreatitis, 156:93
after liver transplantation, 156:1167
AIDS patient, intraabdominal *Mycobacterium tuberculosis* vs *Mycobacterium avium-intracellulare*, 156:487
anorectal tuberculosis (I), 156:870
anterior mediastinum, masses, 157:1171
aorta-bifurcation prosthesis, intrasigmoidal (I), 156:202
aortoenteric fistula, 157:47
appendix, normal (a), 157:1133
brucellosis (I), 156:1323
celiac axis, ligamentous compression of, 156:1101
desmoids, 157:275
disseminated histoplasmosis, 157:955
duodenal ulcer, hemorrhage due to, 157:45
gastrointestinal tract, principles and interpretation, 156:23

- hepatic and splenic lesions, cat-scratch disease, **156:1227**
 lap-belt ecchymosis, children, **157:111**
 nonobstructing periureteric venous ring, **157:997**
 peliosis hepatitis, HIV infection and, **156:91**
 peritoneal metastases, intraperitoneal contrast media improves CT, **157:37**
 pseudotumors, spontaneous disappearance (I), **157:1355**
 rectal intussusception (I), **156:870**
 retrograde jejuno duodenogastic intussusception, complication of gastrostomy tubes, **156:957**
 retroperitoneal fibrosis, **157:321**
 spleen, acquired abnormalities (p), **157:1213**
 splenic hemangioma, **157:44**
 traumatic rupture of diaphragm, **157:17**
CT, aorta, aortic dissection, motion artifact simulating, **157:465**
CT, bladder, transitional cell carcinoma, recurrence after cystectomy, **157:999**
CT, body, CT of trunk (b), **156:326**
CT, bone
 bacterial osteomyelitis (p), **157:365**
 idiopathic myelofibrosis, diffuse intraabdominal lymphoma complicating, **156:1189**
CT, breast
 after breast reconstruction (p), **156:1159**
 preoperative percutaneous localization of lesion, Kopans needle, **157:179**
CT, cranium
 acute cerebral infarction, MR comparison, **157:585**
 benign lymphoepithelial parotid tumors, AIDS patients, **156:1253**
 brain, intraventricular mass lesions (p), **157:1283**
 congenital nasal masses, **156:587**
 double-dose delayed, cerebral metastases, **156:1039**
 ependymoma, fourth ventricle, **157:1278**
 hamartomas of the tuber cinereum, **156:1053**
 intracerebral gangliogliomas, partial complex seizures and, **157:843**
 intracranial cryptococcosis, immunocompromised patients, **156:1245**
 intracranial lipoma (I), **157:887**
 limited slice of paranasal sinus, children, **156:367**
 orbit and its contents, children (p), **156:1219**
 pocket atlas of anatomy (b), **156:1244**
 ruptured intracranial dermoid cyst, **156:807**
 sinonasal carcinoma, spread via eustachian tube (I), **157:888**
 sinuses, optimization of techniques, **157:1093**, **157:1099**
 stroke, coronary artery bypass surgery and, **157:1291**, **157:1295**, **157:1297**
 subarachnoid hemorrhage, nonaneurysmal perimesencephalic, **157:1325**
CT, esophagus
 carcinoma, vs MR, **156:297**
 intramural hematoma dissection, Boerhaave syndrome (I), **157:197**
 mediastinal seroma, after esophagogastricectomy, **156:715**
 perforation (a), **156:643**
CT, extremities, angiosarcoma, associated with chronic lymphedema, **156:543**
CT, fetal, amniography, monoamniotic pair in a triplet pregnancy, **156:559**
CT, head and neck, tubes, alimentary and respiratory tracts (p), **156:1047**
CT, heart, aorta, traumatic injury (I), **157:1123**
CT, hip, iliopsoas bursal distension (a), **156:206**
CT, kidney
 lymphoma (a), **156:645**
 transplants, vascular complications with, **157:449**
CT, knee, osteoarthritis, **157:799**
CT, liver
 biliary system and (b), **156:492**
 choledochojejunostomy, liver transplantation (a), **156:883**
 detection of masses with carcinoma, comparison with MR imaging and sonography, **157:731**
 dual-energy, focal fatty infiltration from low-density masses, **157:721**
 hepatocellular carcinoma, **157:303**
 hydatid cyst, **156:751**
 imaging of tumors (I), **156:867**
 periportal contrast enhancement, **156:313**
 subcapsular hepatic necrosis, **156:981**
 transplanted, low-attenuation periportal collar in, **157:1195**
CT, lung, high-resolution and conventional, chronic diffuse infiltrative lung disease, **157:693**
CT, mediastinum, thymolipoma, **157:468**
CT, neck, posterior cervical space, **157:161**
CT, nose, paranasal aspergillosis (I), **157:416**
CT, pancreas
 after secretin provocation, pancreas divisum (a), **156:643**
 asymptomatic pancreatitis, following endoscopic retrograde cholangiopancreatography (a), **156:206**
 children (p), **157:375**
 microcystic adenoma, presenting with acute hemoperitoneum, **156:749**
CT, pelvis
 after cesarean section, **156:523**
 pelvimetry, **156:527**
CT, pharynx, goitrous cretinism, manifesting as newborn stridor, **157:557**
CT, rectum, lower rectal adenocarcinoma (a), **157:1133**
CT, scrotum, perforated retroperitoneal appendix, Fournier gangrene caused by, **156:341**
CT, spine, cervical, osteosarcoma (I), **157:1357**
CT, spleen
 acute splenic torsion, children with wandering spleen, **156:151**
 acute torsion of wandering spleen, **157:307**
 injuries managed nonoperatively (p), **157:757**
CT, thorax
 amiodarone lung (a), **156:206**
 aorta and inferior vena cava, translumbar access, **156:395**
 aortic aneurysms and dissections (a), **156:645**
 artificial pneumothorax and, origin and extent of tumor, **156:707**
 bronchial carcinoid tumors, adrenocorticotrophic hormone-induced, **156:39**
 broncholithiasis, **157:249**
 calcification, ligamentum arteriosum, pediatric, **156:351**
 collateral venous channels (a), **156:206**
 expiratory
 pulmonary emphysema assessment (a), **157:890**
 suspected pulmonary emphysema (a), **157:1131**
 febrile bone marrow transplant patients (a), **157:421**
 high-resolution
 air trapping, bronchopulmonary sequestration, **157:947**
 chronic diffuse lung disease, **157:1163**
 laceration of thoracic duct, **157:703**
 lymphoma, lung, **156:711**
 mediastinal hemorrhage on chest radiographs and, **156:273**
 mediastinal lymphoma, therapeutic response, **156:265**
 mediastinal masses, high-attenuation, **156:45**
 nonaneurysmal bacterial aortitis, impending rupture (a), **156:645**
 paraquat poisoning, **157:697**
 pericardial effusion, after cardiac surgery, **157:19**
 peripheral carcinoma of lung, bronchus sign, **157:1181**
 pleura, **156:1145**
 small peripheral carcinoma of lung, air bronchograms in, **156:921**
 solitary pulmonary nodules, **156:925**
 ventricular myocardium, noncompaction of, **156:717**
CT, trachea, measurement of tracheal lumen, children and adolescents, **156:371**
CT, ureter
 fibroepithelial polyp, pediatric, **157:1273**
 occult ectopic, girls with urinary incontinence, **156:365**
CT, vagina, reconstruction, rectus abdominis myocutaneous flap, **156:1001**
Cyclosporin A, neurotoxicity induced by, MR imaging of, **157:851**
Cyst, see specific organ or site
Cystadenocarcinoma, biliary (I), **156:1113**
Cystadenoma, biliary (I), **156:1113**
Cystectomy, transitional cell carcinoma recurrence, bladder, CT, **157:999**
Cystinosis, nephropathic, swallowing dysfunction in (a), **156:410**
Cystography
 perforation of the augmented bladder, children and adolescents, **157:1059**
 vaginal filling during, detection (I), **156:406**
Cytology, endoscopic retrograde brush (a), **156:411**
- D**
- Deferoxamine**
 bone dysplasia induced by, thalassemia major with, **156:561**
 therapy, systemic *Yersinia enterocolitica* infection, **157:773**
Dermoid cyst, intracranial, ruptured, CT and MR, **156:807**
Desmoids, abdominal, CT, **157:275**
Diabetes
 abnormalities of the foot, MR imaging (p), **157:813**
 osteomyelitis of the foot in, ¹¹¹In-leukocyte scintigraphy, **157:527**
Diabetes insipidus, MR imaging of brain in, **157:123**
Dialysis
 access planning
 preoperative evaluation of subclavian vein, **156:623**
 subclavian vein and (I), **157:1125**
 acquired renal cystic disease in, **156:501**
Diaphragm
 rupture
 blunt chest trauma (I), **157:411**
 blunt trauma and, **156:51**
 CT, **157:17**
Diffuse alveolar hemorrhage, after bone marrow transplant, **157:461**
Dipyridamole thallium-201
 myocardial imaging, after caffeine infusion (a), **157:1364**
 preoperative screening test (a), **157:1362**
Disk, intervertebral, normal and degenerated, MR (p), **157:93**
Diskectomy, lumbar, automated percutaneous, **156:531**
Diskitis, children (a), **157:652**
Diskography, lower back pain, review, **157:685**
Diverticulitis, jejunum (a), **156:882**
Down syndrome, arthropathy of (a), **156:882**
Drug abuse
 lung disorders and (a), **156:1120**
 maternal, cocaine, neonatal CNS abnormalities, **157:1105**
Drugs, complications related to, infants and children, **157:1039**
Duodenal hematoma, percutaneous management of (I), **156:1112**
Duodenal ulcer disease
 Helicobacter pylori role in (a), **157:421**

- intramural and intraperitoneal hemorrhage due to, **157:45**
Duodenitis, radiologic diagnosis (a), **157:204**
Dural sinus, occlusion, phase-sensitive gradient-echo MR imaging, **157:139**
Dysphagia
 elderly patients without, altered swallowing function, **156:1181**
 post-polio syndrome (a), **157:890**

E

- Echocardiography**
 practical (b), **156:916**
 two-dimensional, cardiac Doppler and (b), **156:14**
Editorials, plagiarism, **157:614**
Embolization, steel-coil, multiple intrahepatic portohepatic venous shunts, **157:971**
Emission computed tomography, exercise, lung thallium-201 uptake (a), **157:652**
Emphysema
 pulmonary
 expiratory CT for (a), **157:1131**
 expiratory CT for assessment of (a), **157:890**
 pulmonary interstitial, jet and conventional mechanical ventilation (a), **157:1364**
Endarterectomy, carotid, predicting the appropriate use of (a), **156:642**
Endocarditis, bacterial, perivalvular pseudoaneurysm, MR detection, **156:1155**
Endometriosis, periumbilical, imaging of (l), **156:636**
Endometrium, cancer, MR imaging, **157:1221**
Endoscopic sinus surgery
 optimization of techniques, **157:1093**, **157:1099**
Endoscopy
 biopsy, larger mucosal samples (a), **157:892**
 fluoroscopy, enteral feeding tube placement, **157:769**
 gallbladder carcinoma (a), **156:881**
 gastrointestinal (a), **157:891**
 insertion, expandable biliary metal stents for malignancies (a), **156:412**
 retrograde cannulation
 cytology (a), **156:411**
 gallbladder (a), **156:412**
 small-bowel, mesenteric vascular insufficiency, **157:1203**
 sonography, upper GI tract (p), **156:63**
 sphincterotomy, bile duct diameter after (a), **156:883**
 therapeutic (b), **157:310**
 transpapillary therapy, disrupted pancreatic duct (a), **157:421**
 ultrasound, pancreatic tumor diagnosis (a), **157:892**
 upper gastrointestinal, predicting the appropriate use of (a), **156:642**
Yersinia enterocolitica enterocolitis (a), **156:881**
Endosonography, anal sphincter, **157:1199**
Endotracheal tube, location, preterm and term neonates (a), **156:1120**
Enteral feeding tube, placement, fluoroscopy and endoscopy, **157:769**
Enteroclysis, inverted Meckel diverticulum (l), **156:1111**
Enterocolitis, *Yersinia enterocolitica*, endoscopy in (a), **156:881**
Enteroscopy, small bowel, gastrointestinal bleeding (a), **156:1331**
Epididymitis, bilateral testicular infarction caused by, **157:517**
Epidural injection, lower back pain, review, **157:685**
Epilepsy, chronic partial, contrast-enhanced MR, **156:605**
ERCP, anatomic variants and artifacts in interpretation (p), **156:975**
Erectile dysfunction, color Doppler sonography, **157:331**
Erythromycin, intravenous, gastric emptying in gastroparesis diabeticorum (a), **156:413**

- Esophagogastrectomy**, mediastinal seroma after, CT, **156:715**
Esophagojejunostomy, total gastrectomy and, complications after, **157:1189**
Esophagus
 abnormal motility, videofluoroscopy and manometry (a), **157:1132**
 Barrett
 prevalence of (a), **156:204**
 radiologic diagnosis, **157:951**
 carcinoma, CT vs MR, **156:297**
 emptying, hiatal hernia and (a), **156:1330**
 evaluation, marshmallow bolus (a), **156:882**
 food impaction, giant thoracic osteophyte, **157:319**
 foreign body, childproof cap on medicine bottle (l), **156:201**
 histoplasmosis, child with immunodeficiency with hyper-IgM, **157:381**
 melanoma, **157:318**
 perforation, CT (a), **156:643**
 squamous cell carcinoma, MR (a), **156:205**
 ulcer, Clinoril-induced, **156:955**
 varices, prophylactic sclerotherapy for (a), **157:1131**
ESWL, see Extracorporeal shock-wave lithotripsy
Ewing sarcoma, osteosarcoma and, response to chemotherapy, **157:825**
Exercise, acute effects on skeletal muscle, MR, **156:765**
Exosurf, respiratory distress syndrome, **157:371**
Extracorporeal membrane oxygenation, posterior fossa intracranial hemorrhage with, infant, sonography, **156:571**
Extracorporeal shock-wave lithotripsy
 assessment of patients (a), **156:1119**
 gallstones, analysis by Markov process (a), **157:1132**
 long-term soft-tissue effects of, **156:73**
 symptomatic gallbladder stones (a), **157:1363**
 ursodiol effects, gallstones (a), **156:641**
 vs cholecystectomy (a), **157:891**
Eye
 disorders, sonography (p), **157:1079**
 malignant uveal melanoma, MR imaging, **157:1087**

F

- Facet-joint injection**, lower back pain, review, **157:685**
Fallopian tubes
 nomenclature (l), **157:415**
 organic vs functional obstruction, hysterosalpingography and selective ostial salpingography, **157:77**
 recanalization, selective salpingography and, **156:33**
Femoral artery
 catheterization, deep to superficial (l), **157:1358**
 ipsilateral antegrade arteriography (l), **157:199**
Fentanyl, midazolam and, sedation for lower-extremity angiography, **157:174**
Fetus
 abdominal wall mass, detection by prenatal sonography, **157:1065**
 anomalies, MR (p), **156:1205**
 death, Doppler assessment of circulation in (l), **156:636**
 trisomic, malformations and aberrant growth detection by sonography (a), **157:1133**
Fibromatosis
 aggressive, MR (a), **156:646**
 MR imaging, **156:539**
Fibrous dysplasia, adamantinoma of the tibia vs, **156:1017**
Filters
 Greenfield, right atrial, percutaneous retrieval (l), **157:199**
 inferior vena caval, **156:813**
 percutaneous retrieval of Greenfield filters (l), **157:199**

- spontaneous fracture of, **157:177**
 transfemoral venous catheterization, **157:967**
 Simon nitinol caval, insertion, antecubital vein approach, **157:521**
Fluoride, therapy, osteoporosis, bone fragility during (a), **156:1119**
Fluoroscopy
 C-arm (l), **157:646**
 endoscopy and, enteral feeding tube placement, **157:769**
Focal high signal, MR images of midbrain (l), **157:1129**
Foot, abnormalities, diabetes mellitus, MR imaging (p), **157:813**
Fournier gangrene, perforated retroperitoneal appendix, CT, **156:341**
Functional residual capacity, determination, digital radiography, neonatal chest, **156:1209**

G

- Gadopentetate dimeglumine**
 brain MR imaging protocols, **157:837**
 enhanced chemical imaging of breast, **157:267**
 enhancement
 MR after brain tumor surgery, children, **156:1237**
 MR of musculoskeletal system, **156:457**
 enhancement of synovial cyst, MR imaging (l), **157:416**
 neurocysticercosis and, **157:393**
 pancreatic transplant dysfunction, **156:1171**
Gallbladder
 calculi, biliary lithotripsy, **157:287**
 carcinoma, endoscopic sonography (a), **156:881**
 contractility, altered after extracorporeal shock-wave variation in, **157:753**
 contraction, ursodeoxycholic acid effects, gallstone patients (a), **156:203**
 endoscopic retrograde cannulation (a), **156:412**
 function, spinal cord injury and (l), **157:412**
 imaging (p), **156:737**
 morphology, after gallstone dissolution (a), **157:651**
 motility, cholesterol gallstone disease (a), **156:643**
 perforation, cholecystographic and sonographic findings (a), **156:1120**
 primary carcinoma (a), **157:204**
 striated thickening of wall, sonography, **156:945**
 variants, imaging (p), **157:1205**
Gallstones: see Cholelithiasis
Ganglioglioma, intracerebral, partial complex seizures and, CT and MR imaging, **157:843**
Gastrectomy, total, esophagojejunostomy and, complications, **157:1189**
Gastric carcinoma, Crohn disease and, **157:311**
Gastric emptying, measurement (a), **156:644**
Gastritis
Campylobacter pylori, diagnosis (a), **156:1119**
Helicobacter pylori (a), **156:1331**
Gastrointestinal bleeding
 obscure origin
 angiography in detection, **156:385**
 small bowel enteroscopy (a), **156:1331**
Gastrointestinal tract
 CT, **156:23**
 endoscopic sonography (p), **156:63**
 lesions, long-distance running and (a), **156:412**
 polyposis syndromes, familial (p), **156:481**
Gastroparesis diabeticorum, gastric emptying in, intravenous erythromycin in (a), **156:413**
Gastroschisis, differentiation from omphalocele, prenatal sonography, **157:1065**
Gastrostomy tube
 migration of, percutaneous needle puncture for (l), **157:885**
 retrograde jejunoduodenogastric intussusception, CT, **156:957**
Gaucher disease, bone scans in (a), **157:422**
Geiger, Andrew H. (m), **156:822**

Gelatin sponge, mimicking of pelvic neoplasm, MR imaging, 157:1227

Genitourinary tract, CT and MR (b), 157:330

Gestational age, sonographic prediction, 157:1275

Goiter, nontoxic, hypervascularity of, color Doppler sonography (l), 156:199

Granuloma, giant-cell reparative, hand and foot bones (a), 156:881

Graves' disease, hyperthyroidism in, optimal iodine-131 dose in (a), 157:652

Growth hormone, idiopathic deficiency, MR, 156:599

Growth plate, cartilage, extension into metaphysis, healing fracture in abused infant, 156:775

H

Hallux rigidus deformity, radiologic assessment (p), 157:1029

Heart

comparative imaging (b), 157:834

congenital disease (b), 156:1154

congenital muscular ventricular septal defects, transcatheter closure of (a), 157:890

interventricular septum, defects, MR imaging (p), 157:943

sonography, fetal, four-chamber view, 156:547

transplantation, pediatric (a), 157:1363

transvenous pacing lead perforation, percutaneous removal, 156:471

Heart disease, procedures, men and women (a), 157:1361

Heart valve, Bjork-Shiley mechanical (a), 157:202

Helicobacter pylori

epidemiology of, asymptomatic population (a), 157:651

peptic ulcer and, children and their families (a), 157:652

Hemangioma

metastasis differentiation, ultrafast MR imaging, 157:727

splenic, CT, 157:44

Hemobilia, control by embolization, hepatic artery, 156:1263

Hemodialysis, arthropathy related to, MR imaging, 157:1023

Hemopericardium, diagnosis, digital subtraction angiography (l), 157:645

Hemoperitoneum, acute, pancreatic microcystic adenoma presenting with, 156:749

Hemophilia, hemarthrosis in, subluxation of humeral head with (l), 157:648

Heparin, low-dose aspirin comparison, myocardial infarction (a), 156:1117

Hepatectomy, partial, recurrent hepatocellular carcinoma after, 156:1177

Hepatic artery, false aneurysm and arterioportal-biliary fistula, hemobilia in, control by embolization, 156:1263

Hepatic vein, duplex Doppler sonography, tricuspid regurgitation, 156:79

Hepatitis, peliosis, HIV and, 156:91

Hepatocellular carcinoma

diagnosis and staging of, CT and sonography, 157:303

parasitization of superior mesenteric artery (l), 157:1357

recurrent, after partial hepatectomy, 156:1177

regression of (l), 156:868

screening methods (l), 156:869

small, fine-needle aspiration biopsy, fatal bleeding (l), 156:1114

Heterotopic ossification, acquired (a), 157:203

Hip

aspiration, girdlestone arthroplasty, 156:545

congenital dysplasia

osteoarthritis and (a), 156:1332

sonography diagnosis in children (a), 156:1332

fracture, risk factors in women (a), 157:890

septic arthritis, rectal tear associated with pelvic fracture, 157:817

total replacement (a), 157:203

Histoplasmosis

disseminated, CT, 157:955

esophageal, child with immunodeficiency with hyper-IgM, 157:381

History page, 157:274, 157:922

Hospitals, radiology practices and, 157:1341

Hughes-Stovin syndrome, radiologic findings (l), 157:1353

Human immunodeficiency virus

children seropositive for, parotid enlargement in, 157:553

peliosis hepatitis with, 156:91

prevalence among university students (a), 156:880

type 1, pulmonary tuberculosis patients (a), 156:1118

Hydatid disease, MR imaging (p), 157:741

Hydrocephalus, congenital, prenatal sonography, 156:359

Hydronephrosis, ureteral compression and, splenosis, scintigraphic diagnosis (l), 156:406

Hyperhomocysteinemia, risk factor for vascular disease (a), 157:889

Hypertension

malignant, coarctation of abdominal aorta associated with (l), 156:201

renal allograft-mediated, iliac artery stenosis causing, 157:513

Hyperthyroidism, Graves' disease, optimal iodine-131 dose in (a), 157:652

Hypothalamus, anatomy and pathology, MR, 156:579

Hyslop, Charles P. (m), 156:622

Hysterosalpingography

review, 157:675

tubal occlusion, 157:77

I

Ileitis, *Yersinia* terminal, sonography, 156:965

Ileum, diffuse stenosis, after ureteroileal interposition, 157:315

Iliac artery

stenosis

renal allograft-mediated hypertension, 157:513

unsuccessful balloon angioplasty and, 156:389

Iliopsoas bursa, distended, hip, MR (p), 156:1025

Impotence, radiologic assessment of, 157:923, 157:932

Infertility

selective salpingography, Fallopian tube recanalization and, 156:33

seminal tract abnormalities, endorectal sonography, 157:337

Infrahyoid portion, neck, lesions, MR imaging (p), 157:155

Interferon- $\alpha 2a$, recombinant, treatment of childhood angiomatous diseases (a), 156:1332

Interleukin-2

systemic therapy, atypical contrast reactions, 156:833

therapy, pulmonary edema during, 156:281

Intestine

chronic bleeding, mesenteric vascular insufficiency, 157:1203

small, amyloidosis, double-contrast radiographs, 156:741

Intraabdominal hemorrhage, arterial, CT, 156:725

Intracerebral hematoma, diversity of temporal pattern in MR imaging, 157:133

Intracranial hemorrhage, posterior fossa, extracorporeal membrane oxygenation treatment and, 156:571

Intrathoracic cyst, transbronchial aspiration of (l), 156:1110

Iohexol

gastrointestinal studies, barium comparison, infants and children, 156:345

intrathecal, reaction to (l), 156:403

oral, hypersensitivity reaction (l), 156:197

Iron, overload, systemic *Yersinia enterocolitica* infection, 157:773

Ischemia, cerebral, MR/spectroscopy, 156:1133

J

Jagodzinski, James A. (m), 157:1258

Jaundice, obstructive (l), 157:197

Jejunum, diverticulitis (a), 156:882

Jugular vein, internal, thrombosis, color Doppler and MR imaging (l), 157:1358

K

Kidney

allograft, biopsy of, arteriovenous fistulas and, 156:507

allograft-mediated hypertension, iliac artery stenosis, angiography, 157:513

arteriovenous malformation, color Doppler sonography, 157:991

autosomal dominant polycystic disease (a), 156:642

caliceal diverticula, stones and infection in, 156:995

failure, radiology of (b), 156:104

fetal, normal length of, sonography, 157:545

lymphoma, CT (a), 156:645

medullary sponge, benign tubular ectasia (l), 156:872

oncocyoma, 156:1144

radiocontrast-associated dysfunction, 157:49, 157:59, 157:66

stones, detection with real-time sonography, 157:975

transplantation

rejection, ^{31}P MR spectroscopy, 156:105

vascular complications with, 157:449

tubular dysgenesis, neonate, 157:383

Knee

arthroplasties, painful or infected, indium 111 leukocyte scanning in (a), 156:644

buckled meniscus (l), 156:200

displaced bucket-handle tear, medial meniscus, sagittal MR images, 156:117, 156:121

high signal in meniscus, MR, 156:333

instability, rupture of anterior cruciate ligament (a), 157:422

MR

meniscomfemoral ligaments (l), 157:1126

multiscreen digital workstation, 157:81

rheumatoid arthritis (l), 157:1128

rheumatoid arthritis, enhanced MR, 156:125

L

Lacunae, urographic finding, chronic obstructive uropathy, 156:985

Lambdoid synostosis, new plain film sign, infant, 156:1215

Latex balloons, anaphylactic reactions to (l), 157:885

Lee, John Joonjae (m), 156:1252

Leukemia

lymphoblastic, acute bone pain, children (a), 156:205

myelogenous, splenic activity (a), 156:413

Ligamentum arteriosum, calcification, CT, pediatric, 156:351

Limb-lengthening procedures, radiology of (p), 156:353

d-Limonene, medical dissolution of gallstones (a), 156:1331

Lipid cyst, classic and atypical appearances (p), 157:271

Lipoma, intracranial, MR imaging and CT diagnosis (l), 157:887

Literature reference, optical character recognition (l), 157:882

Lithotripsy

biliary

gallbladder contractility and, 157:287

gallstone fragmentation during, 156:493

physiochemical determinants (a), 156:881

shock-wave pressures (a), 156:411

endoscopic laser, large bile duct stones (a), 156:204

- extracorporeal shock-wave, *see* Extracorporeal shock-wave lithotripsy
- piezoelectric, symptomatic gallbladder stones (a), **156:411**
- shock-wave, using sonographic guidance (a), **157:1363**
- solitary gallstone, **157:747**
- Liver**
- abscess, percutaneous drainage, **157:1209**
- alcoholic disease, esophageal varices with, prophylactic sclerotherapy for (a), **157:1131**
- blunt injury, liver cell adenoma discovered after (l), **156:1324**
- cancer, embolization of hepatic artery in (l), **157:887**
- chronic acquired failure, MR imaging of the brain, **157:1111**
- detection of tumors
- CT vs MR (l), **156:867**
- sonography (l), **156:867**
- disease, alpha-1-antitrypsin deficiency (a), **156:882**
- fatty infiltration, phase-contrast MR vs biopsy, **156:307**
- focal fatty infiltration, low-density masses, dual-energy CT, **157:721**
- focal nodular hyperplasia, MR, **156:317**
- hepatocellular carcinoma
- hydatid cyst, CT, **156:751**
- masses, patients with carcinoma, sonography, CT and MR imaging comparison, **157:731**
- metastases
- edema adjacent to, MR, **157:499**
- hemangioma differentiation, ultrafast MR imaging, **157:727**
- parasitization of superior mesenteric artery (l), **157:1357**
- periportal contrast enhanced CT, **156:313**
- primary lymphoma (l), **157:413**
- sarcoidosis, MR (l), **156:1324**
- transplantation
- abdominal CT findings after, **156:1167**
- choledochojejunostomy in (a), **156:883**
- CT and sonography, hepatocellular carcinoma, **157:303**
- low-attenuation periportal collar in CT, **157:1195**
- orthotopic, **157:29**
- stenoses of vascular anastomoses after, balloon angioplasty treatment, **157:167**
- subcapsular hepatic necrosis in, **156:981**
- Liver cell adenoma**, discovered after blunt hepatic injury (l), **156:1324**
- Lobular carcinoma in situ**, breast, **157:257**
- Loop, John Wickwire (m)**, **156:1100**
- Lumbar disk**, herniated, automated percutaneous lumbar disectomy, **156:531**
- Lung**
- amiodarone, CT-pathology correlation (a), **156:206**
- bullous disease, digital storage phosphor radiography, **156:467**
- cancer, chest CT combined with artificial pneumothorax in determination of, **156:707**
- chronic diffuse infiltrative disease
- CT comparisons, **157:693**
- high-resolution CT, **157:1163**
- disorders, drug abuse and (a), **156:1120**
- interstitial disease, unknown cause, **156:225**
- lymphoma, CT, **156:711**
- nonfluoroscopic percutaneous needle aspiration, patient with pneumonia (a), **156:410**
- open biopsy, critically ill newborn (a), **156:412**
- peripheral carcinoma, bronchus sign on CT, **157:1181**
- small peripheral carcinoma, air bronchograms, CT, **156:921**
- systemic blood supply, developmental abnormalities, **156:669**
- systemic pathology (b), **157:255**
- thallium-201 uptake, exercise emission computed tomography (a), **157:652**
- transplantation, double, end-stage chronic obstructive pulmonary disease (a), **157:202**
- upper lobe, pulmonary angiography after surgery, **157:471**
- Lymphangiography**, laceration of thoracic duct, **157:703**
- Lymphedema**, chronic, angiosarcoma associated with, CT, **156:543**
- Lymphoma**
- AIDS-related
- CT (p), **156:969**
- infant, **156:1037**
- diffuse intraabdominal, complicating idiopathic myelofibrosis, CT, **156:1189**
- kidney, CT (a), **156:645**
- lung, CT, **156:711**
- mediastinal
- sonography (l), **157:644**
- sonography, CT, and chest radiography compared, **156:265**
- non-Hodgkin's, second cancers after (a), **157:420**
- posttreatment evaluation, mediastinal sonography, commentary, **157:469**
- skeletal, Castleman disease with, **157:1035**
- staging, MR imaging in (a), **157:420**
- M**
- MacPherson, Robert Alexander (m)**, **156:1188**
- Malpractice**
- mammography, **156:475**
- mammography (l), **157:883**
- Mammography**
- after breast reconstruction (p), **156:1159**
- American College of Radiology Accreditation Program, **157:473**
- breast abnormalities, caused by biopsy (p), **156:287**
- breast traction (l), **156:1321**
- lipid cyst (p), **157:271**
- lobular carcinoma in situ, **157:257**
- localization and needle aspiration, breast lesions, **157:711**
- malpractice and, **156:475**
- malpractice and (l), **157:883**
- medicolegal aspects, **156:719**
- palpable vs impalpable lesions, prevalence of carcinoma and, **157:21**
- phyllodes tumor, **157:715**
- quality assurance (l), **157:1354**
- radiographic density, noncalcified breast masses, **157:25**
- residency training in, **156:59**
- self-referred patients, **157:481**
- McCune-Albright syndrome**, scintigraphic abnormality pattern (a), **156:413**
- Meckel diverticulum**, inverted, enteroclysis (l), **156:1111**
- Meckel syndrome**, fetal renal artery blood flow, Doppler velocity waveforms (l), **156:408**
- Mediastinum**
- anterior, masses, CT and MR imaging, **157:1171**
- hemorrhage, angiography, **156:273**
- lymphoma patients
- sonography in posttreatment evaluation, commentary, **157:469**
- sonography (l), **157:644**
- sonography, CT, and chest radiography compared, **156:265**
- mass
- high-attenuation on unenhanced CT, **156:45**
- ultrasonically guided biopsies (a), **157:1361**
- pseudomass, neonates with anterior pneumothorax, **156:145**
- thymolipoma, CT, **157:468**
- Medical decision making**, defining terms for (l), **156:198**
- Medicine in American art**, **156:554**, **156:1180**, **157:280**, **157:720**, **157:974**
- Melanoma**, primary esophageal, **157:318**
- Memorials**
- Andrew H. Geiger, 1956-1990, **156:822**
- Andrew N. Schwartz, 1950-1989, **156:154**
- Charles P. Hyslop, 1924-1990, **156:622**
- Hyman R. Senturia, 1909-1990, **156:400**
- James A. Jagodzinski, 1939-1991, **157:1258**
- John Joonjae Lee, 1940-1990, **156:1252**
- John Wickwire Loop, 1924-1990, **156:1100**
- John W. Turner, 1912-1991, **157:824**
- Robert Alexander MacPherson, 1903-1990, **156:1188**
- Meniscus**
- buckled (l), **156:200**
- high signal, MR, **156:333**
- lateral, pseudotear (l), **157:649**
- medial, displaced bucket-handle tear, MR, **156:117**, **156:121**
- Metaphysis**
- healing injury
- infant abuse, **156:775**
- normal metaphyseal radiologic variants confused with infant abuse (p), **156:781**
- Metatarsal synostosis**, rare form (l), **157:648**
- Methyl tert-butyl ether**
- cholesterol gallstone dissolution by, thin-layer chromatography, **157:33**
- ESWL and, symptomatic gallbladder stones (a), **157:1363**
- Midazolam**, fentanyl and, sedation for lower-extremity angiography, **157:174**
- Midbrain**, enlarged perivascular spaces, focal high signal on MR, **156:157**
- Migraine headaches**, MR imaging, **157:385**
- MR imaging**
- see also* specific type or site
- angiography, renal arteries, **157:981**
- bacterial osteomyelitis (p), **157:365**
- body fat, young women, **157:99**
- central nervous system (b), **156:790**
- claustrophobia induced by, alprazolam and (l), **156:633**
- clinical (b), **157:850**
- contrast-enhanced, advances in, **156:235**
- experimental and clinical oncology (b), **157:1220**
- gamuts and pearls in (b), **157:602**
- gradient echo, portal venous system, **157:297**
- hydatid disease (p), **157:741**
- lymphoma staging (a), **157:420**
- musculoskeletal system (b), **156:784**, **157:526**
- patient comfort, music enhancement of (l), **156:403**
- ³¹P spectroscopy, characterization of tumor by, **157:243**
- sectional anatomy (b), **156:570**
- seminal vesicles (p), **156:989**
- tissue characterization (b), **157:98**
- two-piece wrist surface coil, **156:343**
- vascular anomalies, soft-tissue (p), **157:559**
- velocity-encoded cine, right and left ventricular stroke volume, **157:9**
- vena cava tumor thrombi (a), **156:882**
- MR imaging, abdomen**
- anterior mediastinum, masses, **157:1171**
- barium studies, normal volunteers, **157:761**
- contrast-enhanced, gastrointestinal agents, **156:252**
- pancreatic transplant dysfunction, **156:1171**
- retroperitoneal fibrosis, **157:321**
- MR imaging, adrenal**, Castleman disease, **157:781**
- MR imaging, ankle**, lateral collateral ligament (p), **156:131**
- MR imaging, bladder**, carcinoma of the urinary bladder (b), **157:516**
- MR imaging, bone**
- fossil vertebrae (l), **157:415**
- marrow disease, disappearance of basivertebral vein (l), **157:1129**
- osteosarcoma, preoperative evaluation, **157:347**
- septic sacrolitis (a), **156:1333**
- MR imaging, breast**, gadopentetate dimeglumine enhancement, **157:267**

- MR imaging, cervix**
carcinoma, **156:753**
clinical stage I carcinoma, degree of invasiveness, **156:1191**
- MR imaging, cranium**
acute cerebral infarction, CT comparison, **157:585**
angiography, cervical neural foramen (I), **157:1128**
Behcet disease, neurologic involvement, **157:867**
benign lymphoepithelial parotid tumors, AIDS patients, **156:1253**
brain
carotid artery patency, **157:1299**, **157:1307**
chronic acquired hepatic failure, **157:1111**
diabetes insipidus patients, **157:123**
intraventricular mass lesions (p), **157:1283**
tumor surgery, gadopentetate dimeglumine-enhanced MR after, **156:1237**
brain and spine (b), **157:1324**
brain (b), **157:1282**
cerebral ischemia, **156:1133**
contrast-enhanced, **157:575**
first 24 hours, **157:565**
congenital nasal masses, **156:587**
contrast-enhanced
cerebral metastases, **156:1039**
chronic partial epilepsy, **156:605**
hemorrhagic brain lesions, **157:861**
neurologic applications, **156:239**
nonneurologic applications, **156:245**
conventional neuroangiography (p), **156:1075**
dural sinus occlusion, phase-sensitive gradient-echo, **157:139**
ependymoma, fourth ventricle, **157:1278**
gadopentetate dimeglumine enhancement, intracranial lesions, **157:837**
hamartomas of the tuber cinereum, **156:1053**
hypothalamus, anatomy and pathology, **156:579**
idiopathic growth hormone deficiency, **156:599**
intra- and paraorbital lesions, paramagnetic contrast enhanced, **156:1059**
intracerebral gangliogliomas, partial complex seizures and, **157:843**
intracerebral hematoma, **157:133**
intracranial cryptococcosis, immunocompromised patients, **156:1245**
intracranial lipoma (I), **157:887**
midbrain
focal high signal caused by enlarged perivascular spaces, **156:157**
focal high signal on (I), **157:1129**
migraine headaches, **157:385**
neurocysticercosis, **157:393**
neurotoxicity, cyclosporin A-induced, **157:851**
orbit and its contents, children (p), **156:1219**
pediatric brain (b), **157:122**
phase imaging
intracranial vascular abnormalities, **156:373**
paranasal sinuses, mucosal thickening, **156:381**
practical MR atlas of neonatal brain development (b), **157:842**
proton spectroscopy, multiple sclerosis, **157:1073**
ruptured intracranial dermoid cyst, **156:807**
subarachnoid hemorrhage, nonaneurysmal perimesencephalic, **157:1325**
trochlear nerve neoplasms, **157:595**
white matter hyperintensities, incidental punctate, **157:1317**
- MR imaging, esophagus**
carcinoma, vs CT, **156:297**
squamous cell carcinoma (a), **156:205**
- MR imaging, extremities**
reflex sympathetic dystrophy, **156:113**
vascular grafts, children, **157:1069**
- MR imaging, eye**, pulse sequence and contrast agent, malignant uveal melanoma, **157:1087**
- MR imaging, femur**, avascular necrosis, canine model, **157:341**
- MR imaging, fetal**, anomalies (p), **156:1205**
- MR imaging, foot**, abnormalities, diabetes mellitus (p), **157:813**
- MR imaging, head and neck**
lesions
infrahyoid part of neck (p), **157:155**
suprahyoid part of neck (p), **157:147**
- MR imaging, heart**
bacterial endocarditis, perivalvular pseudoaneurysm, **156:1155**
distal aortopulmonary window, **157:835**
interventricular septal defects (p), **157:943**
- MR imaging, hip**
acetabular residual dysplasia (a), **157:423**
distended iliopsoas bursa (p), **156:1025**
iliopsoas bursal distension (a), **156:206**
- MR imaging, kidney**
amyloid arthropathy, dialysis-related, **157:1023**
morphological and functional MR of the kidneys and adrenal glands (b), **157:776**
- MR imaging, knee**
coronal
meniscomfemoral ligaments (I), **157:1126**
rheumatoid arthritis (I), **157:1128**
gadopentetate dimeglumine-enhanced, rheumatoid arthritis, **156:125**
high signal in meniscus, **156:333**
meniscal abnormalities, asymptomatic marathon runners, **157:1239**
multiscreen digital workstation, **157:81**
osteoarthritis, **157:799**
sagittal images, displaced bucket-handle tear, **156:117**, **156:121**
- MR imaging, leg**, Achilles tendon rupture, polyactic acid implant for repair of, **156:769**
- MR imaging, liver**
biliary system and (b), **156:492**
detection of masses with carcinoma, comparison with sonography and CT, **157:731**
focal nodular hyperplasia, **156:317**
metastasis, edema adjacent to, **157:499**
phase-contrast, vs biopsy, fatty infiltration, **156:307**
sarcoidosis (I), **156:1324**
tumors (I), **156:867**
ultrafast, hemangioma and metastasis differentiation, **157:727**
- MR imaging, mesentery**, sclerosing mesenteritis, **156:517**
- MR imaging, muscle**, exercise effects, concentric vs eccentric actions, **156:765**
- MR imaging, musculoskeletal system**
contrast-enhanced, gadopentetate dimeglumine, **156:457**
teaching file (b), **156:456**
- MR imaging, neck**
internal jugular vein, thrombosis (I), **157:1358**
posterior cervical space, **157:161**
- MR imaging, pelvis**
gelatin sponge mimicking a neoplasm, **157:1227**
malignant Brenner tumor (I), **157:1355**
- MR imaging, pituitary**, posterior fossa, high-intensity signals within, **157:389**
- MR imaging, prostate**, carcinoma, tumor volume, **156:511**
- MR imaging, shoulder**, labral-capsular complex, **157:1015**
- MR imaging, soft tissue**
fibromatosis, **156:539**
myositis ossificans, **157:1243**
sarcoma, **157:353**
synovial sarcoma (p), **156:337**
tumor, paradoxical signals in (I), **157:648**
- MR imaging, spine**
brain and spine (b), **157:1324**
dermal sinus tracts, children, **156:791**
infection, gadolinium-enhanced (a), **156:206**
intervertebral disk, normal and degenerated (p), **157:93**
intraspinous synovial cyst (I), **157:416**
- magnetic susceptibility artifacts and motion effects, cervical neural foramina, **156:1069**
neural foramina, degenerative narrowing, **156:1229**
- MR imaging, thorax**
anterior chest wall, flat coil use in (I), **156:1110**
bronchial carcinoid tumors, adrenocorticotrophic hormone-induced, **156:39**
pleura, **156:1145**
pulmonary infarction (a), **156:1330**
radiation therapy effects, thoracic and lumbar bone marrow, **157:87**
vascular ring, infant (I), **156:1111**
- MR imaging, transaxial**, thoracic inlet (p), **157:707**
- MR imaging, uterus**, endometrium, cancer, **157:1221**
- MR imaging, wrist**, hand and (b), **157:340**
- MR imaging units**, economics and use of in the U.S.
- Mucocoele**, breast, **156:199**
- Mucopolysaccharidosis**, children, arteriopathy and coarctation of abdominal aorta with, **157:819**
- Multiple sclerosis**, proton MR spectroscopy, **157:1073**
- Musculoskeletal system**
cartilaginous tumors (b), **157:1034**
skeletal lesions, percutaneous biopsy of, **157:935**
skeletal lymphoma, Castleman disease with, **157:1035**
stress injury, meniscus, asymptomatic marathon runners, **157:1239**
stress injury (b), **157:1238**
- Mycobacterial infections**, changing epidemiology, United States, **156:255**
- Mycobacterium tuberculosis**, vs *Mycobacterium avium-intracellulare*, AIDS patient, **156:487**
- Myelofibrosis**, idiopathic, diffuse intraabdominal lymphoma and, CT, **156:1189**
- Myocardium**
infarction, heparin and low-dose aspirin for (a), **156:1117**
ventricular, noncompaction of, CT, **156:717**
- Myositis ossificans**, MR, radiologic-pathologic appearance, **157:1243**
- N**
- Nasal masses**, congenital, CT and MR, **156:587**
- Needle-stick injuries**, prevention (I), **157:417**
- Nephropathy**
radiocontrast-associated, **157:49**, **157:59**, **157:66**
uroepithelial malignancy and, **157:69**
- Nephro-urology**, radionuclides in (b), **156:500**
- Neuroangiography**, conventional (p), **156:1075**
- Neuroblastoma**, screening, infant (a), **156:644**
- Neurocysticercosis**, contrast-enhanced MR imaging in, **157:393**
- Neuroimaging**
essentials (b), **157:866**
three-dimensional (b), **157:1072**
- Neuroradiology**, test and syllabus (b), **157:584**
- Neurotoxicity**, cyclosporin A-induced, MR imaging of, **157:851**
- Nuclear medicine**
annual 1990 (b), **156:780**
practical (b), **156:394**
- O**
- Oblique coronal plane**, en face MR imaging in (p), **157:943**
- Ocular melanoma**, prevalence and location, **157:1279**
- Omphalocele**, differentiation from gastroschisis, prenatal sonography, **157:1065**
- Oncocytoma**, renal, **156:1144**
- Orbit**, fat-suppression MR, paramagnetic contrast enhanced, **156:1059**
- Oropharyngeal dysfunction**, elderly patients, videofluoroscopy, **156:293**

- Osler-Weber-Rendu disease**, Doppler sonography (l), 157:413
- Osteitis**, condensing, clavicle, 156:1011
- Osteoarthritis**
congenital dysplasia of hip and (a), 156:1332
hallux rigidus deformity (p), 157:1029
knee, radiography, CT, and MR imaging comparison, 157:799
- Osteochondroma**, radiation-induced, 157:793
- Osteogenesis imperfecta**, child abuse differentiation from (l), 156:634
- Osteomyelitis**
bacterial (p), 157:365
foot, diabetic patients, ¹¹¹In-leukocyte scintigraphy, 157:527
soft-tissue, leukocyte scintigraphy, 157:807
talus, limping in childhood and, 156:785
- Osteonecrosis**, dysbaric (l), 156:1327
- Osteophyte**, giant thoracic, esophageal food impaction, 157:319
- Osteoporosis**
broadband attenuation measurements, sonography (l), 156:1326
fluoride therapy for, bone fragility during (a), 156:1119
noninvasive measurements, bone mass, structure, and strength, 157:1229
physiological basis (b), 156:130
- Osteosarcoma**
cervical spine (l), 157:1357
Ewing sarcoma and, response to chemotherapy, 157:825
preoperative evaluation, enhanced MR imaging, 157:347
- Osteosclerosis**, vertebral sarcoidosis (l), 157:1356
- Ovary**, torsion, pregnancy and (l), 156:871

P

- Pacemaker**, nonfunctioning lead, percutaneous removal, 156:471
- Paget disease**, bone, sarcoma in, 156:1199
- Pancreas**
cancer, superior mesenteric artery involvement, sonography, 156:69
congenital short, polysplenia syndrome with, pediatric, 156:799
CT, children (p), 157:375
cystic tumors, sonography and CT (a), 156:883
microcystic adenoma, presenting with acute hemoperitoneum, 156:749
mucinous tumors (a), 157:422
necrosis, lack of contrast enhancement in CT, 156:93
transplantation, dysfunction, MR, 156:1171
tumor, endoscopic ultrasound in diagnosis (a), 157:892
- Pancreatic duct**, disrupted, endoscopic transpapillary therapy for (a), 157:421
- Pancreatitis**
acute
CT, 156:93
leukocyte infiltration in (a), 156:1119
focal calcifications, 156:1005
percutaneous biopsy of left adrenal masses, 157:777
pseudoaneurysm formation and, interventional radiology, 156:97
- Pancreatography**, fine-needle aspiration (a), 157:420
- Papillomatosis**, common bile duct, ampullary carcinoma and (l), 156:405
- Paranasal sinus**
limited-slice CT, children, 156:367
mucosal thickening, MR images of brain, 156:381
- Paraquat**, poisoning, chest radiography and CT, 157:697
- Parotid gland**
enlargement, HIV-positive children and, 157:553
lymphoepithelial tumors, AIDS patients, CT and MR, 156:1253
- Patellectomy**, partial, displaced patellar fractures (a), 156:644
- Patellofemoral joint**, disorders (b), 156:332
- Pediatric radiology**
acute pyelonephritis, sonography vs ^{99m}Tc-DMSA scintigraphy, 157:539
adrenocortical macrocysts, Beckwith-Wiedemann syndrome, 157:549
angiomatous disease, recombinant interferon alfa-2a (a), 156:1332
anorexia nervosa, decreased bone density in, adolescent girls (a), 156:205
aortic thrombosis, after umbilical artery catheterization, neonate, 156:567
childproof cap on medicine bottle, esophageal foreign body (l), 156:201
choledochal cyst, biliary atresia and, neonate (l), 157:646
congenital dysplasia of hip, sonography diagnosis in children (a), 156:1332
congenital nasal masses, CT and MR, 156:587
congenital short pancreas, polysplenia syndrome with, 156:799
deferoramine-induced bone dysplasia, thalassemia major, 156:561
descending aorta, anomaly of, 156:1033
diskitis in children (a), 157:652
Down syndrome, arthropathy of (a), 156:882
drug-related complications, infants and children, 157:1039
endotracheal tube location, preterm and term neonates (a), 156:1120
esophageal histoplasmosis, with immunodeficiency with hyper-IgM, 157:381
fetal kidneys, normal length, sonography, 157:545
fibroepithelial polyp, ureter, 157:1273
functional residual capacity, digital radiography, neonatal chest, 156:1209
gadopentetate dimeglumine-enhanced MR, brain tumor surgery, 156:1237
gait disturbance, radiology of lower extremities (a), 156:1332
gastrointestinal studies, barium compared with iohexol, 156:345
gestational age, sonography prediction of, 157:1275
goitrous cretinism, manifesting as newborn stridor, 157:557
heart transplantation (a), 157:1363
Helicobacter pylori, peptic ulcer and (a), 157:652
human immunodeficiency virus, parotid enlargement in, 157:553
lambdoid synostosis, new plain film sign, infant, 156:1215
lap-belt ecchymosis, CT findings, 157:111
ligamentum arteriosum, calcification of, CT, 156:351
lung biopsy, open, critically ill newborn (a), 156:412
lymphoblastic leukemia, acute bone pain in (a), 156:205
magnetic resonance imaging of pediatric brain (b), 157:122
mediastinal pseudomass, neonates with anterior pneumothorax, 156:145
mucopolysaccharidosis, arteriopathy and coarctation of abdominal aorta with, 157:819
neonatal CNS abnormalities, maternal cocaine abuse and, 157:1105
neonatal congenital adrenal hyperplasia, sonography, 156:141
neuroblastoma, screening, infant (a), 156:644
occult ectopic ureter, girls with urinary incontinence, CT, 156:365
orbit and contents, children, CT and MR (p), 156:1219
osteomyelitis of the talus, limping and, 156:785
pancreas, CT (p), 157:375
paranasal sinus, limited-slice CT, 156:367
- perforation of the augmented bladder, children and adolescents, 157:1059
pocket atlas of pediatric ultrasound (b), 156:364
posterior fossa intracranial hemorrhage, extracorporeal membrane oxygenation treatment and, 156:571
posthemorrhagic ventricular dilation, asymmetric growth of cerebral ventricle with, infant (a), 156:1333
primary lymphoma, CNS, infant with AIDS, 156:1037
pulmonary interstitial emphysema, jet and conventional mechanical ventilation (a), 157:1364
reflex sympathetic dystrophy (a), 156:204
renal length measurements, sonography, 156:1029
renal tubular dysgenesis, 157:383
Schmid-like metaphyseal chondrodysplasia, simulating child abuse, 156:576
septic arthritis, hip, infant (a), 156:412
sickle cell anemia, cerebrovascular disease in, MR angiography (a), 156:645
sonography of biliary tract, infants and children, 157:1051
spinal dermal sinus tracts, MR, 156:791
splenic size, infants and children, sonography, 157:119
synthetic surfactant, mortality in infants treated with (a), 156:1333
thanatophoric dwarf variant fetus, sonography, 156:149
tracheal lumen, CT measurement, 156:371
tumor vascularity, color Doppler imaging, 157:1267
unilateral hydrocephalus, sonography, 156:359
urethral abnormalities, male neonates with VATER association, 156:137
vascular grafts, MR imaging, 157:1069
vascular ring, infant, MR (l), 156:1111
wandering spleen, acute splenic torsion in, 156:151
- Pelvimetry**, CT, level of ischial spines, 156:527
- Pelvis**
after cesarean section, CT appearance, 156:523
fracture
hemorrhage associated with, 157:1005
imaging of (b), 157:784
rectal tear with, septic arthritis of the hip and, 157:817
- Pentamidine**
inhaled
Pneumocystis carinii pneumonia and (a), 156:409, 880
prevention of pneumonia (a), 157:889
- Peptic disease**, pyloric deformation (a), 156:881
- Percutaneous biliary stricture dilatation**, single-session therapy, general anesthesia, 157:1263
- Pericardial effusion**, after cardiac surgery, CT, 157:19
- Pericardium**, transvenous pacing lead perforation, percutaneous removal, 156:471
- Perinephric hemorrhage**, spontaneous, imaging (a), 157:204
- Perirectal disease**, endorectal sonography (p), 157:503
- Periureteric venous ring**, nonobstructing, CT, 157:997
- Perivalvular pseudoaneurysm**, bacterial endocarditis and, MR detection, 156:1155
- Petrous bone**, deformed, new plain film sign, infant, 156:1215
- Photostimulable phosphor digital imaging**, comparison, 157:533
- Phylloides tumor**, mammography, sonography, and aspiration cytology, 157:715
- Picture archiving and communications systems (PACS)**
cost-effectiveness, 156:177
MR examination of knee, 157:81

- ultrafast network for, 156:835
- Pituitary gland**, posterior fossa, high-intensity signals within, 157:389
- Pleura**
sonography, CT, and MR, 156:1145
transvenous pacing lead perforation, percutaneous removal, 156:471
- Pneumocystis carinii pneumonia**
aerosolized pentamidine against (a), 156:409
AIDS patient, visceral calcification and, 156:745
atypical presentations, patients receiving inhaled pentamidine prophylaxis (a), 156:880
oral therapy for (a), 156:409
- Pneumomediastinum**, spontaneous (a), 157:1131
- Pneumonia**
community-acquired, noninfectious pulmonary diseases masquerading as (a), 157:891
Pneumocystis carinii, inhaled pentamidine for prevention of (a), 157:889
staphylococcal, centrilobular lesions due to (l), 156:1322
- Pneumoperitoneum**
supine abdominal radiography, 156:731
supine abdominal radiography (l), 157:1354
- Pneumothorax**
anterior, neonate, mediastinal pseudomass in, 156:145
artificial, chest CT combined with, 156:707
catamenial, pneumoperitoneum and (l), 156:404
development of, thoracentesis and, 156:917
- Poly-lactic acid**, implant, Achilles tendon rupture repair, 156:769
- Polysplenia syndrome**, congenital short pancreas, pediatric, 156:799
- Popliteal artery**
anatomic relation to vein, accurate angiographic puncture, 157:1259
trifurcation
kissing-balloon technique for angioplasty, 156:823
kissing-balloon angioplasty (l), 157:1359
- Portal vein thrombosis**, color Doppler imaging, 157:293
- Portal venous system**, gradient-echo imaging value in, 157:297
- Portohepatic venous shunts**, multiple intrahepatic, steel-coil embolization treatment, 157:971
- Posterior cervical space**, normal and diseased, 157:161
- Post-polio syndrome**, dysphagia in (a), 157:890
- Pregnancy**
early, vaginal and abdominal sonography (a), 156:1333
ovarian torsion and (l), 156:871
sonography of ureter (a), 157:1363
third trimester, transperineal approach to sonography of the cervix, 157:73
- Prostate**
cancer
prostate-specific antigen in serum (a), 157:889
radioisotope bone scan limitations in (a), 156:203
transrectal sonography (a), 157:1132
carcinoma
MR imaging, 156:511
splenic hemangioma and, 157:44
cystic carcinoma, transrectal sonography, 157:785
transurethral balloon dilatation, 157:509
- Prostatism**
sonographic evaluation of urinary tract in (a), 157:892
transurethral balloon dilatation, prostatic urethra, 157:509
- Pseudoaneurysm**, formation, pancreatitis with, interventional radiology, 156:97
- Pseudoarthritis**, fracture healing (a), 157:1132
- Pulmonary disease**, interstitial (b), 156:680
- Pulmonary edema**
during interleukin-2 therapy, 156:281
noncardiogenic, intravascular contrast media and, 157:255
- Pulmonary emboli**, Wilms tumor and, 156:155
- Pulmonary nodules**, solitary, CT, 156:925
- Pyelonephritis**
acute, CT (a), 156:204
children, sonography vs ^{99m}Tc-DMSA scintigraphy, 157:539
- R**
- Racial differences**, oriental cholangiohepatitis, 157:1
- Radiation**
injury of the brain, 156:689
protection (b), 156:688
- Radiation therapy**
effects on thoracic and lumbar bone marrow, MR, 157:87
high-risk rectal carcinoma (a), 157:419
osteochondroma induced by, 157:793
- Radiculopathy**, lumbosacral, extraspinal causes of (a), 157:1363
- Radiography**, digital, photostimulable phosphor, extremities, 157:533
- Radiography, technique**
chest
functional residual capacity, neonate, 156:1209
history and interpretation (l), 156:197
colon cancer screening, economic implications, 156:939
colonic neoplasms, 156:303
digital storage phosphor, bullous lung disease, 156:467
double-contrast, amyloidosis, small intestine, 156:741
exposure, Fuch's principles (b), 156:954
lower extremities, children with gait disturbance (a), 156:1332
Muhimbili Medical Center, Dar es Salaam, Tanzania (l), 157:195
plain film, bacterial osteomyelitis (p), 157:365
scan equalization, bone imaging with, 157:359
supine abdominal, pneumoperitoneum, 156:731
- Radiologists**
diagnostic, radiologic physics instruction for, 157:409
productivity of, 157:1337
visual acuity testing, commentary, 156:1107
- Radiology**
communication of images, 156:835
diagnostic
aids (b), 156:316
bronchopulmonary dysplasia, 156:681
Christensen's physics of (b), 156:234
environment and (l), 156:863
eye and orbit (b), 156:1218
inappropriate use of significant figures (l), 157:645
information overload and management in, 156:1283
interventional
pancreatitis with pseudoaneurysm formation, 156:97
percutaneous access set, 156:397
interventional (b), 157:166
limb-lengthening procedures (p), 156:353
orthopedic (v), 156:1010
reflections, 157:447
residency training, mammography, 156:59
teaching in developing countries (l), 157:196
trauma (b), 156:774
whose turf is imaging, 156:443
- Radiology Centennial, Inc. (RCI)**, 156:938, 156:944
- Radiology journalism**, 1991 Figley Fellows, 156:448
- Radiology practice**
AIDS risk and risk reduction, 157:911
commentary, 157:919
contracts with hospitals, 157:1341
diagnostic imaging in clinical practice (b), 157:1050
PC-based semiautomated reporting system, 157:1117
- Radiology residents**
mammography, 156:59
physics instruction for diagnostic radiologists, 157:409
teaching method, percutaneous vascular catheterization (l), 157:1125
recommended textbooks (l), 156:863
- Radiology services**, volume and cost in the U.S.
- Radon**, control (b), 156:968
- Receiver-operating-characteristic curves**, understanding of, commentary, 157:1119
- Rectal carcinoma**, effective surgical adjuvant therapy for (a), 157:419
- Rectal disease**, endorectal sonography (p), 157:503
- Rectal intussusception**, CT (l), 156:870
- Rectosigmoid cancer**, local recurrence (a), 156:205
- Rectus abdominis musculocutaneous flap**, breast reconstruction with, mammographic and CT findings after (p), 156:1159
- Rectus abdominis myocutaneous flap**, vaginal reconstruction with, CT, 156:1001
- Reflex sympathetic dystrophy**
children (a), 156:204
extremities, MR imaging in, 156:113
- Renal arteries**
MR angiography, 157:981
stenosis, Wallstent treatment of (l), 156:640
- Renal cell carcinoma**
intratumoral fat in (l), 156:871
vena cava, surgical management (a), 156:1119
- Respiratory distress syndrome**, synthetic vs human surfactants in treatment of, 157:371
- Retinoblastoma**, trilateral (l), 157:198
- Retroperitoneal fibrosis**, review, 157:321
- Retroperitoneal hematoma**, percutaneous management of (l), 156:1112
- Roentgenography**, atlas of measurement (b), 157:498
- S**
- Sacroccocygeal teratoma**, antenatal diagnosis, Doppler sonography and MR (l), 156:1115
- Sacroilitis**, septic, MR (a), 156:1333
- Salpingography**
ostial, tubal occlusion, 157:77
selective, Fallopian tube recanalization and, 156:33
- Sarcoidosis**
gallium-67 distribution in (a), 156:1120
hepatic
hypertrophy of caudate lobe and, sonography (l), 157:886
MR (l), 156:1324
multinodular splenic, CT and sonography (l), 156:1113
retroperitoneal, 156:520
vertebral osteosclerotic (l), 157:1356
- Sarcoma**
Paget disease of bone, 156:1199
soft-tissue, MR imaging vs sonography, 157:353
- Scan equalization radiography**, bone imaging, 157:359
- Schwannoma**, head and neck, angiography, 157:1309
- Schwartz, Andrew N. (m)**, 156:154
- Scintigraphy**
bacterial osteomyelitis (p), 157:365
impotence, 157:923, 157:932
¹¹¹In-leukocyte
osteomyelitis, foot, diabetic patients, 157:527
osteomyelitis, soft-tissue infection, 157:807
regional gut transit, idiopathic constipation (a), 157:891
^{99m}Tc-DMSA, acute pyelonephritis, 157:539
- Sclerosing mesenteritis**, MR, 156:517

Sclerotherapy

- endoscopic, portosystemic shunts of, portal venous system after, **156:85**
- endoscopic variceal, portal pressure in cirrhosis (a), **157:1362**

Seizures, partial complex, intracerebral ganglioglioma, CT and MR imaging, **157:843****Seminal tract**, abnormalities, infertility and, endorectal sonography, **157:337****Seminal vesicles**

- MR (p), **156:989**
- transrectal ultrasound (a), **156:1120**

Senturia, Hyman R. (m), **156:400****Sepsis**, unknown cause, percutaneous cholecystostomy, **156:1163****Sex differences**

- coronary artery disease (a), **157:1361**
- overall fat distribution, young women, MR, **157:99**

Shoulder

- comparison of imaging methods (a), **157:1132**
- impingement syndrome (a), **157:1363**
- labral-capsular complex, MR imaging, **157:1015**

Shuntography, functional positive-contrast, **156:801****Sickle cell anemia**, cerebrovascular disease in, MR angiography (a), **156:645****Sinonasal carcinoma**, spread via eustachian tube (l), **157:888****Sinuses**, screening CT in, **157:1093**

- commentary, **157:1099**

Skeletal hyperostosis, idiopathic, fracture of the spine in (a), **157:892****Skull**, multiple osteolytic defects (l), **157:201****Society for Pediatric Radiology**, European Society of Pediatric Radiology and, International Pediatric Radiology '91, May 1991, **157:1272****Society of Computed Body Tomography**, 14th Annual course, April 1991, **157:615****Society of Gastrointestinal Radiologists**, 20th annual meeting, February 1991, **157:187****Society of Thoracic Radiology**, ninth annual meeting and postgraduate course, May 1991, **157:875****Society of Uroradiology**, tenth meeting and postgraduate course, **156:189****Soft tissue**

- long term effects of ESWL, **156:73**
- tumor, paradoxical signals in (l), **157:648**
- vascular anomalies, MR correlation of (p), **157:559**

Sonography

- artifacts and their origins (p), **156:1267**
- carotid duplex, aortic valvular disease, **157:403**
- color Doppler
 - acute torsion of wandering spleen, **157:307**
 - arteriovenous malformations of the kidney, **157:991**
 - basal cerebral arteries, **157:397**
 - erectile dysfunction, **157:331**
 - hypervascularity of nontoxic goiter (l), **156:199**
 - improved needle-tip visualization by, **156:401**
 - internal jugular, thrombosis (l), **157:1358**
 - intrascrotal pathology (a), **156:644**
 - performance requirements and operational parameters, **156:3**
 - portal vein thrombosis, **157:293**
 - splenic hemangioma, **157:965**
 - testicular (a), **157:423**
 - tumors in children, **157:1267**
- diagnostic medical (b), **157:408**
- Doppler
 - blood-flow indexes (l), **156:1326**
 - cardiac (b), **156:14**
 - circulation in case of fetal death (l), **156:636**
 - duplex (b), **156:984**
 - nomenclature (l), **156:874**
 - Osler-Weber-Rendu disease (l), **157:413**
 - polycystic renal disease (l), **156:408**
 - impotence, **157:923**, **157:932**
 - obstetrics and gynecology (b), **157:544**

Sonography, abdomen

- afferent loop syndrome, **157:41**
- antrooduodenal motility studied by (a), **156:880**
- biliary tract, infants and children, **157:1051**
- duplex Doppler, hepatic vein in tricuspid regurgitation, **156:79**
- early pregnancy (a), **156:1333**
- endoscopic
 - gallbladder carcinoma (a), **156:881**
 - pancreatic tumor diagnosis (a), **157:892**
- gallbladder
 - perforation (a), **156:1120**
 - striated thickening of wall, **156:945**
 - variants (p), **157:1205**
- gastrointestinal tract, endoscopic (p), **156:63**
- sincalide-aided, common bile duct (a), **156:412**
- Yersinia* terminal ileitis, **156:965**

Sonography, adrenal, congenital hyperplasia, neonate, **156:141****Sonography, bone**, broadband attenuation measurements, osteoporosis (l), **156:1326****Sonography, breast**

- equipment and review, **156:449**
- fine-needle aspiration biopsy, carcinoma (a), **156:206**
- phyllodes tumor, **157:715**

Sonography, carotid

- color Doppler conventional (l), **156:873**
- contralateral to severe stenosis (l), **157:200**

Sonography, cranium

- posterior fossa intracranial hemorrhage, extracorporeal membrane oxygenation treatment and, **156:571**
- unilateral hydrocephalus, prenatal, **156:359**
- ventriculomegaly, measurement error effects (a), **157:204**

Sonography, endorectal

- rectal and perirectal disease (p), **157:503**
- seminal tract abnormalities, infertility and, **157:337**
- surgical glove and (l), **156:865**

Sonography, enodvaginal, color flow Doppler, gestational trophoblastic disease, **157:787****Sonography, esophagus**, duplex Doppler, portal venous system, **156:85****Sonography, eye**, eye disorders (p), **157:1079****Sonography, fetal**

- abdominal wall mass, fetus, **157:1065**
- amniotic band syndrome, **156:555**
- gestational age prediction, **157:1275**
- heart, four-chamber view, **156:547**
- kidney, normal length, **157:545**
- major malformations, aberrant growth and, trisomic fetuses (a), **157:1133**
- thanatophoric dwarf variant fetus, **156:149**

Sonography, intravascular

- arteriosclerosis detection, **156:1087**
- histopathologic validation of (a), **157:1131**

Sonography, kidney

- length measurements, children, **156:1029**
- real-time, detection of stones, **157:975**

Sonography, liver

- detection of masses with carcinoma, comparison with MR imaging and CT, **157:731**
- detection of tumors (l), **156:867**
- hepatocellular carcinoma, **157:303**
- high-frequency transducers, cirrhosis patients (a), **157:892**
- sarcoidosis, hypertrophy of caudate lobe and (l), **157:886**

Sonography, lower extremity, deep venous thrombosis (l), **157:1126****Sonography, mediastinum**

- lymphoma (l), **157:644**
- lymphoma patients, posttreatment evaluation, commentary, **157:469**

Sonography, pancreas, superior mesenteric artery thickening, cancer, **156:69****Sonography, soft tissue**, sarcoma, **157:353****Sonography, spleen**

- focal lesions (p), **156:949**

- size, infants and children, **157:119**

Sonography, testicles

- microlithiasis, **157:1003**
- primary lymphoma, **157:1225**

Sonography, thorax

- biopsy guided by, mediastinal masses (a), **157:1361**
- Doppler, cardiovascular application (b), **156:930**
- mediastinal lymphoma, therapeutic response, **156:265**
- pleura, **156:1145**
- Takayasu's arteritis (a), **156:645**
- thoracentesis, pneumothorax associated with, **156:917**

Sonography, transabdominal, transperineal approach, third trimester of pregnancy, **157:73****Sonography, transesophageal**, mediastinal lymph node metastases, lung cancer (a), **156:203****Sonography, translabial**, third-trimester uterine cervix (a), **156:883****Sonography, transperineal**

- pregnancy (a), **157:1364**
- urethra, diverticula of, female, **156:1195**

Sonography, transrectal

- cystic carcinoma of the prostate, **157:785**
- lower rectal adenocarcinoma (a), **157:1133**
- prostate cancer detection (a), **157:1132**
- seminal vesicles (a), **156:1120**

Sonography, transvaginal, color, adnexal masses (a), **157:652****Sonography, umbilical cord**, hematoma (l), **156:1115****Sonography, ureter**

- fibroepithelial polyp, pediatric, **157:1273**
- pregnancy (a), **157:1363**

Sonography, urinary tract

- acute pyelonephritis, **157:539**
- endoluminal, **156:99**
- prostatism patients (a), **157:892**

Spectroscopy

- cerebral ischemia, **156:1133**
- ³¹P MR, renal transplant rejection, **156:105**
- proton MR, multiple sclerosis, **157:1073**

Sphincterotomy, endoscopic, bile duct diameter after (a), **156:883****Spine**

- cervical
 - congenital anomalies (a), **157:204**
 - neural foramina, degenerative narrowing, MR, **156:1229**
 - paraspinal calcification, collagen vascular disease, **157:523**
- dermal sinus tracts, MR, children, **156:791**
- lumbar, imaging (b), **157:684**
- magnetic susceptibility artifacts and motion effects, cervical neural foramina, MR, **156:1069**
- radiology, trauma patients (l), **156:638**
- trauma (b), **156:1036**

Spleen

- acquired abnormalities, CT (p), **157:1213**
- candidal abscesses, **156:474**
- focal lesions, sonography (p), **156:949**
- hemangioma
 - color Doppler sonography, **157:965**
 - CT, **157:44**
- injuries managed nonoperatively, CT appearance (p), **157:757**
- size, infants and children, sonography, **157:119**
- wandering
 - acute splenic torsion in, children, **156:151**
 - CT and sonography, **157:307**

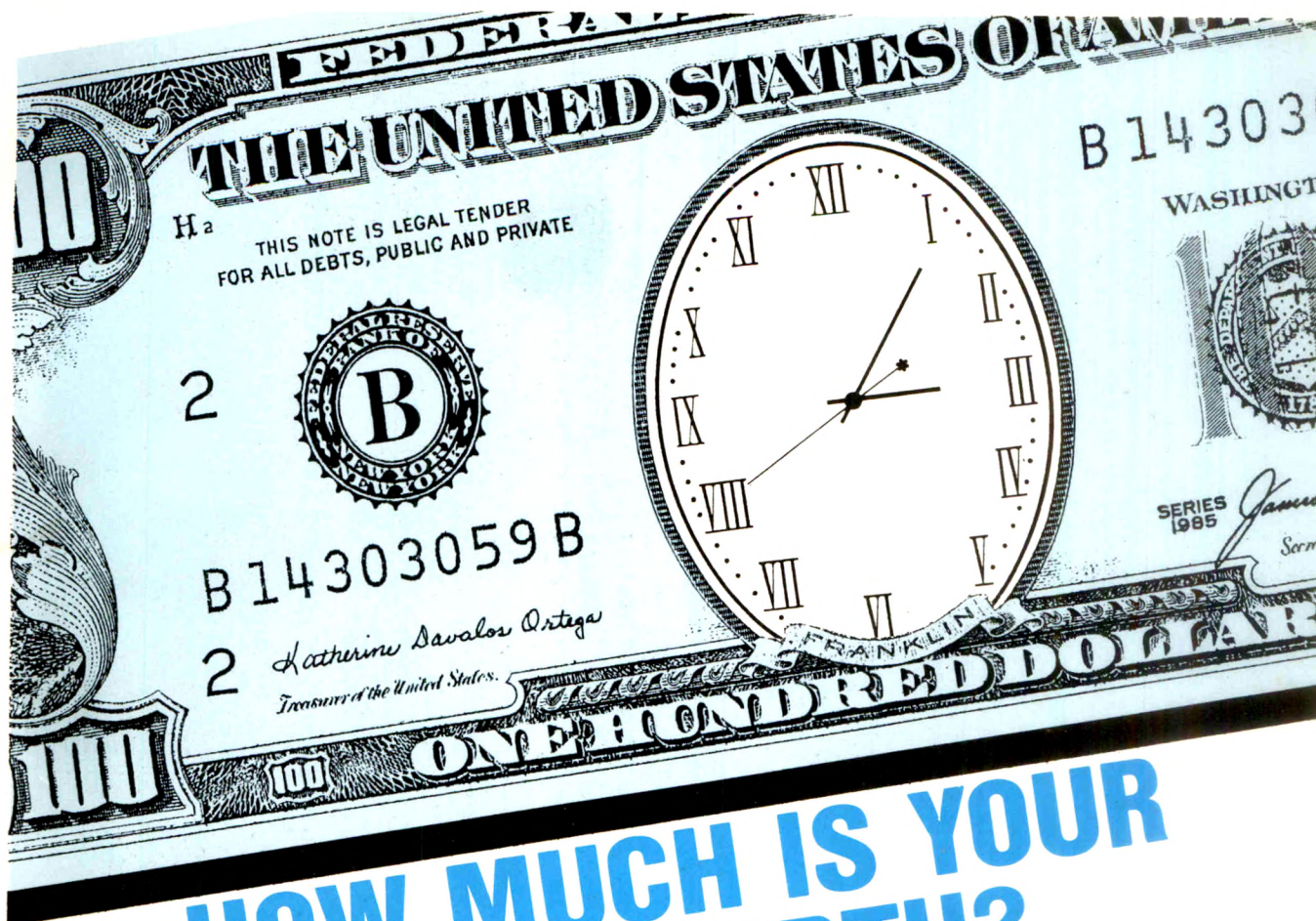
Splenosis, scintigraphic detection, ureteral compression and hydronephrosis (l), **156:406****Spondylolysis**, cervical, CT (l), **156:200**, **157:1127****Squamous cell carcinoma**, base of tongue, liver and bone metastases (l), **156:1328****Stroke**, acute, MR and CT imaging, **157:585****Stroke volume**, right and left ventricular, measurements with velocity-encoded cine MR, **157:9**

- Subarachnoid hemorrhage**, nonaneurysmal perimesencephalic, CT and MR imaging, 157:1325
- Subcapsular hepatic necrosis**, liver transplantation, CT, 156:981
- Subclavian artery**
hemorrhage after removal of catheter, balloon catheter control, 156:1261
percutaneous transluminal angioplasty in, 156:1091
- Subclavian vein**, preoperative evaluation, dialysis access planning and, 156:623
- Subtraction images**, hemorrhagic brain lesions, contrast-enhanced MR imaging, 157:861
- Suprahyoid portion**, neck, lesions, MR imaging (p), 157:147
- Surfactant**
newborns less than 30 weeks' gestation (a), 157:419
synthetic, infants treated with (a), 156:1333
synthetic vs human, respiratory distress syndrome, 157:371
- Surgical glove**, endorectal sonography and (l), 156:865
- Swallowing**
altered function, elderly patients without dysphagia, 156:1181
videofluoroscopy, elderly patients with aspiration (l), 157:647
- Synovial sarcoma**, MR (p), 156:337
- Syphilis**, congenital, hepatic calcifications caused by (l), 156:634
- T**
- Takayasu's arteritis**, carotid duplex sonography (a), 156:645
- Talus**, osteomyelitis, limping in childhood and, 156:785
- Teleradiology**
dial-up digital system, 157:1331
hardware and communications, 156:1279
- Testicles**
bilateral infarction, caused by epididymitis, 157:517
microlithiasis, sonography, 157:1003
primary lymphoma, sonography, 157:1225
- Thalassemia major**, bone dysplasia, deferoxamine-induced, 156:561
- Thallium-201**, reinjection, following delayed imaging (a), 156:882
- Thoracentesis**, pneumothorax associated with, 156:917
- Thoracic duct**, laceration, lymphangiography and CT in, 157:703
- Thoracic inlet**, transaxial MR images (p), 157:707
- Thoracic vent**, Tru-Close, different opinion (l), 156:404
- Thorax**
diseases of (b), 157:692
radiography, paraquat poisoning, 157:697
- Thrombolysis**, pulsed-spray, arterial and bypass graft occlusions, 156:617
- Thrombosis**
deep venous, lower extremity, sonography (l), 157:1126
left-sided vena cava (l), 156:875
- Thymolipoma**, mediastinal, CT, 157:468
- Thyroid**, disease (b), 157:286
- Tibia**, adamantinoma, fibrous dysplasia vs, 156:1017
- Tongue**, primary squamous cell carcinoma, liver and bone metastases (l), 156:1328
- Transcatheter arterial chemoembolization**, recurrent hepatocellular carcinoma, after partial hepatectomy, 156:1177
- Transitional cell carcinoma**, stage D2, bladder (l), 156:1325
- Trauma**
aortic injury, CT (l), 157:1123
blunt
diaphragmatic rupture, 156:51
diaphragmatic rupture due to (l), 157:411
lap-belt ecchymosis, children, CT findings, 157:111
radiology of cervical spine (l), 156:638
thoracic, CT screening, 156:273
- Tricuspid regurgitation**, duplex Doppler sonography, hepatic vein, 156:79
- Trochlear nerve**, neoplasm, MR imaging of, 157:595
- Trophoblastic disease**, gestational, endovaginal color flow Doppler sonography, 157:787
- Tuber cinereum**, hamartomas of, CT, MR, and pathologic findings, 156:1053
- Tuberculosis**
changing epidemiology, United States, 156:255
pulmonary, HIV type 1 in (a), 156:1118
- Tuberous sclerosis**, imaging characteristics (p), 156:1081
- Tubes**, alimentary and respiratory tracts, CT appearance in head and neck (p), 156:1047
- Tumor hypoxia**, ^{31}P MR spectroscopy characterization, 157:243
- Turner, John W. (m)**, 157:824
- U**
- Umbilical artery**
catheterization, aortic thrombosis after, neonate, 156:567
concurrent anomalies, prenatal detection (a), 157:423
- Umbilical cord**, hematoma, sonography (l), 156:1115
- Ureter**
calculi, oblique plain radiographs (l), 156:637
fibroepithelial polyp, pediatric, CT, sonography, and excretory urography, 157:1273
sonographic visualization, pregnancy (a), 157:1363
- Ureteral pseudodiverticula**, uroepithelial malignancy and, 157:69
- Ureteral stent**
antegrade, simplified method for placement, 156:763
Gianturco self-expanding, dilatation of prostatic urethra, 156:757
internal double-J, retrograde replacement of, 156:1007
- Ureteroileal interposition**, diffuse ileal stenosis after, 157:315
- Urethra**
abnormalities, male neonates with VATER association, 156:137
female, diverticula of, transperineal sonography, 156:1195
prostatic, dilatation with the Gianturco self-expanding metallic stent, 156:757
- Urinary diversion**, calculi formed on surgical staples, 157:115
- Urinary tract**
calculi, formed on surgical staples, 157:115
endoluminal sonography, 156:99
- Urinoma**, bilateral, adult (l), 157:414
- Urography**
excretory, fibroepithelial polyp, pediatric, 157:1273
retrograde, ureteral pseudodiverticula, 157:69
- Uropathy**, chronic obstructive, urographic finding in, 156:985
- Uroradiology**, textbook (b), 157:520
- Ursodeoxycholic acid**, gallbladder contraction and, gallstone patients (a), 156:203
- Ursodiol**, ESWL and, gallstones (a), 156:641
- Uveal melanoma**, malignant, MR imaging, 157:1087
- V**
- Vascular grafts**, children, MR imaging, 157:1069
- VATER association**, male neonates, urethral abnormalities with, 156:137
- Veins**, nomenclature, lower extremity (l), 157:200
- Vena cava**
inferior
filters, 156:813
membranous stenosis of (l), 156:639
spontaneous fracture of filter, 157:177
translumbar access, CT, 156:395
left-sided, isolated thrombosis (l), 156:875
thrombus, nonrenal parenchymal malignancy with (a), 156:1332
tumor thrombi, MR (a), 156:882
- Venography**, lower extremity, conventional vs phosphor plate venograms, 156:1095
- Ventriculomegaly**, sonographic evaluation, measurement error effects (a), 157:204
- Videofluoroscopy**
elderly patients, aspiration, 156:293
elderly patients, aspiration (l), 157:647
- Videotape reviews**
MRI of MS and white matter disease, 156:1074
MRI of the brain stem, 156:1052
orthopedic radiology, 156:1010
RSNA today, vol. 4, no. 2, 156:96
RSNA today, vol. 4, no. 3, 156:948
RSNA today, vol. 4, no. 4, 157:380
RSNA today, vol. 4, no. 5, 157:494
RSNA today, vol. 4, no. 6, 157:1064
Wolf-Heidegger's atlas of human anatomy, 156:960
- W**
- White matter**, hyperintensities, MR imaging, 157:1317
- Wilms tumor**, pulmonary emboli and, 156:155
- Wrist**, arthrography, unidirectional joint communications, 157:105
- Wrist surface coil**, two-piece, 156:343
- Y**
- Yersinia enterocolitica**, systemic infection, iron overload and deferoxamine therapy, 157:773
- Z**
- Zollinger-Ellison syndrome**, peptic ulcer perforation (a), 156:1118



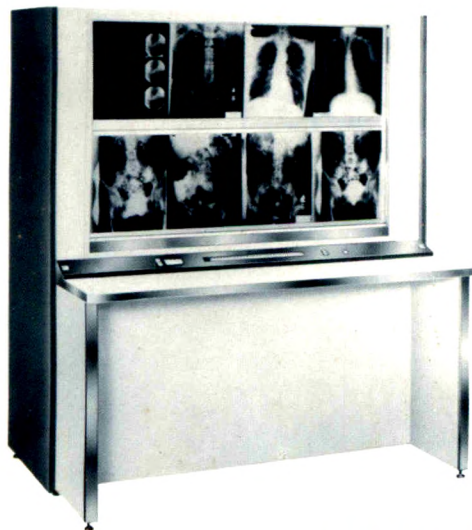
**Statement of Ownership,
Management and
Circulation**
(Required by 39 U.S.C. 3685)

1A. Title of Publication AJR-AMERICAN JOURNAL OF ROENTGENOLOGY		1B. PUBLICATION NO. 0 3 6 1 8 0 3 X		2. Date of Filing 10/1/91
3. Frequency of Issue Monthly		3A. No. of Issues Published Annually 12	3B. Annual Subscription Price \$125.00	
4. Complete Mailing Address of Known Office of Publication (Street, City, County, State and ZIP+4 Code) (Not printers) 428 East Preston Street, Baltimore, Maryland 21202-3993				
5. Complete Mailing Address of the Headquarters of General Business Offices of the Publisher (Not printer) 428 East Preston Street, Baltimore, Maryland 21202-3993				
6. Full Names and Complete Mailing Address of Publisher, Editor, and Managing Editor (This item MUST NOT be blank)				
Publisher (Name and Complete Mailing Address) Williams & Wilkins, 428 E. Preston Street, Baltimore, Maryland 21202-3993				
Editor (Name and Complete Mailing Address) Robert N. Berk, M.D., 2223 Avenida de la Playa, Suite 103, La Jolla, CA 92037-3218				
Managing Editor (Name and Complete Mailing Address)				
7. Owner (If owned by a corporation, its name and address must be stated and also immediately thereunder the names and addresses of stockholders owning or holding 1 percent or more of total amount of stock. If not owned by a corporation, the names and addresses of the individual owners must be given. If owned by a partnership or other unincorporated firm, its name and address, as well as that of each individual must be given. If the publication is published by a nonprofit organization, its name and address must be stated.) (Item must be completed)				
Full Name American Roentgen Ray Society		Complete Mailing Address 1891 Preston White Drive Reston, VA 22091		
8. Known Bondholders, Mortgagees, and Other Security Holders Owning or Holding 1 Percent or More of Total Amount of Bonds, Mortgages or Other Securities (If there are none, so state)				
Full Name NONE		Complete Mailing Address		
9. For Completion by Nonprofit Organizations Authorized to Mail at Special Rates (DMM Section 424.12 only) The purpose, function, and nonprofit status of this organization and the exempt status for Federal income tax purposes (Check one)				
(1) <input checked="" type="checkbox"/> Has Not Changed During Preceding 12 Months (2) <input type="checkbox"/> Has Changed During Preceding 12 Months (If changed, publisher must submit explanation of change with this statement)				
10. Extent and Nature of Circulation (See instructions on reverse side)		Average No. Copies Each Issue During Preceding 12 Months		Actual No. Copies of Single Issue Published Nearest to Filing Date
A. Total No. Copies (Net Press Run)		26560		27816
B. Paid and/or Requested Circulation **SEE BELOW 1. Sales through dealers and carriers, street vendors and counter sales		1554		1648
2. Mail Subscription (Paid and/or requested)		20490		21005
C. Total Paid and/or Requested Circulation (Sum of 10B1 and 10B2)		22044		22653
D. Free Distribution by Mail, Carrier or Other Means Samples, Complimentary, and Other Free Copies		408		328
E. Total Distribution (Sum of C and D)		22452		22981
F. Copies Not Distributed 1. Office use, left over, unaccounted, spoiled after printing		4108		4835
2. Return from News Agents		NONE		NONE
G. TOTAL (Sum of E, F1 and 2—should equal net press run shown in A)		26560		27816
11. I certify that the statements made by me above are correct and complete		Signature and Title of Editor, Publisher, Business Manager, or Owner <i>Alma J. Willis</i> Publisher		



HOW MUCH IS YOUR TIME WORTH?

If, like most Radiologists, you spend 30% or more of your day **handling** films, let us show you how S & S Motorized Viewers eliminate those **COSTLY WASTED HOURS!**



Model MV216

- From 48 up to 324 14" x 17" films can be pre-loaded and stored in proper sequence to be recalled when needed for viewing in as little as 7 seconds—by simply pressing a button!
- All 12 models feature illumination brighter than most other viewers, plus individual panel light controls which promote viewer concentration and increase reading efficiency.
- Some models feature an optional "floating bright spot" which illuminates dense area—at the touch of a button.
- Optional remote controls eliminate need to stand directly in front of viewer to operate it.
- Smaller capacity units on casters provide room-to-room mobility as needed.
- Specially dedicated models are also available for MAMMOGRAPHY, ULTRASOUND, CT and NUCLEAR FILM VIEWING.

Ideal for Teaching, Lecturing or Consultation, S & S Motorized Viewers turn waste into efficiency. **How much is YOUR time worth? Call S & S or your local x-ray dealer today.**

S & S X-RAY PRODUCTS INC.

1101 Linwood Street
Brooklyn, NY 11208
800/347-XRAY
718/649-8500
FAX 718/257-0219



SPECIAL ARTICLE

- 1153 Acute reactions to intravascular contrast media: types, risk factors, recognition, and specific treatment. *Bush WH, Swanson DP*

REVIEW ARTICLES

- 1163 Clinical value of high-resolution CT in chronic diffuse lung disease. *Müller NL*
1171 Masses of the anterior mediastinum: CT and MR imaging. *Brown LR, Aughenbaugh GL*

PULMONARY RADIOLOGY

- 1181 Bronchus sign on CT in peripheral carcinoma of the lung: value in predicting results of transbronchial biopsy. *Gaeta M, Pandolfo I, Volta S, et al.*
1187 Case report. Tuberculous bronchial stenosis: treatment with balloon bronchoplasty. *Nakamura K, Terada N, Ohi M, Matsushita T, Kato N, Nakagawa T*

GASTROINTESTINAL RADIOLOGY

- 1189 Complications after total gastrectomy and esophagojejunostomy: radiologic evaluation. *Levine MS, Fisher AR, Rubesin SE, Laufer I, Herlinger H, Rosato EF*
1195 Low-attenuation periportal collar in transplanted liver is not reliable CT evidence of acute allograft rejection. *Stevens SD, Heiken JP, Brunt E, Hanto DW, Flye MW*
1199 Endosonography of the anal sphincter: findings in healthy volunteers. *Nielsen MB, Pedersen JF, Hauge C, Rasmussen OØ, Christiansen J*
1203 Case report. Chronic intestinal bleeding due to mesenteric vascular insufficiency. *Pollak JS, Bennick M, Denny DF Jr, Markowitz D*
1205 Pictorial essay. Imaging of gallbladder variants. *Meilstrup JW, Hopper KD, Thieme GA*
1209 Percutaneous drainage of hepatic abscesses: comparison of results in abscesses with and without intrahepatic biliary communication. *Do H, Lambiase RE, Deyoe L, Cronan JJ, Dorfman GS*
1213 CT of acquired abnormalities of the spleen. *Taylor AJ, Dodds WJ, Erickson SJ, Stewart ET*

GENITOURINARY RADIOLOGY

- 1221 Cancer of the endometrium: value of MR imaging in determining depth of invasion into the myometrium. *Lien HH, Blomlie V, Tropé C, Kærn J, Abeler VM*
1225 Case report. Sonographic appearance of primary testicular lymphoma. *Moorjani V, Mashankar A, Goel S, Khandelwal K, Patange V, Merchant N*
1227 Case report. Gelatin sponge mimicking a pelvic neoplasm on MR imaging. *Hoeffner EG, Soulen RL, Christensen CW*

MUSCULOSKELETAL RADIOLOGY

- 1229 Review. Noninvasive measurements of bone mass, structure, and strength: current methods and experimental techniques. *Faulkner KG, Glüer C-C, Majumdar S, Lang P, Engelke K, Genant HK*
1239 Do asymptomatic marathon runners have an increased prevalence of meniscal abnormalities? An MR study of the knee in 23 volunteers. *Shellock FG, Deutsch AL, Mink JH, Kerr R*
1243 Myositis ossificans: MR appearance with radiologic-pathologic correlation. *Krandsdorf MJ, Meis JM, Jelinek JS*
1249 Case report. Soft-tissue and osseous lesions caused by bacillary angiomatosis: unusual manifestations of cat-scratch fever in patients with AIDS. *Herts BR, Rafii M, Spiegel G*

VASCULAR AND INTERVENTIONAL RADIOLOGY

- 1253 Dye laser-assisted angioplasty with multifiber catheters: short-term results in the treatment of 29 peripheral arterial occlusions. *Huppert PE, Duda SH, Seboldt H, Claussen CD*

- 1259 Anatomic relationship between the popliteal artery and vein: a guide to accurate angiographic puncture. *Trigaux J-P, Van Beers B, De Wispelaere J-F*
1263 Percutaneous dilatation of benign biliary strictures: single-session therapy with general anesthesia. *Lee MJ, Mueller PR, Saini S, Hahn PF, Dawson SL*

PEDIATRIC AND FETAL RADIOLOGY

- 1267 Vascularity of tumors in children: evaluation with color Doppler imaging. *Taylor GA, Perlman EJ, Scherer LR, Gearhart JP, Leventhal BG, Wiley J*
1273 Case report. Fibroepithelial polyp of the ureter in a child. *Liddell RM, Weinberger E, Schofield DE, Pelman RS*
1275 Sonographic prediction of gestational age: accuracy of second- and third-trimester fetal measurements. *Benson CB, Doubilet PM*

NEURORADIOLOGY

- 1279 The prevalence and location of metastases from ocular melanoma: imaging study in 110 patients. *Lorigan JG, Wallace S, Mavligit GM*
1283 Pictorial essay. Intraventricular mass lesions of the brain: CT and MR findings. *Tien RD*
1291 Stroke associated with coronary artery bypass surgery. *Hise JH, Nipper ML, Schnitker JC*
1295 Commentary. A new role for radiologists in the development of cardiac surgery. *Moody DM*
1297 Commentary. Neuroimaging of cerebral infarction associated with coronary revascularization. *Sila CA*
1299 Assessment of carotid artery patency on routine spin-echo MR imaging of the brain. *Lane JI, Flanders AE, Doan HT, Bell RD*
1307 Commentary. Re: assessment of carotid artery patency on routine spin-echo MR imaging of the brain. *Brant-Zawadzki M*
1309 Angiographic diagnosis and management of head and neck schwannomas. *Abramowitz J, Dion JE, Jensen ME, et al.*
1317 The morphologic correlate of incidental punctate white matter hyperintensities on MR images. *Fazekas F, Kleinert R, Offenbacher H, et al.*
1325 Nonaneurysmal perimesencephalic subarachnoid hemorrhage: CT and MR patterns that differ from aneurysmal rupture. *Rinkel GJE, Wijdicks EFM, Vermeulen M, et al.*

TELERRADIOLOGY

- 1331 Perspective. A dial-up digital teleradiology system: technical considerations and clinical experience. *Templeton AW, Dwyer SJ III, Rosenthal SJ, Eckard DA, Harrison LA, Cook LT*

RADIOLOGY PRACTICE

- 1337 Productivity of radiologists: estimates based on analysis of relative value units. *Conoley PM, Vernon SW*
1341 Radiology practices and their contracts with hospitals, 1989-1990: a representative sample survey. *Sunshine J, Chan WC, Kassinger PJ*

OTHER CONTENT

- 1185 List of book reviews
1198 ARRS 1992 residents' award papers information
1258 Memorial, James A. Jagodzinski
1272 Meeting news. International Pediatric Radiology '91
1278 Radiologic-pathologic conference
1316 Call for papers on neuroradiology
1348 Forthcoming articles
1349 Recognition of manuscript and book reviewers 1991
1352 Letters
1361 Review of current literature
1365 News
1368 American Roentgen Ray Society information
1369 Classified advertisements
1380 Index, Volumes 156-157
A8 AJR business and subscriber information
A21 Guidelines for authors